SEDHYD 2019

Proceedings of SEDHYD 2019: Conferences on Sedimentation and Hydrologic Modeling

Volume 1

Climate Variability and Sediment, Dam Removal or Rehabilitation, Earthen Embankment Erosion Prediction, Extreme Floods and Droughts, Flood Hydrology, Fluvial Geomorphology, Forecasting

Proceedings of SEDHYD 2019: Conferences on Sedimentation and Hydrologic Modeling, 24-28 June 2019 in Reno, NV.

These engineering and scientific proceedings provide much of the latest information on sedimentation and hydrologic modeling (applied research and state of-the-practice) from Federal agencies, universities, and consultants. SEDHYD is the successor to the Federal Interagency Conferences on Sedimentation and Hydrologic Modeling. The Subcommittee on Sedimentation convened the first Federal Interagency Sedimentation Conference (FISC) in 1947. Subsequent FISC conferences were convened in 1963, 1976, 1986, 1991, 1996, and 2001. The Subcommittee on Hydrology convened their first Federal Interagency Workshop, "Hydrologic Modeling Demands for the 90s," in 1993. Subsequent to that workshop, the Subcommittee on Hydrology convened the Federal Interagency Hydrologic Modeling Conferences (FIHMC) in 1998 and 2002. Subsequently, the Subcommittees on Sedimentation and Hydrology began convening the Federal interagency conferences together in 2006 and again in 2010, and 2015. Beginning in 2019, the SEDHYD Conference was hosted by SEDHYD, Inc., a non-profit organization.

Since 1947, the Sedimentation and Hydrologic Modeling Conferences have provided over 3,000 technical papers and extended abstracts and provided engineers and scientists with the opportunity to learn and exchange information about the latest developments and research related to sedimentation and hydrologic modeling. As a continuation of these conferences, SEDHYD provides an interdisciplinary mix of scientists and managers from government agencies, universities, and consultants to present recent accomplishments and progress in research and on technical developments related to sedimentation processes, hydrologic modeling, and the impact of sediment on the environment.

The SEDHYD conference provides a mixed set of formats that include formal technical presentations, poster sessions, field trips, workshops, computer model demonstrations, and a student paper competition. The SEDHYD conference also provides excellent networking opportunities.

The SEDHYD 2019 Conference site was at the Peppermill Hotel and Resort in Reno, Nevada. Reno is situated in a high desert just east of the beautiful Sierra Nevada Mountains. The city lies on the western edge of the Great Basin, at an elevation of 4,400 feet (1,300 meters) above sea level. The Reno downtown area (along with Sparks) occupies a valley informally known as Truckee Meadows. The area offers spectacular desert landscapes and ecosystems, as well as numerous indoor and outdoor recreational opportunities.

Suggested Citation:
In Proceedings of SEDHYD 2019: Conferences on Sedimentation and Hydrologic Modeling, 24-28 June 2019 in Reno, Nevada, USA.

SEDHYD 2019 Planning Committee

Planning Committee Position	Volunteer	Organization
SEDHYD Conference Chair	Jerry Webb	West Consultants
SEDHYD Operations Chair	Jennifer Bountry	Reclamation
SEDHYD Technical Program Chair	Chandra Pathak	USACE
SEDHYD Technical Program Chair (YP)	Will Farmer	USGS
SEDHYD Technical Program	Jerry Bernard	NRCS, retired
Sedimentation Conference Chair	Tim Randle	Reclamation
Sedimentation Program Chair	Eddy Langendoen	ARS
Sedimentation Program Chair (YP)	Joel Sholtes	Mesa State
Hydrologic Modeling Conference Chair	Claudia Hoeft	NRCS
Hydrologic Modeling Program Chair	Jim Barton	USACE, retired
Hydrologic Modeling Program Chair (YP)	Jessica Driscoll	USGS
Student Program Coordinator	Amanda Cox	MWRRC
Proceedings Coordinator	Bob Boyd	BLM
Proceedings Coordinator	Peter Doran	BLM
Poster & Computer Model Demonstration Coordinator	Eddie Brauer	USACE
Short Course Coordinator	Jeff Bradley	ASCE, West Consultants
Short Course Coordinator (YP)	Kevin Denn	USACE, St. Paul Dist.
Field Trip Coordinator	Steve Berris	USGS
Field Trip Coordinator (YP)	Jena Huntington	USGS
Web site Coordinator	Darren Nezamfar	USACE
Registration Coordinator	Penni Baker	USACE
Registration Volunteer	Kathy Randle	
Young Professionals Coordinator	Caroline Ubing	Reclamation
Young Professionals Coordinator	Sara Horgen	Reclamation
Exhibit Coordinator	Molly Wood	USGS
Exhibit Coordinator	Tim Straub	USGS
AV Equipment Coordinator	Jeff Harris	West Consultants
Planning Committee	Jo Johnson	NRCS
Planning Committee	Jon Fripp	NRCS
Planning Committee	Paul Boyd	USACE
Planning Committee	Meg Jonas	USACOE, retired
Planning Committee	Robert R Mason	USGS
Planning Committee	Victor Hom	NOAA

SEDHYD, Inc.

SEDHYD, Inc. Position	Volunteer
SEDHYD President & Board Chair	Jerry Webb
SEDHYD Vice President & Board Member	Jerry Bernard
SEDHYD Treasurer & Board Member	Don Frevert
SEDHYD Secretary & Board Member	Matt Romkens
SEDHYD Board Member	Doug Glysson

Table of Contents

Table of Contents

Table of Contents

Table of Contents

Fluvial Geomorphology (continued)

Table of Contents

Table of Contents

Climate Variability & Sediment

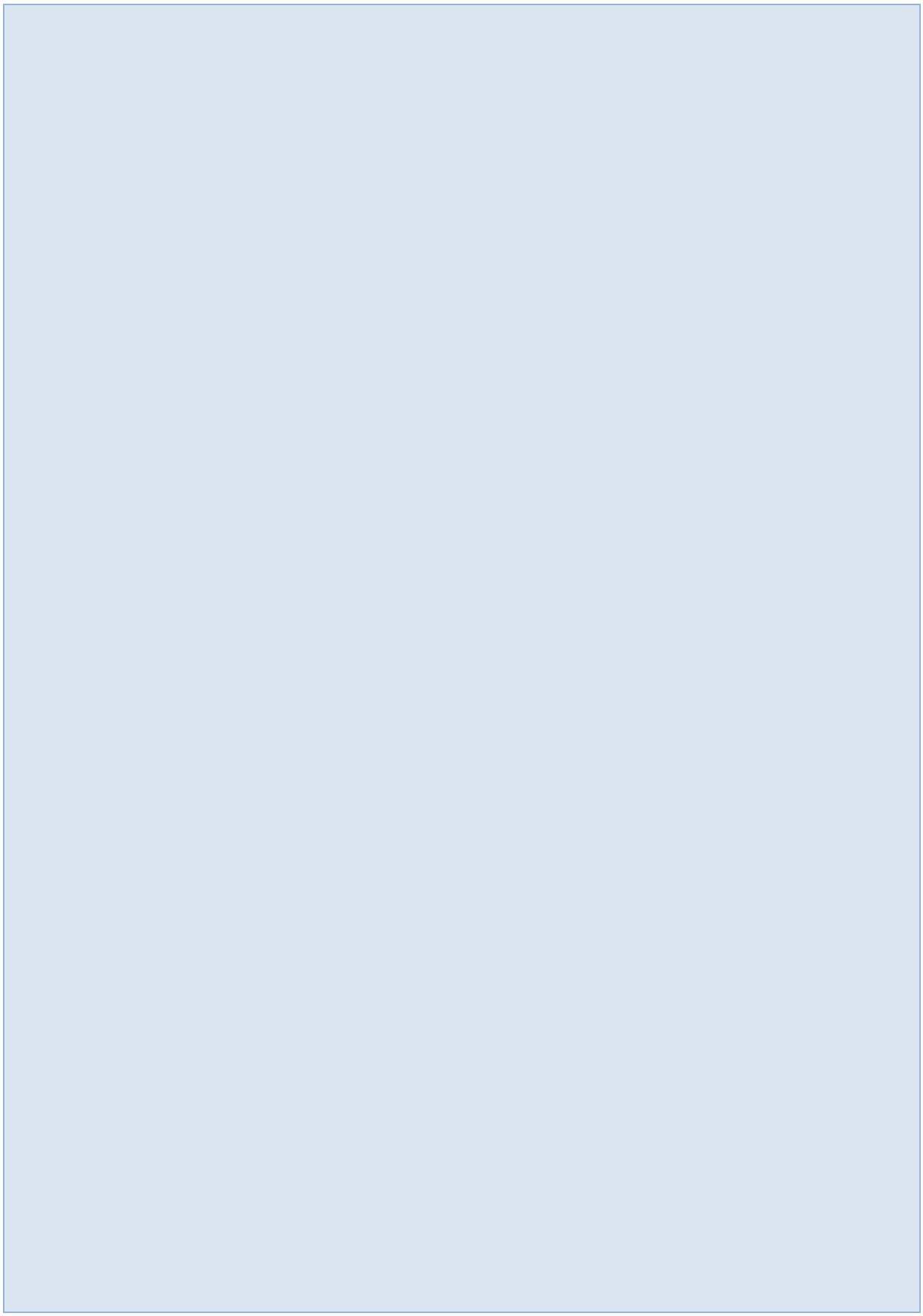

Area of Prairie (Pimple) Mounds in Central Arkansas and Implications for Irrigated Agriculture

Chris King, Geologist, United States Department of Agriculture – Natural Resources Conservation Service, Little Rock, Arkansas, chris.king@usda.gov

Richard Vaught, Soil Scientist, United States Department of Agriculture – Natural Resources Conservation Service, Conway, Arkansas, richard.vaught@usda.gov

Background

Prairie mounds (also known as pimple mounds) are hillocks approximately three feet high and up to 60 feet in diameter found on river and marine terraces across the south-central U.S (Figure 1). Explorers and settlers in western North America noted a peculiar micro-relief called pimple mounds. Four major explanations have been offered, including the work of Native Americans, gophers, ants, and aeolian deposition.

Found throughout the south-central United States, prairie mounds reflect landscape response to protracted late Holocene droughts. Composed of windblown sand and silt, the mounds are formed when a weed or other plant grows and its branches slow the wind, causing deposition. This forms a favorable place for rainfall penetration and further vegetation growth. Thus, the mound grows. The large 30 – 60 feet diameters of these mounds (Figure 2) suggest that arid conditions conducive to growth persisted for decades, possibly even centuries (Quinn, 1961). The existence of prairie mounds throughout the south-central U.S. reflects the severity and duration of late Holocene droughts, which were significantly greater than historically observed climatic variations. Aerial photographs from the 1930's (Bragg and Weir, 2007) show numerous prairie mounds, as well as the vestiges of large prairies on the Pleistocene terraces of southern and eastern Arkansas (Figure 3).

A comprehensive review of paleoclimate literature suggests that droughts more severe than those of the 1930's and 1950's are likely to occur in the future, a possibility that might be exacerbated by climate change. (Booth et al, 2005, Cox et al, 2008, Cox et al, 2004, Denniston et al, 2000, Denniston et al, 2007, Miao et al, 2007, Otvos, 2004, Quinn, 1961, Seifert et al, 2009, Stahle and Cleaveland, 1992, Stahle et al, 2007, Wackerman, 1929, Woodhouse and Overpeck, 1998). A principal difference between major droughts of the twentieth century and major droughts of the more distant past is duration, which is on the order of seasons to years compared to decades to centuries. Dendrochronological records indicate that the period from 1549 – 1577 was likely the worst drought in Arkansas in the past 450 years (Stahle et al, 1985).

Characterized by relatively frequent and severe droughts, tallgrass prairies once covered hundreds of thousands of contiguous hectares across large portions of the state, especially in the Grand Prairie region and west-central Arkansas near Fort Smith (Figure 4). These large prairies were probably legacies of warmer and drier past climates (Bragg and Weir, 2007, Wackerman, 1929). Additional evidence of past aridity is the presence of several "relict species" of plants native to North American desert biomes that still survive today in isolated areas of Arkansas. These include western wallflower (*Erysimum capitatum*) and two cactus species: eastern prickly pear (*Opuntia humifusa*), and western prickly pear (*Opuntia macrohiza*) (Gentry et al, 2013).

Prairie mound sediments from across the south-central United States yield dates between 2400 – 700 years B.P., which correlate with well-documented periods of drought on the Great Plains, as well as the Medieval Climate Anomaly (Cox et al, 2008, Cox et al, 2004, Seifert et al, 2009,). The disappearance of forests during extended droughts likely contributed to severe wind erosion and subsequent mound formation.

A previously unknown area of prairie mounds in the Morrilton, Arkansas area of central Arkansas exhibits a number of these features in a current wetland area (Figures 4, 5, and 6). Arkansas presently receives approximately 50 inches of rainfall annually. Two of these mounds were sampled and the sediment was submitted for grain size distribution analysis at the USDA-NRCS Soil Mechanics Center.

The two samples are fine grained silt with sand and classified as ML soil according to the Universal Soil Classification System (USCS). This is consistent with aeolian sediments. These ML soils are low plastic with a Plasticity Index (PI) of 6 and 2. The sample with a PI of 6 produced a double hydrometer reading of 50 and specific gravity of 2.67. It has 78 percent fines with 22 percent sand. The sample with a PI of 2 produced a double hydrometer reading of 57 and a specific gravity of 2.69. It has 76 percent fines with 24 percent sand. The double hydrometer readings indicate these soils have the potential for dispersion. Both samples had a color of 10yr 5-3.

The fact that arid conditions recurred for extended periods of time in the south-central United States suggests these conditions may occur again in the future, which is potentially bad news for the region's economy. Arkansas relies on irrigation to make it the leading rice producer in the nation. In 2015 Arkansas ranked first in the nation in rice production, third in cotton, and tenth in soybean production (Delp and Shrum, 2017).

A vitally important characteristic of the precipitation climatology is its high variability. In recent years, severe drought episodes occurred in the state during 2005-2007 and again during 2010-2012, interrupted by the wettest year on record in 2009. Arkansas was one of the hardest hit southeastern states during the 2012 drought. Each of the state's 75 counties received a drought-related disaster declaration (NOAA, 2016).

Significance of Prairie Mounds

The historical presence of prairies and prairie mounds indicate that extended periods of aridity are possible in the south-central United States. This is a problem, as the Mississippi River delta leads the nation in rice production. The potential reduction in rice production in the Mississippi River delta is nationally significant. Without adequate water supplies, agriculture in the delta may need to convert to crops less dependent on irrigation.

With well over 6 million cultivated acres in Arkansas, grain production is not only important to the economy of the state, but also makes a significant contribution to national and world food supplies. Arkansas produces the most rice in the nation with approximately 1.5 million acres. Portions of eastern Arkansas also produce vast quantities of soybeans (approximately 3 million acres), cotton (approximately 1 million acres), corn, and milo (USDA NASS, 2017). Without water for irrigation, present production levels of these crops would not be possible.

Arkansas is one the nation's largest water users. Although Arkansas has traditionally received sufficient precipitation to support preferred crops, climatological trends have illustrated a gradual decline in precipitation rates during the peak growing season (June – August). Growers

are affected by decreased rainfall and droughts, even though groundwater presently supplies most of the water used to irrigate crops in Arkansas (Clark et al, 2013).

There is no overall trend in average annual precipitation in Arkansas. The intensity of future naturally occurring droughts is projected to increase because higher temperatures will increase the rate of loss of soil moisture during dry spells. The number and intensity of extreme heat and extreme precipitation events are projected to increase in the future. (NOAA, 2016).

The year 1963 was the driest year on record in Arkansas since 1895 with a statewide average of 32.8 inches of precipitation. The wettest year recorded was 2009, with an average of 72.2 inches of precipitation. In 2009, reported total groundwater use for irrigation in Arkansas was about 5,900 million gallons per day (MGD). The year 2012 was the 10th driest year on record for all of Arkansas, with an average of 39.79 inches of precipitation. As expected, reported total groundwater use for irrigation in 2012 increased significantly from 2009 to about 8,195 MGD (Arkansas Natural Resources Commission, 2013 and 2015; NOAA, 2016).

In 2013, the USGS-produced MERAS model was used to evaluate sustainability of current and projected water use. Modeling results show that current and projected demands for groundwater in the Mississippi embayment in eastern Arkansas are not sustainable. Pumping at higher rates may persist for some time into the future by mining groundwater that is stored in pore space in the alluvial aquifer (Figure 7). Even with this mining approach to groundwater development, production rates decline rapidly as this storage is depleted.

The implications of continued decline in achievable pumping rates and falling water levels have the potential for severe economic impacts. As water levels decline and pumping lifts increase, wells may need to be deepened and pumps replaced. The cost of pumping will also increase due to the increased lift (Clark et al, 2013).

If the alluvial aquifer is allowed to dewater (scenario 1 in the MERAS model), by the year 2050 the model predicts a supply gap in Arkansas of 5,845.5 MGD. If alluvial aquifer pumping is restricted such that water levels cannot go lower than the center of the alluvial aquifer and to the top of the confined aquifers, the supply gap increases significantly to 7,126.4 MGD (Arkansas Natural Resources Commission, 2014).

The impact of this situation could force growers into dryland farming at much lower profit margins, or put consumptive water use at risk from attempts to use deeper aquifers for irrigation purposes. The use of man-made alternatives such as on-farm reservoirs and river-water diversion, when combined with incorporating the production of alternative crops, offers economically feasible scenarios for producers while also conserving the shallow Mississippi River Alluvial Aquifer at sustainable levels.

NRCS irrigation water management practices and associated supporting practices are estimated to reduce water use at a minimum of 10 – 25 percent (USDA NRCS, 2015). Construction of water storage and distribution networks has begun (Figure 8), however further implementation of water conservation measures should be considered, as several times in the last two decades eastern Arkansas has been designated a federal disaster area due to prolonged drought conditions. Fortunately, increased attention has been given in recent years to better utilization of groundwater with greater use of on-farm reservoirs, tail-water recovery, and the adoption of water-conserving practices.

Predictions that climate shifts may result in more frequent droughts and increasingly sporadic rainfall events suggest the agriculture industry should take a proactive position with regards to conservation of groundwater and storage of precipitation. If climatic patterns are shifting, failure to respond to reduced water supplies will result in unsustainable harvests.

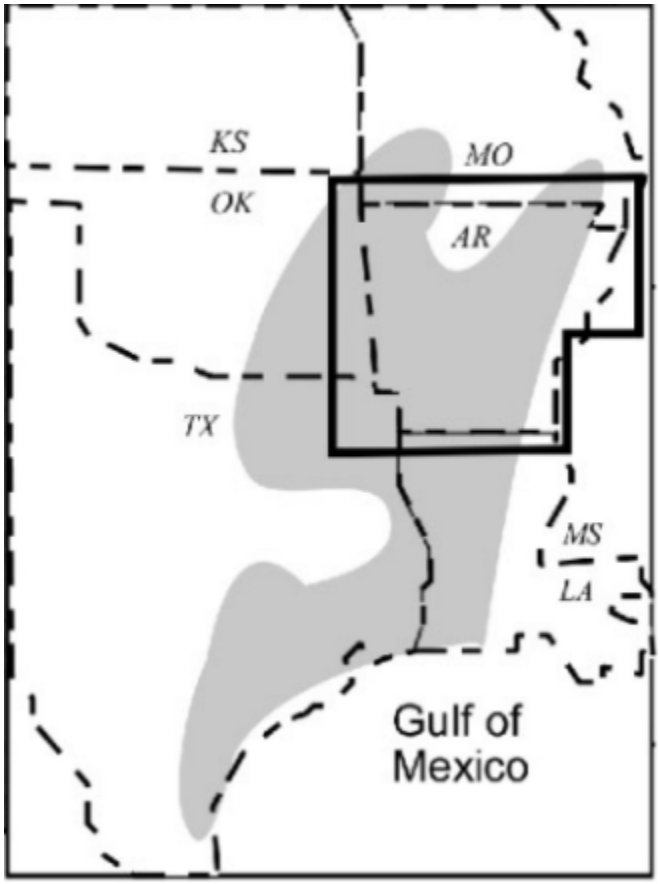

Figure 1. Distribution of prairie mounds in the south-central United States (Seifert, et al, 2009).

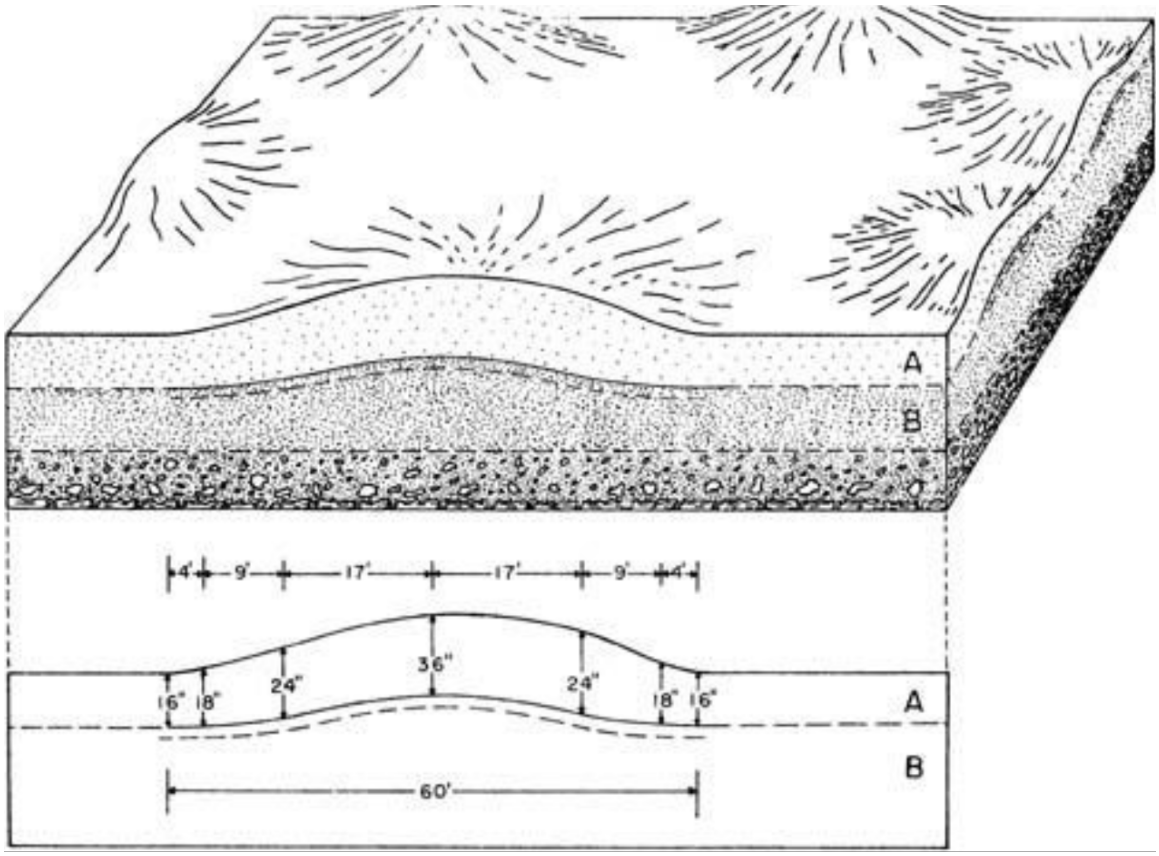

Figure 2. Diagram showing profile and dimensions of a typical prairie mound (Quinn, 1968). The "A" signifies the A horizon, "B" the B horizon, and the dashed line below the B unit indicates the base of the silt unit.

Figure 3. Historical air photo from 11/24/1974 taken just east of Bald Knob in White County, Arkansas. The light dots at the center and right of center are prairie mounds.

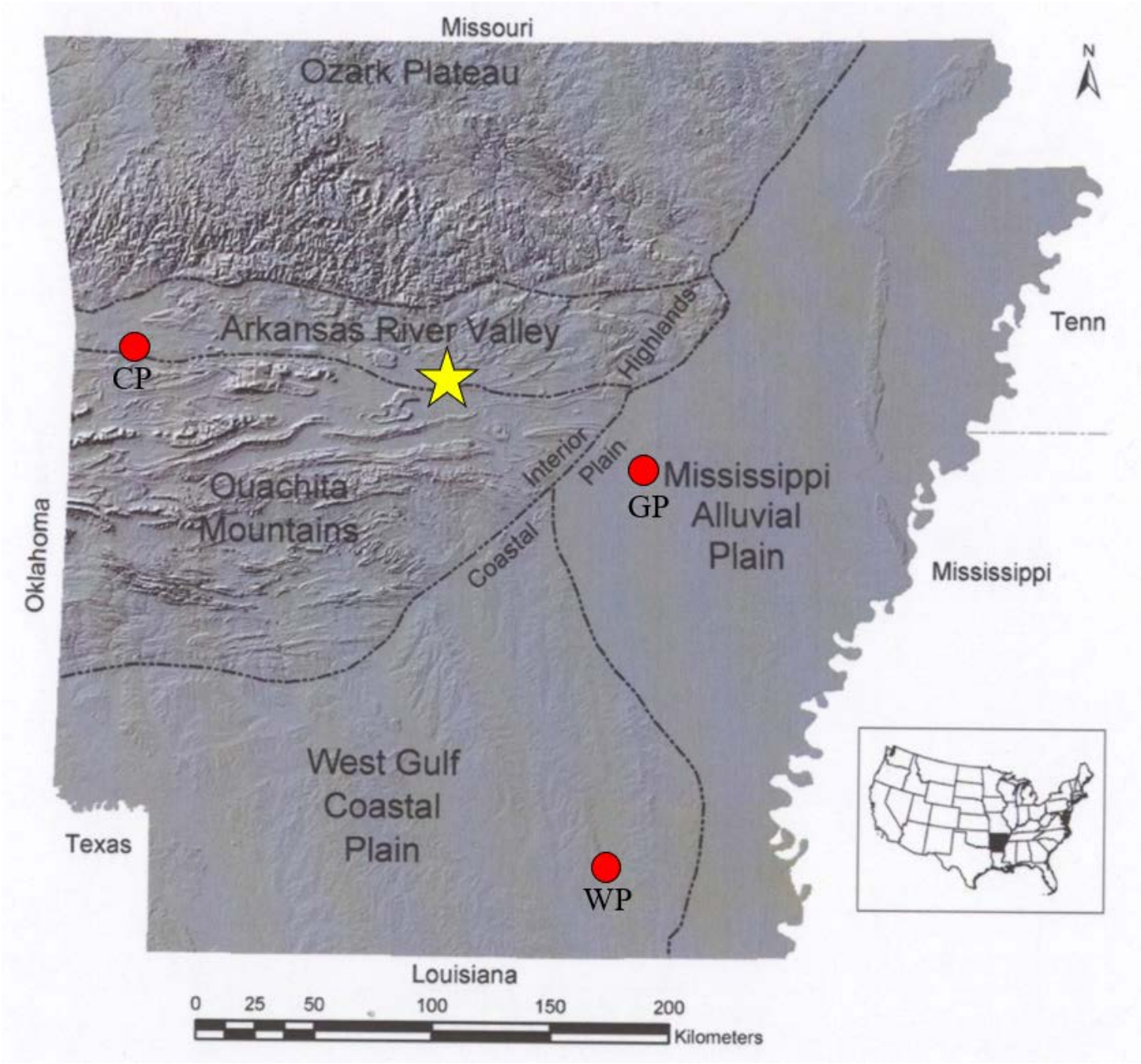

Figure 4. Physiographic map of Arkansas, showing Morrilton Airport (yellow star), Cherokee Prairie (CP), Grand Prairie (GP), and Warren Prairie (WP).

Figure 5. Aerial photograph showing prairie mounds (yellow arrows) next to the Morrilton airport. One-foot contour intervals.

Figure 6. Picture of a prairie mound next to the Morrilton airport. NRCS Soil Scientist Richard Vaught is standing on the crest of the mound.

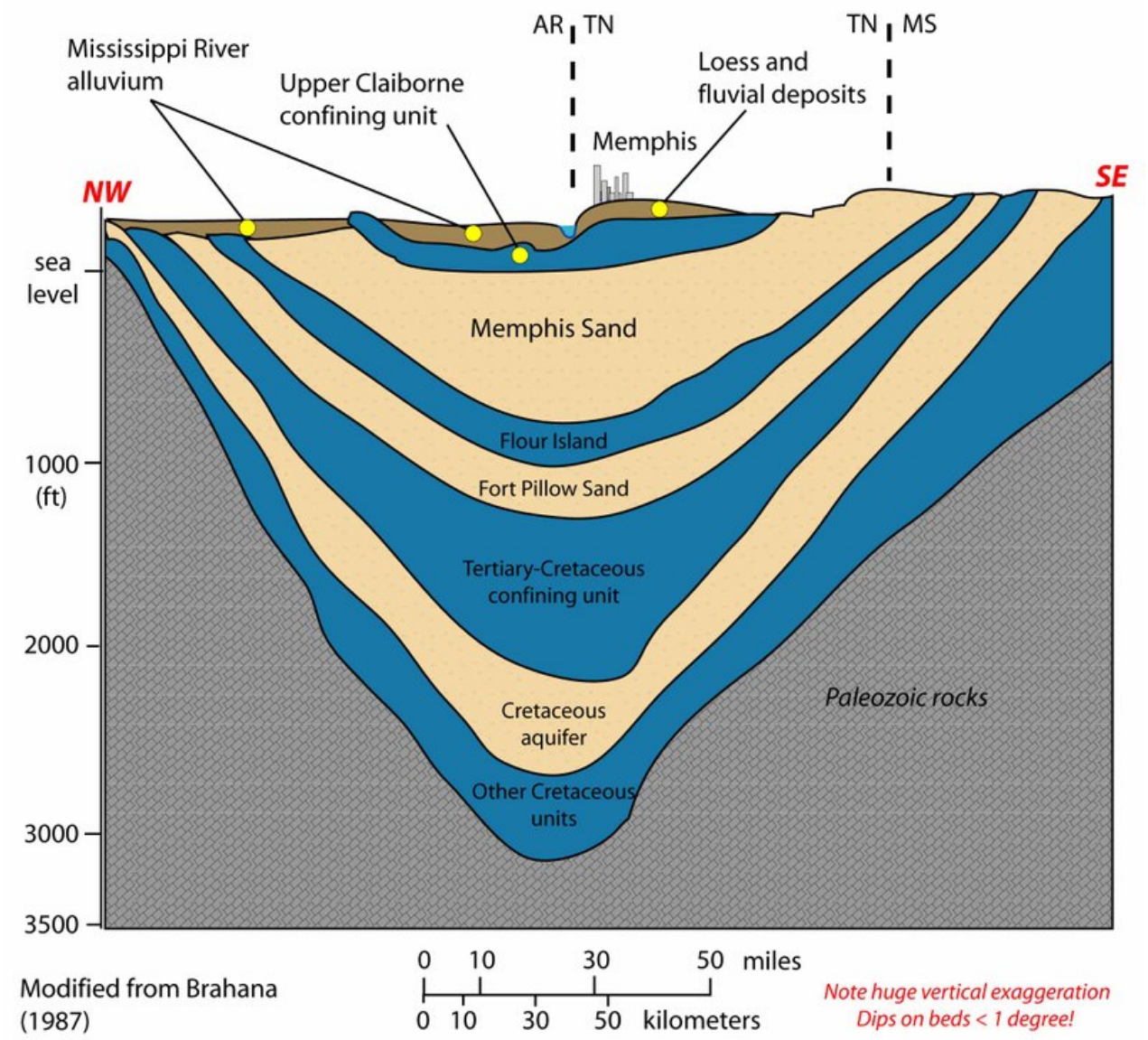

Figure 7. Generalized cross-section showing the Mississippi River Alluvial Aquifer, underlying Sparta (Memphis Sand), and deeper aquifers. Total thickness of the alluvial aquifer in Arkansas ranges from 50 to 150 feet. From Brahana, J.V., W.S. Parks, and M.W Gaydos, 1987. Quality of Water from Freshwater Aquifers and Principal Well Fields in the Memphis Area, Tennessee. U.S. Geological Survey Water Resources Investigations Report 87-4052, 22p.

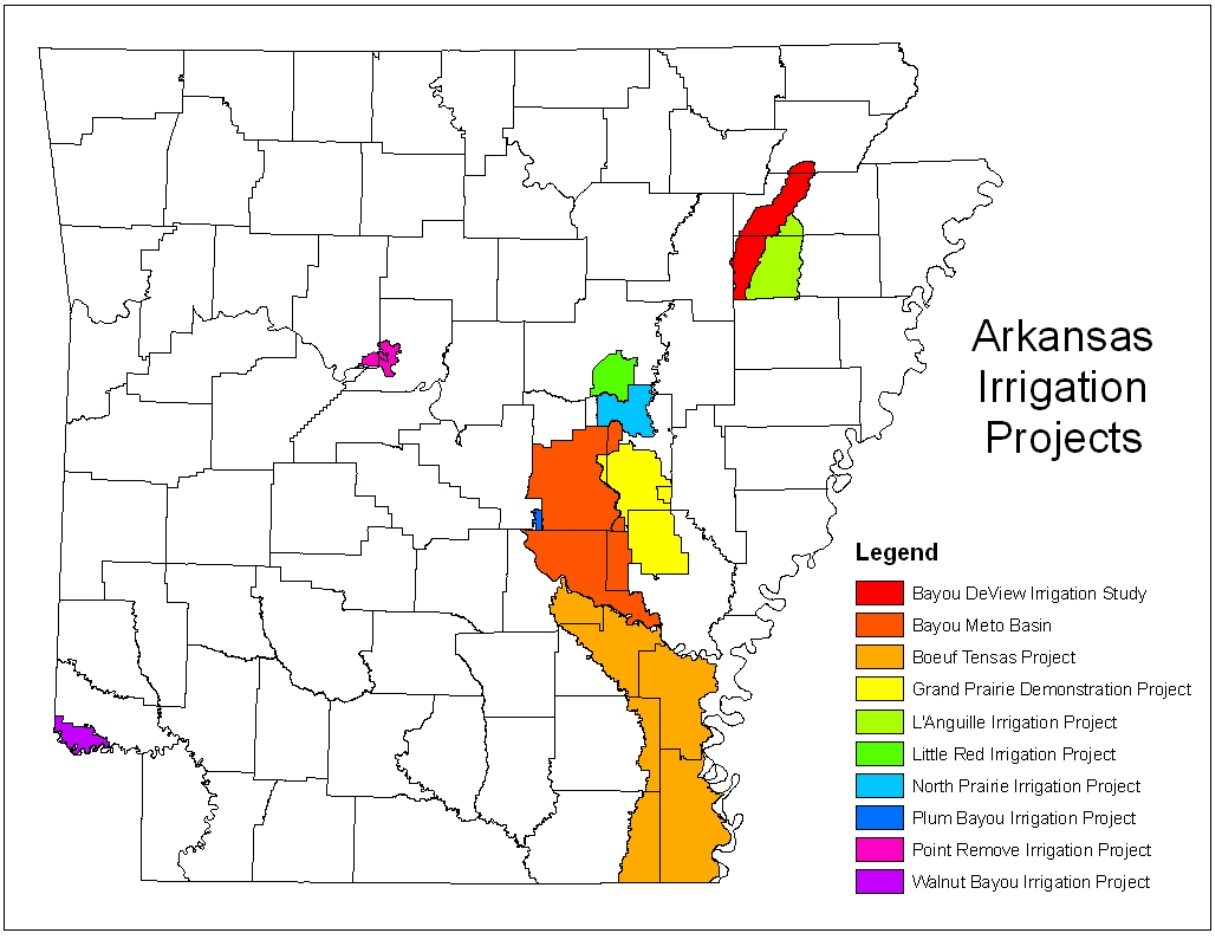

Figure 8. USDA Natural Resources Conservation Service irrigation projects in Arkansas.

References

Arkansas Natural Resources Commission, January 2014. Final Water Availability Report – Arkansas State Water Plan https://www.anrc.arkansas.gov/divisions/water-resources-management/arkansas-water-plan-2014/arkansas-water-plan-2014-update (accessed January 31, 2019).

Arkansas Natural Resources Commission, 2017. Arkansas Groundwater Protection and Management Report for 2016.

Arkansas Natural Resources Commission, 2016. Arkansas Groundwater Protection and Management Report for 2015.

Arkansas Natural Resources Commission, 2014. Arkansas Groundwater Protection and Management Report for 2013.

Booth, R.K., Jackson, S.T., Forman, S.L., Kutzbach, J.E., Bettis, E.A., Kreig, J., and Wright, D.K., 2005. A severe centennial-scale drought in mid-continent North America 4200 years ago and apparent global linkages. The Holocene, 15,3 (2005) pp. 321-328.

Bragg, D.C. and Weir, R.C., 2007. Notable environmental features in some historical aerial photographs from Ashley County, Arkansas. Journal of the Arkansas Academy of Science, 61 (2007), pp. 27-36.

CDM Smith. 2013. Water Demand Forecast Report. Prepared for the Arkansas Natural Resources Commission. September.

Clark, B.R., and Hart, R.M. 2009. The Mississippi Embayment Regional Aquifer Study (MERAS): Documentation of a groundwater-flow model constructed to assess water availability in the Mississippi Embayment. USGS Scientific Investigations Report 2009-5172, 61 p.

Clark, B.R., Hart, R.M., and Gurdak, J.J. 2011. Groundwater availability of the Mississippi embayment. USGS Professional Paper 1785, 62 p.

Clark, B.R., Westerman, D.A., and Fugitt, D.T. 2013. Enhancements to the Mississippi Embayment Regional Aquifer Study (MERAS) groundwater-flow model and simulations of sustainable water-level scenarios. USGS Scientific Investigations Report 2013–5161, 29 p., http://pubs.usgs.gov/sir/2013/5161/

Cox, R.T., Forman, S.L., Seifert, C., and Foti, T., 2008. Pimple mound OSL ages: late Holocene Great Plains drought chronology extended to the south central United States. Joint Meeting of the Geological Society of America, Soil Science Society of America, American Society of Agronomy, Crop Science Society of America, Gulf Coast Association of Geological Societies with the Gulf Coast Section of SEPM.

Cox, R.T., Larsen, D., Forman, S.L., Woods, J., Morat, J., and Galluzzi, J., 2004, Preliminary assessment of sand blows in the southern Mississippi Embayment. Bulletin of the Seismological Society of America, Vol. 94, No. 3, pp. 1125-1142.

Delp, W. and Shrum, C., July 2017. USDA's NRCS assists landowners to overcome water issues. Irrigation Today.

Denniston, R.F., DuPree, M., Dorale, J.A., Asmerom, Y., Polyak, V.J., and Carpenter, S.J., 2007. Episodes of late Holocene aridity recorded by stalagmites from Devil's Icebox Cave, central Missouri, USA. Quaternary Research 68, 45-52.

Denniston, R.F., Gonzalez, L.A., Asmerom, Y., Reagan, M.K., and Recelli-Snyder, H., 2000. Speleothem carbon isotopic records of Holocene environments in the Ozark Highlands, USA. Quaternary International 67, 21-27.

Gentry, J., Johnson, G., Baker, B., Witsell, C.T., and Ogle, J., 2013. Atlas of the Vascular Plants of Arkansas.

Miao, X., Mason, J., Swinehart, J., Loope, D., Hanson, P., Goble, R., and Xiaodong, L., 2007. A 10,000 year record of dune activity, dust storms, and severe drought in the central Great Plains. Geology, 35 (2007), pp. 119-122.

NOAA Centers for Environmental Information, 2016. State Summaries, 149-AR.

Otvos, E., 2004. Prospects for interregional correlations using Wisconsin and Holocene aridity episodes, northern Gulf of Mexico coastal plain. Quaternary Research, 61 (2004), pp. 105-118.

Popp, M., Nalley, L., and Vickery, G., 2009. Going, Going, Almost Gone: How the depletion of the alluvial aquifer will affect cropping decisions in the Arkansas delta. Southern Agricultural Economics Association Annual Meeting.

Quinn, J.H., 1961. Prairie Mounds of Arkansas. Arkansas Archeological Society Newsletter, Vol. II.

Seifert, C.L., Cox, R.T., Forman, S.L., Foti, T.L, Wasklewicz, T.A. and McColgan, A.T., 2009. Relict nebkhas (pimple mounds) record late Holocene megadrought in the forested region of south-central United States. Quaternary Research, 71 (2009), pp. 329-339.

Stahle, D. W., and Cleaveland, M., 1992. Reconstruction and analysis of spring rainfall over the southeastern U.S. for the past 1000 years. Bulletin of the American Meteorological Society.

Stahle, D.W., and Cleaveland, M., and Hehr, J.G., 1985. A 450-year drought reconstruction for Arkansas, United States. Nature, Volume 316, pp. 530-532.

Stahle, D.W., Fye, F., Cook, E., and Griffin, D., 2007. Tree-ring reconstructed megadroughts over North America since A.D. 1300. Climatic Change, 83 (2007), pp. 133-149.

USDA National Agricultural Statistics Service, 2017. Arkansas Crop Production Report: https://www.nass.usda.gov/Statistics_by_State/Arkansas/Publications/Crop_Releases/Crop_Production_Monthly/2017/arcropoct17.pdf

USDA NRCS, 2015. 2015 Upper Cache River Watershed MRBI Fact Sheet: https://www.nrcs.usda.gov/wps/portal/nrcs/detail/ar/programs/landscape/?cid=nrcseprd354822

Wackerman, A., 1929. Why prairies in Arkansas and Louisiana. Journal of Forestry, 27 (1929), pp. 726-734.

Woodhouse, C., and Overpeck, J., 1998. 2000 years of drought variability in the central United States. Bulletin of the American Meteorological Society, 1998, pp. 2693-2714.

Development of the White Mountain Moraine System in New Hampshire and Its Proposed Extension into Vermont, USA

John S. Moore, Retired National Geologist, Natural Resources Conservation Service, US Department of Agriculture, Washington, DC, USA
Home: 7723 Modisto Lane, Springfield, VA 22153 (johnniednm@hotmail.com)
David G. Johnson, Retired Health Physicist, Rhode Island Atomic Energy Commission, Narragansett, RI, USA
Home: One Shadow Ridge Drive, Carolina, RI 02812 (oneshadowridge@gmail.com)

Introduction

The trans-New Hampshire (NH) White Mountain Moraine System (WMMS) is believed to have formed ≈14,000 years B.P. during a short-lived, world-wide cooling interval, the Older Dryas Chronozone, when Laurentide ice recession reached northern New England. Thompson et al. (2017) interpreted this segmented, east-west system as ice front deposition associated with short-lived ice re-advances or stillstands. Hooke and Ridge (2016) draw a WMMS summary line extending 100 kilometers from Bowman, NH westward to Comerford Dam on the Connecticut River, thence northward up the Passumpsic River valley (PRV) terminating near St. Johnsbury, Vermont (VT). This northward extension in the PRV in VT is questionable given the local topography. Studies to determine the extension of the WMMS westward into VT are few and inconclusive. The Connecticut River valley (CRV) and its major north-south tributary, the PRV, are the deepest valleys in the area, and thus must have contained the thickest active ice during recession. These majors valleys along with minor tributaries served as meltwater outlets for Laurentide ice. With progressive ice recession and thinning in these valleys, nearby hills and mountains emerged as nunataks and proglacial Lake Hitchcock formed in the CRV and PRV where varves were deposited (Ridge et al. 2012).

Our field mapping of moraine segments west of the CRV to Marshfield, VT, south to East Ryegate, VT and east to Tinkerville, NH were combined with published data in NH and VT and cross-checked with newly available LIDAR imagery to form a moraine landform record.

To better understand the observed distribution of moraine clusters, theoretical paleo-ice margins were reconstructed by applying Nye's (1952b) legacy equation which defines parabolic, longitudinal profiles of active ice above a glacier's snout. Reconstructions were started from four glacier snout locations in the CRV and one in the PRV and extended up valley along east-west lines every 500 meters with ice edge plot points dictated by the Nye equation.

We conclude that the empirical moraine landform record correlates with the theoretical paleo-ice margin plots in both NH and VT. This correlation provides strong evidence that the WMMS can be extended into VT in time-transgressive fashion during the Older Dryas stade.

Previous Studies

Glacial geological studies are numerous for this region of North America. Significant overviews of the deglaciation of this part of North America are given in Denton (1981), Denny (1982), Clark et al. (1996), Dyke et al. (1982) and Dyke et al. (2002), Parent and Occhietti (1999), Ridge (2003, 2004), Tarasov and Peltier (2004), and Wright (2015).

Thompson (1999) summarized the history of research in the northern NH area from the earliest years through 1940. Ridge et al. (1999), Ridge et al. (2012), and Thompson et al. (1999) referred to the system as the Littleton-Bethlehem (L-B) Moraine Complex. Crosby (1934b) was an early worker who contributed to identifying the complex. Ten kilometers west of Littleton, NH he identified three disconnected moraine

sets along Mullikin Brook valley and near Partridge Lake (figure 9), as well as significant moraines in the Littleton and Bethlehem, NH areas. Ridge (2004) and Bromley et al. (2015) captured the post-1940 history of research.

Varve data near Comerford Dam, East Barnet, VT indicate an absence of 151 varve years (Antevs 1922, 1928, 1939; Lougee 1934, 1935), and later confirmed by Ridge (2004, 2017). Thompson et al. (1999) characterized an outcrop near Comerford Dam, referred to as "section M" in the older literature. The outcrop is 47 meters (155 feet) high within which are a total of 21-meters (70-feet) of two tills intercalated within Lake Hitchcock lacustrine sediments. These workers did not discover moraine *per se* near the dam nor anywhere between the dam and the nearest known moraine fields at Mullikin Brook and Partridge Lake, NH. Nevertheless, many modern workers consider it as evidence of ice re-advance and have demarcated tills as the western-most extension of WMMS. Ridge's (2017) North American Varve Chronology (NAVC) indicates the Littleton-Bethlehem (L-B) readvance (WMMS) reached its maximum 13,984 to 13,833 calibrated years before 2000. This age conforms to the Older Dryas stade in Europe, and suggests Older Dryas cooling triggered deposition of the moraine belt. These data correspond with climate events recorded in Greenland ice cores (Thompson et al. 2017).

Bromley et al. (2015) tentatively extended the WMMS to eastern Maine (ME) because ^{10}Be dates on boulders on the terminal Androscoggin moraine agree well with ^{10}Be dates on boulders on the WMMS. Precision of ^{10}Be dating method varies by $^{+/-}$ 400 years, thus results indicate only broad usability to illustrate that the general direction of WMMS development was from east to west.

Stewart and MacClintock (1969) and Doll (1970) identified hummocky belts of recessional moraine in northeastern VT but concluded that a relationship, if any, with the L-B Moraine Complex (WMMS) in NH was still uncertain. Moore (1974) reported moraine ridges along the south side of Joes Pond and near Cow Hill, West Danville, VT. Moore (2015) mapped numerous moraine ridges and hummocks in Harvey-Symes valley between Harveys Lake and Lower Symes Pond, Ryegate, VT and concluded they were formed by active ice of a short-lived, oscillating outlet valley glacier. Kim et al. (2008) and Springston et al. (2008) identified several moraine ridges in Groton State Forest in Marshfield and Peacham.

Study Objectives

Our primary objective was to determine whether the WMMS of NH extends into adjacent areas of VT and clarify its currently accepted position by two approaches: (1) We would develop a comprehensive, moraine landform record that combines all available previous work in VT and NH and conduct additional mapping in under-mapped areas where the WMMS may have logically occurred in VT and NH. (2) Because there are no moraine mapping records south of Mullikin Brook and Partridge Lake, nor along the densely wooded, steep, east and west flanks of Gardner Range, NH, we would conduct detailed, on-ground mapping along both flanks of Gardner Range and south of Partridge Lake to Tinkerville, NH.

The second objective was to determine whether there are varve sections in the CRV that contain end stage glaciation indicators which would provide irrefutable locations of ice snouts from which we could then reconstruct paleo-ice margins by theoretical analysis using principles of ice physics.

The third objective was to illustrate how these reconstructed margins can provide evidence of time transgressive development of the WMMS.

Methods

Objective 1 Methods: Because moraine ridges are typically less than 6 meters high, they are generally not discernable on 1:24,000 scale US Geological Survey 7.5-minute quadrangles. Hence, mapping was done on foot over a period of 8 field seasons, from 2008 to 2015. As of 2018 in both NH and VT, LIDAR *(Light Detection and Ranging)* imagery became available at a resolution of 0.7 meter (NH GRANITview, 2018; VT Agency of Natural Resources, 2018). LIDAR imagery was used to cross-check location and orientation of all moraine deposits suspected to be associated with the WMMS in our field areas. The senior author conducted on-ground mapping in VT in the vicinity of Joes Pond, West Danville and Harvey-Symes valley near East Ryegate. In NH, the mapping area included both sides of the 32-kilometer long, NNE-trending

Gardner Range. The mapping effort was intended to be sufficiently detailed to identify previously unreported features that may be germane to reconstructing ice margins associated with the WMMS. We visited most moraine segments identified by other workers in VT and NH.

Field maps were seamlessly joined, 7.5-minute, US Geological Survey (USGS) quadrangles printed from National Geographic's software for computer-assisted drawings. The software also was used for track-recording and field navigation by a hand-held Global Positioning System unit. Because some USGS maps use metric units and others use English units for contour elevation and scales, both units with some rounding are provided in this paper.

We collected all relevant published moraine maps in both VT and NH and combined this information with our findings to produce a map of all empirical evidence, the comprehensive moraine landform record.

Objective 2 Methods: To determine the relative timing of minor advances or stillstands that seem to characterize the local events in the Older Dryas Chronozone, we would produce several paleo-ice front determinations. We examined the North American Varve Chronology, NAVC (Ridge et al. 2012, Ridge 2017) in the reach of proglacial Lake Hitchcock between East Ryegate and St. Johnsbury, VT. There are five varve sequences which included end-stage glaciation indicators. These indicators include either basal varves deposited on bedrock or till, or ice-proximal, coarse-grained couplets that can be on the order of a meter thick and indicate commencement of lacustrine deposition usually within no more than a few years of ice recession (Ridge et al. 2012).

Ice snouts and their margins are named after nearby villages: East Ryegate, McIndoe Falls, Barnet, East Barnet, and Passumpsic, VT. Snouts averaged five kilometers apart over a straight-line distance of 20 kilometers. These margins would provide, as a first cut effort, five time-transgressive "snapshots" of the positions leading up to, during, and directly following the short-lived re-advance or stillstand of Laurentide ice. For simplicity, we ignore insolation-related, differential melting where land emerges from thinning ice.

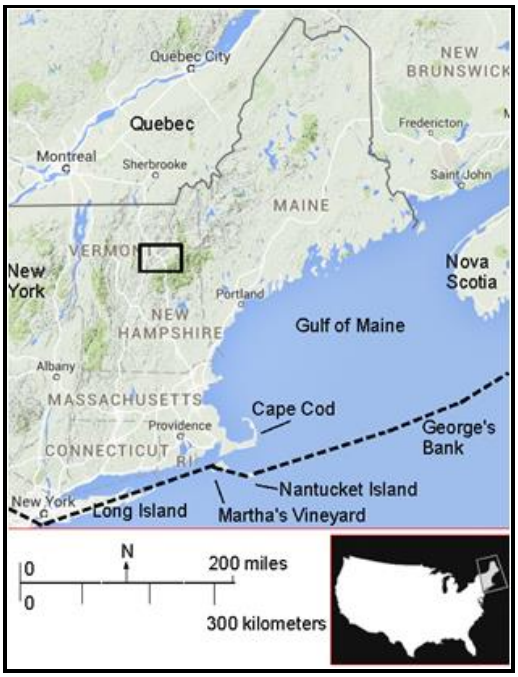

Figure 1 (left). New England and adjacent areas of Canada and New York. Study area within black rectangle. Dashed black line approximate location of Wisconsinan Terminal Moraine, 18,000 years B.P. that marks the Late Glacial Maximum (Oakley and Boothroyd, 2013).

Figure 2 (right). Proglacial Lake Hitchcock, center, at its maximum extent in New England. Study area is within blue rectangle. Blow-ups of study area are in figures 5 through 12. Map after Ridge and Larsen (1990).

The Nye power function equation is considered legacy work in glaciology because it mathematically accounts for mechanics and physics of ice sheet flow (Nye, 1951, 1952a, 1952b, 1952c; Cuffey and Paterson, 2010; Marshall, 2005). Ng et al. (2010) used Nye's equation to inform surface profiles of modern ice masses to inform paleo-glacier reconstructions. Nye's equation defines the longitudinal ice surface profile

of ice sheets and ice cap-glaciers from their maximum elevations. Horizontal driving stress and thus shear stress at the bed are functions of the surface slope of the ice. The fundamental corollary is – no slope, no flow. Ice tends to flow in the direction of maximum surface slope even if the bed slopes in the opposite direction (Cuffey and Paterson, 2010). Conditions of zero slope take effect at ice divides, and when the main ice sheet thins to the point at which exposed ground effectively cuts off ice supply and forces the ice mass to disintegrate into fragments shaped by emerging topography. Fragments then stagnate and melt *in situ*. With exception of ice lingering as mountain glaciers, ice is thickest in valleys where it is last to melt. The equation provides credible matches to actual ice sheet profiles except within approximately 500 meters north of the snout, which is a zone of highly variable dynamics (Nye, 1952c).

We used the National Geographic software to overlay a 500-meter square grid on 1:24,000-scale quadrangles. Using each end-stage glaciation indicator that denoted a snout location and using the Nye-equation to determine ice elevation versus distance up-ice, we plotted ice edge boundaries at 500-meter intervals up to 27.5 kilometers north along the N-S axes of CTV and PRV between Wells River, VT and Lyndonville. Ice edge plots were extended sufficiently to the east and west to provide full coverage of the landform record within the study area. Connecting common points of elevation provided a Nye-generated ice front and revealed emerging nunataks and hill/mountain ridges. Gaps in the ice edge margins are topographic low areas that indicate probable melt-water outlets.

Objective 3 Methods: Combine the findings of the moraine landform record with the plotted Nye generated paleo-margins to reveal possible time transgressive relationships in the PRV and CRV.

Figure 3. Typical cross-sectional view of a moraine ridge in Harvey-Symes valley. Ridge is six to 15 meters high, 20 to 50 meters wide, and 400 meters long. It occurs at the base of and parallel to rock cliffs of Roy Mountain and is likely a lateral moraine of the Harvey-Symes outlet valley glacier. Photo by John S. Moore.

Results

Objective 1 Results: The moraine landform record in three field areas, (marked 'Moore' in figure 4), is illustrated in figures 5, 6, and 7 at a large scale to show individual moraine ridge crests. Each of figures 8 through 12 illustrates the location of the WMMS summary line (in green), eskers (in yellow), and moraine ridges (as red clusters). Continental ice is assumed, but not shown, north of each margin and encircles nunataks. Breaks in a margin are topographic lows or valleys that conveyed meltwater, once ice-free.

Objective 2 Results: Five theoretical paleo-ice margins were reconstructed using the Nye's equation. These are presented in figures 8 through12, sequentially arranged in time and space from south to north, from East Ryegate to Passumpsic, VT over a straight-line distance of 20 kilometers. NAVC data indicate northward recession occurred along this line at a rate of 250 meters/year except for a 150 varve-year break during the East Barnet time frame.

We suspected the northern end of Gardner Range (figure 4) served as a wedge that split ice flow to its east and west flanks. We hypothesized that moraine may have been deposited along Gardner Range at elevations similar to known moraine clusters just a few kilometers west in Harvey-Symes Valley, VT.

East Ryegate Margin marked the beginning of significant active moraine building throughout the study area. The entire Gardner Range was fully emergent and wedge-shaped, narrowing northward. The range has several sub-summits that exceed 600 meters (2000 feet) in elevation and local relief ranges between 460 to 560 meters (1500 to 1800 feet). In VT, high hills in Groton State Forest were emerging nunataks. Directly following or coeval with recession of East Ryegate Margin is a moraine complex of many scores of till ridges and mounds in Harvey-Symes valley and vicinity, figure 5 (Moore, 2015). Many are curvi-linear

with apparent cross-valley counterparts. In NH, numerous linear and hummocky moraines near Tinkerville indicate active ice was clearly present 10 kilometers south of the WMMS summary line (Thompson et al. 2017) at Partridge Lake. Parker Hill, two kilometers south of Tinkerville, marks the southern limit of East Ryegate Margin directly east of Gardner Range. East Ryegate Margin closely conforms to the WMMS from Littleton to Beech Hill and eastward to Jefferson and Bowman, NH.

Significant moraine building occurred in regularly spaced ridge sets during the interval between East Ryegate and McIndoes Margins. McIndoes Margin reveals that Groton State Forest, VT was virtually ice-free while moraine was forming at Harveys Lake. On the east side of Gardner Range, ice penetrated south into narrow Bill Little Brook and Teter Meadow Brook valleys. Moraines between Partridge Lake and the south side of Moore Reservoir, and those in Mullikin Brook valley evidently were deposited within the time interval between the McIndoes and Barnet Margins. Crosby (1934b) and Lougee (1935) discovered the moraine segments near Partridge Lake and Mullikin Brook, but evidently did not visit areas further south. A morphosequence, as described by Koteff (1974) and Koteff and Pessl, Jr. (1981) occurred directly south of the Partridge Lake and Mullikin moraines. The sequence included former ice in the narrow valley occupied today by Dodge Pond and Partridge Lake; and in the narrow valleys drained by Bill Little Brook and Teter Meadow Brook where several eskers formed following the active ice phase. The eskers terminated to the south near Tinkerville (figures 7 and 9) at today's Lake Ogontz and formed a delta in an arm of Lake Hitchcock in Ogontz River valley near Lisbon, NH at elevation 247 meters/810 feet according to calculations by Koteff and Pessl, Jr. (1981).

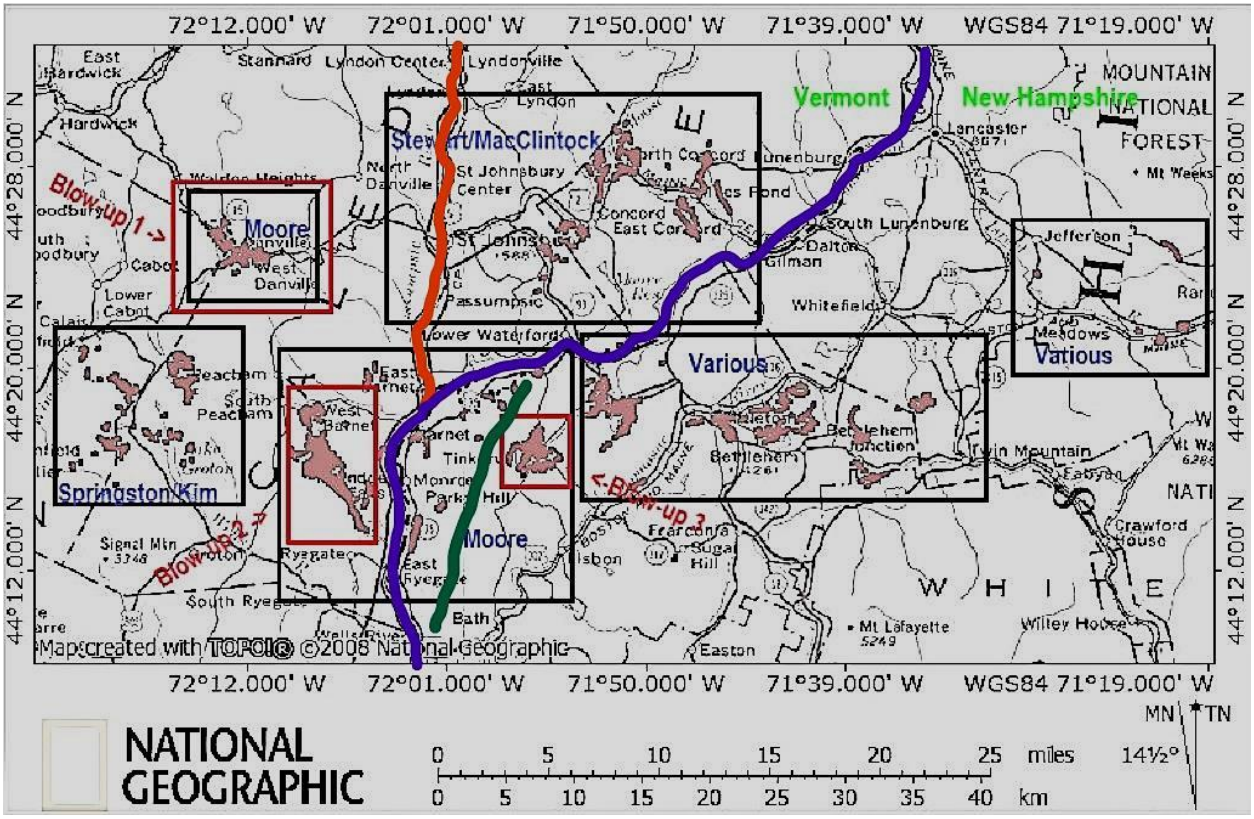

Figure 4. The compiled moraine landform record appears as clusters shown in light red areas. Black enclosures denote mapping areas of workers. "Moore" refers to mapping by senior author; "Stewart and MacClintock"(1969 and Doll (1970); "Springston/Kim" (2008); "Various" include Crosby (1934b), Lougee (1935), Goldthwait (1916), Bromley et al. (2015), Thompson et al. (1998), Thompson et al. (2017), Thompson et al. (1996), Thompson et al. (1999). Red rectangle 1 is the Joes Pond, VT moraine area, (blown-up in figure 5); red rectangle 2 is Harvey-Symes valley, Ryegate, VT area (blown-up in figure 6); red square 3 is the Tinkerville, NH area, (blown-up in figure 7); purple line is CT valley, the border between VT and NH; orange line is Passumpsic valley; green line is axis of Gardner Range, NH.

East of the Mullikin Brook area Barnet Margin falls north of the WMMS summary line. It skirted north of Eustis Hill and across the town of Littleton, through the center of the Bethlehem moraine field and followed an irregular path north of the Beech Hill moraine belt. It skirted northern lower slopes of Mount Martha and continued eastward to Bowman and across Israel River valley to lower slopes of Pliny Range. Many sub-summits of Dalton Range north of Littleton, including Mann Hill, were emerging nunataks (figure 9). Near the summit of Mann Hill in Littleton, NH we encountered several parallel, trapezoidal channels with sides less than one meter high. We infer they most likely formed by melt water channels on the glacier surface that became superposed on the emerging Mann Hill nunatak just prior to the time of the McIndoe Margin.

In VT, Barnet Margin (figure 10) deposited scores of moraine ridges and hummocks along the south side of Joes Pond and toward Mollys Pond. The Kittredge Hills and nine other peaks north to Wheelock Mountain were nunataks. The hilly/mountainous area near Passumpsic, West Waterford, Lower Waterford, and Comerford Dam includes several mountains as high as 559 meters (1834 feet). The area near North Concord as far north as Miles Mountain also had emerging nunataks. In NH, Barnet Margin coincided with the WMMS summary line to the south of Comerford Reservoir along NH Route 135 and thence eastward to within few hundred meters south of Moore Dam. It wrapped around the north side of the exposed Dalton Range where the margin curved southwest to Forest Lake. From there it trended eastward from Whitefield and coincided with the WMMS summary line at Jefferson. Significantly, Barnet Margin indicates approximately when and where a finger of ice re-advanced down CT River valley to Comerford Dam and deposited the till sandwich in the outcrop near the Dam and formed clusters of moraine ridges and thick till (greater than 15 meters/50 feet) on lower west flank of Gardner Range.

In VT, East Barnet Margin (figure 11) marked commencement of moraine building near Duck Pond (Doll, 1970). The valley now occupied by Stiles and Duck Ponds conveyed meltwater southward into Chandler Brook valley that discharged meltwater into proglacial Lake Hitchcock near today's Comerford Reservoir. North of Concord, six mountains were major nunataks.

Passumpsic Margin (figure 12) showed no moraine building near St. Johnsbury, although several kilometers east moraine was starting to deposit near Concord, VT. North of Joes Pond the ridge of Kittredge Hills to Wheelock Mountain had fully emerged as wedge-shaped. As ice continued to recede into St. Johnsbury area, the east-west trending Moose River valley began to open up and captured meltwater that had been discharging through Styles Pond and Chandler Brook valleys from melting ice in the North Concord area. Stewart and MacClintock (1969) considered recessional moraine in this area as a separate major field that they called the "Concord Moraine". However, Passumpsic Margin and younger recessional events indicate the "Concord Moraine" field was simply an integral part of overall recession of Laurentide ice. The formation of eskers soon after the Passumpsic Margin indicates commencement of an ice stagnation front in Passumpsic valley north of St. Johnsbury and its environs.

Objective 3 Results: Co-plots of the moraine landform record with East Ryegate and McIndoes Margins clearly indicate continuity between moraine development in NH and VT. Within this time interval a moraine field developed near Tinkerville, NH where it terminated at Parker Hill (figure 7). The Comerford Dam outcrop containing two interbedded tills and the NAVC 151-year varve data gap can be logically explained by a re-advance down the CRV from the direction of Littleton, NH at the time of the Barnet Margin. However, no re-advance is indicated in NAVC data from the PRV because ice in this valley was starting to stagnate as evidenced by the development of eskers between St. Johnsbury and Lyndonville. The line has been repeatedly drawn, e.g., by Hooke and Ridge (2016, figure 1, p. 400), Ridge et al. (1999, figure 8, p. 88, and figure 15, p. 99), Ridge (2003, figure 3.7, p. 30), Ridge (2004, figures 6 and 7, pp. 174-175), and Ridge et al. (2012, figure 12, p. 705) despite the facts that its position is counter to the laws of ice physics (Cuffey and Paterson, 2010; Marshall et al. 2005) and it is not corroborated by empirical ground evidence in VT.

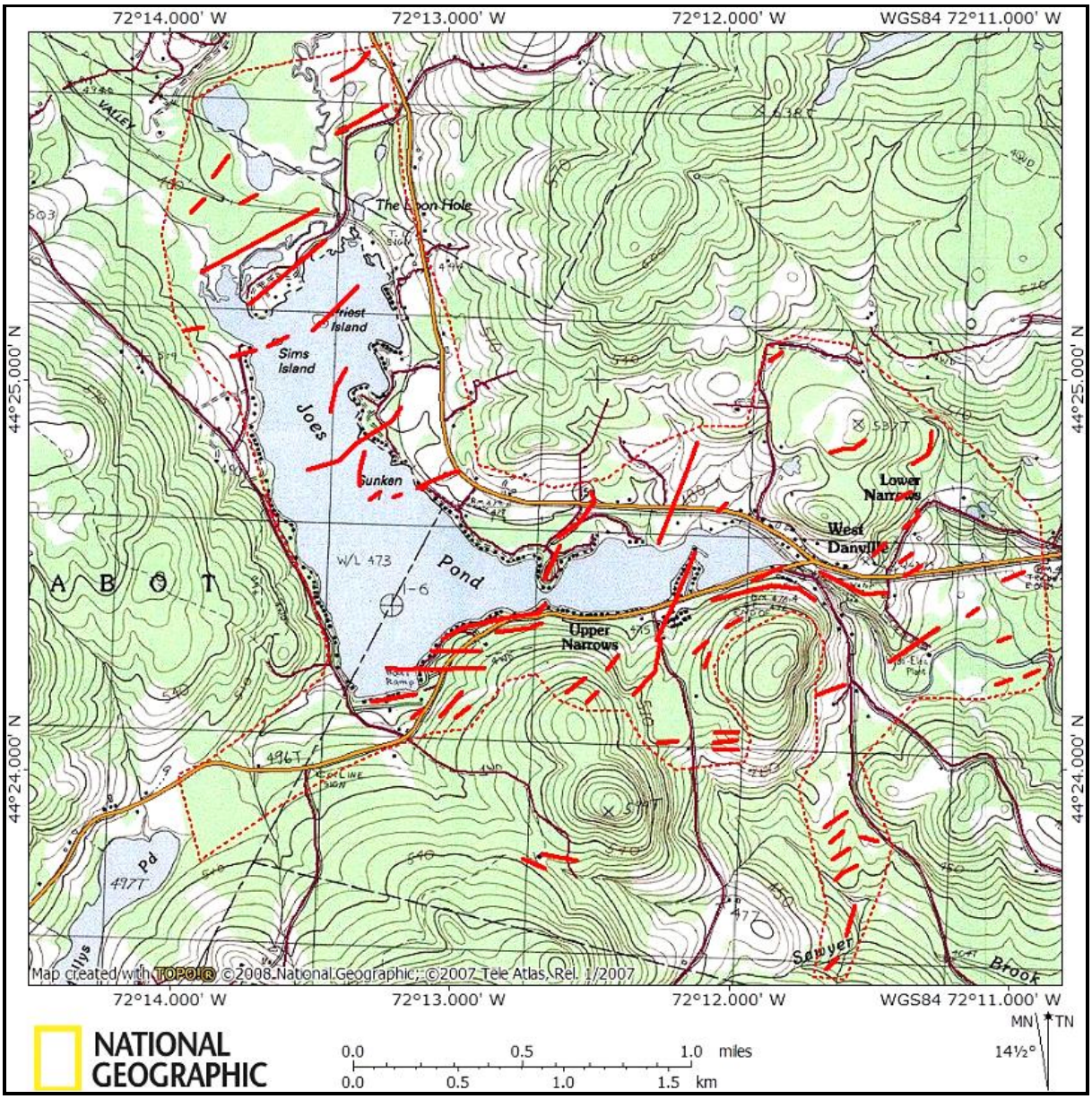

Figure 5. "Blow-up Area 1" (see figure 3 for small scale location) of Joes Pond area, West Danville, VT. Moraine ridge axes shown in solid red lines. Dashed red line encircles area of hummocky till, five to 20 meters thick, according to water well logs. Maximum depth of Joes Pond is 30 meters. The entire south shore of pond and underwater within 300 meters of shoreline are covered with large angular granite boulders that were glacially excavated from the structurally disrupted mixed contact zone of intruded granite and metasediments. The zone is coincident with the three southern basins of Joes Pond as illustrated in Hall's (1959) geology map, and on the geologic map of VT (Ratcliffe et al., 2011).

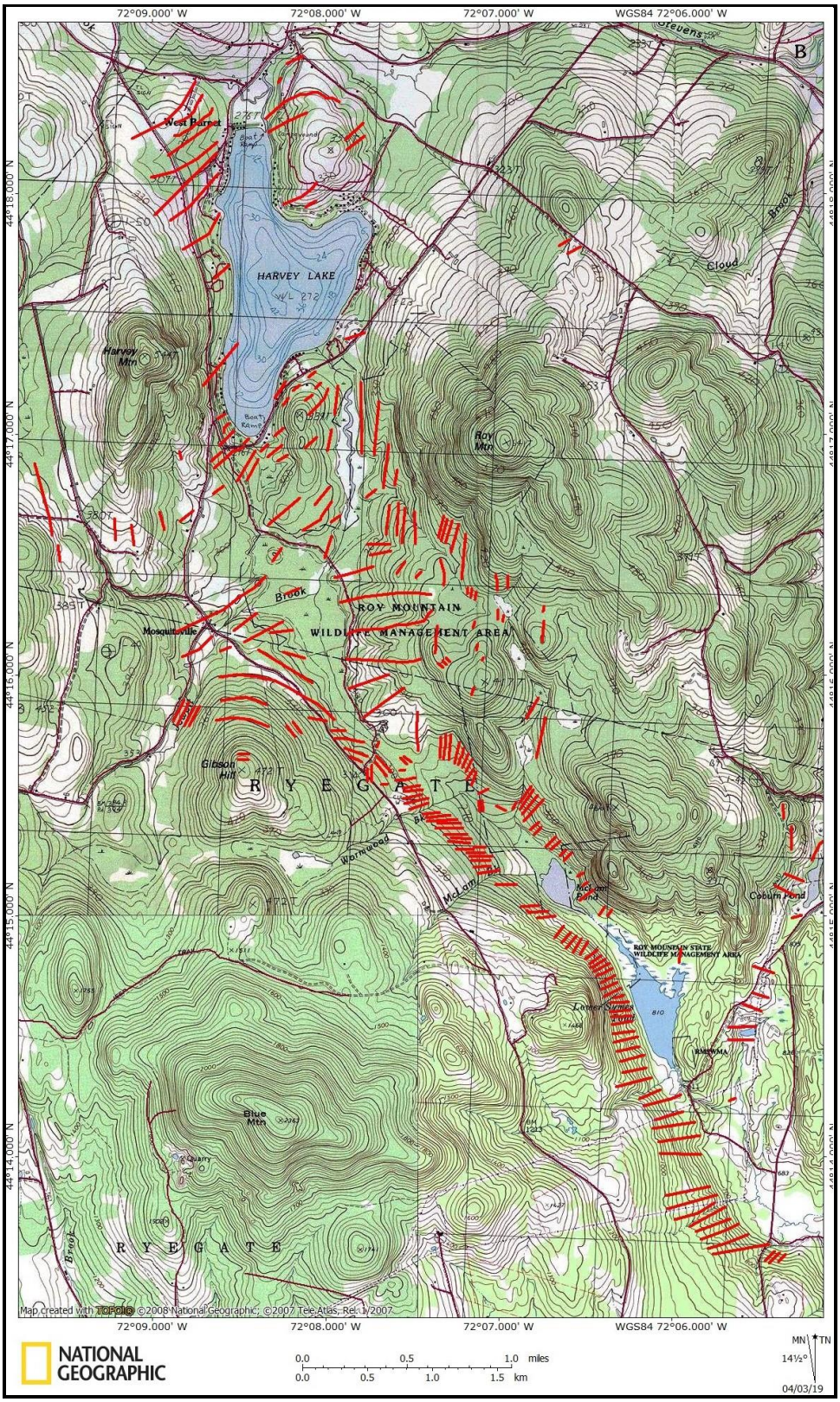

Figure 6. "Blow-up Area 2" (see figure 3 for small scale location) of Harvey-Symes Valley area, near Ryegate, VT. Moraine ridge axes shown in solid red lines. Till is up to 37 meters thick, according to water well logs. Maximum depth of Harveys Lake is 44 meters.

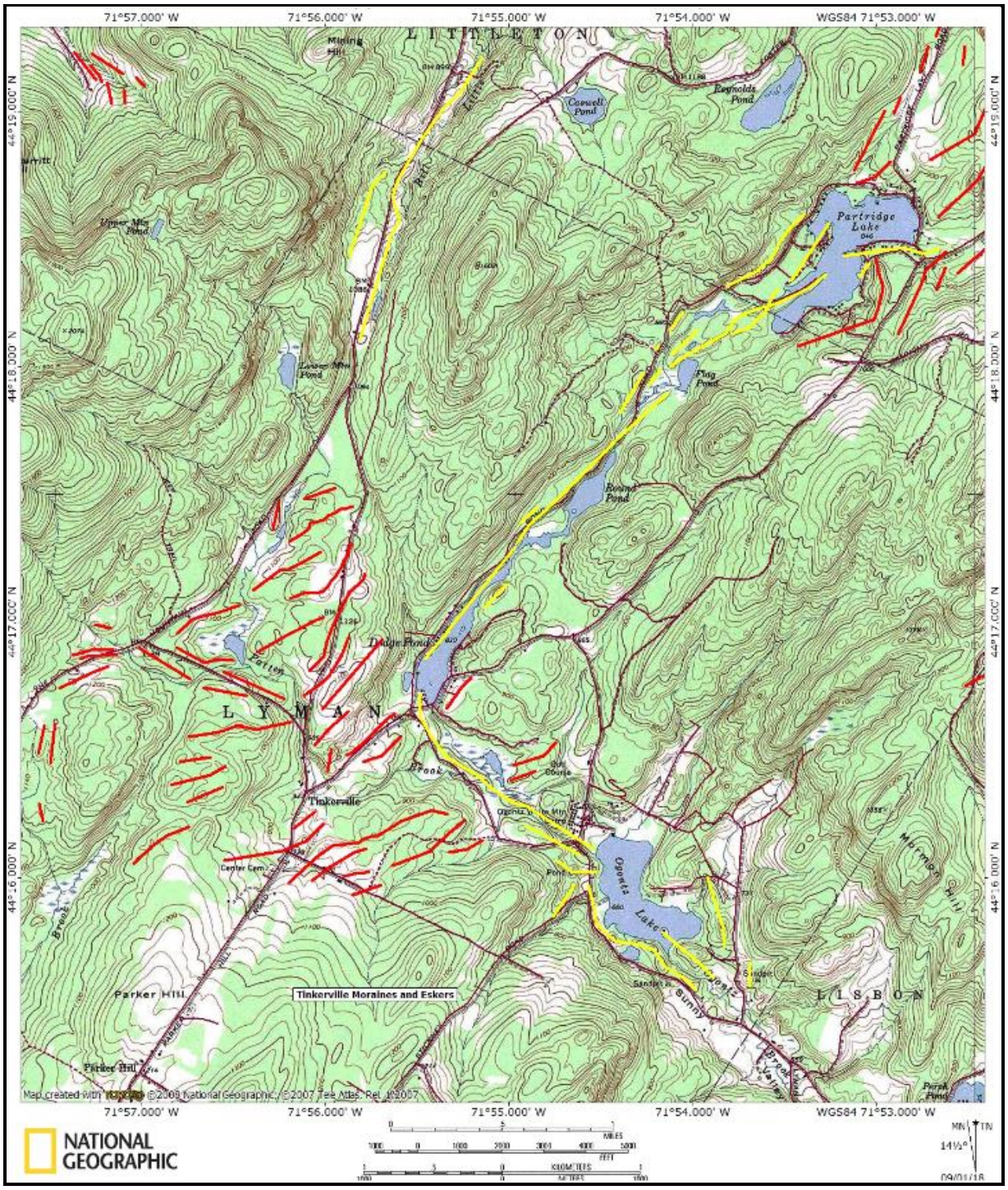

Figure 7. "Blow-up Area 3" (see figure 3 for small scale location) showing axes of moraine ridges and eskers near Tinkerville and Partridge Lake, NH

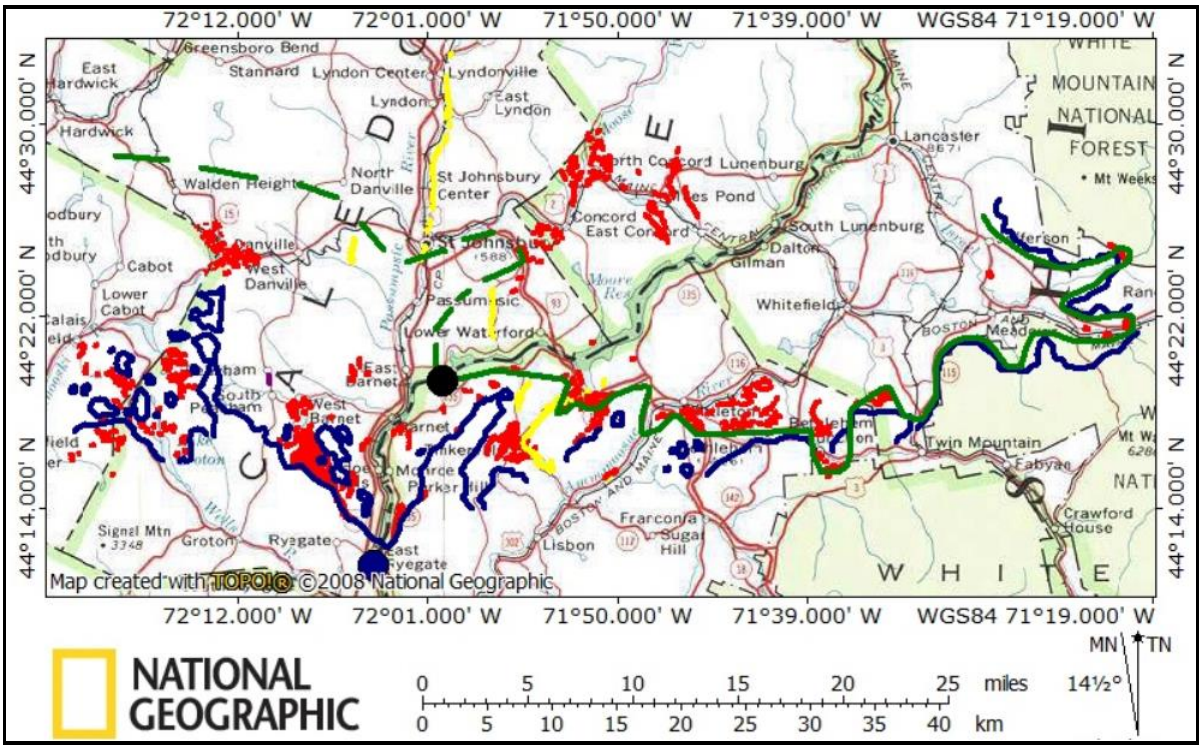

Figure 8. East Ryegate Margin shown in blue lines, enclosed blue areas are emerging nunataks; snout at blue dot; red clusters are moraines; yellow lines are eskers; solid green line is WMMS summary line, dashed green is its VT extension by Hooke and Ridge (2016); black dot is the till outcrop near Comerford Dam

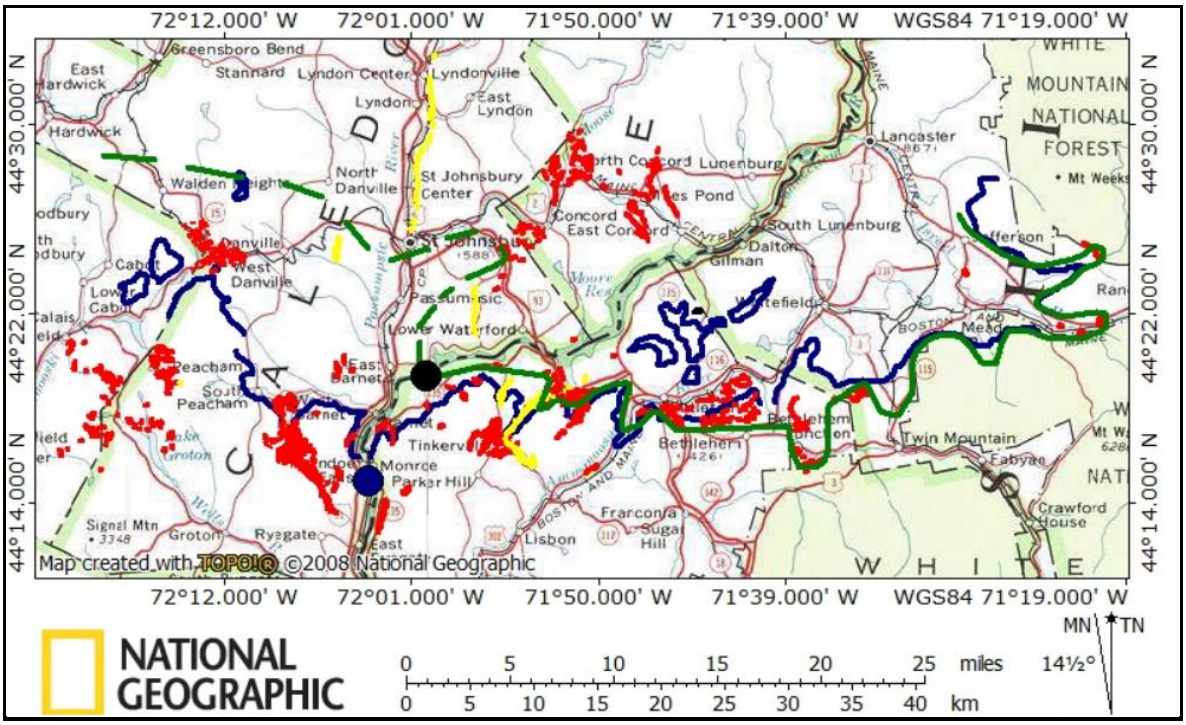

Figure 9. McIndoes Margin shown in blue lines, enclosed blue areas are emerging nunataks; snout at blue dot; red clusters are moraines; yellow lines are eskers; solid green line is WMMS summary line, dashed green is its VT extension by Hooke and Ridge,(2016); black dot is the till outcrop near Comerford Dam

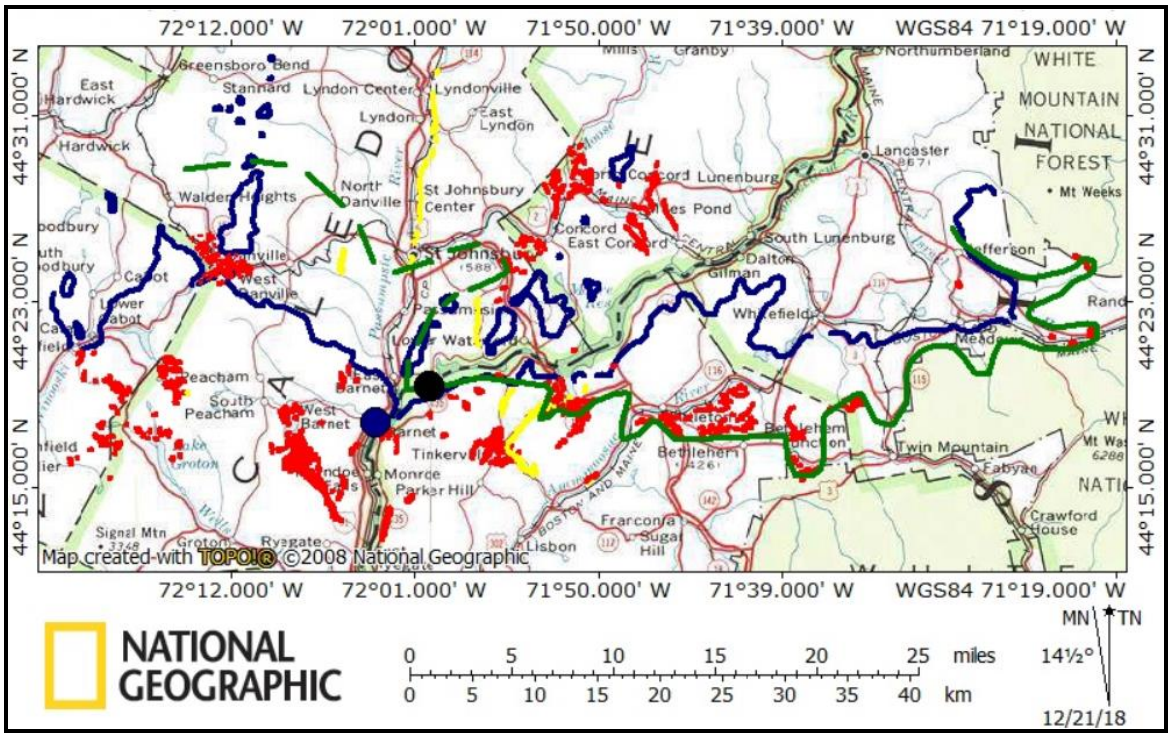

Figure 10. Barnet Margin shown in blue lines, enclosed blue areas are emerging nunataks; snout at blue dot; red clusters are moraines; yellow lines are eskers; solid green line is WMMS summary line, dashed green is its VT extension by Hooke and Ridge,(2016); black dot is the outcrop near Comerford Dam

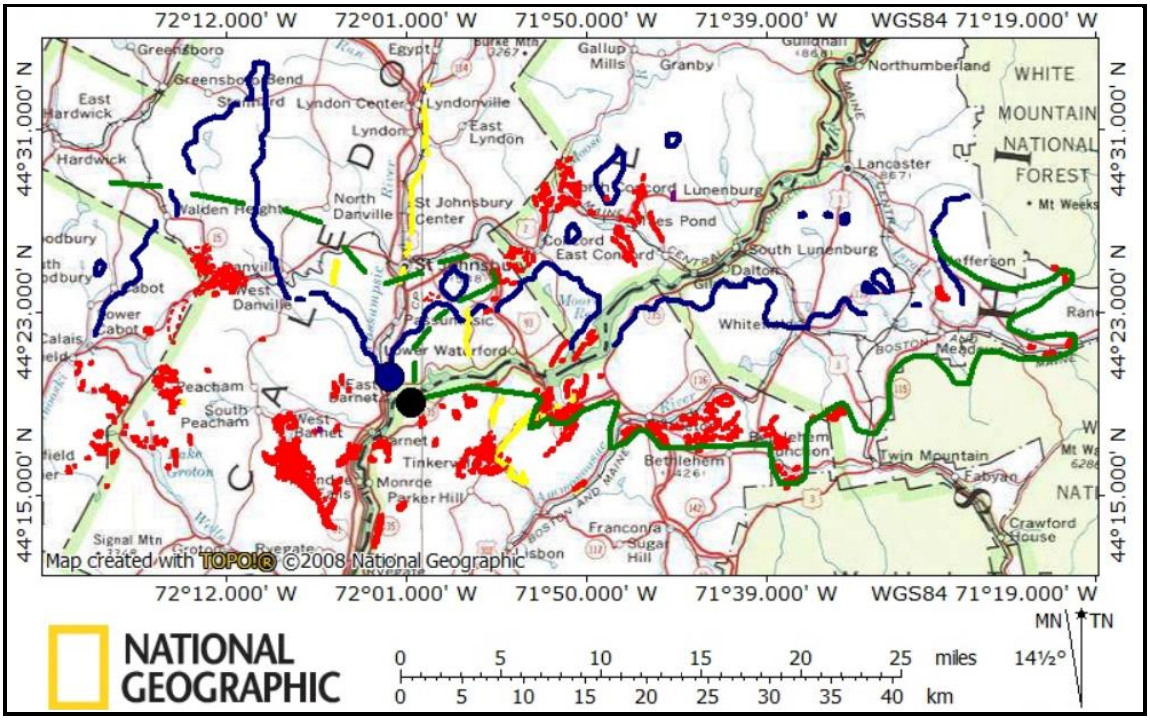

Figure 11. East Barnet Margin shown in blue lines, enclosed blue areas are emerging nunataks; snout at blue dot; red clusters are moraines; yellow lines are eskers; solid green line is WMMS summary line, dashed green is its VT extension by Hooke and Ridge,(2016); black dot is the till outcrop near Comerford Dam

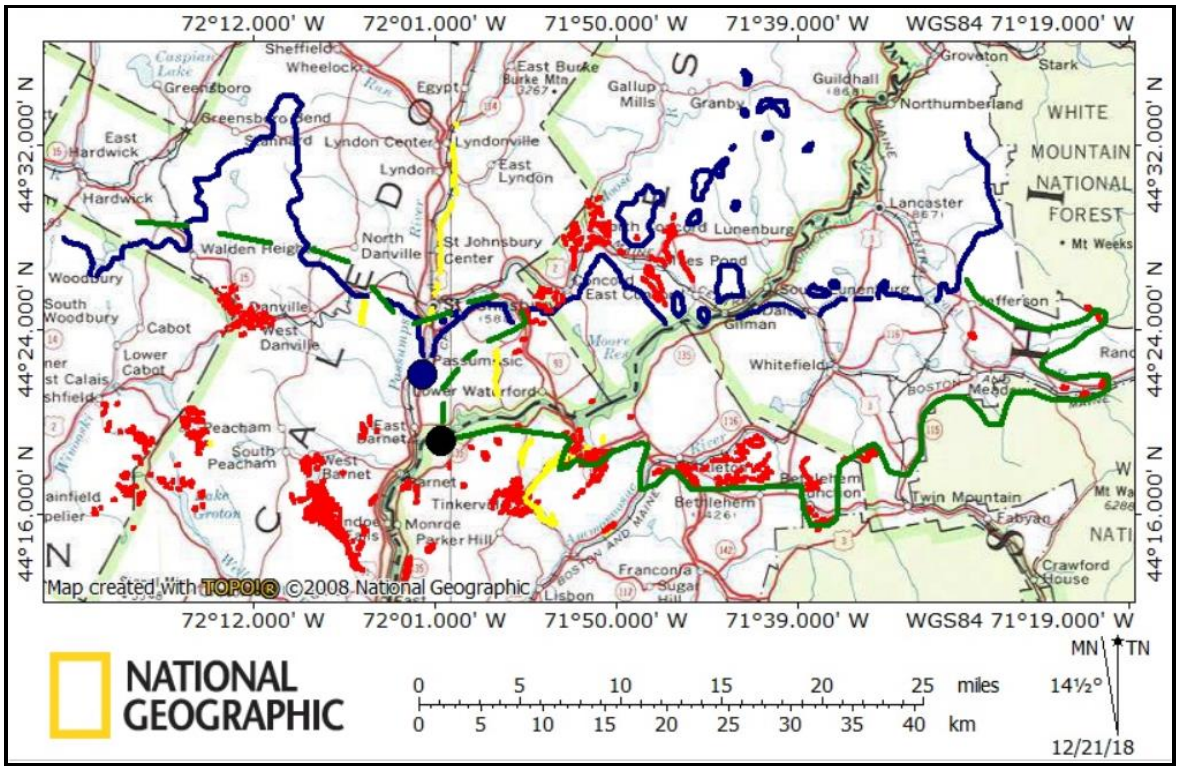

Figure 12. Passumpsic Margin shown in blue lines, enclosed blue areas are emerging nunataks; snout at blue dot; red clusters are moraines; yellow lines are eskers; solid green line is WMMS summary line, dashed green is its VT extension by Hooke and Ridge (2016); black dot is the till outcrop near Comerford Dam

Discussion and Conclusions

Glacial events described in this paper occurred immediately before, during, and soon after the Older Dryas Chronozone, a 200-year cooling period ≈14,000 years B.P. (Ridge, 2004; 2017). Recessional moraine ridges in the moraine landform record are differentiated into five theoretical Nye-generated paleo-margins. The five points of origin for the margins were selected in the CRV and PRV where basal varves or or ice-proximal, couplets are recorded in the NAVC. The south to north ice recession rate was 250 meters/year in this reach of the CRV (Ridge, 2017). The Barnet paleo-margin marks the approximate beginning of an ice re-advance from the direction of Littleton, NH. This interpretation agrees with Crosby's (1934b). However, we disagree with Thompson's et. al (1999) interpretation that the re-advance approached from the north from VT in spite of their pebble counts at Section "M" having a high percentage of VT-sourced clasts, many of which were characterized as fluvial. Our analyses clearly indicate that the numerous hill and mountains up to 559 meters (1834 feet) high in that area presented barriers to a short-term re-advance from directly north of Comerford reservoir. We argue that Chandler Brook valley (which discharges today into Comerford reservoir) was a major melt water channel outlet that would have provided the source material found in their pebble counts. Our analysis agrees with Ridge's (2004, fig 8c) that a re-advance probably terminated in the CRV between the East Barnet and Barnet. Supporting evidence include: (1) several small moraine ridge sets and an area of thick till (> 50 feet/15 meters) that occur along the lower west slopes of Gardner Range just south of Comerford Dam; (2) the upper till unit intercalated within lacustrine deposits in an outcrop called "Section "M" near the dam (Thompson et al. 1999); and (3) the absence of 151 varve-years at the dam (Ridge et al. 2012). Furthermore, within the 60-year time frame between the beginning of the formation of the East Ryegate to the end of the Barnet Margin, moraine segments were being deposited on the eastern side of Gardner Range near Tinkerville, NH. During this same period, segments of the WMMS between Bethlehem and Bowman were under construction. The Barnet Margin extends west and northwest into VT and accounts for numerous moraine ridges near Joes Pond as well as thick till and many till ridges south of Comerford Dam on lower west flanks of Gardner Range.

The dashed green "summary line" of the WMMS is drawn in VT (shown in our figures 8 through 12) in several papers, e.g., by Hooke and Ridge (2016, figure 1, p. 400), Ridge et al. (1999, figure 8, p. 88, and figure 15, p. 99), Ridge (2003, figure 3.7, p. 30), Ridge (2004, figures 6 and 7, pp. 174-175), and Ridge et al. (2012, figure 12, p. 705) which all show the WMMS as abruptly turning north from Comerford Dam, extending along the eastern side of PRV to St. Johnsbury, VT, thence turning west toward Hardwick, VT. Given the local topography, such a configuration erroneously implies that ice persisted in the many hills which are up to 1862 feet (568 meters) east of Passumpsic village while simultaneously the adjacent bottom of the PRV (elevation 540 feet/165 meters) remained ice free. It is commonly understood that ice is thickest in valleys and is therefore last to melt, while higher ground topography emerges first as nunataks. (e. g., Bennett and Glasser, 2009; Cuffey and Paterson, 2010; Marshall et al. 2005). East Barnet and Passumpsic paleo-margins plots (figures 11 and 12) clearly indicate the entire area of hills and mountains east of Passumpsic village and south and southeast of Fairbanks Mountain was ice-free. Thus, the empirical records indicate that this dashed green line is untenable. Moreover, in the PRV north of Passumpsic village are some of Vermont's best-developed eskers. This fact implies there was stagnation zone retreat occurring in front of active ice to the north. Nevertheless, varve deposition continued as proglacial Lake Hitchcock expanded northward another 16 kilometers to terminate at West Burke, VT.

We conclude that the Lower Dryas stade can be constrained by the 60-year period between the beginning of East Ryegate Margin to the end of East Barnet Margin. The time for deposition of East Barnet Margin included ≈150 varve years missing in the NAVC near Comerford Dam. We attribute this gap to a minor re-advance down the CRV from the Littleton, NH area. Thus, we infer the WMMS development persisted for ≈210 years, a value that agrees well with the widely accepted value of ≈ 200 years duration of the Older Dryas stade.

Our study provides strong evidence that moraine segments comprising the discontinuous WMMS were not deposited as a single coeval event; rather, they formed along a broken line from east to west, from Bowman to the west side of Gardner Range near Monroe, NH, and at least 30 kilometers further west to Marshfield, VT. The time interval between East Ryegate and East Barnet Margins was clearly a period of discontinuous moraine segment deposition running generally westward from eastern NH into northeastern VT.

Acknowledgements

We conducted this study over a period of eight field seasons, 2008 through 2015 out of pure academic interest and a long-time attachment to this part of VT and NH. We are both retired and are not actively affiliated with any academic, governmental, or consulting organizations who engage in geological research, so our entire project was self-funded.

References

Antevs, E., 1922. "The recession of the last ice sheet in New England", American Geographical Society Research Series (11):120 p.

Antevs, E., 1928. "The last glaciation with special reference to the ice sheet in North America", American Geographical Society Research Series (17), 292 p.

Antevs, E., 1939. "Modes of ice retreat of the Pleistocene ice sheets", Journal of Geology 47(5):503-508.

Balco, G., Briner, J., Finkel, R., Rayburn, J., Ridge, J., and Schaefer, J., 2009. Regional beryllium-10 production rate calibration for late-glacial northeastern North America", Quaternary Geochronology(4):93-107.

Bennett, M. and Glasser, N., 2009. Glacial Geology: Ice Sheets and Landforms. 2nd ed., Wiley-Blackwell, 385 p.

Bromley, G., Hall, B., Thompson, W., Kaplan, M., Garcia, J., and Schaefer, J., 2015. "Late glacial fluctuations of the Laurentide Ice Sheet in the White Mountains of ME and NH, USA", Quaternary Research, 83(3):522-530.

Clark, P., Licciardi, J., MacAyeal, D., and Jenson, J.W., 1996. "Numerical reconstruction of a soft-bedded Laurentide ice sheet during Last Glacial Maximum", Geology 24(8):679–682.
Crosby, E., 1934a. "Geology of Fifteen-Mile Falls Development", Civil Engineering 4(1):21-24.
Crosby, E., 1934b. "Extension of the Bethlehem, NH moraine", Journal of Geology (42):411-421.
Cuffey, K. and Paterson, W., 2010. Physics of Glaciers. 4th ed., Elsevier, Oxford, Great Britain.
Denny, C., 1982. "Geomorphology of New England", USGS Professional Paper 1208.
Denton, G. and Hughes, T., 1981. "The Last Great Ice Sheets". Wiley-Interscience, NY, 484 p.
Doll, C. (ed.), 1970. "Surficial geologic map of Vermont, 1:250,000", Geology by David P. Stewart, Vermont Geol. Surv.
Dyke, A., Dredge, L. and Vincent, J., 1982. "Configuration and dynamics of the Late Laurentide Ice Sheet during the Late Wisconsin Maximum", Géographie Physique et Quaternaire 36(1-2, fig. 5):5-14.
Dyke, A., Marshall, S., James, T., Clarke, G., 2002. "North American Ice Sheet reconstructions at the Last Glacial Maximum", Quaternary Science Reviews (21):175–192.
Hall, L., 1959. "The geology of the St. Johnsbury Quadrangle, Vermont and New Hampshire", VT Geol. Surv. Bull. 13.
Hooke, R. and Ridge, J., 2016. "Glacial lake deltas in New England record continuous, not delayed, postglacial rebound". Quaternary Research 85:309-408.
Koteff, C. 1974. "The morphosequence concept and deglaciation of southern New England", *In*: The morphologic sequence concept and deglaciation of southern New England, *in* Coates, D. R., ed., Glacial geomorphology: Binghamton, N.Y., State University of New York, Publications in Geomorphology:121-144.
Koteff, C. and Pessl, F., Jr., 1981. "Systematic ice retreat in New England", USGS Prof. Paper 1179.
Lougee, R., 1934. "Time measurements of an ice readvance at Littleton, NH", Science 79(2055): 462.
Lougee, R., 1935. "Time measurements of an ice readvance at Littleton, NH", Proc. National Academy of Science 21(1):36-41.
Marshall, S., 2005. "Recent advances in understanding ice sheet dynamics", Earth and Planetary Sciences Letters 240:191-204.
Moore, J., 1974. "Origin and geolimnology of Joes Pond, Vermont", Unpublished MS thesis, Dept. Geology, University of VT, Burlington, VT: 80 p.
Moore, J., 2015. "Origin of till ridges in a northeastern Vermont valley", Proc. 3rd Joint Federal Interagency Conference on Sedimentation and Hydraulic Modeling, April 19-23, Reno, NV:55-66.
New Hampshire GRANITview, 2018. "LIDAR Imagery", developed by the Earth Systems Research Center, Institute for the Study of Earth, Oceans, and Space, Univ. New Hampshire.
Ng, F., Barr, I., and Clark, C, 2010. "Using the surface profiles of modern ice masses to inform palaeo-glacier reconstructions", Quaternary Science Reviews, 29(23-24):3240-3255.
Nye, J., 1951. "The flow of glaciers and ice-sheets as a problem in plasticity", Proc. Royal Society of London, Series A, 207 (1091):554-572.
Nye, J., 1952a. "A method of calculating the thicknesses of the ice-sheets", Nature, 169:529-530.
Nye, J., 1952b. "The mechanics of glacier flow", Jour. Glaciology, 2(12):82-93.
Nye, J., 1952c. "A comparison between the theoretical and the measured long profile of the Unteraar glacier", Jour. Glaciology, 2(12):103-107.
Oakley, B., and Boothroyd, J., Oct. 2013. "Constrained age of Glacial Lake Narragansett and the deglacial chronology of the Laurentide Ice Sheet in southeastern New England", Journal of Paleolimnology, 50(3):305–317.
Parent, M. and Occhietti, 1999. "Late Wisconsinan deglaciation and glacial lake development in the Appalachians of southeastern Québec", Géographie Physique et Quaternaire, 53(1):117-135.

Ratcliffe, N., Stanley, R., Gale, M., Thompson, P., and Walsh, G., 2011. "Bedrock geologic map of Vermont", USGS Scientific Investigations Series Map 3184, 3 sheets, scale 1:100,000.

Ridge, J., 2003. "The last deglaciation of northeastern United States: A combined varve, paleomagnetic, and calibrated ^{14}C chronology *in* Hart, J., and Creemans, D., editors, Geoarchaeology of Landscapes in the Glaciated Northeast U.S.: New York State Museum Bull. 497: 163-193.

Ridge, J., 2004. "The Quaternary glaciation of western New England with correlations to surrounding areas", *In:* Quaternary Glaciations - Extent and Chronology, Part II: North America. J. Ehlers and P. Gibbard, (Eds.), Developments in Quaternary Science, 2b, Amsterdam, Elsevier:212-231.

Ridge, J., 2017. "The North American Glacial Varve Project". From http://eos.tufts.edu/varves

Ridge, J., Bensonen, M., Brochu, M., Brown, S., Callahan, J., Cook, G., Nicholson, R., and Toll, N., 1999. "Varve, paleomagnetic, and ^{14}C chronologies for late Pleistocene events in New Hampshire and Vermont, U.S.A.", Géographie physique et Quaternaire, 53(1), fig. 8:88.

Ridge, J., Balco, G., Bayless, R., Beck, C., Carter, L., Dean, J., Voytek, E., and Wei, J., Sep 2012. "The new North American Varve Chronology : a precise record of southeastern Laurentide ice sheet deglaciation and climate, 18.2–12.5 kyr bp, and correlations with Greenland ice core records", American Journal Science, 312:685-722.

Springston, G., 2016. "Surficial geology and hydrogeology of the Cabot 7.5 Minute Quadrangle, Vermont", Report, Map plates 1-3, Map plates 4-6, Map plates 7-9 and GIS data. VT Geol. Surv. Open File Report VG2016-3, text plus 9 plates, scale 1:24,000.

Springston, G. and Kim, J., 2008. "Surficial geologic map of the Knox Mountain area, Marshfield and Peacham, VT", VT Geol. Surv. Open-File Report VG08-4, 2 color plates, 1:24,000.

Stewart, D., 1961. "The glacial geology of Vermont". VT Geol. Surv. Bulletin 19.

Stewart, D. and MacClintock, P., 1969. "Surficial geology and Pleistocene history of Vermont", VT Geol. Surv. Bulletin 31.

Stone, J., Schafer, J., London, E., DiGiacomo-Cowen, M., Lewis, R., and Thompson, W., 1998. "Quaternary Geologic Map of CT and Long Island Sound Basin", USGS Open File Report, OF-98-371 (also published as USGS Scientific Investigations Map 2784, 2005).

Tarasov, L. and Peltier, W., 2004. "A geophysically constrained large ensemble analysis of the deglacial history of the North American ice-sheet complex", Quaternary Science Reviews, 23:359-388.

Thompson, W., 1998. "Deglaciation of western Maine and the northern White Mountains (abs.)", GSA, Abstracts with programs, 30(1):79.

Thompson, W., 1999. "History of research on glaciation in the White Mountains, NH", Geographie Physique et Quaternaire, 53(1):7-24.

Thompson, W. and Fowler, B., 1989. "Deglaciation of the Upper Androscoggin River Valley and Northeastern White Mountains, Maine and NH", Maine Geol. Survey, Studies in Maine Geology, 6:71-88.

Thompson, W., Fowler, B., and Dorion, C., 1999. "Deglaciation of the northwestern White Mountains, NH", Geographie Physique et Quaternaire, 53(1):59-77.

Thompson, W., Dorian, C., Ridge, J., Balco, G., Fowler, B., and Svendsen, K, 2017. "Deglaciation and late-glacial climate change in the White Mountains, New Hampshire", Quaternary Research, 87:96-120.

Vermont Agency of Natural Resources, 2018. Department of Environmental Conservation, Vermont Center for Geographic Information LIDAR Program.

Wright, S., 2015. "Late Wisconsinan ice sheet flow across northern and central Vermont, USA", Quaternary Science Reviews, 129:216-228.

Changes in Hydrology and Suspended-Sediment Transport in the Mississippi River Basin over the Past Century

Andrew Simon, Senior Principal, Cardno, Oxford, MS, andrew.simon@cardno.com
Kimberly Artita, Senior Civil Engineer, Sci-Tek Consultants, Inc., Clemson, SC, kartita@scitekanswers.com
Stephen E. Darby, Professor**,** University of Southampton, Southampton, UK, s.e.darby@soton.ac.uk
Julian Leyland, Associate Professor**,** University of Southampton, Southampton, UK, j.leyland@soton.ac.uk
Gail L. Simon, Technician/Specialist, Cardno, Oxford, MS, gail.simon@cardno.com

Abstract

Altered hydrological conditions in the Lower Mississippi River are a result of changes in precipitation, rainfall-runoff relations and anthropogenic factors that play a role in the magnitude and frequency of hydrologic events. Numerous studies have shown the significance of climate change and extreme weather events on peak flows, low-flows, and flooding, etc. Contributing to shifting hydrologic patterns such as precipitation, are human-induced changes to the natural environment such as agriculture, urbanization, channelization, dam construction, etc., that often vary in spatially-systematic ways according to regional demands for water. Changing flow regimes also affect sediment- transport rates and channel stability, challenging on-going efforts in flood protection, stream restoration and water-quality management.

Results of this study show that in general, although most of the Mississippi River Basin is receiving more rainfall than it did 100 years ago, there are vast areas where water yields have decreased significantly, particularly in the western part of the basin and particularly in spring. Precipitation has also shifted temporally such that winter precipitation has significantly decreased in many areas while spring and autumn precipitation has generally increased. Parts of the western basin are experiencing 25 to more than 50% less discharge per unit area than they did 100 years ago. In contrast, the mid-continent is generating considerably more water than it did 100 years ago. In part this can be attributed to increases in precipitation and a greater influence of hurricane-related rainfall, but anthropogenic effects cannot not be minimized. The result is that the lower Mississippi River is receiving more flow from its major HUC-2 tributaries (Ohio, Missouri and Upper Mississippi Rivers) than at the turn of the 20th century. Integrated over an average year and excluding inputs from other smaller tributaries, brings average-annual increase in flows to the Lower Mississippi River to about 1.62 million m^3/s (57.2 million ft^3/s). Average, mean-daily flow contributions from the Ohio, Upper Mississippi and Missouri Rivers have changed from 61%, 23% and 16% in 1930, to 55%, 28% and 18% in 2014, respectively.

Although the direction of the changes (positive or negative) varies across the basin, these effects are widespread and sizeable in magnitude, indicating that anthropogenic influences have been a major determining factor on changes in streamflow regimes over the past century. The direction and magnitude of these influences can clearly be sorted by region. While anthropogenic activities have resulted in increases in water yield in the central part of the basin (increases of

50-100% decreasing eastward to 0-10%), activities at the basin margins have caused decreases in flow. In the west, decreases of 25-100% are typical.

The average-annual delivery of suspended sediment to the Lower Mississippi River has declined by about 300%, from about 600 Mt/y in 1940 to about 100 Mt/y, currently. The largest actual decline is from the Missouri River (about 250 Mt/y) largely due to the trapping of sediment behind impoundments. Decreases in sediment delivery to these reservoirs are also noted. Other researchers have similarly reported on a large decline in suspended-sediment loads discharged by the Mississippi River to the Gulf of Mexico. These reductions in loads have consequences for river stability, protection of hydraulic structures, nutrient transport, and replenishment of coastal wetland areas.

Introduction

Recent years has seen significant hydrologic events affecting the Mississippi River Basin. Flood protection on the lower Mississippi River (below Cairo, IL) is a major focus of the Mississippi Valley Division, U.S. Army Corps of Engineers (CoE). Altered hydrological conditions as a result of changes in precipitation and rainfall-runoff relations must play a role in the magnitude and frequency of flow events from tributary basins (e.g., Yang et al. 2015). Numerous studies have shown the significance of climate change and extreme weather events on peak flows, low-flows, and flooding, etc. Contributing to shifting hydrologic patterns are human-induced changes to the natural environment such as agriculture, urbanization, channelization, dam construction, etc. Changing flow regimes also affect suspended-sediment transport rates and channel stability, challenging on-going efforts in flood protection, stream restoration and water-quality management. To assess and quantify spatial and temporal trends, and anthropogenic effects on hydrologic conditions within the Mississippi River Basin, daily precipitation and streamflow over the past 100 years were analyzed on an annual and seasonal basis. Peak-flow rates over one through 7 days were also investigated. All data was set in the framework of the four-digit hydrologic-unit code basins (HUC4) developed by the USGS to differentiate spatial variability across the major sub-basins. Temporal variability was evaluated over the entire period as the difference between conditions at the beginning and end of the recorded period (i.e., 1900-present). This paper represents an abridged version of a much larger report including data appendences and scores of maps produced for the CoE (Simon et al., in press).

Available Historic Data and Methods

Daily-Precipitation and Hurricane-Related Data

The fundamental data unit for precipitation that was available for this study was daily climate data, some dating back to the mid- to late-1800s, and available through the Global Historical Climatology Network-Daily (GHCND). These were accessed online through NOAA's National Climatic Data Center. The entire GHCND database was downloaded and data for all stations within the study area were extracted for the parameter PRCP (precipitation). Figure 1 (Left) shows the location of all 6,815 GHCND precipitation gages with at least one complete calendar year of data that was used in this study. Additional information on the GHCND database and its contents are available online at (http://www1.ncdc.noaa.gov/pub/ data/ghcn/daily/ghcnd-stations.txt).

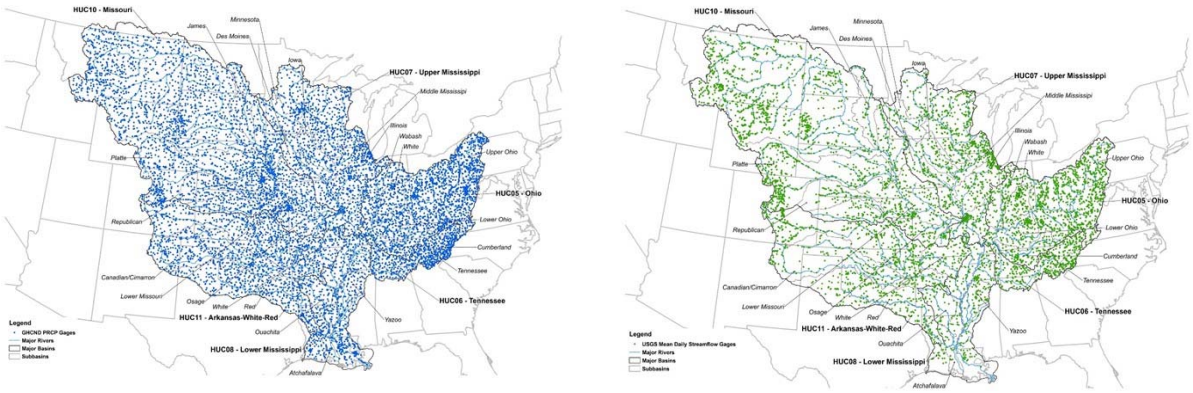

Figure 1. Map of the Mississippi River Basin showing the locations of the precipitation gages (Left) and streamflow gages (Right) used in this study.

Hurricane-related rainfalls were estimated following the methodology outlined in Darby et al. (2013; 2016) using NOAA's International Best Track Archive for Climate Stewardship (IBTrACS) database (version v03r02) (Knapp et al., 2010; available online: https://www.ncdc.noaa.gov /ibtracs/). IBTrACS was used to locate the paths of all recorded hurricanes (at daily time steps), intersecting or passing near the Mississippi Basin for the available period of record, 1950–2014 (Figure 2). The IBTrACS data comprise six hourly best-track positions and intensity estimates. Only storms designated as being in a tropical phase with one-minute maximum, sustained surface-wind speeds exceeding 34-knots (17.5 m/s) are included in the analysis.

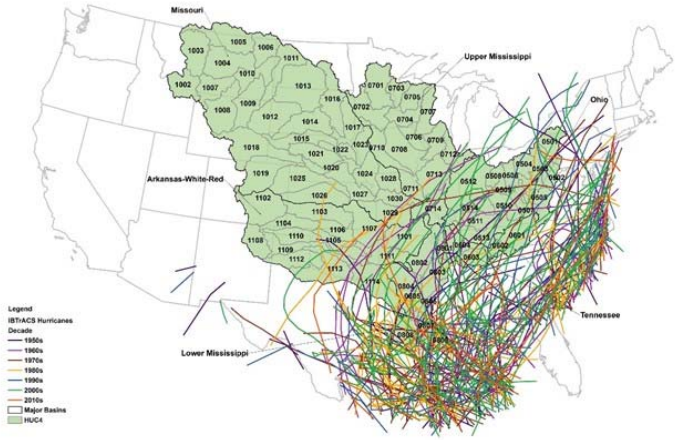

Figure 2. Hurricane Tracks Affecting the Mississippi River Basin (1950-2014).

Mean-Daily and Peak-Annual Streamflow

Mean-daily discharge data were obtained through batch downloads using the USGS Water Services Tool (https://waterservices.usgs.gov/rest/DV-Test-Tool.html). There are 6,186 flow stations with at least one complete calendar year of data within the study area (Figure 1, Right). For the majority of these gages, the drainage or contributing area to the gage is published. Where drainage areas were not defined, areas were estimated using either the USGS online tool, StreamStats version 4 Beta Application (https://streamstatsags.cr.usgs.gov/streamstats/), or for smaller basins, delineating the basin area using GIS. Additional mean-daily discharge data at gages along the Mississippi River main stem were obtained through the CoE River Gages website (http://rivergages.mvr.usace.army.mil/ WaterControl/new/layout.cfm).

Instantaneous, peak-annual discharge data were available at 8,210 USGS gages. However, only 7,118 gages have at least 10 annual observations, which was considered the minimum number required for flood frequency analysis.

Sediment Data: Suspended-Sediment Concentrations

To analyze the spatial distribution of suspended-sediment loads and to investigate how these have changed with time, it was decided to use the raw, concentration and associated discharge data from the time of sampling. Discrete suspended-sediment concentration with corresponding instantaneous flow data were obtained using USGS' Sediment Data Portal (https://cida.usgs.gov/sediment/). Within the study area there are 1,638 gages with at least 10 samples (Figure 3), which was considered the absolute minimum number required for generating sediment transport-rating relations.

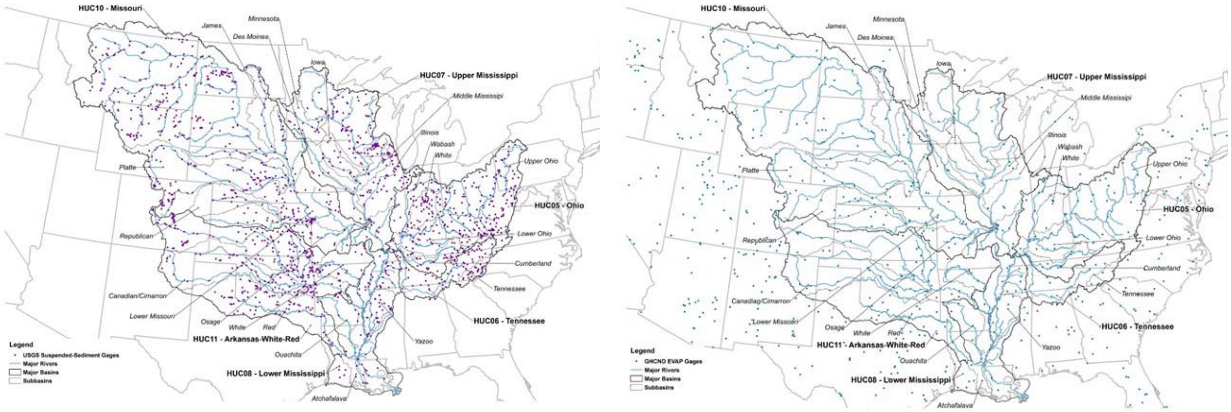

Figure 3. Locations of USGS suspended-sediment stations (Left) and GHCND pan-evaporation gages (Right) used in this study.

Ancillary Data: Dams, Pan-Evaporation and Geospatial

Information on the location, characteristics and construction date of dams is important to the investigation both in terms of understanding changes in flow regimes at particular gages and in determining their role in trends in evaporation and water-yield. These data were obtained from CoE's National Inventory of Dams (NID). Within the study area there are 13,629 impoundments listed in the NID database with published completion dates and data on the surface area of impounded water. This excludes privately-owned dams, and only considers dams owned by Federal, State, or Local Governments, as well as those owned by public utilities or whose ownership type is not listed.

To achieve a better understanding of the role of impoundments in altering hydrology and water availability, evaporation data were required across the basin. In addition to precipitation data, the GHCND database contains Class A pan-evaporation observations stored under the parameter EVAP. Pan evaporation is an empirical measurement of evaporation, which is a function of temperature, wind, humidity, and solar radiation. This parameter can be used to estimate evaporation from open bodies of water (WMO, 1966; Farnsworth and Thompson, 1982). Unlike GHCND precipitation data, pan-evaporation data from the entire continental U.S. were used, with 830 gages having sufficient data for this study (Figure 6).

Additional sources of geospatial data were obtained from the USDA NRCS' Geospatial Data Gateway (https://datagateway.nrcs.usda.gov/). This included delineations of HUC-2s and HUC-4s from the USGS Watershed Boundary Dataset as well as 1:24,000 hydrography networks. All spatial data presented in this study is projected using the Albers equal-area conic projection, USGS version.

General Methodology

All data were sorted by HUC4. Using this database, annual and seasonal values of precipitation and streamflow were computed from mean-daily values for each GHCN and USGS station, respectively. Three gages were established as the minimum within a given HUC4 for a given year (or season) to generate median values of total precipitation, water yield, and normalized water yield (median water yield per median total precipitation) for each of the 84 four-digit hydrologic unit code (HUC4) basins developed by the USGS. If there were greater than 15 years of data, that particular HUC4 was included in the analysis of annual and seasonal trends.

Water Yield and Precipitation Weighted Water Yield: Water yield, the amount of runoff per unit drainage area, is a convenient metric to compare stations of different sizes, providing a measure of runoff production for a given area. Temporal trends in water yield reflect hydrologic changes resulting from the combined effects of changing precipitation regimes as well as landscape changes imposed by humans. For example, if annual water yield is normalized (divided) by total-annual precipitation, any changes in flow due to altered precipitation regimes are removed, revealing the effects of anthropogenic changes on runoff and potentially, sediment yields.

Index Stations: To evaluate changes in absolute values of water discharge (not water yield) provided at the outlets of each HUC-4 and particularly the HUC-2's, trends in streamflow (in m3/s) were examined at select "index" stations. These stations were chosen based on their location along the major rivers or tributaries, period of record, and approximate drainage area. Where drainage area was approximately equal to the drainage area of its encompassing HUC-4 or if smaller, the first upstream gage with an adequate record was selected. Approximately 400 gages where chosen to represent regional (HUC-2) and sub-regional (HUC-4) changes in streamflow. The majority of the streamflow to the Lower Mississippi (~60%) originates in the Ohio River Basin. Contributions from the Upper Mississippi (including the Illinois River) were computed as the difference between flows at Thebes, IL and Hermann, MO. The CoE gage at Hickman, KY (MS113D) was chosen to represent the flows at the upstream boundary of the Lower Mississippi just below the confluence with the Ohio River. Flows at the CoE gage at Tarbert Landing, LA (01100Q) were used to represent flows along the Lower Mississippi,

Analysis of Median-Annual Values: Trends of annual data were analyzed using calendar years and were determined using multiple methods: simple linear regression, annual Kendall tau (Hirsch et al. 1982), and seasonal Kendall tau (Hirsch and Slack 1984) trend tests. The Kendall tau trend test is a non-parametric test for monotonic trends based on Kendall's tau statistic with a continuity correction, and was implemented using the statistical package *R* and the library EnvStats (Millard 2013). It is a common metric utilized by the USGS to assess trends in water quality (Hirsch et al. 1982). In the test, the null hypothesis is tau and is equal to 0 while the alternative hypothesis is that the true tau is not equal to 0, where positive values of tau indicate an increasing monotonic trend and negative values indicate a decreasing trend. The test

statistic itself is *z* and the *p*-value of *z* allows the user to accept or reject the null hypothesis. Although the Kendall tau statistic was used to determine the statistical significance of the trend, the magnitude and rate of change was computed using a linear regression and determining the difference between the calculated values for the first and last years of record for that HUC4.

Annual Trend Analysis with Seasonality: A more complex form of the Kendall- tau trend test accounts for monotonic trends within individual seasons: winter (Dec-Feb), spring (Mar-May), summer (Jun-Aug), and fall (Sept-Nov). The seasonal Kendall-tau trend test is appropriate for testing annual trends when all seasonal trends are in the same direction. When the seasonal Kendall test is not appropriate (e.g., increasing trends in summer and fall seasons but decreasing trends in spring and winter), the determination of the trend defaults to the first Kendall trend test using annual values. As with the analysis of the annual data, total change over the period was determined using linear regression and solving for the difference between the first and last year of record within that season and HUC4.

Determining Annual Suspended-Sediment Yields: Annual suspended-sediment yields at the sub-regional (HUC-4) level were determined using two separate methods. The first method involved calculating the suspended-sediment yield at a discharge that could be used to compare with other sites and that represented a meaningful geomorphic condition. The discharge selected for this purpose was the $Q_{1.5}$, a flow rate that is commonly used to represent the "effective discharge" (Leopold et al., 1964; Dunne and Leopold, 1978; Williams 1978; Castro and Jackson, 2001; Simon et al., 2004). Of course, there can be substantial variability around this average value (Williams, 1978), but it has been shown to be a good measure of this parameter for Level III ecoregions across the United States (Simon et al., 2004). To calculate representative sediment yields at the $Q_{1.5}$ for each sub region (HUC-4) the following procedure was used:

- Select an "index" station for each of the HUC-4 sub-regions representing the most downstream site with an extensive data set;
- Develop a first-approximation sediment-transport rating using a single power function from instantaneous discharge and concentration data;
- Solve the resulting sediment-transport relation using the $Q_{1.5}$ for that station; and
- Divide by drainage area to obtain a suspended-sediment yield in $t/y/km^2$.

Using a constant value of flow frequency allowed for direct comparison between sites and sub-regions as well as investigating how suspended-sediment yield varied at a single site (sub-region) over time. The earliest sampled decade for HUC-4 index stations is the 1930s. Many regions do not have sufficient sampling to determine temporal trends until the 1970s.

The sediment station in each HUC-4 with the greatest drainage area, greatest number of suspended-sediment samples, and longest period of record was selected at the representative "index" station. Transport ratings were developed for each decade of available data to determine whether the transport ratings were shifting with time. Examples from the Arkansas and the Missouri River are shown in Figure 4. The change in sediment load can be easily visualized by noting where the black vertical line (representing the $Q_{1.5}$) crosses each regression line. Using results from only the first and last decades of suspended-sediment observation, load (and yield) at the $Q_{1.5}$ was computed to quantify net change over the period. If a sediment station did not have a calculated $Q_{1.5}$-value from the peak-flow analysis at the same gage, the $Q_{1.5}$ was estimated based on a relation between drainage area and $Q_{1.5}$ for gages within the corresponding HUC-4.

The second method was aimed at providing mean-annual suspended-sediment loads and yields for each sub-region to obtain a spatial distribution of sediment contributions across the basin. In this case, suspended-sediment transport ratings were developed for every sediment station in the database. Instead of automatically accepting the first-approximation rating relation based on a single power function, every relation was visually inspected to determine if in fact, a more accurate representation of the general relation between flow and concentration could be attained using several linear segments (in log-log space). Where necessary, the rating relations were adjusted using one or more additional segments. For sediment stations with associated mean-daily flows (minimum of one complete year), daily sediment loads were calculated. These values were then summed for each year to obtain annual loads, divided by the number of years to obtain an average, and then divided by drainage area to obtain average, annual sediment yield for each station. To then characterize suspended-sediment yields at the HUC-4 level, the median value from all of the stations in the sub region was reported. The data set of sampled suspended-sediment concentrations at each station was considered sufficient if there were a minimum of 10 observations and if the maximum sampled flow was at least 75% of the calculated $Q_{1.5}$.

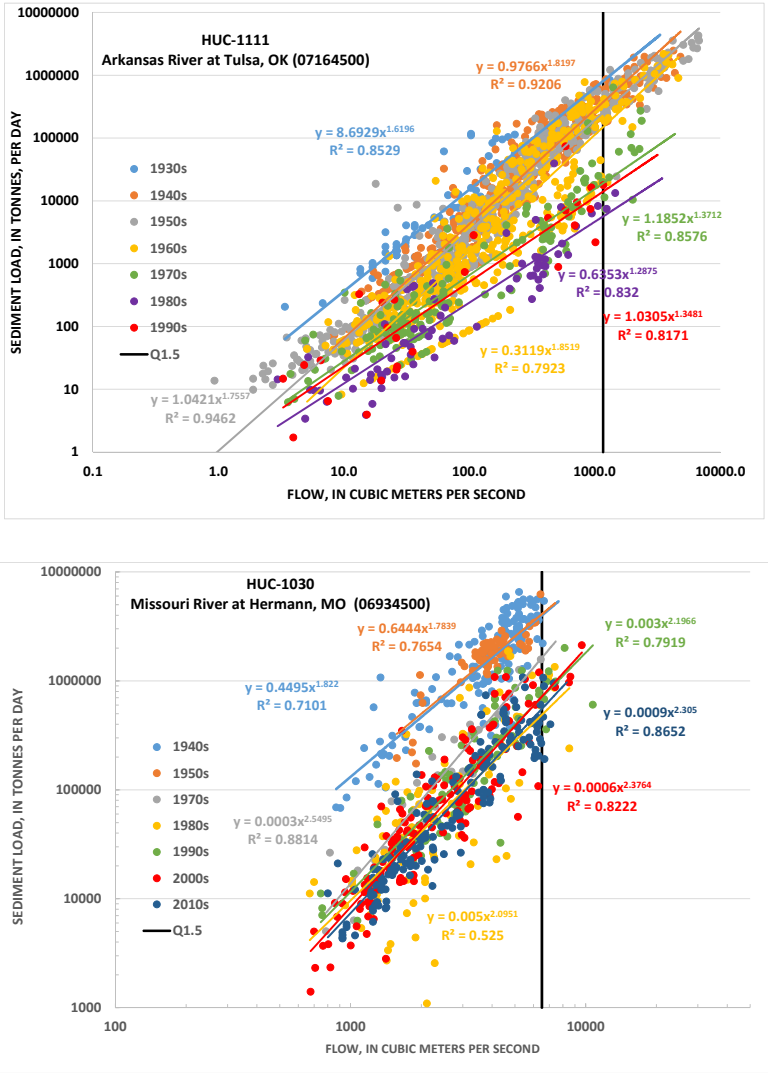

Figure 4. Examples of decadal shifts in sediment-transport ratings from index stations along the Arkansas (Top) and Missouri Rivers (Bottom). Note: the vertical black line represents the $Q_{1.5}$.

Precipitation, Hydrology and Suspended-Sediment Results

Geospatial presentation of results in the form of maps provides a succinct way of visualizing and interpreting spatial and temporal trends in the data. Due to space limitations, however, we can only provide examples of these in the sub-sections to follow.

Summary of Precipitation Results

On an average-annual basis, most of the Mississippi River Basin receives more rainfall than it did 100 years ago (Figure 5). Typical increases are in the range of 10-25%. The largest increases have occurred in the Upper and Lower Mississippi and the Tennessee River Basins, and may exceed 150 mm (about 6 inches). Large percent increases in the Missouri River Basin represent increases of less than 100 mm (about 4 inches) per year. A few of the far-western HUC-4s show decreases in annual precipitation. Peak annual-rainfall totals over 1-, 3-, 5- and 7-days also show increases over most of the basin indicating that inputs of precipitation have become more intense.

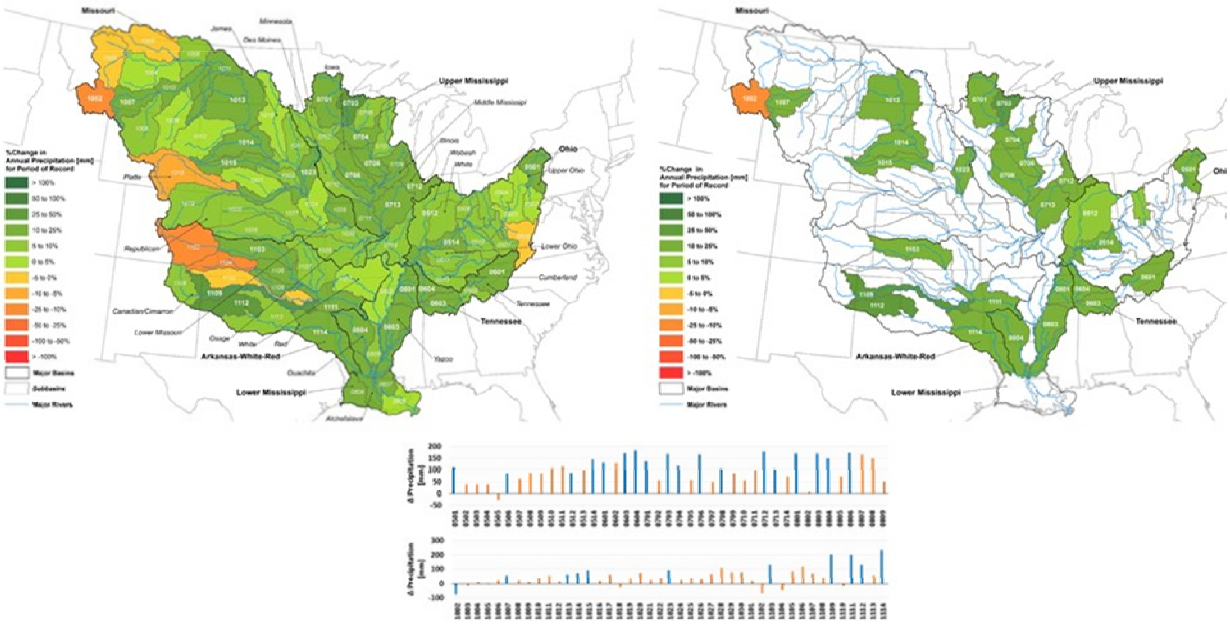

Figure 5. Percent change in annual rainfall for all HUC-4s (Top Left) and for HUC-4s with statistically significant trends only (Top Right). Change for all HUC-4s (Bottom), with significant trends shown in blue.

On a seasonal basis there were:

- Dramatic and significant increases in seasonal precipitation during the fall, with up to 150 mm (about 6 inches) more rainfall in some HUC-4s. Statistically-significant increases are recorded for HUC-4s south and east of a line extending from south-central Oklahoma to southwestern New York (Figure 6). This spatial pattern is similar to the changes (increases) identified in hurricane-related precipitation.
- Moderate increases during spring across the entire basin with decreases in the Red River and upstream areas of the Arkansas;
- Moderate increases during winter in the upper Mississippi and Tennessee, decreases in the Ohio, and little change in the Missouri;

- During summer, small decreases throughout the Missouri and Tennessee, small increases in the Ohio, and moderate increases in the Upper Mississippi, Arkansas and Red River Basins.

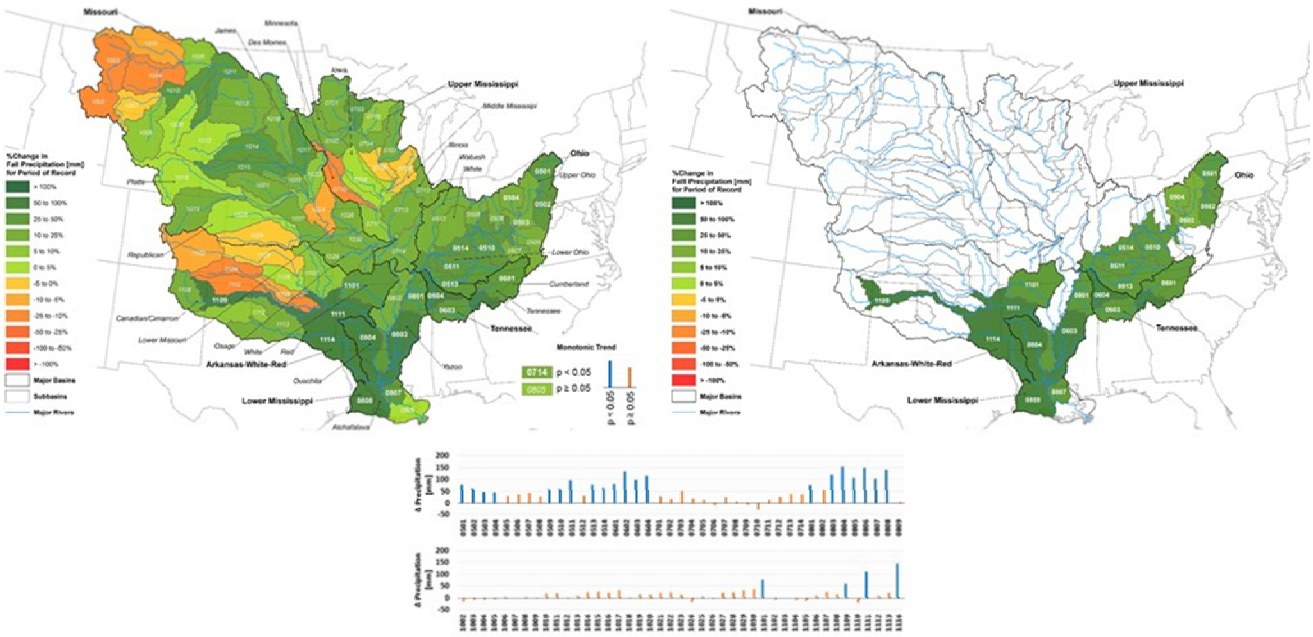

Figure 6. Percent change in Fall rainfall for all HUC-4s (Top Left) and for HUC-4s with statistically significant trends only (Top Right). Change for all HUC-4s (Bottom), with significant trends shown in blue.

Seasonal-peak precipitation mirrors the changes in total precipitation with the exception of important declines in peak-winter precipitation in the Rockies and much of the Missouri Basin. The dramatic increases in fall precipitation along the Appalachians is reinforced by increases in peak values with 3-day totals increasing by hundreds of mm. These results point to an increasing influence of hurricanes in the southeast and the Ohio River Basin. Hurricanes that are making landfall and impacting the Mississippi River Basin are, on average, producing more rainfall on both an annual basis and over one to seven day periods than they did in 1950 (Figure 7). The spatial distribution of these changes seem to indicate a combination of effects related to general circulation patterns and a potential orographic effect from the Appalachian Mountains.

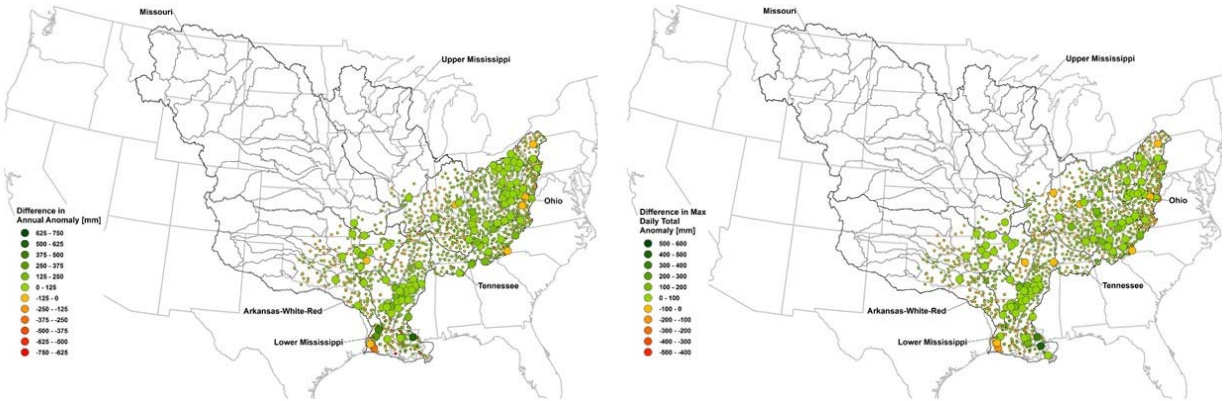

Figure 7. Change in annual (Left) and maximum-annual daily hurricane anomaly (Right), in millimeters.

Summary of Water-Yield Results

Changes in water yield reflect how discharge regimes have changed over the past century and represent a combination of changes in precipitation and anthropogenic influences. Average-annual changes in water yield show stark spatial differences between the central part of the basin where important increases have occurred (particularly in the upper Mississippi) and the contributing western basins (upper Missouri, Arkansas and Red River Basins, as well as the western floodplains of the lower Mississippi) which show large percentage decreases in flow (Figure 8). Increases and decreases in these respective regions can be substantial, in the range of 25-50% or even 50-100%. Similar spatial trends and magnitudes are apparent for the 1-day and 7-day peak water yields, reflecting vast changes in runoff generation and transmission through the river systems. The importance of water withdrawals and flow regulation in causing decreasing water yields is supported by the knowledge that this has occurred in some HUC4s that have experienced increases in precipitation.

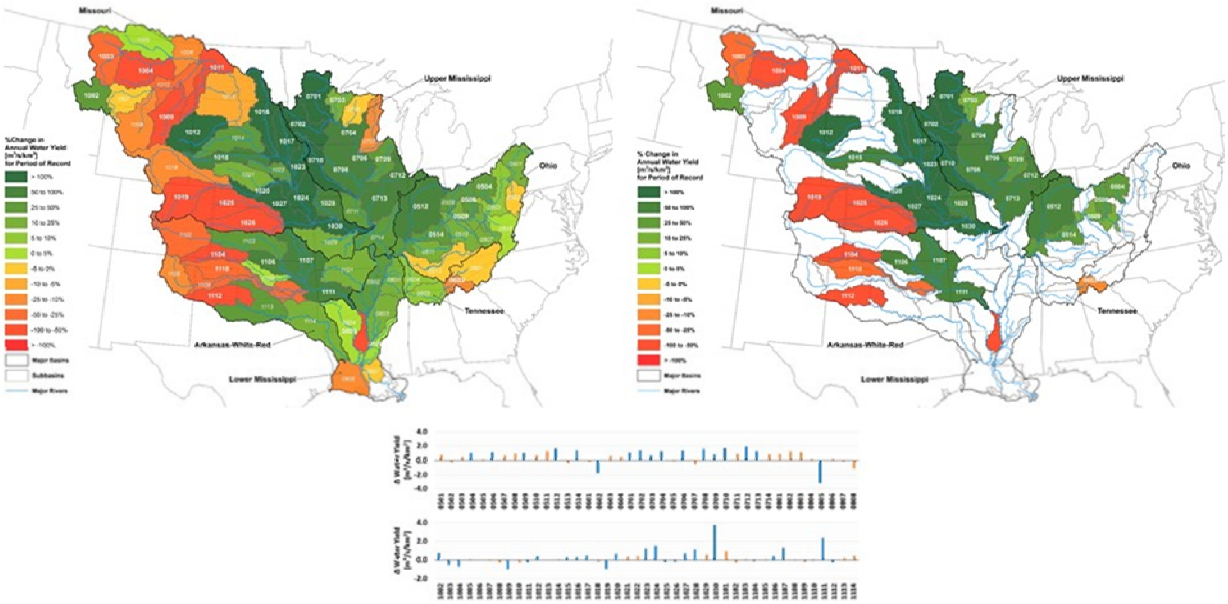

Figure 8. Percent change in annual water yield for all HUC-4s (Top Left) and for HUC-4s with statistically significant trends only (Top Right). Change for all HUC-4s (Bottom), with significant trends shown in blue.

The spatial distribution of changes in seasonal water yields again shows the increase in discharges throughout the mid-continent and the decreases in the western-most parts of the basin. Winter and fall tend to show the greatest areal extent of increases while irrigation withdrawals that peak during the summer months in large parts of the upper Missouri and upper Arkansas and Tennessee Basins, have resulted in important decreases in summer water yields and the amount of water available for ecological processes.

With regard to peak-seasonal water yields, there again are stark spatial differences between the western regions showing decreases across the 1- to 7-day durations, and the central and eastern regions that generally showing increasing peak yields. This clear geographic difference is probably mostly related to differences in how human requirements for water vary spatially across the basin relative to the availability of water while recalling that precipitation increases are larger in the mid-continent and southeastern parts of the basin, particularly in the fall. The fact remains though that peak-annual and peak-seasonal flows have dramatically increased in

the central and eastern parts of the basin. This has implications for channel erosion and flood control.

Summary of Precipitation-Weighted Water-Yield Results: Anthropogenic Influences

Although the direction of the changes varies across the basin, these effects are widespread and sizeable in magnitude, indicating that anthropogenic influences have been a major determining factor on changes in streamflow regimes over the past century. While anthropogenic activities have resulted in increases in water yield in the central part of the basin, activities at the basin margins have caused decreases in flow. The direction and magnitude of these influences can be sorted by region (Figure 9):

- Western-most part of the basin - Decreases: Widespread reductions in water yield due to anthropogenic activities characterize most of these HUC-4s. Decreases in the range of -25% to -100% are typical. This includes most of the upper Missouri (e.g., main stem Missouri down to Oahe, the Yellowstone, Platte, Republican and Smoky Hill Rivers), upper and middle Arkansas and upper Red Rivers (e.g., Canadian and Cimarron Rivers).
- Central part of the basin - Increases: Anthropogenic activities have resulted in significant increases in water yield throughout this region, with the magnitude of the increase generally decreasing from west to east. The largest effects (50-100%) are seen in the middle and lower sections of the Missouri River, the lower Arkansas and parts of the upper Mississippi (e.g., Minnesota and Des Moines), transitioning to moderate increases (10-50%) in the mid-continent and tailing off to 0-10% in the middle Ohio River basin.
- Eastern-most part of the basin- Decreases: Human activities have resulted in mild decreases (generally 0-10%) in water yield in the upper basins of the Ohio and moderate decreases (-10 to -25% in the upper and middle Tennessee River basins.
- Southern-most part of the basin - Decreases: The lower-most sub-basins of the lower Mississippi and Red River have had moderate reductions in water yield as a result of human activities. The greatest decrease has been in the Boeuf-Tensas (0805).

Seasonally, the spatial distribution of anthropogenic influences on water yield look much like those on an annual basis as described in the bulleted points above. Striking differences during the winter in the middle and lower Missouri basin and the Red and Washita Rivers, where winter flow releases are significantly greater now (>100%) than under the natural flow regimes before the dams.

Evaporation behind impoundments has increased drastically over the past century with the construction of thousands of dams which peaked in the 1960s and 1970s. Through the 1930s, evaporation relative to average-annual rainfall was about 0.1%. Starting in the 1960s and certainly by the 1980s, broad swaths of the Arkansas and Red River basins were losing more than 5% of their rainfall from evaporation behind impoundments (Figure 10).

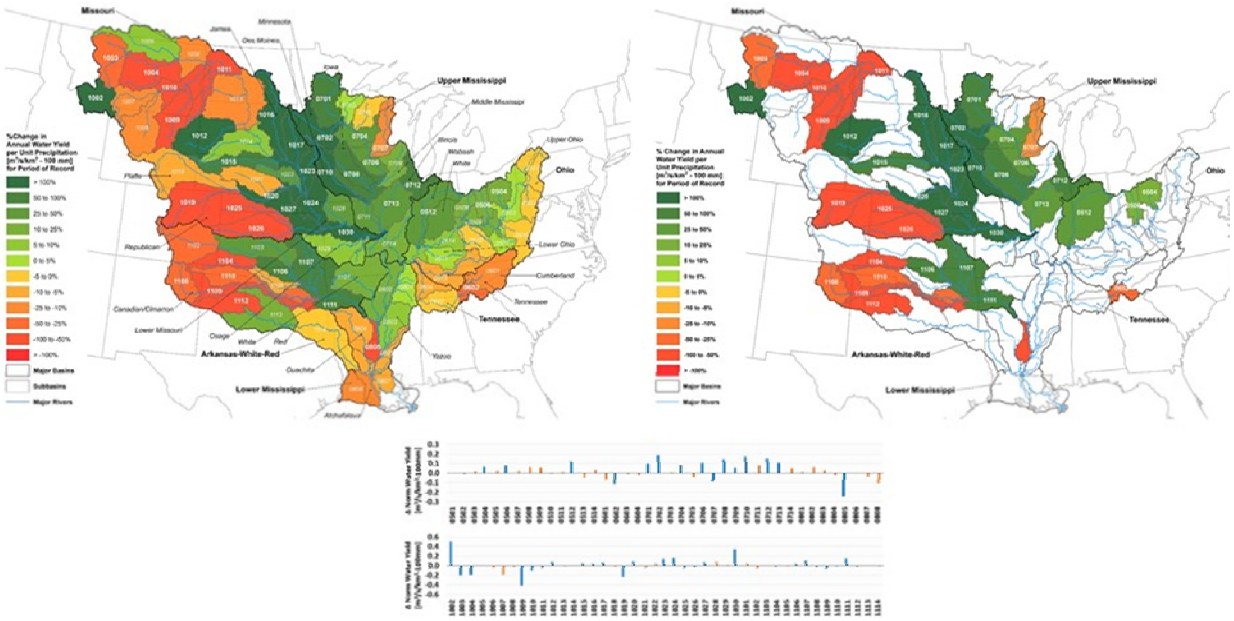

Figure 9. Percent change in annual, precipitation-weighted water yield for all HUC-4s (Top Left) and for HUC-4s with statistically significant trends only (Top Right). Change for all HUC-4s (Bottom), with significant trends shown in blue.

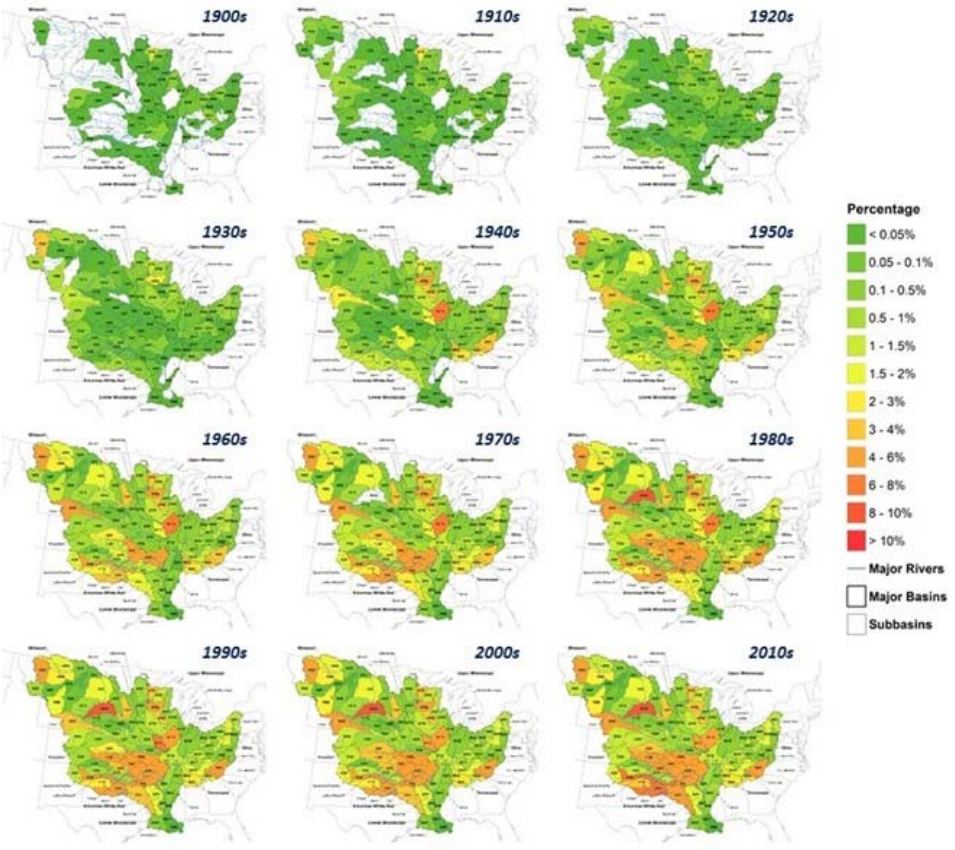

C

Figure 10. Percentage of average-annual potential evaporation from impoundments in specific HUC-4s relative to decadal average-annual rainfall by decade.

Summary of Streamflow Trends from Index Stations

The most important result from the analysis of the HUC-4 index stations is that discharges from much of the interior part of the basin show important increases in annual streamflow over the past century (from 25% to > 100%). Still, some trends of decreasing streamflow for various sub-regions in the upper Missouri and Arkansas River Basins are identified. In the upper parts of the Missouri, Arkansas, Ohio, and Tennessee River Basins, maximum-daily and 7-day streamflows emanating from the HUC-4 index stations were observed to decrease significantly, probably as a result of effective flood-control efforts by dam operations (Figure 11).

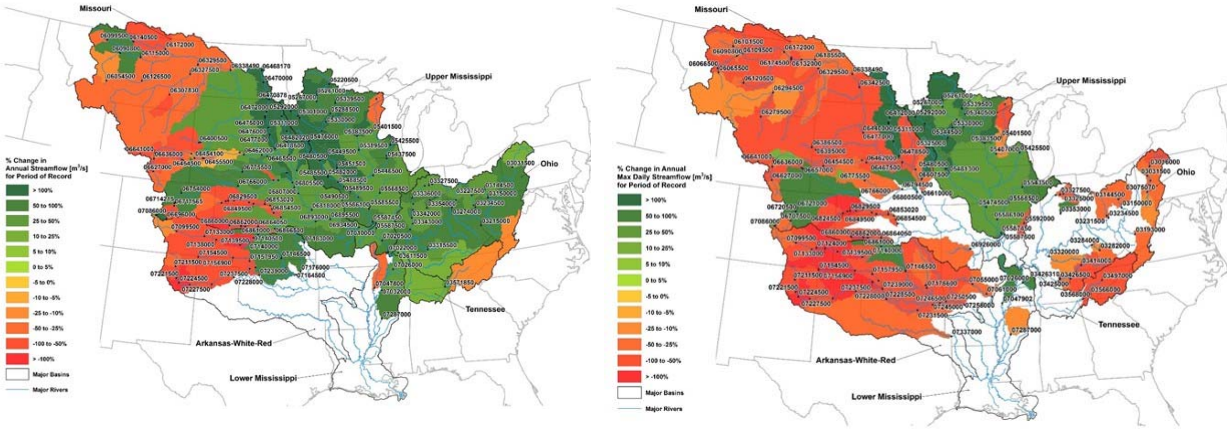

Figure 11. Change in annual (Left) and maximum-daily streamflow at index stations with significant trends over the past century.

HUC-4 seasonal distributions are similar to the annual ones with the exception of during the winter, where increases in flow extend well up into the Missouri Basin, reflecting the release of water under ice-covered rivers. Also striking are the large (25% to > 100%), widespread increases in discharge during the fall throughout the Mississippi River basin with the exception of the upper parts of the Missouri, Arkansas and Red Rivers, which showed decreases during this season.

In 1930, the relative contributions to average- and total-annual flow from the Ohio, Upper Mississippi and Missouri Rivers were 61%, 23% and 16%, respectively. By 2014 contributions from these three major suppliers shifted slightly to 55% from the Ohio, 28% from the Upper Mississippi and 18% from the Missouri. In general, the amount of water being delivered to the Lower Mississippi River has increased over the past century. Total-annual and annual-average flows have increased at all index stations emanating from the major river basins (HUC-2s) over the period of record (Figure 12). The actual, average increases in mean-daily flows from the three main basins to the upstream boundary of the Lower Mississippi River are:

- Ohio River: 1,674 m^3/s (23.8%);
- Upper Mississippi River: 1,767 m^3/s (66.0%); and
- Missouri River: 986 m^3/s (54.8%).

This comes to an increase in average, mean-daily flows, of about 4,427 m^3/s (156,000 ft^3/s). Integrated over an average year and excluding inputs from other smaller tributaries, brings the

average, annual increase in flows to the Lower Mississippi to about 1.62 million m^3/s (57.2 million ft^3/s).

Peak-annual streamflows from the Upper Mississippi River, measured at Thebes, showed significant increases over the period of record, for all durations:

- 1-Day: 2,990 m^3/s, (105,000 ft^3/s);
- 3-Day: 10,300 m^3/s, (364,000 ft^3/s);
- 5-Day: 16,500 m^3/s, (582,000 ft^3/s); and
- 7-Day: 25,000 m^3/s, (882,000 ft^3/s).

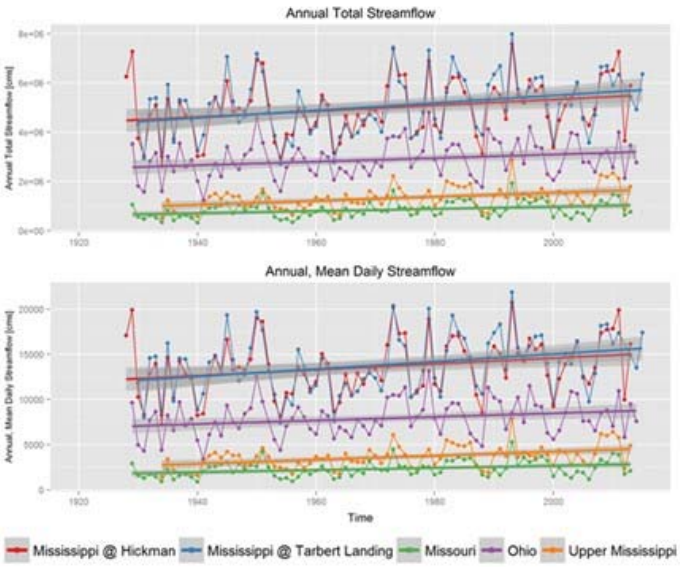

	%Change	p < 0.05
Missouri	55.2%	*
Upper Miss	60.1%	*
Ohio	24.1%	*
Miss @ Hickman	26.1%	*
Miss @ Tarbert Landing	31.6%	*

	%Change	p < 0.05
Missouri	55.2%	*
Upper Miss	60.2%	*
Ohio	24.1%	*
Miss @ Hickman	26.1%	*
Miss @ Tarbert Landing	31.6%	*

Figure 12. Change in total-annual and average-annual streamflow at the major index stations

Increases in seasonal streamflows from the Ohio, Upper Mississippi, and Missouri were detected in all seasons, although flows in the Lower Mississippi were found to increase only during the winter, summer, and fall months.

Summary of Sediment-Yield Results

Suspended-sediment yields were calculated for all stations and all time periods at the $Q_{1.5}$ to represent conditions at the "effective discharge". Maximum values occur in the Yazoo Basin (HUC 0803) with suspended-sediment yields of 154 $t/d/km^2$ and are 2.5 times greater than the next largest yielding region. Other areas of high yields include parts of the Upper Red (HUCs 1112 and 1113), the Kansas and Lower Missouri (HUC 1027 and 1030, respectively) and in two HUCS-4s in Upper Mississippi Rivers (704 and 706). In contrast, low-yielding regions (<0.25 $t/d/km^2$) occur throughout the upper Missouri, the James River (HUC 1016) and the Mississippi Headwaters.

Index stations were used to establish transport relations by decade to evaluate the change in sediment transport over the period of sampling and to determine the spatial distribution of these changes. These are shown at the HUC-4 level in Figure 13. Results show that suspended-

sediment loads at the $Q_{1.5}$ have declined from the outlets of all of the major (HUC-2) tributaries draining to the lower Mississippi River. About 5 million tons per day less sediment is reaching the lower Mississippi River (excluding the Atchafalaya) from its major tributaries at the $Q_{1.5}$:

- Ohio River: -48.5% (286,000 t/d);
- Tennessee River: -46.4% (8,380 t/d);
- Upper Mississippi River: -47.3% (446,000 t/d);
- Lower Mississippi (Atchafalaya River): -30.0% (49,600 t/d);
- Missouri River: -86.1% (3,440,000 t/d);
- Arkansas River: -95.7% (768,000 t/d);
- Red River: -90.5% (775,000 t/d).

Still, there are some sub-regions that are providing greater sediment loads currently than at the beginning of the sampling periods. These are located in the Upper Mississippi basin where about 50% of the index sites (sub-regions) are showing increases in suspended-sediment yields.

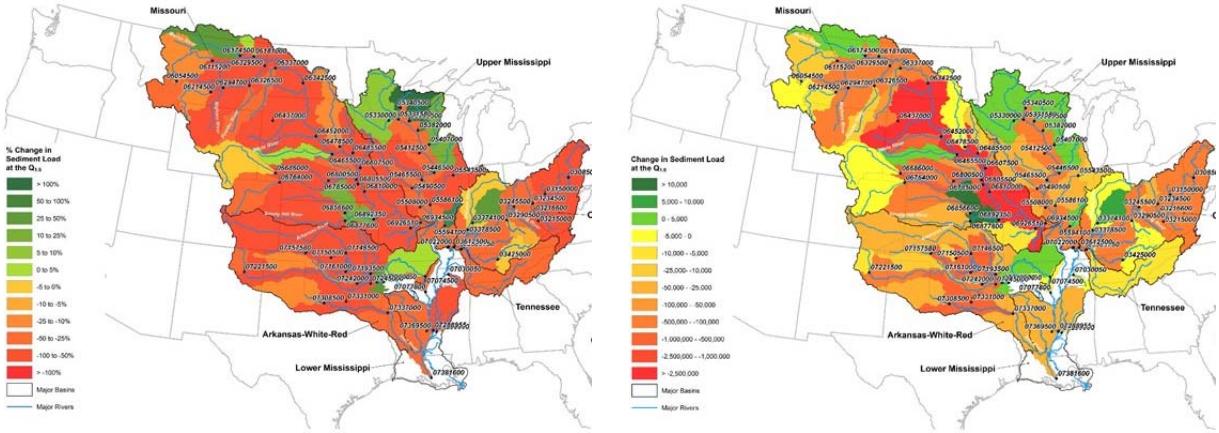

Figure 13. Change in suspended-sediment load at the $Q_{1.5}$ at sediment index Stations, expressed in percent (Left) and in t/d (Right). Blank areas represent a lack of index stations.

Using a data set of 970 gages, median, annual suspended-sediment yields from the sub-regions were found to vary over three orders of magnitude, ranging from 0.6 t/y/km^2 in HUC-1016 (James River) to 514 t/y/km^2 in HUC-1021 (Loup River) (Figure 14). The central 50% of the distribution of median values ranges from 20.1 to 95.1 t/y/km^2. Changes in median-annual suspended-sediment yields within each of the sub-regions reflect a broad range of hydrologic and anthropogenic changes over the past century. Marked decreases are observed across large parts of the Upper Missouri, throughout the Arkansas and Red River basins and in parts of the Upper Ohio and Lower Mississippi River Basins (Figure 15). These decreases are probably the result of land- and water-use practices that result in less water in the channels. In contrast, increases in median-annual yields have occurred throughout much of the mid-continent, including the Upper Mississippi and the lower Missouri Basins.

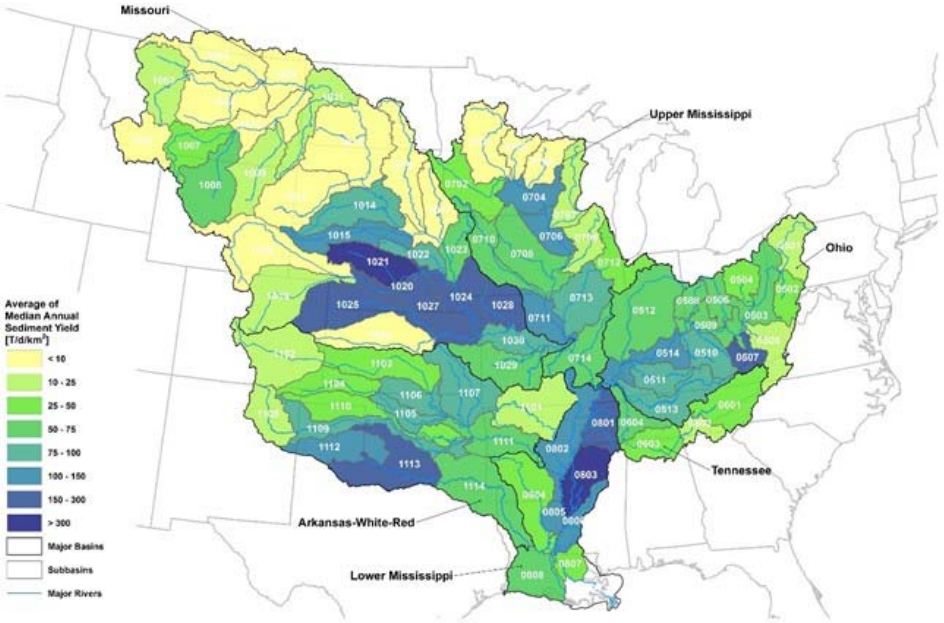

Figure 14. Average annual suspended-sediment yield by HUC-4 from station medians.

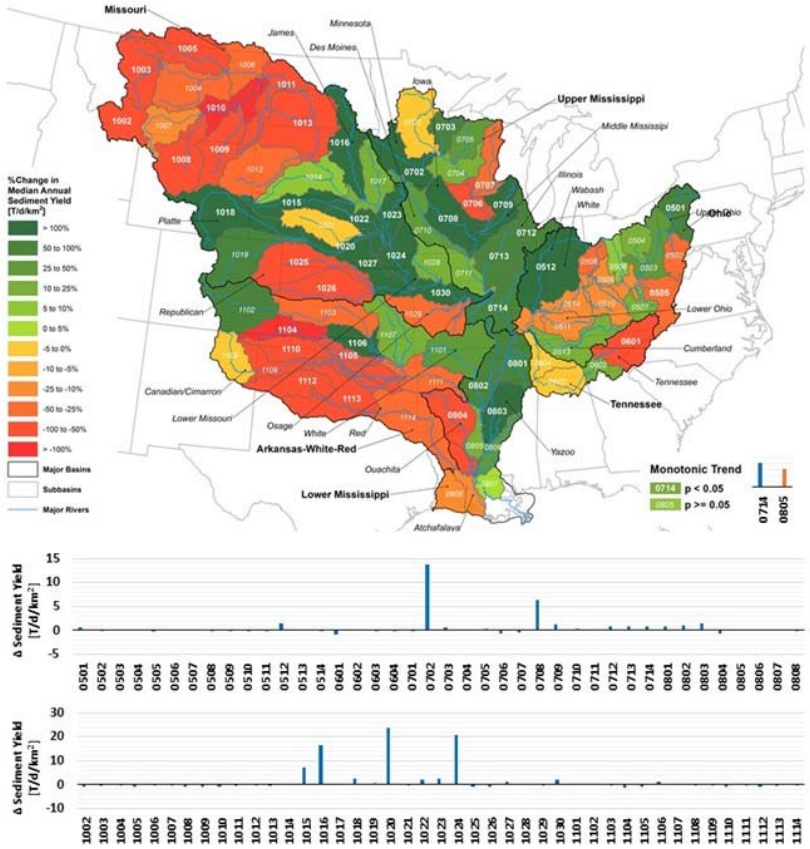

Figure 15. Changes in median-annual suspended-sediment yields over the period of record, by HUC-4.

To provide an evaluation of how sediment delivery to the lower Mississippi River has changed over time, sediment-load data from the outlet of the major contributing rivers was considered. To account not only for changes in hydrology, but also for changes in the relation between flow and sediment- transport rates, shifts in the rating relations were included in the analysis. Decadal sediment-transport curves were developed for the major (HUC-2) index stations and used to determine average-annual values for each decade (Table 1).

Table 1. Decadal average-annual sediment delivery to the Lower Mississippi River.

Decade	Average Annual Sediment Load [Mt]				
	Ohio	Missouri	Upper Mississippi	Arkansas	Total
1940s	49.6	360	47.3*	106	616
1950s	58.7α	268	45.1*	57.0	452
1960s	48.4α	259β	43*	24.9	408
1970s	45.3	99.7	9.4	13.2	168
1980s	30.4	40.7	32.6	15.3γ	119
1990s	29.8	83.7	57.2	4.0	175
2000s	31.4	31.2	21.0	3.1	86.6
2010s	20.8	47.8	27.0	2.3	97.9

α Uses 1940s transport curve; β Uses 1950s transport curve; γ Uses 1970s transport curve

* Estimated from extrapolation of trend from 1970s-2010s, back to 1940s

Sediment delivery to the lower Mississippi River from the HUC-2 basins show drastic, monotonic decreases over the period 1940 to present. The percent reduction in average-annual, suspended-sediment loads are: 61% for the Ohio River, 33% for the Upper Mississippi River, 84% from the Missouri River and 96% for the Arkansas River. About 251 Mt less suspended sediment are discharged per year to the Lower Mississippi River today from the Missouri River than in the 1940s. In total, this represents about a 300% reduction in average-annual, suspended-sediment delivery from the major tributaries to the Lower Mississippi River, from about 616 Mt/y in 1940 to about 98 Mt/y currently (Figure 15). Numerous other researchers have similarly reported on a large decline in suspended-sediment loads discharged by the Mississippi River to the Gulf of Mexico (Keown et al., 1986; Meade and Moody, 2010; Heimann et al., 2011). These reductions in loads have consequences for river stability, protection of hydraulic structures, nutrient transport, and replenishment of coastal wetland areas.

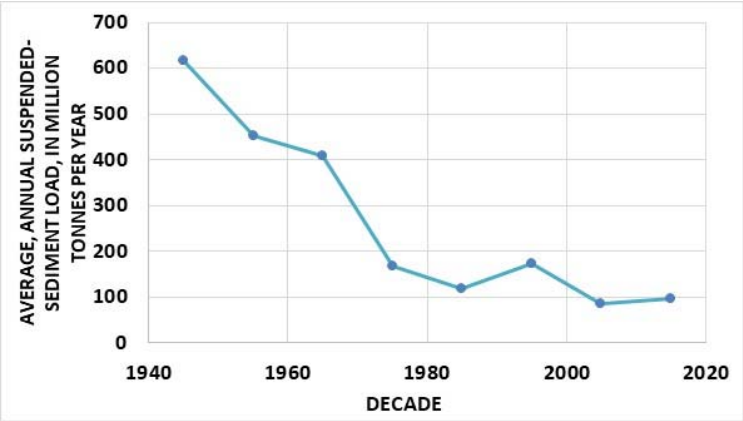

Figure 15. Decline in average-annual delivery of suspended-sediment to the Lower Mississippi River.

Summary

Altered hydrological conditions in the Lower Mississippi River are a result of changes in precipitation, rainfall-runoff relations and anthropogenic factors that play a role in the magnitude and frequency of hydrologic events. Numerous studies have shown the significance of climate change and extreme weather events on peak flows, low-flows, and flooding, etc. Contributing to shifting hydrologic patterns such as precipitation, are human-induced changes to the natural environment such as agriculture, urbanization, channelization, dam construction, etc., that often vary in a spatially systematic way according to regional demands for water. Changing flow regimes also affect suspended-sediment transport rates and channel stability, challenging on-going efforts in flood protection, stream restoration and water-quality management.

Results of this study show that in general, although most of the Mississippi River Basin is receiving more rainfall than it did 100 years ago, there are vast areas where water yields have decreased significantly, particularly in the western part of the basin and particularly in spring. Precipitation has also shifted temporally such that winter precipitation has significantly decreased in many areas while spring and autumn precipitation has generally increased. Parts of the western basin are experiencing 25 to more than 50% less discharge per unit area than they did 100 years ago. In contrast, the mid-continent is generating considerably more water than it did 100 years ago. In part this can be attributed to increases in precipitation and a greater influence of hurricane-related rainfall, but the anthropogenic effects cannot not be minimized. The result is that the lower Mississippi River is receiving more flow from its major HUC-2 tributaries (Ohio, Missouri and Upper Mississippi Rivers) than at the turn of the 20th century. Integrated over an average year and excluding inputs from other smaller tributaries, brings the average, annual increase in flows to the Lower Mississippi River to about 1.62 million m3/s (57.2 million ft3/s). Average, mean-daily flow contributions from the Ohio, Upper Mississippi and Missouri Rivers have changed from 61%, 23% and 16% in 1930, to 55%, 28% and 18% in 2014, respectively.

Although the direction of the changes (positive or negative) varies across the basin, these effects are widespread and sizeable in magnitude, indicating that anthropogenic influences have been a major determining factor on changes in streamflow regimes over the past century. The direction and magnitude of these influences can clearly be sorted by region. While anthropogenic activities have resulted in increases in water yield in the central part of the basin (increases of 50-100% decreasing eastward to 0-10%), activities at the basin margins have caused decreases in flow. In the west, decreases of 25-100% are typical.

Results of this study are in direct contrast with results of McCabe and Wolock (2011) over the same time period. Those authors concluded that precipitation variability accounts for nearly all the variability in observed runoff in the conterminous U.S. based on rainfall-runoff simulations. Similar to the findings of McCabe and Wolock (2014) who determined that streamflow was only weakly correlated to known climate indices, the results of this study show unpredictability of water yields based solely on climate – in this case, precipitation.

Sediment yields were calculated for all stations with available data at the channel-forming discharge (Q1.5) and on an annual basis. Results for both the downstream-most stations in each

sub-region and for average conditions within each sub-region elucidate current rates of suspended-sediment transport as well as changes over the period of record. Suspended-sediment loads at the outlets of most sub-regions have drastically declined. From the major tributaries at the Q1.5, by 30% in the Arkansas, 46-48% in the Tennessee, Upper Mississippi and Ohio Basins, and 86% in the Missouri. Similar results were obtained for annual values. Still, increases in sediment yields are found in some sub-regions impacted by increased precipitation and water yields such as the upper Mississippi, and regions bordering the lower and middle Mississippi and Missouri Valleys where channels are responding to the lowering of the trunk streams downstream from dams or because of channelization activities.

The average-annual delivery of suspended sediment to the Lower Mississippi River has declined by about 300%, from about 600 Mt/y in 1940 to about 100 Mt/y, currently. The largest actual decline is from the Missouri River (about 250 Mt/y) largely due to the trapping of sediment behind impoundments. Decreases in sediment delivery to these reservoirs are also noted. Other researchers have similarly reported on a large decline in suspended-sediment loads discharged by the Mississippi River to the Gulf of Mexico. These reductions in loads have consequences for river stability, protection of hydraulic structures, nutrient transport, and replenishment of coastal wetland areas.

References

Castro, J.M., Jackson, P.L., 2001. Bankfull discharge recurrence intervals and regional hydraulic geometry relationships: patterns in the Pacific Northwest, USA. Journal of the American Water Resources Association 37 (5), 1249–1262.

Darby, S.E., Leyland, J., Kummu, M., Rasanen, T.A., and Lauri, H., 2013. Decoding the drivers of bank erosion on the Mekong River: The roles of the Asian monsoon, tropical storms and snowmelt. Water Resources Research, 49: 2146-2163.

Darby, S.E., Hackney, C.R., Leyland, J., Kummu, M., Lauri, H., Parsons, D.R., Best, J.L., Nicholas, A.P., and Aalto, R. 2016. Fluvial sediment supply to a mega-delta reduced by shifting tropical-cyclone activity. Nature, 539: 276-279.

Dunne, T., Leopold, L.B., 1978. Water in Environmental Planning. Freeman, San Francisco. 818 pp.

Farnsworth, R.K. and Thompson, E.S., 1982, Mean monthly, seasonal, and winter pan evaporation for the United States, NOAA Technical Report NWS 34, National Oceanic and Atmospheric Administration, Washington, DC, p. 85.

Heimann, D.C., Sprague, L.A., and Blevins, D.W., 2011. Trends in suspended-sediment loads and concentrations in the Mississippi River Basin, 1995-2009. U.S. Geological Survey, Scientific Investigations Report 2011-5200, 43 p.

Hirsch, R. M., Slack, J. R., and Smith, R. A. 1982. Techniques of trend analysis for monthly water quality data. Water Resources Res 18(1), 107-121.

Hirsch, R.M. and J.R. Slack. 1984. A Nonparametric Trend Test for Seasonal Data with Serial Dependence. Water Resources Research 20(6), 727-732.

Keown, M.P., Dardeau, E.A., Jr., and Causey, E.M., 1986, Historic trends in the sediment flow regime of the Mississippi River: Water Resources Research, v. 22, p. 1,555–1,564.

Knapp, K.R., Kruk, M.C., Levinson, D.H., Diamond, H.J., and Neumann, C.J., 2010, The international best track archive for climate stewardship (IBTrACS): Unifying tropical cyclone best track data. Bulletin American Meteorological Society, 91, 363–376.

Leopold, L.B., Wolman, M.G., Miller, J.P., 1964. Fluvial Processes in Geomorphology. Freeman, San Francisco. 522 pp.

McCabe, G.J. and Wolock, D.M., 2011. Independent effects of temperature and precipitation on modeled runoff in the conterminous United States. Water Resources Research, 47, W11522, doi10.1029/2011WR010630,2011.

McCabe, G.J. and Wolock, D.M,. 2014. Spatial and temporal patterns in conterminous United States streamflow characteristics. AGU Geophysical Research Letters, 10.1002/2014GL061980, 6889-6897.

Meade, R.H., and Moody, J.A., 2010. Causes for the decline of suspended-sediment discharge in the Mississippi River system, 1940-2007. Hydrological Processes, 24: 35-49. 3916.

Millard, S.P. (2013). EnvStats: An R Package for Environmental Statistics. Springer, New York.

Simon, A., Dickerson, W. and Heins, A. 2004. Suspended-sediment transport rates at the 1.5-year recurrence interval for ecoregions of the United States: Transport conditions at the bankfull and effective discharge? Geomorphology 58, 243-262.

Simon, A., Artita, K., Darby, S.E., Leyland, J., and Simon, G.L., 2019. Changes in hydrology and suspended-sediment transport in the Mississippi River Basin over the past century. US Army Corps of Engineers MRG&P Report, Vicksburg, MS, 258 p., in press.

Williams, G.P., 1978. Bank-full discharge of rivers. Water Resources Research 14 (6), 1141–1153.

World Meteorological Organization, 1966. Measurement and estimation of evaporation and evapotranspiration. Tech. Note No. 83, Working Group on Evaporation Measurement, WMO, Geneva, Switzerland. 121p.

Yang, Q., Tian, H., Friedrichs, M.A.M., Liu, M., Li, X. and Yang, J., 2015. Hydrological responses to climate and land-use changes along the North American East Coast: A 110-year historical reconstruction. J Am Water Resour Assoc. 51(1), 47-67.

Reservoir Sedimentation: Impacts on Water Management and Sustainability

David L. Wegner, Senior Strategic Consultant, Woolpert Engineering,
Retired House of Representatives Senior Staff
David.L.Wegner@gmail.com

Preface

This extended abstract is a summary of a larger paper currently in technical review.

Introduction

Sedimentation in a reservoir created by a dam occurs due to changes in the characteristics of flow and the transport and resulting deposition. The accumulation of sediment in reservoirs is reducing storage capacity and is a significant problem facing dam managers globally. A 1987 World Bank study (McCully 1996) concluded that nearly one percent of global water supply is found in reservoirs. The study went on to state that of the global reservoir storage, it is estimated that approximately one-fifth or 20 percent of that storage has already been lost due to sedimentation. As sediments build up in reservoirs and water storage is replaced by sediments, operational options may be reduced and compromised leading to an increased risk of dam safety.

Reservoirs provide a valuable water source that supports agriculture and cities, protects people and lands from floods, provide sources for the generation of power, provides cooling water for power plants, support river levels for inland navigation, and provide locations for recreation and enjoyment (Hogeboom et al. 2018). Protection of reservoir storage capacity is important however limited resources have been allocated to determine the extent reservoir management is being impacted by sediment accumulation. Federal and state policy needs to be developed and aligned to address the concerns in a timely and cost-effective manner.

This paper was developed to assist water policy experts in identifying the challenges facing water and dam managers. Infrastructure and asset management of the Nation's dams, turbines, and reservoirs requires appropriate identification of the risk and the development of appropriate legislative direction and agency policy.

Identifying the Sedimentation Problem in Reservoirs

Reservoirs fill with sediment resulting in storage loss which leads to reduced water supply reliability, impacts to infrastructure including outlet works, turbines, spillways, river bypasses, water intakes, recreational boat ramps, marinas and water quality. Sediment deposition in the reservoir inflow areas often change the river base level causing deposition that often lead to flooding, channel migration and access to upstream riverine areas. Reservoir sedimentation rates are watershed and site specific and vary across

river basins, ranging from an average annual storage loss of capacity of 2.3 percent in China to 0.2 percent in North America (USBR 2015). Sediment inflow rates will likely increase as climate change brings about more extreme and variable runoff events. Sediment is mobilized more during the rising hydrograph during high flow events with deposition occurring during the descending hydrograph.

In most cases the impact of sediment depositing in reservoirs was not the first concern identified when dams were authorized for construction, designed, built and put into operation. According to the International ICOLD Register of Dams (2019) there is approximately 7,000km3 of reservoir water storage capacity of which approximately 3,000 km3 is classified as *dead storage* below the outlet works. This dead storage is typically where sediment accumulation occurs in reservoirs.

Including all dams (hydro and non-hydro dams) in 2006, 33% of the available reservoir capacity was filled with sediment. It is estimated that by 2050 this proportion of current total reservoir sediment capacity will have risen to 62% (IWPDC 2010). The annual combined global sediment load is estimated to be between 24-30 billion tons for a water inflow of 40,000 km3. Whether this loss of storage capacity is at hydropower, flood control or water supply reservoirs, the potential economic impact will increase due to loss of total reservoir capacity, impacts to dam and hydropower infrastructure, and ultimately increasing the cost of operations and maintenance. In addition, unless dam and reservoir operation manuals and operating procedures recognize the loss of storage capacity, risk in release and storage operations can increase resulting in loss of flexibility in management decisions.

All reservoirs that capture water are impacted by rising sediment levels. Depending on upstream watershed erosion and hydrology, sediments may be impacting storage capacity. Each river system is different in respect to what level of flows will mobilize and transport sediment downstream. Watershed condition and the physical structure and slope of the river channel may help to retard or accelerate sediment transport towards a reservoir. Once the sediment reaches the reservoir, limnological and geomorphic characteristics of the water body will determine how and where the sediment is distributed under the water surface. Typically, the reservoir inflow area and delta will build and shift because of the dynamics between inflow conditions, reservoir elevation, and the composition of the sediment load of the incoming flows.

Hydropower reservoirs can be filled slightly fuller with sediments since their use is dictated by the amount of water above the intakes. However, once reservoir sedimentation reaches 80% operational impacts due to the entrainment of sediment into flow of water driving the turbines occurs. Conversely, flood control and water supply reservoirs are dependent upon maintaining more storage capacity to meet their design functions. Their operational capacity will be hindered once the sedimentation reaches 70% (IWPDC 2010).

Many run-of-river hydropower plants built in sediment-loaded rivers are directly affected by sediment, both by a reduction in the amount of water available for daily peaking power production and by the rapid wear rates of turbines and other mechanical equipment, such

as gates and valves. The erosion rates on the infrastructure assets is directly proportional to the flow velocity. Brekke et al (2002) identified that sediment-induced turbine wear problems cannot be overcome by hydraulic design alone. The extent of damage can be reduced however through careful operational design avoiding rapid accelerations and reducing of turbine velocities. The extent of infrastructure erosion is a function of turbine design, type of surface coating, velocity of flow, reservoir head and sediment characteristics (Bishwakarma 2007)

Global regions and countries experiencing negative issues related to sedimentation in reservoirs by 2050 include:

Middle East – Afghanistan, Iran, Oman, Pakistan, Saudi Arabia,

Europe – Albania, France, Macedonia

Africa – Algeria, Botswana, Kenya, Morocco, Namibia, Sudan, Tanzania, Tunisia

South American – Bolivia, Columbia

Central America – Ecuador, Mexico,

Asia – China, Malaysia, Singapore, Sri Lanka,Uzbekistan

South Pacific – Fiji, New Zealand

Caribbean – Jamaica, Puerto Rico

In the United States small to large reservoirs are being impacted by sedimentation. For multiple reasons a large percentage of reservoirs across the United States have not been surveyed to determine the amount of capacity lost due to sedimentation. Sediment deposition in reservoirs is causing dam and river managers to modify their traditional operational parameters and evaluating ways to mitigate the impact of reservoir sedimentation. Two examples of the types of problems being experienced are the Conowingo Dam on the Susquehanna River in Maryland and Paonia Reservoir in Colorado.

Susquehanna River, Maryland. On the Susquehanna River in Maryland, the Conowingo reservoir is over 90% full of sediment, effectively reducing its ability to capture flood flows or serve as a river regulating facility. Conowingo Dam and reservoir are managed in coordination with two other dams and reservoirs on the lower Susquehanna River, Safe harbor Dam (Lake Clarke) and Holtwood Dam (Lake Aldred). The three reservoirs collectively cover 32 miles of the Susquehanna River and had a combined design water storage capacity of 510,000 acre-feet (acre-ft) at normal pool elevations. The Susquehanna River is the largest tributary to Chesapeake Bay and transports approximately one-half of the total freshwater input and substantial amounts of sediment, nitrogen and phosphorus to the bay (USGS 2015).

The three reservoirs began filling with sediments as soon as they were constructed. Conowingo Dam was completed in 1929 and 2011 estimates indicate that approximately 8 percent remained of the original 146,000 acre-ft of the reservoir storage capacity. As storage capacity in the reservoir is reached, a dynamic-equilibrium condition will exist between incoming and outgoing sediment and nutrient loads discharged downstream to Chesapeake Bay. This has led to increasing nutrient and sediment loading to Chesapeake Bay with subsequent challenges to meeting the established Total Maximum Daily Load mandates for sediment and nutrients (Nitrogen and Phosphorus). Estimates for nutrient and sediment loading are approximately 153 million pounds of nitrogen and 9.1 million pounds of phosphorus carried along with 6,600 million pounds of sediment (USGS 1997).

Paonia Reservoir, Colorado. Paonia Dam was completed in 1962 by the Bureau of Reclamation. The purpose of the dam is to provide water primarily for irrigation with additional benefits accrued to flood control and recreation. Due to upstream erosion, caused by land disturbance and logging, sediment moved into the reservoir basin and accumulated to levels that have reduced the storage capacity and limited the management of the reservoir to basically run-of-river operations. It is estimated that more than 8 million cubic yards of sand, silt, and other particles have accumulated behind the dam (HCN 2017).

The issues of sediment accumulation in reservoirs was not unanticipated by dam engineers and builders. Engineers design reservoirs to function for 50 to 100 years. Many western dams constructed by the federal government are now 60 years or older and nearing the end of their sediment and construction design life. This is requiring federal, state, tribal and water district dam managers to evaluate what alternatives exist to reservoirs that are filling or are filled with sediments.

Managing the Sediment in Reservoirs

Multiple options exist for dam and reservoir managers – none of them are easy or without substantial cost. Regulatory permitting of dam operations often requires the attainment of federal and state approval, adding considerable time to the implementation of operational changes. Traditional approaches have explored flushing, dredging and physical removal of sediments by drawing down the reservoirs and moving the sediments with heavy equipment. Alternative approaches have included physical construction of sediment sluicing gates in dams, retrofitting dams to move intakes above the sediment levels and upstream watershed control of sediment sources. Each of these alternatives are costly and generally need appropriation of funds and appropriate policy and agency support.

Of interest globally is the study of the high sediment loads in many Asian rivers, especially the Yangtze and Yellow rivers in China and the Mekong River in southeast Asia. These

rivers, whose watersheds include the highly erosive loess soils of the Tibetan Plateau, have historically exhibited large seasonal flow and sediment transport events that have tested infrastructure and public safety. Chinese hydrologic engineers and academic experts have developed intricate assessments of sediment loading. Chinese river managers have employed multiple approaches to managing sediment on the Yangtze and Yellow rivers including upstream watershed stabilization, constructing sediment capturing dams on tributaries and construction dams so that large suspended sediment load flows can be routed through reservoirs and through mainstem dams (Yang et al. 2006).

Planning and design considerations when either designing and constructing dams in high sediment yield catchments requires a vision about the possible changes in upstream watershed management and land use. Often not considering potential upstream development will lead to reduced operational flexibility and impacts to infrastructure. Important elements for consideration include:

- Site selection – location, watershed characteristics, and rainfall/runoff patterns
- Data collection – gathering of reliable sediment data that takes into account sampling locations, techniques, frequency, technology and skill of personnel.
- Design of project including efficient sediment flushing options, trapping efficiency of the reservoir, estimated impact of sediment on the infrastructure, and costs associated with flushing or shut down during high sediment transport periods.
- Turbine design – dependent upon sediment load characteristics and anticipated turbine wear, and appropriate turbine design, construction and operation.
- Optimization of sediment exclusion – sediment control and removal of sediments should be identified and addressed during the planning and operational phases of the project.
- Real time sediment monitoring – to provide early warning system regarding sediment concentration and asset management of the physical equipment.

Tasks for Maintaining Sustainable Water Supplies

Sediment accumulation in reservoirs is diminishing their useful life span and operational flexibility. During the dam development era in the United States (1940-1970's) limited thought was given to plan for reservoirs filling up sediment. It was assumed the dead pool area would suffice. That assumption did not consider changing hydrology and upstream land practices and their impact on erosion and sediment transport. Authorizing legislation and subsequent policy and development of operations manuals did not take into consideration the impact of sediment loading into reservoirs, its impact of infrastructure nor a systems perspective on upstream and downstream development.

Research and Risk Assessment. A need exists now, while we have time on the planning horizon, to assess what the impact of reservoir sedimentation will be on river management and dam operations as more extreme weather and resulting hydrologic events lead to increased sediment mobilization and transport to and in reservoirs. Coordinated research and assessment focused on determining the extent of the potential risk at dam assets and to prioritize and assess remediation and mitigation strategies will be value added to protection of our water assets.

System Water Resource Planning. Significant advances in water resource planning have occurred with the advent and adoption of adaptive management, watershed management and integrated water resources management. The foundations for these approaches evolved from early watershed and river basin management. The building of dams has been justified based on dam's ability to provide a constant supply of water for agriculture, municipal, industrial, hydropower, power plant cooling, navigation, downstream flood control, and in some cases for water quality purposes. Justification, design and operation of these reservoirs is predicated on the assumption that the original design capacity of the reservoir will be available to provide project benefits.

To assist water managers and decision-makers in achieving project goals and objectives, significant investments have been made developing and implementing technology to gather data and information to allow for the characterization of the hydrology and other operationally important parameters to populate dam and river management models and operational options. The resulting dam and operation supporting infrastructure provide significant and expected economic and social benefits.

Assessment of Sediment Removal Techniques. One of the largest challenges in sediment management is to have a plan on how to handle deposited sediments from the reservoir basins or settling areas. The removal of the accumulated sediments and their ultimate disposal in an environmentally friendly way need to be considered. Current methods currently include sediment flushing, sediment sluicing systems, removal by pipeline and routing of sediments through reservoir basins.

Limited Monitoring. Unfortunately, most of the large and small reservoirs in the world are not monitored in respect to sediment capture and the resulting build up and lost water storage capacity. Many reservoirs around the globe are experiencing increased sediment build up due to upstream watershed erosion driven by development and variable rainfall and runoff events.

Climate Change. Climate change is significantly increasing watershed-sediment erosion rates and as a result sediment transport rates in rivers and an increase in the rates of reservoir storage capacity loss.

Historically there was generally enough capacity in reservoirs to meet the authorized goals and objectives of dam and river managers. However, with the increase in larger and more frequent extreme weather and hydrology driven events, dam and river managers are faced with challenges in maintaining public safety and water supply.

New Tools. Developing new technology is critical to efficient collection of reservoir sedimentation data. This data needs to be integrated into improved reservoir management models that can assist in sediment management. The U.S. Army Corp of Engineers and others are assessing the use of LIDAR to measure sedimentation in reservoirs (USACOE 2016).

Technical Coordination. Multiple federal, state and academic institutions dialogue on the reservoir sedimentation. The National Reservoir Sedimentation and Sustainability Team provides a forum for the scientific and engineering discussion on sedimentation in reservoirs. Additional support to ensure the information is fed back to policy and decision-makers is critical to ensure that the information is formulated into appropriate policy and action. A National focused forum should be established to ensure that the information generated is carried into the appropriate policy forums.

Policy Support. Providing direction to agencies and groups to initiate data collection, model development and risk assessment often requires direction and support from agencies and appropriators. It is important that appropriate direction and funding is allocated to the agencies to adequately assess the reservoir sedimentation problem and formulate appropriate actions to address.

Recommendations

Under the existing operation and management regimes of the reservoir management community the impact of sedimentation will continue to increase. Not accounting for the reduction in storage capacity in reservoirs due to sediment is already impacting operational efficiency. Sustainable reservoir and water management requires that an improved and coordinated approach to understanding and managing the sediment loads in reservoirs be developed.

While it may be desired to calculate sediment deposition rates and loss of storage capacity for every reservoir it is not cost effective or likely to occur. What is possible however is to develop a risk assessment approach to reservoirs located within specific watersheds/river basins to help prioritize activities. Actions to be taken should include:

1. Develop federal policy to work with the states to aggressively address the issue and develop a set of recommendations for consideration by Congress.
2. Establish a National level Water Commission to help coordinate agency actions and approaches to defining the risk, build linkages between agencies, and to formulate cooperative watershed-based approaches.
3. Charge the Bureau of Reclamation, the U.S. Army Corps of Engineers, Department of Energy and the Federal Emergency Management Administration to evaluate the current state of the knowledge on sediment management in reservoirs including the identification of best practices, research needs, and policy priorities.

4. Establish river basin forums to identify and prioritize reservoirs to be assessed as to loss of reservoir storage capacity due to sedimentation (USBR 2015).
    - Determine the magnitude of the sediment problem
    - Define sediment management options
    - Define stakeholders and constraints
5. Prioritize the identified reservoirs based on their potential impact to public safety, water supply, flood control, access and energy production.
6. Assess the desired level of quality of data that is needed to address the initial assessments
    - Design and implement a sediment management monitoring program
    - Facilitate and invest in remote sensing technology to assess the level of deposition in high risk reservoirs or watersheds.
7. Develop new technologies to gather data
    - Developing new technologies for collecting reservoir sedimentation data
    - Implement data collection and analysis programs to develop quality data sets
    - Design and coordinate pilot studies to test assumptions
    - Integrate data into Geographic Information System for watersheds/river basins
8. Refine and or develop new models.
    - Models to address operational impacts associated with identified reservoirs.
    - Integrate real time data streams into modeling applications
    - Verify and validate the models
9. Update and Refine Operations Manuals
    - Integrate data and reservoir modeling information into operational manuals
    - Develop and implement a sediment management plan
10. Adaptation, Mitigation and Remediation Strategies
    - Develop useful adaptation, mitigation and remediation mitigation strategies
    - Identify methods to both reduce sediment loading to the reservoirs and the potential and cost-effectiveness of sediment removal to improve operational flexibility

References

Bishwakarma, M.B. 2007. Addressing sediment problems. International Water Power and Dam Construction. https://www.waterpowermagazine.com.

Brekke H, Wu Y L and Cai B Y 2002 Design of Hydraulic Machinery Working in Sand Laden Water Abrasive Erosion & Corrosion of Hydraulic Machinery ed C G Duan and V Y Karelin (London: Imperial College Press) 155-233

High Country News. 2017. As sediment builds, one dam faces its comeuppance: Officials at a Colorado reservoir are reckoning with decades of accumulation.

https://www.hcn.org/articles/water-as-sediment-builds-a-colorado-dam-faces-its-comeuppance-paonia-reservoir

Hogeboom, R.J., L. Knook, and A.Y. Hoekstra. 2018. The blue water footprint of the world's artificial reservoirs for hydroelectricity, irrigation, residential and industrial water supply, flood protection, fishing and recreation. Advances in Water Resources. 113. 285-294.

ICOLD (2016). Register of Dams – General Synthesis. Retrieved December 15, 2018, from https://www.icold-cigb.org/GB/world_register/world_register_of_dams.asp.

International Water Power and Dam Construction. 2010. Tackling the growing problem of sedimentation. https://www.waterpowermagazine.com/features/featuretackling-the-growing-problem-of-sedimentation/

McCully, P. (1996). Silenced Rivers: The ecology and politics of large dams. London. ZED Books.

USACOE. 2016. USACE LIDAR capabilities for reservoir sedimentation. https://www.usace.army.mil/Portals/2/docs/civilworks/climate/docs/LiDar_theme_02-29-2016.pdf?ver=2017-11-30-10448-757.

USBR. 2015. Dealing with the inevitable: Sediment in reservoirs: Developing effective guidelines for managing sediment in Reclamation's reservoirs. Bulletin 2015-03. http://usbr.gov/research/docs/updates/2015-03-sediment.pdf.

USGS. 1997. Sediment deposition in Lake Clarke, Lake Aldred, and Conowingo Reservoirs, Pennsylvania and Maryland, 1910-93. USGS Water Resources Investigation Report 96-4048. 14pp.

USGS. 2015. Conowingo dam above 90 percent capacity for sediment storage. https://www.usgs.gov/news/conowingo-dam-above-90-percent-capacity-sediment-storage.

Yang, Z., H.Yang, Y.Saito, J.D., Milliman, K. Xu, S. Qiao, and G.Shi. 2006. Dam impacts on the Changjiang (Yangtze) river sediment discharge to the sea: The past 55 years and after the Three Gorges Dam. Water Resources Research, Vol. 42, W04407, doi:10.1029/2005WR003970.

Dam Removal or Rehabilitation

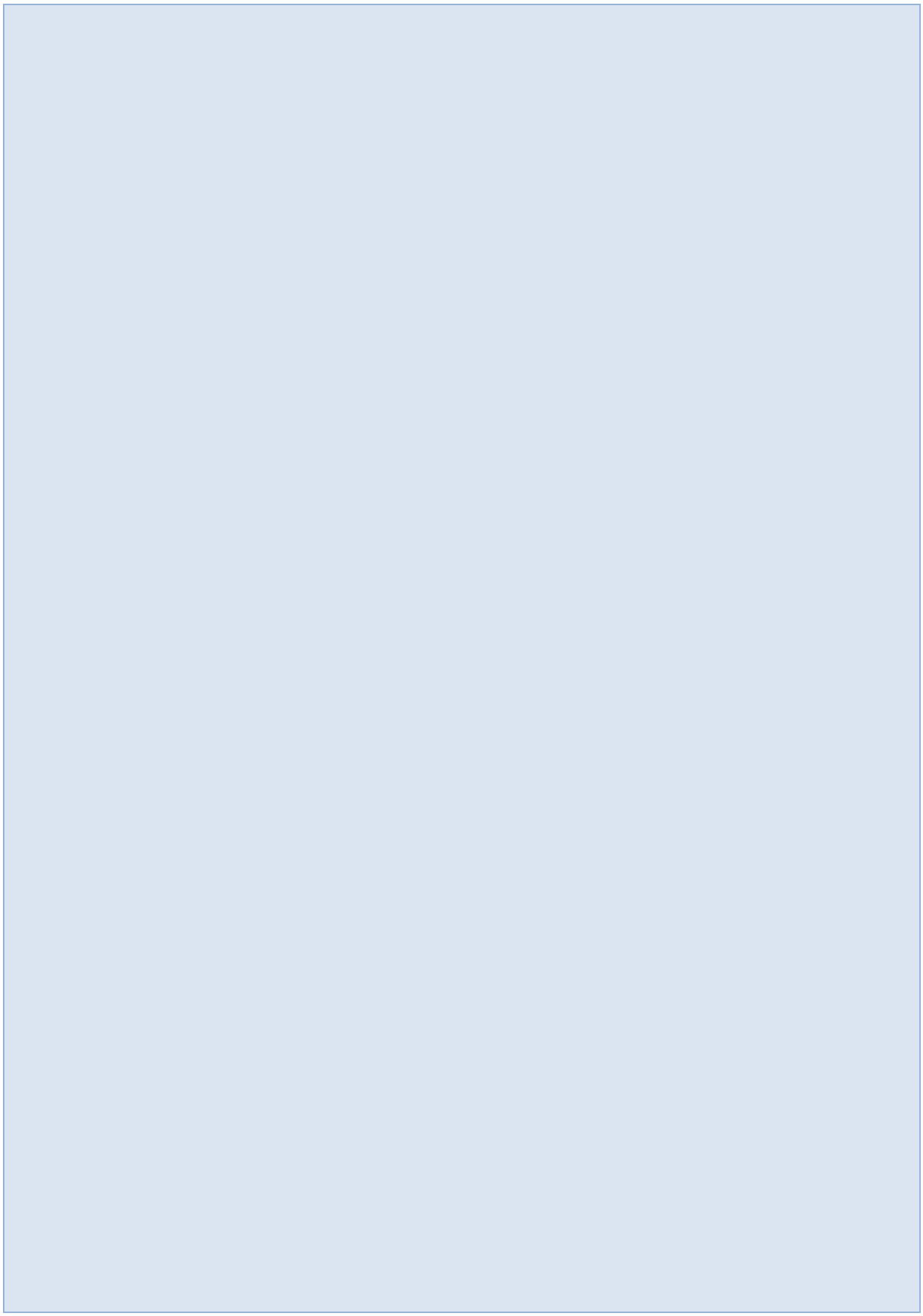

Geomorphic Response to Dam Removals on the Lower Penobscot River, Maine, USA

Mathias J. Collins, Environmental Scientist, NOAA Fisheries, Gloucester, MA, mathias.collins@noaa.gov
Alice R. Kelley, Instructor, School of Earth and Climate Sciences, University of Maine, Orono, ME, akelley@maine.edu
Pamela J. Lombard, Hydrologist, US Geological Survey, Augusta, ME, plombard@usgs.gov
Sean M.C. Smith, Associate Professor, School of Earth and Climate Sciences, University of Maine, Orono, ME, sean.m.smith@maine.edu

Geomorphology studies of dam removals have typically focused on sites with appreciable quantities of stored sediments. There is considerable interest in channel responses to sediment releases because of the potential effects on aquatic and riparian habitats and human uses of these areas (Bellmore et al. 2017). Yet, many dams in the Northeast U.S. have only minor accumulations of sediment because of small impoundments, run-of-river dam design and management configurations (inflow approximately equals outflow), low watershed sediment yield, and/or channel beds dominated by coarse sediment and/or bedrock. The two lowermost dams on Maine's Penobscot River in New England's second largest watershed (~22,000 km^2), removed in 2012-13, were examples of these conditions. Veazie Dam (~10 m) was located just above the head-of-tide and Great Works Dam (~6 m) was ~12 km further upstream (Figure 1). These run-of-river hydroelectric dams did not have substantial water storage capacity. Pre-project geophysical surveys showed little stored sediment in either impoundment, and coarse substrates (cobbles, boulders, and bedrock) dominated the beds of the reservoirs and the reaches up and downstream—functions of reach geology, late Quaternary history, and upstream dams. Nonetheless, the streambed substrata in the impoundments was poorly understood and there was a history of river modifications at the sites, suggesting unexpected geomorphic changes were possible.

To evaluate physical responses to the removals, we did repeat cross-section surveys pre- and post-removal in each impoundment as well as the upstream and downstream reaches. We also measured bed sediment grain-size and collected turbidity data below the dams. Repeat cross-section surveys were accomplished at 13 permanent transects by combining ADCP measurements of channel areas and total station surveys of near-bank and subaerial areas. Some transects in some years had sections too shallow to boat and too deep/fast to wade and thus data were not obtained. The channel geometry data were supplemented with oblique photographs taken at fixed locations and azimuths along each transect to qualitatively record conditions during each survey. Bed sediment grain-size was measured via an experimental method of towing across each transect an underwater video camera mounted on a weighted sled with measuring bars in the field of view. Still images were subsequently extracted from every minute of transect video and the intermediate axes of individual clasts larger than very coarse sand or small pebbles were measured using a grid developed from the measuring bars. Texture and percent cover of interstitial sediment were also estimated. Turbidity was measured in situ via nephelometer every 60 minutes at a US Geological Survey gage downstream of both dams.

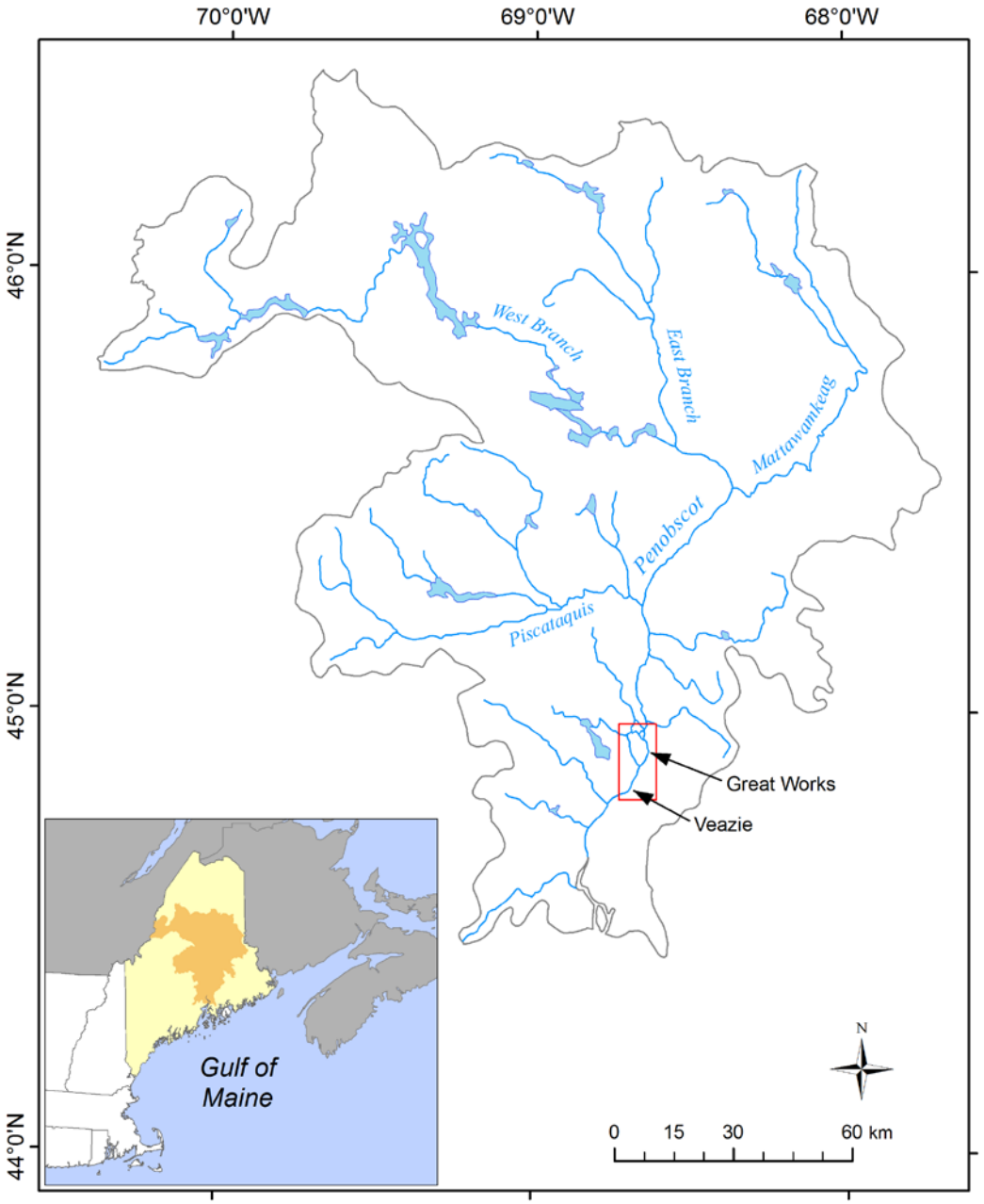

Figure 1. The Penobscot River watershed with the study area (box) and dam locations.

The pre- and post-removal channel geometry surveys confirmed our expectation that bed elevation, channel shape, and channel position would change little in the affected upstream and downstream reaches (e.g., Figure 2). Indeed, changes from one survey to the next at nearly all cross-sections were often within our estimated measurement error. We also confirmed that collecting bed sediment grain-size data is exceptionally challenging in wide, high velocity rivers that are frequently too deep to wade but too shallow and turbulent for many boats. We could only collect reliable video tow data in the impoundments, thus post-removal comparisons were impossible. However, the pre-removal data confirmed that the impoundments were dominated by coarse substrates as sidescan sonar surveys had shown during project feasibility studies. The turbidity data also reflected that the impoundments were dominated by coarse substrates and

stored little fine sediment. Turbidity spikes during the dam removals were of the same magnitude and duration as those produced naturally by the watershed (Tullos et al. 2016).

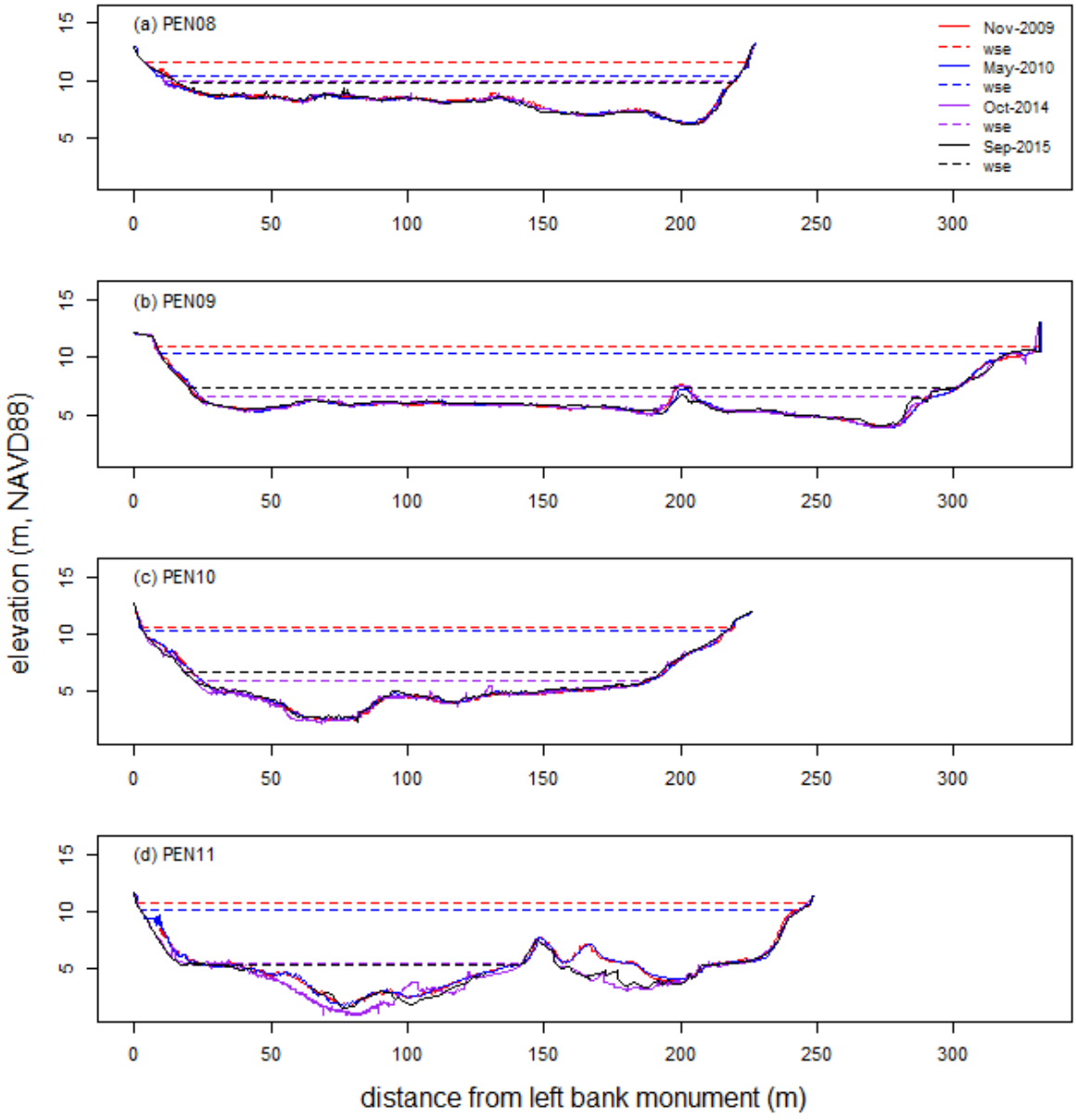

Figure 2. Veazie impoundment before (2009 and 2010) and after removal. PEN11 is closest to the former dam.

Our study shows that physical changes are likely to be minimal when impoundments storing relatively little sediment are removed from erosion-resistant streambeds. Since many dams eligible for removal have these characteristics, the observations are an important case study largely unrepresented in the dam removal response literature to date and suggest that physical monitoring is frequently not necessary in these settings.

References

Bellmore, J.R., Duda, J.J., Craig, L.S., Greene, S.L., Torgersen, C.E., Collins, M.J. and Vittum, K. 2017. “Status and trends of dam removal research in the United States,” WIREs Water, 4: e1164. doi:10.1002/wat2.1164

Tullos, D.D., Collins, M.J., Bellmore, J.R., Bountry, J.A., Connolly, P.J., Shafroth, P.B., and Wilcox, A.C. 2016. “Synthesis of common management concerns associated with dam removal,” Journal of the American Water Resources Association (JAWRA), 52(5): 1179–1206. DOI: 10.1111/1752-1688.12450

Sediment Monitoring during Elwha River Dam Removals: Lessons Learned during the Nation's Largest Dam Removal Project

Christopher A. Curran, Hydrologist, U.S. Geological Survey, Tacoma, WA, ccurran@usgs.gov
Christopher S. Magirl, Assoc. Center Director, U.S. Geological Survey, Tucson, AZ, magirl@usgs.gov
Robert C. Hilldale, Research Engineer, U.S. Bureau of Reclamation, Denver, CO, rhilldale@usbr.gov

The gradual, staged removal of two large dams on the Elwha River located on the Olympic Peninsula, Washington, USA, was the largest dam removal project in U.S. history when it began in September 2011. For almost 100 years, the 32-m tall Elwha Dam, located on the Elwha River 8 km upstream from the river mouth at the Strait of Juan de Fuca, blocked access of anadromous salmonids to the upper watershed. The construction in 1927 of a second dam (64-m tall Glines Canyon Dam located 22 km upstream from the river mouth) further restricted the river and trapped fluvial sediment sourced from the upper watershed. Beginning in September 2011, the incremental removal of both dams resulted in the release of large volumes of sediment that had profound effects on the downstream morphology of the river and posed challenges for scientists tasked with monitoring the transport of sediment. While some changes such as large-scale aggradation of the river bed and the subsequent incision of channel deposits were expected and planned for, other factors such as the timing, magnitude and characteristics of sediment transport were largely unknown. Before dam removals and throughout the duration of the project, a network of U.S. Geological Survey (USGS) streamgages located upstream and downstream of both dams on the Elwha River provided real-time hydrologic information such as stage, discharge and turbidity to managers, engineers and scientists planning for and studying the effects of dam removal. These telemetered data were vital to implementing an adaptive management program used to direct the rate and extent of dam removal to ensure mitigation services such as water treatment operations and levee protection did not exceed design criteria. A bedload impact-plate system installed and operated by the U. S. Bureau of Reclamation (USBR) at the downstream gage location was instrumented with geophones and accelerometers for monitoring coarse bedload (≥ 16mm) transport rates (Hilldale et al. 2015). Physical sediment samples, both suspended and bedload, were collected periodically and opportunistically during the project and were the basis for sediment-surrogate relations used to calculate daily sediment loads. Despite modest runoff during the first three years following the start of dam removal (peak discharges were below the 2-year flood), annual total sediment load in year 2 (7.1 Mt) was the largest of the 5-year study whereas the largest daily suspended-sediment load occurred in year 5 (430 kt) coincident with the timing of the 9.4-year flood discharge (Ritchie et al. 2018a). During the 5 years following initiation of dam removal, a total sediment flux of 18.9 Mt (~65% of trapped reservoir sediment) was recorded at the downstream gage, of which 24 percent was estimated as bedload (Ritchie et al. 2018b).

In the summer of 2011, prior to the beginning of dam removal, nephelometric turbidimeters and pressure transducers for measuring stage were installed at two USGS gages on the Elwha River; one located upstream of both dams (12044900), and one located downstream of both dams (12046260) (Figure 1). A long-term USGS gage (12045500) with more than 100 years of discharge record and located between the former reservoirs (middle gage) was operated throughout the study and recorded river stage using an in-stream pressure transducer until significant channel aggradation required transitioning to a non-contact radar stage sensor.

Figure 1. Elwha River basin prior to the start of dam removals in September 2011, showing the locations of the former Elwha Dam which formed Lake Aldwell and the former Glines Canyon Dam which formed Lake Mills.

At the downstream gage (12046260), an optical backscatter turbidimeter was used to measure exceptionally high turbidity levels beyond the operable range of the nephelometric turbidimeter. Other sediment surrogate technologies used at the downstream gage included a side-looking acoustic Doppler velocimeter (1500 kHz) deployed during the first two years of sediment monitoring, and an acoustic point sensor (LISST-ABS) set near (within 2-m) both turbidity sensors and deployed in 2016. Suspended-sediment concentration (SSC) samples were collected periodically from a pedestrian bridge 350 m downstream from the downstream gage over a

range of discharge and turbidity conditions using standard USGS cross-section sampling methods (Edwards and Glysson 1999). An automated point sampler was used to collect daily composite SSC samples during year 2 of the study and was deployed periodically thereafter for event-based and seasonal sampling. Using the SSC samples, sediment-surrogate regressions were developed using established techniques (Rasmussen et al. 2009; Landers et al. 2016) and suspended-sediment loads were determined at the downstream gage as a product of SSC and discharge from the long-term gage (12045500) adjusted for time of travel and flow contributions from the ungagged reach (Magirl et al. 2015). The bedload impact-plate system at the downstream gage measured the frequency of particle-plate collisions (impulses) from which correlations with physical sample data were developed to estimate the sediment flux of particles ≥16 mm (Hilldale et al. 2015). Due to the cost and complexity of sampling bedload near (within 10-m) the impact-plate system, bedload was sampled much less frequently than SSC although samples were successfully collected during multiple years and at various discharges (Hilldale et al. 2015). Standard USGS stream gaging methods, requiring the collection of continuous stage data and discrete discharge measurements (Rantz 1982), provided the basis for a stage-discharge residual analysis (Anderson and Konrad 2019) at the middle gage (12045500) and was used for assessing the passage of a large sediment wave generated during removal of the Glines Canyon Dam.

Turbidity was the single-most utilized surrogate for continuously monitoring the large range of observed SSC following dam removals. A combination of turbidimeters, one each for low/high SSC conditions, proved reliable surrogates for SSC within their operable ranges. During the 5-year study, the nephelometric turbidimeter measured a range of 0.1 – >1,500 formazin nephelometric units (FNU), although values >1,300 FNU were not used due to accuracy concerns. By comparison, the optical backscatter turbidimeter measured from 2.6 – 3,400 formazin backscatter units (FBU), and values <100 FBU were not used due to accuracy concerns. In combination, the turbidimeters monitored an SSC range of 0.1-21,400 mg/L as determined from log-transformed turbidity-SSC regressions developed for each sensor. Telemetered 15-minute turbidity data provided the additional benefits of informing fisheries managers with water-quality conditions for the successful reintroduction of salmonids and was used by downstream water treatment facilities for maintaining functionality during periods of high sediment loads. Because turbidity was measured at the upstream and downstream gages with identical sensors and consistent calibration protocols (Wagner et al. 2006), direct comparisons between upstream and downstream measurements were possible in assessing progress toward background conditions following dam removals.

As a parameter, river stage provided multiple uses during and long after the 3-year dam removal process. Stage measured at USGS gages provided real-time flood warning for the safe removal of dam structures and the protection of the human population in the downstream floodplain. The stage record at the long-term USGS gage (12045500) was used not only for determination of discharge but also as a proxy for monitoring the aggradation/incision of the channel bed and the detection and tracking of a large-scale dispersive sand wave initiated following the breach of the upstream Glines Canyon Dam (East et al. 2018; Ritchie et al. 2018b). Stage-discharge record at the upstream-most USGS gage (12044900), in combination with pre-dam removal studies (e.g., Curran et al. 2009) provided estimates of background sediment load needed for closure of the

basin-wide sediment budget. When combined with physical bedload samples, impulse-frequency measurements from geophones embedded within bedload impact-plates provided empirical estimates of sediment flux for particles ≥2 mm. The combination of suspended-sediment and bedload monitoring allowed valuable comparisons with volumetric change measurements made in complimentary studies to validate how much sediment had evacuated the reservoir and reached the river mouth. Being able to document when 90% of released sediment reached the river mouth was important for assessing the finality of downstream sediment impacts from dam removal.

References

Anderson, S.W., and Konrad. C.P. 2019. "Downstream-propagating channel responses to decadal-scale climate variability in a glaciated river basin," Journal of Geophysical Research: Earth Surface, 124, 18 p.

Curran, C.A., Konrad, C.P., Higgins, J.L., and M. 2009. Estimates of sediment load prior to dam removal in the Elwha River, Clallam County, Washington. U.S. Geological Survey Scientific Investigations Report 2009-5221, 18 p.

East, A. E., Logan, J. B., Mastin, M. C., Ritchie, A. C., Bountry, J. A., Magirl, C. S., and Sankey, J. B. 2018. Geomorphic evolution of a gravel-bed river under sediment-starved versus sediment-rich conditions: River response to the world's largest dam removal. Journal of Geophysical Research: Earth Surface, 123, 3338–3369.

Edwards, T.K., and Glysson, D.G. 1999. Field methods for measurement of fluvial sediment: U.S. Geological Survey Techniques of Water-Resources Investigations 3–C2, 89 p.

Hilldale, R.C., Carpenter, W. O., Goodwiller, B., Chambers, J.P., and Randle, Timothy J. 2015. "Installation of Impact Plates to Continuously Measure Bed Load: Elwha River, Washington, USA.," Journal of Hydraulic Engineering, 141 (3):06014023-1-5.

Landers, M.N., Straub, T.D., Wood, M.S., and Domanski, M.M. 2016, Sediment acoustic index method for computing continuous suspended-sediment concentrations: U.S. Geological Survey Techniques and Methods, book 3, chap. C5, 63 p.

Magirl, C. S., Hilldale, R.C., Curran, C.A., Duda, J.J., Straub, T.D., Domanski, M., and Foreman, J.R. 2015. "Large-scale dam removal on the Elwha River, Washington, USA: Fluvial sediment load," Geomorphology 246: 669–686.

Rantz, S.E. and others. 1982. "Measurement and computation of streamflow: Computation of discharge," U.S. Geological Survey Water-Supply Paper 2175, vol. 2.

Rasmussen, P. P., Gray, J. R., Glysson, G. D. & Ziegler, A. C. 2009. "Guidelines and Procedures for Computing Time-Series Suspended-Sediment Concentrations and Loads from In-Stream Turbidity-Sensor and Streamflow Data," U.S. Geological Survey Techniques and Methods 3–C4.

Ritchie, A.C., Curran, C.A., Magirl, C.S., Bountry, J.A., Hilldale, R.C., Randle, T.J., and Duda, J.J. 2018a. "Data in support of 5-year sediment budget and morphodynamic analysis of Elwha River following dam removals," U.S. Geological Survey Data Release.

Ritchie, A. C., Warrick, J.A., East, A.E., Magirl, C.S., Stevens, A.W., Bountry, J.A., Randle, T.J., Curran, C.A., Hilldale, R.C., Duda, J.J., Gelfenbaum, G.R., Miller, I.M., Pess, G.R., Foley, M.M., McCoy R., and Ogston, A.S. 2018b. "Morphodynamic evolution following sediment release from the world's largest dam removal," Scientific Reports, vol. 8, no. 13279.

Wagner, R.J., Boulger, R.W., Jr., Oblinger, C.J., and Smith, B.A. 2006. "Guidelines and standard procedures for continuous water-quality monitors—Station operation, record computation, and data reporting," U.S. Geological Survey Techniques and Methods 1–D3, 51 p.

Sediment Transport Simulation of Klamath Dam Removals

Blair Greimann, Hydraulic Engineer, Technical Service Center, Bureau of Reclamation, Denver, CO, bgreimann@usbr.gov

Abstract

Four Klamath River dams in California (Iron Gate, Copco I, Copco II, and J.C. Boyle) currently owned by PacifiCorp are scheduled for removal in 2021 by the Klamath River Renewal Corporation. Prior to the effort led by Klamath River Renewal Corporation, the Department of the Interior through the Klamath Hydroelectric Settlement Agreement conducted a study of the potential effects on the downstream river environment from removing these four dams. A one-dimensional model (SRH-1D) was used to simulate dam removal and the No Action Alternative of continued operation of the dams. With the dam removal eminent, a summary of the most important modeling results will assist in the development of efficient sediment monitoring efforts. It will also help to identify areas where numerical modeling can be improved after monitoring data is available. Lastly, a summary of the analysis will guide future dam removals studies.

The sediment stored in the PacifiCorp reservoirs is approximately 85% silt, clay and organic material that is 80 to 90 % water by volume and highly erodible. The remaining material is mostly sand with a relatively small amount of gravel present. Approximately 15 million cubic yards of sediment projected to be stored in the reservoirs by 2021. Based upon the SRH-1D simulations, drawdown of the four PacifiCorp Dams will release between one- and two-thirds of the approximately during the first year of drawdown. . If there is a wet year, more material will likely be eroded and if there is a dry year, less material will be eroded from the reservoirs. The river is expected to return to its pre-dam alignment at each reservoir and have a similar width to pre-dam conditions. The sediment that is left behind in the reservoirs would raise the floodplain terraces above the pre-dam conditions; as a result, the floodplains within the former reservoirs are expected to be inundated less frequently than typical floodplains in the basin.

Most of the reservoir sediment will be transported to the ocean during the period of concurrent drawdown at the four sites which will last from January 1, 2021 to mid-March, 2021. Silt and clay will be quickly mobilized during drawdown and transported downstream in suspension, temporarily impacting water quality. The maximum sediment concentrations during this period may be more than 10,000 mg/l downstream of Iron Gate, which is the most downstream dam. Tributaries entering Klamath River should significantly dilute these concentrations to less than 2,000 mg/l at the mouth of the Klamath River, approximately 190 miles downstream of Iron Gate Dam. Sediment concentrations are expected to resume to background levels by the end of the summer 2021 regardless of the hydrology over this time period. The erosion of reservoir sediment is limited to the first year because aggressive revegetation of the remaining reservoir sediment is planned immediately following dam removal, which will stabilize the sediment from erosion due to rainfall. In addition, the reservoir sediment dramatically increases its resistance to erosion once it dries out and consolidates.

The bed material within the reservoirs and just downstream of Iron Gate Dam is expected to have a high content (30 to 50 %) of sand immediately following reservoir drawdown until a

flushing flow moves the sand sized material out of the reach. The flushing flow will need to be at least 6,000 cfs , which is approximately a 2-yr flood (Reclamation, 2011), and last several days to weeks to return the bed to cobble and gravel with a sand content less than 20%. After the flushing flow, the bed is expected to maintain fractions of sand, gravel, and cobble, similar to natural conditions.

Introduction

Four dams (J.C. Boyle, Copco No. 1, Copco No. 2, and Iron Gate) constructed on the Klamath River in California between 1918 and 1962 are scheduled for removal in 2021. The dams were built and are currently owned by PacifiCorp and are scheduled for removal by the Klamath River Renewal Corporation. The locations of the dams within the Klamath River watershed are shown in Figure 1 and their characteristics are given in Table 1. The most downstream dam is located approximately 190 river miles upstream of the Pacific Ocean on the Klamath River.

One of the major concerns with large dam removals are the sediment impacts associated with them (Reclamation, 2017). Because of these concerns, the Department of the Interior through the Klamath Hydroelectric Settlement Agreement studied the effects of removing these four dams. Reclamation (2011) documents the detailed hydraulic and sediment studies evaluating the effects of dam removal and the current plan for dam removal is given by Klamath River Renewal Corp (2018).

The goals of summarizing here the most important results presented by Reclamation (2011) are to:

1. Assist the development of efficient sediment monitoring for the project.
2. Clearly document the predicted impacts so that after monitoring data are available they can be easily compared to the predictions and areas where models need to be improved can be identified.
3. Illustrate an example dam removal sediment analysis that can help scope and guide future dam removals.

Table 1. Properties of Klamath River Dams scheduled for removal (From PacifiCorp, 2004).

Item	J.C. Boyle	Copco No. 1	Copco No. 2	Iron Gate
Completion Date	1958	1918	1925	1962
Dam Location (RM)	224.7	198.6	198.3	190.1
Dam Type	Earthfill	Concrete	Concrete	Earthfill
Dam Height (ft)	68	126	33	173
Storage at Normal Pool Elev (acre-ft)	3,495	46,867	73	58,794

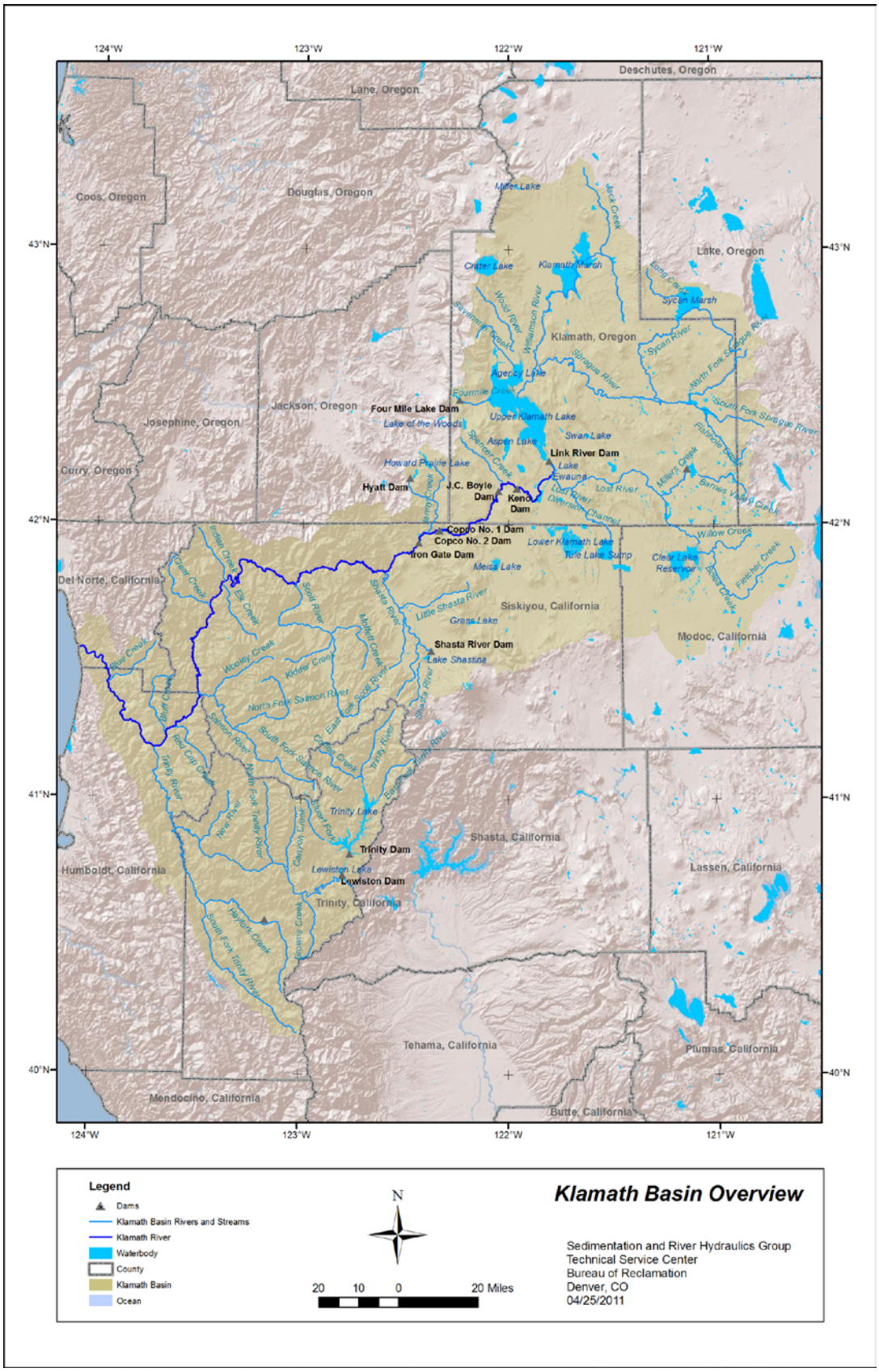

Figure 1. The Klamath River Basin and the dams scheduled for removal.

The Klamath River flows from its headwaters near Crater Lake, Oregon, to its confluence with the Pacific Ocean in northern California. The Klamath Hydroelectric Project (Project) is owned and operated by PacifiCorp, and includes four power generating developments along the mainstem of the Upper Klamath River between river mile (RM) 228 and RM 190, at J.C. Boyle, Copco No. 1, Copco No. 2, and Iron Gate Dams. The smaller East Side and West Side developments are located further upstream at the Bureau of Reclamation's (Reclamation's) Link River Dam at RM 254, and have been previously proposed by PacifiCorp for decommissioning. The Project also includes a re-regulation dam with no generation facilities at RM 233 (Keno Dam), and a small (2.2 MW) generating development on Fall Creek, a tributary to the Klamath River at RM 196.3. The installed generating capacity of the existing Project is 169 MW and, on average, the Project generates 716,800 MWh of electricity annually. PacifiCorp began relicensing proceedings before the Federal Energy Regulatory Commission (FERC) in 2000, with a proposal for continued operation of their facilities with new environmental measures. A Final Environmental Impact Statement (EIS) was issued by FERC in November 2007 which included Mandatory Conditions requiring the installation of new fish passage facilities at each dam, or the consideration of dam removal.

The Klamath Hydroelectric Settlement Agreement (KHSA) was completed in February 2010 for the express purpose of resolving the pending FERC relicensing proceedings by establishing a process for potential facilities removal and operation of the Project until that time (KHSA, 2010). Under the KHSA, the Secretary of the Interior would determine by March 31, 2012 whether the physical removal in 2020 of all or part of each of the facilities, necessary to achieve a free-flowing condition and volitional fish passage, would (a) advance restoration of the salmonid fisheries of the Klamath Basin, (b) be in the public interest, including the potential impacts on affected local communities and Tribes, and (c) not exceed $450 million, which is the total amount to be provided by Oregon and California for facilities removal under the State Cost Cap. The KHSA described the process for engineering and scientific studies, environmental review, and participation by the signatory parties and the public to inform the Secretarial Determination. The KHSA was linked to the Klamath Basin Restoration Agreement (KBRA) that required substantial federal funding to complete. There was subsequently no funding approved for the KBRA and therefore a revised KHSA was completed in 2016 that provides for decommissioning the hydroelectric dams through the traditional Federal Energy Regulatory Commission (FERC) approval process.

The Klamath River Renewal Corporation (KRRC), which is a private non-profit guided by 13 board members, was formed to take ownership of four PacifiCorp dams — JC Boyle, Copco, No. 1 & 2, and Iron Gate — and then remove these dams, restore formerly inundated lands, and implement required mitigation measures in compliance with all applicable federal, state, and local regulations (http://www.klamathrenewal.org). PacifiCorp will continue to operate the dams in the interim. Dams upstream of JC Boyle — Keno and Link River Dams — are not part of the KRRC project. PacifiCorp will transfer Keno Dam to the United States government under the amended KHSA, and both Keno and Link River dams will remain operational.

Methods

The necessary information to make predictions of dam removal impacts include:

1. Reservoir sediment characterization including its volume, distribution and gradations
2. Geometry and hydraulic characteristics of channel
3. Sediment model parameters
4. Reservoir drawdown and hydrologic scenarios

Each of these pieces of information were input into SRH-1D (Huang, J. and Greimann, 2010). SRH-1D (Sedimentation and River Hydraulics - One Dimension) is a one-dimensional mobile boundary hydraulic and sediment transport computer model for rivers and manmade canals. Simulation capabilities include steady or unsteady flows, internal boundary conditions, looped river networks, cohesive and non-cohesive sediment transport, and lateral inflows. The model uses cross section based river information similar to HEC-RAS (Brunner, 2008).

Sediment Characterization

Detailed reservoir sediment investigations were performed by Reclamation (2011) to collect samples of reservoir sediment to determine physical and engineering properties. They were also used to estimate the thickness of reservoir sediment throughout all major sections of each reservoir. Though not discussed in this paper, the collected samples were also used for screening-level analysis of organic and inorganic chemical compounds within the reservoir sediment and, where present, to determine the level and extent of contamination.

Barge and boat-supported drilling/sampling took place at fifty-five locations in J.C. Boyle, Copco No.1, and Iron Gate reservoirs. Sixty-nine samples of reservoir sediment and pre-reservoir deposits were collected for gradation analysis, Atterberg limits, and field moisture content; seventy-three samples of reservoir sediment were collected for chemical analysis; and nineteen undisturbed samples of reservoir sediment were collected in Lexan liners for testing engineering properties such as shear strength. In Copco No. 2 Reservoir, boat-supported sampling of reservoir sediment was performed at sixteen locations, from the dam upstream for about 1,000 feet. No sediment was observed in Copco No. 2 because it operates essentially as an after bay of Copco I and is much smaller. This paper focuses on the physical properties of the sediment and how these were used to simulate the expected sediment transport.

Sediment Thickness, Volume and Gradations

There were close to 30 total drill holes in each reservoir that provided direct measurements of sediment thickness. This information was used to extrapolate the sediment depth throughout the entire reservoir. The specific methods employed for each reservoir are given below. The total reservoir sediment volume measured in 2006 and 2009 was 13.15 million cubic yards with thickness ranging from a few feet up to 10 feet. The gradations were typically silt and clay with localized areas of sand deposition at tributary confluences and along the historical (pre-dam) channel alignments. The total volume is estimated to increase to 15 million cubic yards by 2021.

The sediment depth at J.C. Boyle Reservoir was determined by combining the sediment sample information with field observations. In the upper portions of the reservoir, little or no sediment was found during drilling except in one bend of the historical stream channel. The extent of the deposition was limited to the historical stream channel. The total volume of sediment in J.C. Boyle

Reservoir was estimated to be 990,000 yd^3 and a summary of the physical properties is given in Table 2.

At Copco I and Iron Gate, an equation was developed to extrapolate measured sediment depths to locations without measurements. Beginning with the downstream end of the reservoir, a relative station (X) was calculated for each sample, where is $X = 0$ at the downstream end of the reservoir and $X = 1$ at the upstream extent of the reservoir. The relative depth with respect to each station (Y) was calculated by setting the minimum bed equal to 1 and the highest elevation in the cross section below normal pool equal to 0. The following function (Eq 1) was then fit to the observed data:

$$D = (a - bX^c)Y^d \quad \text{Eq (1)}$$

where, D = sediment depth (ft)

X = relative stationing along reservoir

Y = relative depth within cross section ($=z/H$), where z is the vertical distance from the water surface, and H is the maximum depth at that cross section

a, b, c, d = fitted parameters

For Copco Reservoir, the relationship yielded an R^2 value of 0.84 and a root mean squared error of 1.1 ft. An estimate of the uncertainty of this volume was computed by multiplying the average error of the regression equation by the area of the reservoir. This equated to an uncertainty of 1.5 million yd^3, or 20 %. For Iron Gate Reservoir, the relationship yields an R^2 value of 0.54 and a root mean squared error of 1.0 ft. This equated to an uncertainty of 1.3 million yd^3 or 29 %. The absolute error was similar between Copco and Iron Gate, but the relative error at Iron Gate was significantly higher because the sediment thickness were significantly lower.

Maps of the final sedimentation depth in Copco I and Iron Gate are given in Figure 2 and 3. Notable in the maps of sediment deposition is the lack of large coarse deltas because little coarse sediment is supplied to this reach. Upper Klamath Lake traps all of the coarse material in the upper watershed. Further, there is a long, low gradient section of the Klamath River below Upper Klamath Lake that stores sediment. There are some tributaries that feed small amounts of coarse material to J.C. Boyle, but that is all trapped in J.C. Boyle. There are no large tributaries between J.C. Boyle and Copco I. Jenny Creek and a Lower Tributary supply some coarse sediment into Iron Gate Reservoir as evidenced by the relative thicker and coarser deposit at the delta location (Figure 3). The data collected at these tributaries were analyzed separately.

The average sediment size gradations of the sediment were based upon the gradations of the sampled drill cores. The samples were separated into the upper and lower sections of each reservoir and the major tributaries were also analyzed separately. The average gradation data of each of these zones is given in Table 2.

The sediment stored in the PacifiCorp Reservoirs is approximately 85 % silt, clay and organic material that is 80 to 90 % water by volume and, as a result, has an unusually low dry bulk density of about 20 lb/ft^3. The only locations with high sand content are at the head of J.C. Boyle Reservoir and in the tributary deltas in Iron Gate. There is also gravel present in the tributary deltas such as Spencer Creek in J.C. Boyle Reservoir, Jenny Creek at Iron Gate Reservoir, and other small watersheds that contribute sediment, but it is difficult to estimate the volume because it is much smaller than the volume of fine material.

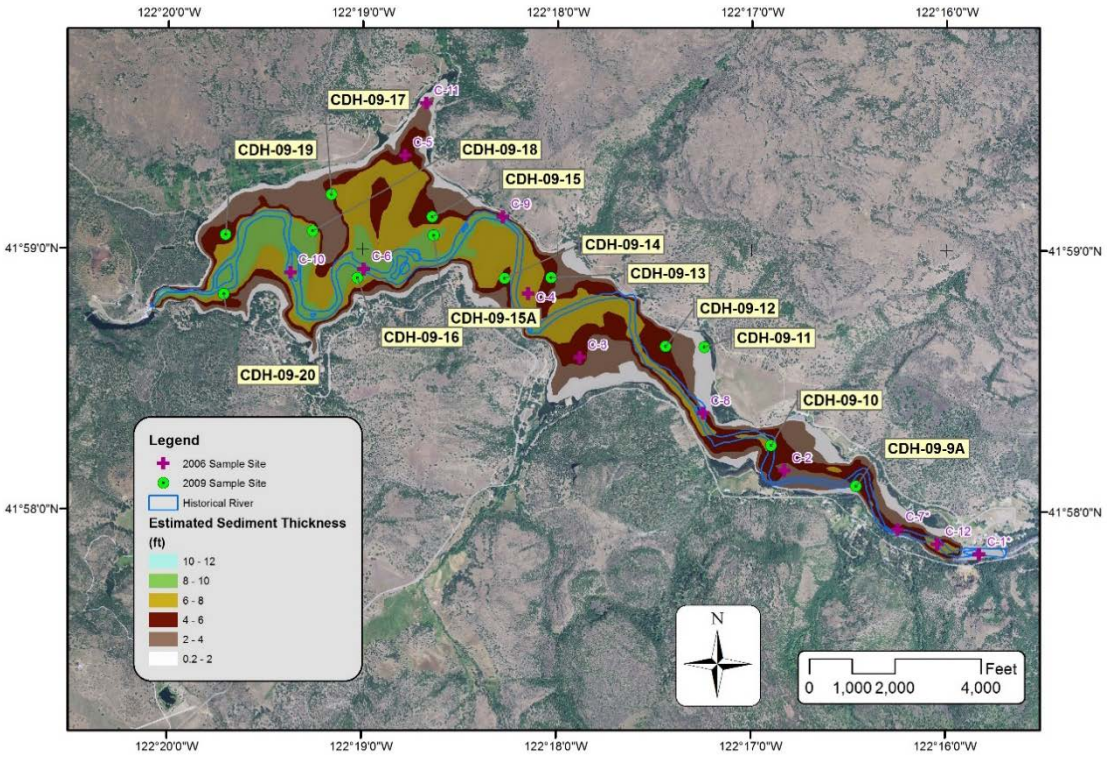

Figure 2. Copco I estimated sediment thickness and sample site locations and historical (pre-dam) river alignment.

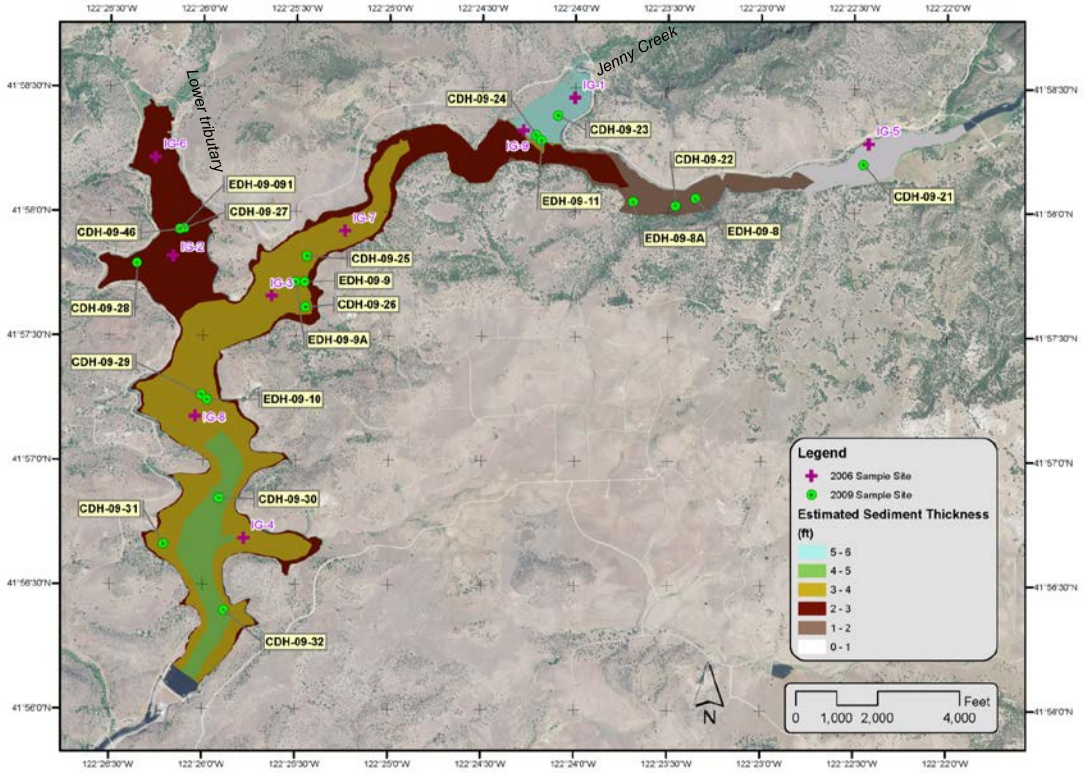

Figure 3. Iron Gate Reservoir estimated sediment thickness and sample site locations.

Table 2. Estimated Physical properties of reservoir sediment for Klamath River Dams as measured in 2006 and 2009.

Reservoir	Location	Volume (yd^3)	Silt and Clay (%)	Porosity (-)	Dry Bulk Density (lb/ft^3)	Estimated Dry Weight (tons)
JC Boyle	Upper	380,000	44	0.82	29.5	151,000
	Lower	620,000	88	0.90	16.3	136,000
Copco I	Upper	810,000	73	0.88	19.2	210,000
	Lower	6,630,000	88	0.88	18.7	1,674,000
Iron Gate	Upper	830,000	78	0.83	27.0	303,000
	Lower	2,780,000	86	0.88	19.8	743,000
	Jenny Creek	300,000	75	0.73	44.4	180,000
	Lower Trib	800,000	94	0.88	19.3	208,000
All		**13,150,000**	**85**	**0.87**	**20.3**	**3,605,000**

Erodibility

The timing and magnitude of predicted reservoir sediment transport is controlled by the erosive forces applied to the sediment and its erodibility. The equation used to predict the erosion of cohesive sediment erosion in SRH-1D is:

$$E = k_d(\tau - \tau_c) \quad \text{Eq (2)}$$

where E = erosion rate,

k_d = erosion rate constant,

τ = shear stress, and

τ_c = critical shear stress.

For SRH-1D modeling, the constants in the above equation were directly measured using a jet test as described in Simons et al. (2010). The samples were collected by a 9-inch Ponar sampler. These samples were repacked in the lab and tested using a jet test device described in Simons et al. (2010). The results from the repacked samples of Simons et al. (2010) are shown in Figure 4 and the range of results is given in Table 3. Both wet (~80% water content similar to field conditions) and dried samples were tested and as expected dried samples showed significantly less erodibility than the wet samples. The simulations of erosion during drawdown used the Moist Sample's results. The base SRH-1D simulation used the median erodibility parameters; then a sensitivity analysis was performed using the 25th and 75th percentiles. The volume and timing of predicted reservoir sediment erosion in SRH-1D was not significantly affected by changing the erodibility parameters within this range. This is because the erosive forces computed in the 1D hydraulic model under riverine conditions are significantly higher than the range of measured critical shear

stress. The rate of sediment erosion is largely dependent upon the drawdown rate and whether the sediment is exposed to flowing water. It is less dependent upon small changes to the critical shear stress and erosion rate constant.

Table 3. Summary of jet tests on sediment from all reservoirs from Simons et al. (2010).

	τ_c (Pa)	k_d (cm^3/N-s)
Moist Sample		
Minimum	0.000	0.23
25th Percentile	0.032	0.57
50th Percentile	0.21	0.82
75th Percentile	1.18	1.23
Max	4.83	5.6
Dry Samples		
Minimum	1.2	0.04
25th Percentile	2.7	0.12
50th Percentile	5.9	0.16
75th Percentile	17.8	0.32
Max	113.6	0.59

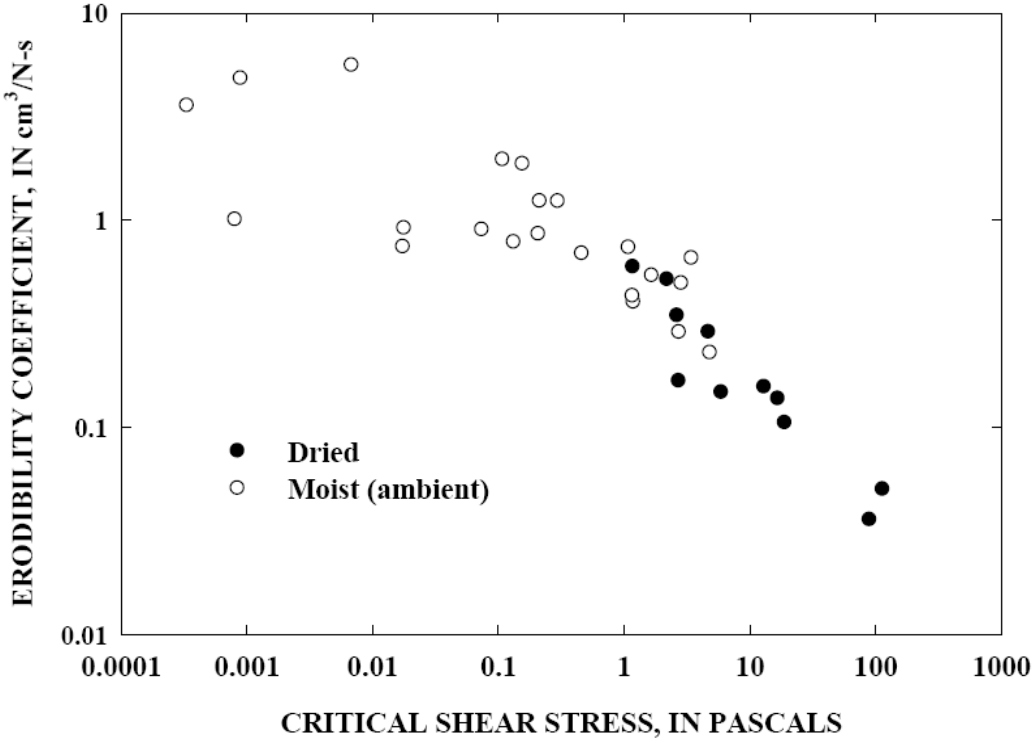

Figure 4. Measured critical shear stress (τ_c) and erodibility coefficient (k_d) for moist and dried samples (From Simon et al. 2010).

Fall Velocity

The fall velocity is used to determine the deposition rate of the sediment when shear stresses are low. During drawdown, the sediment eroded from the upper portion of the reservoir can redeposit in the lower pool. Deas et al (2010) collected samples of the sediment contained in the water column at one site upstream of Copco Reservoir, three sites within Copco Reservoir and one river site downstream of Iron Gate Dam. The samples were taken to a lab where the fall velocity of the particles were measured with a Laser In-Situ Scattering and Transmissometry with Settling Tube (LISST-ST) in a bench-top setting. The LISST-ST measures the settling rates and particle size distribution of the samples. The mean settling rate of the sediment sampled from the reservoir sites was 0.55 m/d (0.006 mm/s) and the average for the river sites was 2.7 m/d (0.03 mm/s).

Geometry and Hydraulic Characteristics of Channel

The model extents were from about 10 miles upstream of JC Boyle Dam and to approximately 17 miles downstream of Iron Gate Dam. The model includes both riverine and reservoir sections. The channel geometry is taken from LiDAR collected in 2010 and bathymetry collected by boat in the river as described in Reclamation (2012). The reservoirs were surveyed in 2001 by JC Headwaters, Inc. (2003). A continuous terrain was then generated by combining the LiDAR with the bathymetric data. Cross sections were then generated at an interval of approximately every 500 ft for the first 8 miles downstream of the Iron Gate and then increasing to 1000 ft downstream of that.

Channel and overbank roughness were calibrated to two different datasets. Channel roughness was calibrated to longitudinal profile data that was collected during the bathymetric survey, and the overbank roughness was calibrated to stream gage data. Daily flow data from the United States Geological Survey (USGS) gages (#11516530, 11520500, 11517500, 11519500) corresponding to the data collection period (10/11/09 – 10/18/09) were run in the hydraulic model. A range of channel roughness values were applied to the geometry and the resulting water surface elevations were compared to the measured water surfaces from the survey. One value for channel roughness from Iron Gate Dam to Happy Camp was unable to match the surveyed water surfaces. A relationship between reach-average bed slope and roughness was developed such that the modeled water surface elevations matched the surveyed water surface elevations to an acceptable level. The channel roughness ranged from 0.03 to 0.05. Generally, the higher slope reaches had higher roughness due to the larger bed material and presence of bedrock outcrops.

Sediment model parameters

There are several sediment model parameters necessary as input into the model. A brief description of the most important ones is given below.

Tributary sediment supplies were computed from results of Stillwater (2010), who estimated the annual loading to the Klamath River from tributaries. sediment rating curve was developed in the form of $Q_s = aQ^b$, where Q_s is the sediment load and Q is the flow rate, such that the annual loads are reproduced by the flow duration curve. The value of b was fixed at 2.3 based upon developing best matches to the observed sediment rating curves in the mainstem. The value of a was computed to match the annual sediment load.

There were four bed layers used to represent the reservoir sediment and river bed sediment. In the reservoir, the upper two layers represented the reservoir sediment and the bottom two layers represented the pre-reservoir sediment.

The sediment size classifications range from 0.00002 mm to 2048 mm in diameter. One size class is used to represent the silt/clay fractions, which is assumed to be all sediment smaller than 0.0625 mm. Sediment larger than 0.0625 mm is separated into size classes separated by powers of two starting at 0.0625 mm. The bulk density was taken from the average bulk density in Table 2, while the bulk density assumed for the non-cohesive material was 100 lb/ft^3, which is typical for sandy material. Bed material gradations for the river reaches are taken from Reclamations sampling in 2009 downstream of Iron Gate and PacifiCorp's (2004) bed material information upstream of Iron Gate (Reclamation, 2012).

The reservoir sediment thicknesses were taken from the estimates described previously. Because the sampling occurred in 2006 and 2009, but the removal was planned to occur in 2020, the thicknesses were increased to estimate the thickness in 2021, when dam removal will occur. This increases the sediment volumes in the reservoirs by 24% at Iron Gate, 12% at Copco, and 22 % at J.C. Boyle. It is estimated that there will be 15 million yd^3 of sediment stored behind the three reservoirs by 2020. SRH-1D allows the definition of bedrock and the pre-reservoir sediment in the reservoir reaches was assumed to be non-erodible bedrock.

The erosion rate of the cohesive fractions is controlled by Eq. 1 as described previously. For non-cohesive sediment (assumed to be all sediment greater than 0.0625 mm) the Parker (1990) bedload equation is used to predict sediment transport movement if D50 is greater than 2 mm, while the Engelund and Hansen (1972) formula is used to predict the movement if the D50 is less than 2 mm.

The above water angle of repose is important to defining the stability of the reservoir sediment. Geotechnical tests indicated that the angle of repose was above 25º, but Strauss (2010) indicated that this is likely an upper estimate and that the actual value could be significantly lower. Samples indicated the samples rapidly increase in shear strength when drained. As a simple test, a container of the moist sample was tipped at a 15º a day after placement. The slope was maintained and the sediment did not show any significant movement. Therefore, as long as the sediment is freely drained, the sediment should an angle of 15º or greater shortly after drawdown and the assumed angle of repose is 15º for most simulations, but some model sensitivity of this parameter is conducted using an angle of repose ranging down to a value of 5º.

The time step was chosen by decreasing the time step until results were not significantly affected. The chosen time step was 0.1 hours. The downstream end of the model is a fixed rating curve based upon a larger scale hydraulic model.

Reservoir drawdown and hydrologic scenarios

The SRH-1D model is run in unsteady mode meaning that the storage effects of the reservoir are taken into account. The input flows to the model were taken from a separate hydrologic routing model called RiverWare that accounted for project operations at Link Dam and Keno Dam located upstream of JC Boyle. The model uses historical measured inflows into Upper Klamath Lake and then operates Link Dam (impounding Upper Kalmath Lake) according to assumed operational rules. Details on the hydrologic assumptions and model is found in Reclamation (2012). Two sets of simulations were performed:

1. Forty-eight separate simulations of the reservoir drawdown extending into following year. The forty-eight simulations represented the range of observed water year types between

water year (WY) 1961 and 2008. These simulations were used to assess the short term impacts of dam removal, particular the sediment concentrations in the first two years following dam removal.

2. Three 50-year simulations with the reservoir drawdown occurring the first year. Three simulations were performed using representative Wet, Dry, and Median WY types. The representative Wet, Dry, and Median WY were defined as the 90%, 50%, and 10% exceedance of the March to June flow volume at Keno Dam on the Klamath River. The Dry, Median, and Wet WY were 2001, 1976, and 1984, respectively.

The primary objective of the preferred drawdown scenario was to limit the period of high sediment concentrations to the months of January to early March. Details of the deconstruction can be found in the Detailed Plan Report (Reclamation, 2010). The preferred drawdown scenario has the following activities for each dam. These scenarios are what was simulated in this paper, but the actual drawdown scenarios and the year of removal will be different as described in KRRC (2018).

At J.C. Boyle Reservoir, the drawdown is assumed to begin January 1, 2020 and would occur through the penstocks and gated spillway from a normal pool elevation of 3793 feet to 3780 feet at a rate not to exceed 3 ft/d. On January 13, one of the low level outlets of J.C. Boyle Dam would be opened by removing the concrete stoplogs that block the outlet and the reservoir would be drawdown to an elevation of 3770 feet. The second of the low level outlets would be opened January 20, 2020 and the reservoir would be drawdown to an elevation of 3762 feet.

The drawdown at Copco Reservoir is assumed to begin November 1, 2019 at rate of 1 ft/d from normal pool of about 2606 feet to 2590 feet, which is 3 feet below spillway crest. The spillway gates and superstructure would be removed once the pool is lowered below the crest and their removal would be complete by January 1, 2020. The original low level outlet used for stream diversion during the construction of Copco No.1 Dam would be used to bring the reservoir level below the spillway crest.

The drawdown of Copco Reservoir would resume January 1, at a rate of approximately 1.75 ft/d to an elevation of 2529. Below an elevation of 2529, the drawdown rate would be increased to 2.25 ft/d until it reaches the pre-dam river elevation. The drawdown at Copco Reservoir would primarily occur through the low level outlet. The dam would be notched by removing concrete sections and the spillway will be removed to ensure that the drawdown rates are accomplished and the reservoir does not refill.

Drawdown at Iron Gate Dam is assumed to initiate on January 1, 2020 at a rate not to exceed 3 ft/d. The low level outlet at Iron Gate would be used to drawdown the reservoir. The earthen embankment would be removed in July and August of 2020.

Results

Three main results are summarized here: the erosion and deposition volumes, the sediment concentrations and the bed material changes. The primary reach of impact will be below Iron Gate Dam to the Shasta River and this reach is shown in Figure 5 showing Iron Gate Reservoir and tributaries to the Klamath River which are used for reference in the following sections.

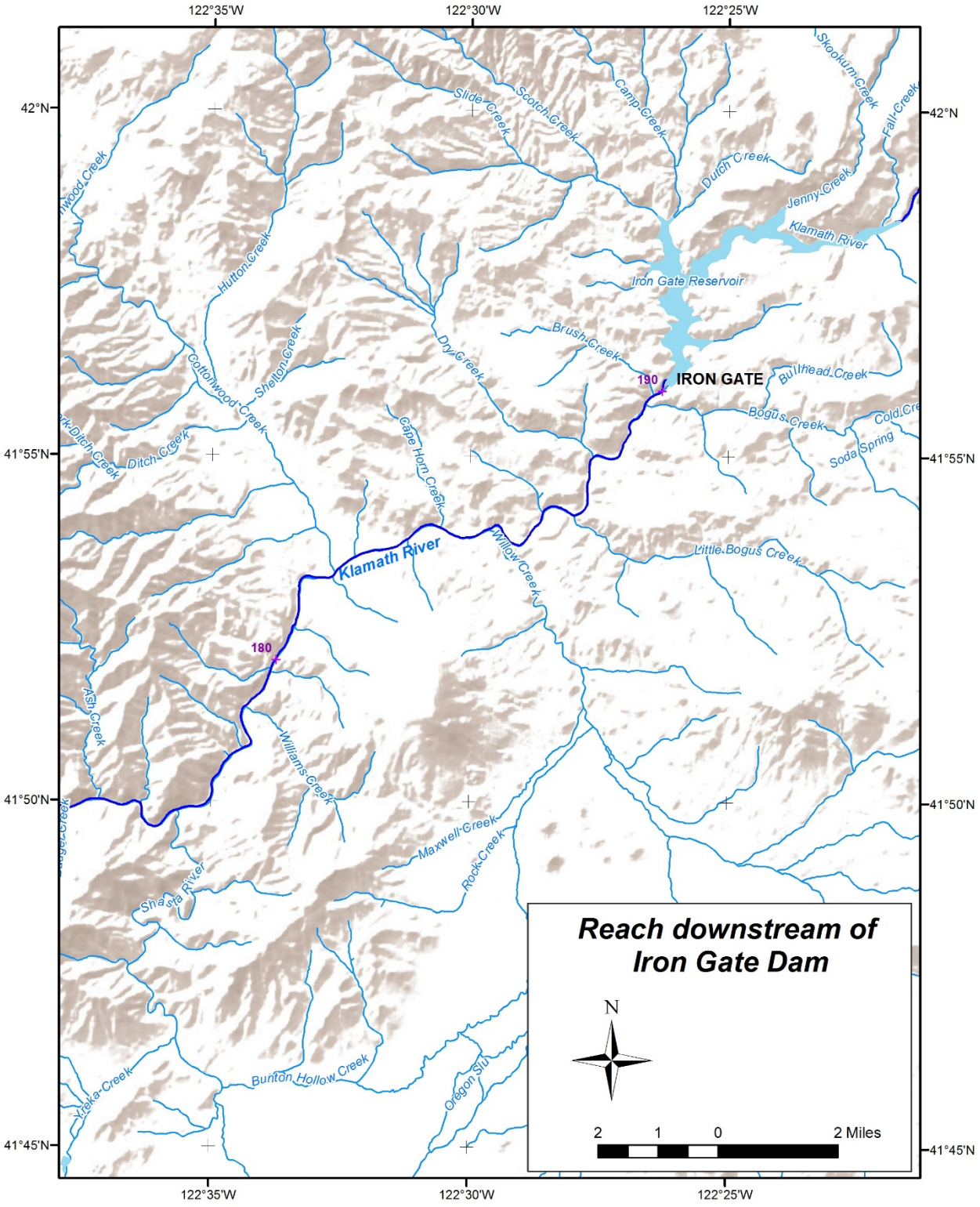

Figure 5. Klamath River reach below Iron Gate Dam, which is the most downstream dam being removed.

Reservoir Erosion and Downstream River Deposition

Based upon the SRH-1D simulations, drawdown of the four PacifiCorp Dams will release between one- and two-thirds of the approximately 15 million cubic yards of sediment projected to be stored in the reservoirs by 2021 (Figure 6). If there is a wet year, more material will likely be eroded and if there is a dry year, less material will be eroded from the reservoirs. The river is expected to return to its pre-dam alignment at each reservoir and have a similar width to pre-dam conditions. The sediment that is left behind in the reservoirs may raise the floodplain terraces above the pre-dam conditions and the floodplains are expected to be inundated less frequently than typical floodplains in the basin. High flows are expected to gradually widen the floodplain through bank erosion and surface erosion, but this process may occur slowly over several decades depending on the frequency and magnitude of floods. This two-phase process where the majority of sediment is first eroded during the initial drawdown and then additional erosion occurs only during episodic flows is similar to that described by East et al. (2018) and Collins et al. (2017).

After dam removal, the model predicted an average of 1.5 feet of streambed deposition from Bogus Creek to Willow Creek (0.5 to 4 miles downstream of Iron Gate Dam), and less than 1 foot of deposition from Willow Creek to Cottonwood (4 to 8 miles downstream of Iron Gate Dam). Downstream of Cottonwood Creek at all locations, there was less than 0.25 feet of deposition predicted and is considered not significant. The results for a dry start year and wet start year are very similar.

The deposition is expected to be relatively permanent as gravel is resupplied to the reach because it is likely that likely that some amount of streambed erosion has occurred downstream of Iron Gate Dam and natural resupply of gravel to the reach would be expected to restore the bed profile that was there prior to dam construction.

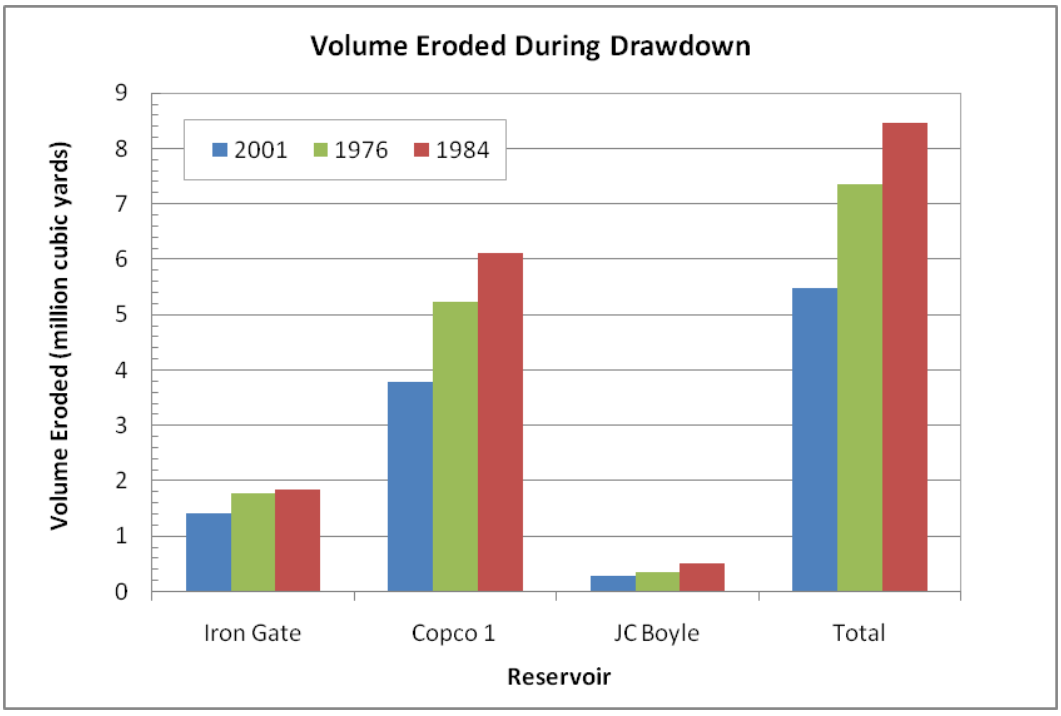

Figure 6. Estimated erosion volumes from each reservoir during drawdown period. WY2001 is a dry year, WY 1976 is a normal year, and WY 1984 is a wet year.

Sediment Concentrations

The sediment concentration immediately downstream of Iron Gate Dam (the most downstream dam) are shown for the Dry, Median and Wet WY types in Figure 7, 8, and 9, respectively. The highest concentrations and longest durations occur during the Dry WY because there is less water to dilute the reservoir sediment. Because the sediment is fine and quite erodible, even low flows are able to erode significant amounts of sediment. The peak concentrations in the Dry WY exceed 10,000 mg/l while the peak concentrations during the wet year are below 8,000 mg/l. Most of the reservoir material will be transported to the ocean during the period of drawdown which will last from January 1, 2021 to mid March, 2021. Sediment concentrations are expected to return to background levels by the end of the summer 2021 regardless the hydrology over this time period. Aggressive revegetation of the reservoir material is planned immediately following dam removal, which will stabilize the sediment from erosion due to rainfall. In addition, the reservoir sediment dramatically increases its resistance to erosion once it dries out.

Assuming average flows from the tributaries during the drawdown, it is likely that the peak concentrations will be less than 2,000 mg/l at the mouth of the Klamath River. It is assumed that the majority of the fine material (silts and clays) will not deposit in the Klamath River and they will behave as essentially wash load.

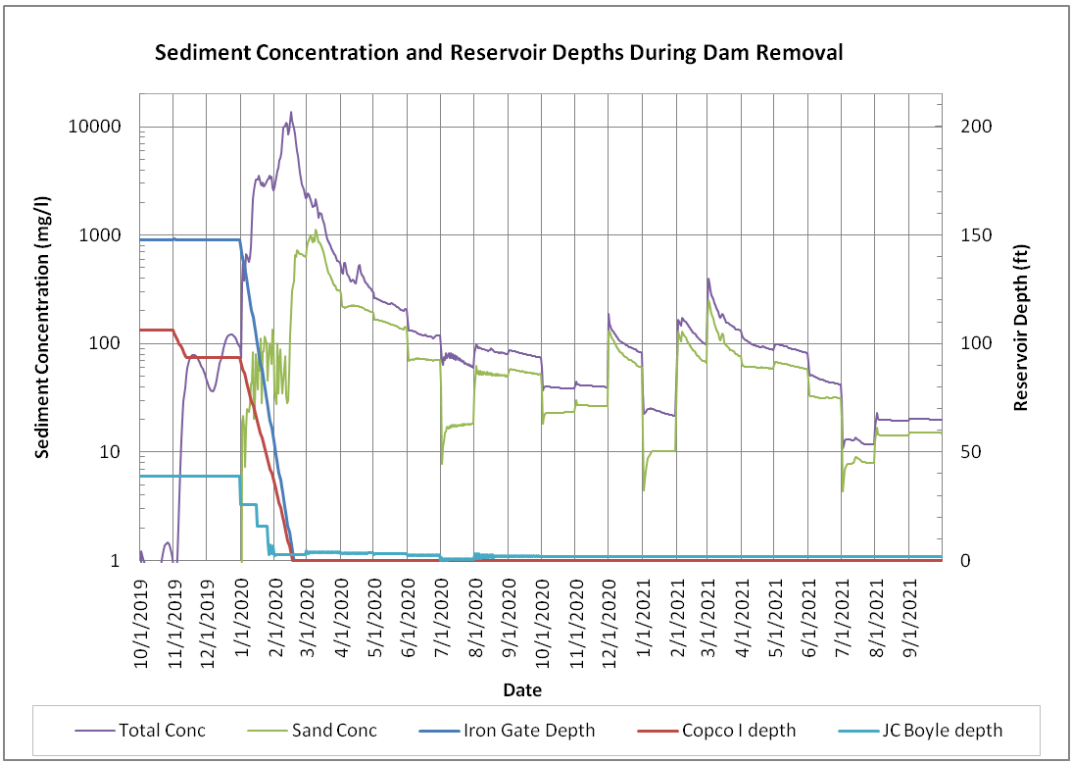

Figure 7. Estimated sediment concentrations downstream of Iron Gate Dam resulting from reservoir drawdown during Dry Water Year.

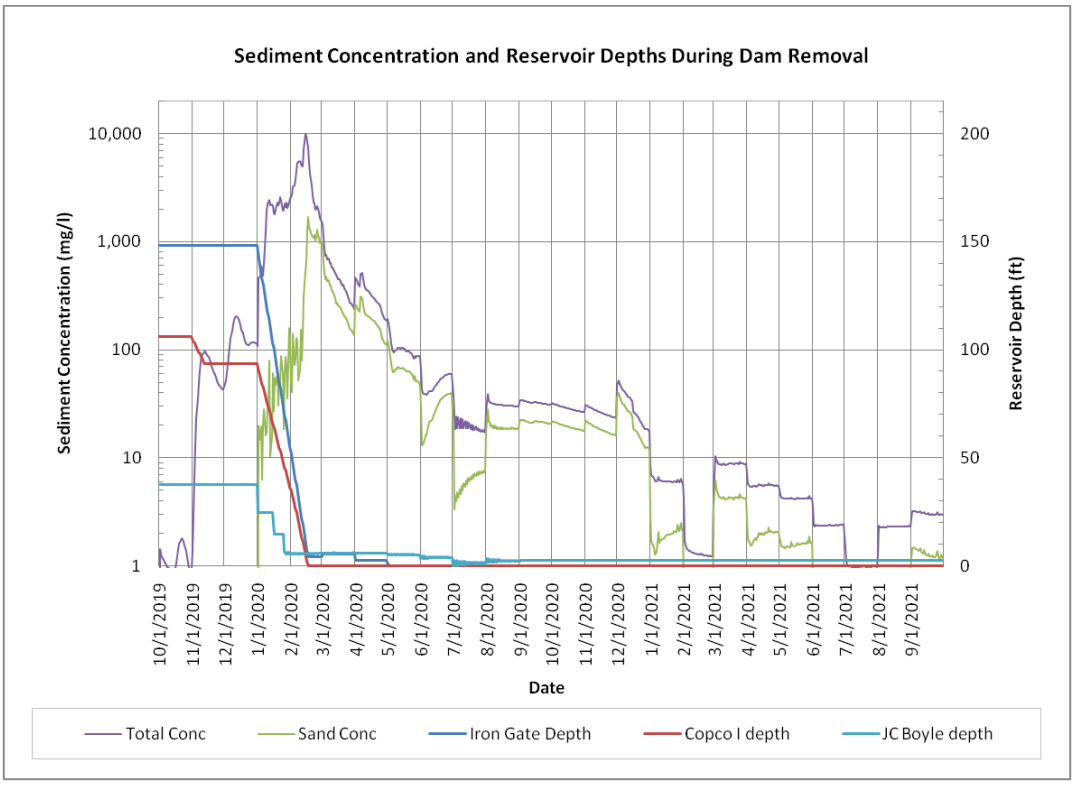

Figure 8. Estimated sediment concentrations downstream of Iron Gate Dam resulting from reservoir drawdown during the Median Water Year.

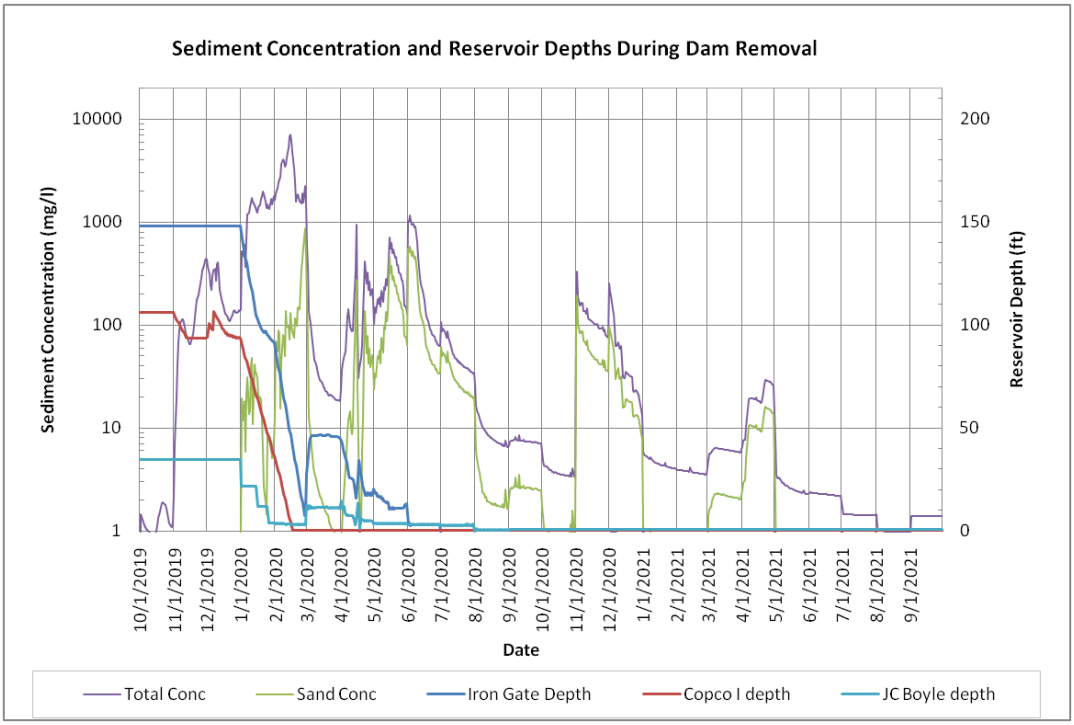

Figure 9. Estimated sediment concentrations downstream of Iron Gate Dam resulting from reservoir drawdown during the Wet Water Year.

Bed Material

While the vast majority of the reservoir deposit is silt, clay and organic material, approximately 15% of the 15 million cubic yards or 2.3 million cubic yards is sand. There is also some gravel expected to be present in the reservoir deposit, but it is difficult to get an estimate of it because the relative volume of the gravel is so much smaller. The modeling assumed that the gravel would be supplied at the transport capacity based upon the measured bed material in the reaches downstream of Iron Gate.

The percentages of bed material within various size classes in the reach downstream of Iron Gate to Willow Creek (approximately 4 miles) for the simulations with the Median and Wet WY are given in Figure 10 and Figure 11. The bed material within this reach is expected to have a high content (30 to 50 %) of sand immediately following reservoir drawdown until a flushing flow moves the sand sized material out of the reach. The flushing flow is expected to have to be at least 6,000 cfs and occur for several days to weeks to return the bed to dominantly cobble and gravel with a sand content less than 20%. After the flushing flow, the bed is expected to maintain fractions of sand, gravel, and cobble similar to natural conditions.

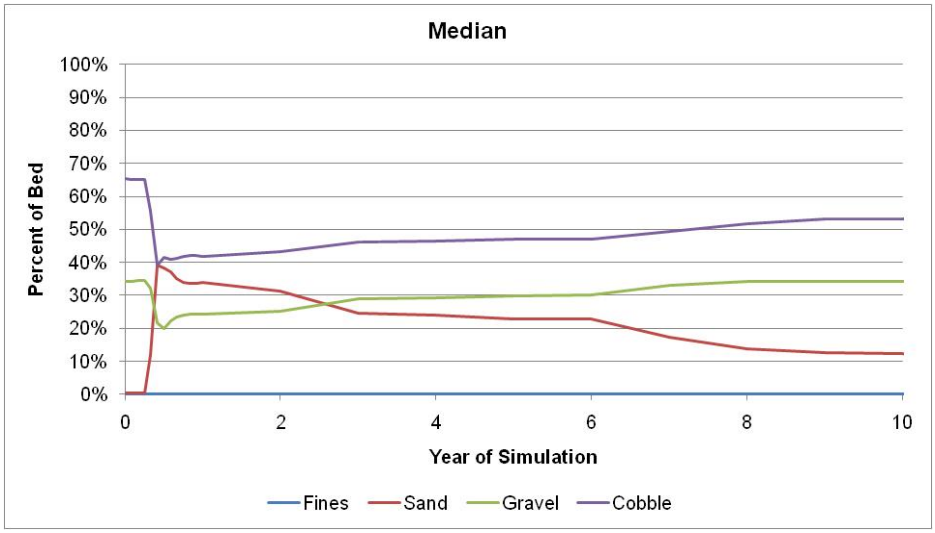

Figure 10. Percentage of bed material in various size classes in the reach between Iron Gate Dam and Willow Creek as a function of time from start of dam removal for the Median Water Year start.

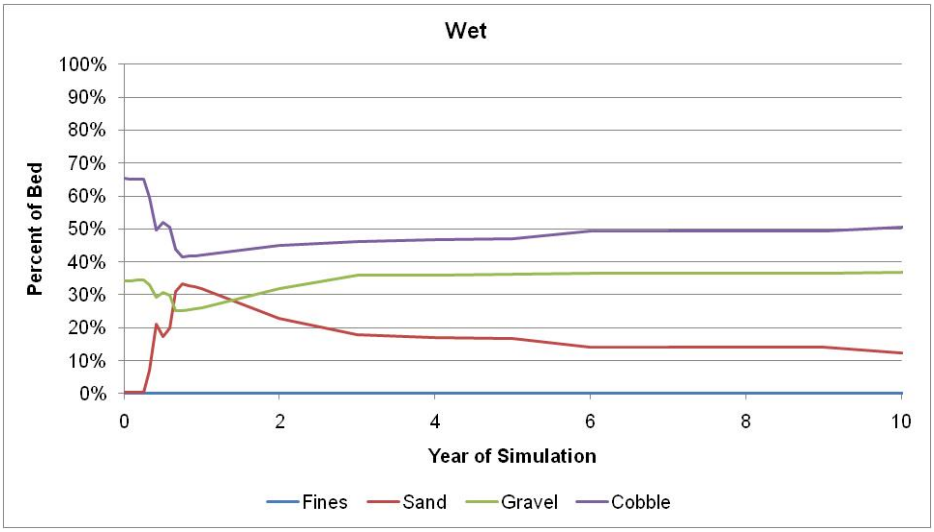

Figure 11. Percentage of bed material in various size classes in the reach between Iron Gate Dam and Willow Creek as a function of time from start of dam removal for the Wet Water Year start.

Conclusions

The PacifiCorp dams Iron Gate, Copco I, Copco II, and J.C. Boyle located on the Klamath River are scheduled for removal in 2021. Reclamation (2011) detailed the sediment transport dynamics expected after dam removal based on SRH-1D model simulations. The most important results from that study have been summarized here to assist in the development of monitoring plans for the project, to provide clear expectations against which the monitoring results can be compared, and to summarize the analytical procedures so they can be referenced in future large dam removal studies.

It is expected that the high concentration of sediment resulting from dam removal will mostly be confined to the drawdown period because the sediment stored behind the dams is very erodible and has a high water content. The expected concentrations will largely be a function of the flow rates during the drawdown period as this will determine the dilution of the eroded sediment. The remaining reservoir sediment is expected to have dramatically increased resistance to erosion once reservoir drawdown is complete because it will consolidate and be aggressively revegetated.

Some deposition of sandy material is expected in the reach immediately downstream of Iron Gate dam, but normal (2-yr) flood flows should restore the river bed to an equilibrium condition dominated by gravel with less than 20% sand in the surface bed material. There will also be some permanent aggradation of this reach, but this is expected to be no more than 1 to 1.5 ft and is the result of the natural resupply of gravel material to the reach from further upstream.

References

AECOM Technical Services, Inc., CDM Smith, and River Design Group (2018), *Definite Plan for the Lower Klamath Project*, prepared for the Klamath River Renewal Corp, http://www.klamathrenewal.org/.

Brunner, G.W. (2008), HEC-RAS River Analysis System User's Manual, US Army Corps of Engineers, Hydrologic Engineering Center, Davis, CA.

Collins, M. J., Snyder, N. P., Boardman, G., Banks, W. S. L., Andrews, M., Baker, M. E., Conlon, M., Gellis, A., McClain, S., Miller, A., and Wilcock, P. (2017) "Channel response to sediment release: insights from a paired analysis of dam removal." *Earth Surf. Process. Landforms*, 42: 1636– 1651. doi: 10.1002/esp.4108.

Deas, M., Vaugh, J., Limanto, E. 2010. "Copco Reservoir and Klamath River Particulate Matter Settling Pilot Study: 2008," memo dated 10-8-2010 submitted to PacifiCorp.

East, A.E., Logan, J.B., Mastin, M.C., Ritchie , A.C., J. A. Bountry, J.A., Magirl, C.S., Sankey, J.B. (2018). "Geomorphic Evolution of a Gravel-Bed River Under Sediment-Starved Versus Sediment-Rich Conditions: River Response to the World's Largest Dam Removal," *Journal of Geophysical Research*, Volume 123, Issue 12, pp. 3338-3369 https://doi.org/10.1029/2018JF004703.

Huang, J. and Greimann, B. (2010). *User's Manual for SRH-1D, Sedimentation and River Hydraulics – One Dimension Version 2.6*, Technical Report SRH-2010-25, Technical Service Center, US Bureau of Reclamation, Denver, CO

Klamath River Renewal Corp (2018), *Definite Plan for the Lower Klamath Project*, prepared by AECOM, CDM Smith, and River Design Group.

J.C. Headwaters, Inc. (2003). Bathymetry and Sediment Classification of the Klamath Hydropower Project Impoundments. Prepared for PacifiCorp By J.C. Headwaters, Inc.

PacifiCorp (2004a). *Final License Application, Volume I, Exhibits A, B, C, D, and H*. Klamath Hydroelectric Project, FERC No. 2082.

Phillip Williams and Associates, Ltd (2009). A *River Once More: Restoring the Klamath River Following Removal of the Iron Gate, Copco, and J. C. Boyle Dams*, California State Coastal Conservancy and California Department of Fish and Game.

Reclamation (2011). "Hydrology, Hydraulics and Sediment Transport Studies for the Secretary's Determination on Klamath River Dam Removal and Basin Restoration," Technical Report No. SRH-2011-02. Prepared for Mid-Pacific Region, US Bureau of Reclamation, Technical Service Center, Denver, CO

Reclamation (2017). *Dam Removal Analysis Guidelines for Sediment, Bureau of Reclamation*, Technical Service Center, Denver, CO. Prepared for the Advisory Committee on Water Information Subcommittee on Sedimentation.

PacifiCorp (2004). *Water Resources Final Technical Report*, Klamath Hydroelectric Project, FERC No. 2082

Simon, A., Thomas, R.E., and Bell, R.B. 2010. *Erodibility Characteristics of Bottom Deposits from Three Klamath River Reservoirs*, USDA-ARS National Sedimentation Laboratory, Oxford, MS.

Stillwater Sciences (2008) *Klamath River dam removal study: sediment transport DREAM-1 simulation*. Technical Report, Prepared for California Coastal Conservancy, 1330 Broadway, 13th Floor, Oakland, CA 94612, 73 pages, October.

Stillwater Sciences (2010). *Anticipated sediment release from Klamath River dam removal within the context of basin sediment delivery*. Prepared by Stillwater Sciences, Arcata, California for California Coastal Conservancy, Oakland, California.

Strauss, T., (2010). *Results of Geotechnical Laboratory Studies of Reservoir Sediment – Klamath Dam Removal Study*, California and Oregon, Bureau of Reclamation, Technical Service Center Memorandum dated July 20, 2010.

Tools for Evaluating Sediment Impacts from Dam Removal – Qualitative Guidance

S. Kyle McKay, Research Civil Engineer, USACE Engineer Research and Development Center, Vicksburg, MS, Kyle.McKay@usace.army.mil
Tahirih Lackey, Research Hydraulic Engineer, USACE Engineer Research and Development Center, Vicksburg, MS, Tahirih.C.Lackey@usace.army.mil
Susan Bailey, Research Civil Engineer, USACE Engineer Research and Development Center, Vicksburg, MS, Susan.E.Bailey@usace.army.mil
Waleska Echevarria-Doyle, Research Civil Engineer, USACE Engineer Research and Development Center, Vicksburg, MS, Waleska.Echevarria-Doyle@usace.army.mil
Earl Hayter, Research Civil Engineer, USACE Engineer Research and Development Center, Vicksburg, MS, Earl.Hayter@usace.army.mil

Abstract

Dam removal has become a frequently applied river management technique, which is increasingly used to meet a variety of goals. Objectives for dam removal range from removing aging infrastructure and reducing flood risk to opening recreational pathways and restoring riverine ecosystems. The resulting release of sediment poses risks related to sediment erosion, deposition, and turbidity including the quantity, location, and timing of each as well as sediment quality. This study provides a brief overview of sediment transport due to dam removal and reviews the applicable tools, models, and associated capabilities. In particular, we review tools designed to answer two questions: (1) How much sediment is stored behind a dam? (2) What are the geomorphic implications of removal? The answer to each of these questions is dependent on site specific characterization and our ability to input sufficient information to these tools and utilize them to produce accurate results. A large range of tools are available which can be used to infer or quantify the geomorphic implications of dam removal prior to removal. We summarize predictive methods ranging in complexity from simple, conceptual models to complex, hydrodynamic and sediment transport models. Qualitative guidance is provided for selecting appropriate tools depending on issues such as focal questions, data availability, and analytical resources (e.g., time, funding, and expertise).

Introduction

The management, operations, maintenance, and long-term fate of dams has emerged as a central issue in both public infrastructure management and aquatic ecosystem restoration in the United States. FEMA (2011) estimated 85% of the 84,000 large dams in the US will have exceeded their design lifespan by 2020. ASCE's "Infrastructure Report Card[1]" gave dams a grade of D, noting that 15,500 dams are high hazard potential with 2,170 of those structures structurally deficient. ASCE estimates that $64 billion is needed to rehabilitate dams nationwide, and the USACE estimates its 694 dams will require $25 billion to address

[1] https://www.infrastructurereportcard.org/

deficiencies. While other management alternatives exist (e.g., repair, reconstruction), dam removal has emerged as a crucial tool for asset management and ecosystem restoration with more than 1,200 dam removals nationwide (Figure 1, Bellmore et al. 2016).

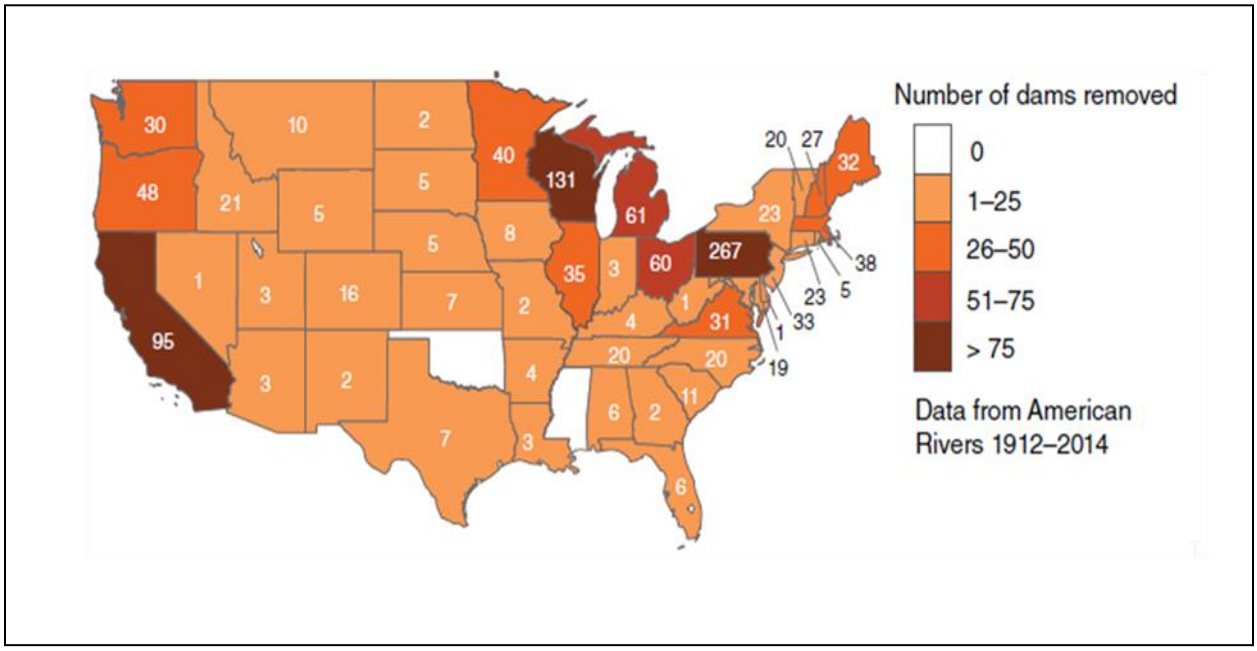

Figure 1. Dam Removal in the United States (Bellmore et al. 2016)

Dam removal represents a significant opportunity to restore geomorphic and ecological function in disturbed ecosystems. Restoration benefits associated with dam removal may not be evident for years, or even decades, and this will likely vary between components of the ecosystem (e.g., migratory pathways for fish vs. sediment storage) and as a function of various factors (e.g., dam size and type, impoundment volume, sediment quantity and grain size, sediment chemistry, removal method, etc.). In fact, decision makers must consider the potential for dam removal to cause temporary or even irreversible degradation to specific ecosystem attributes. The goal should be to minimize the negative impacts of a removal as well as to maximize the rate of recovery of the physical and ecological systems. Understanding sediment processes and geomorphic responses to various dam removal actions is central to achieving this goal.

One significant impediment to executing dam removal projects is prediction of morphological response and the consequent impacts and benefits of that response. Management of sediment stored in a reservoir is an important consideration in any dam removal project. Numerous management options exist and a number of factors contribute to the identification of the best approach(es). Tools are needed to better predict erosion, transport and deposition of sediments, geomorphic change associated with sediment release, short- and long-term ecological ramifications of sedimentation processes and potential contaminant release. A number of existing models and tools have been (or could be) applied to dam removal projects to assess the sediment storage, sediment processes (erosion, transport and deposition), and geomorphic response of a system to various decommissioning strategies. Within this paper, we qualitatively review models and tools designed to answer two important questions: (1) How much sediment is stored behind the dam? (2) What are the geomorphic implications of removal?

Models and Tools Associated with Dam Removal

Trade-offs in model selection

Generally speaking, all modeling efforts require balancing needed resolution and accuracy with available resources and time. To focus our discussion of tools associated with dam removal, we will compare modeling efficiency with the resolution of the information produced by modeling (Figure 2). In this case, modeling efficiency is defined as how quickly modeling results can be obtained and analyzed. Modeling resolution is defined as the degree of accurate information that can be obtained from the simulation (both spatially and temporally). Understanding these basic characteristics is essential when selecting an appropriate modeling strategy for a given dam removal project. For example, one-dimensional numerical models (e.g., HEC-RAS) are often the most practical tools available for understanding reach-averaged channel responses of non-cohesive reservoir sediment deposits following dam removal for planning purposes. However, even simpler models of geomorphic response (e.g., conceptual models, sediment budgets) might be appropriate in some cases such as extremely small dam removals with unconfined, uncontaminated sediment. Conversely, cases involving complex transport phenomena or cohesive sediments may require application of two- and three-dimensional sediment models (e.g., GSMB) containing dynamically linked hydrodynamic and sediment transport models. Unfortunately, such models may require additional site specific data, have much longer run time, and subsequently cost more to develop.

It is understood that all models require some level of site specific data, however the amount can vary widely. A simple box model may require information on sediment characteristics such a grainsize distribution or even general information that sediment is either fine or coarse material. However, when using a three-dimensional sediment model such as GSMB, the best case scenario is that data should be obtained from sediment cores which can be analyzed to determine the sediment grainsize distribution for the variation within the vertical layers of the bed. In addition, analysis of critical shear stress should be obtained from the cores to accurately depict erosion and deposition.

It should also be mentioned that the approach to model applications can also be varied based on the context of a particular study. Sensitivity analyses can systematically vary key input parameters to bracket outcomes, stochastic model runs could be executed across a range of potential inputs, or multiple simulations could be applied to understand a problem in its entirety. For example if site specific data for critical shear stress is unavailable for a Lagrangian particle tracking model, multiple simulations can be performed using a range of a given parameter (e.g., a reasonable minimum and maximum) to bracket potential results.

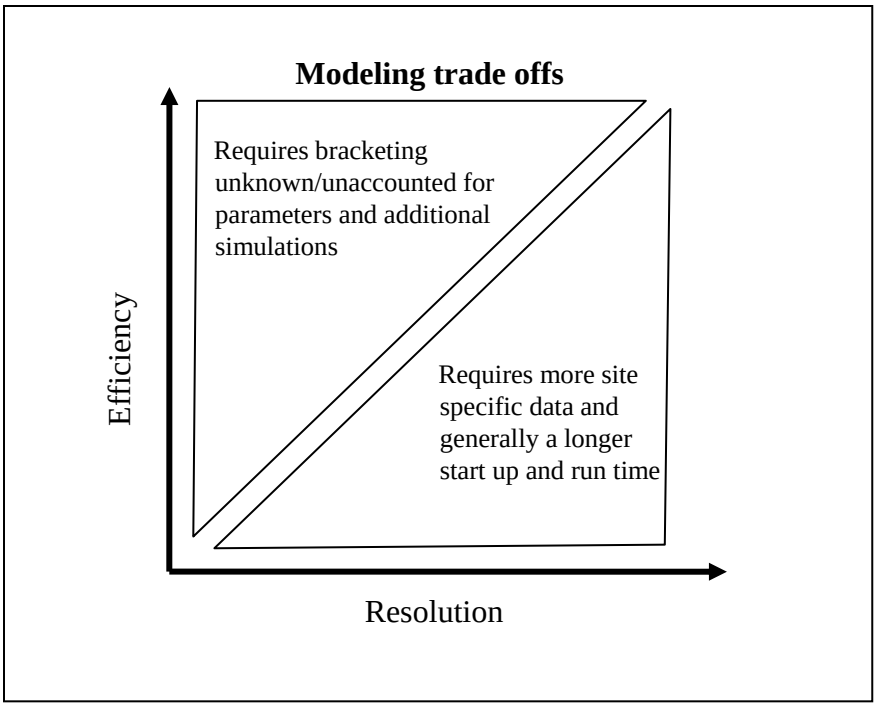

Figure 2. Model tradeoff diagram

Reservoir sediment storage

Reservoir sedimentation is a well-acknowledged technical challenge for both reservoir management and dam removal applications (Morris and Fan 2009). Sediment infill of reservoirs is a constraint on the life span and long-term viability of a structure (Juracek 2014), and stored sediment can also have beneficial or undesirable impacts upon release. The relative volume of stored reservoir sediment (i.e., the ratio of stored sediment volume to average annual volumetric sediment loading rate) has been identified as an important metric for predicting potential effects of sediment release from dam removal (Major et al. 2017) and serves as a key screening criteria for risk-based sediment analysis (Randle and Bountry 2017). It should be mentioned that in addition to volume storage, the character, quality, and gradation of sediment is also relevant. Although a key factor, volume alone is not enough to inform a model setup. Figure 3 shows an example of a reservoir sediment profile. A complex system with a variety of spatially varying sediment types can exist.

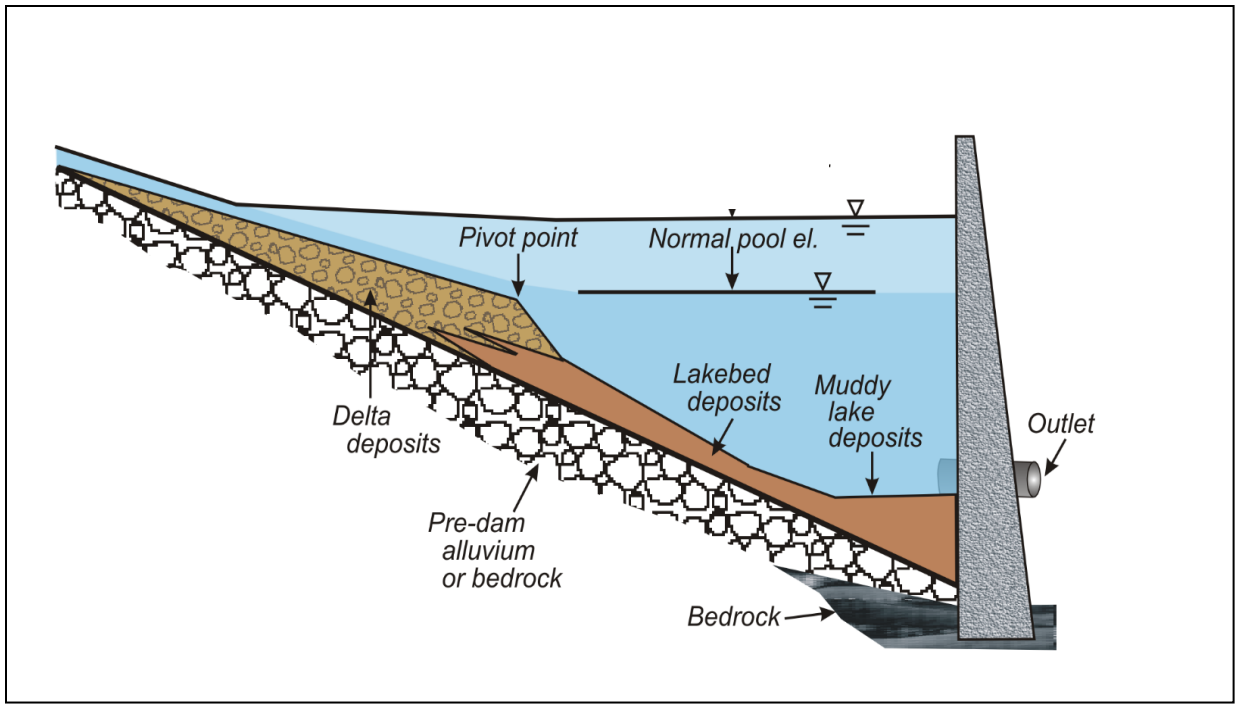

Figure 3. Example of reservoir sediment profile adapted from Randle and Bountry, 2017

Sediment volume may be estimated directly or indirectly through a variety of mechanisms (Strand and Pemberton 1982), which typically take one of four approaches based on Equation 1.

$$V_{s,t} = V_0 - V_t = Q_s t P \quad (1)$$

Where $V_{s,t}$ is reservoir sediment volume at time t, V_o is total initial reservoir volume, V_t is total reservoir volume at time t, Q_s is annual volumetric sediment loading rate, t is age of the reservoir (in years), and P is sediment trapping efficiency over the life of the reservoir.

First, sediment volume may be estimated directly using existing empirical databases such as the reservoir sedimentation database RESSED (Ackerman et al. 2009, Gray et al. 2010, Cooper 2015) and Reservoir Sedimentation Information (RSI) database (Pinson et al. 2016). The RESSED database is a large database with national coverage containing bathymetric and topographic surveys of reservoirs. Although powerful resources, databases tend to emphasize larger structures and only cover 2-3% of large dams (i.e., ~2,000 structures of the ~90,000 in the National Inventory of Dams, NID).

Second, site-specific surveys can be undertaken using techniques such as bathymetric mapping (Pinson et al. 2016), longitudinal profiling (Gartner et al. 2015), probing reservoir deposits, or ground penetrating radar surveys (Santaniello et al. 2013).

Third, estimates of the sediment loading rate (Alighalehbabakhani et al. 2017), structural age, and trapping efficiency (Brune 1953, Churchill 1948, Randle and Bountry 2017) can be combined into a sediment volume. Generally these methods are utilized by extracting a value for the estimate of sedimentation from an analytically developed curve. Both Brune's curve

(Figure 4) and Churchill's curve are extensively utilized, differing based on the specifics of the curve equation and added parameterization.

Fourth, total reservoir volume can be used as a proxy for the maximum volume of sediment stored in a reservoir. Notably, these methods result in varying levels of information about the levels of compaction or layering at a site, which can be important determinants of geomorphic change following removal.

Reservoir volumes, bathymetric surveys, and sedimentation rates all represent crucial data gaps at a national scale, and data compilation and standardization (e.g., Cooper 2015, Pinson et al. 2016) are important continuing needs. In particular, data are notably missing on small, non-Federal reservoirs, which are more typically the focus of dam removal (Bellmore et al. 2016).

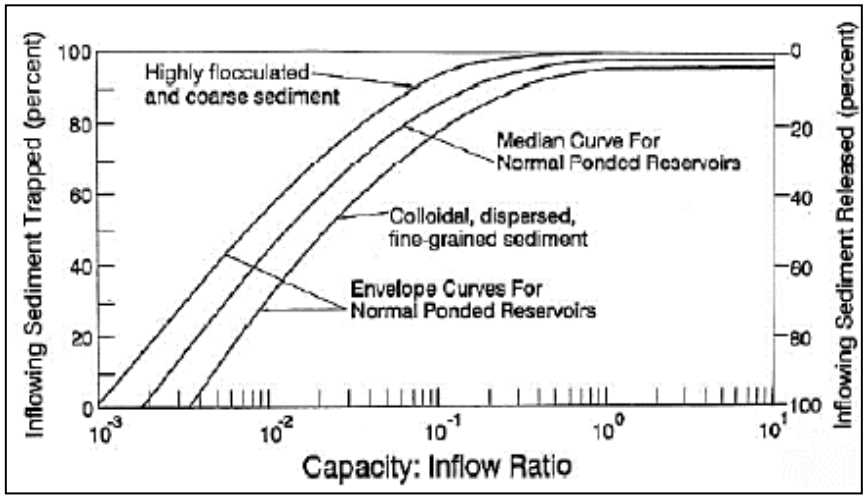

Figure 4. Brune's curve (1953)

Geomorphic implications of removal

The influence of dams on geomorphic processes has been a focus of river management for more than 65 years (Leopold et al. 1954), and the short- and long-term mobilization and fate of sediments is often a key uncertainty surrounding management decisions about dam removal. Using a database of published dam removal studies (Bellmore et al. 2015, Duda et al. 2018), Tullos et al. (2016) synthesized seven common management concerns (CMC) associated with dam removal, four of which are directly related to sediment management and geomorphic change (Table 1).

Table 1. Common management concerns for dam removal directly related to sediment. Framework adapted from Tullos et al. (2017) and supplemented with guiding questions and key driving variables from Foley et al. (2017a), Major et al. (2017), and Randle and Bountry (2017).

Management Concern	Guiding Questions	Key Issues Affecting Biophysical Response
CMC1: Degree and rate of reservoir sediment erosion	• How much of the sediment impounded within a reservoir will erode? • How quickly will the eroded sediment move through the downstream river corridor?	• High % fine grained sediment • Width (sediment deposit) / Width (channel) > ~2.5 • Phased removal • Degree of base level drop
CMC2: Excessive channel incision upstream of reservoirs	• Will a "knick point" form and propagate upstream? If so, how far? • Will upstream infrastructure be affected (e.g., bridge piers)?	• Reach-scale incision downstream • High % fine grained sediment • Phased removal • Coarse delta • Ephemeral flow • Channel slope (e.g., degree of base level drop, presence of grade control features)
CMC3: Downstream sediment aggradation	• Where will sediment deposit longitudinally (on average and specifically around infrastructure)? • Will bedforms be affected (e.g., pool filling)? Will sediment fill interstitial spaces (i.e., embeddedness)? Will channel complexity be reduced? • Will flood levels increase? • Will downstream water bodies be impacted?	• Proximity to dam • Low slope / unconfined channel • High relative sediment volume (ratio of stored sediment volume to average annual volumetric sediment loading rate) • Coarse grain size • Sediment pulse dispersion or translation (Pace et al. 2016)
CMC4: Elevated turbidity	• Will suspended sediment exceed ecological or regulatory thresholds? • Will turbidity influence human uses of the river (e.g., recreation, water intake)?	• High % fine grained sediment • High relative sediment volume • Rapid reservoir drawdown • Background turbidity levels

Table 1 emphasizes the complex interplay of geomorphic processes functioning across multiple time scales (short- vs. long-term), large and small spatial scales (e.g., long reaches vs. within a cross-section), and basin locations (e.g., upstream vs. downstream of a dam). Furthermore, each of these challenges is differentially affected by highly site-dependent variables such as removal strategy, topography, sediment properties, sediment volume, hydrologic conditions, valley morphology, and watershed characteristics (Major et al. 2017). Given these complexities, it is not surprising that a large range of tools may be used to infer or quantify the geomorphic implications of dam removal.

The following section summarizes some available techniques ranging in complexity from simple, conceptual models to complex, hydrodynamic tools. This list is not meant to be exhaustive but to describe some models/tools which have been or are in the process of being used for dam removal assessments. This list focuses on predictive, forecasting tools and families of modeling approaches (rather than monitoring tools and specific hydrodynamic codes, respectively). Notably, geomorphic tools should be selected in line with the project objectives, risks, data availability, and analysis time for a given dam removal; furthermore, multiple tools can be applied to a single site as an analysis proceeds from preliminary screening to permit application (Randle and Bountry 2017). Regardless of the project complexity, a site-specific conceptual

model should be developed to document expected geomorphic change (Randle and Bountry 2017), which is consistent with guidelines for other types of ecosystem restoration projects (Fischenich 2008). Table 2 then summarizes a few specific hydrodynamic and geomorphic tools, which have particular relevance for dam removal applications.

Conceptual models: Generalized and site-specific conceptual models can inform short and long-term effects of sediment release, which can draw from response to other geomorphic phenomena (Doyle et al. 2002, Pizzuto 2002, Cannatelli and Curran 2012, Zunka et al. 2015).

Generalized rules: Empirical rules for system response to dams can indicate the sensitivity or vulnerability to sediment release (Schmidt and Wilcock 2008, Sawaske and Freyburg 2012, Major et al. 2017, Tullos et al. 2017).

Geomorphic analysis: Qualitative insight (e.g., pre-dam topography, sediment volume, grain size) may be gained from historical aerial photographs, soil maps, historical accounts, and field reconnaissance (Tonitto and Riha 2016, Randle and Bountry 2017).

Preliminary sediment analysis: A variety of simple, desktop analyses may be executed such as longitudinal analysis of stream power and transport capacity (Randle and Bountry 2017), sediment budgets (Warrick et al. 2015, Collins et al. 2017), sediment wave models (Doyle et al. 2002, Pace et al. 2016), and application of Exner equations (Gartner et al. 2015).

1-D sediment transport modeling: Reach-averaged hydraulic tools provide an important mechanism for assessing longitudinal change, but the data needs and outcomes can be widely variable (Downs et al. 2009, Gartner et al. 2015). Some tools are also incorporating higher order assumptions to account for channel dynamics (Boyd and Gibson 2014). Modeling of this type tends to be focused on total volume transported and reach-averaged response as opposed to spatially-explicit, cross-channel representation of deposition. Figure 5 shows layout for a HEC-RAS Dam Break simulation study (USACE 2014). Results for volumetric transport can be calculated at each cross section.

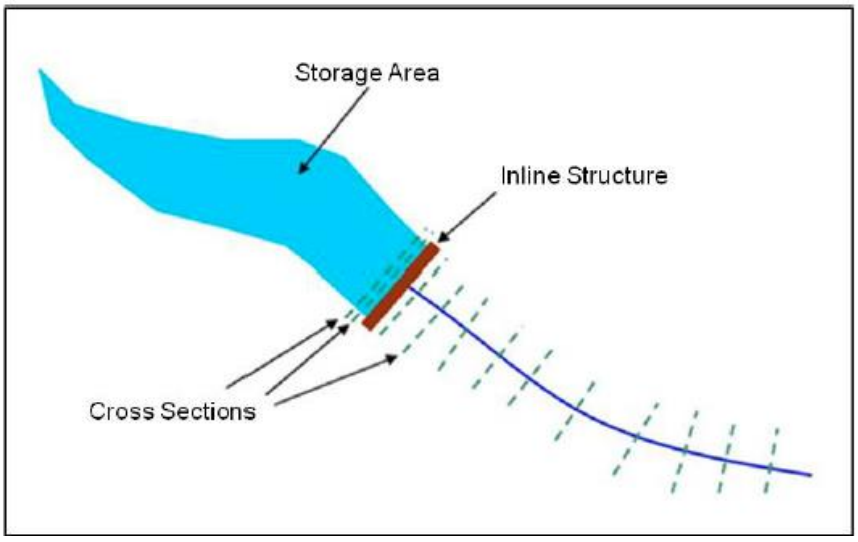

Figure 5. Example of Storage Area and Cross Section Layout for HEC-RAS Dam Break study (USACE 2014)

2-D Sediment transport modeling: Lateral movement of channels and cross-sectionally distributed outcomes require use of two-dimensional, depth-averaged tools (Wang and You 2016). Depth-averaged solutions are formulated with the assumption that there is no vertical stratification. This type of modeling works better when flow is not density stratified and when structures do not have a major impact on the model. Models of this type begin to allow for better assessment of sediment characterization addressing the issue of bed composition transition.

Lagrangian sediment transport modeling: Lagrangian sediment models can assess specific locations of sediment deposition, which could be extremely useful in dam removal applications (MacDonald et al. 2006, Gailani et al. 2016). This modeling style allows users to visualize sediment pathways and can be both qualitative and quantitative.

3-D sediment transport modeling: Three-dimensional models have not (to our knowledge) been applied in the context of dam removal, likely because of computation requirements. However, high risk or extremely sensitive applications could warrant their application. This method is best utilized when detailed knowledge of sediment characterization, bathymetry, sediment sources, and boundary conditions are known or can be obtained readily. Model start up and run time can be significantly longer than other methods but results should be more accurate and spatially resolved, allowing users to better understand detailed and site specific issues, such as water quality near habitat or bed morphology changes at specific locations of importance. GSMB has been applied by ERDC in several coastal, estuarine and riverine modeling studies (Hayter et al. 2012; Chapman et al. 2014; Chapman et al., 2015; Hayter et al. 2015; Hayter et al. 2016; and Bunch et al. 2018). The cohesive and noncohesive sediment transport and morphologic change models are dynamically linked to the hydrodynamic model.

Physical models: Flume studies have informed a number of dam removal assessments (Downs et al. 2009), and their use is likely to continue, particularly for enhancing understanding of key sediment processes and dynamics.

Table 2. Select hydrodynamic models with relevance to dam removal

Tool/Model	Description	Reference
CONCEPTS	Channel evolution model, simulates unsteady, one-dimensional flow, graded-sediment transport, and bank erosion processes in stream corridors	Langendoen (2000,2002)
Dream-1 & 2	1-D sediment transport models that simulate pulsed transport in rivers and address issues following dam removal. DREAM-1 simulates non-cohesive fine sediment. DREAM-2 simulates fine and coarse sediment transport. Spatial resolution output limited to 1-D.	Cui et al. (2006a,b)
HEC-RAS	1-D quasi-unsteady and unsteady sediment transport model that performs transport/movable boundary calculations in rivers and reservoirs. Simulates potential scour and deposition trends in rivers and reservoirs. Provides erosion bed change options for reservoir flushing drawdown or dam removal	Gartner et al (2015), Rumschlag and Peck (2007), Tullos et al (2010), Epstein (2009)
SEDMOD	1D steady state model. Simulates transport in networks of channels and computes resultant scour and fill. Uses hydrographs as stepwise steady state. Sediment size is limited.	Bennett (2001), Syed et al (2005)
FLUVIAL12	1D model simulates spatial and temporal variations in water-surface elevation, sediment transport, and channel geometry	Chang (1988, 2008)
River2D, River 2D-Morophology (R2DM)	2D Depth-averaged finite element two-dimensional hydrodynamic-morphological and gravel transport model	Kwan et al (2010)
MIKE -21C	2D comprehensive modeling system for the simulation of hydraulics and hydraulic-related phenomena. Applied to any two-dimensional free-surface flows where stratification can be neglected	DHI (1996)
SRH-2D	2D hydraulic and sediment transport model for river systems and Watersheds. Uses a layered hybrid approach	Lai (2005), Lai (2006),
PTM	Lagrangian Particle Tracking Model. Determines 3-D sediment fate and pathways in both large and small scale scenarios. Best used in dam removal if we just want to know where sediment is potentially going to go. Can run multiple scenarios easily, and can make up for lack of data.	MacDonald et al.(2006), Gailani et al. (2016)
GSMB (LTFATE)	Fully 3D unsteady multi-block sediment transport model. Determines bed morphology change, dynamically linked hydrodynamic and sediment transport modules, and easily depicts areas of deposition and erosion.	Hayter et al. (2012); Chapman et al. (2014); Chapman et al. (2015); Hayter et al. (2015); Hayter et al. (2016); and Bunch et al. (2018)

Conclusions

Dams often represent crucial pieces of water resources infrastructure critical to meeting societal needs for freshwater. However, dam removal has grown in prominence as a river management technique as the Nation's aging infrastructure portfolio intersects with a growing interest in ecosystem restoration. Sediment release associated with dam removal has the potential to impact both human and ecological outcomes. Here, we have qualitatively reviewed a variety of models and tools that could inform dam removal decisions, with a particular emphasis on two sediment related questions: (1) How much sediment is stored behind the dam? (2) What are the geomorphic implications of removal? In reviewing these tools, we emphasize that no single tool is required for all dam removal studies, but instead scientists and engineers must balance competing needs for model accuracy and resolution with efficiency, time, and resources. This paper provides a brief menu of analytical options for those tasked with selection of models and tools for assessing the potential effects of sediment release associated with dam removal.

References

Ackerman K.V., Mixon D.M., Sundquist E.T., Stallard R.F., Schwarz G.E., and Stewart D.W. 2009. RESIS–II—An updated version of the original Reservoir Sedimentation Survey Information System (RESIS) database: U.S. Geological Survey Data Series 434, available only online at http://pubs.usgs.gov/ds/ds434.

Alighalehbabakhani F., Miller C.J., Baskaran M., Selegan J.P., Barkach J.H., Dahl T., and Abkenar S.M.S. 2017. Forecasting the remaining reservoir capacity in the Laurentian Great Lakes watershed. Journal of Hydrology, 555, 926-937.

American Society of Civil Engineers (ASCE). 2017. Infrastructure report card: A comprehensive assessment of America's infrastructure. Accessed 30 August 2017. http://www.infrastructurereportcard.org/.

Bellmore J.R., Vittum K.M., Duda J.J., and Greene S. 2015. USGS Dam Removal Science Database (ver. 1.3, July 2015). U.S. Geological Survey, https://doi.org/10.5066/F7K935KT.

Bennett J.P., 2001, User's guide for mixed-sized sediment transport model for networks of one-dimensional open channels: U.S. Geological Survey Water-Resources Investigations Report 01-4054, 33 p.

Boyd P.M. and Gibson S.A. 2014. Regional Sediment Management (RSM) modeling tools: Integration of advanced sediment transport tools into HEC-RAS. ERDC/CHL CHETN-XIV-36. U.S. Army Engineer Research and Development Center, Vicksburg, Mississippi.

Bunch, B., Hayter, E., Kim, S-C., Godsey, E., and Chapman, R. 2018. "Three Dimensional Hydrodynamic, Water Quality, and Sediment Transport Modeling of Mobile Bay," ERDC Letter Report to the USACE Mobile District.

Brune G.M. (1953) Trap Efficiency of Reservoirs. Trans. Am. Geophysical Union 34(3), 407-418.Cannatelli K. and Curran J. 2012. Importance of hydrology on channel evolution following dam removal: Case study and conceptual model. Journal of Hydraulic Engineering, 138 (5), 377-390.

Chapman, R.S., P.V. Luong, S.C. Kim, and E.J. Hayter. 2014. "Development of Three Dimensional Wetting and Drying Algorithm for the Geophysical Scale Transport Multi-Block Hydrodynamic, Sediment and Water Quality Transport Modeling System ," Technical Note, Dredging Operations and Environmental Research Program, U.S. Army Engineer Research and Development Center, Vicksburg, MS.

Chapman, R.S., Luong, P., Kim, S.C., and Hayter, E.J. 2015. "Development of a Three Dimensional Vegetative Loss Mechanism for the Geophysical Scale Transport Multi-Block Hydrodynamic Sediment and Water Quality Transport Modeling System (GSMB)," Technical Note, DOER.Churchill M.A. (1948) Discussion of "Analysis and Use of Reservoir Sedimentation Data", Proceedings of Federal Interagency sedimentation Conference, edited by L. C. Gottschalk, Denver, pp. 139-140, USA.

Chang, H. H. 1998. Generalized computer program: FLUVIAL-12 mathematical model for erodible channels, San Diego State Univ., San Diego

Chang HH. 2008. Case study of fluvial modeling of river responses to dam removal. J Hydraul Eng. 134:295–302. doi:10.1061/(ASCE)0733-9429(2008)134:3(295).

Collins M.J., Snyder N.P., Boardman G., Banks W.S.L., Andrews M., Baker M.E., Conlon M., Gellis A., McClain A., and Wilcock P. 2017. Channel response to sediment release: Insights from a paired analysis of dam removals. Earth Surface Processes and Landforms, doi: 10.1002/esp.4108.

Cooper D. 2015. USACE Reservoir Sedimentation Survey Database (RESSED) Oracle Conversion. Proceedings of the 10th Federal Interagency Sedimentation Conference, Reno, Nevada.

Cui, Y., Braudrick, C., Dietrich, W.E., Cluer, B., and Parker, G., Dam Removal Express Assessment Models (DREAM), Part 2: Sample runs/sensitivity tests, Journal of Hydraulic Research, 43(3), 308-323, 2006.

Cui, Y., Wooster, J., Baker, P., Dusterhoff, S., Sklar, L., and Dietrich, W.E., Theory of fine sediment infiltration into immobile gravel bed, submitted to Journal of Hydraulic Engineering

DHI. (1996). MIKE 21 hydrodynamic module users guide and reference manual. Danish Hydraulic Institute.

Downs P.W., Cui Y., Wooster J.K., Dusterhoff S.R., Booth D.B., Dietrich W.E., and Sklar L.S. 2009. Managing reservoir sediment release in dam removal projects: An approach informed by physical and numerical modelling of non-cohesive sediment. International Journal of River Basin Management, 7 (4), 433-452.

Doyle M.W., Stanley E.H., and Harbor J.M. 2002. Geomorphic analogies for assessing probable channel response to dam removal. Journal of the American Water Resources Association, 38 (6), 1567-1579.

Duda J.J., Johnson R.C., Wieferich D.J., and Bellmore J.R. 2018. USGS Dam Removal Science Database v2.0. U.S. Geological Survey. https://doi.org/10.5066/P9IGEC9G.

Environmental Advisory Board (EAB). 2006. Environmental benefits and performance measures: Defining National Ecosystem Restoration and how to measure its achievement. Chief of Engineers Environmental Advisory Board, U.S. Army Corps of Engineers. Access 30 August 2017. http://www.usace.army.mil/Portals/2/docs/Environmental/EAB/ebpm_mar07.pdf.

Epstein, JA 2009. Upstream geomorphic response to dam removal: The Blackfoot River, Montana. MS thesis, University of Montana.

Fischenich J.C. 2008. The application of conceptual models to ecosystem restoration. ERDC TN-EBA-TN-08-1. U.S. Army Engineer Research and Development Center, Vicksburg, Mississippi.

Foley M.M., Bellmore J.R., O'Connor J.E., Duda J.J., East A.E., Grant G.E., Anderson C.W., Bountry J.A., Collins M.J., Connolly P.J., Craig L.S., Evans J.E., Greene S.L., Magilligan F.J., Magirl C.S., Major J.J., Pess G.R., Randle T.J., Shafroth P.B., Togersen C.E., Tullos D., and Wilcox A.C. 2017a. Dam removal: Listening in. Water Resources Research, 53, doi: 10.1002/2017WR020457.

Gailani, Joseph & C. Lackey, Tahirih & B. King, David & Bryant, Duncan & Kim, Sung-Chan & Shafer, Deborah. (2016). Predicting dredging-associated effects to coral reefs in Apra Harbor,

Guam - Part 1: Sediment exposure modeling. Journal of Environmental Management. 168. 16-26. 10.1016/j.jenvman.2015.10.027.

Gartner J.D., Magilligan F.J., and Renshaw C.E. 2015. Predicting the type, location and magnitude of geomorphic responses to dam removal: Role of hydrologic and geomorphic constraints. Geomorphology, 251, 20-30.

Gray J.R., Bernard J.M., Stewart D.W., McFaul E.J., Laurent K.W., Schwarts G.E., Stinson J.T., Jonas M.M., Randle T.J., and Webb J.W. 2010. Development of a National, dynamic reservoir sedimentation database. Proceedings of the 9th Federal Interagency Sedimentation Conference, Las Vegas, Nevada.

Hayter E.J., Chapman, R.S, Luong, P.V., Smith, S.J., and Bryant, D.B. 2012. "Demonstration of Predictive Capabilities for Fine-Scale Sedimentation Patterns within the Port of Anchorage, AK," Final Report prepared for USACE Alaska District, Anchorage, AK.

Hayter E.J., Chapman, R.S, Luong, P.V., Mausolf, G., and Lin, L. 2015. "Sediment Transport Modeling for the St. Louis River Estuary 40th Avenue Shoals and Island Design." Letter Report prepared for USACE Detroit District, Detroit, MI.

Hayter. E., R. Chapman, P. Luong, and G. Mausolf. 2016. "Modeling Sediment Transport using the Geophysical Scale Hydrodynamic and Sediment Transport Modeling System (GSMB)," *14th Estuarine and Coastal Modeling Conference*, Kingston, RI, June 13-15, 2016.

Juracek K.E. 2014. The aging of America's reservoirs: In-reservoir and downstream physical changes and habitat implications. Journal of the American Water Resources Association, doi: 10.1111/jawr.12238.

Kwan, S., Vasquez, J. Millar, R., and Steffler, P. (2010) "A two dimensional finite element hydrodynamic river morphology and gravel transport model" Proceedings Second Joint Federal Interagency Hydrologic Modeling Conference, June 27-July 1, 2010 Las Vegas, NV

Lai, Y.G. (2005). "River and watershed modeling: current effort and future direction," USCHINA Workshop on Advanced Computational Modeling in Hydroscience & Engineering, Sept. 19-21, 2005, Oxford, MS, USA.

Lai, Y.G, Holburn, E.R., and Bauer, T.R. (2006). "Analysis of sediment transport following removal of the Sandy River Delta Dam," Project Final Report, Technical Service Center, Bureau of Reclamation, Denver, CO.

Langendoen, E. J., and Simon, A. (2000). "Stream channel evolution of Little Salt Creek and North Branch West Papillion Creek, eastern Nebraska." Report, US Department of Agriculture, Agricultural Research Service, National Sedimentation Laboratory, Oxford, MS.

Langendoen, E.J., 2002. CONCEPTS: A process-based computer model of instream hydraulic and geomorphic processes. Hydrologic Modeling for the 21st Century, Proceedings Second Joint Federal Interagency Hydrologic Modeling Conference, June 27-July 1, 2010 Las Vegas, NV, on CDROM.

Leopold L.B., and Maddock T.M. 1954. The flood control controversy, big dams, little dams, and land management. Geomorphological Review, 45 (2), 301-303.

MacDonald N.J., Davies M.H., Zundel A.K., Howlett J.D., Demirbilek Z., Gailani J.Z., Lackey T.C., and Smith J. 2006. PTM: Particle Tracking Model Report 1: Model theory, implementation, and example applications. ERDC/CHL TR-06-20, U.S. Army Engineer Research and Development Center, Vicksburg, Mississippi.

Major J.J., East A.E., O'Connor J.E., Grant G.E., Wilcox A.C., Magirl C.S., Collins M.J., and Tullos D.D. 2017. Geomorphic response to dam removal in the United States: A two decade perspective. Gravel-bed Rivers: Processes and Disasters (Ed. Tsutsumi and Laronnw), John Wiley & Sons Ltd.

Morris G.L. and Jiahua, F. 1997. Reservoir sedimentation handbook (Vol. 15). New York: McGraw-Hill.

Pace K.M., Tullos D., Walter C., Lancaster S., and Segura C. 2016. Sediment pulse behavior following dam removal in gravel-bed rivers. River Research and Applications, doi: 10.1002/rra.3064.

Pinson A., Baker B., Boyd P., Grandpre R., White K.D., and Jonas M. 2016. U.S. Army Corps of Engineers reservoir sedimentation in the context of climate change. Civil Works Technical Report, CWTS 2016-05, U.S. Army Corps of Engineers, Washington, D.C.

Pizzuto J.E. 2002. Effects of dam removal on river form and process. BioScience 52 (8), 683–691.

Randle T.J. and Bountry J. 2017. Dam removal analysis guidelines for sediment. Technical Service Center, Bureau of Reclamation, Denver, Colorado.

Revel, M T K, N & P G R Ranasiri, L & M C R K Rathnayake, R & Pathirana, Kariyawasam Pathiranage. (2013). Experimental Investigation of Sediment Trap Efficiency in Reservoirs. Engineer: Journal of the Institution of Engineers, Sri Lanka. 47. 10.4038/engineer.v47i2.6863.

Rumschlag, J.H. and Peck, J.A. 2007. Short-term sediment and morphologic response of the middle Cuyahoga River to the removal of the Munroe Falls Dam, Summit County, Ohio. J. Great Lakes Research, 33 (Special Issue 2): 142-153.

Santaniello D.J., Snyder N.P., and Gontz A.M. 2013. Using ground-penetrating radar to determine the quantity of sediment stored behind the Merrimack Village Dam, Souhegan River, New Hampshire. Reviews in Engineering Geology XXI, 45-57.

Sawaske S.R. and Freyberg D.I. 2012. A comparison of past small dam removals in highly sediment-impacted systems in the U.S. Geomorphology, 151, 50-58.

Schmidt J.C. and Wilcock P.R. 2008. Metrics for assessing the downstream effects of dams. Water Resources Research, 44 (W04404), doi:10.1029/2006WR005092.

Strand, R.I., and E.L. Pemberton, 1982. Reservoir Sedimentation, Technical Guideline for Bureau of Reclamation, Sedimentation and River Hydraulics Branch, Denver, CO.

Syed, A.U., Bennett, J.P., and Rachol, C.M., 2005, A pre-dam-removal assessment of sediment transport for four dams on the Kalamazoo River between Plainwell and Allegan, Michigan: U.S. Geological Survey Scientific Investigations Report 2004-5178, 41 p.

Tonitto C. and Riha S.J. 2016. Planning and implementing small dam removals: Lessons learned from dam removals across the eastern United States. Sustainable Water Resources Management, doi: 10.1007/s40899-016-0062-7.

Tullos D.D., Collins M.J., Bellmore J.R., Bountry J.A., Connolly P.J., Shafroth P.B., and wilcox A.C. 2016. Synthesis of common management concerns associated with dam removal. Journal of the American Water Resources Association, doi: 10.1111/1752-1688.12450.

Wang Y.H., You G.J.Y. 2016. Evaluation of fluvial geomorphic responses to the removal of dams with the consideration of hydrological uncertainty: A case study in Shihgang Dam. 12th International Conference on Hydroscience & Engineering, Tainan, Taiwan.

Warrick J.A., Bountry J.A., East A.E., Magirl C.S., Randle T.J., Gelfenbaum G., Ritchie A.C., Pess G.R., Leung V., and Duda J.J. 2015. Large-scale dam removal on the Elwha River, Washington, USA: Source-to-sink sediment budget and synthesis. Geomorphology, 246, 729-750.

Zunka J.P.P., Tullos D.D., and Lancaster S.T. 2015. Effects of sediment pulses on bed relief in bar-pool channels. Earth Surface Processes and Landforms, doi: 10.1002/esp.3697.

Earthen Embankment Erosion Prediction

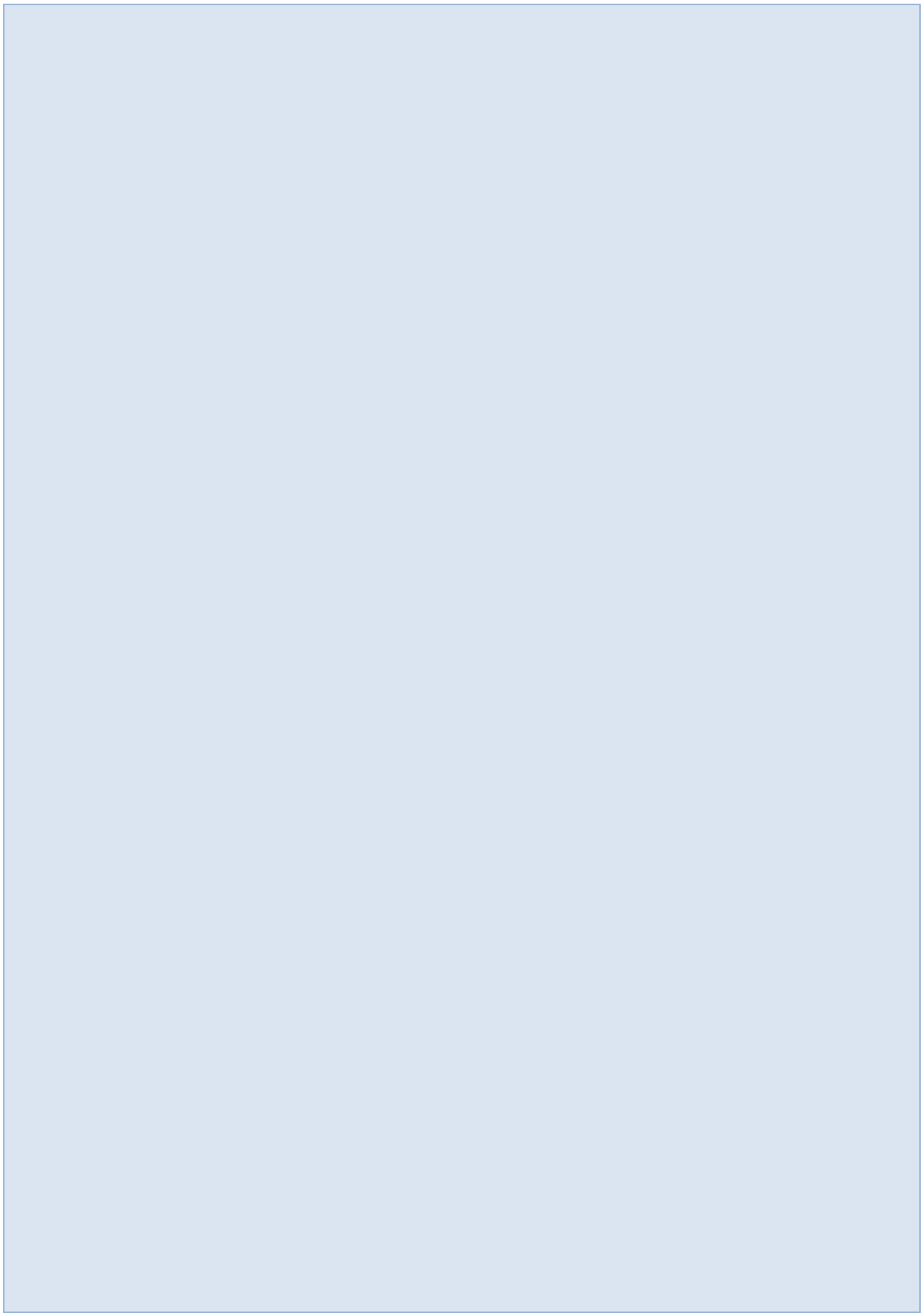

Erosion Assessment of Sacramento and American River Levees

Todd Rivas, Lead Civil Engineer, U.S. Army Corps of Engineers, Sacramento, California, Todd.M.Rivas@usace.army.mil

Shyamal Chowdhury, Lead Civil Engineer, U.S. Army Corps of Engineers, Sacramento, California, Shyamal.B.Chowdhury@usace.army.mil

Jonathan AuBuchon, Regional Sediment Specialist, U.S. Army Corps of Engineers, Albuquerque, New Mexico, Jonathan.Aubuchon@usace.army.mil

HienDung Nguyen, Hydraulic Engineer, U.S. Army Corps of Engineers, Sacramento, California, Hiendung.Nguyen@usace.army.mil

Eddy Langendoen, Research Hydraulic Engineer, U.S. Department of Agriculture, Agricultural Research Service, Oxford, Mississippi, Eddy.Langendoen@ars.usda.gov

Mick Ursic, Hydraulic Engineer, U.S. Department of Agriculture, Agricultural Research Service, Oxford, Mississippi, Mick.Ursic@ars.usda.gov

Moosub Eom, Regional Technical Specialist, U.S. Army Corps of Engineers, Los Angeles, California, Moosub.Eom@usace.army.mil

Morteza S. Majd, Senior Hydraulic Engineer, U.S. Army Corps of Engineers, Los Angeles, California, Morteza.ShakeriMajd@usace.army.mil

Freda Y. Cheung, Hydraulic Engineer, U.S. Army Corps of Engineers, Sacramento, California, Freda.Y.Cheung@usace.army.mil

Abstract

The Water Resources Development Act of 2016 (WRDA 2016) authorized more than $1.5 billion to improve, among other things, the erosion protection for the Sacramento and American river levees that provide flood damage risk reduction to the city of Sacramento. To balance the need to protect the city of Sacramento with the habitat and recreation benefits of the rivers, risk-informed decisions need to be made when selecting and designing erosion protection sites. Quantifying the estimated bank retreat in a stochastic manner provides information to make risk-informed decisions that include the uncertainty of bank retreat estimates. The U.S. Department of Agriculture, Agricultural Research Service's (USDA-ARS) dynamic Bank Stability and Toe Erosion Model (BSTEM) is utilized to estimate total bank retreat from a combination of (1) shear exceeding the critical shear stress of the soil and (2) slope instability.

The use of BSTEM to accurately and objectively estimate bank retreat for a historical period needs to be verified prior to relying on stochastic BSTEM results to inform risk-based decisions. Calibration of the dynamic BSTEM model is illustrated for two sites on the American River to simulate the recorded bank retreat data between 2008 and 2017. To provide the best fit to the observed bank retreat information, calibration of the BSTEM models for the variables with the greatest variation – such as the erodibility coefficient, critical shear stress, and effective hydraulic shear stress on the banks – was performed through the process described in this

paper. The calibration process includes a deterministic calibration followed by a check of the stochastic bank retreat estimate. An additional site is illustrated to validate the application of calibrated soil erodibility parameters to another site with similar soil properties. This procedure demonstrates proof of concept for using dynamic BSTEM erosion performance assessments on both the American and Sacramento rivers to provide objective and reliable stochastic bank retreat estimates for making risk-informed erosion decisions. However, additional work is needed to confirm the initial findings.

Background

Sacramento, California, is located near the confluence of the Sacramento and American rivers and is one of the highest flood risk urban areas in the United States. Large floods in 1986 and 1997 caused substantial erosion of the levees along the American and Sacramento rivers. To reduce flood risk to Sacramento, the selected plan from the American River Common Features (ARCF) General Reevaluation Report (GRR) included adding erosion protection (Figure 1). The ARCF GRR was authorized and funded as part of WRDA 2016.

The Sacramento and American rivers provide valuable habitat and recreation opportunities for the Sacramento area. The American River is a state and federally designated Wild and Scenic River. The erosion protection proposed by WRDA 2016 needs to protect the Sacramento area while preserving these important habitat and recreation opportunities. The bank erosion assessment is intended to balance these needs by informing risk-based erosion decisions.

Bank Erosion Assessment

Bank erosion occurs as a result of the interaction of two processes – hydraulic and geotechnical (Langendoen 2018). The hydraulic process, fluvial erosion, involves the ability of the applied erosive forces from the water to erode the bank material above a designated threshold, the critical velocity or critical shear. The geotechnical process, mass wasting, requires insight into the strength of the soil to resist mass instabilities.

By comparing the critical shear or the critical velocity against a representative shear stress or velocity from a numerical model, or by utilizing a table of permissible velocities (Fischenich 2001), it is possible to assess whether bank erosion will occur or not. The rate of erosion can also be assessed if values for the erodibility rate of the soil are pulled from literature (Briaud 2007). These assessments, while they are useful tools, rely considerably on published values, which may or may not be representative of the heterogeneity of a specific site. Because of site variations, it is useful to calibrate the erosion potential at a site using observed lateral migration rates, as has been proposed by Briaud and Montalvo-Bartolomei (2017).

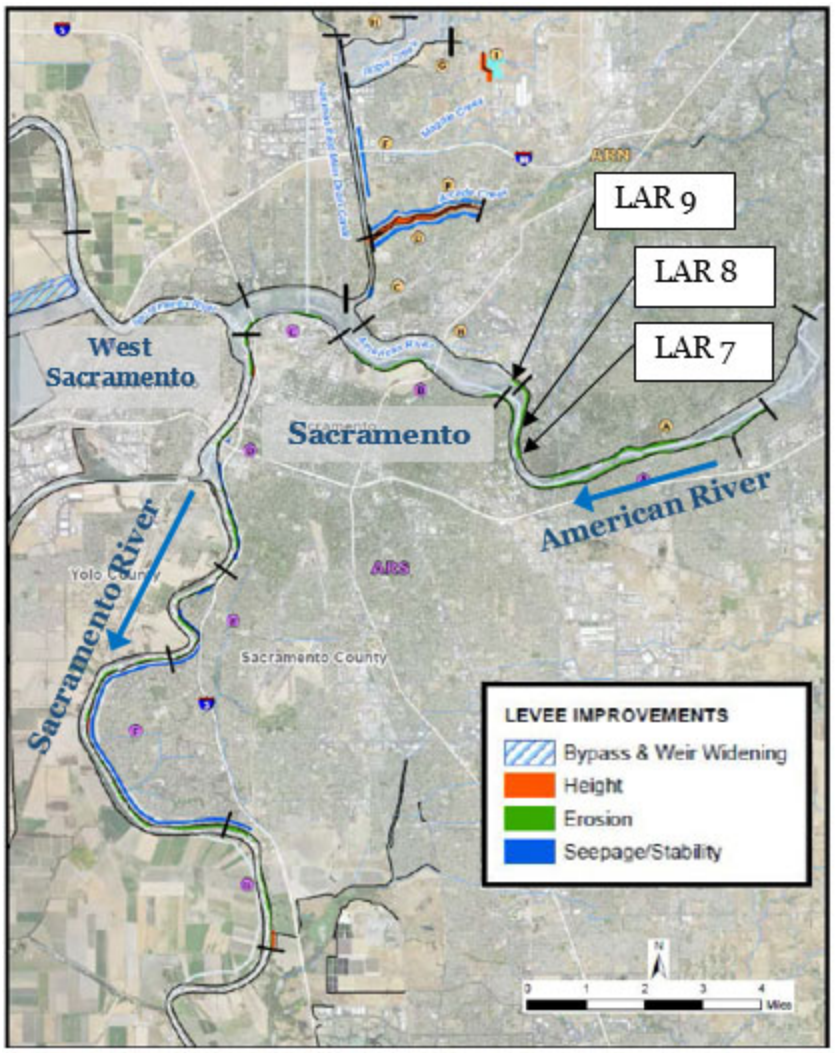

Figure 1. Overview Map of American River Common Features.
The features represent feasibility level locations.

BSTEM, which uses a critical shear stress approach, was developed by the USDA-ARS in Oxford, Mississippi. The model was chosen for this project to assess the bank erosion potential on the American and Sacramento rivers because it incorporates both fluvial erosion and mass wasting processes. The dynamic BSTEM model was modified for this effort to allow the user to input the probabilistic distribution of key erosion parameters and run multiple random combinations to provide stochastic estimates of bank retreat based on uncertainties of the input parameters. BSTEM's anticipated primary use is to help confirm recommendations from initial erosion assessments, including sites where the need for erosion protection may not initially be obvious. This includes sites that may not have experienced erosion during past events, but may experience erosion during a larger design flood. By informing risk-based erosion decisions, the BSTEM model can help balance the need to reduce the flood risk for Sacramento with the need to protect the environmental and recreational values in the project area.

BSTEM parameters

The dynamic version of BSTEM (version 3.1.1) was used in the test scenarios described in this paper. The geometry for the BSTEM model was developed from a meshing of aerial

photography, LiDAR, and sonar bathymetric measurements. These were processed into a digital elevation model from which the cross section geometry at the desired bank locations was extracted. Because the BSTEM model only includes 23 points for the geometry input, the extracted geometry was further trimmed such that all points were monotonically increasing, and the selected points were spaced to reasonably represent the bank geometry from the channel thalweg to the crest of the levee. Five bank layers were identified based on previous borehole information. The bank geometry matches the thicknesses ascribed in the five bank layers. The water surface elevation and the energy gradient on daily time steps were extracted from a 1-dimensional HEC-RAS model for the period 2008 – 2017 on a daily time step, then input and run within the BSTEM model. This period of record was chosen because of observed erosion during this time.

The long-term lateral retreat of the bank is primarily driven by the fluvial erosion, which in BSTEM is estimated using the excess shear stress equation as shown in Equation 1.

Equation 1. Effective hydraulic shear stress (Hanson and Cook 2004)

$$\epsilon_r = k_d(\tau_e - \tau_c)$$

where ϵ_r= the rate of erosion (ft/hr), k_d = the erodibility coefficient (ft^3/lb-hr), τ_e = the effective hydraulic shear stress (lb/ft^2) and τ_c = the critical shear stress (lb/ft^2).

This equation has three unknowns: critical shear stress (τ_c), erodibility coefficient (k_d), and effective hydraulic shear stress (τ_e). Significant research (Hanson and Cook 2004; Briaud 2007; Wahl 2016) has been conducted in recent decades to measure values of both τ_c and k_d through site-specific soil tests. The tests consist of a series of known or estimated stresses/velocities acting on the soil, with resulting erosion rates measured or inferred based on the specific testing procedure. The results of these tests are combined with an erosion model equation from which the erodibility parameters – critical shear stress/critical velocity and the erodibility rate of the soil – are estimated.

The majority of the tests completed to date on the American and Sacramento rivers are for the Jet Erosion Test (JET) and mini-JET. Typically, results from these tests are interpreted using the Blaisdell method (Bankhead et al. 2010; Wibowo and Robbins 2012; Wibowo and Robbins 2017). Other methods (Wahl 2016), however, such as the regression method, may also be used to analyze test results. The regression method (Langendoen, E., written communication 2018) fits the best linear relationship between the observed test results (shear stress and erosion rate) and, typically, results in a higher τ_c value than the corresponding Blaisdell method. The τ_c value from the Blaisdell method is more representative of erosion conditions closer to the incipient motion of soil, when the amount of erosion may be relatively small. In contrast, the regression method is more representative of erosion conditions occurring during active erosion that controls the amount of bank retreat. In initial calibration test sites on the American River, the τ_c values associated with the regression method were found to be more representative of the observed bank retreat that occurred between 2008 and 2017, confirming that the regression method provides τ_c values that are more representative of erosion conditions controlling bank retreat. The regression method was therefore used for the BSTEM analysis on the American and Sacramento rivers.

In addition to evaluating test results using the regression method, previous JETs and mini-JETs were screened to ensure the evaluated test adequately defined the erosion potential associated with a jet-type test (JETs and mini-JETs). Field tests (JETs and mini-JETs) were screened

using the following three criteria: (1) more than two points on the erosion curve, (2) reduction in the erosion rate with time, and (3) erosion induced by a submerged jet. Test results from the Erosion Function Apparatus (EFA) were screened using only criteria one and two. These erosion tests are the basis for determining the values for τ_c and k_d for BSTEM modeling. Multiple erosion test results for a given soil type are combined to help define the stochastic modeling input parameters.

Model Calibration, Validation, and Applicability

Since τ_c and k_d are obtained from tests along the American and Sacramento rivers, the effective hydraulic shear stress then became the primary calibration parameter. The dynamic version of BSTEM relies upon a 1-dimensional (straight reach, uniform flow) numerical hydraulic solution for the boundary shear stress. Its values cannot represent the 3-dimensional nature of the flow due to cross circulation, turbulent fluctuations, and variations in the properties of the fluid itself. Vegetation on the bank also confounds the effective hydraulic shear stress applied at the bank, and while established vegetation may provide some additional soil erosion resistance through effective cohesion, woody vegetation may also obstruct the flow and cause a local impingement point on the bank.

Three sites were identified for the purposes of conducting a calibration and validation on the American River: HEC-RAS cross sections 5.25 (LAR 9) and 6.16 (LAR 8) for calibration; and LAR 7 for validation purposes (Figure 1). These sites were chosen because survey data exists for them, and noticeable lateral retreat has occurred.

While an adjustment parameter associated with the effective hydraulic shear stress was the primary calibration parameter, the specific τ_c and k_d parameters are not always available at each site. The collected τ_c and k_d data, therefore, was used to estimate representative soil parameters for the three sites. Representative values used for the BSTEM scenarios are shown in Table 1. The first quartile, mean, and third quartile values are listed for the critical shear stress and erodibility coefficient. This provides a range of applicable parameters that were used to provide an initial step (the mean) and a range (between the first and third quartiles) for use within the calibration process described below.

Table 1. Representative soil parameters used for calibration of the American and Sacramento River sites

Soil Parameter	Representative Soil Values by Soil Type			
	Sand	**Silty Sand**	**Silt**	**Clay***
Saturated unit weight (lbs/ft^3)	120	114	108	
Effective cohesion (lbs/ft^2)	0	25.5	45	
Friction angle (deg)	32	26	31	
Suction angle (deg)	10	10	10	
Hydraulic conductivity (ft/day)	18	1.3	.06	.007
Critical shear† stress (lbs/ft^2)	0.079 (Q1:0.039/ Q3:0.11)	0.17 (Q1:0.073/ Q3:0.25)	0.20 (Q1:0.11/ Q3:0.26)	0.12 (Q1:0.068/ Q3:0.28)
Erodibility coefficient† (ft^3/lbf-sec)	19.91 (Q1:8.50/ Q3:29.69)	8.61 (Q1:4.05/ Q3:12.57)	16.41 (Q1:4.97/ Q3:14.56)	0.44 (Q1:0.05/ Q3:0.55)

Notes:
*— Limited data in the clay soil types, so silt and clay values are lumped together.
†— Listed values are means. Q1 are the first quartile values. Q3 are the third quartile values.

While defining general soil parameters by soil layer was helpful for calibrating and validating the model sites, the bank sites are known to be significantly heterogeneous, based on collected information. To better quantify the inherent uncertainty of erosion estimates, leading to better risk-informed erosion decisions, a stochastic evaluation was conducted within BSTEM (Monte Carlo realizations). To conduct this assessment, a probability distribution based on erosion test data was defined for each soil parameter listed in Table 1, plus the expected variability of the boundary roughness through the effective Manning parameter (n_e). Values used in the assessment are listed in Table 2. Initial assessment on the assigned stochastic realization values estimated that a minimum of 100 realizations are needed to mirror the variability found in the assessed sample values.

Table 2. Stochastic parameters

Soil Parameter	Distribution Type	Soil Type	Stochastic Parameters			
			Min	Max	Param a*	Param b†
Saturated unit weight (lbs/ft³)	Gamma	Sand	98.4	163.8	16.5	7.4
		Silty sand	91.6	145.9	68	1.7
		Fines (silts and clays)	96.2	121.8	230	0.5
Effective cohesion (lbs/ft²)	Uniform	Sand	0	0	---	---
	Gamma	Silty sand	0.0001	338.3	0.6	189.9
	Gamma	Fines	0.0001	172	0.6	75.9
Friction angle (deg)	Uniform	Sand	32	35	---	---
	Uniform	Silty sand	19.1	32	---	---
	Gamma	Fines	26.9	36.2	92.9	0.3
Suction angle (deg)	Uniform	Sand	15	15	---	---
	Uniform	Silty sand	10	20	---	---
	Gamma	Fines	5.05	24.95	3.5	3.3
Hydraulic conductivity (ft/day)	Gamma	Sand	0.02000	1417.00	1.00	450.00
	Gamma	Silty sand	0.00341	85.00	1.20	80.00
	Gamma	Silt	0.00425	5.66	3.50	0.20
	Gamma	Clay	0.00009	1.69	2.00	0.10
Critical shear stress (lbs/ft²)	Gamma	Sand	0.00852	0.15998	1.036956	0.076343
	Gamma	Silty sand	0.0114	0.5159	1.848233	0.094461
	Gamma	Silt	0.0238	0.4282	2.01937	0.098841
	Gamma	Clay	0.0326	0.5957	1.163643	0.187527
Erodibility coefficient (ft³/lbf-sec)	Gamma	Sand	0.349891	42.72779	0.54425	36.57258
	Gamma	Silty sand	0.468448	19.79302	1.841666	4.675274
	Gamma	Silt	0.347617	81.54159	0.807292	20.32631
	Gamma	Clay	0.011389	1.473347	0.543307	0.813525
n_e (s/m$^{1/3}$)	Gamma	All	0.03	0.07	8.519027	0.004126

Notes:
*— Parameter a is needed for normal (mean), lognormal (mean of the ln of values), gamma (shape parameter), and triangular (mode).
†— Parameter b is needed for normal (standard deviation), lognormal (standard deviation of the ln of values), and gamma (scale parameter).

Calibration Steps

With three potential calibration parameters, a consistent, objective, and repeatable calibration method is needed for BSTEM. A calibration process was developed for this purpose and applied to two sites: LAR 8 and LAR 9 along the American River. Both of these sites have observed bank retreat data and JET results are available. These sites were calibrated using the following steps:

1. Correct effective hydraulic shear stress, τ_e, as calculated in HEC-RAS, to account for helical flow around river bends. This step is only applied, if needed, after an evaluation of the planform shape. For BSTEM, this correction is applied to the energy slope (or water surface energy slope).

2. Select initial values for critical shear stress,τ_c, and erodibility coefficient, k_d, based on the probability density function (PDF) of the soil type.
3. Select effective Manning's parameter, n_e, based on "base n" [=0.03 for American River bare ground according to Chow (1959) and the HEC-RAS manual (Brunner 2016)]. Make adjustments for site vegetation.
4. To fine tune τ_c, review graphs of average toe shear stress and maximum retreat with water surface elevation in the BSTEM model output. If needed, change τ_c within the interquartile range (25% to 75%) to bring the estimated bank retreat closer to the observed value.
5. If estimated bank retreat is not close to the observed bank retreat, adjust k_d within the interquartile range (25% to 75%), as needed, to bring the estimated bank retreat closer to the observed value.
6. If additional adjustments are still needed to provide a reasonable match between the estimated and observed bank retreat, then change n_e slightly. This is the deterministic BSTEM result.
7. Once the deterministic BSTEM result is obtained, perform a stochastic simulation. Evaluate the percent range in which the deterministic BSTEM result falls.

Calibration step 1 is a visual inspection of the fluvial planform. Where planform curvature was noted, such as at LAR 9, the applied hydraulics estimated by the 1-dimensional model was adjusted to account for observed increases in hydraulic boundary shear on the outer bank within bends, according to Equation 2.

Equation 2. 1-dimensional model adjustment
to account for increases in shear stress in a bend (Sclafani et al. 2012)

$$K_{bend-shear} = 2.47\left(\frac{R_c}{TW}\right)^{-0.235}$$

where $K_{bend\text{-}shear}$ = the bend shear correction factor, R_c = the measured centerline radius of curvature (feet), and TW = the approximate bankfull channel top width.

The BSTEM hydraulic inputs from the 1-dimensional model are water surface elevation (from which water depth is calculated), and slope. Both water depth and slope are directly correlated to the applied normal shear stress (USACE 1994), so the bend shear correction factor was applied directly to the 1-dimensional model slope values from HEC-RAS to provide a better estimate of the 3-dimensional hydraulics through the bend.

Calibration step 2 utilizes the screened, field-collected values to estimate a starting value for τ_c and k_d. Based on the initial two calibration sites, LAR 8 and LAR 9, it was determined that using the mean from the sample distribution was a good starting point, primarily because a lower τ_c resulted in large estimated bank retreat lengths at flow conditions when no noticeable bank erosion was observed in the field. The mean tends to be on the higher end of the PDF than the median, so this was the chosen starting value. The first and third quartiles were then chosen as being representative of the bulk of the field-tested values and used to provide a reasonable range to adjust τ_c and k_d for a given soil layer. An example of these relationships is shown in Figure 2 for silty sands within the study area.

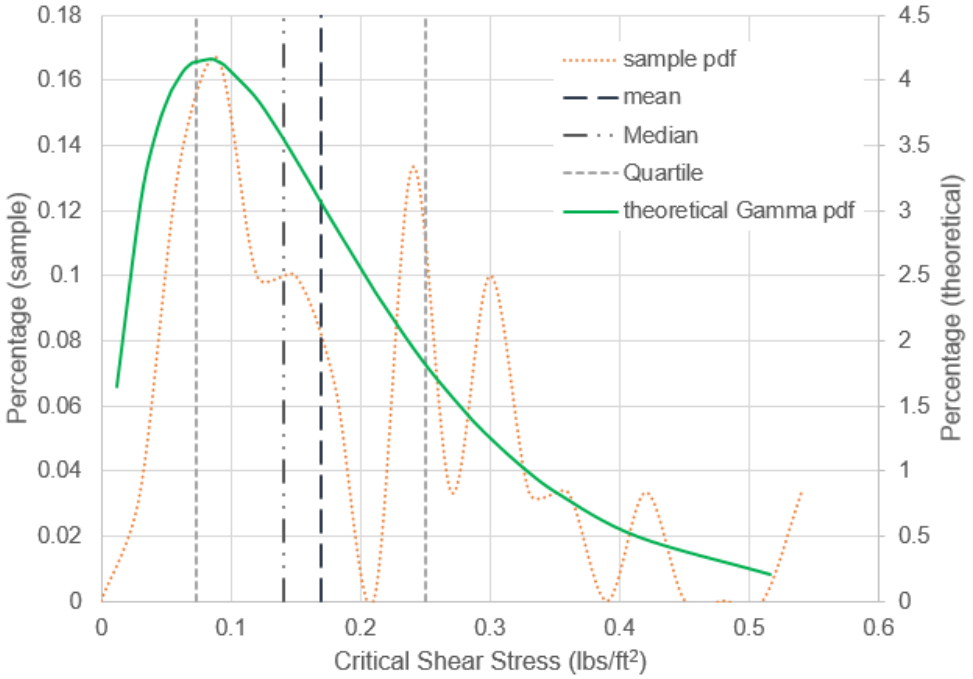

Figure 2. Silty sand PDF, with mean, median, and quartiles one and three shown. Both the sample PDF and the theoretical gamma PDF given in Table 2 are shown.

Calibration step 3 involves the determination of the effective hydraulic shear stress acting on the soil, which is calculated in BSTEM using Equation 3.

Equation 3. Effective hydraulic shear stress adjustment (Hanson 1989; Temple et al. 1987)

$$\tau_e = \tau_o \left(\frac{n_s}{n_e}\right)^2$$

where τ_e is as previously defined, τ_o = the normal bed shear stress (lb/ft²), n_e = the effective Manning parameter, and n_s = Manning's roughness associated with median soil grain roughness for the identified soil layer.

The values for τ_o and n_s are calculated internally within BSTEM, given hydraulic inputs (water surface elevation and slope) and soil information (median grain based on the input τ_c for that soil layer). The lowest limit in BSTEM for n_s is 0.0156, which relates to a .011-mm-size particle.

Since vegetation strongly influences how the effective hydraulic shear stress acts on the soil, experiments conducted by the Natural Resources Conservation Service, NRCS (2007a), were utilized to provide a relationship between a bare earth (base) n value (n_b) for the American and Sacramento rivers (0.03) and the modifying influence of vegetation. The vegetal cover factor (C_f) found by the NRCS (2007a) was found to relate to Manning's roughness by $\sim \frac{1}{\sqrt{1-C_f}}$. NRCS (2007a) found that C_f varies between zero (no vegetation) and one (maximum effects of vegetation). Applying this relationship, along with the base n (n_b) results in an adjustment to the effective Manning parameter, as shown in Equation 4.

Equation 4. Effective Manning's roughness acting on the soil, incorporating a vegetal cover factor

$$n_e = \frac{n_b}{\sqrt{1 - C_f}}$$

where n_e, n_b and C_f are as defined previously.

Using the base n as a starting roughness, photographs of the vegetation cover are utilized to provide an estimate for n_e. Photographs of the vegetation at the calibrated sites will be coupled with the calibrated n_e values to provide a means of estimating this value at other sites on the American and Sacramento Rivers.

Calibration step 4 involves the adjustment of τ_c within the first and third quartile range mentioned previously. Two graphs, provided within BSTEM, are useful when adjusting τ_c. The first graph (Figure 3) shows local maximum retreat versus water surface elevation (WSE). When there is estimated bank retreat at lower flows (smaller WSE values in Figure 3) τ_c is too low and should be adjusted higher. Figure 4 shows the local maximum retreat versus WSE graph at LAR 8 after final adjustment of τ_c. The second graph (Figure 5) is the average toe shear stress versus WSE. This graph helps assess the magnitude of the adjustment that is needed to reduce the occurrence of bank retreat at lower flows.

Calibration step 5 adjusts the k_d values within the identified first and third quartile range to assess if the estimated bank retreat can be adjusted closer to the measured value. BSTEM provides the ability to graph existing and estimated bank profiles with an observed bank profile (as shown in Figure 6 at LAR 8).

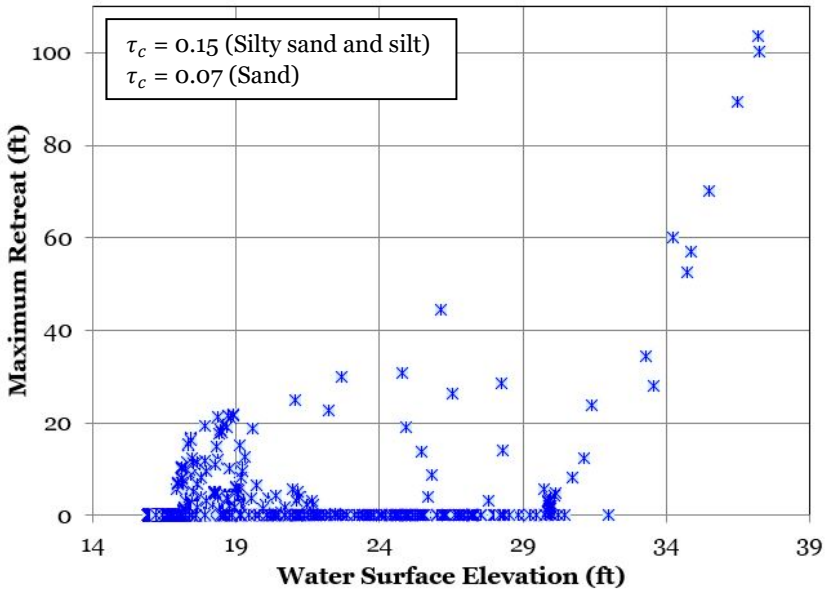

Figure 3. Local maximum bank retreat versus WSE with a critical shear stress that is too low at LAR 8

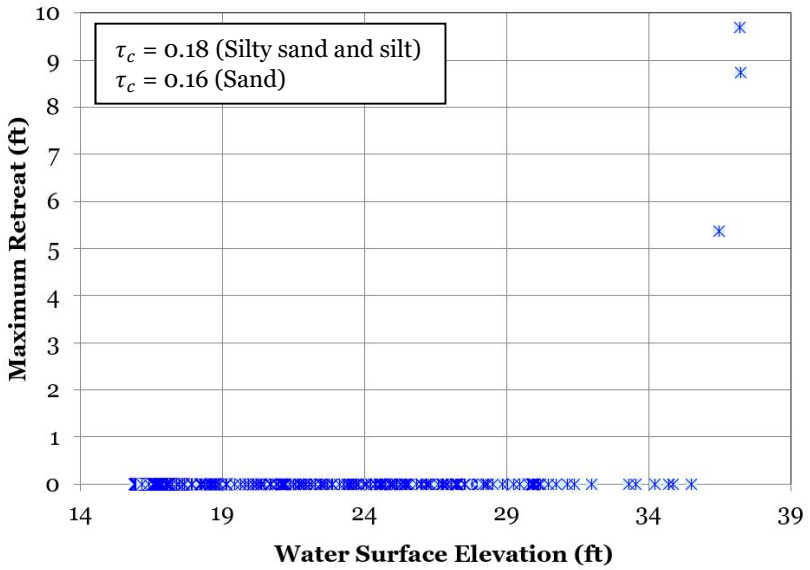

Figure 4. Local maximum bank retreat versus WSE with a critical shear stress at LAR 8 that is set so retreat happens at the higher flow events when documentation of the bank retreat occurs

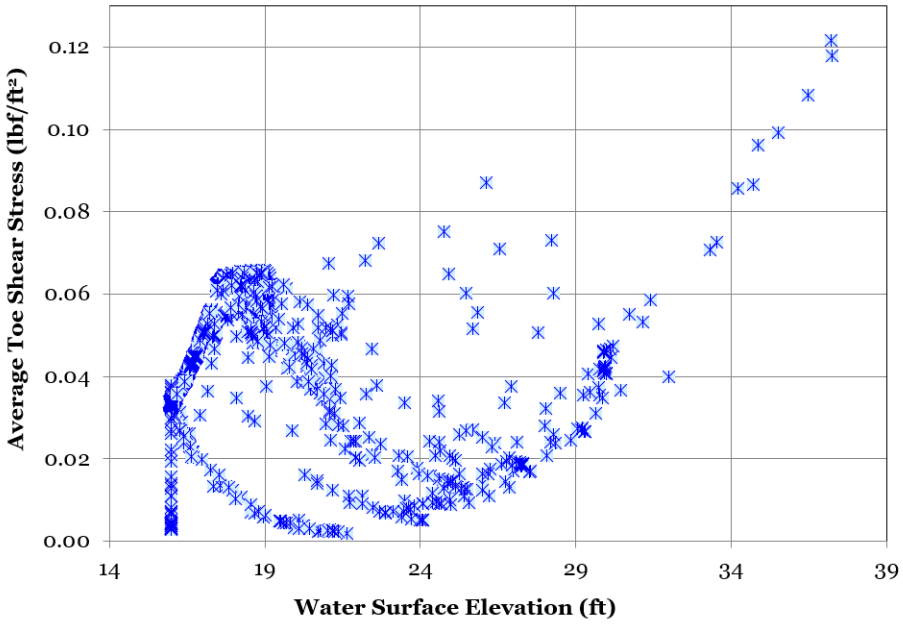

Figure 5. Average toe shear stress versus WSE with the final critical shear stress used at LAR 8

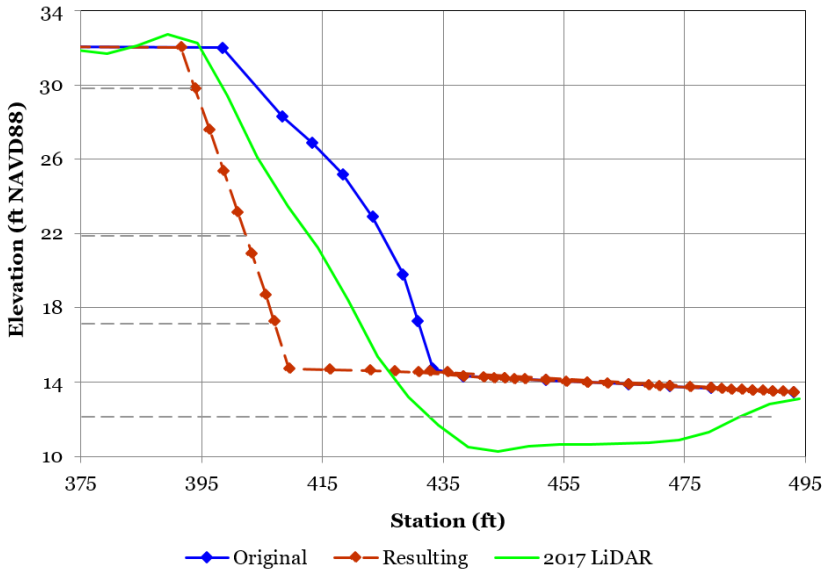

Figure 6. Comparison of estimated bank retreat (resulting line) and the observed bank retreat (2017 LiDAR). The original surface (2008 condition) is provided along with the approximate boundaries of the three lower soil layers at LAR 8.

If the estimated bank retreat still doesn't match the observed values, then calibration step 6 is pursued. By varying n_e within BSTEM until the estimated bank retreat closely matches the observed bank retreat, the effective hydraulic shear stress can be calibrated. Once the effective hydraulic shear stress is calibrated, Equation 4 can be used to estimate the resulting vegetal cover factor. The coupling of this calibrated cover factor with bank photographs provides a database from which to estimate C_f at other sites on the American and Sacramento rivers where bank retreat has not been observed, but bank photographs of the vegetation are available. Table 3 provides values for n_e and C_f at LAR 8 and LAR9, two calibration sites on the American River. A library of C_f values makes it possible to estimate n_e from vegetation cover, extending the BSTEM analysis to other sites where observation data is not known.

Table 3. Evaluated n_e and C_f factors for LAR 8 and LAR 9

Site	n_e	C_f	Bank Vegetation
LAR 8	.035	0.26	Sparse grass
LAR 9	.03	0	Bare earth
LAR 7	0.39	0.40	Grasses and woody shrubs on bank

The final calibration step, step 7, evaluates the stochastic bank retreat response. A stochastic analysis, using the parameters listed in Table 2, has been incorporated into BSTEM to estimate the variability of bank retreat estimates given the soil parameter uncertainties. Figure 7 and Figure 8 show the stochastic results of bank retreat, along with the deterministic BSTEM result for LAR 8 and LAR 9, respectively. It should be noted that the profile simulated with the deterministic model for LAR 8 falls within the 25% and 50% results for all layers except the bottom layer. The deterministic result for LAR 9 falls within the 25% to 75% range of the stochastic results.

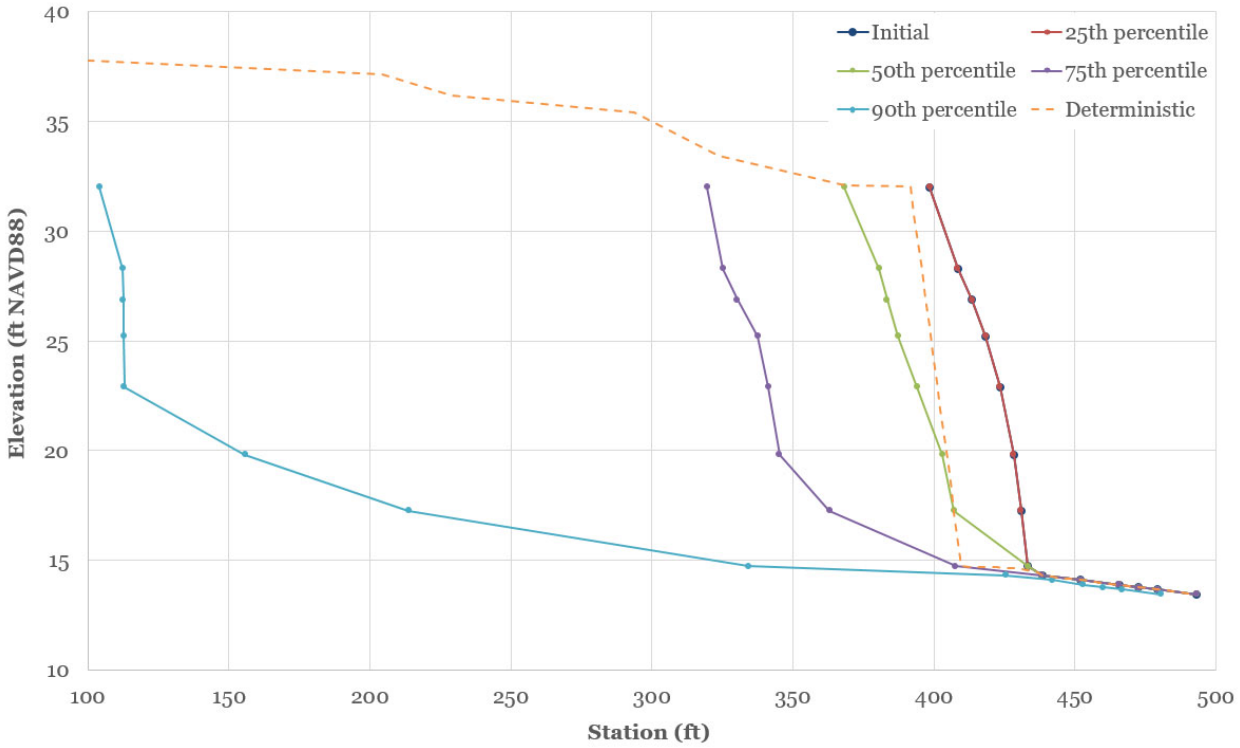

Figure 7. Stochastic and deterministic BSTEM results at LAR 8

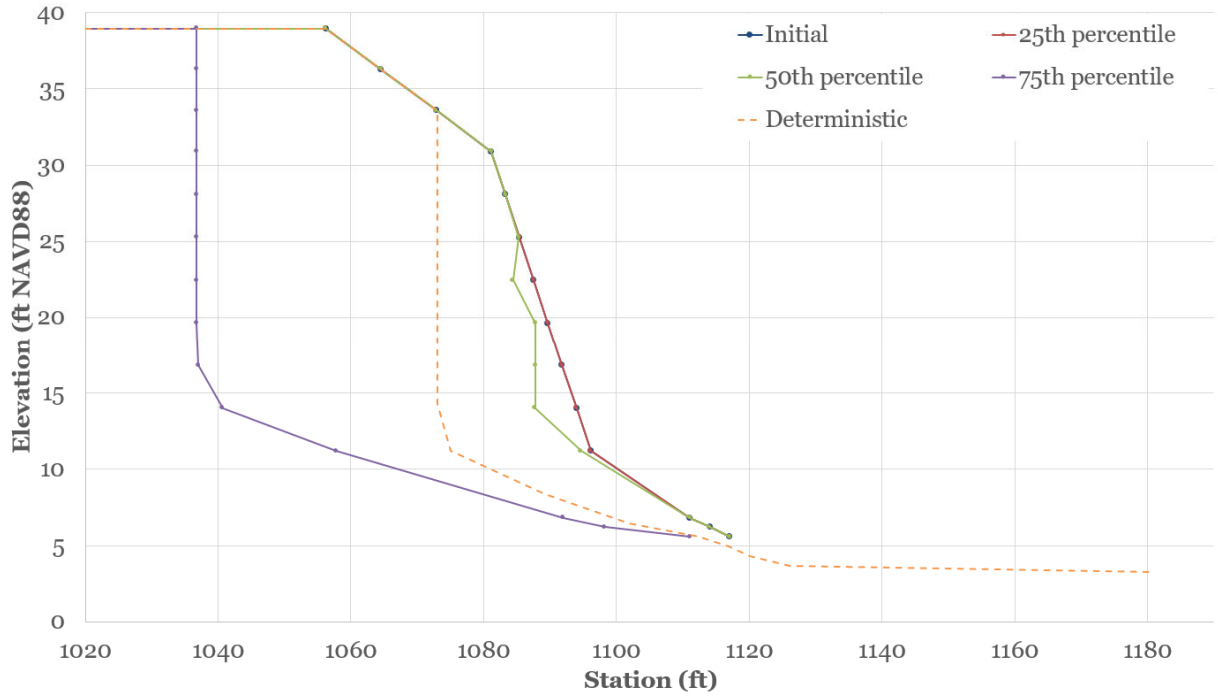

Figure 8. Stochastic and deterministic BSTEM results at LAR 9

Validation Steps

After the BSTEM model was set up – a process which included extracting the cross section profile, determining the five soil layers, and estimating the soil parameters from available data – the validation followed these six steps:

1. Estimate τ_c and k_d from calibrated model results for similar soil types for the deterministic model.
2. Assess cover factor for the site based on vegetation cover, and back-calculate n_e for the deterministic model.
3. Run deterministic and stochastic BSTEM models.
4. Compare proximity of estimated bank retreat in the deterministic model to the observed bank retreat.
5. Compare where deterministic and observed profiles fall in the percent range of stochastic results.
6. If the deterministic estimated bank retreat is reasonably similar to the observed bank retreat, and the deterministic bank retreat falls within the stochastic percent ranges found during assessment of the calibration sites, then the model is validated.

Validation steps were performed at LAR 7. Since soil layers for LAR 7 are similar to those found at LAR 8 and LAR 9, the calibrated τ_c and k_d values from those sites for the appropriate soil layers were applied to the deterministic model. LAR 7 was more vegetated than either LAR 8 or LAR 9. A C_f was chosen for LAR 7 based on site photographs showing the bank vegetation and the estimated C_f factors of 0.40. This was used to estimate a n_e for LAR 7. The deterministic results for LAR 7 were approximately 50 feet of the observed bank retreat at the toe and approximately 15 feet of the observed bank retreat at the top of the bank. In essence, BSTEM predicted more lateral bank retreat at the top of the bank and less at the toe of the bank than what was observed. Figure 9 shows that the deterministic and 2017 profiles fall within the 25% to 50% range, which is similar to the deterministic and stochastic results for LAR 8 and LAR 9.

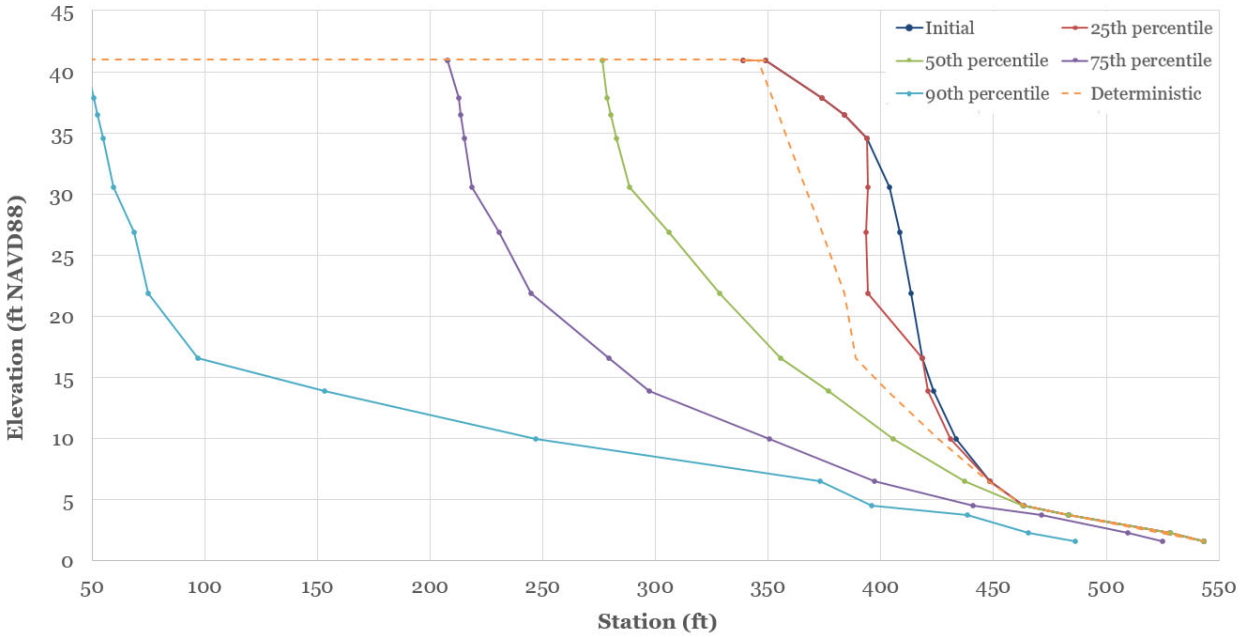

Figure 9. Stochastic and deterministic BSTEM results at LAR 7

Conclusion and Discussion

BSTEM predicts bank retreat by fluvial erosion and geotechnical stability of banks. BSTEM's ability to perform deterministic and stochastic bank retreat estimates makes it a useful tool for making risk-informed erosion decisions during analysis and design. Initial results for the bank erosion work under WRDA 2016 indicate that a conceptual framework for calibration/validation of sites is viable for the American and Sacramento rivers.

A method was developed to calibrate the BSTEM model using measured bank retreat and JET results and applied to two sites, LAR 8 and LAR 9, along the American River. This method accounts for flow around a bend, and effects of vegetation. The calibration effort covered a few soil types such as silty sand, silt, and sand. Based on limited calibration, validation was carried out at LAR 7, which had measured bank retreat but no JET test results. Results of the calibration indicate the proposed calibration process may provide a method to consistently calibrate BSTEM to observed erosion using JET test results and adjusting for flow around bends and vegetation cover. The results for the validation run indicate calibrated erosion parameters can possibly be used at nearby sites with similar soils. However, additional calibration and validation runs are needed and planned to confirm these initial findings.

During the bank erosion effort conducted to date around Sacramento, it was found that the regression method for analyzing JET erosion parameters provides a good estimate of the threshold and rate of fluvial erosion for the American River. Additional soil testing is ongoing to provide a larger sample pool for the critical shear stress and erodibility coefficient, in order to improve stochastic bank retreat estimates.

The stochastic results for the three assessed sites on the American River (LAR 8, LAR 9, and LAR 7) indicate that the 25% to 50% range is a reasonable approximation for the estimated bank retreat possible during a 1/10 Annual Chance Exceedance event on the American River (2017 flood event). Given the uncertainty of soil parameters, the stochastic calibration results indicate BSTEM is suitable for a stochastic framework. Current plans are to utilize this framework with a larger design event scenario, to provide bank retreat estimates and inform risk-based decisions for hydrologic events that have yet to occur on the American and Sacramento rivers.

References

Bankhead, N., Simon, A., Thomas, R., Klimetz, L., and Klimetz, D. 2010. "Sediment Loadings from Streambanks and Levees Along the Sacramento River and Selected Tributaries." U.S. Department of Agriculture, Agriculture Research Service, National Sedimentation Laboratory, Oxford, Mississippi.

Briaud, J-L. 2007. "Case Series in Soil and Rock Erosion: Woodrow Wilson Bridge, Brazos River Meander, Normandy Cliffs, and New Orleans Levees." The 9th Ralph B. Peck Lecture, Journal of Geotechnical and Geoenvironmental Engineering of the American Society of Civil Engineers, College Station, Texas.

Briaud, J-L. and Montalvo-Bartolomei, A.M. 2017. "Meander Migration: the observation method." *Can. Geotech. J.*, NRC Research Press, 1-14.

Brunner, G.W. 2016. HEC-RAS, River Analysis System Hydraulic Reference Manual. U.S. Army Corps of Engineers, Hydrologic Engineering Center, Davis, California.

Chow, V.T. 1959. Open Channel Hydraulics. McGraw-Hill, New York, New York.

Fischenich, C. 2001. Stability thresholds for stream restoration materials, EMRRP Technical Notes Collection. U.S. Army Corps of Engineers, Engineer, Research, and Development Center, Vicksburg, Mississippi.

Hanson, G.J. 1989. “Channel erosion study of two compacted soils.” Transactions of the ASAE 32(2), 485-490.

Hanson, G.J. and Cook, K.R. 2004. “Apparatus, Test Procedures, and Analytical Methods to Measure Soil Erodibility In Situ.” Applied Engineering in Agriculture. American Society of Agricultural Engineers, 20(4). 455-462.

Langendoen, E.J. 2018. “Channel Erosion Width Adjustment: Importance, Mechanics, and Assessment.” Powerpoint presentation by U.S. Department of Agriculture, Agricultural Research Service, Oxford, Mississippi.

NRCS. 2007a. “Chapter 7 Grassed Waterways.” *Part 650 Engineering Field Handbook*. U.S. Department of Agriculture, Natural Resources Conservation Service. Washington, D.C.

Scalafani, P., Thornton, C.I., Cox, A.L., and Abt, S.R. 2012. Methodology for Predicting Maximum Velocity and Shear Stress in a Sinuous Channel with Bendway Weirs using 1-D HEC-RAS Modeling Results, Colorado State University for the U.S. Department of the Interior, Bureau of Reclamation, Ft. Collins, CO.

Temple, D.M., Robinson, K.M., Ahring, R.M., and Davis, A.G. 1987. Stability design of grass-lined open channels. USDA Agricultural Handbook No. 667. U.S. Department of Agriculture, Washington, D.C.

USACE. 1994. Hydraulic Design of Flood Control Channels, EM-1110-2-1601. U.S. Army Corps of Engineers, Washington, D.C.

Wahl, T.L. 2016. “The Submerged JET Erosion Test: Past-Present-Future.” Proceedings of the USSD International Symposium on the Mechanics of Internal Erosion for Dams and Levees, Salt Lake City, Utah.

Wibowo, J.L. and Robbins, B.A. 2012. “Laboratory JET Erosion Tests on American River Soil Samples.” U.S. Army Corps of Engineers, Engineer, Research, and Development Center, Geotechnical and Structures Laboratory, Vicksburg, Mississippi.

Wibowo, J.L. and Robbins, B.A. 2017. “Laboratory JET Erosion Tests on the Lower American River Soil Samples,” Sacramento, California – Phase 2. U.S. Army Corps of Engineers, Engineer, Research, and Development Center, Geotechnical and Structures Laboratory, Vicksburg, Mississippi.

Multi-Pronged Evaluation of Spillway Erosion at Pipestem Dam

Roger L. Kay, P.E., Chief, Hydraulics Section, U.S. Army Corps of Engineers, Omaha, NE, Roger.L.Kay@usace.army.mil

Introduction

Erosion of the spillway at nearby Cottonwood Creek Dam in 2009 raised concern over the erodibility of the spillway at Pipestem Dam in North Dakota. However, quantifying the risk of spillway erosion can be difficult, so several approaches were used in evaluation of spillway erosion potential to improve confidence in the results. Pertinent background information and the methods used are presented herein; specific results of the analysis are not presented in this paper.

Pipestem Dam Background

Pipestem Dam was constructed by the U.S. Army Corps of Engineers, Omaha District and is a high hazard potential dam located in Stutsman County, on Pipestem Creek, about four miles northwest of Jamestown, North Dakota. The project is approximately seven miles above the confluence of Pipestem Creek and the James River. Jamestown Dam, owned and operated by the Bureau of Reclamation (USBR), is located approximately three miles southeast of Pipestem Dam. Jamestown Dam is a high hazard potential dam located on the James River. Both Pipestem and Jamestown Dams are operated as a system to manage flood risk on the James River. The location of Pipestem and Jamestown Dams is shown below (Figure 1).

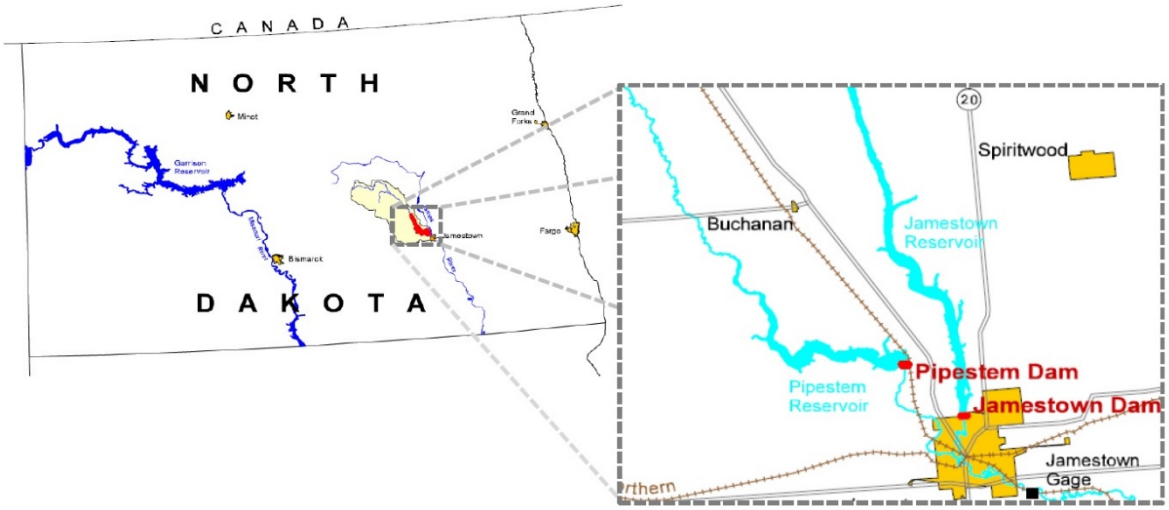

Figure 1. Location Map, Pipestem Dam near Jamestown, ND.

Project Features: Construction of Pipestem Dam was completed between spring 1971 and late fall of 1973, with initial impoundment of waters beginning in March 1974. Pipestem Dam consists of a zoned earthfill dam, an emergency spillway, and an outlet works. The main embankment is about 4,000 feet long and has a crest width of 30 feet with a design crest elevation of 1,507.5 feet Local Project Datum (LPD). The foundation is comprised of alluvium

and glacial drift underlain by Pierre Formation shale bedrock. The 3,100-foot-long, 1,500-foot-wide emergency spillway consists of an ungated earth channel excavated in the right abutment overburden with a crest elevation of 1,496.8 feet LPD. The outlet works consists of a concrete intake drop structure, a 621-foot-long gated reinforced concrete conduit, and a stilling basin. A five-foot thick compacted clay blanket extends into the left and right abutment areas to reduce seepage through the abutments. Reservoir storage to the spillway crest is 142,000 acre-feet.

Watershed Characteristics: The Pipestem Creek basin, in general, is a relatively flat plain, sloping gradually from about elevation 1,800 feet LPD at the headwaters of the creek to about elevation 1,400 feet LPD at the reservoir. The Pipestem basin is located in the prairie pothole region where there are numerous kettle lakes formed by glaciers, which contributes uncertainty into the drainage area above the dam. The estimated contributing drainage above Pipestem Dam was 594 square miles, with roughly 400 square miles of non-contributing drainage area based on original design documents in 1965; however, the contributing area was revised downward to 400 square miles in 1967, although 594 square miles continued to be used as contributing drainage area for all design activities through construction (USACE 1975). A 2010 study estimated the contributing drainage basin as 611 square miles, with 399 square miles of non-contributing drainage area. During the 2017 Inflow Design Flood (IDF) update, the contributing drainage was found to vary with surface storage and effective basin precipitation, with 904 square miles contributing runoff to the updated IDF.

Regional Geology: The Jamestown and Pipestem reservoirs lie within the Drift Prairie section of the Interior Lowland Province. The youngest geological formations in the area are the alluvial deposits in the valleys of both streams. Most of this material was deposited by post-glacial streams flowing through the deeper valleys and filling them to the level of the present valley floors. The alluvial deposits prevail over a relatively small portion of the surface area, and in the vicinity of Jamestown extend to a maximum depth of approximately 100 feet. The most important formation is glacial drift, which blankets the entire basin and is composed of coarse sand and gravel interlaced with seams of clay. Outcroppings of the underlying Pierre Formation shale, which forms bedrock for practically the entire area, are rare. Underlying the Pierre Formation, in successive order, are the Niobrara and Benton shales and the Dakota sandstone. Groundwater is continually percolating through the coarse glacial drift, and in some instances is found only a few feet below the surface. This flow is generally independent of streamflow, having been sealed off by mud and silt deposited by the stream.

Climate: The climate of the Pipestem basin is classified as dry subhumid, as the basin is located near the geographical center of the North American continent and is subject to extreme variations in temperature. Precipitation is moderate and fluctuates widely from year to year. Mean annual precipitation is 19.0 inches, with more than 75% of the annual precipitation occurring between April and September. However, nearly all major floods in the basin are the result of snowmelt, typically occurring in the months of March or April, although occasionally into the month of May. Snowmelt floods are often, but not always, augmented by rainfall.

Pipestem Dam Spillway

Design of Dam and Spillway

Geology: Initial geological investigations of the dam site began as early as 1944, approximately 4300 feet downstream of the present dam embankment. However, the overburden data from this investigation was not readily assimilated with borings associated with

the dam design in the 1960s and were not considered further. 52 borings were completed in the fall of 1967, including 21 in the spillway itself, but only 3 of these extended to top of bedrock and were the only 3 borings extending more than 35 feet below the spillway floor, with only 2 others extending more than 16 feet deeper than the spillway floor. These borings were made to determine the type of material to be excavated as well as to ensure the base of the spillway excavation would be in erosion resistant material. There were 3 test pits also dug in the spillway to investigate the percentage of plus 4 inch material that may be suitable for providing embankment riprap. The borings and test pits showed some erodible material may be present at the proposed spillway floor, so further exploration was recommended to better define the extent of erodible material present at the bottom of the spillway excavation. General Design Memorandum JP-3 (USACE 1969) noted that materials in the spillway were similar to those in the abutments but more impervious with depth.

An additional 82 borings were completed, including 22 in the spillway, in 1970. The large number of additional borings was primarily related to relocating the proposed embankment 1900 feet upstream to its constructed location. The depths of these additional borings ranged in depth from 8 to 183 feet; however, none of the additional borings in the spillway appear to have been made more than 20 feet below the spillway floor elevation. The additional borings helped to define an area of surficial sands and silt that were removed from the spillway floor and replaced with clay fill, with about 200,000 yds^3 of material removed and placed (Figure 2). The materials removed from the spillway excavation were used to construct the dam embankment, with 80% of the excavated material comprising lean and sandy clays, and 10% each clayey sand and silty sand (USACE 1969, 1970).

Figure 2. Areal Extent of Surficial Sands Removed from Spillway During Construction.

Hydrology: Pipestem Dam was designed to retain all the volume of floods up to and including the Standard Project Flood (SPF) (USACE 1967). Since the period of record did not contain any significant rises in discharge resulting solely from rainfall, an investigation of snowmelt floods was undertaken to determine an appropriate unit hydrograph. Accordingly, the 1950 flood was selected as the largest flood of record, the most data comprehensive and did not appear to have any rainfall component. Since most snowmelt occurs in the daylight hours, the first 12 hours of melt was considered the runoff for the 6 hours ending at noon and the melt of the second 12 hours the 6 hour runoff ending at 6 p.m.

The SPF was then developed using the derived unit hydrograph with an index rainfall of 8.6 inches, yielding a runoff volume of 139,500 acre-feet and peak flow of 20,700 cfs. This resulting flood was used to determine the spillway crest elevation, assuming the entire SDF was stored with a starting pool at base of flood control pool. This spillway crest elevation was initially at 1495.4 feet LPD but was revised to 1496.3 feet LPD when the final embankment location was selected.

A Probable Maximum Flood (PMF) was selected as the spillway design flood (SDF) for Pipestem Dam. The rainfall was developed from Hydrometeorological Report No. 33, with an index rainfall of 20 inches for a 200 square mile area. An arrangement of 1.2 inches rainfall in the first 12 hours, followed by 2.0 inches in 6 hours, followed by 12.6 inches in 6 hours, with 2.4 inches in the final 24 hours, resulted in a PMF with a peak discharge of 51,500 cfs and runoff volume of 348,460 acre-feet. The resulting peak pool of 1502.0 feet LPD was revised to 1502.5 feet LPD when the final dam location was selected, with 5 feet of freeboard added to set the final embankment crest elevation.

A memorandum dated 09 June 1971 in response to 2nd Indorsement to Design Memorandum No. JP-5 noted that the maximum surcharge elevation of 1502.5 was based on a hydrograph with incorrect time scale, resulting in a routing of 666,920 acre-feet, rather than the 348,460 acre-feet stated. Routing with the corrected volume of 348,460 acre-feet lowered the maximum pool from 1502.5 to 1502.3 feet LPD. The memorandum further states that developing the SDF in accordance with EM 1110-2-1405 increased the peak flow at the dam from 51,500 cfs to 58,000 cfs. This change in SDF hydrograph increased the peak pool from 1502.3 to 1502.8 feet LPD.

A pool probability curve for Pipestem Reservoir was derived based on routing 17 years of record in accordance with the proposed reservoir regulation schedule. Since the flood of 1950 was the largest since 1883, the plotting position of the 1950 flood was plotted at the 0.83% annual chance exceedance (ACE) rather than 4.0% ACE. The resulting plot showed the spillway crest was at a 0.1% ACE (or 1000-year return interval).

Hydraulics: Initial design of the spillway consisted of a 1,200 foot bottom width with 1 on 3 sideslopes, with a 200-foot flat crest near the upstream end at elevation 1495.4 feet LPD (USACE 1969). The spillway channel downstream of the crest was to have a slope of 0.002 with an overall length of 3,100 feet. A Manning's n of 0.030 was selected to allow for variations in vegetative growth and localized erosion. It was assumed that critical depth would occur where the spillway channel emerges from the hillside, resulting in subcritical flow through the entire length of spillway, with velocities becoming progressively less in the upstream direction. The Design Memorandum JP-3 stated that any erosion that would start at the downstream end must

progress the entire length of the spillway before lowering of the crest could occur; however, the Design Memorandum does not assess the erodibility of the spillway materials and may discount the likelihood of erosion based on the assumed frequency of spillway flow (<0.1% ACE). Subsequent revision to the location of the embankment and spillway in Design Memorandum JP-5 resulted in a change in bottom width to 1,500 feet and raise of crest to elevation 1496.3 feet LPD but no changes in discussion of erodibility (USACE 1970).

A Close Call

The flood of 1950 was somewhat unusual compared to other historic floods at the time of construction, comprised of two distinct snowmelt periods, one in mid-April and the other in mid-May. A reconstituted flood routing of the 1950 flood at the time of design showed the pool would have raised to approximately elevation 1475 feet LPD after the mid-April snowmelt with an ultimate pool of 1487.3 feet LPD following the mid-May snowmelt. This routing assumed no outflow from Pipestem until the peak pool had been achieved.

Prior to the winter of 2008-2009, the highest pool realized at Pipestem had been 1487.01 feet LPD on 11-May-1997. The 1997 spring runoff season was similar to that of 1950 with two distinct rises in discharge, with one in early April and the other in late April. However, releases had not been held to zero as had been assumed in the reconstituted 1950 flood routing. The spring flood of 2009 likewise was comprised of two distinct rises in flow, with the first in late March augmented by a rainfall event that changed over to a raging blizzard, with additional snowfall accumulations contributing to the later rise in discharge following a return to more moderate temperatures, culminating in a peak pool of 1492.2 feet LPD on 24-Apr-2009. The flood potential of this event was known with some certainty in advance because of the large snowpack, which resulted in advance measure levees being constructed in Jamestown, North Dakota, which allowed releases from Jamestown and Pipestem to be made well in excess of channel capacity. Without this capability to make larger releases, it is likely that the spillway of Pipestem would have experienced flow.

Cottonwood Creek Dam: Cottonwood Creek Dam is located about 60 miles south of Pipestem Dam in a similar geologic formation which includes glacial till soils. Like the Pipestem Dam spillway, the spillway at Cottonwood Creek Dam consisted of a relatively flat exit channel which daylighted into a steep valley wall. Prior to the 2009 event, Cottonwood Creek Dam had a 700-foot-long and 100-foot-wide trapezoidal spillway excavated through the right abutment at a 1% slope. The spillway channel excavation daylighted and dropped approximately 40 feet to the valley floor. In 2009, a headcut advanced through the spillway exit channel for a distance of approximately 450 feet over a 5-day period with a peak discharge of approximately 500 cfs (5 cfs/ft of width). Final erosion depths were estimated to be 30 to 40 feet with the ultimate headcut advancing within 40 feet of the crest. Several methods of intervention were attempted, ranging from dropping large sandbags from helicopters into the top of the headcut in an attempt to arrest upstream migration of the headcut, to dumping and bulldozing material (riprap) from the left sidewall over the crest of the spillway to reduce flow over the spillway, to cutting an additional channel into the right sidewall of the spillway in an attempt to divert water from the pool into the spillway channel downstream of the headcut. The final advancement of the spillway erosion headcut is shown in Figure 3.

Several similarities exist between the Cottonwood Creek and Pipestem Dam spillways allowing comparisons between the two projects regarding spillway performance. The most significant

commonality is that both spillways are located within the same geologic region and are composed of similar geologic materials. Configurations are also similar between the two spillways as both are trapezoidal earth-cut, uncontrolled, grass-lined spillways without any positive cutoff or sill. Both spillway excavations daylight into valleys with steep exit slopes. Both spillways included the excavation of granular material (and replacement with select fill) within the spillway excavation.

The primary difference between the Pipestem Dam spillway and the Cottonwood Creek Dam spillway is that the upper soil layers at Cottonwood Creek were thought to consist primarily of glacial till, with no underlying layer of glacio-fluvial sands in the upper portion that was eroded, based on all borings taken prior to construction and visual inspection following erosion. Glacio-fluvial sands may be present at Cottonwood Creek Dam, but at a lower depth than at Pipestem.

Figure 3. Post-flood aerial imagery of Cottonwood Creek Dam. Orange arrow calls out upper extent of head cut, approximately 40 feet from the crest.

Subsequent Investigations

Geologic and Geotechnical: Prior to the erosion of the Cottonwood Creek spillway in 2009, spillway erosion had been identified as a possible failure mechanism at Pipestem Dam during the Screening Portfolio Risk Assessment done in 2007. However, no analysis of the erosion potential had been conducted prior to 2009.

Following the erosion of the Cottonwood Creek spillway in 2009, awareness of the potential for spillway erosion was greatly heightened. In 2011, some preliminary spillway erosion analyses were performed using SITES (USDA 2004), assuming some generic physical soil properties typical of glacial till. Results showed the Pipestem spillway would fail not only under PMF conditions, but also under a low flow, long duration event with a flow volume estimated at a

0.2% ACE (or 500-year return interval). One of the recommendations of the study was to collect additional soil data to create a more detailed model of the subsurface layers and properties.

As a result of this recommendation, a field investigation was conducted in 2013 to support the study and model. Due to the size of the area and known variability of the subsurface materials, it was determined that the most efficient approach would be to first conduct a geophysical investigation of the entire spillway area using both 2D resistivity profiles and seismic refraction microtremor (ReMi) soundings. The geophysical results were then reviewed by the Omaha District geophysicist and dam safety engineer and targeted geotechnical boring locations were identified to verify and calibrate the geophysical data. This stepped approach was selected to provide maximum coverage of the spillway area with the geophysical data and confirmation and correlation of the geophysical results with the geotechnical borings. The geotechnical investigation was performed in August 2013 by the Omaha District drill crew.

A Headcut Erodibility Index Analysis Report was then prepared in 2013 using data from the geotechnical and geophysical reports. After the report was prepared however, additional laboratory testing was completed on samples collected during the 2013 geotechnical field investigation. In 2016, the original 2013 drilling logs and geologic profiles from the geotechnical field investigation report were revised to incorporate the results of the lab testing, which resulted in several changes to the geologic classifications.

In general, the geotechnical investigations show a discontinuous layer of surficial sands and silts, underlain by layers of glacial till clay and glacio-fluvial sands over the shale bedrock. These investigations appear to show a layer of glacio-fluvial sands over the shale bedrock under the entire spillway, ranging in thickness from 5 to more than 30 feet. A layer of glacial till then covers this layer of sands. However, beginning about one-third of the way across the spillway from right to left, a second layer of glacio-fluvial sands begins to appear, with a continuous layer from upstream to downstream extending over the left one-third of the spillway, with the thickness of the layer increasing and depth to layer decreasing from right to left. A representative profile is shown in Figure 4 and 3D representation in Figure 5. Overall results of the geotechnical investigations into the surficial sands, glacial clay tills and glacio-fluvial sands are presented in Table 1.

Table 1. Erodibility index and soil parameters of soil layers in spillway.

Material	Erodibility Index, K_h	Range % Passing #200 Sieve	Average % Passing #200 Sieve	Range % Clay-sized Particles	Average % Clay-sized Particles	Estimated dry density, lb/ft^3
Surficial Sand	0.05	14-77	32	4-18	10	110-115
Glacial Clay Till	0.10	48-99	69	16-66	34	90-105
Glacio-fluvial Sands	0.05	6-38	12	2-16	5	100-115

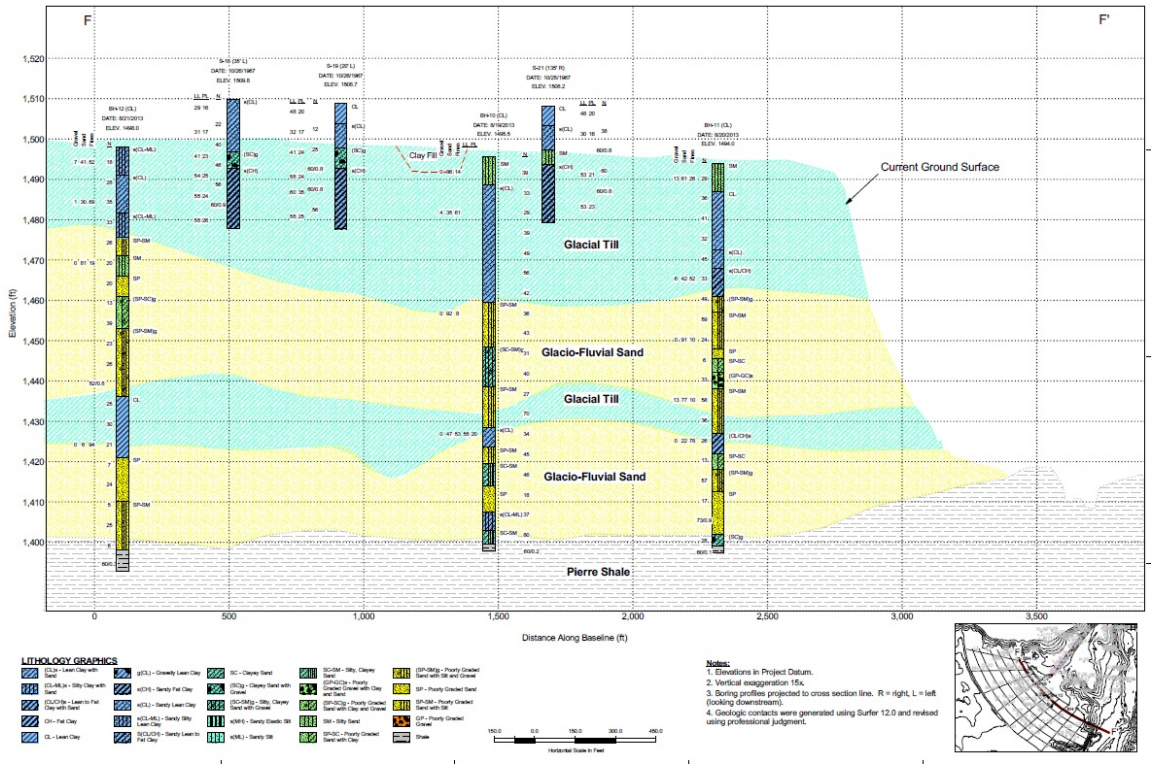

Figure 4. General soil layer representation along left side of spillway channel, showing layers of glacial till and glacio-fluvial sands.

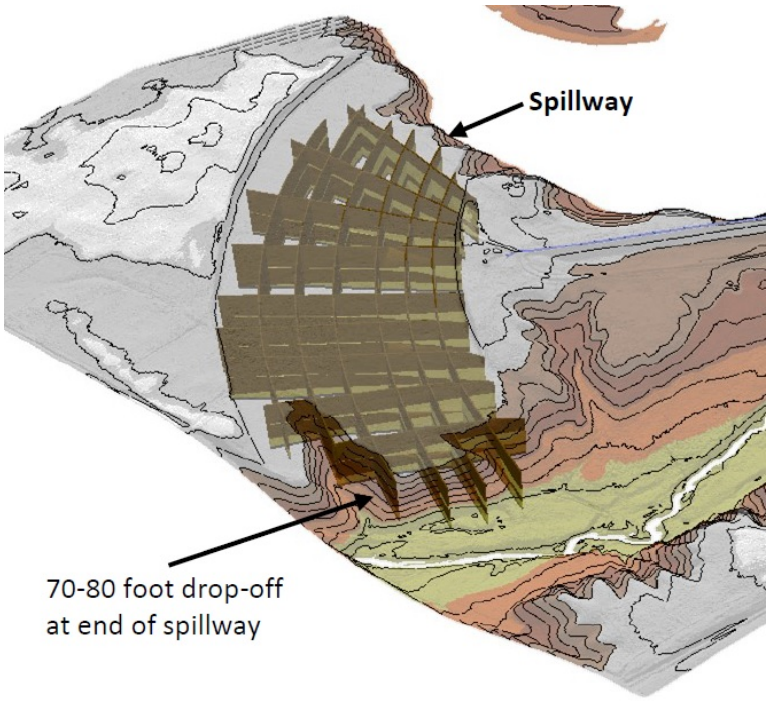

Figure 5. 3D Model with Fence Diagram Showing Spillway Geology (greenish-yellows represent glacio-fluvial sands, browns represent glacial till clays).

Hydrologic: As part of the Pipestem Issue Evaluation Study (IES), the IDF and hydrologic loading curve were updated in order to better assess hydrologic risk using current state of the practice methodologies. There were several reasons for updating the original IDF: 1) The original PMF was a rainfall only event with a basin average rainfall of 18.2 inches over 48 hours, while the updated all-season Probable Maximum Precipitation (PMP) had a basin average rainfall of 18.6 inches over 72 hours; 2) Although the original IDF was developed using a unit hydrograph derived from a 1950 snowmelt flood, antecedent Snow Water Equivalent (SWE) was not considered, so an antecedent SWE grid was developed for modeling the updated IDF; 3) ER 1110-2-8(FR) requires that the inflow unit hydrographs be peaked 25%-50% to account for expected non-linearity during extreme events, which was not done for the original IDF determination; 4) Infiltration rates in the original IDF were 0.3 in/hr, which was much higher than the calibrated loss rate of 0.02 in/hr for rain on snow events and 0.1 in/hr for rainfall only events determined during calibration; and 5) In the original IDF, Pipestem had a drainage area of 594 square miles, but, due to changes in the watershed and incorporation of surface storage into the hydrologic model, the updated drainage area (up to 1,028 square miles) was modeled as a dynamic parameter that varies with changes in assumed initial surface storage and effective basin precipitation.

Two runoff events were considered in updating the IDF: rainfall only and rain on snow. For a rainfall only PMF, an all-season PMP was developed according to Hydrometeorological Report (HMR) 52 standards with consideration of more recent events with a resulting basin average of 18.6 inches over 72 hours. Two rain on snow events were considered, April and May, and analysis showed that the April PMF was the critical rain on snow scenario. The April PMF utilized a 1% antecedent SWE of 8 inches, a seasonal April PMP developed using HMR 53 with a basin average rainfall of 9.6 inches over 72 hours, and an augmented temperature sequence derived from snowmelt temperatures in April 2009. The April rain on snow PMF utilized an antecedent pool at top of conservation storage (1442.5 ft), and the rainfall only PMF utilized an antecedent pool of 1499 ft. Infiltration rates varied for each runoff event based on calibration and sensitivity analysis. In the absence of a detailed unit hydrograph peaking study to better define a peaking factor, unit hydrograph peaking of 50% was applied to each subbasin. The rain on snow runoff event using 50% peaked unit hydrographs was recommended as the new IDF. The resulting Pipestem peak inflow is 124,950 cfs and the peak pool is 1507.4 feet LPD which provides 0.4 feet of freeboard, less than the minimum required of five feet. The peak 10-day volume is 653,810 ac-ft. Spillway flows would occur for approximately 20 days, assuming no breach and no outlet works releases, with a peak flow of 109,620 cfs.

Derivation of the updated hydrologic loading curve consisted of several steps. The first step involved computation of inflow volume-frequency curves for durations from 1-day to 20-days. Two gages on Pipestem Creek upstream of Pipestem Dam were used to extend the observed period of record back to 1950, and estimates of historic floods in 1882, 1897, 1902, 1919 and 1948 were used as perception thresholds. Results of the inflow-volume-duration analysis, as well as daily pool elevation since 1974, were then utilized in a stochastic model, RMC-RFA, to simulate multiple inflow hydrographs, which are then routed to obtain a multitude of peak pool values, which are then used to produce the best estimate of stage frequency. The results of the updated loading curve show the spillway crest to be exceeded on average once every sixty years, while the top of the dam could be expected to be reached on average once every 43,900 years.

Spillway Erosion Analysis

HEC-RAS (1-dimensional and 2-dimensional)

A steady flow, one-dimensional HEC-RAS model of the spillway was developed using survey data for the spillway, extending from the pool downstream to the valley floor at the terminus of the spillway exit channel. The downstream boundary condition was set to critical depth at the end of the exit channel. The actual downstream boundary is irregular and two-dimensional; forcing the downstream boundary at critical depth at a single cross-section was a simplification, but does not have a major effect on the computed energy slope in the upstream 0.2% exit channel. Manning's n values were set to 0.03 (as used in the original design). It should also be noted that the Manning's n value of 0.03 is considered appropriate for vegetal retardances 'C' and 'D' as the product of velocity and hydraulic radius approach 10+. For lower discharges where the roughness of the vegetation impacts flow in the channel, "n" values developed from retardance curves were also analyzed. The energy slope and maximum flow depth were determined from the HEC-RAS model.

A 2-dimensional HEC-RAS model of the Pipestem spillway was constructed to estimate the spatial variations in velocity and shear stress across a range of flows for the spillway. The downstream limit of the excavated spillway channel was used as the downstream boundary condition to eliminate to the greatest extent possible model instabilities created by overly steep terrain where the spillway channel drops into the valley of Pipestem Creek. The basic mesh was created with 50-ft by 50-ft elements; the mesh was refined with breaklines where there were significant breaks in slope at the edge of road features found crossing the spillway channel. Terrain data was taken from a Digital Elevation Model (DEM) with 1-meter resolution. The upstream boundary condition was assigned a flow hydrograph, while the downstream boundary condition was assigned a normal depth slope of 0.0025, slightly greater than the general slope of the spillway channel. Critical depth would be the optimal downstream boundary condition; however, 2D areas in HEC-RAS do not allow for a critical depth boundary condition. Steady flows between 500 and 50,000 cfs were modeled, as well as the PMF hydrograph. The 2D mesh is shown in Figure 6.

Computing Permissible Velocity, Erosional Effective Shear Stress and Stream Power: The erosion process can be described in three phases: 1) erosion through the vegetal cover; 2) vertical erosion of the material directly below the vegetal cover; and 3) upstream advancement of the head cut through the length of the spillway. The 1D and 2D HEC-RAS models were utilized to compute velocity, shear stress and stream power, which can be considered surrogates for indirectly estimating each of the three phases. The 1D model was used to estimate these three parameters on the steep exit slope, while the 2D model was used to estimate these three parameters at the heads of three gullies (see Figure 6 for locations) and on the 0.2% slope from the reservoir pool to the break in grade at the downstream extent of the 0.2% slope.

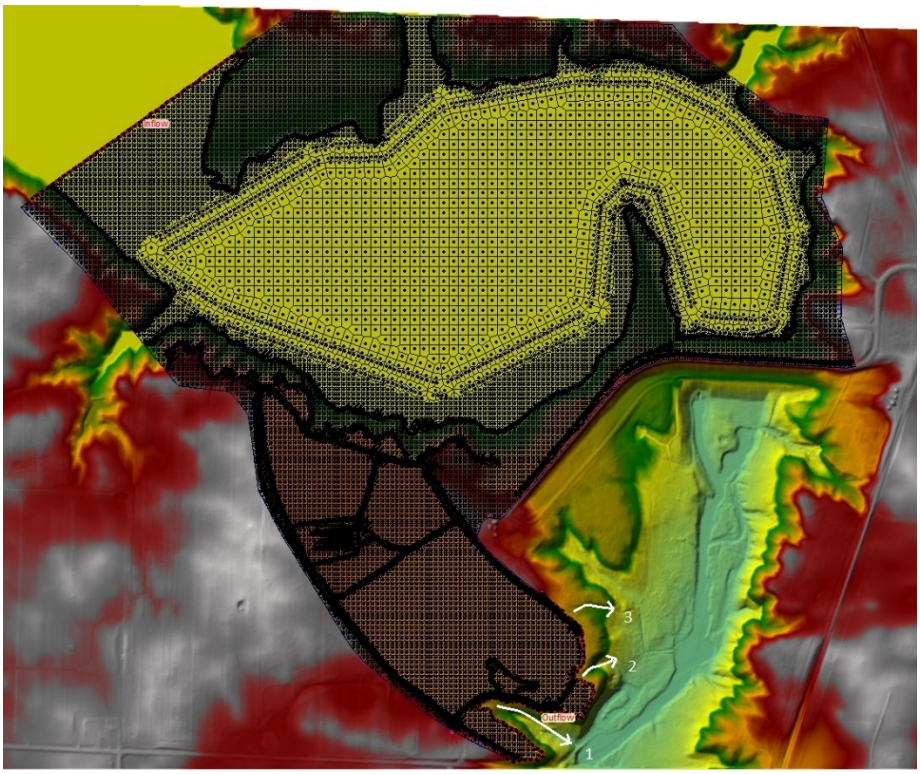

Figure 6. 2D HEC-RAS Mesh and Locations of Three Gullies at Spillway Exit.

Values for maximum permissible velocities of vegetated channels were taken from SCS-TP-61 (SCS, 1947), EM 1110-2-1601 (USACE, 1991) and Stream Restoration Design (NRCS, 2007) and compared against the HEC-RAS results. Results in excess of the maximum permissible velocity could be considered capable of vegetal cover removal. 1D results on the steep exit slope demonstrated that vegetal cover could be removed at flows in excess of 1,000 cfs (neglecting effects of flow concentration due to existing gullies), while the 2D model showed vegetal cover could be removed at the head of Gully 3 when flows exceed 500 cfs, at the head of Gully 1 when flows exceed 1,000 cfs and at the head of Gully 2 only when flows exceed 3,000 cfs. Velocities sufficient to remove vegetal cover along the entire length of the spillway do not occur until flows exceed 20,000 cfs. It is important to note that the headcut phase can progress upstream even if upstream vegetal cover has not yet been removed, however. Similar results were found when using shear stress and stream power in evaluating downcutting (soil detachment) and headcut advancement, respectively.

Pros and Cons of Using HEC-RAS: A 1D model is advantageous in that it is quick and easy to set up and evaluate velocity/shear stress/stream power. The 1D model however can only show variability of these parameters in the longitudinal direction, not the lateral direction. The advantage of utilizing 2D HEC-RAS was that it allowed for a spatially varied assessment of differences in velocity/shear stress/stream power in both the lateral and longitudinal directions. This was especially effective for Pipestem spillway, as the results demonstrated that the highest values of velocity/shear stress/stream power were on the entire left side of the spillway, co-located with the shortest erosion path and most erodible materials, over the entire range of flows modeled. It had the added benefit of being able to visually present the results of the analysis to the entire team in a manner in which the team could understand (see Figure 7 for

examples of velocity plot). The 2D results also highlighted the potential for erosion in Gully 3, which had not previously been considered a gully of concern due to its less pronounced appearance in comparison to Gullies 1 and 2. The disadvantage of both 1D and 2D HEC-RAS is that these models cannot directly estimate the erosion rate of the various materials in order to predict whether the spillway would breach or not. WinDAM, described below, was used to estimate erosion rate of the spillway and predict possible breach of the spillway crest.

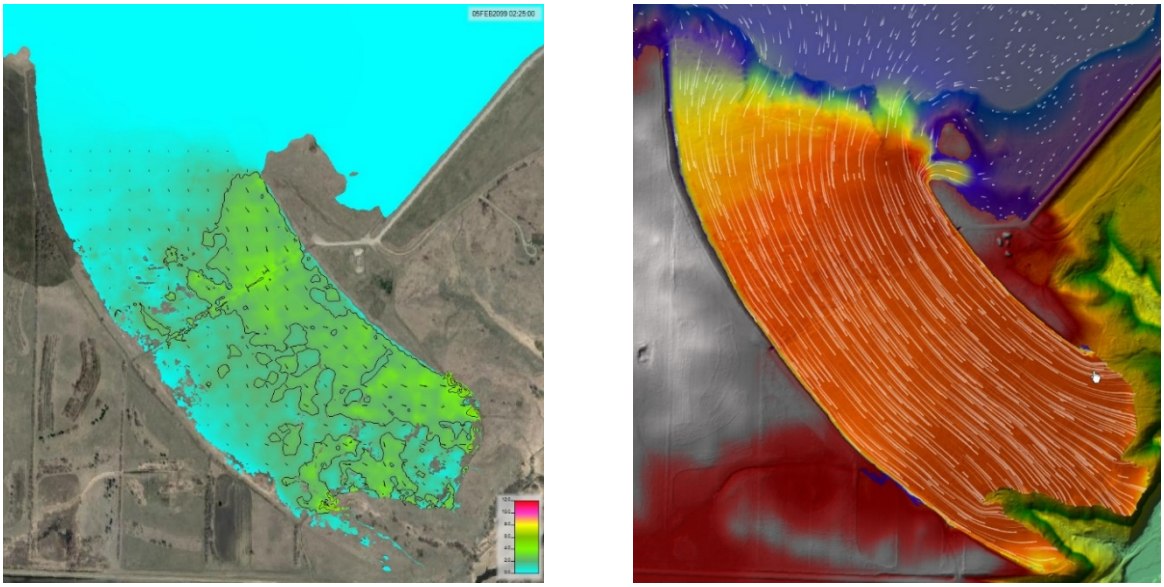

Figure 7. Visualizing Velocity: Velocity Vectors and Contours, 2,000 cfs (left), and Particle Tracing and Velocity Magnitude shading, PMF Pool (right).

WinDAM

WinDAM can be used to model erosion in earthen embankments as well as erosion in earthen auxiliary spillways of dams. The program utilizes a three-phase erosion model: Phase One of the erosion or failure process is failure of the vegetal cover and development of concentrated flow; Phase Two is downward erosion in the area of concentrated flow, resulting in headcut formation; and Phase Three is downward and upstream movement of the headcut, potentially breaching the spillway or embankment. Each phase is described by a set of threshold-rate relationships based on the process mechanics. A headcut erodibility index (K_h) describes the resistance of the exposed geologic materials to erosive attack during the third phase of the process.

Spillway erosion modeling for Pipestem Dam had previously been performed in 2011 and 2015, which indicated the spillway would be expected to fail under PMF flow conditions. However, there was a reduced level of confidence in the model results showing failure at long duration, low flow conditions. In order to improve confidence in the modeling of spillway erosion at Pipestem Dam, calibration to the observed 2009 Cottonwood Creek Dam spillway erosion was performed. The results of the calibration were then used to inform the modeling of the Pipestem spillway.

Cottonwood Creek Calibration: There was limited information available, so best estimates of spillway geometry, spillway flow and material properties based on satellite imagery,

photos, brief survey notes, Pipestem geotechnical information, and as-built drawings were made. The duration of flow through the spillway was estimated at 354 hours, without breaching; however, it is unknown if the various methods of intervention actually prevented breach. WinDAM is not able to simulate the intervention methods attempted. Very little is known about the depth or quantity of flow in the first two-thirds of the flow event, and there is conflicting information about the quantity of flow over the final one-third of the event.

A single layer of glacial till material was assumed. Various soil parameters are required, including dry bulk density, percent clay, headcut erodibility, plasticity index, and particle diameter. Values from Pipestem borings were input to the WinDAM model to evaluate the sensitivity of each parameter to the modeled time to breach; the range in values for some of these parameters is shown in Table 2. All combinations of parameters tested resulted in the spillway breaching in much less than 354 hours. A literature search was performed to determine the most likely absolute minimum and maximum values for lean clay (CL), which was what the limited boring information from Cottonwood Creek spillway showed for material type, and these ranges in values are also shown in Table 2.

Table 2. Range for subsurface materials used for Cottonwood Creek Dam.

	Headcut Erodibility Index	Percent Clay, %	Dry Density, lb/ft^3
From Pipestem Dam	0.05-0.1	5-34	90-115
Absolute Minimum and Maximum from Literature	0.05-0.17	4-66	60-148

Further sensitivity testing demonstrated that the three parameters shown in Table 2 had the greatest impact on the computed time to breach, so all further computations focused on varying just these three parameters. Various combinations of these three parameters that did not result in breach in 354 hours were determined. Two combinations that most closely matched the observed final headcut approaching within 50 feet of the crest were: 1) using the absolute maximum values for headcut index (0.17) and percent clay (66%) with a dry density of 120 lb/ft^3, and 2) using Pipestem maximum values for headcut index (0.1) and percent clay (34%) with a dry density of 139 lb/ft^3. A visual representation of the spillway erosion modeled by WinDAM for the second combination is shown in Figure 8.

Modeling Pipestem Dam spillway erosion: The most critical erosion path was determined to be 3,300 feet in length, based on results of the 2D HEC-RAS modeling which showed the left side of the spillway with the highest velocities, as well as having the greatest total depth of glacio-fluvial sands based on the geotechnical investigations. The spillway profile was modeled with two layers each of glacial till and glacio-fluvial sands, similar to that shown in Figure 4. Material values based on the 2013 geotechnical investigations were used to estimate the erodibility of the spillway, with the headcut index and percent clay showing the most sensitivity to the rate of erosion.

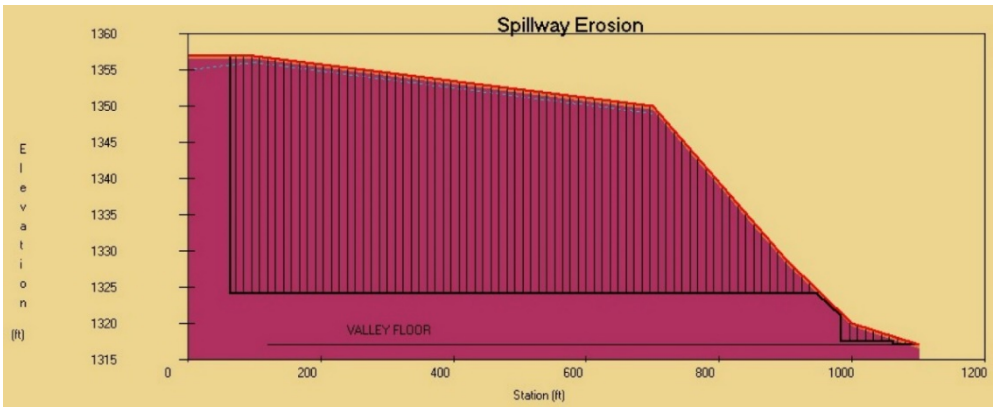

Figure 8. WinDAM representation of Cottonwood Creek spillway erosion (hatched area) with Pipestem maximum values for headcut index and percent clay with dry density of 139 lb/ft^3.

For purposes of the risk assessment, headcut index values were increased by 50% above the maximum values reported in the geotechnical report, since the absolute maximum values used to calibrate the Cottonwood Creek spillway erosion modeling were about 50% greater than the maximum Pipestem values computed in the geotechnical report. Inflow hydrographs were based on scaling the rain only PMF and rain on snow PMF hydrographs to produce a peak spillway flow of 1,000 cfs, 7,500 cfs, 15,000 cfs, 30,000 cfs, 45,000 cfs, 60,000 cfs, 120,000 cfs or 180,000 cfs, with the antecedent pool at either the conservation pool or the spillway crest; various combinations of ranges of parameters were utilized as well. The results could then be presented either in tabular or graphical format showing time to breach for each flow condition (Figure 9, left) or in a graphical hydrograph format that visually showed where the breach might occur relative to the timing of the peak outflow (Figure 9, right). The WinDAM results showed that breach of the spillway is likely to highly likely when the pool exceeds a 1% ACE pool level.

	Peak Discharge, Kcfs							
	1 K	7.5 K	15K	30 K	45 K	60 K	120 K *	180 K *
HIGH	No Breach	267	207	163	144	126	90	80
MEDIUM	No Breach	230	190	154	137	123	89	80
LOW	298	213	180	148	133	122	89	80

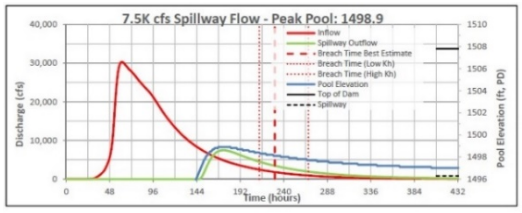

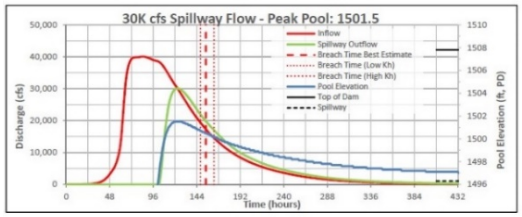

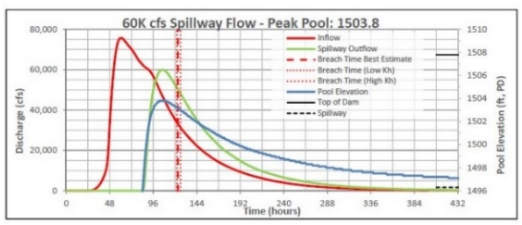

Figure 9. Different Ways in Which Spillway Breach Information Could Be Represented, with Results over Full Range of Flows (left) and Specific Flows (right).

Conclusions

Pipestem Dam has an unlined earthen spillway with no positive cutoff to prevent erosion. The nearby Cottonwood Creek Dam, with similar geology and no positive cutoff, suffered extensive erosion at low flow rates, raising concerns for the unlined spillway at Pipestem Dam and leading to studies of erosion potential at Pipestem. 1D and 2D HEC-RAS models of the spillway were used to evaluate velocity, shear stress and stream power in the spillway channel. Results of the 2D model were particularly beneficial in identifying a new potential headcut initiation point at the spillway exit, as well as identifying the areas where allowable and permissible velocities and shear stress were first exceeded, as well as the discharges when vegetation and soil removal would initiate, and that these discharges correlated well with the results of the calibrated WinDAM model. The results of the 2D model demonstrated that the areas most likely to first experience erosive flows coincided with the areas of the spillway with surficial sands present as well as greatest depth of the highly erodible subsurface glacio-fluvial sands. WinDAM results demonstrated that spillway erosion may be a concern at flows in excess of 1,000 cfs and that the spillway may breach at frequent pool levels. The results of this multi-pronged approach to evaluating spillway erosion were extremely useful in identifying spillway erosion as a dam safety risk above Tolerable Risk Guidelines, leading to a recommendation to proceed to a Dam Safety Modification Study to develop alternatives to address spillway erosion. The methods presented herein should be applicable to evaluating erosion of other unlined spillways.

References

North Dakota State Water Commission 1972. "Cottonwood Creek Project No. 1515 As-Built Drawings," North Dakota State Water Commission, Bismarck, ND.

NRCS 2007. "Stream Restoration Design, U.S. Department of Agriculture, Natural Resources Conservation Service, National Engineering Handbook, Part 654," Washington, D.C.

SCS 1947. "SCS-TP-61, Handbook of Channel Design for Soil and Water Conservation," Soil Conservation Service, U.S. Department of Agriculture, Washington, D.C., Revised 1954.

U.S. Army Corps of Engineers 1991. "Engineer Manual 1110-2-1601, Hydraulic Design of Flood Control Channels," U.S. Army Corps of Engineers, Washington, D.C., Revised 1994.

U.S. Army Corps of Engineers 1967. "Pipestem Creek Dam and Reservoir, Design Memorandum (DM) No. JP-1," U.S. Army Corps of Engineers, Omaha, NE.

U.S. Army Corps of Engineers 1969. "Pipestem Creek Dam and Reservoir, General Design Memorandum No. JP-3," U.S. Army Corps of Engineers, Omaha, NE.

U.S. Army Corps of Engineers 1970. "Pipestem Creek Dam and Reservoir, Design Memorandum No. JP-5," U.S. Army Corps of Engineers, Omaha, NE.

U.S. Army Corps of Engineers 1975. "Preliminary Reservoir Regulation Manual for Pipestem Dam and Lake, North Dakota," U.S. Army Corps of Engineers, Omaha, NE.

U.S. Army Corps of Engineers 2017. "Headcut Erodibility Index Analysis, Pipestem Dam Emergency Spillway, Final Revised Report," U.S. Army Corps of Engineers, Omaha, NE.

U.S. Army Corps of Engineers, Hydrologic Engineering Center 2016. "HEC-RAS, River Analysis System User's Manual, Version 5.0," Hydrologic Engineering Center, Davis, CA.

U.S. Department of Agriculture, et al 2004. "SITES Spillway Erosion Analysis with Latin Hypercube Sampling (SSEA + LHS), Beta Version, User's Manual," U.S. Department of Agriculture, Washington, D.C.

U.S. Department of Agriculture, Agricultural Research Service and Kansas State University 2012. "WinDAM-B, Version 1.1, Computer Program Release," U.S. Department of Agriculture, Washington, D.C.

Soil Characteristics of Selected Earthen Dams in the State of Mississippi

Yavuz Ozeren, Research Assistant Professor, NCCHE, The University of Mississippi, University, MS, yozeren@ncche.olemiss.edu
Mustafa Altinakar, Research Professor, NCCHE, The University of Mississippi, University, MS, altinakar@ncche.olemiss.edu
Dusty Myers, Chief of the Dam Safety Division, Mississippi Department of Environmental Quality, Jackson, MS, dmyers@mdeq.ms.gov
Daniel Wren, Research Hydraulic Engineer, USDA-ARS National Sedimentation Laboratory, Oxford, MS, Daniel.Wren@ars.usda.gov

Abstract

As part of a multi-component research project that concerns the improvement of semi-empirical equations used to estimate breach parameters for embankment dams, a series of field surveys were carried out at sixteen earthen dams throughout the state of Mississippi. Soil samples were collected at each dam for jet testing, bulk density measurements, and soil texture analysis. The jet testing was used to find the critical shear stress and erodibility coefficient of the soil. Bulk density measurements, sieve analysis and pipette testing for soil texture for finer particles were performed at the USDA-ARS National Sedimentation Laboratory. The data will be used in a numerical model study to develop parametric breach equations that take in to account geophysical and geotechnical characteristics of dams. This paper summarizes the results of these field and laboratory tests.

Measurements and Results

Soil samples were collected at sixteen earthen dams in the state of Mississippi. 6-in diameter, 6-in high cylindrical cores were collected from each dam for jet testing (JET), and 2-in diameter, 2-in long cylindrical cores were collected for soil texture and bulk density (BD) measurements. The list of dams and number of collected samples are presented in Table 1.

Table 1. List of dams and the total number of collected samples

State ID	County	# of JET samples	# of BD samples
MS02667	Lauderdale	3	9
MS02756	Lauderdale	3	6
MS06155	Lauderdale	3	6
MS03385	Oktibbeha	3	6
MS00344	Oktibbeha	3	6
MS02473	Forrest	2	4
MS00132	Lamar	2	4
MS02472	Forrest	2	4

State ID	County	# of JET samples	# of BD samples
MS01305	Rankin	2	4
MS03249	Hinds	2	4
MS01743	Hinds	2	4
MS01790	Hinds	2	4
MS01259	Rankin	2	4
MS03104	Lafayette	2	4
MS02734	Panola	2	4
MS03301	Lafayette	2	4

Both JET and BD samples were collected approximately 6 inches below the surface of the dam, near the mid-section. One of each JET and BD samples were collected from the downstream sloping face of each dam. The soil tests were performed at the USDA-ARS, National Sedimentation Laboratory in Oxford, MS. The 2-in diameter samples were used to obtain bulk-density, soil texture through pipette analysis, and particle-size distribution through sieve analysis. The 6-in dimeter samples provided erosion characteristics of each soil sample thorough standard Jet Erosion Test (Hanson and Cook, 2004).

The analysis results showed that the bulk densities of the soils varied between 1.1 g/cm^3 and 1.7 g/cm^3. Figure 1 shows the distribution of the 2-in samples on the soil texture triangle. The type of soils vary significantly across the selected sites but the sand and silt content was moderately high for some sites.

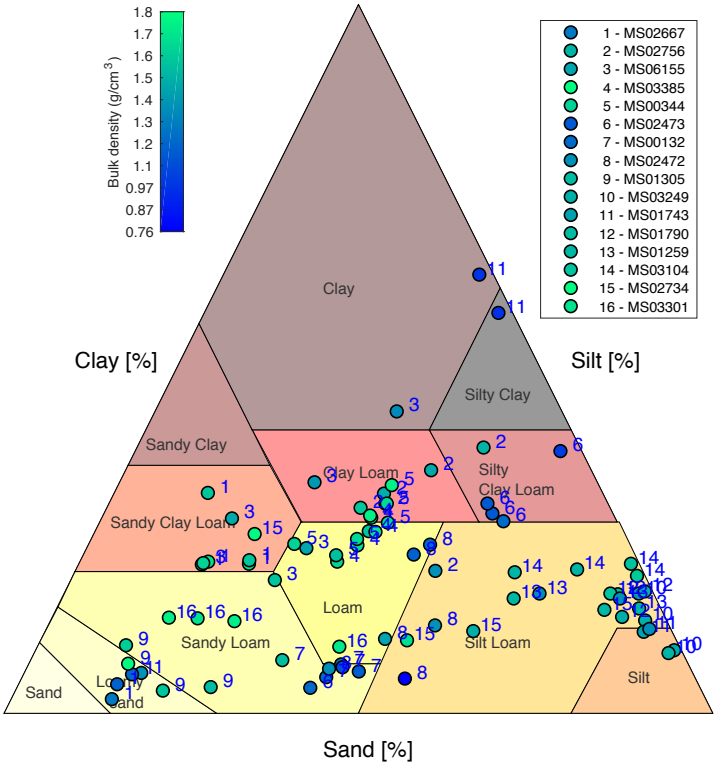

Figure 1. Soil texture and bulk density of soil samples from earthen embankments in Mississippi. The site numbers in the legend correspond with those in Table 1.

Preliminary results show that JET measurements strongly depended on the initial head chosen. If the initial head was too high, the soil specimen eroded too quickly, preventing the collection of sufficient data for predicting erosion parameters. Dense, fibrous root networks in the soils limited soil detachment in the upper layers and reduced erodibility. Consolidated soils with high clay content were eroded slowly and created shallow scour holes using the standard jet test device. The small values of scour depth for the high-clay samples, which were difficult to measure accurately, led to higher measurement errors. Figure 2 shows the erodibility coefficients, and Figure 3 shows the critical shear stresses of the 6-in samples based on three methods used to determine the erodibility coefficient, k_d, and the critical shear stress, τ_c. In Blaisdell method, the equilibrium depth was determined using a nonlinear regression of a

logarithmic-hyperbolic function to the scour depth time series, and the erodibility coefficient, k_d was determined by curve-fitting measured values of scour depth versus time, and minimizing the error of the measured time versus the predicted time. In iterative method, first, k_d and τ_c values were determined using the Blaisdell solution. Then, an upper bound was computed for τ_c. Finally, a simultaneous solution that minimized the root-mean-square error between the measured and predicted time was obtained for both k_d and τ_c. Linear method simply used a logarithmic fit to the erosion rate and time data to estimate the k_d and τ_c values.

In spite of the uncertainties involved, the data revealed that there is an inverse relationship between the erodibility coefficient and critical shear stress estimates from the jet erosion tests. Older dams with consolidated clay had relatively lower erodibility and higher critical shear stress. Erodibility and critical shear stress estimates in these plots vary within an order of magnitude, and in general there is an inverse relationship between the critical shear stress and the erodibility coefficient, such that the soils with critical shear stress tend to have lower erodibility coefficients. The results demonstrate the potential for measuring the erodibility of dams through laboratory testing and also provide a database that can be used in efforts to model breaches in existing dams.

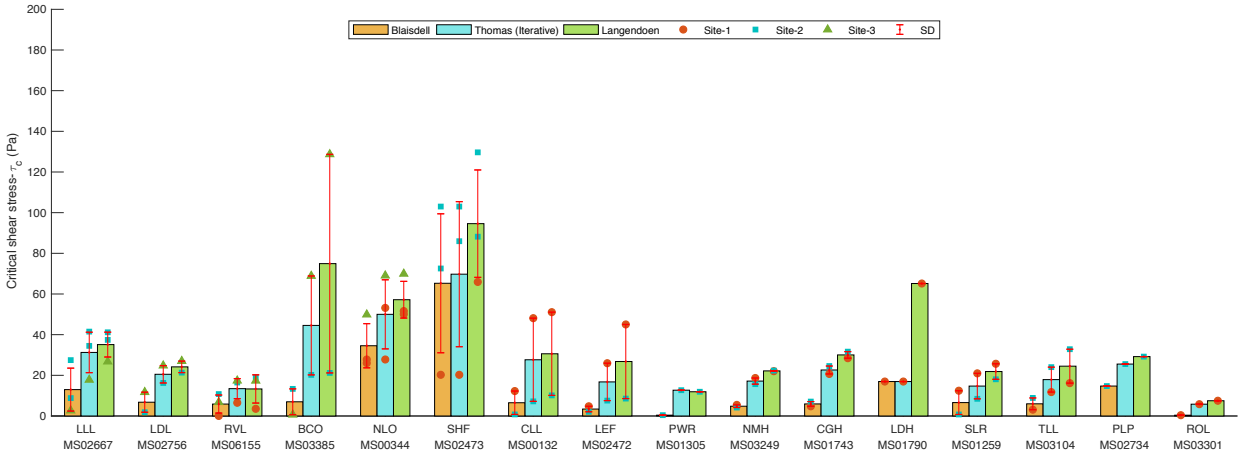

Figure 2. Critical shear stress estimates from JET tests on intact soil samples collected from 16 earthen dams in Mississippi.

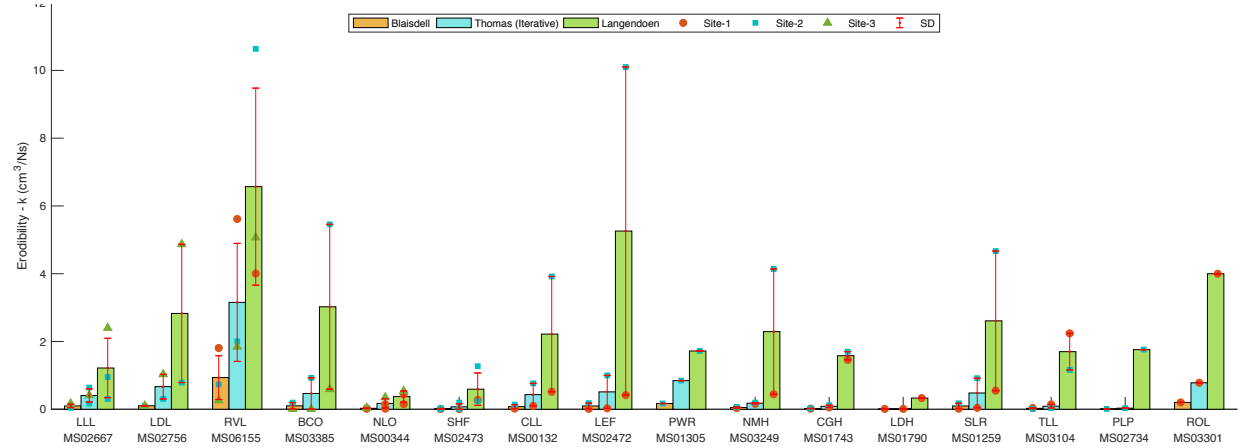

Figure 3. Soil erodibility estimates from JET testing of earthen dams in Mississippi.

References

Hanson, G. J., and Cook, K. R. 2004. “Apparatus, test procedures and analytical methods to measure soil erodibility in situ,” Applied engineering in agriculture, 20(4), 455–462.

Toutle River Debris Flows Initiated by Pacific Northwest Atmospheric Rivers: November 2006

Adam R. Mosbrucker, US Geological Survey, Vancouver, WA, amosbrucker@usgs.gov
Kurt R. Spicer, US Geological Survey, Vancouver, WA, krspicer@usgs.gov
Jon J. Major, US Geological Survey, Vancouver, WA, jjmajor@usgs.gov

Introduction

In early November, 2006, an atmospheric river brought heavy rainfall and high freezing levels to the Pacific Northwest. Without snowpack to buffer the hydrologic response, the storm caused widespread landslides and debris flows in drainages sourced from every central Cascades volcano. At Mount St. Helens, in southwestern Washington State, intense rainfall in the crater of the volcano caused at least two mass failures with an aggregate volume of 4.5 million m^3, which spawned a series of debris flows with velocities as great as 11 m/s. The debris flows incised Loowit Creek as much as 9 m and traveled 16 river km before transforming to hyperconcentrated flow via rapid dilution at the confluence of North Fork Toutle River (NFT), Castle Creek, and Maratta Creek (Figure 1). Reduced channel gradient downstream lowered velocity enough to transform to sediment-laden streamflow less than 40 km from the source, where suspended-sediment concentration (SSC) peaked at 177,000 mg/L. Heavy rain persisted for several days, producing over 100 cm of rainfall in upper NFT basin which caused immediate remobilization of surface deposits; half of the annual suspended-sediment discharge (SSQ) for water year (WY) 2007 was transported in 5 days, despite a relatively low 7-year flood recurrence interval.

This analysis expands upon Major et al. (2005), Pitlick et al. (2007), and Olsen (2011) to document the largest suite of rainfall-triggered debris flows identified to date at Mount St. Helens. We investigate debris flow initiation, velocity, deposition, and downstream sediment flux in the NFT basin by integrating data from near real-time monitoring stations, remote sensing, terrestrial surveying, and fluvial sediment samples.

Study Area Background

The cataclysmic eruption of Mount St. Helens on 18 May 1980 devastated the 378-km^2 upper NFT basin and severely altered the hydrogeomorphic regime in the upper 24 km of the river where a 2.5-km^3 debris avalanche buried the valley to a mean depth of 45 m. Syneruptive debris flows caused by local liquefaction of the avalanche deposit transported 120–140 million m^3 of sediment more than 100 km downstream (Major et al. 2005).

Formed in fall 1980, Loowit and Step Creeks, headwaters of the NFT, originate as glacier meltwater and magmatically-heated springs on the crater floor. The steep upper channels, incised into non-cohesive pyroclastic flow, debris-avalanche, and ancient lava-dome deposits, have been a primary sediment source for many post-1980 debris flows. Some debris flows were caused by episodic, eruption-triggered floods developed from rapid snowmelt. The largest (10–20 million m^3), on 19 March 1982, was caused by the breaching of an eruption-induced meltwater lake in the crater (Waitt et al. 1983). Since the late 1980s, debris flows have been unrelated to eruptive activity, instead caused by rainfall-triggered landslides or glacial outburst

floods. For example, on 16 September 1997, intense rainfall elevated groundwater pressures and caused two large failures near the head of Loowit channel spawning a series of debris flows with an aggregate volume ~200,000 m^3 (Major et al. 2005), which traveled 2–3 km and left 10-m-tall levees along Loowit channel before its deposit avulsed the creek into Spirit Lake to the east. A smaller debris flow in October 2004 avulsed the creek back to the NFT where it remained until it returned to a previously occupied channel to the north during a debris flow/flood event in November 2006.

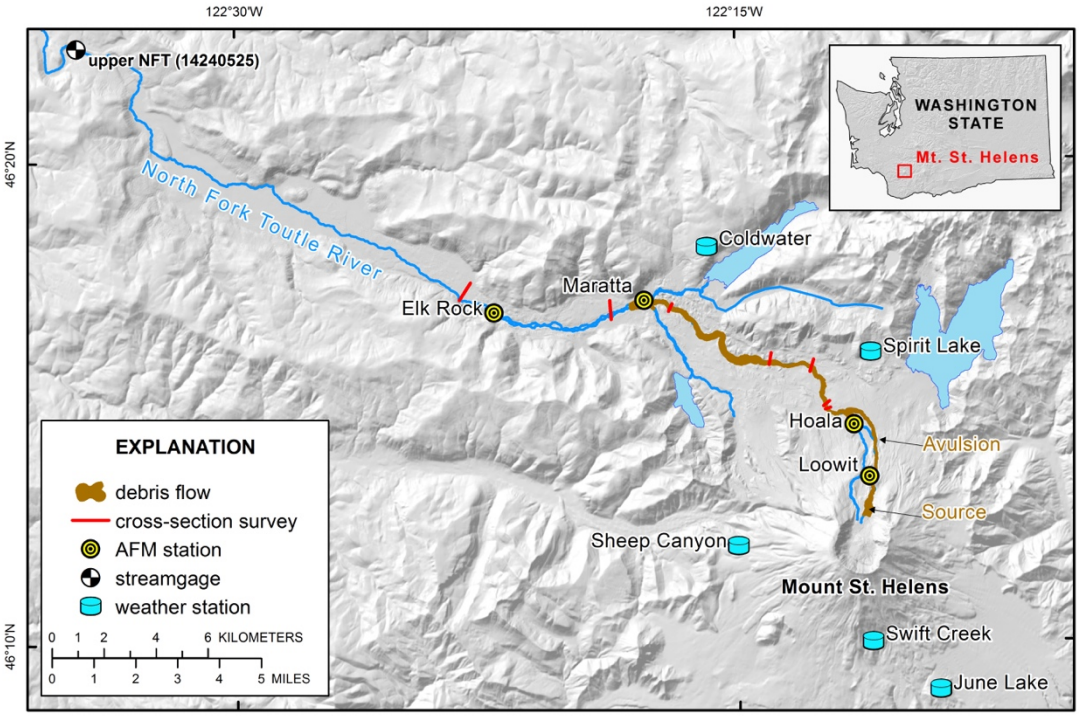

Figure 1. Location map of North Fork Toutle River showing source of debris flows and runout, acoustic flow monitoring (AFM) stations, weather stations operated by Natural Resources Conservation Service and Northwest Avalanche Center (five additional stations are beyond map extent), channel cross sections, and upper NFT gage.

Precipitation

Weather stations at Mount St. Helens provide detailed information about an exceptional atmospheric-induced storm in November 2006 (Neiman et al. 2008). A temperature inversion above an elevation of 1,200 m kept regional snow levels nearly 500 m above the summit for the duration of the storm; a cold front lowered the snow level to 1,000 m elevation on 9 November (Figure 2). Typical of atmospheric river events, stations recorded a directional component; south-facing slopes received the greatest amount of rainfall where maximum daily precipitation was 37.1 cm on 6 November (Figure 1; June Lake; 1,050 m elevation). Storm total rainfall in the NFT basin was 39 cm in the valley and 101 cm in the crater based on spatial interpolation between weather stations (n=10), representing 20–30% of mean annual precipitation (1981–2010).

Debris Flows

Cascades volcanoes continue to experience frequent debris flows unassociated with volcanic activity (Burns et al. 2015). Deposits from many of these events are not easily distinguished after a few months. Research at Mount St. Helens is supported by an extensive network of long-term hydrologic and geomorphic monitoring stations, field surveys, and remote sensing data collections, which we leverage here.

To identify the primary source area of the 2006 debris flows and calculate initial volume, we used aerial photographs acquired on 21 October and 6 December 2006. The photographs provide evidence of two mass failures in the head of Loowit channel. Structure-from-Motion photogrammetry methods were used to construct digital surface models for each date. We calculated an aggregate mass failure volume of 4.5 million m^3 by differencing these pre- and post-event surface models.

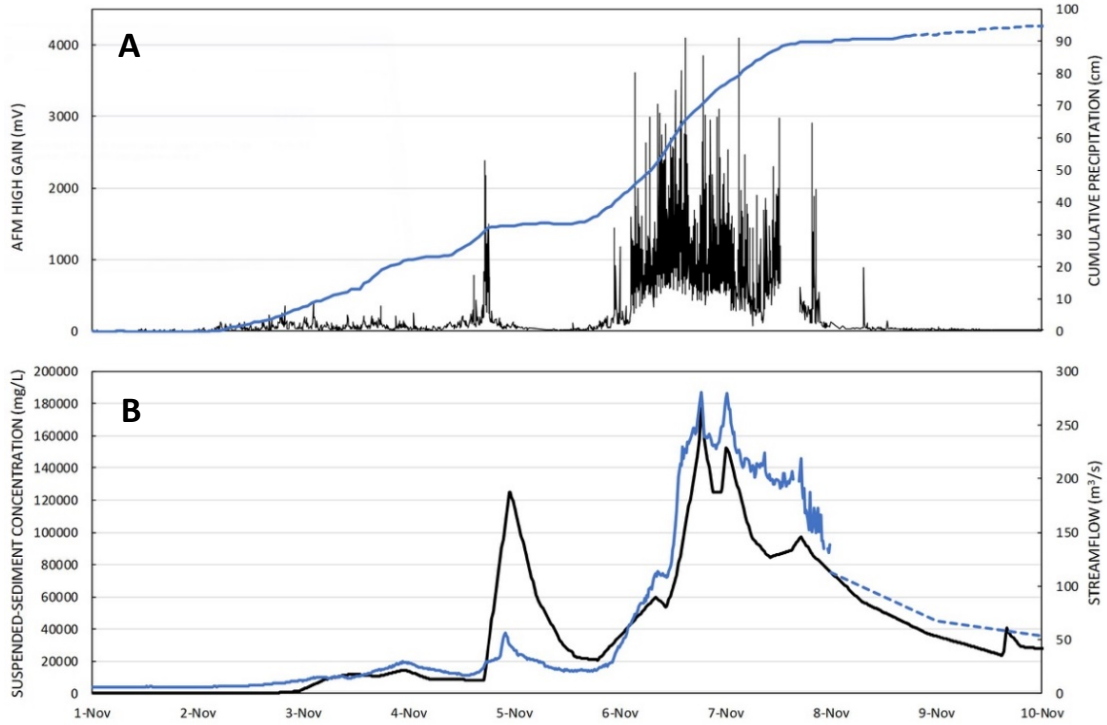

Figure 2. Time series of monitoring station data including (A) ground vibration at Loowit AFM (6-minute) and precipitation at Swift Creek (hourly; 1,350 m elevation; dashed line denotes transition to snowfall), and (B) suspended-sediment concentration and streamflow at the upper NFT gage (15-minute; dashed line denotes estimated daily streamflow due to instrument damage).

Debris flow velocity was calculated using time and distance between three acoustic flow monitor (AFM) stations located along Loowit Creek and NFT (Figure 1). AFM stations record amplitude, frequency, and duration of ground vibration caused by passing flows. The first flow was detected by Loowit AFM at 15:00 PST on 4 November (Figure 2). This discrete signal lasted 3 hours and was followed by a series of debris flows for nearly 44 additional hours (6–7 November). Velocities of these flows were 1.0–11.1 m/s in the steep upper reach (0.106 channel gradient; Loowit to Hoala AFM) and 1.3–6.3 m/s in the middle reach (0.038 gradient; Hoala to Maratta

AFM); mean velocity was 3.2 m/s. Debris flow likely transformed to hyperconcentrated flow in the lower reach (0.023 gradient) before reaching Elk Rock AFM, which was lost to bank erosion.

To map the extent of the debris-flow deposits, we used remote-sensing feature-extraction methods, lidar-surface differencing, and cross-sectional analysis. Feature-extraction combined object-based image analysis and supervised classification methods with artificial intelligence "learning" techniques to classify airborne lidar data integrated with multispectral satellite imagery. Classification resulted from training area characteristics being applied to this integrated dataset to extract, or identify, similar features throughout the channel. Surface roughness metrics (n=5), spectral signatures (n=8, 0.45–12.5 μm,), and lidar-return intensity were characterized at four field-surveyed training areas (0.024 km^2 total). Classification results (0.28 km^2 total) and lidar-differencing maps were field checked in September 2012; subsequent interpolation between deposits resulted in 1.79 km^2 of affected area following the avulsion of Loowit Creek (Figure 1).

Repeat stream-channel cross-section surveys, in addition to cross sections extracted from lidar data, allowed us to evaluate changes to cross-sectional area, erosion, and deposition at seven locations along Loowit Creek and upper NFT (Figure 1). We found channel incision at the upper four sections (2.5–9.0 m; 300–1,110 m^2 area increase) and deposition at the lower three sections (0.5–3.0 m; 70–90 m^2 area decrease). While this transition from erosion to deposition suggests flow bulking, it is difficult to quantify given the intensity and duration of rainfall across the basin which surely drove additional sediment production during and immediately after the debris flow events.

Streamflow and Suspended Sediment

During WY 2007, the USGS operated three surface water and suspended sediment gages in the Toutle River basin: the upper NFT gage (14240525), South Fork Toutle River gage (14241500), and the mainstem Toutle River gage (14242580). Annual mean water discharge at the NFT gage is 22.2 m^3/s, representing 37% of the annual mean at the Toutle River gage based on 30 years of cross-correlated record. During the November 2006 storm, water flow at the NFT gage had two discrete peaks (Figure 2). The initial flood surge (56.9 m^3/s peak streamflow at 22:00 PST followed by 125,000 mg/L maximum SSC at 23:00 PST) arrived 6 hours after the first debris flow was detected at Loowit AFM on 4 November, an average flow velocity of 2 m/s along 40 river km. The second and largest flood surge, at 18:30 PST on 6 November (281 m^3/s streamflow peak; 7-year recurrence interval), arrived 8 hours after the larger series of debris flows began. Maximum instantaneous SSC for the second peak reached 177,000 mg/L (9.6 vol% total suspended particles; 1.85 g/cm^3 debris avalanche bulk density). A sample of the peak flow deposit collected at the high-water line had a fine particle (<0.062 mm) concentration of 15.6 wt%, suggesting the hyperconcentrated flow upstream had likely transitioned to sediment-laden flood at the gage. Five days (6–10 November) account for 8% of the annual water discharged at the NFT gage but 47% of the annual SSQ during WY 2007 (6.38 million Mg). Frequent debris flows are just one process that elevates average annual suspended-sediment yields from the Toutle River basin (4,720 Mg/km^2) above pre-eruption yields.

Conclusions

In early November, 2006, an atmospheric river brought heavy rainfall and high freezing levels to the central Cascades volcanoes. Intense rainfall in the crater of Mount St. Helens caused at least

two mass failures with an aggregate volume of 4.5 million m^3, which sent a series of debris flows into the upper North Fork Toutle River. With velocities as great as 11 m/s, debris flows incised the channel as much as 9 m and traveled 16 river km before transforming to hyperconcentrated flow via rapid dilution at the confluence of two tributaries. Reduced channel gradient downstream lowered velocity enough to transform flow to sediment-laden streamflow less than 40 km from the source, where suspended-sediment concentration peaked at 177,000 mg/L. With persistent heavy rainfall (>100 cm) in the basin, half of the annual suspended-sediment discharge for water year 2007 was transported in 5 days.

Our results indicate that November 2006 debris flows were significantly more fluid than September 1997 flows due to the storm having three times greater rainfall intensity. Although both events initiated in the head of Loowit channel as mass failures, the 1997 flows traveled only a few km despite having similar velocity (Major et al. 2005). The 2006 flows caused little disturbance to the tall 1997 levees and traveled at least 16 km downstream with an aggregate volume ~20 times greater.

Atmospheric rivers occur regularly in the Pacific Northwest, but antecedent conditions, such as snowpack and soil saturation, can affect the magnitude of disturbance and subsequent sediment yield from streams draining Cascades volcanoes.

References

Burns, S.F., Pirot, R., Williams, K., and Sobieschezk, S. 2015. “Massive debris flow event on Pacific Northwest volcanoes, USA, November 2006—Causes, effects, and relationship to climate change,” Proc. International Association of Engineering Geology and the Environment XII Congress, Torino, in Lollino, G. et al. (eds). 2015. Engineering Geology for Society and Territory-Volume 2. Springer, Cham.

Major, J.J., Pierson, T.C., and Scott, K.M. 2005. “Debris flows at Mount St. Helens, Washington, USA,” in Jakob, M. and Hungr, O. 2005. Debris-flow Hazards and Related Phenomena. Springer, Berlin, Heidelberg.

Neiman, P.J., Ralph, F.M., Wick, G.A., Kuo, Y.-H., Wee, T.-K., Ma, Z., Taylor, G.H., and Dettinger, M.D. 2008. “Diagnosis of an intense atmospheric river impacting the Pacific Northwest—Storm summary and offshore vertical structure observed with COSMIC satellite retrievals,” Monthly Weather Review, 136:4398–4420.

Olsen, K.V. 2012. “Inventory and initiation zone characterization of debris flows on Mount St. Helens, Washington initiated during a major storm event in November, 2006,” Portland State University M.S. thesis.

Pitlick, J., Mueller, E.R., Spicer K., and Major J.J. 2007. “Response of the North Fork Toutle to November 2006 rainfall and flooding,” Proc. Geological Society of America Annual Meeting, Denver, Colorado, 39(6):178.

Waitt, R.B., Pierson, T.C., MacLeod, N.S., Janda, R.J., Voight, B., and Holcomb, R.T. 1983. “Eruption-triggered avalanche, flood, and lahar at Mount St. Helens—Effects of winter snowpack,” Science, 221:1394–1397.

Extreme Floods & Droughts

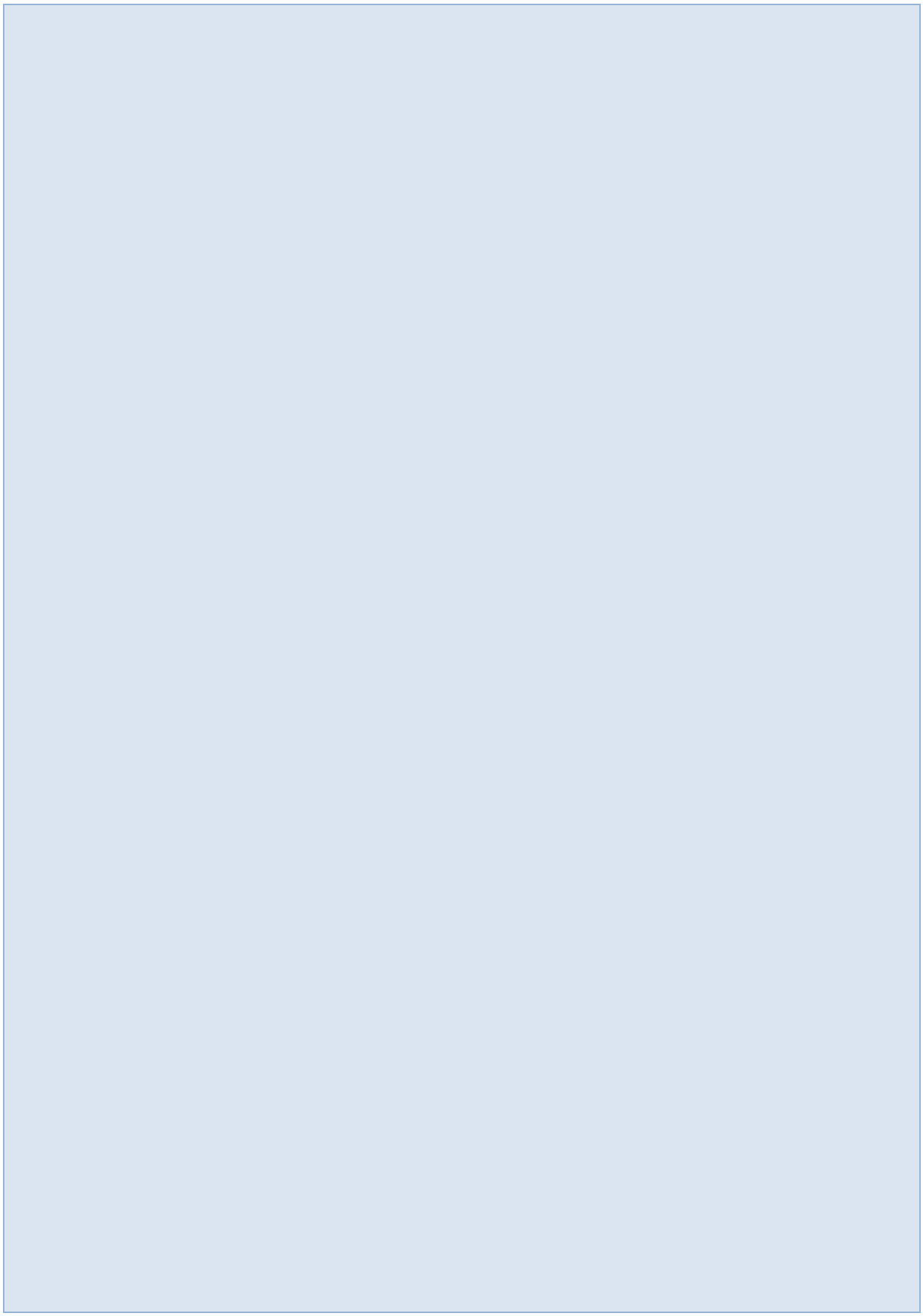

A Spatial Analysis of Extreme Precipitation in the Columbia River Basin

Brian Skahill, Civil Engineer, USACE Coastal and Hydraulics Laboratory, Portland, OR, Brian.E.Skahill@usace.army.mil
Angela Duren, P.E., P.H., Senior Hydrologist, USACE Northwestern Division, Portland, OR, Angela.M.Duren@usace.army.mil
Luciana Cunha, Ph.D., P.H., Senior Engineer, West Consultants, Folsom, CA, lcunha@westconsultants.com
Chris D. Bahner, P.E. D.WRE, Senior Project Manager, West Consultants, Salem, OR, cbahner@westconsultants.com

Abstract

Current Columbia River Basin (CRB) hydrology studies managed by the Northwestern Division of the US Army Corps of Engineers (USACE-NWD) include a key project task directed at the development of precipitation frequency estimates to support planning analyses throughout the CRB. The deployment of traditional L-moments based Regional Frequency Analysis (RFA) requires the study area to be decomposed into homogeneous sub-regions and this is highly problematical for the CRB hydrology studies due to the basin size and the physiographic and climatological variability which exists within the CRB. Moreover, depth-area reduction factors (ARFs) which are used to convert point rainfall depths to areal average depths for the same duration and recurrence interval suffer from being the same for all watersheds falling within a large region and they also do not provide a pattern of rainfall variation over space within the watershed. These technical barriers of traditional RFA are overcome by applying relatively recent advances in extreme value theory (EVT) which directly model the observed dependence among the pointwise maxima which must be accounted for to properly assess risk. These recent advances have demonstrated the capacity to efficiently, flexibly, and credibly model spatial extremes of pointwise maxima using max-stable processes, the stochastic process extension of EVT. With their application one can not only compute traditional pointwise return level maps leveraging readily available and relevant spatial and temporal covariate data for the trend surface modeling, but also by modeling the joint distribution, more complex areal-based assessments of risk such as

$$\Pr\left\{\int_{\mathcal{B}} \Upsilon(x)dx > z_{crit}\right\},$$

where $\Upsilon(x)$, $\mathcal{B}$, and z_{crit} denote the joint distribution, a sub-basin, for example, and a critical quantity greater than zero, respectively. Additionally, adherence to EVT enables for a mathematically consistent extrapolation beyond the range of the data. We will summarize the calculation of pointwise and areal-based exceedance probabilities of observed precipitation for the Columbia River Basin using a spatial max-stable process model and observed pointwise maxima data. In particular, we will discuss data collection and processing, analysis methods and their application, study products and their intended uses, and opportunities for future related work. Figures 1 – 6 relate to these noted activities and products that will be discussed and presented in more comprehensive detail during our presentation at SEDHY 2019. Of course, flood risk management in the CRB also requires the consideration of cool season processes. Comparable extreme value analysis of snow water equivalent data has yielded additional useful products to support cool season risk-informed hydrologic planning analyses across the CRB (Figure 7).

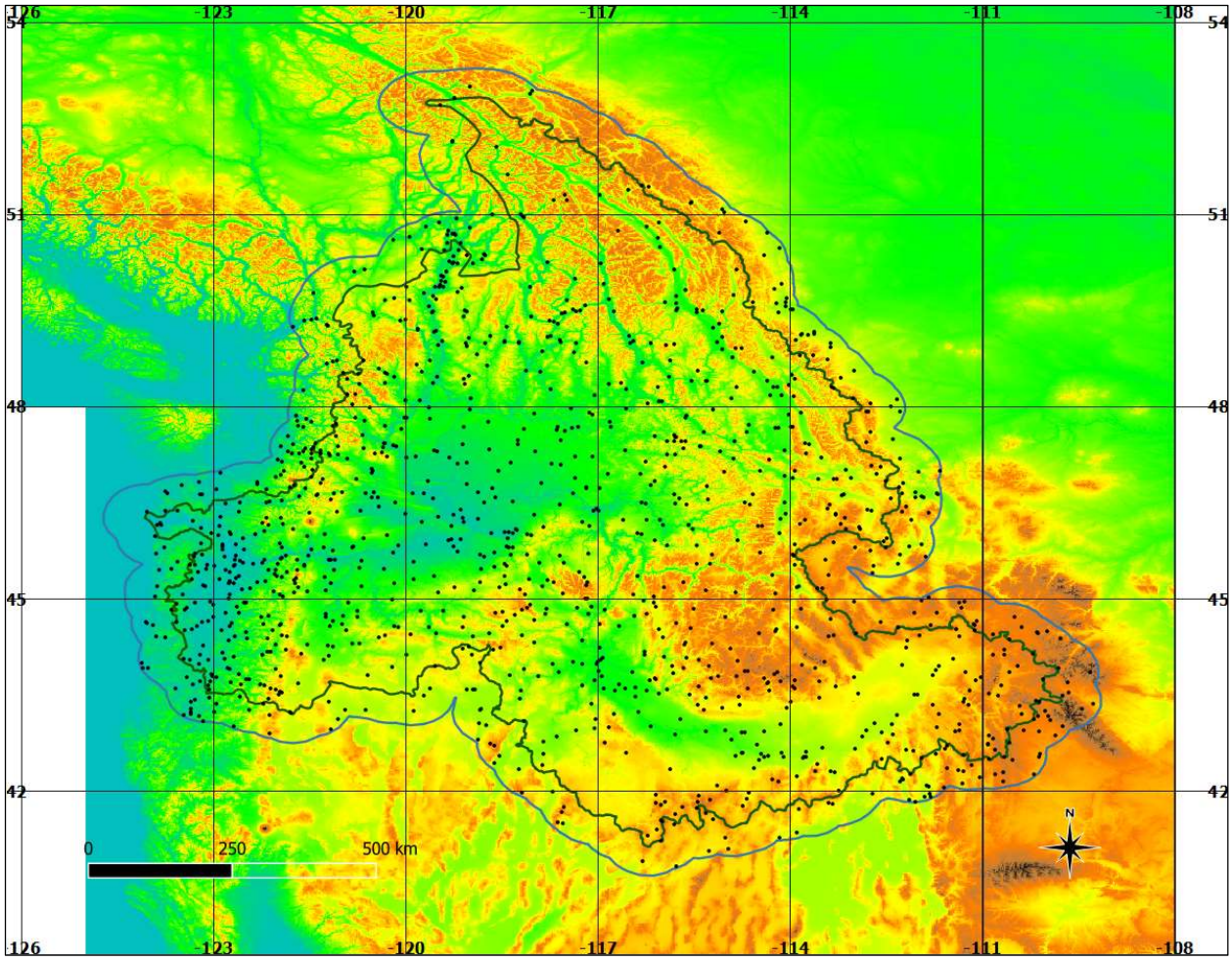

Figure 1. Digital elevation model, Columbia River Basin (CRB) boundary, and sample sites of cool season daily duration block maxima precipitation data with at least 20 years of record located within a 50km buffer of the CRB.

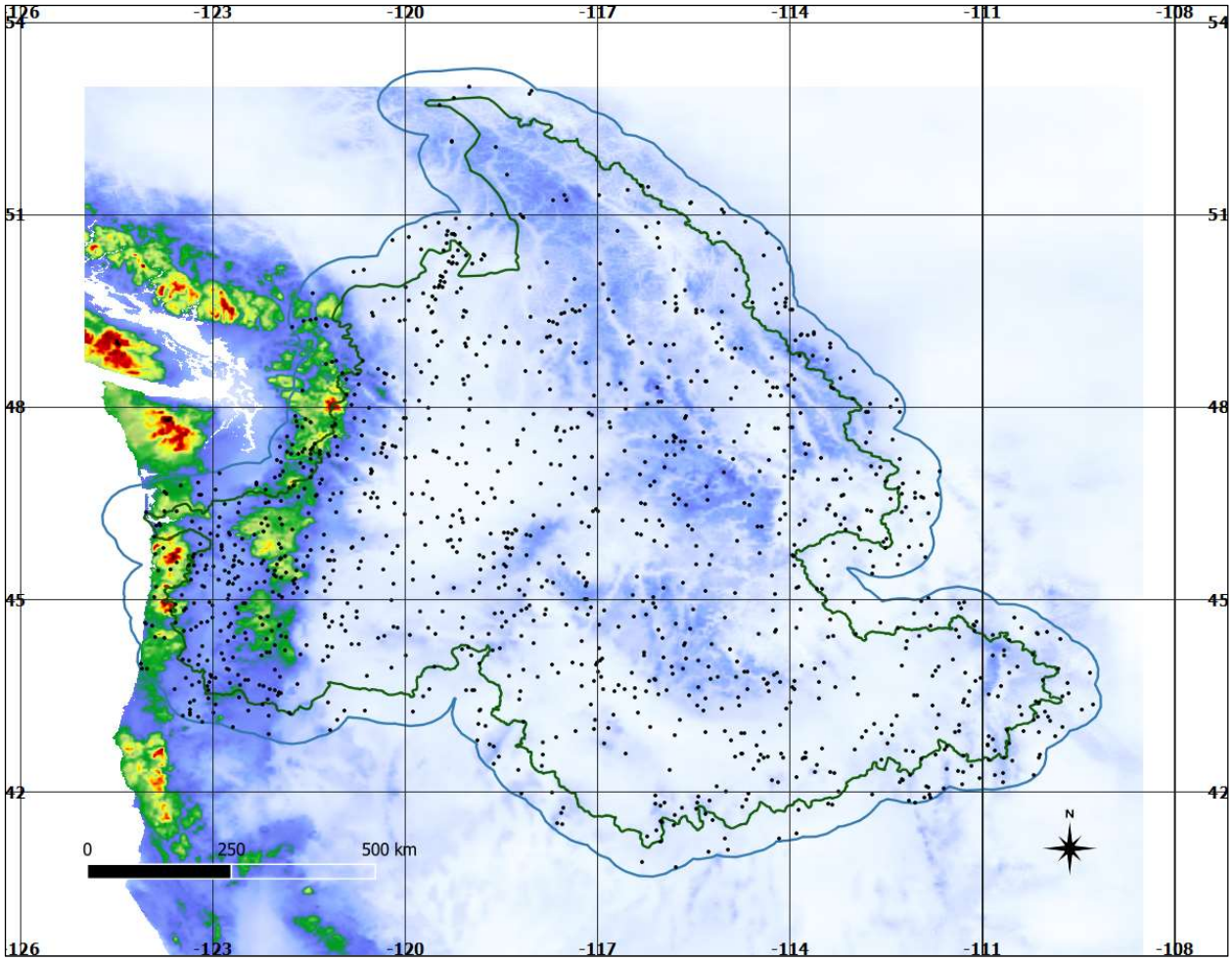

Figure 2. 100-year pointwise return level map of extreme cool season daily precipitation across the CRB.

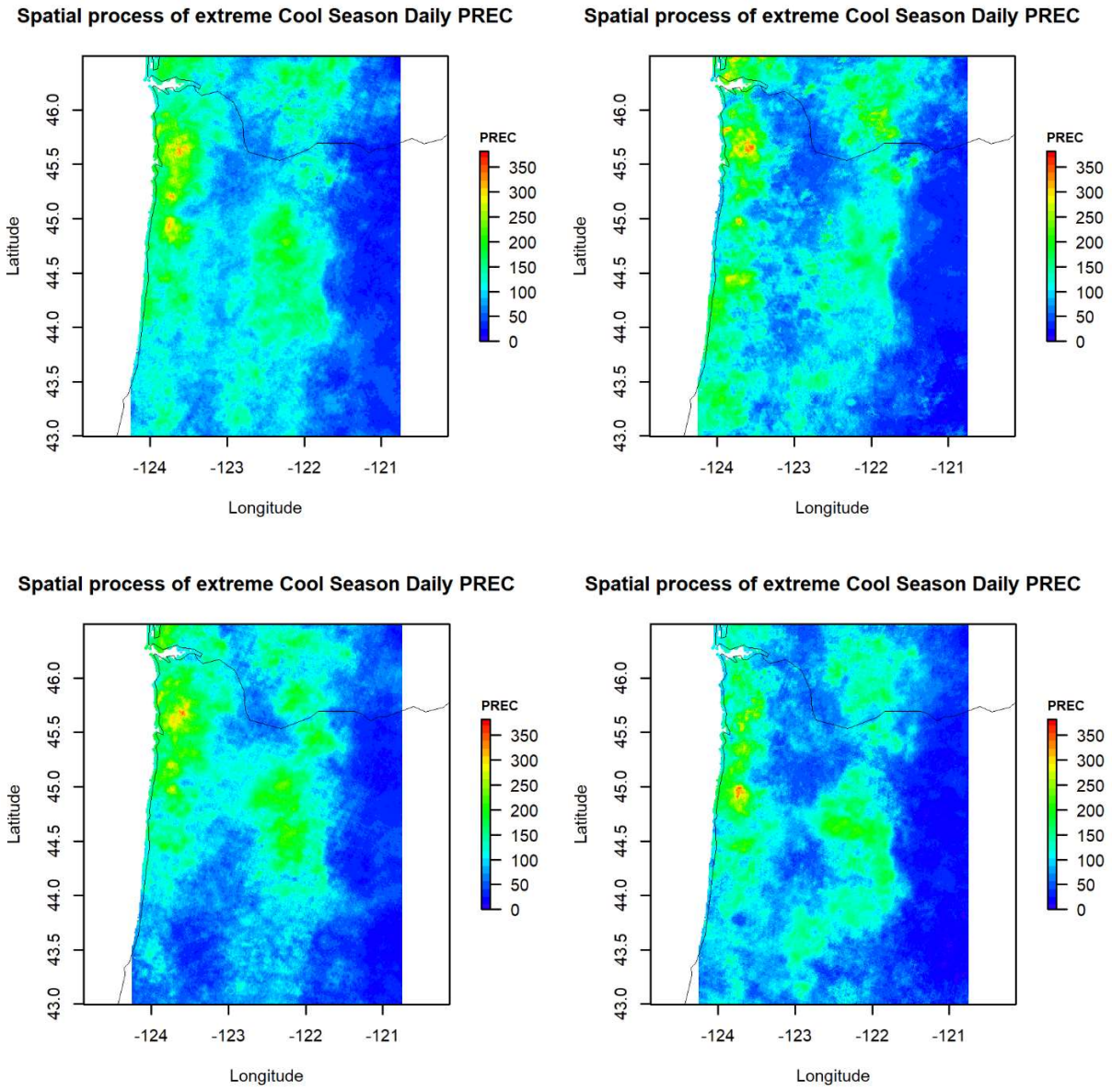

Figure 3. Simulated independent copies from a fitted max-stable process model for cool season daily precipitation block maxima data across the CRB for a 3 by 3 degree domain that contains the Willamette River Basin.

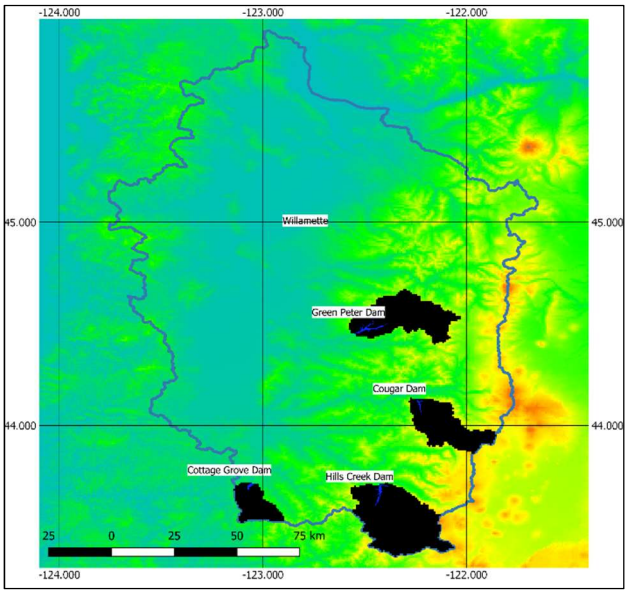

Figure 4. Digital elevation model and delineated drainage areas for four projects located within the Willamette River Basin, Oregon.

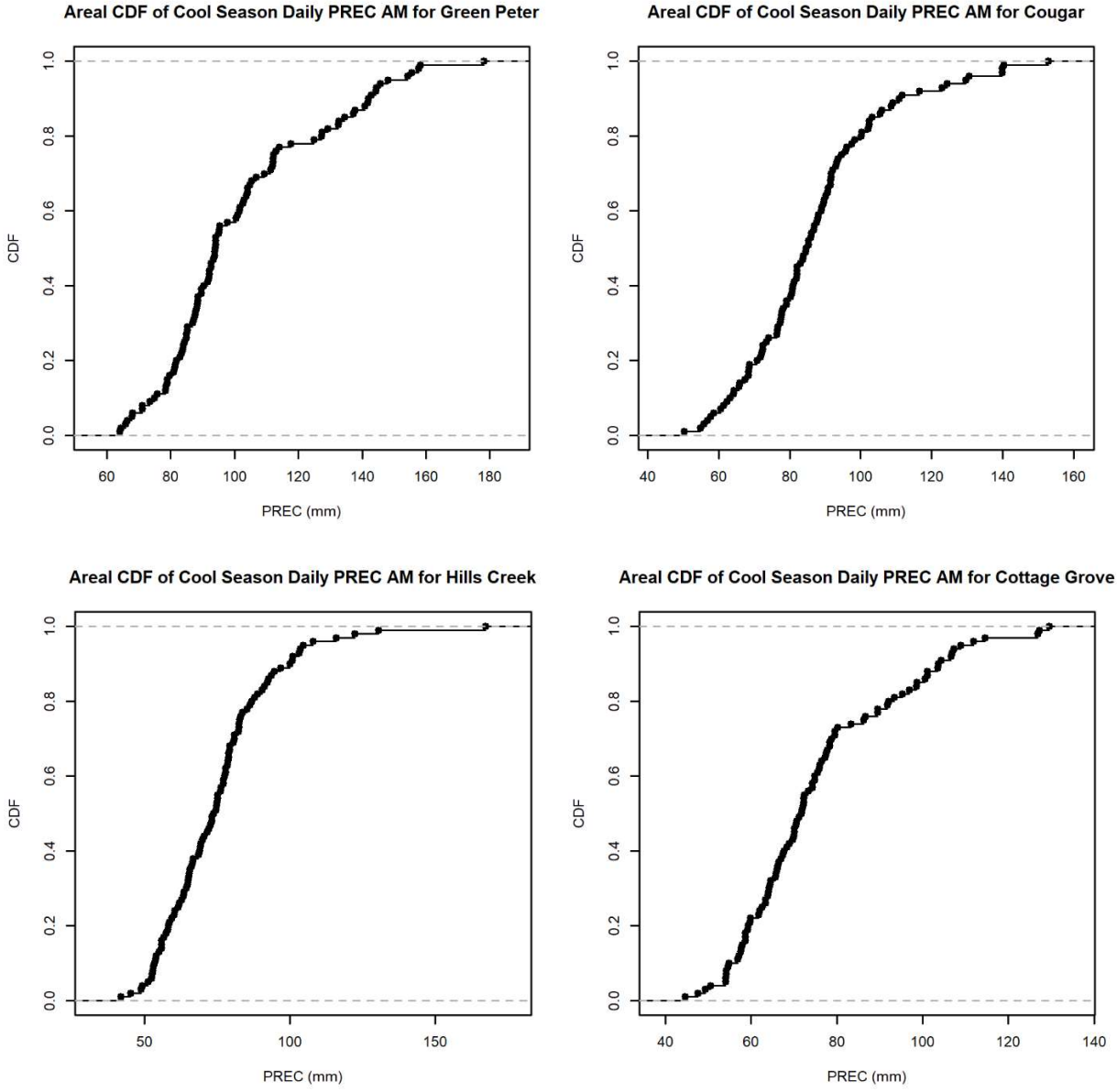

Figure 5. Areal-based probabilities of cool season daily precipitation data for the four drainages depicted in Figure 4 for four USACE projects located within the Willamette River Basin, Oregon.

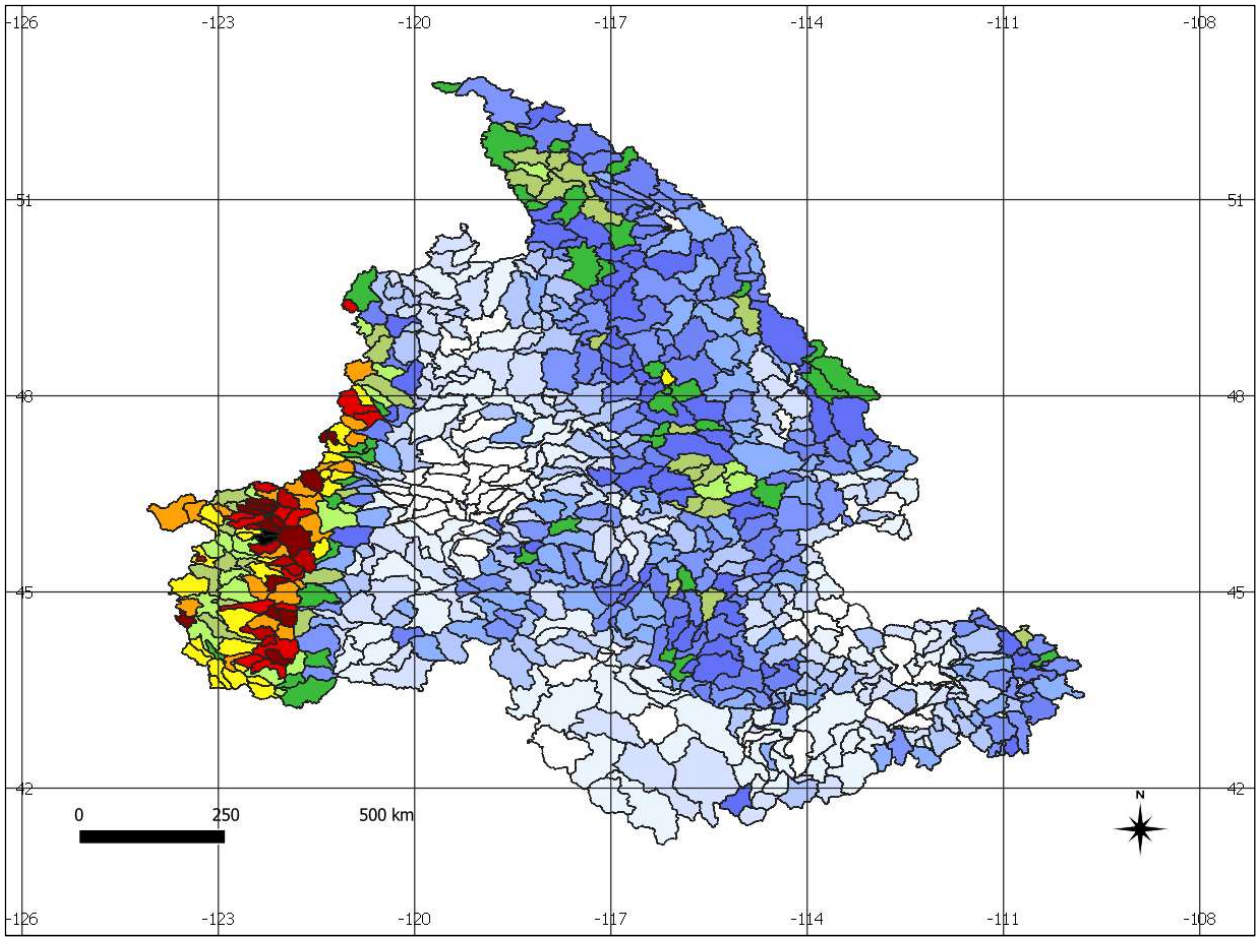

Figure 6. Plot of areal-based 100-year exceedances for cool season daily precipitation for 758 delineated basins in the CRB.

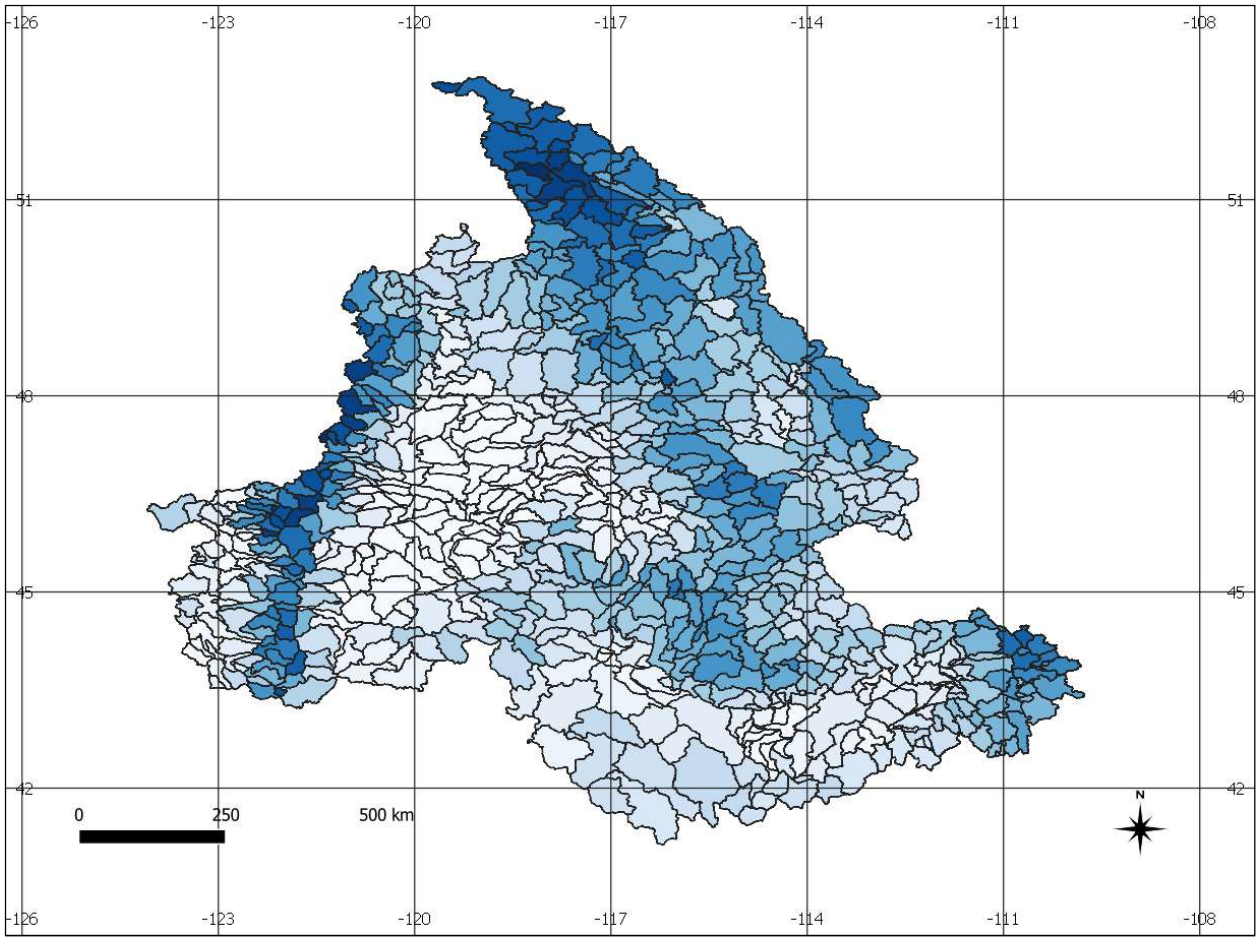

Figure 7. Plot of areal-based 100-year exceedances for water year snow water equivalent for 758 delineated basins in the CRB.

Determining Extreme Flows Using Entropy Theory

Drew Allan Loney PhD PE, USACE ERDC, Vicksburg, MS drew.a.loney@usace.army.mil
Aaron Byrd PhD PE, USACE ERDC, Vicksburg, MS aaron.r.byrd@usace.army.mil
Joseph Gutenson PhD, USACE ERDC, Vicksburg, MS joseph.l.gutenson@usace.army.mil
Edward Race PE, USACE ERDC, Vicksburg, MS edward.e.race@usace.army.mil

Abstract

Accurate estimation of extreme weather and hydrologic events with greater than 100 or 500-year recurrence intervals is essential in planning and maintaining civil infrastructure. Recent hydrologic events, such as Hurricane Harvey, have led researchers and the public to question the accuracy of existing recurrence interval estimates. Typical gage sites have a record spanning about 40 years and many have a smaller reference frame. These gage records can give the hydrologist a reasonable approximation of flows with short recurrence intervals. However, accurate extrapolation of this data to the less frequently observed, long recurrence interval events in the distribution tail is a challenge and is often subject to the assumptions built into the statistical models.

Shannon Entropy theory applied to the watershed extremes analysis has significant promise for improving frequency characterization over existing methods. The entropy approach provides an independent estimate of event frequency from current statistical methods that rely solely on the local or regionalized historical record. This approach is also insensitive to the assumptions used to construct the tail region of existing statistical approaches from which extreme events are taken. Moreover, as the concepts of available states and maximum entropy underpin the given method, more information can be extracted about the potential parameter states available to the watershed.

Extension of the method to low frequency events requires subsequent research to demonstrate that the large magnitude states predicted by the method are in fact realizable. Further research is required to compare the entropy derived recurrence estimates to that from traditional historical record statistical analysis, particularly in the low frequency region that is poorly characterized by the latter. In addition, while the developed method is expected to generalize broadly across other watershed parameters beyond discharge, the validity of this method must also be demonstrated under these cases.

Due to the large impacts of recent extreme weather events, there is a significant demand to improve the prediction of extreme event frequency to facilitate planning and construction of mitigating infrastructure. Building on Shannon Entropy theory, the technique described in this research demonstrates that it is possible to estimate the potential maximum states available to a watershed from only the historical minimum, mean, and maximum annual time series through the derivation of an entropy parameter. If the time series are weakly correlated, the marginal probability distribution of each parameter can be used to combinatorially produce a likelihood surface for the maximum event magnitude. Collapsing the likelihood surface results in a return period curve which estimates the likelihood of an annual maximum event magnitude. The researchers hypothesize that the described procedure yields an improved estimate of extreme event magnitudes given its use of watershed states and reduced reliance on long-tail behavior to derive the likelihood of low frequency events.

Introduction

Accurate estimation of extreme weather and hydrologic events with greater than 100 or 500-year recurrence intervals is essential in planning and maintaining civil infrastructure (Ross & Lott, 2003) (Kvocka, Falconer, & Bray, 2016). The Geological Survey (USGS) Gages II dataset contains gage locations in the United States for which there are either 20+ complete (not necessarily continuous) years of data or as of water year 2009 are active (USGS, 2011). The average Gages II gage site has an average record length of about 40 years as of 2009. Figure 1 describes the distribution of the number of complete years for each gage in the Gages II dataset. These gage records can give the hydrologist a reasonable approximation of flows with short recurrence intervals. However, accurate extrapolation of this data to the less frequently observed, long recurrence interval events in the distribution tail is a challenge and is often subject to the assumptions built into the statistical models.

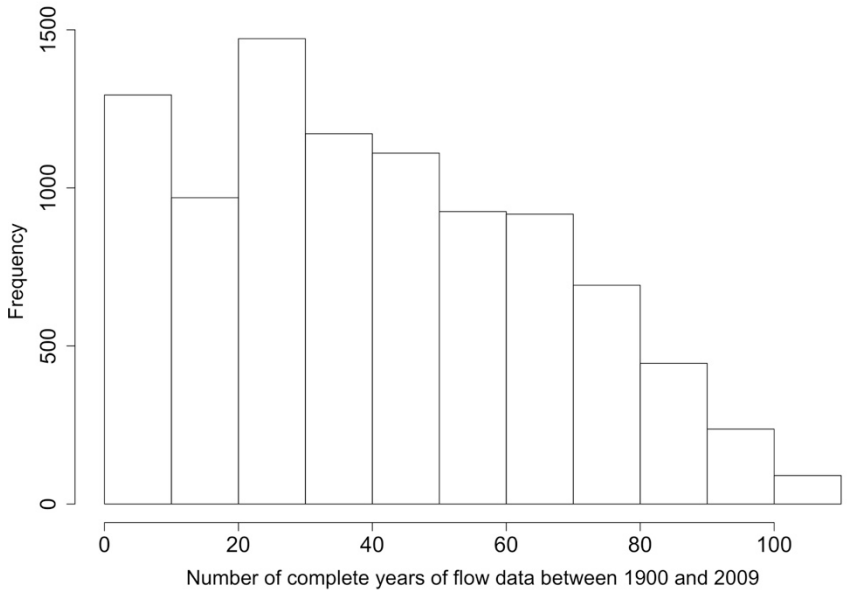

Figure 1: Histogram of the number of complete years of flow data at USGS Gages II locations.

The typical approach to determining the likelihood of extreme hydrological events is through statistical analysis of the historical record, which may have some regionalized information incorporated to extend its temporal coverage or improve its accuracy. (Büchele, et al., 2006; Castellarin, Merz, & Blöschl, 2009) This approach entails that the hydrologist fit a statistical distribution to the historical dataset, typically through the use of probability plots, and extrapolate the likelihood of large magnitude parameter occurrences. The fitting process relies upon the assumption that the historical data points are independent, temporally stationary, and follow the same statistical distribution (Chow, Maidment, & Mays, 1988). Moreover, the distribution used to characterize a historic dataset can vary and is, to a certain degree, subjective. For example, the United States (U.S.) Water Resources Council (USWRC) developed Bulletins 15, 17B, and 17C, with each being a revision of the previous. (Water Resources Council, 1967; Interagency Advisory Committee on Water Data, 1982; Advisory Committee on Water Information, 2015) The implementation of the most recent update, Bulletin 17C, utilizes a log-Pearson Type III (LP-III) distribution with regional skew coefficients to estimate flood flows and frequencies using the magnitudes of historic yearly maximum discharges. Because the Bulletin

17C methodology assumes a representative historic record, observations of extreme events within the historical record is crucial in accurately estimating future extremes. Bulletin 17C methodology can under-predict the occurrence of large event magnitudes when large events are not present in the historical record.

The probable maximum event is another common method to characterize extreme events. The probable maximum precipitation (PMP) is the greatest accumulation of precipitation over a given area and time of year that is meteorologically possible (World Meteorlogical Organization, 2009). To determine the PMP, modelers force numerical weather models with inputs that will lead to the greatest amount of precipitation for a given period and watershed. Many regulatory agencies, such as the U.S. Army Corps of Engineers (USACE), establish design criteria for dam design to account for the Inflow Design Flood (IDF). To find the inflow design flood (IDF) from the PMP, the engineer must model both runoff and routing processes. Because of the synthetic nature of the PMP process, there can be difficulty determining the return period or likelihood of these events.

The traditional methods of statistical extremes analysis, such as analysis of the historical record and PMP, leave knowledge gaps that can be supplemented by other approaches to characterize hydrological extremes. The purpose of this paper is to demonstrate a method of estimating the frequency of hydrological extremes based on the Shannon Entropy (AghaKouchak, 2014) (Singh, Hydrologic Synthesis Using Entropy Theory, 2011) (Singh, Byrd, & Cui, Flow Duration Curve Using Entropy Theory, 2014). Entropy methods are thought to circumvent many of the limitations of traditional statistical approaches by considering the full parameter space of a variable beyond the single realized historical sequence given by the gage record. This work begins by introducing and extending the entropy analysis given by Singh et al (2014) into an entropy-based methodology for extremes characterization. This research demonstrates the application of the entropy-based method for the characterization of extreme flow behavior within the Brazos River watershed. Finally, this research outlines additional work required to validate the predictive capability of entropy-based approaches for extremes analysis.

Methodology

Entropy is a system property that, when taken as a random variable, describes uncertainty in the state of a system through the range of the potential states available to that system. Shannon (1948) derived an entropy formulation which measures system entropy in terms of the state likelihood and the number of states, given as:

$$H(p) = -K \sum_{i=1}^{N} p(x_i)\, log\left(\frac{p(x_i)}{m(x)}\right) \quad (1)$$

where $H(p)$ is the entropy function, N is the number of system states, $p = \{p_i, i = 1, 2, \dots, N\}$ is the probably distribution giving the likelihood of the system being in a given state, K is a property of the logarithm base, and $m(x)$ is a function that maintains invariance under changes of coordinates (Shannon, 1948) (Singh, Hydrologic Synthesis Using Entropy Theory, 2011) (Singh, Byrd, & Cui, Flow Duration Curve Using Entropy Theory, 2014). If the number of states is large and the likelihood is diffused across the states, H will be relatively large in magnitude. If the number of states is small and the likelihood is concentrated on only a few states, H will be relatively small in magnitude. The magnitude of H therefore captures the system uncertainty as a single value by aggregating the number and likelihood of each available system state.

Entropy has seen significant use in water resources analysis, an overview of which is provided by Singh (2011). Applications of entropy theory have centered on improving the ability to model specific physical processes, such as infiltration, soil moisture, flow duration curves, and groundwater as well as capture various physical geometries. (Zehe, Blume, & Bloeschl, 2010; Eltahir & Gong, 1996; Hou, Huang, Leung, Lin, & Ricciuto, 2012; Woodbury & Ulrych, 1996; Moramarco & Singh, 2010) Most cases utilize maximum entropy theory to determine distributions which represent the likely state of a process or geometry of interest from the known information while not imposing artificial constraints on the parameter range. Cases also consider single subsystems and variables due to the complexity arising from multiple interacting physical processes.

The present work extends entropy theory into the estimation of extremes for watershed analysis. As traditional entropy theory considers a sample to be representative of the likely parameter state, the historical record can be considered as a single realization of all likely event sequences for a watershed. Other event sequences are similarly plausible given perturbations in the weather conditions or alternative historical sequences of hydrometeorlogical phenomena. This premise supposes that there exists a finite number of potential states that the parameter may assume that, when sampled repeatedly, would create a realization of an event sequence. Exploration of the underlying watershed states and production of valid historical sequences from the potential states has been the subject of much ongoing work due to the difficulty in accurately constructing and sampling the state space. Analysis of extremes using entropy theory greatly simplifies characterization of the potential states by capturing only the range of possible states and neglecting the exact behavior of any sequence realization.

The characterization of flow duration curves by Singh et al. (2014) forms the foundation on which entropy methods can be extended for extremes analysis of watershed parameters. Singh et al. applied Shannon entropy together with the principle of maximum entropy to evaluate flow duration curves by relating the range of states and the annual mean flow to the anticipated maximum flow. The proposed method follows directly from Singh et al (2014) and the result maximum entropy analysis as given by:

$$\frac{\bar{Q}}{Q_{max}} = \frac{1}{M} + \frac{\frac{Q_{min}}{Q_{max}} \exp\left(-\frac{MQ_{min}}{Q_{max}}\right) - \exp(M)}{\exp\left(-\frac{MQ_{min}}{Q_{max}}\right) - \exp(M)} \tag{2}$$

where $\bar{Q}$ is the average yearly flow, Q_{max} is the maximum yearly flow, Q_{min} is the minimum yearly flow, and M is the entropy parameter. Under the assumption that $Q_{min} \cong 0$, Equation 2 reduces to:

$$\frac{\bar{Q}}{Q_{max}} = \frac{1}{M} - \frac{\exp(-M)}{1 - \exp(M)} \tag{3}$$

The entropy parameter, M, is a dimensionless constant that is directly proportional to the range of possible maximum flow states with respect to the average and maximum flow states. A larger value for M indicates a larger range of discharge rates for that year. Utilizing the available historical record, M is calculated from the annual flow characteristics.

The analysis of extremes begins with Equation 3. Let $f(\bar{Q})$ and $g(M)$ be continuous random variables fit to the historical records for $\bar{Q}$ and M, respectively. Furthermore, let $F(\bar{Q})$ and $G(M)$ be defined as the cumulative distributions of the fits $f(\bar{Q})$ and $g(M)$. The exact distribution used

to model each may be chosen such that each parameter is characterized with the least error. Given the assumptions that:

1. The magnitude of M is uncorrelated with the magnitude of $\bar{Q}$
2. The range of M uncorrelated with the magnitude of $\bar{Q}$

it follows that any value of M is equally likely to apply to any value of $\bar{Q}$. If the assumptions are not upheld, the remainder of the analysis can still be conducted so long as the form of the dependency between M and $\bar{Q}$ is properly formulated. $Q_{max}(M, \bar{Q})$ may then be rewritten as function of both random variables using Equation 3, yielding:

$$Q_{max} = Q_{max}(G^{-1}(M), F^{-1}(\bar{Q})) \tag{4}$$

A surface characterizing Q_{max} can be produced by independently sampling $G^{-1}(M)$ and $F^{-1}(\bar{Q})$ with a sufficiently small interval to make subsequent operations independent of the sampling resolution. The Q_{max} surface represents the maximum extent of the event magnitude range for each combination of M and $\bar{Q}$. The frequency at which a given Q_{max} value occurs therefore gives the likelihood of encountering a given Q_{max} in a given year. A frequency distribution $p(Q_{max})$ for Q_{max} is obtained by binning and counting the occurrence of values on the Q_{max} surface. One may then optionally fit a distribution to the $p(Q_{max})$ histogram to simplify subsequent operations. This method results in a frequency estimate for Q_{max} which, while informed by the historical record, does not limit the potential states of the watershed to those present within the historical record and is separate from traditional annual maximum statistical estimation methods.

Results and Discussion

The proposed entropy method for extremes estimation is illustrated with discharge information from USGS Station 08082500 on the Brazos River near Seymour, Texas. The Brazos River was selected as it is well-gaged with 98 gage stations along its reach. The selected station has a contributing drainage area of 15,467 km^2 (5,972 mi^2) as shown in Figure 2 (USGS, 1990). Much of the watershed is cropland and pasture, particularly in the upper reaches (USGS, 2008).(USGS, 2008). The climate of the Brazos River basin is typical for the southcentral United States ranging from temperate to subtropical (Brazos River Authority, n.d.). The watershed provides a diverse range of flows, including extremes related to droughts and hurricanes. This gage station provided data including minimum, average, and maximum yearly flows available from 1924 to 2016.

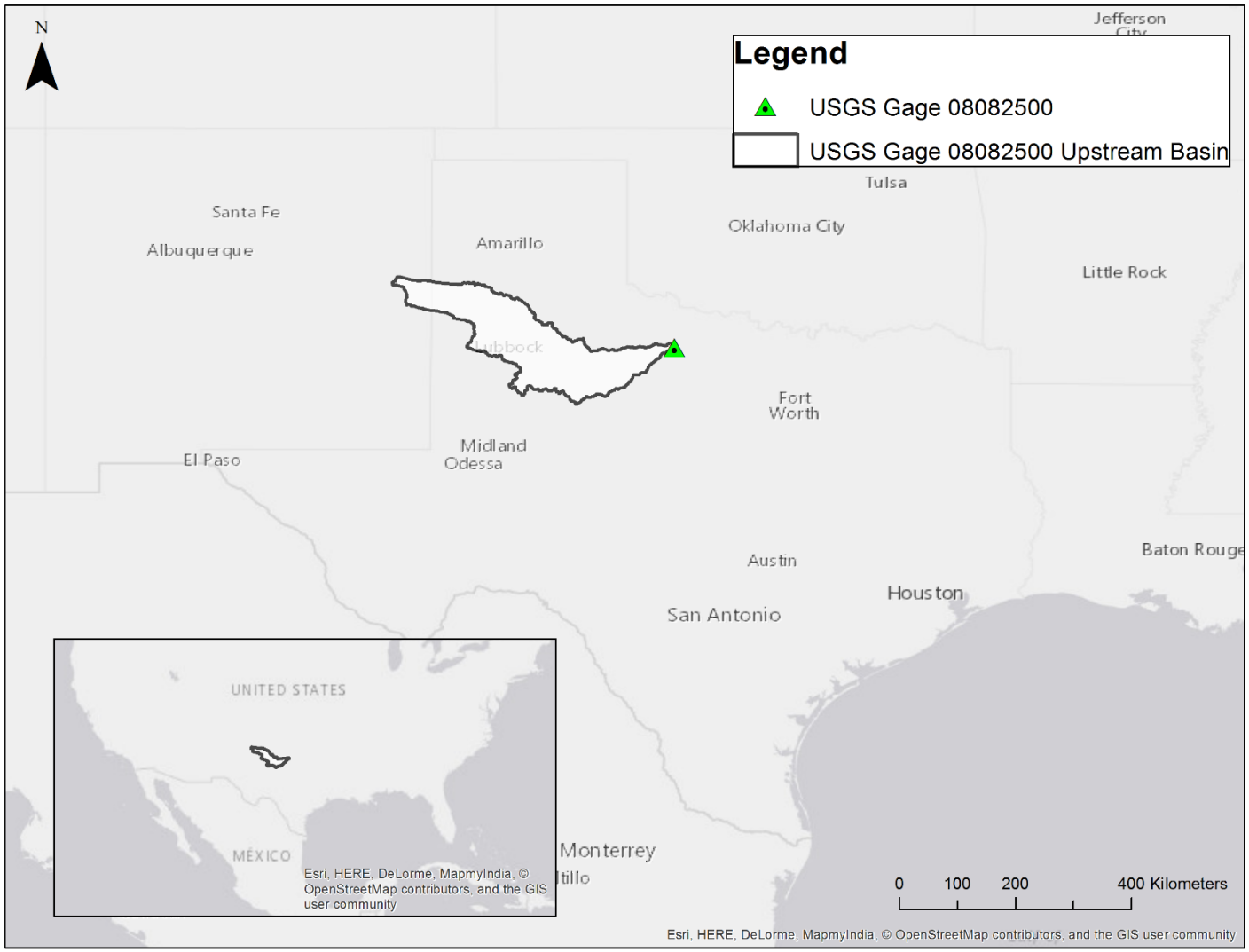

Figure 2: Map of upstream drainage area of gage 08082500

Historical values of M were calculated for each year from the mean and maximum following Equation 3. The independence of M and $\bar{Q}$ was verified with Figure 3 and by calculating the correlation between the series. As the correlation coefficient is low at 0.077, the parameters can be considered sufficiently independent for non-joint characterization.

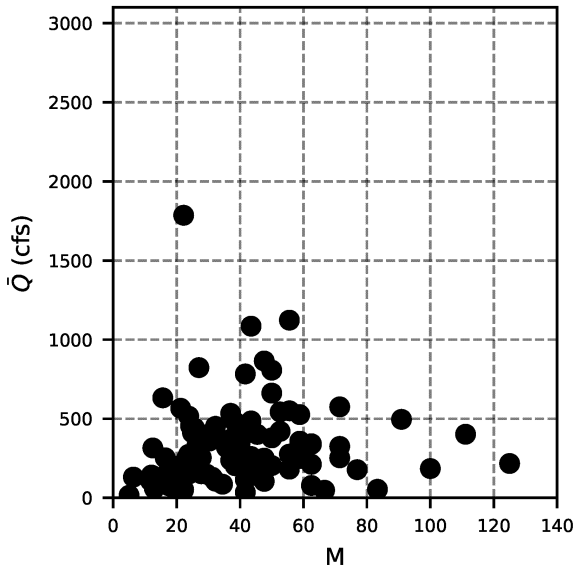

Figure 3: Test for correlation between $\bar{Q}$ and M within the Brazos River basin. The parameters are uncorrelated with a σ=0.077. $\bar{Q}$ is given in units of cubic feet per second (cfs).

Distributions were then fit to M and $\bar{Q}$ to enable parameter sampling. Best fits were achieved using the gamma distribution to characterize M and the Burr distribution to characterize $\bar{Q}$, achieving R^2 of 0.775 and 0.986, respectively. The full forms of both fits are given in Equations 5 and 6 with depictions of each illustrated in Figure 4.

$$f(M) = \frac{\left(\frac{M-c}{b}\right)^{a-1} \exp\left(-\frac{M-c}{b}\right)}{b\Gamma(a)} \qquad \begin{matrix} a = 3.494 \\ b = -0.369 \\ c = 11.774 \end{matrix} \tag{5}$$

$$g(\bar{Q}) = cd\left(\frac{\bar{Q}-m}{k}\right)^{-(c+1)}\left(1+\left(\frac{\bar{Q}-m}{k}\right)^{-c}\right)^{-(d+1)} \qquad \begin{matrix} c = 2.918 \\ d = 0.556 \\ k = -1.661 \\ m = 359.303 \end{matrix} \tag{6}$$

The surface characterizing Q_{max} was generated by sampling the inverse cumulative probability distributions for M and $\bar{Q}$ on the interval $0 \leq x \leq 0.999$ and solving Equation 3, the results of which are given in Figure 5. The dotted lines within the figure are probability contours which divide the surface into 25 regions of equal likelihood. The spacing between the contours

indicates the frequency at which Q_{max} values would be drawn from that region of the surface. Likely Q_{max} values bias strongly toward low mean flows and the lower portion of the entropy value range as these are the average conditions experienced within the Brazos watershed. Additionally, the historic Q_{max} are plotted with the color of each dot corresponding to the magnitude. The magnitude of the calculated surface strongly reflects the historical data which gives confidence that the entropy model correctly characterizes the historically sampled portion

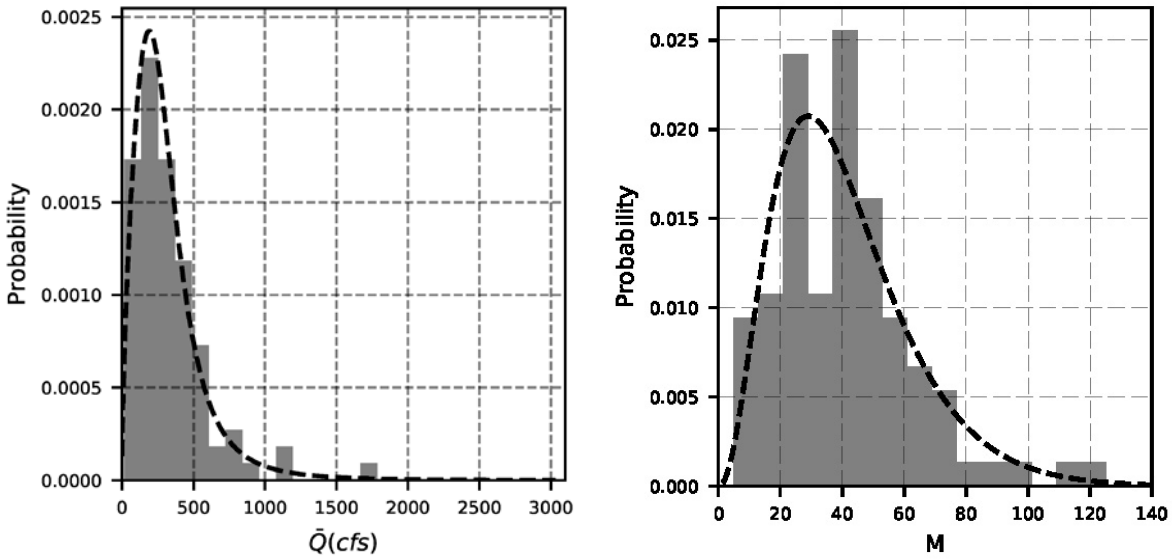

Figure 4: Left – Histogram and fit of the gamma distribution to $\bar{Q}$. Right – Histogram and fit of the Burr distribution to M.

of the state space. However, the historic measurements occupy only the lower magnitude, high sampling the likelihood region of the predicted state space. The predicted existence of a higher magnitude region suggests that there are discharge states available to the watershed that have not been sampled by the historical event sequence. If the accessibility of watershed parameters to some portion of the predicted high magnitude state space can be established, extreme event frequency estimates could be improved using the new state information over the historic record alone.

If accessibility to the full state space can be established, the surface characterizing Q_{max} can be applied in two useful manners. First, the annual likelihood of a given Q_{max} can be determined by finding the frequency of Q_{max} values on the surface, as given in Figure 5

significantly different behavior for low frequency events. Whereas the historical fit asymptotes to a constant, the entropy fit continues to increase with larger return periods.

. A Log-Pearson Type III (LP III) (R^2=0.965) as in Equation 7 characterized the occurrence of Q_{max} in this circumstance with least error (Figure 6). The distribution obtained for the occurrence of Q_{max} represents an improved estimate of the extreme event frequency as it more fully captures the range of states and the various watershed mechanisms which lead to similar parameter magnitudes.

$$P(Q_{max}) = \frac{1}{\sqrt{w\pi}\sigma Q_{max}} \exp\left(-\frac{(\log_{10} Q_{max} - \mu)^2}{2\sigma^2}\right) \qquad \begin{matrix}\mu = 9.041 \\ \sigma = 1.009\end{matrix} \qquad (7)$$

The surface can compare the statistical analysis of historical event sequence, as done in Figure 7. The empirical and LP III fit frequency estimates of the historical record are given by the circles and solid line, respectively. The empirical and LP III fit frequency estimates of the values occurring on Q_{max} surface are given by the squares and dotted line, respectively. The LP III fit to the historical record poorly characterizes the empirical historical estimate beginning at the 10-year return period. This causes extrapolations to longer return period events to have a large uncertainty range. The LP III fit to the Q_{max} surface frequency performs better but also under predicts the empirical distribution. Additionally, the Q_{max} frequency estimate demonstrates

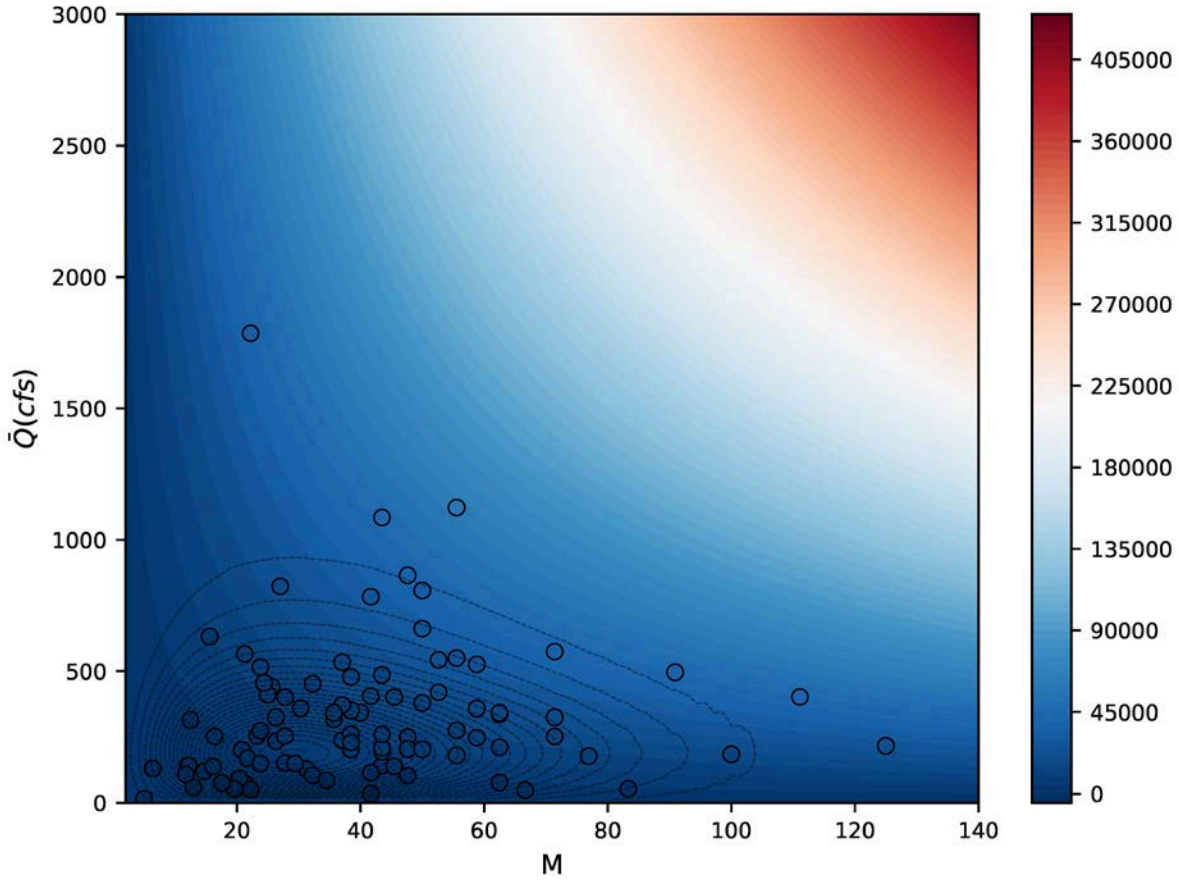

Figure 5: Predicted variation of Q_{max} as a function of M and $\bar{Q}$ produced by sampling the distributions and solving Equation 3. The color bar gives the magnitude of Q_{max} across the parameter space. The dotted contours divide the surface into 25 equally likely bins. Historical measured values are superimposed on the surface as the circle.

significantly different behavior for low frequency events. Whereas the historical fit asymptotes to a constant, the entropy fit continues to increase with larger return periods.

The difference between the historical and entropy fits is a product of the greater number of high magnitude states predicted by the entropy analysis. If these predicted states prove accessible to

the system, the difference between the fit curves would also characterize the information gained through the entropy analysis. In addition, the results portrayed in Figure 6 demonstrate that the empirical distribution of the Q_{max} surface and the LP III fit to the Q_{max} surface capture the largest event at Gage 08082500. The largest observed Q_{max} is approximately a 100-year return period event. These results indicate potential that the predicted states are accessible to the system and that the entropy-based surface is a viable indicator of extreme event magnitude. However, because of poor performance from 10-year to 100-year return period, additional research is necessary.

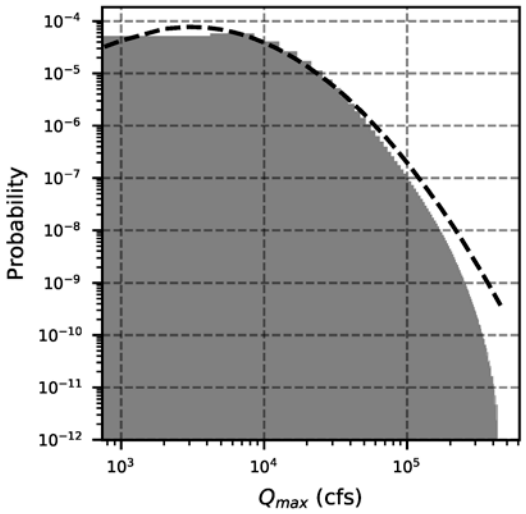

Figure 6: Histogram and fit of the LP III distribution to Q_{max}, giving the annual likelihood of Q_{max} being the maximum discharge within the Brazos River watershed. The distribution was created by counting the frequency of Q_{max} values on the surface in Figure 4.

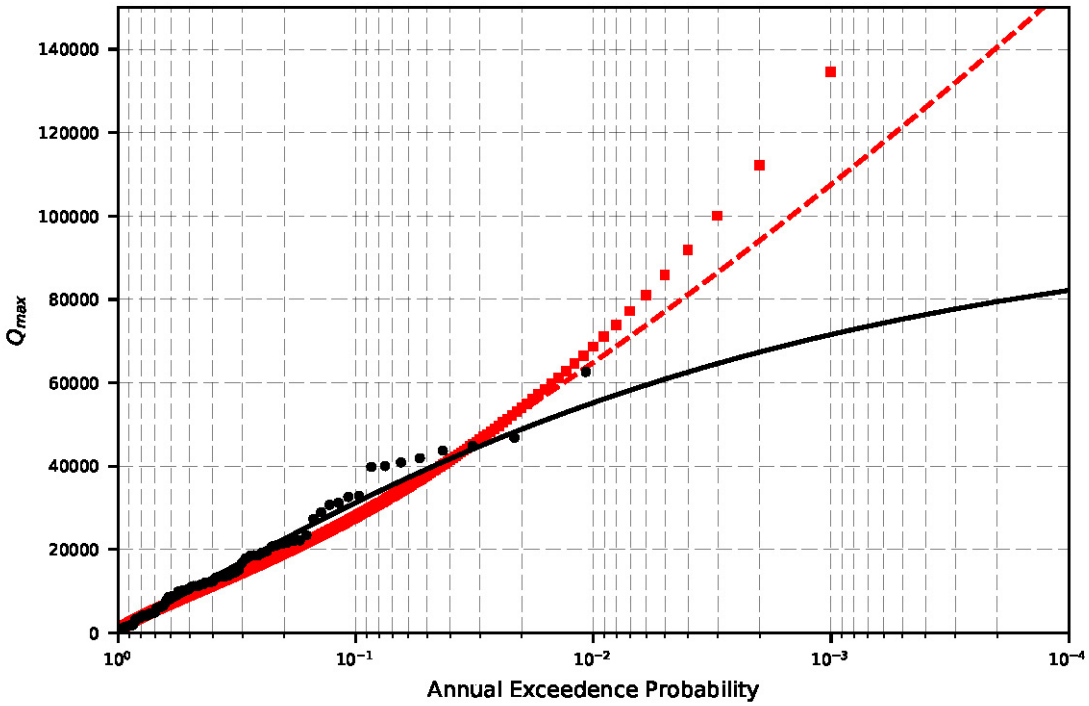

Figure 7: Estimation of the annual exceedance probability from the Q_{max} surface. The circles and solid line give the empirical and LP III fit for the historical record, respectively. The squares and dotted line give the empirical and LP III fit for the values occurring on the Q_{max} surface, respectively.

Conclusion

This work formulated and demonstrated an entropy-based approach to hydrologic analysis within the Brazos River watershed for estimating extreme event frequency. Expanding on the work of Singh et al. (2014), a method for characterizing the mean state and range of states available to watershed parameters was developed. These distributions were then sampled to create a magnitude surface that can be used to characterize the likelihood of the annual peak event magnitude.

Entropy theory applied to the watershed extremes analysis has significant promise for improving frequency characterization over existing methods. The outlined approach provides an independent estimate of event frequency from current statistical methods that rely solely on the local or regionalized historical record. This approach is also insensitive to the assumptions used to construct the tail region of existing statistical approaches from which extreme events are taken. Moreover, as the concepts of available states and maximum entropy underpin the given method, more information can be extracted about the potential parameter states available to the watershed.

At a minimum, an entropy-based extremes analysis can be useful to verify and provide an uncertainty estimate to the historical event sequence. Extension of the method to low frequency events requires subsequent research to demonstrate that the large magnitude states predicted by the method are in fact realizable. In addition, while the outlined method is expected to generalize broadly across other watershed parameters beyond discharge, the validity of this method must also be demonstrated under these cases.

References

Advisory Committee on Water Information. (2015). *Guidelines for Determine Flood Flow Frequency (draft).* Reston, VA: US Geological Survey.

AghaKouchak, A. (2014). Entropy-Copula in Hydrology and Climatology. *Journal of Hydrometeorology, 15*(6), 2176-2189.

Büchele, B., Kreibich, H., Kron, A., Thieken, A., Ihringer, J., Oberle, P., . . . Nestmann, F. (2006). Flood-risk mapping: contributions towards an enhanced assessment of extreme events and associated risks. *Natural Hazards and Earth System Sciences, 6*(4), 485–503.

Brazos River Authority. (n.d.). *What is the Brazos River?* Retrieved June 25, 2017, from Brazos River Authority: https://www.brazos.org/About-Us/Education/Water-School/ArticleID/265

Castellarin, A., Merz, R., & Blöschl, G. (2009). Probabilistic envelope curves for extreme rainfall events. *Journal of Hydrology, 378*(3-4), 263-271.

Chow, V. T., Maidment, D. R., & Mays, L. W. (1988). *Applied Hydrology.* Tata McGraw-Hill Education.

Eltahir, E., & Gong, C. (1996, May). Dynamics of wet and dry years in West Africa. *Journal of*

Climate, 9(5), 1030-1042.

Hou, Z., Huang, M., Leung, L., Lin, G., & Ricciuto, D. (2012, August 10). Sensitivity of surface flux simulations to hydrologic parameters based on an uncertainty quantification framework applied to the Community Land Model. *Journal of Geophysical Research-Atmospheres, 117*.

Interagency Advisory Committee on Water Data. (1982). *Guidelines for Determining Flood Flow Frequency.* Reston, VA: US Geological Survey.

Kvocka, D., Falconer, R., & Bray, M. (2016). Flood Hazard Assessment for Extreme Flood Events. *Natural Hazards, 84*(3), 1569-1599.

Moramarco, T., & Singh, V. (2010, October). Formulation of the Entropy Parameter Based on Hydraulic and Geometric Characteristics of River Cross Sections. *Journal of Hydrologic Engineering, 15*(10), 852-858.

Rajsekhar, D., Mishra, A., & Singh, V. (2013). Regionalization of Drought Characteristics Using an Entropy Approach. *Journal of Hydrologic Engineering, 18*(7), 870-887.

Ross, T., & Lott, N. (2003). *A Climatology of 1980-2003 Extreme Weather and Climate Events.* US Department of Commerce. Asheville: National Climatic Data Center.

Shannon, C. E. (1948). *The Mathematical Theory of Communications I and II.* Bell Systems Tech Journal.

Singh, V. J. (1996). The Use of Entropy in Hydrology and Water Resources. *Hydrological Processes, 11*, 587-626.

Singh, V. J. (2011). Hydrologic Synthesis Using Entropy Theory. *Journal of Hydrologic Engineering, 16*(5), 421-433.

Singh, V. J., Byrd, A. R., & Cui, H. (2014). Flow Duration Curve Using Entropy Theory. *Journal of Hydrologic Engineering, 19*(7), 1340-1348.

USGS. (1990). *Largest Rivers in the United States.* Department of the Interior. USGS.

USGS. (2008, October 8). *Brazos Watershed*. Retrieved 06 25, 2017, from EDNA Derived Watersheds for Major Named Rivers: http://edna.usgs.gov/watersheds/ws_ws_chars.php

USGS. (2011). *Geospatial Attributes of Gages for Evaluation Streamflow.* Reston, Virginia: United States Geological Survey (USGS).

Water Resources Council. (1967). *A Uniform Technique for Determining Flood Flow Frequencies.* Washington, D.C.: Water Resources Council.

Woodbury, A., & Ulrych, T. (1996, September). Minimum relative entropy inversion: Theory and application to recovering the release history of a groundwater contaminant. *Water Resources Research, 32*(9), 2671-2681.

World Meteorlogical Organization. (2009). *Manual on Estimation of Probable Maximum Precipitation (PMP).* Geneva, Switzerland: World Meteorlogical Organization.

Zehe, E., Blume, T., & Bloeschl, G. (2010, May 12). The principle of 'maximum energy dissipation': a novel thermodynamic perspective on rapid water flow in connected soil structures. *Philosophical Transactions of the Royal Society B-Biological Sciences, 365*(1545), 1377-1386.

Effectively Utilizing Stochastic Hydrologic Loadings for Risk Analysis and Risk-Informed Design

Amanda Stone, Engineer, Bureau of Reclamation, Denver, CO, astone@usbr.gov
Walter Heyder, Engineer, Bureau of Reclamation, Denver, CO, wheyder@usbr.gov
Jonathan East, Engineer, Bureau of Reclamation, Denver, CO, jeast@usbr.gov
Keil Neff, Engineer, Bureau of Reclamation, Denver, CO, kneff@usbr.gov
Frank Dworak, Engineer, Bureau of Reclamation, Denver, CO, fdworak@usbr.gov
Subhrendu Gangopadhyay, Engineer, Bureau of Reclamation, Denver, CO, sgangopadhyay@usbr.gov

Abstract

The Bureau of Reclamation (Reclamation) currently utilizes stochastic methods in hydrologic modeling as part of a multiple-method approach to develop flood frequency estimates for use in risk analyses and risk-informed design for Reclamation dams and appurtenant structures. Broadly, the use of stochastic methods allows for improved characterization of uncertainty and development of more realistic hydrologic loadings over deterministic methods. Stochastic methods are employed within the modeling framework by sampling hydrological and meteorological datasets as well as model parameters using a Monte-Carlo simulation framework (MCSF). The MCSF allows for model inputs and parameters to be varied within physically realistic ranges for the study area and preserves co-variability of model inputs. The model can then be run thousands of times sampling from historical data and precipitation-frequency curves to simulate hypothetical annual maximum floods representing thousands of years of record. The underlying premise of this approach is that, the simulated hydrographs from a stochastic hydrologic model represent a broad frequency space and better characterize the inherent uncertainties in a flood frequency analysis. However, the large number of hydrographs developed as part of a stochastic study can pose technical, communication, and data management challenges to a team. While traditional methods typically presented one or a few hydrograph shapes, such as Probable Maximum Floods (PMFs), with which to support design or risk analysis, use of many realizations of potential flood hydrographs can make these processes far more complex. The methods and communication framework presented in this paper can support effective implementation of stochastic hydrologic modeling results in support of risk analysis and risk-informed design.

Introduction

Stochastic methods are being increasingly used by the Bureau of Reclamation's Technical Service Center to improve characterization of uncertainty and to develop representative hydrologic loadings relative to deterministic methods. Simply put, stochastic methods treat model parameters and inputs as random variables rather than fixed values. Monte-Carlo simulation framework (MCSF) simulations samples from probability distributions of these parameters to better describe uncertainty in the model. Historically, deterministic methods were used to develop Inflow Design Floods (IDFs) including Probable Maximum Floods (PMFs) which were used to support design and risk assessment of Reclamation dams. Use of stochastic methods employed within the modeling framework by sampling hydrology and meteorology

datasets and model parameters can allow for parameters and inputs to be varied within physically realistic ranges for the study area. This approach provides an improved representation of the potential variations in hydrologic conditions in a watershed of interest relative to those defined using deterministic methods where model inputs and parameters are largely specified as constants.

Flood frequency estimates from stochastic modeling studies are used to support risk analyses and inform design or operational modifications for Reclamation dams and appurtenant structures. The benefits associated with stochastic methods include an improved characterization of uncertainty in hydrologic modeling, improved confidence over estimates derived using limited datasets or deterministic methods, and potentially minimization of cost associated with physical design and/or operational modifications due to more refined hydrologic loads. The level of effort associated with stochastic models may not always be needed depending on the level of risk or confidence in estimates from an earlier study, so determination of the need for these methods should be defined in early project planning and risk screening studies. However, with these improved methods come challenges in application of the results of such stochastic models.

Relative to traditional methods in practice (e.g., use of IDFs or PMFs), stochastic hydrologic model results present communication and data management challenges and can limit their usefulness in situations where results are not effectively communicated. Traditionally, design and risk analysis team members were typically presented with just a handful of hydrographs for design and risk analysis. When presented with a suite of hundreds or thousands of hydrographs, team members are presented with the challenges of interpreting, understanding and using this information to support design and risk analysis. The response to these challenges may be for the team to either refer back to simplified methods; or, to improperly apply results to designs; or, to simply ignore the stochastic hydrologic modeling results.

To address these challenges, a robust communication plan between the team conducting the hydrologic modeling and those performing the design and risk assessment becomes a critical path - the critical path to bringing the stochastic hydrologic modeling results from theory to practice (Rubin et al. 2018). The objective of this paper is to define a robust communication plan for the development and application of stochastic hydrology models, and for them to be effectively implemented in risk analysis and risk-informed design decisions.

History of Hydrologic Loadings

Historically, dam design and analysis of risk was completed using a designated “design flood” such as an IDF or PMF. Use of this one design flood made for a simplified handoff of the design hydrograph from the hydrology team to the design or risk analysis team. This one flood was meant to represent extreme flood conditions with which the design team could be reasonably confident that the dam could handle the hydrologic risk posed to the facility. Often that one flood hydrograph shape was used to represent floods across the frequency spectrum by simply scaling it to estimates of frequency peak inflows or volumes. However, use of just one hydrograph for risk analysis is inadequate as it does not portray any of the uncertainty and natural variability of hydrologic responses, especially across the range of frequencies of interest for risk analysis.

Limitations with Use of "Design Flood"

There are several limitations and issues related to use of a single hydrograph that need to be addressed using more modern methods and data for a risk team to be confident in hydrologic loads being presented. The first issue is that, many design floods were developed several decades ago and therefore relied on minimal flow data available at that time. Often, stream gage sites were only established a couple of years before or even after a dam was built, limiting the observed floods available to support development of design floods. The second issue is the lack of quality precipitation datasets available at the time of design flood development. Over time, the spatial network of precipitation gages has grown as has the length of precipitation records. The availability of new precipitation data varied both spatially and temporally provides a higher confidence in precipitation-frequency estimates. Furthermore, many Probable Maximum Precipitation (PMP) and precipitation-frequency products available previously have been superseded by updated products leveraging new data. Many PMFs were developed based on limited precipitation data using Hydrometeorological Reports developed in the 1960s through 1990s. Potential increases in PMP estimates with recent data means that, many of the calculated PMFs may be underestimated (Gangrade et al. 2017). An overall limitation is that, hydrologic response is inherently complex due to the natural variability of factors such as soil conditions, storm intensity, storm aerial distribution, snowpack, etc. Natural meteorological variability further contributes to complexity of the response, including such variables as spatial distribution, temporal distribution, intensity, and temperature driving rain-snow partitioning. One single hydrograph realistically cannot capture the complexities of this natural variability of a hydrologic system.

Use of the historical "design flood" metric may generally seem overly conservative, which may be appealing from the perspective of risk reduction, but this poses potential problems from both risk and cost perspectives. From a risk perspective, previously estimated design floods may not actually be overly conservative. One such example would be if modern precipitation observations approach or exceed historically determined PMP values, such as in the case where extreme rainfall events approach or exceed existing PMP values (e.g. Kao et al. 2019). Another example would be if a different hydrograph shape representing the inherent variability of the hydrologic system may result in elevated risk compared to the design flood. From a cost perspective, use of an overly conservative flood load for design or modification can mean the difference between a project being cost prohibitive or feasible. These reasons highlight the importance of shifting from using deterministic design floods to using frequency floods developed from stochastic modeling approaches.

Hydrologic Hazard Curves

Hydrologic hazard curves are used to help determine hydrologic risk at a dam. The hydrologic load is the inflow hydrograph to the reservoir. These curves represent a relationship between hydrologic load and likelihood of that load or a response, otherwise known as annual exceedance probability (AEP). Common curve types (i.e. hydrologic loadings) include probabilistic peak inflow, maximum water surface elevation, volume, or duration of overtopping. Which curves are important is dependent on the characteristics of the facility, reservoir, watershed, meteorology as well as specific project needs and potential failure modes of concern. For the purposes of risk analysis within the Bureau of Reclamation's dam safety program, the AEPs of interest are typically 1/10,000 to 1/1,000,000.

These curves are typically developed using multiple methods where data allows in order to maximize the credible extrapolation to support risk analysis. Use of multiple methods improves understanding of uncertainty in loadings estimates and allows for estimations for rarer AEPs. A summary of typical methods and limits of credible extrapolation are summarized in Table 1. The additional of stochastic hydrologic models can further extend the optimal credible extrapolation AEP beyond what is listed there. Typically, these curves are developed by fitting a distribution to an annual peak stream gage series and then extrapolating out to the AEPs of interest. As most stream gage records are ~100 years in length, extrapolating out to a 1,000,000-year event results in very high uncertainty. Paleoflood data usually improves confidence and reduces uncertainty of rare flood frequency estimates for hydrologic hazard curves, but uncertainty associated with paleoflood and non-exceedance estimates can still be high and may not be available at all sites. These methods are described in detail in Bulletin 17C (England et al. 2018). The use of stochastic hydrologic models in conjunction with stream gage records and paleoflood data can improve estimates for rare flood events and better represent the uncertainty to support risk analysis and any subsequent modification decisions.

Table 1. Hydrometeorological data types and extrapolation limits for flood frequency analysis (Adapted from Swain et al, 1998)

Type of Data Used for Hydrologic Hazard Curve Development	Limit of Credible Extrapolation for AEP	
	Typical	Optimal
At-site streamflow data	1/100	1/200
Regional streamflow data	1/750	1/1,000
At-site streamflow and at-site paleoflood data	¼,000	1/10,000
Regional precipitation data	½,000	1/10,000
Regional streamflow and regional paleoflood data	1/15,000	1/40,000
Combinations of regional data sets and extrapolation	1/40,000	1/100,000

Stochastic Modeling Overview and Challenges

Basics of Stochastic Hydrologic Modeling

The current practice to better understand uncertainty and represent the inherent variability of a watershed and its climatic forcings is through use of stochastic hydrologic modeling (Reclamation & USACE 2015; Sayers et al. 2014; England et al. 2014). Stochastic methods are employed within the modeling framework by sampling hydrological and meteorological datasets as well as model parameters using a MCSF. The MCSF allows for model inputs and parameters to be varied within physically realistic ranges for the study area and preserve co-variability of the model inputs. Examples of parameters that can be varied within the hydrology model include infiltration rates, subsurface storage, and flow timing. In addition to model parameters, meteorological forcings can be varied as well. Examples include rainfall duration and intensity, spatial distribution, and orographic parameters impacting snowfall and snowpack characteristics. Precipitation can be sampled from a regional precipitation-frequency curve along with its associated uncertainty and scaled to reflect representative spatial and temporal storm patterns for the study basin. Traditional design hydrology is typically far more simplistic

and may not represent a suite of storms and associated responses. Variation of these parameters allow the hydrologic modeler to simulate a more realistic hydrologic responses compared to typical design hydrology methods.

Use of the MCSF allows for many thousands to hundreds of thousands of simulations to develop synthetic datasets representing thousands of years of hypothetical floods. Typical flood frequency curves are developed using a series of annual peak flows from a stream gage. However, in best-case scenarios, this is at most ~150 years of data (more often it is ~20-50 years of data). This can be further complicated by stream gages being discontinued or upstream regulation impacting peak timing and volume. Further, non-stationarity issues may impact gage records such as land-cover changes, fire disturbance, or climate change to name a few. The problem with extending a flood frequency curve out to a return period of interest for risk analyses from ~50 years of data is the large uncertainty associated with these estimates beyond credible extrapolation (refer to Table 1). This is where the PMF or IDF have historically played a significant role, but still with large uncertainty. Development of a large number of hydrographs allows for the team to better quantify uncertainty and gain insight into flood frequency characteristics beyond what is credible for analysis using only peak streamflow gages.

Another beneficial characteristic of stochastic modeling for risk analysis for dams is the ability to route the floods by varying initial water surface elevations in the reservoir. Historically, with use of a single hydrograph, reservoir routing analyses assumed a pre-determined set of initial water surface elevation, such as top of operating pool. In the Western US, reservoir water surface elevations can vary significantly and may not reach the top of active conservation pool value every year as many are purposed to store snowmelt (which varies annually). Therefore, use of a high initial water surface elevation that does not represent the seasonal variability inherent to reservoir operations may be unnecessarily conservative. Through the use of stochastic modeling, reservoir initial water surface elevation associated with the routing can be varied as well and tied to antecedent conditions such as snow pack, soil moisture, or simply randomly sampled from historical observations during the flood period of interest. This method of sampling the initial water surface from a historical distribution during flood season rather than simply choosing a design elevation allows for more realistic representation of the system and improved quantification of uncertainty.

The Challenges of Using Stochastic Modeling Results

One of the key challenges associated with the use of stochastic hydrology model results for risk assessment and design is knowledge and data transfer. Stochastic hydrology modeling often produces thousands to hundreds of thousands of hydrographs and reservoir routings. This can be a challenge for data transfer from the hydrology team to the rest of the risk analysis team or the design team. These datasets can be very large in size where old design hydrographs were typically table of hydrograph ordinates in report appendix and/or accompanying digital file. Datasets could be transferred via physical hard drives or network sharing; however, it presents the challenge of how to archive in a way that makes the data accessible for future use, especially if an archive management system has been focused on either paper copies or scans of documents. From a hydrologic loading perspective, these hydrographs could be used to simply develop frequency hazard curves, however, for more detailed studies, designers typically need to use hydrographs to simulate scenarios for modification of design or operations. This is where a data management challenge becomes a much larger communication challenge.

First, just the large amount of data relative to legacy methods like the PMF can be difficult to understand. Second, sometimes evolving past these legacy methods can be difficult, especially with those who have become accustomed to using a certain type of dataset (PMF, IDF, scaled hydrographs, etc.). Conversely, some design tasks do not readily lend themselves to stochastic approaches, necessitating development or selection of a small subset of hydrographs that effectively characterize uncertainties. This requires communication-oriented and opposite to the discussion above (designer to modeler) to clarify these needs. Communicating how stochastic hydrologic modeling works and why it is a more realistic representation of the system and better understanding of uncertainty becomes important. Finally, working with the entire multidisciplinary team to determine what are the needs at the facility of interest and how to use the hydrographs properly becomes one of the most important parts of the process.

Communication Framework

For stochastic modeling results to be properly implemented in a project, a robust communication framework should be developed at the onset of the project. This framework has been divided into three distinct phases: (1) planning, modeling, and baseline risk assessment; (2) design and analysis using results from phase 1 using a small subset of the generated hydrographs (e.g., 50-100, depending on project application); and (3) verification of acceptable risk from design/operations developed in phase 2 using the full suite of generated hydrographs (e.g., 10,000 or more).

Phase 1:

Phase 1 is the first important component of the study where the team is assembled, the stochastic modeling is completed, and the baseline risk is identified. Figure 1 illustrates the makeup of the teams involved in the process. A summary of the major tasks and subtasks associated with this phase are shown in the bulleted list below and in Figure 2. The overall plan for the project should be laid out during pre-project planning. The key players on the teams should be identified. The three elements of this type of study should include three teams – (i) hydrology team, (ii) risk analysis team, and (iii) design team. The hydrology team consists of members performing the stochastic hydrologic modeling, the design team uses the results to inform decision making in any design or operations modification, and the risk analysis team ultimately analyzes the overall risk at the facility using the results of the stochastic hydrology model. The teams need to communicate frequently throughout the process to meet the goals identified for the study. The hydrology study portion is complete when the hydrographs and hydrologic hazard curves are developed. The routing portion of the study (a task that could be shared between the hydrology and design team) uses all the hydrographs developed in the hydrology study and routes them through the reservoir. This includes sampling from a distribution of historic initial water surface elevations reflecting current operations and routing hydrographs through the dam using pre-determined existing routing scenarios. The result of the routing is generally a hydrologic hazard curve representing return periods for water surface elevations. Finally, after all the hydrologic hazard curves have been developed, the results go to baseline risk assessment to determine existing hydrologic risk.

- Pre-project planning
    - Identification of key team members

        - Identified in this report as “Hydrology Team,” “Risk Analysis Team,” and “Design Team”
        - Identify leads for each team for communication
    - Development of a communication plan
        - Who is leading what
        - How frequent should meetings be and what should the content be
        - What are the key deliverables
    - Identification of goals
        - What kind of study: design, modification, operations, or baseline risk analysis
        - What hydrologic hazard curves need to be developed (maximum water surface elevation, peak inflows, peak outflows, duration of overtopping)
        - What operations should be simulated
        - How will routing be completed? Inside stochastic model versus by team outside of hydrology team? This is dependent on the complexity of flood routing rules for a given facility as this may impact the computational requirements for data sets with significant numbers of hydrographs.
- Hydrology study
    - Development of inflow frequency hydrographs
    - Deliverable of hydrologic hazard curves for peak inflows and volumes
    - Archive of full set of hydrographs for future use
- Routing
    - Routing based on operations identified in pre-project planning
    - Review of initial reservoir elevations
- Baseline Risk Assessment
    - Use of hydrologic hazard curves to determine hydrologic risk.
    - Determination whether hydrologic risk at acceptable level
        - If yes, archive hydrographs for potential future use
        - If no, move onto phase 3
        - If design or operational modification project, move onto phase 2

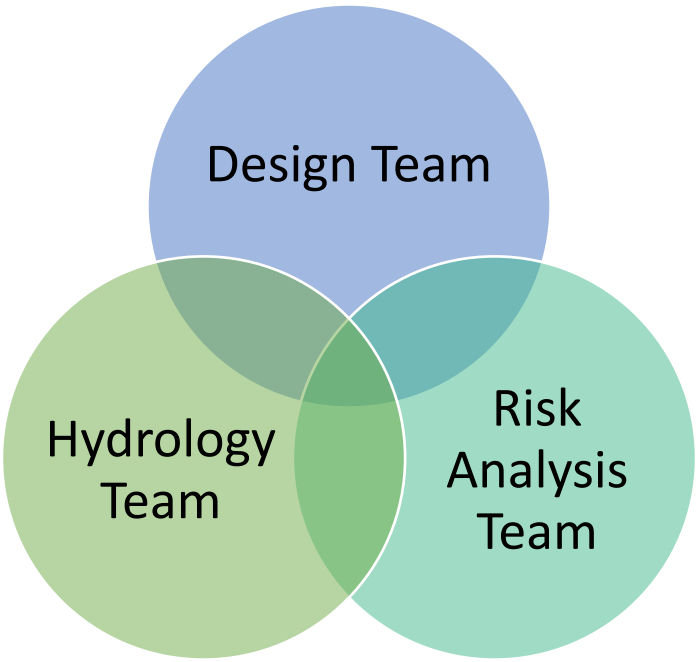

Figure 1. Venn diagram illustrating collaboration framework between the three teams involved in use of hydrologic loadings

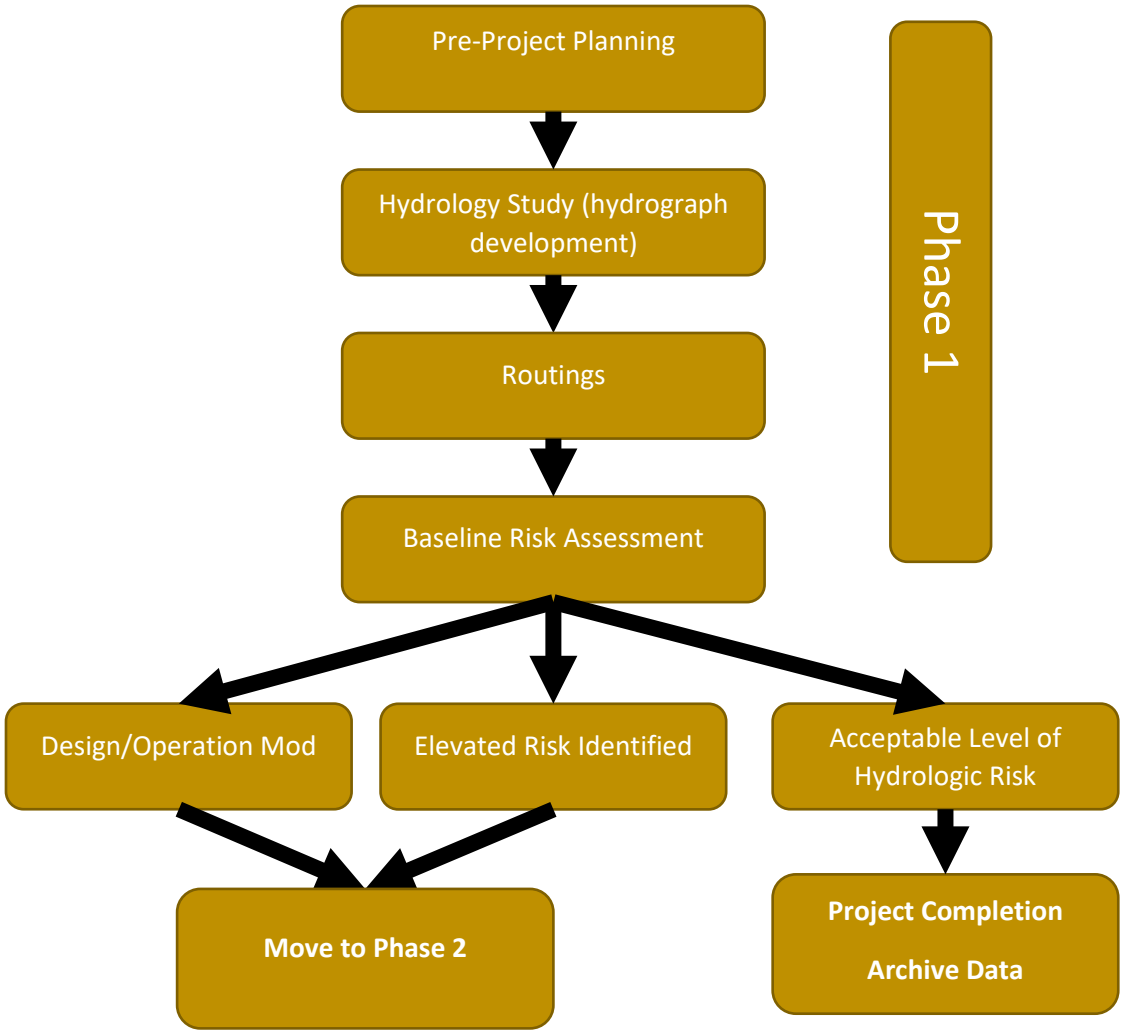

Figure 2. Summary of Phase 1 of stochastic hydrology study

Phase 2:

Phase 2 represents use of the hydrographs developed as part of Phase 1. Projects which either have identified elevated hydrologic risk for further analysis or have the need for any modifications move on to this phase. The main tasks and subtasks for Phase 2 are listed below and illustrated in Figure 3. The hydrology team in discussion with the design team extracts a subset of representative hydrographs around the AEPs of interest identified by the risk analysis and design teams for use in the design process, as described in the previous section. These hydrographs should be manageable for the design team to do screening level development of a variety of design and/or operations alternatives.

- Use of subset of hydrographs from Phase 1
  - Extract subset of hydrographs representative of important return periods identified by full project team – should be a small manageable number for use by design team
  - Extraction based on specific needs identified by design team

- Use subset of hydrographs to define design alternatives or operational changes
- Development of preliminary design/operations

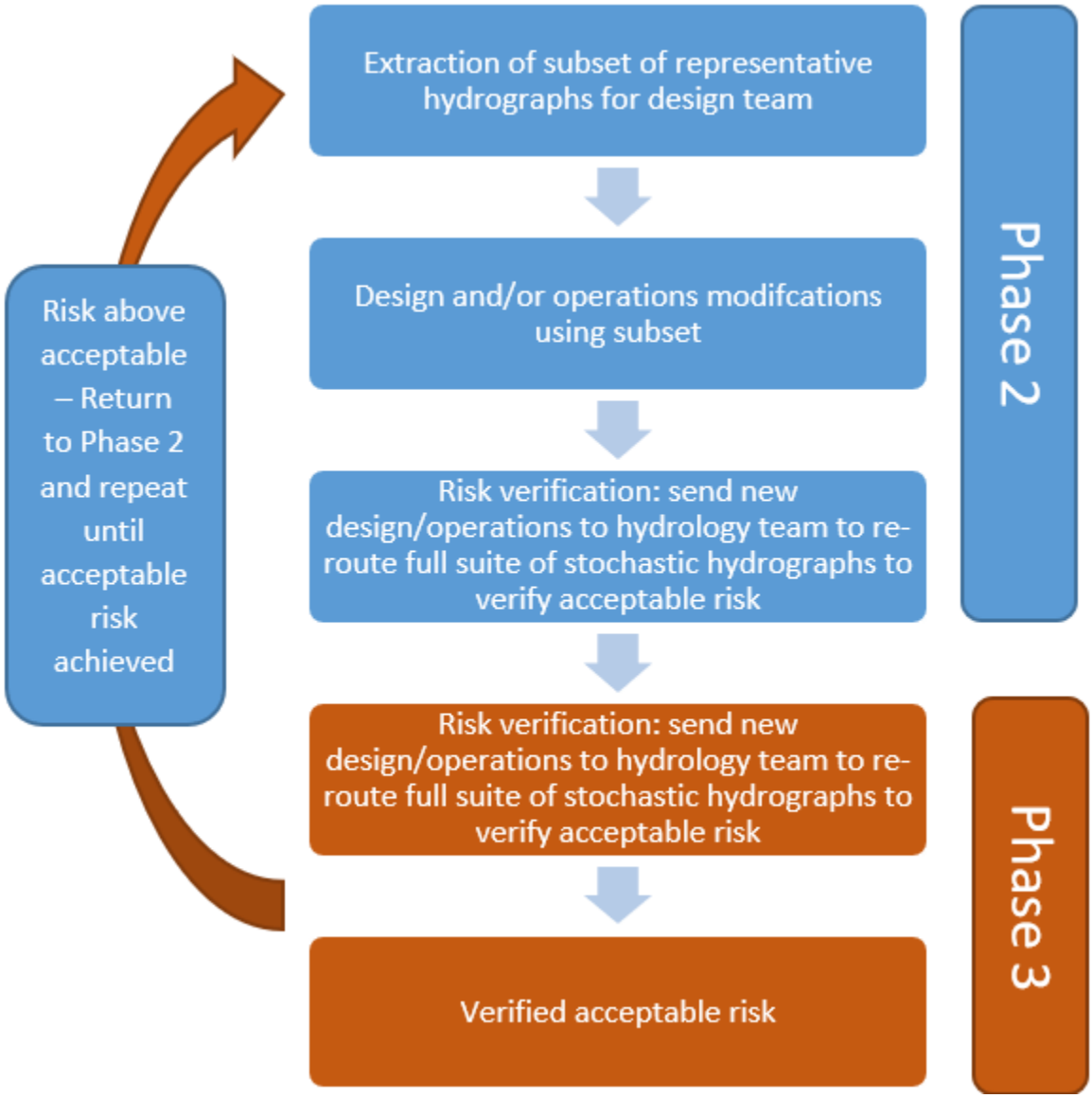

Figure 3. Summary of phases 2 and 3 of stochastic hydrology study

Phase 3:

Phase 3 immediately follows completion of design alternatives in Phase 2 (or as an iteration of the design process), illustrated in Figure 3. The goal of this phase is to evaluate if the risk associated with the design alternatives is acceptable for the risk analysis team. To complete the risk verification, the full suite of hydrographs developed in Phase 1 should be re-routed using the new alternatives to verify that risk is considered acceptable for the new design. If the full routings still indicate elevated risk, the hydrology and design teams return to Phase 2 to identify

additional hydrographs or different criteria for hydrograph selection to support the design process.

- Verification of acceptable risk
    - Using new design alternatives or operations, hydrology team re-runs routings of full set of hydrographs from Phase 1 with routing settings (e.g., storage-discharge curves) provided by the design team
    - If risk level acceptable, design team moves forward
    - If risk level not acceptable, design team re-visits design or operational changes to re-submit to hydrology team for verification
        - Hydrology team may need to provide different or larger subset of hydrographs in support of the proposed design

Three hypothetical but representative project situations with variations in the communication framework are presented below:

- Through the screening level risk analysis, it was identified that Dam A had high hydrologic risk, although there was high uncertainty in the hydrologic loading estimates. A team is convened to perform a detailed stochastic hydrology study. The stochastic hydrology study changed the estimates and reduced the uncertainty in the hydrologic loads, bringing the hydrologic risk below guidelines. No modification of the facility is required due to hydrologic loads and the detailed study improved confidence and range of uncertainty in previous estimates.
- Dam B requires operations modification. Given high uncertainty in previous hydrologic hazard estimates, a detailed stochastic hydrology study is completed. A subset of hydrographs is extracted for the design team to develop operations alternatives. The operations alternatives are then used to route the entire suite of hydrographs developed during the stochastic hydrology study to verify acceptable risk. The risk analysis team determines that the operations modifications maintain an acceptable level of risk, allowing the design team to move forward with the proposed operations.
- Dam C is slated for a raise to increase storage capacity. Because of the high cost of the dam raise, a detailed stochastic hydrologic study is completed to maximize spillway capacity, other design consideration, and operations such that post-modification is risk-neutral. A subset of hydrographs is extracted for the design team to develop design alternatives. The proposed design alternatives are then used to route the full suite of hydrographs from the stochastic hydrology study for risk verification. The routing indicated that one of the alternatives results in elevated risk slightly above guidelines. The design team goes back to the hydrology team for additional hydrographs to support modification of the current design. Following modification, the design alternative is then re-verified through routing of the full suite of hydrographs, confirming acceptable risk of the modified design. The design team can then move forward with the proposed designs modifications.

Selection of Subset of Representative Hydrographs

While use of the full suite of hydrographs to support development of hazard curves for risk analysis is important, often the design team needs just a subset of representative hydrographs to develop design or operations changes. Choosing a subset of representative hydrographs can be a challenging task, especially if someone outside of the hydrologic modeling team is simply

presented with many data files representing hydrographs with no guidance. Instead, the hydrologic modelers should work with the design team to determine the needs to support the design process. This process will look different for different facilities but following some general guidance can streamline this process.

The process to select a subset of hydrographs to support any design or operations modification can be divided into three parts. The first part is identifying a “risk window”, where the risk analysis and design teams identify what level of risk, or what return period, is critical for further analysis at that facility (Reclamation 2018). Also, what level of uncertainty is important to know? For example, accounting for factors such as population downstream and facility type, perhaps the risk analysis team is interested in looking at flood risk from the 100,000- to 1,000,000-year return periods. Perhaps the 90th percentile of uncertainty is deemed appropriate for risk analysis. This is then the risk window identified for further study.

The second part is up to the hydrology modeling team to determine what the inherent variability of the system is and how to identify hydrographs to represent the spectrum of natural variability for the watershed. For large and complex watersheds, such as those representing heavy snowfall mountainous regions adjacent to arid regions or those with extensive regulation, this may be a very large subset. For smaller, simpler basins, this will likely be a much smaller selection. For smaller projects, this could be completed simply with manual analysis and visual inspection. For larger projects, methods such as principal component analysis (PCA) could be used to identify clusters of similar hydrographs. Methods that could be applied beyond manual inspection or visual analysis include options such as PCA, self-organizing maps, or multivariate clustering approach (Hotelling 1933; Kohonen 1990). The applicable methods should be determined based on both an objective multivariate analysis coupled with judgement from the teams.

Finally, the design team should determine what is a manageable number of hydrographs to work with to refine designs. Ideally, this number should be large enough to be able to represent the natural variability of the system but small enough for the design team to efficiently test any modifications. If representative hydrographs are properly selected, proposed designs and operations should be able to pass the final verification process of routing the entire suite of hydrographs. Taking adequate care during this process can minimize the need to return to the hydrograph selection process after preliminary designs are completed.

Summary

When applied with multiple lines of evidence such as stream gage records and paleoflood data, use of stochastic methods in hydrologic modeling can improve confidence and improve characterization of uncertainty in hydrologic loading estimates to support risk analysis and the design process. Results from stochastic hydrology models are generally more realistic of existing hydrologic conditions in the watershed relative to deterministic methods employed in the past. Uncertainty is often better constrained for the extremely rare flood events of interest for management of risk. However, to foster use of stochastic modeling results in practice, additional effort must be given to planning and communication during the process. The large datasets and complex methods may appear confusing, overwhelming, or not conservative enough to those accustomed to traditional methods of developing hydrologic hazard estimates. The methods and framework provided here can be used in practice to support adoption of the methods as a standard practice in support of risk analysis and design for facilities.

The goal of this paper, through the communication plan and methods presented here, is to improve understanding of stochastic hydrologic model results and to provide a robust communication framework to utilize these tools in analysis, and risk-informed decision making. By implementing these tools at the onset of a project and throughout the study process, probabilistic flood hydrographs developed using stochastic hydrology models can be effectively implemented.

References

England, J.F., Julien, P.Y., and Velleux, M.L. 2014. "Physically-Based Extreme Flood Frequency with Stochastic Storm Transposition and Paleoflood Data on Large Watersheds," Journal of Hydrology, 2014. 510: p. 228-245. doi: 10.1016/j.jhydrol.2013.12.021

England, J.F., Jr., Cohn, T.A., Faber, B.A., Stedinger, J.R., Thomas, W.O., Jr., Veilleux, A.G., Kiang, J.E., and Mason, R.R., Jr., 2018. Guidelines for determining flood flow frequency – Bulletin 17C, U.S. Geological Survey Techniques and Methods, book 4, chap. 5, 148 p.

Gangrade, S., Kao, S., Naz, B., Rastogi, D., Ashfaq, M, Singh, N., and Preston, B. 2017. "Sensitivity of probable maximum flood in a changing environment," Water Resources Research: 54. doi: 10.1029/2017WR021987

Hotelling, H. 1933. "Analysis of a complex of statistical variables into principal components," Journal of Educational Psychology: 24(417-441). doi: 10.1037/h0071325.

Kao, S, DeNeale, S.T., and Watson, D.B. 2019. "Hurricane Harvey Highlights: Need to Assess the Adequacy of Probable Maximum Precipitation Estimation Methods," Journal of Hydrologic Engineering: 24(4) doi: 10.1061/(ASCE)HE.1943-5584.0001768.

Kohonen, T. 1990. "The Self-Organizing Map," Proceedings of the Institute of Electrical and Electronics Engineers. 78(9), 1464-1480. doi: 10.1109/5.58325

Rubin, Y., Chang, C.F., Chen, J., Cucchi, K., Barken, B., Heße, F., and Savoy, H. 2018. "Stochastic hydrogeology's biggest hurdles analyzed and its big blind spot," Hydrology and Earth System Sciences: 22(5675-5695). doi: 10.5194/hess-22-5675-2018

Reclamation, and U.S. Army Corps of Engineers (USACE). 2015. "Best practices in dam and levee safety risk analysis (Version 4.0)," Probabilistic hydrologic hazard analysis, Chapter li-2: Denver, CO.

Reclamation. 2018. "Reservoir operations pilot study: Washita Basin Project, Oklahoma," Accessed March 8, 2019 at: https://www.usbr.gov/watersmart/pilots/docs/Final_Reservoir_Operations_Pilot_Report-Washita_Basin_Project_OK.pdf

Sayers, P., Nathan, R., Rodda, H., Tomlinson, E., and Bowles, D. 2014. "Comparison of Flood Hazard Estimation Methods for Dam Safety - Phase 1," C. International, Editor. 2014: Montreal, Canada.

Swain, R.E., Bowles, D., and Ostenaa, D. 1998. “A framework for characterization of extreme floods for dam safety risk assessments,” Proceedings of the 1998 USCOLD Annual Lecture, Buffalo, NY. August, 1998.

Flood Inundation Mapping Cadre Process and Procedures by the USACE's Modeling, Mapping, and Consequence Production Center (MMC)

Wesley Crosby, P.E., Modeling Technical Coordinator, U.S. Army Corps of Engineers, Vicksburg, MS, Wesley.A.Crosby@usace.army.mil

Abstract

The USACE Modeling Mapping and Consequences Production Center (MMC) provides hydraulic modeling, mapping and consequence analysis for USACE dams and Levees in support of the USACE Dam & Levee Safety and Critical Infrastructure Protection and Resilience (CIPR) Programs. The MMC has developed processes, tools and standards for creating dam and levee breach hydraulic models for use in emergency action plans (EAP), during real-time flood events, and in support of the Corps Dam & Levee Safety and Security programs. As a result of this experience, the MMC also provides Flood Inundation Modeling support during real-time flood events with its Flood Inundation Mapping Cadre (FIM). The mission of the FIM Cadre is to assist districts and other government agencies when called upon to run real-time hydraulic models, prepare forecast inundation maps, and develop consequence estimates for significant flood events. Since supporting the flooding efforts during the 2011 flood of record on the Mississippi River and the 2011 flood on the Missouri River, the FIM Cadre has been called in to support multiple flood events across the nation, including support during some hurricanes. To date the MMC FIM Cadre has supported at least 14 flood events since 2011, including 7 Hurricane Events.

This presentation will provide information on the purpose, processes, and procedures for production of inundation mapping products within the USACE. The use of mapping during extreme events (floods, droughts, hurricanes, etc.) has provided, and continues to provide, critical situational, and real-time information for emergency responders, decision makers, and key stakeholders. This information is helpful not only to USACE, but also to federal, state, local, and emergency responder partners. This presentation will discuss the modeling, mapping, consequence products produced during a flood event. In addition, this presentation will provide case studies where the MMC FIM Cadre has supported flood inundation modeling during flood events. Over the years, the MMC FIM Cadre has supported 19 districts, multiple states, and FEMA.

Since the passage of the Flood Control Act of 1917, USACE has played a significant role in managing flood risk nationwide. After supporting the 2011 Mississippi River flood, the MMC worked to develop a national FIM Cadre team that could assist districts with producing hydraulic models, inundation maps, and consequence estimates for flood events across the nation. These products during an extreme flood event, provide critical situational and real-time information that can be used by decision makers, emergency responders, and other key stakeholders. In order to provide consistent products across all USACE districts, the MMC has developed a Standard Operation Procedure (SOP) for Flood Inundation Mapping. The initial draft was created in 2016 and the latest version was finalized in early 2018. Some of the information provided in the SOP is the FIM Cadre Team structure, roles and responsibilities for

team members, planning and coordination between members and districts/divisions/HQ, data collection, model and software selection, typical model scenarios, typical mapping products, data standards, mapping standards, upward reporting, product release, data management etc. In addition, the MMC has worked with the Hydrologic Engineering Center to develop ways to communicate model quality/confidence and uncertainties within our models on our map products.

References

U.S. Army Corps of Engineers, MMC Flood Inundation Mapping SOP, 2018.

Hurricane Florence Shows Us a Need For a New Classification System to Categorize Flooding and Damages

Dr. Frank Reckendorf,
Fluvial Geomorphologist
Reckendorf and Associates
Salem, OR
(503) 551-2130
frecken@mac.com

Abstract

Over the years flooding is usually associated with rivers and streams where flood water has overtopped streambanks.. Other flooding was observer but seldom identified. Wetlands flood when there is heavy rainfall and are referred to as ponding. Water accumulation in lakes sometimes exceeds the lakes capacity, so water accumulates around the lake. Water from rivers and flood plains, along with that from wetlands and lakes eventually reaches estuaries where the accumulation exceeds the banks of the estuary causing flooding. Along the ocean significant waves and storm surge wash over land areas to cause local flooding. The geomorphic expression (i.e. the topography) associated with all these types of flooding can be placed in USFWS wetland classification (Circular 39, 1979). If we modify the wetland classification to only look at the flood component, the flood classes are: Riverine, Lacustrine, Palustrine Estuarine, and Marine. Historically Riverine flooding has been defined (Reckendorf, 1973) as that floodplain with alluvial land adjacent to a river that can be flooded by the occasional great flood such as the 1% chance event. This would be consistent with FEMA maps based on a base flood with a 1% chance event. Lacustrine flooding would be that which occurs along typical wetland and adjacent flat areas.. Palustrine flooding would be typical of flooding around lakes. Estuarine flooding includes flooded areas around estuaries and lagoons and would include river stage, tidal flooding and storm surge. Marine flooding includes all areas around coastlines that could be flooded by significant waves , storm surge, and associated run-up. The landscape developed during the Holocene to Recent set a geomorphic low topography that has a historical record of flooding. This topography along the North and South Carolina Coast has flooded many times. It is unknown if the duration and depth of flooding of the equivalent areas flooded during hurricanes or tropical storms has increased because of climate change impacts along the North and South Carolina coast. It is known that slower hurricanes can dump more rain in an equivalent area , which is reflected in Hurricane Florence flooding. Hurricane Florence made land fall as a Category 1 hurricane. Inland it changed to a tropical storm, and than to a tropical depression. Florence has changed how we need to look at flooding. The slow movement (2 mph) was a major cause for the Lacustrine and Palustrine flooding, which adds to the Riverine Flooding. The Swansboro Rain Gage recorded 33.89 inches of precipitation for the event compared to 24.86 inches for the Floyd Hurricane. Hurricane Florence caused inland flooding where it has never occurred before. Flood peaks along rivers in North and South Carolina greatly exceeded prior flood peaks ,

Introduction

Flooding throughout the world has been recognized as a problem for over 100 years. The subject is complex and is described differently depending on the conditions where the flooding occurs. This paper shows a new template to categorize all types of flooding. The focus will be on flooding in the United States of America and include the natural condition of the landscape flooding and the encroachment of infrastructure that has caused natural flooding to increase.

The topography (geomorphology) along rivers and streams, lakes, estuaries, and coastlines has developed over geologic time of Holocene and Recent. The Holocene Period, is basically the last 10,000 years. The Recent period represents the last 2,000 years, but in the later part of the Recent time frame, flooding has been modified and often increased, because of changes in the watershed natural landscape and encroachment into the floodplain.

To reflect the topography for both the natural condition and the modified condition the author proposes a new template. The template proposed is a modification of the US Fish and Wildlife Service system for categorizing wetlands published in Circular 39 (USFWS, 1979). The system divides wetlands into Riverine, Lacustrine, Palustrine, Estuarine, and Marine Classes. Circular 39 does has an important vegetative component of the classification system. The vegetation criteria for that component will be ignored is this classification system designed to represent the aerial extent of flooding by the 1% chance event.

Background information about the conditions that caused Florence hurricane flooding will be presented before a discussion of the new classifications system and their applicability to Florence and in the US. Also discussed will be the evolvement of FEMA.

Background

Weather and Rainfall

Tropical Cyclone Florence became Hurricane Florence on September 6, 2018, and was the sixth named hurricanes, and the first major hurricane of the 2018 hurricane season. At one time Florence was classified as a Category 4 hurricane, but slowed to be classified as a Category 1 hurricane (sustained winds of 74 to 95 mph) when it made landfall just south of Wrightsville Beach North Carolina on September 13, 2018 (Wikipedia, Hurricane Florence, October 2, 2018). Within a day it transitioned to a Tropical Storm and then to a Tropical Depression. During the storm bands of the circulation had different intensites of rainfall. Florence slowly drifted inland over a wide area such that tropical force winds occurred out 195 mi. from the hurricane's eye (Rhodan, 2018).

A ridge of high pressure over eastern North America stalled Florence'a forward motion for several days. It moved forward at only 2-3 mph and dumped heavy rainfall from the outer rain bands between September 13th. to 15 th. By September 15th, the storm had stalled only a few miles from Wilmington NC. A rainfall total near Swansboro NC of 30.58 inches broke the all time record rainfall for a tropical system. The prior record was 24.06 inches during Hurricane Floyd.

A recent paper from Penn State (Mann, 2018), states that unusual warmth in the Arctic causes jet streams, the rivers of air in the atmosphere that push or pull the weather systems, to slow down stall or meander in strange ways, When the undulations of the jet stream lock in place, weather systems can be trapped in place and cause havoc like extreme flooding from long duration storms.. The extremes and unusual jet stream patterns are known as "quasi-resonant amplification". The paper indicated this effect on the jet stream is increasing because of climate change brought about by the burning of fossil fuels.

On June 8, 2018 the Science Daily reported that some hurricanes are moving more slowly. They state that according to a June 6, 2018 article in the Journal Nature a study has measured translation speed, which measures how quickly a storms moves over an area. Between 1949 and 2016 tropical cyclone translation speeds declined 10 percent word wide. In another study James Kossin, a climate scientist with NOAA measured how fast a storm moved over the landscape and found that tropical cyclones were slowing down. He also states that steering winds are responsible for moving hurricanes along their path, as hurricanes are carried passively by the winds that are sitting in, somewhat like a cork in a stream. He goes on to state that the steering winds draw power from the temperature differences between tropics and the poles. However, because of climate change that temperature difference is declining, which weakens the winds and therefore hurricanes move more slowly. An article by Doyle Rice on September 29,2018, that appeared in USA today, reported on a new study of Atlantic Ocean temperatures. He reported that the 2017 hurricane season, that included Hurricanes Harvey, Irma, and Maria, was fueled in part by warm ocean water. In 2017 six major hurricanes formed which was twice the average. Sea water in main hurricane development area averaged 0.7 degrees warmer than normal for the entire hurricane season. Quoting Hiro Murakami, climate scientist and hurricane expert at National Oceanic and Atmospheric Administration (NOAA), " We show that the increase in 2017 major hurricanes was not primarily caused by La Nina conditions in the Pacific Ocean, but mainly by pronounced warm sea water conditions in the tropical North Atlantic".

Geology, Soils, Topography, and Trees

North Caroline lies to the north of South Carolina. They both have a topography characterized by a large coastal plan on the east side. During the Cenozoic Era the ocean covered the lowlands, and subsided repeatedly , creating terraces each time. Eleven marine terraces can be found in South Carolina representing higher sea levels. Extensive back barrier marsh deposits occur and some estuarine and delta deposits. These soils would tend to have drainage problems and this along with high water tables means that these soils and the sandy soils can easily be saturated with high rainfall. Runoff was responsible for gradually shaping the coastal plain's gradual downward slope, and rivers cut down to the existing sea level. Several rivers have their headwaters in North Carolina and than flow through South Carolina at their lower end.

The trees on the North Carolina Coastal plain include Loblolly Pine, Oak, Red maple, Yellow Popular, Lealand Cypress, Bedford Pear, and Sassafress. South Carolina's Coastal Plain trees are mostly Oak, Maple, Pine, Palm, Bald Cypress, and barkless trees. Spanish Moss tends to accumulate on Oaks and Bald Cypress.

Hydrology

As Florence moved inland from September 15 to 17, 2018, the heavy rainfall caused widespread flooding inundating cities such as Fayetteville, Smithfield. Lumberton, Durham and Chapel Hill, as major rivers such as the Neuse River, Eno River, Cape Fear River, and Lumber River overtopped their banks. In Fayetteville, NC, the Cape Fear River crested at 61.4 ft some 26 ft. above its normal flood level which is 21 ft. (Rhodan, 2018). A larger area has flooded than was flooded in Hurricane Mathew two years ago. The Neuse River reached a new peak height of 25.8 ft, with a major flood peak being 21 ft. The Cape Fear River near Fayetteville NC had a flood peak of 61.4 ft, which was 25 ft. above flood stage. A larger area flooded from Florence than was flooded in Hurricane Mathew two years prior. Florence is projected to be classified as a 500 to 1000-yr. average recurrence interval event for some rivers in North and South Carolina. Flood stages for riverine areas reached new highs.

Damages

Hurricane Florence currently (September, 2018) ranks 6th, >$38,000 million in damages (Wikipedia, October 1, 2018). It is still too early to get a final total on damages, but current estimates will be much higher if one builds in the loss of commerce because of the flooded roads, especially I-40, I-95, and US Routes 70 and 401, and Sate Highway 76. Their was an extensive flood fight in both NC and SC and there were 42 deaths attributed to Hurricane Florence..

FIA, FEMA, and Floodplain Zoning

With the passage of the National flood Insurance Act (FIA) in 1968 the author started to do Flood Insurance Studies in Oregon, starting with a Type 2 study to identify communities that had flood problem. The first field study was a Type 10 Flood Insurance on the Applegate River in Jackson County in Oregon (Reckendorf and Taylor, 1971). That study established a floodway and a flood fringe, and included a economic evaluation of flood damages. The study established at each cross section what was the height of water in the floodway if the cross sections was constricted so that the water in the floodway was increased in increments from 1.0 ft. to 2.5 ft. These results were plotted on curves presented in the report as " Increasing Depth Remaining Width Curves". That report never got beyond the Draft Stage as the Flood Insurance Administration was so anxious to see what a flood insurance study looked like that they accepted the draft report as a final and no further work was done. The constriction analysis was done to determine how much freeboard to add to the base flood to be shown as flood fringe on the maps. The author worked with the SCS national staff and FIA in determining the criteria for a Flood Insurance Study.

The Federal Emergency Management Agency (FEMA) was created in 1978 and 1979 (Wikippedia, 12/22/2018). FEMA made Flood Insurance Rate Maps (FIRM) which show Special Flood Hazard Areas (SFHA) defined as areas inundated by a base flood event having a 1% chance of being equaled or exceeded in any given year, often referred to as 100-year flood zones. The SFHAs are separated into flood zones such as areas flooded by Riverine flooding in 1% chance events, areas of minimal flood hazard outside the SFHA, and areas flooded in the 0.2% chance event. In the early 1980's the author was part of the team that evaluated what should be recommended for the first floor elevation for development above the base flood, and be designated as the flood fringe on floodplain maps. The author's position was that the elevation needed for development should be 2-3 feet of freeboard above the stage determined for the 100-year average

recurrence interval event. A few government agencies used the 2-3 feet criteria in their development of the floodplain zoning ordinances. However, for economic reasons, the FIA chose to recommend the one foot above base flood for development for the flood fringe. The author thinks that this was a major mistake by FIA, as it allowed for so little freeboard to accommodate any mistakes in the analysis and did not accommodate the higher flood events that might come in the future because of upstream development that would decrease the time of concentration of flood waters or for climate change.

Classification System

Riverine Flooding

Runoff during the Holocene shaped valleys to form a sequence of terraces and floodplains. Former floodplains became terraces as the rivers down-cut during the Holocene. For those streams tributary to the ocean, the rivers cut lower floodplains because their base level was lowered as ocean levels dropped. For streams not influenced by a lowering base level, streams down-cut to form lower floodplains due to high volumes of runoff. Ice and snow remaining from glacial conditions of the Pleistocene and Holocene caused high runoff to initiate down-cutting to form a sequence of terraces and floodplains. The floodplains developed had geomorphic form and features in the landscape.

For this new classification systems to describe flooding for FEMA studies, Riverine floodplain flooding is that alluvial land that can be flooded by the occasional great flood, that has a 1% chance of occurrence in any given year (Reckendorf, 1973). This definition would be consistent with the base flood on Flood Boundary Maps and Floodway Map (FBFM) and mapped on FIRM maps. It would also be applicable to the floodplain zone mapping done by units of government, that show the area flooded by the base flood, plus one foot or higher above the base flood required by the unit of government. Floodplains have been defined otherwise such as by Leopold (1994). He defined floodplain as a level area near a river, constructed by the river in the present climate and overflowed by moderate flow events.

Leopold later described the floodplain in a video on bankfull flow as the first depositional surface along a river and floods with an average recurrence interval of about 1.5 to 2 yrs. (Leopold, 1994). Rosgen (1996) and others call higher floodplains along the river as terraces, defined as former floodplains where downcutting has occurred. Restricting the definition of the floodplain to that overtopped in bankfull flow was very useful in the development of the Rosgen Stream Classification (1996), and for field identification of the first flat depositional surface. However it is not useful when classifying areas flooded by large events such as that which occurs in a 1% chance event. The thousands of square miles of floodplain shown on floodplain boundary maps and floodplain rate maps FIRMs developed under FIA and FEMA for over 50 years, are based on a frequency of flooding in a 1% chance event, so that definition needs to be the working definition of floodplain for floodplain rate mapping.

The author has done floodplain mapping since 1966, on close to a million acres spread throughout OR, AL, WA, and AZ. These studies have been done for flood hazard analysis, flood insurance studies, floodplain zoning maps, comprehensive plans, river basin studies, and for litigation. He has also made numerous flood observations in 20

states. The author has determined that there are extensive intermediate floodplains that occur above the first flat depositional surface floodplain but below the floodplain flooded in the 1% chance event. In OR, this intermediate floodplain is flooded by about the 10% chance event. Above the intermediate floodplain is the high floodplain that in western OR is flooded with a 2% chance of occurring in an given year as well as well as flooding in the 1% chance event. The difference in width is minimal as the 1% chance event is just deeper water, and is higher on the scarp break. In the Oregon, it was established that the floodplain outside scarp break to a terrace was high enough to confine the 500-year average recurrence inter flood, i. e. a 0.2% chance event. The height of the outside scarp between 1% chance event and 0.2% chance event is not consistent across the country. In some states 500-year average recurrence interval flood event would put flood water up on a terrace, where it can spread out for miles.

The geomorphic features used in the authors floodplain mapping, were explained in a paper entitled "Geomorphic Features of Oregon Streams and Floodplains" (Reckendorf, 1969). The methodology used in the mapping was published as "Methods for Identification and Mapping of Flood Plains" (Reckendorf, 1968, and Reckendorf, 1973).

The author's floodplain mapping has been incorporated into FBFM, FIRM and floodplain zoning ordinances, in several Willamette Valley Counties in Oregon. The author mapped a total of about a half a millions acres of Riverine floodplains in Oregon. He later mapped 231,000 acres of Riverine flooding on nine streams in Alaska, as well as doing studies and floodplain mapping along streams in Washington and Arizona. Extensive mapping has given the author an opportunity to examine flooding in a broad context. He has observed the various types of flooding in this classification system, but there was no comprehensive system for mapping the various types of flooding as the programs developed by the Federal Government primarily focused on Riverine flooding. Today there are millions of acres along Riverine streams that have FBFM, and FIRM maps of the area flooded in the base flood. Boundaries for rate maps are marked "A" for approximate floodplain and "AE" for detailed mapping floodplains

The flood problems along rivers has partly occurred because the infrastructure developed along rivers to facilitate transportation. Once roads developed and needed to cross rivers, people often placed a fill on the floodplain to elevate both the approach and the bridge over the river. The bridge opening was often not large enough to pass large flood flows so backwater occurred. In addition, bridges were often built at the grade of the land which was much lower that that flooded in a 1% chance event. Therefore the cross section at the bridge had limited capacity to pass flood water. To offset the limited capacity the units of government sometimes excavated below the bridge. This excavation tended to start a head-cut that migrated upstream, often undermining the foundation of upstream bridge. To offset the flood damages to infrastructure that was occurring from building roads and railroads that crossed river, engineers started building dams to store flood runoff, and or channelizing the river to try and increase the velocity to pass through the reach. This channelization was only partly successful, as river channels tended to re-meander by down-cutting and widening to return the river to a dynamic equilibrium condition.

With the passage of the National flood Insurance Act (FIA) in 1968 the author started to do Flood Insurance Studies in Oregon, starting with a Type 2 study to identify communities that had flood problem. His first field study was a Type 10 Flood Insurance

study on the Applegate River in Jackson County in Oregon (Reckendorf and Taylor, 1971). That study established a floodway and a flood fringe, and included a economic evaluation of flood damages. The study established at each cross section what was the height of water in the floodway if the cross sections was constricted so that the water in the floodway was increased in increments from 1.0 ft. to 2.5 ft. These results were plotted on curves presented in the report as " Increasing Depth Remaining Width Curves". That report never got beyond the Draft Stage as the Flood Insurance Administration was so anxious to see what a flood insurance study looked like that they accepted the draft report as a final and no further work was done. The constriction analysis was done to determine how much freeboard to add to the base flood to be shown as flood fringe on the maps. The author worked with the SCS national staff and FIA in determining the criteria for a Flood Insurance Study.

The author has extensive experience in field flood plain mapping, so he is an authority on the subject, and is well suited to evaluate if our present floodplains as represent on FEMA maps are adequate He has been involved in 15 litigations concerning flood plain boundaries, and the associated streambank erosion. Most of the authors mapping has become part of later studies published by FEMA. The authors floodplain mapping has been incorporated into floodplain zoning ordinances, in several Willamette Valley Counties in Oregon. The author mapped about a half a millions acres of Riverine floodplains in Oregon. He later mapped 231,000 acres of Riverine flooding on nine streams in Alaska, as well as studies along streams in Washington and Arizona.

If any single date can be assigned to the importance of floodplain encroachment in the US it is January 22, 1936. On that date Congress passed the Federal Flood Control Act. The Act recognized that flood problems where national in scope and resulted in national policies which placed primary reliance on flood control structures. to solve the flood problems. Between 1936 and 1998 the Federal Government invested more than seven billion dollars in building dams and doing channelization. However the flood damage was greater in 1966 than it was in 1936 (Reckendorf 1973). In 1965 the Bureau of the Budget appointed a task force on flood control policy. The task force report was printed as House Document 465, entitled "A Unified National Program for Managing Flood Losses", U.S. Congress (1966). The report directed that: (1) all towns with a flood problem be identified; (2) flood plains were to be outlined on aerial photographs; (3) there should be an accelerated program of floodplain mapping and reports by Federal Agencies. With the passage of the Federal Flood Insurance Program in 1968 a local unit of government could request through the U.S. Department of Housing and Urban Development (HUD) Federal Insurance Administration (FIA) that subsidized floodplain insurance be made available, if minimum floodplain management requirements were met by the unit of government (HUD, 1968).

In the decade of the 1990's, with flood damages at an all-time high, and with upward spiraling disaster relief costs that began to strain national budgets, new approaches were attempted to reduce flood damages. The Midwest Flood of 1993 served as a catalyst to recognize the value and benefits of floodplains as natural resources, and pointed the way toward restoration and wise management of these beneficial resources as part of the overall strategy to reduce flood losses. In the wake of the 1993 Midwest Flood, many of the flooded communities began to develop and implement a new strategy of voluntary buyouts and relocation of homes out of the floodplain. Since than, many other communities across the country have followed suit. These actions represent a major change in attitude and approach toward addressing flood problems, with significant

benefits to people at risk and taxpayers, as well as not having adverse environmental impacts (Conrad, et. al. 1998).

The prime candidates for voluntary buyouts and relocations are properties that are considered to be "Repetitive Loss Property". The National Flood Insurance Program (NFIP) defines any insured property that has sustained two or more flood losses in a 10 year period as a "Repetitive Loss Property" (Conrad et. al, 1998). In the time period between 1978 and 1995, the repetitive loss properties only represented two percent of all insured properties, but claimed 40 percent of the NFIP payments. Nearly one out of every ten repetitive loss properties has had cumulative flood insurance claims that exceed the value of the property. (Reckendorf et. al. 2012). In spite of the large investment in flood control, and in flood insurance, flood damages from large floods have continued to rise. In the area flooded by Hurricane Florence it is estimated that less than 3% of the people had flood insurance. To make matters worse, recent floods in the area of NC and SC are estimated to have 500 to 1000-year average recurrence intervals.

In North Carolina, 16 major rivers were out of bank because of Florence. The Coastal Plain topography in both NC and SC, is such that once rivers are out of bank they can flood for miles. Some rivers such as the Cape Fear River and the Neuse River in North Carolina reached all-time highs and long duration flooding did extensive damage to homes, commercial and industrial areas as well as agricultural land and livestock. Power was out for 343,000 people in NC alone. In NC and estimated 1.7 million chickens were killed because of flooding. Crops at harvest such as cotton and peanuts were extensively damaged and an estimated half of the tobacco crop was flood damaged. Some local flood control structures, such as levees, had been installed but many were flanked or overtopped. The City of Lumberton had a protective levee but there was an opening in the levee for the CSX railroad tracks. Flood waters came through the gap as it had earlier in Hurricane Matthew. This is an unresolved conflict between the railroad and local officials as to how to provide some flood protection and keep the railroad operational. The Weather Channel showed a steel railroad bridge over the Lumber River with flood water up on the side of the bridge, creating backwater and accumulated woody debris. Many roads were flooded, such as Highway 76, by the Lumber River. A low area of I-95 in North Carolina, at the exit to Fayettville, flooded closing the interstate in both directions.

Lacustrine Flooding

Lacustrine flooding is that flooding that occurs on wetlands and adjacent flat land. The soils under wetlands are classified by the Natural Resources Conservation Service (NRCS) as Poorly or Imperfectly Drained. Adjacent well drained soils may not typically pond because of their good drainage but, if the soil is saturated because of long duration rainfall, than well drained soil cannot be readily separated from poorly or imperfectly drained soils. Any soil impediment to drainage can cause water to pond on the surface and can create mapped Lacustrine flooding. FIRM maps show Lacustrine flooding with map symbol AH to represent surface ponding. What is shown as AH is not the equivalent of Riverine flooding in the 1% chance event. One would need a statistical analysis of precipitation gages to determine a 1% chance storm, and that analysis is not being done. The largest data base of Lacustrine flooding areas is that shown by state in the National Wetland Inventory. What is shown as Lacustrine flooding can be used as a first approximation of the extent of Lacustrine flooding in local areas not previously mapped.

However there is no flood frequency associated with the Lacustrine flooding as the maps are only showing that from wetlands and do not show the additional flooding because of obstructions to runoff that road and railroad fills, as well as fills for housing and industrial developments cause. NRCS soil survey maps show poorly and imperfectly drained soils. A map of these soils would also give an approximation of Lacustrine flooding but with no flood frequency.

In the 1970's the State of Alaska was examining sites that might be suitable to relocate the State Capitol from Juneau. The Soil Conservation Service was asked in 1975 to do a study of the area east of Fairbanks, called Delta Junction, as a possible site for the relocation. The author was asked to do the floodplain mapping of the proposed area. He mapped 231,100 acres of Riverine flooding along nine streams. In addition he mapped 135,471 acres which would be classified now as Lacustrine flooding. In this case, the impermeable soils were because of the shallow permafrost that caused to water to pond on the surface every year. No frequency was assigned to the 37% of the area flooded due to Lacustrine flooding.

The author from visual date of NC shown by the Weather Channel in their coverage of Hurricane Florence noted that long before rivers overtopped their streambanks, large areas were flooded a few feet deep. The author interpreted this situation that thousands of acres were Lacustrine flooding, as the area being shown were 6-7 miles to the nearest stream. For the area south of Mechlenbuerg NC in Union Co., it was stated that the area had never flooded before. The area was receiving 2-3 inches per hour of rainfall, and at the time had accumulated 12" of rainfall. The author interpreted this flooding as Lacustrine flooding.

Palustrine Flooding

Palustrine Flooding would be that area flooded around lakes. The largest data base of Palustrine flooding would be the National Wetlands Inventory. These maps can be used as a first approximation of Palustrine flooding. What is shown would have the same limitations as mentioned for Lacustrine flooding, that no frequency is assigned to the flooding.

In the authors field work in Alaska in 1971 he visited lakes in the vicinity of Point Barrow. These lakes were described to be part of the oriented lakes. The water in the Lakes was almost to the level of the adjacent cotton grass tundra. Snow melt alone would provide standing water around the lakes that could not drain off. The underlying restriction to any infiltration was the permafrost leading to Palustrine flooding.

The Sanford dam breach on boiler Springs Lake in NC, had Palustrine flooding as the reservoir flooded adjacent areas that were not planned as part of its capacity. The Headwater Dam above Creston N. C. also filled to capacity and caused adjacent Palustrine Flooding. During the Weather Channel flood coverage of Florence one location visited was a reporter near Lumberton, N. C. The reporter repeatedly reported that there was no river for 5-6 miles and no overbank flooding. However he noted that there was a lake about a mile away that had filled to capacity and that any water that would have flowed into the lake now spread out on to the adjacent ground. The author has interpreted this situation near Lumberton, NC as Palustrine. Flooding.

Estuarine Flooding

As with Lacustrine and Palustrine flooding, an approximation of the Estuarine flooding can be obtained by looking at the National Wetland Inventory maps for each state. The estuaries at the mouth of the major rivers in North Carolina and South Carolina had extensive high water for many days. The Little Pee Dee and Lumber Rivers join near Nicholes, SC, which is near the head of the estuary. Nicholes had severe flooding from Hurricane Mathew in SC causing 600 residents to evacuate Only 400 returned to live is this flood prone area.. Some 4-6 feet of floodwaters again inundated Nicholes from Hurricane Florence Estuarine flooding. In general, Estuarine flooding is not separated from Riverine AE, and A on FIRM maps or from Marine flooding V and VE on FIRM maps.

Marine Flooding

Marine flooding along the coast of North Carolina and South Carolina during Florence occurred during storm surge. In some parts of NC, 20 inches of rain fell on areas of high tides and a storm surge. The expected storm surge at the mouth of the Pee Dee River was 20 ft. Deposition of beach sand inland is an indication of the extent of storm surge. At Surf City, NC, sand deposition from the Florence storm surge was observed several blocks inland. Hurricane Hugo produced 12.5 ft. of storm surge along the South Carolina Coast. On the FIRM maps these areas are mapped as V and VE. An approximation of the extent of Marine flooding can be obtained from the National Wetland Inventory maps. There is a projection of as much as 3 inches of seal level rise along the Carolina coast by 2100, to increase the flood problem. Flooding from Significant Waves has been ignored in flood studies along the Carolinas. In Oregon Significant Waves average 12.8 times average wave height (Komar, 1997).

Discussion

Hurricane Florence was directly or indirectly responsible for 42 death. One can ask if Hurricane Fluorence flooding was natural flooding that should be expected or was it just an extreme event in a long-term record? In addition was it enhanced by climate change? The ocean temperature was very warm in the tropics where Hurricane Florence originated. Research is needed to establish if the ocean temperatures that generated Florence represent a new condition. A big problem was the slow movement of the hurricane rain bands at 2-3 mph for a long duration over local areas. Some gages reported rainfall of over 60 inches for the event. The high rainfall and lack of drainage ditch capacity and adequate outlets, caused ponding (Laciustrine flooding) that has not in general been documented.

Hurricane Florence is likely to be one of the worst flood disaster in terms of area flooded, that the nation has experienced. Part of this is that some of the flooding was a none traditional type like Lacustrine flooding because the soils in some areas were saturated, the drainage ditches were full and there was no way for water to infiltrate or run off. The capacity of some lakes and reservoirs were maxed out causing Palustrine flooding of surrounding areas. On some NC and SC streams, Riverine flooding occurs with flood stages that only occur in very extreme floods like those with 500 to 1,000 year average recurrence intervals. The Riverine, Lacustrine, and Palustrine flooding eventually reached estuarine causing Estuarine flooding. Where Florence made landfall there was also a storm surge which caused Marine flooding.

The FEMA floodplain maps were not adequate to represent the extent of potential flooding, which made it difficult to understand the extent of the problem from Hurricane Florence In addition the denial of local people of the potential flood hazard, and the cost of flood insurance caused resulted in a low percent of people with flood insurance. Also the denial of local people to recognize the flood problem caused a need for extensive search and rescue, and the need for over 3,000 people having to reside in shelters in North Carolina, The Hurricane Florence flood fight and rescue operations were greatly hampered by flooding over roads, and down trees and power lines. Some of the road flooding was Lacustrine flooding because of inadequate road ditches, and culverts to move the surface ponded water over to drainage outlets that had not yet reached flood stage.

During Hurricane Florence a lot of trees were blown down along roads bringing down power lines in the process. In addition hundreds of trees were blown down along stream banks. These blown down trees and other Large Woody Debris (LWD) restricted flood runoff and caused backwater effects that increased flooding and its duration. It is unknown if the trees blown down in Florence were shallow rooted or deep rooted species. If the problem was deep rooted trees were blown over because the soils were saturated than those areas needs evaluation for better drainage. In addition a better evaluation is needed if trees have been planted in the past to minimize blow down.

The author has mapped about a half a millions acres of Riverine floodplains in Oregon. He later mapped 231,000 acres of Riverine flooding on nine streams in Alaska, as well as studies along streams in Washington and Arizona. Most of the authors mapping has become part of later studies published by FEMA. The authors floodplain mapping has also been incorporated into several floodplain zoning ordinances, in the Willamette Valley in Oregon.

The author's extensive experience in floodplain mapping leads him to present a new way to discuss and map flooding. These new categories are Riverine, Lacustrine, Palustrine, Estuarine, and Marine. A better understanding of these other types of flooding, especially Lacustrine flooding, may help us understand how to manage this overall water accumulation. Lacustrine flooding is more of a drainage problem because of impermeable soils or saturated soils that local drainage districts must deal with in terms of ditch size, vegetation maintenance, and culvert size.. The rainfall caused ponding has not in general been documented This may be because Riverine studies are being done using HEC-RAS to only document water surface profiles along river cross sections.

The author believes that to adequately map Lacustrine, Palustrine, Estuarine and Marine flooding one needs high resolution Lydar aerial imagery, and drone flights over these types of flooding events. However there are Federal Aviation Administration (FAA) restrictions on where drones can fly. FAA restrictions applied during Florence prevented getting the coverage needed to represent any type of flooding.

We need to take a hard look at the encroachment by development that has changed what would occur as natural flooding to one modified by encroachment. Often streams are abandoned and put in a straight ditch with no floodplain and with inadequate culverts.

Three ways to evaluate how to constrain encroachment is flood proofing, relocation and buyouts. A part of flood proofing is to raise the elevation of structures above the

base flood. The author led a study in Washington of a large river basin that had a long history of flooding where these solutions have been used. (Reckendorf et al, 2012).

The Chehalis River and the Skookumchuck River were formed by runoff from the Pudget Glaciation and have been subject to periodic flood flows ever since. The Centralia newspaper has documented reports of 34 flood events from 1887 to 2007 in Lewis County, 27 of which included the Chehalis Basin. USGS stream gages have documented 35 flood events in the Chehalis Basin that cover from 1930 to 2010. With this extensive flood history, how the local have dealt with floods is worthy of consideration. There are no flood control structures, channel works or major dikes to mitigate flood hazards. Since 1993, the Cities of Centralia, and Chehalis in Lewis County worked with individual landowners to reduce flood hazard. This work was done with the support of FEMA, Washington State Emergency Management Division, and the Small Business Administration (SBA) which invested several million dollars to acquire or elevate many flood prone residential structures in Lewis County (FEMA 2008). Between 1994 to 2004 Lewis County, Centralia, and Chehalis combined flood proofed 230 structures, and removed 61 flood prone structures. (Brown and Caldwell, 2008). To determine the effectiveness of this non-structural program, FEMA in 2008 developed a study on residential structures located in Centralia that had been flood proofed. The study focused on 35 structures that were elevated after being flooded in 1996 and 1997. Detailed flood elevation data was obtained on these 35 structures following the December 2007 flood event. The total mitigation cost for the 35 structures was estimated to be $1,906,000. The flood damages prevented from 2007 flood on these 35 structures exceeded the project cost by almost 2 to 1 (FEMA, 2008).

In addition to the projects listed above, since 2006 Lewis County has assisted in raising 105 homes within both the Chehalis and Cowlitz Basins. Also, Lewis County demolished 29 flooded homes after the December 2007 flood on the Chehalis River. Of the homes that were damaged in the December 2007 flood event, 85% were not located in a FEMA map flood zone.

In the Chehalis Basin, Lewis County Conservation District has flood proofed land areas for livestock, called critter pads. The fill is placed above a certain flood elevation for both livestock and equipment. Critter pads have also been used Tillamook County, OR to get livestock and equipment above of expected flood stages.

To offset the flood damages to infrastructure that was occurring throughout the United States engineers started building dams to store flood runoff, and or channelizing the river to try and increase the velocity to pass through the reach. This was only partly successful, as river channels down-cut and widen to return the river to a dynamic equilibrium condition.

We have been trying to solve flood problems for close to 100 years. Unfortunately, the flood problem has become a moving target, because of encroachment, modified watersheds from pavement in the watershed, fires, and clear-cutting. Some possible increase in flooding may be occurring because of climate change that we do not fully understand.

Conclusion

Scientists can do a better job of preparing maps of potential flooding and the classification suggested in this paper could help in that characterization. The names are Riverine, Lacustrine, Palustrine, Estuarine, and Marine. Some flood types like Riverine have a standard hydraulic procedure when used for FEMA studies. There are no standard procedures for evaluating ponding on flat ground (Lacustrine) or for that around lakes (Palustrine), or estuaries (Estuarine) or for flooding above the beach by tidal surge, storm surge and that from significant waves (Marine). These types of procedures need to be developed. Use of drones for aerial mapping during flood events would greatly help in establishing flood boundaries. In addition updating the land topography with high resolution Lydar would allow updated flood maps to be drawn with good topographic control. The author is unsure if FBFM and FIRM mapping is being done using high resolution Lydar at the resolution being used by the Oregon Consortium. That lydar exceeds the lydar requirements being used by USGS.

Waterway conveyance constraints such as bridges, culverts, floodplain encroachment, and climate change have resulted in flooding being a “moving target” in term of expected area, depth, and duration. Studies are needed to update existing maps of flooding.

There needs to be a statistical analysis of rainfall gages to establish 100 year average recurrence interval events, that cause flooding of Lacustrine, Palustrine , and Estuarine areas.

Flooding and flood damages are likely to increase again in the future so our needs for accurate maps means built in updated studies.

The options to deal with the extensive flood problems involve integrating all of the solutions (flood control, flood proofing, relocation, increasing ditch and culvert capacity, and planting appropriate trees to minimize blow down) in a comprehensive way.

In the uplands, there is a need for an evaluation by U. S. Forest Service and the Bureau of Land Management to find ways to manage forest and rangeland to reduce runoff and erosion. Research could be provided by the Agricultural Research Service.

For all flooding there is a need for another national task force like the one in House Document 465, “ A Uniform National Program for Managing Flooding in US “ . The same agencies (e.g. USCOE, NRCS, USGS, and TVA) that developed House Document 465 are needed as well as FEMA, SBA, NOAA, NWS USFHA, FAA, USBR as well as representation from soil , water , and atmospheric Professional societies. They need to provide direction to upgrade data collection on precipitation, runoff, and mapping of flooding of all types.

At the state level water resources departments, natural resources departments, departments of transportation, flood control districts, drainage districts as well as soil and water conservation districts need a task force to evaluate what can be done to reduce overall flooding that floods state highways, and that along drainage ditches. Counties and cities need a task force to determine how to reduce flooding along roads from inadequate drainage ditches, and culverts. This should include representation from drainage districts and Soil and Water Conservation Districts. NRCS can help establish areas of poorly and imperfectly drained soils.

There is a need for local arborist and foresters to have a task forces to evaluate if the correct species to reduce tree throw have been installed in the past and will be replanted in areas of extensive blow down during flood events. This should involve consultation with NRCS on soil differences that can influence tree root systems and the ability to remain upright in high winds.

These various task forces are needed to establish policy and procedures for reducing storm and flood damage. The approach needs to be that we are in this together and cooperative evaluation is a necessity. The coordination of all these various task forces should be placed under FEMA, which should be responsible for preparing legislation to go to the U. S. Congress for future evaluation and mapping of Riverine, Lacustrine, Palustrine, Estuarine, and Marine flooding. Block grants to states could be authorized and set up a program to do the field mapping.

References

Brown and Caldwell Consulting, 2008. Lewis County Comprehensive Flood Plain Management Plan. Prepared for Lewis County, Washington. Seattle, WA.

Conrad, D., McNitt, B., and Stout, M., 1998. Higher Ground. A Report of Voluntary Property Buyouts in the Nations Floodplains, A Common Ground Solution Serving People At Risk, Taxpayers, and the Environment. National Wildlife Federation, Chehalis, WA

Cowardin, L. M., Carter, V., Golet, F. C., and LaRoe, E., T., 1979. Classification of Wetlands and Deepwater Habitats of the United States. US Department of the Interior, Fish and Wildlife Service, Washington, DC, Jamestown, ND Northern Prairie Wildlife Research Center Home Pate. http:///www.npwrc.usgs.gov/resource/1998/classwet.htm (Version 04DEC98).

FEMA, 2008. Evaluating Losses Avoided through Hazard Mitigation. City of Centralia, FEMA. Washington, DC

Komar, P., 1997. The Pacific Northwest Coast. Duke University Press, Durham, NC

Leopold, L., 1994. A Guide to the Field Identification of Bankfull Stages in the Western United States. USDA Forest Service Rocky Mountain Forest and Range Experiment Station, Stream Systems Technology center, CD, (31 minute Video).

Mann, M., 2018, Controlling future summer weather extremes still within our grasp. Penn State. Science Daily, October 31, 2018

Reckendorf, F., Renner, D., Amrine, R., Verd, K., Wilson, N., Stevens, M., and Fenwick, D., 2012. Chehalis River Basin Studies, Inventory and Evaluation. Lewis County Conservation District, in Cooperation with USDA, Natural Resources, Conservation Service, and Washington State Conservation Commission.

Reckendorf, F., 1998, Use of Geomorphic Surfaces in Floodplain Mapping as Modified by Land Use Changes, and Reflecting the Adequacy of FEMA Mapping and Guidelines,

as well as Oregon Land Use Goals. Environmental, Groundwater, and Engineering Geology: Applications from Oregon. Star Publishing. Belmont, CA.

Reckendorf, F, and Styner, W., 1978., Flood Hazard Analyses, Delta Study Area, Alaska. USDA, Soil Conservation Service, Anchorage Alaska

Reckendorf, F., 1973, Techniques for Identifying Floodplains in Oregon. PhD Thesis, Corvallis, Oregon State University. 344 pages, leaves.

Reckendorf, F. and Taylor, P., 1971. Draft, Type 10 Flood Insurance Study, Applegate River Portion of Applegate River in Jackson, CO, OR. Report for Flood Insurance Administration, USDA, SCS, Portland, OR.

Reckendorf, F., 1969, Geomorphic Features of Oregon Streams and Floodplains. American Society of Civil Engineers, Hydraulic Specialty Conference, Logan, Utah. August 20-22, 1969.

Reckendorf, F., 1968. Methods of Identification and Mapping of Floodplains. American Society of Agricultural Engineers, Annual Meeting. June 18-21, 1968.

Rhodan, M., 2018, When the Rivers Rise. Hurricane Florence pounds the Carolina coast, leaving residents at nature's mercy. Time Magazine, pp 32-35.

Rippey, B., 2019. Weatherwatch, Weatherwise Magazine, January/ February 1019. Philadelphia, PA.

Rosgen, D., 1996, Applied River Morphology, A Classification of Natural Rivers. Wildland Hydrology, Pogosa Springs, Colorado.

U.S. Congress, House Committee on Public Works, 1966, "A Unified National Program for Managing the Nations Flood Losses", 89th Congress, Second Session, House Document 465. Washington, D.C.

U.S. Department of Housing and Urban Development, 1968. National Flood Insurance Act of 1968, HUD Washington D. C. 28p.

U.S. Department of Homeland Security, Federal Emergency Management Agency, 2018, FEMA Policy Standards for Flood Risk Analysis and Mapping. Washington, DC.

Hydrologic Risk Analyses for Willamette River Basin Dams

Chris Bahner, Project Manager, WEST Consultants, Inc., Salem, Oregon,
Phone (503) 485-5490, Fax (503) 485-5491, cbahner@westconsultants.com

Angela Duren, Portland District's Hydrologist, U.S Army Corps of Engineers, Portland District, Portland, Oregon, Phone (503) 808-4964,
Angela.M.Duren@usace.army.mil

Abstract

The U.S. Army Corps of Engineers' (USACE) vision is to achieve safe, secure, and more resilient civil works infrastructure by enhancing its protection in order to prevent, deter, or mitigate the potential for dam failure and improve preparedness, response, and rapid recovery in the event of an attack, natural disaster, and other emergencies. A major initiative within this effort involves the updating of hydrologic data for the 700 plus USACE impoundment structures and dams. It is expected that this effort and its hydrologic results can be utilized to reduce the uncertainty in the assessment of hydrologic risk for a given dam as well as to provide a basis for design, if needed.

Several studies have been completed to assess the hydrologic risk for seven of the USACE dams located within the Willamette River Basin. Studies based on traditional approaches included the determination of the Probable Maximum Precipitation (PMP) and Probable Maximum Flood (PMF) for each dam facilities. Analyses completed in support of the PMP\PMF estimation included the evaluation of the precipitation gages in the Pacific Northwest to identify key regional storms after the publication of HMR 57; the development of the depth-area-duration relationships for the key storm events; development of HEC-HMS hydrologic models of the Willamette River Basin; calibration and validation of the HEC-HMS models; and development of HEC-WAT models to simulate the HEC-HMS with the HEC-ResSim used for operations of the dam facilities. Some unique components of the PMP estimation included the consideration of uncertainty in defining the PMP and using a regional approach to define the PMP for the entire Willamette River Basin.

USACE has also been working on the development of hydrologic loading curves that takes into account epistemic and aleatory uncertainty of the precipitation, snowmelt processes, hydrographic responses, and initial starting elevation. Interim curves were estimate using the Flood Risk Analysis (FRA) and Hydrologic Sampling capabilities of the HEC-WAT software and finalized using RMC-RFA.

Introduction

The U.S. Army Corps of Engineers' (USACE) vision is to achieve safe, secure, and more resilient civil works infrastructure by enhancing its protection in order to prevent, deter, or mitigate the potential for dam failure and improve preparedness, response, and rapid recovery in the event of an attack, natural disaster, and other emergencies. A major initiative within this effort involves the updating of hydrologic data for the 700 plus USACE impoundment structures and dams. It is expected that this effort and its hydrologic results can be utilized to reduce the uncertainty in the assessment of hydrologic risk for a given dam as well as to provide a basis for design, if needed.

The USACE operates 13 dams in the Willamette River Basin (WRB) as part of water resource management system that provides flood risk management, power generation, water quality improvement, irrigation, fish and wildlife habitat, and recreation on the Willamette River and many of its tributaries. Seven of the 13 USACE dams located in the WRB have been identified to have hydrologic failure modes from a risk assessment of the facilities. As a result, these dams are considered to be in the Issue Evaluation Study (IES) Phase 2 stage. This indicates that complex analysis on the hydrologic details of the failure modes is required to further reduce the uncertainty in hydrologic risk. The final products from the IES study are the PMF and a hydrologic loading curve with associated confidence limits for each of the dams.

This paper presents general information related to the WRB, analyses completed in support of PMP\PMF for each of the dams, and development of interim hydrologic loading curves. Information is also provided about the HEC-WAT software, which was an important tool in completing the hydrologic assessment of the WRB.

Willamette River Basin

The study area is the WRB located in Oregon. A location map for the study area and the USACE dams within the basin is provided as Figure 1. The Willamette River and its watershed lie in the greater Cascades Geological Province, which extends from British Columbia to northern California. The river has a watershed area of about 11,478 mi^2. The watershed's runoff fluctuates dramatically from heavy precipitation in the winter months, snowmelt in the spring months, and relatively rain-free summers. The Willamette River watershed is about 180 miles in length and roughly 100 miles wide. The river bed is approximately 450 feet above sea level at the southern end of the valley and ten feet above sea level at its confluence with the Columbia River. The four main tributaries to the Willamette River are the McKenzie River, Long Tom River, Santiam River, and Clackamas River. The majority of the tributary area is located on the east side of the Willamette River. The watershed is comprised of nine general regions: (1) Coast Fork Willamette River, (2) Middle Fork Willamette River, (3) McKenzie River, (4) Long Tom River, (5) Middle Willamette River, (6) South Santiam River, (7) North Santiam River, (8) Lower Willamette River East Side, and (9) Lower Willamette River West Side.

The Willamette River basin is bounded on the west by the relatively low Coast Range, with Mary's Peak being its highest point (4,097 feet), and the Cascade Range on the east, with Mt. Jefferson (10,497 feet) being the highest point that has an influence on the watershed's unique

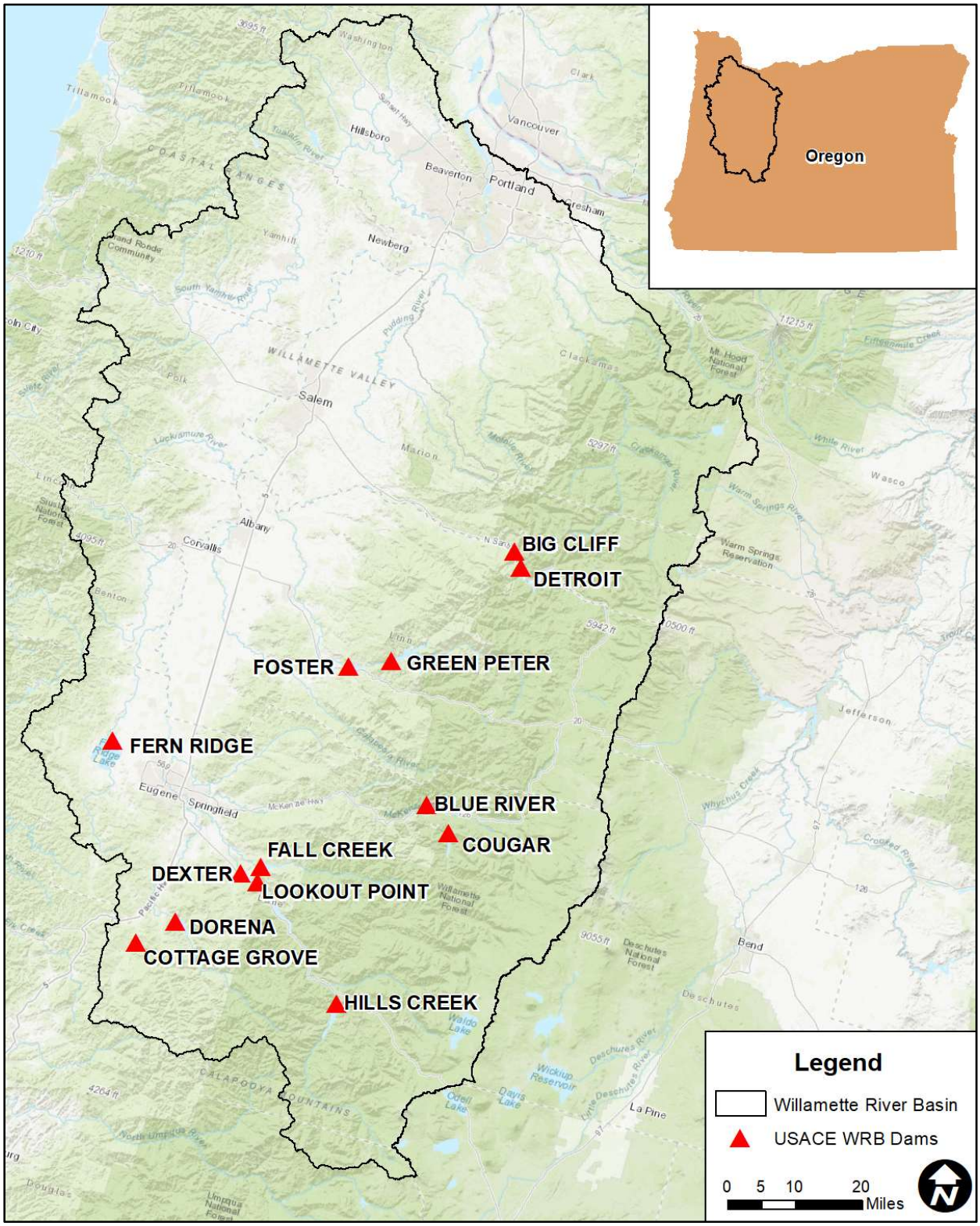

Figure 1. Location Map of the Willamette River Basin and USACE Dams

temperature and precipitation range. The regional climate is shaped by maritime influences—northward and southward seasonal ocean currents and prevailing eastward winds. Warm, moist air blowing in from the southwest produces heavy precipitation in the late fall, winter, and early spring months in the Coast Range, producing intense seasonal rains with light, transitory snowfall at the higher elevations. The Cascade Range to the east has an equally significant seasonal precipitation. Most of it, however, occurs as snowfall, resulting in large snowfields and some permanent glaciers. The Cascades also provide a buffer from continental climatic influences, creating a unique blend of topographic relationships that shape the regional climate. There are thirteen USACE dams located in the Willamette River basin (Figure 1).

Each dam contributes to a water resource management system that provides flood risk management, power generation, water quality improvement, irrigation, fish and wildlife habitat and recreation on the Willamette River and many of its tributaries. Seven dams are considered to be in the IES Phase 2 stage that requires hydrologic analyses be conducted to further reduce the uncertainty in hydrologic risk.

HEC-WAT

USACE policy states that USACE will analyze water resource projects, including flood risk management projects, using a risk framework that incorporates watershed and systems approaches. USACE's Hydrologic Engineering Center (HEC) developed the Watershed Analysis Tool (HEC-WAT). HEC-WAT helps a study team perform the necessary hydrologic, hydraulic, and consequence planning analyses by integrating water resources software that is commonly applied by a multidisciplinary study team when conducting a water resources study. Many pieces of software within the HEC suite of tools are implemented within HEC-WAT, thus allowing a study team to perform many of the necessary hydrologic, hydraulic, and planning/consequence from a single interface. HEC-WAT software (US ACE-HEC, 2017)can interface with HEC-HMS (hydrology), HEC-RAS (hydraulics), HEC-ResSim (reservoir operations), HEC-SSP (statistical analyses), and HEC-FIA (flood consequences).

HEC-WAT software also includes a flood risk analysis (FRA) compute option. The FRA compute builds on the HEC-WAT framework to provide a convenient method of implementing a Monte Carlo analysis across multiple HEC models to perform plan formulation or system performance analyses while incorporation risk and uncertainty analyses. The Monte Carlo simulation provides a method for incorporating a probabilistic description of inputs (i.e., boundary conditions, initial conditions, model parameters) into an analysis while making use of detailed deterministic models. During a Monte Carlo simulation, the single-valued inputs are replaced with randomly sampled values as defined by probability distributions. In turn the sampled model information is repeated over and over to span the possible range of model inputs to quantify uncertainty in model results (USACE-HEC, 2017).

The HEC-WAT FRA compute is implemented as a two-level nested process to account for the two kinds of uncertainty: (1) epistemic uncertainty, or knowledge uncertainty, is based on that fact that random variables are not know exactly, and it exist when it is impossible to make an accurate estimate of the input value, i.e., hydraulic roughness, hydrologic losses, and flood

likelihood; and (2) aleatoric uncertainty, or natural variability, is based on fact that random variables vary spatially or event-to-event, and it exist when the outcome of a natural process is random, i.e., flood magnitude and forecasts. Iterations in the inner loop (referred to as events) randomly sample from natural variability uncertainty (aleatoric). A realization is created when enough events have been sampled to create a frequency curve. The outer loop randomly samples the knowledge uncertainty to define uncertainty parameters that are held for all events in a realization (USACE-HEC, 2017).

The HEC-WAT FRA includes the following plugins that might be used for an FRA compute:

(1) Hydrologic Sampling is used for sampling of the hydrology to create the hydrologic sequence for the FRA compute. The hydrologic sampling will generate hydrologic information, such as precipitation or flow frequency curves, cross correlations between curves, and hyetograph or hydrograph based on historic or synthetic events (USACE, 2017).
(2) Fragility Curve Sampler is used to sample levee failure potential defined from a levee fragility curve.
(3) Performance Metrics is used to define metrics to describe the system for accommodating a single event (Assurance) and for a full range of events (Annual Exceedance Probability and Long-Term Exceedance Probability).

Two types of HEC-WAT models were developed. An HEC-WAT was developed for the entire WRB to integrate the hydrologic response of the watershed estimated using HEC-HMS with the reservoir operation capabilities of HEC-ResSim software. The HEC-HMS model was developed to determine the runoff hydrograph from the watershed for rainfall and snowmelt processes. The HEC-HMS model is a detailed, distributed model comprised of averaged subbasin parameters. The model was calibrated to five winter flood events and four spring flood events, and validated to two winter flood events and two spring flood events.

The operations of the Willamette River Basin Reservoirs are simulated using HEC-ResSim software (USACE-HEC, 2013). HEC-ResSim is used to model reservoir operations at one or more reservoirs for a variety of operation goals and constraints. The software simulates reservoir operations for flood risk management, low flow augmentation and water supply for planning studies, detailed reservoir regulation plan investigations, and real-time decision support. The HEC-ResSim model of the Willamette River Basin was developed by the USACE Portland District. The model was calibrated using event information provided in the Water Control Manual (WCM) for each reservoir.

Separate HEC-WAT models were also developed for completing an FRA of the seven dams considered for the IEPR Phase 2 study: (1) McKenzie River system (Cougar Dam and Blue River Dam), (2) South Santiam River system (Green Peter Dam and Foster Dam); and (3) Middle Fork Willamette River system (Hills Creek Dam, Lookout Point Dam, and Fall Creek Dam).

Hydrologic Studies for Phase 2 Issue Evaluation Study

As previously mentioned, seven of the WRB dams are in the IES Phase 2 stage. The final products from the IES study are the PMF and a hydrologic loading curve with associated confidence limits for each of the dams. The PMF required multiple studies to be conducted. These studies and information related to the hydrologic loading curve are briefly discussed in the remainder of this paper.

Probable Maximum Flood (PMF)

Several studies were completed in support of the PMF estimated at each dam. These studies are briefly discussed in the following paragraphs.

Extreme Storms Analysis: An extreme storms analysis (USACE-NWP, 2016b) was conducted in support of the WRB PMP study. This study involved analyzing the precipitation gages located in Oregon, southern Washington, and northern California to identify key regional storms that occurred after the publication of HMR 57 (NWS, 1994). Ten key storms were identified: (1) February 1996, (2) March 1997, (3) November 2006, (4) December 2007, (5) January 2012, (6) February 1982, (7) November 1996, (8) December 2008, (9) December 2014, and (10) January 1983. Half of the events originated in the subtropical region and the other half formed in the mid-latitude region. Additionally, the extreme storms analysis included the development of depth-area-duration (DAD) curves for the key storm events using procedures documented in *Manual for Depth-Area-Duration Analysis of Storm Precipitation* (WMO, 1969). Curves were developed for durations of 1-, 3-, 6-, 12-, 18-, 24-, 30-, 36-, 42-, 48-, 54-, 60-, 66-, 72-, and 96-hours.

Hydrologic Model Calibration and Validation: An HEC-WAT model (USACE-NWP, 2016c) of the WRB was developed to integrate the hydrologic response of the watershed estimated using HEC-HMS (USACE-HEC, 2016) with the reservoir operation capabilities of HEC-ResSim software. The HEC-HMS model was developed to determine the runoff hydrograph from the watershed for rainfall and snowmelt processes. The HEC-WAT results were evaluated to ensure that the HEC-HMS and HEC-ResSim models were correctly linked and to finalize the HMS/ResSim calibration. The evaluation focused on reservoir elevations and the discharge hydrographs at the main streamflow gages located downstream of the reservoirs. This evaluation mainly involved minor modifications to the operations of the reservoirs and some of the local inflow locations defined within the HEC-ResSim model. Changes to the HEC-ResSim operations were completed by the USACE Portland District for the four winter calibration events. The adjustments made to operations for the various events are related to maximum downstream control releases and ramping rates.

Probable Maximum Precipitation (PMP): A site-specific PMP study was completed in support of determining the PMF for the USACE dams of interest in the WRB. The Willamette River dams operate as a system for flood control which add another layer of complexity to analyzing the PMP at individual dams. The main issue is related to defining the coincident rainfall depths throughout the watershed, given the significance of downstream local inflows on reservoir system operations. Additionally, due to the nature of the meteorology in this region,

rainfall is generally widespread over most of the Cascades during significant events, and does not occur as isolated storm centers over one given headwater watershed. Therefore, the WRB dams were analyzed using a regional PMP approach for the entire WRB watershed with consideration for the individual dam watersheds. The uncertainty in Sea Surface Temperature (SST) and transposition locations were quantified and are captured in the estimate of an average, upper, and lower estimate of the PMP at any given dam.

Probable Maximum Flood (PMF): The PMP was utilized with the WRB HEC-WAT model to define the PMF for the WRB dams. A total of six spatial precipitation distributions were initially considered based upon the significance of runoff in the winter season. An evaluation was conducted to identify the three spatial precipitation distributions within the initial six, with the highest average precipitation depth within the watersheds above the seven WRB dams of interest. The normalized raster for a given spatial distribution was used to derive normalized depths, and the weighted average depth within the watershed above the dam was computed for each dam. The spatial distribution with the three highest normalized depths for the majority of the seven dams were selected for sensitivity testing and for estimating the final PMF. Initially, a total of ten temporal distributions were considered: Seven event-based distributions and three patterns based upon guidance given in HMR 57 (NWS, 1994). The temporal distributions were then further narrowed down from ten to six events, with five event-based distributions and one HMR 57 distribution.

The PMF determination also took into account of the initial pool elevation of each reservoir and changes to the calibrated Clark Unit Hydrograph (UH) parameters. Two initial pool elevation conditions were considered: (1) full flood control level, and (2) pool level prevailing five days after the last significant rainfall of a storm that produces one-half the PMF. The initial pool elevation and outflow releases for the first condition (Full Flood Control Pool) were defined from the WCM for each dam and were applied to all dams in the WRB at the same time in any given routing scenario. The spatial and temporal condition that defined the inflow PMF hydrograph for each dam was determined from the analysis for the first pool elevation condition. Using the 'Ratio' option under the Compute tab of HEC-HMS, precipitation was scaled iteratively until the resulting PMF inflow reflects the ½ PMF hydrograph for each of the dams. The ½ PMF hydrograph was routed through the reservoirs with a starting pool level at the top of the conservation pool. The pool elevation five days after the maximum 15 minute time increment of the PMP hyetograph was extracted from the HEC-ResSim results. For this starting elevation condition, this was first determined at each of the dams in the WRB. Then, the respective ½ PMF starting elevation for each of the dams was in turn the starting elevation condition of all of the dams as the final simulation of the ½ PMF condition.

The Clark Unit Hydrograph parameters should be adjusted to account for the fact that they are based on calibration events significantly smaller than the PMF event. The USACE has general guidance of using Clark Unit Hydrograph (UH) peaking factors between 1.25 and 1.50 for PMF events (USACE, 1991).

Two approaches were considered in revising the Clark UH parameters: (1) UH peaking based upon precipitation intensity of a given spatial pattern and (2) the standard approach of UH peaking between 25-50% at a given dam. The first approach relates the peaking factor to the total rainfall intensity of a given spatial pattern. The UH peaking factors were defined for each of the spatial distributions that were considered. For each spatial distribution, the raster for the event was normalized by dividing the raster by the average depth over the entire WRB. The

unique UH peaking factor was then calculated for each subbasin using linear interpolation defined by the normalized pattern inflections defined for each spatial event. After the determination of the UH peaking factor for each subbasin, the time of concentration and storage coefficient were adjusted to obtain a peaking of the unit hydrograph in the subbasin by the specified percent.

The second approach is based on the general USACE guidance (USACE, 1991) of using UH peaking factors between 1.25 and 1.50 that are relative to the dam inflow hydrograph. This approach was considered only for the subbasins located above each of the seven dams, and UH peaking factors for the downstream areas are the same as determined for the first approach. The Clark UH parameters were adjusted iteratively in HEC-HMS until a reservoir inflow unit hydrograph peaking of 1.25, 1.33, and 1.50 was achieved.

The uncertainty in PMP, starting water surface elevations, and Clark UH parameters was utilized to define the lower and upper limit of the PMF hydrograph as reflected in Figure 2 for one of the WRB dams.

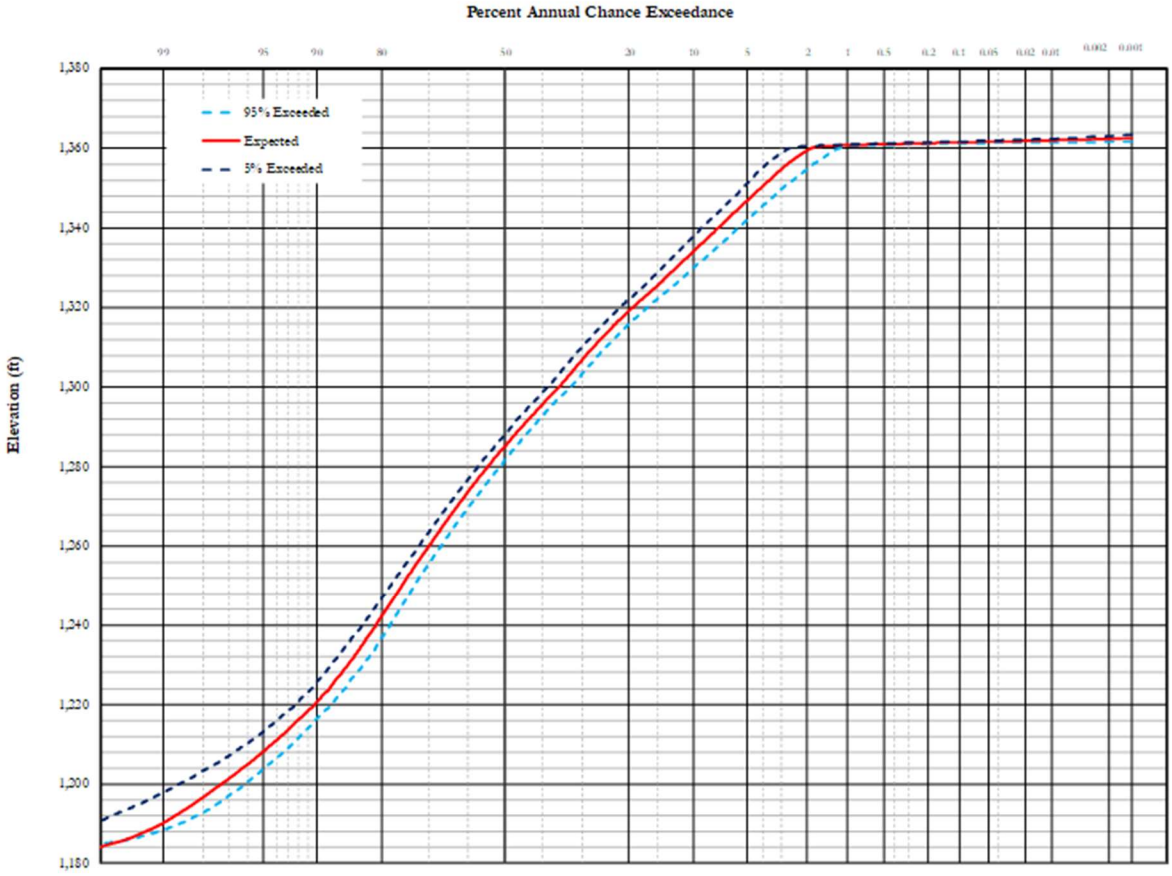

Figure 2. Example PMF Hydrograph Developed for One of the WRB Dams

Hydrologic Loading Curves

A hydrologic loading curve defines the reservoir elevation over a range of exceedance probabilities with associated confidence limits. The development of this curve must account for meteorologic, hydrologic, and operational uncertainties. The stage-frequency curves are extended to the elevation that characterizes the upper uncertainty of the PMF by leveraging site-specific meteorologic and hydrologic studies, development of calibrated hydrologic and reservoir operations models, and the use of stochastic models.

Interim hydraulic loading curve was developed for the seven WRB dams using the FRA and Hydrologic Sampling capabilities of the HEC-WAT software. Separate HEC-WAT models were developed for: (1) McKenzie River system (Cougar Dam and Blue River Dam), (2) South Santiam River system (Green Peter Dam and Foster Dam); and (3) Middle Fork Willamette River system (Hills Creek Dam, Lookout Point Dam, and Fall Creek Dam). Two FRA's were completed for each of HEC-WAT models. Information about each FRA is summarized in Table 1.

Table 1. Information about HEC-WAT FRA Analyses

Item	Method 1	Method 2
Sampling Method	Correlated 7-day inflow volume-frequency relationship (USACE, 2016) and initial reservoir elevation distribution defined by USACE (USACE, 2017c)	Basin average precipitation-frequency relationship (USACE, RMC 2017) and initial reservoir elevation distribution defined by USACE (USACE, 2017c)
Event Sampling	A normal distribution with a mean of January 31, a standard deviation of 30 days, a start date of October 31, and an end date of March 31	Uniform distribution for the entire year
Primary Location Probability Distribution	Log Pearson Type III (LPIII) distribution	Kappa distribution
Secondary Locations	None	Hyetographs and temperature patterns per HEC-HMS subbasins
Cross Correlation Matrix	Based on the correlation analysis completed by USACE (USACE, 2017c)	N.A.
Shape Set	Based on the winter calibration events (USACE, 2016)	Eighteen spatial and temporal distributions (USACE, 2016)
Shape Summary	Equivalent probabilities were defined for each of the winter calibration events	Equivalent probabilities were defined for each shape set
Additional Comments	None	FRA was completed for two initial SWE conditions (1% ACE and average) and a variety of debris blockage of the spillway (no blockage, 10% to 50% blockage, and complete blockage)

Each FRA consisted of 100,000 years in a realization and a maximum of 100 realizations for a total of 10,000,000 simulation events. Due to the number of simulation events, the FRA was run on the Amazon Web Service (AWS) Cloud Compute Services (CCS) using the distributed compute capabilities of HEC-WAT. Per each FRA simulation, a network of 100 machines were used to complete the simulation. The FRA simulation for one of the systems took an average of

two weeks. HEC-WAT has the capabilities to generate frequency relationships from the FRA results. However, a script was created to extract and process because of the number of regions utilized in the AWS CCS network. An example relationship from the HEC FRA is provided in Figure 3.

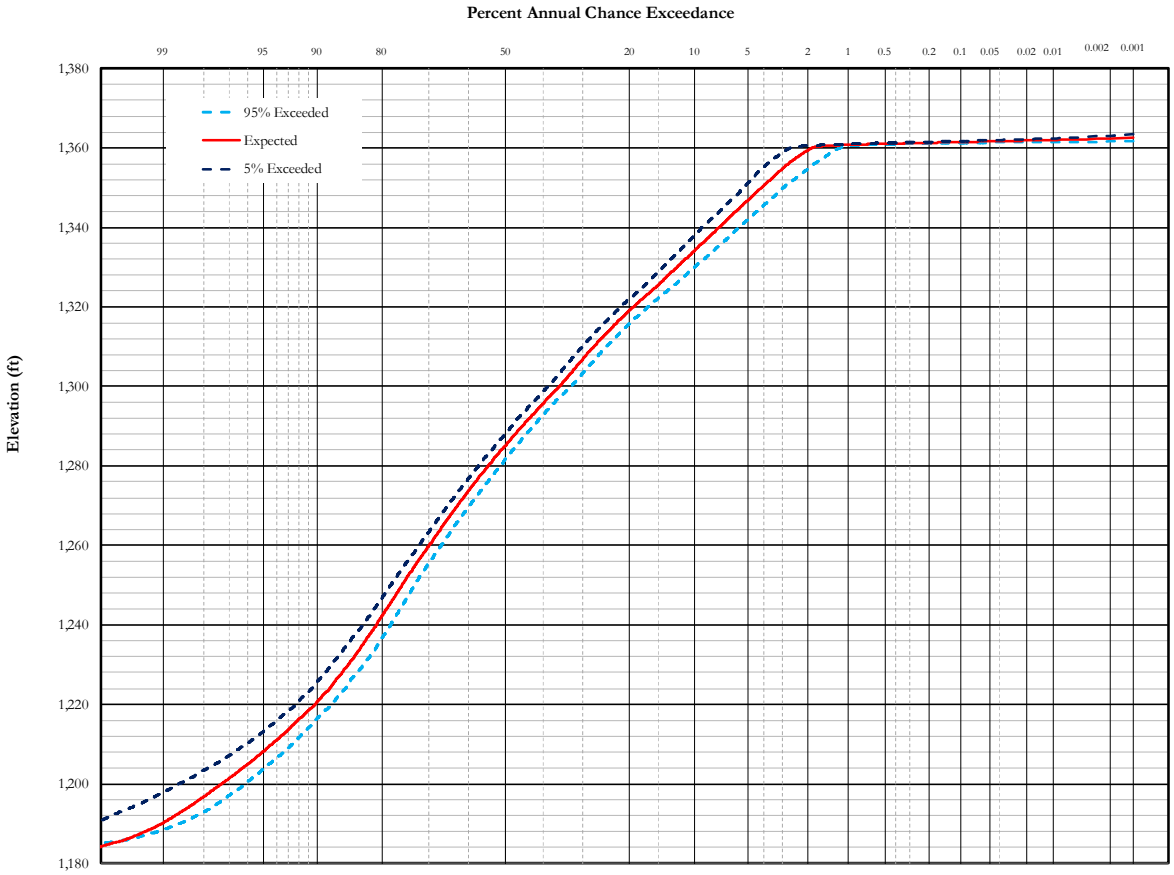

Figure 3. Example Hydrologic Loading Curve from HEC-WAT Flood Risk Analysis

The final hydraulic loading curves were established using RMC Reservoir Frequency Analysis (RMC-RFA) software with the precipitation and volume-duration-frequency information as the primary input. The volume-duration-frequency relationship was derived from a Bayesian method that incorporated non-standard data, such as regional precipitation information, censored historical and paleoflood data, and causal information, such as rainfall-runoff results and expert opinion. RMC-RFA produces an inflow volume-based stage-frequency curve with uncertainty bounds by utilizing a deterministic flood routing model while treating the seasonal occurrence of inflow events, antecedent reservoir stage, inflow volume, and inflow hydrograph shape as uncertain variables rather than fixed values. RMC-RFA employs a two looped, nested Monte Carlo methodology, similar to the HEC-WAT software (USACE-NWP, 2019). The RMC-RFA software was adopted in lieu of the HEC-WAT software since the RMC-RFA took a significantly shorter time to complete the computations and the resulting relationship perform well in fitting the expected probability curve derived from observed annual maximum stages. An example relationship determined from the RMC-RFA analysis is provided in Figure 4.

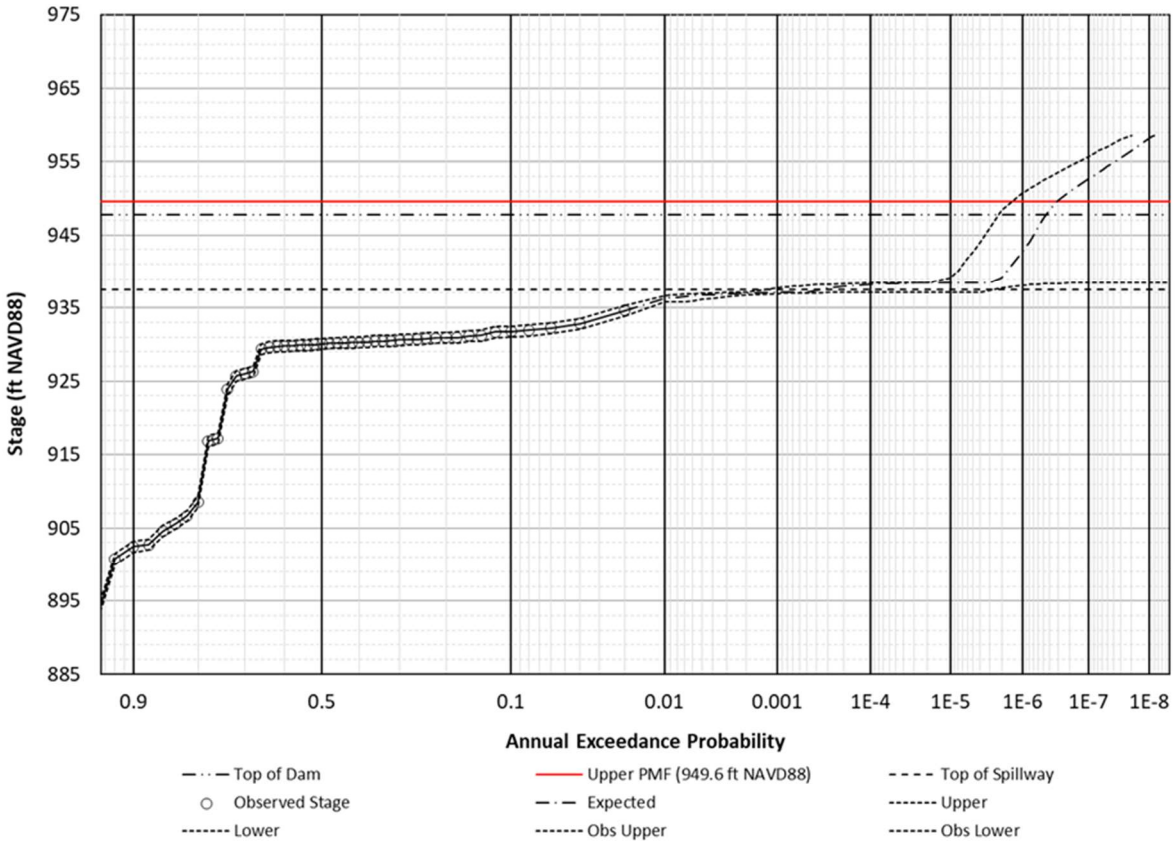

Figure 4. Final Hydrologic Loading Curve for One of the WRB Dams

Conclusions

USACE has completed several studies to assess the hydrologic risk for seven of the USACE dams located within the WRB. Several of the studies are summarized in this paper. Some unique components include the consideration of uncertainty in defining the PMP and using a regional approach to define the PMP for the entire WRB, and utilization of the AWS CCS in developing hydrologic loading curves that takes into account epistemic and aleatory uncertainty of the precipitation, snowmelt processes, hydrographic responses, and initial starting elevation.

References

U.S. Army Corps of Engineers. 1991 (March). "Engineering Regulation, 1110-8-2(FR), Inflow Design Floods for Dam and Reservoirs".

U.S. Army Corps of Engineers, Hydrologic Engineering Center (HEC). 2013 (May). "HEC-ResSim, Reservoir System Simulation, User's Manual, Version 3.1".

U.S. Army Corps of Engineers, Hydrologic Engineering Center (HEC). 2015 (July). "HEC-HMS, Technical Reference Manual, Version 4.1".

U.S. Army Corps of Engineers, Hydrologic Engineering Center (HEC). 2017 (September). "HEC-WAT, Watershed Analysis Tool, User's Manual, Version 1.0".

U.S. Army Corps of Engineers, Portland District (NWP). 2013 (October). "Willamette Basin HEC-ResSim Model Documentation Report, ESA BiOp Modeling, Portland, OR.

U.S. Army Corps of Engineers, Portland District (NWP). 2016a (February). "Memorandum for Record, Willamette Headwater Dams Critical Flow Duration".

U.S. Army Corps of Engineers, Portland District (NWP). 2016b (August). "Extreme Storms Report".

U.S. Army Corps of Engineers, Portland District (NWP). 2016c (December). "Hydrologic Model Calibration and Validation Report".

U.S. Army Corps of Engineers, Portland District (NWP). 2017a (January). "PMP Report".

U.S. Army Corps of Engineers, Portland District (NWP). 2017b (January). "PMP Temporal Distribution Memorandum".

U.S. Army Corps of Engineers, Portland District (NWP). 2017c (March). "Memorandum for Record, Reservoir Elevation Distributions and Correlation Analysis for Stochastic Sampling"

U.S. Army Corps of Engineers, Portland District (NWP). 2019 (January). "RMC-RFA Models Temporal Distribution Memorandum".

U.S. Army Corps of Engineers, Risk Management Center (RMC). 2017 (May). "RMC-TR-2017, Regional 72-Hour Precipitation Frequency Analysis". Prepared for Northwest Division, Portland District.

U.S. Department of Commerce, National Oceanic and Atmospheric Administration (NOAA), National Weather Service (NWS), 1994 (October). "Hydrometeorological Report No. 57, Probable Maximum Precipitation – Pacific Northwest States", Water Management Information Division, Office of Hydrology, National Weather Service, Silver Spring, MD, in cooperation with U.S. Department of Interior, Bureau of Reclamation, and U.S. Department of Army, Corps of Engineers.

World Meteorological Organization (WMO). 1969. "Manual for Depth-Area-Duration Analysis of Storm Precipitation".

Risk Informed Inundation Mapping

David C. Curtis, Senior Vice President, WEST Consultants, Folsom, CA,
dcurtis@WESTconsultants.com
Brent Travis, Director of Applied Research, WEST Consultants, Tempe, AZ,
btravis@WESTconsultants.com
Gyan Basyal, Staff Engineer, WEST Consultants, Tempe, AZ,
gbasyal@WESTconsultants.com

Abstract

Risk informed inundation mapping provides information and context to rare low probability high consequence events. Traditional deterministic hydraulic modeling produces a single water surface mapped to the local terrain, even though there are significant uncertainties in some of the underlying model parameters. In the case of dam breach modeling, parameter choices such as breach geometry (bottom width, elevation, and side slopes), the weir coefficient, breach formation time, and initial piping elevation can all significantly impact the breach discharge hydrograph and influence stages routed downstream. Choices for channel and overbank roughness, bridge parameters, culverts, in-line structures and floodplain encroachments further impact downstream stages and mapped areas.

For purposes of dam breach inundation mapping these breach parameters are often assumed at their most conservative values. This creates a worst-case scenario for the potential extent of inundated areas. However, given that a dam breach is likely to be a low-probability event (often less than the 1% chance event), this worst-case scenario will substantially lower this probability. This may be inconsistent with the risk tolerance of the decision makers.

Understanding the impacts of the range of possible parameter choices provides important context to the mapped results. One way to evaluate this context is through a direct simulation of through a Monte Carlo approach. This approach, which varies the parameters according to their distributions and typically executed with thousands of scenarios to stabilize the statistics, facilitates risk assessments of the resulting inundation maps.

Examples of risk-based inundation mapping will be presented and discussed. The results provide important context to risk to specific floodplain structures and support improved prioritization of mitigation resources.

Introduction

Probabilistic Mapping Approach

Traditionally, selection of the breach parameters is done deterministically by

1. Estimating the size, shape, and timing of the dam breach using empirical equations;
2. Performing a sensitivity analysis assuming a reasonable range of these parameters; and,

3. Selecting conservative values (e.g. those values that appear to increase the magnitude of the breach outflow hydrograph).

This three-step approach may well represent the worst-case scenario but given the inherent unlikelihood of these worst-case features all occurring at once does not match most reasonable risk-based decisions.

A reasonable, alternative method for selecting the breach parameters is a probabilistic approach. This approach varies the dam breach parameters through predefined probability density functions. By considering a large set of model simulations (events), statistical distributions of outcomes of interest can be generated. Examples include the dam breach hydrographs, floodwave arrival times, and stage hydrographs, among others.

Studies such as Vorogushyn, Merz, Lindenschmidt, and Apel, (2010) and Tsai, Yeh, and Huang (2019) have shown that statistical consideration of these outcomes can have a pronounced impact on downstream flood mapping. These studies utilized specifically developed software that coupled stochastic input and 1-dimensional and 2-dimensional floodplain delineation. As proof of concept this work is critical, but from a practical standpoint difficult to apply to engineering studies where existing, publicly available freeware models such as the United States Army Corps of Engineer's Hydrologic Engineering Center's River Analysis System (HEC-RAS) are standard and accepted by numerous government agencies. Probabilistic floodplain mapping is thus more easily implemented using HEC-RAS or other accepted hydraulic and hydrologic modeling software.

Assuming agency acceptance of the floodplain mapping software, the first step in probabilistic consideration becomes the careful selection of the corresponding dam and levee breach statistical distributions. This often involves meeting with project stakeholders such as the dam owners, the Federal Emergency Management Agency (FEMA), the Federal Energy Regulatory Commission (FERC), and others. After consideration of the potential failure mode statistical distributions, stakeholders can discuss the distributions and corresponding factors to determine if they are appropriate given the failure mode, construction of the dam, inflow hydrograph, reservoir size, applicable guidelines, and other factors. Assuming a consensus is achieved, modeling by Monte Carlo simulation can then executed to developed probabilistic outcomes.

Modeling Procedures

In recognition of the need to improve flooding risk assessment for dam and levee breach evaluations, new software was developed that directly incorporates probabilistic aspects of all major components consistent with Monte-Carlo type simulations. The resulting product, tentatively named RiskRAS (formerly SimRAS 2D), is a multipurpose, graphical user interface (GUI) based HEC-RAS simulation tool with a simple graphical interface. It allows the user to assign a statistical distribution to one or more key parameters in the chosen HEC-RAS 1D or 2D model (see examples shown in Figure 1 below).

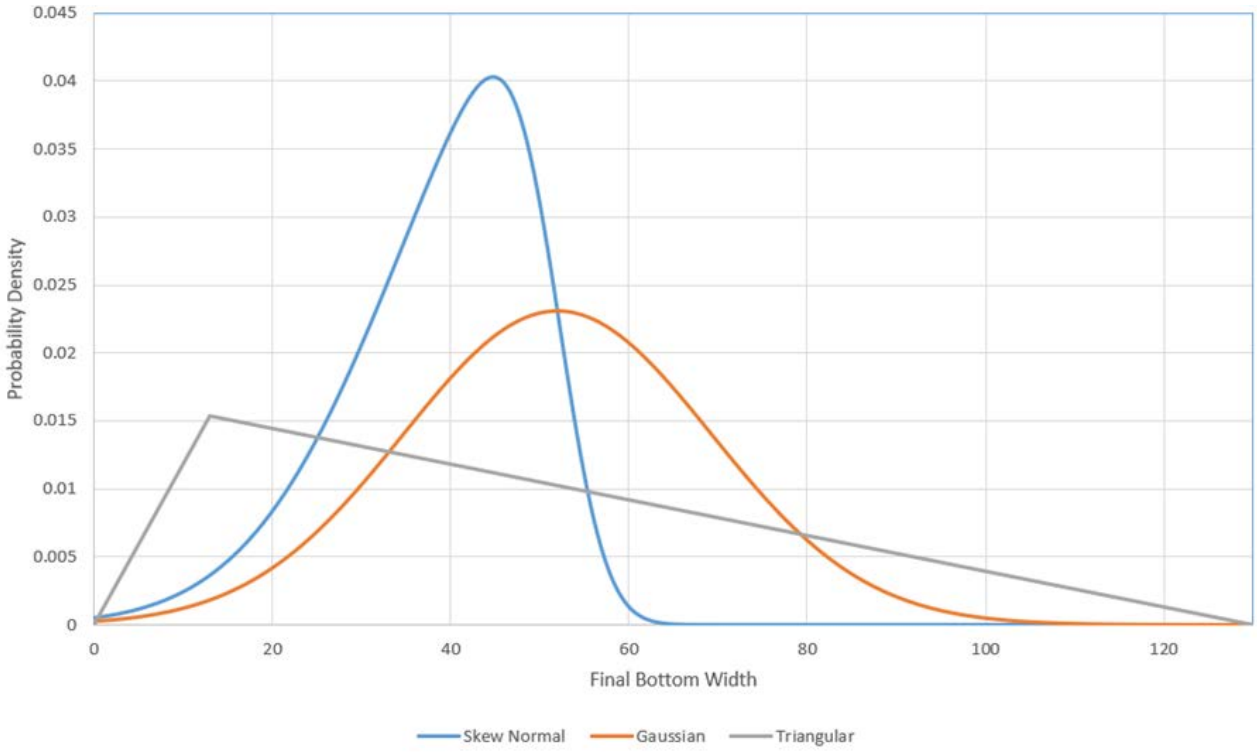

Figure 1. Example available statistical distributions in RiskRAS

Completely automated, RiskRAS runs the HEC-RAS model multiple times, selecting randomized values of the key parameters for each run (consistent with a Monte Carlo analysis). When complete, the results can be used to determine the risk of a particular event occurring, evaluate parameter sensitivity, and/or determine most likely outcomes. RiskRAS is written in Python language utilizing reliable and well tested libraries. Some specific features are as follows:

- Easy to use GUI interface minimizing the learning curve, promoting efficient, error-free simulations.
- Facilitation of statistical distribution type and parameter selection with dynamic plots.
- Guided input selection.
- Instant results reported through dynamic tables and figures.
- Python based programming allows easy modification for individual projects.
- Live feedback during simulation.
- Utilizes HEC-RAS standard database (HEC-DSS) for all parameter and results storage.

Beyond the present application, RiskRAS can also be used for:

- Dam Break Modeling
- Levee Breach Modeling
- River Model Sensitivity Analyses
- Emergency Action Planning
- Uncertainty Analysis
- Risk Analysis
- Design of Simulated Experiments
- Floodplain Delineation

The results of a RiskRAS application (each typically referred to as a realization) are stored within the HEC-DSS database along with the randomly generated parameters. Thus, all vital simulation information can be easily accessed from within HEC-DSSVue. Further analysis of the results can be accomplished both through HEC-DSSVue (e.g., tabulation, plotting) as well as via the currently implemented RiskRAS post-processing tools. These tools include direct floodplain mapping and statistical analyses. For example, Figure 2 displays the results of one RiskRAS study of flow exceedance (e.g., the 1% flow exceedance is equivalent to the 100-year storm) due to five stochastically selected breach parameters: final bottom width, left side slope, right side slope, weir coefficient, and formation time. A pronounced, albeit statistically noisy, relationship is seen between final bottom width and formation time. The former parameter indicates the breach width appears to be positively correlated with the rarity of the flood event. The latter displays the opposite effect, specifically that rarer storms tend to be exceeded by shorter progression times. The other factors appear to have little effect. Note that this analysis was for only one dam; other locations will likely have different outcomes.

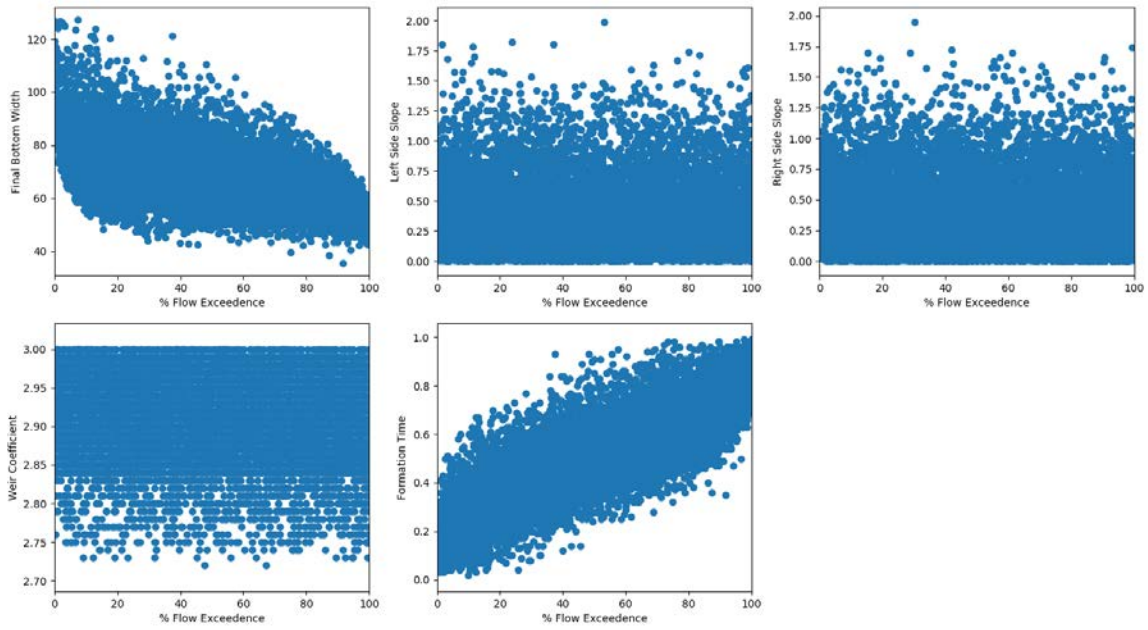

Figure 2. Examples of the post-processing capabilities in RiskRAS

Application of Probabilistic Mapping

As a test of the overall approach to risk informed inundation mapping in general and RiskRAS in particular, probabilistic analysis was performed at a hydroelectric, concrete gravity dam located in Montana (Figure 3). The first step of this ongoing project is to understand how high flows downstream of the dam might vary due to a breach and then determine how these flows relate to an exceedance risk.

Figure 3. Aerial photo of the Montana hydroelectric project

Following development of the hydrology and a HEC-RAS hydraulic model, RiskRAS was utilized for the risk analysis. Specifically, 10,000 Monte Carlo scenarios were executed with the outflow tracked as the outcome of interest. [Details of this effort will be described within as the Travis, Basyal, Bahner and Wahlin (in press) conference paper accepted for the Proceedings of United States Society on Dams 2019 Conference and Exhibition, April 8 – 11, 2019.] The results were ranked and the risk of exceedance of each assigned accordingly. Overall, high variation was seen among the outflows (Figure 4). In particular, it is seen that the breach outflow risk becomes quite sensitive in the design range, with the 1% chance of exceedance breach outflow of 18,500 cfs about 20% higher than the median breach outflow of 15,500 cfs, and the 0.01% chance of exceedance flow even higher at 20,500 cfs. Hence, the risk analysis indicates that the deterministic value originally chosen for the project (25,500 cfs) would correspond to a chance of exceedance far smaller than 0.01%. The comparison to hydrology would be that the deterministic value is far greater than 10,000-year hydrologic event.

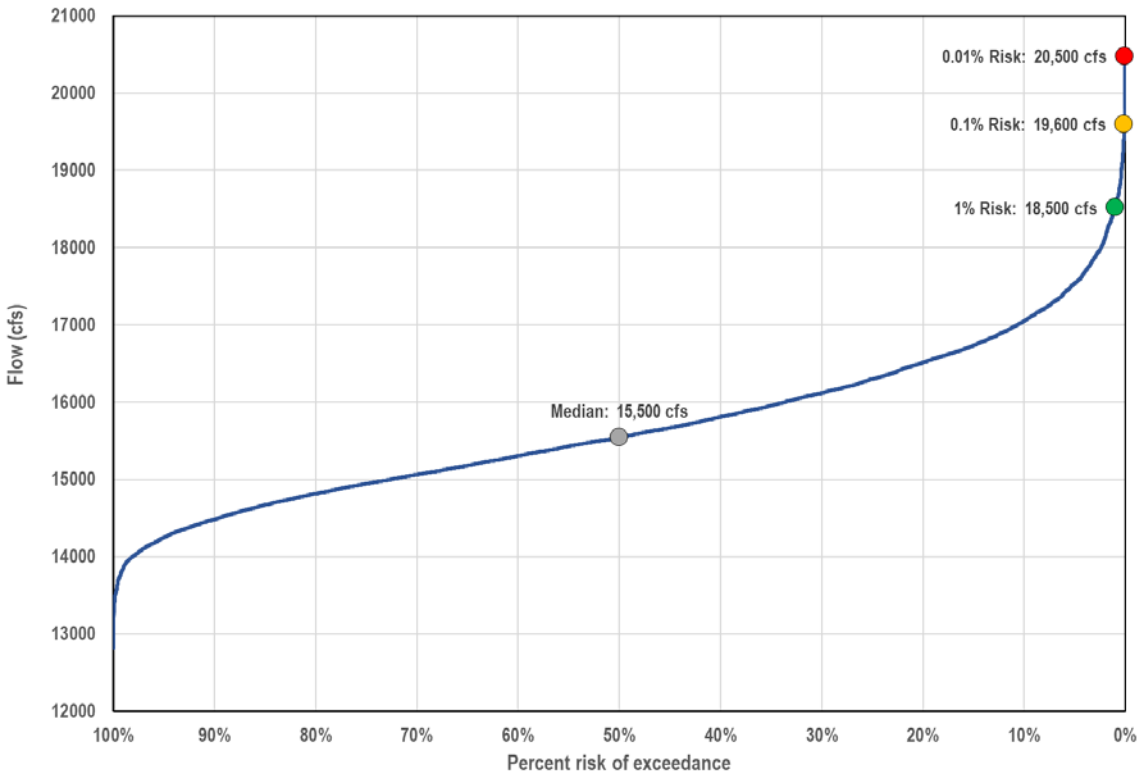

Figure 4. RiskRAS risk analysis results for Montana Dam

Following identification of flow exceedance risk, floodplain mapping proceeded as normal for each of the flows of interest. The results for a particular section of the floodplain is shown in Figure 5. The worst-case (25,500 cfs), 1% risk (18,500 cfs), and median risk (15,500) floodplain delineation are shown.

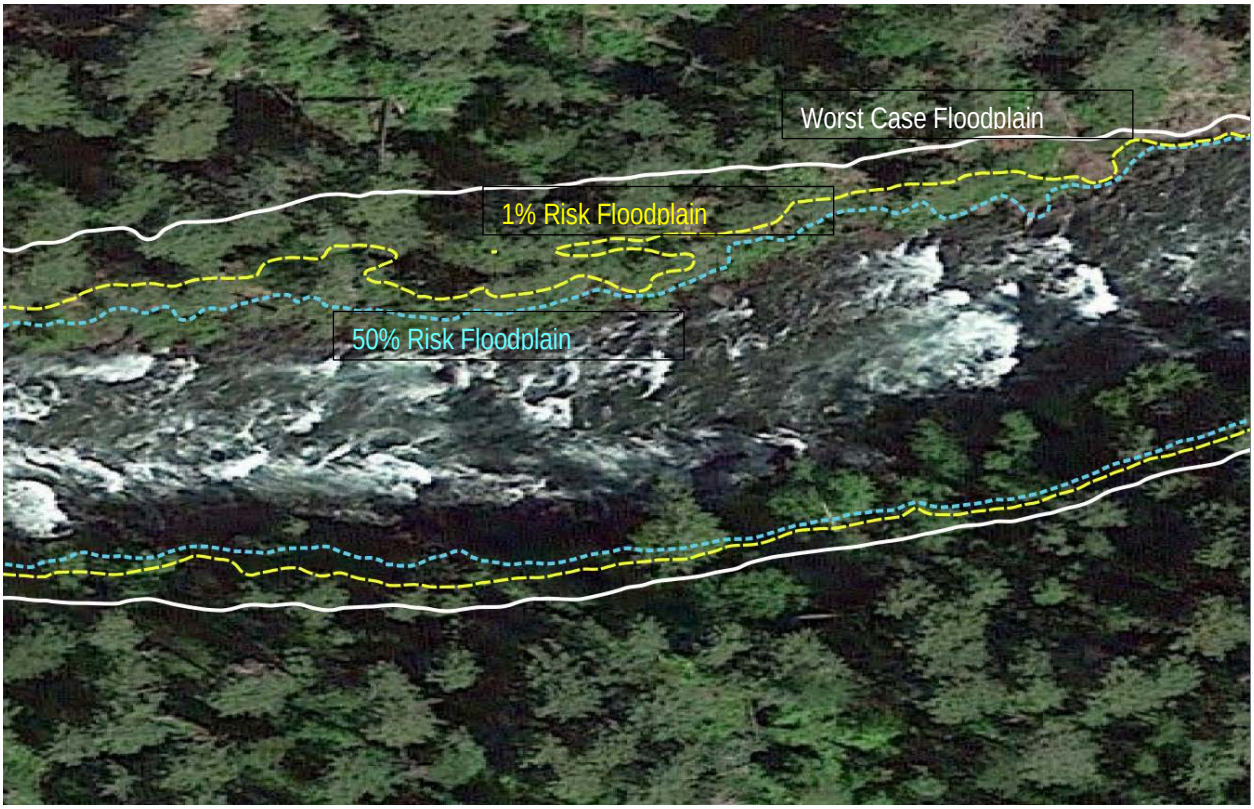

Figure 5. Probabilistic mapping example

Conclusion

This general overview of probabilistic floodplain mapping shows how the procedure can assist floodplain managers make informed, risk-based decisions regarding floodplain extents from typically highly uncertain dam breach scenarios. The associated tool – RiskRAS – can facilitate the approach which, by directly accounting for individual breach component uncertainty, provides direct, quantitative results well suited for risk-based floodplain management.

References

Travis, B., Bahner, C., Basyal, G., and Wahlin, B. (in press). "Dam and levee break modeling with HEC-RAS simulation and risk analysis (SimRAS)", in Proceedings of United States Society on Dams 2019 Conference and Exhibition, April 8 – 11, 2019, Chicago, IL.

Vorogushyn, S., Merz, B., Lindenschmidt, K.-E., and Apel, H. (2010), A new methodology for flood hazard assessment considering dike breaches, Water Resour. Res., 46, W08541, doi:10.1029/2009WR008475.

Tsai, C.W., Yeh, JJ. & Huang, CH. Stoch Environ Res Risk Assess (2019) 33: 91. https://doi.org/10.1007/s00477-018-1636-8.

Strategies for Improving Accuracy and Efficiency in Emergency Flood Inundation Modeling

Stephanie Bell, Hydraulic Engineer, USACE, Vicksburg, MS, stephanie.a.doyal@usace.army.mil

Extended Abstract

During a declared emergency, such as a dam or levee safety incident, hurricane, a flood, or a potential flood event, inundation modeling is conducted by USACE district offices in collaboration with NWS or by the MMC through the national flood inundation mapping (FIM) cadre to support real-time flood fighting effort. This includes the production of dynamic GIS data to provide real-time flood inundation mapping to the public in support of flood fighting activities as well as making the public aware of potential consequences. The two dimensional capabilities of HEC-RAS, which allow the inclusion of localized flooding due to rainfall in addition to riverine flooding, have allowed for the production of detailed flood inundations in as few as 24 - 48 hours. These detailed inundation maps, which show conditions throughout the watershed, are quickly becoming one of the preferred products of leadership and those coordinating flood fighting and emergency response. However, there are a few major issues that challenge the FIM cadre.

One of the major challenges for hydraulic modelers is being to produce and share inundation maps before the peak flooding occurs and with enough time to allow warnings to be released and preparations to be made. Under normal circumstances, it may take weeks or months to build, calibrate, and run a hydraulic model. During a flood event, this timeline is compressed significantly and results must be obtained in days. Under these circumstances, it can take up to as many as four days to obtain and process data, construct a hydraulic model, run model simulations, and prepare and upload inundation maps. Therefore, it is key that flood inundation modeling be initiated as soon as a major threat, such as a hurricane or potential dam or levee breach, is identified. This timeline can be reduced by about two to three days if there is an existing hydraulic model that can be used with minimal or no modifications.

Decision making capability is another key factor that affects the time it takes to produce a flood inundation map. Key deliverables and the level of detail required for each deadline need to be established at the time modeling is initiated and communicated to the modeler by leadership.

For example, a map that provides a statewide overview of flood extents and identifies areas at high risk for localized flooding may be required for a briefing twenty four hours before a hurricane landfall and more detailed maps for individual cities and counties may be required twenty four hours post landfall to aid in emergency response efforts. Each of these situations requires a different level of detail and the modeling effort should be adjusted accordingly to meet each deadline. Hydraulic modelers need to be able to anticipate the time required for each step of the flood inundation map production process and be able to make decisions on when each step needs to be completed in order to meet the established deadlines. Being able to decide what should be included to produce the best quality inundation map in such a short time takes experience or the guidance of an experienced modeler. For this reason, it is imperative that modelers document processes used and lessons learned during the flood event or immediately after so that the knowledge and experience gained can be shared. With each flood event, the cadre build their level of experience, make improvements to the FIM cadre's standard operating procedures, and share lessons learned through after action reports, webinars, and conferences. This has resulted in increased efficiency and a reduction in map delivery time.

The availability and ability to process and transfer data is another major issue that often hinders the production of flood inundation maps. The two-dimensional HEC-RAS models that are commonly used for flood inundation modeling rely upon large terrain datasets. These large datasets often require a significant amount of time to download and process before they can be used. For example, during Hurricane Florence in 2018, terrain download and processing accounted for 36 of the 46 hours required to produce an initial map for a major watershed in North Carolina. Large data transfers are facilitated by the use of network folders with organization-wide access and file exchanges. Model and data libraries are also being continually updated in order to reduce the amount of time needed to obtain data and build models.

There are key pieces of data that are critical for the development hydraulic models. These key data include flow and stage data, observed and forecast precipitation, antecedent conditions, and the dimensions and locations of dams and levees. These data are not always readily available and if they are, it often takes days to acquire. Modelers should organize, label, and store the data that was gathered during the event so that it can be used for future modeling efforts. This investment of time and resources can significantly reduce the time it takes for data collection for the next flood event.

Social media is one source of data that can be used when time is limited. A search of recent social media posts for the area of interest can provide insight on the current conditions in the watershed. During Hurricane Harvey, social media posts were used to verify model outputs of coastal flooding that seemed unreasonable at first glance. User posted photos of major highways and coastal towns were comparable to the model outputs. During another dam breach modeling effort, social media was also use as a data gathering tool. At the time the dam breach modeling was initiated, the dam was still under construction. As a result, the height of the embankment dam, one of the most important dam breach parameters, was unknown. Official requests for data did not initially yield any information. Through a social media search, a Facebook group related to the dam was found. In this group, regular updates were being posted by the construction workers at the dam detailing their progress. These posts revealed information about the dam height and gate operability which was then used for the dam breach model. This information was then verified later by on-site personnel. While caution should always be used when using social media as a data source, it is still preferable to a blind estimate or assumption. The ability to visually examine the project is invaluable to modelers. This creative method of gathering data when no other data sources are immediately available has allowed modelers to produce preliminary results under emergency conditions in as few as 24 hours.

Valuable lessons are learned from every flood event and that information is used to improve the efficiency of the team and the quality of the flood inundation products. As data processing and transfer capabilities are improved and modelers gain more experience, the time required to provide these products will decrease, and hopefully, a delivery time of 24-48 hours or less will become the new standard.

Flood Hydrology

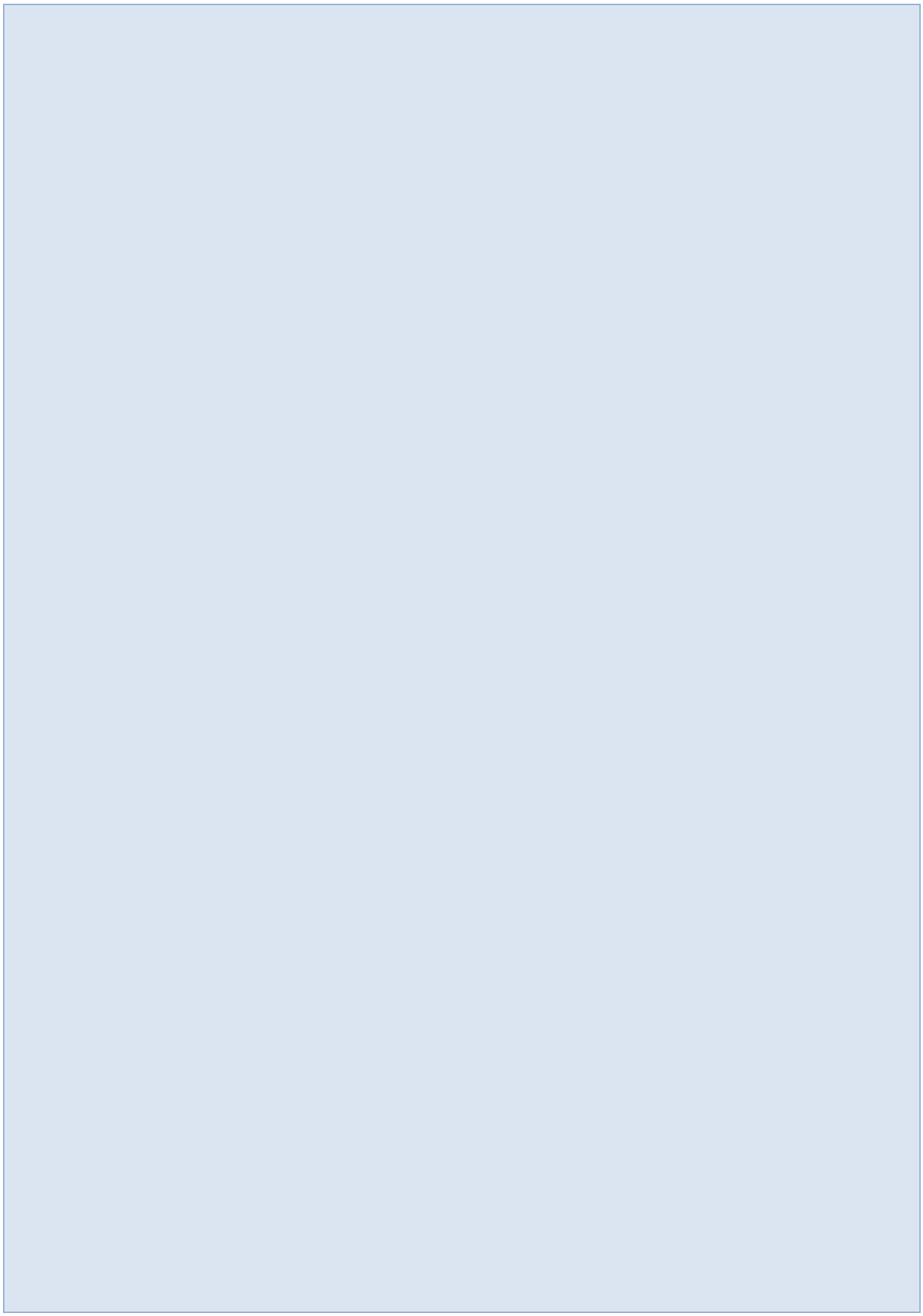

A Modified Temperature-Based Method to Spatially Simulate Frozen Ground within GSSHA and HEC-HMS

Dr. Michael Follum, P.E., Hydraulic Engineer, U.S. Army Corps of Engineers, Engineer Research and Development Center, Coastal and Hydraulics Laboratory, 3909 Halls Ferry Rd, Vicksburg, MS 39180; 601-634-2639; Michael.L.Follum@usace.army.mil
Dr. William Scharffenberg, Hydraulic Engineer, U.S. Army Corps of Engineers, Institute for Water Resources, Hydrologic Engineering Center, 609 Second Street, Davis, CA 95616; 530-302-3691; William.Scharffenberg@usace.army.mil.
Dr. Jeffrey Niemann, P.E.; Professor, Department of Civil and Environmental Engineering, Colorado State University, Campus Delivery 1372, Fort Collins, CO 80523; 970-491-3517; Jeffrey.Niemann@colostate.edu

Introduction

More than one-sixth of the world's population relies on meltwater from glaciers and seasonal snowpack for their water supply (Barnett et al., 2005). Thus, the volume and timing of snowmelt-derived streamflow is crucial for water managers to make water supply and flood protection decisions. Frozen ground can affect the hydrologic response (volume and timing) within watersheds by reducing infiltration and increasing runoff (Bayard et al., 2005; Dunne and Black, 1971; Stähli et al., 1999), which can lead to flooding as well as increased sediment erosion (Johnson and McArthur, 1973). Hydrologic models are often utilized by water managers, but frozen ground has proven difficult to simulate due to complex interactions of energy and water between the atmosphere, snowpack, ground cover, and soil (Dun et al., 2010; Kennedy and Sharratt, 1998; Lin and McCool, 2006). Energy-balance approaches to simulate frozen ground are available and can capture the heterogeneity of frozen ground (Flerchinger and Saxton, 1989; Jansson 2001; Chen et al., 2007), but often have large parameter and forcing data requirements (e.g. wind speed, relative humidity, short- and long-wave radiation) which limit their applicability. Temperature-based approaches to simulate frozen ground (Molnau and Bissell, 1983; Rekolainen and Posch, 1993) are also available, but typically only simulate the presence of frozen ground, not the depth of frozen ground. Additionally, temperature-based approaches only vary the presence of frozen ground due to elevation and the depth of snowpack, whereas frozen ground is known to be highly-variable temporally and spatially (Campbell et al., 2010; Shanley and Chalmers, 1999; Stähli, 2017). This paper discusses ongoing modifications to a temperature-based frozen ground model within U.S. Army Corps of Engineers (USACE) hydrologic models to more accurately simulate the temporal and spatial heterogeneity of frozen ground while limiting the number of forcing data required. Ultimately, these improvements are aimed at improving the streamflow simulations within USACE hydrologic models used by water managers in data austere environments.

USACE Hydrologic Models: GSSHA and HEC-HMS

The USACE has two primary hydrologic models: Hydrologic Engineering Center – Hydrologic Modeling System (HEC-HMS; Scharffenberg and Fleming, 2006) and the Gridded Surface Subsurface Hydrologic Analysis model (GSSHA; Downer and Ogden, 2004). GSSHA is a fully-distributed hydrologic model that solves conservation of mass and energy equations on a structured grid. HEC-HMS is used operationally by every USACE District and has the option to simulate hydrological processes using a lumped, semi-distributed, or fully-distributed (gridded)

domain. Both GSSHA and HEC-HMS provide numerous methods/options to simulate hydrological processes (often dictated by available data). GSSHA has two frozen ground methods: an advanced energy balance method that requires numerous forcing data, use of Richard's Equation infiltration, and several calibration parameters; and the temperature-based continuous frozen ground index (CFGI; Molnau and Bissell, 1983) method that requires minimal inputs but varies the frozen ground only with elevation. HEC-HMS does not have a frozen ground method. This paper provides and overview of modifications to the CFGI frozen ground method (referred to as modCFGI) to improve the spatiotemporal estimation of frozen ground. The modCFGI method is currently an option within GSSHA (Follum et al., 2018) and is currently being implemented into HEC-HMS. The following sections discuss the drivers of frozen ground, how these drivers are included within the modCFGI frozen ground method, and the planned test cases of modCFGI within HEC-HMS.

Drivers of Frozen Ground

Mass (water) and energy balances drive the presence and depth of frozen ground. When the temperature of the soil falls below freezing for extended periods of time the moisture within the soil begins to freeze creating pore ice (frozen ground). Frozen ground can begin to thaw when geothermal and atmospheric energy are available to melt the water content within the soil. Several factors (drivers) control the spatial pattern, presence, and depth of frozen ground, including the following:

- Soil moisture (Fox, 1992; Willis et al., 1961)
- Physical properties of the soil (e.g. thermal conductivity) (Farouki, 1981; Johansen, 1977)
- Insulation from the snowpack (Pearson, 1920; Willis et al., 1961)
- Vegetation (Campbell et al., 2010; Kienholz, 1940; Shanley and Chalmers, 1999)
- Woody debris, and leaf litter (Brown, 1966; Diebold, 1938; Fahey and Lang, 1975; MacKinney, 1929; Sartz, 1973; Stähli, 2017)
- Solar shading (from vegetation and topography) (Wilcox et al., 1997)
- Topography (elevation, aspect, slope) (Flerchinger et al., 1990; Seyfreid and Wilcox, 1995; Shanley and Chalmers, 1999)

Physics-based (i.e. energy balance) approaches can account for all of the drivers of frozen ground listed, but have large parameter and forcing data requirements. Temperature-based approaches require less data, but only account for elevation and insulation from the snowpack (which also varies only with elevation in temperature-based snow models). Because frozen ground can drastically impact hydrologic runoff, a method is needed within USACE hydrologic models to accurately simulate the temporal and spatial pattern of frozen ground while limiting the forcing data requirements (e.g. most watersheds do not have measurements of solar radiation, pressure, relative humidity, etc.).

modCFGI Frozen Ground Model

The CFGI model is commonly used within operational hydrologic models as a simple degree-day method to account for the presence of frozen ground. Degree-day methods accumulate daily temperatures as a frost index (F, °C-days). When F exceeds a calibrated threshold ($F_{Threshold}$, °C-days), the ground is assumed frozen and infiltration is restricted. Because snow can insulate the ground from sub-freezing temperatures, the CFGI method adjusts the affect that daily temperatures have on F by accounting for the depth of the snow. A detailed description of the CFGI method is given in Molnau and Bissel (1983). The following sections briefly describe the modCFGI method, with more details provided in Follum et al. (2018).

Use of a Proxy Temperature to Represent Available Energy and Improve Spatial Snowpack Simulation

Follum et al. (2015) proposed using an hourly proxy temperature (T_{rad}, °C) instead of air temperature to represent available energy at the snow surface (Figure 1). The modCFGI method replaces daily averages of air temperature with daily averages of T_{rad} in the calculation of F. Through simple relationships between radiation (shortwave and longwave) and topography/vegetation, the net solar radiation can be calculated for each cell within a distributed hydrologic model. Using the Stefan-Boltzmann law to relate radiated energy to a temperature, T_{rad} is calculated hourly and accounts for variations in latitude, time of day, topography (slope, aspect, elevation, shading) and vegetation (shading, downwelling longwave radiation from canopy). The forcing data requirements include air temperature, precipitation, and cloud cover. Air temperature and precipitation are common requirements of hydrologic models. Cloud cover is measured operationally at airports within the U.S. as part of the local climatological data (NCEI, https://www.ncdc.noaa.gov/) as well as estimated from satellites (NCEI).

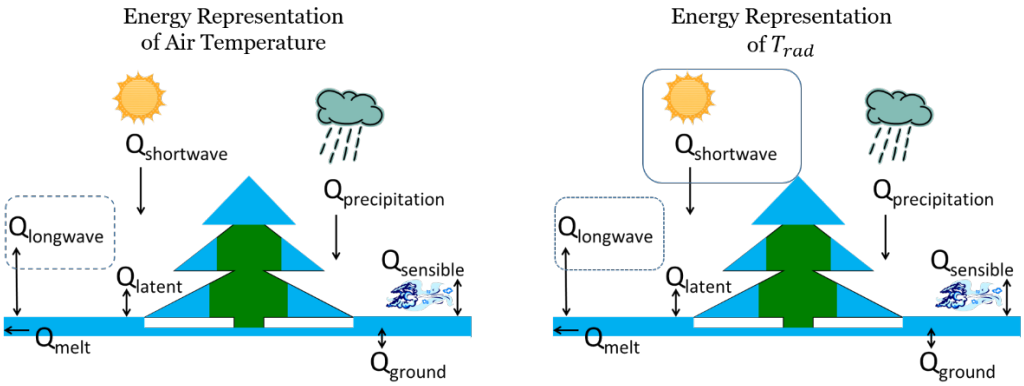

Figure 1. Diagram of the energy fluxes ($\boldsymbol{Q}$) affecting the snowpack, with boxes around the energy fluxes captured by air temperature (downwelling $\boldsymbol{Q_{longwave}}$ from atmosphere) and $\boldsymbol{T_{rad}}$ ($\boldsymbol{Q_{shortwave}}$ and downwelling $\boldsymbol{Q_{longwave}}$ from atmosphere and vegetation). $\boldsymbol{Q_{longwave}}$ is net longwave radiation, $\boldsymbol{Q_{shortwave}}$ is net shortwave radiation, $\boldsymbol{Q_{melt}}$ is advected heat removed by meltwater, $\boldsymbol{Q_{precipitation}}$ is advected heat from precipitation, $\boldsymbol{Q_{ground}}$ is ground heat flux, $\boldsymbol{Q_{latent}}$ is latent heat flux, and $\boldsymbol{Q_{sensible}}$ is sensible heat flux. Figure 1 is modified from a figure in Follum (2018).

Air temperature was replaced with T_{rad} within the commonly-used SNOW-17 snow model (Anderson, 1973; 2006) and tested at Senator Beck Basin in Colorado. The modified snow model, referred to as the Radiation-derived TI snow model (RTI), showed improved accuracy in simulation of snow water equivalent (SWE) at two point locations and basin-wide snow covered area (SCA). The spatial patterns of SWE produced by the RTI snow model (Follum et al., 2015; 2018; Follum, 2018) better follow the known controls of large-scale distributions of the snowpack (Fassnacht et al., 2017; Jost et al., 2007). Additionally, use of the RTI snow model improved the simulated streamflow indicating that the RTI snow model better captured the basin-wide SWE (Follum, 2018). Use of the RTI model to simulate the snowpack when using the modCFGI frozen ground method provides improved spatial and temporal simulation of the snowpack, which better accounts for the snowpack insulation of the ground.

Ground Cover as Insulator of the Soil

Vegetation, woody debris, and leaf litter all insulate the ground from freezing, yet are often not considered in frozen ground methods. Follum et al. (2018) proposed adding ground cover (encompasses everything on the ground surface) as an additional insulator within the modCFGI model. The depth of ground cover is approximated based on land cover maps, such as the 2006 National Land Cover Database (Fry et al., 2011). The insulating properties of the ground cover are calibrated parameters. As shown in Follum et al. (2018), the inclusion of ground cover as an insulator was a key reason the modCFGI model outperformed the CFGI model at six test sites within the Sleepers River Experimental Watershed in Vermont.

Soil Moisture and Soil Properties

Aside from calibrating $F_{Threshold}$, neither the CFGI nor modCFGI methods account for soil moisture or soil properties (e.g. thermal conductivity of the soil) in the presence of frozen ground. As shown in Follum et al. (2018), the F value calculated from the modCFGI model can be used within a modified Berggren Equation (as described in DeWalle and Rango (2008)) to simulate the depth of frozen ground. The modified Berggren Equation accounts for both soil moisture and the thermal conductivity of the soil (an additional model input). Because the presence of frozen ground may be more important than the depth of frozen ground within hydrologic models, the calculation of frozen ground depth is left as an option within GSSHA and HEC-HMS.

Future Projects / Testing

The modCFGI frozen ground method is currently available within GSSHA and has been tested at two watersheds: Sleepers River Experimental Watershed in Vermont (Follum et al., 2018), and the Hubbard Brook Experimental Watershed in New Hampshire. The RTI snow model is currently being implemented within HEC-HMS, for release in HEC-HMS v4.4. Once RTI is fully implemented, the modCFGI frozen ground model will be implemented within HEC-HMS. Initial testing of the modCFGI model within HEC-HMS will use the Mill Creek watershed model (part of the USACE Walla Walla District). Additional tests are also planned for watersheds in the upper-Midwest United States (part of the USACE St. Paul District).

References

Anderson, E.A., 1973. National Weather Service River Forecast System - Snow Accumulation and Ablation Model. Technical Memorandum NWS Hydro-17, 217 pp.

Anderson, E.A., 1976. A point of energy and mass balance model of snow cover. U.S. National Oceanic and Atmospheric Administration NOAA Technical Report NWS 19, Silver Spring, MD.

Barnett, T.P., Adam, J.C. and Lettenmaier, D.P., 2005. Potential impacts of a warming climate on water availability in snow-dominated regions. Nature, 438(7066), p.303.

Bayard, D., Stähli, M., Parriaux, A., Flühler, H. 2005. The influence of seasonally frozen soil on the snowmelt runoff at two Alpine sites in southern Switzerland. Journal of Hydrology 309(1), 66-84.

Brown, J., 1966. Influence of vegetation on permafrost, In: Woods, K.B. (Ed.), Permafrost International Conference, National Academy of Sciences-National Research Council, NRC Div. Bldg., Ottawa, Canada, 6 pp.

Campbell, J.L., Ollinger, S.V., Flerchinger, G.N., Wicklein, H., Hayhoe, K., Bailey, A.S., 2010. Past and projected future changes in snowpack and soil frost at the Hubbard Brook Experiment Forest, New Hampshire, USA. Hydrological Processes, 24, 2465-2480.

Chen, R.S., Kang, E.S., Ji, X.B., Yang, Y., Zhang, Z.H., Qing, W.W., Bai, S.Y, Wang, L.D., Kong, Q.Z, Lei, Y.H, Pei, Z.X., 2007. Preliminary study of the hydrological processes in the alpine meadow and permafrost regions at the headwaters of Heihe River. Journal of Glaciology and Geocryology, 29(3), 387-396.

DeWalle, D.R., Rango, A., 2008. Principles of snow hydrology. Cambridge University Press.

Diebold, C.H., 1938. The effects of vegetation upon snow cover and frost penetration during the March 1936 floods. Journal of Forestry, 36(11), 1131-1137.

Downer, C.W., Ogden, F.L., 2004. GSSHA: Model to simulate diverse stream flow producing processes. Journal of Hydrologic Engineering, 9(3): 161-174.

Dun, S., Wu, J., McCool, D., Frankenberger, J., Flanagan, D., 2010. Improving frost-simulation subroutines of the Water Erosion Prediction Project (WEPP) model. Transactions of the ASABE, 53(5), 1399-1411.

Dunne, T., Black, R.D., 1971. Runoff processes during snowmelt. Water Resour. Res., 7, 1160–1172.

Fahey, T.J., Lang, G.E., 1975. Concrete frost along an elevational gradient in New Hampshire. Canadian Journal of Forest Research, 5(4), 700-705

Farouki, O.T., 1981. The thermal properties of soils in cold regions. Cold Regions Science and Technology, 5(1), 67-75.

Fassnacht, S. R., López-Moreno, J. I., Ma, C., Weber, A. N., Pfohl, A. K. D., Kampf, S. K., and Kappas, M., 2017. Spatio-temporal snowmelt variability across the headwaters of the Southern Rocky Mountains. Front. Earth Sci., 11(3), 505-514.

Flerchinger, G., Cullum, R., Hanson, C., Saxton, K., 1990. Soil freezing and thawing simulation with the SHAW model. Frozen Soil Impacts on Agricultural, Range, and Forest Lands: 77-86.

Flerchinger, G., Saxton, K.E., 1989. Simultaneous heat and water model of a freezing snow-residue-soil system I, theory and development. Transactions of the ASAE, 32(2), 565-571.

Follum, M.L., 2018. Spatial simulation of snow and frozen ground using a modified temperature-based model. PhD Dissertation, Department of Civil and Environmental Engineering, Colorado State University, Fall 2018.

Follum, M.L., Downer, C.W., Niemann, J. D., Roylance, S. M., and Vuyovich, C. M., 2015. A radiation-derived temperature-index snow routine for the GSSHA hydrologic model. J. Hydrol., 529, 723–736.

Follum, M.L., Niemann, J.D., Parno, J.T., Downer, C.W., 2018. A simple temperature-based method to estimate heterogeneous frozen ground within a distributed watershed model. Hydrology and Earth System Sciences, 22(5), 2669.

Fry, J.A., Xian, G., Jin, S., Dewitz, J.A., Homer, C.G., Limin, Y., Barnews, C.A., Helold, N.D., Wickham, J.D., 2011. Completion of the 2006 national land cover database for the conterminous United States. Photogrammetric Engineering and Remote Sensing, 77(9): 858-864.

Fox, J.D., 1992. Incorporating freeze-thaw calculations into a water balance model. Water Resources Research, 28(9), 2229-2244.

Jansson, P.E., 2001. Coupled heat and mass transfer model for soil-plant-atmosphere systems.

Johansen, O., 1977. Thermal conductivity of soils. CRREL-TL-637, Cold Regions Research and Engineering Laboratory, Hanover, NH.

Johnson, C.W., McArthur, R.P., 1973. Winter storm and flood analyses, northwest interior. Hydraulic Engineering and the Environment. ASCE, pp. 359-369.

Jost, G., Weiler, M., Gluns, D.R., Alila, Y., 2007. The influence of forest and topography on snow accumulation and melt at the watershed-scale. Journal of Hydrology, 347(1), 101-115.

Kennedy, I., Sharratt, B., 1998. Model comparisons to simulate soil frost depth. Soil Science, 163(8), 636-645.
Kienholz, R., 1940. Frost depth in forest and open in Connecticut. Journal of Forestry, 38(4): 346-350.
Lin, C., McCool, D., 2006. Simulating snowmelt and soil frost depth by an energy budget approach. Transactions of the ASABE, 49(5), 1383-1394.
MacKinney, A., 1929. Effects of forest litter on soil temperature and soil freezing in autumn and winter. Ecology, 10(3), 312-321.
Molnau, M., Bissell, V.C., 1983. A continuous frozen ground index for flood forecasting. Proceedings 51st Annual Meeting Western Snow Conference, Canadian Water Resources Association, Cambridge, Ontario, 109-119.
National Centers for Environmental Information (NCEI), https://www.ncdc.noaa.gov/.
Pearson, G.A., 1920. Factors controlling the distribution of forest types, Part I. Ecology, 1(3), 139-159.
Rekolainen, S., Posch, M., 1993. Adapting the CREAMS model for Finnish conditions. Hydrology Research, 24(5), 309-322.
Sartz, R.S., 1973. Effect of forest cover removal on depth of soil freezing and overland flow. Soil Science Society of America Journal, 37(5), 774-777.
Scharffenberg, W.A. and Fleming, M.J., 2006. Hydrologic modeling system HEC-HMS: User's manual. US Army Corps of Engineers, Hydrologic Engineering Center.
Seyfried, M., Wilcox, B., 1995. Scale and the nature of spatial variability: Field examples having implications for hydrologic modeling. Water Resources Research, 31(1): 173-184
Shanley, J.B., Chalmers, A., 1999. The effect of frozen soil on snowmelt runoff at Sleepers River, Vermont. Hydrological Processes, 13(13), 1843-1857.
Stähli, M., 2017. Hydrological significance of soil frost for pre-alpine areas. Journal of Hydrology, 546, 90-102.
Stähli, M., Jansson, P-E., Lundin, L-C., 1999. Soil moisture redistribution and infiltration in frozen sandy soils. Water Resources Research 35(1), 95-103.
Wilcox, B.P., Newman, B.D., Brandes, D., Davenport, D.W., Reid, K., 1997. Runoff from a semiarid ponderosa pine hillslope in New Mexico. Water Resources Research, 33(10), 2301-2314.
Willis, W., Carlson, C., Alessi, J., Haas, H., 1961. Depth of freezing and spring run-off as related to fall soil-moisture level. Canadian Journal of Soil Science, 41(1), 115-123.

Advances in Snowmelt Modeling in the Midwest, Red River of the North

Ann Banitt, Senior Hydraulic Engineer, US Army Corps of Engineers, St Paul, MN
ann.m.banitt@usace.army.mil
Kevin Denn, Senior Hydraulic Engineer, US Army Corps of Engineers, St Paul, MN
kevin.d.denn@usace.army.mil
Emily Moe, Senior Hydraulic Engineer, US Army Corps of Engineers, St Paul, MN
emily.l.moe@usace.army.mil
Carrie Vuyovich, Hydrological Sciences Laboratory, NASA
Goddard Space Flight Center Greenbelt, MD, carrie.m.vuyovich@nasa.gov

Abstract

The Red River of the North (RRN) basin is a hydrologically-complex area bordering eastern North Dakota and western Minnesota. Positioned in low-lying glacial Lake Agassiz, the RRN flows northward over very flat terrain (2.64 m per km; Schwert, 2003). The watershed is vulnerable to snowmelt floods due to its flat terrain and low permeability soil. High river discharges pose a threat to communities along the RRN, inundating sections of land extending out several miles from the river's main channel.

The St Paul District USACE in partnership with the USACE Cold Regions Laboratory (CRREL) utilized the temperature index method of HEC-HMS to simulate the snowmelt across the watershed, focusing on the March 2009 flooding event that was the basin's second-worst in modern history. The flood severity was due to a combination of highly saturated soils resulting from above-average rainfall the previous fall, above-average winter snowpack, and increased rainfall and unseasonably warm temperatures in late March (Macek-Rowland and Gross, 2011). Flood levels persisted for two months after peak stage, causing $55M USD in damage to the region (National Weather Service, 2010). Real-Time Mesoscale Analysis (RTMA) is a NOAA/NCEP high-spatial and temporal resolution analysis/assimilation system for near-surface weather conditions. RTMA was used for the temperature series, and SNODAS was used to generate an "observed" snow water equivalent (SWE) time series for each HMS subbasin for calibration purposes.

Regional suitability of snowmelt parameters can be used to group regions across the 46,000 square mile watershed that can be parameterized similarly. This approach is described and a case study presents how a suite of snowmelt parameters can be applied across a basin with metrics, such as the Nash Sutcliffe Efficiency parameters, calculated and displayed spatially using GIS software. Calibrated parameters for regulated basins can be reviewed against the visual relationships discovered in the regional processing.

Future snow modeling efforts can take advantage of several new ground observation and remotely sensed data products available. These data are expected to provide additional sources of information on ground state and moisture as well as SWE and snow melt estimates. By improving current modeling capabilities, parameter estimation techniques and incorporating additional soil and snow data we hope to improve our ability to simulate snowmelt in the RRN.

Introduction

The St Paul District USACE in partnership with the USACE Cold Regions Laboratory (CRREL) utilized the temperature index method of HEC-HMS to simulate the snowmelt across the watershed, focusing on the March 2009 flooding event that was the basin's second-worst in modern history. The flood severity was due to a combination of highly saturated soils resulting from above-average rainfall the previous fall, above-average winter snowpack, and increased rainfall and unseasonably warm temperatures in late March (Macek-Rowland and Gross, 2011). Flood levels persisted for two months after peak stage, causing $55M USD in damage to the region (National Weather Service, 2010). Real-Time Mesoscale Analysis (RTMA) is a NOAA/NCEP high-spatial and temporal resolution analysis/assimilation system for near-surface weather conditions. RTMA was used for the temperature series, and SNODAS was used to generate an "observed" snow water equivalent (SWE) time series for each HMS subbasin for calibration purposes.

Basin Overview

The Red River of the North (RRN) basin is a hydrologically-complex area bordering eastern North Dakota and western Minnesota. Positioned in the low-lying glacial Lake Agassiz, a pre-historic lake which no longer exists, the RRN flows northward over very flat terrain (2.64 m per km; Schwert, 2003). The watershed is vulnerable to snowmelt floods due to its flat terrain and low permeability soil. High river discharges pose a threat to communities along the RRN, inundating sections of land extending out several miles from the river's main channel. Performing snowmelt modeling in this watershed helps to inform communities how the various tributaries route and combine, as the melt progresses from the upstream basins in the south to the Canadian border in the north. Snowmelt floods happen over the course of several weeks, and allow for some planning and emergency construction of sandbag levees or other flood closures in communities at risk.

The Landscape: Within the Red River of the North, the road network follows the sections of land. In such a flat watershed, the section roads are the highest feature on the landscape for miles and perpendicularly crosshatch the watershed in a grid pattern. Culverts provide the hydraulic connections between the ditches within the sections. During spring runoff, culverts may initially be filled with ice and snow, and may cause the sections of land to become individual square-shaped reservoirs. The hydraulic connectivity of the watershed complicates the snowmelt hydrology and calibration of flow rates within a hydrologic model. **Figures 1a and 1b** shows a reach of the Red River of the North immediately upstream of Fargo, North Dakota and Moorhead Minnesota on the Red River the North. The fact that the watershed flows from south to the north into Canada also adds a complicating factor as the melt water flows north into areas that are colder and at times ice covered. Ice jams can be a problem in the river system.

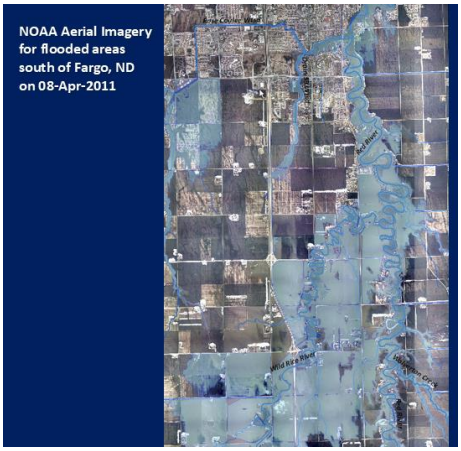

Figure 1a

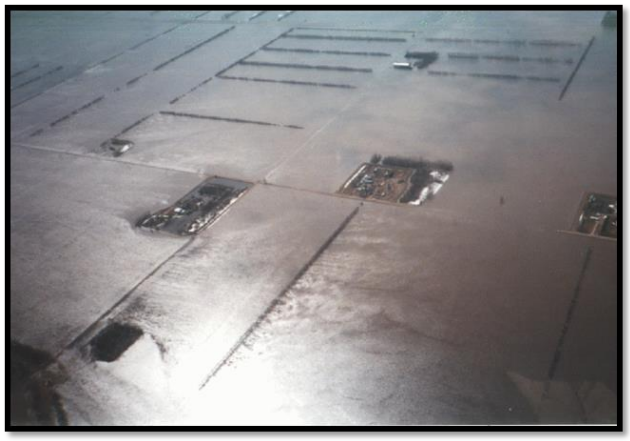

Figure 1b

Figures 1a and 1b. Section flooding in the Red River of the North Watershed
a) USACE Unsteady HEC-RAS 2011 flood inundation overlay on aerial imagery
b) Typical Section Flooding, 1997 Spring Flood Imagery, Red River of the North

Soils of the Red River of the North: The soils in the Red River of the North are dense clays. The Red River of the North soil as clay with very low infiltration rates. (NRCS SSURGO, USACE EM 1110-2-1417) Depending on the snow cover and prevailing winter temperatures, the soil column freezes down to a depth of 30 inches. The antecedent soil moisture plays a part in the snowmelt and runoff in the basin. When the clay is substantially dry, large cracks form in the soil column. These cracks have been observed in the field (**Figure 1**), and have been surmised to be the connection to soil storage that in some snowmelt seasons, is responsible for large volumes of runoff that never materialize in the channel.

Figure 1. Clay fissures in dry watershed conditions (West Consultants, 2012)

Red River of the North Climate Data Summary

The Red River of the North mean annual snowfall at Fargo Hector International Airport, ND from (1981-2010) is approximately 50 inches, with the majority of the snowfall occurring in November – March (https://www.ndsu.edu/ndsco/data/snow/#c343720). Snow Water Equivalent (SWE) values vary over the wind-swept midwest plains, but the SWE values that prevailed prior to recent snowmelt floods were on average about 4 inches in 2009 and in 2011 with a few tributaries (especially near the Sheyenne River and North Dakota's Wild Rice River) with patches of SWE up to 6 inches.

The temporal melt pattern has been investigated by engineering firms and the St Paul District, US Army Corps of Engineers. The temperature records from climatological stations across the watershed were analyzed to estimate the threshold date, on average, when three consecutive above-freezing days occurs. This threshold was used to estimate when melt would initiate. In years with the highest runoff in the Red River of the North, melt started in the beginning of April in the most upstream portion of the watershed (in the Bois de Sioux watershed), on approximately April 15th in the portion of the watershed along the Canadian border, and on April 19th in the far western tributaries (Sheyenne and Park Rivers). (**Reference** Phase 1 Red River Integrated Watershed Study)

Although temporal patterns can be used to show averaged behavior of snowmelt across a watershed, each season presents its own character in the rate and timing of spring melt. Snow melt may pause until the end of the March and then warm to melting and continue to warm until the snow was gone). The freezing and thawing of the snow during the cycling of daytime and nighttime have an effect on the snowmelt runoff in this basin.

Modeling Data Sources

Snowmelt modelers of Midwestern basins are at a fundamental disadvantage compared to modelers in the western U.S. basins, where much of the snowmelt research and model application takes place, because of the lack of observed data. While SWE in the mountainous areas are notably greater than SWE in the Midwest, the vast majority of regional floods in the Midwest are driven by intense rainfall occurring on a ripened snowpack, indicating that SWE information is no less important in the Midwest. Within the 46,000 square mile Red River of the North watershed, there are approximately two SWE observation sites. The dots in **Figure 2** represent SWE gages maintained by the National Resource Conservation Service (NRCS) recording observed data, with the vast majority of the gages concentrated in the mountainous western United States.

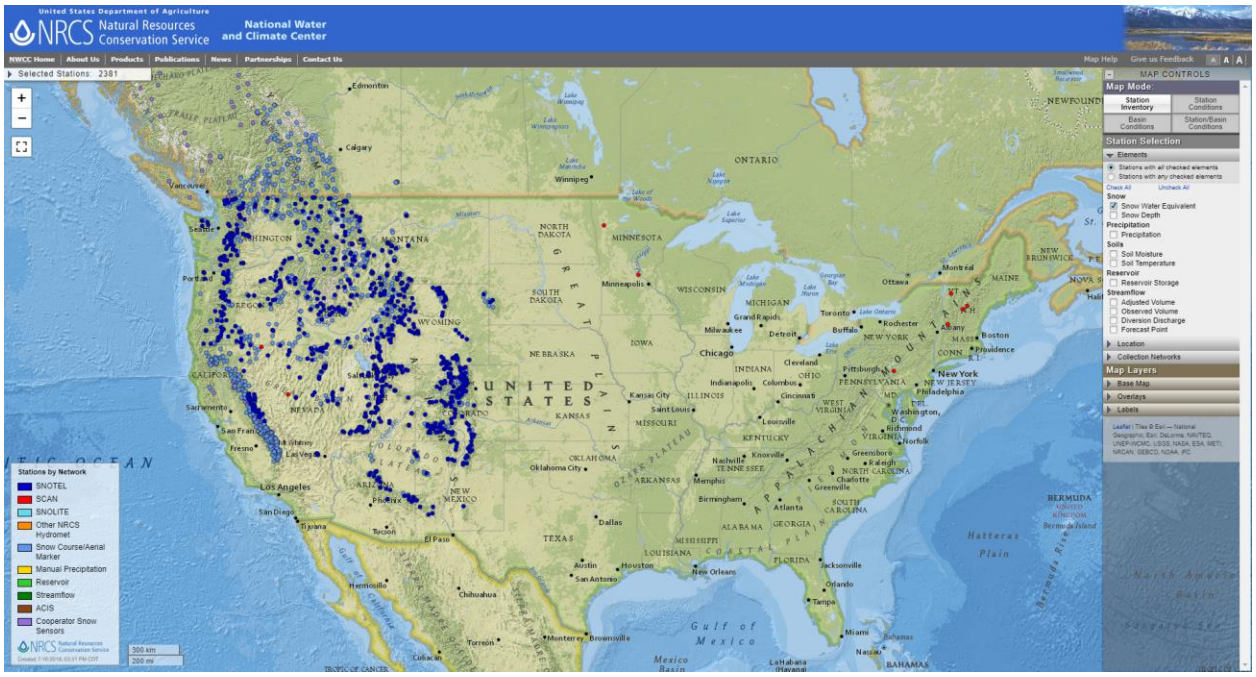

Figure 2. Observed Snow Data Availability throughout the United States from the NRCS.

Historically, the National Operational Hydrologic Remote Sensing Center (NOHRSC) has flown flight lines and collected satellite imagery to verify SWE estimates and snow cover extents. Site personnel from USACE projects and NWS reconnaissance engineers field-verify approximate areal snow coverage and snow depths. Remote sensing and snow modeling has continued to evolve within the Federal Agencies. Current modeling efforts combine remote sensing and field measurements to update and validate hydrologic model simulations of snow accumulation and melt. The NOHRSC SNOw Data Assimilation System (SNODAS) product combines snow estimates based on an energy balance model with ground observations and satellite based snow extent data to provide daily SWE and snow depth estimates on a gridded basis throughout the United States. This product is widely used as a surrogate for observed SWE data where gages do not exist.

Modeling Approach

Model Calibration: An HEC-HMS model of the RRN was constructed during a Corps Water Management System (CWMS) production effort and was initially calibrated to rainfall events. When updated snowmelt algorithms were added to the CWMS modeling suite, the HMS model's calibration was extended to snowmelt for two years, 2009 and 2011, when heavy snow and spring rain led to significant flooding in the region. The HMS snow model was calibrated initially by comparison to SNODAS modeled SWE, averaged over each subbasin area using HEC-MetVue. The snowmelt simulations were initiated in March, using the SNODAS modeled SWE estimate as the initial condition, before the main snowmelt commenced. SNODAS estimates were compared to ground measurements where possible for reasonableness. Adjustments to the snow and hydrologic model parameters were then made to best match the observed discharge.

The Temperature Index method within the HMS model was used for snowmelt modeling. The Temperature Index method first discriminates between snow and rain, updates antecedent

temperature indexes, calculates the meltrate, melts snowpack based on the temperature, and performs a mass balance with rain, meltwater and previous liquid water. Melting happens at the bottom of the snowpack.

The primary parameter adjusted in the snowmelt calibration for each major tributary or groups of tributaries was the Antecedent Temperature Index (ATI) melt rate factor. Several melt rate tables and patterns were tested during calibration, however a constant melt rate factor was found to give as good or better results when compared with SNODAS and observed discharge data. A second HMS snowmelt parameter that was adjusted was called PX temperature. The PX temperature discriminates between rainfall and snowmelt, and can be changed to reflect local conditions. The third snowmelt relationship that was adjusted during calibration trials was the ATI coldrate relationship. The ATI coldrate relationship represents the amount of energy needed to raise the temperature of the snowpack to the melting point.

Snowmelt Parameter Variation: Modeling multiple years of snowmelt in the Red River of the North illustrated that the melt rate can vary from year to year depending on the timing and pattern of the warm-up period (i.e., temperatures rise above freezing to begin melt, and then drop below freezing again. **Figures 3a and 4b** illustrate the variation of two regional temperature gages during a snowmelt event. Melt rates are also affected by whether the melt happens due solely to temperature increases, or if the melt is accelerated by rain falling on the ripening snowpack. Some of the most challenging spring floods to predict include double-peaked events in the valley where a melt is initiated, followed by a very cold period that refreezes the melt for a time and then resumes the warming to melt out the snowpack.

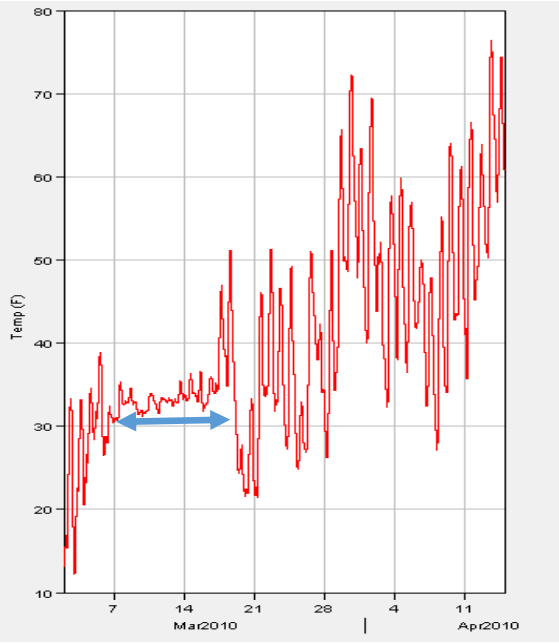

Figure 4a

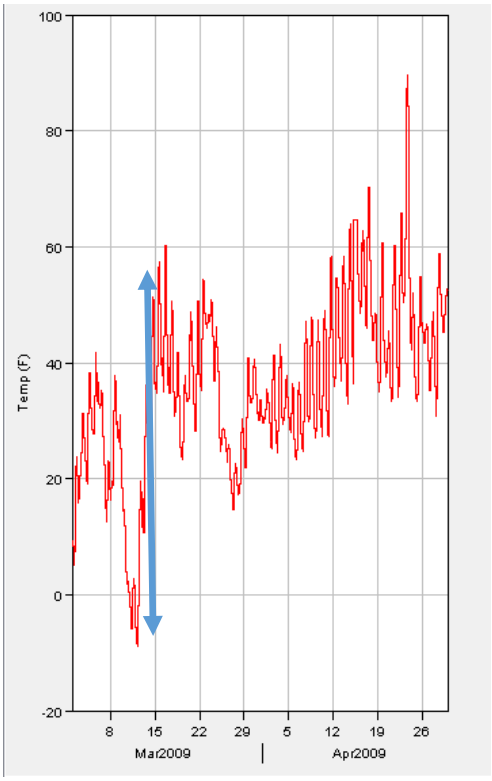

Figure 4b

Figures 3a and 4b. Spring Warm-Up Period Variation
a) Temperatures hover around freezing for a week or more ripening snowpack
b) Temperatures vary from -8 Degrees F and dramatically warm into the 50's over the course of 5 days.

SNODAS Corrections: The accuracy of the SNODAS data in the plains region can be lacking, in particular when reported depths of SWE are significantly higher than exist in reality. Reviewing SNODAS data during calibration reveals that "corrections" are made at a point in time (e.g. the SNODAS SWE estimates are reduced by 4 inches in a day to match observed ground data) and notes are made on the NWS website. During calibrations, a modeler has the luxury to review the notes during the data collection phase, and can adjust the SWE grids to "correct" for the error. During real time snowmelt calibration, the errors in SNODAS may not be caught until after the event. Checking with the local NWS office for their SWE estimates, where they have personnel on the ground to verify snow depths, may help provide insight and improve accuracy of the snowmelt modeling. Our modelers also discovered the nationally distributed SNODAS grids have areas of "no data" over the frozen lakes. Some portions of the Midwest prairies have large "prairie potholes" areas or lakes with large surface areas. Missing the snowpack over frozen lakes in "SNODAS" can result in a significant underestimation of the water in the watershed during the melt period.

Regional Assessment

Currently, snowmelt calibration in large basins is difficult, time consuming, and relies significantly on modeler judgment. Due to the size and complexity of large Midwestern basins being modeled at present, a novel approach that allowed for systematic and objective snowmelt parameter calibration was developed. This approach was initially applied to two watersheds in the Upper Midwest: the Red River of the North and the Upper Mississippi River. Since the development of this technique, it has been adopted by numerous snowmelt modelers throughout the United States. The technique relies on a simple workflow involving the hydrologic model, a spreadsheet, and a geographic information system (GIS). The end product of the technique is a series of maps that display the appropriateness of the calibration using widely-accepted metrics that remove modeler bias. The following paragraphs present the current state of snowmelt calibration, a detailed overview of the regional assessment process, and a case study showing the effectiveness with which the process can be deployed. While the following paragraphs focus on the use of the process for the HEC-HMS snowmelt model, the process can be easily adapted to any hydrologic model that can output time-series SWE data for each subbasin modeled.

Current State of Snowmelt Calibration Process for Midwestern Basins:

A current limitation within HEC-HMS is that snowmelt model parameters are defined at a basin level, with each individual subbasin using the exact same snowmelt parameters as every other subbasin within the model. Therefore, finding parameters that allow for the proper calibration of snowmelt models with dozens of subbasins across large, diverse watersheds is of paramount importance. However, determining the appropriateness of the calibration effort requires the modeler to individually select and review time series output, as shown in **Figure 4** where the modeled basin is shown on the left and the results of an individual subbasin are shown on the right, with the blue line indicating the modeled results and the red line indicating the observed results. When dozens of subbasins exist within the model, this turns into a time-consuming process. Additionally, determining the appropriateness of the calibration is fairly subjective if simply comparing the modeled values to the observed values in order to see if they are "close enough".

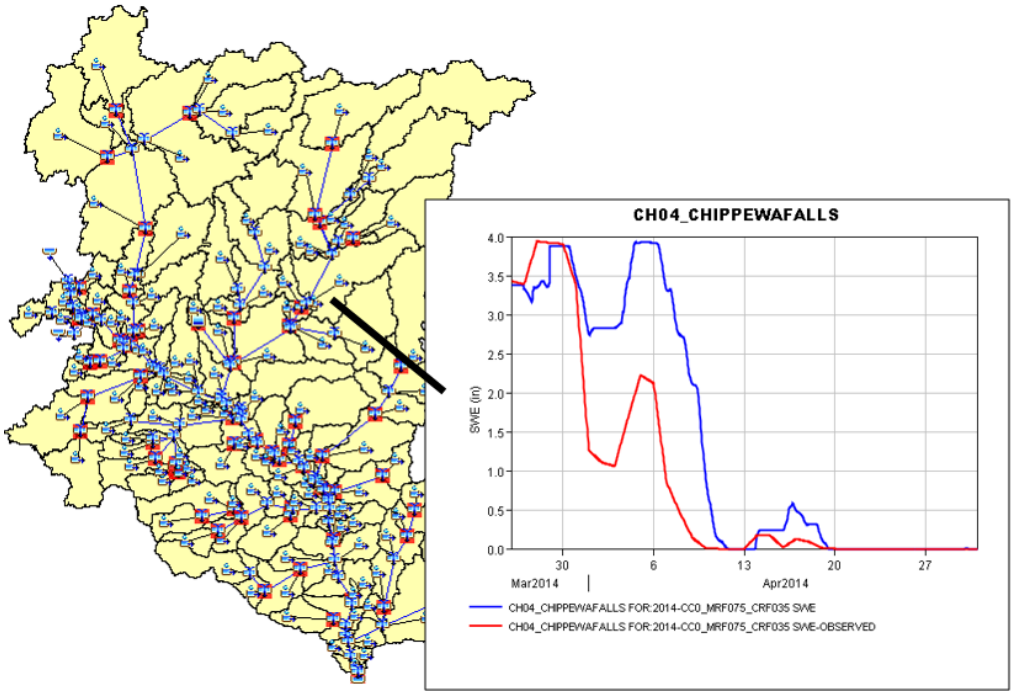

Figure 4. Example of current process to evaluate snowmelt calibration appropriateness

Regional Assessment Process: A regional assessment process was developed to address three goals:

1. Use defined metrics to determine "goodness of fit" of modeled data against observed data;
2. Allow the user to clearly see the "goodness of fit" spatially across all subbasins that constitute the overall modeled basin; and
3. Reduce the amount of time needed to perform a snowmelt model calibration

The first challenge was to define "goodness of fit" that removed modeler judgment from the process. For this, the Nash-Sutcliffe Efficiency (NSE) metric was selected. The NSE metric is commonly used in hydrologic modeling and was deemed suitable for use in defining "goodness of fit" for snowmelt modeling. A study conducted by Moriasi et al. (2007) determined that the statistically-based performance rating chart displayed in **Table 1** is appropriate for hydrologic models. Generally, a NSE equal to a value of 1 indicates a perfect match between the modeled and observed data, NSE values between 0.4 and 1 indicate "Satisfactory" performance or better, and an NSE less than 0 indicates that the mean observed value serves as a better predictor of the modeled parameter than does the hydrologic model.

Table 1. Performance Ratings for Calibration for a Daily and Weekly Time Step (Moriasi et al., 2007)

Performance Rating	NSE
Very Good	0.65<NSE≤1
Good	0.55<NSE≤0.65
Satisfactory	0.40<NSE≤0.55
Unsatisfactory	NSE≤0.40

It is recommended that the NSE metrics for the meteorologic model calibration be calculated for the primary melt timeframe (if one exists) rather than for the entire simulation timeframe. In the Midwestern United States, one melt timeframe is the main contributor to high flows. This will ensure that the selected calibration parameters best simulate this primary melt period and that the NSE statistic is not artificially skewed by the time period when no SWE exists in both the observed and modeled data.

The second challenge of allowing modelers to spatially view "goodness of fit" across the modeled basin was accomplished through a simple two-step process involving a spreadsheet and GIS software. A spreadsheet was developed that simply requires the modeled and observed SWE values to be copied from the model output into a tab within the spreadsheet. From there, the spreadsheet automatically calculates the NSE for each individual subbasin. The developed spreadsheet is easily portable from one project to the next and only requires minimal modification at the outset of each project based primarily on the number of subbasins present in the modeled basin. Once the NSE values for each subbasin are calculated, they are copied into a GIS attribute table for the shapefile layer showing the polygon extents of each subbasin. A simple formatting of the shapefile layer display settings to show the four performance rating categories of very good, good, satisfactory, and unsatisfactory based on the NSE value allows for a rapid viewing of the performance of the selected calibration parameters.

The third challenge is to ensure that the process reduces the amount of time necessary to conduct the calibration effort. The ease of use of the spreadsheet greatly assists in accomplishing this task. The other important components to ensuring that the process reduces the necessary effort are that the model allow for numerous simulation alternatives to be established and that the modeler generally understands the parameters to which the model results are sensitive. Within HEC-HMS, a modeler has the ability to quickly establish a number of snowmelt alternatives with different input parameters. Additionally, the authors have found that for Midwestern basins, two parameters typically drive the calibration: (i) the meltrate function, which controls how quickly the snowpack warms/melts and (ii) the coldrate function, which controls how quickly the snow absorbs cold temperatures. Therefore, a large number of alternatives can be rapidly established in which reasonable ranges of meltrate and coldrate functions can be simulated. The authors have found that within an hour or two, 20 alternatives can be set up, run, and spatially evaluated for "goodness of fit" without modeler bias, significantly reducing the amount of time necessary to hone in on the appropriate calibration values compared to the traditional approach. From there, refinements to the less-sensitive model parameters can be made to increase the "goodness of fit" using the same general approach.

Case Study: A case study is presented in the paragraphs below to illustrate the regional assessment approach. The case study uses a basin in the same general hydrologic setting as the Red River of the North basin: the Upper Mississippi River basin. The meltrate function parameter was the first parameter investigated. The results of the alternatives using four different meltrate functions (keeping all other variables constant) are shown in **Figure 6a**, where green indicates the best "goodness of fit" and red is the poorest fit. As shown in the black circled areas in **Figure 6a**, a clear divide was noted within the basin where different meltrate functions performed adequately. The subbasins within the black circled areas are defined as the "upper" area while the remaining subbasins are termed the "lower" area.

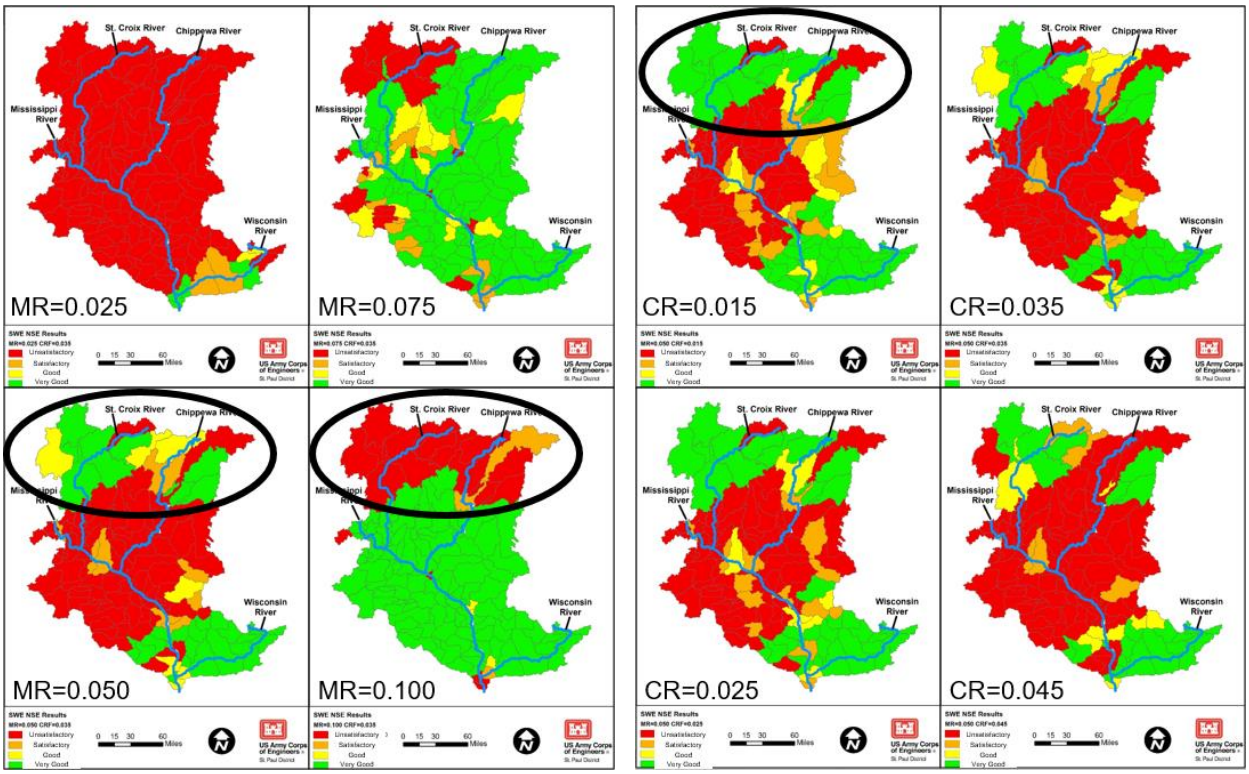

Figure 6a and 6b. Regional assessments
a) Adjusting meltrate function and holding all other variables constant
b) Calibrating upper area with constant meltrate function (0.050 in/deg F-day) and adjusting coldrate function

The calibration for the "upper" area continued with altering the coldrate function values while keeping the meltrate function at a value of 0.050 in/deg F-day, with the results shown in Error! Reference source not found.. This calibration showed that the coldrate function of 0.015 in/deg F-day in combination with the meltrate function value of 0.050 in/deg F-day yielded the best results for that area.

The calibration for the "lower" area then commenced by again adjusting the coldrate function values while keeping the meltrate function at a value of 0.100 in/deg F-day, with the results shown in **Figure** . This calibration showed that the results were not highly sensitive to the coldrate function; generally, a coldrate function of 0.035 in/deg F-day in combination with the meltrate function value of 0.100 in/deg F-day yielded the best results for that area.

Using this approach, the final meltrate and coldrate function combinations determined via the regional assessment methodology were concluded to provide the best modeled versus observed SWE calibration. **Figure 8** shows the final maps for the "upper" and "lower" area, with the "upper" area defined in the figure as the purple hatched area. At this time, HMS requires that one set of snowmelt parameters be applied to the entire basin. To handle disparate parameterizations, the HMS model was divided into separate basins, applying the upper area runoff hydrographs as input to the lower area streams.

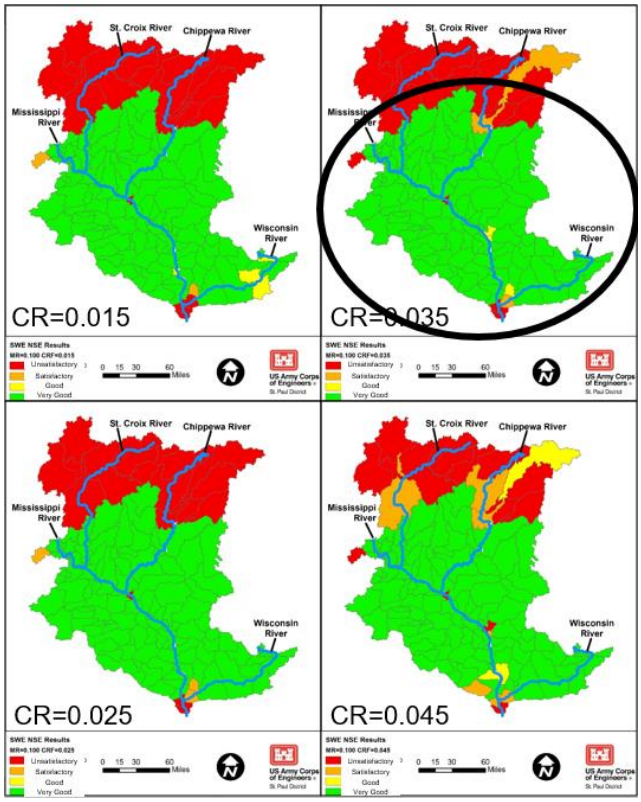

Figure 7. Regional assessments when calibrating lower area using constant meltrate function of 0.100 in/deg F-day and adjusting coldrate function

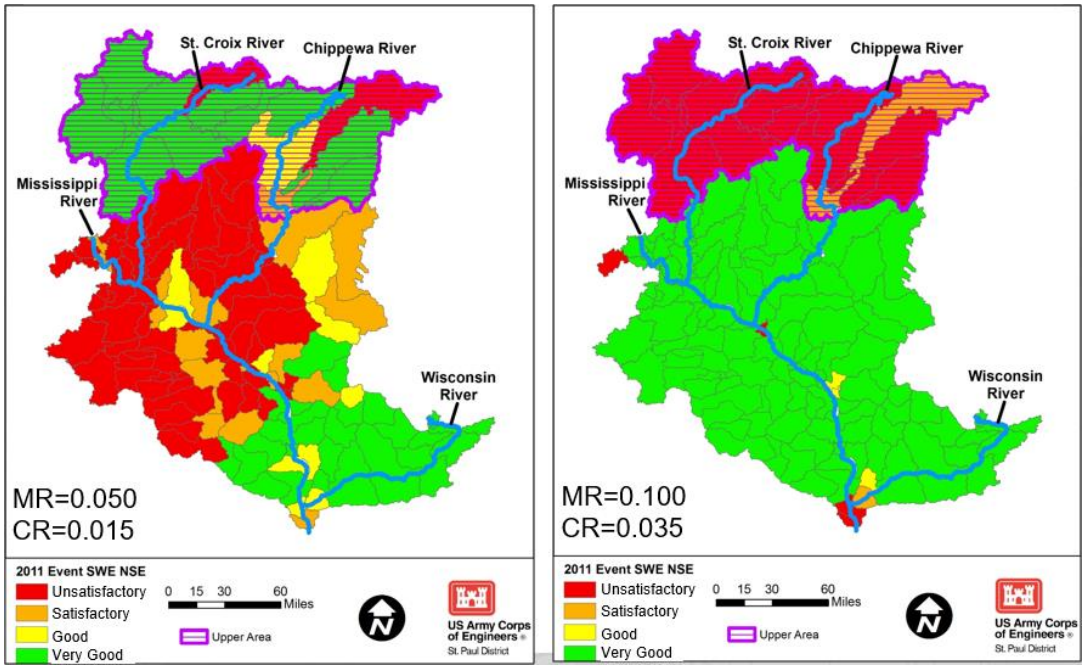

Figure 8. Final regional assessments for upper and lower areas (The left figure is the recommended parameterization for the upper watershed, and right is the parameterization for the lower watershed.)

This case study exhibits the ease with which the regional assessment process can be used as well as the effectiveness in establishing regional variability in snowmelt modeling parameters. Future releases of HEC-HMS will incorporate flexibility in selecting snowmelt parameters at the subbasin level or within groupings of subbasins, called "zones", which will further benefit from an approach similar to the one described above.

Informed Hydrologic Modeling - Next Steps

Although the ability to model snowmelt in the Red River of the North remains challenging, there are new data sets that have recently become available to enhance the understanding and offer up new capabilities to model snowmelt in the watershed.

Soil Moisture and Temperature Probe Measurement: The Silver Jackets Interagency partnership of State and Federal Agencies in the Red River of the North Watershed installed 13 soil moisture probes across the Red River of the North Watershed in 2016. Soil moisture probes were added to thirteen gage sites in the basin both in the valley and in the high lands spread out over the entire basin. This new data provides insight on the prevailing soil moisture going in to winter freeze up of the soil column. Tying the observations of clay crack formation to soil moisture can help inform how the available storage in the soil may change from one year to another.

Remote Sensing of Antecedent Soil Moisture: The antecedent moisture can also be assessed by using remote sensing data. The following data sources are starting to be used by the US Army Corps of Engineer offices to further investigate soil moisture states. NASA has a soil Moisture Active Passive (SMAP) 3 hour product that has a period of record from March 2015 to present. This product is generated from a satellite that orbits the earth and measures the top 5 centimeters of soil moisture from land surface microwave emission and radar backscatter. The top 1 meter of soil moisture is computed with a land surface model (GEOS-5 Catchment Land Model). The final SMAP product takes the SMAP measurements and the land surface model data and are assimilated into an improved product.

Passive Microwave Remote Sensing of SWE and snow melt: Passive microwave remote sensing provides an opportunity to remotely sense SWE and snow melt over large spatial extents. Passive microwave data is expressed as a brightness temperature and is sensitive to the presence of a snow cover at certain frequencies which allows for the estimation of SWE. The physical properties of the snowpack change the way the microwave signal is scattered. Any liquid in the snow eliminates scattering of the signal and the SWE estimates go to zero, which has been used to indicate snow melt onset. The data are unaffected by cloud cover and day/night and there are occasional swaths of no data due to orbit. Recent investigations of the USACE Cold Regions Research and Engineering Laboratory focused on utilizing NASA's MEaSUREs high resolution Calibrated Enhanced-Resolution Passive Microwave Brightness Temperature (CETB) data in the RRN. The CETB data and meteorological data (T, P) were combined in an algorithm to compute SWE, investigate how the snowpack ripens and when the melt onset occurs. SWE signals lose strength during periods of wet snow and could be an indicator for a melt signal. Results from CRREL's application of this method to the March 2009 snowmelt period, shows that passive microwave data changed in the days preceding the flood (**Figure 9**). Along the valley of the RRN mainstem and some of the south-eastern subbasins, the change in CETB data indicates heterogeneous behavior in the spatial distribution of the initial melt onset. This data is not yet available for use in real-time analysis.

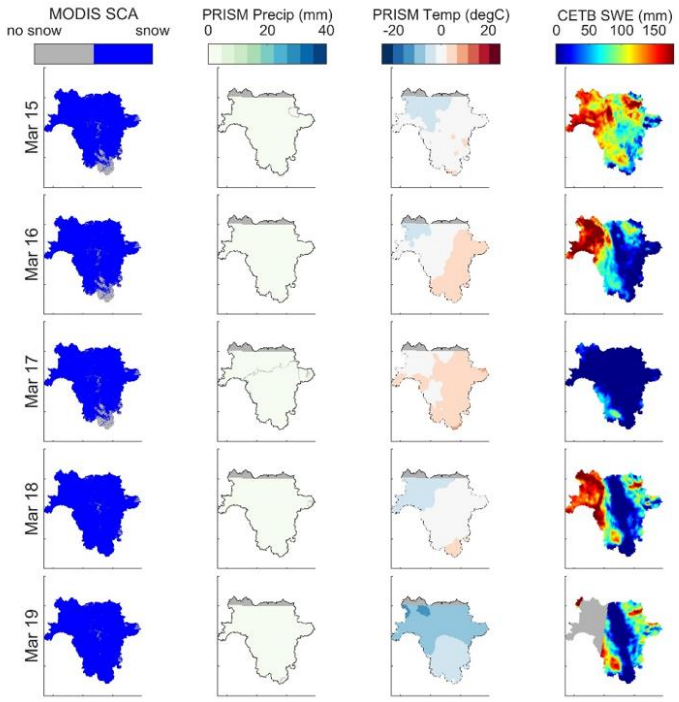

Figure 9. Precipitation (MODIS SCA), temperature (PRISM), and SWE (CETB) in the Red River of the North (March 15-March 19, 2009)

References

Houston Engineering Inc. "Fargo-Moorhead Metro Basin-Wide Modeling Approach- Hydrologic Modeling. HEC-HMS model Development Various Tributaries above the Red River of the North at Halstad, MN" 23December 2011.

"Interactive Snow Information" National Operational Hydrologic Remote Sensing Center 01January2019, https://www.nohrsc.noaa.gov/interactive/html/map.html?ql=.

Macek-Rowland, K.M., and Gross, T.A., 2011. 2009 Spring floods in North Dakota, western Minnesota, and northeastern South Dakota: U.S. Geological Survey Scientific Investigations Report 2010–5225, 41 p.

"Monthly Climate Summaries" North Dakota State Climate Office, North Dakota State University, 01Janurary 2019, https://www.ndsu.edu/ndsco/data/snow.

Moriasi, D. N., Arnold, J. G., Van Liew, M. W., Bingner, R. L., Harmel, R. D., and Veith, T. L. 2007. "Model Evaluation Guidelines for Systematic Quantification of Accuracy in Watershed Simulations," Transactions of the American Society of Agricultural and Biological Engineers, 50(3), 885-900.

National Weather Service (NWS), 2010. Flood Damages Suffered in the United States During Water Year 2009. Annual Flood Loss Summary Reports. National Oceanic and Atmospheric Administration (NOAA).

Natural Resources Conservation Service (NRCS), United States Department of Agriculture. Soil Survey Geographic (SSURGO) Database. https://sdmdataaccess.sc.egov.usda.gov.

Schwert, D.P., 2003. A geologist's perspective on the Red River of the North: history, geography, and planning/management issues. Proceedings 1st International Water Conferences, Red River Basin Institute, Moorhead, MN.

U.S. Army Corps of Engineers. (1994). Engineer Manual 1110-2-1417, Flood-Runoff Analysis. Washington, D.C.: USACE.

West Consultants, 2012. Geomorphology Study of the Fargo, ND & Moorhead, MN Flood Risk Management Project.

Application of a Markov Chain Monte Carlo Sampler to Infer Parameter Uncertainty Distributions Using HEC-HMS

Angela Duren, P.E., P.H., District Hydrologist, U.S. Army Corps of Engineers, Portland, OR, Angela.M.Duren@usace.army.mil
Brian E. Skahill, Ph.D., Research Civil Engineer, U.S. Army Corps of Engineers, Engineer Research and Development Center, Coastal and Hydraulics Laboratory, Vicksburg, MS Brian.E.Skahill@usace.army.mil
William Scharffenberg, Ph.D., Senior Hydraulic Engineer, U.S. Army Corps of Engineers, Hydrologic Engineering Center, Davis, CA, William.Scharffenberg@usace.army.mil

Abstract

This study makes use of version 4.3 of HEC-HMS software which now includes a Markov Chain Monte Carlo (MCMC) sampler to support simultaneous HEC-HMS model optimization and inference for risk-informed hydrologic analyses. These tools are used to explore the HEC-HMS model posterior parameter distributions inferred using different data likelihood formulations; from either multiple discrete event calibrations, two season-specific calibrations, or use of continuous simulation. The parameters from the multi-parameter calibration parameter sets are explored individually to use as the basis of uncertainty distributions in a stochastic analysis for dam safety studies and also as a means for characterizing hydrologic uncertainty in developing a deterministic design flood hydrograph.

Introduction

Hydrologic models often contain parameters that cannot be measured directly either because they have no physical basis, it would be impractical, or due to an incompatibility of scales, among other possible reasons. Hence, hydrologic model parameters are inferred by adjusting their values until an acceptable level of agreement is achieved between a set of historical observations of the real world system that the model represents and their simulated counterparts. While manual model calibration is certainly one approach to the problem, it is subjective, labor-intensive, and may also suffer from a lack of consistency and/or repeatability, among others. Computer-based calibration of hydrologic models is an active area of research and development (see; for example, Baggett and Skahill, 2010a, b; Skahill et al. 2009, Skahill and Doherty, 2006; Doherty and Skahill, 2006, and references cited therein) which has resulted in numerous automatic calibration methods that are readily available (see Matott et al. 2009 and references cited therein). The Corps of Engineers is fully committed to implementing risk-informed engineering methodologies to capture uncertainty and transparency of insufficient knowledge and parameter variability.

Background

As mentioned, hydrologic models are typically calibrated by adjusting parameters encapsulated in the simulator until there is an acceptable level of agreement between a set of historical data and their model simulated counterparts. The parameters obtained via calibration are often then used by the model to predict system behavior for one or more pre-defined scenarios of interest to different groups whose life or livelihood is rooted in the local model study area. Regardless of the calibration method employed and the type (e.g., empirical or physics-based) of model used, some if not all of the parameter values obtained through the calibration process possess a degree of quantifiable

uncertainty. This is because the observed data contain measurement errors and the model never perfectly represents the watershed system or exactly fits the observation data. Where model parameters are uncertain so too are model predictions. In particular, quantifying uncertainty supports, among others, the following hydrologic modeling activities (Schoups and Vrugt, 2010; Schoups et al., 2010):

1. Model comparison and selection,
2. Identification of the best water management strategies that reflect the likelihood of outcomes,
3. Data collection aimed at improving hydrologic predictions and water management, and
4. Regionalization and extrapolation of hydrologic parameters to ungauged basins.

Model uncertainty, characterized by the model covariance matrix calculated using the model Jacobian (Skahill and Doherty, 2006) evaluated at the best estimate for the model, can be quantified by employing a traditional linear analysis. However, this approach is local, which does not dovetail well with the understanding that for hydrologic models there may exist many effectively equally acceptable models; i.e., it is difficult to identify a unique best estimate. In addition, it relies on a linearity assumption that is often violated in hydrologic modeling practice. Bayesian-based approaches to model calibration, wherein a prior distribution for the model is proposed and the vector of adjustable model parameters is treated as a random variable with a target probability distribution conditioned with observed data, are a formal means to obtain a realistic and reliable estimate of model uncertainty. In particular, Markov Chain Monte Carlo (MCMC) simulation, which is by far more efficient than other Monte Carlo methods, is used for inference, search, and optimization with hydrologic models (Harmon and Challenor, 1997; Kuczera and Parent, 1998; Campbell et al., 1999; Campbell and Bates, 2001; Makowski et al., 2002; Qian et al., 2003; Kanso et al., 2003; Vrugt et al., 2003a; Vrugt et al., 2003b; Vrugt et al., 2008). With MCMC we are interested in a target probability distribution and its key elements. These key elements include exploration of this distribution by way of some sort of random walk or diffusion process. This distribution must be initialized in an arbitrary way because we don't know a priori where good places necessarily are in terms of parameter space.

Case Studies

A by-product of the use of MCMC in HEC-HMS for auto-calibration and uncertainty is the ability to explore the individual parameter distributions for a given event or composite event. The singular marginal distribution of a parameter from the MCMC results can be used deterministically to inform a semi-quantitative assessment of uncertainty of a model or design flood hydrograph. In this paper we discuss a watershed in which the posterior distribution of a parameter changes by combining events in the MCMC simulation. We also explore the use of the uncertainty around a singular parameter distribution as a basis of a semi-quantitative uncertainty around a design flood hydrograph.

Single-Event versus Composite Event

A small (174 square mile) watershed hydrologic model located in the Willamette Basin, located in central Oregon, was used to evaluate the current deployment of MCMC in the latest HEC-HMS software version. The small watershed is located in the South Santiam River basin (which is part of the larger Willamette Basin) on the western-facing slopes of the Cascades. This watershed is largely forestland with some high elevations and runoff

that includes both snowmelt and rainfall. The hydrologic model in this region was developed and calibrated manually in HEC-HMS and then also calibrated using MCMC. For this watershed, we compare two separate single-event MCMC calibrations for one event and compare the posterior distributions between the events of a couple of parameters with a 'composite' simulation in which we run the two events back-to-back.

For the simulations there are 50,000 iterations and convergence was determined by using the weight of evidence approach with likelihood plots, trace plots, and the Gelman-Rubin index. In general, convergence was reached by the end of the first 20,000 iterations. Examining the unit hydrograph parameters, time of concentration and storage coefficient, the single-event marginal distributions were distinctly different from each other (Figure 1). The storage coefficient for both events formed a normal distribution with different mean and standard deviation (Figure 1). For time of concentration, the posterior distribution between both events are different distributions. For the hydraulic conductivity parameter for soil loss, both events fall under a uniform distribution for each single-event simulation (Figure 2).

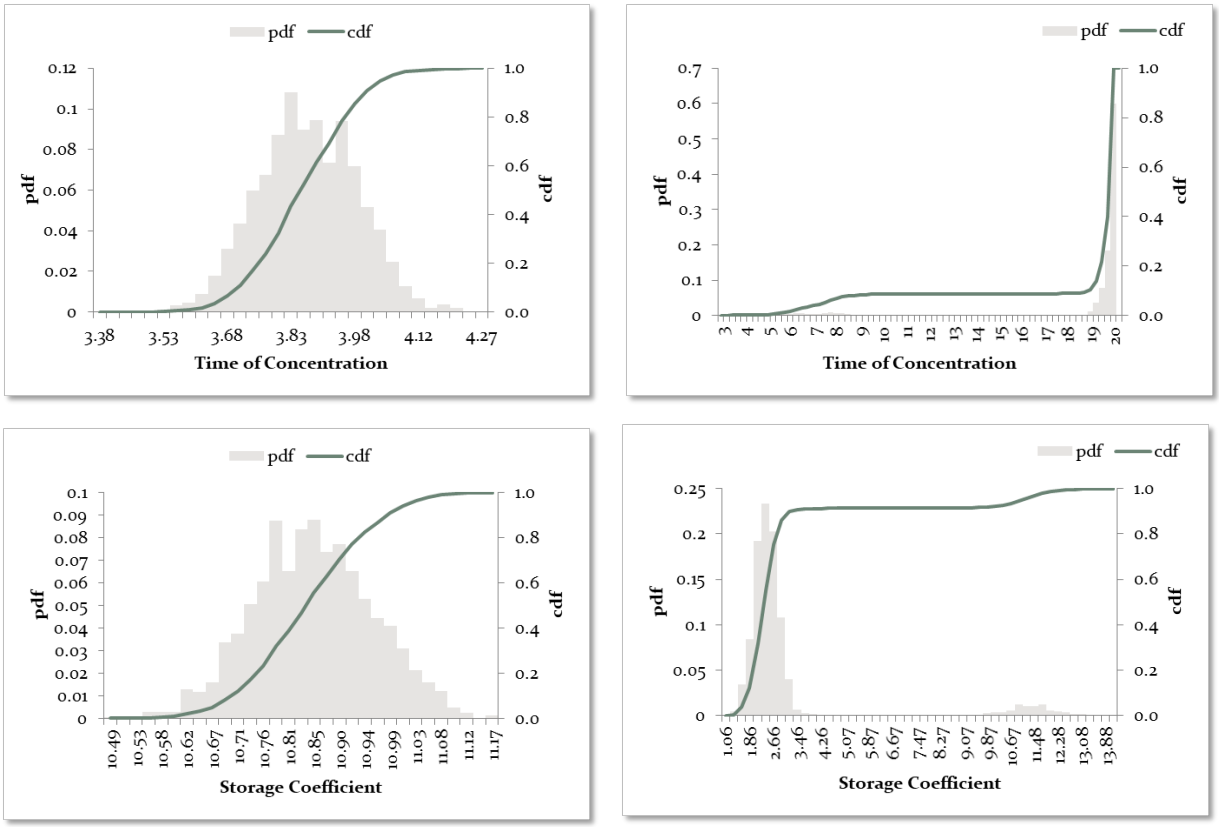

Figure 1 Time of Concentration Marginal Distribution for Event 1 (top left) and Event 2 (top right); Storage Coefficient Marginal Distribution for Event 1 (bottom left) and Event 2 (bottom right)

Under the composite event scenario, the time of concentration and storage coefficient parameters converge to a normal distribution with unique distribution parameters (Figure 3). For the hydraulic conductivity, use of the composite event resulted in converging from a uniform distribution to a normal distribution, which results in better parameter inference (Figure 3).

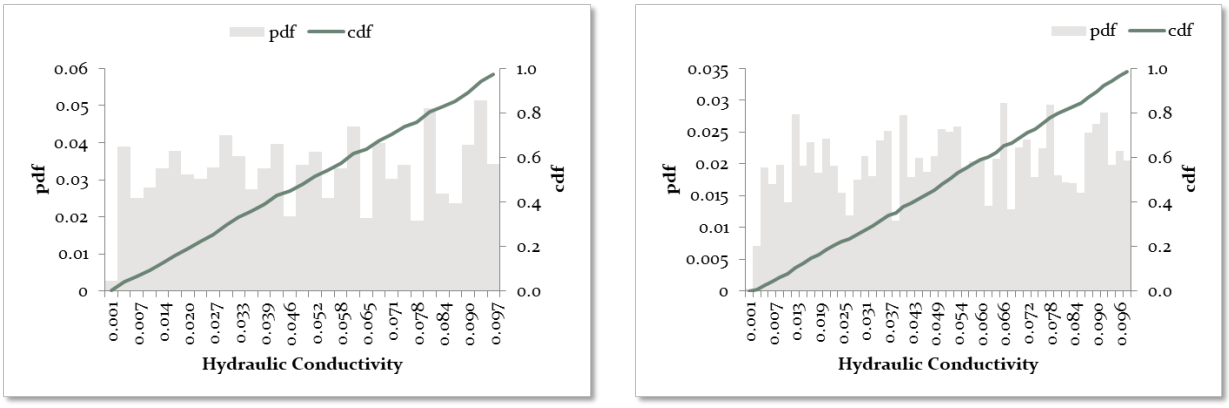

Figure 2 Hydraulic Conductivity Marginal Distribution for Event 1 (left) and Event 2 (right)

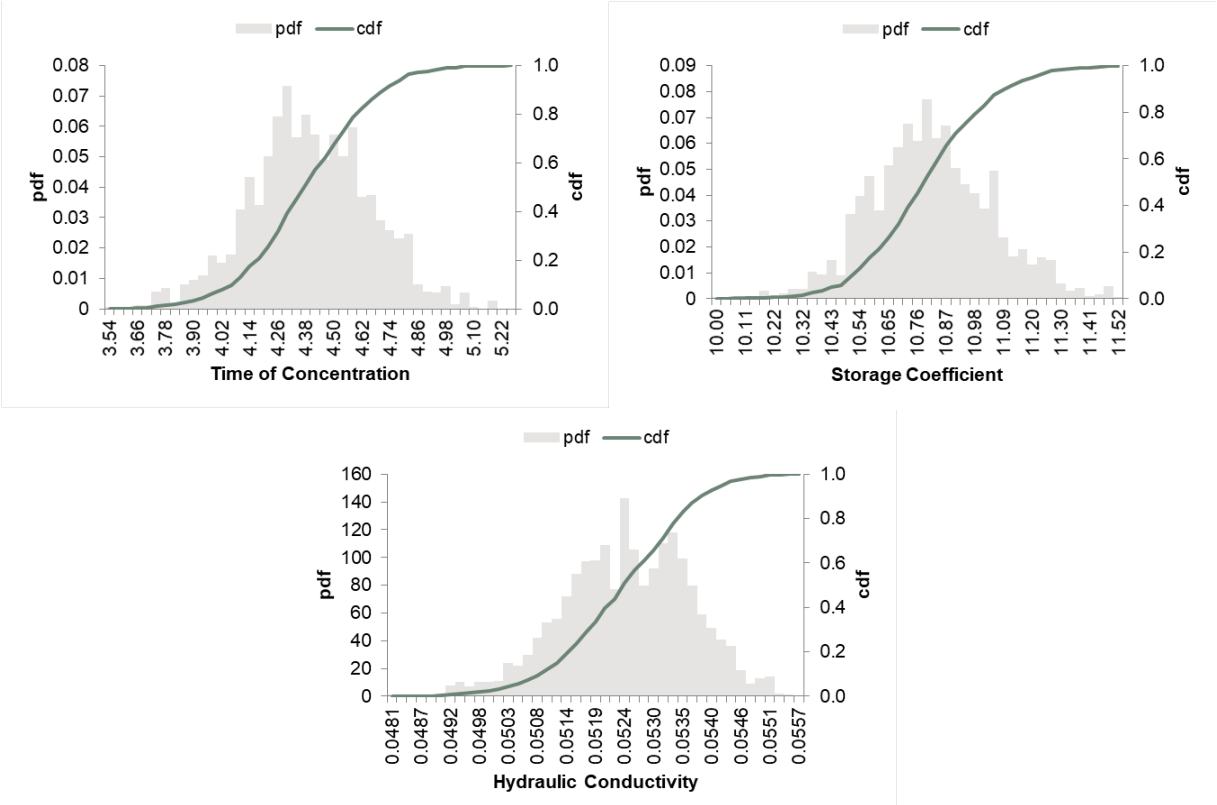

Figure 3 Posterior Distributions of Parameters for Composite Events for Time of Concentration (top left), Storage Coefficient (top right), and Hydraulic Conductivity (bottom)

Design Flood Uncertainty

In another case study, MCMC in HEC-HMS is used to characterize the uncertainty distribution around a critical parameter in a calibrated hydrographic model. The parameter distribution is sampled as part of the deterministic design flood hydrograph to obtain an estimate of the uncertainty around design flood hydrograph.

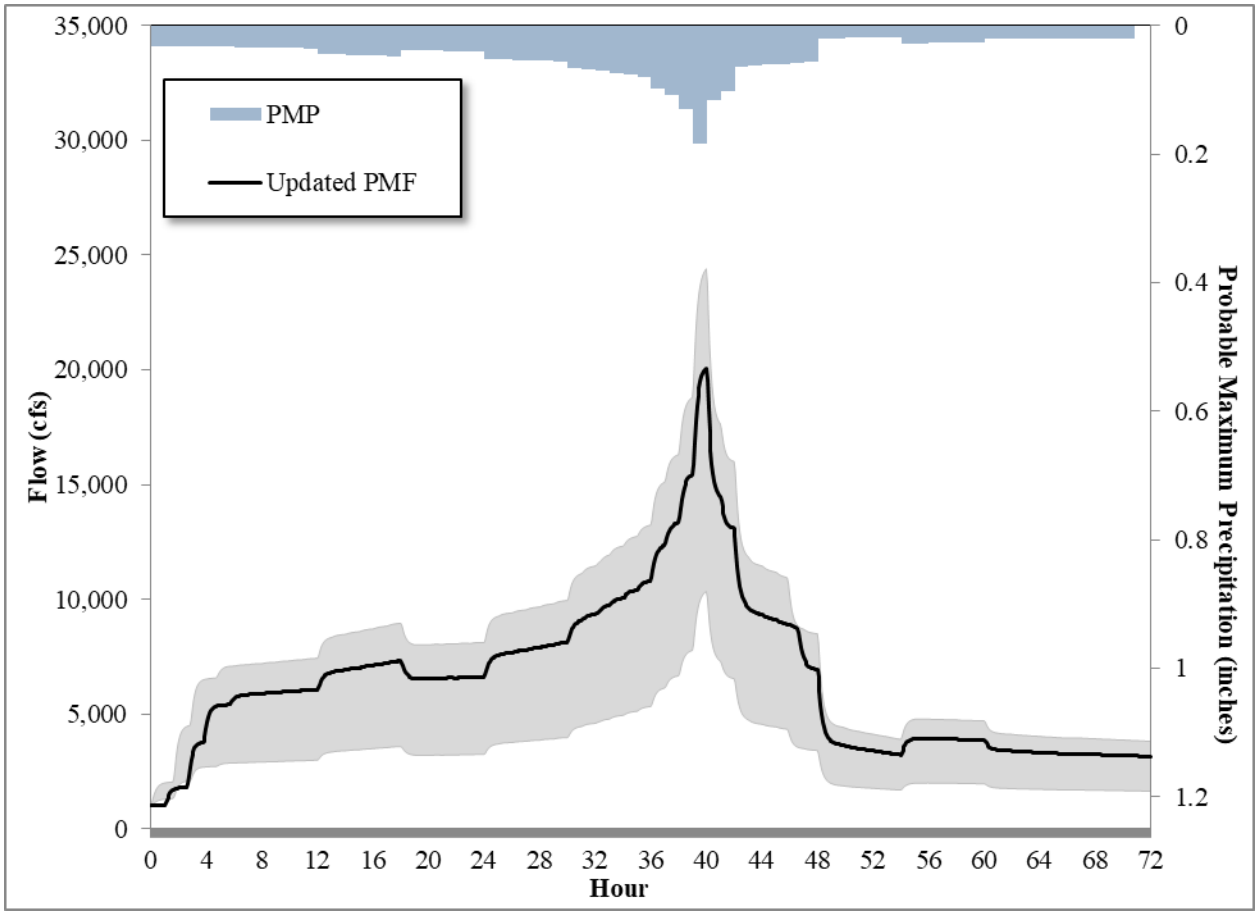

Figure 4 PMF Hydrograph with Semi-Quantitative Hydrologic Uncertainty

Conclusions

MCMC is a powerful tool for use in both hydrologic model calibration and characterizing hydrologic model uncertainty, which is consistent with the risk-based decision-making paradigm. Compared with single event MCMC simulation parameter posterior distributions, parameters from composite events (events run back-to-back) can converge to a posterior distribution that differs from the single-event posterior distribution. This suggests that allowing for the ability of the additional parameter space exploration, one can arrive at a potentially more informative parameter posterior distribution.

References

Baggett, J., and B. E. Skahill. 2010a. *Hybrid Optimization using Evolutionary and Approximate Gradient Search for Expensive Functions*. (Submitted to Engineering Optimization).

Baggett, J., and B. E. Skahill, 2010b. *Hybrid Optimization using Evolutionary and Approximate Gradient Search for Expensive Functions*. In: Proc. 2nd Int. Conf. Eng. Opt.

Box, G. E. P., and G. C. Tiao. 1973. *Bayesian Inference in Statistical Analysis*. Reading, AM: Addison-Wesley.

Campbell, E. P., D. R. Fox, and B. C. Bates. 1999. A Bayesian approach to parameter estimation and pooling in nonlinear flood event models. *Water Resource. Res*. 35 (1) 211-220.

Campbell, E. P., and B. C. Bates. 2001. Regionalization of rainfall-runoff model parameters using Markov Chain Monte Carlo samples. *Water Resource. Res*. 37 (3), 731-739.

Doherty, J., and B. E. Skahill. 2006. An Advanced Regularization Methodology for Use in Watershed Model Calibration. *Journal of Hydrology*, (327), 564– 577.

Duan, Q. S., S. Sorooshian, and V. K. Gupta. 1992. Effective and efficient global optimization for conceptual rainfall runoff models. *Water Resource. Res*. 28 (4), 1015–1031.

Duan, Q., V. K. Gupta, and S. Sorooshian. 1993. A shuffled complex evolution approach for effective and efficient global minimization. *J. Optim. Theory Appl*. 76 (3), 501–521.

Gallagher, M., and J. Doherty. 2007. Parameter estimation and uncertainty analysis for a watershed model. *Environmental Modelling and Software* (22), 1000-1020.

Gelman, A., and D. B. Rubin. 1992. Inference from iterative simulation using multiple sequences. *Stat. Sci.*, 7, 457-472.

Gupta, H. V., S. Sorooshian, T. S. Hogue, and D. P. Boyle. 2003. Advances in automatic calibration of watershed models. In: Duan, Q., Gupta, H., Sorooshian, S.,

Rousseau, A., Turcotte, R. (Eds.), Water Science and Application Series 6, 197–211.

Hansen, N. 2006. The CMA Evolution Strategy: A Comparing Review. In J.A. Lozano, P.

Larrañga, I. Inza and E. Bengoetxea (Eds.). Towards a new evolutionary computation. Advances in estimation of distribution algorithms. pp. 75-102,
Springer

Harmon, R., and P. Challenor. 1997. A Markov chain Monte Carlo method for estimation and assimilation into models. *Ecological Modelling*, 101, 41-59.

Hastings, W. K. 1970. Monte Carlo sampling methods using Markov chains and their applications. *Biometrika*, 57, 97-109.

Kanso, A., M. C. Gromaire, E. Gaume, B. Tassin, and G. Ghebbo. 2003. Bayesian approach for the calibration of models: application to an urban stormwater pollution model. *Water Science and Technology* 47 (4) 77-84.

Kuczera, G., and E. Parent. 1998. Monte Carlo assessment of parameter uncertainty in conceptual catchment models: The Metropolis algorithm. *J. Hydrol.*, 211, 69-85.

Makowski, D., D. Wallach, and M. Tremblay. 2002. Using a Bayesian approach to parameter estimation; comparison of the GLUE and MCMC methods. *Agronomie* 22, 191-203.

Matott, L. S., J. E. Babendreier, and S. T. Purucker. 2009. Evaluating Integrated Environmental Models: A Survey of Concepts and Tools. *Water Resources Research*, vol. 45, W06421, doi: 10.1029/2008WR007301

Metropolis, N., A. W. Rosenbluth, M. N. Rosenbluth, A. H. Teller, and E. Teller. 1953. Equations of state calculations by fast computing machines. *J. Chem. Phys.*, 21, 1087-1091.

Powell, M. J. D. 1992. The theory of radial basis function approximation in 1990, Advances in Numerical Analysis, Volume 2: Wavelets, Subdivision Algorithms and Radial Basis Functions, W. Light Ed., London, U.K., Oxford Univ. Press, 105-210.

Qian, S. S., C. A. Stow, and M. E. Borsuk. 2003. On Monte Carlo methods for Bayesian inference. *Ecological Modelling* 159, 269-277.

Schoups, G., and J. A. Vrugt. 2010. A formal likelihood function for parameter and predictive inference of hydrologic models with correlated, heteroscedastic and non-Gaussian errors. *Water Resources Research*, doi:10.1029/2009WR008933, In Press.

Schoups, G., J. A. Vrugt, F. Fenicia, and N. C. van de Giesen. 2010. Inaccurate numerical implementation of conceptual hydrologic models corrupts accuracy and efficiency of MCMC simulation. *Water Resources Research*, doi:10.1029/2009WR008648, In Press.

Skahill, B. E., and J. Baggett. 2010. More efficient Bayesian-based optimization and uncertainty assessment of hydrologic model parameters. (in preparation – 75% complete – to submit to the Journal of Hydrology, Environmental Modelling & Software, or Water Resources Research).

Skahill, B. E., J. Baggett, S. Frankenstein, and C. W. Downer. 2009. Efficient Levenberg-Marquardt Method Based Model Independent Calibration. *Environmental Modelling & Software* (24): 517–529.

Skahill, B. E., and J. Doherty. 2006. Efficient accommodation of local minima in watershed model calibration. *Journal of Hydrology*, (329): 122-139.

Vijayakumar, S., A. D'Souza, and S. Schaal. 2005. Incremental Online Learning in High Dimensions. *Neural Computation*. 17(12): 2602-2634.

Vrugt, J. A., H. V. Gupta, W. Bouten, and S. Soorooshian. 2003a. A shuffled complex evolution metrolopolis algorithm for optimization and uncertainty assessment of hydrologic model parameters. *Water Resourc. Res.* 39(8): 1201-1215.

Vrught, J. A., H. V. Gupta, L. A. Bastidas, W. Bouten, and S. Sorooshian. 2003b. Effective and efficient algorithm for multiobjective optimization of hydrologic models. *Water Resourc. Res.* 38(8): 1214-1233.

Vrugt, J. A., C. J. F. ter Braak, M. P. Clark, J. M. Hyman, and B. A. Robinson. 2008. Treatment of input uncertainty in hydrologic modeling: Doing hydrology backward with Markov chain Monte Carlo simulation. *Water Resources Research*, 44, W00B09, doi:10.1029/2007WR006720.

Evaluation of Flood Mitigation Strategies in an Agricultural Watershed in Iowa using Physically-Based Modeling

Antonio Arenas Amado, Assistant Research Engineer, IIHR - Hydroscience & Engineering, The University of Iowa, Iowa City, Iowa, antonio-arenasamado@uiowa.edu

Marcela Politano, Research Engineer, IIHR - Hydroscience & Engineering, The University of Iowa, Iowa City, Iowa, marcela-politano@uiowa.edu

Maral Razmand, Graduate Research Assistant, IIHR - Hydroscience & Engineering, The University of Iowa, Iowa City, Iowa, maral-razmand@uiowa.edu

Larry Weber, Professor, IIHR - Hydroscience & Engineering, The University of Iowa, Iowa City, Iowa, larry-weber@uiowa.edu

Abstract

Each one of Iowa's 99 counties has been impacted by flooding events that exceeded the state's capacity to respond and that ultimately led to flood-related presidential disaster declarations (FRDD). In the last three decades, the total number of FRDD in Iowa counties has exceeded 900 making flooding one of the most prominent environmental challenges that Iowa faces. Physically-based watershed modeling was used to evaluate the flood reduction benefits expected from both nature-based and structural mitigation strategies. Model baseline conditions were determined using a 15-year continuous simulation. The model was forced with hourly climatological data and simulated streamflow hydrographs were compared against measurements taken at USGS stations. The model was able to reproduce satisfactorily the measured hydrographs as well as seasonal and annual trends. Model baseline parameters were modified to simulate implementation of cover crops and native vegetation (e.g. tall-grass prairie) in the study area. In addition, the watershed model was used to evaluate the flood reduction benefits associated to a system of distributed storage built with ponds located in the watershed's headwater catchments. This work presents quantifications of changes in watershed's hydrology as well annual peak flow reductions.

Introduction

Each one of Iowa's 99 counties has been impacted by flooding events that exceeded the state's capacity to respond and that ultimately led to flood-related presidential disaster declarations (FRDD). In the last three decades, the total number of FRDD in Iowa counties has exceeded 900, making flooding one of the most prominent environmental challenges that Iowa faces. (Figure 1). In January 2016, the state of Iowa received a $97 million award for the Iowa Watershed Approach project (IWA, https://www.iowawatershedapproach.org/). The grant was part of the U.S. Department of Housing and Urban Development's (HUD) National Disaster Resilience Competition, which funds cutting-edge projects to address unmet needs from past natural disasters and reduce Americans' vulnerability to future disasters. The IWA project will accomplish six specific goals: reduce flood risk; improve water quality; increase community flood resilience; engage stakeholders through collaboration, outreach, and education; improve quality of life and health for Iowans, especially for vulnerable populations; and develop a program that is scalable and replicable throughout the Midwest and United States. This project will end in September 2021. The eight watersheds selected to participate in the IWA project are presented in Figure 1.

Within the work of the IWA project, physically-based hydrologic modeling was used to evaluate the flood reduction potential of different land use changes and structural Best Management Practices (BMPs). Model results were used to quantify the potential effects of three different flood mitigation strategies: 1) conversion of 100% of the rowcrop acres to native vegetation, 2) adoption of both no-till and cover crops in 100% of the rowcrop acres, and 3) a distributed storage system built with ponds located in the headwater catchments. This paper presents results of the hydrologic analyses performed in the Upper Iowa River watershed (see watershed in red in Figure 1).

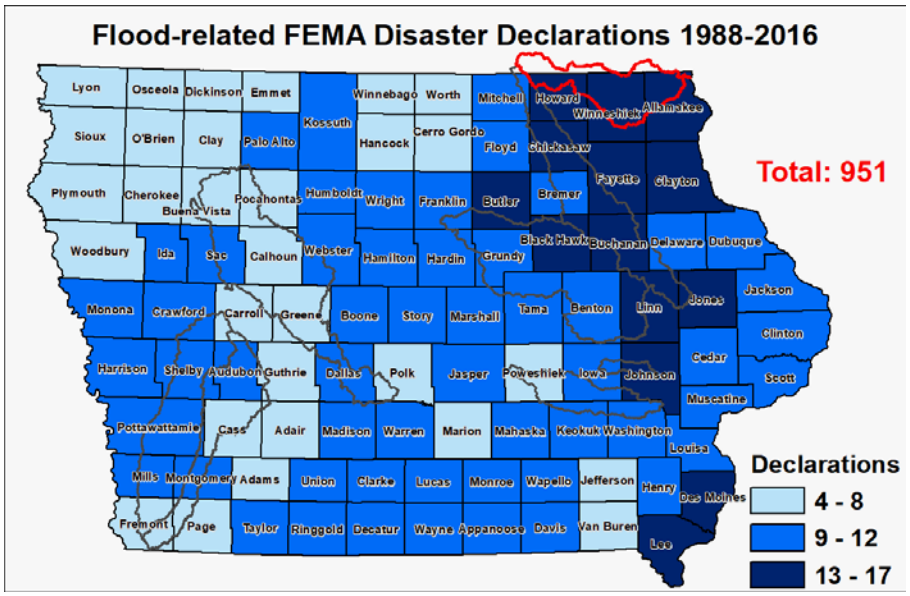

Figure 1. Number of flood-related federally declared disasters in Iowa counties (1988–2016). Data source: https://www.fema.gov/.

Study Area

The Upper Iowa River Watershed (UIRW) is located in North-East Iowa and South-East Minnesota. UIRW encompasses approximately 1,000 square miles and it drains into the Mississippi River at the Iowa and Wisconsin border. The watershed boundary falls within seven counties; however, most of the watershed area lies within Allamakee, Winneshiek, Howard Counties. Elevations range from approximately 1,500 feet above sea level to 600 feet above sea level in the downstream portion of the watershed. Land use in the UIRW is mainly agricultural, dominated by cultivated crops (corn/soybeans) at approximately 44.3% of the acreage, followed by grass/pasture at approximately 25.7%. The remaining acreage in the watershed is about 20.5% forest, 5% developed land, 3.7% crops other than corn/soy and 0.4% open water and/or wetlands, per the 2017 USDA/NASS Cropland Data Layer (Figure 2).

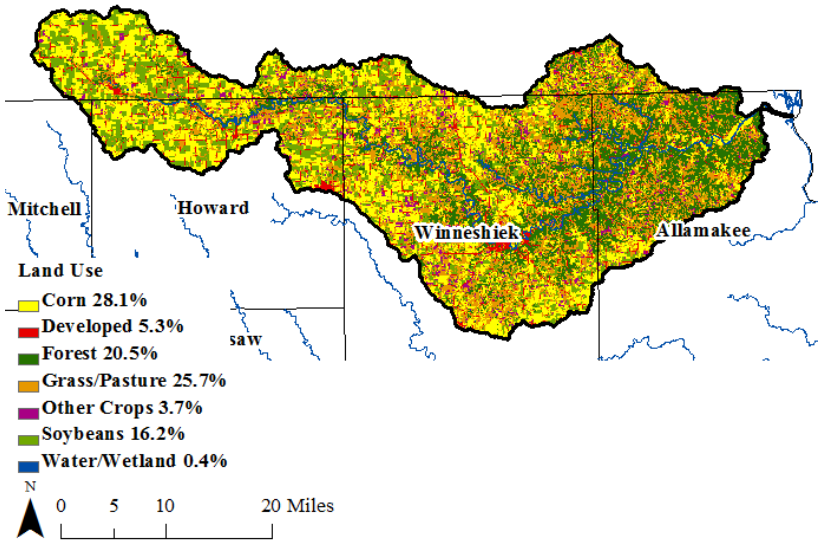

Figure 2. Land use composition in the Upper Iowa River Watershed. 2017 USDA Cropland Data Layer.

Hydrologic Model Description

The modeling activities described in this paper were performed using Generic Hydrologic Overland-Subsurface Toolkit (GHOST) which is a physically-based integrated model recently developed by IIHR-Hydroscience & Engineering. This model considers Iowa's varied topography, soils, and land use and simulates the hydrologic responses at watersheds over time periods in the order of decades. GHOST is based on the open source hydrologic code MM-pihm (Qu and Duffy 2007, Yu et al. 2013), which fully couples surface and subsurface water systems to predict streamflow and groundwater movement for normal and extreme rainfall and snowmelt events. Figure 3 presents the major hydrologic processes modeled in GHOST. Specific modules were developed at IIHR and incorporated into the code to properly predict water budgets for the long-term simulations required for the large-scale IWA watersheds. Publicly available data on land use, soil type, and surface elevations were used to spatially describe surface and subsurface domains. Stage IV radar rainfall estimates (NCEP/EMC 4KM Gridded Data (GRIB) Stage IV Data) were used as the precipitation input for simulation. Other meteorological data such as air temperature, relative humidity, wind speed, shortwave/longwave radiation and surface pressure were obtained from North American Land Data Assimilation System Phase 2(NLDAS-2) products. The temporal resolution of all the used forcing data was hourly. The ground surface was discretized using 8,185 triangular elements and the river network captured by the model is made of 1,653 linear segments. A view of the mesh is presented in Figure 4. The same figure shows the approximately 180 points (see red points) at which hourly climate data were available.

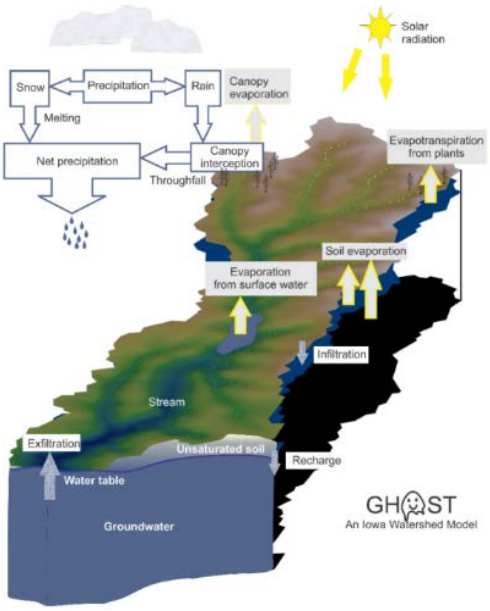

Figure 3. Hydrologic processes modeled in GHOST.

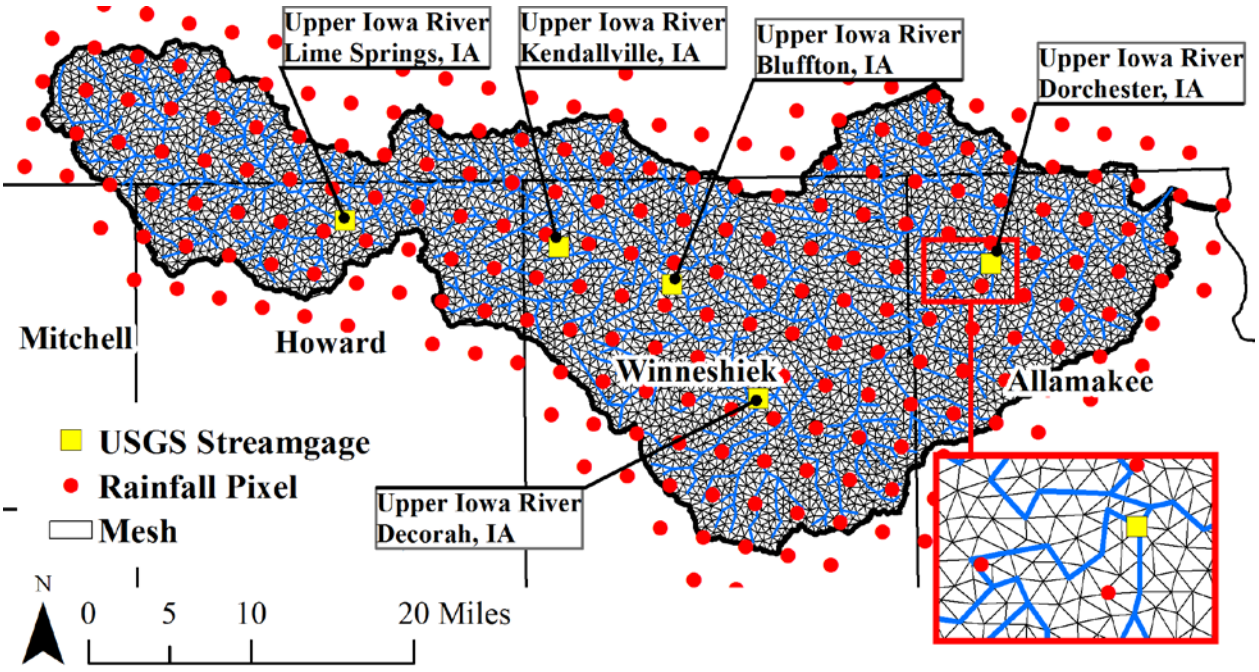

Figure 4. Computational mesh and rainfall/climate pixels.

Hydrologic Model Calibration and Validation

Model calibration was carried out for a nine-year period (2002-2010) and during the validation process the model performance was evaluated using measurements taken between 2011 and 2016. Simulated flows were compared against observed flows at two USGS stream-gage stations: Upper Iowa River at Decorah: USGS 05387500 and Upper Iowa River near Dorchester: USGS 05388250 (see Figure 5). For 2002, measured data at Decorah have significant gaps therefore those data were omitted from the analysis presented below.

Figure 5 shows observed and simulated time series for both the calibration and validation periods at Dorchester. Overall, model predictions match the measurements adequately. This figure displays both periods where the simulated values follow measured data closely, and others when they do not. Given that a hydrologic model is a simplified representation of the actual watershed, some level of mismatch between the simulation results and measured data is to be expected. Based on Moriasi et al., (2007) model simulations can be judged as satisfactory if Nash-Sutcliffe efficiency (NSE) > 0.50, Percent bias (PBIAS) ± 25% for streamflow, and the coefficient of determination (R^2) values are close to 1. Table 1 presents common metrics used in hydrologic model performance evaluation. The UIRW model results for both the calibration and validation periods display metrics that meet those criteria.

In the UIRW monthly runoff depths display a marked seasonal cycle with the window between April and August showing the highest runoff depths (Figure 6). Model results show a slight tendency to underestimate runoff at Decorah for the wettest months (May-July). This trend is less apparent when making comparison between simulated and observed flow near Dorchester. Figure 6 shows that simulated runoff during the winter and fall is also slightly underestimated by the model. Overall, simulated monthly runoff values match observations closely with values of $R^2>0.95$.

To assess the model ability to predict flood characteristics in the Upper Iowa River simulated and observed annual peak flows were compared at Decorah and near Dorchester (see Figure 7). Model results show no bias and annual peaks are both slightly under-predicted and over-predicted (data on both sides of the one-to-one line).

Table 1. Hydrologic model evaluation metrics for both the calibration and validation periods. Nash-Sutcliffe efficiency (NSE), Percent bias (PBIAS), and coefficient of determination (R^2).

	NSE		PBIAS		R^2	
	Cal	Val	Cal	Val	Cal	Val
Decorah	0.82	0.81	4.89	8.81	0.90	0.91
Dorchester	0.77	0.82	-0.40	2.25	0.89	0.91

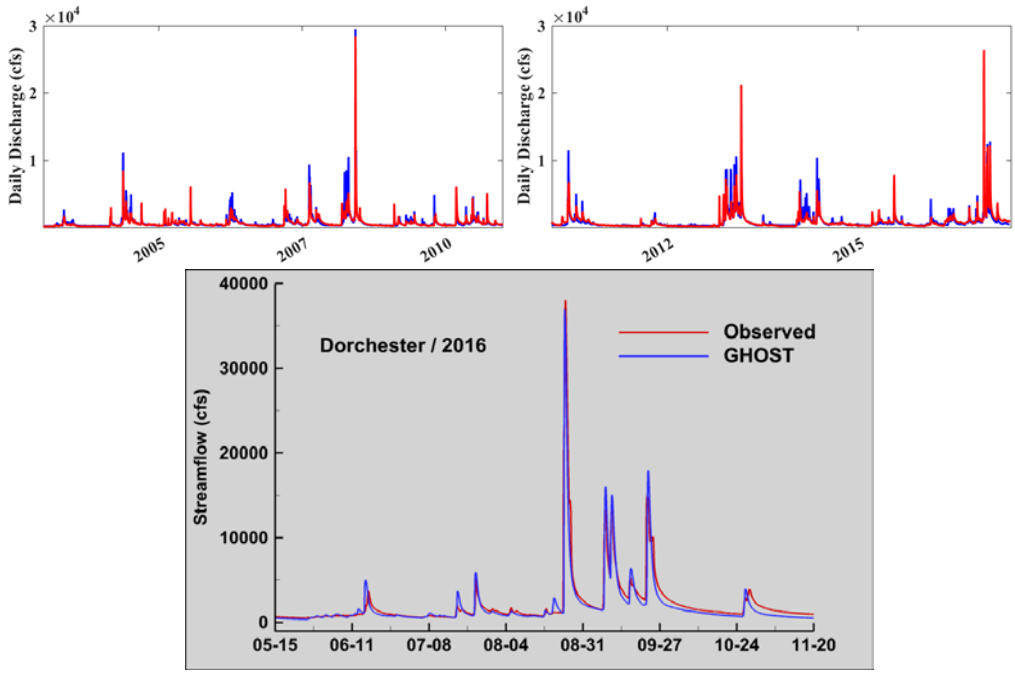

Figure 5. Observed and simulated time series at Dorchester (see Figure 4).

Scenarios

The GHOST model of the UIRW was used to investigate the potential impacts of alternative flood mitigation strategies in the watershed as well as the consequences of projected increases in heavy downpours in Iowa and the Midwest for the mid and late 21st century described in the latest Climate Science Special report (see Figure 8). The main focus of these scenarios was placed on understanding the impacts of (1) increasing infiltration/transpiration in the watershed and (2) implementing a system of distributed storage projects (ponds) across the landscape. In this section, we examine two different alternatives to reduce runoff through land use changes and soil quality improvements. One hypothetical land use change would be the conversion of row crop agriculture back to native tall-grass prairie. Another possible land use change would be improvements to agricultural conditions that would result from planting cover crops during the dormant season as well as adoption of no-till in 100% of the rowcrop acres. These are hypothetical examples and are only meant to illustrate the potential effects on flood reduction. The examples are also not project proposals; they are either economically undesirable or not practically feasible. Still, these hypothetical examples provide valuable benchmarks on the limits of flood reduction benefits that are physically possible with broad-scale land cover changes. Modifications to baseline model parameters to represent land use changes (e.g. native vegetation and cover crops/no-till) were based on information reported by several studies: Baschle, (2017); Mohamoud, (1991); VanLoocke et al., (2012); Kang et al. (2003); Baron et al. (1993), Bharati et al. (2002); Yimam et al. (2015), and Cronshey, (1986).

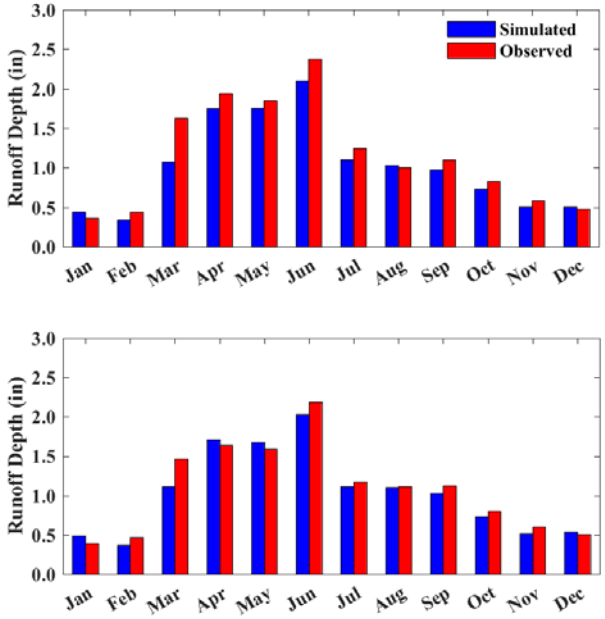

Figure 6. Observed and simulated average monthly runoff depth (in inches) for the Upper Iowa River Watershed. Results are shown for both the calibration and validation periods. Top: Decorah (USGS 05387500) and bottom: Dorchester (USGS 05388250).

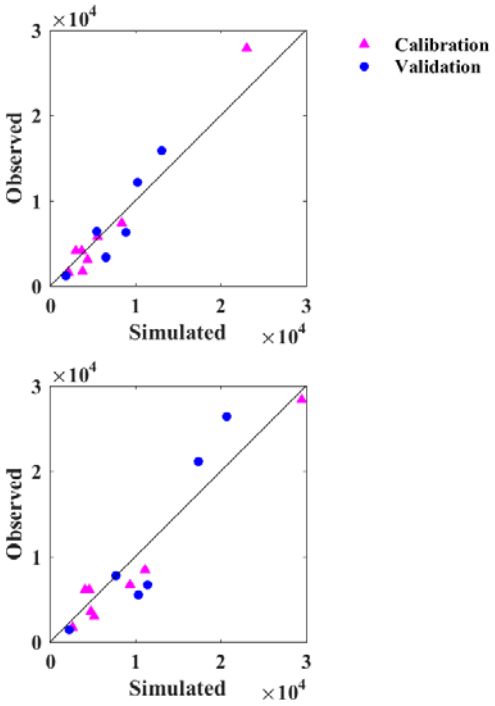

Figure 7. Simulated versus observed annual maximum peak daily discharges (cfs). Top: Decorah (USGS 05387500) and bottom: Dorchester (USGS 05388250).

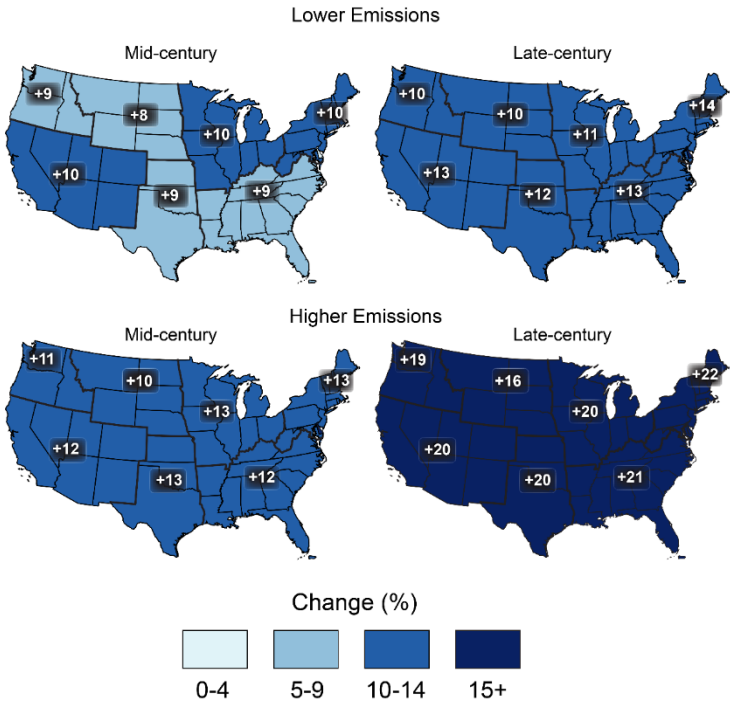

Figure 8. Projected change in heavy precipitation. Twenty-year return period amount for daily precipitation for mid- (left maps) and late-21st century (right maps). Results are shown for a lower emissions scenario (top maps; RCP4.5) and for a higher emissions scenario (bottom maps, RCP8.5). Figure taken from The Climate Science Special Report (Easterling et al. 2017) (https://science2017.globalchange.gov/).

Increased Precipitation and Index Points

A simple approach was followed to generate forcing data for simulations with increased precipitation (IP). Daily rainfall accumulations for each one of the rainfall pixels (see Figure 4) were calculated using observed hourly data from 2002 to 2016 . The days were ranked and hourly precipitation values for the wettest 5% of the non-zero-rain days were increased by 10%. No other meteorological data were modified for the IP simulations. For the 15 years of available data, precipitation for approximately 95 days was altered.

The hydrologic model made predictions at approximately 1,600 locations along the stream network. Six index points were selected to present the results of different watershed scenarios (Table 2). These points were chosen based on several criteria including the location of the existing USGS gauging stations, areas with high risk potential and/or proximity to a community, and to demonstrate the model results at different spatial scales.

Table 2. Index points (see Figure 9).

Index Point	Represents
1	Upper Iowa River at Lime Springs
2	Upper Iowa River at Kendallville
3	Upper Iowa River into Decorah
4	Near outlet of Trout Creek (HUC 12 near Decorah/Freeport)
5	Canoe Creek (HUC10)
6	Upper Iowa River at Dorchester

Mitigating the Effects of High Runoff with Native Vegetation

One of the proposed scenarios was to replace all current rowcrop acres with native tall-grass prairie. The simulation results from this scenario are not intended to be a recommend flood mitigation strategy; rather these results are meant to provide the theoretical maximum of the flood reduction benefits that can be expected from land use changes.

A flood frequency analysis was conducted at the index points for three different simulations: baseline, native vegetation, and native vegetation plus increased precipitation. Figure 10 shows the 15 annual maximum peak discharges and a sample estimate of the exceedance probability. Results show that for all the 15 years and under both historic and increased precipitation conditions, the adoption of native vegetation significantly reduces peak discharges at all six locations. We mapped average peak reductions at the chosen index points in Figure 9.

In each one of the panels in Figure 10, the average peak flow reduction is reported for both Baseline vs. Native Vegetation and Baseline vs. Native Vegetation + IP. Peak flow reduction along the Upper Iowa River mainstem (points 1, 2, 3, and 6) decreases as one moves downstream. The highest average peak flow reductions were found at the index point 1 and the lowest at point 6. Under historic precipitation conditions, the average peak flow reduction in the Upper Iowa River at Decorah (index point 3) is 46% whereas in the IP simulations is 33%.

The transformation of rainfall into runoff is known to be a highly non-linear process and therefore increases in precipitation volumes by a given percentage are not expected to result in similar increases in peak flow magnitudes. In other words, a 10% increase in heavy precipitation does not necessarily create floods with 10% larger peaks. Model predictions show that for the most severe floods (see Figure 10, exceedance probabilities < 20%, scenario vs. scenario + IP), increases in peak discharges due to increases in heavy precipitation are up to approximately 40%.

Mitigating the Effects of High Runoff with Cover Crops/Soil Health/No-Till

The purpose of this hypothetical scenario is to investigate the impact of improved agricultural management practices could have on reducing flood peak discharges throughout the watershed. Planting cover crops across all agricultural areas in the watershed during the dormant (winter) season is hypothesized to lower the runoff potential of these same areas during the growing season (spring and summer) due to increased soil health and fertility. This scenario does not represent the conversion of the existing agricultural landscape to cover crops. Rather, the existing agricultural landscape is kept intact, but its runoff potential during the growing season has been reduced by planting cover crops in all rowcrop acres.

Based on the model results, cover crops/no-till practices reduce peak discharges for all the years at all index points when using measured precipitation data (Figure 11, green circles below the blue squares). This is largely true for the model results of the simulations with cover crops/no-till plus increased precipitation. However, at all index points the maximum annual peak discharge values for the simulations with increased precipitation is larger than those of the baseline condition (black circles above the blue squares). The largest and the smallest average peak flow reductions were found at points 1 and 6, respectively.

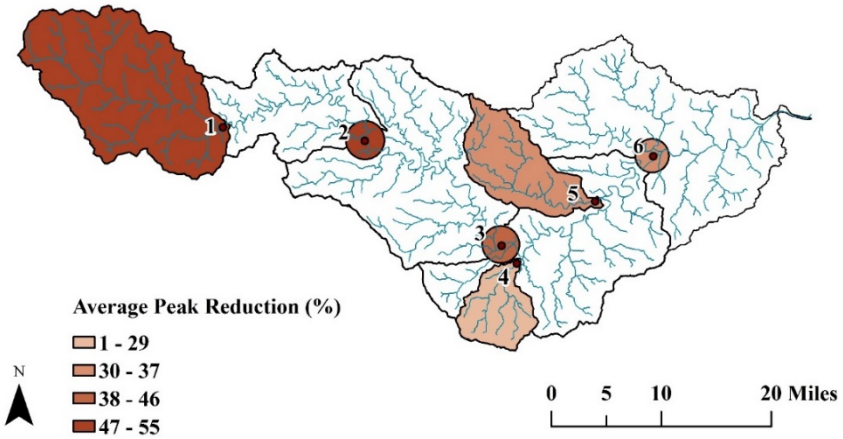

Figure 9. Average peak discharge reduction (%) for index points in the Upper Iowa River Watershed. Baseline vs. Native Vegetation (historic precipitation).

Mitigating the Effects of High Runoff with Distributed Storage

For this analysis, 735 ponds were simulated in the UIRW (Figure 12). A "typical" pond was developed for use for the Upper Iowa River Watershed using the existing data on farm ponds in Iowa and NRCS Technical References as guidance. The geometry of this typical pond consists of a 6-inch pipe outlet as the principal spillway with a 10-foot wide emergency spillway set at an elevation above the pipe inlet to provide a flood storage of 20 acres-feet. Site topography will actually dictate the placement of the emergency spillway and the potential dam height. The stage-storage relationship of a pond also depends on local topography and is highly variable from site to site. There certainly are opportunities to design and construct ponds at locations in subbasins that have not been used in this analysis. Furthermore, some of the locations selected for ponds may be far from ideal. Therefore flood reductions presented below do not represent the theoretical maximum of the flood reduction benefits that can be expected from construction of ponds throughout the watershed.

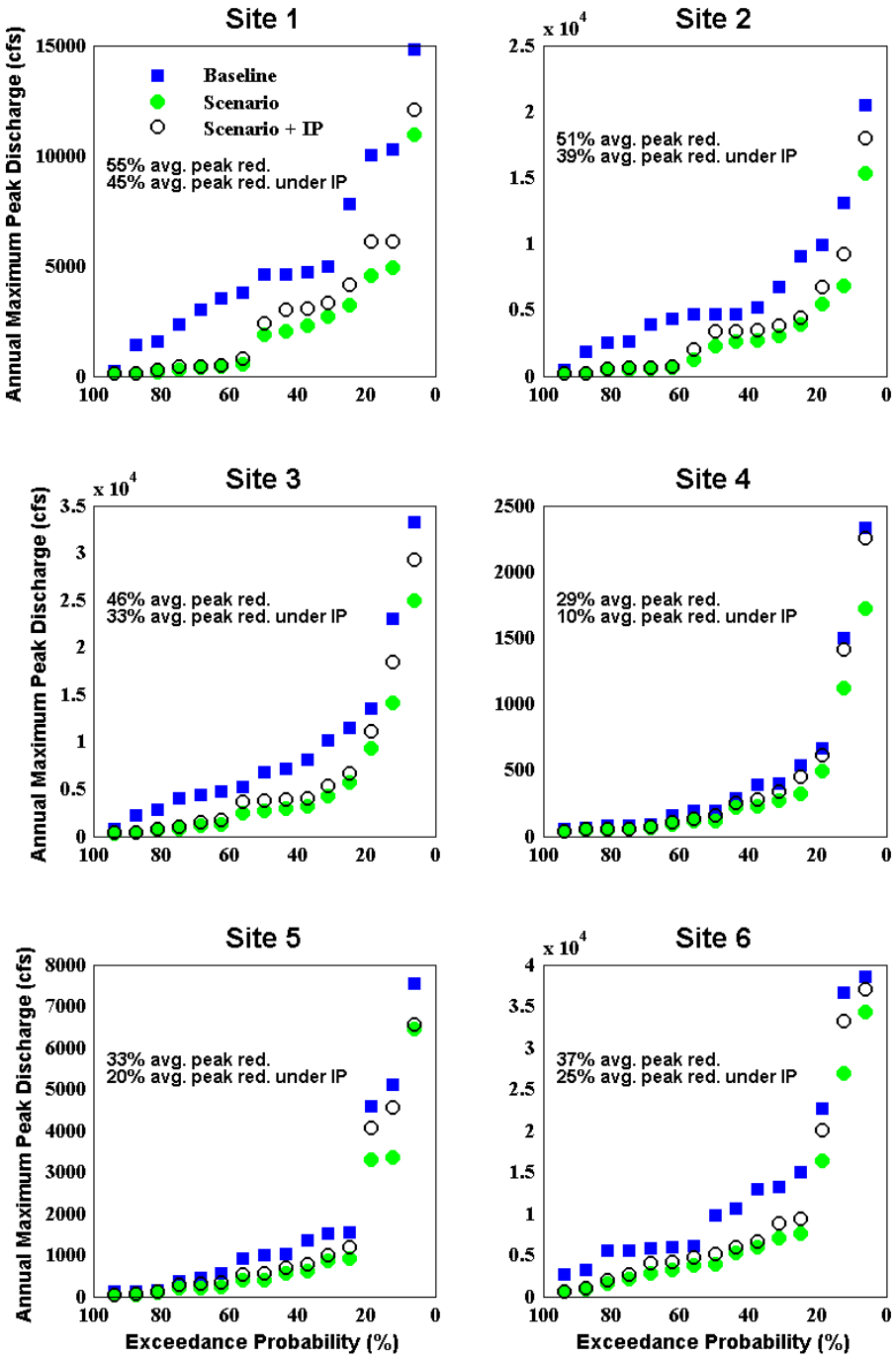

Figure 10. Sample probability distribution of annual maximum peak discharges for the baseline, native vegetation, and native vegetation plus increased precipitation simulations. Results are shown at the six index points displayed in Figure 9. Baseline corresponds with the calibrated model.

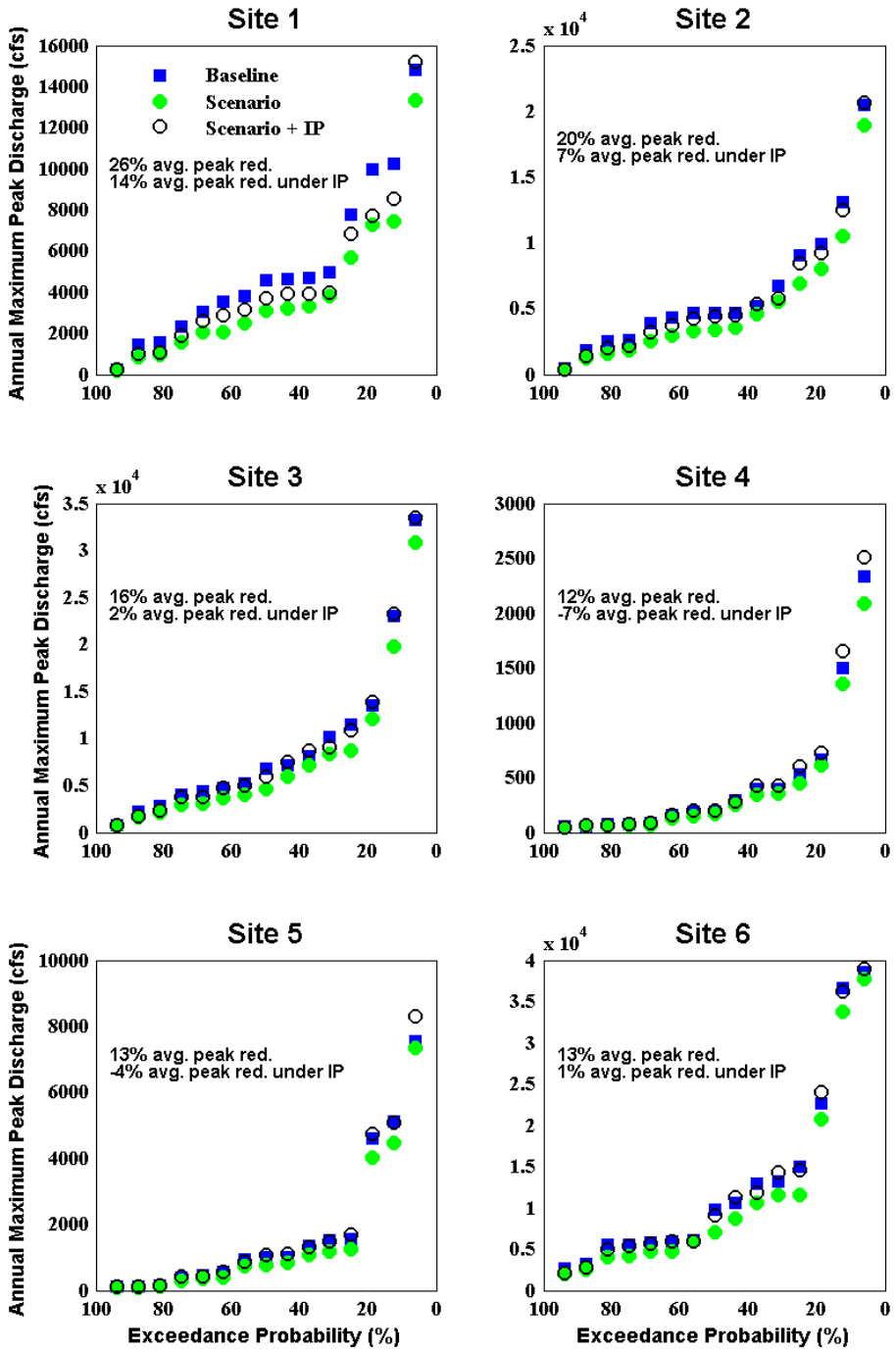

Figure 11. Sample probability distribution of annual maximum peak discharges for the baseline, cover crops/no-till, and cover crops/no-till plus increased precipitation simulations. Results are shown at the six index points displayed in Figure 9. Baseline corresponds with the calibrated model.

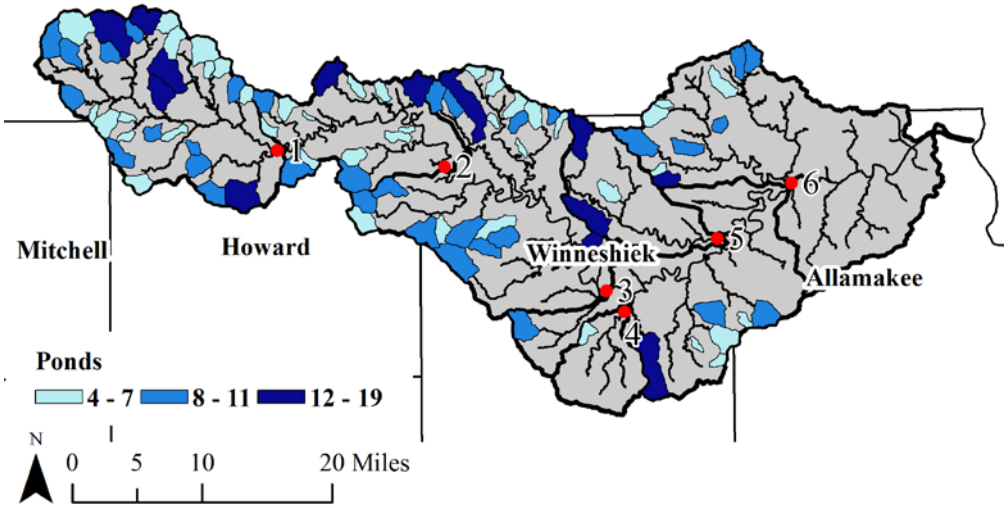

Figure 12. Ponds (735) placement in the Upper Iowa River Watershed.

Information on annual peak discharge reduction is presented in Table 3 and Figures 13. The 735 ponds result in average peak flow reductions at all index points, under historic precipitation conditions, that range between 5% and 11%. However, these reductions are smaller than those of the cover crops/no-till and native vegetation scenarios. As expected, reductions for the index points along the Upper Iowa River mainstem decrease in the downstream direction (Index Points 1, 2, 3, and 6).

Simulation results with increased precipitation conditions show no positive average peak flow reductions at any of the index points (Table 3). In other words, on average the ponds are insufficient to keep the peak flows below the baseline conditions (under IP conditions). However, for the highest annual streamflow peaks the model predicts a lower peak flow value (under increased precipitation conditions with the ponds) at all points except at index point 4 (Figure 13). It is worth mentioning that for index point 4 the ratio between the total drainage area and the area regulated by the ponds (Table 3, DAR/DA) is just 0.04 and a higher level of protection can be expected by increasing the number of ponds upstream from this point.

Table 3. Average peak flow reduction at the index points.

Index Point	Drainage Area (DA) (mi^2)	Number of Ponds	Drainage Area Regulated (DAR) (mi^2)	DAR/DA	Avg. Peak Reduction (%)	Avg. Peak Reduction under IP (%)
1	182	249	74	0.41	10	-1
2	281	353	102	0.36	9	-3
3	490	549	157	0.32	7	-6
4	38	6	1	0.04	5	-21
5	66	32	11	0.17	11	-3
6	767	651	193	0.25	5	-7

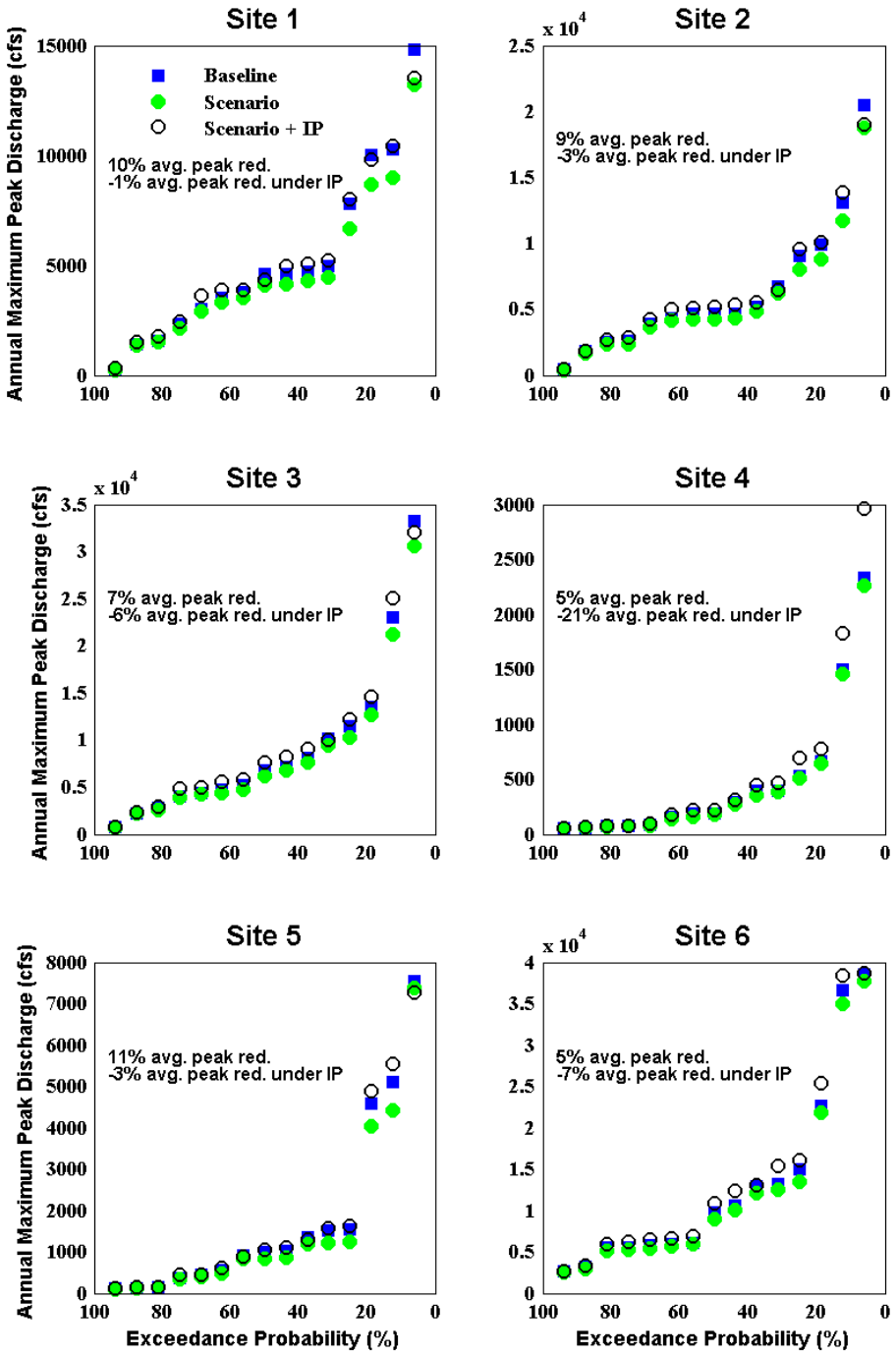

Figure 13. Sample probability distribution of annual maximum peak discharges for the baseline, distributed storage, and distributed storage plus increased precipitation simulations. Results are shown at the six index points displayed in Figure 9 Baseline corresponds with the calibrated model.

Summary and Conclusions

We used physically-based hydrologic modeling to evaluate the flood reduction benefits of three different flood mitigation strategies in an agricultural watershed. Hydrologic modeling results presented in this paper can be used to perform loss-avoidance and cost-benefit analyses to assist watershed stakeholders and policy makers in making decisions to reduce flood damages. Furthermore, our modeling results highlight the flood reduction benefits of maintaining a vegetation cover all year round and more generally the potential of implementing nature-based flood protection systems.

References

Baron, V.S., Dick, A.C., Najda, H.G. and Salmon, D.F., 1993. Cropping systems for spring and winter cereals under simulated pasture: yield and yield distribution. Canadian Journal of Plant Science, 73(3), pp.703-712.

Basche Andrea, Turning Soils into Sponges: How Farmers Can Fight Floods and Droughts, Union of Concerned Scientists, 2017, http://www.ucsusa.org/foodagriculture/advance-sustainable-agriculture/turning-soils-sponges#.WZyYRyiGOUk

Bharati, L., Lee, K.H., Isenhart, T.M., Schultz, R.C., (2002). "Soil-water infiltration under crops, pasture, and established riparian buffer in Midwestern USA," Agroforest. Syst. 56 (3), 249–257.

Cronshey, R., 1986. Urban hydrology for small watersheds. US Dept. of Agriculture, Soil Conservation Service, Engineering Division.

Kang, S., Gu, B., Du, T. and Zhang, J., 2003. Crop coefficient and ratio of transpiration to evapotranspiration of winter wheat and maize in a semi-humid region. Agricultural water management, 59(3), pp.239-254.

Mohamoud, Y.M., 1992. Evaluating Manning's roughness coefficients for tilled soils. Journal of hydrology, 135(1-4), pp.143-156.

Moriasi, D.N., Arnold, J.G., Van Liew, M.W., Bingner, R.L., Harmel, R.D. and Veith, T.L., 2007. Model evaluation guidelines for systematic quantification of accuracy in watershed simulations. Transactions of the ASABE, 50(3), pp.885-900.

Qu, Y. and Duffy C.J. 2007. A closed-form equation for predicting the hydraulic conductivity of unsaturated soils. *Soil science society of America journal* 44.

VanLoocke, A., Twine, T.E., Zeri, M. and Bernacchi, C.J., 2012. A regional comparison of water use efficiency for miscanthus, switchgrass and maize. Agricultural and Forest Meteorology, 164, pp.82-95.

Yimam, Y.T., Ochsner, T.E. and Kakani, V.G., 2015. Evapotranspiration partitioning and water use efficiency of switchgrass and biomass sorghum managed for biofuel. Agricultural Water Management, 155, pp.40-47.

Yu, X., Bhatt, G., Duffy C. and Shi Y. 2013. Parametrization for distributed watershed modeling using national data and evolutionary algorithm. *Computer and Geosciences* 58.

Extreme Weather in Iowa and the Midwest June 2018 – May2019

Antonio Arenas Amado, Assistant Research Engineer, IIHR - Hydroscience & Engineering, The University of Iowa, Iowa City, Iowa, antonio-arenasamado@uiowa.edu

Chad Drake, Postdoctoral Research Scholar, IIHR - Hydroscience & Engineering, The University of Iowa, Iowa City, Iowa, chad-drake@uiowa.edu

Daniel Gilles, Water Resources Engineer, IIHR - Hydroscience & Engineering, The University of Iowa, Iowa City, Iowa, daniel-gilles@uiowa.edu

Nathan Young, Research Engineer, IIHR - Hydroscience & Engineering, The University of Iowa, Iowa City, Iowa, nathan-young@uiowa.edu

Iris Brenner, Graduate Research Assistant, IIHR - Hydroscience & Engineering, The University of Iowa, Iowa City, Iowa, iris-brenner@uiowa.edu

Abstract

Between June 2018 and May 2019, extreme weather has taken a heavy toll on Iowa and the Midwest. We have seen: significantly above normal rainfall, reservoirs close to uncontrolled releases, flash flooding and tornados, an extremely cold (e.g., the Polar Vortex) and snowy winter, powerful and rare events known as bomb cyclones, rivers spilling out of their banks and flooding communities due to "ice dams", levees crumbling or being overtopped reminding us of our limited ability to control mother nature, massive flooding along the Missouri River and its tributaries, and extended periods of major flood conditions as well as flood stage records along the Mississippi River among others. Each of these extreme weather events is noteworthy, and some of them are even record-setting. However, in our opinion, it is equally (and perhaps more) remarkable that all these events happened within a 12-month window. For at least three decades, scientists have been predicting increasingly frequent extreme weather. The last year provides a frightening glimpse of the devastating, and in some cases deadly, consequences that extreme weather can have for Iowa and its residents.

Introduction

In this article, we present information on recent (June 2018-May 2019) extreme weather events. Most of the information presented focuses on Iowa, but data on other midwestern states and other parts of the country are also documented. We included information, in chronological order, on extreme precipitation, reservoirs and flooded rivers, shallow groundwater, snowfall accumulations, snow water equivalent, air and soil temperature, presidential disaster declarations, and financial losses from flooding. Most of the text and figures were taken from www.hydroiowa.org/timeline, which is an online timeline the authors created.

June and July 2018

For significant portions of Iowa, June 2018 was a month with above-average precipitation. The place with the highest departure from normal was found in Osceola County near Shelby in northwest Iowa. In June 2018, this area received more than 3.5 times the normal precipitation

(June normal: 4.5", June 2018: 16.5"). Counties with widespread above-normal precipitation (in June 2018) include Osceola, Lyon, Sioux, Dickinson, Obrien, Winnebago, and Madison. On June 29, engineers tested the inflatable crest gates of Saylorville reservoir (upstream from Des Moines, IA), which give the dam six additional feet of protection. On July 9, 2018, the Saylorville Lake reservoir recorded its sixth highest crest — approximately 6 feet below the highest level reported in 1993 (Figure 1). Precipitation data for July 2018 do not show above-normal precipitation statewide. However, some areas in central Iowa were affected by heavy rain. Between June 30 and July 1, the Des Moines metro area received 5–9 inches of rainfall, with a National Weather Service station in Ankeny reporting 8.7 inches. On July 1, major flooding was reported around the Des Moines metro area, and some of the creeks draining to the Des Moines River experienced record flooding (Figure 2). On July 20, multiple tornados impacted Iowa. The most severe damages occurred in Pella, where the Vermeer Corporation took a direct hit, and in Marshalltown, where several buildings, including the historic courthouse, suffered damages.

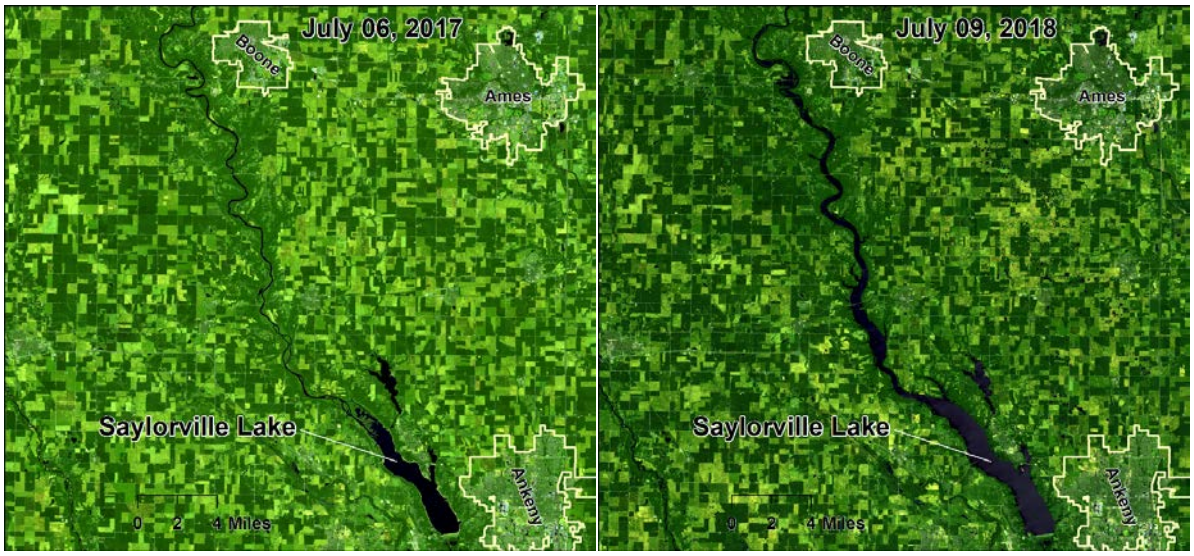

Figure 1. Saylorville Lake. Highest level in 2018 and at normal pool elevation in July 2017. Raw data: https://www.sentinel-hub.com/

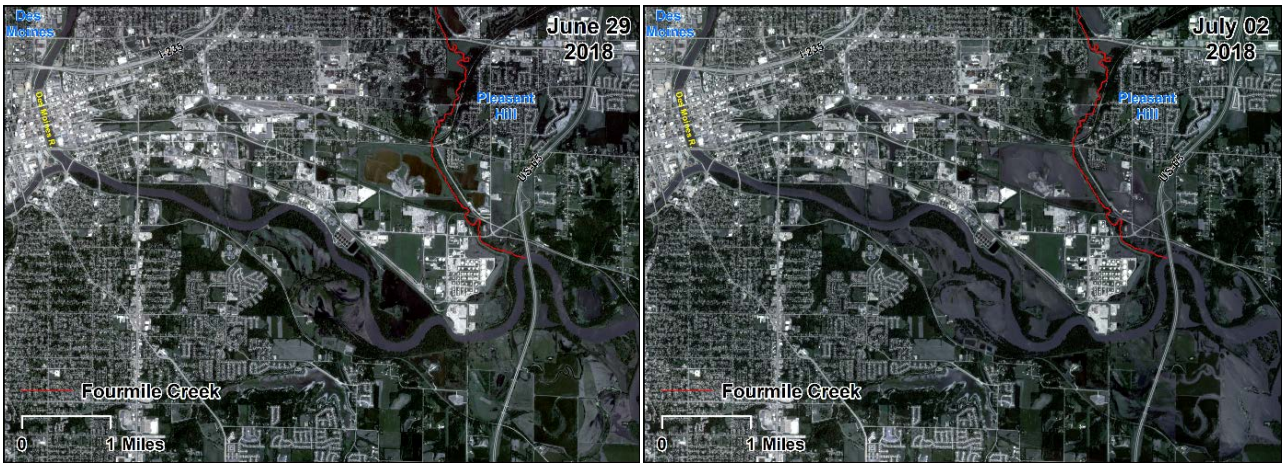

Figure 2. East Des Moines and Pleasant Hill. Raw data: https://www.planet.com/

A Soggy Fall for Iowa

Data for 2018 show statewide above-normal precipitation between August 1 and October 31. On average, Iowa received twice as much precipitation as normal (Aug–Oct), with less than 5% of the state recording only slightly above-normal precipitation. Northeast and north central Iowa received significantly above-normal precipitation. Some areas in Butler, Bremer, and Clayton counties received more than three times the normal amount of precipitation. Remarkably, some of those areas received close to a year's worth of normal precipitation in the window between August and October

Coralville Reservoir came very close to allowing uncontrolled releases (e.g., activation of the emergency spillway). On October 19, 2018, the reservoir crested at 710.93 ft., just one foot below the emergency spillway elevation. Records show higher reservoir stages for just four years: 2008, 1993, 1969, and 1984. The two satellite images in Figure 3 show the reservoir two days after it crested in 2018 and one year before that in 2017 (under conservation pool conditions).

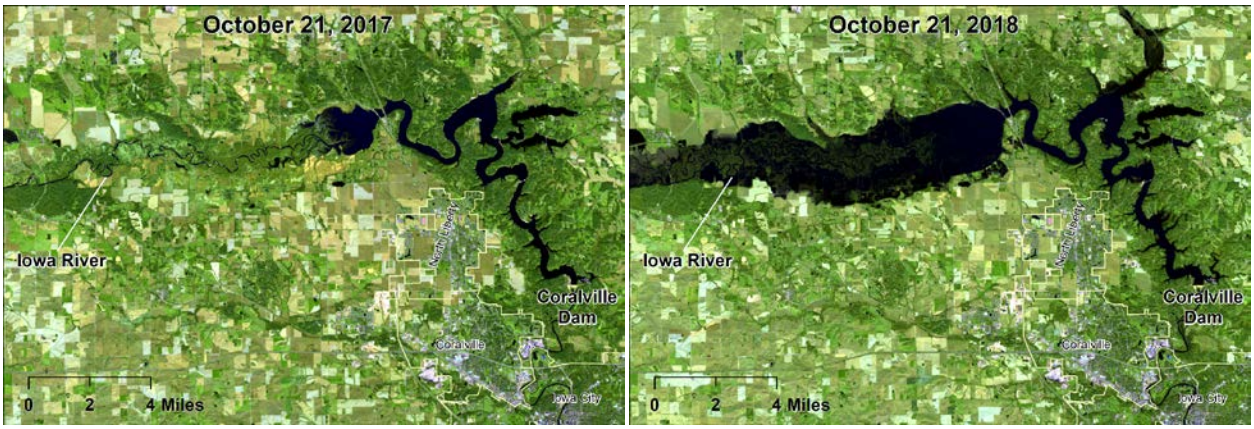

Figure 3. Coralville Reservoir. Raw data: https://www.sentinel-hub.com/

Precipitation Records Broken in 2018

According to NOAA (https://www.ncdc.noaa.gov/sotc/national/201813): "2018 was the third wettest year on record for the nation, and the sixth consecutive year with above-average precipitation." Several states experienced above-normal precipitation — notably, about three quarters of Iowa and Nebraska had a 25% or greater departure from normal precipitation (Figure 4). In Iowa, the highest departure (91.4%) was found in Sioux County near the town of Rock Valley. The continental United States comprises approximately 3,100 counties. Based on 2018 data, 13 Iowa counties appear in the top 100 counties nationwide with high departure from normal precipitation values: Osceola (16), Chickasaw (26), Dickinson (28), Bremer (39), Floyd (47), Lyon (56), Emmet (64), Hancock (65), Butler (70), Sioux (77), Wright (85), Webster (93), and Cerro Gordo (99).

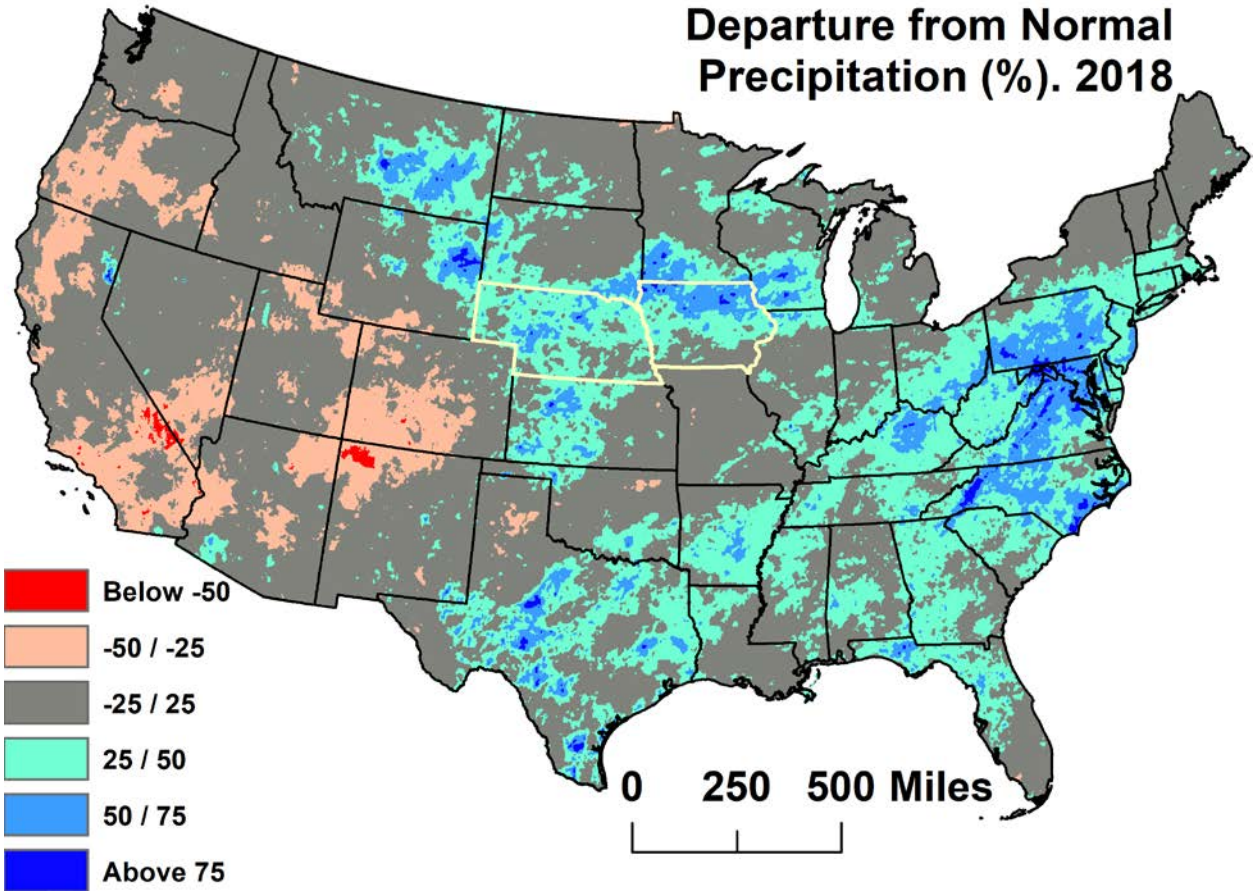

Figure 4. Departure from normal precipitation. 2018. Raw data: http://www.prism.oregonstate.edu/

Watersheds Have Long Memories

Because of above normal precipitation in 2018, eastern and midwestern U.S. states began 2019 with abundant shallow groundwater storages. The blue areas in Figure 5 have significantly more groundwater than expected for the month of December (in comparison to Decembers between 1948–2012). At the beginning of 2019, approximately 70% of Iowa and 60% of Nebraska had shallow groundwater conditions wetter than 95% of the historical record. Note that areas on both sides of the Missouri River along the Nebraska-South Dakota and Nebraska-Iowa borders had significantly wetter than average conditions. The same is true for the Mississippi River along the Wisconsin-Iowa border, as well as the upper part of the Illinois-Iowa border. Consistent with the very high precipitation values in the fall of 2018, the seven counties with the highest shallow groundwater wetness are in northeast Iowa (Winneshiek, Chickasaw, Floyd, Clayton, Bremer, Dubuque, and Black Hawk).

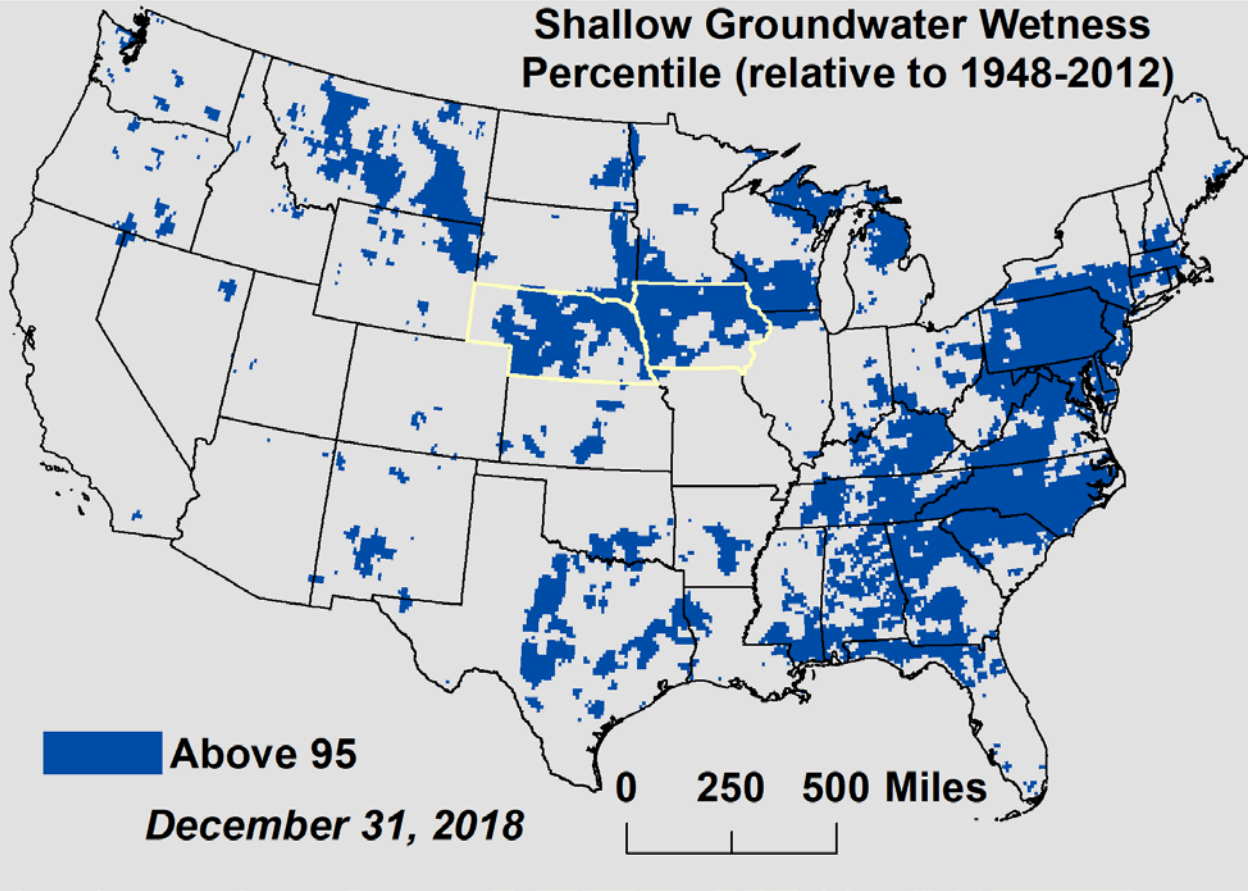

Figure 5. Shallow groundwater wetness percentile. Raw data: https://nasagrace.unl.edu/

Long, Cold, and Snowy Winter

During the winter months, it is not uncommon for Iowa to have days with maximum temperatures below 32 F. Data for the last four decades show that January and February are the months with the highest number of cold days (e.g., maximum T below 32 F). Depending on the location, January can have, on average, between 10 and 20 cold days.

Several atmospheric factors affect snowmelt, including air temperature, prevalence of sunshine, wind speed, and precipitation, among others. Melting can occur even on days with air temperature below freezing. However, melting on cold days is likely to be small in comparison to warmer days.

Some parts of Iowa and the Midwest recorded arctic temperatures on the last two days of January 2019. The so-called Polar Vortex triggered temperatures as low as -20 F in Des Moines and -24 F in Waterloo, with some areas of northeast Iowa reporting even colder temperatures. With the wind chill factored in, some numbers went as low as -50 F. For Iowa, February 2019 was colder than normal, especially in the western part of the state. Most of the days had maximum temperatures below 32 F — a pattern that extended into early March. Between February 5, 2019, and March 9, 2019, only six days had maximum temperatures above 32 F for limited areas located

mostly in southern Iowa. From March 12 on, maximum temperatures stayed above 32 F, and Iowans observed rapid snowmelt.

Heavy Snowfall

In Iowa, normal snowfall varies between approximately 2.0 and 3.5 ft. Early season snowfall was recorded in mid-October 2018. However, despite this early start, at the end of January 2019, about two-thirds of the state had snowfall accumulations below normal. Most of the places with above normal snowfall were in south-central Iowa. February 2019 was a very snowy month throughout the upper Midwest. For this month alone, these cities in Iowa received close to or more than an entire season's worth of snowfall: Ames, Carroll, Fort Dodge, Marshalltown, Shenandoah, and Waterloo, among others. In the same way that extreme fall precipitation pushed 2018 to its status as one of wettest in the weather books, snowfall in February 2019 broke records and labelled the 2018–19 winter as one of the snowiest in history.

Figure 6 shows snowfall accumulation values from September 30, 2018, for the states draining into the Missouri River Basin (see dashed line) at Brownville (just downstream of the Iowa-Missouri border). As of March 2019, some counties in northeast and north central Iowa had the highest (> 5 ft.) snowfall accumulation records: Allamakee, Mitchell, Howard, Kossuth, Worth, Winneshiek, and Winnebago. Out of the nine counties bordering the Missouri River, Fremont had the highest (55") snowfall accumulation. Remarkably, some places in northern Minnesota and Wisconsin, the Dakotas, Montana, Wyoming, and Colorado show areas with snowfall accumulation values in excess of 100 inches.

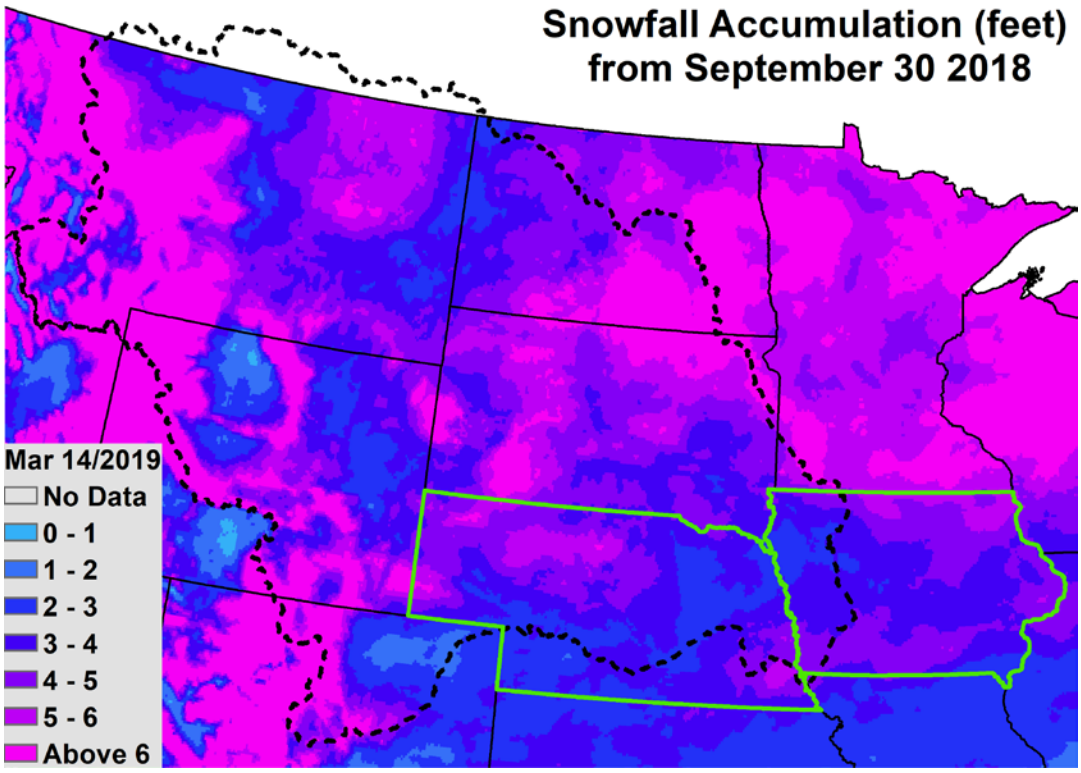

Figure 6. Snowfall accumulation. Sep 30, 2018 – Mar 14, 2019. Raw data: https://www.nohrsc.noaa.gov

Snow Water Equivalent (SWE)

SWE represents the amount of liquid water stored in the snowpack. It can also be defined as the surface runoff expected from instantaneous snow melt. At the beginning of January 2019, some small areas in northwest Iowa had up to 1.5 inches of SWE, but most of the state remained snow free. At the end of January after several cycles of relatively low snowfall and melting, Iowa had on average a little more than an inch of SWE, while some limited areas had up to 4 inches of SWE. Most of the melting happened in the first half of the month. SWE conditions in some of Iowa's neighboring states were as follows: Nebraska was virtually snow free, except for the southeast corner of the state (SWE below 2.0"); Minnesota had on average 2.5 inches of SWE, but some areas had up to 10 inches; and South Dakota SWE values were similar to Iowa's.

After some melting in the first weeks of February 2019, SWE values went up for Iowa and the other states with areas draining to the Missouri River Basin upstream from Brownville. On March 11, 2019, statewide averages were as follows: Minnesota, 5.5"; Montana, 4.4"; Wyoming, 4.2"; Colorado, 4.1"; North Dakota, 3.4"; South Dakota, 3.3"; Iowa 2.6"; and Nebraska, 1.2". Iowa counties with averages above 4" of SWE (on March 11, 2019) include: Winnebago, Worth, Mitchell, Dickinson, Hancock, Pocahontas, Osceola, Cerro Gordo, Chickasaw, Howard, Floyd, Palo Alto, Hamilton, Emmet, Greene, Kossuth, Franklin, and Calhoun.

Between March 11 and March 17, significant snow melt occurred in Iowa, Nebraska, and the southeastern corner of South Dakota. On March 17, more than two-thirds of Nebraska and Iowa were free of snow. In contrast, significant amounts of water were still stored in the snowpack in eastern North Dakota, Minnesota, and northern Wisconsin; snowmelt from these areas, along with spring rains, generated major flooding conditions along the Mississippi River in April and May 2019.

Figure 7 shows SWE (in inches) for the states draining into the Missouri River Basin (see dashed line) at Brownville (just downstream of the Iowa-Missouri border). Data are presented for 2 days March 11, 2019, and March 17, 2019.

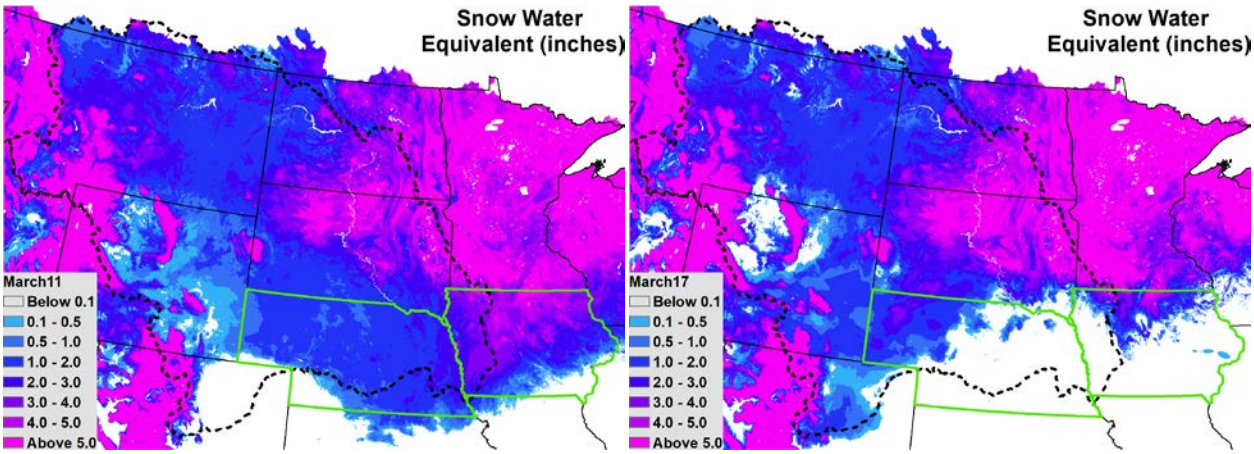

Figure 7. Snow Water Equivalent. March 11, 2019 and March 17, 2019. Raw data: https://nsidc.org/data/g02158

Bomb Cyclone and Ice Dams

Between March 13 and 14, heavy rains, strong winds, and blizzard conditions impacted the central United States, adding, in some areas, to the ongoing runoff produced by snow melt. Large areas of eastern Nebraska and portions of southeastern South Dakota received up to 3.5" of precipitation. Most of the precipitation in eastern Nebraska, Iowa, eastern South Dakota, and Minnesota came as rainfall.

In Iowa, most of the rain fell in the part of the state that drains to the Missouri River. The 10 counties with the highest average rainfall accumulations were as follows: Monona, Crawford, Ida, Woodbury, Lyon, Sioux, Obrien, Plymouth, Cherokee, and Dickinson. With the exception of some small areas of Monona County (with accumulations above 2.5"), Iowa received relatively small rainfall amounts from this extreme weather event. This underscores the important effect that frozen ground conditions, snow melt, and levee failures had on mid-March flooding in the areas of the state unaffected by high levels in the Missouri River. Figure 8 shows precipitation (03/13-03/14) for the states draining into the Missouri River Basin (see dashed line) at Brownville (just downstream of the Iowa-Missouri border).

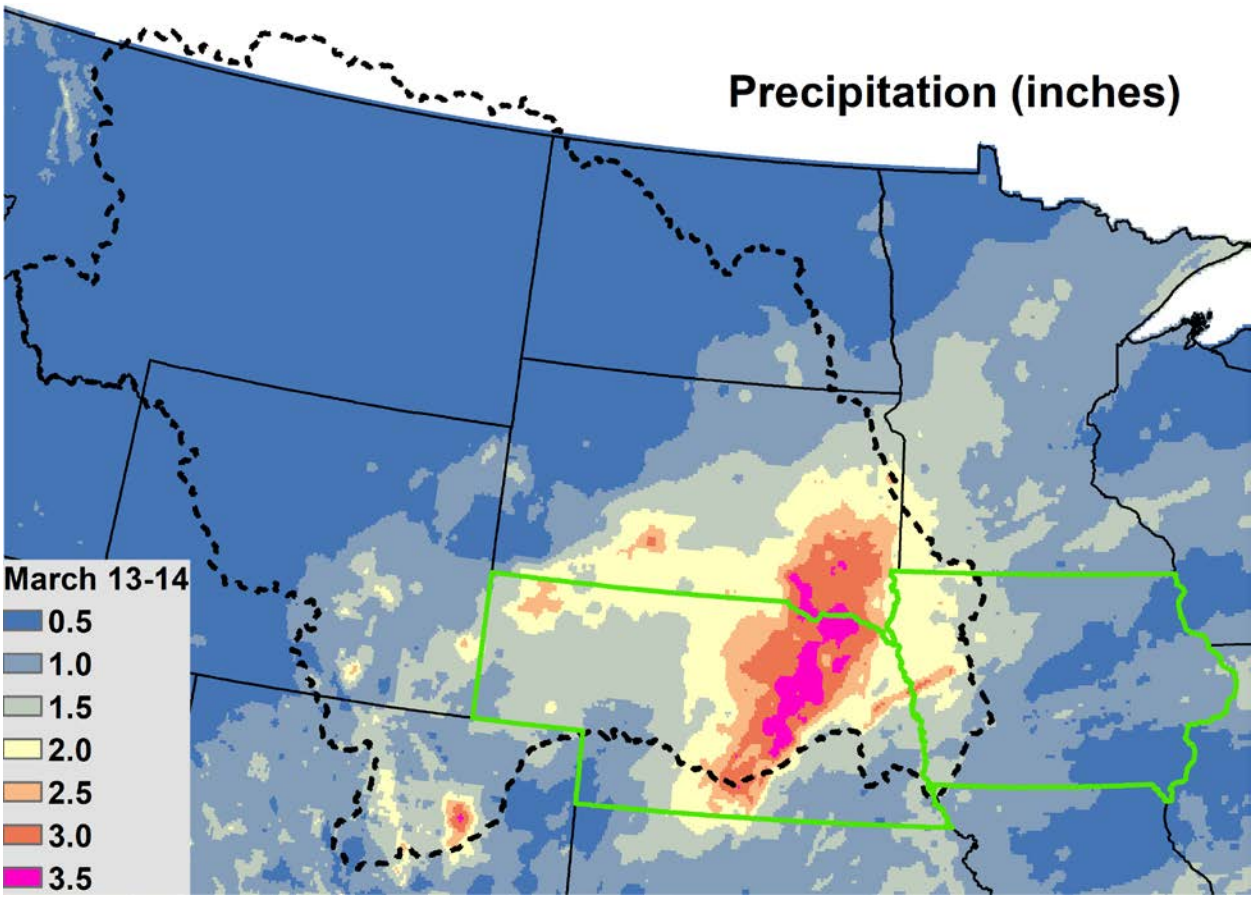

Figure 8. Precipitation. Missouri River Basin. March 13-14, 2019. Raw data: http://www.prism.oregonstate.edu/

During extended periods of below freezing temperatures, it is common to see ice formation on top of lakes and relatively slow moving and shallow creeks and streams. As temperatures gradually warm up, the ice layers slowly melt away and break up without significantly affecting river levels.

Iowa recorded below normal temperatures and above normal snowfall values in January, February, and early-March 2019. This period was followed by a rapid warm-up that started around March 12. Rapid snowmelt and the Bomb Cyclone storm generated runoff that elevated water levels, which in turn broke ice layers. Ice chunks flowed downstream, and some areas with river bends, bridges, confluences, narrow passages, and other flow constrictions saw the creation of ice dams. This further elevated river levels, producing major flooding.

Several communities across Iowa reported significant flooding because water levels in ice-choked rivers rose up. The two satellite images in Figure 9 show areas around Des Moines, IA for two days in March, one in 2018 and the other in 2019. The image taken on March 13, 2018, displays ice accumulations on Saylorville Lake, but Lake Red Rock appears ice-free. In contrast, the image captured on March 18, 2019, displays areas with significantly more ice accumulations. These include: North Raccoon River flowing into Des Moines; Des Moines River between Saylorville and Red Rock Lakes; both Saylorville and Red Rock lakes; and South Skunk River near Colfax. Remarkably, this image shows approximately 11 miles of accumulated ice upstream from the Red Rock Dam.

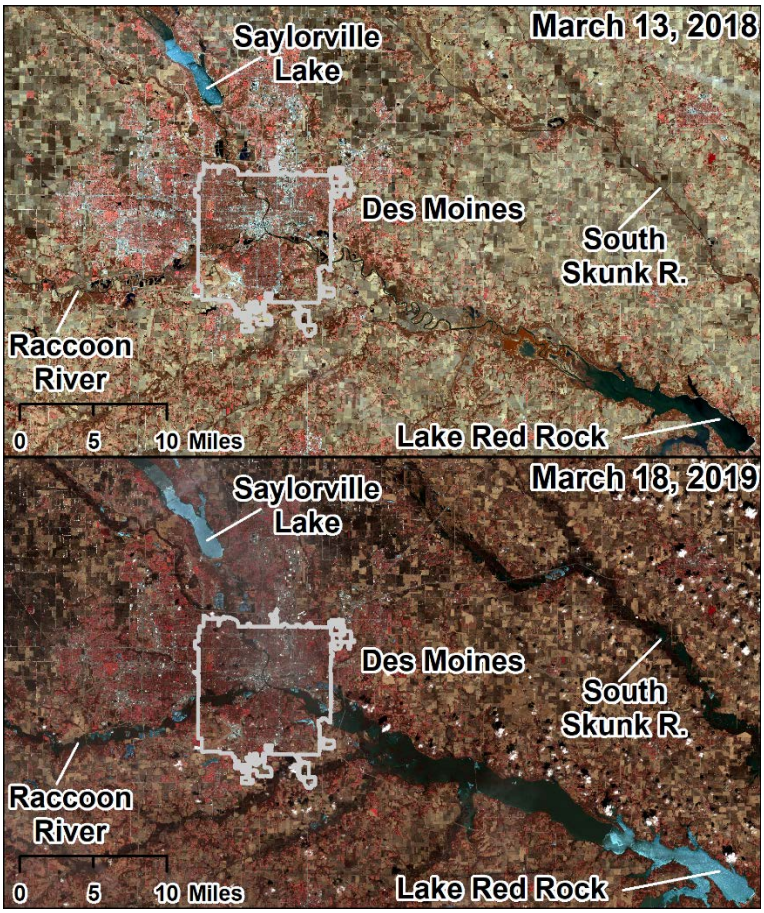

Figure 9. Ice accumulations around Des Moines, IA. Raw data: https://www.sentinel-hub.com/

Flood Extent

By March 2019, conditions in the Midwest were primed and set for a flooding disaster. The question wasn't if, but where and when the flood water would begin disrupting and displacing people. All that was required was a moderate spring storm to send events into motion. With the arrival of the March 13–14 Bomb Cyclone, those in the Missouri River Basin got much more than a moderate spring storm event.

The red lines in Figure 10 show U.S. Army Corps of Engineers (USACE) levees, and areas that flooded in March 2019 are presented in blue (flooded areas in Nebraska are shown in light blue). Purple areas represent the "man-made" floodplain or the areas to which levees are supposed to keep the Missouri River constrained.

Widespread riverine and flash flooding severely impacted southwest Iowa (Cass, Fremont, Mills, Montgomery, Page, and Pottawattamie counties). The March 2019 event flooded a total area of approximately 185,000 acres or 285 square miles in southwest Iowa (see blue areas in the image). Of this area, approximately 130,000 acres or 200 square miles of crops were inundated, based on the 2018 Cropland Data Layer. There were 29 zip codes and 15 communities directly impacted by riverine flooding, and likely additional areas affected by flash flooding.

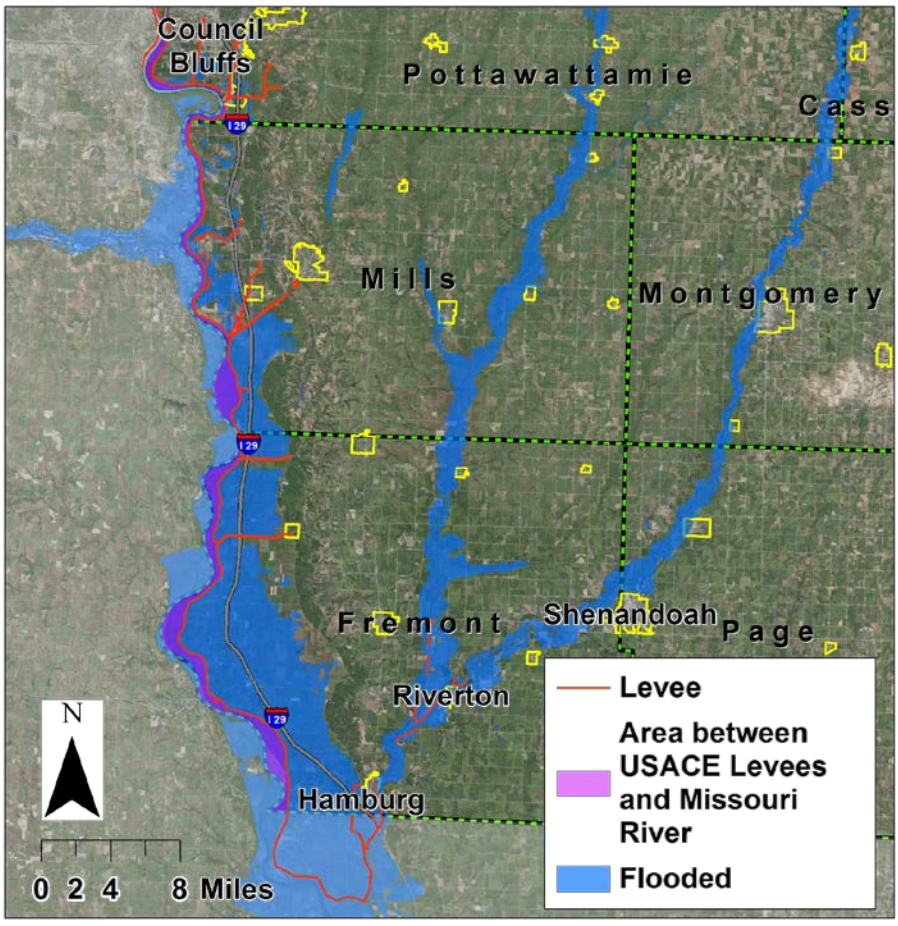

Figure 10. Flooding in southwest Iowa. March 2019. Raw data: https://www.sentinel-hub.com/

The Missouri River floodplain had the largest area of widespread flooding despite the existence of a USACE levee system along the river channel. Levee breaches inundated 135 square miles of Iowa land along the Missouri River from Council Bluffs to the southern Iowa border. This flooded area dwarfs the 25 square miles of Iowa land between the Missouri River and the levee system (see purple areas in the image). The flooded area between the Missouri River and I-29 was approximately 75 square miles.

The Mississippi River

In 2019, high levels in the Mississippi River have broken historic records for flood duration and flood stage. These high levels are caused by the combined effect of snow melt and spring rains. At Clinton, Iowa, the USGS has kept daily flow records of the Mississippi River for almost 150 years. 2019 already appears as the year with the highest number of days (29) with flows above 200,000 cfs (e.g., major flooding as of May 7, 2019). Other years with many days include: 2001 (28), 1888 (27), 1881 (22), and 1993 (19).

Figure 11 shows two images of approximately 40 miles of the Mississippi River upstream from Clinton, Iowa. The two satellite images were taken one year apart. On April 19, 2018, the flow was approximately 80,000 cfs. One year later, the flow was about 2.5 times higher.

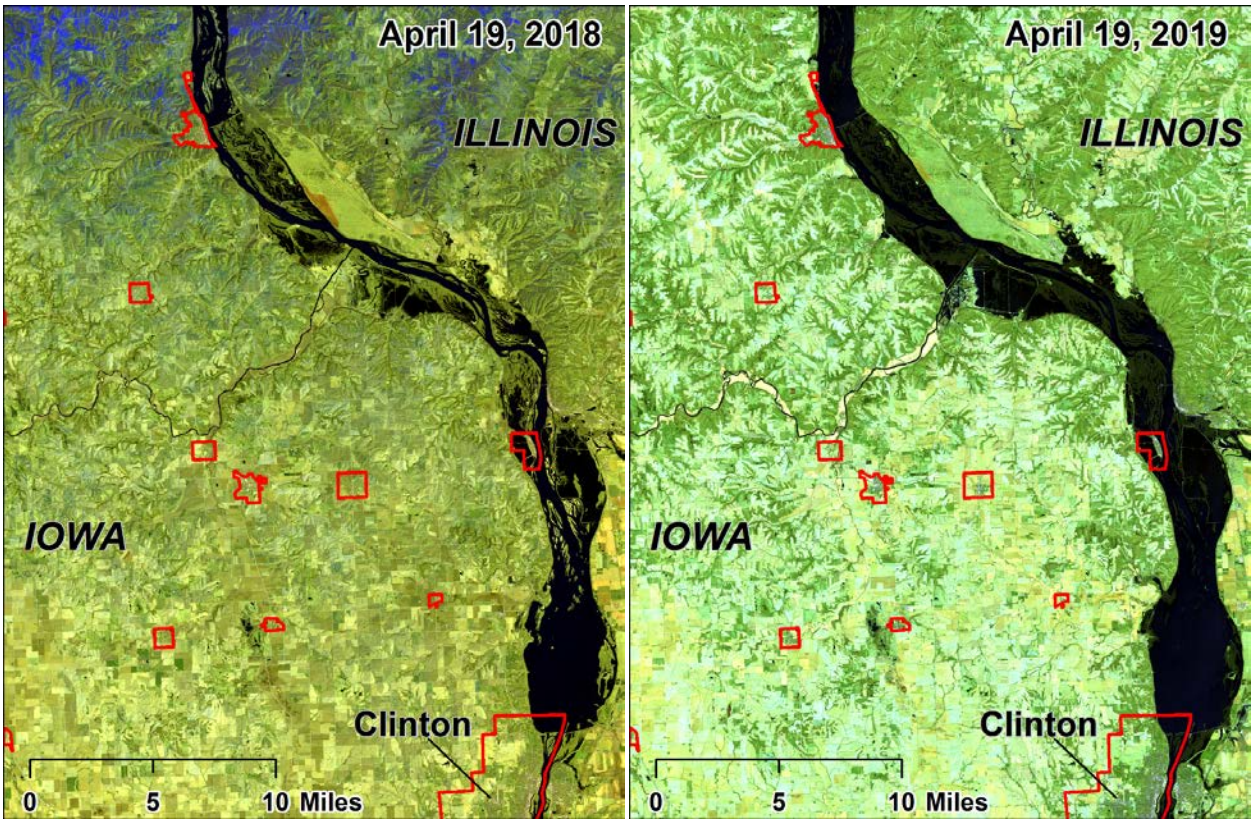

Figure 11. The Mississippi River upstream from Clinton, Iowa. Raw data: https://www.sentinel-hub.com/

Downtown Davenport Floods

On May 2, 2019, the Mississippi River at the Quad Cities (Davenport, Bettendorf, Moline, and East Moline) set an all-time record, cresting at 22.63 ft and surpassing the levels recorded in 1993. On April 30, 2019, high levels in the Mississippi River caused a temporary barrier breach that flooded several blocks of downtown Davenport. Figure 12 shows the Davenport-Rock Island area on two different days. In the image captured on May 4, 2019, the flooded areas can be seen.

Figure 12. Davenport-Rock Island area. Raw data: https://www.planet.com/

Final Remarks

Iowa is not a stranger to extreme weather–related disasters. Approximately five years after the territory of Iowa became the 29th state in the union, heavy rain led to widespread flooding in areas draining to the Des Moines, Cedar, Iowa, Skunk, and Maquoketa rivers. Flooding was not limited to Iowa; areas of Nebraska and the southern Mississippi region were also affected. The record-setting rainfall and subsequent flooding came to be known as The Great Flood of 1851.

Iowa's more recent history illustrates that flooding continues to be a major issue. FEMA records show that between 1988 and 2016, Iowa counties received more than 900 flood-related disaster declarations (Figure 13). Estimated losses accumulated between 1988 and 2015 are staggering. The SHELDUS database reports $13.5 billion in direct property losses and $4.1 billion in direct crop losses (Figure 14 and 15). These numbers continue to increase. Because of the March 2019 flood, 58 Iowa counties received presidential disaster declarations, and preliminary flood damage estimations show that at least $1.6 billion are needed for recovery efforts. https://www.thegazette.com/subject/news/government/iowa-16-billion-flood-damage-estimate-probably-low-governor-kim-reynolds-says-20190409

It is correct to say that flooding has always been a problem in Iowa. However, a dispassionate look at scientific data reveals an unmistakable trend toward more extreme weather that will only accelerate and exacerbate the cycle of "flood-rebuild-repeat" that the state is currently in.

In our opinion, Iowa will not break this cycle without making significant investments and tough decisions. We may need to acknowledge that, in some places, our dream of achieving a floodless floodplain is just that, a dream. Building ponds and wetlands, implementing cover crops, restoring native vegetation where possible, and more generally, restoring Iowa's landscape resilience, is going to be both difficult and expensive.

However, we need to keep in mind that inaction is a very costly proposition as well (that has cost us at least $20 billion in the last 30 years), and decision-makers considering investments in conservation must take into account the fact that the cost of doing nothing is not zero.

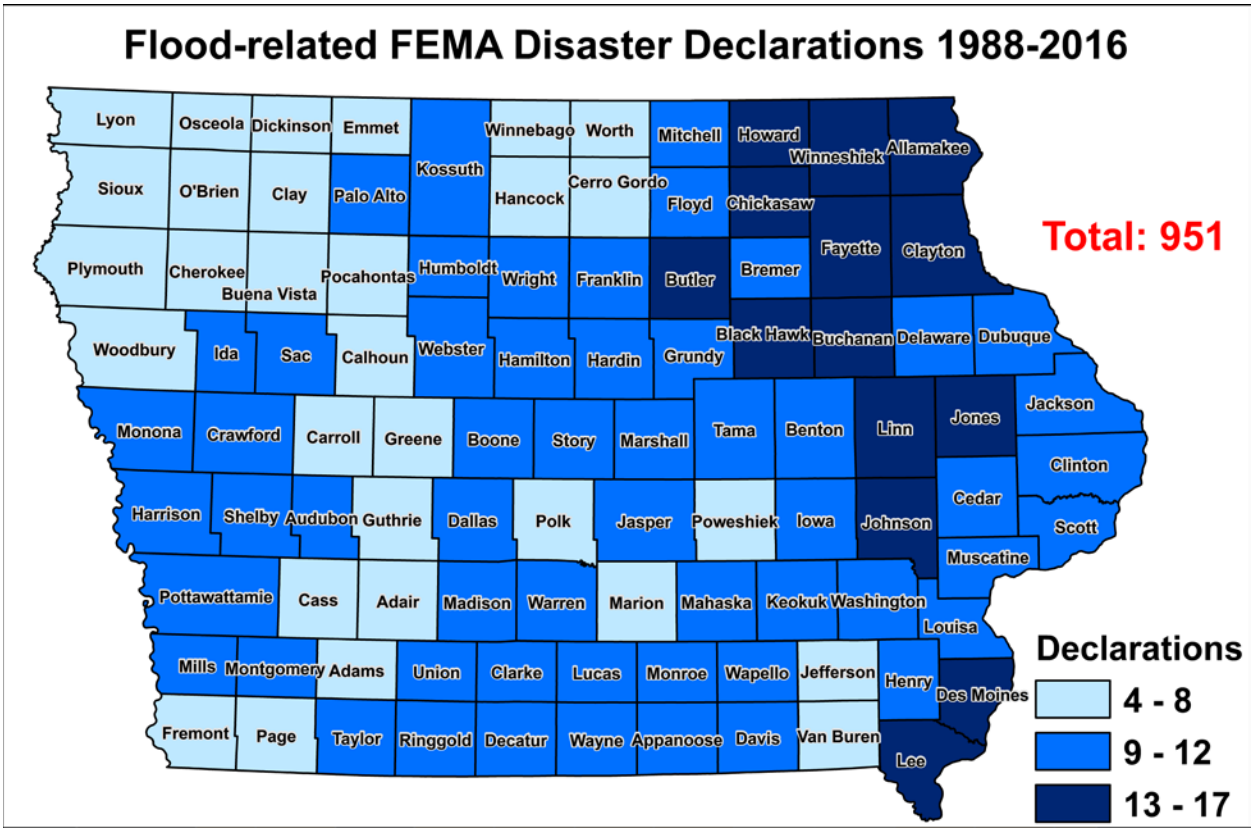

Figure 13. Flood-related disaster declarations in Iowa counties. 1988-2016. Raw data: https://www.fema.gov/

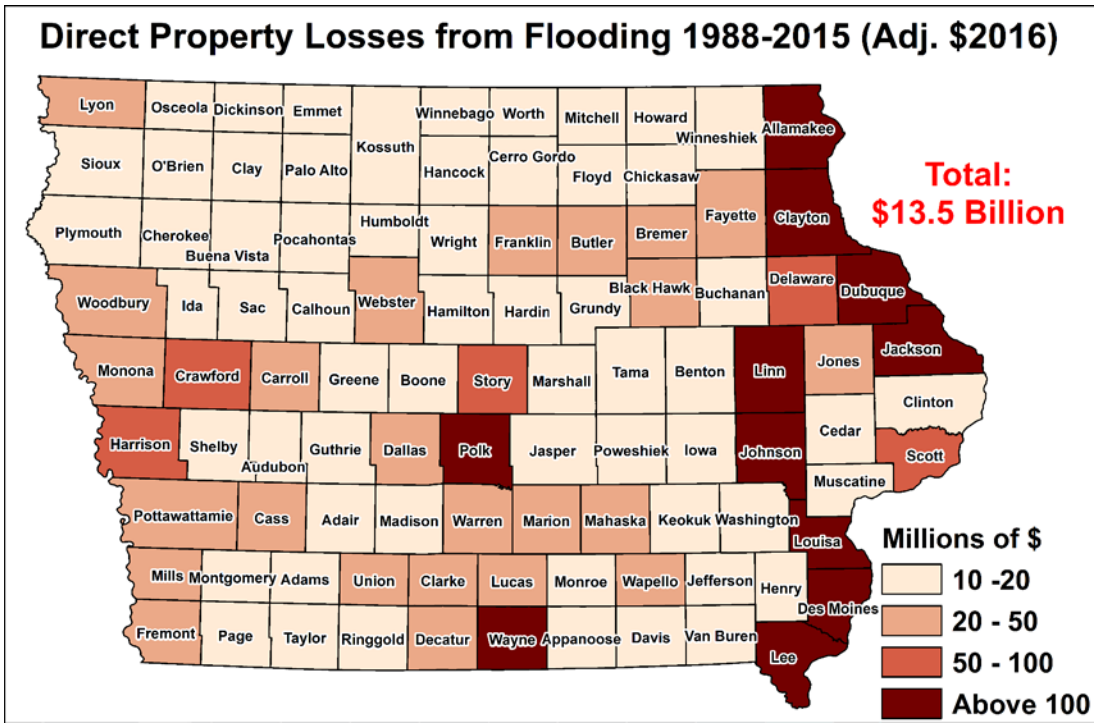

Figure 14. Iowa direct property losses from flooding. Raw data: https://cemhs.asu.edu/SHELDUS/

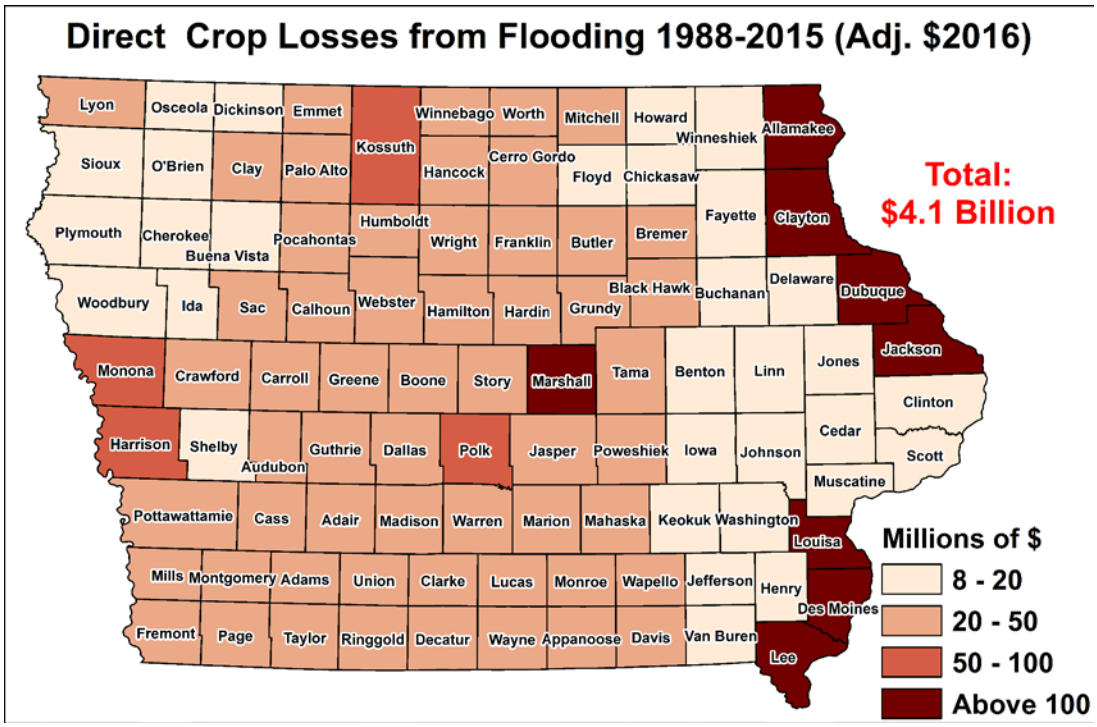

Figure 15. Iowa direct crop losses from flooding. Raw data: https://cemhs.asu.edu/SHELDUS/

Flood-Inundation Mapping of a Steep, Gravel Desert Stream in Death Valley National Park, California

Christopher Morris, Hydrologist, US Geological Survey, Henderson, Nevada, cmmorris@usgs.gov
Toby Welborn, Geographer, US Geological Survey, Portland, Oregon, tlwelbor@usgs.gov

Extended Abstract

Introduction

In desert landscapes, flooding can result in dramatic changes to streams. However, the frequency, magnitude, and geomorphic effects of floods in such environments are less understood compared to wetter environments (Tooth, 2000). In desert landscapes, steep slopes and sparse vegetation result in runoff and flashy flood peaks, often lasting for only a few hours. Many floods are the result of isolated, convective thunderstorms that cannot be predicted easily in advance and frequently occur at night. Therefore, direct observations or measurements of streamflow during floods often are limited, with data collection mostly occurring after the event. In ephemeral streams, limited vegetation within channels and on overbanks result in large stream velocity and higher probability for erosion during flooding. Moreover, flood occurrence in desert streams is often highly variable and some sites may go for years without streamflow, complicating flood frequency analyses. Finally, data sets in desert environments are often short and have few long-term, systematic collection sites.

Grapevine Canyon, located in the northeast part of Death Valley National Park in the Mojave Desert of California, drains the steep, sparsely vegetated slopes of the Grapevine Mountains. The stream channel is very steep, with an average 0.05 slope and drainage area of about 48 square miles. Channel material is predominately gravel. Except for short reaches supported by springs, the stream is ephemeral and only flows in response to heavy rainfall. The canyon is also the site of Scotty's Castle, a historic ranch and popular tourist attraction in the national park. Several buildings, a road, parking lot, and bridge occupy the canyon bottom. On October 18, 2015 an intense thunderstorm produced nearly an entire year's worth of rainfall in just a few hours. The resulting flash flood caused substantial damage to several buildings, roads, powerlines, and water infrastructure. In some locations, several feet of sand, gravel, and cobble were deposited, while elsewhere up to 10 ft. of channel incision occurred and new channels were created. The area is expected to be closed to the public until at least 2020, and cost $50 million to repair.

To help the National Park Service better understand the potential of future flooding and associated risk to historic park structures in Grapevine Canyon, the U.S. Geological Survey mapped current flood-inundation boundaries for the 4, 2, 1, 0.5, and 0.2-percent annual exceedance probability (AEP) streamflows.

Methods

Streamflow measurements in Grapevine Canyon were limited to two, post-flood indirect measurements (1968 and 2015) and an estimated streamflow (1976). Two streamgages were installed at the site (in Grapevine Canyon and Tie Canyon, a tributary canyon) in 2016, however,

as of April 2019, no streamflows have occurred. The existing data were not enough to perform a site-specific flood frequency analysis, therefore regional peak streamflow regression equations for the desert regions of California were used to estimate the 4, 2, 1, 0.5, and 0.2-percent AEP streamflows (Gotvald and others, 2012). The estimated discharges ranged from about 3,900 to 41,300 cubic feet per second. The October 18, 2015 flood was estimated to be between a 4 and 2-percent AEP streamflow.

In addition to the lack of hydrologic data, the study area also lacks high resolution topographic data. In July 2016, a terrestrial laser scanner (TLS) was used to collect ground based lidar at 38 locations. The TLS locations were then surveyed to georeference each scan, and the collected data were combined into a 3-dimensional point cloud of the area. Over 83 million topographic points were collected during the TLS survey. From this point cloud, filtering was used to eliminate extraneous data such as vegetation, fences, powerlines, and atmospheric interference to create a digital terrain model of the area.

Finally, friction losses due to roughness of the channel bed and vegetation must be accounted for when modeling streamflow. When streamflows are directly measured, roughness can be computed via Manning's equation, however, in the absence of direct measurements, roughness must be estimated. Three approaches were used in this study to estimate channel roughness. First, the site was visually compared to other locations where the roughness has been directly computed (Phillips and Ingersoll, 1998). Secondly, the roughness was estimated using tables for channel material and adjusting for channel irregularities, obstructions, and vegetation (Chow, 1959). Finally, five Wolman style pebble counts were performed to determine channel bed particles sizes, and roughness was estimated using the measured particles size in empirically derived equations (Rickenmann and Recking, 2011).

The combination of the hydrologic, topographic, and roughness data were used to create a one-dimensional HEC-RAS hydraulic model. A total of 539 cross-sections were extracted from the digital terrain model over the approximately 5,000 ft. model reach. Model calibration was limited to the 2015 flood event high-water marks due to the lack of streamflow since that event and the large channel changes that occurred because of the 2015 flood, limiting the applicability of previously collected data.

Results and Conclusions

The model results indicated that at the highest computed streamflows, inundation would cover nearly the entire canyon bottom, impacting several historic buildings, parking lots, and roads. However, the main building of Scotty's Castle would not be inundated by any computed floods as it was built on a higher terrace. At the 0.2-percent AEP streamflow, a bridge and embankment could be overtopped by almost 6 feet of total depth.

Even at lower computed streamflows, some infrastructure would be inundated. Sections of the road and parking lot were inundated by every modeled streamflow as they are located directly within the stream channel. One building was situated in the direct path of streamflow as channel

changes caused by the 2015 flood, have redirected the main channel toward the building. Additionally, at the 2 AEP, the bridge and embankment would be overtopped.

Model results must be viewed with an understanding of several assumptions and uncertainties. Except for areas with very dense vegetation and at the constriction of the bridge, the entire modeled reach computes as super-critical flow with very high velocities which have been questioned as unrealistic in other steep channel computations (Jarrett, 1984; Costa and Jarrett, 2008). The channel is subject to unknown erosion and deposition during floods. Since topographic data was limited to post flood conditions, using such data could result in over or under estimates of actual channel dimensions and inundated areas.

Due to the lack of site specific hydrologic data, regional regression equations were used to compute the AEP streamflows. This also adds uncertainty as the difference in computed streamflows between the latest (2012) and previously published equations (1977) are a 10-50% decrease in streamflow.

Finally, focusing on streamflow in main channels did not account for flooding potential from small tributaries, gullies, or overland flow. In the 2015 flood, many smaller channels flowed, however, drainage is mostly non-existent at Scotty's Castle, with several channels simply ending at building walls or parking lots.

References

Chow, V.T. 1959. Open-channel hydraulics: New York, McGraw-Hill, 680 p.

Costa, J.E. and Jarrett, R.D. 2008. "An evaluation of selected extraordinary floods in the United States reported by the U.S. Geological Survey and implications for future advancement of flood science.", U.S. Geological Survey Scientific Investigations Report 2008-5164, 232 p.

Gotvald, A.J., Barth, N.A., Veilleux, A.G., and Parrett, Charles. 2012. "Methods for determining magnitude and frequency of floods in California, based on data through water year 2006", U.S. Geological Survey Scientific Investigations Report 2012–5113, 38 p.

Jarrett, R.D. 1984. "Hydraulics of high-gradient streams", Journal of Hydraulic Engineering, 110(11):1519-1539.

Phillips, J.V. and Ingersoll, T.L. 1998. "Verification of roughness coefficients for selected natural and constructed stream channels in Arizona", U.S. Geological Survey Professional Paper 1585, 77 p.

Rickenmann, D. and Recking, A. 2011. "Evaluation of flow resistance in gravel-bed rivers through a large field data set", Water Resources Research, 47(7):1-22.

Tooth, S. 2000. "Process, form, and changes in dryland rivers: a review of recent research.", Earth-Science Reviews 51:67-107.

Flood Potential in the Southern Rocky Mountains Region and Beyond

Steven E. Yochum, Hydrologist, U.S. Forest Service, Fort Collins, Colorado
970-295-5285, steven.yochum@usda.gov

prepared for the SEDHYD-2019 conference, June 24-28th, Reno, Nevada, USA

Abstract

Understanding of the expected magnitudes and spatial variability of floods is essential for managing stream corridors. Utilizing the greater Southern Rocky Mountains region, a new method was developed to predict expected flood magnitudes and quantify spatial variability. In a variation of the envelope curve method, regressions of record peak discharges at long-term streamgages were used to predict the *expected flood potential* across zones of similar flood response and provide a framework for consistent comparison between zones through a flood potential index. Floods varied substantially, with the southern portion of Eastern Slopes and Great Plains zone experiencing floods, on average for a given watershed area, 15 times greater than an adjacent orographic-sheltered zone (mountain valleys of central Colorado and Northern New Mexico). The method facilitates the use of paleoflood data to extend predictions and provides a systematic approach for identifying extreme floods through comparison with large floods experienced by all streamgages within each zone. A variability index was developed to quantify within-zone flood variability and the flood potential index was combined with a flashiness index to yield a flood hazard index. Preliminary analyses performed in Texas, Missouri and Arkansas, northern Maine, northern California, and Puerto Rico indicate the method may have wide applicability. By leveraging data collected at streamgages in similar-responding nearby watersheds, these results can be used to predict expected large flood magnitudes at ungaged and insufficiently gaged locations, as well as for checking the results of statistical distributions at streamgaged locations, and for comparing flood risks across broad geographic extents.

Introduction

Greater insight into the expected magnitudes and spatial variability of floods is needed to more effectively manage our resources and build more sustainable communities. However, our understanding of floods is limited and hazards can be poorly communicated by technical specialists to decision makers and the public.

Generally, hydrologists and engineers rely on three methods for estimating flood magnitudes: 1) flood frequency methods that fit statistical distributions to annual peak discharge data and extrapolate these data to ungaged locations in regional regression studies; 2) rainfall-runoff based analyses; and 3) empirically-derived relationships between flood discharges and watershed characteristics (frequently implemented as envelope curves). Two of these methods rely directly on streamgage data. However streamgage databases can be problematic due to widely variable record lengths and periods, and mixed distributions of runoff mechanisms and flood magnitudes; this can be tricky for analyses and induces prediction uncertainty. As with other problems where predictions have substantial uncertainty, it's preferable to utilize multiple approaches. To this end, a new method was developed to help enhance understanding and communication of expected flood magnitudes and spatial variability.

Based on an analysis performed in the greater Southern Rocky Mountain region and preliminarily verified in several other regions of North America and Puerto Rico, a new method was developed using a space for time substitution to predict expected flood magnitudes at any given location given the streamgage record in similarly-responding nearby watersheds. Regressions of record peak discharges using drainage area and additional explanatory variables were fit across areas with similar flood records, with these areas referred to as *zones*. (The term zone is intentionally used to differentiate from regional regressions, which typically predict flood frequency relationships from streamgage analyses.) From these zonal regressions, a *flood potential index* was developed to rank flood hazards between zones, and a variability index was developed to quantify within-zone variability. Additionally, in combination with a flashiness index, an overall flood hazard index was developed. The method allows users to predict flood magnitudes and understand which areas tend to experience larger or smaller floods. This assists practitioners with answering such questions as:

- What magnitude of floods can be expected at a given ungaged location and how reasonable are predictions from the USGS regional regression equations?
- Is a streamgage flood frequency analysis providing reasonable results, or are the results biased due to such issues as the presence or absence of a large flood?
- Considering such applications as enhanced understanding of the geomorphic form and erosion hazard of stream corridors, the inherent risk of stream restoration, the impacts of wildfires, and the variability in probable maximum precipitation, what areas are prone to larger or smaller magnitude floods?
- Given the record of floods in the area, is a specific flood extreme in magnitude?
- Is a watershed that has only experienced relatively small floods in a precipitation shadow or has this watershed not yet experienced a larger flood that its neighboring watersheds indicate as being likely?

Methods

The primary study area consisted of the greater Southern Rocky Mountains, from the Great Plains of eastern Colorado to the Great Salt Lake, and from Casper, Wyoming to Albuquerque, New Mexico, with additional analyses on the Edwards Plateau (Texas Hill Country), the Ozark Plateau, northern Maine, Northern California, and northern Puerto Rico.

Streamgage data were obtained from the U.S. Geological Survey (USGS 2017a; USGS 2018a), a variety of state agencies, and the U.S. Bureau of Reclamation. Watershed areas up to 8600 km^2 (3320 mi^2) were evaluated. All streamgages with at least 40 years of record were required to be included in the analysis, with exceptions for redundant gages and gages dominated by attenuation from upstream reservoirs that have little or no pre-impoundment data. In areas with insufficient long-term streamgage data, streamgages with substantial floods but with records as short as 10 years were also used. Additional peak flow data were obtained for the 2013 Colorado Front Range flood (Jarrett, pers. comm. 2014, Schram 2014, Kimbrough and Holmes 2015, Moody 2016, Brogan et al. 2017, and Yochum et al. 2017).

Zones of relatively consistent flood magnitudes were developed, with the boundaries being approximate and often similar to the hydrologic region boundaries for regional regression equations (Miller, 2003; Kenney et al. 2007; Waltemeyer, 2008; Capesius and Stephens, 2009; Kohn et al., 2016). These boundaries were based on physiographic provinces and sections, watershed boundaries and topographic features, and flood flashiness.

Drainage area and other watershed characteristics were tested as regression predictors. Watersheds were delineated from modifications of HUC12 boundary datasets (USGS, 2017b). Arithmetic mean elevation, maximum elevation, and arithmetic mean slope and aspect

calculated in ArcGIS from 30 meter national elevation datasets (USGS 2017b). Annual and monthly area-weighted precipitation was computed from 30-year, 800 meter PRISM grids (Daly et al. 2008; PRISM 2018).

Four indices were used for comparing floods between zones. The flood potential index (P_f) is:

$$P_f = Average\left({Q_{20}}/{4.15} + {Q_{200}}/{21.0} + {Q_{2000}}/{106}\right)$$

, where Q_{20} is the fitted discharge (m^3/s) for a 20 km^2 watershed for the zone of interest (which is divided by the fitted discharge for a 20 km^2 watershed in zone 2), and with 200 and 2000 noting similar computations for 200 and 2000 km^2 watersheds. The variability index (V_f) is the ratio of the regression intercepts for maximum likely flood potential and the expected flood potential, specifically:

$$V_f = {a_{mlf}}/{a_{efp}}$$

, where $Q = aA^b$. Flashiness was determined using the Beard flash flood index (F; Beard 1975), which is computed as the standard deviation of the natural logarithms of the annual peak flow for each streamgage. A flood hazard index (H_f) was computed as:

$$H_f = P_f * F$$

Regressions were performed using the R software package. Natural logarithmic transformations were applied, which generally provided good adherence to regression assumptions of linearity, homoscedasticity, and independent and normally-distributed residuals. Where encountered, outliers were assumed to not be errors and were identified using Cook's distance (D) measurement of influence. High outliers were typically retained to maintain conservative predictions. In zones where low outliers were excluded, these points were identified where $D >$ 1.9*(mean D). Low outliers exclusion was necessary to avoid developing models with less conservative flood predictions.

Additional details on the methods utilized in the analysis are provided in Yochum et al. (in review).

Results and Discussion

Enhanced understanding of the magnitude and spatial variability of flood hazards and simpler language for communicating these hazards with managers and the public are needed to help protect lives, property, and infrastructure. Data exploration of streamgage annual peak discharge data revealed a spatial pattern in experienced floods. Regressions of the maximum (record) peak discharges (Q) using watershed area (A), topographic, and climatologic predictors were performed across zones of similar flood response, with high levels of explained variance (Table 1). The method facilitates understanding of floods that, given these precedents, are likely to occur in the future across each zonal extent. Detailed analyses have been completed for the greater Southern Rocky Mountains region and preliminary analyses were performed in diverse regions across the United States.

In the greater Southern Rocky Mountains region (Figure 1), regressions were performed for eleven zones of similar flood responses. The analyses included 463 streamgages with watershed areas ranging from 1.5 to 8550 km^2 (0.58 to 3300 mi^2). Each of these regressions define the *expected flood potential* for each zone using a method independent of flood frequency analyses; Figure 2 provides example plots for four zones, with additional information available in Yochum et al. (in review). Up to 93% of the variance in the record peak discharges was explained using up to two predictors, with the prediction equations provided on each plot. Using a space for time substitution, this method predicts flood magnitudes that can be expected in specific watersheds

(within the derived watershed area range) given the streamgage record of appropriate neighboring watersheds, providing a complimentary approach to flood frequency/regional regression and rainfall-runoff models, and potentially reducing uncertainties in predicting the size of large floods.

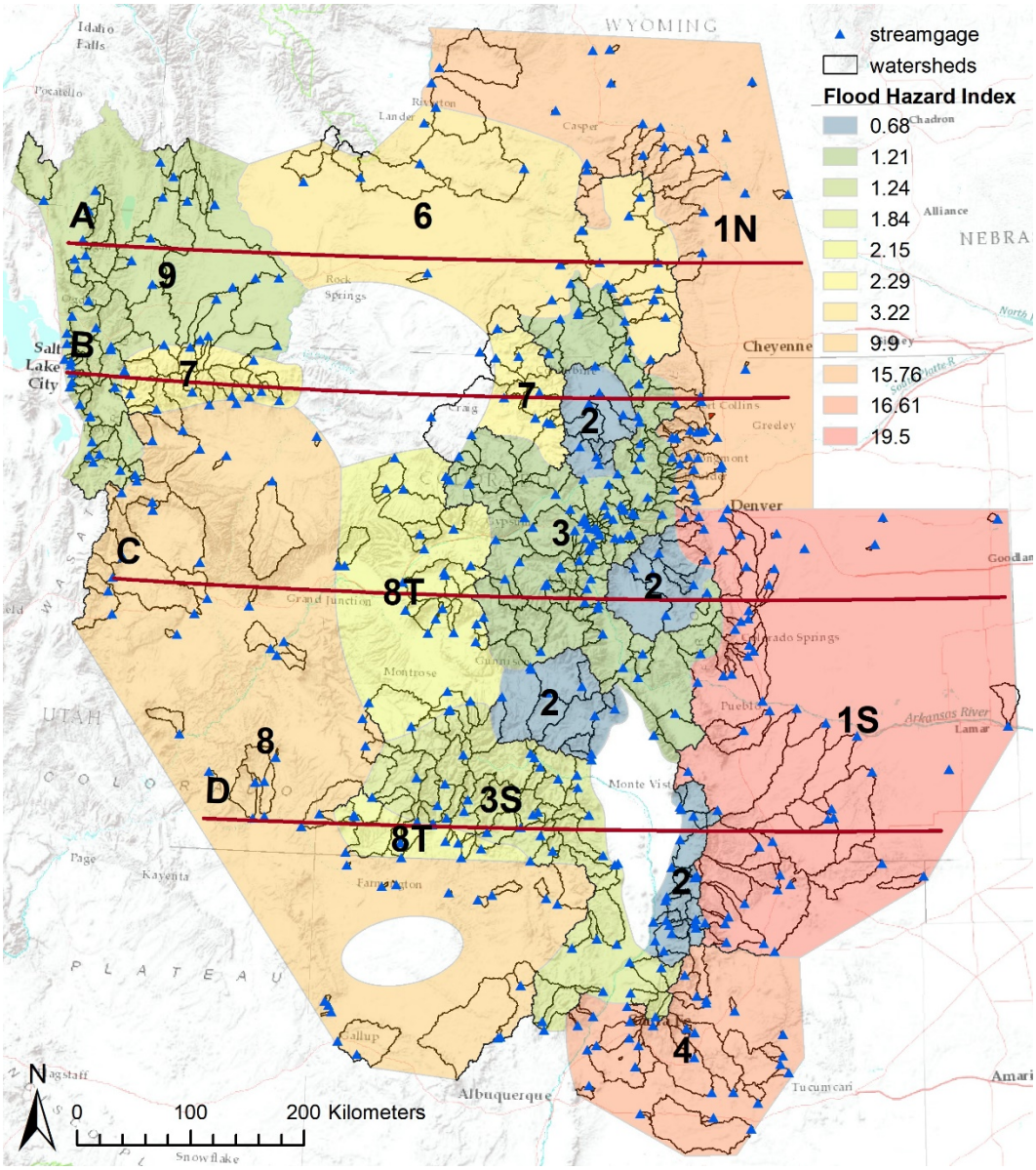

Figure 1. Greater Southern Rocky Mountains analysis extent, with zone boundaries, utilized streamgages, and watershed boundaries. The colors represent the flood hazard index value for each zone. Embedded areas with insufficient data do not have any coloring. Section lines are also indicated.

Table 1: Expected flood potential analysis results, where n is the number of streamgages in each regression, R^2 is the explained variance, P_f is the flood potential index, F is the Beard flash flood index, and H_f is the flood hazard index.

	Zone	ID	n	R^2	P_f	V_f	F	H_f
Southern Rocky Mountains Region	Eastern Slopes & Great Plains, South	1S	45	0.70	15.0	2.77	1.30	20
	Eastern Slopes & Great Plains, North	1N	41	0.75	13.8	1.76	1.14	16
	Orographic Sheltered	2	36	0.89	1.0	1.52	0.69	0.7
	Southern Rocky Mountains	3	90	0.93	2.3	1.62	0.53	1.2
	Southern Rocky Mountains, South	3S	45	0.71	3.0	1.94	0.61	1.8
	Southern Transition	4	25	0.85	14.0	1.97	1.19	17
	Wyoming Basin	6	21	0.90	3.6	1.43	0.90	3.2
	Northwest Mountains	7	21	0.85	4.7	1.38	0.49	2.3
	Colorado Plateaus	8	42	0.74	9.0	1.88	1.10	10
	Colorado Plateaus Transition	8T	27	0.81	2.7	1.50	0.80	2.2
	Wasach and West Basins	9	41	0.79	1.9	1.78	0.65	1.2
Preliminary Analyses	Great Basin Transition	22	29	0.87	2.9	----	1.10	3.2
	Sierra Nevada Mountains	23	56	0.91	12.7	----	1.07	14
	California Coastal Ranges	25	30	0.98	33.3	----	0.71	24
	Eastern Klamath Mountains	26	15	0.98	17.2	----	0.84	14
	Midwest, Central Lowlands	51	16	0.95	22.7	----	0.72	16
	Ozark Plateaus	52	19	0.92	34.0	----	0.82	28
	Edwards Plateau	61	16	0.98	79.4	----	1.90	151
	New England, Coastal Lowlands and Uplands	95	19	0.96	5.5	----	0.39	2.1
	Puerto Rico	101	21	0.97	117	----	0.88	103

Upper 95% prediction limits were utilized to understand flood variability within each zone, with this limit dubbed the *maximum likely flood potential*. Floods above this level are unlikely but still possible, and are considered extreme – this method provides a tool for quantitatively and consistently defining extreme floods. The amount of departure above the maximum likely flood potential denotes the degree of extremity. For example, in the Eastern Slopes and Great Plains South (zone 1S; Figure 1; Figure 2-A), an area that has experienced the largest and most variable flood magnitudes within the greater Southern Rocky Mountains analysis extent, four extreme floods occurred at the evaluated streamgages. The most extreme flood was experienced on Jimmy Camp Creek, CO in June of 1965 (Q = 3510 m^3/s = 124,000 ft^3/s; A = 169 km^2 = 65 mi^2), with the second most extreme flood occurring on Kiowa Creek in May of 1935 (Q = 1230 m^3/s = 43,500 ft^3/s, A = 74 km^2 = 29 mi^2). Generally, extreme floods tend to be associated with intense thunderstorms, squall lines, and shortwave troughs developed within or influenced by synoptic-scale weather systems, and are often associated with atmospheric blocking patterns (Hirschboeck, 1987).

There is substantial variability in the expected flood potential across this regional analysis extent (Figure 3); Table 2 provides expected flood potential and maximum likely flood potential predictions for a standard 1000 km^2 watershed size. This variability is despite these zones relatively close (or adjacent) proximity to each other (Figure 1, Figure 4) and may be due to watershed characteristics, such as bedrock exposure, thin soils, vegetative conditions, and steep relief (Osterkamp & Friedman 2000; O'Connor & Costa 2004), as well as flood type (rainfall versus snowmelt), orographic blockage (rain shadow), water vapor sources, rainfall rates, and convective storm sizes.

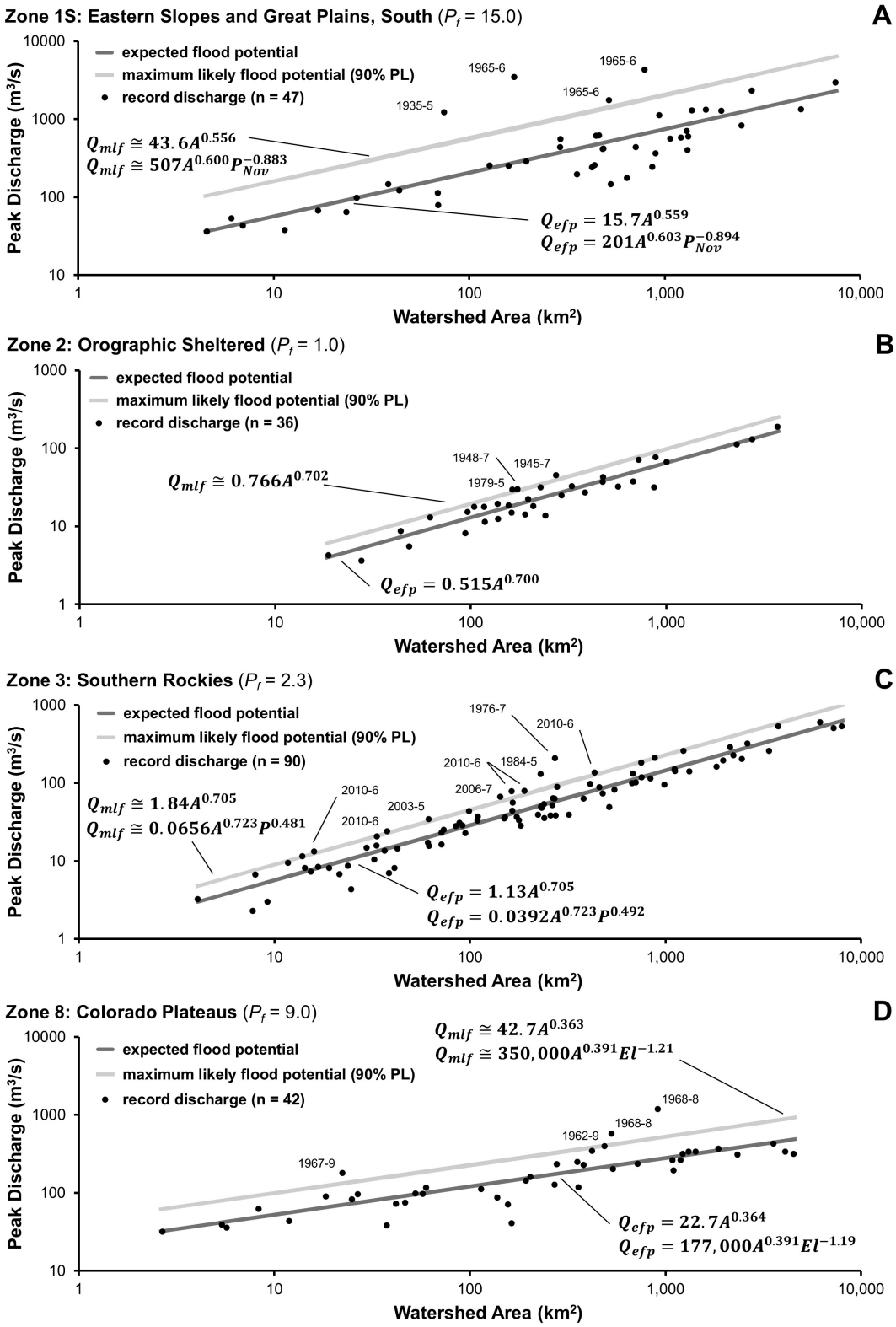

Figure 2. Selected zone plots of long term streamgage record peak discharges (black dots), expected flood potential (regression fit), and the maximum likely flood potential (90% prediction limit). Dates of extreme floods are also provided. A: watershed area (km²); P: average annual precipitation (mm); P_{Nov}: average November precipitation (mm); El: average watershed elevation (m).

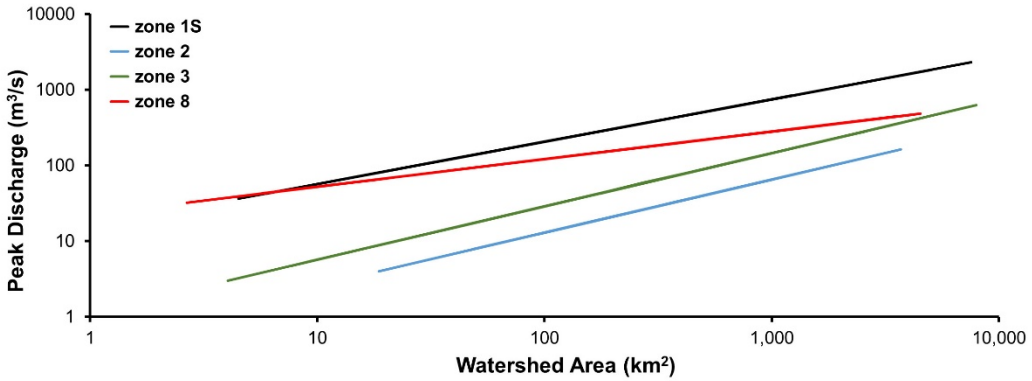

Figure 3. Expected flood potential for zones 1s (Eastern Slopes and Great Plains, South), 2 (Orographic Sheltered), 3 (Southern Rockies), and 8 (Colorado Plateaus).

Table 2. Expected flood potential and maximum likely flood potential flood magnitude estimates for a standard 1000 km² (386 mi²) watershed.

		Expected Flood Potential		Maximim Likely Flood Potential	
Zone	**ID**	(m^3/s)	(ft^3/s)	(m^3/s)	(ft^3/s)
Eastern Slopes & Great Plains, South	1S	750	26,000	2,000	71,000
Orographic Sheltered	2	65	2,300	98	3,500
Southern Rocky Mountains	3	150	5,100	240	8,500
Colorado Plateaus	8	280	9,900	520	18,000

Indices were used to quantify the spatial variability of flood hazards across diverse topographic areas. The *flood potential index* (P_f) compares the expected flood potential to the zone with the smallest experienced floods (zone 2, Orographic Sheltered). Zone 2 is composed of the high-elevation rain-shadowed valleys of central Colorado and northern New Mexico, specifically North Park, South Park, and the upper Gunnison, San Luis, and Taos valleys (Figure 1). This index varied from 1.0 to 15 for the core study area (Table 1), with the highest flood potential zone (1S) experiencing floods, on average, 15 times greater than the adjacent Orographic Sheltered zone. The *flood variability index* (V_f) quantifies the variability of the within-zone record discharges (Figure 2); the greatest variability was in zone 1S and the least in zone 7 (Northwest Mountains). The *Beard flashiness index* (F) was utilized to quantify how unexpectedly large a flood can be compared to more typical floods. The zonal average F varied from 0.49 to 1.30 (in zone 1S), with higher values indicating greater flashiness. The *flood hazard index* (H_f) is the product of P_f and F, and accounts for both the flood magnitude and flashiness. H_f varied from 0.7 to 20, with the least flood hazards in zone 2 and the greatest in zone 1S. Other areas of the greater Southern Rocky Mountains region with highest flood potential and hazard are zones 1N and 4, with zone 8 also being of note (Figure 1). These zones include numerous urban areas, including cities along the Colorado Front Range (Denver, Colorado Springs, Fort Collins, Boulder), Casper and Cheyenne, WY, as well as Pueblo and Trinidad, CO, Santa Fe and Farmington, NM, and Moab, UT.

Four cross sections were cut from west to east across the study area (Figure 1), to illustrate how flood potential varies with topographic landforms (Figure 4). The eastern and southwestern portions of the study area have the highest flood potential, while the highest elevations (and the embedded valleys) have the lowest flood potential. These differences may likely be the result of dominant meteorological processes induced by the mountainous terrain of the study area.

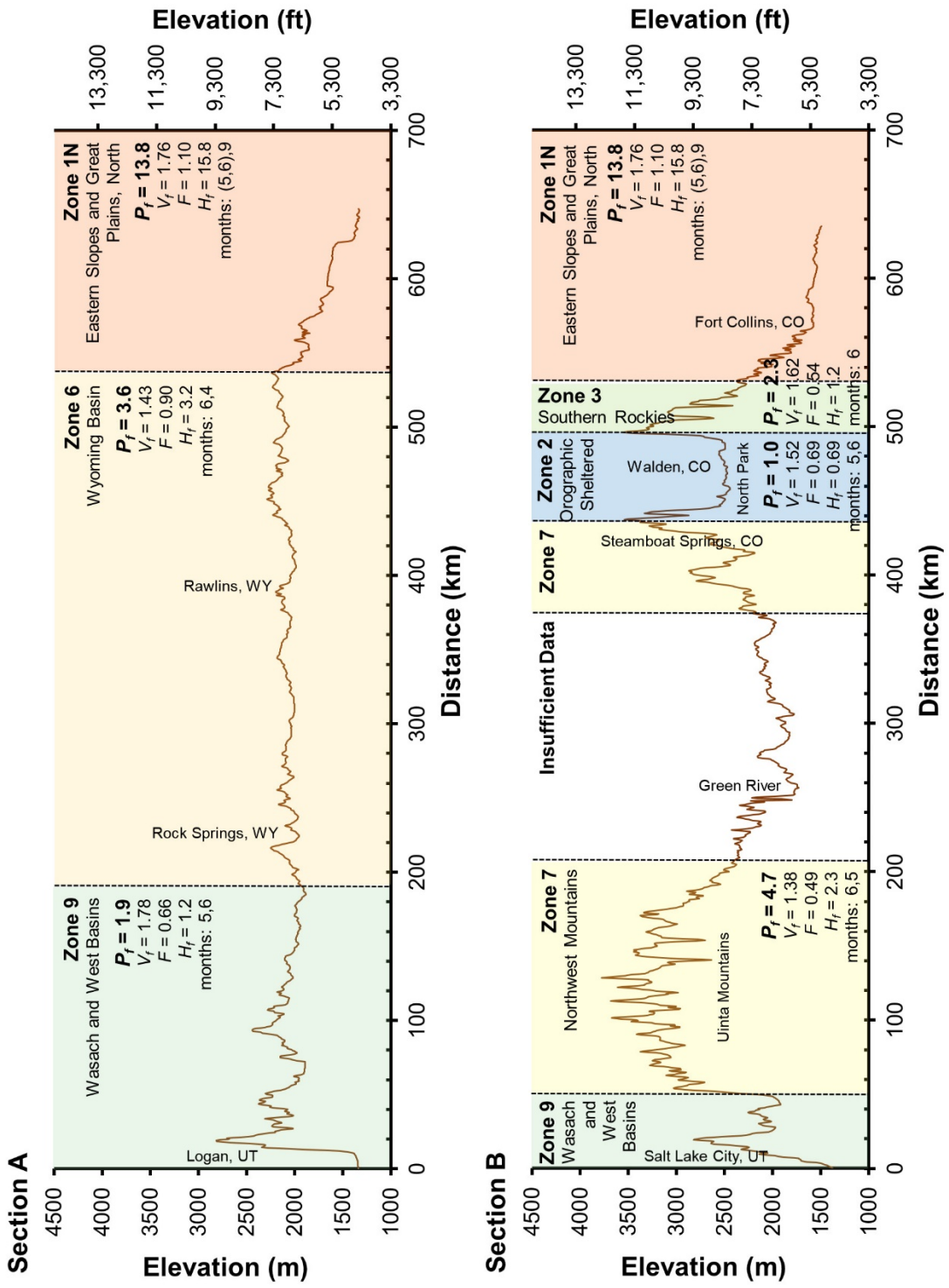

Figure 4a. Cross sections across the study area, from west to east, showing relief as well as flood potential and other indices. Warmer and cooler colors indicate higher and lower flood potential, respectively.

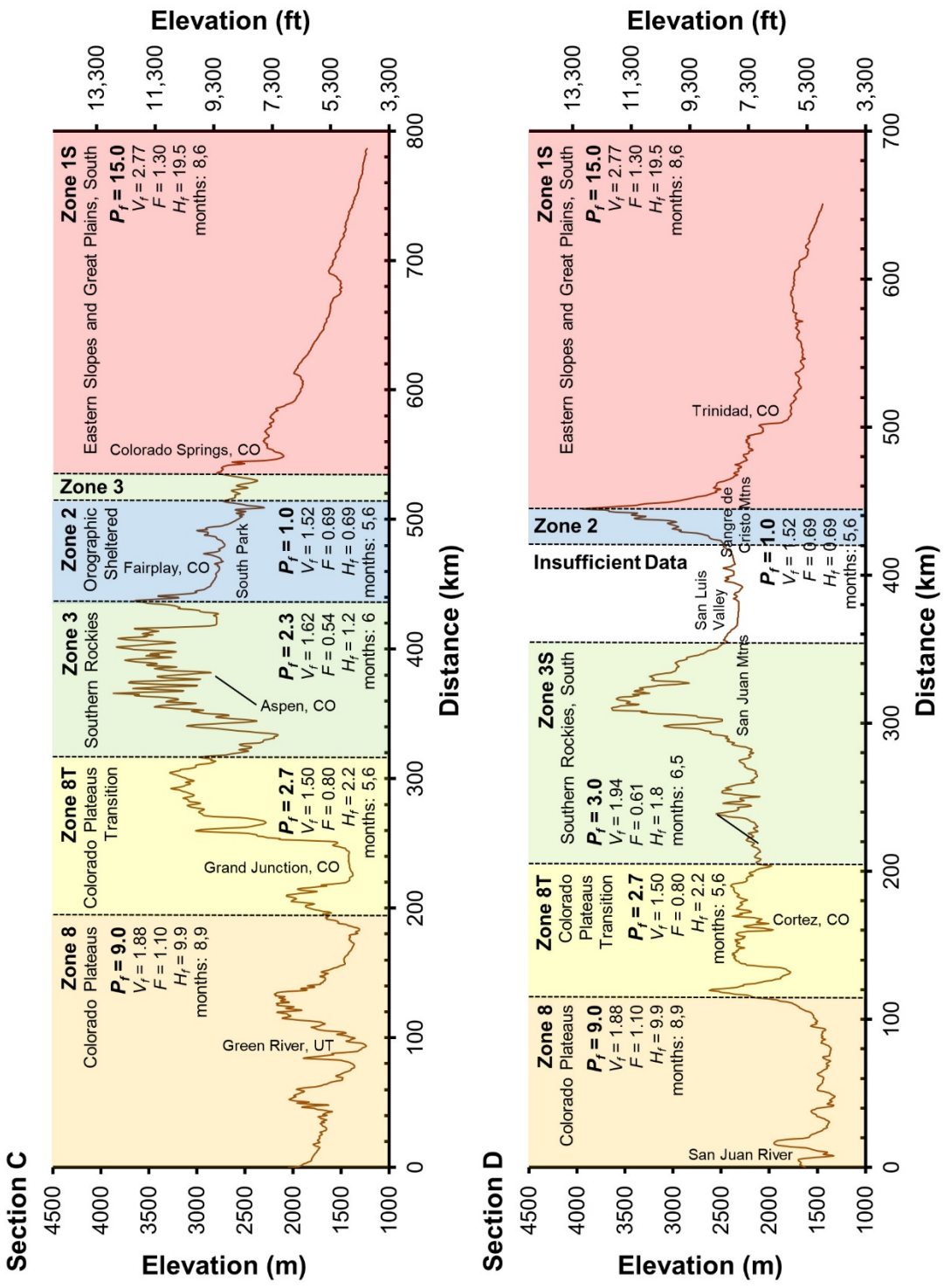

Figure 4b. Cross sections across the study area, from west to east, showing relief as well as flood potential and other indices. Warmer and cooler colors indicate higher and lower flood potential, respectively.

Northern Colorado Front Range Floods

The northern Colorado Front Range is part of zone 1N (Eastern Slopes and Great Plains, North). This area is of special interest due to the well-known Big Thompson Flood of 1976 and 2013 Colorado Front Range floods (Gochis et al. 2015; Yochum et al. 2017). Initially, the 2013 floods were referred to by the National Weather Service as an event with "biblical rainfall amounts" (Koronowski 2013), with rainfall on the order of a 1000-year storm (NWS 2013). Such overly sensational language is problematic in that, upon hearing this, citizens frequently react by considering the flooding to be an aberration, discounting the possibility of future occurrences and inhibiting the development of more resilient stream valley communities. Flood potential analyses allow us to place a flood event into a broader perspective that considers other floods that have been measured in neighboring (zonal) watersheds.

The expected flood potential regression is illustrated in Figure 5, which includes the record peak discharges (black dots), the maximum likely flood potential (dark gray line), and a number of the most substantial peak flow estimates collected after the 2013 (and 1997) floods (marked with a "+"). The most extreme floods (Figure 6), in decreasing order of extremity, were on Sand Creek, WY (August 1955), the Spring Creek Flood in Fort Collins, CO (July 1997), and the Big Thompson flood (July 1976). The other extreme floods were experienced in September of 2013 in the St. Vrain Creek and in Little Thompson River watersheds. Other areas impacted by the 2013 flood experienced magnitudes that were similar to (or less than) the expected flood potential. Hence, most portions of the 2013 flood extent did not experience extreme floods, but rather flood magnitudes that can be considered expected given the available zonal streamgage records.

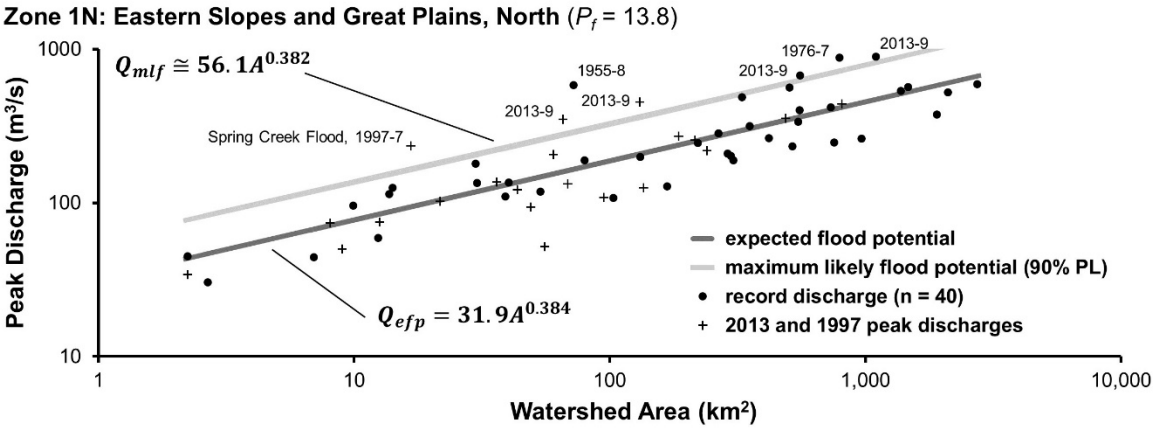

Figure 5. Zone 1N plot of long term streamgage record peak discharges (black dots), expected flood potential (regression fit), and the maximum likely flood potential (90% prediction limit). Floods greater than the maximum likely flood potential are considered extreme, with the departure indicating the degree of extremity. Flood peaks at non-streamgaged locations are marked with a "+". Dates of extreme floods are also provided.

An interesting characteristic of the Colorado Front Range is that, at higher elevations as the continental divide is approached, flood potential decreases. Traditionally, a rule of thumb that a 2300 m (7500 ft) elevation contour is the approximate boundary between snowmelt (zone 3) and rainfall-dominated floods (Follansbee & Sawyer 1948, Jarrett 1990), with the rainfall floods having much greater flood potential. It has been hypothesized that as a warm, moist airmass is forced upslope by the mountains, this topography initially intensifies precipitation rates due to orographic lifting (as illustrated by the eastern portions of the sections in Figure 4), but as the airmass rises still higher further west, available moisture in the air column tends to decrease and precipitation rates decrease (Hansen et al., 1988, Osterkamp & Friedman, 2000). However,

large magnitude 2013 flooding in higher-elevation areas of the Big Thompson watershed indicated the limitations of this rule of thumb. Additional exceptions to the 2300 m hypothesis were noted by Smith et al. (2018). Reflecting this, the zonal boundary between zone 1N and 3 (Figure 6) is not a contour but is, instead, a series of topographic features that appear to block moisture availability and reduce convection and precipitation intensity.

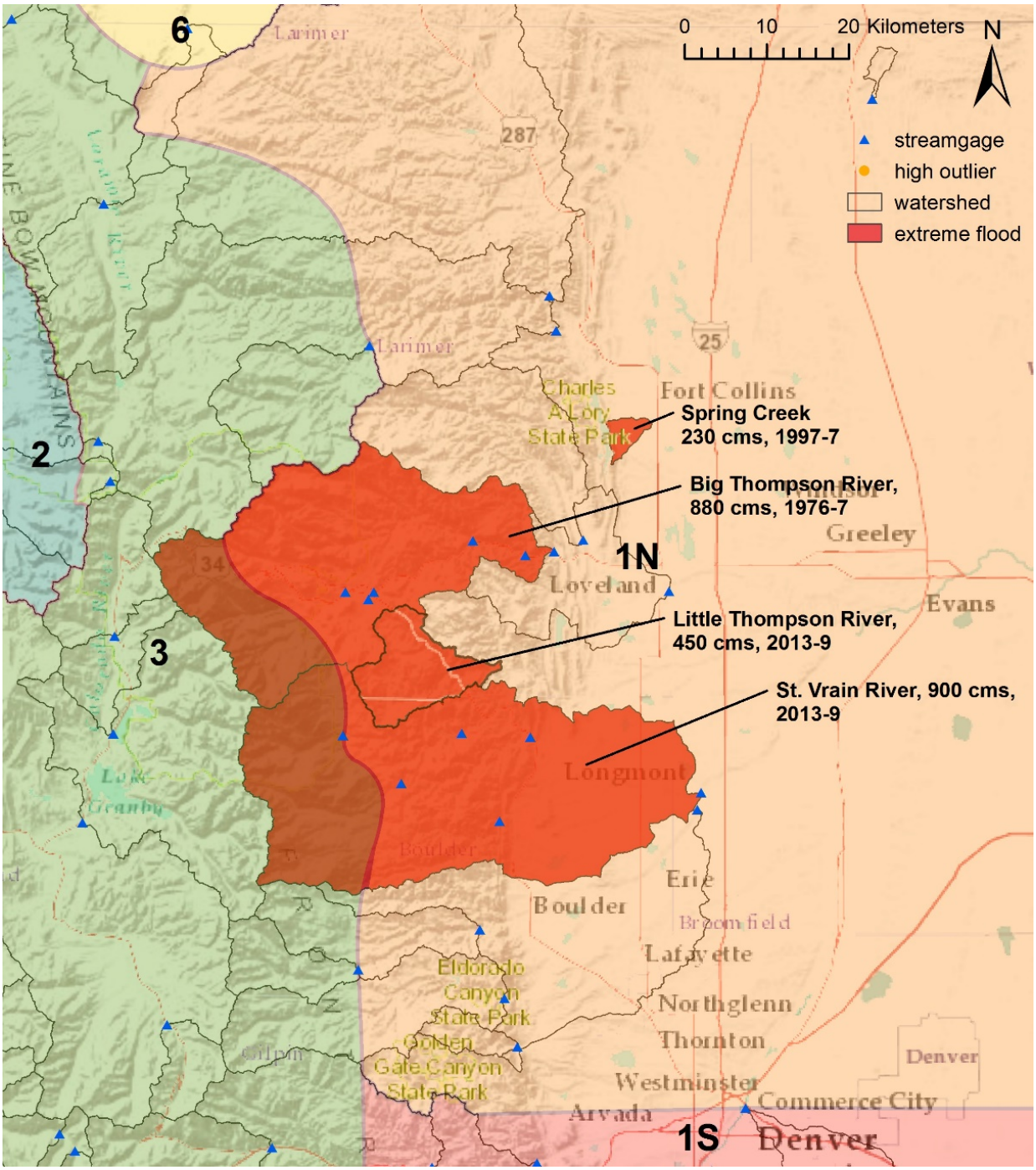

Figure 6. Portion of zone 1N (Eastern Slopes and Great Plains, North) impacted by the floods of 1976 (Big Thompson), 1997 (Spring Creek), and 2013 (Colorado Front Range flood). Watersheds that experienced extreme floods are highlighted in red. The most extreme flood in this zone was experienced outside this map extent, on Sand Creek, Wyoming.

Broader Application

Preliminary analyses were performed across diverse areas of the United States, to assess broader applicability of the technique. These areas included the southern Midwest, northern New England, central Texas, northern California, and Puerto Rico (Figure 7). Distinct zonal variability in flood potential was identified with high-levels of explained variance (Table 1). Preliminary flood potential indices varied from the low values of 2.9 (Great Basin Transition, leeward side of the Sierra Nevada and southern Cascade Mountains) and 5.5 (northern New England), with increased flood potential in the Sierra Nevada Mountains (P_f = 13), the California Coastal Ranges (P_f = 33), and the southern Midwest (P_f = 34 in the Ozarks). Still higher flood potential was quantified on the Edwards Plateau of Texas (P_f = 79) and Puerto Rico (P_f = 117), which has experienced the largest floods within the current investigation. Additionally, this method allows the simple comparison of flood potential between any two zones. For example, the Edwards Plateau (which includes the Texas hill country) experiences, on average for a given watershed area, 79 times larger floods than the index zone and 79/15 = 5.3 times larger floods than the zone with the largest flood magnitudes in the greater Southern Rocky Mountains region, the Eastern Slopes and Great Plains, South (zone 1S). This method shows promise for comparing flood variability on a continental scale.

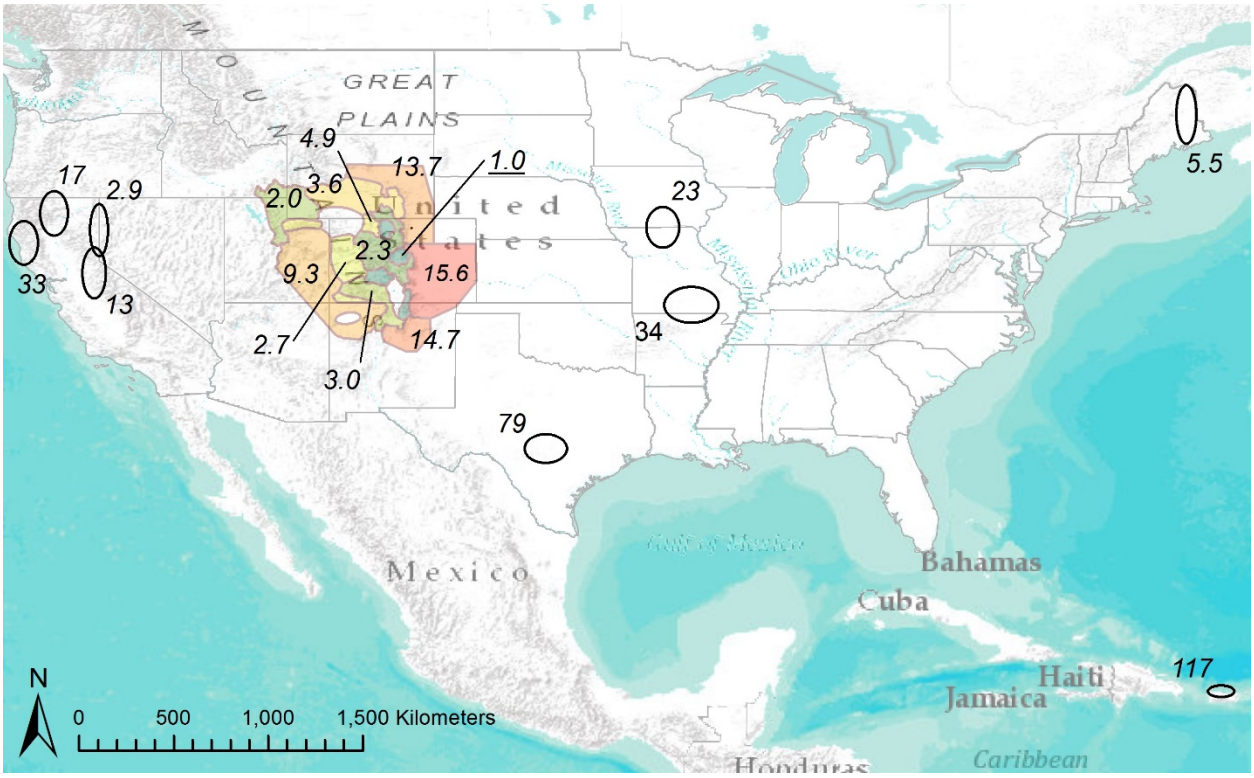

Figure 7. Flood potential index values for the greater Southern Rocky Mountains region analysis extent and the broader application areas (preliminary). The ovals represent the general area of analyses, not specific zone extents. The underlined 1.0 value indicates the index zone (large Central Colorado and northern New Mexico mountain valleys).

Flashiness also varied between the different analyzed zones. The lowest flashiness is experienced in northern New England (F = 0.39) and the highest on the Edwards Plateau (F = 1.90). The variability in both flood potential and flashiness is illustrated in Figure 8, which shows preliminary results for all currently analyzed areas. Zones in the upper-right portion of this figure have the greatest flood hazard (61 – Edwards Plateau, 101 – Puerto Rico), while zones in

the lower-left portion of the figure have the least flood hazard (3 – Southern Rocky Mountains, 7 – Northwest Mountains of the greater Southern Rocky Mountain region, 95 – northern New England). The flood hazard index subsumes this into a single numerical value, with the Edwards Plateau indicating the greatest flood hazard (H_f = 151) and the index area zone 2 (Orographic Sheltered) having the least hazard (H_f = 0.7) across the current analysis extent.

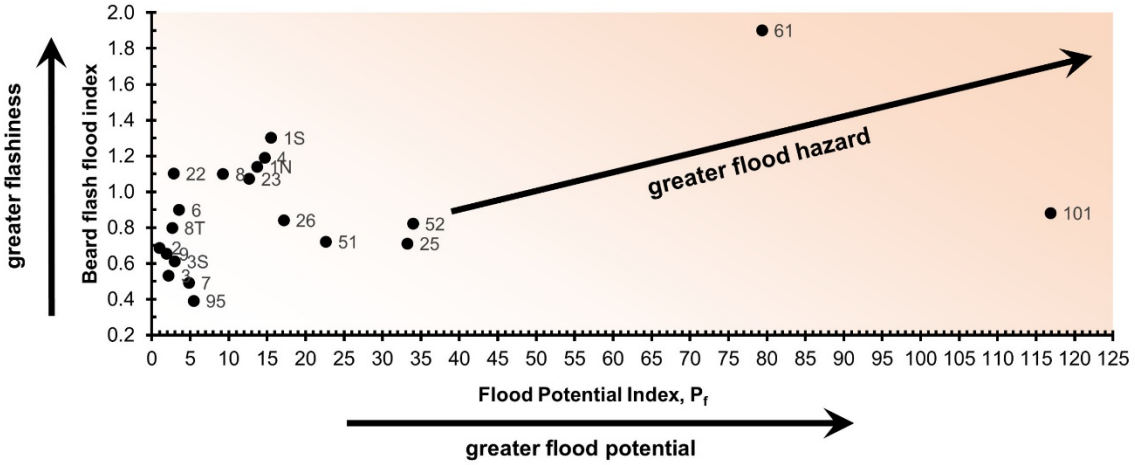

Figure 8. Flood hazard comparison of analyzed zones (identified by the provided ID numbers), with hazard composed of the flood potential and the Beard flash flood indices. The greatest flood hazard index for these preliminary extended analyses is the Edward Plateau (zone 61), Texas (H_f = 151).

Conclusions

Using streamgage records at long term stations, regressions of record peak discharges across zones of similar flood response were utilized to define the *expected flood potential*, a term developed to help understand and communicate what flood discharge magnitudes can be expected given the streamgage records of nearby watersheds. These zones were delineated using physiographic provinces, watershed boundaries and topographic features, and flood flashiness. The method was developed for the greater Southern Rocky Mountain region, with additional preliminary analyses performed across diverse areas of the United States. Upper 90% prediction limits were used to define the *maximum likely flood potential* and to assess flood variability. The 90% prediction limits also identify extreme floods, with departure above this level denoting the degree of extremity. Indices were used to quantify the variability of flood hazards, with the areas with the greatest hazards (in increasing magnitude) being the Southern Rocky Mountains eastern slopes and adjacent Great Plains, the California Coastal Ranges, the Ozark Plateau, Puerto Rico, and the Edwards Plateau of Texas. This methodology shows promise for providing practitioners, managers, and the public with valuable additional information for developing more resilient stream valley communities. Additionally, this method provides indices and language that can enhance communication among scientists, for developing greater understanding of the mechanisms that cause large floods and how these mechanisms may change over time due to global warming.

Acknowledgements

Julian Scott and David Levinson contributed to this work; their efforts are highly valued. Additionally, both David Levinson and Ann Banitt are appreciated for their reviews of this report.

References

Beard, L.R. 1975. Generalized evaluation of flood potential. University of Texas, Austin, Center for Research in Water Resources. CRWW-124, pp 1-27.

Brogan, D.J., Nelson, P.A., MacDonald, L.H. 2017. Reconstructing extreme post-wildfire floods: a comparison of convective and mesoscale events. Earth Surface Processes and Landforms 42, 2505-2522, doi:10.1002/esp.4194.

Capesius, J.P., Stephens, V.C. 2009. Regional regression equations for estimation of natural streamflow statistics in Colorado. U.S. Geological Survey Scientific Investigations Report 2009–5136.

Daly, C., Halbleib, M., Smith, J.I., Gibson, W.P., Doggett, M.K., Taylor, G.H., Curtis, J., and Pasteris, P.A. 2008. Physiographically-sensitive mapping of temperature and precipitation across the conterminous United States, International Journal of Climatology, 28: 2031-2064.

Follansbee, R., & Sawyer, L.R. 1948. Floods in Colorado. U.S. Department of Interior, Geological Survey. Water Supply Paper 997.

Gochis, D., Schumacher, R., Friedrich, K., Doesken, N., Kelsch, M., Sun, J., Ikeda, K., Lindsey, D., Wood, D., Dolan, B., Matrosov, S., Newman, A., Mahoney, K., Rutledge, S., Johnson, R., Kucera, P., Kennedy, P., Sempere-Torres, D., Steiner, M., Roberts, R., Wilson, J., Yu, W., Chandrasekar, V., Rasmussen, R., Anderson, A., & Brown, B. 2015. The Great Colorado Flood of September 2013. Bulletin of the American Meteorological Society, 96, 1461–1487.

Hansen, E.M., Fenn, D.D., Schreiner, L.C., Stodt, R.W., & Miller, J.F. 1988. Probable maximum precipitation estimates – United States between the continental divide and the 103rd meridian. National Oceanic and Atmospheric Administration, Hydrometeorological Report No. 55A.

Hirschboeck, K.K. 1987. Catastrophic flooding and atmospheric circulation anomalies, in Mayer, L. and Nash, D.B., eds., Catastrophic Flooding, Allen & Unwin, pp 23-56.

Jarrett, R.D. 1990. Paleohydrolgic techniques used to define spatial occurrence of floods. Geomorphology 3, 181-195.

Jarrett, R.D. 2014. personal communication, Applied Weather Associates.

Kenney, T.A., Wilkowske, C.D., Wright, S.J. 2007. Methods for estimating magnitude and frequency of peak flows for natural streams in Utah. U.S Geological Survey Scientific Investigations Report 2007–5158.

Kimbrough, R.A., Holmes, R.R. 2015. Flooding in the South Platte River and Fountain Creek Basins in Eastern Colorado, September 9-18, 2013. U.S. Department of Interior, U.S. Geological Survey, Scientific Investigations Report 2015-5119.

Kohn, M.S., Stevens, M.R., Harden, T.M., Godaire, J.E., Klinger, R.E., Mommandi, A. 2016. Paleoflood investigations to improve peak-streamflow regional-regression equations for natural streamflow in Eastern Colorado, 2015. U.S. Geological Survey Scientific Investigations Report 2016-5099.

Koronowski, R. 2013 'Biblical' Amounts Of Rainfall Slam Colorado, Causing Death, Destruction, And Massive Flooding. https://thinkprogress.org/biblical-amounts-of-rainfall-slam-colorado-causing-death-destruction-and-massive-flooding-422e62aaa260/.

Miller, K.A. 2003. Peak-flow characteristics of Wyoming streams. U.S Geological Survey Water-Resources Investigations Report 03-4107.

Moody, J.A. 2016. Estimates of Peak Discharge for 21 Sites in the Front Range in Colorado in Response to Extreme Rainfall in September 2013. U.S. Geological Survey Scientific Investigations Report 2016-5003, doi:10.3133/sir20165003.

National Weather Service (NWS) 2013. Exceedance Probability Analysis for the Colorado Flood Event, 9 - 16 September 2013. National Oceanic and Atmospheric Administration, National Weather Service, Hydrometeorological Design Studies Center.

O'Connor, J.E., Costa, J.E. 2004. Spatial distribution of the largest rainfall-runoff floods from basins between 2.6 and 26,000 km2 in the United States and Puerto Rico. Water Resources Research 40, W01107, doi:10.1029/2003WR002247.
Osterkamp, W.R., Friedman, J.M. 2000. The disparity between extreme rainfall events and rare floods – with emphasis on the semi-arid American West. Hydrological Processes 14, 2817-2829.
PRISM Climate Group, Northwest Alliance for Computational Science and Engineering, 30-Year Normals. http://www.prism.oregonstate.edu/normals/ (accessed August 2018).
Schram, H., Wulliman, J.T., Rapp, D.N. 2014. Hydrologic Evaluation of the St. Vrain Watershed: Post September 2013 Flood Event. Prepared for the Colorado Department of Transportation, Region 4 Flood Recovery Office. Jacobs Engineering, Denver, Colorado.
Smith, J.A., Cox, A.A., Baeck, M.L, Yang, L., & Bates, P. 2018. Strange floods: The upper tail of flood peaks in the United States. Water Resources Research. doi:10.1029/2018WR022539.
U.S. Geological Survey (a). Peak Streamflow for the Nation. Retrieved from https://nwis.waterdata.usgs.gov/usa/nwis/peak (accessed August 2017).
U.S. Geological Survey (b). Peak Streamflow for the Nation. Retrieved from https://nwis.waterdata.usgs.gov/usa/nwis/peak (accessed October 2018).
U.S. Geological Survey (b). Watershed Boundary Dataset. Retrieved from https://nhd.usgs.gov/wbd.html (accessed December 2017).
Waltemeyer, S.D. 2008. Analysis of the magnitude and frequency of peak discharge and maximum observed peak discharge in New Mexico and surrounding areas. U.S Geological Survey Scientific Investigations Report 2008-5119.
Yochum, S.E., Sholtes, J.S., Scott, J.A., Bledsoe, B.P. 2017. Stream power framework for predicting geomorphic change: The 2013 Colorado Front Range flood. Geomorphology 292, 178-192.
Yochum, S.E., Scott, J.A., Levinson, D.H. In review. Methods for Assessing Expected Flood Potential and Variability: Southern Rocky Mountains Region. Water Resources Research.

Hydrologic Hazard Curve Development for Final Design and Risk Assessment

Keil J. Neff, Bureau of Reclamation, Technical Service Center, kneff@usbr.gov
Frank Dworak, Bureau of Reclamation, Technical Service Center, fdworak@usbr.gov
Amanda Stone, Bureau of Reclamation, Technical Service Center, astone@usbr.gov

Abstract

The Bureau of Reclamation (Reclamation) uses risk-informed decision-making to manage dam safety risks for over 350 high and significant hazard dams in the Western U.S. Hydrologic hazard curves represent loading conditions for dams and are developed to associate peak flows, flood volumes, and reservoir water surface elevations with annual exceedance probabilities (AEPs). These hazard curves and resultant frequency hydrographs are used in design of dam modifications and in risk analyses evaluating hydrologically-induced potential failure modes. Reclamation is currently implementing a phased approach for hydrologic hazard curve development using multiple methods dependent on the specific needs of the project/decision, available data, level of confidence and understanding of uncertainty needed, and complexity of the hydro-meteorological controls of the basin. One method/tool Reclamation has recently been using is the U.S. Army Corps of Engineer's Reservoir Frequency Analysis software (USACE RMC-RFA) to develop a reservoir elevation frequency with uncertainty bounds. This approach includes 1) defining critical flood seasons and critical durations within these flood seasons; 2) performing volume frequency analyses for critical durations in defined seasons; 3) representing appropriate reservoir routing characteristics and antecedent reservoir conditions; 4) developing representative flood hydrographs from historic record; and 5) running Monte Carlo simulations stochastically sampling inflow volume, hydrograph shape, seasonal occurrence, and antecedent reservoir water surface elevation. Development of reservoir frequency information using RMC-RFA will be presented in the context of Reclamation's development of hydrologic hazard curves for final design and dam safety risk assessments.

INTRODUCTION

Since 1995, Reclamation has used risk-informed decision-making to assess the safety of dams, recommend safety improvements, and prioritize capital improvements for over 370 high and significant hazard dams in its portfolio. As part of Reclamation's risk-based Dam Safety process, the need for hydrologic loading information for each dam is essential. From a hydrologic perspective, risk estimates require an evaluation of a full range of hydrologic loading conditions and possible failure mechanisms tied to consequences of failure (Reclamation, 2006). The flood loading input used in a dam safety risk analysis is typically a Hydrologic Hazard Curve (HHC) that is developed from a Hydrologic Hazard Analysis (HHA) (Reclamation, 2006). HHCs include frequencies related to peak inflow, volume, and reservoir water surface elevation (RWSE) and are plotted with respect to their Annual Exceedance Probability (AEP). Information derived in HHAs, including HHCs and associated flow and stage frequency hydrographs, can be used to assess the risk of hydrologically-influenced potential failure modes (PFMs).

When evaluating hydrologic hazards, a systematic means of developing flood frequency information is used for risk-based assessments (Reclamation, 2004). The nature of the PFM,

and characteristics of the dam, reservoir and watershed dictate the type of hydrologic information needed. The selected approach also considers available hydrologic data, potential analysis techniques, resources for analysis, and an acceptable level of uncertainty. For estimating less frequent AEPs, multiple types of data and methods of analysis are generally combined, and information are expanded temporally, spatially and causally (Merz & Blöschl, 2008).

In order to understand the potential range of hydrologic loadings, state-of-the-practice flood frequency relationships include an estimate of the uncertainty around the recommended flood loadings estimate (Beven and Hall, 2014). As the AEP decreases, the uncertainty in the loading increases; and for extreme floods, the uncertainty is commonly quite large and challenging to quantify. Floods may result from unusual combinations of hydrologic conditions generally not represented in the flood history at a particular location. Uncertainties occur because of limitations in hydrometeorological data, imperfect understanding of the physical processes, and numerical inadequacy to represent these processes (Beven and Hall, 2014). Uncertainty in flood loading estimates is typically represented by statistically-derived confidence intervals (often defining the 5% and 95% confidence limits). Understanding the uncertainty in the hydrologic loadings can become an important factor when the risk associated with hydrologically-driven PFMs is within an order of magnitude of the guidelines for annualized failure probability of the dam or annualized life loss (FERC, 2014).

Reclamation is currently implementing a phased approach of hydrologic hazard curve development using multiple methods dependent on the specific needs of the project/decision, available data, level of confidence and understanding of uncertainty needed, and complexity of the hydrometeorological controls of the basin. Reclamation primarily uses the following methods, and associated data, for flood frequency estimation: 1) Statistical flood frequency analyses (systematic stream gage data, historical flood data, paleoflood data); 2) Statistical precipitation frequency analysis and rainfall-runoff modeling (systematic precipitation data, systematic stream gage data, data describing physical basin characteristics (often geospatial; e.g. soils, land-use, elevation), paleoflood data); and 3) rainfall-runoff modeling (geospatial data, systematic stream gage data, systematic climate station data, SNOTEL data, paleoflood data, reservoir and routing information).

One tool Reclamation has recently been using is the Reservoir Frequency Analysis software (RMC-RFA; see Smith et al. 2018) to develop a reservoir elevation frequency with uncertainty bounds. This study reports flood frequency information derived using RMC-RFA in the context of Reclamation's development of hydrologic hazard curves for final design and dam safety risk assessments.

METHODS

The U.S. Army Corps of Engineer's Reservoir Frequency Analysis software (RMC-RFA; see Smith et al., 2018) was used to develop reservoir stage frequency with uncertainty bounds. This included 1) defining critical flood seasons and critical durations within these flood seasons; 2) performing volume frequency analyses for critical durations for defined seasons; 3) representing appropriate reservoir routing characteristics and antecedent reservoir conditions; 4) developing representative flood hydrographs from historic records; and 5) running stochastic simulations using Monte Carlo sampling to randomly sample inflow volume, hydrograph shape, seasonal occurrence, and antecedent reservoir water surface

elevation. Monte Carlo simulation samples from probability distributions of these parameters to better describe the uncertainty in the frequency model. The resulting flood hydrographs were routed considering a reservoir model (i.e. stage-storage-discharge curve). The peak reservoir elevation for each stochastic event was recorded and subsequently ranked to define annual exceedance probabilities of critical reservoir elevations.

Hydrometeorological Characterization

The subject dam and its large storage reservoir are located in Northern California. The watershed for the dam is large and spatially heterogeneous with respect to climate and hydrogeologic controls. Additionally, there is upstream regulation in the watershed in the form of dams/reservoirs and irrigation storage and conveyance. Northern California is well known for flooding events caused by heavy precipitation during winter storms or later in the season when snowpack at higher elevations melts (Reeves and Rotunno, 2008). The bulk of annual precipitation across the western United States occurs during winter months when the North Pacific storm track is most active, producing storms that can last for several days or more (Higgins et al., 2000). These storm systems interact with local terrain, producing regional characteristics in precipitation and flooding. A majority of cool-season precipitation in northern California occurs with landfalling atmospheric rivers and terrain-locked Sierra barrier jets (Ralph et al., 2016) interacting with complex topography.

Input Data

Data for reservoir stage frequency analysis included:

- Deregulated mean daily time series inflow record developed by the USACE as part of the 2002 Sacramento and San Joaquin River Basins Comprehensive Study (USACE 2002). This deregulated time series spans from October 1925 through July 2018 (figure 1).

- Daily mean reservoir stage data obtained from the California Data Exchange Center (figure 2). For this study, the vertical datum of the elevations reported are based on the 1988 North American Vertical Datum (NAVD88).

- Hourly 7-day inflow hydrographs of large floods in WY 1938 and 1940 flood developed from detailed records collected by the USGS. The 1938 flood hydrograph was recorded tabularly in the USGS Water-Supply Paper 843 (McGlashan and Briggs, 1939). The 1940 flood hydrograph was received via email communication with the USGS (2018).

Inflow Volume-Duration Frequency

For the evaluation of inflow volume frequency, annual maximum volumes for various durations were generated from the mean daily time series (see figure 1). These were generated considering the water year calendar (October 1–September 30) for the annual series and considering multiple potential critical seasons based on dominant storm systems and snow melt: December–March, January–April, December–May, and December–April. The inflow volume-frequency estimates were computed by fitting a Log-Pearson Type-III (LP III) distribution to the series of annual maximums (see Bulletin 17 C, England et al., 2018). The volume frequency-duration analysis was performed using the Hydrologic Engineering Center's Statistical Software Package (HEC-SSP Version 2.1.1; USACE, 2017).

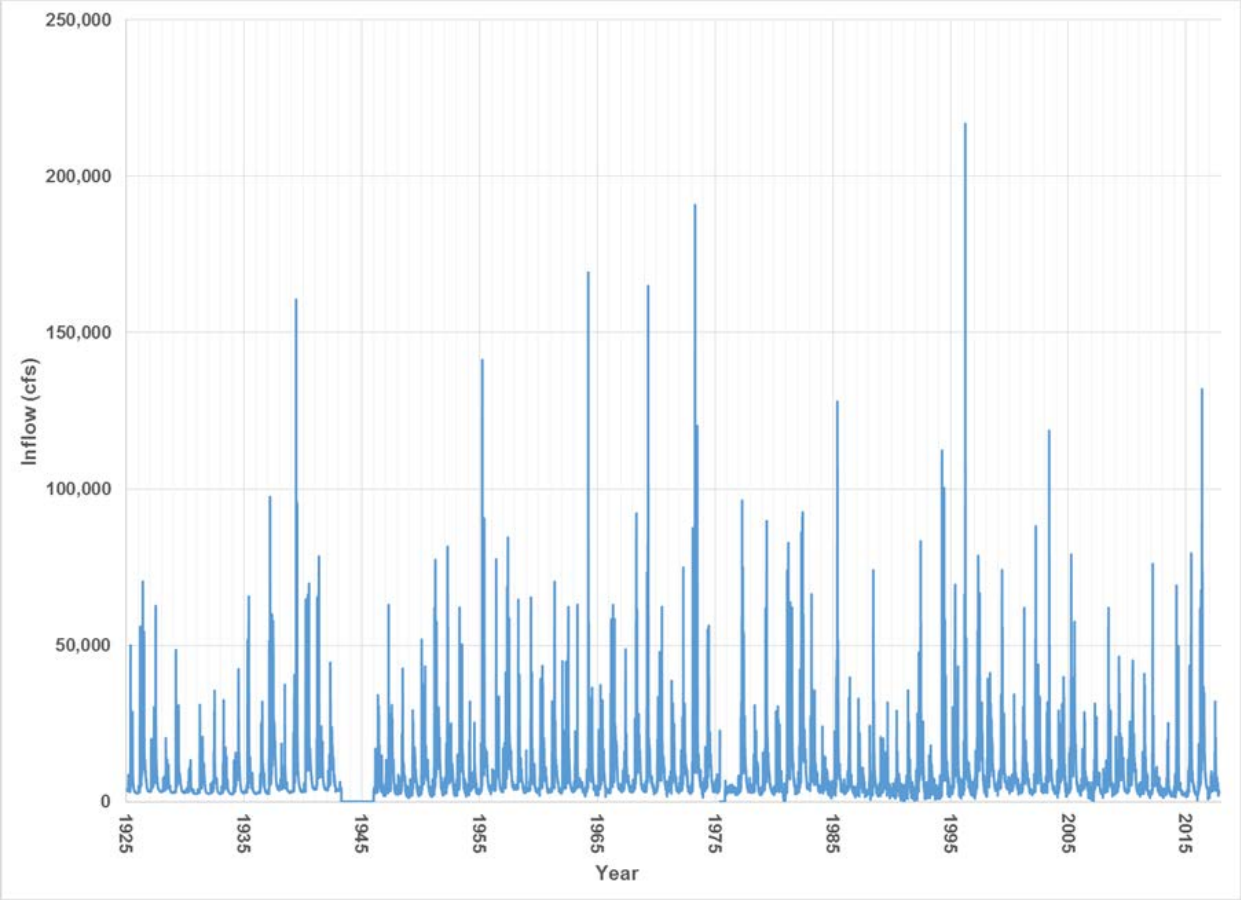

Figure 1. Mean daily time series inflow record.

Flood Seasonality and Critical Duration

The flood seasonality and critical flood duration are defined to best represent historic reservoir empirical data and hydrometeorological character of large floods impacting the site. Flood seasonality describes the frequency of occurrence of largest floods on a seasonal basis. In RMC-RFA, a starting reservoir stage is based on seasonality consistent with the time of year when floods are likely to occur. One important consideration is that the seasonal operations of the reservoir greatly influence the annual maximum stage, and for most years the maximum stage occurs a month or two later than when the peak inflows occur. Therefore, seasonality was evaluated for both peak inflow and reservoir stage. Also, the flood seasonality is dependent on the defined flood duration. The critical flood duration is the duration that results in the highest water surface elevation on average. Multiple flood durations considering water year annual maximums as well as in multiple flood seasons were evaluated with respect to historic observations and the influence on reservoir elevations.

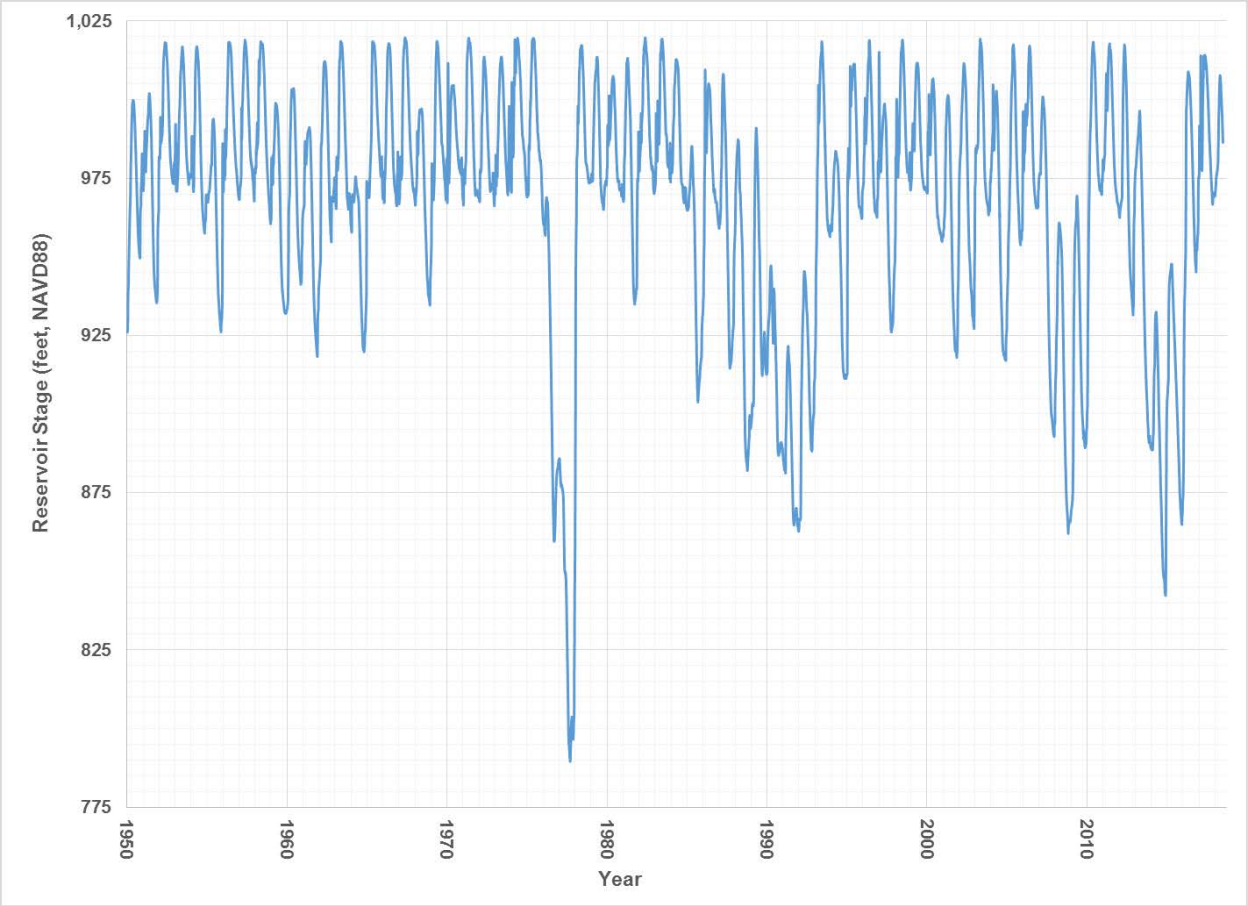

Figure 2. Daily mean reservoir water surface elevation.

Using an iterative process, the flood seasonality and critical duration were selected based on the loadings on the dam (evaluated in RMC-RFA for specified inflow volume-duration frequencies) and with respect to hydrometeorological conditions in the watershed.

Reservoir Model

Modified Puls is used as the reservoir routing method in RMC-RFA. This level-pool reservoir routing method requires specifying the storage and discharge associated with subject dam's reservoir pool elevations. As the operations are complex, multiple discharge rating curves were developed based on deterministic hydrographs and different initial reservoir water surface elevations. Within the range of discharge rating curves, a final elevation–discharge relationship for the existing condition (Figure 3) was defined based on an iterative approach to calibrate model results to empirical stage data in RMC-RFA.

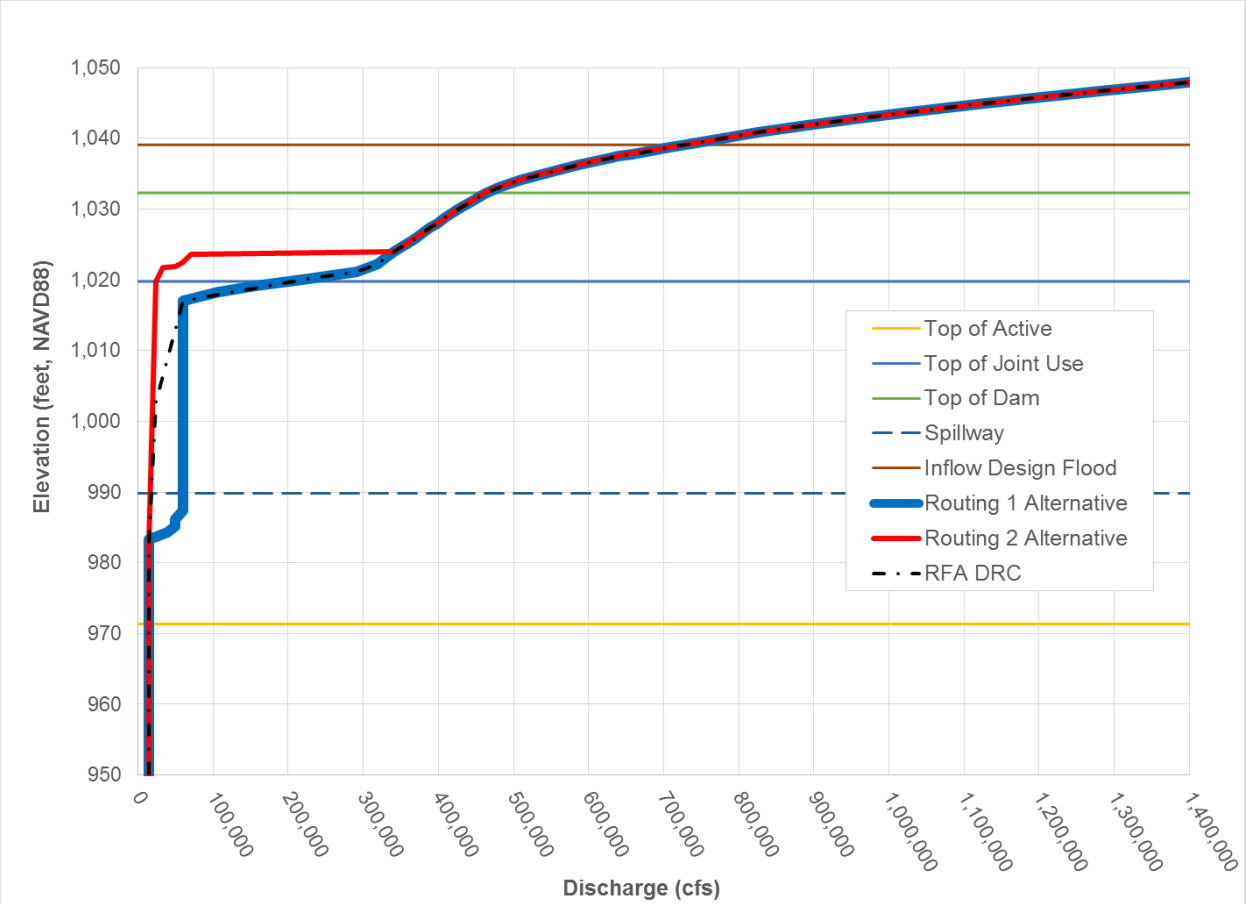

Figure 3. Discharge rating curve for subject dam.

Inflow Hydrographs

The WY 1938 and 1940 hourly 7-day flood hydrographs (figure 4) were selected to use for scaling the sampled inflow flood events because: (1) these were the only inflow hydrographs with less than a one day time step; (2) they occurred before construction of the subject dam and therefore did not require deregulation; and 3) were two of the largest floods of the historic record, representative of basin response to large storms. Historic daily inflow hydrographs from multiple years were also modeled in RMC-RFA to substantiate use of 1938 and 1940 hourly hydrographs. Considering daily hydrographs, using 1938 and 1940 daily hydrographs produced higher elevations than using deregulated daily hydrographs. Results using the selected hourly flood hydrographs produced the highest stage frequency elevations – at 10^{-4} AEP, elevations were approximately 1.5-ft higher for hourly 1938/1940 hydrographs than for daily 1938/1940 hydrographs. The two hydrograph shapes were given equal probability of occurrence in the RMC-RFA simulation since there was limited hydrograph data available for large events in the watershed to suggest a different weighting scheme. Results indicate that the stage-frequency curve was not particularly sensitive to these hydrograph shapes.

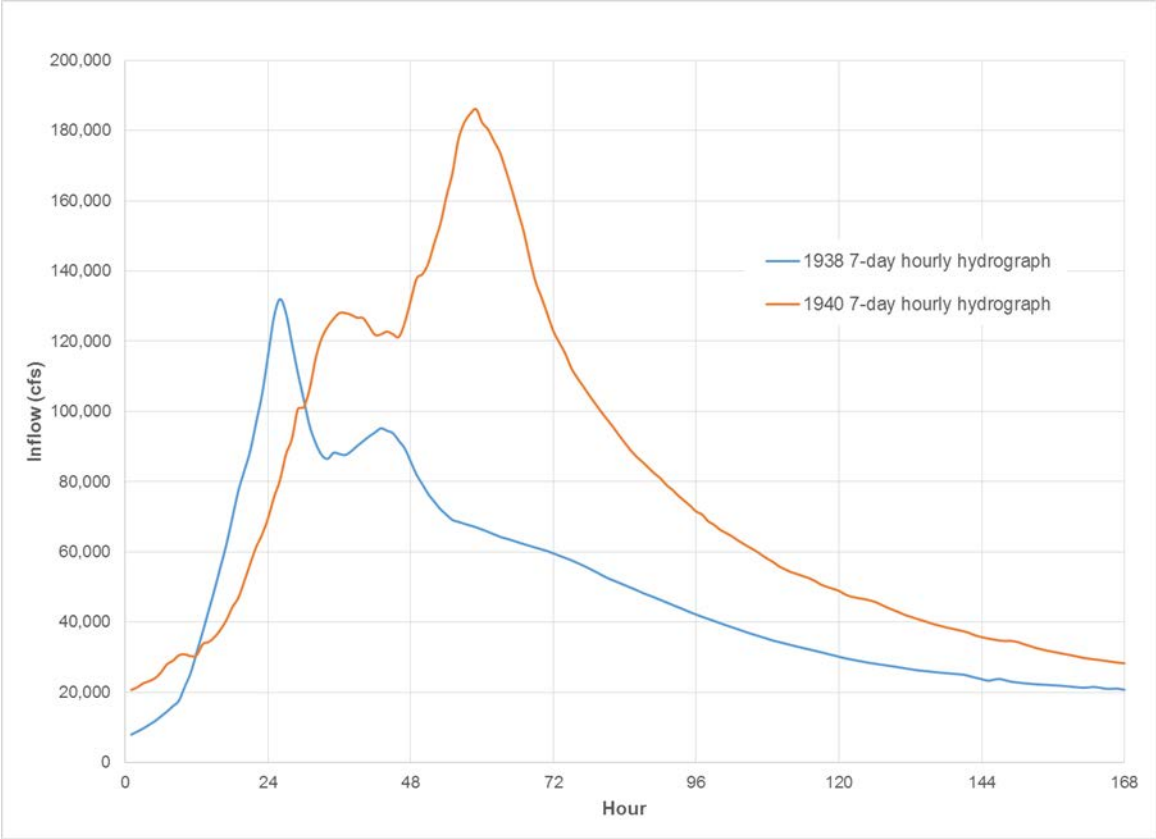

Figure 4. 1938 and 1940 7-day hourly inflow hydrographs.

Reservoir Stage-Frequency Analysis

The RMC-RFA model was used to produce reservoir stage frequency curves with uncertainty bounds considering seasonality based upon both peak stage and peak inflow. RMC-RFA utilizes a deterministic flood routing model while treating the inflow volume frequency, flood hydrograph shape, seasonal occurrence of the flood event, and antecedent reservoir stage as random variables rather than fixed values. The expected curves are considered the "best estimate" from the RMC-RFA simulations because it implies that on average the estimated probability for a given reservoir stage is correct. Additionally, frequency hydrographs were extracted from the simulations to be externally routed considering complex operational considerations.

Results

Inflow Volume-Duration Frequency

The mean, standard deviation, and skew coefficient were estimated from the available sample data; moments for the different durations are presented in Table 1.

Table 1. Inflow volume-duration frequency moments.

	Duration	Mean	SD	Skew
Annual	1-day	4.737	0.252	-0.18
	3-day	4.639	0.246	0.035
	5-day	4.569	0.246	0.036
	7-day	4.511	0.256	-0.218
	10-day	4.456	0.247	-0.227
	15-day	4.386	0.25	-0.403
	25-day	4.306	0.237	-0.448
	30-day	4.281	0.233	-0.436
Dec-April	1-day	4.735	0.25	-0.001
	3-day	4.63	0.257	-0.079
	5-day	4.563	0.254	-0.028
	7-day	4.511	0.252	-0.026
	10-day	4.456	0.242	-0.03
	15-day	4.38	0.256	-0.43
	25-day	4.302	0.242	-0.435
	30-day	4.277	0.237	-0.427

Flood Seasonality and Critical Duration

Based upon investigation of historic flood hydrographs considering the duration and timing of primary floods into the reservoir, and simulated peak reservoir stages in RMC-RFA, the critical flood duration was found to be 7 days with the critical season being from the beginning of December through the end of April. The flood seasonality histogram developed for this analysis can be seen in Figure 3. As the historic operations of the reservoir also greatly influence reservoir elevations, the occurrence of the highest reservoir elevations were also defined for the December–April flood season, in which approximately 85% of the peak stages occur in April (see Figure 4).

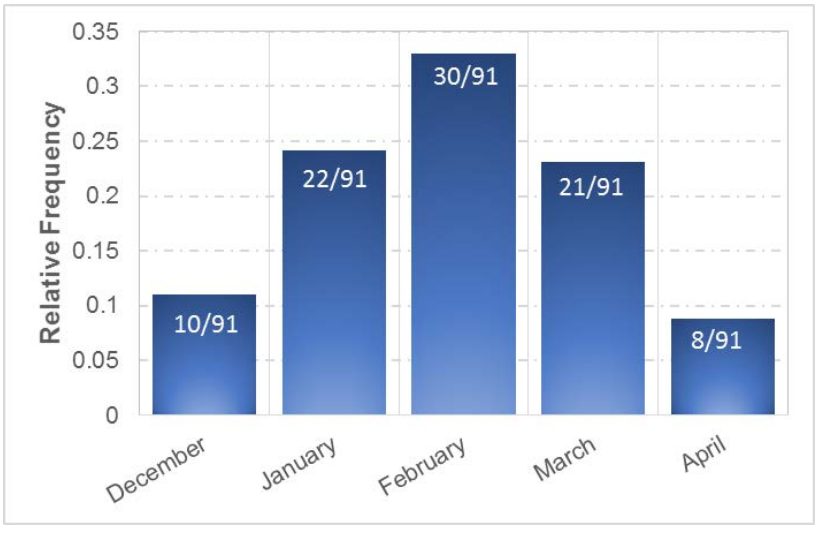

Figure 3. Flood seasonality histogram based on peak inflows into the reservoir during the December–April flood season.

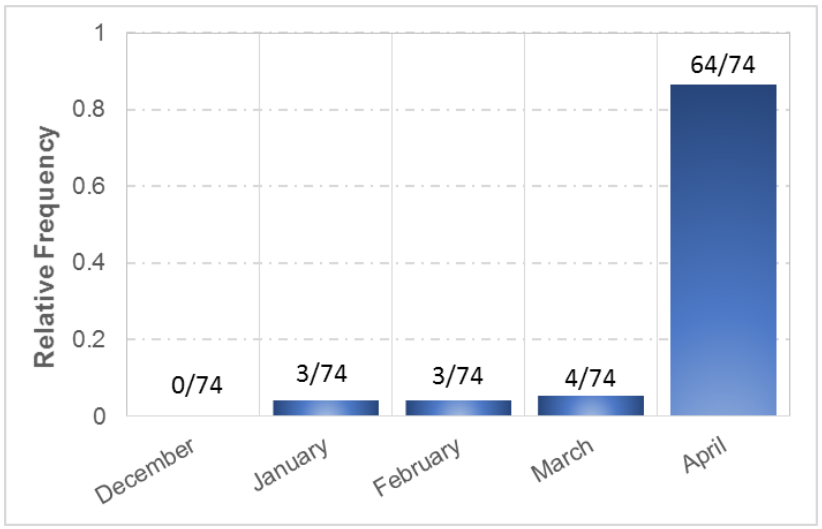

Figure 4 Flood seasonality histogram based on peak reservoir water surface elevations during December–April flood season.

Based on the critical flood season and duration, the volume-duration-frequency curve described above based on LP III distribution has a mean (of log) of 4.5110, a standard deviation (of log) of 0.2520, and a skew (of log) of -0.0260, with an effective record length defined as 93 years. Figure 5 shows the 7-day volume frequency relationship (median) and the 90-percent confidence interval (lower, 5%; upper, 95%) for the reservoir.

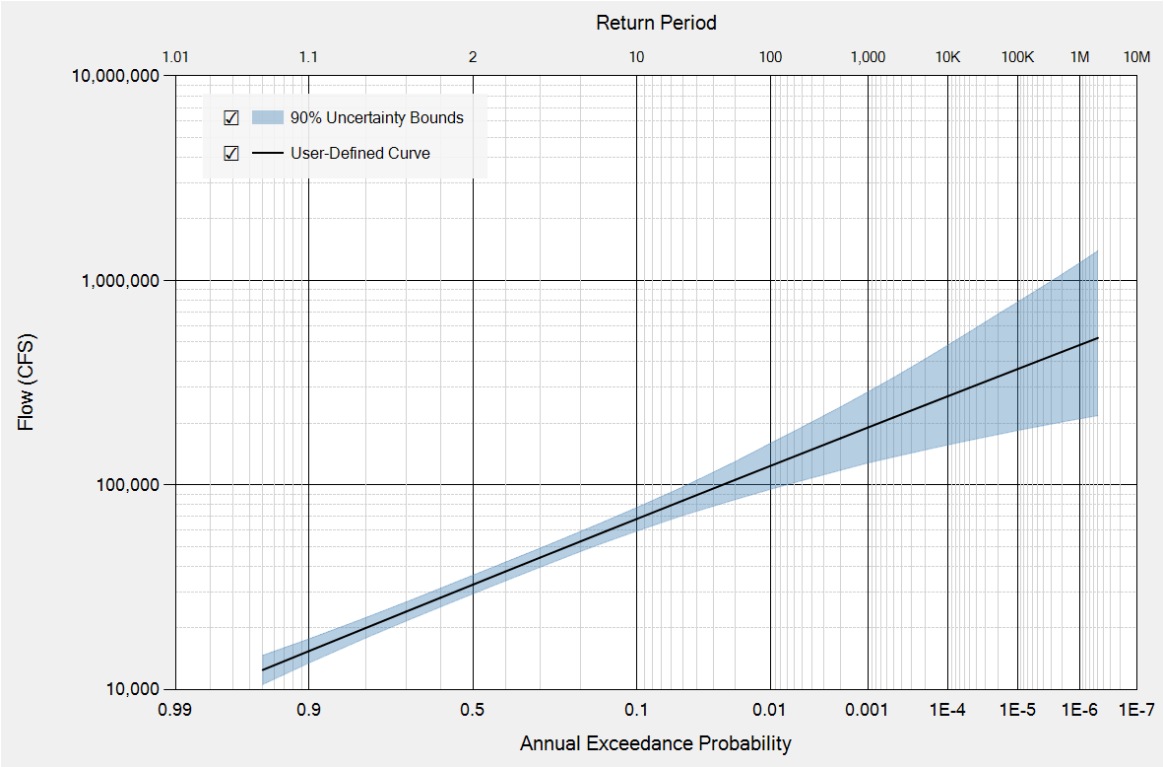

Figure 5. December through April 7-day volume frequency relationship.

Reservoir Stage-Frequency Results

Results for the existing condition are shown in Figure 6 (peak stage seasonality) and Figure 7 (peak inflow seasonality). Frequency hydrographs were developed from the expected reservoir frequency curve derived with peak stage seasonality as it corresponded well with empirical stage data.

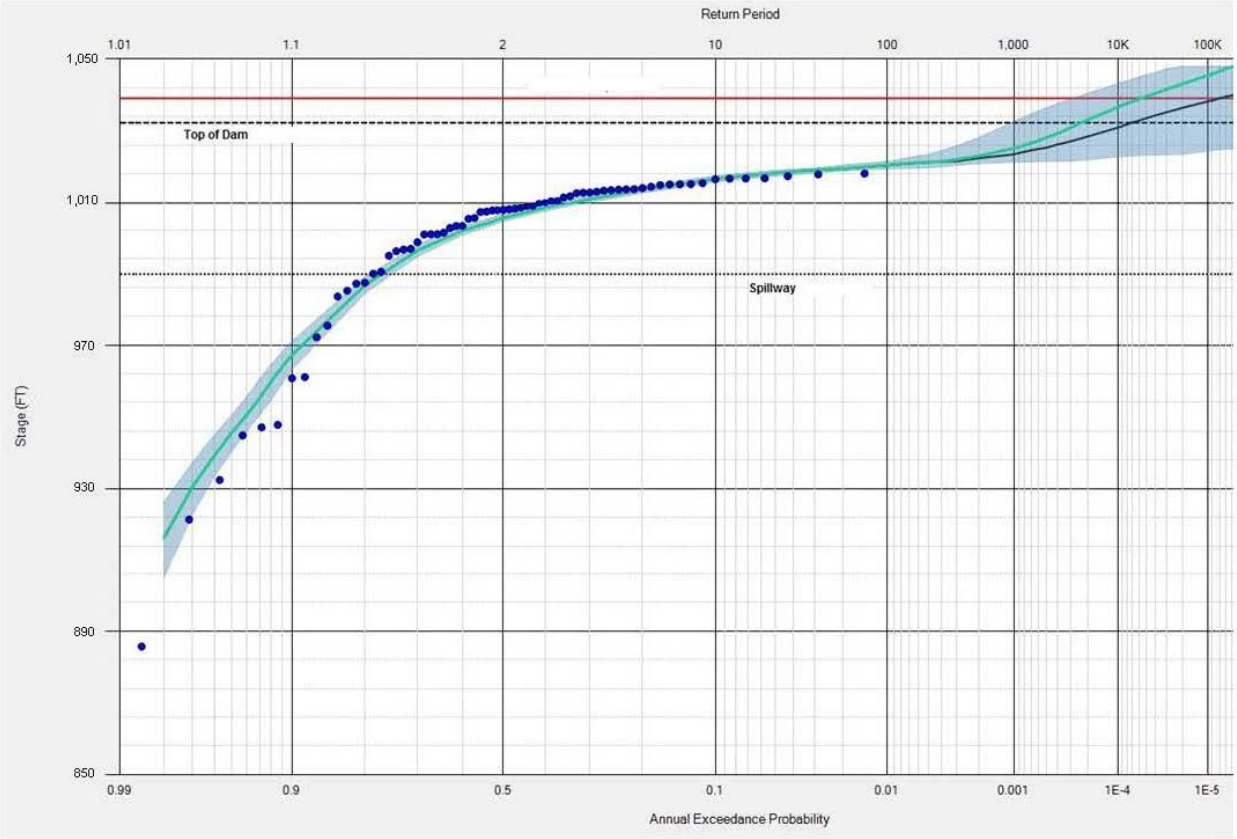

Figure 6. Stage frequency results considering stage seasonality. The expected curve (green line) and median curve (black line) are inside 90% uncertainty bounds (grey shaded area).

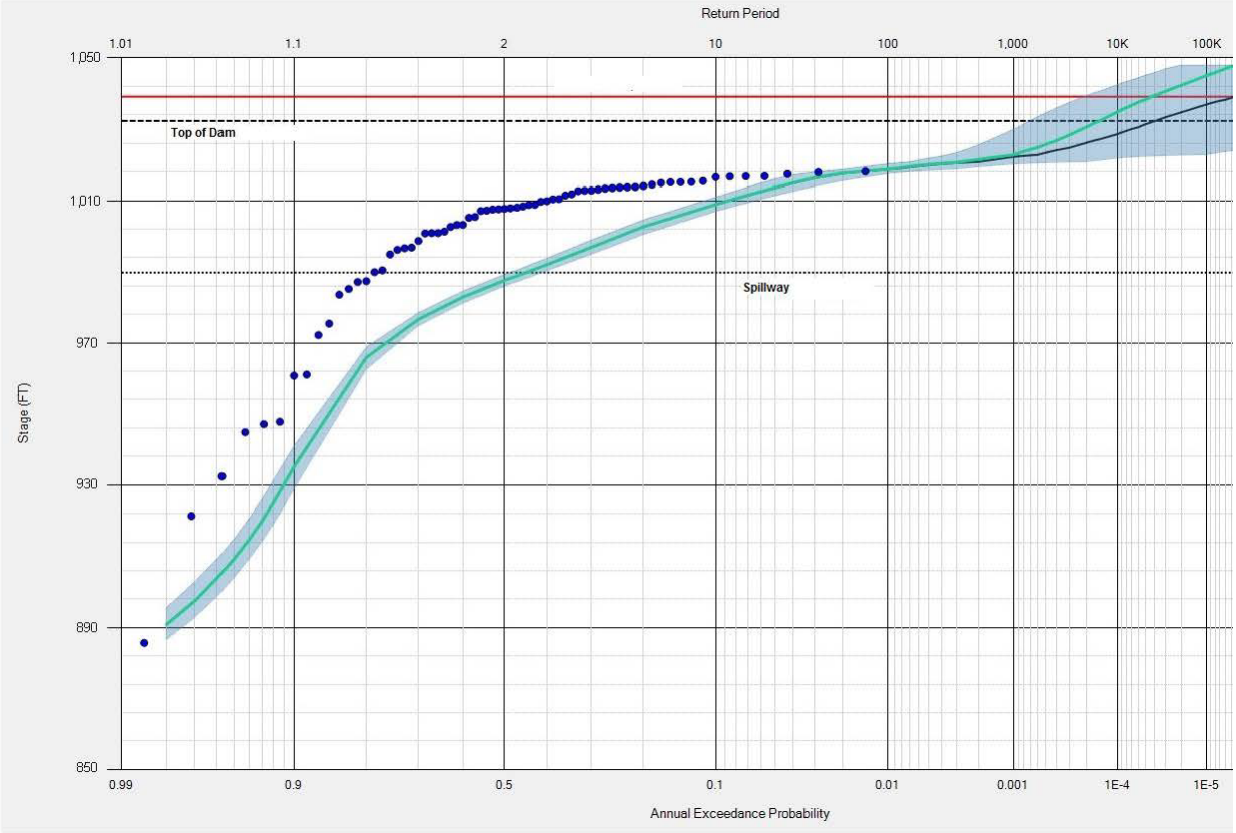

Figure 7. Stage frequency results considering inflow seasonality. The expected curve (green line) and median curve (black line) are inside 90% uncertainty bounds (grey shaded area).

DISCUSSION

The volume frequency analysis represented a comprehensive analysis using observed hydrologic data. Using RMC-RFA (Smith et al., 2018), and a 7-day critical duration and seasonality specific to the operations of the dam, frequency hydrographs developed from the expected reservoir frequency curve matched the empirical stage data quite well (see Figure 6). This is due to operational controls (seasonal guide curve) considering water availability and flood risk. Having the historic stage frequency observations represented well by the model provided confidence in the results. For more rare events, the flood frequency associated with peak inflow seasonality would be expected to control. Integrating the frequency curves derived from the different seasonality cases will be considered in a later phase of this project.

For this project, Reclamation used multiple methods to develop hydrologic hazard curves and associated frequency hydrographs. Multiple methods were applied to reduce the uncertainty and improve confidence of the results considering the complexity of the hydrometeorological and operational complexity of the watershed and reservoir. In addition to developing volume frequency and performing reservoir frequency analysis using RMC-RFA, Reclamation 1) performed a statistical flood frequency analysis using systematic stream gage data, historical flood data, and paleoflood data following techniques described in Bulletin 17C (England et al., 2018); and 2) applied statistical precipitation frequency analysis (L-moments, see Hosking and Wallace) and spatiotemporal storm templates developed from simulation of historic storms

using Weather, Research, and Forecasting (WRF) model (see Skamarock et al., 2008) and snowmelt model into rainfall-runoff model in an AEP-neutral framework. Although a stochastic rainfall-runoff component was not utilized due to project scheduling constraints, using the RMC-RFA model and the methodology outlined in this paper provided useful flood frequency estimates with uncertainty which could be used to inform design and risk assessment decisions.

REFERENCES

Beven, K. and Hall, J. (2014). Applied Uncertainty Analysis for Flood Risk Management, World Scientific Publishing Company, Imperial College Press, 684 p.

Bureau of Reclamation (Reclamation), (2004). "Hydrologic hazard curve estimating procedures, dam safety research program (DSO-04-08)," U.S. Department of the Interior, Bureau of Reclamation, Technical Service Center.

Bureau of Reclamation (Reclamation), (2006). "Guidelines for evaluating hydrologic hazards," U.S. Department of the Interior, Bureau of Reclamation, Technical Service Center.

England, J.F., Jr., Cohn, T.A., Faber, B.A., Stedinger, J.R., Thomas, W.O., Jr., Veilleux, A.G., Kiang, J.E., and Mason, R.R., Jr., (2018). Guidelines for determining flood flow frequency—Bulletin 17C, U.S. Geological Survey Techniques and Methods, book 4, chap. 5, 148 p.

Federal Energy Regulatory Commission (FERC), (2014). "Probabilistic Flood Hazard Analysis, Chapter 19, Ferc Engineering Guidelines, Risk-Informed Decision Making (Draft)," U.S. Department of Energy. p. 37.

Higgins, R.W., Schemm, J-K.E., Shi, W., and Leetmaa, A. (2000). "Extreme Precipitation Events in the Western United States Related to Tropical Forcing," Journal of Climate, 13, 793-820.

Hosking, J.R.M., and Wallis, J.R., (1997). "Regional frequency analysis - an approach based on L-moments," Cambridge University Press, New York, 224 p.

McGlashan, H.D., and Briggs, R.C. (1939). "Floods of December 1937 in Northern California, Water-Supply Paper 843," U.S. Geological Survey, Washington, D.C., 497 p.

Merz, R. and Blöschl, G. (2008). "Flood Frequency Hydrology: 1. Temporal, Spatial, and Causal Expansion of Information," Water Resources Research, 44(8).

Ralph, F.M., Cordeira, J.M., Neiman, P.J., Hughes, M. (2016). "Landfalling Atmospheric Rivers, the Sierra Barrier Jet, and Extreme Daily Precipitation in Northern California's Upper Sacramento River Watershed," Journal of Hydrometeorology, 17, 1905-1914.

Reeves, H.D. and Rotunno, M. (2008). "Dynamic Forcing and Mesoscale Variability of Heavy Precipitation Events over the Sierra Nevada Mountains," Monthly Weather Review, 135, 62-77.

Skamarock, W.C., Klemp, J.B., Dudhia, J., Gill, D.O, Barker, D.M., Duda, M.G, Huang, Y., Wang, W., and Powers, J.G., (2008) "A Description of the Advanced Research WRF Version 3," NCAR Tech. Note NCAR/TN-475+STR, 113 pp.

Smith, H., Bartles, M., and Fleming, M. (2018). "Hydrologic Hazard Methodology for Semi-Quantitative Risk Assessments – An Inflow Volume-Based Approach to Estimating Stage-Frequency for Dams," U.S. Army Corps of Engineers, Institute for Water Resources Risk Management Center.

United States Army Corps of Engineers (USACE), (2002). Sacramento and San Joaquin River Basins Comprehensive Study, Technical Studies Documentation. Appendices A through G. Sacramento District, California.

United States Army Corps of Engineers (USACE), (2017). Statistical Software Package, HEC-SSP, Version 2.1.1, June 2017. U.S. Army Corps of Engineers, Davis, California.

Improved Flow Frequency Techniques with Frequency-Based Storms and Bulletin 17C

Katherine Werner, Hydrologic Engineer, U.S. Army Corps of Engineers, Omaha, NE, Katherine.M.Werner@usace.army.mil

Introduction

This paper summarizes the hydrologic evaluation performed by the United States Army Corps of Engineers (USACE), Omaha District as part of the Elkhorn Basin Flood Plain Management Services (FPMS) Flood Risk Identification Study. The Elkhorn Basin FPMS Study is a collaborative effort between the Nebraska Department of Natural Resources (NeDNR), the USACE, and the Federal Emergency Management Agency (FEMA) Region VII. The Elkhorn River is located in northeastern Nebraska, covers approximately 7,000 square miles, and includes 11 Federally Constructed Levees, 5 high hazard dams, and dozens of NFIP participating communities. Previous flood risk information in the basin was developed specific to different communities or decisions, such as National Flood Insurance Program (NFIP) Mapping and levee management (O&M, risk screening, NFIP certification, and 408 modifications). Unfortunately these different studies used various methods which lead to inconsistent data. One of the reasons for no previous basin wide evaluation is the basin itself, with a large area and precipitation gradient, basin modeling is a challenge. With efforts to remap the area in the NFIP, expected levee certification efforts, transportation improvement efforts, and recent flooding in 2010, it was recognized that there was a need for updated, consistent information.

The purpose of the hydrologic analysis was to develop peak flow frequencies (2-, 5-, 10-, 25-, 50-, 100-, 200-, 500-year, and 100-plus) and corresponding hydrographs throughout the Elkhorn River Basin. Peak flow frequencies were estimated at over a dozen gages throughout the watershed using Bulletin 17C guidelines. Additionally, a gridded hydrologic model of the Elkhorn watershed using Hydrologic Engineering Center Hydrologic Modeling System (HEC-HMS) was developed, calibrated, and simulated with frequency-based design storms to estimate peak flow frequencies and associated hydrographs at 372 computation points throughout the watershed. This paper is based on a more detailed 2018 report (USACE 2018).

Flow Frequency

In the United States, the guidelines for conducting statistical flow frequency analysis were updated with the release of Bulletin 17C (England Jr., et al. 2015). For the Elkhorn Basin sufficient length of record was defined as gages having at least 20 years of peak streamflow data. Sufficient length of record enables the development of statistically based frequency estimates of reasonable reliability. Long-term data is extremely valuable and generally provides the most reliable basis for frequency determinations.

In many cases the statistical-analysis procedures of Bulletin 17C are of limited use for estimating discharge because few streams are gaged, there are insufficient length of records, and the procedures do not provide information about runoff volume and timing. Consequently, in many cases an alternative analysis procedure is required. A common alternative analysis procedure

relies upon the use of rainfall of a specified annual exceedance probability (AEP), coupled with a model that transforms rainfall to runoff (USACE 2000). With this method, the rainfall AEP is often assumed to equal the AEP of runoff. However, in addition to rainfall, runoff is a function of loss rates and baseflow, the magnitudes of which vary with time and antecedent moisture conditions. The runoff generated by a particular storm will be a function of the state of the watershed when the storm occurs. A major storm occurring on a very dry watershed can result in moderate runoff, and a moderate storm on a saturated watershed can result in substantial runoff. Streamflow peaks of a specified frequency can be caused by an infinite number of combinations of storms and watershed states. Due to the uncertainty of the design-storm runoff frequency, it is best to utilize statistically based frequency information wherever possible to 'calibrate' the exceedance frequency with particular combinations of design storms and loss rates (USACE 1994).

This report documents the Bulletin 17C flow frequency analysis that was performed for all gages with at least 20 years of data and the use of the Bulletin 17C results to calibrate the HEC-HMS model that utilized NOAA Atlas 14 frequency-based hypothetical storms. The report highlights the development of the frequency-based design storms with particular emphasis on how the Hydrologic Engineering Center Meteorologic Visualization Utility Engine (HEC-MetVue) software was utilized.

Hydrologic Model

The Elkhorn River extends from the headwaters located in the eastern Sandhills and enters the Platte River as a left bank tributary just southwest of Gretna, Nebraska. The Elkhorn River subbasins were delineated based on NeDNR hydrography and HUC12 boundaries using the Hydrologic Engineering Center Geospatial Hydrologic Modeling Extension, HEC- GeoHMS (USACE 2013). Additional delineations were created based on stream gage locations, levees, and several dams of interest. Peak flow frequencies and hydrographs were created for 372 computation points which were comprised of 265 subbasin outlets, 5 reservoirs, and 102 stream convergences. Figure 1 illustrates the final watershed delineations of the Elkhorn Basin.

The gridded hydrologic model was created using the Green and Ampt soil loss method, the ModClark transform method, the recession and linear reservoir baseflow methods, the simple surface method, and the Muskingum routing method. Due to its ability to capture surface-groundwater interaction and its mass volume conservation, the linear reservoir baseflow was utilized to capture the unique hydrology of the Nebraska Sandhills. The Sandhills cover portions of the western Elkhorn River Basin where average soil hydrologic conductivity values range up to 7 inches per hour.

2010 Calibration

The hydrology model was calibrated to the June 2010 event; the flood of record for several gages. The 2010 event calibration was completed to identify which parameters should initially be calibrated as well as to formulate a foundation of better initial parameter estimates. The June 2010 event was modeled using hourly Multisensor Precipitaion Estimates (MPE) (Seo and Maidment 1998) (Krajewski 1987) that were further temporally distributed based on fifteen minute National Centers for Environmental Information (NCEI) (DOC/NOAA/NESDIS/NCDC 2016) precipitation data taken from eleven rain gages throughout the Elkhorn basin. Watershed parameters were adjusted to best reproduce the timing, peak, and volume of the observed flood

hydrographs at nine gages. The calibrated parameters included storage, initial content, ModClark storage coefficient, groundwater layer one and two coefficient, recession, ratio, Muskingum K, and loss fraction. Overall, the event calibration was very good with seven of the eight gages having a Nash-Sutcliffe Efficiency (NSE) value over 0.7.

Frequency-Based Hypothetical Storms

Once the model was calibrated to the June 2010 event, the frequency-based hypothetical storms were developed. These design storms are necessary inputs for HEC-HMS to determine the peak flow frequencies and corresponding hydrographs at the hundreds of computation points throughout the Elkhorn River Basin. The frequency-based hypothetical storms were developed based on NOAA Atlas 14 point frequency precipitation.

Precipitation Gradient

Over the Elkhorn Basin, an east-west precipitation gradient is present, and for the 24-hour, 100-year event the point precipitation varies up to two inches across the watershed. To capture the precipitation gradient over the watershed, a compatible gridded version of the NOAA Atlas 14 point precipitation was developed. Figure 2 illustrates the ArcGIS model used to obtain the gridded Hydrologic Engineering Center Data Storage System Visual Utility Engine (DSS) output, a format that HEC-HMS can recognize and use.

Temporal Disaggregation

A common approach to temporally distribute precipitation is a balanced hyetograph where the depth for each duration interval of the storm keeps the relation between the depth and duration for a given frequency. Although such storms do not preserve the random character of natural storms, using the alternating block method ensures an appropriate frequency depth regardless of the time-response characteristics of a particular watershed (USACE 1994).

When using the HEC-HMS frequency-based hypothetical storm, HEC-HMS uses the alternating block method to automatically temporally disaggregate the user specified point precipitation depths. However, a frequency-based hypothetical storm developed in HEC-HMS is limited by the watershed size (maximum of 400 square miles). Due to the size of the Elkhorn Basin, the frequency-based hypothetical storms were temporally distributed outside of HEC-HMS. A temporal pattern that would later be applied to all the hypothetical storms was created in HEC-HMS using NOAA Atlas 14 point precipitation depths for a central location (100 year, 24 hour duration event). Using the frequency storm method, a hyetograph pattern was developed which would be used to distribute all the precipitation grids.

To apply the hyetograph pattern to the NOAA Atlas 14 precipitation depths, the DSS file containing the gridded depths was loaded into HEC-MetVue. Each storm was temporally disaggregated using the hyetograph pattern tool shown in Figure 3. The aggregate Triangulated Irregular Network (TIN) start and end dates were arbitrarily selected but defined to be one day (24 hours) apart. The output type was selected as “SHG grid in DSS file”; and after the DSS paths and location were defined, the tool was run for each return period.

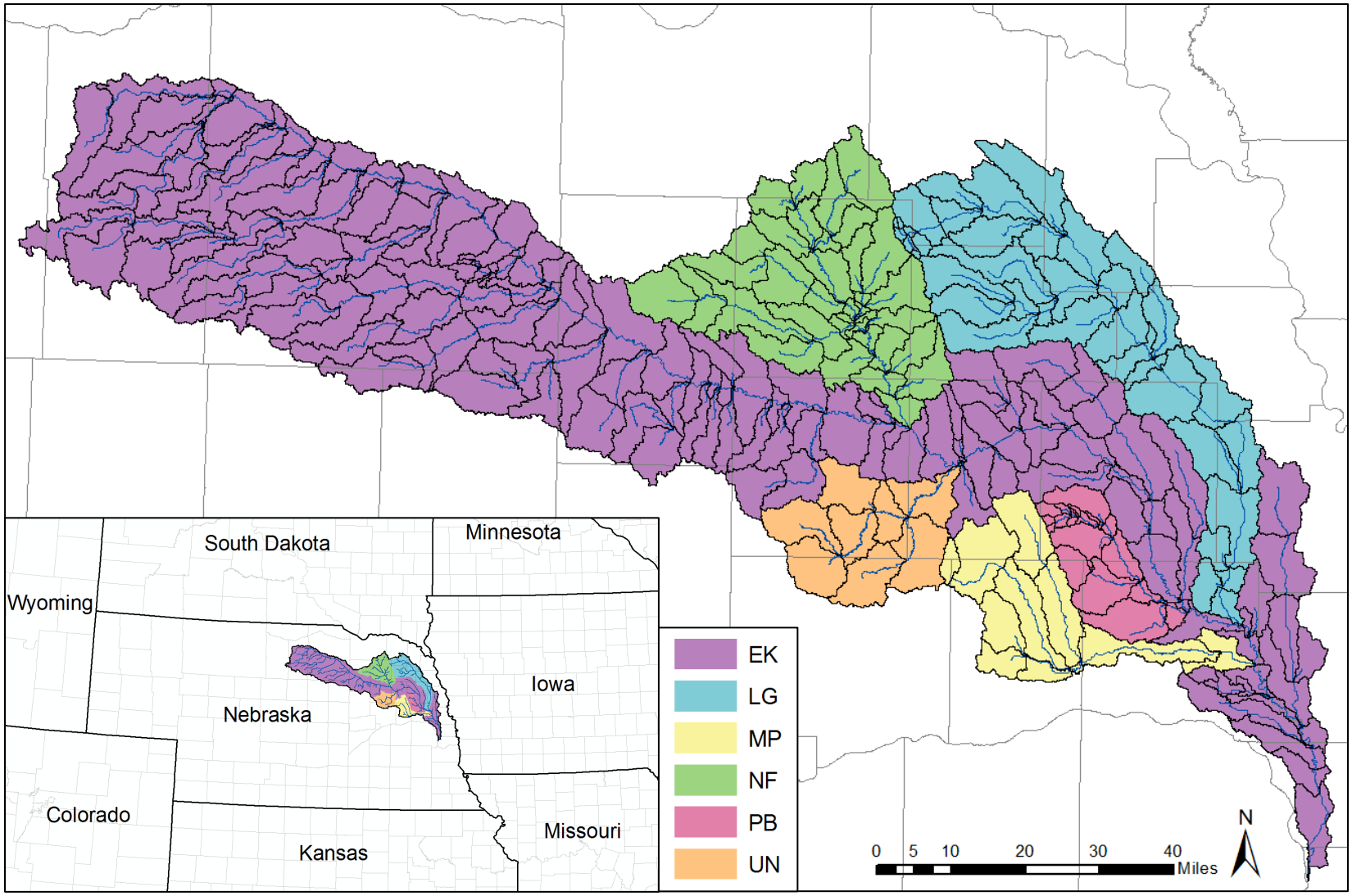

Figure 1. Final subbasin delineations of the Elkhorn Basin located in northeastern Nebraska.

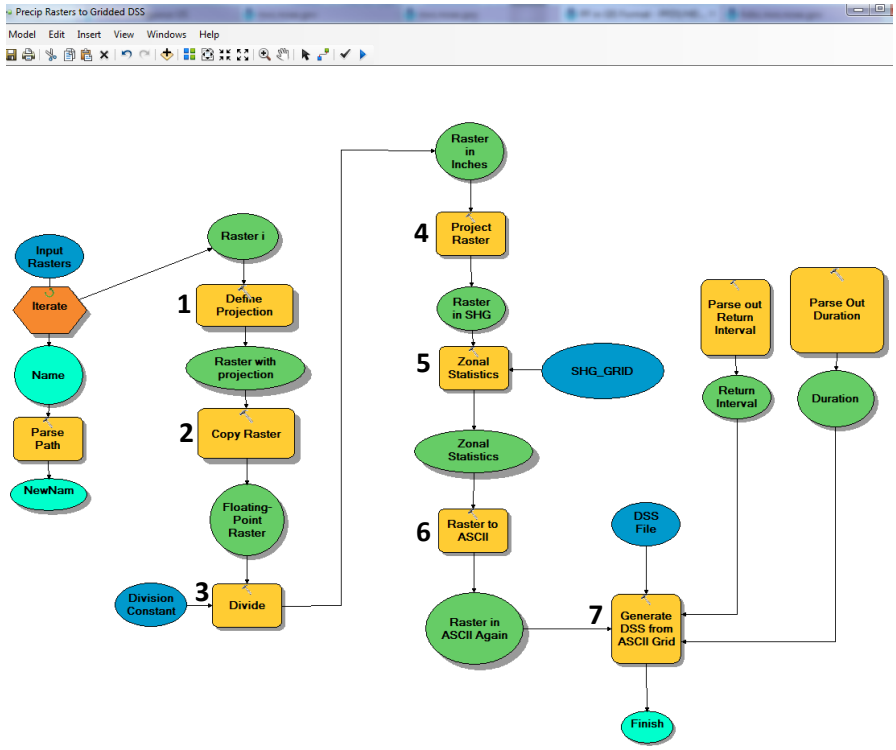

1. Define Projection (Projection was defined as GSC_North_American_1983.)
2. Copy Raster (The raster data was converted into floating-point values.)
3. Divide (The raster values were divided by a division constant (1000) to obtain inches.)
4. Project Raster (The raster was projected to the SHG coordinate system.)
5. Zonal Statistics (The average point precipitation was found for each SHG zone/grid cell. The SHG zones/grid cells were based on a file created during the GeoHMS processing that are 2,000 x 2,000 meters.)
6. Raster to ASCII (The final raster was converted to ascii format.)
7. Generate DSS from ASCII Grid (The ascii file was converted and saved to a DSS file.)

Figure 2. The GIS model implemented to batch process the NOAA Atlas 14 point precipitation depths. The numbered steps correspond to those in the text.

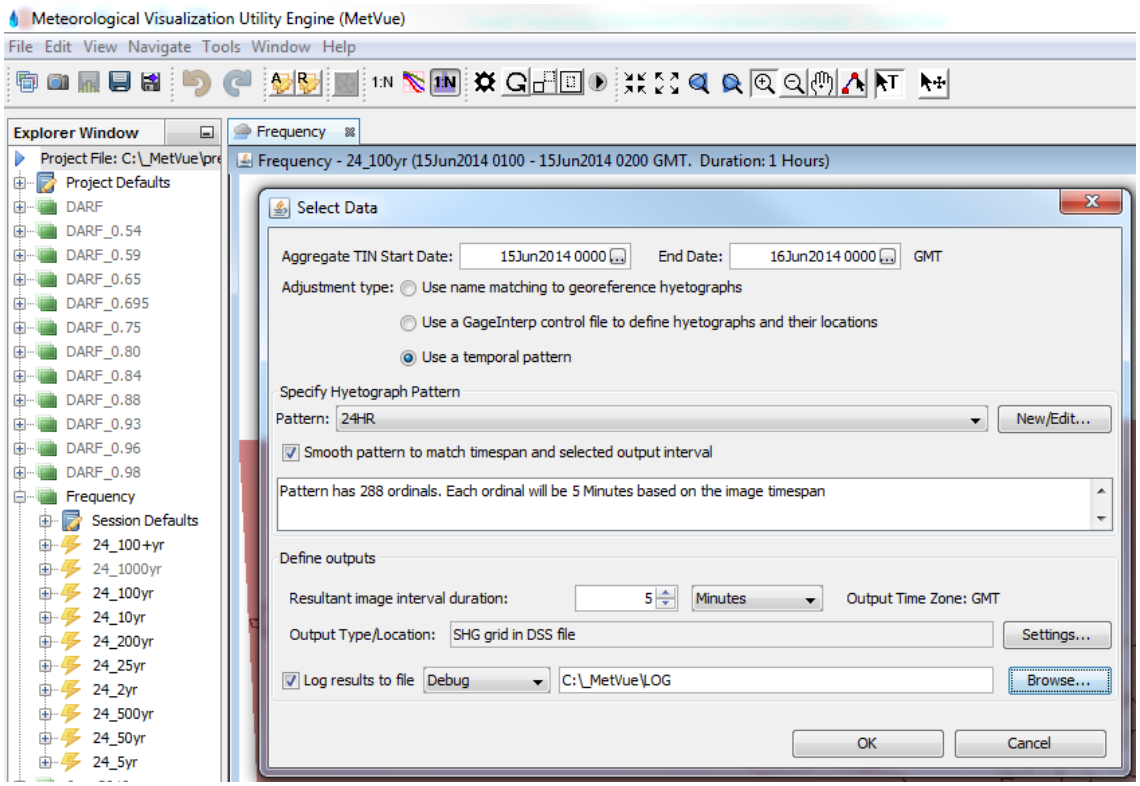

Figure 3. HEC-MetVue window where a hyetograph temporal pattern is applied to SHG precipitation depth.

Depth-Area Reduction

In order to appropriately apply the NOAA Atlas 14 point frequency precipitation, areal reduction factors are used to transform a point rainfall depth to an equivalent rainfall depth over a given area. In HEC-HMS, these areal reduction factors are built in for drainage areas up to 400 square miles. However, due to the size of the Elkhorn Basin (7,000 square miles), it was necessary to develop a site specific depth-area reduction curve which would be applied outside of HEC-HMS.

Dozens of storms across a region with similar hydrometeorological characteristics were analyzed based on gridded hourly MPE data. Figure 4 illustrates the approximate regional boundary, along with the approximate centers of the storms that were initially considered. Figure 5 shows the three major steps in the analysis of each storm which included the spatial examination of the storm to create isohyets, the development of the depth-area curve, and the generation of the final depth-area reduction factors. The spatial analysis and depth-area curve development for each storm was done prior to this study as part of an ongoing effort by USACE to develop an extreme storm database. The storm's depth-area reduction factors were found by dividing the depths (from the depth-area curve) by the storm's corresponding maximum rainfall depth.

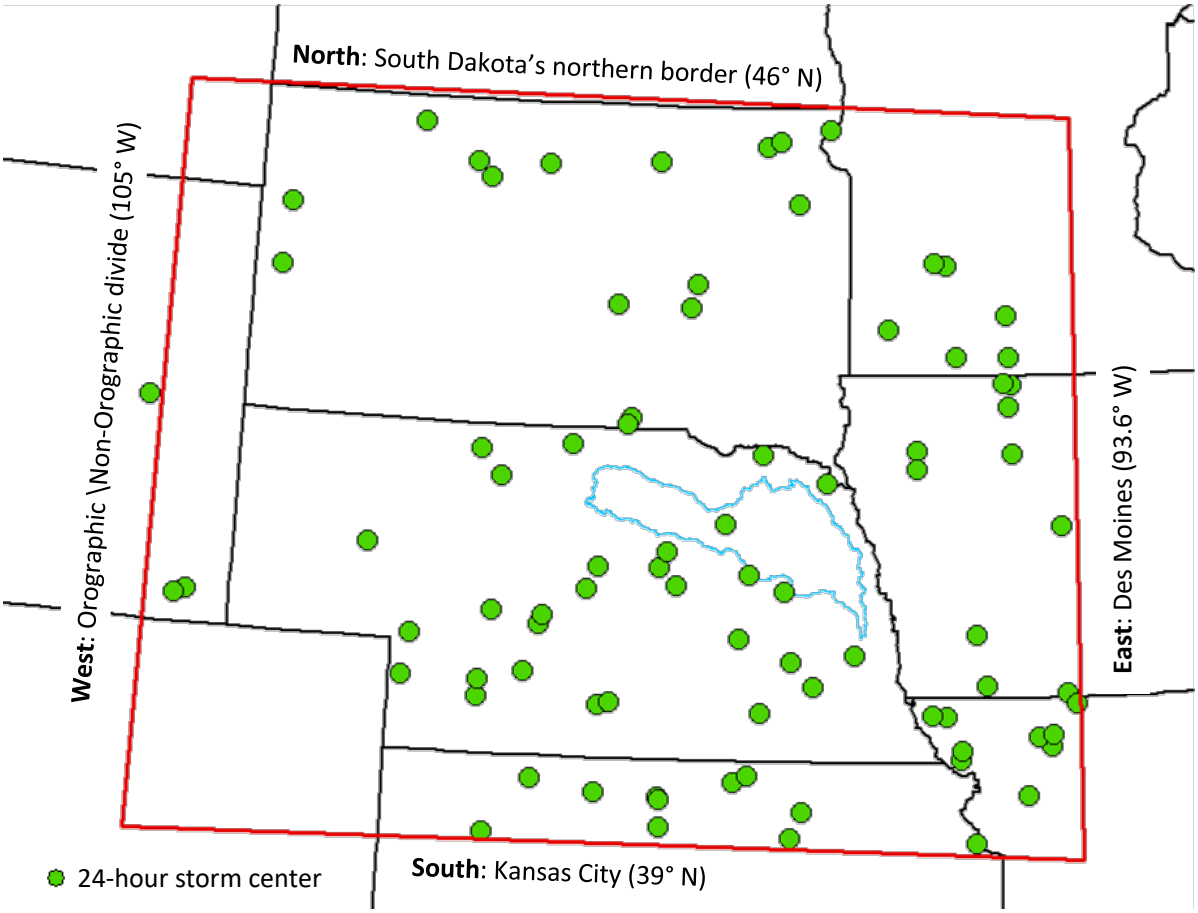

Figure 4. The 24-hour historical storm centers in green; with the Elkhorn Basin boundary in blue and the approximate storm boundary in red.

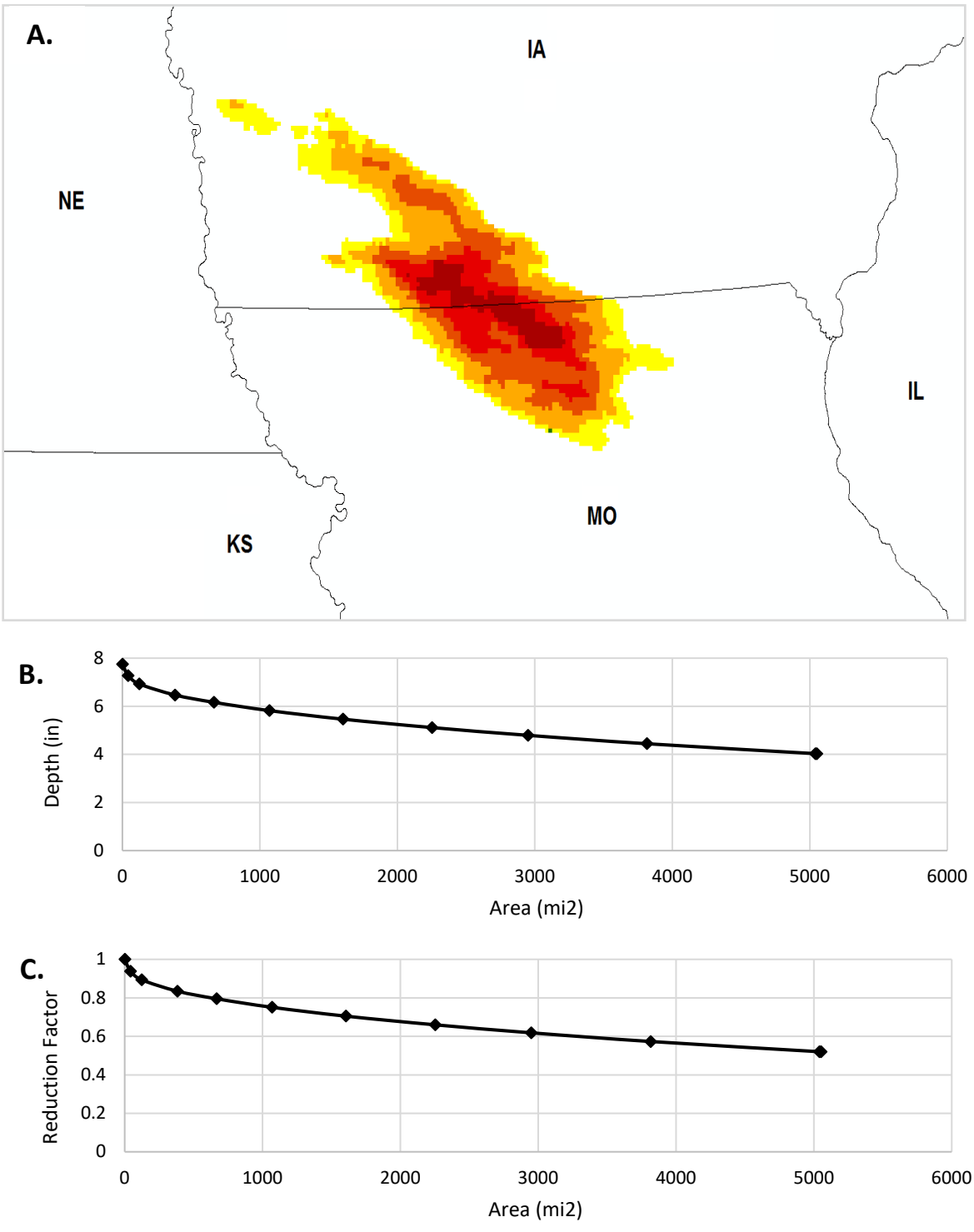

Figure 5. The analysis for each storm included: (A) spatial analysis of the storm to create isohyets, (B) development of depth-area curves, and (C) generation of the final depth area reduction curves.

The site specific 24-hour depth area reduction curve was based on an analysis of 84 storms. To provide a conservative but representative curve, a number of the lower storms were omitted. Based on the remaining storms and with more weight on those storms closer to the Elkhorn Basin, a new areal reduction curve was developed and determined to be the best representation for the Elkhorn Basin. For modeling purposes, a step function was developed to break the smoothed depth-area reduction curve into nearly a dozen area increments. The stepped area increments reasonably represent the depth-area reduction values for all the computation points (within 3%) and significantly reduces the number of model runs necessary to produce results for all the computation points.

Figure 6 displays the depth-area reduction curves of all the 24-hour storms that were analyzed and indicates the low curves that were excluded. Additionally, the figure shows the adopted curve and corresponding stepped curve used for modeling. The computation points are also plotted along the adopted curve to provide a visual comparison to the stepped curve.

Using the stepped 24 hour depth-area reduction curve, rainfall depths are reduced by as much as 41% depending on the drainage area. For tributary areas less than 20 square miles, no area correction was applied. Between 20 and 30 square miles, a 2% reduction was applied to all upstream basins. Between 30 and 60 square miles, a 4% reduction was applied to all upstream basins. This process continues as shown in Table 1 for all the computation points in the model to determine the appropriate precipitation reduction ultimately used to determine the appropriate peak discharge.

The depth-area reduction factors were applied to the temporally distributed, gridded frequency storms within HEC-MetVue. By right clicking and selecting “Adjustment Measurement Values for entire TIN”, the depth-area reduction factor was applied with “Multiply Measurement by a Constant Value” selected. Figure 7 shows this step in MetVue which was done for each return period (2-, 5-, 10-, 25-, 50-, 100-, 200-, 500-year, and 100 plus), for each Depth Area Reduction Factor (DARF) (0.98, 0.96, 0.93, 0.88, 0.84, 0.80, 0.75, 0.695, 0.65, and 0.59). Therefore, a total of 99 hypothetical storms (9 return periods x 11 DARFS) were created and saved. An HEC-HMS model was created for each DARF which each contained the nine frequency events. The outputs of each simulation were filtered with python scripts to obtain only the pertinent flows.

Bulletin 17C Analysis

The Bulletin 17C analysis was performed using Hydrologic Engineering Center Statistical Software Package (HEC-SSP) version 2.1. Bulletin 17C uses annual maximum discharge to calibrate a log-Pearson Type III statistical model and uses the computed statistical curve to predict flows of particular annual exceedance probabilities (England Jr., et al. 2015). For each gage, a weighted skew was determined utilizing the station skew and a regional skew taken from Soenksen, et al. (Soenksen, et al. 1999). The Bulletin 17C analysis was performed for fourteen streamgages within the Elkhorn River Basin. Figure 8 indicates the location, Table 2 lists the pertinent information, and Table 3 provides the peak flow results for each gage.

Frequency Calibration

Once the Bulletin 17C analysis was completed and the frequency-based hypothetical storms were developed, the HEC-HMS model was calibrated to Bulletin 17C peak flows. Engineering Manual 1110-2-1417 Flood-Runoff Analysis states that it is best to utilize statistically based frequency

information wherever possible to calibrate the exceedance frequency with particular combinations of design storms and loss rates (USACE 1994). Therefore, the 2010 HEC-HMS model was further calibrated using the results from the Bulletin 17C analysis. The Bulletin 17C analysis also included several additional gage locations which improved the calibration.

Table 4 gives the calibrated peak flows along with the Bulletin 17C analysis peaks for the suite of return intervals. The table also provides the percentage of how much higher (positive) or lower (negative) the calibrated peak flows are in comparison to the Bulletin 17C results. According to FEMA's Guidance for Flood Risk Analysis and Mapping, the proposed base flood discharges from the rainfall-runoff model are considered reasonable if they are generally within one standard error (68-percent confidence interval) of the regression or gaging station estimates (FEMA 2018). Thus, the objective for this calibration was to have the modeled peak flows within one standard error or closer to the Bulletin 17C peak flows.

Nearly all of the gages and return periods met this objective, and those flow that did not were considered not applicable and not included in the report. The peak flows for the 2-, 5-, and 10-year events were underestimated along the main stream where drainage areas are greater than 2,500 square miles. As described further in the full report, the high frequency events are likely caused by intense, localized events; thus, their results are not applicable and are not included.

Flow Frequency Results

After the model was calibrated to the Bulletin 17C peak flows, it was used to predict peak discharges for the suite of return periods including the 2-, 5-, 10-, 25-, 50-, 100-, 200-, and 500-year and the 100 plus at the hundreds of computation points throughout the Elkhorn River Basin.

A comparison to several Flood Insurance Studies (FIS) within the Elkhorn Basin was completed as part of the FPMS study. The FIS peak flows were all estimated about 20 to 50 years ago using methods that have since been superseded. Because of the updated methods and increased period of record, the new Bulletin 17C and HMS peak flows differ greatly from those currently in the FIS reports. Figure 9 plots the HMS, FIS, Bulletin 17C, and regression peak flows for the 100-year event. The figure also includes the 68% confidence intervals for Bulletin 17C and regression.

All of the HMS peak flows with Bulletin 17C results, fall within the 68% CIs. Many of the HMS peak flows also fall within the regression 68% CIs. For nearly all the HMS peak flows that do not fall within the regression CIs, the HMS estimates are closer to the regression CIs than the FIS estimates. Additionally, half of the locations that have Bulletin 17C results have HMS peak flows that fall within the Bulletin 17C 68% CIs, but not the regression CIs. This indicates that the regression estimates may be overestimating or underestimating the peak flows in various locations. With this in mind, it was concluded that the peak HMS flows are considered reasonable.

A final note is that caution should be taken to ensure the proper use of this model and results. There are a multitude of complexities and assumptions built into the model that are not readily apparent. These limitations are further detailed in the full report.

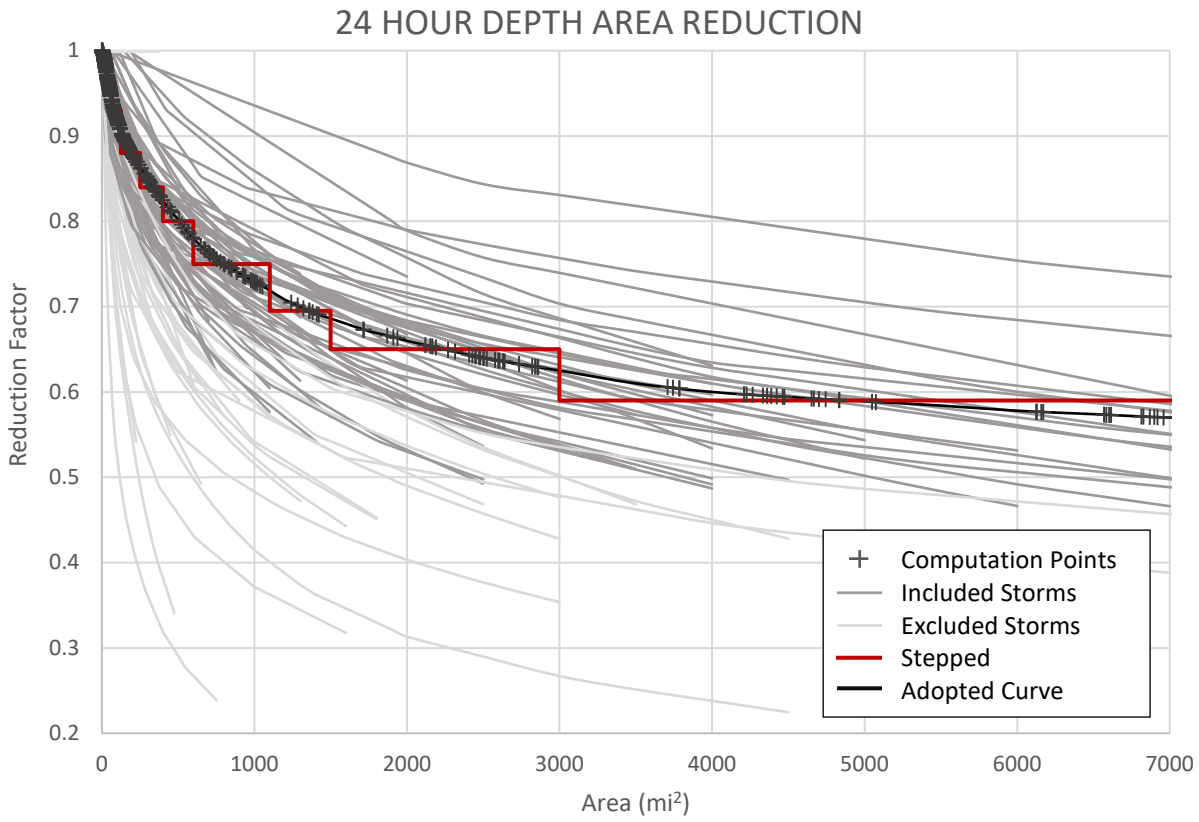

Figure 6. The depth-area reduction curves of regional 24-hour storms and the final depth-area reduction curves.

Table 1. Stepped area increments and depth area reduction factor.

Area Range (mi²)		DARF
0	20	1.0
20	30	0.98
30	60	0.96
60	125	0.93
125	250	0.88
250	400	0.84
400	600	0.80
600	1100	0.75
1100	1500	0.695
1500	3000	0.65
3000	7000	0.59

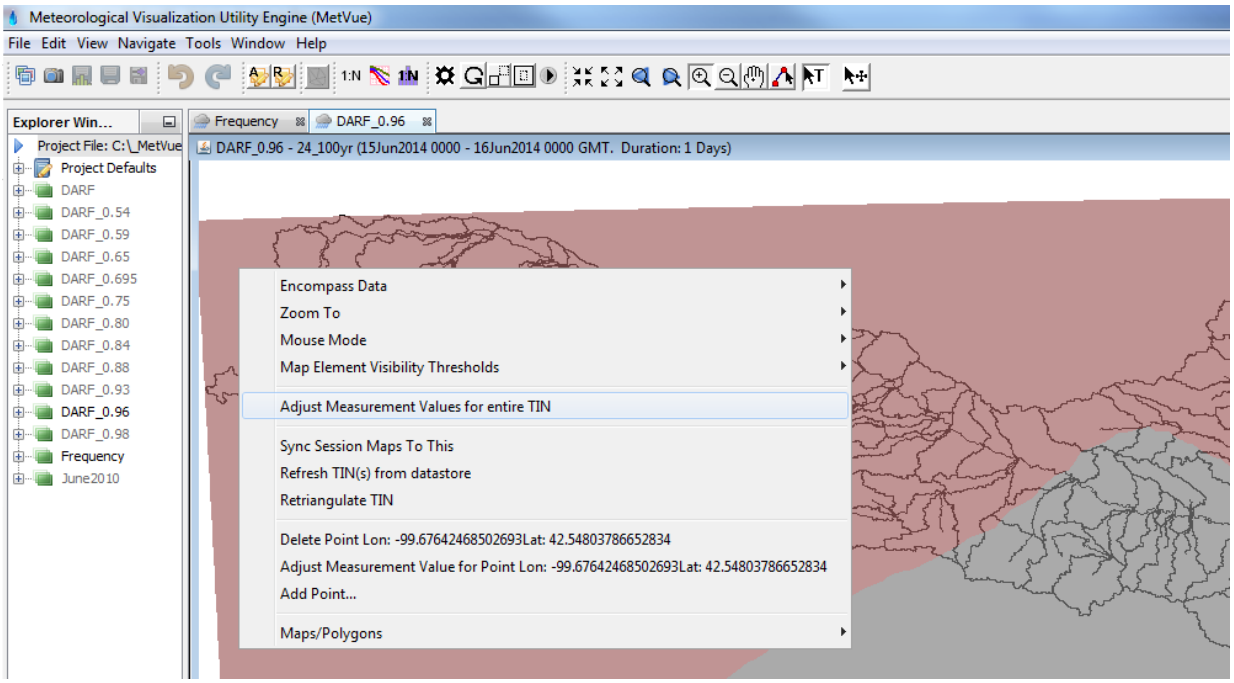

Figure 7. Applying the DARFs within HEC-MetVue by adjusting the measurement values for the entire TIN.

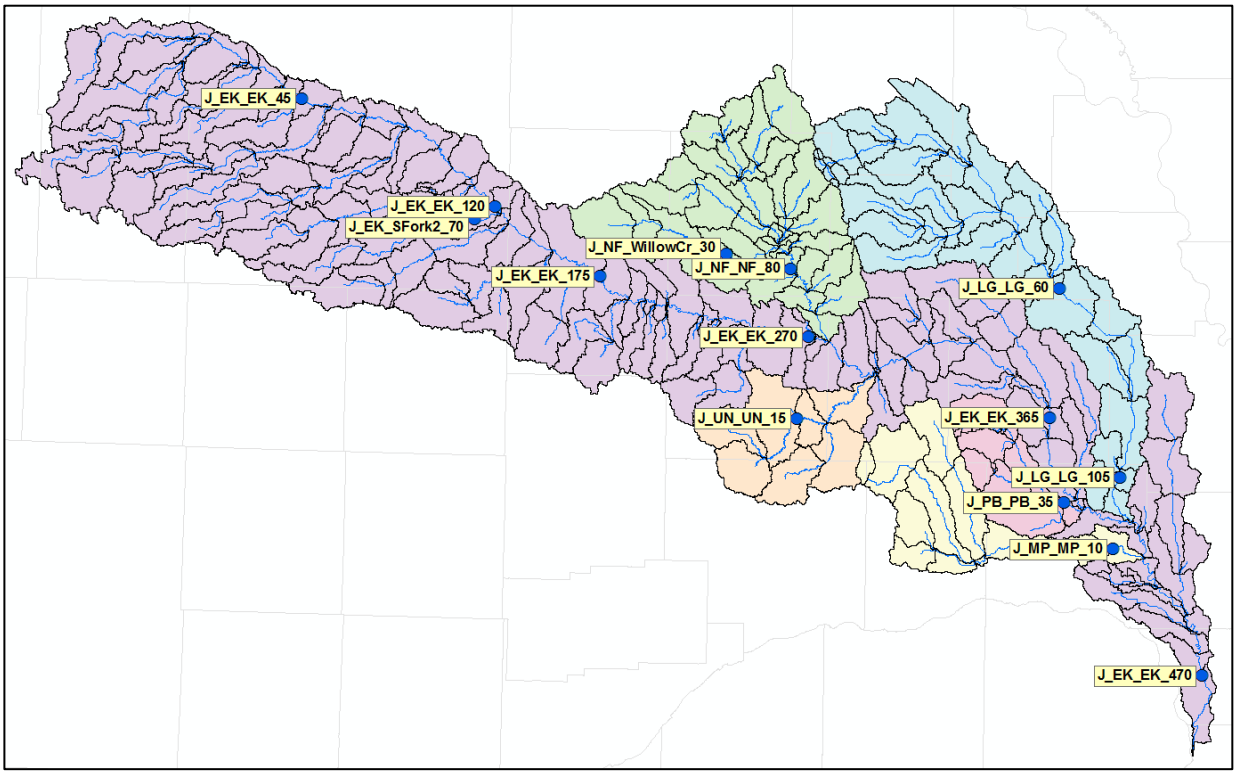

Figure 8. Locations of the fourteen streamgages within the Elkhorn Basin used for the Bulletin 17C analysis, all meeting the threshold of at least 20 years of annual peak flows.

Table 2. Fourteen streamgages within the Elkhorn Basin used for the Bulletin 17C analysis with corresponding pertinent information.

Location	Gage ID	JUNCTION	Lat.	Lon.	Start	End	No. of Events	Regional Skew	MSE	Upstream Area (mi^2)	DARF
Atkinson	06796973	J_EK_EK_45	42.486	-98.911	1983	2015	33	-0.01	0.024	570	0.80
Ewing	06797500	J_EK_EK_120	42.268	-98.339	1943	2015	68	-0.03	0.024	1409	0.695
Ewing	06798000	J_EK_SFork2_70	42.241	-98.398	1943	2015	58	-0.04	0.024	278	0.84
Neligh	06798500	J_EK_EK_175	42.125	-98.031	1932	2015	83	-0.05	0.024	2270	0.65
Norfolk	06799000	J_EK_EK_270	42.004	-97.426	1897	2015	83	-0.23	0.024	2840	0.65
Pierce	06799100	J_NF_NF_80	42.149	-97.479	1961	2015	55	-0.17	0.024	707	0.75
Foster	06799080	J_NF_WillowCr_30	42.177	-97.667	1976	2015	40	-0.07	0.024	139	0.88
Madison	06799230	J_UN_UN_15	41.831	-97.455	1979	2015	37	-0.3	0.024	174	0.88
West Point	06799350	J_EK_EK_365	41.839	-96.727	1961	2015	55	-0.31	0.024	4651	0.59
Scribner	06799385	J_PB_PB_35	41.659	-96.684	1979	2015	37	-0.28	0.024	207	0.88
Pender	06799450	J_LG_LG_60	42.114	-96.702	1966	1993	50	-0.33	0.024	737	0.75
Uehling	06799500	J_LG_LG_105	41.713	-96.522	1940	2013	75	-0.3	0.024	1008	0.75
Nickerson	06800000	J_MP_MP_10	41.561	-96.541	1944	2015	64	-0.24	0.024	372	0.84
Waterloo	06800500	J_EK_EK_470	41.293	-96.284	1899	2015	96	-0.2	0.024	6919	0.59

Table 3. Bulletin 17C computed peak flows (cfs) for given percent ACEs at various gages throughout the Elkhorn watershed.

ACE (%)	Atkinson	Ewing	Ewing SFork	Neligh	Norfolk	Pierce	Foster	Madison	West Point	Scribner	Pender	Uehling	Nickerson	Waterloo
0.2	25,564	35,149	15,603	46,559	42,079	17,560	1,685	28,691	74,438	74,830	46,237	27,787	28,979	96,259
0.5	17,879	25,108	10,951	33,638	33,740	13,662	1,330	22,459	62,263	58,802	38,405	24,454	23,506	79,483
1	13,292	19,015	8,184	25,746	28,036	11,077	1,091	18,249	53,522	47,883	32,755	21,926	19,713	67,689
2	9,601	14,030	5,960	19,241	22,831	8,785	877	14,462	45,184	37,997	27,355	19,385	16,210	56,641
4	6,676	10,002	4,195	13,934	18,103	6,765	686	11,088	37,241	29,136	22,216	16,823	12,986	46,307
10	3,791	5,919	2,441	8,474	12,541	4,484	466	7,241	27,318	18,974	15,834	13,372	9,133	33,667
20	2,221	3,615	1,474	5,329	8,812	3,025	322	4,774	20,188	12,439	11,313	10,658	6,501	24,774
50	790	1,404	566	2,209	4,380	1,395	156	2,055	10,954	5,247	5,647	6,690	3,303	13,489
80	277	544	219	924	2,109	625	74	832	5,689	2,054	2,627	4,023	1,620	7,140
90	159	331	134	588	1,421	407	50	505	3,968	1,220	1,711	3,030	1,100	5,062
95	101	219	90	405	1,019	283	36	330	2,919	781	1,183	2,375	793	3,788
99	42	101	42	203	537	142	19	144	1,603	325	570	1,470	421	2,166

Table 4. Peak flows (cfs) for the calibrated suite of events at various streamgages, along with the Bulletin 17C results, and a comparison table giving the percentage of how much greater (positive) or lower (negative) the calibrated peaks are compared to the 17C peaks.

CALIBRATED HMS PEAK FLOWS (cfs)

Return Interval (yr)	Atkinson	Ewing	Ewing Sfork	Neligh	Norfolk	Pierce	Foster	Madison	West Point	Scribner	Pender	Uehling	Nickerson	Waterloo
100+	26,068	36,375	15,765	45,868	47,682	18,124	1,712	28,056	71,872	75,925	46,458	27,813	29,428	97,085
500	26,189	36,615	15,986	46,242	48,125	18,280	1,776	29,478	74,302	75,577	47,243	28,404	30,018	100,017
200	17,909	26,122	11,452	34,961	37,025	13,993	1,370	23,216	63,764	60,163	39,468	25,068	24,172	83,389
100	13,771	19,862	8,397	27,454	30,330	11,340	1,130	18,782	54,648	49,382	34,138	22,463	20,071	70,908
50	9,928	14,687	6,082	20,049	24,389	9,025	915	15,109	46,338	39,163	29,043	19,914	16,333	60,598
25	6,813	10,458	4,261	14,834	18,958	6,853	709	11,658	37,811	30,305	23,253	16,981	13,306	49,077
10	3,918	6,045	2,480	8,956	12,672	4,614	484	7,614	NA	19,615	16,595	13,479	9,356	NA
5	2,244	3,664	1,482	5,660	9,288	3,084	335	5,001	NA	12,802	11,751	10,831	6,717	NA
2	800	1,422	574	2,337	4,565	1,434	NA	2,173	NA	5,410	5,919	6,898	3,394	NA

BULLETIN 17C PEAK FLOWS (cfs)

Return Interval (yr)	Atkinson	Ewing	Ewing Sfork	Neligh	Norfolk	Pierce	Foster	Madison	West Point	Scribner	Pender	Uehling	Nickerson	Waterloo
500	25,564	35,149	15,603	46,559	42,079	17,560	1,685	28,691	74,438	74,830	46,237	27,787	28,979	96,259
200	17,879	25,108	10,951	33,638	33,740	13,662	1,330	22,459	62,263	58,802	38,405	24,454	23,506	79,483
100	13,292	19,015	8,184	25,746	28,036	11,077	1,091	18,249	53,522	47,883	32,755	21,926	19,713	67,689
50	9,601	14,030	5,960	19,241	22,831	8,785	877	14,462	45,184	37,997	27,355	19,385	16,210	56,641
25	6,676	10,002	4,195	13,934	18,103	6,765	686	11,088	37,241	29,136	22,216	16,823	12,986	46,307
10	3,791	5,919	2,441	8,474	12,541	4,484	466	7,241	27,318	18,974	15,834	13,372	9,133	33,667
5	2,221	3,615	1,474	5,329	8,812	3,025	322	4,774	20,188	12,439	11,313	10,658	6,501	24,774
2	790	1,404	566	2,209	4,380	1,395	156	2,055	10,954	5,247	5,647	6,690	3,303	13,489

COMPARISON BETWEEN HMS AND 17C PEAKS (%)

Return Interval (yr)	Atkinson	Ewing	Ewing Sfork	Neligh	Norfolk	Pierce	Foster	Madison	West Point	Scribner	Pender	Uehling	Nickerson	Waterloo
500	2	4	2	-1	14	4	5	3	0	1	2	2	4	4
200	0	4	5	4	10	2	3	3	2	2	3	3	3	5
100	4	4	3	7	8	2	4	3	2	3	4	2	2	5
50	3	5	2	4	7	3	4	4	3	3	6	3	1	7
25	2	5	2	6	5	1	3	5	2	4	5	1	2	6
10	3	2	2	6	1	3	4	5	NA	3	5	1	2	NA
5	1	1	1	6	5	2	4	5	NA	3	4	2	3	NA
2	1	1	1	6	4	3	NA	6	NA	3	5	3	3	NA

NA: not applicable

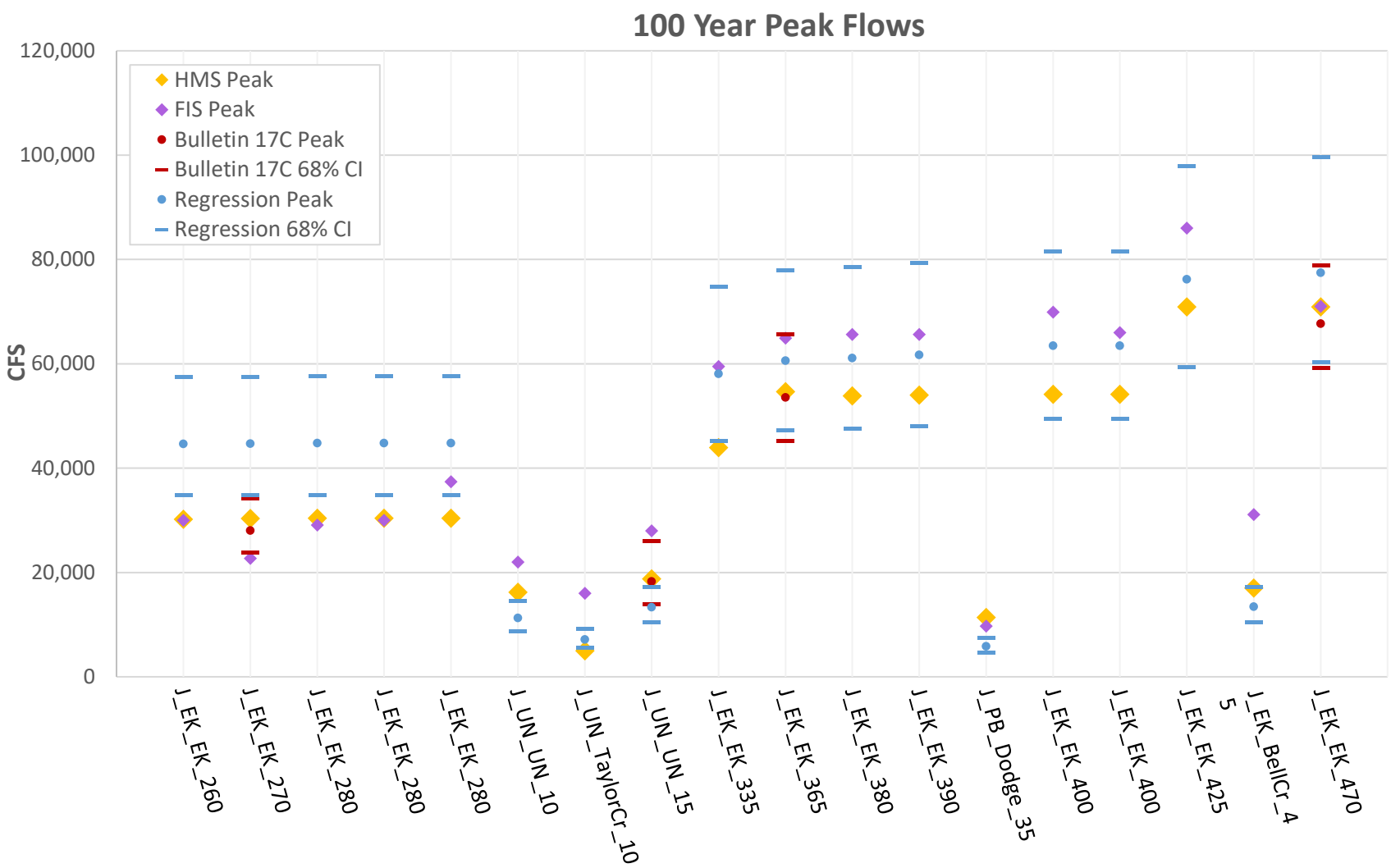

Figure 7. Comparison between FIS (purple) and HMS (orange) 100 year peak flows. Bulletin 17C (red) and regression (blue) peak flows (circles) and 68% CIs (dashes) are also given for comparison.

References

DOC/NOAA/NESDIS/NCDC. 2016. *National Climatic Data Center.* Prod. NOAA, U.S. Department of Commerce NESDIS. July 05.

England Jr., J. F., T. A. Cohn, B. A. Faber, J. R. Stedinger, W. O. Thomas Jr., A. G. Veilleux, J. E. Kiang, and R. R. Mason. 2015. "Guidelines for Determining Flood Flow Frequency - Bulletin 17C." U.S. Geological Survey Techniques and Methods 4-BXX. http://dx.doi.org/10.3133/tm4–BXX/.

FEMA. 2018. "General Hydrologic Considerations." Guidance for Flood Risk Analysis and Mapping.

Krajewski, W. F. 1987. "Cokriging of radar rainfall and rain-gauge." *J. Geophys. Res* 9571-9580.

Seo, S. M., and D. R. Maidment. 1998. "Real-time estimation of rainfall fields using radar." *J. Hydrol* 37-52.

Soenksen, P. J., L. D. Miller, J. B Sharpe, and J. R. Watton. 1999. "Peak-Flow Frequency Relations and Evaluation of the Peak-Flow Gaging Network in Nebraska." Water-Resources Investigations Report 99–4032, Lincoln, Nebraska.

USACE. 2018. *Elkhorn Basin FPMS Flood Risk Identification: Elkhorn Hydrologic Report.* Hydrologic Engineering Branch, Omaha, NE: U.S. Army Coprs of Engineers.

USACE. 1994. "Engineer Manual 1110-2-1417 Flood-Runoff Analysis." Engineer Manual, Department of the Army, United States Army Corps of Engineers, Washington, DC.

USACE. 2016. *Engineering and Construction Bulletin 2016-25: Guidance for Incorporating Climate Change Impacts to Inland Hydrology in Civil Works Studies, Designs, and Projects.* Engineering and Construction Bulletin, United States Army Corps of Engineers.

USACE. 2017. *Guidance for Detection of Nonstationarities in Annual Maximum Discharges. Engineer Technical Letter, ETL 1100-2-3.* Washington, DC: USACE.

—. 2013. "HEC-GeoHMS, Version 10.2." Davis, California: U.S. Army Corps of Engineers, Hydrologic Engineering Center, February.

—. 2000. *Hydrologic Modeling System HEC-HMS Technical Reference Manual.* Davis, California: U.S. Army Corps of Engineers, Hydrologic Engineering Center.

Pawnee Dam Inflow Design Flood (IDF) Update and Stage-Frequency Curve Development Using RMC-RFA

Jennifer Christensen, P.E., Hydrologic Engineer, U.S. Army Corps of Engineers, Omaha, Nebraska, Jennifer.P.Christensen@usace.army.mil

Joshua Melliger, P.E., Chief of Hydrology, U.S. Army Corps of Engineers, Omaha, NE, Joshua.J.Melliger@usace.army.mil

Abstract

Pawnee Dam is one of the ten Salt Creek Dams designed and built in the 1960s to mitigate flooding in Lincoln, Nebraska. This short paper illustrates the update of the Pawnee Dam inflow design flood (IDF) through calibration to recent high flow events and the development of its stage-frequency or hydrologic loading curve with the U.S. Army Corps of Engineers' Risk Management Center Reservoir Frequency Analysis (RMC-RFA) model. The IDF update follows Engineering Regulation 1110-8-2, Inflow Design Flood for Dams and Reservoirs, including unit hydrograph peaking and two antecedent pool elevations. Background information on the original design of the dam is presented and the original and updated unit hydrographs are compared. Some sensitivity analyses related to the influence of volume duration parameters and RFA inputs are also illustrated. This short paper is based on a more detailed report written for the Pawnee Dam periodic assessment in 2018. Note that this site was very data-limited in that it did not have a stream gauge at the site, historic data particular to the dam, or paleoflood data.

Introduction

As part of their risk-informed approach to dam periodic assessments (PA) and semi-quantitative risk assessments (SQRA), the U.S. Army Corps of Engineers develops a stage-frequency curve or hydrologic loading curve. This curve provides an estimated annual probability of the pool elevation reaching specific elevations. One of these elevations is the maximum pool elevation of the inflow design flood (IDF) which is why the update of the IDF is also presented. The main guidance document for this work was the *Hydrologic Hazards Methodology for Semi-Quantitative Risk Assessments RMC-TR-2018-03, An Inflow Volume-Based Approach to Estimating Stage-Frequency for Dams (USACE, 2018)*.

Pawnee Dam is one of the ten Salt Creek Dams designed and built in the 1960s to mitigate flooding in Lincoln, Nebraska. The drainage area of Pawnee Dam is 33.7 square miles of mainly rural area, making it the second largest of the ten Salt Creek Dams in the system, and it is located on the North Branch of Middle Creek about 10 miles upstream of Salt Creek which flows through the city of Lincoln. The dam was completed in 1965 and was constructed primarily in response to the May 9, 1950 flood that produced a peak flow of 27,800 cfs at the Salt Creek at Lincoln stream gauge below the current location of all ten dams. The city has experienced around one hundred floods along Salt Creek and its tributaries since 1900 with the majority caused by high intensity thunderstorm rainfall (USACE, 1960).

Figure 1 shows the location of Pawnee Dam along with the nine additional Salt Creek Dams upstream of Lincoln. Figure 2 shows a conceptual drawing of key Pawnee Dam pool elevations. Pawnee Dam is a U.S. Army Corps of Engineers (USACE) Standard 1 high hazard dam. A Standard 1 dam places human life at risk or results in catastrophic consequences if it fails; it is designed to pass the probable maximum flood (PMF) as its IDF. It is a fill and spill dam with a 42-inch outlet and a 200-foot spillway crest length. The downstream non-damaging discharge for this project is 3,000 cfs and the maximum discharge over the spillway and top of dam with the updated IDF is 76,300 cfs.

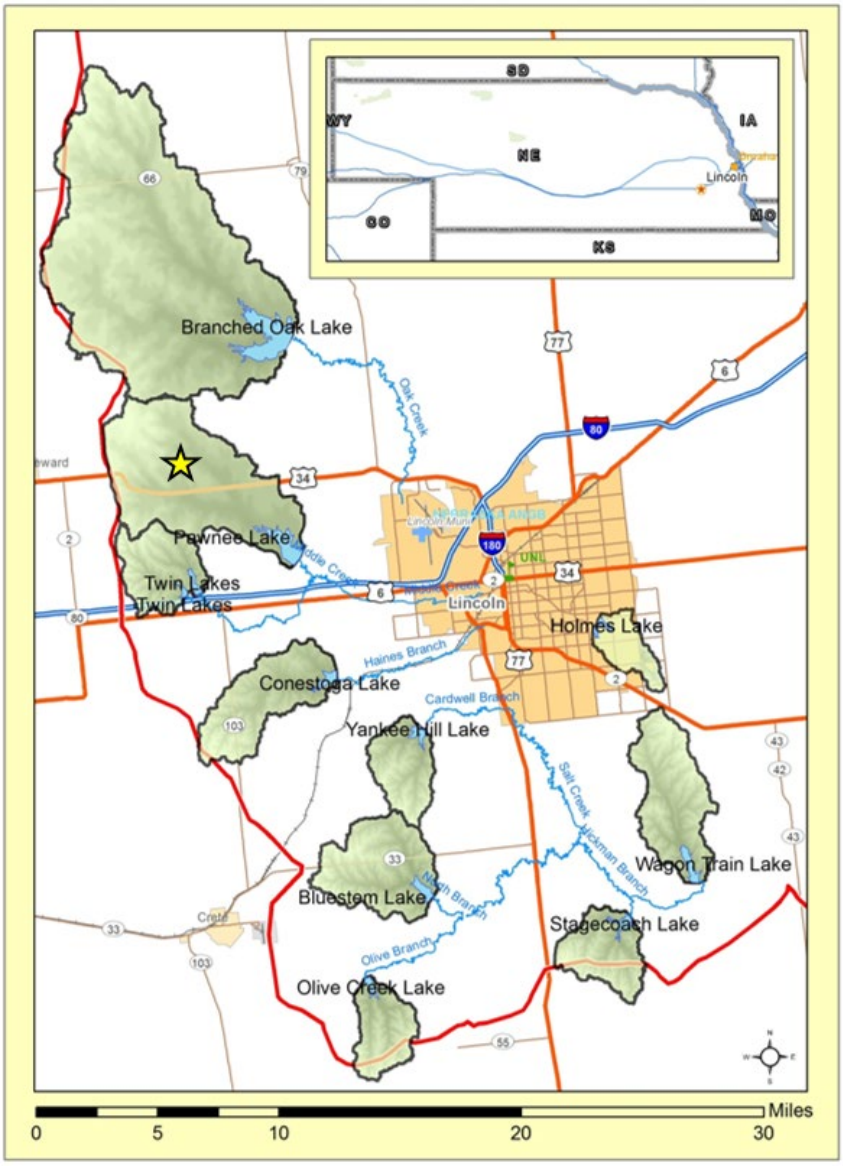

Figure 1. Pawnee Dam location

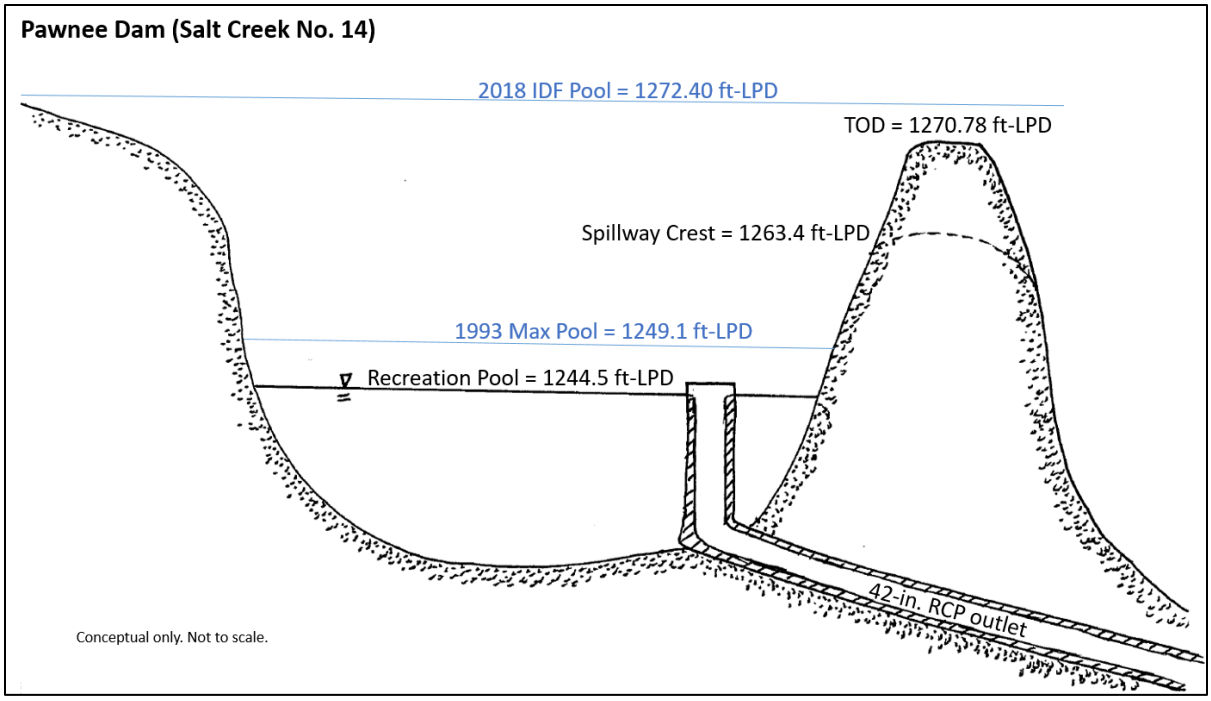

Figure 2. Pawnee Dam key pool elevations. LPD = local project datum

Inflow Design Flood

The original 1960s inflow design flood (IDF) for Pawnee Dam spillway was developed from estimates of a probable maximum flood (PMF) using precipitation estimates from Hydrometeorological Report No. 23 (HMR No. 23) and a 1-hour unit hydrograph from a regional analysis because detailed stream flow and flood records of historic floods were not available (USACE, 1960). The maximum possible precipitation was a 35.6 square mile, 6-hour storm with a total rainfall of 22.2 inches with a runoff of 20.37 inches. Neither the 1963 Pawnee Dam Design Memorandum (USACE, 1963) or the General Design Memorandum for all ten dams (USACE, 1960) state why a 6-hour duration storm was used in the original design.

The inflow design flood (IDF) update used updated guidance from Engineering Regulation 1110-8-2, Inflow Design Floods for Dams and Reservoirs; updated probable maximum precipitation (PMP) from HMR 55A; updated soil losses; and an updated 15-minute unit hydrograph calibrated to three inflow events.

The May 7, 2015 inflow event was selected as the main calibration inflow because this event created a peak flow of 34,800 cfs downstream at the Salt Creek at Lincoln gauge that resulted in a peak stage of 28.9 feet, which is just below major flood stage (29 feet) when the levees start to overtop (NWS, 2017). This event also had verified hourly inflow data and radar rainfall data. The other two calibration events were the June 10 and 14, 2015 events. The selection of calibration events was limited to the hourly discharge record, and all had radar data. Note that Pawnee Dam is an ungauged watershed and the inflow record was calculated from a record of pool elevations at the dam site. The Corps Water Management Systems (CWMS) was the source of the calibration data; these data are labeled as “observed” in the figures but were actually calculated from change in storage and dam discharge. In general, this calculated hourly inflow record had little confidence except for a handful of events where peak inflows had been verified by the

Omaha District Water Control Section. Verification events were limited to average daily data due to the short record of confident hourly data.

Figure 3 through Figure 5 show the calibration to the three events, Figure 6 shows the comparison of the 15-minute unit hydrographs from the original 1960s design memorandum and the update. The design memorandum's unit hydrograph has a 1-hour duration but was transformed to a 15-minute duration for comparison by calibrating Clark unit hydrograph parameters to the 1-hour Design Memorandum (DM) unit hydrograph and then running the model with 15-minute time steps to determine the 15-minute equivalent of the 1-hour unit hydrograph in the 1960s DM.

Based on ER 1110-8-2 guidance (USACE, 1991), the unit hydrographs determined through calibration with unit hydrograph methods like Clark UH should be peaked 25 to 50 percent. Figure 7 shows this 15-min unit hydrograph peaking with a pulse of 1 inch of rainfall over 15 minutes. The 50-percent peaked unit hydrograph at the subbasin was adopted for this IDF update. This resulted in the inflow at the dam being peaked over 25 percent.

The updated PMP from HMR 55A was a 24-hour duration storm with a total depth of 29.8 inches with an excess of 24.6 inches. A balanced hyetograph pattern was used. The 24-hour duration PMP was checked against results for the 72-hour and the maximum pool elevation was not sensitive to the longer PMP. Also, past documentation show that most historic events are 24-hours in duration or shorter.

Figure 8 shows the updated IDF using HMR 55a PMP depths, updated soil losses, and the updated 50-percent peaked 15-minute unit hydrograph determined through calibration to the May 2015 and two June 2015 events. Table 1 summarizes the calibrated and adopted watershed parameters. Table 2 shows the peaked unit hydrograph parameters.

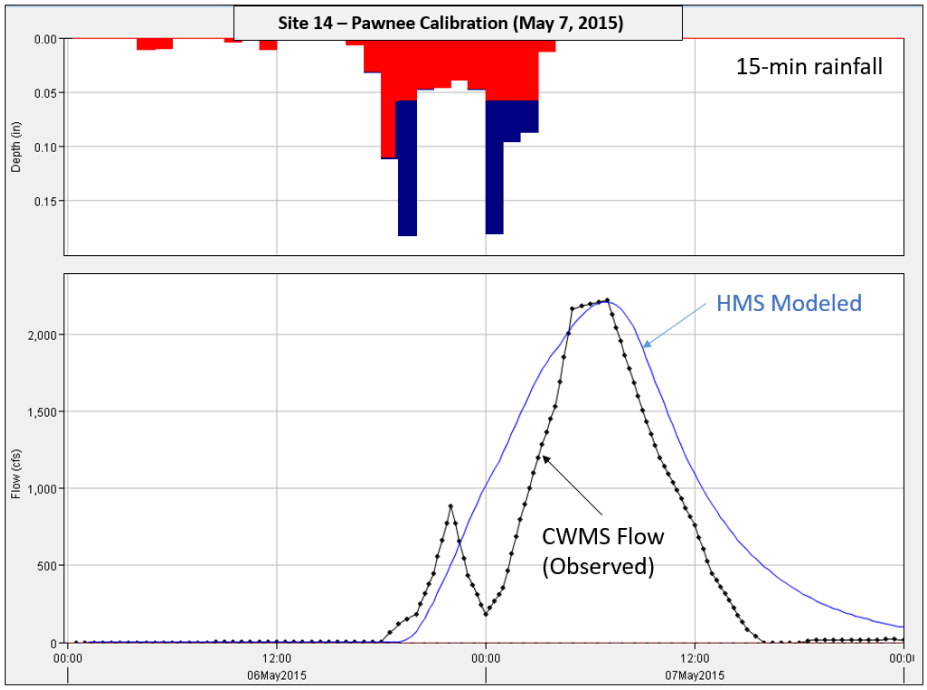

Figure 3. May 2015 calibration. Corps Water Management System (CWMS) was the source of data with which to calibrate. While labeled "observed" these data were actually calculated from the observed pool and discharge data. Nash-Sutcliffe 0.783.

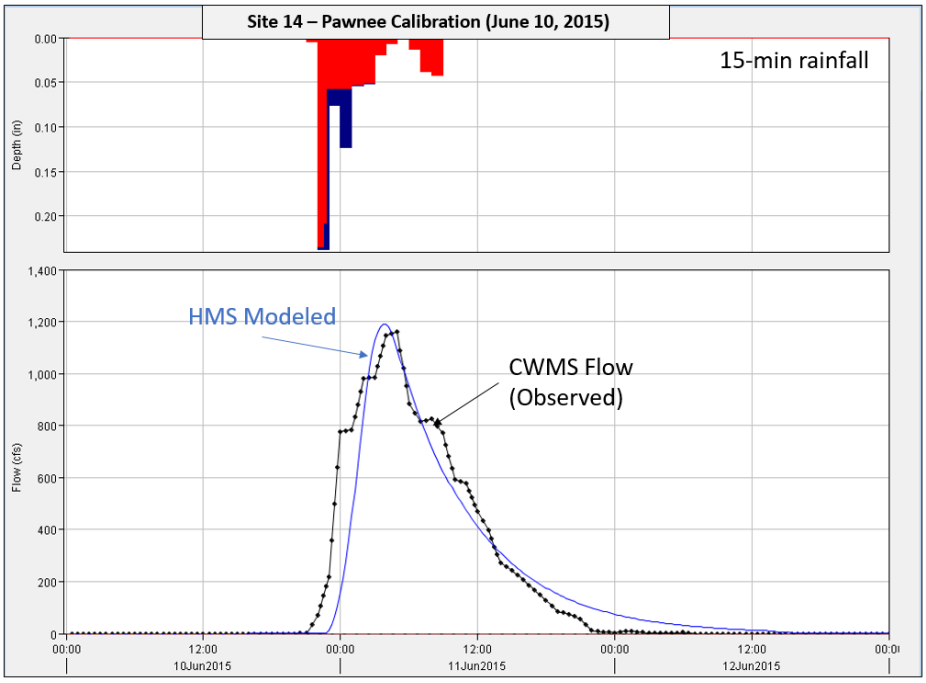

Figure 4. June 10, 2015 calibration. Corps Water Management System (CWMS) was the source of data with which to calibrate. While labeled "observed" these data were actually calculated from the observed pool and discharge data. Nash-Sutcliffe 0.914.

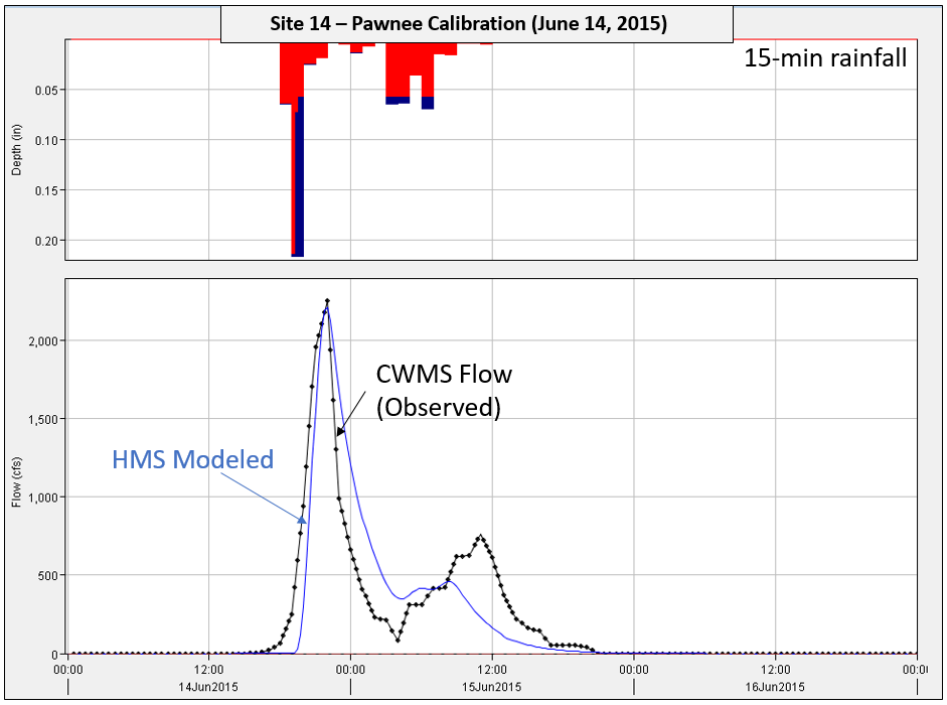

Figure 5. June 14, 2015 calibration. Corps Water Management System (CWMS) was the source of data with which to calibrate. While labeled "observed" these data were actually calculated from the observed pool and discharge data. Nash-Sutcliffe 0.773.

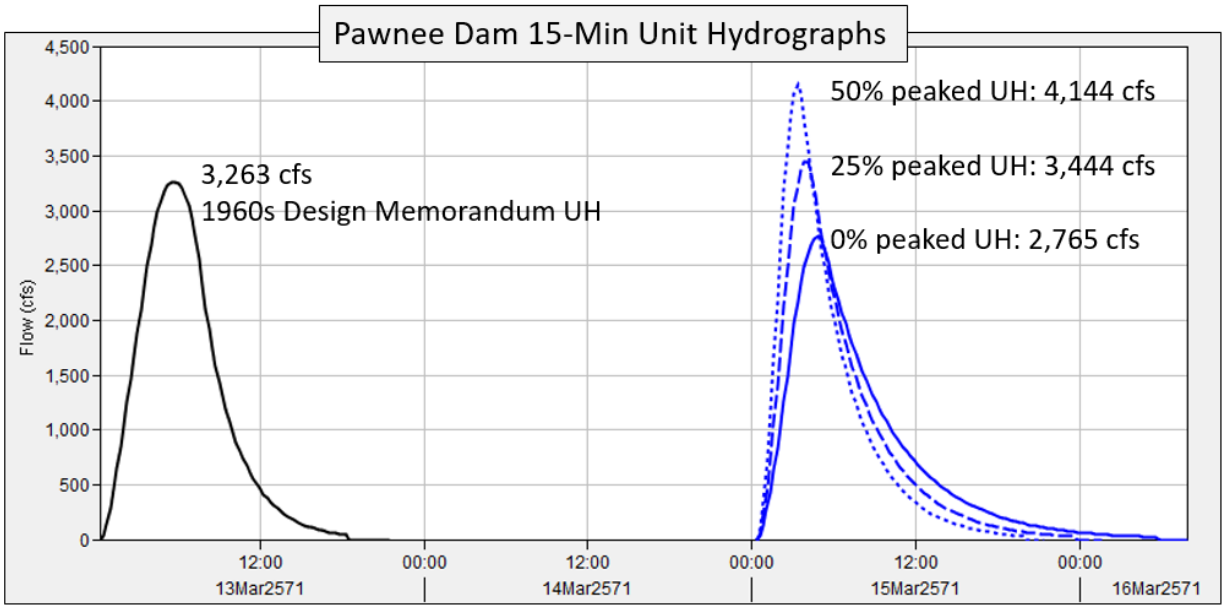

Figure 6. Comparison of 15-minute unit hydrographs (Design Memorandum and 2018 update)

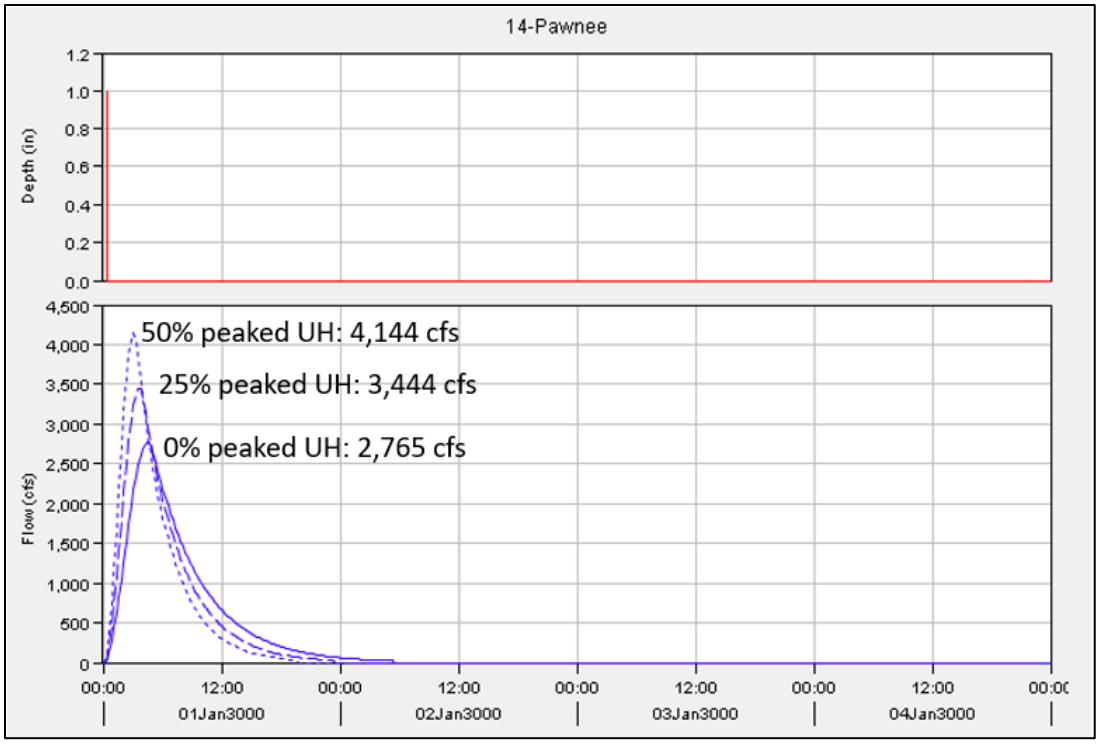

Figure 7. 15-min duration unit hydrograph peaking. One inch of rainfall applied over 15-minutes with no soil losses.

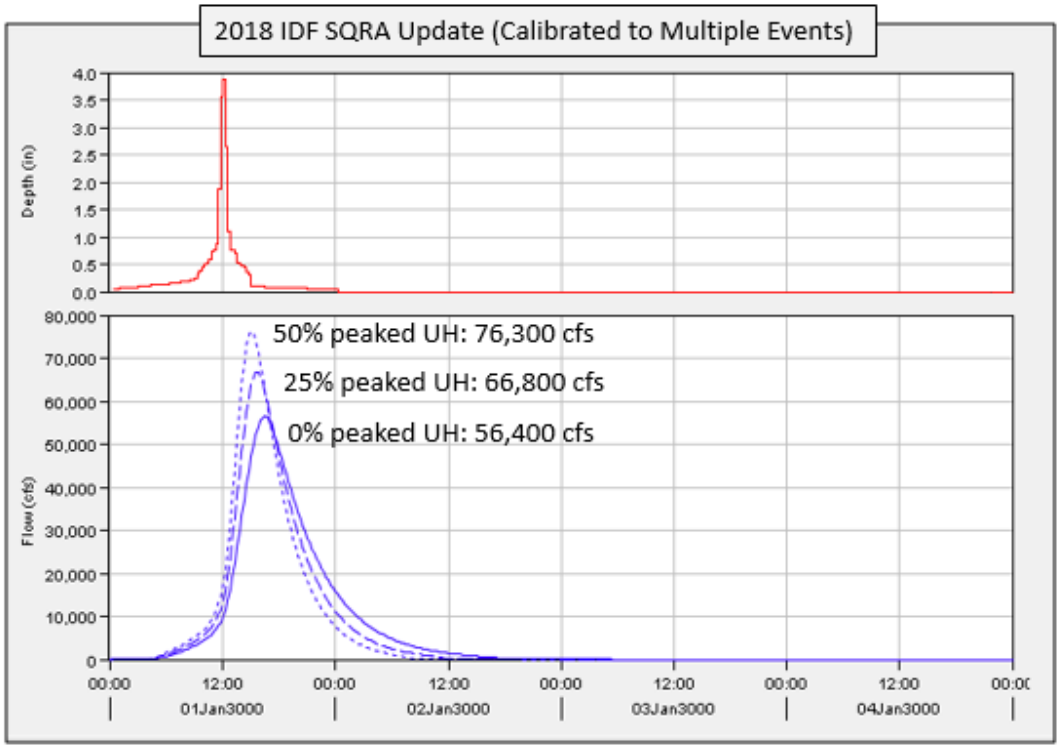

Figure 8. Updated inflow design flood assuming varying peaked unit hydrographs.

Table 1. Calibrated and adopted watershed parameters

Calibration Event	Tc (hr)	R (hr)	Initial Loss (in)	Constant Loss (in/hr)
7-May-15	8	5	0.65	0.23
10-Jun-15	4	7	0.7	0.23
14-Jun-15	2.5	3	0.5	0.23
Adopted	**4.8**	**5**	**0***	**0.23**

*This initial loss rate was used because another Salt Creek watershed calibrated at this initial loss which indicates conditions of zero initial loss could occur for Pawnee as well

Table 2. Peaked UH parameters

Amount of Peaking	None	25%	50%
T_c (hr)	4.8	3.84	3.19
R (hr)	5	4.00	3.33

Critical Inflow Duration

The critical inflow duration for this analysis was determined to be one day. Critical inflow duration is the duration of the inflow in days that creates the largest rise in pool elevation. This duration is important to the analysis because it focuses the analysis to one volume duration frequency curve in the calculation of the stage frequency.

The critical inflow duration for Pawnee Dam was determined from four inflow events (July 1993, March 1987, June 1984, and June 1998). The reservoir inflow, reservoir stage, and discharge hydrograph for each event was plotted together and then a visual assessment was preformed to determine the critical inflow duration for each event. Critical duration is estimated by measuring the time from the rise in the stage to when the inflow drops below the outflow. Figure 9 and Figure 10 show an example of one estimate using both the daily average and hourly data. Hourly data were not available for all events. Based on the analysis of all four events, the critical inflow duration varied from four days to one day or less. All but one of the events had an inflow of one day or less, so a critical duration of one day was adopted.

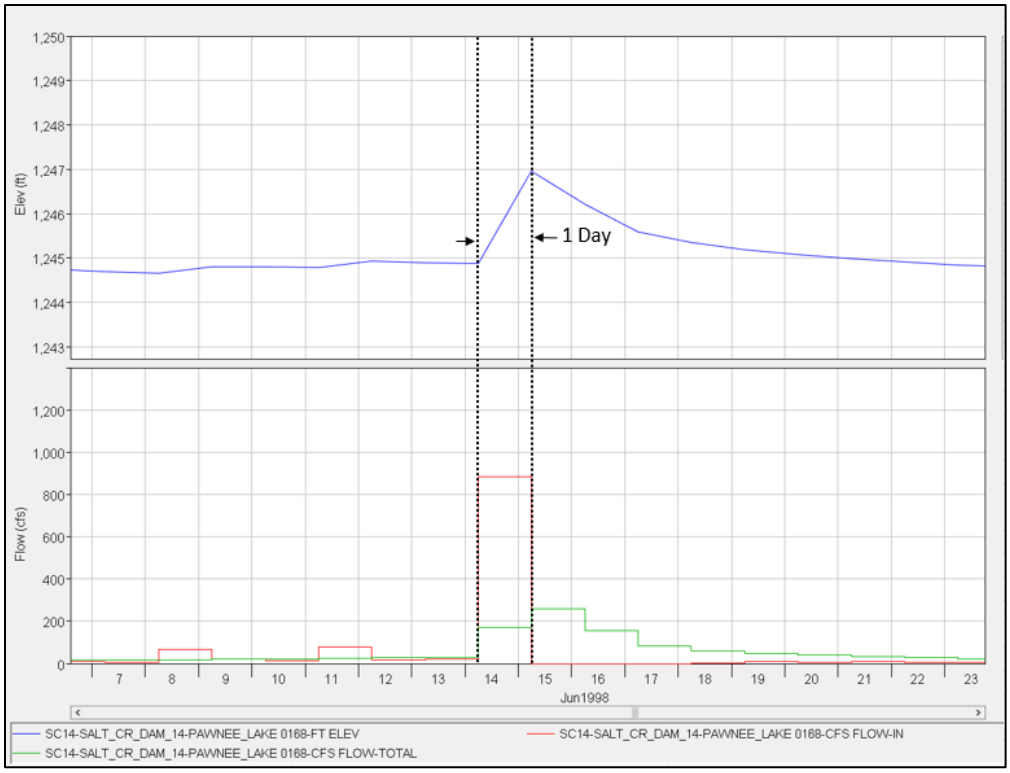

Figure 9. Critical duration for June 1998 event (daily average data)

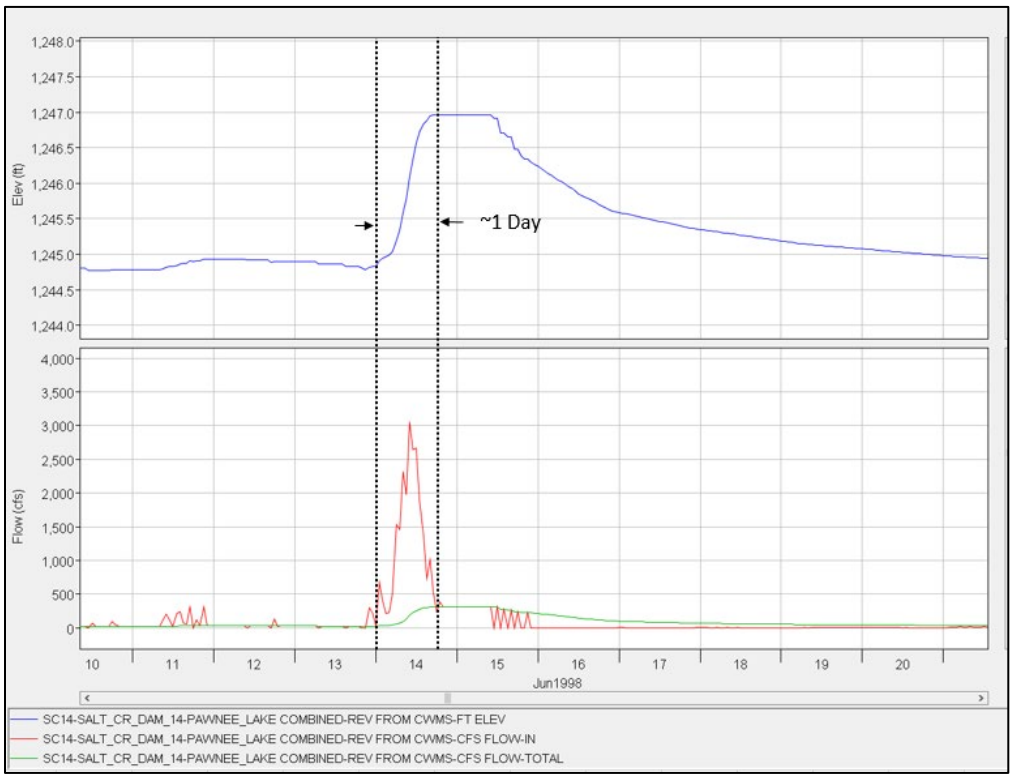

Figure 10. Critical duration for June 1998 event (hourly data)

Volume Duration Frequency Curve

The volume duration frequency curve is important to this analysis because it is one of the inputs into RMC-RFA for the determination of the stage-frequency curve. This family of curves defines the annual probability of the reservoir reaching or exceeding a certain flow for a variety of durations (e.g., 3-, 7-, 15-, 30-, 60-, 90-, 120-, and 183-day are common). The volume duration frequency curve with the critical duration determined previously (1 day) is the input needed for RMC-RFA, but a family of curves (with durations 1-, 2-, 3-, 4-, and 5-day) was developed in order to smooth the statistics of the curves and determine the most appropriate moment statistics for the 1 day duration.

Daily average inflows for Pawnee Dam were used to calculate inflow volume-frequency curves. The period of record for the daily average inflows is 1966 through 2017 (51 years). The inflow data were imported into the Statistical Software Package developed by the Hydrologic Engineering Center (HEC-SSP 2.1.1) and the 1- through 5-day inflow volume durations were developed. While investigation of the critical inflow duration resulted in a one day duration, other durations are included for purposes of smoothing the volume duration curves. The volume frequency analysis in SSP was used to extract the annual maximums for each duration and then Bulletin 17C methods were used to determine the mean, standard deviation, and skew for each. These statistics were then smoothed and added back into the volume frequency analysis to generate the smoothed curves.

A regional skew was referenced from a regional skew map in the USGS publication *Peak-Flow Frequency Relations and Evaluation of the Peak-Flow Gaging Network in Nebraska* (USGS, 1999) for the Southeastern region. This skew applies to instantaneous flows but according to guidance can be applied to the 1- to 3-day durations (USACE, 2018). The referenced regional skew was -0.2 with a mean square error (MSE) of 0.018. This regional skew was used for the 1- through 3-day durations in this study as recommended in the guidance.

While historic flow data are available downstream in Lincoln, NE historic flow data for the Pawnee site itself were not available. Flows in Lincoln, NE are influenced by multiple tributaries so a translation of peak flow to the upstream site could not be used. The only town on Middle Creek between the dam and Lincoln, NE is Emerald and no flood history could be found related to this area. The USGS stream gauge on Middle Creek downstream of the dam has only been operated since 1994 and its peak stage was from the May 7, 2015 event.

Peak flow data were not available at this site as there is low confidence in the hourly inflow dataset because inflows are calculated from pool elevations readings and not screened for errors on a continuous basis.

The inflow volume-frequency statistics generated by HEC-SSP for the final curves using the complete record with historical and regional skew are provided below in Table 3. Because the critical inflow duration was 1 day, the 1-day inflow volume-frequency curve of the set of final curves developed was selected to inform the stage-frequency curve. This selected curve is shown by itself in Figure 11. The figure shows the curve with station skew. The 1-day station skew was adopted in this study over the weighted skew because the regional skew study is dated and the station skew was less negative and considered more conservative and applicable.

Table 3. Inflow volume-frequency statistics

Statistic	Peak	1 day	2 day	3 day	4 day	5 day
Mean	N/A	2.39	2.238	2.089	2.019	1.953
Standard Deviation	N/A	0.434	0.423	0.447	0.410	0.412
Computed (Station) Skew	N/A	-0.150	-0.829	-1.192	-0.240	-0.232
Regional Skew (Peak flow) (District, if available)	N/A	-0.20	-0.20	-0.20	N/A	N/A
MSE for Regional Skew		0.018	0.018	0.018	N/A	N/A
Weighted Skew	N/A	-0.193	-0.219	-0.220	N/A	N/A
Adopted Skew	N/A	-0.150	-0.219	-0.220	-0.240	-0.232
Effective Years*	N/A	51	36	38	51	51
Smoothed Standard Deviation	N/A	0.434	0.423	0.420	0.410	0.400
Smoothed Skew	N/A	-0.193	-0.219	-0.220	-0.240	-0.25

*Note: Effective years determined by subtracting the number of low outliers from the historical period estimated by HEC-SSP Bulletin 17C Analysis.

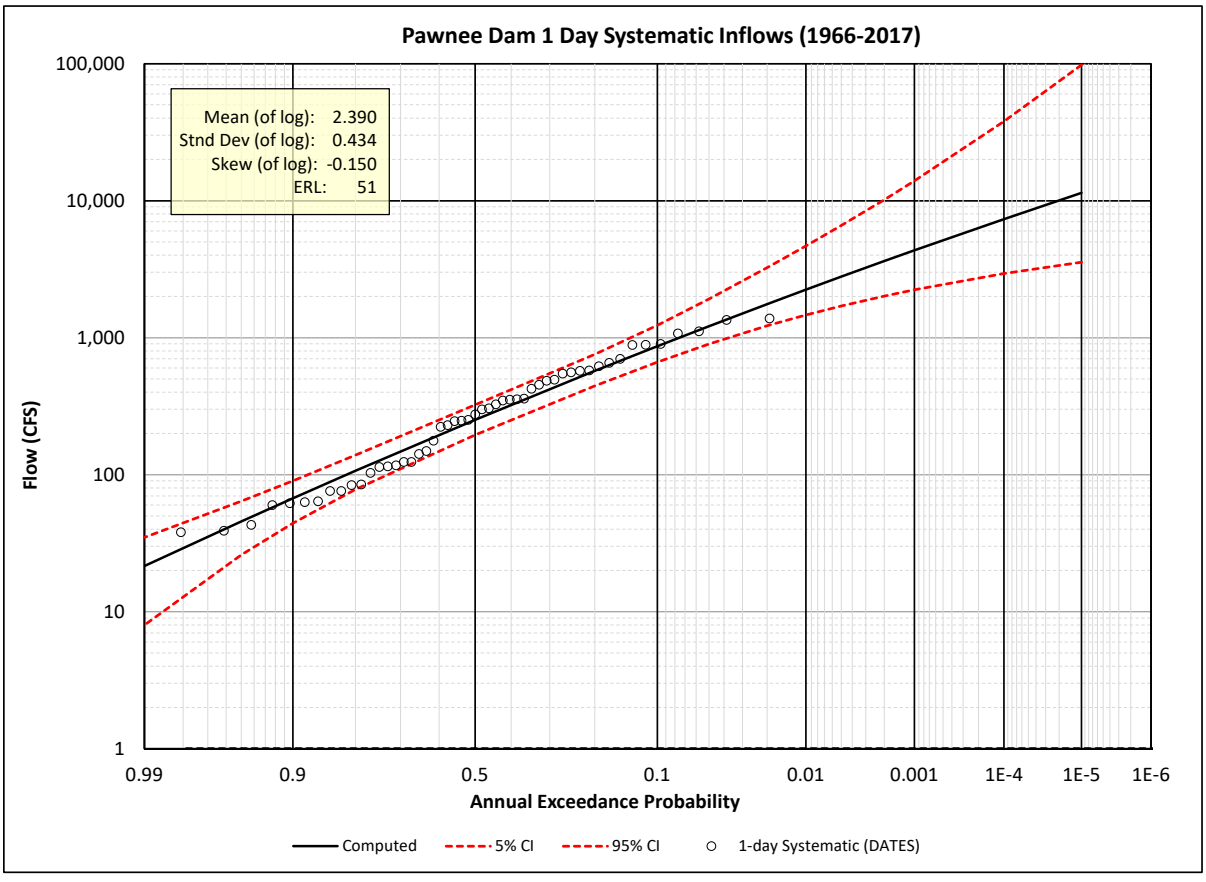

Figure 11. 1-Day inflow volume-frequency relationship (station skew adopted). Period of record 1966-2017; no other historic data or paleoflood data available for site.

Stage Frequency Curve (Hydrologic Loading Curve)

The stage frequency curve or hydrologic loading curve for Pawnee Dam was developed using the RMC-RFA software. A stage frequency curve is important in dam safety studies because it estimates the annual chance of a pool elevation being equaled or exceeded.

RFA is a Monte Carlo simulation model that generates a series of observed inflow hydrographs scaled to peak flows from an empirical frequency curve and routes them through a reservoir with a variable starting pool. Inputs to RMC-RFA include the volume frequency analysis curve for the critical duration, flood seasonality or pool stage-duration curves, a reservoir elevation-storage-discharge curve, a starting stage duration curve, inflow hydrograph patterns, and an empirical frequency curve. The main output of RFA is the stage frequency curve. This stage-frequency curve can then be graphed along with the empirical frequency curve and several hypothetical frequency events molded with NOAA Atlas 14 rainfall depth as a check.

Several RFA expected stage-frequency curves are shown in Figure 12; some use the weighted 1-day duration skew in the volume duration and some use the station skew only in the volume duration. The two curves with the weighted skew have two scenarios, one with the 42-inch diameter outlet at the recreation pool and one for results with the outlet fully blocked. The lower level outlet has a maximum discharge of 340 cfs at 1263.4 ft-LPD (spillway crest). These scenarios are summarized below:

- RFA expected – no outlet: volume duration with weighted skew (-0.193) and reservoir outlet blocked
- RFA expected – outlet: volume duration with weighted skew (-0.193) and reservoir outlet works operating as designed
- RFA expected (statG) – no outlet: volume duration with station skew (-0.15) and reservoir outlet blocked
- RFA expected (statG) – outlet: volume duration with station skew (-0.15) and reservoir outlet works operating as designed

Figure 12 and Table 4 show the sensitivity testing results with the different skews (station and weighted) and with and without the 42-inch outlet in operation.

Figure 13 shows the adopted stage-frequency curve from Pawnee Dam. Based on 51 years of effective record length but no historical or paleo data, this SQRA-level H&H analysis estimates the expected best frequency of the 2018 PMF is 1/100,000 cfs using the station-skew 1-day duration with the outlet operational. Results with the reservoir outlet works open was selected during advanced hydrologic review because this is how the dam would operate during inflow events. This is counter to how the IDF was modeled where the worst-case scenario of the outlet works not functioning was adopted.

Table 5 shows the results of the adopted stage frequency curve.

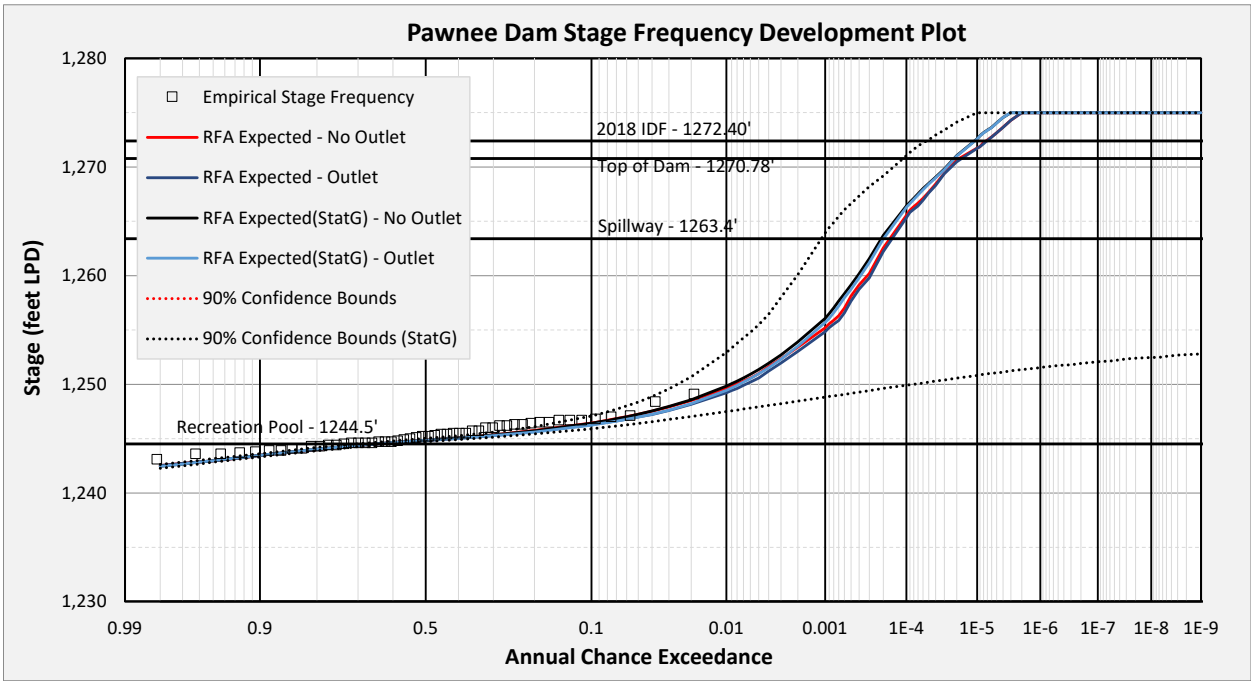

Figure 12. Development plot with sensitivity tests

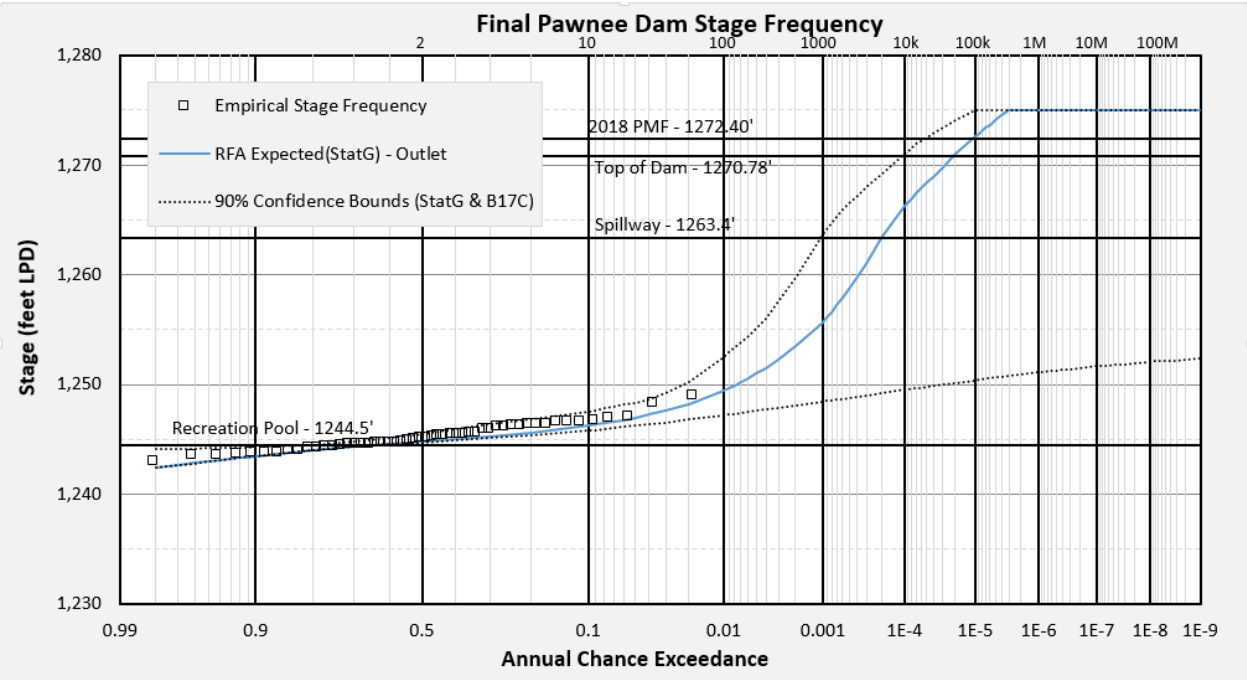

Figure 13. Adopted stage-frequency curve

Table 4. Sensitivity test results

Scenario	Elevation	Best Estimate			
	(ft-LPD)	Station G, Outlet	Station G, No Outlet	Weighted G, Outlet	Weighted G, No Outlet
2018 IDF/PMF	1272.4	1/100,000	1/100,000	1/160,000	1/160,000
Top of Dam	1270.78	1/50,000	1/50,000	1/60,000	1/60,000
Spillway Crest/Top of Flood Control Pool	1263.4	1/5,000	1/5,000	1/6,500	1/6,500
Pool of Record (July 1993)	1249.1	1/100	1/70	1/100	1/70

Table 5. Adopted stage-frequency results (with station skew -0.15 and reservoir outlet)

Scenario	Elevation (ft-LPD)	Annual Exceedance Probability (AEP)		
		Upper	Best Estimate	Lower
Top of Dam	1270.78	1/10,000	1/50,000	<1/1,000,000
2018 IDF/PMF	1272.40	1/20,000	1/100,000	<1/1,000,000
Spillway Crest/Top of Flood Control Pool	1263.4	1/1,000	1/5,000	<1/1,000,000
Pool of Record (July 1993)	1249.1	1/30	1/100	1/3,000

Conclusions

This short paper illustrated the update of the Pawnee Dam inflow design flood (IDF) through calibration to recent high flow events and the development of its stage-frequency or hydrologic loading curve. This site was very data-limited in that it did not have a stream gauge of observed data, historic flood data specific to the dam, or paleoflood data to improve the confidence of the results. It was also a relatively small site (drainage area 33.7 square miles) with sub-daily hydrographs. Sensitivity testing of the volume duration curve skew (weighted versus station) showed the station skew to produce more conservative stage-frequency curve results. These results were selected over the weighted skew results because they shifted the loading curve closer to the observed data. Sensitivity testing with the outlet open or closed resulted in very little impact to the analysis. The scenario with the 42-inch outlet open was selected because that is the most likely way the dam would be operated during large events.

References

NOAA. 1988. Hydrometeorological Report No. 55A. Probable Maximum Precipitation Estimates-United States Between the Continental Divide and the 103rd Meridian. Accessed Jan 2019 at: http://nws.noaa.gov/oh/hdsc/studies/pmp.html.

NWS. 2017. Advanced Hydrologic Prediction Service. Accessed July 2017 at: http://water.weather.gov/ahps2/.

USACE. 1960. Salt Creek and its Tributaries General Design Memorandum No. MSC-1 General Channel Improvements and Reservoirs for Flood Control. U.S. Army Corps of Engineers Omaha, NE. December 1960.

USACE. 1963. Salt Creek and its Tributaries Design Memorandum No. MSC-13 Dam and Reservoir Site 14. U.S. Army Corps of Engineers Omaha, NE. February 1963.

USACE. 1991. Inflow Design Floods for Dams and Reservoirs. U.S. Army Corps of Engineers. Accessed on Jan 2019 at: https://www.publications.usace.army.mil/USACE-Publications/Engineer-Regulations/u43546q/313131302D382D32/.

USACE. 2017. Hydrologic Engineering Center Statistical Software Package (HEC-SSP). Version 2.1.1.

USACE. 2018. Hydrologic Hazard Methodology for Semi-Quantitative Risk Assessments RMC-TR-2018-03 An Inflow Volume-Based Approach to Estimating Stage-Frequency for Dams. U.S. Army Corps of Engineers Institute for Water Resources Risk Management Center. May 2018.

USGS. 1999. Peak-Flow Frequency Relations and Evaluation of the Peak-Flow Gaging Network in Nebraska. Water-Resources Investigation Report 99-4032. U.S. Geological Survey.

Snowmelt Simulation Enhancements within HEC-HMS

Michael Bartles, P.E., Hydraulic Engineer, U.S. Army Corps of Engineers, Institute For Water Resources, Hydrologic Engineering Center, 609 Second Street, Davis, CA 95616; 530-302-3706; Michael.D.Bartles@usace.army.mil.

Dr. William Scharffenberg, Hydraulic Engineer, U.S. Army Corps of Engineers, Institute For Water Resources, Hydrologic Engineering Center, 609 Second Street, Davis, CA 95616; 530-302-3691; William.Scharffenberg@usace.army.mil.

Dr. Michael Follum, P.E., Hydraulic Engineer, U.S. Army Corps of Engineers, Engineer Research and Development Center, Coastal and Hydraulics Laboratory, 3909 Halls Ferry Rd, Vicksburg, MS 39180; 601-634-2639; Michael.L.Follum@usace.army.mil

Introduction

The accumulation of a snowpack and the subsequent melt occurs throughout the United States ranging from the Sierra Nevada Mountains to the Great Plains to the Appalachian Mountains. In many watersheds, especially in the mountainous western United States, snowmelt and rain-on-snow events are the primary sources of runoff as well as the main source of flood hazards. Significant resources have been expended constructing water resources projects with the intention of mitigating flood risks as well as capturing runoff due to snowmelt and rain-on-snow events. However, watersheds that experience snowmelt runoff and rain-on-snow events are oftentimes unique due to dissimilarities in topography, data availability, and predominant weather patterns (amongst other factors). As such, it is in the national interest to continue the advancement of knowledge about snowpack accumulation/melt and expand the tools available to all engineers to simulate snow hydrology.

The processes involved in snowpack accumulation, melt, and rain-on-snow were first studied in great detail by the Federal government in the 1940s. One of the most fruitful studies was the *Cooperative Snow Investigation Program* which was a joint venture between the U.S. Army Corps of Engineers (USACE) and the U.S. Weather Bureau that lasted approximately 15 years. This program established multiple snow laboratories (one of which is still operational) and studied, in detail, the accumulation, evolution, and melt of snow throughout the mountainous west. Voluminous technical reports, research notes, and guidance was developed from this program. Examples of the output from this program include *Snow Hydrology* (U.S. Army Corps of Engineers, 1956) and *Engineer Manual 1110-2-1406* (U.S. Army Corps of Engineers, 1960), each of which form an important cornerstone of nearly all snow hydrology applications that have been undertaken in the last 60 years. Finally, this program (along with subsequent research), led to the derivation of nearly all conceptual snowmelt models that are still used to this day.

One of the benefactors of this research has been the Hydrologic Engineering Center's Hydrologic Modeling System (HEC-HMS). This software is designed to simulate the precipitation-runoff processes of dendritic watershed systems (U.S. Army Corps of Engineers, 2018). HEC-HMS is meant to be applicable in a wide range of geographic areas for solving the widest possible range of problems including large river basin water supply and flood hydrology and small urban or

natural watershed runoff. HEC-HMS is a generalized modeling system capable of representing many different watersheds simultaneously. These watersheds can be discretized by separating the hydrologic cycle into manageable pieces. One of these pieces is the meteorology of the watershed, which includes snow accumulation and melt.

Evolution of Snow Accumulation and Melt Simulations within HEC-HMS

Since version 3.0, HEC-HMS has contained the temperature index (TI) method which is a relatively simple snowmelt/accumulation modeling approach. Within this method, air temperature is used as a proxy for the energy available for heating or melting the snowpack. While this method is relatively simple, it is incredibly flexible, easily adjusted through model calibration, and has seen wide use throughout the U.S. to design and operate water supply and flood risk management infrastructure.

However, assuming that air temperature is the only means for heating or melting the snowpack is not applicable for all applications and problems. For example, several studies have shown that net radiation is the primary source of energy for melt (Aguado, 1985), of which shortwave radiation (solar) is often the dominant source of energy for snow melt (Dewalle & Rango, 2008). Non-linear effects of rain falling on snow and convective transfer of sensible and latent heats from the atmosphere to the snow can significantly increase the rate at which accumulated snow melts, exacerbate flooding, and lead to extensive damage. Also, cloud cover and wind speed can significantly affect the evolution and melt of snow. In the past few decades, advancements in computing technology and hydrologic data collection have made it possible to more accurately and efficiently utilize increasingly complex snowmelt algorithms, when warranted.

Enhancements to HEC-HMS are currently under development that can aid engineers when simulating snowmelt and rain-on-snow events. In addition to the existing temperature index method, future versions of HEC-HMS will contain two new snow accumulation/melt methods: a radiation-derived temperature index (RTI) method and an energy balance (EB) method.

While the TI method relies solely upon air temperature to estimate energy available to melt accumulated snow, the RTI method utilizes additional factors to compute a proxy energy available for snowmelt. This representative energy is derived from a radiation balance computation that includes simple calculations of net shortwave and longwave radiation (Follum, Downer, Niemann, Roylance, & Vuyovich, 2015). Net shortwave radiation includes topographic, cloud cover, vegetation, and albedo effects while net longwave radiation includes contributions from the air, vegetation, cloud cover, and approximate snow temperature. Compared to the TI method, the RTI approach requires only a few additional meteorological inputs. However, the RTI method has not been as widely used as the TI method within USACE.

The EB method is the most complicated and data intensive snowmelt/accumulation modeling approach within HEC-HMS. This method utilizes a generalized energy balance approximation of all energy fluxes into and out of the snow in order to simulate the growth, evolution, and melt of a snowpack. This method has the ability to potentially outperform the two previously described methods when air temperature and/or net radiation are not the primary sources of energy available for snowmelt. For instance, both the TI and RTI methods do not implicitly include means for incorporating energy from turbulent heat transfer. However, the EB method

suffers from the need for a large amount of highly accurate meteorologic inputs that are not readily available in most watersheds (U.S. Army Corps of Engineers, 1998).

The addition of these two new methods that can be used to accumulate and melt snow allow for users to choose a relatively simple method with only a few required boundary conditions, a moderately complex method that requires additional parameters, and an intricate method with numerous required meteorological inputs. All three methods include means to discriminate between precipitation falling as rain or snow, form a snowpack, melt the snowpack, reformulate the snowpack when temperatures drop below a defined threshold, and eventually melt the entire snowpack. Also, users have the ability to employ all three methods at either a subbasin scale (i.e. lumped) or within gridded (i.e. distributed) implementations.

Furthermore, improvements to existing tools will be made in order to refine distributed snow accumulation/melt parameters as well as aid in model calibration. For instance, future versions of HEC-HMS will allow for the definition of temperature index parameters at the subbasin scale as opposed to defining these parameters for the entire modeling domain. These new modeling capabilities will provide much needed flexibility when predicting snowmelt and runoff in a wide range of applications including flood forecasting, feasibility, and dam/levee safety studies.

Example Projects

Multiple projects are currently underway to evaluate the effectiveness of these additional snow accumulation/melt methods. These include a very large application in the Pacific Northwest and a moderately sized application in the Sierra Nevada Mountains.

HEC-HMS models have been developed for the approximately 250,000 square mile Columbia River watershed in support of the Columbia River Treaty and study applications by USACE Districts within the northwest. These models span one of the geographically most diverse areas in North America which includes glaciated valleys, 14,000+ foot mountain peaks, and arid deserts (to name a few). The primary driver of runoff within this watershed is snowmelt which, when combined with the diverse hydrologic regions prevalent throughout the modeling domain, lends itself well to having multiple choices available for use when modeling the meteorology. HEC-HMS was effectively used to accurately and efficiently simulate the precipitation-runoff process throughout the entire Columbia River watershed, as shown in Figure 1, over four discrete water years (1997, 2011, 2012, and 2017).

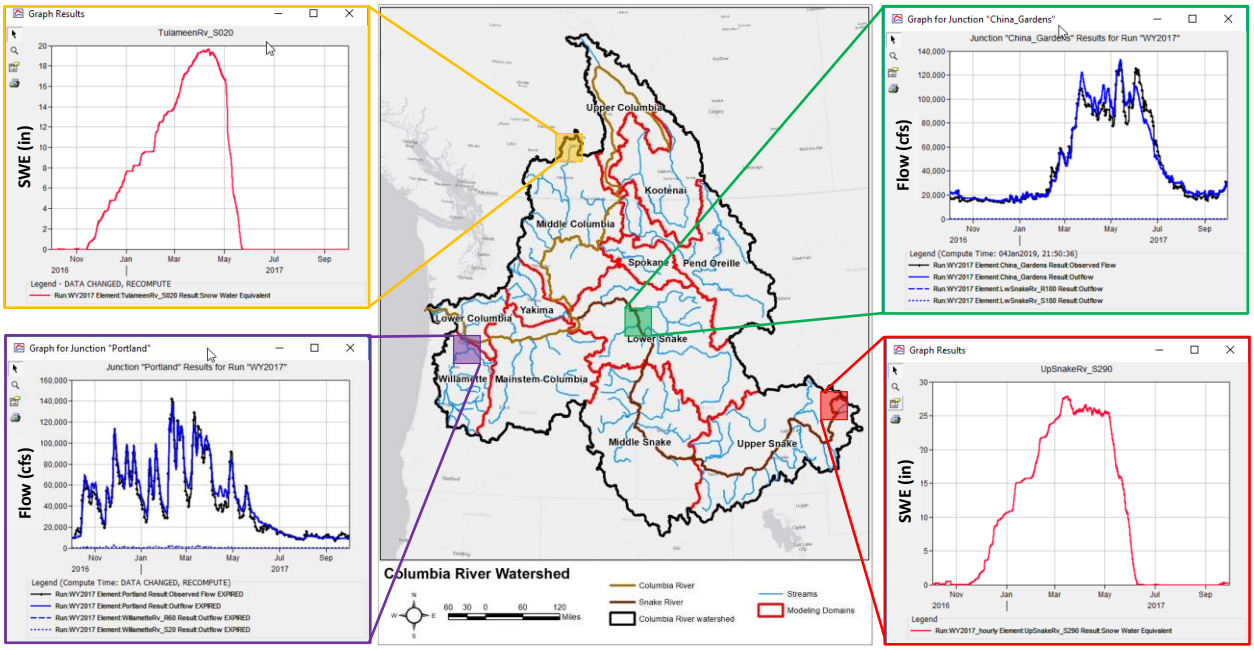

Figure 1. Columbia River HEC-HMS Modeling

Additionally, an HEC-HMS model is under development for the Truckee River, which originates along the eastern side of the Sierra Nevada Mountains in California and eventually reaches its terminus in Nevada. While the Truckee River provides a major source of water for the 350,000 inhabitants of its watershed, the river is also prone to significant flooding. Substantial damage to large population centers like Reno and Sparks, NV has occurred during large scale and widespread rain-on-snow flood events in 1996-1997, 2005-2006, and 2016-2017 (amongst others). Numerous state and federal water supply and flood risk management projects have been constructed within this watershed to harness runoff and mitigate potential flooding risks. The Truckee River watershed offers an excellent opportunity to compare and contrast the three snowmelt modeling techniques contained within HEC-HMS in a watershed that contains an extremely large amount of meteorological, snow, and river observation stations, as shown in Figure 2.

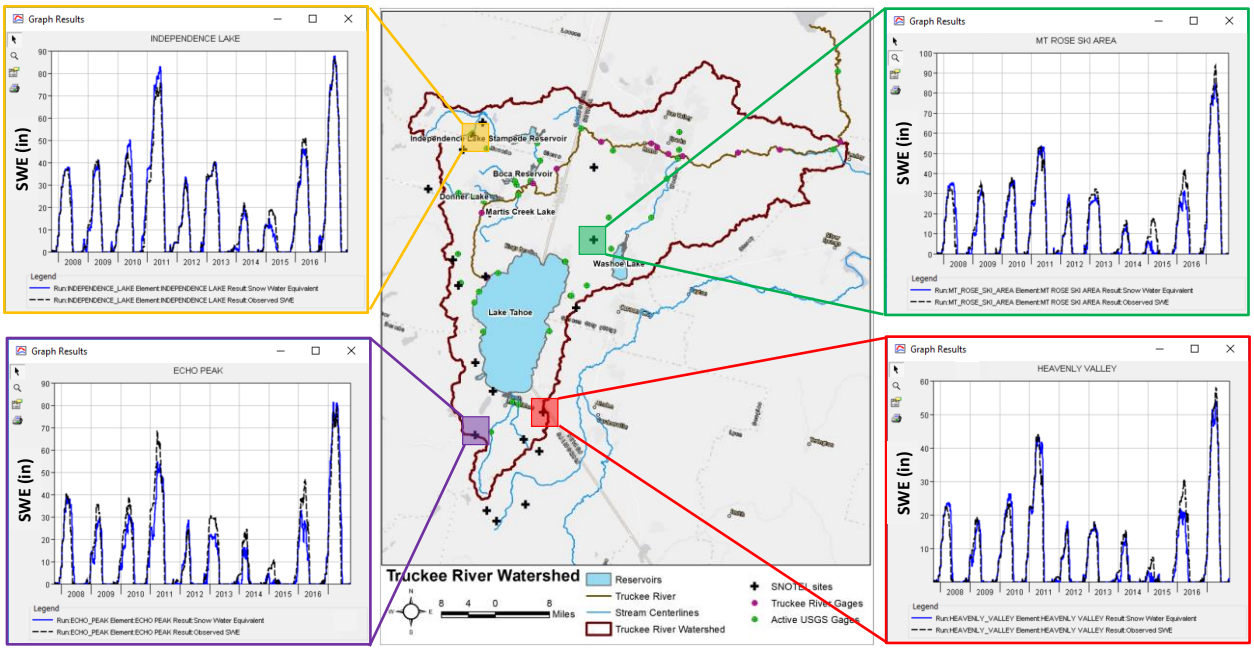

Figure 2. Truckee River HEC-HMS Modeling

References

Aguado, E. (1985). Radiation Balances of Melting Snow Covers at an Open Site in the Central Sierra Nevada, California. *Water Resources Research*, 1649-1954.

Dewalle, D. R., & Rango, A. (2008). *Principles of Snow Hydrology*. Cambridge University Press.

Follum, M. L., Downer, C. W., Niemann, J. D., Roylance, S. M., & Vuyovich, C. M. (2015). A Radiation-Derived Temperature-Index Snow Routine for the GSSHA Hydrologic Model. *Journal of Hydrology*, 723 - 736.

U.S. Army Corps of Engineers. (1956). *Snow Hydrology*. Portland, OR: North Pacific Division.

U.S. Army Corps of Engineers. (1960). *Engineer Manual 1110-2-1406 Runoff from Snowmelt*. Washington, D.C.: U.S. Army Corps of Engineers.

U.S. Army Corps of Engineers. (1998). *Engineer Manual 1110-2-1406 Runoff from Snowmelt*. Washington, D.C.: U.S. Army Corps of Engineers.

U.S. Army Corps of Engineers. (2018). *Hydrologic Modeling System HEC-HMS, User's Manual, Version 4.3*. Davis, CA: Hydrologic Engineering Center.

Using Multiple Methods to Estimate Frequency Hydrology for Shasta Dam

Frank Dworak, Hydrologic Engineer, Bureau of Reclamation, Denver, CO fdworak@usbr.gov

Keil Neff, Hydrologic Engineer, Bureau of Reclamation, Denver, CO kneff@usbr.gov

Amanda Stone, Hydrologic Engineer, Bureau of Reclamation, Denver, CO astone@usbr.gov

Jeffrey Niehaus, Hydrologic Engineer, Bureau of Reclamation, Denver, CO jniehaus@usbr.gov

Katie Holman, Hydrologic Engineer, Bureau of Reclamation, Denver, CO kholman@usbr.gov

James Gilbert, Hydrologic Engineer, Bureau of Reclamation, Denver, CO jmgilbert@usbr.gov

Lindsay Bearup, Hydrologic Engineer, Bureau of Reclamation, Denver, CO lbearup@usbr.gov

Subhrendu Gangopadhyay, Hydrologic Engineer, Bureau of Reclamation, Denver, CO sgangopadhyay@usbr.gov

Abstract

The Bureau of Reclamation (Reclamation) is designing a dam raise for Shasta Dam, CA. An important part of this study is providing hydrologic loadings to inform risk based design for the dam raise. The Water Resources Engineering and Management Group is using multiple methods and a phased approach to best estimate hydrologic loadings for Shasta Dam. One of the many challenging aspects of this project is an aggressive time schedule with approximately five months to provide initial hydrologic loadings to the design group.

Three somewhat independent methods are being used for this study; Expected Moments Algorithm (EMA), Risk Management Center's Reservoir Frequency Analysis (RMC-RFA), and rainfall-runoff modeling using HEC-HMS using L-moment precipitation frequency estimates. EMA is a statistical method using an unregulated systematic record from multiple stream gages and paleoflood estimates to develop a peak discharge frequency curve for the Shasta Dam location. Initially, the EMA analysis will include available gage records and preliminary paleoflood data. The second method, RMC-RFA, uses a series of data developed from the systematic gage record available for Shasta Dam. RMC-RFA produces a reservoir stage-frequency curve with confidence bounds by utilizing a deterministic flood routing model while treating the inflow volume, the inflow flood hydrograph shape, the seasonal occurrence of the flood event, and the antecedent reservoir stage as uncertain variables rather than fixed values. In order to quantify both the natural variability and knowledge uncertainty in reservoir stage-frequency estimates, RMC-RFA employs a two looped, nested Monte Carlo methodology. The natural variability of the reservoir stage is simulated in the inner loop defined as a realization, which comprises many thousands of simulated flood events, while the knowledge uncertainty in the inflow volume frequency distribution is simulated in the outer loop, which comprises many realizations. The third method, rainfall-runoff modeling, applies a model originally developed by the U.S. Army Corps of Engineers for the Sacramento and San Joaquin River Basins Comprehensive Study. The model uses an AEP-neutral approach utilizing L-moment precipitation frequency and four historic storm templates. The model leverages parameter sensitivity and precipitation frequency uncertainty to estimate overall uncertainty. The second phase of the study will build on the results of the first phase and incorporate detailed site-specific paleoflood data into the analyses.

The strengths and weaknesses of each method within the phased multi-method framework will be discussed and used to recommend appropriate hydrologic loads for risk informed design for

Shasta Dam. Use of multiple methods and datasets allows for greater confidence in load estimates and associated uncertainty in support of risk informed design for Shasta Dam.

Introduction

Objective

The Bureau of Reclamation (Reclamation) is designing a dam raise for Shasta Dam, CA. A key component of dam design, and the focus of this paper, is the hydrologic loadings used for dam raise design and subsequent risk analysis. Reclamation utilizes a risk informed design process which allows the designers to incorporate important risk factors when considering design alternatives. For Shasta Dam an important risk factor is the high population located downstream of Shasta Dam, which is located on the Sacramento River approximately 11 miles north of Redding, CA. Flood flows would follow the Sacramento River through the entire Central Valley, through Sacramento, and into Suisun Bay near just east of San Francisco. This risk factor plays an important role in selecting an appropriate flood load for the dam raise.

There are some unusual aspects to this study that make it particularly challenging. The Pit River drainage makes up a majority of the contributing area while contributing less than a majority of the overall inflow. Characterizing the Pit River basin for extreme flood analysis and the actual contribution to the system was a complex challenge. Another challenging aspect of the project was the schedule. Work for the project began in May, 2018, based on funding availability, and due to hydrologic loadings being a critical path for final design, the completion date for inflow hydrographs was December, 2018.

Approach

To appropriately characterize the hydrologic hazard and uncertainty for the Shasta Dam raise project, Reclamation used a multiple methods approach. A multiple methods approach improves understanding the effects of mixed populations, non-contributing drainage areas, seasonal controls, and the range of model and data uncertainty. The analysis methodologies include

(1) Peak discharge frequency analysis using the Expected Moments Algorithm (EMA; Cohn et al., 1997). The EMA analysis was performed using the computer program PeakfqSA (Cohn and England, 2016) to compute the moments of a Log Pearson Type III distribution using a time series of systematic, historic, and paleoflood information.

(2) Volume frequency analysis using HEC-SSP (Hydrologic Engineering Center – Statistical Software Package; USACE, 2017b) applied in stochastic simulation of inflow volume, hydrograph shape, seasonal occurrence, and antecedent reservoir water surface elevation using appropriate reservoir routing characteristics and antecedent reservoir conditions (Risk Management Center – Reservoir Frequency Analysis (RMC-RFA); Smith et al., 2018).

(3) Frequency rainfall-runoff modeling: a regional precipitation frequency analysis was developed using L-moments (Hosking and Wallis, 1997), and applied to historic storm templates to incorporate in runoff modeling and flood event analysis using the U.S. Army Corp of Engineers' (USACE) HEC-HMS (Hydrologic Engineering Center – Hydrologic Modeling System; USACE, 2017a).

One of the most challenging part of this project was the expedited schedule. The schedule did not change the overall multiple methods approach but did change how we approached each method. The focus of this paper will be on the unique challenges within each method and the steps that were taken to complete the hydrologic modeling in a timely manner.

An important aspect to highlight is that due to time constraints a phased approach was identified for final hydrologic loadings. The original scope of the study included a robust paleoflood analysis to identify and characterize historic floods and non-exceedance values. Completion of this work and incorporating the results into the hydrologic analysis was outside the possible scope for the desired completion date. Therefore a phased approach was utilized to allow an initial estimate of flood loadings to be completed using available data in the first phase of the project. A second phase of the study would incorporate paleoflood findings to verify the findings in the first phase of the study. The second phase will build on the results of the first phase and incorporate detailed site-specific paleoflood data into the analyses. A further objective of the second phase is to conduct additional data analysis, modeling, and model development needed to support the recommended hydrologic loadings from the first phase of the study. The second phase of the project will also investigate causality using a Bayesian approach to integrate results from the multiple methods.

Watershed and Climate

The watershed contributing to Shasta Dam (Figure 1) has a drainage area of nearly 6,600 square miles. Shasta Dam is located about 11 miles north of Redding, California. Elevation in the watershed ranges from 1,078 feet at the dam crest to 14,179 feet at the top of Mount Shasta. Vegetation is variable throughout the watershed and varies from sparse scrub to heavy coniferous forest.

Shasta Dam is located at the northern tip of California's Central Valley, which is one of the most agriculturally productive regions in the world, and emphasizes the importance of water and water measurement in this region. Consequently, this region is data rich in hydrologic information and supports the data requirements for the various analysis methodologies presented here.

The Shasta watershed is located within a transitional climate zone where conditions vary significantly. The western portion of the basin is influenced by the Pacific Ocean and Coast Mountain Range while the eastern portion is protected from the ocean influence and is in the mountain rain shadow. Depending on altitude and local conditions, there is significant daily and seasonal temperature variability with cold/wet winters and warm/dry summers.

As with most of California, dry summers are due to the northward migration of the semi-permanent North Pacific High with most storm tracks deflected far to the north. The North Pacific High decreases in intensity in winter and moves further south, permitting storms to move into the region producing widespread rain at low elevations and snow at high elevations. Occasionally the broad-scale circulation pattern permits a series of storm centers to move into California from the southwest. This type of storm pattern (atmospheric river) is responsible for extreme precipitation events. An example of an atmospheric river extreme precipitation event was in 1955 when over 32-inches of precipitation was recorded over a 4-day period in part of the watershed.

Average annual precipitation within the watershed ranges from less than 15 inches to over 85 inches. Most precipitation occurs in the western mountainous portion of the basin with extremely

dry conditions in most of the eastern plateau areas. Annual maximum one-day precipitation events typically occur during the cool season, specifically October through April. Basin-wide average monthly high temperatures (degrees Fahrenheit) range from the upper-40s in the winter to upper-80s in summer and lows range from the mid-20s in winter to upper-40s in summer.

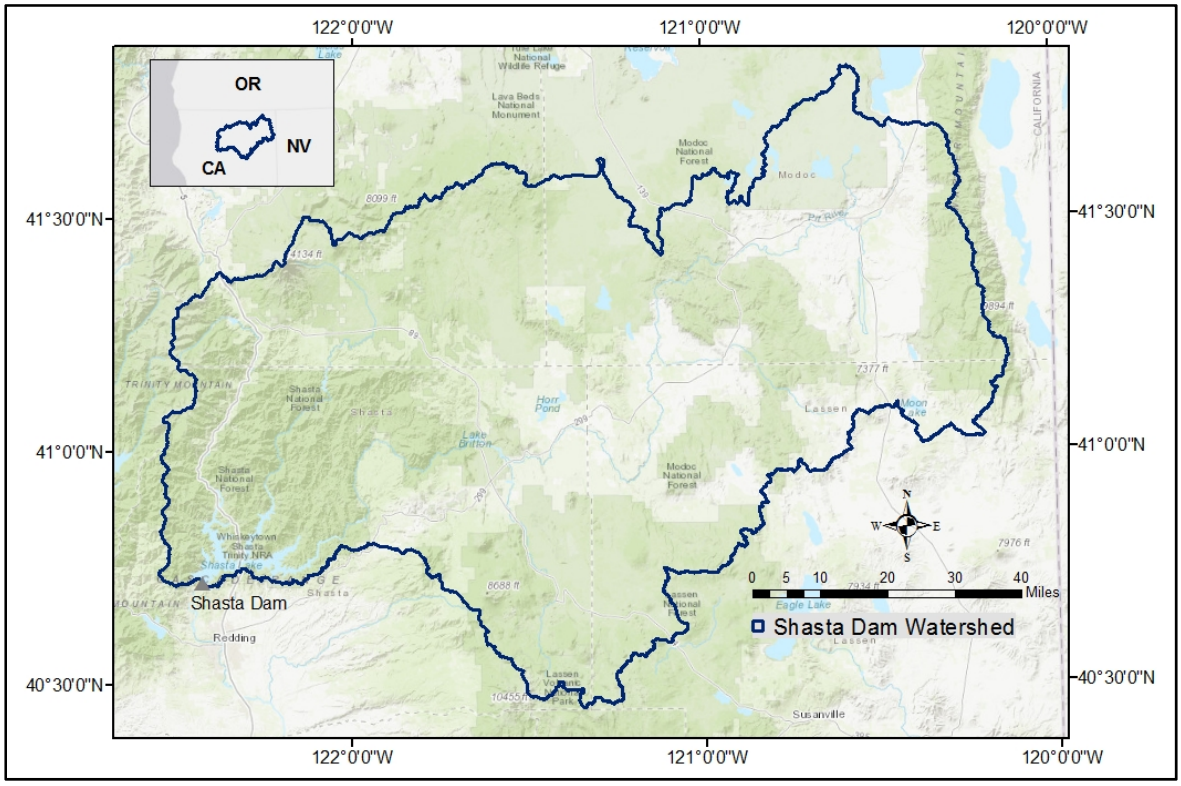

Figure 1. Location of Shasta Dam (gray triangle) and associated watershed, which controls runoff from ~6,590 square miles.

Methodology

Multiple methods were used in an attempt to fit a distribution to a relatively small sample of observed data with the intent to extrapolate that data to extremely rare annual exceedance probabilities (AEPs). Each method and its associated dataset have a credible range of extrapolation that generally is significantly limited. However, when the methods and datasets are used together, the collection of results increases the credible range of extrapolation. The methods used in the Shasta Dam study use somewhat independent datasets allowing each method to produce independent results. Trends in the magnitude and skew of each individual resulting frequency curve builds confidence in the validity of the results and extrapolation techniques used.

Bulletin 17C Flood Flow Frequency Analysis

A peak discharge frequency relationship was developed based on Bulletin 17C techniques (England et al., 2018) and use the Expected Moments Algorithm (EMA). The objective of EMA analyses is to utilize the longest available timeseries of instantaneous annual peak flows in which to fit with a distribution. The Shasta Dam EMA analysis is based on 137 records including one revised paleoflood record from a previous Reclamation study.

The main focus of the Shasta Dam EMA analysis was on data acquisition and validation. As stated previously, the Shasta Dam region is data rich with a large network of stream gaging stations. The stream gages utilized for the EMA analysis are shown in Figure 2. While data was not used directly from each stream gage station shown in Figure 2, data from the upstream network of gages was used to build a storyline of flows to validate observations recorded at gages representative of Shasta Reservoir inflows. Some of the largest flood events were found to have published values that conflicted depending on the source of the information. The largest flood values are critical in controlling the shape of the upper portion of a frequency curve responsible for estimating peak discharge properties for rare floods. Therefore, the validation of peak flow for the largest events was important to the overall shape of the frequency curve.

Similarly, Reclamation uses paleoflood data as an additional important basis for extending the flood frequency curve. Paleofloods are floods estimated from geologic and geomorphological information combined with hydraulic modeling. Paleoflood studies also try to identify ranges of non-exceedance data representing a period when flow values have not been exceeded at a given location. The data is used to extend the timeseries of available annual peak flows. EMA incorporates the paleoflood and non-exceedance data as a single value or a range of values. Previous paleoflood and non-exceedance estimates were developed for Shasta Dam in 2007. The data were revisited for this study using carbon dating and one-dimensional hydraulic modeling that was not completed during the prior study. The updated paleoflood analysis helped to refine the data for incorporation to the EMA model.

The EMA analysis resulted in a peak discharge frequency curve developed from 137 years of concurrent annual peak flows and a paleoflood with an age greater than 680 years before present time.

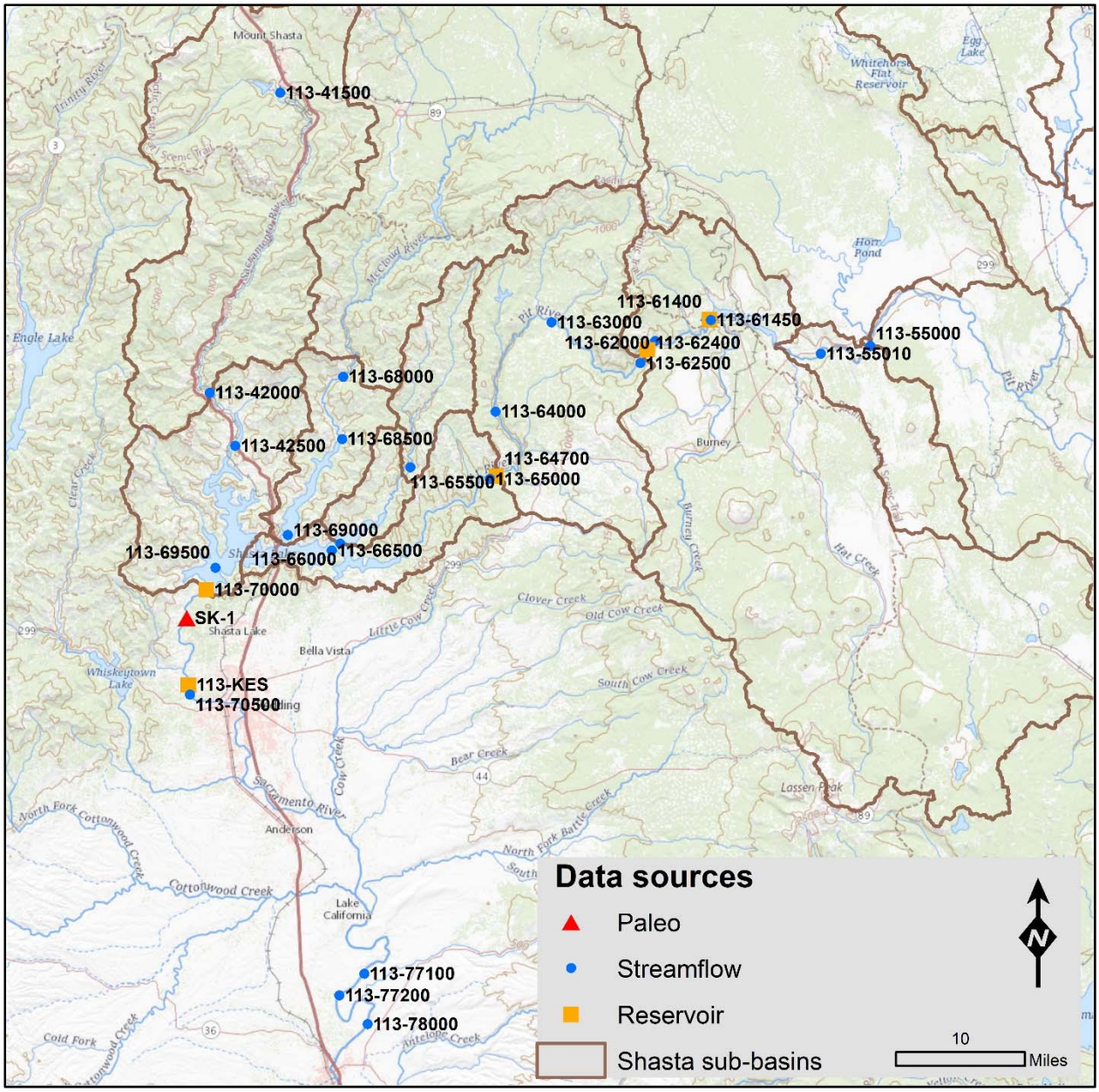

Figure 2. Location of stream gages used to develop annual peak flow timeseries.

Reservoir and Volume Frequency Analysis

The reservoir frequency analysis is an iterative analysis and includes a two-step process consisting of, (1) volume frequency analysis, and (2) reservoir frequency analysis (RFA) that is informed with the volume frequency analysis in addition to other inputs such as seasonality, critical duration, reservoir stage and stage-storage-discharge relationships. The objective of the RFA analysis is to use a combination of daily flows, historic reservoir operations, and sub-daily inflow hydrographs to better understand the probability of the reservoir reaching a stage of interest.

Daily unregulated inflows are one of the most important pieces of data needed to develop volume frequency for an RFA analysis. A long record of unregulated inflow is difficult to acquire for a heavily regulated watershed like the one for Shasta Dam. Fortunately, an extensive 93 year dataset of daily unregulated inflows to Shasta Dam was available based on reanalysis performed by the USACE during the 2002 Sacramento and San Joaquin River Basins Comprehensive Study (USACE 2002). The dataset has been reviewed and used extensively within basin studies and was appropriate for use in the RFA analysis for Shasta Dam.

An important focus of the RFA analysis is understanding and developing the model around the seasonality of the system. While the dominant storms occur during the winter and early spring, the reservoir is operated to have the most flood storage available during the same season. Maximum reservoir stage is reached following the dominant storm season to reduce the probability of flooding while maximizing storage for irrigation season. Therefore, a critical analysis period for RFA modeling is the shoulder season when large floods are still possible but reservoir storage is increasing. Much effort was spent identifying possible scenarios that would result in the greatest reservoir stage.

Again, due to the data rich aspect of the region, several sub-daily hydrographs were available from the USGS through direct contact and within water supply papers. Real hydrographs are critical to characterize the shape and volume of inflow representative of big floods at Shasta Dam.

Rainfall-Runoff Modeling

An AEP-neutral approach (AEP is annual exceedance probability) to rainfall-runoff modeling was used to develop Shasta Dam flood loadings. AEP-neutrality assumes the AEP of the flood is equal to the AEP for the rainfall input. Proper modeling of the precipitation and basin runoff need to reach to validate this assumption. In the current study, precipitation frequency estimates and historic storm templates were developed for application in the rainfall-runoff model. Following calibration of the hydrologic model, precipitation totals in the storm templates were scaled to match specific precipitation magnitudes sampled from the precipitation frequency relationship. The frequency-based templates were routed through the model to simulate flood conditions under rare conditions. Sensitivity analyses were used within the rainfall runoff model varying sensitive runoff parameters as well as the temporal and spatial distribution of precipitation for each storm template. Understanding the full range of resulting flows for each precipitation frequency helped to estimate the AEP neutral results.

Regional Precipitation Frequency Analysis: A basin-average precipitation frequency relationship was developed by applying the regional frequency method (L-moments) of Hosking and Wallis (1997) to historical point precipitation observations in the meteorological region of interest. The precipitation frequency analysis is highly dependent on seasonality and duration. The seasonality is based on the time of year when large precipitation events, atmospheric river events (e.g., Ralph and Dettinger, 2011; Dettinger, 2013; Rutz et al., 2014), occur for the Shasta Dam watershed. Historically, atmospheric river events have produced heavy precipitation totals and flooding in the region. Precipitation-frequency duration is based on understanding the number of precipitating days during heavy precipitation events in the watershed. For the Shasta

Dam basin, 4-day annual maximum precipitation events occur between late-fall and late-spring, specifically October through April, were used.

The Generalized Extreme Value (GEV) distribution best characterizes the seasonal maximum precipitation observations within the meteorological region of interest. The basin-average precipitation frequency relationship was developed by scaling the GEV distribution fit to the point observation data (in the form of a unitless regional growth curve) by an at-site mean (ASM) precipitation total and an areal-reduction factor (ARF) for the Shasta Dam watershed. An uncertainty analysis providing 5th and 95th percent confidence limits was performed using a bootstrap resampling approach.

Storm Templates: HEC-HMS storm template files were generated using output from a numerical weather prediction model, the Weather, Research, and Forecasting (WRF) model. The WRF model is designed to solve the governing equations (e.g., conservation of mass, conservation of momentum, conservation of energy) based on initial and transient conditions provided at domain boundaries. Initial and transient boundary conditions were provided by the Climate Forecast Reanalysis System (CFSR; Saha et al., 2010) at six-hour intervals during each 15-day simulation. Four historical precipitation events were simulated in the WRF model – modeled events began in February 1986, March 1995, December 1996, and February 2004.

Output from WRF was used to develop two types of storm template files—best-estimate and frequency-based estimates. Best-estimate storm templates were based on raw WRF output. Specifically, sub-basin-average precipitation, 2 m air temperature, and 10 m wind speed time series were computed during each hour by averaging each field across each sub-basin. Frequency-based storm templates were based on scaling WRF precipitation output by a frequency-based ratio. The frequency-based ratio, which varies by event and return period, was computed as the ratio of basin-average precipitation sampled from a basin-average precipitation-frequency relationship to basin-average precipitation from WRF. The frequency-based storm templates only include changes to precipitation; all other variables remain the same.

Runoff Modeling: Storm templates and the basin-average precipitation frequency relationship were used to develop inputs to a rainfall-runoff model (HEC-HMS) to simulate the hydrologic response of the Shasta Dam watershed. To conduct this analysis, the precipitation was spatially and temporally distributed throughout the basin according to historic storm patterns (i.e., output from WRF). The four selected historic events, identified here by water year as 1986, 1995, 1997, and 2004, were used to represent a range of precipitation events that impacted the watershed.

The Upper Sacramento River HEC-HMS model originally developed by the USACE (Dunn et al., 2001; USACE, 2002) was adapted and used in this study for rainfall-runoff modeling. The original model developed for the 2002 USACE Sacramento and San Joaquin River Basins Study has been extensively reviewed and used since its development.

The original HEC-HMS model was modified allow data inputs developed specifically for the Shasta Dam hydrology study. Similarly, the model was recalibrated and validated using the four historic precipitation events used for storm template development (1986, 1995, 1997, and 2004).

Results

Results from the multiple methods analysis were used to build a case for recommending the most representative frequency flood inflows to Shasta Dam. The independent nature of each of the methods lead to unique results representative of different flood properties. The EMA analysis results in a peak discharge frequency curve, RFA results in a volume and stage frequency curves, and the rainfall-runoff modeling results in hydrographs representative of the precipitation frequency. In order to compare the results in a trend analysis they needed to be converted to describe similar metrics. Trends were explored based on peak inflow and 7-day volume.

Peak inflow was estimated for the RFA model results using the peak of the representative scaled hydrograph corresponding to specific frequencies. Peak inflow is a direct output from the EMA and rainfall runoff methods. The peak discharge from all three methods resulted in a similar skew. The magnitudes of the peak inflow varied between the methods with the EMA method producing the lowest peak inflows, the rainfall runoff method producing the highest peak inflows, and the RFA method having results somewhere in between.

To compare 7-day volume, the EMA results were scaled to the peak discharge of the 1940 historic hydrograph. Similar to the peak discharge results, the 7-day volume from the multiple methods had a similar skew but varied in magnitude, with the EMA method producing the lowest 7-day volumes and the rainfall runoff producing the highest 7-day volume.

A positive aspect of the results were the similar trends in skew between the results of the independent methods. The similar trend in the skew could be associated with how the results are being extrapolated. If the skew varied between the methods, the difference in the values could increase greatly for rarer events. Or the curves could cross at some point. Having frequency curves with similar skew results in somewhat parallel frequency curves that gives more confidence that the data is being extrapolated appropriately. Similarly, it builds confidence that similar hydrologic processes are being captured by the independent datasets.

While the results had similar shapes, the magnitudes varied, making it challenging to recommend specific frequency results and set of hydrographs to be used for hydrologic loadings. All of the results are supported with historic observations, calibrated modeling, and current state-of-the-practice methodologies. Therefore, a combination and weighting approach was used with the recommended results representing a range of uncertainty based on the median values from each method.

References

Cohn, T.A., W.L. Lane, and W.G. Baier, 1997. “An Algorithm for Computing Moments-Based Flood Quantile Estimates When Historical Flood Information Is Available.” Water Resources Research, 33, 9, 2089–2096.

Cohn, T.A. and J.F. England, 2016. PeakfqSA Program, Version 0.998.

Cudworth, A.G., 1989. “Flood Hydrology Manual, A Water Resources Technical Publication.” U.S. Department of the Interior, Bureau of Reclamation, Denver, Colorado, 243 p.

Daly, S.F.R. Davis, E. Ochs, and T. Pangburn, 2000. “An Approach to Spatially Distributed Snow Modelling of the Sacramento and San Joaquin Basins, California.” Hydrological Process, 14, 3257–3271.

Dettinger, M.D., 2013. “Atmospheric Rivers as Drought Busters on the U.S. West Coast.” Journal of Hydrometeorology, 14, 1721-1732, https://doi.org/10.1175/ JHM-D-13-02.1.

Dunn, C., M. Hurst, H. Dotson, M. McPherson, J. Doan, and T. Evans, 2001. "HEC-HMS for the Sacramento and San Joaquin River Basins Comprehensive Study." U.S. Army Corps of Engineers, Sacramento District and Hydrologic Engineering Center, California.

England, J.F., Jr., Cohn, T.A., Faber, B.A., Stedinger, J.R., Thomas, W.O., Jr., Veilleux, A.G., Kiang, J.E., and Mason, R.R., Jr., 2018. "Guidelines for determining flood flow frequency—Bulletin 17C," U.S. Geological Survey Techniques and Methods, book 4, chap. B5, 148 p., https://doi.org/10.3133/tm4B5.

Hirsch, R.M., 1982. "A Comparison of Four Streamflow Record Extension Techniques." Water Resources Research, 18, 4, 1081-1088.

Hosking, J.R.M. and J.R. Wallis, 1997. "Regional Frequency Analysis: An Approach Based on L-Moments." Cambridge University Press, 224 p.

Livneh B., E.A. Rosenberg, C. Lin, B. Nijssen, V. Mishra, K.M. Andreadis, E.P. Maurer, and D.P. Lettenmaier, 2013. "A Long-Term Hydrologically Based Dataset of Land Surface Fluxes and States for the Conterminous United States: Update and Extensions." Journal of Climate, 26, 9384–9392.

Ralph, F.M. and M.D. Dettinger, 2011. "Storms, Floods, and the Science of Atmospheric Rivers." Eos, Transactions, American Geophysical Union, 92, 265–266.

Rawls, W.J., D.L. Brakensiek, and N. Miller, 1983. "Green-Ampt Infiltration Parameters From Soils Data." Journal of Hydraulic Engineering, 109, 1, 62-70.

Rutz, J.J., W.J. Steenburgh, and F.M. Ralph, 2014. "Climatological Characteristics of Atmospheric Rivers and Their Inland Penetration Over the Western United States." Monthly Weather Review, 142, 905-921.

Saha, S. et al., 2010. "The NCEP Climate Forecast System Reanalysis." Bulletin of the American Meteorological Society, 91, 1015–1058, https://doi.org/10.1175/2010BAMS3001.1.

Smith, H., M. Bartles and M. Fleming, 2018. "Hydrologic Hazard Methodology for Semi-Quantitative Risk Assessments – An Inflow Volume-Based Approach to Estimating Stage-Frequency for Dams." U.S. Army Corps of Engineers, Institute for Water Resources Risk Management Center.

United States Army Corps of Engineers (USACE), 2002. "Sacramento and San Joaquin River Basins Comprehensive Study, Technical Studies Documentation." Appendices A through G. Sacramento District, California.

United States Army Corps of Engineers (USACE), 2017a. Hydrologic Modeling System HEC-HMS, Version 4.2.1, Build 28, March 2017. U.S. Army Corps of Engineers, Davis, California.

United States Army Corps of Engineers (USACE), 2017b. Statistical Software Package, HEC-SSP, Version 2.1.1, June 2017. U.S. Army Corps of Engineers, Davis, California.

Fluvial Geomorphology

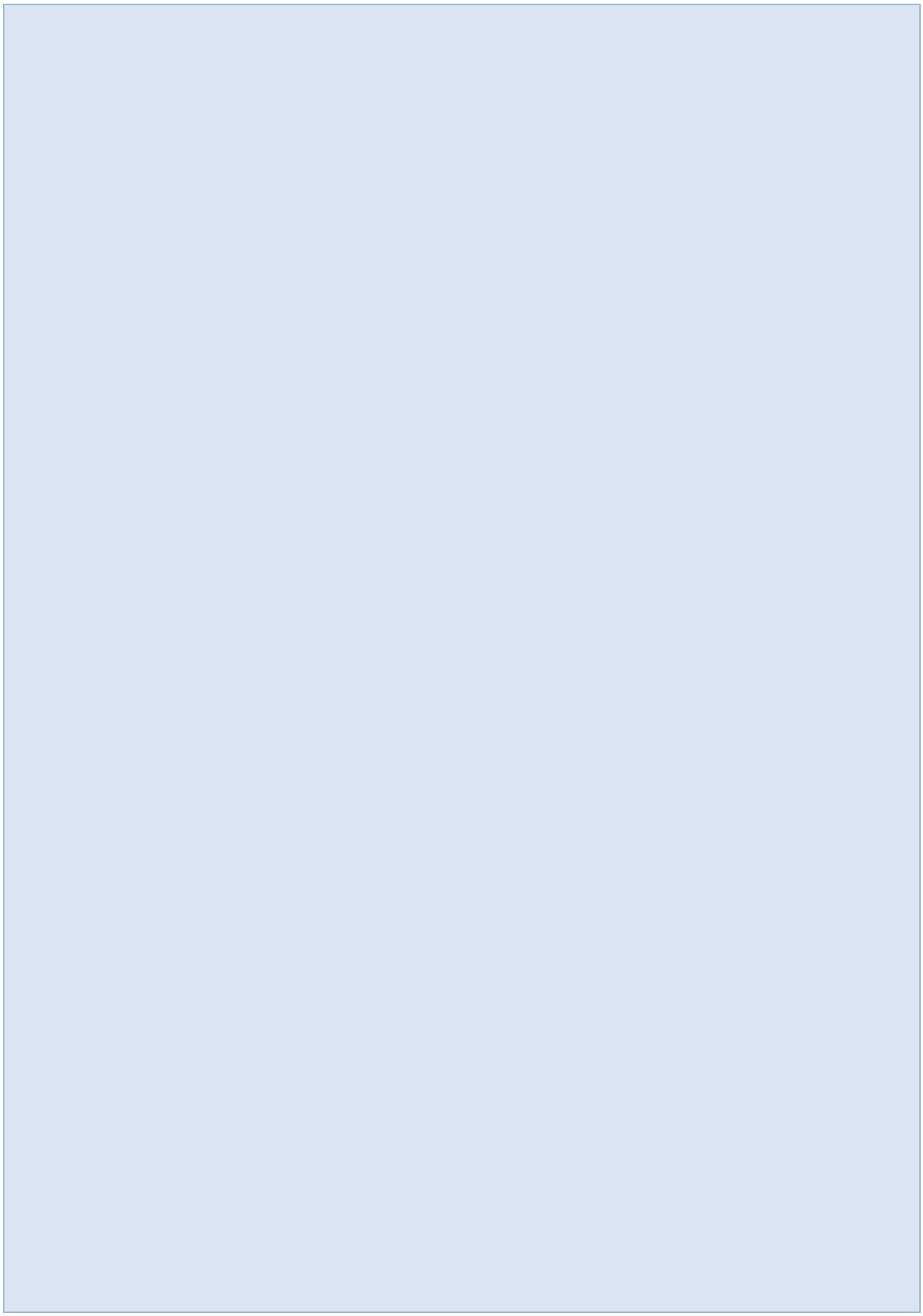

An Assessment of a LiDAR-Based Approach for Estimating Regional and Hydraulic Geometry Relationship Curves for the Southern Driftless Area of the Midwest

Christopher P. Haring, Research Physical Scientist,
ERDC-River Engineering Branch, Vicksburg, MS,
Christopher.P.Haring@@usace.army.mil

Abstract

The development of empirical equations and curves based on Hydraulic Geometry Relationships (HGR) for use in natural channel design and stream assessments is an important and evolving field in geomorphology and river engineering research. Regional specific HGR describing relations of bankfull channel characteristics for width, depth, cross-sectional area, and discharge are used extensively across the United States for stream geomorphic assessments, stream rehabilitation, and design (Castro and Jackson, 2001). Two types of commonly developed HGR are regional and regime curves. Regional curves are regression equations that correlate bankfull channel dimensions and discharge to watershed drainage area. Regime curves are constructed from regression equations that relate bankfull stream channel width, mean depth, cross-sectional area, and mean velocity to bankfull discharge.

Regional and regime curves have been developed for many parts of the country and around the world but have not been developed for the Southern Driftless Area of the Midwest. This study details the results of a new Light Detection and Ranging (LiDAR) and HGR based methodology for developing bankfull regional and regime curves for the Southern Driftless Area streams of the Midwest. LiDAR is an optical remote-sensing technique that uses laser light to densely sample the surface of the Earth, producing highly accurate x, y, and z measurements.

The typical protocol for developing regional curves incorporates extensive field data collection and surveys that can be time consuming and costly. Researchers, river engineers, and restoration specialists may not have the resources or funding available to gather bankfull channel dimensions, floodplain bench elevations and extents, or additional natural channel features. If efficient ways of gathering geomorphic channel data are not available, then research and project designs suffer due to lack of applicable or credible data. Based on this need, a LiDAR-HGR methodology was developed to construct both regional and regime curves using LiDAR-high resolution terrain data. The LiDAR-HGR approach integrates the more traditional geomorphic channel survey techniques and data interpretation with high resolution terrain data to save time, reduce cost, reduce potential field data collection error, and offer a relatively rapid approach for developing HGR.

In this study, traditional geomorphic stream channel survey data from previous studies and newly collected geomorphic channel surveys are used to evaluate the LiDAR-HGR based approach of developing regional and regime regression equations. The results of this study demonstrate that the LiDAR-HGR based methodology can be used to replace or supplement the more time and resource consuming field-based procedures used in previous studies. The new methodology may not only reduce time and cost, but in some cases also be capable of providing similar accuracy for channel and floodplain data collection.

Introduction

Stream systems develop a regular progression of channel form and morphology that naturally balance upstream watershed inputs. Stream channel forming flow or bankfull discharge provides hydraulic geometry relationships that develop from balancing and maintaining a quasi-equilibrium state and balance between sediment supply, slope, channel shape, channel planform, vegetation, soil types, geology, and other factors. In a stable stream, bankfull discharge fills the channel to the active floodplain level, delineating a morphological feature which defines the channel forming discharge and informs sediment transport processes and depositional features on a floodplain (Dunne and Leopold, 1978; FISRWG, 1998). To mimic natural channel conditions, bank-full channel geometry and discharge are commonly estimated using regression analysis and graphical plots that relate bankfull channel characteristics such as width, mean depth, cross-sectional area, and discharge to drainage area and are referred to as "regional curves."

In parts of the United States stream research and restoration specialists use generalized regional and regime curves from other regions potentially introducing error using data derived from a differing hydro-physiographic region (Sherwood and Huitger, 2005). In the Southern Driftless Area of the Midwest, where regional, sub-regional, or statewide regional and regime curves are not available, regional curves published by Dunne and Leopold (1978) are used by federal, state, and local governments, and private organizations to estimate bankfull channel geometry and discharge. Though widely used, these curves (Dunne and Leopold, 1978) are developed from sites of unknown localities (Emmett, 2004), and the accuracy of these curves when applied to streams in the Midwest is unknown.

The development of HGR curves and equations requires bankfull channel dimensions based on stable riffle cross-over locations and the LiDAR data collection techniques do not penetrate the water surface; lower discharge and wadable stream conditions were considered desirable to provide the least amount of depth error. Riffle cross-over locations (Figure 1) are typically active channel areas with the least amount of depth at low flow and bankfull discharges. Pools are the deep channel areas between the riffle cross-over locations. In flows of bankfull and lower, riffles have steeper slopes, and pools have relatively flat slopes. As discharge increases, the pool slopes become steeper, and the riffle slopes become flatter. These relationships are very important to sediment transport and the formation of channel forming bankfull discharge signatures at the channel margins. The representative riffle or run segment of a stream is the location where erosional features are at a minimum, so bankfull indicators and other geomorphic characteristics will be present. The bankfull indicators will typically be an active floodplain or some other geomorphic channel-forming discharge marker such as vegetation or erosional lines on the channel margins.

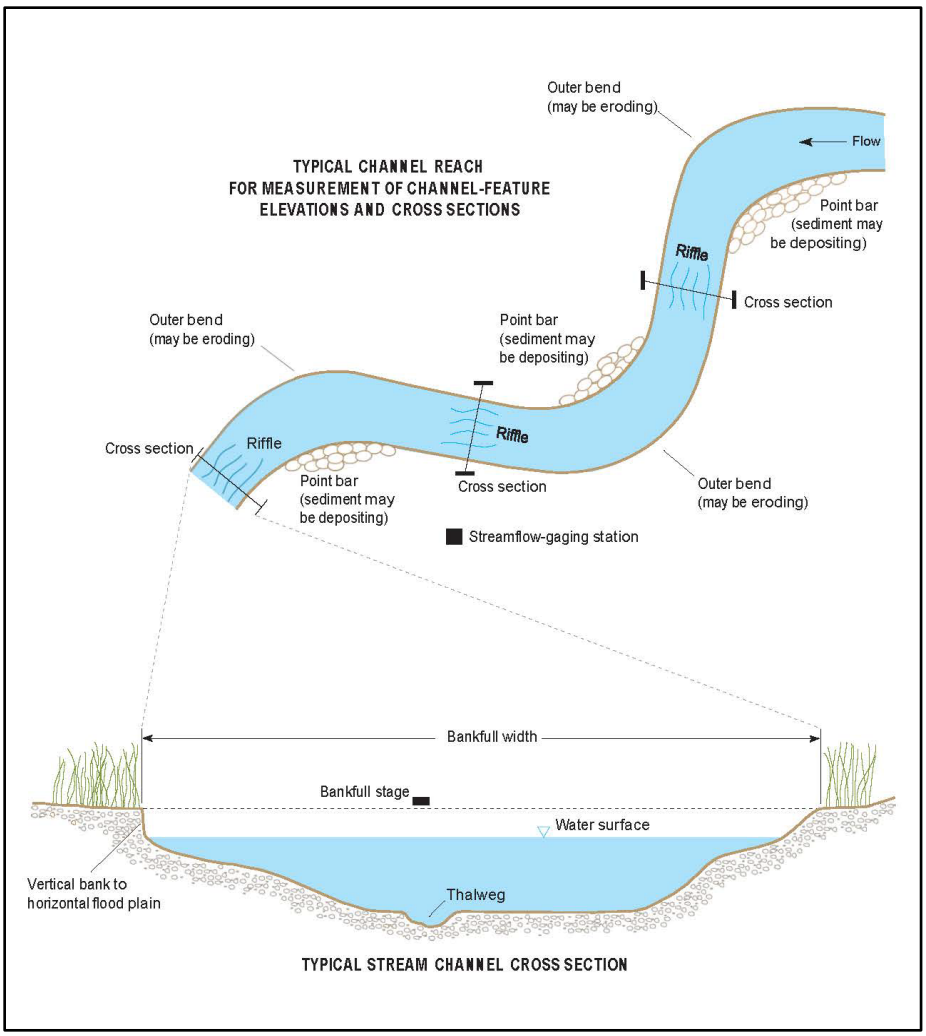

Figure 1 Typical Stream Reach and Cross-section Locations for Channel Features (From Lawlor 2004)

In the design of a HGR curve study, an area, region, or sub-region is typically selected based on a variety of common hydro-physiographic factors. The selection of the region for this study originally included the entire Driftless Area of the Midwest. The United States Environmental Protection Agency (EPA) divides the United States into Ecoregions (Level III) that offer a basis for analyzing patterns and composition of the geographic areas. However, upon further investigation, the Driftless Area was thought to be too large and extensive from a hydro-physiographic range perspective. If a selected region has too much natural variability in the underlying geology, soils, channel and watershed slopes, vegetation, precipitation, resulting runoff rates and other factors, then the regionally derived geomorphic channel data will have significant inconsistencies and wide error bands. Splitting the Driftless Area into two regions, north and south and analyzing the Southern Driftless Area sub-region alleviated some of the common geomorphic channel data variability. The final Southern Driftless Area delineation for the split between the two sub-regions was decided through the selection of a group of USGS gage site locations. The selected Southern Driftless Area Region along with the gage sites and associated stream reaches are displayed in Figure 2. There were 28 Southern Driftless Area USGS gage site locations identified for this study to provide the appropriate level of hydrologic and hydraulic data required for regional and regime curve development. In addition, existing

NRCS geomorphic stream channel survey data were available from four previously completed stream surveys ranging from less than one square mile to approximately 40 square miles. Four other stream channel surveys were completed on USGS gage station locations ranging from approximately one square mile to 125 square miles. The two sets of gage analysis locations provide geomorphic channel data for testing the LiDAR-HGR approach. Overall, the 28 Southern Driftless Area sites were developed exclusively with the LiDAR-HGR approach to develop the HGR regression equations and curves.

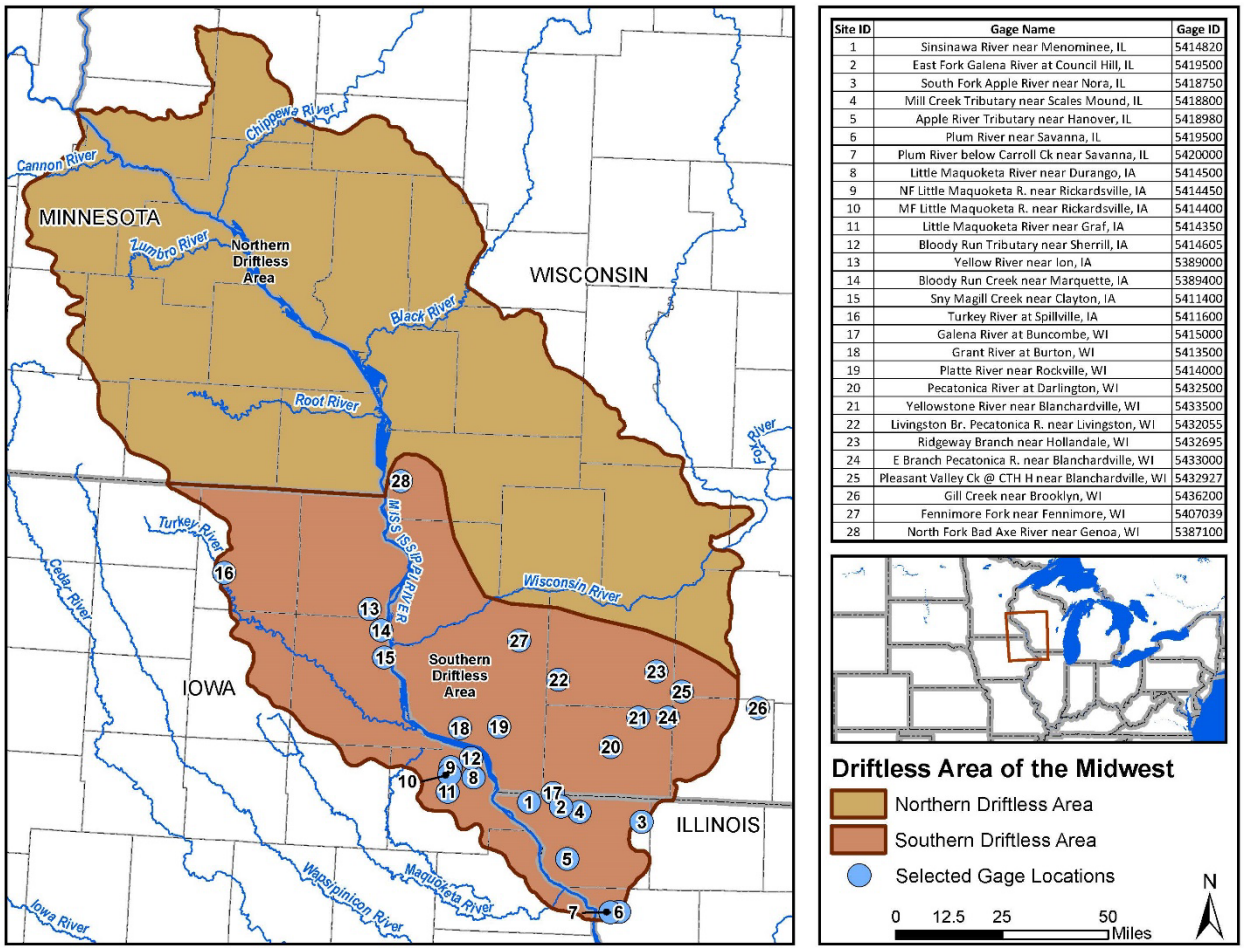

Site ID	Gage Name	Gage ID
1	Sinsinawa River near Menominee, IL	5414820
2	East Fork Galena River at Council Hill, IL	5419500
3	South Fork Apple River near Nora, IL	5418750
4	Mill Creek Tributary near Scales Mound, IL	5418800
5	Apple River Tributary near Hanover, IL	5418980
6	Plum River near Savanna, IL	5419500
7	Plum River below Carroll Ck near Savanna, IL	5420000
8	Little Maquoketa River near Durango, IA	5414500
9	NF Little Maquoketa R. near Rickardsville, IA	5414450
10	MF Little Maquoketa R. near Rickardsville, IA	5414400
11	Little Maquoketa River near Graf, IA	5414350
12	Bloody Run Tributary near Sherrill, IA	5414605
13	Yellow River near Ion, IA	5389000
14	Bloody Run Creek near Marquette, IA	5389400
15	Sny Magill Creek near Clayton, IA	5411400
16	Turkey River at Spillville, IA	5411600
17	Galena River at Buncombe, WI	5415000
18	Grant River at Burton, WI	5413500
19	Platte River near Rockville, WI	5414000
20	Pecatonica River at Darlington, WI	5432500
21	Yellowstone River near Blanchardville, WI	5433500
22	Livingston Br. Pecatonica R. near Livingston, WI	5432055
23	Ridgeway Branch near Hollandale, WI	5432695
24	E Branch Pecatonica R. near Blanchardville, WI	5433000
25	Pleasant Valley Ck @ CTH H near Blanchardville, WI	5432927
26	Gill Creek near Brooklyn, WI	5436200
27	Fennimore Fork near Fennimore, WI	5407039
28	North Fork Bad Axe River near Genoa, WI	5387100

Figure 2: Map of the Driftless Area of the Midwest and the 28 Southern Driftless Area Gage Study Sites

Geomorphic Setting of the Southern Driftless Area

The Driftless Area of the Midwest is a mostly unglaciated region that lies largely in southwestern Wisconsin, but also includes small portions in SE Minnesota, NE Iowa, and NW Illinois (Knox and Leigh 1990). The Driftless Area covers an area of nearly 15,000 square miles, 13,360 square miles of that lie in Wisconsin with the remainder extending into Minnesota, Iowa, and Illinois (Figure 2). The LiDAR-HGR study area covers the southern portions of the Driftless Area that have similar geology, physiography, vegetation, climate, soils, land-use, and hydrology. The Driftless Area physiographic section is in the Central Lowland physiographic province that is within the Interior Plains major physiographic division (Omernik, 1987).

The Iowa section is referred to as the Paleozoic Plateau, having been influenced (to varying degrees) by glaciation, with evidence of glacial till and outwash in certain areas. Iannicelli (2010) provides a summary of the geologic data that supports the pre-Illinoian glaciation of parts of the Driftless Area, specifically the NE Iowa section and describes the chances of finding till as "*extremely remote*." The generalized bedrock geology of the Southern Driftless Area watersheds range from Cambrian sandstones to Ordovician dolomite, shale, and limestone, to Silurian dolomites (Figure 3).

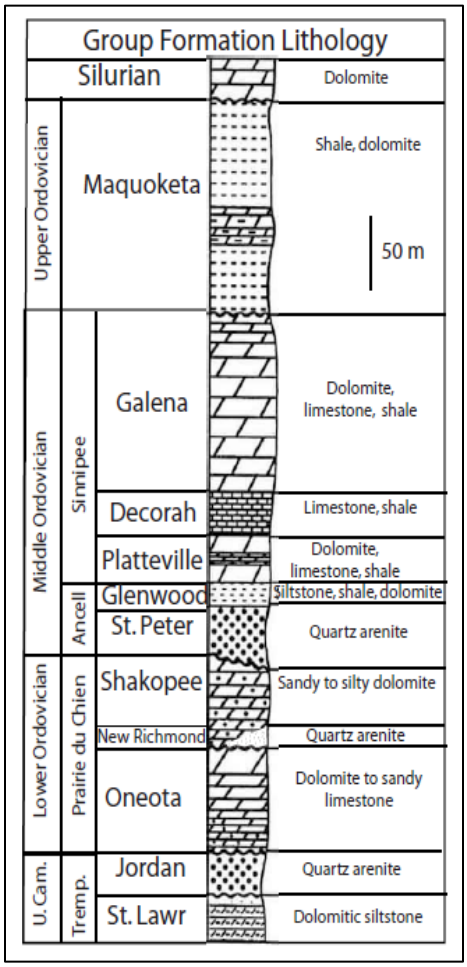

Figure 3. Generalized Stratigraphic Column for the Sourthern Driftless Area of the Midwest (Modified from Robins, 2005; Smith and Simo, 1997)

For the Southern Driftless Area, in Wisconsin and northeastern Iowa, the major karst formations are located in the Lower Ordovician Oneota Formation and Middle Ordovician Galena and Platteville Formation carbonates. For northern Illinois and eastern Iowa, the karst areas are in the Middle Ordovician (Galena and Platteville) carbonates and Silurian dolomites. In southwestern Wisconsin, Day (1986) describes the karst-cave extents as occurring, "*mostly located on the hilltops and hillsides and represent remnants of formerly more extensive cave systems now dismembered by valley incision.*" The majority of the caves are stranded in the vadose or unsaturated zone, most within 10 meters of the ground surface. The northeastern Iowa watersheds have karst regions that are more extensively developed with direct hydrologic connections. Some stream systems have been identified with "*losing streams*" on the Upper

Iowa River. A losing or influent stream loses water as it flows downstream with the water infiltrating into the ground recharging the near surface aquifer. In these areas, the water table is below the stream bottom, so the porous material moves water down and to the sides, losing flow at the channel boundaries. Losing streams are very common in the desert and karst landscapes. Karst influences to the regional curve development should be minimal in most areas of the Southern Driftless Area, but watersheds in northeast Iowa should be investigated further to determine to what extent the karst areas may influence watershed hydrology and associated stream channel dimensions.

The bedrock in the Paleozoic Plateau controls the shape of the landform with upland and lowland flat areas in agriculture, valley slopes and steeper slopes in pasture or forest. The region's distinctive topography is marked by fertile farms on the plateaus; deeply carved valleys with tall, steep bluffs of dolomite; numerous caves; springs; and cold-water streams. The hills and sharp ridges are underlain by dolomitic strata and sweeping slopes, and wide valleys are generally eroded into less resistant underlying shale (Frankie and Nelson, 2002). Loess (windblown silt), in which the modern soils developed, covers the less resistant underlying shale. Land-use practices of the 1800's and early 1900's led to wide-scale erosion, flooding, and the altering of its streams and valleys with the deposition of dozens of feet of soil at many locations (Frankie and Nelson, 2002). The highest point in the Driftless Area is West Blue Mound at 1,719 ft. msl. The Driftless Area streams are typically gravel-cobble bed with the larger systems being small gravel to sand and silt. The streams in this study are mostly wadable in low flow, with drainage areas ranging from approximately 0.5 to 300 square miles.

Purpose and Scope of Approach

This study takes the stream channel geomorphology analysis a step further by combining the LiDAR in-channel terrain data with USGS gage flow statistics to develop regional and regime curves. The regional and regime curves are focused on capturing bankfull riffle cross-over location data that provide bankfull stream channel dimensions and discharge for statistical analysis. The riffle cross-over locations have the lowest amount of depth error if the LiDAR data are collected during low flow times that in many cases occurs during leaf-off LiDAR data collection times. There are potential limitations to this method such as the timing of when the LiDAR data is collected, timing between the LiDAR data collection and geomorphic channel studies, and the lack of depth data for some larger watersheds that have streams with deeper riffle cross-over sections. However, given our current working knowledge of the applications and interpretation of LiDAR terrain data, and combined with traditional geomorphic field methods, a LiDAR-based methodology for producing regional and regime curves has great potential.

In the selection of the Southern Driftless Area watershed study sites, criteria include assembling a widespread range of watershed sizes that were mostly wadable with USGS gages ranging from0.5 to approximately 300 square miles in area. The best watershed size data should have sizes equally distributed for the entire population of data sites. Unfortunately, for this region there are very few or non-existent gage sites ranging from 50 to 120 square miles water-sheds. Another smaller watershed size gap identified was from five to 15 square miles. There were supplemental gages identified in the five to 15-square-mile range and at least one additional gage from the 50 to 120-square-mile watershed size, but data have not been collected for the additional sites for this study. The selected watershed sites include 28 USGS gage locations, comprised of 12 streams in SE Wisconsin, nine streams in NE Iowa, and seven streams in NW Illinois. Six of these streams had previous geomorphic channel surveys completed in 2009

(NRCS study sites) and 2017 geomorphic channel surveys, while the other 22 sites were visited in the field in 2016, 2017, and 2018 to review the site conditions.

The goals and objectives of the Southern Driftless Area of the Midwest study are to:

1) Assess the LiDAR-HGR approach using 28 USGS stream gage sites for estimating bankfull channel geometry and discharge. The compilation of 28 sites fulfill a commonly followed practice that at least 24 gages be used for regional and regime curve development. The watersheds were also limited to those within the Southern Drift-less Area to maintain the same hydro-physiographic region. There are 12 sites in SE Wisconsin, 9 in NE Iowa, and 7 in NW Illinois.

2) Compare LiDAR-HGR based 2008 channel surveys to existing 2017 geomorphic channel surveys to investigate potential error between the methods. There were two existing geomorphic channel surveys available for smaller stream system comparisons, the Site 3-South Fork Apple River (1.93 square mile) and Site 1-Sinsinawa River (39.6 square mile) sites. Because the study is investigating watersheds up to approximately 300 square miles in area, larger watersheds were added to investigate a wider range of sizes. Since the Site1-Sinsinawa River was the largest site at just under 40 square miles, two larger watersheds were selected to fill the gap based on doubling and tripling the 40-square-mile watershed. Site 28-North Fork Bad Axe River (80.8 square miles) and Site 17-Galena River (125 square miles) were chosen to expand the analysis to larger watersheds. The LiDAR data were gathered on December 31, 2008, and the geomorphic channel surveys were completed in November 2017.

3) Compare LiDAR-HGR based 2008 channel surveys to existing 2009 NRCS geomorphic channel survey data. In 2009, NRCS geomorphic channel surveys were collected for Site 4-Mill Creek Tributary (0.86 square miles), Site 5-Apple River Tributary (1.55 square miles), Site 3-South Fork Apple River (1.93 square miles), and Site 1-Sinsinawa River (39.6 square miles). Bankfull channel dimensions of width, mean depth, cross-sectional area and discharge were compared from the NRCS data to determine differences with values derived from the LiDAR-HGR. The LiDAR data was gathered on December 31, 2008, and the NRCS surveys were completed June 1 through June 6, 2009.

4) Compare LiDAR-HGR based regional curves to existing USGS regional curves from the Eastern United States, Indiana (three curves), Ohio (two curves), and Southern Michigan. The Eastern United States regional curves are used extensively for geomorphic channel comparison and analysis in many parts of the Midwest (Sherwood and Huitger, 2005). This broad application of the curves likely adds a large amount of geomorphic channel dimension and engineering design error because it involves applying curves too far removed from their original hydro-physiographic region. This analysis will provide a test as to whether the Eastern United States curves are indeed applicable on a wider basis or if the Southern Driftless Area LiDAR-HGR-based regional curves approach provides a more suitable alternative. Evaluation of possible relationships be-tween the Southern Driftless Area to the Indiana, Ohio, and Southern Michigan USGS curves allow for additional comparisons to determine if other Midwest hydro-physiographic regions might have similar bankfull channel dimensions and watershed characteristics.

5) Assess the capability of the LiDAR-HGR methodology to predict HGR at chosen sites in Indiana and Ohio developed for USGS Indiana and Ohio regional curves. The Indiana regional curves were developed on ungaged streams, so channel dimensional analysis without converting

USGS gage-stage discharge relationships is not required. The Ohio regional curve sites were developed at USGS gage stations and required gage analysis. Four sites from Indiana and three Ohio gage sites were chosen with watershed sizes ranging from 4.7 to 88.8 square miles.

Methods

The LiDAR-HGR approach and the geomorphic channel surveys completed for the four 2017 geomorphic channel surveys and the four 2009 NRCS channel surveys followed the common ground survey techniques outlined in Harrelson et al. (1994), Leopold (1994) and the USDA Stream Corridor Restoration Manual (1996). The datum used for surveys was the local gage datum. For many of the gages, this is an arbitrary datum established below the elevation of the lowest expected range of the stage-discharge rating curve and typically established near the stream bottom. Benchmarks and reference marks were used during geomorphic channel surveys at each gage location to tie into the local datum. Data were converted as required at all gage locations using the Corpscon6 Program to National Geodetic Survey Datum 1988 (NGVD88). NGVD88 is the datum that the LiDAR survey data was collected in. Survey notes were taken to identify specific geomorphic data on channel profiles, cross-sections, and bankfull geomorphic indicators.

Cross-sections for the geomorphic channel surveys and LiDAR-HGR were taken at representative riffles, runs, or cross-over locations. Channel morphological features were surveyed including top of bank, bankfull indicators, left and right water edge, thalweg, and channel bottom (Harrelson et al., 1994). A minimum of two and a maximum of seven representative stream-channel reference cross-sections were identified at riffle locations along the stream profile for both the geomorphic channel surveys and the LiDAR-HGR methods. Harrelson et al. (1994) recommends cross-sections located in stable reaches between channel bends where the riffle cross-over locations are located (Figure 1). A reach had a minimum of two reference cross-sections, in that data were averaged to provide reach-representative values of bankfull width, mean depth, cross-sectional area, mean velocity, wetted perimeter, width-to-depth ratio, and others.

The LiDAR data were collected for the 28 study sites by airborne methods for Iowa in 2007 and 2010, for Illinois in 2008, and for Wisconsin in 2010 and 2011. The Southern Driftless Area LiDAR point cloud datasets vertical accuracies (bare ground) ranged from 0.23 to 0.89 ft. The corresponding 95-percent confidence levels for all Southern Driftless Area LiDAR vertical accuracies ranged from 0.59 to 1.19 ft. The horizontal accuracy is less than 0.4 tenths of an inch. The 2017 geomorphic channel surveys were collected using a Javad GNSS Triumph-1 GPS. The typical errors for the High Resolution GPS traditional geomorphic channel surveys are as little as 0.05 ft (1.5 cm) horizontal and 0.1 ft (3 cm) vertical (Billings, 2017). The 2017 geomorphic channel surveys average errors were approximately 0.2 ft (6.0 cm) vertical and 0.05 ft (1.5 cm) horizontal. Error values commonly vary point to point depending on survey equipment tolerance settings. A CST-Berger LMH “C” Rotary Laser Level was used to collect the 2009 NRCS geomorphic channel survey data. The typical vertical error at 100 ft (30 m) is plus or minus 0.1 ft (3 cm). As the survey distance increases for the laser levels so do the typical error range from 0.1 ft (3 cm) to 0.5 ft (15.24 cm). The vertical and horizontal errors are assumed to be within the range of typical laser level survey errors for this analysis. For this study, the high resolution GPS and laser level geomorphic channel surveys are considered to be the baseline that the 2008 LiDAR data is measured against. For this study the original LiDAR point cloud data was

collected for each site and reprocessed to remove hydro-flattening that removes the water surface slope. By reprocessing and removing the hydro-flattening water surface slopes can be derived. New reprocessed LiDAR DEMs were completed to 1 ft vertical resolution.

After the data were collected and analyzed, regression analysis defining equations and graphing were completed for curve development. Cross-section five from Site 1-Sinsinawa River (Figure 4) illustrates the cross-section plotting for both the 2017 geomorphic channel survey and the 2008 LiDAR data that were used for analysis. The largest differences occur with the in-channel thalweg section where the water is deepest. There are also slight differences below the bankfull elevation between the geomorphic channel survey and the LiDAR interpretation. The geomorphic channel survey included 32 elevation points with variable spacing compared to the LiDAR-HGR that had 384 elevation points on 0.33 foot spacing for the same surveyed cross-section. One major note on the two datasets is the LiDAR data were gathered on December 31, 2008, and the geomorphic channel surveys were completed in November 2017. It is quite likely that some of the differences between the two datasets represent active erosion of the thalweg along the left bank with deposition on the right bank point bar channel margin. The channel in this area is very stable with cobble and gravel substrate, so the channel depth would likely be very similar for both datasets collected. The difference in the overbank floodplain elevations is a bit more puzzling as there are no obvious indications of mass deposition. However, two of the largest flood events on record occurred in July 2010 and again in July 2011. The final orientation of cross-section five likely has somewhat differing and altered alignment when comparing the geomorphic channel survey to the LiDAR data. There could be slight errors in both surveying methods that would also intro-duce slight elevation and stationing differences.

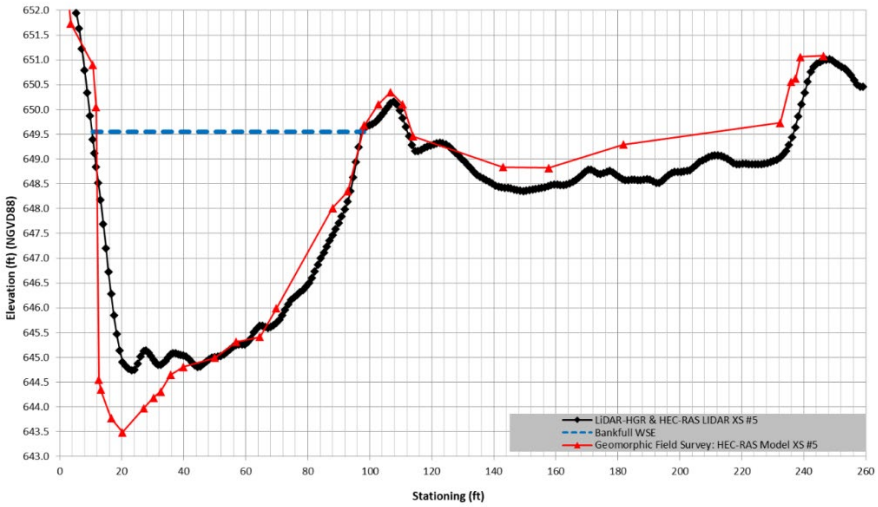

Figure 4. Site 1-Sinsinawa River (05414820) Gage Site Cross-section #5: Geomorphic Channel Survey (red) and LiDAR-HGR (black), Bankfull Water Surface Elevation (blue)

The basis of the LiDAR-HGR bankfull geomorphic channel mapping requires the collection of detailed topographic bankfull indicators. To provide a method to objectively derive bankfull channel characteristics from LiDAR based topographic floodplain indicators, Faux et al. (2009) used a method of comparing hydraulic depth. Hydraulic depth is flow area divided by flow width. The LiDAR-HGR approach uses the existing water surface as captured by LiDAR as a function of flow height (elevation) for each cross-section. The hydraulic depth test provides the maximum value as the function indicates a sudden increase in flow width at the elevation where water spills onto the floodplain thereby signifying geomorphic floodplain connection. Faux et al.

(2009) noted that their approach was originally proposed by McKean et al. (2005) and is discussed in bankfull determination approaches from Williams (1978). Figure 5 shows the hydraulic depth function for the Sinsinawa River gage site cross-section five from Figure 4.

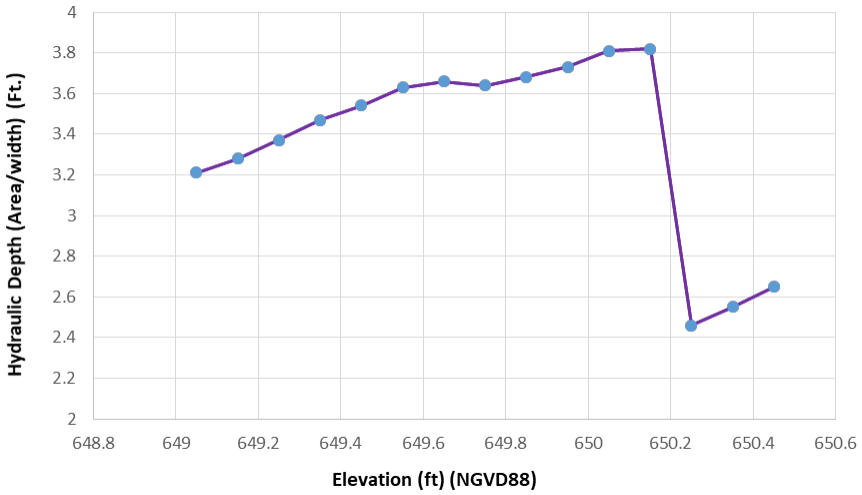

Figure 5. Example Hydraulic Depth Function for the Site 1-Sinsinawa River (05414820) Gage Site Cross-section #5

In Figure 5, hydraulic depth increases from 3.21 ft. and elevation 649.05 ft. (NGVD88) until it reaches elevation 649.65 ft. (NGVD88) with a hydraulic depth of 3.66 ft. The next tenth of a foot increase in elevation increases to 649.75 ft. (NGVD88), decreases the hydraulic depth to 3.64 ft., and stays relatively flat until elevation 650.15 ft. (NGVD88) and hydraulic depth 3.81 ft. The hydraulic depth significantly decreases between elevation 650.15 (3.82 ft.) and 650.25 (2.46 ft.) (NGVD88). This is caused by the extended channel width and area relationship change once the flow overtops the existing berm. Site specific determinations of hydraulic depth and associated bankfull channel forming discharges have to be determined for each gage site and the hydraulic depth tool provides an objective tool for determining bankfull elevations and associated floodplain elevations. When possible, it is certainly recommended to have geomorphic channel surveys to confirm bankfull elevations and other geomorphic channel features to provide more confidence in the data developed for bankfull hydraulic geometry relationships.

The longitudinal profile and bankfull indicators upstream and downstream were used to validate bankfull and floodplain geomorphic features. An example of the longitudinal bankfull indicators along the profile is depicted in Figure 6.

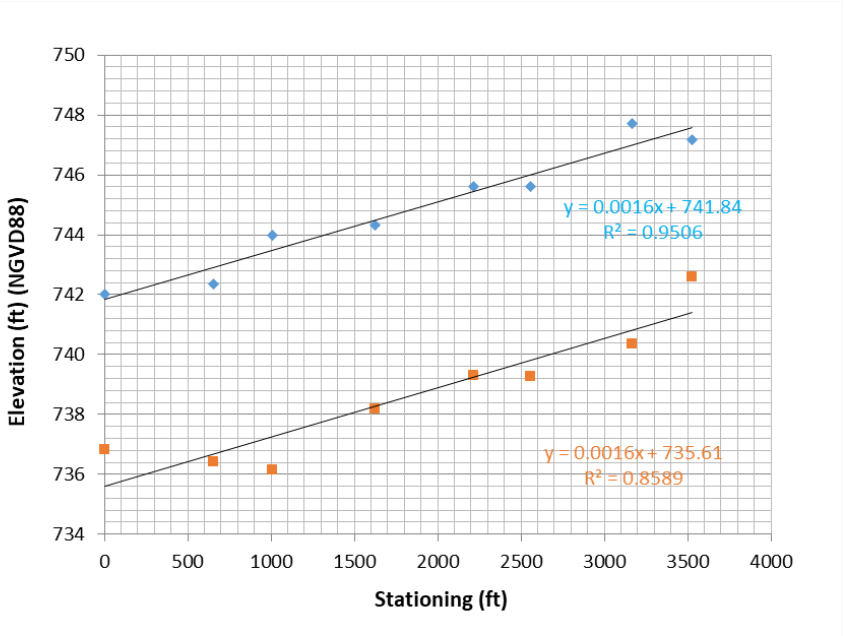

Figure 6. Little Maquoketa River Bankfull Indicators: LiDAR water surface slope (Orange) and Bankfull indicators (Blue) Water surface slopes

The bank-full elevation is determined to be the first leveling of the hydraulic depth at approximate elevation 649.6 ft. (NGVD88). Sherwood and Huitger (2005) describe similar bankfull channel indicators in their study as, "Interpretation was necessary because interpreted bankfull elevations frequently did not match what appear to be the active floodplain elevations." Natural levees may not be readily apparent in the field but are readily captured in the detailed LiDAR cross-sections. This could potentially lead to bankfull elevation errors between the field collection of data or lack there-of and the detail that the LiDAR can provide. Sherwood and Huitger (2009) described natural levees and the potential masking from vegetation that may be hard to detect in the field. The Sinsinawa gage site cross-sections had multiple field site visits, so the elevation for this particular cross-section is field validated. Reach analysis determined that the berm is inconsistent along the right bank, and the riffle location has allowed the narrow floodplain to propagate from geomorphic bankfull channel discharge.

At all 28 sites, the bankfull discharge was chosen from the gage stage-discharge relationship and the corresponding bankfull geomorphic feature that was typically a floodplain surface. For both the active gage and discontinued gage sites, the most recent stage-discharge rating curve was used to determine bankfull discharge. Bankfull discharge was determined from the established gage rating table elevation that corresponded to the geomorphic floodplain feature present in the gage pool or where the gage rating curve was developed. This was the primary method for calculating bankfull discharge, and the resulting HGR equations reflect this input. When possible, the channel forming discharge was estimated just downstream of the gage pool, typically at a riffle low-water rating station where the channel has freedom to freely adjust from typical bridge pool station influence. In many cases the USGS gage vertical datum had to be converted from 1912 and NGVD29 to the current LiDAR vertical datum NGVD88. In several instances, the Iowa and Wisconsin gage datum elevations had to be re-collected from existing gage site benchmarks to appropriately calibrate the gage's established vertical datum to the LiDAR NGVD88 elevation datum.

Based on gage-stage discharge relationships from the established rating tables at each gage and NGVD88 elevation data from LiDAR, bankfull dimensions and characteristics were calculated: width, mean depth, cross-sectional area, maximum depth, mean velocity, hydraulic radius (riffles only), stream power, shear stress, and mean n-values. The data were then examined in R, DPlot, and Microsoft Excel for regression analysis, plotting, and HGR curve development.

The U.S. Army Corps of Engineers Hydrologic Engineering Center's River Analysis System (HEC-RAS) was used to analyze the study sites. Hydraulic geometry, discharge, and water surface slopes were compared for the four traditional geomorphic channel survey sites listed in red in Table 8 to LiDAR-HGR. The HEC-RAS model uses a standard-step method for calculating water surface profiles based on defined bankfull channel discharge. Cross-section report files for each stream reach were created and imported into HEC-RAS. Channel geometry details were then entered into the HEC-RAS model, such as distance between cross-sections, channel roughness (Manning "*n*" values), and the starting water surface elevations. Bankfull discharge was estimated for each of the 28 sites using Manning's open channel flow equation. Manning's equation and the specific energy equation were used to determine critical, subcritical, and supercritical flows that are essential for testing the assumption of uniform, steady flow conditions. For the LiDAR-HGR analysis, the bankfull water surface slope (S) was approximated by comparing geomorphic channel features and the LiDAR water surface slope at riffle cross-sections. Jarrett (1984) reports that the use of the water surface slope in place of the energy or friction slope, S, is a common practice. The LiDAR-HGR geomorphic bankfull water surface slopes were estimated using the slope of a best-fit line through the geomorphic bankfull indicator elevations at the surveyed cross-section locations

Results

Two additional sub-regions were identified during the analysis. They were the Lower Southern (LS) Driftess Area (Sites 1-5, 8-12, 17-19), and the Little Maquoketa River (sites 8-12) sub-regional curves. Based on standard linear regression modeling the average values for all 28 sites used in developing the Southern Driftless Area HGR curves ranged from 23 to 112 ft. for bankfull width, 1.0 to 8.1 ft. for bankfull mean depth, and 31 to 696 ft^2 for bankfull cross-sectional area. Bankfull channel discharges ranged from 71 to 3298 cfs., and mean velocity ranged from 2.3 to 7.4 ft/sec. The Southern Driftless Area regional curve regression equations for drainage area as the independent variable (x) versus dependent variables (y) bankfull width, bankfull mean depth, bankfull cross-sectional area, and bankfull discharge are show in Table 1.

The simple regression analysis for this study used two separate statistical analysis packages, Microsoft Excel based spreadsheet for data analysis, and R code for calculating and plotting statistical relationships, which follow standard regression analysis procedures as outlined in Helsel and Hirsch (2002). Plots of residuals, R^2, adjusted R^2 values, p-values, and other statistical indicators of model fit and validity were analyzed.

(1) Determination of whether the LiDAR-HGR approach was suitable for defining regional and regime curves for the Southern Driftless Area of the Midwest based on comparisons with existing studies with respect to bankfull recurrence interval's, bankfull dimensional analysis, bankfull channel discharge versus drainage area, and standard regional curve theory.

The bankfull mean recurrence interval for all of the 28 Southern Driftless Area sites is a 1.47 year event. The bankfull mean recurrence interval for the LS Driftless Area and the Little Maquoketa River is a 1.43 year event. The recurrence interval analysis align with the

approximate 1.5 year recurrence interval that the Rosgen (1996) and Dunne and Leopold (1978) data suggest.

Table 1. Regional LiDAR-HGR Regression Equations for the Southern Driftless Area, Lower Southern Driftless Area, and Little Maquoketa River within the Lower Southern Driftless Area of the Midwest.

Equation Number	Regression Equation	R^2
	Southern Driftless Area (28 sites)	
19	$W = 28.4 * DA^{0.22}$	0.69
20	$D = 1.5 * DA^{0.22}$	0.65
21	$A = 40.9 * DA^{0.44}$	0.75
22	$Q = 111.6 * DA^{0.55}$	0.75
23	$W = 4.9 * Q^{0.38}$	0.83
24	$D = 0.2 * Q^{0.40}$	0.84
25	$A = 1.1 * Q^{0.78}$	0.94
26	$V = 1.02 * Q^{0.22}$	-
	Lower Southern Driftless Area (13 sites)	
27	$W = 32.4 * DA^{0.23}$	0.86
28	$D = 1.7 * DA^{0.24}$	0.89
29	$A = 54.6 * DA^{0.48}$	0.97
30	$Q = 150.3 * DA^{0.60}$	0.93
31	$W = 5.1 * Q^{0.38}$	0.87
32	$D = 0.3 * Q^{0.38}$	0.85
33	$A = 1.3 * Q^{0.76}$	0.96
34	$V = 0.65 * Q^{0.24}$	-
	Little Maquoketa River Watershed (5 sites)	
35	$W = 27.5 * DA^{0.27}$	0.99
36	$D = 1.7 * DA^{0.27}$	0.97
37	$A = 45.7 * DA^{0.54}$	0.98
38	$Q = 141.5 * DA^{0.67}$	0.99
39	$W = 3.8 * Q^{0.40}$	1.00
40	$D = 0.2 * Q^{0.40}$	0.98
41	$A = 0.8 * Q^{0.81}$	0.99
42	$V = 1.32 * Q^{0.20}$	-

Nomenclature: D = bankfull depth (ft). Q = bankfull discharge (cfs). A = bankfull cross-sectional area (ft^2). DA = drainage area (mi^2). V = bankfull mean velocity (fps). W = bankfull width (ft). R^2 = coefficient of determination.

The Southern Driftless Area curves developed by this study provide great insight into the regional and sub-regional bankfull channel dimensions and discharge. The average watershed size decreased from approximately 84 (Southern Driftless Area-28 sites) to 63 (LS Driftless Area-13 sites) to 44 (Little Maquoketa River-5 sites) square miles. The decrease in watershed

size was accompanied by an increase in discharge from the Southern Driftless Area curve set of 1181 cfs to the LS Driftless Area of 1411 cfs to 1558 cfs, and the watershed runoff rates increased from 14.1 to 22.8 to 35.4 cfs/sq. mile. The smaller drainage areas with the sub-watersheds signifies closer stream channel morphology and a more concentrated hydro-physiographic influence with the smaller more focused sample size of streams in the selected watersheds.

Consistent with the findings reported by similar regional curve studies (Harmon et al., 2000; USDA-NRCS, 2007), discharge not drainage area was the basin characteristic that accounts for the largest proportion of variance in bankfull channel characteristics for the Southern Driftless Area regional curves. However, discharge was found to be relatively equivalent to drainage area for the results of the smaller sample sized sub-regional curves, the LS Driftless Area and Little Maquoketa River curves.

The Coefficient of Determination (R^2) for the Southern Driftless Area curves range from 0.65 to 1.0. Recent USGS regional curve studies from Indiana (Robinson 2013), Ohio (Sherwood and Huitger, 2005), and Southern Michigan (Rachol and Boley-Morse, 2009) have reported R^2 values ranging from 0.28 to 0.94. Comparisons in the R^2 statistical analysis for this study provide reasonable results when compared to results from other traditional field based geomorphic studies.

(2) Determine if the LiDAR-HGR approach provides accurate results as compared to traditional geomorphic field-based methods. Assuming that the traditional geomorphic field-based methods are the correct baseline condition, identify a range of typical errors between the two methods. The results of the analysis for comparing bankfull channel dimensions between the LiDAR-HGR to the 2017 geomorphic channel surveys determined an error range from one to 19%. These error ranges compare similarly to Dietterick et al. (2012) that reported 90% of the surveyed cross-sections provided width measurements within 20% of the channel surveyed values and routinely underestimated bankfull depth. The bankfull mean depth error for the LiDAR-HGR is one to 19%.

The results of the LiDAR-HGR bankfull channel data versus 2009 NRCS geomorphic channel surveys indicate the range of error from zero to 25%. The error compares similarly with traditional geomorphic survey errors described from Wahl (1977) with up to a 30% error from experienced personnel and Roper et al. (2002) who reported plus or minus 15% error in determination of bankfull channel dimensions.

An assessment of the advantages and disadvantages of the LiDAR HGR methodology was also investigated in this study. Based on literature review, study findings, and goals and objectives of other water resource projects that may integrate the LiDAR-HGR methodology, some of the common advantages and disadvantages are:

Time and cost savings:

Time and cost comparisons of the traditional high resolution GPS geomorphic surveys to LiDAR geomorphic survey yields interesting insight from the dike study outlined in Mayfield (2015). Mayfield (2015) compared the time spent for surveying 25 miles (40.2 km) of dike with conventional GPS surveys to airborne LiDAR surveys for 153 miles (246 km) of the same levee system. Mayfield (2015) found that 1,921 hours were spent collecting 26,241 measurements or 13.75 measurements per hour for the conventional GPS survey. In contrast, 373 hours were spent on collecting and producing a much larger area of interest that yielded 2.9 billion

measurements or a little more than 7.7 billion measurements per hour (Mayfield, 2015). This provides a good comparison when considering how much more data at relatively the same resolution can be produced by collecting LiDAR data. The cost to complete and provide the 25 miles (40.2 km) of dike survey was approximately $106,000 with a cost-per-line mile of $4225.00 (Mayfield, 2015). Mayfield (2015) provided the cost to complete the 153 miles (246 km) of dike survey using airborne LiDAR at $75,500 and $493.00 cost-per-line mile. One might expect the cost of the airborne technology to be more expensive than traditional survey methods, but putting professionals in the field with significant expenses for surveying, trucks, ATV's, fuel, and other equipment can be costly.

LiDAR surveys are becoming more economically viable and traditional geomorphic field surveys can be very expensive and time consuming. The accessibility of high-resolution, high-quality terrain data using LiDAR from existing local, state, and federal databases is becoming increasingly available and utilized by natural resource managers to research, plan, investigate, evaluate, monitor, and develop solutions to water resource issues.

Data Resolution:

LiDAR data collection systems are becoming more accurate as reported by Dietterick et al., (2012) with substantial sensor pulse rate resolution improvements from 20,000 pulses per second in 2002 to 150,000 pulses per second in 2010. Faux and others (2009) describe improvements in LiDAR from technological advances in pulse densities, GPS accuracy, and ground classification methods.

From the LiDAR DEM data, user-defined point spacings can provide detailed channel elevation data at cross-section, water surface, and longitudinal bank profiles. In contrast, geomorphic field surveys are limited to only data collected during the site visit, that even in the most rigorous surveys are constrained due to availability, time, user error or lack of training, and resource constraints.

One of the more important aspects of developing hydraulic geometry relationships are gathering bankfull channel dimensions at riffle, run, or cross-over locations. These are the areas that are between deeper pool areas and have less depth. For the Southern Driftless Area streams the cross-over locations in many instances are only tenths of a foot deep so there was very little depth dimension lost. A relative channel depth can be verified by checking the LiDAR acquisition dates against site location gage records to determine if local hydrologic flow conditions were higher stages or representative of low water collection periods. Low water is the preferred condition as very little depth will be lost for this condition. For the 28 Southern Driftless Area study sites the gage records indicate low-water conditions. The majority of the LiDAR data collected for this study were collected during leaf-off vegetation, no ice or snow, and low flow stream channel conditions.

As an example of the potential depth resolution that was gained from reprocessing the original LiDAR point cloud data and processing the associated new DEM to 1 ft vertical resolution, Figure 7 shows Site 1-Sinsinawa River that captures the boulder and cobble substrate located in the riffle cross-over locations in the reach at cross-section two and three. The red areas within the channel margins show areas of higher local slope depicting the channel substrate and riffle locations. The dark blue areas within the channel represent areas of low slope and signify flat pool areas. This was visually verified for the Sinsinawa River site as the author was present for both field survey visits to this site. The riffle cross-over locations are effectively located using

the LiDAR reprocessing method to check for cross-section locations for the LiDAR-HGR approach.

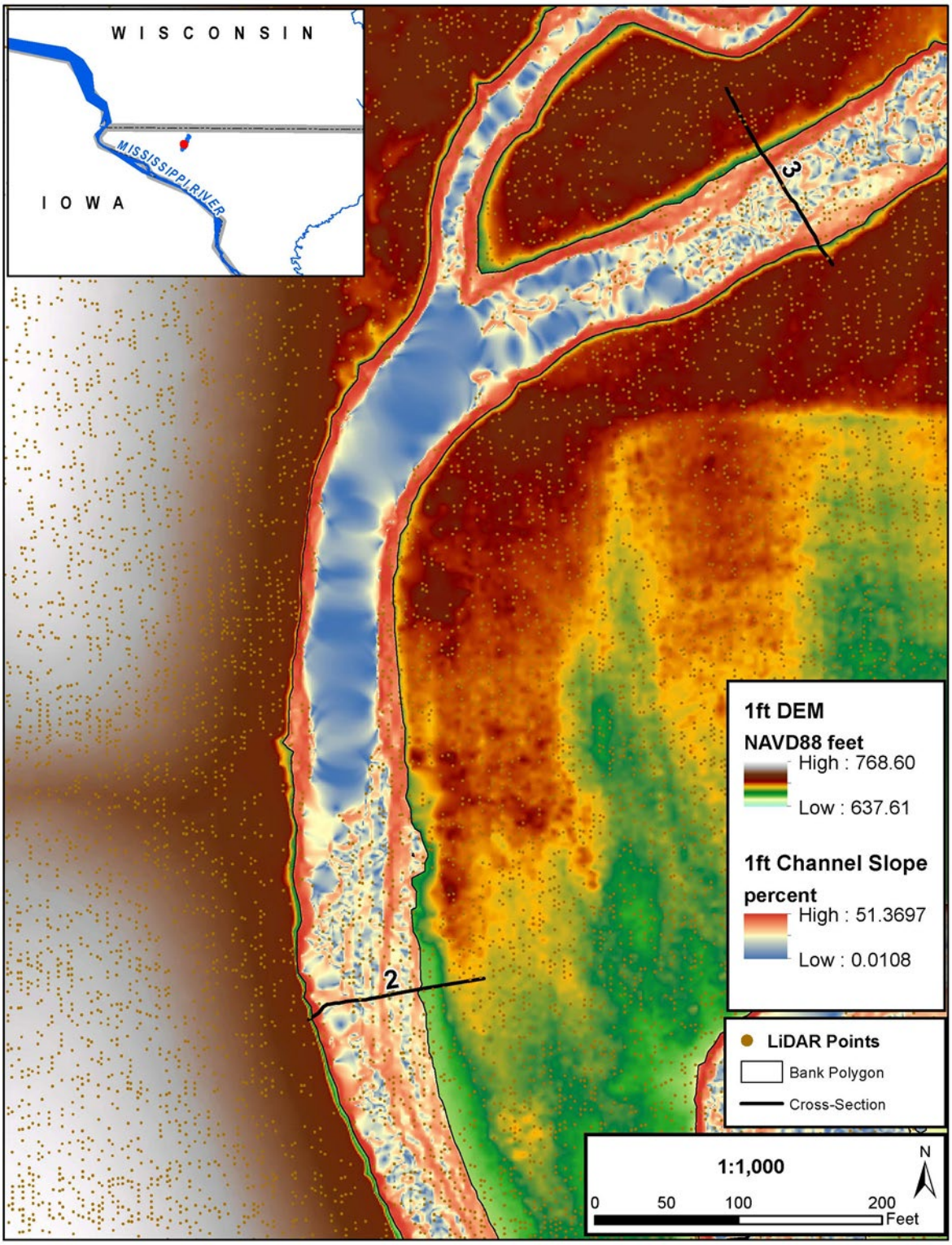

Figure 7. 1 ft DEM of Site 1-Sinsinawa River-near Menominee, IL (05414820, 39.6 mi2) (from Illinois Geospatial Data Clearinghouse, 2008 LiDAR)

By cutting the LiDAR-HGR cross-sections at riffle locations, there is the least amount of depth loss between the LiDAR water surface and traditional geomorphic field surveys. Riffle cross-over locations provide the closest interpretation to channel depth, and are least affected by depth error at these locations. The obvious limiting factor is as the size of the watershed increases and corresponding channel depth increases in the cross-over locations.

Data Collection Consistency:

Geomorphic field-based surveys have reported errors ranging from five to 30% (Wahl 1977; Hammer 1981; Roper et al., 2002; Eaton and Church, 2007; Faux et al., 2009) in data collection and estimation of bankfull channel dimensions. Similar ranges of data error have been verified in this study and in previous literature for LiDAR-based analysis. In summary, geomorphic field surveys may be used to supplement LiDAR-HGR based studies and vice versa. Field validation for the LiDAR-HGR gage sites is an important addition in validation of the method. Additional enhancements for the LiDAR-HGR approach include further field validation to include depth measurements, bankfull indicator confirmation, pebble counts, bank erosion analysis, and the stability of the reach if analysis and many more metrics as time allows. This cross-pollination of methods would provide a truly robust method for evaluation and validation of geomorphic channel, floodplain, and watershed characteristics.

Spatial Analysis:

LiDAR DEMs provide spatially continuous data that can be used to measure a variety of channel, floodplain, and watershed characteristics at user defined intervals along the stream system. This analysis makes available a large amount of data that offers improved quantifying of the spatial variability of stream reaches and watershed conditions. If LiDAR data analysis is completed on an annual basis, then the same cross-section or specific site reaches in a watershed can be monitored for geomorphic channel change and watershed analysis.

Temporal Analysis:

Based on the precision that LiDAR DEMs provide, temporal changes in channel geometry, floodplain, and watershed characteristics can be evaluated at identical cross-section or longitudinal profile locations using the same x, y, z coordinates. This provides a repeatable and verifiable method to reduce data collection errors and also a technique for capturing temporal changes in the channel geometry, floodplain, and watershed. However, it should be noted that because of the rapid technological advances in LiDAR data collection methods, multi-temporal analysis requires the understanding of the differences in precision and resolution of the underlying data from differing LiDAR datasets (Faux et al., 2009). This is a very important when comparing differing LiDAR data from different collection dates, resolutions, and differing study goals and objectives that may have led to conflicting methods, metrics, and precision measurement.

(3) Assess the applicability and possible relationships between the Southern Driftless Area regional, Lower Southern Driftless Area and Little Maquoketa River sub-regional curves with the Eastern United States, Indiana, Ohio, and Michigan regional curves. The newly derived Southern Driftless Area curves and the other Midwest curves are plotted and data are compared in table format for evaluation.

A comparison was completed of the LiDAR-HGR-based Southern Driftless Area and sub-regional curves to USGS regional curve studies for Indiana, Ohio, Southern Michigan, and the

Eastern United States (Dunne and Leopold, 1978). The Southern Indiana regional curve which has similar topography, geology, and climate to the Southern Driftless Area exhibited the closet relationships with the LS Driftless Area and Little Maquoketa River regional curves. As discussed previously, the Eastern United States regional curves are used by many specialists in the Midwest to predict bankfull channel dimensions mainly due to the lack of available regional curve datasets. The results of this study show that the Eastern United States regional curves are not applicable to the Southern Driftless Area regional curves. However, the Eastern United States regional curves do show a common association to the LS Southern Driftless Area sub-regional curve for 100 to 300 square mile watersheds and the Little Maquoketa River sub-regional curve for watersheds ranging from 100 to 130 square miles.

(4) Evaluate the applicability of the LiDAR-HGR procedure to measure and predict stream channel dimensions and discharge at USGS gage sites from existing regional curves studies in Indiana and Ohio. Four sites in Indiana and three sites in Ohio in watersheds ranging from 4.7 to 90 square miles were analyzed to determine the applicability of the LiDAR-HGR method.

The LiDAR-HGR method provided very close geomorphic channel dimension and discharge values in the comparisons of six of the seven Indiana and Ohio study sites. The slight differences in the analysis are likely attributed to differences in the date of the LiDAR data compared to the date of the geomorphic channel surveys and also a depth error for the larger Sandusky River site in Ohio. Fluvial systems are not static but very dynamic in nature, so relative changes can occur over a short period of time, and much larger changes can be expected over larger time frames. The LiDAR-HGR method should be used to test and further develop regional curve relationships for additional regional curve studies.

Conclusions

Based on the results of this study, the LiDAR-HGR Southern Driftless Area regional and regime curves can be applied to ungaged stream systems with watershed sizes up to approximately 300 square miles. The curves can be used to determine typical hydraulic geometry dimensions for bankfull width, mean depth, cross-sectional area, mean velocity, and discharge. The range of values for regional curves varies greatly within the region and only provides a guide that will require verification for each stream reach application. There are dynamic variants in natural stream hydraulic geometry and resulting channel form that will lie above and below the general regression lines and equations defined by the curves. Users are cautioned to validate regional curve data to the local hydro-physiographic area in question prior to application to a specific study reach. Based on the analysis in this study, the Eastern United States regional curves from Dunne and Leopold (1978) should not be applied to ungaged sites and watersheds within the Southern Driftless Area.

As a cautionary note, it should be noted that for any application of regional bankfull-channel-dimension curves, it is important that the user recognize that most often there is significant natural variability contained within the datasets used to establish the regional relationships. The best fit line represents the central tendency of the measured data, and it is readily apparent that many of the measured data do not fall on the best fit line. In fact, many of the data points are well off of the best fit line. Therefore, while a best-fit line can be identified and a regression equation describing that line presented, it is important for the user to consider the many

variables that may influence channel dimensions and the scale of variability that may be present in the channel dimensions of any natural waterway.

In summary, the results of this study indicate when compared to traditional geomorphic channel surveys the LiDAR-HGR method produced similar or less error, and provides an efficient, low-cost, rapid assessment approach to developing regional and regime curves for additional hydro-physiographic regions where appropriate data are available.

References

Billings, S., 2017. Triumph-LS Cluster Average and Relative Accuracy. Javad Website: https://support.javad.com/index.php?threads/triumph-ls-cluster-average-and-relative-accuracy.2619/

Castro, J.M. and P.L. Jackson, 2001. Bankfull Discharge Recurrence Intervals and Regional Hydraulic Geometry Relationships: Patterns in the Pacific Northwest, USA. Journal of the American Water Resources Association 37(5):1249-1262.

Contreras, M.A., Staats, W., Yiang, J., and Parrott, D., 2017. Quantifying the Accuracy of LiDAR-Derived DEM in Deciduous Eastern Forests of the Cumberland Plateau. Journal of Geographic Information System, 2017, 9, 339-353. Scientific Research Publishing. http://www.scirp.org/journal/igisDay, M., 1986. Caves in the Driftless Area Of Southwestern Wisconsin. University of Wisconsin-Milwaukee. 10 p.

Dietterick, B.C., White, R., and Hilburn, R. 2012. Comparing LiDAR-Generated to ground-surveyed channel cross-sectional profiles in a forested mountain stream. Gen. Tech. Rep. PSW-GTR-238. Albany, CA: Pacific Southwest Research Station, Forest Service, U.S. Department of Agriculture. pp. 639-648.

Dunne, T., and Leopold, L.B., 1978. Water in Environmental Planning. W.H. Freeman and Co., San Francisco, CA.

Eaton, B.C., and Church, M. 2007. Predicting downstream hydraulic geometry: a test of rational regime theory. Journal of Geophysical Research: Earth Surface 112(F03025): 1-18p.

Emmett, W.W. 2004. A Historical Perspective on Regional Channel Geometry Curves. Stream Systems Technology Center-Stream Notes, Rocky Mountain Research Station, Fort Collins, Colorado.

Faux, R.N., Buffington, J.M., Whitley, M.G., Lanigan, S.H., and Roper, B.B., 2009. Use of airborne near-infrared LiDAR for determining channel cross-section characteristics and

monitoring aquatic habitat in Pacific Northwest rivers: A preliminary analysis [Chapter 6]. PNAMP: pp 43-60.

FISRWG (Federal Interagency Stream Restoration Working Group). 1998. Stream Corridor Restoration: Principles, Processes and Practices. National Technical Information Service. U.S. Department of Commerce, Springfield, VA.

Frankie, W.T., and Nelson, R.S., 2002. Guide to the Geology of the Apple River Canyon State Park and Surrounding Area of NorthEastern Jo Daviess County, Illinois. Department of Natural Resources and Illinois State Geological Survey, Field Trip Guidebook.

Hammer, R.G., 1981. Streamflow estimates using channel width: Missoula, Mont., U.S. Forest Service, Northern Region, Soil, Air, and Water Notes 81-3, 6p.

Harman, W.A., Wise D.E., Walker, M.A., Morris, R., Cantrel, M.A., Clemmons, M., Jennings, G.D., Clinton, D., and Patterson, J., 2000. Bankfull Regional Curves for North Carolina Mountain Streams. In: Water Resources in Extreme Environments Proceedings, D. L. Kane (Editor). American Water Resources Association Speciality Conference, Anchorage, Alaska. AWRA TPS-00-1, pp. 185-190.

Harrelson, C.C., Rawlins, C.L., and Potyondy, J.P., 1994. Stream Channel Reference Sites: An Illustrated Guide to Field Technique. Gen. Tech. Rep. RM-245. Fort Collins, CO: U.S. Department of Agriculture, Forest Service, Rocky Mountain Forest and Range Experiment Station.

Helsel, D.R., and Hirsch, R.M., 2002, Statistical methods in water resources: U.S. Geological Survey Techniques of Water-Resources Investigations, book 4, Hydrologic analysis and interpretation, chap. A3, 510 p., http://pubs.usgs.gov/twri/twri4a3/pdf/twri4a3-new.pdf.

Iannicelli, M., 2010. Evolution of the Driftless Area and Contiguous Regions of Midwestern USA Through Pleistocene Periglacial Processes. The Open Geology Journal, V4, 35-54.

Jarrett, R.D., 1984, Hydraulics of high-gradient streams: Journal of Hydraulic Engineering, American Society of Civil Engineers, v. 105, no. 11, p. 1519–1539.

Knox, J. C., and Leigh, D. S., 1990. Valley trenching at the Driftless Area Boice Site." Geological Society of America, North Central Section Field Trip Guidebook. pp. F26–F31.

Lawlor, S.M., 2004, Determination of channel-morphology characteristics, bankfull discharge, and various design-peak discharges in western Montana: U.S. Geological Survey Scientific Investigations Report 2004–5263, 19 p.

Leopold, L.B., 1994. A View of the River. Harvard University Press, Cambridge, Massachusetts.

Mayfield, B., 2015. The Mapping Match: LiDAR verse Traditional Topo. Point Of Beginning: Website: https://www.pobonline.com/articles/97670-the-mapping-match-lidar-v-traditional-topo

McKean J.A., Isask, D.J., and Wright, C.W., 2005, Mapping channel morphology and stream habitat with a full wave-form green lidar: EOS Transactions, American Geophysical Union, v. 86, no. 52, Fall Meeting, Suppl. Abstract H34B-05.

Omernik, J.M., 1987. Ecoregions of the Conterminous United States, Annals of the Association of American Geographers, DOI: 10.1111/j.1467-8306.1987.tb00149.x, 77:1, p. 118-125.

Rachol, C.M., and Boley-Morse, K., 2009, Estimated bankfull discharge for selected Michigan rivers and regional hydraulic geometry curves for estimating bankfull characteristics in southern Michigan rivers: U.S. Geological Survey Scientific Investigations Report 2009–5133, 300 p.

Robins, C., 2005. The Geology of the New Richmond Sandstone, Prairie du Chein Group, Southeastern Minnesota. Carlton College, Northfield, MN, USA

Robinson, B.A., 2013. Regional bankfull-channel dimensions of non-urban wadeable streams in Indiana: U.S. Geological Survey, Scientific Investigations Report 2013–5078, 33 p.

Roper, B.B., Kershner, J.L., Archer, E., Henderson, R., and Bouwes, N., 2002. An evaluation of physical habitat used to monitor streams: Journal of the American Water Resources Association, v. 38, p. 1637-1646.

Rosgen, D.L., 1996. Applied River Morphology. Pagosa Springs, CO. Wildland Hydrology.

Sherwood, J.M., and Huitger, C.A., 2005, Bankfull characteristics of Ohio streams and their relation to peak streamflows: U.S. Geological Survey Scientific Investigations Report 2005–5153, 38 p.

Smith, G.L., and Simo, J.A., 1997. Carbonate Diagenesis and Dolomitization of the Lower Ordovician Prairie du Chein Group: Geoscience Wisconsin, V. 16, 16 p.

Stream Corridor Restoration: Principles, Processes, and Practices, 1996. United States Department of Agriculture.

United States Department of Agriculture, Natural Resources Conservation Service (USDA-NRCS). 2007. Developing Regional Relationships for Bankfull Discharge using Bankfull Indices. Part 654, National Engineering Handbook-Tech Supplement 5.

Wahl, K.L., 1977. Accuracy of channel measurements and implications in estimating streamflow characteristics: U.S. Geological Survey Journal of Research, v. 5, no. 6, p 811-814.

Williams, G.P., 1978. Bankfull discharge of rivers. Water Resources Research 14:1141-1154

Aquatic, Riparian, and Avian Habitat Improvement within Escondida Burn Area

Chi Bui, Bureau of Reclamation, Sacramento, CA, cbui@usbr.gov

Abstract

In June of 2016 a wildfire in Escondida, New Mexico, burned approximately 524 acres in the Bosque. The 3-mile long reach of the Middle Rio Grande through the burn area was severely incised and left the abandoned floodplains with an average depth to the water surface elevation of 8 feet. Without mechanical interference, it was unlikely that native vegetation and wildlife would be able to re-establish.

A habitat restoration project was developed to improve habitat qualities on the burn scar of the floodplain. Various analyses were performed, including the existing biological, hydraulic, hydrologic, geomorphic and sediment conditions to develop a final design that was both economical and engineering sound. The objective of the project was to ensure the longevity of the constructed features that would serve as an aquatic habitat for an endangered species, the Rio Grande Silvery Minnow, and a riparian habitat for native vegetation and avian habitat for another endangered species, the Southwestern Willow Fly Catcher. The final design components included bank sloping and lowering of a terrace in an arroyo fan to be inundated at 300-cfs as a nurturing habitat, improvement of a side channel to be inundated at 300-cfs as a passage for fish to avoid high in-channel velocities, and monitoring of the habitat features to assess the functionality and longevity of the constructed aquatic features. It is expected that vegetation will develop within the constructed aquatic habitat features, leading it to eventually become a terrestrial habitat.

Methodology

The hydrologic analysis of the current condition identified the median flow magnitudes that would be exceeded 50% of the time for the four unique hydrologic seasons of a year that were found to be significant based on biological preferences of the different life stages of the Rio Grande Silvery Minnow. The four hydrologic seasons include pre-runoff (March-April), spring runoff (May-June), post-runoff (July-October), and winter (November-February) (Dudley and Platania 1997). The hydrologic analysis also identified the median flow magnitude of a 14-day duration spring runoff that was found as the minimum requirement for the Rio Grande Silvery Minnow's eggs to hatch and develop into functioning larvae juvenile (Bureau of Reclamation 2017b). These median flow magnitudes derived from the hydrologic analysis were used in the hydraulic analysis to identify the design elevation of the different habitat features for the different life stages of the Rio Grande Silvery Minnow.

River sediment investigation with 1-D sediment transport modeling with HEC-RAS suggested that the reach in the project vicinity could be classified as stable to degradational. 2-D HEC-RAS transport modeling of the design condition showed that seasonal deposition could occur after

monsoonal runoff events, but there would be a balance of sediment when spring snowmelt runoff could mobilize sediments deposited by summer monsoonal events.

Quantification of the existing and design conditions for the habitat of the Rio Grande Silvery Minnow were determined according to three categories identified for a similar project along the lower reach of the Middle Rio Grande. The three aquatic habitat categories that characterize suitable in-channel velocity and depth conditions that provide habitat for the different life stages of the RGSM are summarized hereafter and in Table 1:

Table 1. Ideal, Suitable, and Unsuitable RGSM Habitat Criteria

Life Stage	Ideal		Suitable	Unsuitable
	Depth	Velocity	Velocity	
Egg/Larvae	0< depth < 11.8 in	≥0.37 in/s	≥0.37 in/s	All other wetted areas
Larvae/Juvenile	2-19.9 in	0.39-11.8 in/s	0.39-11.8 in/s	All other wetted areas
Adults	2-19.9 in	0.39-15.7 in/s	0.39-15.7 in/s	All other wetted areas

- "Ideal Habitat": meeting both the depth and velocity criteria (Bureau of Reclamation 2017a)
- "Suitable Habitat": meeting only the velocity criteria (Bureau of Reclamation 2017a)
- "Unsuitable Habitat": meeting neither the depth nor velocity criteria (Bureau of Reclamation 2017a)

Results

The overall theoretical habitat created for the different RGSM life stages by the lowering of the arroyo fan and side channel is illustrated in Figure 1. This figure does not have the information of unsuitable habitat.

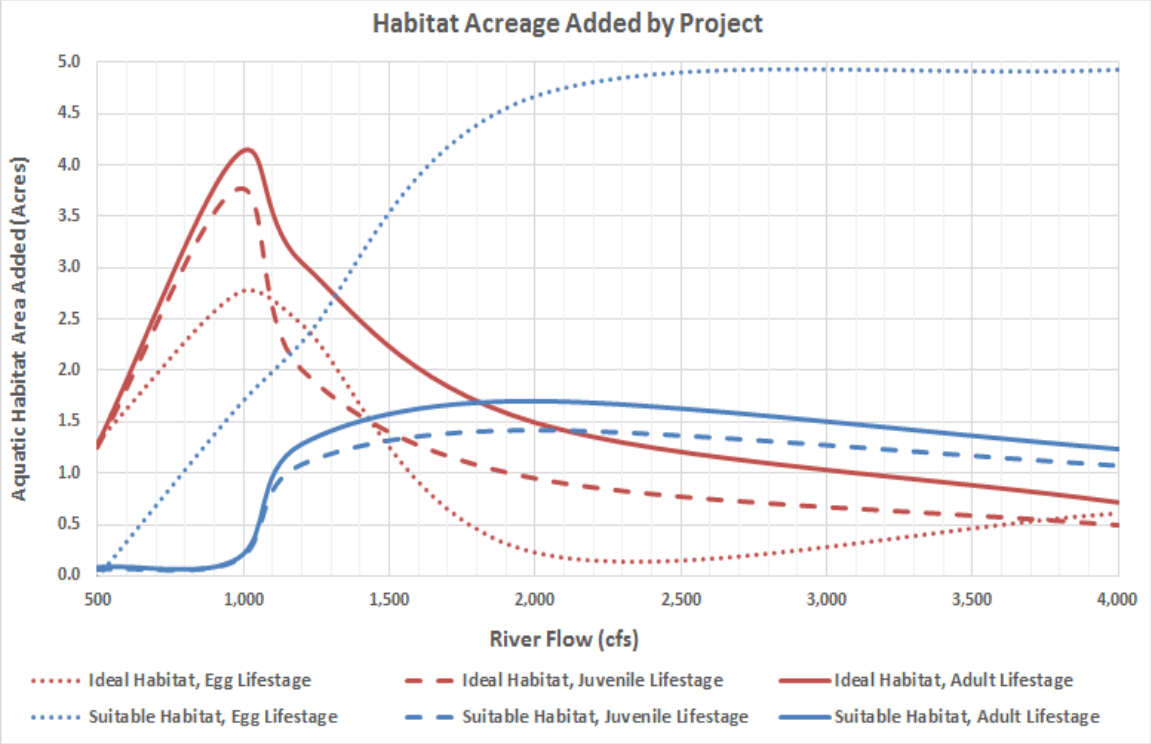

Figure 1. Habitat acreage added by lowering the arroyo fan and side channel

In general, the created ideal habitat for the Rio Grande Silvery Minnow's three life stages (egg to larvae, larvae to juvenile, adult stage) peaks around 1,000 cfs and decrease as flows increase above 1,000 cfs. The created ideal habitat is dominant at flows less than 1,000 cfs. Between 1,000 cfs and 2,000 cfs there is a transition from an ideal-habitat dominant environment to a suitable-habitat dominant environment. After 2,000 cfs, there is more created suitable habitat than ideal habitat. As flows increase above 2,000 cfs, the velocities and depths of the design habitat features exceed the ranges defined by the biological and hydraulic criteria for habitat assessment as summarized in Table 1 (Bureau of Reclamation 2017a) to support habitat and thus the habitat acreage decreases as flows increase above 2,000 cfs. As the primary goal of the project was to create habitat at flows that occurred most frequently in the reach (less than 1,000 cfs), the increase of the habitat at flows less than 1,000 cfs could justify the decrease in habitat at flows larger than 2,000 cfs.

Continuing Monitoring

The construction of the project was completed in April,2018, and was tested with a week-long period with three monsoonal flash flood events of which instantaneous discharges had a difference in an order of magnitude from the mean values of the instantaneous discharge records of the Rio Grande at Bridge near Escondida (USGS 08355050). Continuing monitoring of the project has been performed by visual observations and surveys of the topography and biology to assess the development of the different features over time and how well they serve the biological and hydraulic purposes of the project. It was observed that there was a 1-foot to 2-foot deposition along the alignment of the improved side channel and the lowered arroyo. Most of this deposition was fine sands and silts. Bathymetric surveys after the coming spring runoff of

2019 will help to identify if the 2019 spring runoff will have mobilized the sediment deposition as it was projected in the sediment transport analysis. In some locations, sedimentation can be prevented by adjusting angles of flow entrances and exits, or building woody debris configurations to induce strategic scour. This will be considered on a case-by-case basis. However, sedimentation will only be adaptively managed to a degree because sedimentation is natural, and it is expected that eventually the aquatic habitat will be transformed into willow (avian) habitat.

References

Bureau of Reclamation. (2017a). *Technical Note - Habitat Targets for BDA Realignment Pilot Modeling Analysis*.

Bureau of Reclamation. (2017b). *Central Socorro Bosque Restoration Project Environmental Assessment*.

Dudley, R. K., and Platania, S. P. (1997). *Habitat Use of Rio Grande Silvery Minnow*. New Mexico Department of Game and Fish, Santa Fe New Mexico; United States Bureau of Reclamation, Albuquerque, New Mexico.

Can Wood Placement in Degraded Channel Networks Result in Large-Scale Water Retention?

Tim Abbe, Chief Science Officer, Natural Systems Design (NSD), Port Angeles, WA, tim@naturaldes.com
Susan Dickerson-Lange, Senior Scientist, NSD, Seattle, WA, susan@naturaldes.com
Mike Kane, President, Kane Natural Resources, Port Townsend, WA, kanenaturalresources@gmail.com
Pete Cruickshank, Nat. Resources Specialist, Chelan County DNR, pete.cruickshank@co.chelan.wa.us
Mike Kaputa, Director, Chelan County DNR, mike.kaputa@co.chelan.wa.us
John Soden, Senior Scientist, NSD, Bellingham, WA, john@naturaldes.com

Introduction

In forested channel networks wood can be the dominant control on grade and shear stress partitioning. In these systems a loss of wood triggers channel incision that results in a lowering of alluvial groundwater tables and loss of water storage within a watershed. It also speeds up the routing of water out of channel network. Alluvial channels consist of two distinct channels conveying water: i) a surficial channel of open channel flow and ii) a subsurface hyporheic groundwater "channel" of flow moving through a porous medium of alluvial sediment. The velocity of water moving through these two pathways varies by up to five orders of magnitude. Thus, the subsurface flow volume can have a significant role in water retention within basin as well as supplementing baseflows. Channel incision leads to a substantial reduction or even complete loss of subsurface water capacity by lowering water tables and evacuating alluvial sediment. Shields et al (2009) report that 60-90% of sediments leaving many watersheds are due to channel incision. There are several major causal mechanisms triggering channel incision (e.g., Schumm et al. 1984). Dams cut off sediment supply which will drive downstream incision without a major reduction in peak flows (e.g., Galay 1983, Williams and Wolman 1984, Ligon et al 1995, James 1997, Kondolf 1997). Another mechanism of channel incision is changes in flow regimes that increase the magnitude and frequency of peak flows such as urbanization (e.g., Hamer 1972, Booth 1990). Large scale forest clearing can increase channel drainage networks and the frequency of bankfull or bed mobilizing peak flows which can result in channel incision (e.g., Wemple et al. 1996, Prosser and Moufi 1998, Marden et al. 2005, Perry et al. 2016). Channelization and shortening the length of channels also contributes to incision by increasing hydraulic gradients and sediment transport capacity (e.g., Simon 1989, Simon and Rinaldi 2006). In North America, the historic removal of beaver contributed to channel incision through the loss of in-stream wood dams beavers created (e.g., Pollock et al. 2007, 2012, 2014). We believe the most wide-spread cause of channel incision involves the forest clearing and the loss of in-stream wood either by direct removal or clearing (e.g. Prosser and Soufi 1998, Collins et al. 2002, Brooks et al. 2003, Marden et al. 2005, Stock et al. 2005, Brummer et al. 2006, Montgomery and Abbe 2006, Sear et al 2010, Phelps 2011, Abbe et al. 2016). By definition, this has led to an extensive loss of the natural alluvial and surface water storage that once existed. Figure 1 illustrates a recent example of rapid incision and gully formation after industrial logging. The ecologic benefits of wood placement are well established and are being used around the world (e.g., Abbe and Brooks 2011, USBR and ERDC 2016, Bridges et al. 2018). They can also help to attenuate flood peaks (Anderson 2006, Nisbet 2012, Abbe et al. 2016, Bridges et al. 2018) and reduce organic contaminants (Peter et al. 2019). The focus of this paper is highlight the potential role wood placements can have on raising water tables and substantially increasing the water storage within a channel network.

The Role of Wood in Storing Alluvium and Water

Wood has two important hydrologic influences, it can slow downstream routing resulting in "spreading out a hydrograph" (Anderson 2006) and store large volumes of alluvium within stream valleys, enlarging subsurface channels (e.g., Abbe 2000, Abbe and Montgomery 2003; Montgomery and Abbe 2006). The role of wood on stream channel grade has been well established. Veatch (1906), Guardia (1933) and Harvey et al. (1988) documented 5 meters (15 ft) of channel incision in the Red River of Louisiana after logjam removal. Hartopo (1991) showed that a major expansion of Lower Colorado River delta in Matagorda Bay occurred after logjams were removed from the Little Colorado River in the Texas coastal plain, corresponding to deposition of approximately 14,000,000 cubic meters of sediment in a 29 year

period after logjam removal (Abbe 2000). Removal of logjams in the Ozette River (1951-52) lowered Lake Ozette 4.5 ft (Brummer et al. 2006). This resulted in 30,000 ac-ft of lost storage in the lake. Logjam clearing contributed to simplification in the Upper Cowlitz River in the West Cascade mountains of Washington where the number of forested islands per km in the river reduced from over 5 to 2 (Abbe et al. 1997). Brooks et al. (2003) demonstrate how riparian forest clearing in southeast Australia resulted in a 240% increase in channel slope, 360% increase in depth and 700% increase in channel capacity, evacuating alluvium that had been stored for 27,000 years. Brooks and Brierley (2002) describe a "mediated equilibrium" of river morphology dependent on wood and vegetation. In the Olympic and Cascade mountains we have both observational evidence and detailed documentation of channel incision following the removal of in-stream wood. Brummer et al (2006) describe the role of wood in the vertical stability of channels and how wood removal can lead to two meters or more of incision followed by lateral channel migration that evacuates alluvium that had been in long-term storage. Abbe et al. (2013, 2015) documented up to 3 meters (9 ft) of incision in the South Fork Nooksack River draining the western Cascades in northern Washington State. The upper basin has no dams, urbanization, or channelization. Landuse within the basin is primarily industrial timber harvest which tends to increase peak flows and sediment supply and decrease in-stream loading of functional wood. Despite increases in sediment supply, the South Fork Nooksack has experienced significant incision. We believe the causal mechanism has been removal of in-stream wood and a subsequent increase in the effective basal bed shear stress. Katz et al. (2019) document over a meter (3 ft) of incision in the South Fork Newaukum River, another system with extensive industrial timber land and no dams or urbanization. Stock et al. (2005) attributed two meters (6 ft) of incision in the West Fork Teanaway River in the eastern Cascades of central Washington over the last century entirely due to wood removal. This incision not only included evacuation of all the alluvium once stored in the streambed, but a meter of erosion into the underlying bedrock. Over the last decade there has been considerable work on the role of beaver on water storage and reversing channel incision (e.g., Pollock et al. 2007, Beechie et al. 2008, Fouty 2013, Pollock et al. 2012, 2014). It is important to remember that beaver dams account for just one subset of the types of wood accumulations that occur from a variety of physical processes such as bank erosion, landslides, and windthrow (e.g., Abbe and Montgomery 2003).

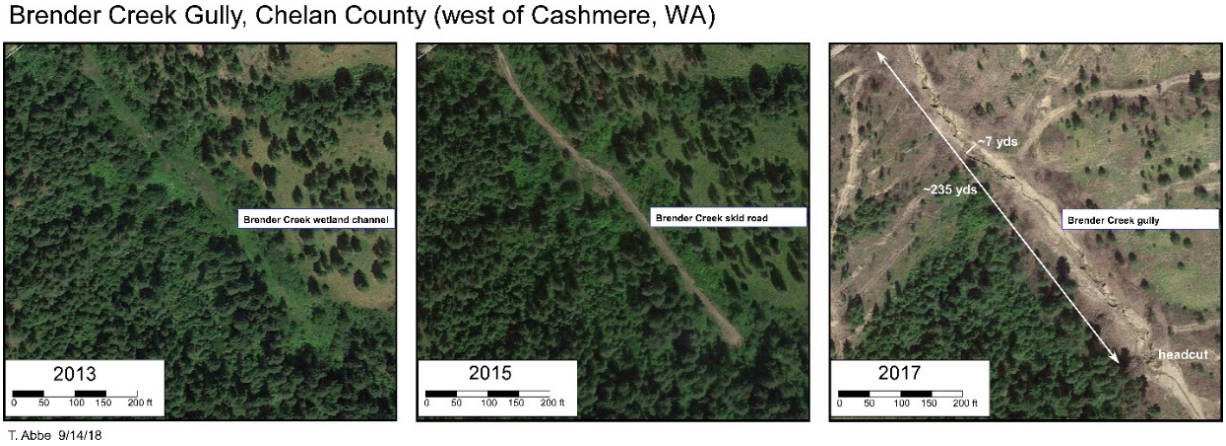

Figure 1a: Example of timber harvest disturbance to second order subsurface alluvial channel, Brender Creek south of the Wenatchee River, Chelan County. Timber skid road was routed up a second order alluvial valley with subsurface runoff (no open water channel). Shortly after logging, a gully formed and evacuate more than 25,000 m^3 of alluvium, converting the channel from subsurface to overland flow.

Figure 1b. Close up showing gully incision in Brender Creek (previous figure), 2017. Up to 7 m (21 ft) of downcutting happened in 2017, shortly after the site was logged (Figure 1a). Photo courtesy of Washington Department of Fish and Wildlife and Chelan County Natural Resources.

Our primary hypothesis is that restoring channel spanning wood accumulations increases water retention within a channel network. When extrapolated to the scale of human landscape disturbance, we believe channel networks once naturally retained much more water than present day conditions that rivaled or exceeded the water retention of large dams. Our secondary hypothesis is that by storing alluvium that would otherwise not be retained, wood is essential in creating and sustaining large subsurface alluvial channels which slow water export (movement out of basin), supplement downstream flows, improve water quality, and enhance riparian forest health. Conversely, channel incision leads to loss of water storage and rapid water export from the basin.

The images in Figure 1 convey an important message regarding the impact of incision on the routing of flow through a channel network. The original surface water channel was shallow and wide (evident by the skid road within the channel). Prior to logging channel was heavily vegetated (first panel of Figure 1a). After the gully formed the channel deepened, widened and became smoother. Surface water flow through the gully moved about eight times faster than the pre-existing vegetated channel. The gully also destroyed a large sub-surface groundwater channel conveying flow through the alluvium. Flow through porous media move much slower, by 4-5 orders of magnitude, than flow through a surface channel. Flow in surface channels is commonly expressed by the Manning's equation

$$(1) \qquad U = \frac{(R^{2/3}\, S^{1/2})}{n}$$

U = flow velocity, m/s
R = hydraulic radius, m
S = hydraulic gradient
n = Manning's roughness coefficient (0.035 for smooth channel, 0.09 for very rough channel)

Flow through a porous medium is commonly expressed by Darcy's equation:

$$(2) \qquad U = \frac{K}{p}\,\frac{\Delta h}{\Delta L}$$

K = hydraulic conductivity of material, m/s. This varies by orders of magnitude
p = porosity of the material
$\Delta h/\Delta L$ = hydraulic gradient (S)
Δh = hydraulic head (vertical change in water elevation over distance ☐L), m
ΔL = horizontal distance of flow path

Subsurface flow not only reduces the rate at which water is exported from a basin, but it plays a major role in cooling and cleaning the water. This can be a critical role for the ecology of salmon streams.

Table 1 illustrates the difference in routing times of flow through a stream valley 10 km in length with a valley gradient of 0.03 and filled with a well-graded alluvium of silt, sand and gravel. The presence of alluvium creates subsurface groundwater channels that have a significant effect on the rate water is exported out of a basin and thus potential contributions to recessional dry season stream flows. Natural variations in bedrock valley constrictions can be a factor in forcing subsurface flow back to the surface.

Table 1 – Routing times within a 10 km alluvial stream with a 3% gradient.

Flow Condition	Routing time (3% grade over 10 km)	
	hours	days
Surface water through incised channel	0.4	0.01
Surface water through natural channel	3.2	0.13
Subsurface water through alluvium*	14,854	619

*subsurface flow diminishes substantially for incised channel due to lower water table and evacuation of alluvium from the valley. Subsurface flow can be effectively eliminated when incision reaches bedrock. Subsurface flow assumes no significant macropores or preferential flow paths.

Research on the hydraulic effects of wood has demonstrated the importance of wood not only in storing sediment, but in reducing sediment transport capacity by shear stress partitioning that reduces the effective shear stress available for grain mobilization (Shields and Gippell 1995, Buffington and Montgomery 1999, Manga and Kirchner 2000). Relatively small accumulations of wood within a streambed can have a substantial influence on reducing the shear stress available for grain mobility (sediment transport). This reduces the stream's capacity to move larger grains and sediment volumes, resulting in a finer streambed (lower median grain size) and bed aggradation. This is consistent with fact that many streams with high wood loading have multiple shallow channels with large volumes of floodplain sediment deposition (Abbe et al. 1996, Abbe and Montgomery 2003, Montgomery and Abbe 2006, Sear et al. 2010). Wood can store sediment in channel with gradients over 15% (Abbe 2000, Abbe and Montgomery 2003).

$$\tau_0 = \tau_{GS} + \tau_{LWD} \quad (3)$$

τ_0 = total bed shear stress = $\rho g R S$

τ_{GS} = grain stress that is effective shear stress available to sediment transport

τ_{LWD} = shear stress acting on wood

ρ = water density

g = gravity

R = hydraulic radius

S = slope of energy grade line

Channel and floodplain deposition enlarges the subsurface channel where water is moving much slower. The fact that groundwater flow is moving so much slower means that increased groundwater storage and flow has a net effect of slowing the export of water from the watershed. The headwaters of a channel network typically start with convergent topography ("channels") filled with colluvium where flow is entirely subsurface. Wood and vegetation increase the length of subsurface flow in a channel network which slows the rate that water is exported from the watershed, supplementing flows in dry periods. Incision not only increases water velocities in the stream and speeds the export of water out of the basin, but it can cut down to underlying bedrock and entirely eliminate the alluvial subsurface channel (e.g. Schanz et al. 2019). The lower invert of the incised channel lowers the adjacent groundwater table which drains a substantial portion of water stored in the alluvium. Prior to incision, channel connectivity to the floodplain was reflected in a relatively flat-water surface gradient across the valley. The principal gradient would have been down the valley. After incision the groundwater gradient rotates toward the channel (i.e., perpendicular to the valley) and increases. Water quickly drains from the alluvial aquifer into the

incised channel where it is rapidly routed downstream (Table 1). Prior to incision flow moved much slower down valley, retaining water within the watershed. This same process explains how subsurface tributary channels can maintain flows in downstream channels well into dry seasons and why gullies dry up so quickly. Basic definitions of the surface and subsurface channel and incision are illustrated in Figure 2.

Restoration within about 2 km of Poison Creek, a tributary to Mission Creek in north central Washington, resulted in this exact scenario. After wood placement , the channel aggraded, filling with sand and fine sediment. Water levels also increased, extending across large portions of the valley bottom in places. Portions of the channel and floodplain remained wetted through the summer and into the winter. Several restoration projects focused on in-stream wood placement illustrate this (Figures 3-4). Similar post-project conditions were observed in Toppenish Creek, a snow-dominated, moderate gradient tributary to the Yakima River in Yakima County, Washington (Figure 3) and the South Fork Nooksack, a rain-dominated river southwest of Mount Baker in northwest Washington (Figure 4). Another important influence of wood and vegetation goes back to the discussion of sediment transport capacity. The finer the sediment being deposited, the lower the hydraulic conductivity and rate of subsurface water flow. To illustrate the importance of grain size and how the grain size of a porous medium influences the flow of water down through surface area resistance, consider that gravel has a surface area of 15 cm^2/cm^3. Sand is 150 cm^2/cm^3, silt is 1500 cm^2/cm^3 and clay is 8,000,000 cm^2/cm^3. In summary, in streams dominated by a large subsurface alluvial channel, water moves much slower, thereby raising water tables and increasing water storage. The slower moving alluvial groundwater can supplement flow in downstream portions of the channel network, sustaining higher base flows.

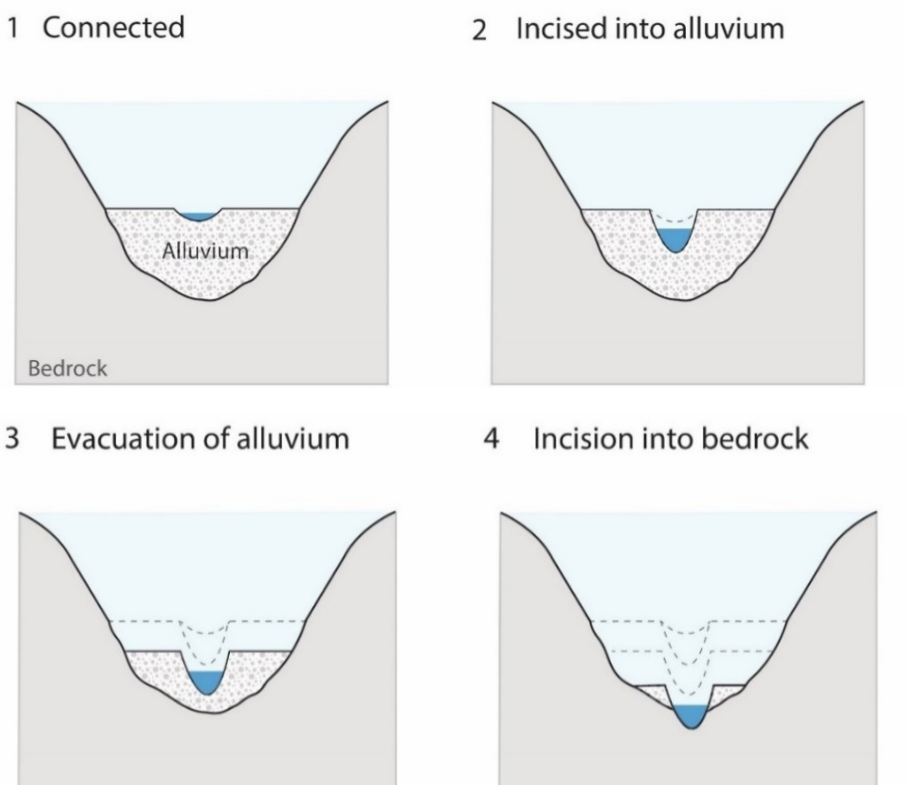

Figure 2. Illustration of depicting an alluvial channel consisting of a surface water channel and subsurface alluvial groundwater channel (1). Channel incision (2-4) has three key impacts: 1) lowering the water table, 2) enlargement and smoothing of the surface water channel, and 2) reduction of the alluvial subsurface channel and export of alluvium that may have taken thousands of years to accumulate. Water storage is lost by lowering the water level of the alluvial reservoir and routing it more quickly out of valley.

Flow Augmentation

Summer baseflows are currently too low and too warm in many streams across the Columbia River basin, resulting in a range of water scarcity problems, from water rights curtailment of irrigators to fish mortality from high stream temperatures (Ecology and U.S. Department of the Interior, 2012; Malloch and Garrity, 2012; Schneider and Anderson, 2007). Baseflows are projected to decrease further in many tributaries as climate warms and snowpack and soil moisture water storage are reduced (Elsner *et al.*, 2010). For example, average unregulated August streamflow in the Wenatchee River (modeled at Monitor, WA) is projected to decrease by 50-65% by the end of the century (Hamlet *et al.*, 2013). Current and future water scarcity are motivating proposals for new water storage projects, such as dams, that introduce new risks and impacts to aquatic ecosystems (Ecology and U.S. Department of the Interior, 2012). Restoration actions offer a viable alternative to increase water storage and dampen climate change impacts on the baseflow hydrograph, while simultaneously providing many ecosystem benefits.

As channel incision proceeds, overbank flow becomes less frequent, which reduces water storage in adjacent wetlands and floodplains. In addition to reduced groundwater recharge via overbank flow, the shallow groundwater is essentially drawn down by the lowered stream channel. This in-turn reduces the down-valley flow of groundwater that existed prior to incision. In gaining reaches, the hydraulic gradient between the subsurface groundwater stored in the floodplain and the surface water stored in the channel increases with the vertical distance between the two water surfaces. A steeper gradient drives flow from the groundwater to the channel, leading to faster and earlier seasonal lowering of the local groundwater table (Schilling *et al.*, 2004). Reduced surface and subsurface water storage within the river network subsequently results in lower baseflows, and mortality of shallow rooted riparian vegetation (Beechie *et al.*, 2008; Loheide and Gorelick, 2005; Wilcox, 2005).

Extensive restoration of incised streams has the potential to increase storage of alluvial sediment and water, and to augment low flows during the dry season. Restoration also has a suite of ecological benefits that have been widely recognized and supported as part of salmon recovery efforts in the Columbia River basin (Honea *et al.*, 2009; Katz *et al.*, 2007). Less recognized, however, are the critical benefits of the increased water storage and baseflow contributions that river restoration provides to water resources, aquatic habitat, and forest health. Although the idea has been intermittently proposed across the western United States (Van Haveren, 2004; Ponce and Lindquist, 1990) and assessed in California (Emmons, 2013; Loheide and Gorelick, 2006; Tague *et al.*, 2008; Wilcox, 2005), work to consider and quantify the effects of restoration on water resources in the Pacific Northwest is sparse (Fouty, 2013).

Figure 3. Toppenish Creek in Yakima River basin of central Washington in June 2015 prior to restoration (a). Same location in Toppenish Creek on October 4th, 2017 after restoration using channel spanning wood placements (b). Photo was taken at end of summer during period of

minimum flows yet channel is largely full of water. The estimated increase in water storage following restoration is 20 acre-ft over a 500 m reach and 240 m wide valley (76 ac-ft/mile).

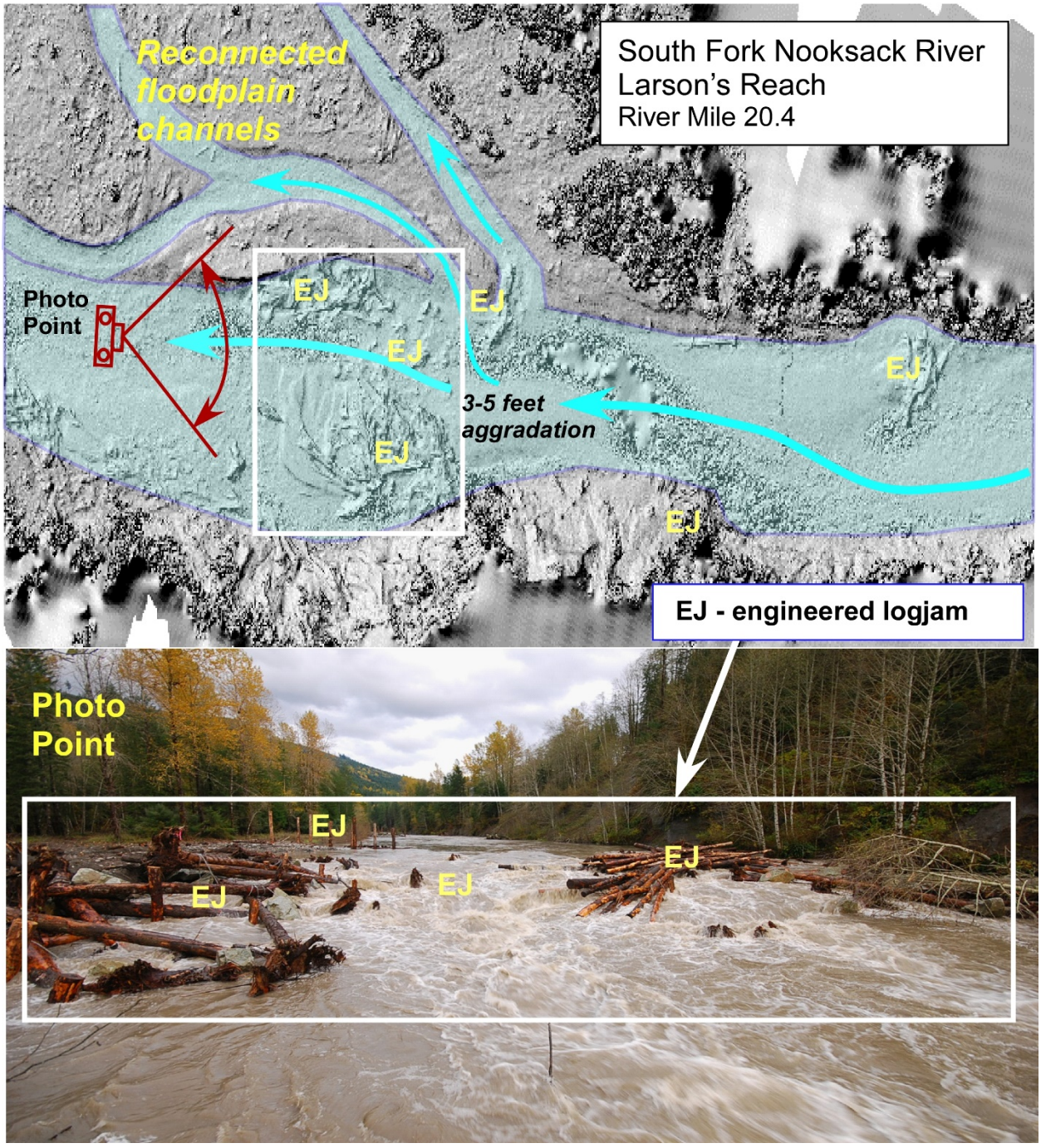

Figure 4. The South Fork Nooksack River, a large montane river draining the west Cascades in Skagit and Whatcom Counties. Prior to restoration wood placement, this reach of the river had experienced three meters of incision (Abbe et al. 2015). Channel spanning engineered wood placements in 2016 raised water levels about 1.5 meters, reconnecting 25 acres of floodplain, forming one km of new side channels within a 0.6 km segment of the valley. The instream structure corresponds to the white water in the photo (looking upstream). Restoration within the treatment area created 30 ac-ft (102 ac-ft/mile) of additional water storage.

Restoration approaches to store water and sediment

Restoration actions that implement channel-spanning structures or barriers constructed from natural materials are designed to re-aggrade the channel bed through the trapping of sediments and improve hydrologic connectivity between the channel and the surrounding floodplain (Figure 3). Approaches range from installing engineered log jams (Abbe *et al.* 2003, 2015; Abbe and Brooks 2011) to beaver dam analogs (Pollock *et al.*, 2012) to creation of small earthen dams (i.e. 'pond and plug') (Wilcox, 2005), but the underlying concept is similar: partially block the channel to increase hydraulic roughness, slow and impound streamflow, and capture and store sediment.

Backwatered areas created by the stream impoundments act as surface water storage, which raise the local surface water elevation and, consequently, the surrounding groundwater elevation (Figure 2). The lower flow velocities initiate deposition of sediment, which raises the elevation of the channel bed and reduces local stream gradient (Abbe and Montgomery, 2003; Abbe and Brooks, 2011; Brummer *et al.*, 2006). Backwater pools formed by channel-spanning structures are therefore temporary in any one location, because channel aggradation is the primary geomorphic goal when restoring incised streams. However, the channel aggradation drives a long-term increase in local groundwater storage (Hammersmark *et al.*, 2008; Schilling *et al.*, 2004; Tague *et al.*, 2008) and improved geomorphic function, which includes natural wood recruitment processes that create new backwatered areas (Collins *et al.*, 2012). Thus, a restored stream will sustain increased surface and subsurface water storage even though locations of backwater pools will shift through time.

Re-aggradation of the incised channel raises the in-channel water surface elevation, which results in a newly saturated wedge of subsurface floodplain sediments in a gaining stream (Figure 2). Local groundwater-surface water interaction vary longitudinally with position in the watershed, and locally with subsurface characteristics (Payn *et al.*, 2012); however, reaches above the mountain-to-valley transition (i.e., mountain front recharge zone) tend to be net gaining with baseflow contributions from groundwater (Covino and McGlynn, 2007). Thus, widespread restoration throughout the upper watershed has the potential to increase surface and subsurface water storage. The approach has been considered in California, where Emmons (2013) estimated 97,000 acre-feet of "restorable" groundwater storage if all impaired reaches were re-aggraded in the montane meadows of the Sierra Nevada. Within the Columbia River basin, Fouty (2013) estimated an increase in surface and subsurface water storage of 40-53 acre-feet/mile from restoration actions on Camp Creek, an incised stream in the Wallowa-Whitman National Forest in Oregon. The analysis was based on analysis of channel and valley morphology and soil types along a 0.75-mile reach.

Restoration of in situ water storage has been shown to increase instream water quantity and improve water quality. Both observational and modeling studies have demonstrated at the reach-scale that re-aggradation of incised streams can result in a 10-20% increase in baseflow early in the dry season (Ohara *et al.*, 2014; Tague *et al.*, 2008). The additional contribution is a result of the raised water surface elevation in the re-aggraded channel. The hydraulic gradient between the shallow groundwater elevation and the in-channel water surface elevation is reduced, which slows the drainage of the shallow groundwater reservoir (Fouty, 2013; Loheide and Gorelick, 2006). The reduced rate of groundwater inflow subsequently extends the duration of the baseflow contribution of these inflows, which contributes to more and colder water later in the season. Loheide and Gorelick (2006) combined stream temperature measurements with coupled groundwater-surface water modeling to demonstrate elevated groundwater inflow through a restored reach in a Sierra Nevada meadow. In the restored reach streamflow persisted several weeks after adjoining reaches were dry and stream temperatures were more than 3 °C lower than in adjoining, untreated reaches. Wondzell and Swanson (1999) show how breaching of wood jams led to incision of a 200 m long study reach, transforming a multi-channel morphology to a simple single channel. This reduced hyporheic exchange lowered groundwater oxygen and dissolved organic carbon.

There is consensus in the literature that stream restoration addressing incision increases local groundwater storage. Some studies have demonstrated increased baseflow contributions, but others have

suggested that gains in baseflow may be partially or fully offset by increased water use from riparian vegetation. The lowering of the groundwater table from channel incision has been observed to cause vegetation mortality or a conversion from a wetter ecosystem to a drier one (Loheide et al., 2009). Therefore, the increased amount and longer duration of water storage in the shallow groundwater likely improves the health of the riparian vegetation (e.g., Fouty, 2013; Loheide and Gorelick, 2006). For example, Tague et al. (2008) analyzed streamflow measurements above and below a restored reach and found that baseflow was increased downstream of the restored reach early in the summer season, but increases in baseflow were diminished by late summer. The authors suggested that the change was due to increased evapotranspiration from restored riparian vegetation. Another study in a northern California meadow utilized hydrologic modeling to assess restoration effects and found that although groundwater storage increased, local in-meadow baseflow decreased due to increased evapotranspiration while downstream baseflow increased and altered groundwater flow paths (Hammersmark et al., 2008). In contrast, Essaid and Hill (2014) found that modeled baseflow decreased both in-meadow and below the restored meadow, which they attribute to increased evapotranspiration. Despite local variations in hydrological fluxes, all studies demonstrate additional groundwater storage and most demonstrate groundwater input to the stream, which suggests that, at a minimum, restoration actions will result in healthier riparian vegetation and lower summer stream temperatures (Bogan et al., 2003; Baird et al., 2005; Loheide et al., 2009). It is noteworthy that restored stream segments are likely to retain more organic matter which can increase water holding capacity of alluvial material (Hudson 1994, Libohova et al. 2018). Hudson (1994) shows that when organic matter content increased from 0.5 to 3% the available water content of the alluvium more than doubled for three different grain sizes of soil (sand, silt-loam and silty clay loam).

In addition to variable recharge and transpiration rates, the volume of restorable water storage and related benefits to water resources depends on the extent of channel incision and/or valley lowering that has occurred. Incision on the order of one to several feet has been widely observed across the Washington State (Abbe et al. 2009, 2013, 2015, ; Beechie *et al.*, 2008; Fouty, 2013; Pollock *et al.*, 2014). However, the almost complete loss of alluvial sediments and subsequent valley down-cutting has also been documented in the Teanaway River, in central Washington (Stock et al. 2005, Schanz et al. 2019). Successful restoration of incised river channels has been widely documented, and the restoration of lowered river systems is also theoretically possible. For example, Pollock *et al.* (2014) present a conceptual model of how beaver dams (or analogous structures) raise both the channel and valley elevation, and the amount of alluvial sediment and water stored. River restoration has been shown to aggrade channels where there is sufficient sediment supply from upstream or adjacent hillslopes (e.g., Abbe et al. 2013).

Methods

We present a framework for evaluating potential water storage using simple geometric computations of valley alluvium and water content, estimates of channel incision and assumptions of alluvium characteristics using field observations. Our analysis includes a GIS based analysis of digital elevation models (DEMs), aerial imagery, and analysis of field data that includes topography, water levels, sediment, vegetation, and how these attributes change over time.

We began with a reach-scale geomorphic assessment of stream incision and utilized field-derived and spatial data to estimate watershed-scale water storage potential through restoration in Mission Creek, which flows into the Wenatchee River near Cashmere, Washington (Figure 5). The 240 km^2 Mission Creek watershed is located relatively low on the eastern slopes of the Cascade Range, with snowmelt-fed spring streamflow and dry conditions in late spring and summer. The watershed is steep with a mean slope of 44% and relief of 1843 m with elevations from 241 to 2085 m. Summer water quantity and quality impact the availability of irrigation water to orchards along the mainstem as well as the health of the Endangered Species Act-listed spring Chinook salmon and summer steelhead runs. Both Mission Creek and the Wenatchee River are on the Clean Water Act 303(d) list of impaired water bodies for water temperature exceedances. Field inspections of Poison Creek, a second order channel draining into Mission Creek revealed incised channel segments lacking wood and segments where wood still maintains stream grade and creates wetlands, as well as incised segments (Figure 6).

As part of the work we developed a semi-automated GIS analysis to provide initial predictions of incision and potential water storage using DEMs and segmented stream networks with drainage area attributes (Figure 6). The GIS analysis computed stream gradient, delineated valley bottoms and widths, and estimated incision (with a high resolution one meter DEM). Using valley width, reach length, extent of incision and stream gradient, we then compute the restorable sub-surface water volume, flow contribution per reach length, surface water storage and minimum treatment density. This assessment of water storage through river restoration in Mission Creek represents a pilot project led by Chelan County Natural Resources Department to evaluate the feasibility of a multi-benefit strategy to address current and future water quantity and quality. In contrast to the suite of new dams and reservoirs that are currently proposed in Washington and across the west to buffer projected climate impacts (Ecology, 2016; Ecology and U.S. Department of the Interior, 2012), a water storage strategy based in re-initiation of natural processes includes additional benefits, rather than impacts, to aquatic and terrestrial ecosystems. To support a robust comparison of water storage strategies, we developed and applied methodology for estimating potential reach and watershed scale water storage from the restoration of incised channels.

To estimate water storage potential from restoration in Mission Creek, we completed a geomorphic assessment in three study reaches, from which we estimated water storage potential at the reach-scale. We subsequently extrapolated the reach-scale estimates to the watershed-scale in order to estimate the potential for water storage and baseflow contribution from extensive restoration. We conceptualized the restorable subsurface volume as a wedge of sediments (Emmons 2013) that would become saturated when the channel bed elevation was raised, extended along the length of the alluvial valley (Figure 7). The shape of this wedge depends on the water surface elevation in the channel, which we approximated as the channel bed elevation during baseflow and on the groundwater surface elevation at the edge of the floodplain, which we approximated as the surface elevation at the hillslope-valley transition.

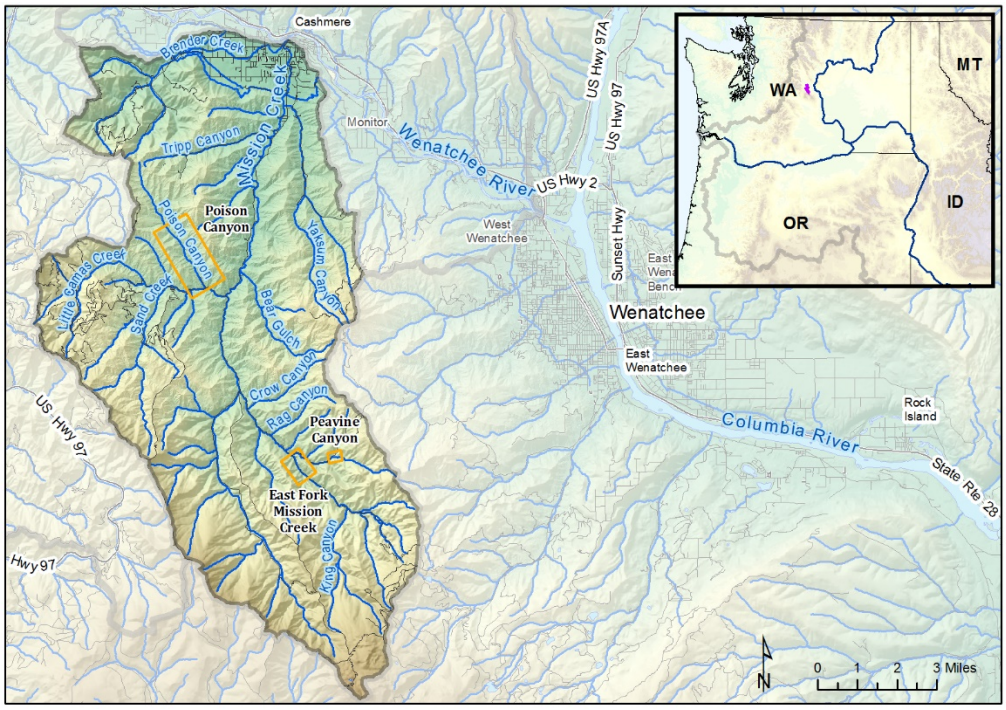

Figure 5. Map of the Mission Creek Watershed, with the three study areas indicated in gold rectangles. Inset map shows location in the Pacific Northwest, the Columbia and Snake Rivers indicated as blue lines and the boundary of the Columbia River basin indicated as a gray line.

To estimate surface water storage from backwatered areas triggered by in-channel wood structures, we computed the ideal density of structures along the reach and estimated a water storage volume per

structure. Similar to an artificial impoundment, surface water storage volume from in-channel wood structures is positively correlated to valley width and structure spacing (i.e., area of potential storage) and negatively correlated with valley slope. Thus, low-relief reaches with wider valley bottoms will have greater surface water storage potential per in-channel wood structure versus steeper channels with naturally confined valleys where storage potential is low. We therefore estimated additional surface water storage based on the average reach gradient and a target aggradation height to estimate the backwater influence of each structure and the maximum treatment density.

We averaged the reach-scale results for restorable water storage (i.e., combined volume of surface and subsurface water storage per length of stream restored) to the watershed-scale in order to estimate the potential to restore water storage if restoration actions were implemented across incremental fractions of the stream network. The analysis assumes that the incised conditions observed in the study reaches are representative of conditions across the watershed and neglects spatial variability in channel and valley morphology. We utilized existing channel location data from the National Hydrography Dataset, and excluded reaches in agricultural valleys and reaches with a stream gradient higher than 10%.

Figure 6 - 4-panel figure – a) Photos of wetland reaches in Poison Canyon showing wood as the downstream hydraulic control (a) and shallow height (0.5-1') from water surface to bank (b). Photos of severely incised reaches in Poison Canyon. (c and d)

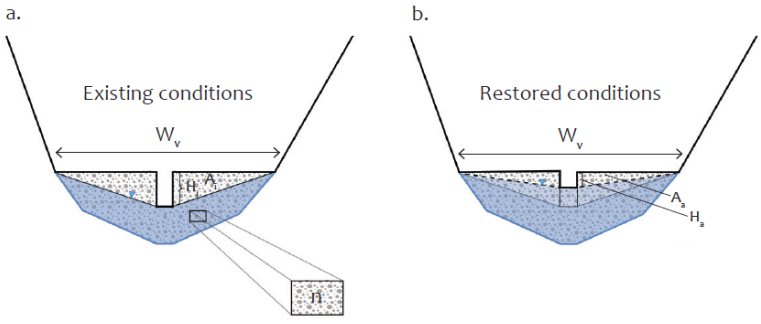

Figure 7a, b. Graphical definitions of influence of incision on alluvial water storage.

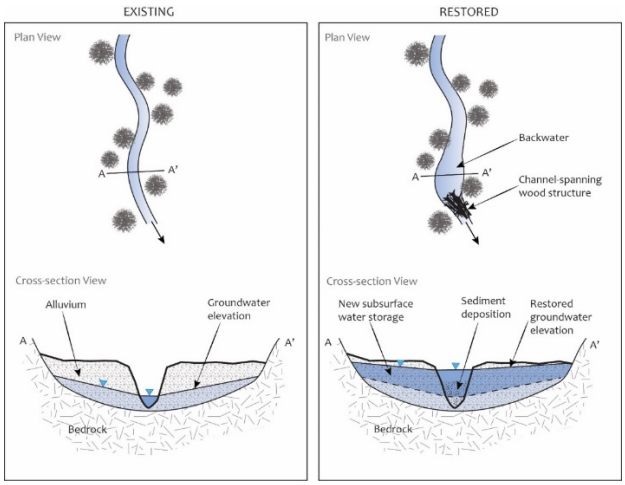

Figure 7c. Illustration of restoring alluvial water storage.

Estimates of water storage (m^3/km or acre-feet/mile of stream restored) were converted to a baseflow contribution by computing the flux of water from the shallow groundwater to the channel. The baseflow contribution is based on assumptions of homogeneous sediments with a uniform saturated hydraulic conductivity, and a constant hydraulic gradient. Flux was computed through the wetted area of the channel wall (assuming a baseflow water depth of 0.15 m) to represent groundwater inflows only, and therefore neglects upwelling and downwelling hyporheic exchange through the stream bed.

Preliminary Results

We have applied the GIS model to several small watersheds draining to the Wenatchee River in Chelan County totaling 791 km^2 and 596 km of stream. Our preliminary estimate of potential water storage for this area came to approximately 13.6 million m^3 (11,000 acre-ft). An example of results for the 240 km^2 Mission Creek watershed are presented in Figure 8. Given these results are for low-order montane streams with relatively narrow valley bottoms, we believe the results are conservative (low) with regards to extrapolating to larger areas.

The geomorphic assessment of three study reaches yielded observations of substantial upland sediment sources, widespread channel incision, and in-channel large wood contributing to local sediment storage. Historical photos from Mission Creek indicate that hillslope and channel erosion was widespread around the 1930s-1950s, and was likely due to grazing and logging activities combined with friability of the underlying sandstone bedrock. In response, the Civilian Conservation Corps (CCC) constructed terraces and wooden check dam structures to slow erosion; Peavine Canyon is thought to be the location of some of these historical structures (Matt Karrer, USFS, personal communication).

Channel and floodplain sediments are dominated by sand and gravel. Channel bed sediments consist of 10-40% sand, 10-90% gravel, and 5-40% cobbles. We observed sandstone bedrock in the channel in one location in both East Fork Mission Creek and Poison Canyon. Floodplain sediments characterized by test pits consist primarily of sand from 0 to 0.61 m (0-2 ft) depth. Based on the field assessment and geologic context of the watershed, we applied a constant value of 0.35 for the porosity (i.e., interstitial space) of the floodplain sediments (sand). This simplification is based on published values for sand and gravel (Morris and Johnson, 1967), the location of the field site within two similar geologic formations (i.e., the Chumstick and Swauk Formations), and observations of homogeneous floodplain sediments.

Estimate for potential surface water storage in Poison Canyon and East Fork Mission Creek from backwatered areas are 3,065 and 12,260 m^3/km (4 and 16 acre-feet/mile), respectively. The differences between the two reaches reflect differences in channel gradient, valley width, and longitudinal extent of incision. We estimated the volume of surface water behind each structure at 160 to 345 m^3 (0.13 to 0.28

acre-feet) per channel-spanning structure based on the geometry of a stream gradient, a 1.2 m impoundment height, and a ponded width equal to half of the valley width (9 and 20 m, respectively). Based on the channel morphology and gradient, the maximum treatment density is 35 structures per km.

Reach-average subsurface alluvial water storage from channel restoration is estimated at 1,456 and 8,274 m^3/km (1.9 and 10.8 acre-feet/mile) in Poison Canyon and East Fork Mission Creek, respectively. The restorable reach-average alluvial water storage is an order of magnitude higher in East Fork Mission Creek due to the larger valley width and the longitudinally continuous incised condition. The estimate for Poison Canyon is based on the observation and delineation of three geomorphic conditions in Poison Canyon, ranging from no incision (i.e., the wetland complexes) to severe incision. Thus, the amount of restorable groundwater storage from channel aggradation was highest in the most severely incised reaches, but we computed a reach-average value that includes all three conditions. In contrast, we observed longitudinally continuous incision in East Fork Mission Creek, and estimated restorable water storage for the reach based on reach-average values of incision. Whereas channel restoration in Poison Canyon and East Fork Mission Creek represent a range of low scenarios for restorable water storage in Mission Creek, we additionally estimated high scenarios from hypothetical valley restoration, for which the entire alluvial is raised. Since restoration of alluvial across the valley substantially raises the vertical dimension of the subsurface wedge of saturated sediments, the restorable subsurface alluvial water storage is higher. Estimated combined values for channel and valley aggradation are 8,660 and 22,140 m^3 (11.3 and 28.9 acre-feet/mile) for Poison Canyon and East Fork Mission Creek, respectively. When looking at incised channels in larger alluvial valleys, the potential storage goes up substantially. For example in Toppenish Creek (Figure 3), wood placement rose the water table an average of 2.8 ft, resulting in 76 acre-ft/mile of additional water storage. For the South Fork Nooksack example (Figure 4), the water table was raised 4.9 ft, resulting in 180 ac-ft/mile of water storage. The work in Misson, Toppenish and South Fork Nooksack only involved wood placement. Work by the US Forest Service in Staler Creek, Willamette National Forest (Powers et al. 2018) had even more incision (>9 ft) and took an aggressive restoration approach that filled the incised channel, the estimated increase in water storage (using same Mission Creek methodology) is 350 acre-ft/mile. These estimates make a strong case for restoring incised channels simply based on the potential water retention.

We applied the estimated combined surface and subsurface water storage values for Poison Canyon and East Fork Mission Creek under the channel and valley restoration scenarios to extrapolate to watershed-scale restoration. Poison Canyon and East Fork Mission Creek represent a range of geomorphic conditions and morphology, and therefore water storage potential. Thus, the range of the two estimates applied to the stream network is intended to reflect some of the spatial variability in restorable water volumes. In the Mission Creek watershed we estimate that there are 8 km (5 miles) of stream network that have a stream gradient less than 5% and are not adjacent to a road, and 40 km of stream network that have a stream gradient less than 10% and are not adjacent to a road. Based on extrapolating the mean volume per length of restoration values derived in the reach-scale estimates to the length of treatable stream network, we estimate the total potential surface and subsurface water storage of treating all 8 km with an average stream gradient less than 5% to be 370,000-789,400 m^3 (300-640 acre-feet) in the low and high restoration scenarios, respectively. In the context of this linear extrapolation, water storage scales with length treated, so restoration applied to 10% of the feasible stream network would result in 10% of the water storage. The magnitude the streamflow flux provided by additional alluvial water storage scales with the length of the treated stream network. The additional streamflow contributions following the restoration actions range from $5.7x10^{-4}$ - $4.8x10^{-2}$ cms (0.02 to 1.7 cfs). Additional flow can be supplied to the stream (above base flow) for three or more months depending on the extent of the restoration.

Feasibility of restoration approach in Mission Creek

Geomorphic assessment of the two study reaches in conjunction with widespread effects from historic impacts suggest that incision and channel disconnection from the floodplain is common in the Mission Creek watershed. Under these impaired conditions, Mission Creek is likely transporting more water and

sediment out of the channel network earlier in the season as compared to reference (historic) conditions. Therefore, historic and on-going channel incision contribute to downstream impacts including decreased baseflows, higher stream temperatures, and increased sediment loads.

Identification of wetland complexes in Poison Canyon demonstrates that placement of in-channel large wood is likely to initiate channel bed aggradation and the storage of both alluvial sediment and water. The average stream gradient of 4.1% the Poison Canyon study reach would be considered relatively high for some restoration approaches. However, the existence of two wetland complexes provides local examples of the role of wood for providing hydraulic control and storing alluvial sediment in this watershed at these gradients. Beavers typically build dams in perennial stream channels with slopes of less than 6%. The buried check dam structures in Peavine Canyon illustrate sediment storage potential in steeper (gradient = 6.8%) ephemeral reaches and suggest that the total amount of stream network that could be treated is closer to 24.8 miles (40 km) with gradient < 10%, opposed to 8 miles (13 km) with gradient < 5% in Mission Creek.

Observations of two locations with in-channel bedrock exposure combined with a large hillslope sediment source further suggest that valley-lowering may have occurred, and that there is high potential to capture and store sediment. In this case, the higher estimates may be more accurate reflections of the long-term water storage benefit. Restoration of a lowered valley would require repeated restoration actions through time combined with riparian forest restoration and the re-initiation of large wood recruitment processes.

Comparison with Built Infrastructure

The analysis presented herein indicates that widespread restoration may be a feasible approach to improve water storage and increase baseflow, and comparison with previous cost estimates for traditional dam structures demonstrate that the approach may also be cost-effective. Previous assessments of potential for water storage and low flow augmentation from surface water impoundment identified three project locations within Mission Creek (Montgomery Water Group, 2006). In particular, two sites for off-channel reservoirs and one site for an instream reservoir were identified. The potential reservoirs would provide 51, 95, and 926 acre-feet of storage for an estimated construction cost of $25,000, $58,000 and $8,000/acre-foot, respectively. The estimated instream flow benefit ranges from 0.5 cfs to 12.9 cfs for 30 days for during the summer (Montgomery Water Group, 2006).

For comparison, we estimate a cost of $4700/acre-foot of additional surface and subsurface water storage from restoration. This estimate is based on an estimated cost of $1000/in-channel structure and an implementation density of 53 structures/mile, along with estimated mean surface and subsurface water storage of 11.4 acre-feet/mile. Note that costs associated with operations and maintenance (O&M), potential negative habitat impacts, and increased downstream risks are not included in either estimate, but are likely to be much higher for a traditional engineering approach than a restoration approach.

Accounting for Evaporative Losses

The estimates of water storage for Mission Creek neglect uncertainties related to how evapotranspiration rates and timing may change with an increase in the elevation of the shallow groundwater (Tague et al., 2008). Although more water will theoretically be available, the additional water storage will be partitioned between baseflow augmentation and transpiration by riparian vegetation. Further study is needed to understand how transpiration rates, in the short-term, and plant communities, in the long-term, may shift with increased shallow groundwater availability in this watershed.

Although more transpiration represents a loss to baseflow from a water budgeting perspective, more robust riparian vegetation and forests are more resilient to drought, fire, and insect outbreaks (Allen, 2009; Grant et al., 2013; Polvi and Wohl 2013, Millar and Stephenson, 2015). Healthy riparian forests additionally provide a source for abundant in-channel wood that repeatedly creates backwater effects and prevents incision (Collins et al., 2012). In contrast to evaporation off the water surface of a reservoir, the

water that is consumed by the transpiration process contributes to the health of riparian vegetation and river function. Wetted valley bottoms and healthy trees increases fire resilience. Riparian vegetation and hyporheic flow also have a significant role in lowering stream temperatures (e.g., Johnson 2004, Seixas et al. 2018) and improving water quality (e.g., Peter et al. 2019).

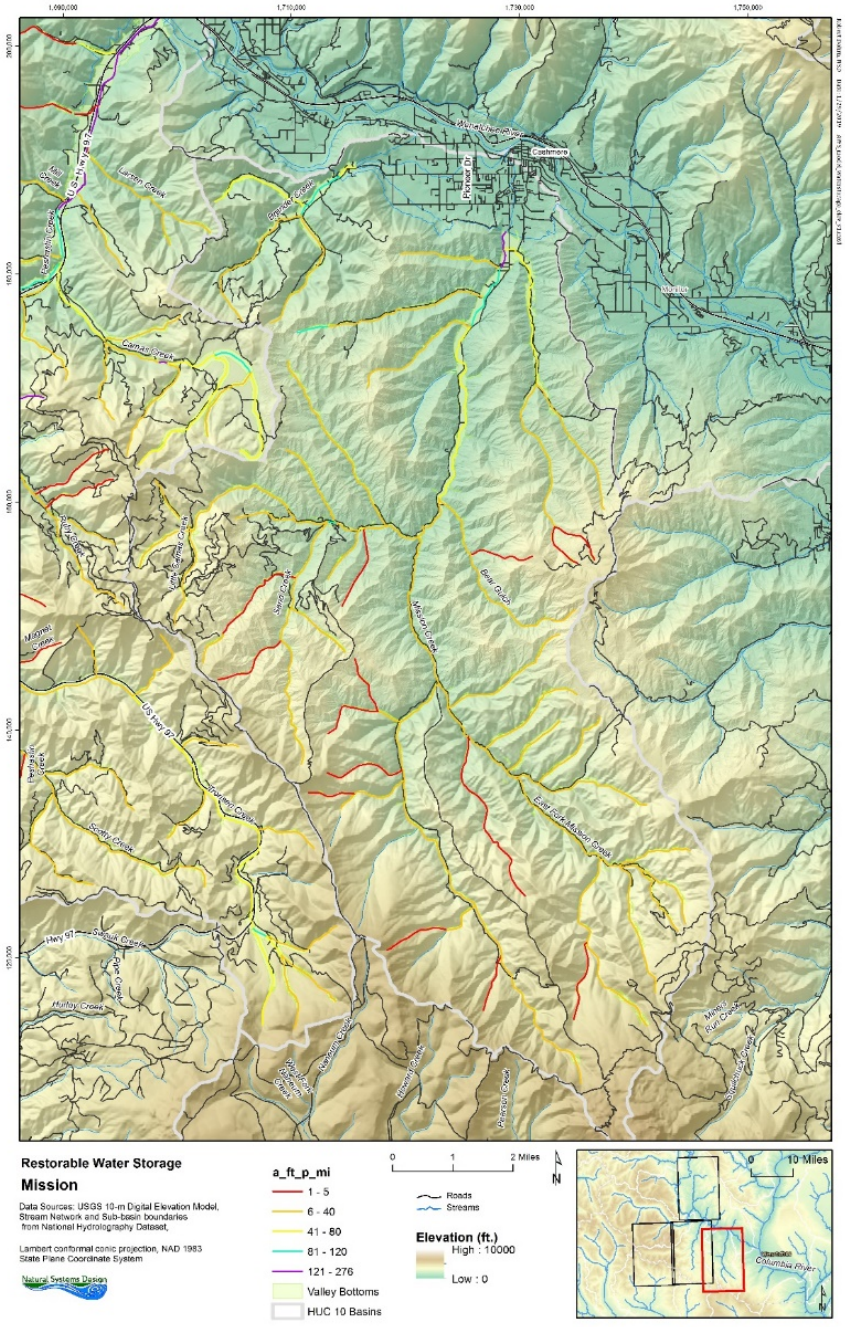

Figure 8 Water storage potential estimates based on 10m digital elevation model of 209 km^2 Mission Creek basin in Chelan County on eastside of Cascade mountains, north central Washington.

Implications for water storage in the Western U.S.

The assessment of water storage potential in Mission Creek represents a replicable approach that could have substantial benefits to baseflow quantity and water quality in the context of the Wenatchee River watershed or even the Columbia River basin. The Mission Creek watershed constitutes a relatively small portion of the Wenatchee River watershed, but the analysis presented herein suggests that the water resources benefits from extensive restoration are on par with the estimated benefits of more traditional approaches. As stated in our preliminary results, we show a range of 11 to 29 acre-ft/mile for small alluvial valleys and 76 to 350 ac-ft/mile for intermediate sized alluvial valleys. Washington State has about 74,000 miles of perennial channels and more than twice that of ephemeral channels. Assuming a range of 20 to 250 ac-ft/mile and just using perennial channel length, there could be 1.5 to 18 million ac-ft of potential water storage. Including Oregon these numbers more than double. Applying same methods to California alone yields 12 to 150 million ac-ft. Given that this approach is also applicable to ephemeral channels (e.g. Fouty 2013) and that they account for twice the length of perennial channels, we believe our estimates for potential water storage are conservative. We acknowledge there is a great deal of uncertainty but believe these estimates further support the value of stream restoration and stress the importance of additional research into restoring incised channels and channel spanning wood placement. Restoring natural water storage processes represent a sustainable, multi-benefit strategy to address water scarcity, with benefits to salmon recovery and forest resilience. The volume and baseflow contributions of stream restoration are more difficult to quantify than built infrastructure such as reservoirs, but the numerous ecosystem benefits and virtual absence of negative impacts of restoration make restoration for water storage a compelling approach. This analysis provides a quantitative estimate of the water storage and baseflow augmentation benefits of stream restoration in Mission Creek together with supporting example of other regions that serves as a starting point for thorough consideration of innovative water resource solutions in the Western United States.

Acknowledgements

Editorial comments by G. Hudson and and T. Rowley improved the manuscript.

Citations

Abbe, T.B., 2000. Patterns, Mechanics, and Geomorphic Effects of Wood Debris Accumulations in a Forest River System. University of Washington. 222 p.

Abbe, T., B. Anderson, C. Carlstad, D. Devier, K. Fetherston, S. Dickerson-Lange, L. Embertson, S. Higgins, S. Katz, L. Lestelle, K. Knox Machata, M. Nelson, J. O'Neal, K. Patrick, M. Reinhart, C. Riordan, M. Stepp, P. Trotter and R. Ventres-Pake. 2016. Preliminary Scientific and Technical Assessment of a Restorative Flood Protection Approach for the Upper Chehalis River Watershed. Report to by Natural Systems Design submitted to the Washington State Department of Ecology, Olympia, WA.

Abbe, T., M. Aubele, C. Miller and S. Blanton. 2009. Self-mitigating protection for pipeline crossings in degraded streams: A case study from Woodard Creek, Washington. Proceedings of the 2009 International Rights-of-Way Symposium. 13 p.

Abbe, T. and P.D. Brooks, 2011. Geomorphic, Engineering, and Ecological Considerations When Using Wood in River Restoration. A. Simon, S. J. Bennett, and J. M. Castro (Editors). Stream Restoration in Dynamic Fluvial Systems: Scientific Approaches, Analyses, and Tools. American Geophysical Union, Washington, DC, pp. 419–451.

Abbe, T., B. Belby, and F.D. Shields. 2016. Geomorphology and hydrology considerations. Chapter 4 in Bureau of Reclamation and U.S. Army Engineer Research and Development Center. National Large Wood Manual: Assessment, Planning, Design, and Maintenance of Large Wood in Fluvial Ecosystems: Restoring Process, Function, and Structure. 628 p. + Appendix. www.usbr.gov/pn/ and http://naturaldes.com/resources/

Abbe, T., M. Ericsson and L. Embertson. 2013. Geomorphic assessment of the Larson Reach of the South Fork Nooksack, NW Washington. Report submitted to Lummi Indian Nation.

Abbe, T., M. Ericsson and L. Embertson. 2015. Channel incision and floodplain abandonment due to historic wood removal in Washington State, USA. International Conference on Wood in World Rivers Conference. University of Padova, Padova, Italy.

Abbe, T.B. and D.R. Montgomery, 2003. Patterns and Processes of Wood Debris Accumulation in the Queets River Basin, Washington. Geomorphology 51:81–107.

Abbe, T.B., G. Pess, D.R. Montgomery, and K.L. Fetherston, 2003. Integrating Engineered Log Jam Technology into River Rehabilitation. In D. R. Montgomery, S. M. Bolton, D. Booth, and L. Wall (Editors). Restoration of Puget Sound Rivers. Center for Water and Watershed Studies, Seattle, WA pp.443-490.

Abbe, T.B., D.R. Montgomery, and C. Petroff. 1997. Design of Stable In-Channel Wood Debris Structures for Bank Protection and Habitat Restoration: An Example from the Cowlitz River, WA. pp. 809-816 in: S.S.Y. Wang, E.J. Langendoen, and F.D. Shields Jr. (eds.), Proceedings of the Conference on Management of Landscapes Disturbed by Channel Incision. University of Mississippi, University, Mississippi.

Allen, C.D., 2009. Climate-Induced Forest Dieback: An Escalating Global Pheno.? Unasylva 60:43–49.

Beechie, T.J., H. Imaki, J. Greene, A. Wade, H. Wu, G. Pess, P. Roni, J. Kimball, J. Stanford, P. Kiffney, and N. Mantua, 2012. RESTORING SALMON HABITAT FOR A CHANGING CLIMATE. River Research and Applications 22:n/a-n/a.

Beechie, T.J., M.M. Pollock, and S. Baker, 2008. Channel Incision, Evolution and Potential Recovery in the Walla Walla and Tucannon River Basins, Northwestern USA. Earth Sur. Proc. and Land. 33:784–800.

Beedle, D., 1991. Physical Dimensions and Hydrological Effects of Beaver Ponds on Kuiu Island in Southeast Alaska. Oregon State University.

Bridges, T.S., E.M. Bourne, J.K King, H.K. Kuzmitski, E.B. Moynihan and B.C. Suedel. 2018. Engineering with nature; an atlas. ERDC/EL SR-18-8. Vicksburg, MS. U.S. Army Engineer Research and Development Center.

Brooks, A.P. and Brierley, G.J. 2002. Mediated equilibrium: the influence of riparian vegetation and wood on the long-term character and behavior of a near pristine river. Earth Surface Processes and Landforms 27, 343-367.

Brooks, A.P., Brierley, G.J. and Millar, R.G. 2003. The long-term control of vegetation and woody debris on channel and floodplain evolution: insights from a paired catchment study between a pristine and disturbed lowland alluvial river in southeastern Australia. Geomorphology 51, 7-29.

Brummer, C.J., Abbe, T.B., Sampson, J.R. and Montgomery, D.R. 2006. Influence of vertical channel change associated with wood accumulations on delineating channel migration zones, Washington, USA. Geomorphology 80, 295-309.

Buffington, J.M. and Montgomery, D.R. 1999. Effects of hydraulic roughness on surface textures of gravel-bed rivers. Water Resources Research 35, 3507-3521.

Collins, B.D., D.R. Montgomery, K.L. Fetherston, and T.B. Abbe, 2012. The Floodplain Large-Wood Cycle Hypothesis: A Mechanism for the Physical and Biotic Structuring of Temperate Forested Alluvial Valleys in the North Pacific Coastal Ecoregion. Geomorphology 139–140:460–470.

Collins, B.D., D.R. Montgomery, and A.D. Haas, 2002. Historical Changes in the Distribution and Functions of Large Wood in Puget Lowland Rivers. Canadian Journal of Fisheries and Aquatic Sciences 59:66–76.

Covino, T.P. and B.L. McGlynn, 2007. Stream Gains and Losses across a Mountain-to-Valley Transition: Impacts on Watershed Hydrology and Stream Water Chemistry. Water Resources Research 43. doi:10.1029/2006WR005544.

Ecology, W.D. of, 2016. Chehalis Basin Strategy - Draft Programmatic EIS. http://chehalisbasinstrategy.com/eis-library/.

Ecology, W.D. of and U.S. Department of the Interior, 2012. Yakima River Basin Integrated Water Resource Management Plan - Final Programmatic Environmental Impact Statement. https://www.usbr.gov/pn/programs/yrbwep/reports/FPEIS/fpeis.pdf.

Elsner, M.M., L. Cuo, N. Voisin, J.S. Deems, A.F. Hamlet, J.A. Vano, K.E.B. Mickelson, S.-Y. Lee, and D.P. Lettenmaier, 2010. Implications of 21st Century Climate Change for the Hydrology of Washington State. Climatic Change 102:225–260.

Emmons, J.D., 2013. Quantifying the Restorable Water Volume of Sierran Meadows. Univ. CA, Davis.

Essaid, H.I. and B.R. Hill, 2014. Watershed-Scale Modeling of Streamflow Change in Incised Montane Meadows. Water Resources Research 50:2657–2678.

Fouty, S., 2013. A Strategic Response to Climate Change: Restoring Water Storage Capability to Stream Ecosystems on Public Lands with the Help of Beavers, Wolves, and Fire. River Restoration Northwest. http://www.rrnw.org/wp-content/uploads/201311_Fouty.pdf

Galay, V.J. 1983. Causes of river bed degradation. Water Resources Research 19 (5), 1057-1090.

Grant, G.E., C.L. Tague, and C.D. Allen, 2013. Watering the Forest for the Trees: An Emerging Priority for Managing Water in Forest Landscapes. Frontiers in Ecology and the Environment 11:314–321.

Guardia, J.E.. 1933. Some results of log jams in the Red River. The Bull. of the Geog. Soc. of Philadelphia 31(3), 103-114.

Hamer, T.R. 1972. Stream channel enlargement due to urbanization. Water Res. Res. 8 (6), 1530-1540.

Hamlet, A.F., M.M. Elsner, G.S. Mauger, S.-Y. Lee, I. Tohver, and R.A. Norheim, 2013. An Overview of the Columbia Basin Climate Change Scenarios Project: Approach, Methods, and Summary of Key Results. Atmosphere-Ocean 51:392–415.

Hammersmark, C.T., M.C. Rains, and J.F. Mount, 2008. Quantifying the Hydrological Effects of Stream Restoration in a Montane Meadow, Northern California, USA. River Res. and App. 24:735–753.

Hartopo. 1991. The effect of raft removal and dam construction on the Lower Colorado River, Texas. M.S. Thesis, Texas A & M University.

Harvey, M.D, D.S. Biedenharn, and P. Combs. 1988. Adjustments of Red River following removal of the Great Raft in 1873 [abs.]. EOS (Transactions of the American Geophysical Union) 69(18), 567.

Hudson, B.D., 1994. Soil organic matter and available water capacity. Journal of Soil and Water Conservation, 49(2), pp.189-194.

James, L.A. 1997. Channel incision on the lower American River, California, from streamflow gage records. Water Resources Research 33 (3), 485-490.

Johnson, S.L. 2004. Factors influencing stream temperatures in small streams: substrate effects and a shading experiment. Canadian Journal of Fisheries and Aquatic Science 57, 30-39.

Kondolf, G.M. 1997. Hungry water: effects of dams and gravel mining on river channels. Environmental Management 21 (4), 533-551.

Libohova, Z., C. Seybold, D. Wysocki, S. Wills, P. Schoeneberger, C. Willams, D. Lindbo, D. Stott, and P.R. Owens. 2018. Reevaluating the effects of soil organic matter and other properties on available water-holding capacity using the National Cooperative Soil Survey Characterization Database, Journal of Soil and Water Conservation 73(4), 411-421.

Ligon, F.K., W.E. Dietrich and W.J. Trush. 1995. Downstream ecological effects of dams. BioScience 45 (3), 183-192.

Loheide, S.P., R.S. Deitchman, D.J. Cooper, E.C. Wolf, C.T. Hammersmark, and J.D. Lundquist, 2009. A Framework for Understanding the Hydroecology of Impacted Wet Meadows in the Sierra Nevada and Cascade Ranges, California, USA. Hydrogeology Journal 17:229–246.

Loheide, S.P. and S.M. Gorelick, 2005. A Local-Scale, High-Resolution Evapotranspiration Mapping Algorithm (ETMA) with Hydroecological Applications at Riparian Meadow Restoration Sites. Remote Sensing of Environment 98:182–200.

Loheide, S.P. and S.M. Gorelick, 2006. Quantifying Stream–Aquifer Interactions through the Analysis of Remotely Sensed Thermographic Profiles and In Situ Temperature Histories. Environmental Science & Technology 40:3336–3341.

Malloch, S. and M. Garrity, 2012. Yakima River Basin Integrated Water Plan, Strange Bedfellows take risks, find common ground. The Water Report.

Millar, C.I. and N.L. Stephenson, 2015. Temperate Forest Health in an Era of Emerging Megadisturbance. Science 349:823–6.

Manga, M. and Kirchner, J.W. 2000. Stress partitioning in streams by large woody debris. Water Resources Research 36(8). 2373-2379.

Marden, M., Arnold, G., Gomez, B. and Rowan, D. 2005. Pre- and post-reforestation gully development in the Mangatu Forest, East Coast, North Island, New Zealand. River Research and Applications 21, 757-771.

Montgomery, D.R. and Abbe, T.B. 2006. Influence of logjam-formed hard points on the formation of valley-bottom landforms in an old-growth forest valley, Queets River, Washington, USA. Quaternary Research 65, 147-155.

Montgomery, D.R., B.D. Collins, J.M. Buffington, and T.B. Abbe, 2003. Geomorphic Effects of Wood in Rivers. American Fisheries Society Symposium.

Montgomery Water Group, 2006. Multi-Purpose Water Storage Assessment in the Wenatchee River Watershed. Kirkland, Washington.

Morris, D.A. and A.I. Johnson, 1967. Summary of Hydrologic and Physical Properties of Rock and Soil Materials, as Analyzed by the Hydrologic Laboratory of the US Geol. Survey, 1948-60. Washington, DC.

Nisbet, T.2012. Modelling the hydraulic impact of reintroducing large woody debris into watercourses. Flood Risk Management 5(2), 164-174.

Peter, K.T., S. Herzog, Z. Tian, C. Wu, J.E. McCray, K. Lynch, and E. Kolodziej. 2019. Evaluating emerging organic contaminant removal in an engineered hyporheic zone using high resolution mass spectrometry. Water Resarch 150, 140-152.

Powers, P.D., M. Helstab and S.L. Niezgoda. 2018. A process-based approach to restoring depositional river valleys to Stage 0, an anastomosing channel network. River Research and Applications 1-11, http://doi.org/10.1002/rra.3378

Prosser, I.P. and Soufi, M. 1998. Controls on gully formation following forest clearing in a humid temperate environment. Water Resources Research 34 (12), 3661-3671.

Ohara, N., M.L. Kavvas, Z.Q. Chen, L. Liang, M. Anderson, J. Wilcox, and L. Mink, 2014. Modelling Atmospheric and Hydrologic Processes for Assessment of Meadow Restoration Impact on Flow and Sediment in a Sparsely Gauged California Watershed. Hydrological Processes 28:3053–3066.

Payn, R.A., M.N. Gooseff, B.L. McGlynn, K.E. Bencala, and S.M. Wondzell, 2012. Exploring Changes in the Spatial Distribution of Stream Baseflow Generation during a Seasonal Recession. Water Resources Research 48. doi:10.1029/2011WR011552.

Perry, G., Lundquist, J. and Moore, R.D. 2016. Review of the potential effects of forest practices on stream flow in the Chehalis River basin. Prepared for Washington State Department of Ecology, Chehalis Basin Strategy. University of Washington, Seattle, WA. 46 p.

Phelps, J.D., 2011. The Geomorphic Legacy of Splash Dams in the Southern Oregon Coast Range. University of Oregon.

Pollock, M.M., Beechie, T.J. and Jordan, C.E. 2007. Geomorphic changes upstream of beaver dams in Bridge Creek, an incised stream channel in the interior Columbia River basin, eastern Oregon. Earth Surface Processes and Lanforms 32, 1174-1185.

Pollock, M.M., T.J. Beechie, J.M. Wheaton, C.E. Jordan, N. Bouwes, N. Weber, and C. Volk, 2014. Using Beaver Dams to Restore Incised Stream Ecosystems. BioScience 64:279–290.

Pollock, M.M., J.M. Wheaton, N. Bouwes, C. Volk, N. Weber, and C.E. Jordan, 2012. Working with Beaver to Restore Salmon Habitat in the Bridge Creek Intensively Monitored Watershed Design Rationale and Hypotheses. Seattle, WA.

Polvi, L.E. and E. Wohl. 2013. Biotic drivers of stream planform: implications for understanding the past and restoring the future. Bioscience, 63(6), 439-452.

Ponce, V.M. and D.S. Lindquist, 1990. MANAGEMENT OF BASEFLOW AUGMENTATION: A REVIEW. Journal of the American Water Resources Association 26:259–268.

Schanz, S.A., D.R. Montgomery, and B.D. Collins. 2019. Anthropogenic strath terrace formation caused by reduced sediment retention. Proceedings of the National Academy of Sciences. www.pnas.org/cgi/doi/10.1073/pnas.1814627116

Schilling, K.E., Y.K. Zhang, and P. Drobney, 2004. Water Table Fluctuations near an Incised Stream, Walnut Creek, Iowa. Journal of Hydrology 286:236–248.

Schneider, D. and R. Anderson, 2007. Wenatchee River Watershed Temperature Total Maximum Daily Load-Water Quality Report. Olympia, WA. https://fortress.wa.gov/ecy/publications/documents/0710045.pdf.

Schumm, S.A., M.D. Harvey, and C.C. Watson, 1984. Incised Channels: Morphology, Dynamics, and Control. Water Resources Publications.

Sear, D.A., Millington, C.E., Kitts, D.R. and Jeffries, R. 2010. Logjam controls on channel: floodplain interactions in wooded catchments and their role in the formation of multi-channel patterns. Geomorphology 116, 305-319.

Seixas, G.B., T.J. Beechie, C. Fogel and P.M. Kiffney. 2018. Historical and future stream temperature change predicted by a Lidar-based assessment of riparian condition and channel width. Journal of the American Water Resources Association 54(4). 974-991.

Shields, Jr. F.D and Gippel, C.J. 1995. Prediction of effects of woody debris removal on flow resistance. Journal of Hydraulic Engineering 121, 341-354.

Shields Jr. F.D., Simon, A. and Dabney, S. 2009. Streambank dewatering for increased stability. Hydrological Processes 23, 1537-1547.

Simon, A. 1989. A model of channel response in disturbed alluvial channels. Earth Surface Processes and Landforms 14, 11-26.

Simon, A. and Rinaldi, M. 2006. Disturbance, stream incision, and channel evolution: the roles of excess transport capacity and boundary materials in controlling channel response. Geomorphology 79, 361-383.

Stock, J.D., Montgomery, D.R., Collins, B.D., Dietrich, W.E. and Sklar, L. 2005. Field measurements of incision rates following bedrock exposure: implications for process controls on the long profiles of valleys cut by rivers and debris flows. Geological Society of America Bulletin 117 (11/12), 174-194.

Tague, C., S. Valentine, and M. Kotchen, 2008. Effect of Geomorphic Channel Restoration on Streamflow and Groundwater in a Snowmelt-Dominated Watershed. Water Resources Research 44:n/a-n/a.

USBR and ERDC (Bureau of Reclamation and U.S. Army Engineer Research and Development Center). 2016. National Large Wood Manual: Assessment, Planning, Design and Maintenance of Large Wood in Fluvial Ecosystems: Restoring Process, Function and Structure. 628 p.

Van Haveren, B.P., 2004. Dependable Water Supplies from Valley Alluvium in Arid Regions. Environmental Monitoring and Assessment 99:259–266.

Veatch, A. C. 1906. Geology and underground water resources of Northern Louisiana and Southern Arkansas. Washington D.C. United States Geological Survey Professional Paper 46.

Wemple, B.C., Jones, J.A. and Grant, G.E. 1996. Channel network extension by logging roads in two basins, Western Cascades, Oregon. Water Resources Bulletin 32 (6), 1195-1207.

Wilcox, J.G., 2005. Water Management Implications of Restoring Meso-Scale Watershed Features. International Conference on Headwater Control VI: Hydrology, Ecology and Water Resources in Headwaters. Bergen, Norway.

Williams, G. and Wolman, M.G. 1984. Downstream effects of dams on alluvial rivers. U.S. Geological Survey Professional Paper 1286.

Wondzell, S.M. and Swanson, F.J. 1999. Floods, channel change, and the hyporheic zone. Water Resources Research 35 (2), 555-567.

Estimates of Gravel Transport Rates in Mountain Streams for Normal ($Q_{1.5}$) High-Flow Events

Kristin Bunte, Research Scientist, Department of Civil and Environmental Engineering, Colorado State University, kbunte@engr.colostate.edu
Kurt W. Swingle, Environmental Scientist, Boulder, CO, kskb@ix.netcom.com
Steven R. Abt, Prof. emer., Department of Civil and Environmental Engineering, Colorado State University, sabt@engr.colostate.edu
Dan A. Cenderelli, Hydrologist, USDA Forest Service, National Stream and Aquatic Ecology Center, Fort Collins, CO, dcenderelli@fs.fed.us
Robert Ettema, Prof., Department of Civil and Environmental Engineering, Colorado State University, rettema@engr.colostate.edu

Abstract

This study takes an empirical approach to address the problem of predicting gravel transport rates in mountain streams. A total of 96 worldwide datasets on gravel transport relations versus water discharge were compiled including the writers' measurements and datasets from the literature. Unit rates of gravel transport occurring during a common high-flow event $q_{B,1.5}$ were computed for each dataset and plotted vs. a modified stream power parameter $\omega_{1.5}$'. Most of the data pairs, $q_{B,1.5}$ vs. $\omega_{1.5}$', fell along the plot's central zone about two orders of magnitude wide. Within that zone, $q_{B,1.5}$ increased with $\omega_{1.5}$' following a power function. Data falling above or below the central zone were found to be associated with exceptionally high or low sediment supply, respectively. The plotted relations of $q_{B,1.5}$ vs. $\omega_{1.5}$', together with qualitative information of a site's watershed's and channel's situation of sediment supply, can then be used to obtain estimates of $q_{B,1.5}$ for unsampled streams. Estimates of $q_{B,1.5}$ also provide a context for evaluating measured or predicted transport rates relative to values for other streams.

Introduction

Knowledge of gravel transport rates in mountain streams is important for studies concerning fluvial research, channel restoration, watershed management and assessments of channel response to changes in water or sediment yield. Transport rates that occur during common high-flow events, such as the annually to biennially recurring flood are often of specific interest. However, reliable information on gravel transport is difficult to obtain in mountain streams.

Various studies (e.g., Gomez and Church, 1989; Johnejack and Megahan, 1991, Martin and Ham, 2005) have found that bedload transport equations—typically based on flume experiments—grossly mispredict bedload transport rates in gravel-bed streams through steep terrain. The equations are not designed for flow tumbling over rocks and steps, and they cannot account for large differences in bed mobility and sediment supply between streams. Computed transport rates are not only highly uncertain but also lack context; i.e., a user is offered no insight on whether a computed transport rate is high or low for a given stream with its specific characteristics. A study may conduct its own field measurements, but this approach is laborious and likely error-prone if expertise and suitable field equipment are not available.

To mitigate the prediction problem for gravel transport rates in mountain streams, this study takes an empirical approach and evaluates a large compilation of gravel transport relations (transport rates vs. discharge) measured in a variety of streams. Most measurements were made in mountain streams, and all measurements were taken with samplers suitable for gravel bedload. Based on the compiled transport relations, the study plotted transport rates predicted for commonly occurring high-flow events in relation to a modified stream-power parameter. In combination with a qualitative assessment of a channel's sediment supply, the resulting plots serve to estimate gravel transport rates for a common flood for a study stream. The plots also provide a reference that allows a user to compare gravel transport rates measured in a study stream to rates expected in other streams.

Several arguments speak for focusing the analyses on transport rates associated with a commonly occurring high-flow event such as the 1.5-year recurrence interval flow ($Q_{1.5}$). The ability to conduct field measurements and then to predict a certain transport rate from them was the main reason. Transport is often still measurable with physical samplers at flows near $Q_{1.5}$, and a transport relation measured to only 50-70% of the $Q_{1.5}$ flow can often be reasonably extrapolated to the $Q_{1.5}$ flow. By contrast, bedload samples can usually not be collected in very large events such as the Q_{20}. Besides, transport rates associated with a Q_{20} flow are highly variable between events because transport may be controlled by external sediment input (e.g., debris flows, bank collapse) or retention (e.g., in debris dams or overbank). Transport rates for the Q_{20} flow are therefore not inferable from a transport relation measured accurately to the $Q_{1.5}$ flow.

The study selected the hydrologically defined $Q_{1.5}$ flow as a basis for analyses because $Q_{1.5}$ can often be computed with more certainty than the morphologically determined bankfull flow. While several writers noted close similarities between the $Q_{1.5}$ flow and bankfull flow (Dury, 1976; Leopold, 1994; Castro and Jackson, 2001), the similarity holds only for streams with active gravel floodplains, but not for gravel-bed streams in which the cross-section is carved into largely immobile banks or is shaped by the largest flood events. It also does not hold when water or sediment supply have changed. Another complication is that a stream's bankfull flow level may be determined morphological, graphical, or hydraulically, and resulting bankfull estimates may differ widely between methods and also between operators (Williams, 1978; Johnson and Heil, 1996; Radecki-Pavlik, 2002), which lead Williams (1978) to conclude that no firm ratio exists between the $Q_{1.5}$ flow and bankfull flow. Owing to this lack of clarity, this study focuses on the hydrologically defined $Q_{1.5}$ rather than morphologically, graphically, of hydraulically defined bankfull flow.

Methods

Data compilation

Data for this study are partially based on the gravel transport relations sampled by the writers in 12 high-elevation Rocky Mountain streams and one stream in the Eastern Cascades (Bunte and Swingle, 2019). Most of the writers' bedload samples were collected with bedload traps (Bunte et al., 2004, 2007, 2008); a large-frame net sampler was used at one site (Bunte, 1996) and pit traps at another site (Bunte, 1997).

To extend the database numerically and geographically, the writers compiled a worldwide set of 70 gravel transport relations, predominantly from mountain streams, where bedload was measured with samplers suited for coarse beds: bedload traps, vortex samplers, pit-type samplers, unflared wide-mesh basket samplers, hanging baskets and large-frame net samplers. Bedload measurements made with a Helley-Smith sampler (or other pressure difference samplers such as the Elwha and the TR2 samplers) were not included in this study, because Helley-Smith measurements greatly over-predict actual rates when transport is low and under-predict them when particles are streaming into the sampler and exceed mid-sized gravel sizes (Bunte et al., 2019, this volume).

Geographically, the literature data represent streams in many mountain areas worldwide. Within Canada, data come from the interior of British Columbia (*Harris Creek*: Hassan & Church 2001; Church & Hassan 2005; *Elk* and *Cotton Creek*: Green et al. 2013, 2014a) and the Alberta Rocky Mountains (*Bridge Creek*: Nanson 74). Within the U.S., there are data from the Pacific North-West (*Oak Creek*: Milhous 1973; *Flynn Creek*: Estep and Beschta, 1985; Beschta 1981; *N.F. Caspar Creek*: Hassan et al., 2014); the Northern Rocky Mountains of WY and MT (*East Fork River*: Emmett, 1980; Leopold and Emmett, 1997; *Dupuyer Creek*: Whitaker and Potts 2007 a and b); the Great Basin (*Hobble Creek*: Hinton 2012) and the South-East (*Goodwin Creek*: Kuhnle, 1992; R. Kuhnle, pers. comm.; the Goodwin Creek tributaries *WS13* and *WS14*: Kuhnle, 1991; 1992); and *Little Turkey Creek*: McMahon, 2013).

The European Alps are presented by data from Austria (the *Pitzbach*: Hofer 1987; Turowski & Rickenmann, 2009; the *Rofenache*: Habersack et al., 2015a; Gattermayr, 2013; the *Urslau*: Kreisler et al., 2016; *Fischbach* and *Ruetz*: Rickenmann, 2018); from Switzerland (the *Riedbach*: Schmid 2011; Schneider et al. 2015b; the *Erlenbach*: Rickenmann et al., 2012); from Italy (*Rio Cordon*: Lenzi et al., 1999, 2004, 2006; *Saldur Bach*: L. Mao, per. comm., Dell'Agnese et al., 2014); as well as in the Spanish Pyrenees (*Tordera*: Garcia et al., 1996, Laronne et al., 2001).

Steep mountain streams in other areas of the world include the New Zealand Alps (*Torlesse Creek*: Hayward, 1980; Hayward and Sutherland, 1974), the Chinese Yunnan Province in the southeastern Himalaya (*Diaoga*: Yu et al., 2009), the Chilean Andes (*Estero Morales*: L. Mao pers. comm.; Ravazzolo et al., 2019); southern Brazil (*Arvoresinha*: G. Merten, pers. comm.), the Karakorum (the *Talo*, *Gosak*, *Gulshanabad*, *Duber*, and *Kandia* streams: Palt, 2001); and central Japan (*Yotagiri*, Uchida et al., 2018; *Hirakawa* and *Kamanashigawa*: Handa et al., 2013; Mitsunaga et al., 2015; Sakurai et al., 2016).

Besides mountain streams, the data include channels in Israel's Negev desert (*Nahal Yatir* and *Nahal Eshtemoa*: Reid et al., 1995, 1996; Powell et al., 1998; Laronne et al. 2003; Bergmann et al., 2007; Cohen et al., 2010; Alexandrov et al., 2007); as well as pool-riffle streams in northern Italy (*Virginio Creek*: Tacconi and Billi 1987; Cencetti et al., 1994); in Great Britain (*Turkey Brook*: Reid et al., 1985, 1986 a, b; *Avon*: Downs et al., 2016; Soar and Downs, 2017), and in Canada (*Elbow River*: Hollingshead, 1971).

The data include measurements from a few large-valley streams, draining catchments of 800 - 2200 km² in the Alps (the *Isel* and *Drau*: Habersack et al., 2015b, Habersack et al., 2016), the *Elwha River* in the Pacific NW (Hilldale et al., 2014; Magirl et al., 2015), and the *Vedder River* in British Columbia (McLean '80; Martin and Church '95). The data compilation also includes large foreland streams draining 6,000 – 250,000 km²: (the *Danube* in Slovavia: Holubova et al., 1998, 2004; Camenen et al., 2011, Liedermann et al., 2012); the *Rhine* in Switzerland: Nesper, 1937; Meyer-Peter et al., 1937) and the *Fraser River* in Canada: McLean et al., 1999; Ferguson and Church, 2009).

Data analysis

Determining the $Q_{1.5}$ flow: In the writers' study streams, the $Q_{1.5}$ flow was determined from long-term flow records or from scaling a flow record from a gauging station reasonably close to the study stream. Datasets from the literature were more likely to provide information on bankfull flow (and its channel dimensions) rather than referring to the $Q_{1.5}$ flow, and some publications use the term bankfull in the sense of "boardfull" (i.e., as flow overtopping the banks) in which case the reported bankfull flows may be significantly larger than $Q_{1.5}$. This study carefully evaluated whether reported bankfull flow values represented $Q_{1.5}$ and, if needed, estimated $Q_{1.5}$ by searching the publication for comments on the relative magnitude of the measured event or turning to other publications about the same stream. For some sites, information on $Q_{1.5}$ was found in hydrological publications, or $Q_{1.5}$ was estimated from a published multi-year hydrograph. Sometimes, a plotted cross-sectional profile together with an estimate of the stream's active width from Google Earth images gave clues about the $Q_{1.5}$ level; and, in some cases, bankfull values or estimated $Q_{1.5}$ values were evaluated against plotted regional relations of $Q_{1.5}$ vs. basin area, A.

Establishing a gravel transport relation: A gravel transport relation was determined for each measured set of field data by fitting a power function in the form of to measured gravel transport

$$Q_B = a \cdot Q^b \qquad \text{(Eq. 1)}$$

rates (Q_B) and instantaneous discharge (Q). The coefficient a and the expo-nent b were empirically determined and refer to Q_B in units of g/s and Q in m³/s. When several down-stream locations were sampled at a study stream or when a site was resampled in a later year, two power functions were fitted to one stream's data. Two power functions were also fitted when the transport rela-tion displayed notable hysteresis following changes in intra-seasonal sediment supply. By contrast, litera-ture data collected over multiple years were usually combined to one dataset, unless the study specifically pointed out inter-annual differences.

Transport relations measured by the writers in Rocky Mountain streams exhibited steep, straight trends in log-log space over the entire range of sampled flows, allowing standard curve-fitting (Eq.1) to be applied. Adjustments to a standard curve-fitting approach were required when a plotted dataset exhibited large scatter or data were scant, when the trend was curved in log-log scale, or when data were not presented in a log-log plotting scale. To avoid an overly flat relation that results when a power function is fitted to log-log plots with scattered data or only a short range of sampled flows, the data envelope was used as a guide to fit a trend line by eye which often represented the data trend better. Curve fitting was then applied to

two or more points on the visually fitted line. Two power functions were fitted to transport relations with a curved trend in log-log space, one to the steep initial increase and one to the upper, flattened part. For data presented as plots in log-linear or linear-linear scales, geometric (or arithmetic) mean values of Q_B were visually estimated for several increments of Q and a power function was then fitted to the estimated means. In all, 26 transport relations were derived from the sites sampled by the writers mainly in the Rocky Mountains and 70 transport relations were derived from datasets published for streams worldwide.

Calculating $q_{B,1.5}$: The cross-sectional, gravel transport rate associated with the $Q_{1.5}$ flow, $Q_{B,1.5}$, was determined for each dataset by solving Eq. 1 for $Q_{1.5}$. The unit gravel transport rate $q_{B,1.5}$ was obtained by dividing the predicted $Q_{B1.5}$ by stream width $w_{1.5}$ and multiplying by a bias-correction factor F_{bias} to counteract the inherent under-prediction of y-values from x-values in power functions (Eq. 2); i.e.,

$$q_{B,1.5} = a \cdot Q_{1.5}{}^{b} / w_{1.5} \cdot F_{bias} \qquad \text{(Eq. 2)}$$

Various approaches are possible to compute F_{bias} (Hirsch et al., 1992); this study applied the one by Ferguson (1986, 1987) to most of the writers' datasets. Bias-correction factors generally increase with data scatter and ranged from 1 to 3 for the writers' study streams. Depending on a visual assessment of scatter in plotted data, values of 1.5 to 2.5 were assigned to datasets for which F_{bias} was not provided.

Developing a suitable parameter to predict $q_{B,1.5}$: A suitable flow-based parameter that showed a close relation to $q_{B,1.5}$ needed to be devised to compare measured $q_{B,1.5}$ between sites and predict $q_{B,1.5}$ for unsampled sites. Ryan (2007) has shown that, for a sequence of sites along a Rocky Mountain channel system, bankfull bedload transport rates increased in close correlation to the size of the basin area, A. The typically tight relation between Q and A within a stream system suggested that a simi-larly tight relation exists between $q_{B,1.5}$ and $Q_{1.5}$, or $q_{1.5}$. Plotted data from this study showed a relation be-tween $q_{B,1.5}$ and $q_{1.5}$ (Figure 1a), and most data pairs fell into a central band three orders of magnitude wide. However, the large width of the central data field and its curved trend (in log-log space) that cannot be described by simple curve-fitting makes ` the relation of $q_{B,1.5}$ vs. $q_{1.5}$ not well suited for comparison and prediction of $q_{B,1.5}$, albeit that a power function can be fitted to the lower data branch representing mountain channels with $q_{1.5}$ <1 m³/m·s.

Bagnold's (1977) stream power per unit width $\omega = \rho \cdot q \cdot S$, where ρ is the fluid density, q is the discharge per unit width, and S is a reach-averaged channel gradient in m/m, is sometimes used for comparison of bedload transport relations (Q_B vs. ω) between streams (e.g., Martin and Church, 2000). However, ω was not a suitable parameter for the diverse streams compiled in this study: In the plotted relation of $q_{B,1.5}$ vs. $\omega_{1.5}$ with data of all study sites, steep streams plotted to the right of lower-gradient streams (Figure 1b), suggesting that for the same stream power, low-gradient streams have much larger $q_{B,1.5}$ than steeper channels. The reason is an overly large numerical influence of stream gradient. In our data compilation, S covered a 100-fold range (0.1 to 0.001 m/m) among mountain streams and controlled a study site's $\omega_{1.5}$ value much more than $q_{1.5}$ which covered a 10-fold range (0.2 to 2 m²/s). Besides, even among sites of similar channel gradients, the scatter of $q_{B,1.5}$ with $\omega_{1.5}$ was too wide to permit prediction of $q_{B,1.5}$.

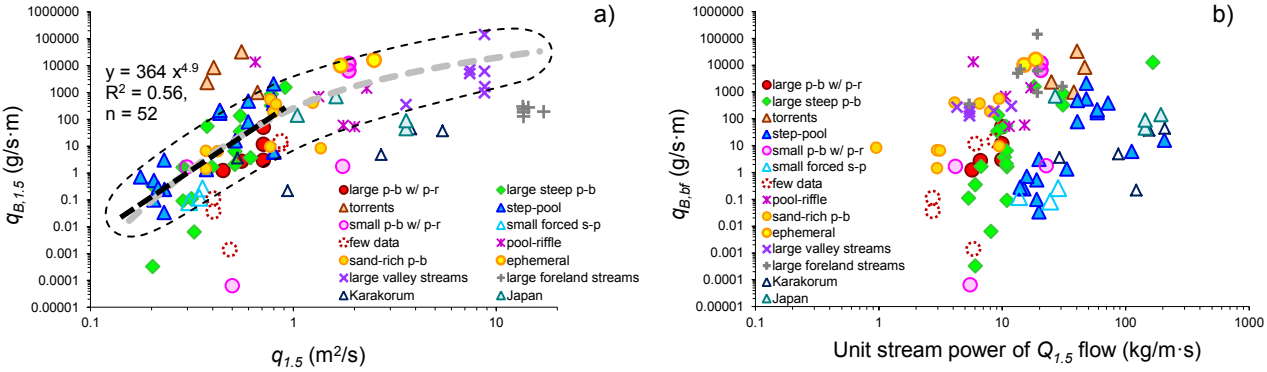

Figure 1. Relation of $q_{B,1.5}$ vs. unit discharge $q_{1.5}$ (a) and vs. unit stream power $\omega_{1.5}$ (b). Streams are grouped by stream type.

Based on this experience, the writers developed a modified unit stream power expression $\omega_{1.5}$' that incorporated the promising parameter $q_{1.5}$ (Figure 1a) and diminished the overly strong influence that S exerts on $\omega_{1.5}$ (Figure 1b) by take the square root of S which balances the numerical influences of $q_{1.5}$ and S

$$\omega_{1.5}' = \rho \cdot q_{1.5} \cdot S^{0.5} \cdot \%D_{sub<8} \quad \text{(Eq. 3)}$$

Here, $q_{1.5}$ is $Q_{1.5}$ per unit width; S is square rooted to limit the range of its numerical values; and, $\%_{Dsub<8}$ is the percentage of subsurface fines <8 mm. Units are kg, m and s, while subsurface fines are entered as percent value (e.g., as 25 for 25%). Compared to Bagnold's stream power ω, the lowered effect of S in the modified ω' reflects the dissipation of a large portion of the flow energy in mountain streams. For this reason, Nitsche et al., (2011) had suggested using S as its square root to describe flow hydraulics in steep streams. The writers also note that common flow velocity relations (e.g., Manning and Chezy) relate mean velocity of open-channel flow directly to $S^{0.5}$.

This study's parameter $\omega_{1.5}$' includes a term for bed mobility: $\%D_{sub<8}$ was added because the presence of sand and fine gravel in a streambed enhances particle mobility and transport rates of all particle sizes, including coarse gravel (Ikeda and Iseya, 1987; Wilcock et al., 2001; Wilcock and Kenworthy, 2002). In the data for this study, $\%D_{sub<8}$ ranged from 12-82% and was found to be largely independent of hydraulic or channel geometry parameters but slightly positively related to surface sediment's ratio of % fines <8 mm to D_{84}: $\%D_{sub<8} = 45\ (\%D_{surf<8}/D_{84})^{0.2}$, $r^2 = 0.41$.

The $\%D_{sub<8}$ is ideally determined from a cumulative grain-size distribution of large volumetric sediment samples. Sample collection techniques and necessary sample volumes are explained in Bunte and Abt (2001). For the writers' study sites, $\%D_{sub<8}$ was computed from detailed field samples and values of $\%D_{sub<8}$ ranged between 16 and 34%, with a mean near 25%. Several datasets in the compilation likewise provided cumulative grain-size distributions for subsurface sediment.

If needed, the surface grain-size distribution served as a guide to estimate a value for $\%D_{sub<8}$. Surface and subsurface size-distributions have similar coarse ends, and a subsurface distribution curve—although elevated—has a curvature that is typically similar to that of the surface distribution. Photos from the study site and Google Earth images give some indication of the relative abundance of fine surface sediment and hence suggest whether subsurface fines are scant or abundant. Also, the grain-size distribution of bedload collected near $Q_{1.5}$ may represent the finer and central portion of the subsurface size distribution. A loose relation was noted between $\%D_{sub<8}$ and channel type within the data compilation and those values may help to guide an estimate: $\%D_{sub<8}$ was lowest in steep plane-bed streams (12-40%), slightly higher (15-45%) in step-pool channels, mountain torrents, and low-gradient plane-bed channels, and again slightly higher in pool-riffle channels (20-45%). Sand-rich gravel-bed streams had the highest values (50-80%).

Data grouping: For visual comparison among streams, plotted data of $q_{B,1.5}$ vs. $\omega_{1.5}$' were grouped by channel type following the gradient-based classification proposed by Montgomery and Buff-ington (1997), but also noting other stream types. Separate symbols were used to differentiate between step-pool channels, steep plane-bed streams with occasional mini-steps, lower-gradient plane-bed streams with occasional or forced pool-riffle sequences, and pool-riffle channels. Those channel-type-specific symbols were then used with various color schemes to differentiate between subtypes of streams within the same gradient class: For example, low-gradient plane-beds with occasional pool-riffles con-tained three groups: 1. Relatively large Rocky Mountain channels sampled by the writers with less than desirable sample size, 2. Ephemeral desert streams, and 3. Sand-rich streams with notably large amounts of surface sand. Also marked as groups were large valley streams with gradients of 0.001 to 0.004 m/m draining mountain watersheds in the Alps, the Pacific NW, and British Columbia with basin areas 800-2100 km² and large foreland streams with gradients of 0.0003 to 0.0009 m/m and basin areas >6000 km². A second layer of grouping categorized mountain streams by geographical location. The study dif-ferentiated between the writers' sites located mainly in the U.S. Rocky Mountains (CO, WY, MT), steep streams in the Pacific NW and British Columbia, as well as mountain streams in the European and New Zealand Alps, the Canadian Rockies, the Karakorum, the Chinese Yunnan Province in the SE Himalaya, and central Japan. The few streams not falling into any of the categories above were labeled "other".

Results

Relation of unit gravel transport rates $q_{B,1.5}$ flow vs. modified stream power $\omega_{1.5}$'

Data from writers' Rocky Mountain streams: For the writers' Rocky Mountain data, values of $q_{B,1.5}$ plotted vs. $\omega_{1.5}$' in log-log space showed a positive, straight trend. Most data fell within a central envelope two orders of magnitude wide (Figure 2). The few outlier data (transport rates below or above the central data envelope) were explainable based on the writers' familiarity with their study sites: overly low values of $q_{B,1.5}$ resulted from upstream gravel entrapment behind beaver dams, woody debris, and within a large pool and also resulted from the limited competence of the $q_{1.5}$ flow to mobilize beds in oversized cross-sections. By contrast, sediment release from a logjam into a stream that was already well supplied from a watershed mostly above tree-line resulted in an overly high value of $q_{B,1.5}$. This finding indicated that the streams within the envelope had neither extremely high nor extremely low $q_{B,1.5}$.

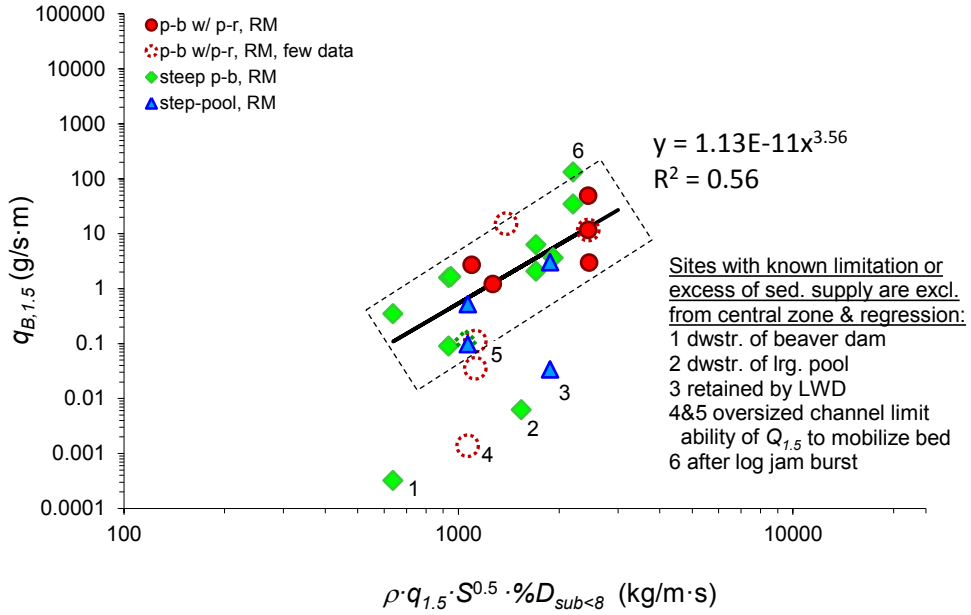

Figure 2: Unit gravel transport rates $q_{B,1.5}$ for the $Q_{1.5}$ flow measured mainly with bedload traps and a large net-frame sampler in central Rocky Mountain streams and plotted vs. a modified stream power parameter $\omega_{1.5}$'. Most of the data fall within the dashed envelope. Outlier data are annotated.

Intrinsic natural variability due to intra-seasonal hysteresis and annually-variable sediment supply explained a data scatter at the writers' sites over two orders of magnitude within the central envelope. For example, the bed of a steep plane-bed stream ran out of sediment supply at the end of a long and large high-flow season. Another example comes from a low-gradient plane-bed stream: the study site sampled across an active point bar produced higher $q_{B,1.5}$ than the site sampled at a pool-exit 10 m upstream during the same high-flow season. In both cases, $q_{B,1.5}$ varied by 3- to 20-fold within one season. Between-year differences in $q_{B,1.5}$ were even higher: Five of the writers' sites were sampled over two high-flow seasons, and $q_{B,1.5}$ varied by factors of 3-100 between years.

The steady increase of $q_{B,1.5}$ with $\omega_{1.5}$' for the 26 data from Rocky Mountain streams that fell within the central data envelope (Figure 2) was expressed by a fitted power function

$$1.13\text{ E-}11\ \omega_{1.5}'^{\,3.56},\ r^2 \text{ of } 0.56 \qquad \text{(Eq. 4)}$$

This empirical function facilitates a rough estimate of $q_{B,1.5}$ from a modified stream power parameter $\omega_{1.5}$' to within ± an order of magnitude in central Rocky Mountain streams.

Data combined from Rocky Mountain and worldwide streams: Moderate sedi-ment supply within the central data envelope The 70 worldwide datasets were added to the plot of $q_{B,1.5}$ vs. $\omega_{.5}$' in Figure 2. Of the literature data, ⅔ fell into the data envelope that was extrapolated from the Rocky Mountain streams and slightly widened to a little over two orders of magnitude (Figure 3). Among the worldwide streams that fell within the envelope were high-elevation Alpine step-pool and plane-bed streams, pool-riffle streams in Canada, England, and northern Italy, sand-rich gravel-bed streams in the Pacific NW, Wyoming, and the Eastern U.S., a small step-pool stream in the interior of British Columbia, and even many of the large valley and foreland streams. The interpretation of "normal" sediment supply for values of $q_{B,1.5}$ from Rocky Mountain streams within the central data envelope (Figure 2) was extended to the worldwide data because exceptionally high or low sediment supply could also be documented for worldwide sites falling above and below the central zone.

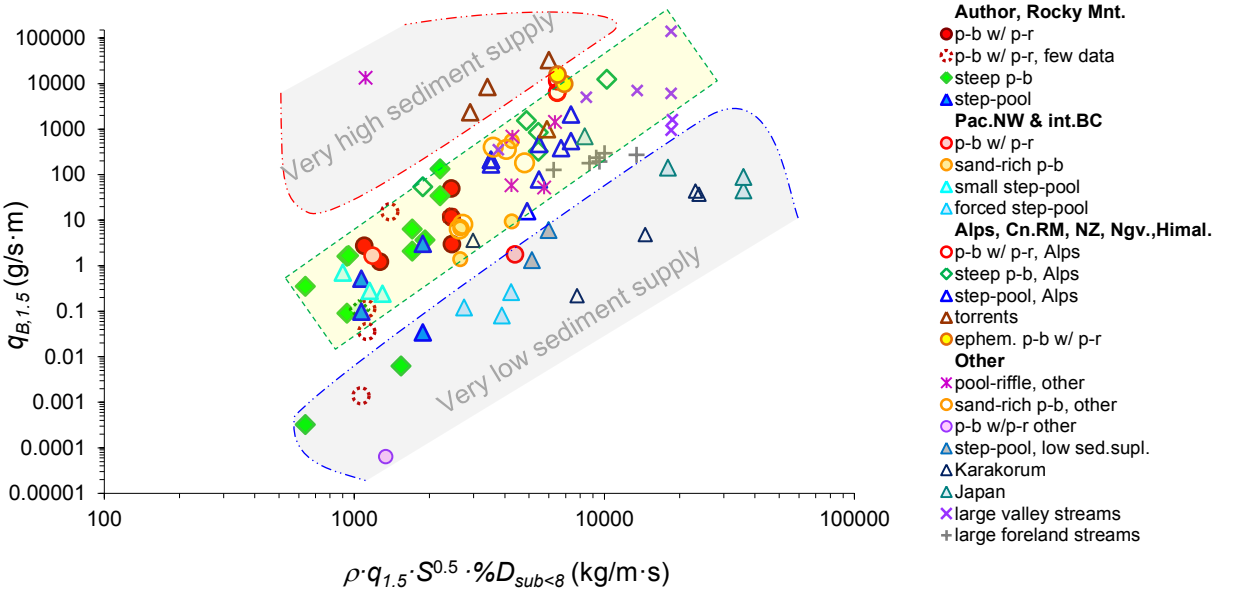

Figure 3. Unit gravel transport rates $q_{B,1.5}$ plotted vs. a modified stream power parameter $\omega_{1.5}$': Most worldwide data fall into the data envelope extrapolated from the Rocky Mountain streams encircled in a dashed green line.

Very high sediment supply The few worldwide datasets of $q_{B,1.5}$ vs. $\omega_{1.5}$' that plotted notably above the central data envelope included three mountain torrents: one was a steep pro-glacial stream draining a recently deglaciated valley in the Canadian Rockies (Nanson, 1974); another was a small torrent in China's Yunnan Province in the SE Himalaya draining a highly anthropogenically disturbed catchment underlain by crumbly sedimentary lithology (Yu et al., 2009); and, the highly active Erlenbach gulch (Rickenmann, 2012) that is subject to heavy summer thunderstorms and drains a small catchment with unstable, creeping hillslopes in the Swiss Flysch zone (crumbly marine sediments). Exceptionally high gravel transport rates were also reported for a pool-riffle stream in the northern Montana Front Range where steep, ephemeral washes are incised into faulted sedimentary lithology. Flashy flows transport large amounts of coarse sediment and boulders from unstable headwaters to intermittent channels and on to perennial streams (Whitaker and Potts, 2007 a, b). A borderline-high sediment supply was produced in two ephemeral streams in the Negev desert (Reid et al. 1995, 1996; Powell et al., 1998; Laronne et al., 2003) and in a stream in the Austrian Alps located at the confluence of three highly productive, glacier-fed tributaries (Kreisler et al., 2016). In all of those streams, the very high transport rates during commonly occurring high-flow events were associated with enormous sediment supply from catchments that were either poorly vegetated, had naturally unstable lithology, or experienced major anthropogenic hillslope destabilization. These findings confirm the large role lithology plays in setting transport rates (Ryan 2007).

Very low sediment supply The worldwide data points that fell below the central data envelope included a small step-pool stream down an escarpment in agricultural land in southern Brazil (G. Merten, pers. comm.) where tobacco fields produced little gravel supply. An unexpectedly low $q_{B,1.5}$ in a step-pool stream in the Chilean Andes was caused by an annually developing calcium carbonate crust that kept bed particles cemented during commonly occurring events (L. Mao, pers. comm.; Ravazzolo et al., 2019). Borderline-low transport rates were also measured in a low-gradient plane-bed stream with pool-riffles sequences in central British Columbia (Hassan and Church, 2001; Church and Hassan, 2005). Here, stone-ring bed-structures kept much of the cobble-bed channel stabilized during commonly occurring high-flow events. Several sites along a small step-pool stream in southern British Columbia also plotted within the lower zone. Here, numerous log steps retained sediment and dissipated flow energy (Green et al. 2013, 2014a, b). A stream in Utah, degraded to an urban ditch and cut off from its upstream sediment supply, also had extremely low transport rates (Hinton, 2012). In all of these streams, very low transport rates during commonly occurring high-flow events were caused by bed-material stabilization, as well as sediment storage and energy dissipation associated with log steps, absence of upstream supply as well as due to upstream sediment retention. Very low gravel transport rates at the $Q_{1.5}$ flow were also measured in steep streams in subtropical environments. In central Japan (Uchida et al., 2018, Sakurai et al., 2015, Mitsunaga et al., 2015; Handa et al., 2013), typhoons cause multiple very large flood events each year that seem to leave little sediment available for transport during a $Q_{1.5}$ event. Furthermore, $q_{1.5}$ values are high (water yields $Q_{1.5}/A$ are 10-20 and up to 100 times higher, respectively compared to the Alpine and Rocky Mountain streams in the data compilation), which makes $\omega_{1.5}$' values high and shifts plotted data for those sites towards the right side in **Figure 3**. Similarly, frequent large monsoon floods seem to sweep channels clear of mobile sediment in some large Karakorum streams (Palt, 2001). Those data suggest that the $q_{B1.5}$ vs. $\omega_{1.5}$' relation may shift downward for mountain regions with frequent high-intensity rainstorms.

Empirical transport relation for steep worldwide streams with no extreme conditions of sediment supply: For the 64 datasets of worldwide streams that plotted within the central data envelope, a fitted power function yielded the regression relation

$$q_{B,1.5} = 4.0\text{E-}12\ \omega_{1.5}'^{3.7},\ r^2 = 0.80 \qquad \text{(Eq. 5)}$$

The regression function (Eq. 5) is generally similar to the one fitted to the writers' Rocky Mountain data (Eq. 4), but has a higher r^2 because a wider range of $\omega_{1.5}$' and of more data. Study results show that unit gravel transport rates $q_{B,1.5}$ are sufficiently closely related to $\omega_{1.5}$' to predict $q_{B,1.5}$ using a simple power function to within ± an order of magnitude in gravel and cobble-bed streams when sediment supply is neither exceptionally low nor exceptionally high.

Prediction of gravel transport rates $q_{B,1.5}$

From observation to explanation: Evaluation of gravel transport rates that fell within, above, and below the central zone had indicated that notable watershed and channel processes needed to have happened for a measured $q_{B,1.5}$ to fall above or below the central zone. Sites with $q_{B,1.5}$ higher than in the central zone were associated with unstable hillslopes, high sediment supply and direct connectivity to the stream channel, whereas sites plotting below the central zone were associated with low rates of sedi-ment supply or supply exhaustion, upstream sediment retention, bed stabilization and energy dissipation.

From explanation to prediction: The obvious connection of a site's gravel transport rates $q_{B,1.5}$ with sediment supply, delivery, retention, bed stability and energy dissipation can be used to guide estimation of $q_{B,1.5}$ for unsampled streams. Aerial photography (Google Earth or other images) is useful to qualitatively assess the magnitude of a watershed's sediment supply (e.g., from visible hillslope instability), the directness of hillslope-channel connections, sediment supply contributed by productive tributaries and active bank erosion, as well as the downstream gravel conveyance potential (e.g., its obstruction by lakes, ponds, log jams, and beaver dams). Closer to the study site, field visits can clarify if sediment has recently been retained by logjams and beaver dams (or was released therefrom). Site visits also can ascertain if repeated energy dissipation occurs on weirs, drop structures, and logs, and how much resistance to entrainment a channel bed may offer to common high-flow events (e.g., due to a coarse pavement, stone rings, or an oversized cross-section).

Once the necessary data have been compiled to compute $\omega_{1.5}$' from Eq. 3 for an unsampled site, the assessment of a site's watershed, channel conveyance, and study reach as producing or receiving unremarkable, very high or very low sediment supply suggests whether the $q_{B,1.5}$ for the study site with a specified $\omega_{1.5}$' will fall into the central envelope, or above or below it. On a finer scale, estimates of $q_{B,1.5}$ (to within± one order of magnitude around Eq. 4) inside the central zone may likewise be narrowed, and results from visual assessment of watershed, channel, and reach conditions may guide the decision whether a site's $q_{B,1.5}$ might fall towards the upper border of the central envelope, the envelope's central portion, or towards the envelope's lower border. A study site's classification into one of the three zones is not necessarily permanent. While the upper border may be more firm than the lower border, common natural variability may occasionally shift gravel transport rates from sites that had plotted within the central zone in one year across the border in other years.

Gravel concentrations and gravel yield

Other than by the parameter $q_{B,1.5}$, gravel transport intensity may also be expressed as gravel concentration (transport rates $Q_{B,1.5}/Q_{1.5}$ flow) or as gravel yield ($q_{B,1.5}/A$). The argument may be posed that the relative magnitude of transport rates at the $Q_{1.5}$ flow might be more meaningfully evaluated for transport rates that are related to the discharge or the basin area that produced them. To determine differences and suitability of those approaches, analyses described in Section 3.1 for unit gravel transport rates $q_{B,1.5}$ were likewise applied to gravel transport expressed in terms of $Q_{B,1.5}/Q_{1.5}$ and $q_{B,1.5}/A$.

Relation of $Q_{B,1.5}/Q_{1.5}$ with $\omega_{1.5}$': The plot of gravel concentration $Q_{B,1.5}/Q_{1.5}$ vs. $\omega_{1.5}$' (Figure 4) looks quite similar to the plot of $q_{B,1.5}$ vs. $\omega_{1.5}$' (Figure 3) with ⅔ of the data falling into a central data zone and some data falling above and below. Most of the sites that had fallen within the central zone of the relation $q_{B,1.5}$ vs. $\omega_{1.5}$' (Figure 3) likewise fell within the central zone of the relation $Q_{B,1.5}/Q_{1.5}$ vs. $\omega_{1.5}$'and the vertical width of the central zone also extended over just slightly more than two orders of magnitude. Differences compared to the relation $q_{B,1.5}$ vs. $\omega_{1.5}$' were that the ephemeral Negev streams and the Austrian stream near the confluence of three productive tributaries moved from the upper border well into the central data field. By contrast, along the lower border, all large foreland streams dropped out of the central zone, and only the better-supplied large valley streams remained within the central zone.

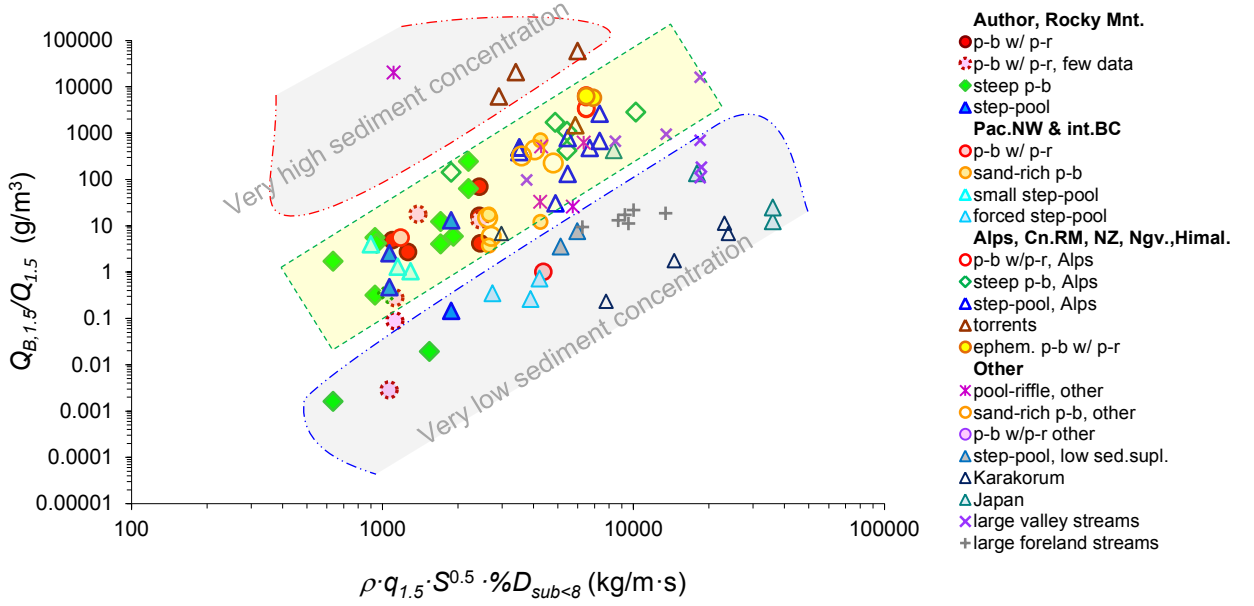

Figure 4. Gravel concentrations $Q_{B,1.5}/Q_{1.5}$ plotted vs. a modified stream power parameter $\omega_{1.5}$': A distinct segregation into the three zones similar to Figure 3 is evident.

Overall, the relation of $Q_{B,1.5}/Q_{1.5}$ vs. $\omega_{1.5}$' revealed a clear separation of gravel concentrations within the central zone from those that are extremely high and extremely low. A power function regression fitted to the data points in the central zone of $Q_{B1.5}/Q_{1.5}$ vs. $\omega_{1.5}$' yielded the equation

$$Q_{B,1.5}/Q_{1.5} = 8.7\text{E-}11\ \omega_{1.5}'^{3.4},\ r^2 = 0.76,\ n = 64 \qquad \text{(Eq. 6)}$$

which was almost as steep and as tightly defined as Eq. 5.

It is not known whether the clearer segregation of the data in the plot of $Q_{B,1.5}/Q_{1.5}$ vs. ω' into the three zones is entirely inherent or somewhat incidental. The use of similar parameters, $Q_{1.5}$ and $q_{1.5}$ on the two axes may contribute to the zonal segregation. In any case, the plotted relation of $Q_{B,1.5}/Q_{1.5}$ vs. $\omega_{1.5}$' confirmed the general classification of three zones of gravel transport: extremely high, moderate, and extremely low.

Prediction of $q_{B,bf}/A$ from $\omega_{1.5}$': The familiar segregation into the three zones was likewise evident in the plotted relation of $q_{B1.5}/A$ vs. $\omega_{.5}$' (Figure 5). Most of the sites contained within the central zone in the relation of $q_{B1.5}$ vs. $\omega_{1.5}$' also populated the central zone in the relation of $q_{B1.5}/A$ vs $\omega_{.5}$', and the central zone was likewise just slightly wider than two orders of magnitude. A power function regression is fitted to the cohort of sites within the central zone and yields the equation

$$q_{B,1.5}/A = 4.5\text{E-}15\ \omega_{1.5}'^{4.2},\ r^2 = 0.78,\ n = 54 \qquad \text{(Eq. 7)}$$

However, the plot of $q_{B1.5}/A$ vs. $\omega_{1.5}$' sorted streams by their basin area size: streams with small basins generally plotted slightly higher than larger streams, while streams with large basin areas shifted downward. As a result, most of the large valley streams and all of the foreland streams dropped out of the central zone into the zone of extremely low gravel yield. This shift suggest that the relation $q_{B1.5}/A$ vs. $\omega_{1.5}$' in Eq. 7 is best applied to small mountain streams with basin areas less than about 200 m².

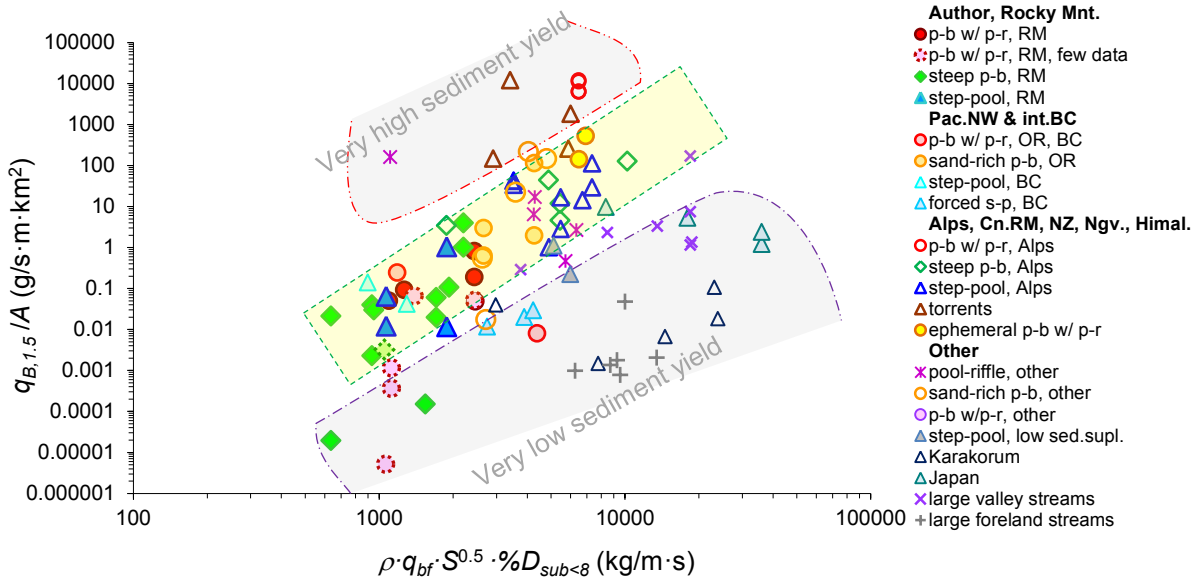

Figure 5. Unit gravel yield $q_{B,1.5}/A$ for the $Q_{1.5}$ flow plotted vs. a modified stream power parameter $\omega_{1.5}$': A segregation into the three zones similar to Figure 3 is evident.

Summary and Discussion

This study compiled 96 gravel transport relations (measured by the writers in mainly Rocky Mountain streams and studies reported in the literature for streams worldwide) to produce a plotted relation be-

tween unit gravel transport rates for a commonly occurring high-flow event ($q_{B,1.5}$) vs. a modified stream power parameter ($\omega_{1.5}$') (Figure 3). The plot reveals a central data zone about two orders of magnitude wide within which the majority of the data fall. Variability of $q_{B,1.5}$ within that zone is attributed to common natural variability in sediment supply as well as to errors in measurements and computations. Within the central zone, $q_{B,1.5}$ increases with $\omega_{1.5}$' following a simple and well-defined ($r^2 = 0.8$) power function. The study revealed that for a specified value of $\omega_{1.5}$', the magnitude of measured $q_{B,1.5}$—and hence the zone into which a study site falls—is associated with the watershed's and channel's situation regarding sediment supply. This connection is instrumental in guiding an estimate of the magnitude of $q_{B,1.5}$.

To apply results from this study for estimating $q_{B,1.5}$ to an unsampled site, a user first computes $\omega_{1.5}$' (Eq. 3) for that site. A user then employs interpretation from aerial photography (e.g., Google Earth images) and field information to assess the watershed's ability to generate gravel supply, the transfer of that supply from hillslopes to the channel, and the channel's potential to convey or retain that sediment in order to arrive at a qualitative categorization of a site's sediment supply as unremarkable, very high, or very low. With $\omega_{1.5}$' computed and the study site's sediment supply situation categorized, Figure 3 can be consulted to graphically determine the most likely zone (central, high or low) for a study site's estimate of $q_{B,1.5}$. Alternatively, a user may estimate a site's gravel concentration $Q_{B,1.5}/Q_{1.5}$ using Figure 4 or gravel yield $q_{B,1.5}/A$ using Figure 5. If a site's unremarkable situation of sediment supply has already been established, Eqs. 5, 6, or 7 may be applied directly.

Recommendation for using this study's approach to estimating gravel transport rates. A study site's gravel transport rate is best estimated (or evaluated) by applying all three expression of gravel transport: unit gravel transport rates, gravel concentrations and gravel yield. Considering that the database for this empirical study stems mainly from small and midsized streams in basins with temperate climates and from largely unaltered channels, this study's approach is foremost intended for streams in those climates.

Is differentiation of the magnitude of gravel transport into three zones real?
Several arguments support the visual segregation of the relations between $q_{B,1.5}$ and $\omega_{1.5}$' into the three zones and that the segregation reflects actual differences in gravel transport and sediment supply. 1) The outline of the central zone was initially determined from the writers' stream sites for which the sediment supply situation in the year of sampling was well known (Figure 2). 2) The trend of the central zone extrapolated from the writers' Rocky Mountain sites holds for plotted relations of $q_{B,1.5}$ vs. $\omega_{1.5}$' from many of the worldwide streams (Figure 3), and the extremely high or low sediment supply situations for worldwide datasets falling below or above the central zone are explainable from information provided in the study or from an assessment of a watershed's and channel's situation of sediment supply. 3) The segregation of plotted relations of gravel transport vs. $\omega_{1.5}$' into three zones (central, above and below) appears to be general—holding regardless of whether gravel transport is expressed in terms of unit transport rates (Figure 3), gravel concentration (Figure 4), gravel yield (Figure 5), or simply as a relation between $q_{B,1.5}$ and $q_{1.5}$ (Figure 1a). 4) The segregation is numerically robust in that the number of sites within each zone remains similar for all transport expressions: 4-7% of the data are above the central zone and 20-30 % of the data below. And even the zones' data cohorts remain largely similar for the various expressions of gravel transport: The only shifters between zones are sites with very high sediment supply, as well as large foreland and large valley streams.

Systematic difference between stream types? Within the central zone, the magnitude of $q_{B,1.5}$ was not determined by stream type (and hence not by stream gradient). The exceptions are mountain torrents and ephemeral streams, both of which exhibited very large transport rates at the $Q_{1.5}$ flow. Similarly, a stream's runoff yield, $Q_{1.5}/A$, appears to exert only a small influence on $q_{B,15}$. Within the central zone, however, sites close to the tree-line tended to have larger $q_{B,1.5}$ values than do sites in fully forested basins.

The effect of data errors on the plotting position of $q_{B,1.5}$ vs $\omega_{1.5}$'. Potential errors in values estimated for $q_{1.5}$ from measured field data cannot be quantified, because true values of $q_{1.5}$ are unknown. Errors in $q_{1.5}$ are assumed to be below 20% for most of the sites, but might reach 50% for a few sites with scant hydrological information. Subsequent errors in $\omega_{1.5}$' progress linearly because $q_{1.5}$ is a simple multiplier in $\omega_{1.5}$'. By contrast, errors in the estimates of a site's $q_{1.5}$ cause misprediction in $q_{B,1.5}$ that increase

with the steepness of a stream's transport relations. For a rating curve exponent of 6, errors in $q_{1.5}$ of ±20% and ±50% results in 3-4 fold misprediction of $q_{B,1.5}$ and more than an order of magnitude, respectively. For a rating curve exponent of 12, errors in $q_{1.5}$ by +20% and ±50% mispredict $q_{B,1.5}$ by about one order of magnitude and 2-3 orders of magnitude, respectively. Being aware of the potential errors, great care was taken in determining $q_{1.5}$ and in accurately fitting transport relations.

While an error in $q_{1.5}$ may greatly affect a site's value of $q_{B,1.5}$, the resulting error in the plotted relation of $q_{B,1.5}$ vs. $\omega_{1.5}$' is typically less severe because any error in $q_{1.5}$ affects both $q_{B,1.5}$ and $\omega_{1.5}$' by shifting a plotted data point diagonally. The increase of $q_{B,1.5}$ with $\omega_{1.5}$' followed a power law with an exponent of 3.7 (Eq. 5). Consequently, for gravel transport relations with exponents in that range, any error in $q_{1.5}$ shifts a data point diagonally within its original zone. For flatter or steeper rating curves, the shift is still diagonal but it may transfer a data point into a neighboring transport zone.

Acknowledgement The many years of the writers' field data collection work, and the extensive data compilation of the worldwide datasets "on-the-side," was funded by the U.S.D.A. Forest Service's National Stream and Aquatic Ecology Center in Fort Collins, CO. The writers say "A big thank you!" to Yuko Asano (Univ. of Tokyo) for her generous help with gathering the data from Japan.

References

Alexandrov, Y., J.B. Laronne, and Reid, I. 2007. "Intra-event and inter-seasonal behaviour of suspended sediment in flash floods of the semi-arid northern Negev, Israel," Geomorphology 85: 85–97.

Bagnold, R.A., 1977. "Bed load transport by natural rivers," Water Resour. Res. 13(2): 303-312.

Bergman, N., Laronne, J.B., and. Reid, I. 2007. "Benefits of design modifications to the Birkbeck bedload sampler illustrated by flash-floods in an ephemeral gravel-bed channel," Earth Surf. Process. Landforms 32, 317–328, DOI: 10.1002/esp.1453

Beschta, R.L., 1981. "Increased bag size improves Helley-Smith bed load sampler for use in streams with high sand and organic matter transport," In: Erosion and Sediment Transport Measurement. IAHS Publ. no. 133: 17-25.

Bunte, K. and Abt, S.R. 2001. "Sampling Surface and Subsurface Particle-Size Distributions in Wadable Gravel- and Cobble-Bed Streams for Analysis in Sediment Transport, Hydraulics, and Streambed Monitoring," U.S.D.A. Forest Service, Rocky Mnt. Research Station, Fort Collins, CO, General Techn. Report RMRS-GTR-74, 428 pp.

Bunte, K., Abt, S.R., Potyondy, J.P., and Ryan, S.E. 2004. "Measurement of coarse gravel and cobble transport using a portable bedload trap," J. Hydraul. Engineer., 130(9): 879-893.

Bunte, K., Swingle, K.W., Ettema, R., Abt, S.R., and Cenderelli, D.A. 2019. "Helley-Smith sampler's mismeasurement of gravel transport rates and particle sizes," Proc., SEDHYD 2019, 11th Federal Interagency Sedimentation and 6th Hydrologic Modeling Conf., June 24-28, 2019, Reno, NV. USA

Bunte K. and Swingle, K.W. 2019. "The Bedload Database," Report in preparation. U.S.D.A. Forest Service, Rocky Mountain Research Station, Fort Collins, CO. (84 spreadsheet files, 14 photo folders, 12 study site reports).

Bunte, K., 1996. "Analyses of the temporal variation of coarse bedload transport and its grain size distribution (Squaw Creek, Montana, USA)," U.S.D.A., Forest Service, Rocky Mountain Forest and Range Experiment Station, General Technical Report RM-GTR-288, 123 pp.

Bunte, K., 1997. "Development and field testing of a bedload trap for sand and fine gravel in mountain gravel-bed streams (South Fork Cache la Poudre Creek, CO)," Report submitted to the Stream Systems Technology Center, U.S.D.A. Forest Service, Rocky Mountain Forest and Range Experiment Station, Fort Collins, CO, 53 pp.

Bunte, K., Swingle, K.W., and Abt, S.R. 2007. "Guidelines for using bedload traps in coarse-bedded mountain streams: Construction, installation, operation and sample processing," General Techn. Report RMRS-GTR-191, Fort Collins, CO, U.S.D.A., Forest Service, Rocky Mountain Research Station, 91 pp. http://www.fs.fed.us/rm/pubs/rmrs_gtr191.pdf

Bunte, K., Abt, S.R., Potyondy J.P., and Swingle, K.W. 2008. "A comparison of coarse bedload transport measured with bedload traps and Helley-Smith samplers," Geodinamica Acta 21(1/2): 53-66.

Camenen, B., Holubova, K., Lukac, M., Le Coz, J., and Paquier, A. 2011. "Assessment of methods used in 1D models for computing bedload transport in a large river: the Danube River in Slovakia," J.Hydraul. Engineer. 137(10): 1190-1199.

Castro J.M. and Jackson, P.L. 2001. "Bankfull discharge recurrence intervals and regional hydraulic geometry relationships: patterns in the Pacific Northwest, USA," J. Am. Water Res. Assoc., 37 (5): 1249-1262.

Cencetti, C., Tacconi, P., del Prete, M., and Rinaldi, M. 1994. "Variability of gravel movement on the Virginio gravel-bed stream (central Italy) during some floods," In: Variability in Stream Erosion and Sediment Transport. L.J. Olive, R.J. Loughran and J.A. Kesby (eds.), IAHS Publ. 224: 3-11.

Church, M. and Hassan, M. 2005. "Upland gravel-bed rivers with low sediment transport," In: Catchment Dynamics and River Processes: Mediterranean and Other Climatic Regions, p. 141 – 168. C. Garcia and R.J. Batalla (eds.). Elsevier, B.V., Amsterdam, The Netherlands.

Cohan, H. and Laronne, J.B. 2005. "High rates of sediment transport by flashfloods in the Southern Judean Desert, Israel," Hydrol. Process. 19: 1687-1702; doi: 10.1002/hyp.5630.

Dell'Agnese, A., Mao L., and Comiti, F.2014. "Calibration of an acoustic pipe sensor through bedload traps in a glacierized basin," Catena 121: 222–231.

Downs, P.W., Soar, P.J., and Taylor, A. 2016. "The anatomy of effective discharge: the dynamics of coarse sediment transport revealed using continuous bedload monitoring in a gravel-bed river during a very wet year," Earth Surf. Process. Landforms 41, 147–161, DOI: 10.1002/esp.3785

Dury, G.H., 1976. "Discharge predictions, present and former, form channel dimensions," J. Hydrology 30: 216-245.

Emmett, W.W., 1980. "A Field Calibration of the Sediment Trapping Characteristics of the Helley-Smith Bedload Sampler," Geol. Survey Prof. Paper 1139, Washington, DC.

Estep, M.A. and Beschta, R.L. 1985. "Transport of bedload sediment and channel morphology of a southeast Alaska stream," Pacific Northwest Forest and Range Experiment Station, Research Note PNW-430, 15 pp.

Ferguson, R.I., 1986. "River loads underestimated by rating curves," Water Resour. Res. 22(1): 74-76.

Ferguson, R.I., 1987. "Accuracy and precision of methods for estimating river loads," Earth Surf. Process. Landforms 12: 95-104.

Ferguson, R., and Church, M. 2009. "A critical perspective on 1-D modeling of river processes: Gravel load and aggradation in lower Fraser River, " Water Resour. Res., 45, W11424, doi: 10.1029/2009WR007740.

Garcia, C., Laronne, J.B., and Sala, M. 2000. "Continuous monitoring of bedload flux in a mountain gravel-bed river," Geomorphology 34: 23-31.

Gattermayr, W., 2013. "Das hydrographische Regime der Ötztaler Ache," Publikationen Alpine Forschungsstelle Obergurgl – 3: 121 - 155.

Gomez, B. and Church, M. 1989. "An assessment of bed load sediment transport formulae for gravel bed rivers," Water Resour. Res. 25(6): 1161-1186.

Green, K.C., Brardinoni, F. , and Alila, Y. 2013. "Channel morphology and bed-load yield in fluvial, formerly-glaciated headwater streams of the Columbia Mountains, Canada," Geomorphology 188: 96–109.

Green, K.C., Alila, Y., and Brardinoni, F. 2014. "Patterns of bedload entrainment and transport in forested headwater streams of the Columbia Mountains, Canada," Earth Surf. Process. Landforms DOI: 10.1002/esp.3642

Habersack, H., Aigner, J., Kreisler, A., Rindler, R., and Seitz, H. 2015a. "Geschiebemessung an der Rofenache." Bericht 2008 - 2014," Bundesministerium für Land- und Forstwirtschaft, Umwelt und Wasserwirtschaft, Wien, Austria, 55 pp.

Habersack, H., Aigner, J., Kreisler, A., Rindler, A., Seitz, H., and Tritthart, M. 2015b. "Geschiebemessung an Drau und Isel 2007 – 2012," Endbericht. Bundesministerium für Land- und Forstwirtschaft, Umwelt und Wasserwirtschaft, Wien, Austria, 105 pp.

Habersack , H., Kreisler, A., Rindler, R., Aigner, J., Seitz, H., Liedermann, M., and Laronne, J.B. 2016. "Integrated automatic and continuous bedload monitoring in gravel bed rivers," Geomorphology 291: 80–93.

Handa, K., Chinaka, H., Ishikawa, K., and Miyazawa, K. 2013. "Himekawa River basin on sediment transport monitoring," Sabo gakkaishi 66(2): 74-78.

Hassan, M.A. and Church, M. 2001. "Sensitivity of bedload transport in Harris Creek: Seasonal and spatial variation over a cobble-gravel bar," Water Resour. Res. 37(3): 813-825.

Hassan, M.A., Robinson, S.V.J., Voepel, H., Lewis, J., and Lisle, T.E. 2014. "Modeling temporal trends in bedload transport in gravel-bed streams using hierarchical mixed-effects models," Geomorphology 219: 260-269.

Hayward, J.A. 1980. "Hydrology and stream sediments in a mountain catchment," In: Tussock Grasslands and Mountain Lands Institute Special Publ. no. 17, 236 pp.

Hayward, J.A., and Sutherland, A.J. 1974. "The Torlesse stream vortex-tube sediment trap," J. Hydrol. (N.Z.) 13(1): 41-53.

Hilldale, R.C. 2015. "Continuous bed load measurement with impact plates on the Elwha River, Washington," Proc., Joint 5th Fed. Interagency Hydrol. Modeling & 10th Fed. Interagency Sediment. Conf., April 19 - 23. Reno, NV.

Hinton, D.D., 2012. "Complexity of Bedload Transport in Gravel Bed Streams: Data Collection, Prediction, and Analysis," Ph.D. Diss., Dept. of Civil and Environment. Engineer., Brigham Young University, UT, 99 pp.

Hirsch, R.M., Helsel, D.R., Cohn, T.A., and Gilroy, E.J. 1992. Statistical treatment of hydrologic data. In: Handbook of Hydrology, D.R. Maidment, ed. McGraw-Hill, New York.

Hofer, B. 1987. "Der Feststofftransport von Hochgebirgsbächen am Beispiel des Pitzbaches," Oesterreichische Wasserwirtschaft 39(1/2): 30-38.

Hollingshead, A.B. 1971. "Sediment transport measurements in gravel rivers," J. Hydraulics Div., ASCE, 97 (HY1): 1817-1834.

Holubová, K., Klúcovská J., and Szolgay, J. 1998. "Environmental impact of hydroelectric power generation on an anastomosing reach of the River Danube," In: Gravel-Bed Rivers in the Environment. P.C. Klingeman, R.L. Beschta, P.D. Komar, and J.B. Bradley, eds., 293-312, Water Res. Publ. LLC, Highlands Ranch, Colorado.

Holubová, K., Capeková, Z., and Szolgay, J. 2005. "Impact of hydropower schemes at bedload regime and channel morphology of the Danube River," In: River Flow 2004: Proc. Second Intl. Conf. on Fluvial Hydraulics, Napoli, Italy, June 23-25, 2004. M. Greco, A. Carravetta, R. Della Morte (eds.) A.A. Balkema, Leiden, p. 135-142.

Ikeda, H. and Iseya, F. 1987. "Thresholds in the mobility of sediment mixtures," In: International Geomorphology, Part I. V. Gardiner (ed.), John Wiley & Sons, Chichester, p. 561-570.

Johnejack, K.R. and Megahan, W.F. 1991. "Sediment transport in headwater channels in Idaho," In: Proc. Fifth Fed. Interagency Sedimentation Conf., March 18-21, 1991, Las Vegas, NV., p. 4.155-4.161.

Johnson, P.A. and Heil, T.M. 1996. "Uncertainty in estimating bankfull conditions," Water Res. Bull. 32(6): 1283-1291.

Kreisler, A., Moser, M., Aigner, J., Rindler, R., Tritthart, M., and Habersack, H. 2016. "Analysis and classification of bedload transport events with variable process characteristics," Geomorphology, 291: 57-68.

Kuhnle, R.A. 1991. "Bed load transport in two small streams," Proc. Fifth Fed. Interagency Sedimentation Conf., March 18-21, 1991, Las Vegas, NV, p. 4/139-4/146.

Kuhnle, R.A. 1992. "Bedload transport during rising and falling stages in two small streams," Earth Surf. Process. Landforms 17: 191-197.

Kuhnle, R.A. 1992. "Fractional transport rates of bedload on Goodwin Creek," In: Dynamics of Gravel Bed Rivers. P. Billi, R.D. Hey, C.R. Thorne and P. Tacconi (eds.), John Wiley, Chichester, p. 141-155.

Laronne, J.B., Garcia, C, and Reid, I. 2001. "Mobility of patch sediment in gravel bed streams: patch character and its implications for bedload," In: Gravel-Bed Rivers V, M.P. Mosley (ed.), New Zealand Hydrological Society Inc., Wellington, New Zealand. ISBN 0-473-07486-9. 2001., pp. 249-289.

Laronne, J.B., Alexandrov, Y., Bergman, N., Cohen, H., Garcia, C., Habersack, H., Powell, D.M., and Reid, I. 2003. "The continuous monitoring of bed load flux in various fluvial environments," In: Erosion and Sediment Transport Measurement in Rivers: Technological and Methodological Advances. J. Bogen, T. Fergus and D.E. Walling (eds.), IAHS-Publ. 283, p. 134-145.

Lenzi, M.A., D'Agostino, V., and Billi, P. 1999. "Bedload transport in the instrumented catchment of the Rip Cordon. Part I: Analysis of bedload records, conditions and threshold of bedload entrainment," Catena 36: 171-190.

Lenzi, M.A., Mao, L., and Comiti, F. 2004. "Magnitude-frequency analysis of bed load data in an Alpine boulder bed stream," Water Resour. Res. 40, W07201, doi:10.1029/2003WR002961.

Lenzi, M.A., Mao, L., and Comiti, F. 2006. "Effective discharge for sediment transport in a mountain river: Computational approaches and geomorphic effectiveness.," J. Hydrology 326: 257–276.

Leopold, L.B. 1994. A View of the River. Harvard University Press, Cambridge, Massachusetts, 298 pp.

Leopold, L.B. and Emmett, W.W. 1997. "River hydraulics and sediment transport: inferences from the East Fork River, Wyoming," U.S. Geol. Survey Prof. Paper 1583, 52 pp.

Liedermann, M., Gmeiner, P., Niederreiter, R., Tritthart, M., and Habersack, H. 2012. "Innovative Methoden zum Geschiebemonitoring am Beispiel der Donau," Österreichische Wasser- und Abfallwirtschaft 64:527–534.

Magirl, C.S., Hilldale, R.C. Curran, C.A., Duda, J.J., Straub, T.D., Domanski, M., and Foreman, J.R. 2015. "Large-scale dam removal on the Elwha River, Washington, USA: Fluvial sediment load," Geomorphology, 246: 669-686.

Martin, Y. and M. Church, 1995. "Bed-material transport estimated from channel surveys: Vedder River, British Columbia," Earth Surf. Process. Landforms 20: 347-361.

Martin, Y. and Church, M. 2000. "Re-examination of Bagnold's empirical bedload," Formulae, Earth Surf. Process. Landforms 25, 1011-1024.

Martin Y. and Ham, D. 2005. "Testing bedload transport formulae using morphologic transport estimates and field data: lower Fraser River, British Columbia," Earth Surf. Process. Landforms 30: 1265–1282,

McLean, D.G. 1980. "Flood control and sediment transport study of the Vedder River," M.S. Thesis, Univ. of British Columbia, 266 pp.

McLean, D.G., Church, M., and Tassone, B. 1999. "Sediment transport along lower Fraser River. 1. Measurements and hydraulic computations," Water Resour. Res. 35(8): 2533-2548

McMahon, P.L. 2013. "Bedload Transport Sampling, Characterization and Modeling on a Southern Appalachian Ridge and Valley Stream," Ph.D. Diss., University of Tennessee.

Meyer-Peter, E., E. Hoeck and R. Mueller, 1937. "Die internationale Rheinregulierung von der Illmündung bis zum Bodensee. II. Beitrag der Versuchsanstalt für Wasserbau an der E.T.H. Zürich zur Loesung des Problems," Schweizerische Bauzeitung 110(18): 212-219.

Milhous, R. 1973. Sediment transport in a gravel-bottomed stream. Ph.D. thesis, Oregon State Univ., Corvallis, USA.

Mitsunaga, T., Moriya, T., Uchida, T., Tomita K., and Ye, Z. 2015. Observations of sediment discharge in the district of the Fujikawa Sabo Office. Sabo Gakkaishi 68(1): 83-87.

Montgomery, D.R. and Buffington, J.M. 1997. Channel-reach morphology in mountain drainage basins. Geol. Soc. Am. Bull. 109 (5): 596-611.

Nanson, G.C. 1974. "Bedload and suspended-load transport in a small, steep, mountain stream," Am. J. Science 274: 471-486.

Nesper, F. 1937. "Die international Rheinreguliering von der Illmündung bis zum Bodensee. III. Ergebnisse der Messungen über Geschiebe- und Schlammführung des Rheins an der Brugger Rheinbrücke," Schweizerische Bauzeitung 110(12):143-164.

Nitsche, M., Rickenmann, D., Turowski, J.M., Badoux, A., and Kirchner, J.W. 2011. "Evaluation of bedload transport predictions using flow resistance equations to account for macro-roughness in steep mountain streams," Water Resour. Res., 47, W08513, doi:10.1029/2011WR010645.

Palt, S. M. 2001. "Sedimenttransportprozesse im Himalaya-Karakorum und ihre Bedeutung für Wasserkraftanlagen," Ph.D. Dissertation, Universität Fridericiana zu Karlsruhe (TH), Germany, 257 pp.

Powell, D.M., Reid, I., Laronne J.B., and Frostick, L.E. 1998. "Cross stream variability of bedload flux in narrow and wide ephemeral channels during desert flash floods," Gravel-Bed Rivers in the Environment. P.C. Klingeman, R.L. Beschta, P.D. Komar, and J.B. Bradley, eds., 177-196, Water Res. Publ., LLC, Highlands Ranch, Colorado.

Radecki-Pawlik, A. 2002. "Bankfull discharge in mountain streams: theory and practice," Earth Surf. Process. Landforms 27: 115-123.

Ravazzolo, D., Mao, L., Escauriaza, C., Pastén, P., and Montecinos, M. 2019. "Rusty river: Effects of tufa precipitation on sediment entrainment in the Estero Morales in the central Chilean Andes," Science Total Environ. 652: 822-835.

Reid, I., Frostick, L.E., and Layman, J.T. 1985. "The incidence and nature of bedload transport during flood flows in coarse-grained alluvial channels," Earth Surf. Process. Landforms, 10: 33-44.

Reid, I. and Frostick, L.E. 1986a. "Dynamics of bedload transport in Turkey Brook, a coarse grained alluvial channel," Earth Surf. Process. Landforms, 11: 143-155.

Reid, I. and Frostick, L.E. 1986b. Turkey Brook bedload data-base. Birkbeck College, University of London, Malet St., London WCIE 7HX, UK.

Reid, I., Laronne J.B., and Powell, M. 1995. "The Nahal Yatir bedload database: sediment dynamics in a gravel-bed ephemeral stream," Earth Surf. Process. Landforms 20: 845-857.

Reid, I., Powell D.M. , and Laronne, J.B. 1996. "Prediction of bed-load transport by desert flash floods," J. Hydraul. Engineer. 122(3): 170-173.

Rickenmann, D. 2018. "Variability of bed load transport during six summers of continuous measurements in two Austrian mountain streams (Fischbach and Ruetz)," Water Resour. Res., 54: 107–131.

Rickenmann, D., Turowski, J.M., Fritschi, B., Klaiber, A., and Andreas, L. 2012. "Bedload transport measurements at the Erlenbach stream with geophones and automated basket samplers," Earth Surf. Process. Landforms, 37(9); 1000-1011.

Ryan, S.E. 2007. "The role of geology in sediment supply and bedload transport patterns in coarse grained streams," In: Advancing the Fundamental Sciences. Proc., Forest Service National Earth Sciences Conf., San Diego, CA, 18-22 Oct. 2004, M. Furniss, C. Clifton, and K. Ronnenberg (eds.). PNW GTR-689, Portland, OR: U.S.D.A., Forest Service, Pacific Northwest Research Station.

Sakurai, W., Uchida, T., Tanaka, Y., Uchi, T., and Kambara, J. 2016. "Recent advances in sediment discharge and hydrological observation at mountain rivers of Japan," Techn. Note No. 887, National Institute for Land and Infrastructure Management. Ministry of Land, Infrastructure, Transport and Tourism, Japan. ISSN 1346-7328.

Schmid, B. 2011. Geschiebetransportuntersuchungen in einem Gebirgsbach. Messungen und Berechnungen für den Riedbach im Kt. Wallis. M.S. thesis at the Swiss Federal Institute of Technology, Zürich, Switzerland.

Schneider, J.M., Rickenmann, D., Turowski, J.M., and Kirchner, J.W. 2015b. "Self-adjustment of stream bed roughness and flow velocity in a steep mountain channel," Water Resour. Res., 51, 7838–7859,

Soar, P.J. and Downs, P.W. 2017. "Estimating bedload transport rates in a gravel-bed river using seismic impact plates: Model development and application," Environm. Modelling & Software 90: 182-200.

Tacconi, P. and Billi, P.1987. "Bed load transport measurement by a vortex-tube trap on Virginio Creek, Italy," In: Sediment Transport in Gravel-Bed Rivers. C.R. Thorne, J.C. Bathurst, and R.D. Hey (eds.), John Wiley, Chichester, p. 583-615.

Turowski, J.M. and Rickenmann, D. 2011: "Measuring the Statistics of Bed-Load Transport Using Indirect Sensors," J. Hydraulic Engineering 137 (1): 116–121.

Uchida, T., Sakurai, W., Iuchi, T., Izumiyama, H., Borgatti, L., Marcato, G., and Pasuto, A. 2018. "Effects of episodic sediment supply on bedload transport rate in mountain rivers. Detecting debris flow activity using continuous monitoring," Geomorphology, 306: 198–209.

Whitaker, A.C. and Potts, D.F. 2007a. "Coarse bed load transport in an alluvial gravel bed stream, Dupuyer Creek, Montana," Earth Surf. Process. Landforms 32: 1984-2004.

Whitaker, A.C., and Potts, D.F. 2007b. "Analysis of flow competence in an alluvial gravel bed stream, Dupuyer Creek, Montana," Water Resour. Res., 43, W07433, doi:10.1029/2006WR005289.

Wilcock, P.R., and Kenworthy, S.T. 2002. "A two fraction model for the transport of sand/gravel mixtures," Water Resour. Res. 38 (10), 1194, doi:10.1029/2001 WR000684, 2002.

Wilcock, P.R., Kenworthy S.T., and Crowe, J.C. 2001. "Experimental study of the transport of mixed sand and gravel," Water Resour. Res., 37(12): 3349-3358.

Williams, G.P. 1978. "Bank-full discharge of rivers," Water Resour. Res., 14(6): 1141-1154.

Yu, G., Wang, Z., Zhang, K., Chang, T., and Liu, H. 2009. "Effect of incoming sediment on the transport rate of bed load in mountain streams," Internatl. J. Sed. Res. 24(3): 260–273.

Rapid Watershed Assessment Tools Based On High Resolution Terrain Data

Christopher P. Haring, Research Physical Scientist, ERDC-River Engineering Branch, Vicksburg, MS, Christopher.P.Haring@@usace.army.mil
Charles H. Theiling, Research Ecologist, ERDC-Environmental Branch, Vicksburg, MS, *Charles.H.Theiling@usace.army.mil*
Michael P. Dougherty, Geographer, USACE-Rock Island District, M*ichael.P.Dougherty@ usace.army.mil*

Purpose

The goal of this project was to develop rapid watershed assessment methods to estimate channel stability and sediment transport potential using high resolution terrain data to support USACE watershed planning. This project developed a suite of tools based on advanced remote sensing (RS) technologies (LiDAR) that use off-the-shelf, high resolution terrain data to rapidly assess watershed condition at the channel, floodplain, valley, and watershed scales. The widespread availability of high resolution terrain data provides an opportunity to assess watershed conditions in great detail over large spatial extents. Automated geomorphometric tools for extracting key floodplain, valley, and watershed scale metrics are widely developed and available. However, existing toolsets have yet to automate and identify many of the well-established fluvial geomorphological principles and related empirical relationships at the channel scale. For this project, a channel assessment method was developed using a new LiDAR-Hydraulic Geometry Relationship (HGR) based tool for developing regional curves. Regional curves relate bankfull channel dimensions and discharge to watershed drainage area and are the basis for analyzing and defining channel metrics at large spatial scales within a watershed for this rapid watershed assessment method.
The goals and objectives of this project are:

Goals

- Provide a USACE Planning method for rapid watershed assessments by developing geomorphic analysis tools using high resolution terrain data and existing fluvial geomorphic principles
- Develop a USACE Ecological Planning model based on rapid watershed assessment metrics to define restoration and mitigation benefits

Objectives

- Develop a suite of planning analysis tools to rapidly assess and identify sediment sources, pathways, and sinks for watershed analysis.
- Use existing geomorphic principles to develop metrics for analyzing LiDAR-derived channel, floodplain, valley, and watershed characteristics.
- Develop an approach to relate channel, floodplain, valley, and watershed characteristics to Ecosystem Restoration (ER) habitat evaluation and benefits.

This project developed a new toolbox for extracting many common channel, floodplain, valley, and watershed geomorphology metrics. The tools apply to common watershed assessment tasks by developing repeatable data analysis and processing workflows. The study developed and applied these workflows using several test watersheds located throughout the country to

determine the applicability to a wide range of hydro-physiographic conditions and input data quality.

The rapid watershed assessment approach was developed to better quantify the benefits of streambank stabilization to protect downstream habitats in the Illinois River impacted by excessive sedimentation. The method allows quantification of the potential stream stabilization requirements in a watershed by mapping fluvial geomorphic channel metrics. The various channel metrics map stream reaches by relative channel stability that is based on high, medium, and low erosion potential for the entire watershed as support to watershed planners. The approach also supports Ecosystem Restoration (ER) habitat evaluations that demonstrate links between fisheries data and high-resolution terrain-derived stream channel characteristics and the quality of aquatic habitat. This framework will use geomorphic channel characteristics as predictor variables of aquatic health measured by fish community metrics. Success with linking ecological indicators to a rapid watershed assessment package will provide a powerful RS tool to estimate fisheries potential and test alternative management plans.

In addition, tools created for watershed assessments will support project reconnaissance, regulatory permitting, design, and adaptive management phases with increased spatial coverage and accuracy of geomorphic channel, floodplain, and watershed data. The assessment approach will provide more advanced design information to feasibility alternative evaluation and cost-benefit analysis studies. Maps and data summaries will support USACE engagements and communication of watershed plans across the spectrum of lay and technical audiences.

Introduction

The Illinois River Basin Restoration (IRBR) Program (WRDA 2007, Section 519 (b) & (c)) established the authority to implement watershed restoration studies to reduce sediment transport to Illinois River backwaters, side channels, and wetlands. Early project planning revealed differences in the broad scope of the watershed plan under one policy guidance (USACE watershed policy, EC1105-2-411) and project implementation under a different guidance (USACE 2000). Watershed assessment “may mean including downstream areas that are otherwise technically not in the local watershed or perhaps including a much broader, more regional watershed to adequately capture the full ranges of influence...” (USACE watershed policy, EC1105-2-411). Planning at the project level may consider “...resources that would be directly, indirectly, or cumulatively affected by alternative plans . . . often called the affected area” (USACE 2000). Consequently, it was discovered during early IRBR project planning that USACE methods for stream restoration and ecological benefit analysis were insufficient to document off-site sediment reduction benefits provided by stream stabilization in the watershed. In addition, USACE environmental project cost-benefit analysis (USACE 2000) requires measurable improvement in local habitat conditions (i.e., Habitat Units) that may not be substantial in stream stabilization projects because the projects do not typically capture ecological improvement as much as they stabilize existing conditions to reduce future or off-site impacts.

USACE project planning also includes a host of real estate implications concerning land ownership that precludes taking benefits outside of the project area in Federal ownership or easement. As a result, stream restorations evaluate habitat benefits over small stream reaches or “project areas,” rather than over decades of sediment transport reduction benefits to the downstream reaches. With hundreds of potential small watershed projects in the Illinois Basin

alone (or any USACE watershed study), there is a need to rapidly define sediment management needs with high resolution over large areas. The USACE emphasis on habitat outcomes requires better capacity to evaluate stream habitat over large spatial scales so there is also a direct need for a planning tool to that provides high resolution stream habitat indicators.

Conceptual Framework

A landscape approach was used for this study to define an analytical hierarchy of channel, floodplain, valley, and watershed metrics (Figure 1). The information at each level or in various combinations can be used to classify stream condition for watershed assessments. Floodplain, valley, and watershed metrics define the source of overland flow and the external supply of sediment to streams. Channels and floodplains can be sediment sources, pathways, or sinks depending on local physical conditions that can be characterized as Functional Process Zones (FPZ). Thorp et al. (2006) defined FPZ's in River Ecosystem Synthesis, which conceptualized the physical-ecological relationships inherent in watersheds, streams, and rivers as catchments driven by climate and geology. The FPZ's are shaped as "linked, discontinuous hierarchies of patch dynamics" formed by physicochemical characteristics that affect ecosystem structure and function.

Recent USACE watershed-scale planning initiatives emphasize integration of landscape ecology principles. Hierarchical landscape principles support science, planning, design, implementation, and monitoring of watershed plans by identifying the function and connectivity of habitat patches relevant to natural resource managers and the public. Williams et al. (2015) reported a wide range of geomorphic watershed characteristics to consider, so this study adopted the spatial hydro-geomorphic variables recommended for U.S. databases applicable across the USACE areas of responsibility as a first level evaluation.
As an example, by evaluating channel slope and width-to-depth ratios, the RS analysis tools can provide insight on distribution of stream power and sediment transport potential within the watershed stream network. These relationships are mapped at the channel, floodplain, valley, or watershed scale and potential locations of sources, pathways, and sinks can be identified. In combination with additional variables, they directly influence floodplain and watershed characteristics. The development of RS tools that measure channel HGR's in combination with existing landscape ecological principles (Thorp et al. (2006); Williams et al. (2015)) provides tools to rapidly assess watersheds.

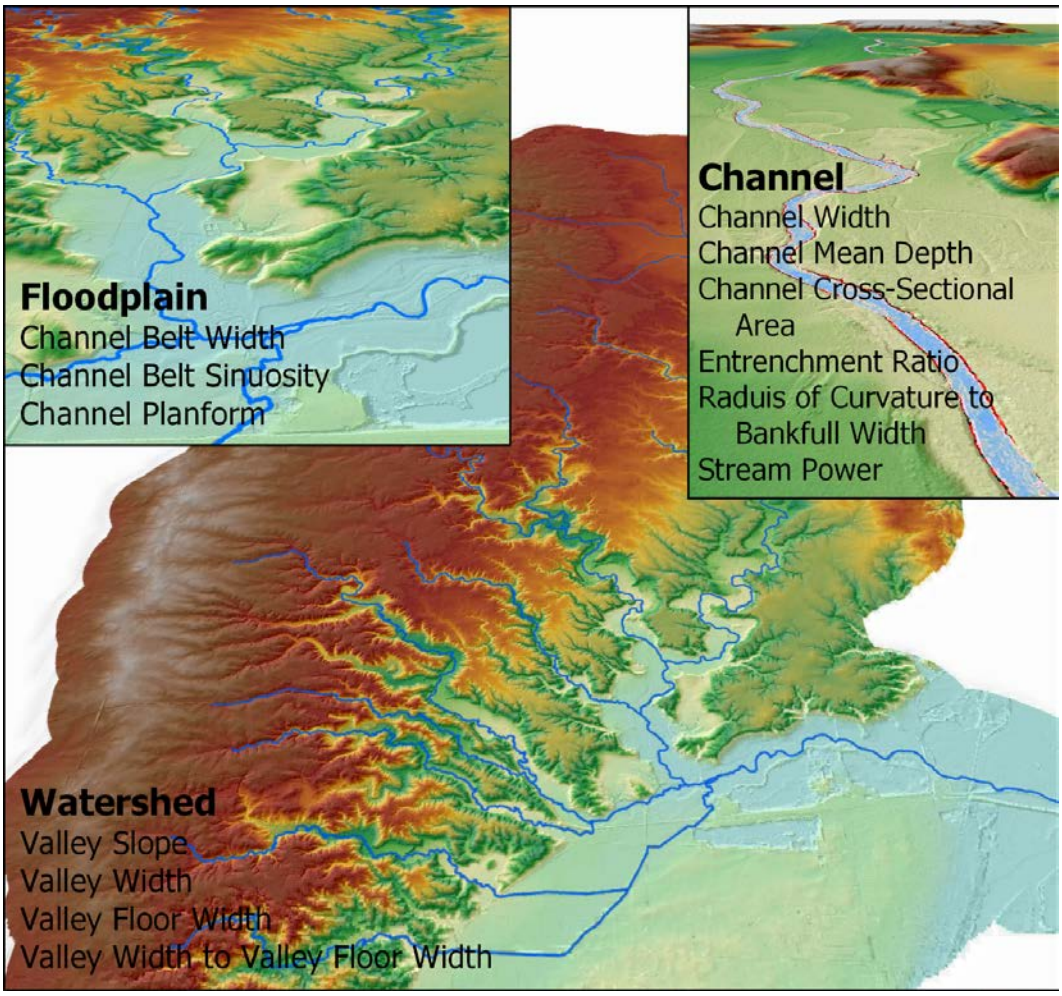

Figure 1. Watershed Analysis Workflow

Regional Curve Development

Stream systems develop a regular progression of channel form and morphology that naturally balance watershed inputs. Channel forming or bankfull HGR develop from balancing and maintaining a quasi-equilibrium state between sediment supply, slope, channel shape, planform, vegetation, and other factors. In a stable stream, bankfull discharge fills the channel to the active floodplain level providing a delineating morphological feature defining channel forming discharge, sediment transport processes, and depositional features on a floodplain (Dunne and Leopold, 1978; FISRWG, 1998). Information about bankfull channel geometry and discharge is important to researchers, Federal, State, and local governments and private organizations involved in construction of roadways, bridges, infrastructure projects, stream stabilization and restoration projects, and watershed assessments. Over the past four decades, stream analysis, research, and design of restoration and stabilization projects have largely focused on using a natural-channel design (NCD) approach that is reliant on estimates of bankfull channel geometry and discharge rather than traditional river engineering practices that may involve straightening, widening, deepening, concrete lining, or hardening banks and channels.

A common method for analyzing geomorphic channel stability is to evaluate channel dimensions relative to regional curves which relate bankfull channel dimensions and discharge relative to drainage area through linear regression analysis. The resulting regression models provide morphological channel dimensions that directly relate to channel forming discharge, sediment transport processes, and depositional channel features. Watershed assessments and stream restoration design techniques suffer from lack of coverage of regional curves for specific hydro-physiographic regions and sub-regions which limits our capacity to analyze many un-gaged watersheds lacking this data.

LiDAR-HGR based regional curves can be developed by combining existing and discontinued stream gage data, rating curves, and datum conversions with high resolution terrain data to capture natural geomorphic channel characteristics. Standard regional curve development is based on traditional geomorphic field surveys capturing bankfull channel dimensions at stable riffle or channel cross-over locations. The LiDAR-HGR methodology also assembles riffle data surveys which provide the least amount of bankfull mean depth error. Similarly, LiDAR-HGR requires an adequate number of gages within a hydro-physiographic region of interest to effectively capture the variation of fluvial geomorphic bankfull conditions. Once the LiDAR-HGR regional curves are assembled, departure analysis comparing channel dimensions from the existing un-gaged watershed to the LiDAR-HGR regional curve can be completed. If the channel dimensions at the un-gaged watershed location are within the 90% confidence interval, than the channel is considered to be stable. If the channel dimensions fall outside the 90% range then further analysis is required from other channel and planform matrices. The process for constructing a regional curve is depicted in the flow diagram below (Figure 2).

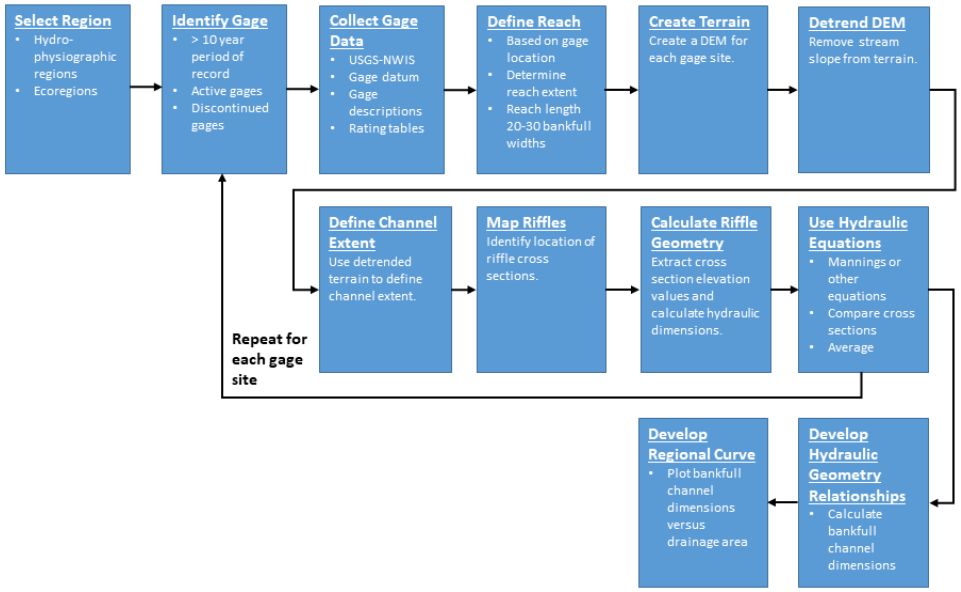

Figure 2. LiDAR-HGR Regional Curve Workflow

Channel Metrics

This study incorporates open source geospatial tools to support channel, floodplain, valley, and watershed geomorphic analysis. Traditional geomorphic field-based data collection methods,

out of necessity, gather and measure channel dimensions and slope using well-established ground survey methods (Harrelson et al., 1994). The traditional field surveys are often limited with constraints on time, funding, and the availability of appropriate survey personnel. In addition, recent literature regarding stream restoration indicates that traditional field survey methods for gathering bankfull channel dimensions may be error prone with reported errors ranging from 5 to 25 percent (Hammer (1981); Wahl, (1977)). Conversely, this rapid watershed assessment method uses existing high-resolution spatial data that can greatly increase the spatial extent and precision of stream assessments thereby reducing time and cost.

An ArcGIS fluvial geomorphology toolbox was developed exclusively for this study to process high-resolution terrain data, extract channel dimensions, and use existing empirical relationships to provide rapid watershed analysis. The toolbox and resulting channel metrics are all based on the concept of bankfull discharge and its effectiveness in shaping the dimension, pattern, and profile of the channel, floodplain, valley, and watershed. Dunne and Leopold (1978) are credited with the commonly accepted and universally applicable definition of bankfull discharge as: "*The bankfull stage corresponding to the discharge in which the channel maintenance is most effective, that is, the discharge that is moving sediment, forming or removing bars, forming or changing bends and meanders, and generally doing work that result in the average morphological characteristics of channel*s." The bankfull discharge and associated channel dimensions are the defining analysis tools that quantify channel metrics relative to empirical relationships known to support stable, intermediate, or unstable stream channel conditions. For example, the sinuosity metric is measured by stream length divided by valley length and values less than 1.8 may indicate channelization, coupled with a width-to-depth ratio of less than 10 may indicate channel instability in the form of channel bed degradation.

The stream channel metrics are described in Table 1 and are based on bankfull channel dimensions to include width, mean depth, cross-sectional area, discharge, water surface slope, width-to-depth ratios, entrenchment ratios, sinuosity, radius-of-curvature, stream power, and additional planform matrices.

Table 1. Bankfull Channel dimension and planform geometry metrics derived from LiDAR.

Channel Dimension	
Width, Mean Depth, Cross-sectional Area	Required for Regional Curve Development: Dimensions of bankfull width (ft) and mean depth (ft), cross-sectional area, and discharge (cfs) to drainage area (square miles)
Width to Depth Ratio	Shape of the channel based at bankfull width (ft) and mean depth (ft) at bankfull discharge because it is the most erosive condition.
Entrenchment Ratio	Depicts relative access to the active floodplain. Typically, for channel stability at 2 times the maximum bankfull depth, the water surface should be at least 2.5 times the water surface width at bankfull depth. Incised or degraded channel reaches will continue to laterally erode and build floodplains until the entrenchment ratio reaches 2.5
Planform Geometry:	
Sinuosity	Sinuosity is the ratio of stream length to valley length. It can also be described as the ratio of valley slope to channel slope for defined reaches. Less than 1.8 likely means a channelized reach

	and combined with the W/D ratio less than 10 may indicate incised channel reaches.
Radius of Curvature(R_C)/ Bankfull Width	The ratio value of R_C to bankfull width is commonly used as a diagnostic test for channel planform stability. The ranges that can occur in nature are highly variable but in general if the R_C/Bkfl ratio is less than 1.8 (<1.8), then the outside bend-channel banks will likely be eroding very agressively as the channel bend progresses erosion in a downvalley direction.
Energy:	
Stream Power (S x Q)	Stream Power is the slope (S) x discharge (Q) Q_sQ_{50} ~ SQ; Lanes-Balance of Dynamic River Forces

FluvialGeomorph Toolbox

The FluvialGeomorph toolbox is designed to provide a comprehensive set of tools for transforming raw terrain data into a set of synthetically derived stream characteristics to derive common fluvial geomorphic metrics (Table 1). The toolbox contains purpose-built Python tools (Table 2) designed to run within ESRI ArcGIS Desktop or ArcPro (ESRI, 2018) to perform geospatial analysis. Some of these Python tools call custom R (R Core Team, 2018) functions to perform statistical analysis and graphing. This modular design allows flexibility to support both geospatial analysis and automated report generation. TauDEM (Tarboton, 2018) is used for many of the hydro-modification steps. This toolbox was heavily influenced by the currently inactive and closed source River Bathymetry Toolkit (McKean et al. 2009).

Table 2. FluvialGeomorph tools.

Tool	Description
Burn Cutlines	Burns cutlines into DEM to ensure water flows across terrain
Contributing Area	Calculates the up-slope area for each DEM pixel
Stream Network	Develops synthetic stream network from hydromodified DEM
Gradient	Calculates stream slope and sinuosity
Create Flowline	Constructs a smooth flowline route
Stream Profile Points	Converts flowline to points and calculates elevation
Detrend DEM	Creates a DEM with valley slope removed
Channel Extent	Creates a channel extent polygon
Channel Slope	Calculates a channel extent slope raster
Centerline	Creates a centerline from channel extent
XS Layout	Creates a set of regularly spaced cross sections
XS Watershed Area	Calculates drainage area for each cross section

XS Assign River Position	Calculates the longitudinal position of each cross section
XS Create Station Points	Converts cross sections to points and calculates elevation
XS Dimensions	Calculates cross section hydraulic dimensions
Reach Bankfull Graph	Graphs sensitivity analysis results for a specified bankfull elevation for selected regions
Reach Geometry Graph	Graphs the hydraulic geometry dimensions for a specified bankfull elevation
XS Plot	Graphs a single cross section for a specified bankfull elevation

FluvialGeomorph tools must be organized into a series of ordered steps which we refer to as workflows. This project has so far developed two workflows: rapid watershed assessment and regional curve development. For example, Figure 3 is a flow model of the individual steps for the Watershed Analysis workflow described in Table 2. Within each workflow step, one or more FluvialGeomorph tools may be required to accomplish that step. The modular design of the FluvialGeomorph toolbox allows new tools to be created to support a new tasks, modify existing workflows, and move to new watersheds.

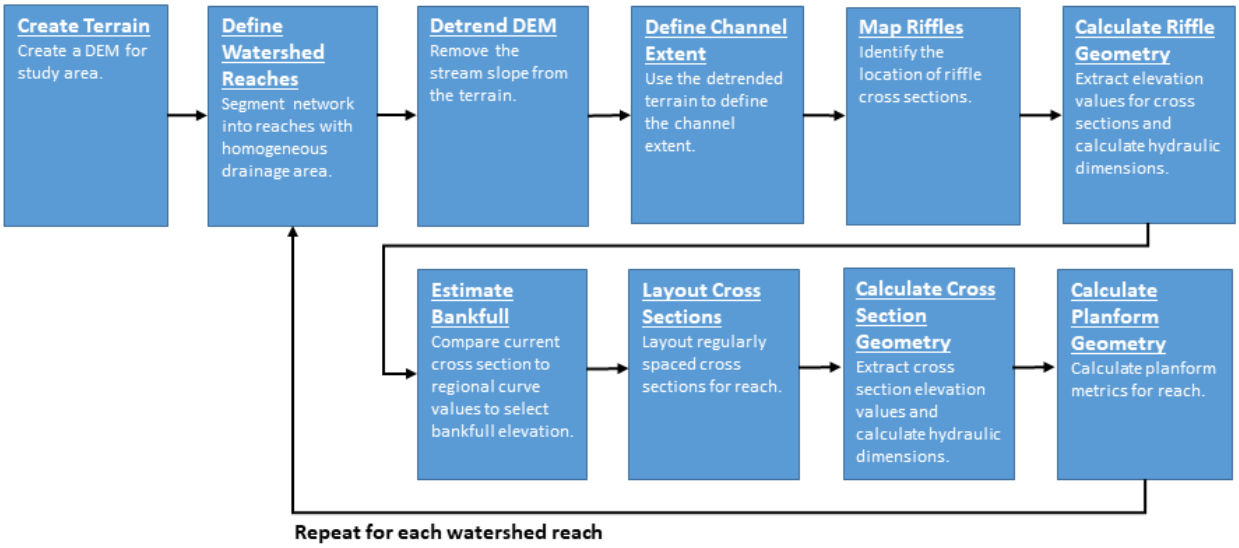

Figure 3. Watershed Analysis Workflow

Stream Habitat Relationships

Given the fidelity of LiDAR-derived stream metrics described in this study, these stream characteristics should serve as strong predictors of aquatic habitat. To make the link between terrain-derived stream characteristics and the quality of aquatic habitat, this study will use stream metrics as predictor variables of aquatic health measured by such metrics as Index of Biological Integrity (IBI) scores. Machine learning methods will be used to train and test this

habitat response model in Minnesota River Basin streams to demonstrate that our watershed, valley, floodplain, and channel metrics can predict fish community characteristics. We will select a subset of available fish sample sites to characterize the Minnesota River Basin across several physiographic regions. The correlations can be validated against remaining sites to define relationships for extrapolation throughout the basin.

If stream metrics prove to be good predictors of IBI scores for the existing condition, then Future Without Project (FWOP) and project alternatives can be analyzed for habitat impacts using this model. This approach makes the most use of existing LiDAR and state-level IBI data making it feasible in a rapid assessment framework.

Conclusion

Developing habitat relationships is important for USACE Ecosystem Restoration planning and watershed analysis and this project provides an efficient rapid watershed assessment methodology. Integrating channel, floodplain, valley, and watershed-wide RS data analysis with existing biological data is more efficient relative to quantitative hydrologic models and can provide high resolution information during the earliest steps of watershed planning. For this project, existing Minnesota River biological data is used to estimate fisheries potential and to evaluate alternative management plans.

The rapid watershed assessment approach integrates channel metrics and biological data to identify potential benefits of stream restoration alternatives and downstream habitats impacted by excessive sedimentation. The analysis approach uses existing regional curves or develops new curves based on the LiDAR-HGR methodology to analyze geomorphic channel metrics that detect channel stability issues identifying watershed-wide locations. Once unstable channel locations or reaches are identified, cumulative steps toward alternative restoration plans and project completion could be conceived and quantitatively evaluated for sediment retention potential and habitat analysis.

The rapid watershed assessment provides efficiency desired for modern USACE District planners and may also be used for disaster and hazard assessment in fire damaged landscapes. While designed for watershed habitat restoration assessment, the watershed assessments may be used to support regulatory cumulative effects analysis. In conditions where main-stem river backwater sedimentation issues exist or navigation channel dredging is impacted, potential sources and locations of sediment delivery from the watershed can be provided based on the geomorphic watershed analysis. Once the potential sediment sources are located in the tributary streams, then focused watershed and habitat restoration projects can be investigated and implemented.

The approach provides a relatively quick, thorough, geomorphic-based, watershed-wide assessment capability that has not been provided elsewhere to the best of our knowledge. This is particularly useful for watersheds that lack biological data to support habitat evaluations as is common in most project sites. The integration of the rapid watershed assessment and biological data will produce a plan that compiles results into a habitat benefits model for nationwide application. The analysis method provides the ability to produce high resolution, quantitative geomorphic assessments over large spatial extents.

References

Dunne, T., and Leopold, L.B., 1978. Water in Environmental Planning. W.H. Freeman and Co., San Francisco, CA.

ESRI 2018. ArcGIS Desktop (version 10.5.1). Redlands, CA: Environmental Systems Research Institute.

FISRWG (Federal Interagency Stream Restoration Working Group). 1998. Stream Corridor Restoration: Principles, Processes and Practices. National Technical Information Service. U.S. Department of Commerce, Springfield, VA.

Hammer, R.G., 1981. Streamflow estimates using channel width: Missoula, Mont., U.S. Forest Service, Northern Region, Soil, Air, and Water Notes 81-3, 6p.

Harrelson, C.C., Rawlins, C.L., and Potyondy, J.P., 1994. Stream Channel Reference Sites: An Illustrated Guide to Field Technique. Gen. Tech. Rep. RM-245. Fort Collins, CO: U.S. Department of Agriculture, Forest Service, Rocky Mountain Forest and Range Experiment Station.

R Core Team 2018. R: A Language and Environment for Statistical Computing (version 3.5.1). Vienna, Austria: R Foundation for Statistical Computing, https://www.R-project.org

McKean, J., Nagel, D., Tonina, D., Bailey, P., Wright, C.W., Bohn, C., Nayegandhi, A., 2009. Remote sensing of channels and riparian zones with a narrow-beam aquatic-terrestrial lidar. Remote Sensing, *1*, 1065-1096; doi:10.3390/rs1041065.

Tarboton, David 2018. Terrain Analysis Using Digital Elevation Models (TauDEM, version 5.3.7). Logan, UT: Utah State University, http://hydrology.usu.edu/taudem/taudem5/

Wahl, K.L., 1977. Accuracy of channel measurements and implications in estimating streamflow characteristics: U.S. Geological Survey Journal of Research, v. 5, no. 6, p 811-814.

Assessing the Effects of Dike Systems on Channel Morphology of the Lower Mississippi River

Casey Mayne, Research Hydraulic Engineer, US Army Corps of Engineers, Vicksburg, MS, Casey.M.Mayne@erdc.dren.mil
David Biedenharn, Research Hydraulic Engineer, US Army Corps of Engineers, Vicksburg, MS, David.S.Biedenharn@erdc.dren.mil
David May, Research Hydraulic Engineer, US Army Corps of Engineers, Vicksburg, MS, David.P.May@erdc.dren.mil

Extended Abstract

A detailed geometric data analysis was conducted for the Lower Mississippi River (LMR) within the U.S. Army Corps of Engineers (USACE) Vicksburg and Memphis Districts from River Mile (RM) 325 to 954 Above Head of Passes. The purpose of the study was to document long-term trends in the channel geometry with an emphasis on the influence of dike systems within the study reach. The results of this study will be part of a detailed geomorphic assessment of the Mississippi River to be conducted as part of the on-going Mississippi River Geomorphology and Potamology Program sponsored by the U.S. Army Corps of Engineers Mississippi Valley Division (MVD) Science and Technology Office.

Previous studies have employed a sedimentation database, developed under the direction of MVD in 1987, in order to quantify sedimentation trends and determine the effects of the LMR dike fields on channel characteristics (Biedenharn et al., 2000). While previous assessments using the dataset provided valuable insights into the effects of dikes on the LMR, there were concerns about moving forward using the methodology described by Cobb and Magoun (1985). In response, this study proposes an alternative method for assessing the effects of training structures on channel morphology in the Lower Mississippi River. A flexible template for channel delineation and a database of historical hydrographic survey data were used to determine spatial and temporal variations in geometry and volume for the defined sections of the channel. The approach utilizes ArcGIS to extract bathymetric data from historical hydrographic surveys to compute geometric and volumetric parameters at various water surface elevations. The channel delineation in this study is based primarily on the channel improvement boundary set by Vicksburg and Memphis jurisdictional districts (Figure 1). The channel alignment provides a reproducible delineation boundary that can quickly and effectively define the “Main Channel” and “Dike Field” areas for the entire study reach, which reduces the uncertainty of manually defining channels areas based on specific channel characteristics. In addition, the method eliminates the need for individual templates based on specific dike systems, which streamlines the process and extends the spatial range for the assessments. Using the proposed approach, the analysis can be flexibly scaled using individual cross sections positioned every 0.2-RM and 1-RM volumetric sections. With the adjustable scaling and removal of reach boundaries, the data can be collected, grouped, and analyzed at various spatial and temporal scales.

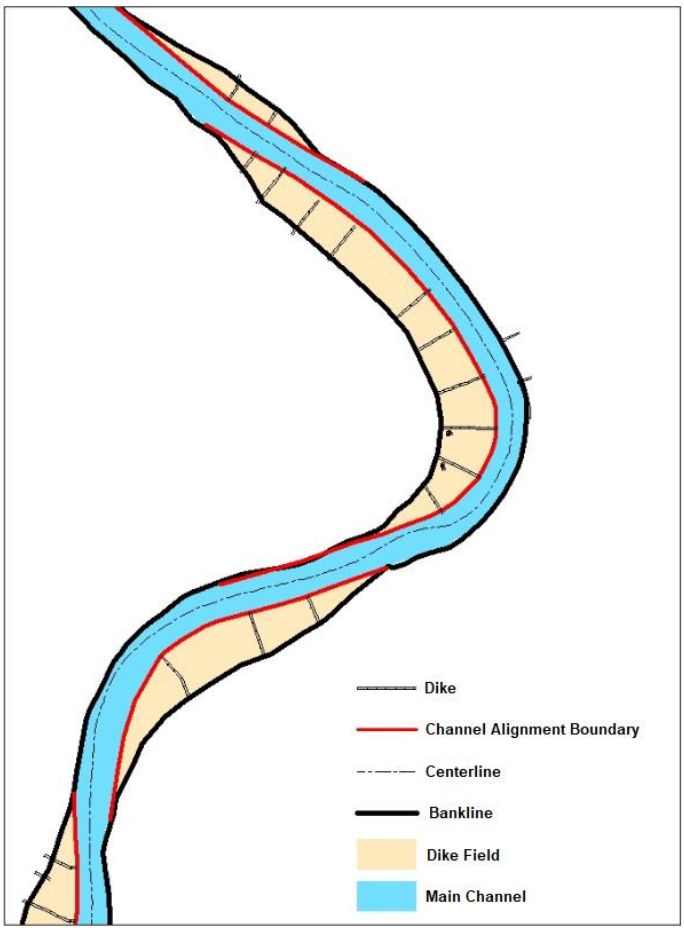

Figure 1. Illustrative sketch of the proposed channel delineation using channel improvement boundary

The developed database allows for the analysis of geometric and volumetric parameters (area, depth, width, conveyance, volume, etc.) over various water surface elevations and time periods, ranging from 1948 to 2015. In order to demonstrate the utility and efficacy of the methodology, preliminary results were produced for cross sectional area and channel volume changes between the 1988 and 2015 surveys at a water surface elevation of 20 feet referenced to the 2007 Low Water Reference Plane (LWRP). For the main channel cross sectional area data in Figure 2, the computed values were grouped into 5-mile representative reaches and median of differences were determined to provide a general representation of the dominant processes occurring on a reach level. The plot incorporates a bar plot with a secondary axis referring to the linear feet of dike construction per reach for the entire study area. The color scheme and bar graph were used to qualitatively relate the observed changes with the long-term system processes and dike construction for each reach.

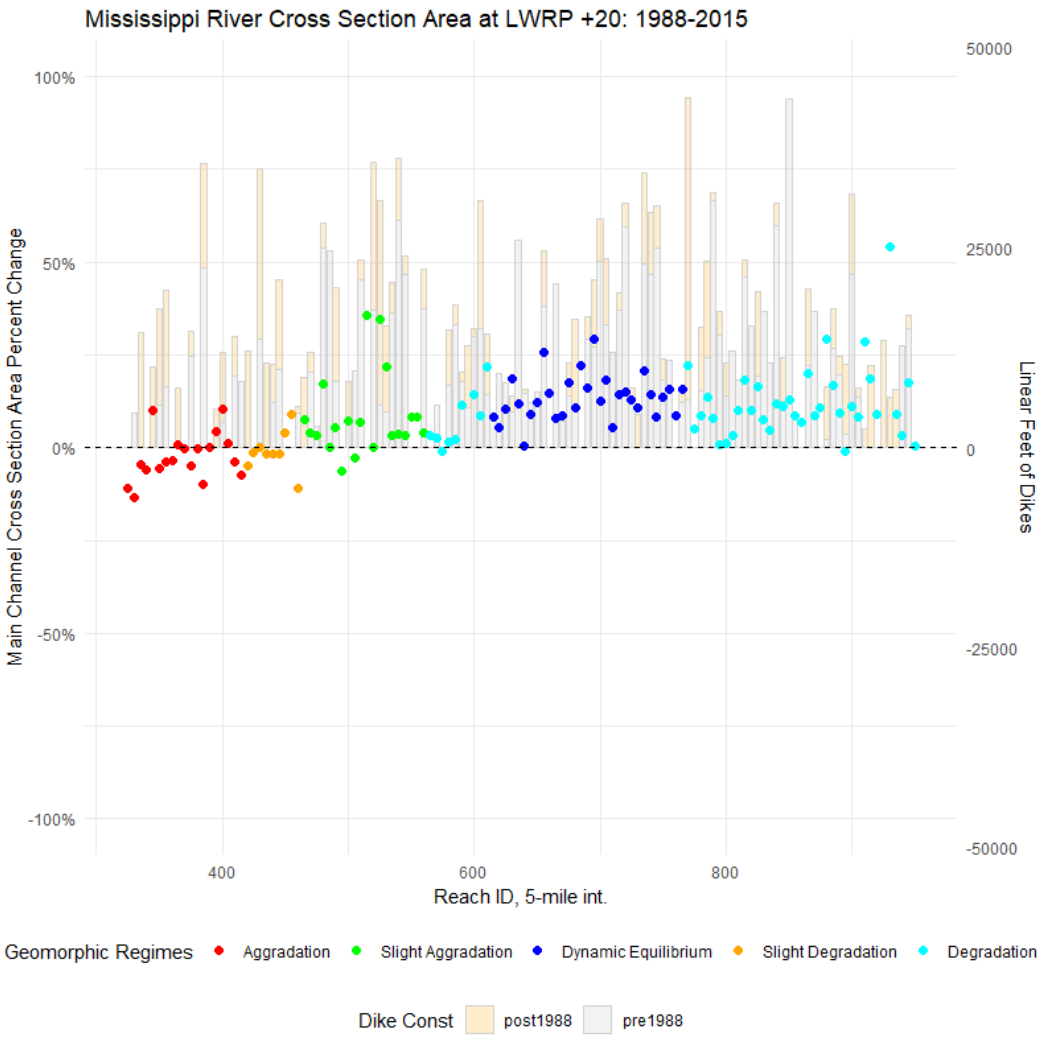

Figure 2. Percent Change in main channel cross section area at LWRP +20 from 1988 to 2015 for LMR RM 325 to 953

Using similar procedures described by Little et al. (2015), cumulative volume change curves for each delineated section were developed to determine the spatial extents of the average volumetric change rates over time (Figure 3). The slope of the curves can be used to describe the average rate of erosion or deposition per mile for the study reach between the two successive hydrographic surveys. The cumulative volume change curves developed using the proposed delineation template allow for further examination of the dike field and main channel areas in relation to the overall changes occurring along the reach.

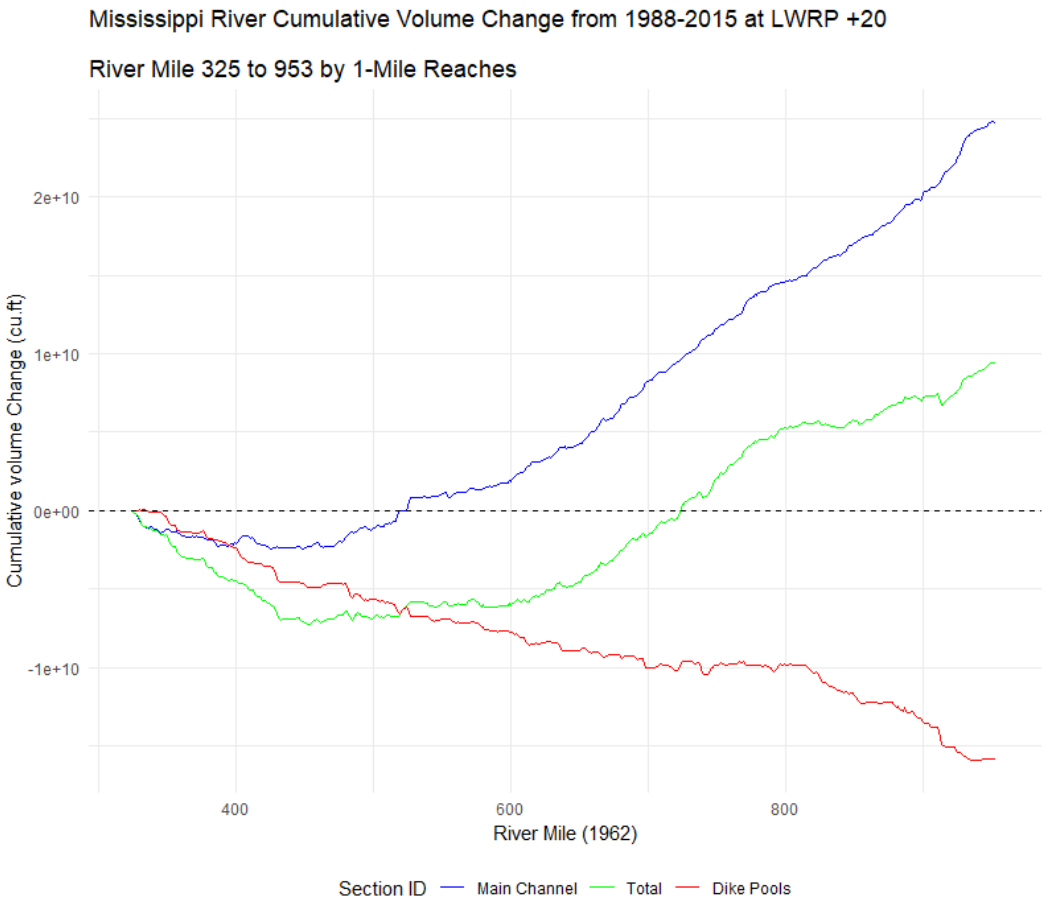

Figure 3. Cumulative volume at LWRP +20 from 1988 to 2015 for LMR RM 325 to 953

Although the database and improved methodology represents a major advancement in our ability to assess the morphologic trends in the Lower Mississippi River, it is by no means considered complete. Rather, it should be viewed as a framework which can be further enhanced as the database continues to be expanded and improved. For these reasons, the preliminary results presented should only be considered as one component of a systematic research program to assess the morphologic impacts of dike structures on the Lower Mississippi River.

References

Biedenharn, D.S., Hubbard, L., and Hofman, P.H., 2000, Historical Analysis of Dike Systems on the Lower Mississippi River. US Army Corps of Engineers Draft Report to U.S. Army Engineer Research and Development Center, Coastal and Hydraulics Laboratory, Vicksburg, MS, 172 p.

Cobb, S.P., and Magoun, A. D., 1985, "Physical and hydrologic characteristics of aquatic habitat associated with dike systems in the Lower Mississippi River, River Mile 320 to 610, AHP," Lower Mississippi River Environmental Program, Report 5, December 1985, P176.

Little, C.D. Jr., Biedenharn, D.S., Watson, C.C., Allison, M.A., McCullough, T., and Wofford, K., 2015, Channel Geometry Trends of the Mississippi River, Old River Control Complex to St. Louis, MO. Mississippi River Geomorphology & Potamology Program Report, USACE Mississippi Valley Division Science & Technology, and ERDC Coastal & Hydraulics Laboratory, (in press).

Channel Curvature and Sediment Supply Controls on the Morphology and Surface Grain Sorting of Meandering Gravel-Bed Rivers: Experimental Insights

Ryan Brown, Graduate Research Assistant, Colorado State University, Fort Collins, CO, now at River Design Group, Corvallis, OR, rbrown@riverdesigngroup.com
Peter Nelson, Associate Professor, Colorado State University, Fort Collins, CO, peter.nelson@colostate.edu

Introduction

Straight and meandering gravel bed rivers develop bar-pool bed topography and distinct bed sorting patterns. Field and flume observations have shown that straight channels with alternate bars tend to display coarse bar tops and fine pools (e.g., Mosley and Tindale, 1985; Lisle and Madej, 1992), while curved channels develop point bars that are finer than adjacent coarse pools (e.g., Bluck, 1971; Bridge and Jarvis, 1976; Whiting and Dietrich, 1991, Clayton and Pitlick, 2007). This reversal of the dominant bed sorting pattern is clearly linked to channel curvature, but we still do not fully understand how the flow field and bed topography in curved channels influence mixed-grain-size sediment transport to produce these patterns.

This extended abstract focuses on two experiments (low discharge and high discharge) conducted in a 20-degree curved channel under differing hydraulic and sediment boundary conditions. These are two experiments in a series of curved channel experiments to be conducted which all aim to document and provide insight on the mechanisms controlling bed topography and sorting in meandering gravel-bed rivers.

Methodology

These experiments were conducted in a 16-ft wide basin at the Colorado State University hydraulics lab. A 1.35-meter-wide curved channel was constructed in this basin with a 20-degree crossing angle as shown in Figure 1. The curve was based on a sine generated trace defined by $\phi = \omega \, sin\left(2\pi \frac{s}{m}\right)$ where ϕ is the angle the channel centerline makes with the horizontal down valley axes, ω is the angle the crossing angle of 20-degrees, s is the streamwise distance and m is the meander wavelength (Whiting and Dietrich, 1993). The downstream end had a metal tailbox with an adjustable tailgate to collect sediment transport out of the channel and control

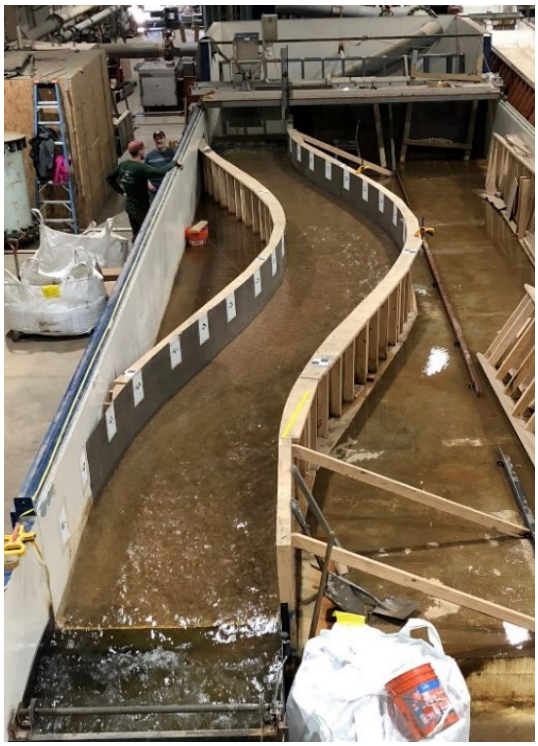

Figure 1. The channel where both experiments were conducted. Flow is from the top of the photo to the bottom. Sediment feeder is visible on scaffolding at upstream end.

the downstream water surface elevation. The rate of sediment leaving the flume was determined by drying and weighing the sediment collected in this tailbox at the end of each timed run. A sediment auger-type feeder was placed above the channel at the upstream end and fed sediment at a constant rate for the entire experiment. The remaining hydraulic, geometric, and sediment related parameters for both experiments are shown in Table 1.

Table 1. Experimental parameters for both the low discharge and high discharge experiments.

		Experiment Version	
Category	Parameter	Low Discharge	High Discharge
Geometry	channel length	15.2 m	15.2 m
	channel width	1.35 m	1.35 m
	wavelength	12.2 m	12.2 m
	crossing angle (ω)	20°	20°
	slope	0.005 m/m	0.007 m/m
Hydraulics	width-to-depth ratio	20	15
	mean depth	0.07 m	0.09 m
	discharge	0.04 cms	0.10 cms
	mean boundary shear stress (τ)	3.36 Pa	5.45 Pa
Sediment	bed material	sub-angular gravel	sub-angular gravel
	D_{16}	1.8 mm	1.8 mm
	D_{50}	3.3 mm	3.3 mm
	D_{84}	5.0 mm	5.0 mm
	mean Shields stress (τ^*)	0.065	0.105
	excess shear ratio (τ^*/τ^*_c)	1.6	2.6
	upstream feed rate	59 kg/hr	230 kg/hr

Each experiment was run under steady discharge and steady feed conditions until the bed reached dynamic equilibrium. We determined that dynamic equilibrium had been reached when the rate of sediment leaving the flume equaled the rate being fed at the upstream end, and when the bed exhibited a steady slope with no substantial areas of aggradation or degradation. The rate of sediment leaving the flume was determined by weighing the dried sediment collected in the tailbox after each timed run. Both the low and high discharge experiment reached this condition after 25 hours of run time.

During the initial 25 hours of runtime, the flume was drained periodically to allow for topographic bed surveys. These surveys were accomplished through structure-from-motion photogrammetry (Morgan, 2017). For the high flow experiment, the resulting point clouds had approximately one-millimeter spatial resolution and overall registration accuracies of less than one-centimeter. The low flow experiment point clouds are of slightly lower quality due to a different photographing and processing procedure. A final topographic survey was conducted at the end of the measurement period described below. To better visualize the bed morphology, the detrended elevation is computed by removing the reach average slope from the original topographic model.

Once the bed reached equilibrium, we collected extensive measurements of relevant morphodynamic metrics. Measurements included detailed water surface profiles, velocity profiles, and bedload measurements. These measurements were collected at cross sections spaced about half a channel width apart (0.7 m). The water surface profiles and velocity data are not presented in this abstract. It is important to note, because the bed was at equilibrium, we can compute the cross-stream bedload transport rates from the downstream rates measured by the Helley-Smith bedload sampler (Dietrich and Smith, 1984; Nelson et al., 2010). Finally, a series of photos were taken near the bed to be photo sieved (Graham et al., 2005) to determine the surface grain size distribution. A roughness index (Wilson et al., 2007) was also computed from the point cloud and used as a proxy for the distribution of relative grain sizes.

Results and Discussion

Both experiments produced the characteristic bar-pool morphology of curved channels, with two pools and one fully formed bar (Figure 2). In both cases, one pool was located just downstream of the bend apex, as expected, and one was located upstream against the right bank just at the start of the curve. This upstream pool was an artifact of the single bend geometry, as the first initiation of the bend acted as a bend apex, forcing the formation of a pool. Without the full bend, a fully developed point bar was not able to form at the upstream end of the channel.

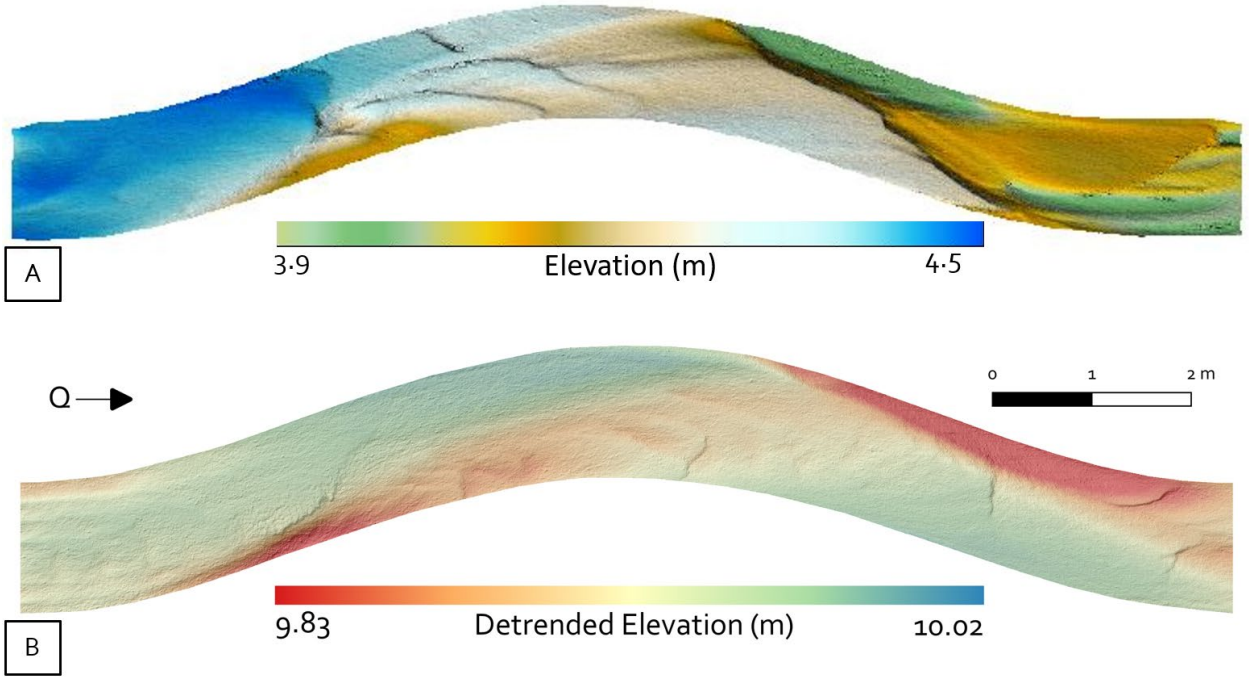

Figure 2. Equilibrium bed topography for the low flow (panel A) and high flow (panel B) experiments (panel A from Hanson (2016)).

Overall, the general morphology was very similar between the two experiments, despite having twice the discharge and nearly four times the sediment feed in the second design. This suggests that the formation of the bar pool morphology is primarily controlled by the channel geometry and is not a function of width-to-depth ratio (a function of discharge) or sediment supply. Morphologic differences between the two experiments include the fact that the bar top and the bottom of the pool are both located further downstream in the high flow experiment than they were in the low flow experiment. There are also minor differences in the amplitude of the bars

relative to their adjacent pool. In the low flow experiment, there was a slightly larger elevation difference between the pool and adjacent bar (approximately 0.4 m). In the high flow experiment, the bar amplitude was slightly less (approximately 0.2 m). Therefore, while the general morphology is a function of channel geometry, the discharge and sediment supply appear to control the size and shape of the expected morphology.

In general, the expected sorting patterns observed in curved channels have been attributed to secondary flow paths (Parker and Andrews, 1985; Ikeda, 1989; Clayton and Pitlick, 2007). However, our understanding of this process is limited. One key question that has not previously been addressed is identifying the threshold degree of curvature necessary for the expected sorting pattern of coarse pools and fine bars to initiate. Surface grain size data from the low and high flow experiments (Figure 3) demonstrate the difference in the characteristic sorting pattern. The low flow surface grain sizes estimated from automatic photo sieving show very little coherent sorting throughout the bed (Figure 3A). Observations of the flume bed at 25 hours confirm the lack of any substantial sorting patterns (Hanson, 2016). Initial results from the high flow experiment (Figure 3B) suggest that the expected sorting pattern formed under high discharge, high sediment feed conditions. Figure 3B results show the roughness of a 2 mm DEM created from the high-resolution point cloud; coarse areas exhibit higher roughness than fine areas. Roughness is defined here as the largest inter-cell vertical difference of a central pixel and its adjacent pixels (Wilson et al., 2007). In the region of the pool, the DEM is rougher, indicating that the pool is coarser than the bar top. Observations of the bed at the end of the 25-hour high flow run support the presence of these sorting patterns. Relative roughness is used for the high flow experiment because automatic photo sieving has not been completed yet.

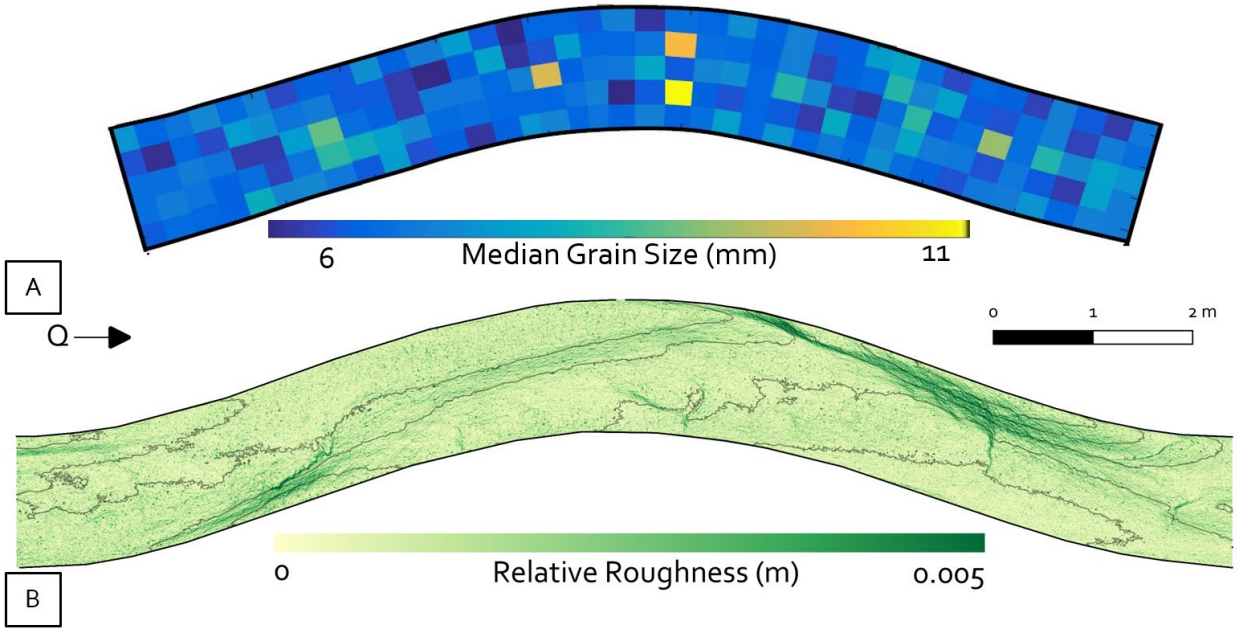

Figure 3. Median grain size determined via automatic photosieving for the low flow experiment (panel A) and relative roughness from a 2 mm raster for the high flow experiment (panel B).

These sorting results suggest that the formation of the characteristic curved channel sorting pattern is not solely a function of curvature, which remained constant between the two experiments. Rather, the expected sorting pattern requires not just a certain degree of curvature, but high enough sediment supply, and enough flow to transport the high sediment supply. Given the overall coarsening of the bed during the low flow experiment, we also

speculate that the sediment supply was low enough to cause armoring of the bed, as the slope was not allowed to adjust.

Conclusions

Comparing bed morphology and surface sorting in two experiments with identical geometry but differing hydraulic and sediment conditions allows us to evaluate geomorphic and hydraulic controls on channel morphology and surface sorting. Although channel curvature determines the overall morphologic patterns (point bars and pools), the sediment supply and width-to-depth ratio control specific meandering channel morphology and sorting patterns. Furthermore, we conclude that sufficient sediment supply is necessary to develop characteristic sorting patterns, in addition to channel curvature.

We have also collected large bedload transport and velocity profile datasets for both the low and high flow experiments presented here. We expect that these data will provide insight into the hydrodynamic and morphodynamic processes in river bends that control bar-pool formation and characteristics. These experiments will represent the first near-field scale flume experiments in which detailed velocity measurements can be coupled with bedload transport data. With these data we hope to identify any coupling between size selective cross-stream sediment transport and secondary flow patterns.

Acknowledgements

We would like to thank the U.S. National Science Foundation (grant EAR-1455259) and Colorado State University for funding this project, as well as Tess Hanson for the use of her data and personal observations, Danny White and David Cortese for assistance with the flume, and Annette Patton for her feedback on this project.

References

Bluck, B. J. 1971. “Sedimentation in the meandering River Endrick,” Scottish Journal of Geology, 7:93-138.

Bridge, J. S. and Jarvis, J. 1976. “Flow and sedimentary processes in the meandering River South Esk, Glen Clova, Scotland,” Earth Surface Processes, 1(4):303-336.

Clayton, J. A. and Pitlick, J. 2007. “Spatial and temporal variations in bed load transport intensity in a gravel bed river bend,” Water Resources Research, 43(2).

Dietrich, W. E. & Smith, J. D. 1984. “Bed load transport in a river meander,” Water Resources Research, 20(10):1355-1380.

Graham, D. J., Reid, I., and Rice, S. P. 2005. “Automated sizing of coarse grained sediments: Image-processing procedures,” Math. Geol., 37(1):1–28.

Hanson, T. C. 2016. Flow, sediment transport, and bed topography in straight and curved gravel-bed channels. Diss. Colorado State University. Libraries.

Ikeda, S. 1989. "Sediment transport and sorting at bends,” River Meandering, American Geophysical Union Water Resources Monograph. (pp. 103-25). Washington, DC: American Geophysical Union.

Lisle T. E. and Madej, M. A. 1992. “Spatial variation in armouring in a channel with high sediment supply,” In Billi, Hey, Thorne, & Tacconi (Eds.), Dynamics of Gravel-Bed Rivers. (pp. 277-93). Chichester, UK: John Wiley & Sons.

Morgan, Jacob A., Daniel J. Brogan, and Peter A. Nelson. "Application of Structure-from-Motion photogrammetry in laboratory flumes." Geomorphology 276 (2017): 125-143.

Mosley, M. P. and Tindale, D. S. 1985. “Sediment variability and bed material sampling in gravel-bed rivers,” Earth Surface Processes and Landforms, 10(5):465-482.

Nelson, P. A., Dietrich, W. E., and Venditti, J.G. 2010. “Bed topography and the development of forced bed surface patches,” Journal of Geophysical Research, 115.

Parker, G. and Andrews, E. D. 1985. “Sorting of bed load sediment by flow in meander bends,” Water Resources Research, 21(9):1361-1373.

Whiting, P. J. and Dietrich, W. E. 1991. “Convective accelerations and boundary shear stress over a channel bar,” Water Resources Research, 27(5):783-796.

Whiting, P. J. & Dietrich, W. E. 1993. “Experimental constraints on bar migration through bends: Implications for meander wavelength selection,” Water Resources Research, 29(4):1091-1102.

Wilson, Margaret FJ, et al. "Multiscale terrain analysis of multibeam bathymetry data for habitat mapping on the continental slope." Marine Geodesy 30.1-2 (2007): 3-35.

Field-Scale Sediment Feed Flume: Upper Santa Ana River, California

Scott A. Wright, U.S. Geological Survey, California Water Science Center, Sacramento CA, sawright@usgs.gov
J. Toby Minear, Cooperative Institute for Research in Environmental Sciences, University of Colorado, Boulder, CO, tminear@colorado.edu

Extended Abstract

The Santa Ana River moves water and sediment from the headwaters in southern California's San Gabriel and San Bernardino Mountains to the Pacific Ocean near Newport Beach. Along the San Bernardino Valley, the river decreases in slope, increases in width, and deposits particles from boulders to sand as it loses transport capacity. Episodic rainfalls feed very large winter floods, but dry summer and fall periods lead to extensive dry alluvial reaches due to surface water infiltration into subsurface aquifers. Within one of these dry reaches, a small inset channel has developed to effectively convey year-round wastewater discharges. The inset channel is about 10-m wide, and during dry phases, is the only surface water present within the larger 250-m wide flood channel (Figure 1). This flow creates a coarse bed substrate composed of gravel and cobble that is home for diatoms and algae, the diet for the Santa Ana Sucker, a threatened native fish. Below we explore the sediment transport dynamics and conditions necessary to maintain a coarse bed substrate to host food for the Santa Ana Sucker.

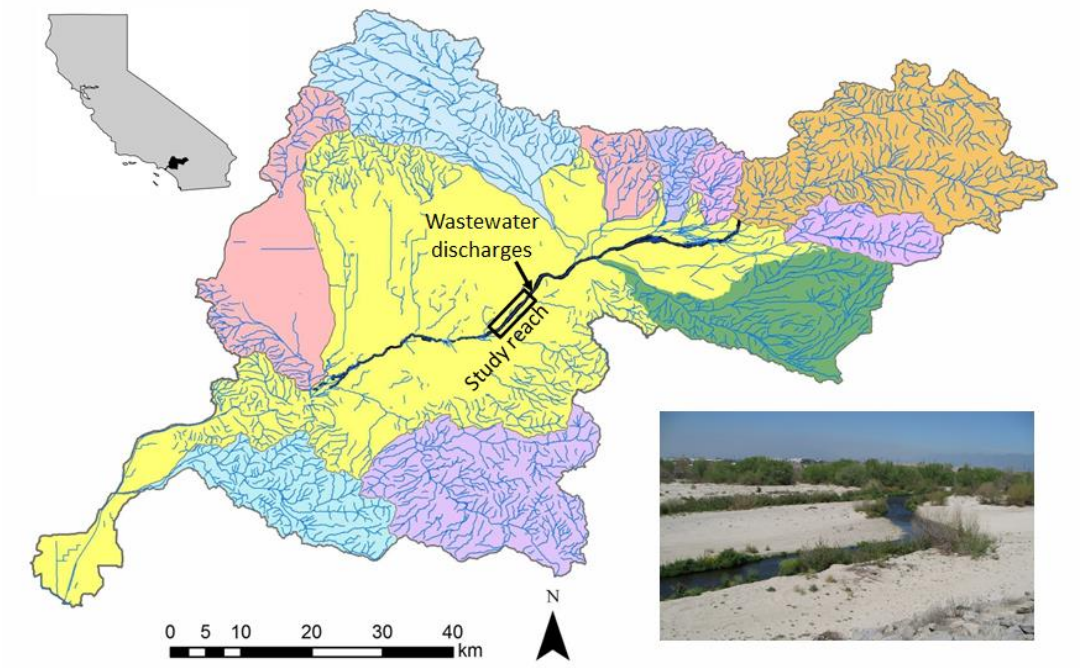

Figure 1. Map of the Santa Ana watershed showing the location of the wastewater discharges and the study reach. The study reach is in the San Bernardino Valley at an elevation of about 300 m; the high elevations in the tributary basins exceed 3000 m. Photo shows the inset channel immediately downstream from the wastewater discharges.

We began with a conceptual model in which the inset channel behaves like a sediment feed flume, with upstream supplies of water and sediment that are mostly independent. Sediment (primarily sand during most flows) moves into the reach with infrequent upstream flow during winter runoff. During these events, the inset channel can fill almost completely with sand, and/or avulse across the floodplain. During the dry season, the previously deposited sands are winnowed from the inset channel by constant, clear-water releases from the wastewater plants, exposing gravel and cobble.

This conceptual model is based in well-established theory, and supported by field-based observations:

- Shear stresses in the inset channel are capable of transporting sand as bedload, but not gravel and cobble. Bedload measurements (at several locations and times under wastewater discharge conditions) indicate that about 90% of the bedload is sand. The median grain size of bedload samples is consistently in the 0.5–1-mm range with little longitudinal variability.

- The upstream supply of sand decreases through time as winnowing proceeds in the downstream direction. Bedload transport rates increase in the downstream direction by an order of magnitude over just 7 km, despite the fact that water discharge decreases downstream due to infiltration (typically by 25–50% over the 7-km reach).

- The location of the gravel-to-sand bed transition is variable from year to year and is related to the amount of time that has elapsed since the most recent upstream runoff event. These events supply new sediment to the reach and reset the winnowing process.

- Direct observations of the inset channel following upstream runoff events revealed many instances of large areas of substantial sand deposition in the channel, in areas that were previously entirely gravel and cobble sizes.

In summary, the bed substrate of the inset channel at any given time and location is a function of 1) the distance downstream from the wastewater discharges, 2) the time since the most recent upstream sediment-supplying runoff event, and 3) the wastewater discharge levels and infiltration rates in the reach. The wastewater discharge levels are of particular interest to local managers because proposals have been made to change release levels. Altering the discharge levels could affect the amount of coarse sediment (gravel and cobble) available or the amount of time required to expose the coarse sediment, impacting native fish.

To assess this effect, we are developing a one-dimensional model of bedload transport and bed substrate in the study reach. Preliminary results indicate that the winnowing process is quite sensitive to wastewater discharge levels, a likely result of the non-linear relationship between bedload transport and shear stress. The calibrated model can be used to assess how treatment plant discharge levels might be used to strategically manage winnowing rates and the amount of gravel and cobble exposed on the bed in the reach. Future model applications will be focused on evaluating the effects of various discharge scenarios on winnowing rates and coarse sediment exposure.

Fluvial Geomorphology in an Arid Environment: A Case Study

David T. Williams, PhD, PE, PH, CFM, CPESC, D.WRE
David T. Williams and Associates: david@dtwassoc.com
And **Joanna Czarnecka, EIT**
Watermia Consulting, LLC

Abstract

The Galisteo Creek Watershed, a 669-square mile drainage basin (428,160 acres), is located in central New Mexico, spanning west San Miguel County, south-central Santa Fe County and eastern Sandoval County. It is part of what is considered the Middle Rio Grande Basin, also termed the Albuquerque Basin. A fluvial geomorphology study was requested by the U.S Army, Los Angeles District, on behalf of the Kewa Pueblo Tribe, to determine future conditions of the Creek meanders and their migration and extension rates in order to safely locate potential infrastructure.

The primary methodology use was from FHWA (2004b) and supplemental NCHRP Report 533 (FHWA 2004a), "Handbook for Predicting Stream Meander Migration." The GIS tools cited in these documents (Data Logger and Channel Migration Predictor) are no longer available but the methodology used in these references is still valid. The approach is similar to HEC-20 method (FHWA 2012).

The low flow channel alignments were prepared with drawing tools using ArcGIS software (ESRI 2011).

Introduction

A fluvial geomorphology study was requested by the U.S. Army, Albuquerque District, on behalf of the Kewa Pueblo Tribe, to determine future conditions of the Galisteo Creek meanders and their migration and extension rates in order to predict future locations of the channel. The future conditions were for the 25- and 50- year projections so that the Tribe could use the results for planning of their infrastructure.

Site Description

General Description

The Galisteo Watershed, a 669-square mile drainage basin (428,160 acres), is located in central New Mexico, spanning west San Miguel County, south-central Santa Fe County and eastern Sandoval County. It is part of what is considered the Middle Rio Grande Basin, also termed the Albuquerque Basin. The Galisteo Watershed is part of the Rio Grande Santa Fe hydrologic unit (HUC: 13020201) (Earth Works Institute 2005).

The Galisteo Watershed is located immediately south of Santa Fe, New Mexico and is bounded on the west by La Bajada Hill, Cerrillos Hills, and the heights of San Marcos; on the east by Glorieta Mesa (sometimes called Rowe Mesa); and on south by the Ortiz Mountains and the escarpment of the Estancia Basin. A Vicinity map of the study area is shown in Figure 1.

Figure 1: Fluvial Geomorphology *Vicinity Map*

Galisteo Creek is an ephemeral creek (defined as a stream that flows only during and immediately following a period of rainfall in the immediate locality) and is subject to extremes between dry conditions and flash floods. The variable hydrologic regime creates a stream dynamic where banks tend to be unstable and new meanders can suddenly cut through established riparian areas. To prevent this, channel stabilization or re-directive methods would be needed.

Overview of Channel Characteristics within the Study Area Limits

Water quality in the Galisteo Creek is reduced by stream bottom sediment, caused by the cumulative and historical impacts of grazing, urban development and major stream modifications related to railway and agriculture in the past 125 years. The Galisteo Creek is an ephemeral stream in short parts but is mostly an intermittent stream of which flows include both snowmelt and summer storm flows. Only about 10 percent of the stream length is perennial.

In many places, the stream is incised in the landscape, which leads to dried out grasslands, dissected by gullies, and susceptible to erosion. Ongoing urban development in the upper watershed leads to annually increasing rates of stormwater runoff and peak flows in the Galisteo Creek. The changes in the ecological and cultural landscapes over the years have contributed to declining ecological health of the stream. It also has led to poor vegetation cover and diversity and accelerated levels of erosion through lateral movement of the meanders. The watershed experiences constant flooding, erosion issues and water table drawdown.

Grain size of D_{50} (median diameter value of particle size distribution) in the vicinity of the project generally consists of particles 2 mm or less. The main channel width varies from 25 ft. to 2,000 ft. wide. Vegetation consists mostly of shrubs and bushes, including Tamarisk and Russian Olives. These problems are addressed by continuous studies and support from the local Galisteo Watershed Partnership (GWP) watershed association established in 2005.

Hydraulic characteristics of the study area were collected from USGS StreamStats Version 4.1.2 (USGS 2017). Output is based on the USGS regression equation for New Mexico from the USGS (2008).

For the purpose of this study, the 5-year discharge was used as the dominant discharge, often characterized as the channel forming discharge. This relatively high frequency event is appropriate for arid and semi-arid regions. Based on the cited information and using StreamStats, the 5-year flow for the basin upstream of I-25 and below the Galisteo Dam is 4,030 cfs. Note that this value does not take into consideration the peak flow attenuation due to Galisteo Dam located upstream of the project site.

The 5-year peak flow of 4,030 cfs from StreamStats is comparable to an HEC-HMS model results for the 5-year, 6-hour storm of 3,218 cfs. For further analysis, the HEC-HMS result of 3,218 cfs was used as the channel forming (dominant) discharge.

GIS Aerial Mapping Overlays

Data Collection

Data collection includes aerial photography, imagery and map resources representing multiple records over the years for comparison and evaluation of the Creek geomorphology.

Sources of the aerial photography and other physical date for this study included:

- Google Earth: version 7.1.7.2606, Build Date: October 6, 2016
  https://www.google.com/earth/explore/products/

- Earth Data Analysis Center (EDAC) at the University of New Mexico
  http://edac.unm.edu/image-archive/

- New Mexico Resource Geographic Information System (RGIS is part of the EDAC), hosted and managed by the Earth Data Analysis Center at University of New Mexico http://rgis.unm.edu/

- New Mexico Bureau of Geology and Mineral Resources, interactive maps
  http://geoinfo.nmt.edu/maps/

- The aerial imagery was obtained from Google Earth Pro software (https://www.google.com/earth/download/gep/agree.html) for the following years: 1996, 2006, 2009, 2014, and 2016.

- The historic imagery for year 1935 was obtained from Resource Geographic Information System (RGIS) at: http://rgis.unm.edu/getdata/#.

- Digital terrain model was supplied by Bohannan-Huston Inc. (2016), through their ftp site.

Other resources not referenced above were investigated to compare the quality of available data. The decision was made to use only the data referenced due to availability and quality of data.

Google historical imagery was downloaded for good representation of channel alignment changes. Markers were placed on Google maps at strategic locations and points were registered. After images were overlaid using GIS software, images were geo-referenced to known location with use of these registration points. After the images were scaled and geo-referenced, all the maps were traced in GIS for the location of the low flow channel (termed Centerline) and channel overbanks (bank lines) based on visual inspection of the image. Quality of the images played a crucial part in this step of the

process. All six historic images (1935, 1996, 2006, 2009, 2014, and 2016) were used for the initial evaluation.

After careful evaluation, it was decided that to best represent historical changes within this watershed and considering the quality of the data, index three years of record imagery would be used for evaluation of the fluvial geomorphology of the Creek. The years chosen for that purpose were images from years 1935, 1996, and 2016.

Aerial Imagery with Stream Centerline Alignment and Bank Lines

As an example, the channel centerline and right and left bank lines that were traced over the 2017 aerial photography and were geo-referenced into the GIS ArcMap 10.5 software are shown below in Figure 2.

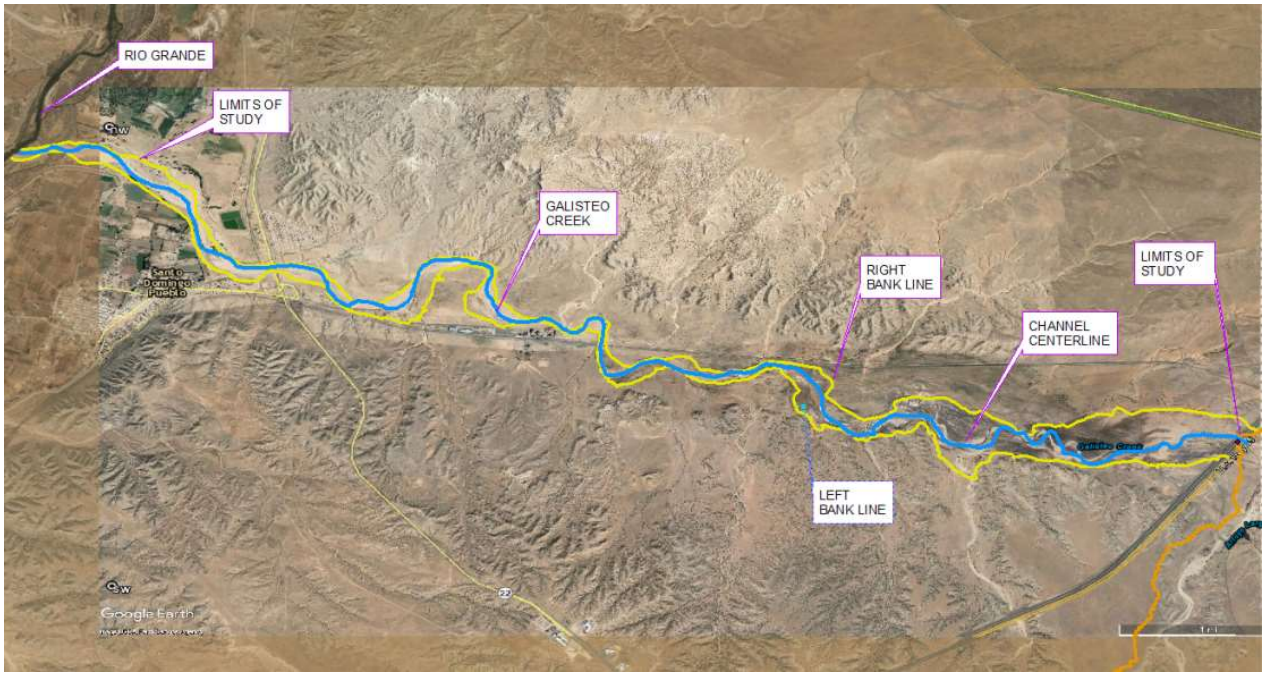

Figure 2: Bank Lines and Channel Centerline, Aerial 2017

Key Points of Study Interests

The key objective of this study is to determine future conditions of the Creek meanders and their migration and extension rates in order to predict future locations of the channel. The following assessments are made:

- Predict the Creek's future planform locations.
- Assess potential for floodplain creation or abandonment and potential for incision or aggradation.
- Document significant possible sites of sediment inflow that could influence the planform movement of the Creek.

The key parameters determined for this study are listed below and described in detail in the following sections:

- Sinuosity index (a dimensionless term representing the ratio of the sinuous length over the straight length of the channel)
- parameter (a measurement of the number of bars or islands in a channel)
- Existing Channel Slope

Methodology

Document Sources

Historic "threads" (thalweg) of the Creek were determined from the sources presented earlier. Other relevant Creek features evaluated for current conditions and over time (if discernible), were (but not limited to) average active bank widths and locations, depths, sinuosity index, braiding parameter, and slope. These Creek features were similar to those described in "Stream Stability at Highway Structures" (FHWA 2012). The technique for evaluation of future meander changes over time was based upon FHWA (2004b).

The validation of the prediction technique utilized the document "Sediment and Erosion Guide," AMAFCA (1994) starting on page 3-66 and generally utilizing the procedures starting on page 3-74. The timing of the lateral movement was determined by analysis of the historic lateral movement over time and projected to the maximum lateral erosion, similar to the method in the NCHRP document. This analysis procedure is from section 3.4.3 of the AMAFCA manual (1994). The technique for additional validation of historic meander change over time was based upon (FHWA 2004a), Chapter 6.3.2. Where applicable, the methods from FHWA (2004b) and AMAFCA (1994) were compared for reasonableness of the results.

Calibration and Confirmation

There is very little site-specific information on meander migration or lateral movement of channels for use in the calibration or confirmation process. This means that regional analysis is the only way to determine if the study results are reasonable. A literature search was conducted for the arid southwest to obtain regional data and to identify potential transferability of that data to the project, based upon climate, watershed altitude, drainage area, cover and soils, and other relevant physical parameters. However, the literature search resulted in very little usable information. Engineering judgment, evaluation of meander tendencies and prediction, and the AMAFCA document were the basis for the evaluation of the reasonableness of the results.

Sinuosity Index Calculations

Sinuosity of the channel measures the deviation of a line representing the channel centerline from the shortest path along the valley and is calculated by dividing the total length of the channel by this shortest possible path. A straight channel would have a sinuosity index equal 1.

To calculate sinuosity of channel centerlines at different times, Creek centerlines were drawn in GIS. The Python toolbar "Calculate sinuosity" was downloaded from ArcGIS website (ESRI 2011) (https://www.arcgis.com/home/item.html?id=00e708a448b74810a0e805c4a97f9d46). The results of this analysis at historic times are presented in Table 1.

The difference in elevations at the ends of the project varied slightly over time but was held constant at 204.1 feet to compute the channel slope. The valley length also varied slightly over the years but was held constant at 35,006 feet. The results showed a gradual increase in the sinuosity, indicating that meandering is gradually increasing also.

Table 1: Sinuosity Index and Channel Slope Results

Year	Total Channel Length (ft)	Sinuosity Index	Channel Slope
1935	43319	1.238	0.00471
1996	44714	1.278	0.00456
2006	46158	1.319	0.00442
2009	48009	1.372	0.00425
2014	45785	1.308	0.00446
2016	46397	1.325	0.00440

Soil Map

The soils map was obtained from the New Mexico GIS data website (http://rgis.unm.edu/getdata/) (University of New Mexico 2016) and includes shapefiles from the Soil Survey 2013.

Based on this map, the majority of soils within the study area are type Qa – Latest Pleistocene to Holocene Alluvium Undifferentiated, Quaternary alluvium (Stewart and Carlson geologic unit). These types of soils represent unconsolidated sediment and are easily eroded. Since the Creek meander belt is almost wholly contained in the area represented by soil type Qa, the meander predictions would not be affected by encountering different types of soils that would have different strength characteristics. Harder soils in the meander belt were very sparse and did not present a consistent barrier to meander migration.

Lateral Migration Analysis

Lateral Migration of Existing Base Flow Channel

The lateral migration rate of the low flow channel, as defined by the channel centerline, was calculated based on the method outlined in NCHRP Document 67, “Methodology for Predicting Channel Migration,” 2004 and supplemental NCHRP Report 533, “Handbook for Predicting Stream Meander Migration,” 2004. GIS tools cited in these documents (Data Logger and Channel Migration Predictor) are no longer available but the methodology used in these references is still valid. The approach is similar to HEC-20 method, “Stream Stability at Highway Structures” (FHWA 2012).

Three separate low flow channel alignments were prepared with drawing tools using ArcGIS software (ESRI 2011). These outlines of channel centerlines, fitting circles and bank lines for aerial photography were performed for years 1935, 1996 and 2016 with 1935 shown in Figure 3 for illustration. Fitting circles and how they are drawn are described later.

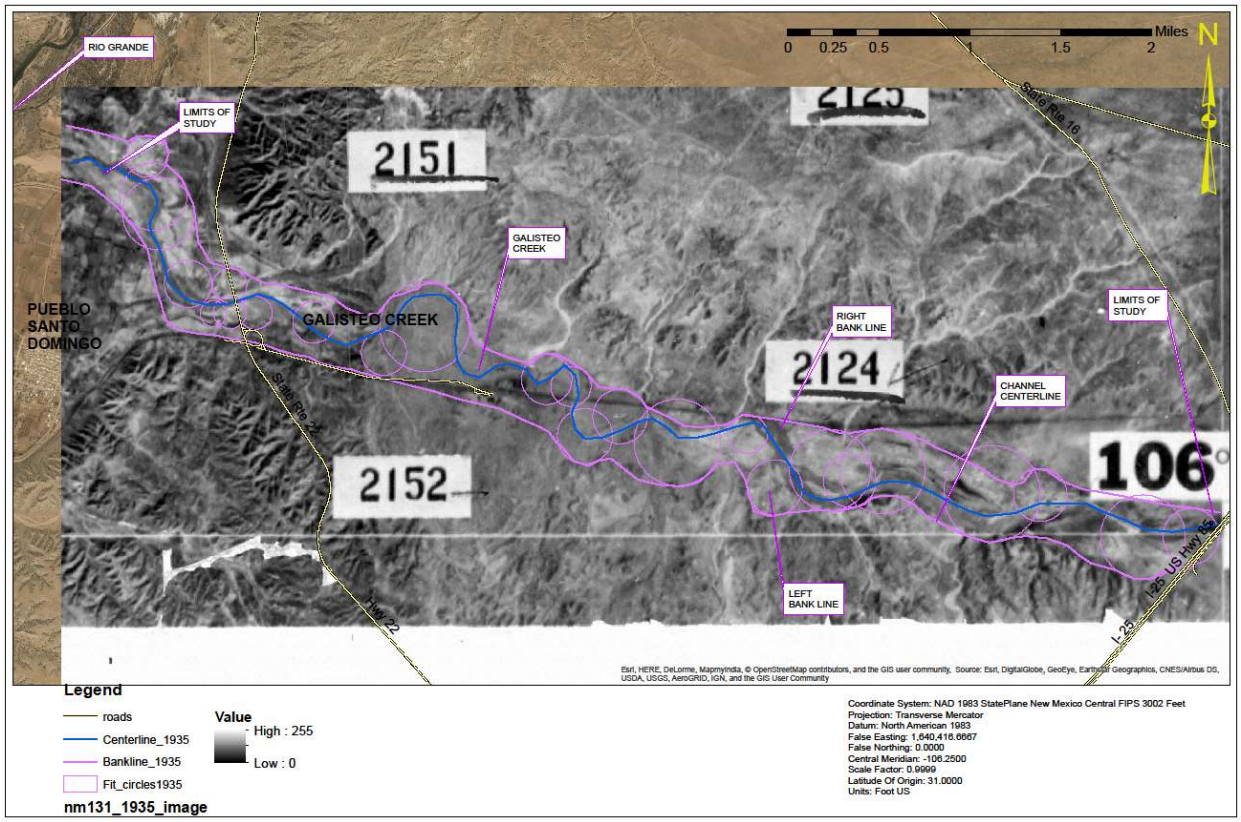

Figure 3: The 1935 Aerial with Centerline, Fitting Circles and Bank Lines

Methodology for Fitting Circles

Based on the NCHRP method, best fit circles were drawn using GIS at meandering loops for all the aerial photographs. These circles are best fit to each bend and are drawn tangential to the outer banks at the apex of the loop. For detailed descriptions of circle fitting, see the NCHRP manuals referenced above or the HEC-20 document.

Each of the bank lines and circles for a given year share the same color for easy differentiation while comparing between different years. After circles were identified in the ArcGIS software while still using separate imagery for each of the alignments, circles, and bank lines, the files were transferred to the CAD software. AutoCAD Civil 3D was used to further evaluate the stream geomorphology. For all three representative years, 1935, 1996, and 2016, at each bend, circle centers were identified and arrows were drawn to represent the direction of change in the channel morphology.

Two separate time comparisons were used based on the fact that Galisteo Dam was built in 1970s. The first time period captures the years 1935 to 1996 and second, the years 1996 to 2016. The first period represents the changes in the Creek geomorphology before the dam was built and the second after dam was built. Ideally, the time division between the two periods would have been the year 1970 (equal durations for each time period); however, good quality data was not available near that time. The next step was to include diameters of these circles for further evaluation of changes to the channel. Width of the channel was captured at this step at various locations.

Comparisons between years 1935 and 1996 are shown in **Figure 4**.

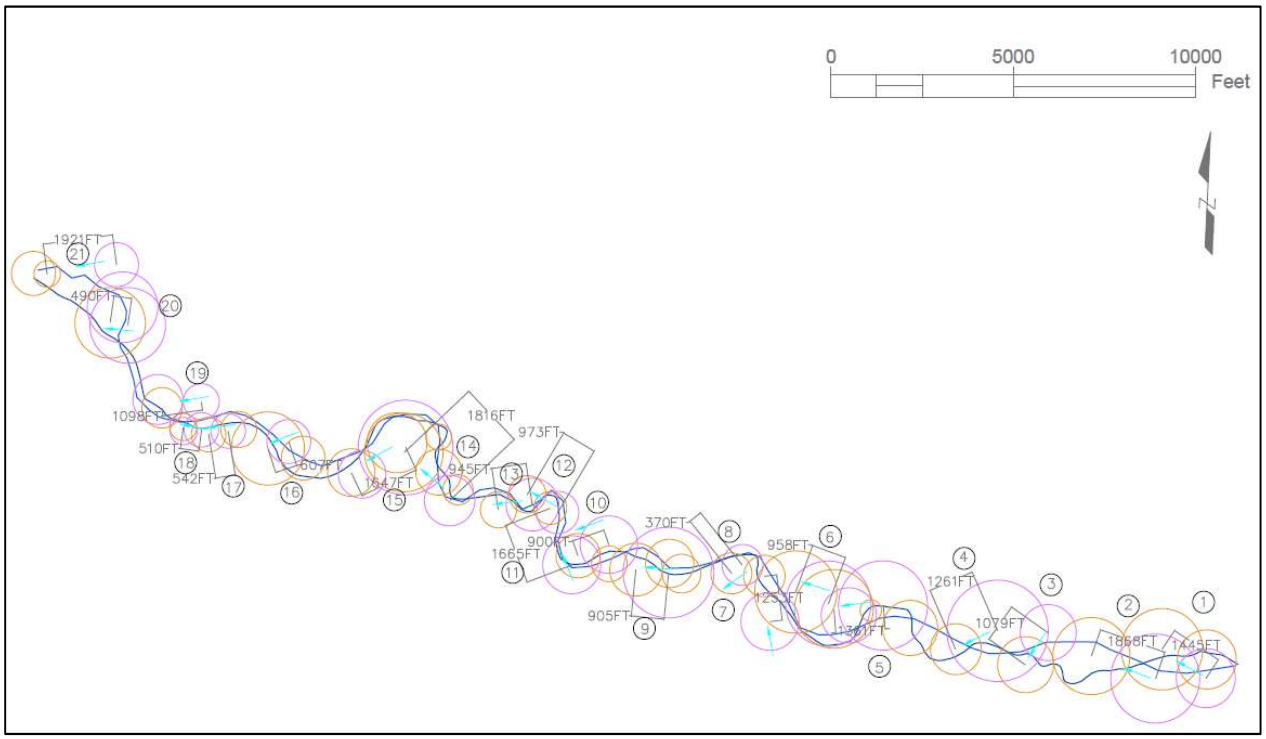

Figure 4: 1935 and 1996 Bank Line and Fitting Circles Changes

For all three years, the radius of curvature and distance between circle centers were recorded. Two tables were prepared to compare the results for pre- Galisteo Dam and post-Galisteo Dam conditions. The projections to 25 and 50 years into the future (from 2016) are discussed in the next section. Results are presented in Tables 2 and 3.

Table 2: Results for Radius and Bend Migration 1935 to 1996 and 25- and 50-Year Predictions

Circle ID	Radius R		Distance between centers 1935-1996	Change in radius 1935-1996	Radius change per year (in 61 years)	Center migration per year	New Center and Radius in 25 years		New Center and Radius in 50 years	
	1935	1996								
No.	ft	ft	ft	ft	ft	ft	Radius 25 yrs(ft)	Distance 25 yrs (ft)	Radius 50 yrs(ft)	Distance 50 yrs (ft)
1	808	1119	1445	-311	-5.1	23.7	-127.5	592.2	-254.9	1184.4
2	1221	1058	1868	163	2.7	30.6	66.8	765.6	133.6	1531.1
3	767	767	1079	0	0.0	17.7	0.0	442.2	0.0	884.4
4	1390	700	1261	690	11.3	20.7	282.8	516.8	565.6	1033.6
5	1224	1079	1361	145	2.4	22.3	59.4	557.8	118.9	1115.6
6	1171	1129	958	42	0.7	15.7	17.2	392.6	34.4	785.2
7	796	567	1253	229	3.8	20.5	93.9	513.5	187.7	1027.0
8	562	562	370	0	0.0	6.1	0.0	151.6	0.0	303.3
9	1247	724	905	523	8.6	14.8	214.3	370.9	428.7	741.8
10	787	606	900	181	3.0	14.8	74.2	368.9	148.4	737.7
11	796	450	1665	346	5.7	27.3	141.8	682.4	283.6	1364.8
12	578	512	973	66	1.1	16.0	27.0	398.8	54.1	797.5
13	724	495	945	229	3.8	15.5	93.9	387.3	187.7	774.6
14	694	1079	1816	-385	-6.3	29.8	-157.8	744.3	-315.6	1488.5
15	1298	650	1647	648	10.6	27.0	265.6	675.0	531.1	1350.0
16	602	1004	607	-402	-6.6	10.0	-164.8	248.8	-329.5	497.5
17	477	474	542	3	0.0	8.9	1.2	222.1	2.5	444.3
18	474	373	510	101	1.7	8.4	41.4	209.0	82.8	418.0
19	493	555	1098	-62	-1.0	18.0	-25.4	450.0	-50.8	900.0
20	1038	969	490	69	1.1	8.0	28.3	200.8	56.6	401.6
21	604	362	1921	242	4.0	31.5	99.2	787.3	198.4	1574.6
							Year 2041	Year 2041	Year 2066	Year 2066

Table 3: Results for Radius and Bend Migration for years 1996 to 2016 and 25- and 50-Year Predictions

Circle ID	Radius R		Distance between centers 1996-2016	Change in radius 1996-2016	Radius change per year (in 20 years)	Center migration per year	New Center and Radius in 25 years		New Center and Radius in 50 years	
	1996	2016								
No.	ft	ft			ft	ft	Radius 25 yrs(ft)	Distance 25 yrs (ft)	Radius 50 yrs(ft)	Distance 50 yrs (ft)
1	808	808	195	0	0	9.75	0	243.75	0.0	487.5
2	1119	1119	133	0	0	6.65	0	166.25	0.0	332.5
3	1058	1058	682	0	0	34.1	0	852.5	0.0	1705.0
4	767	767	105	0	0	5.25	0	131.25	0.0	262.5
5	700	844	639	-144	-7.2	31.95	-180	798.75	-360.0	1597.5
6	757	470	881	287	14.35	44.05	358.75	1101.25	717.5	2202.5
7	1079	1079	161	0	0	8.05	0	201.25	0.0	402.5
8	1129	567	666	562	28.1	33.3	702.5	832.5	1405.0	1665.0
9	567	562	875	5	0.25	43.75	6.25	1093.75	12.5	2187.5
10	562	1171	962	-609	-30.45	48.1	-761.25	1202.5	-1522.5	2405.0
11	724	724	103	0	0	5.15	0	128.75	0.0	257.5
12	487	487	118	0	0	5.9	0	147.5	0.0	295.0
13	606	595	162	11	0.55	8.1	13.75	202.5	27.5	405.0
14	450	450	90	0	0	4.5	0	112.5	0.0	225.0
15	512	512	113	0	0	5.65	0	141.25	0.0	282.5
16	495	495	101	0	0	5.05	0	126.25	0.0	252.5
17	415	415	73	0	0	3.65	0	91.25	0.0	182.5
18	631	587	201	44	2.2	10.05	55	251.25	110.0	502.5
19	354	453	290	-99	-4.95	14.5	-123.75	362.5	-247.5	725.0
20	824	824	196	0	0	9.8	0	245	0.0	490.0
21	650	650	161	0	0	8.05	0	201.25	0.0	402.5
22	602	602	465	0	0	23.25	0	581.25	0.0	1162.5
23	1004	1004	933	0	0	46.65	0	1166.25	0.0	2332.5
24	474	373	651	101	5.05	32.55	126.25	813.75	252.5	1627.5
25	555	373	186	182	9.1	9.3	227.5	232.5	455.0	465.0
26	969	881	173	88	4.4	8.65	110	216.25	220.0	432.5
27	604	604	487	0	0	24.35	0	608.75	0.0	1217.5
							Year 2041	Year 2041	Year 2066	Year 2066

Lateral Migration for 25- and 50- years Projections

Two future time frames were chosen for evaluation of the movement of the meanders in Galisteo Creek, 25- years and 50- years. The base year was 2016 and future years are 2041 and 2066.

In these time frames, each of the bends will migrate to a new location as predicted by the methodology. The radius of the circles will change also. Only the time period between 1996 and 2016 will be used for the evaluation of the migration of the meanders since the time period between 1935

and 1996 included time before construction of Galisteo Dam, and the radius change and center of circle migration were not affected by the Dam in that earlier time period.

Based on the results in Table 3, some of the radius changes for the fitted circles are negative. In those areas, the fitted circles produce significant overlaps of the meanders represented by the fitted circles, and connection of these circles result in drawing a severe meander.

When the sinuosity reaches approximately 3.7, the meander "folds" on itself and a cutoff would occur, resulting in a bend that is slightly straightened out and thus producing a negative bend radius change. Figure 5 shows an illustration of this phenomenon. After the cutoff is naturally created, the old bend ("Oxbow" in Figure 5) will disappear over time.

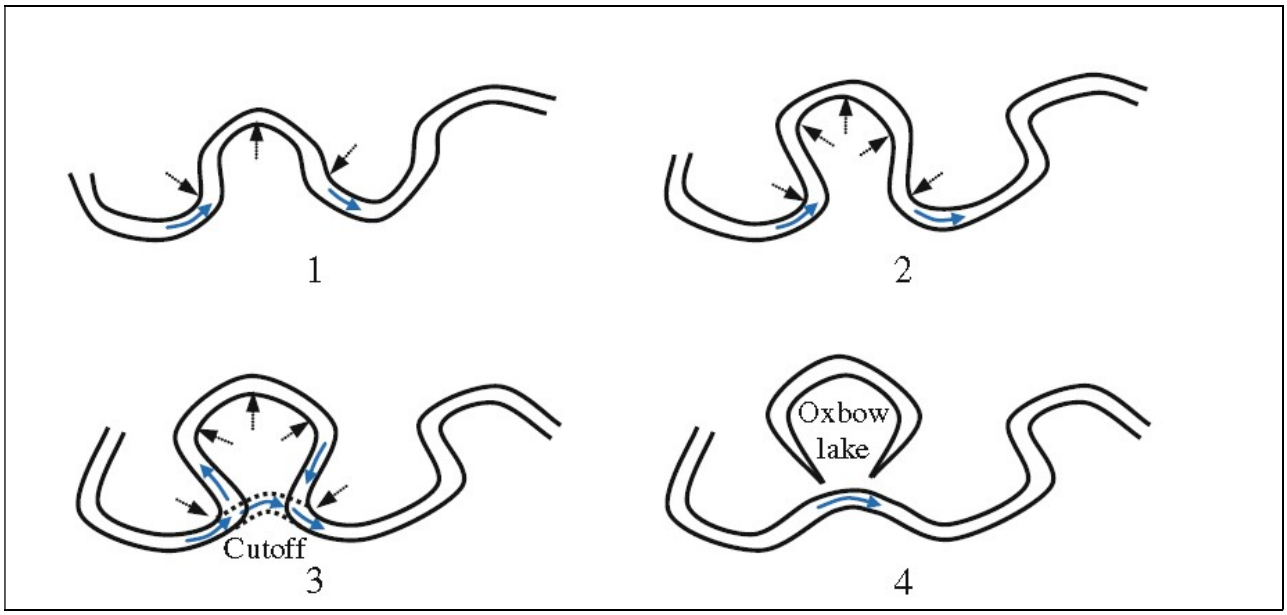

Figure 5: Illustration of the Formation of a Cutoff

In the 1996 to 2016 time period based results which were used for both 25- and 50- year migration predictions, three of the bends are predicted to be reduced and are present in Table 3 as negative numbers for the change in radius.

The migration of the channel meanders is also control by hard structures such as bridges, roads or bank stabilization. If the channel meanders migrate to these "hard" locations, the channel migration will stop. These controls were not taken into account for this study.

The 25-year prediction of the meanders for a portion of the channel is shown in Figure 6. Note that "R" designated the radius of the circle drawn and the arrow designates the direction of the meander movement. Also, it may appear that a circle goes beyond the predicted backline; however, that is because another part of that circle is the advancing part of the meander.

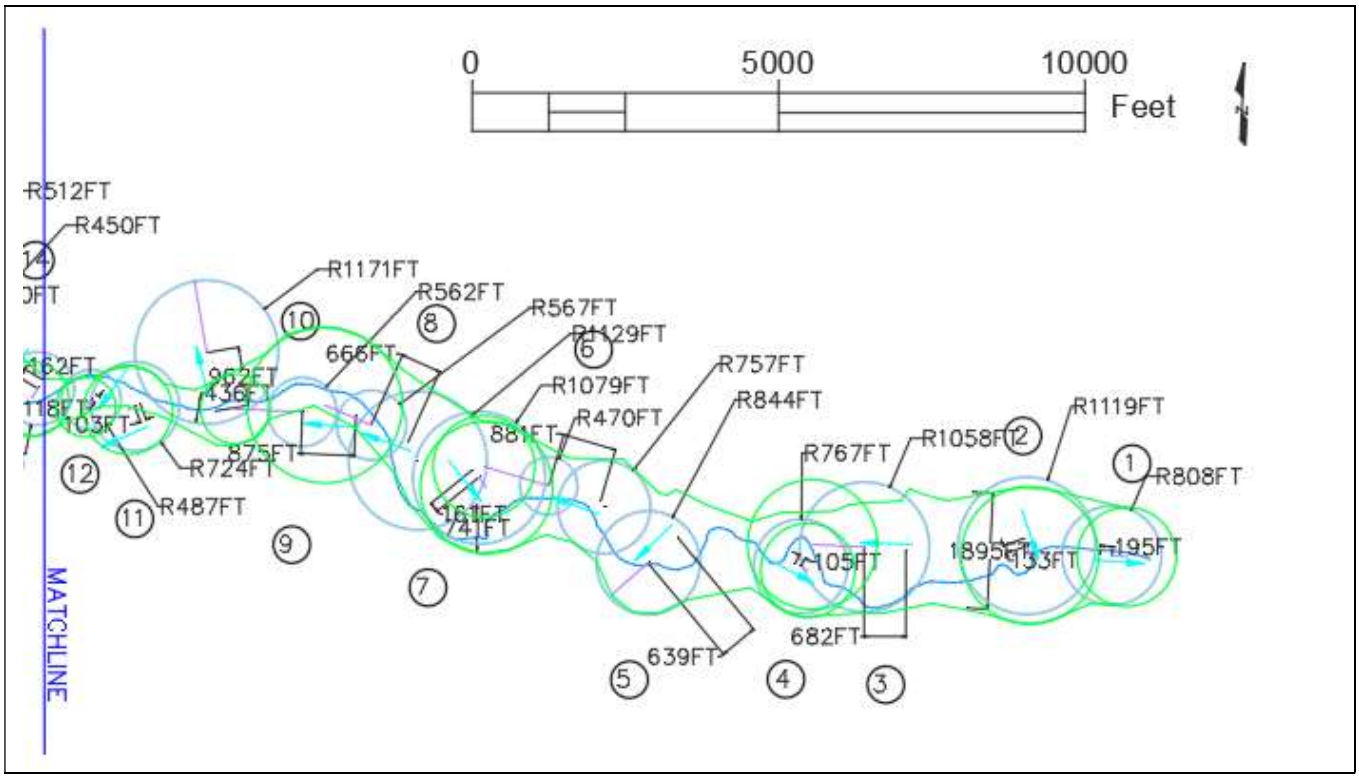

Figure 6: The 25-Year Prediction of the New Bank Lines

Checks for Meander Prediction Technique

Equilibrium Slope Calculation

From the 2016 topography, the length of the main thread of the channel was 46,397 feet between the project limits and had a vertical difference from each end of 188 feet, resulting in a slope of 0.0041.

Equilibrium slope is a theoretical slope that could be attained within decades or thousands of years. Using various methodologies and a channel forming discharge of 3,218 cfs (5-year, 6-hour storm from HEC-HMS), equilibrium slopes were calculated using the spreadsheet by Williams and Kreymborg (2008) ranged from 0.00067 to 0.00022. Since the existing slope is greater than the equilibrium slope(s), the Creek's tendency would be to reach this equilibrium slope and to do this, the channel length would need to increase and result in higher sinuosity. This tendency is demonstrated in Table 4 (Table 1 with 25- and 50- year predictions), which shows that the sinuosity index generally increases with time. This reinforces the results of the meander analysis showing extension of the meanders (lengthening of the stream centerline) as they progress toward equilibrium.

For meandering river systems that extend and elongate over time, the tendency for the sinuosity index is to increase and the channel slope to decrease. The decrease in the channel slope over historic time (as well as for the predictions) is expected since the equilibrium slope is lower than the existing and predicted channel slopes. This adds validity to the 25- and 50- year meander projection methodology. Note that relatively small increases in the sinuosity index do not necessarily imply that there are only incremental changes in the lateral movement of the Creek. There can be large changes to the planform of the meanders as illustrated in Figure 6; however, the formation of the cutoffs

locally decreases the overall channel length, resulting in a lowering of the sinuosity index and increasing the channel slope.

Table 4: Sinuosity Index and Channel Slope Results and Predictions

Year	Total Channel Length (ft)	Sinuosity Index	Channel Slope
1935	43,319	1.238	0.00471
1996	44,714	1.278	0.00456
2006	46,158	1.319	0.00442
2009	48,009	1.372	0.00425
2014	45,785	1.308	0.00446
2016	46,397	1.325	0.00440
25 yr. prediction	46,601	1.331	0.00438
50 yr. prediction	48,697	1.391	0.00419

Braiding Parameter

The braiding parameter is the measure of the number of bars or islands in a channel. The parameter is defined as the number of major bars or islands per meander wavelength. Based upon aerial photos and field inspections, the braiding parameter was approximately one to two throughout the project, which is representative of a mainly single thread meandering channel. The Galisteo Creek, based upon the small braiding index, is almost entirely meandering although there are some localized instances of braiding and small mid-channel bar/island formation. This indicates the channel is not in a predominately avulsion/braiding zone; therefore, the usage of the prediction method for meander migration is appropriate for determining future conditions.

Floodplain Creation/Abandonment and Potential for Incision and Aggradation

In a meander, the deepest part of the channel (incision/thalweg) is at the outside of the bend. This deeper part of the channel is approximately 2 to 4 feet deeper than the average elevation of the main channel. As the meander extends, this deeper part of the channel is the lead portion of the extension and incises into the channel during its movement. The inside of the bend, as the meander continues to extend, will slowly aggrade after moderate to high flow events. In the interim, the floodplain areas will increase but will over time reduce back to their original size due to the aggradation on the inside of the bend.

The areas that have the highest probability to create and/or abandon floodplains are at the locations where the predicted meander extensions (radius change) are the greatest. From Table 3, these

locations are at ID No. 6, 8, 24, and 25. Note that the greatest change is at ID No. 8, which has a 50-year prediction of 1,405 feet extension of the meander (radius).

Summary of Meander Predictions

The final locations of bend movement and size of the bend circles were captured in CAD drawings for both 25-year and 50-year predictions. For the 25-year period, the maximum migration extension is 1,202.5 ft. and 2,405 ft. for the 50-year period with the assumption of linear time extension. Predicted bank lines were drawn using the new outline for fit circles based on calculations included in Table 2 and 3.

An assumption was made that the meander movements are unhindered by "hard" points that may influence the movement. This assumption aids in the identification of future meander locations that may endanger existing and future infrastructure. If a more detailed study is to be performed, the locations of dependable hard control points such as bridges, bedrock and bank rock outcrops, hardened embankments of railroads and roads, as well as bank stabilization efforts which would prevent the movement of the channel, must be identified (see Figure 7). If this is the case, the advancing parts of the circle should be stopped at the limits of the hard points, and adjacent locations of the meander must be adjusted accordingly for continuity.

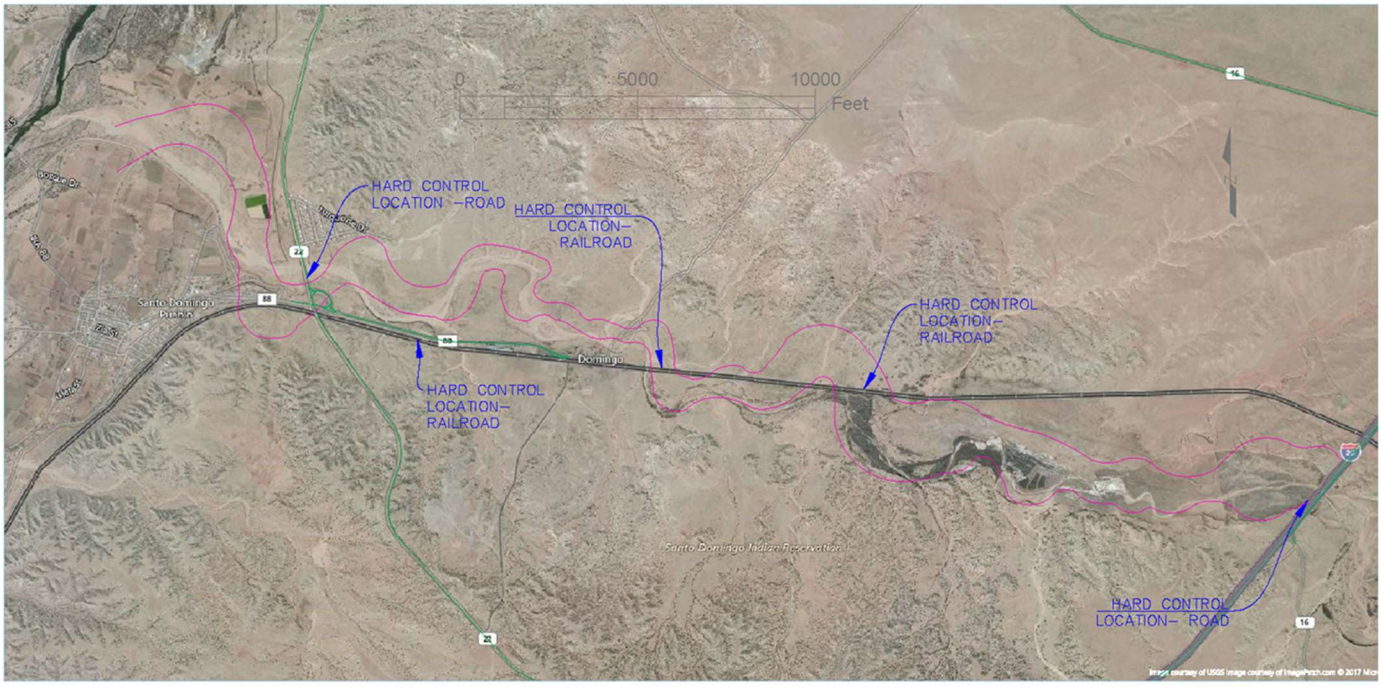

Figure 7: 50-Year Predicted Bank Line (Pink Line)

The final predicted bank line alignments for the 50-year projections, with aerial photography as backdrops and showing locations of easily identified "hard points," are presented in Figure 7 above. Note that there are large predicted movements of the bank lines near the Creek's confluence with the Rio Grande. These movements may be minimized if the confluence location is kept stable by either natural or artificial means.

Recommendations

Projected 25-year and 50 -year meanders vary greatly from the current alignment. Significant lateral movement is visible in many areas, but it should be kept in mind that some of this movement will be prevented by hard control points in the Creek and its banks such as bridges, roads, existing drop structures (if any) and existing (or proposed) bank stabilization a shown in Figure 7. The areas where little or no meander movement is predicted should be the first options for any infrastructure placement. The terrace immediately downstream of a stabilizing structure such as a bridge is another ideal location to place infrastructure. The meander movement in the downstream direction is away from this area, and the extension of the loop is prevented by the stabilizing structure. The upstream terrace is to be avoided since the downstream movement of the meander would "collapse" this area if the meander is close.

If wetlands creation in the floodplain is an option, these should be placed where the meanders are moving away from these proposed locations (inside of the bend) and are moving at a relatively slow rate. However, these inside of the bend locations may fill up with sediment in subsequent flood events. If the meander movement rate is high, the wetland areas could be abandoned by the Creek and would not be sustainable without human intervention. Optimal locations for wetlands are adjacent to meander inflection points, i.e., "crossover" points where meanders change their curvature. These locations are the most stable in a meandering stream.

For the protection of the land and banks if the projected meandering locations are not acceptable, it is recommended to use bank and toe stabilization measures with the possibility of laying back some of the vertical banks, installation of riprap and grouted or ungrouted boulder edging, and if appropriate, integration of biotechnical methods with "hard" methods such as riprap or Mechanically Stabilized Earth (MSE). Other possible bank protection methods are re-directive measures such as bendway weirs and vanes.

References

AMAFCA, 1994, "Sediment and Erosion Design Guide, Section 3," Albuquerque Metropolitan Arroyo Flood Control Authority, Resource Consultants & Engineers, Inc.

Bohannan-Huston Inc. 2016. Bed gradations of Galisteo Creek, Albuquerque, NM.

Earthwork Institute 2005. "Watershed Restoration Action Strategy for the Galisteo Creek Watershed," Santa Fe, NM.

ESRI. 2011. Environmental Systems Research Institute, ArcGIS Desktop, Redlands, CA.

NCHRP. 2004a. "Report 533, Handbook for Predicting Stream Meander Migration," National Cooperative Highway Research Program, Washington, DC.

NCHRP. 2004b. "Methodology for Predicting Channel Migration," National Cooperative Highway Research Program, Washington, DC.

NCHRP. 2012. "Archived River Meander Bend Database CD," National Cooperative Highway Research Program, Transportation Research Board, Washington, DC.

FHWA. 2012. "Hydraulic Engineering Circular No. 20, Stream Stability at Highway Structures, Fourth Edition," Federal Highway Administration, Washington, DC.

University of New Mexico. 2016. Earth Data Analysis Center, Albuquerque, NM.

USGS. 2008. "Analysis of the Magnitude and Frequency of Peak Discharge and Maximum Observed Peak Discharge in New Mexico and Surrounding Areas," USGS, Scientific Investigations Report 2008-5119, U.S. Geological Survey, Reston, VA.

USGS. 2017. "StreamStats, Version 4.1.2.," U.S. Geological Survey, Reston, VA.

Williams, David T. and Kreymborg, Leonardo. 2008. "PBS&J Scour Spreadsheet," San Diego, CA.

Geomorphic Evolution in a Volcanically Disturbed River System—Relative Significance of Vertical Versus Lateral Adjustments

J.J. Major, U.S. Geological Survey, Cascades Volcano Observatory, Vancouver, WA, jjmajor@usgs.gov
S. Zheng, State Key Laboratory of Water Resources and Hydropower Engineering Science, Wuhan University, Hubei, China
A.R. Mosbrucker, U.S. Geological Survey, Cascades Volcano Observatory, Vancouver, WA
K.R. Spicer, U.S. Geological Survey, Cascades Volcano Observatory, Vancouver, WA
T. Christianson, U.S. Geological Survey, Cascades Volcano Observatory, Vancouver, WA
C.R. Thorne, School of Geography, Nottingham University, Nottingham, UK

A 2.5-km^3 landslide and subsequent pyroclastic flows during the 1980 eruption of Mount St. Helens buried upper North Fork Toutle River (NFTR) valley. Since then, a new drainage network has evolved. A suite of cross-sectional surveys over nearly 40 years at 16 locations along a 20-km reach of river valley documents channel evolution. We analyze spatial and temporal changes in channel evolution using two new metrics: (1) a shape index that defines the degree of U-shaped or V-shaped valley geometry (Figure 1); and (2) an alluvial phase-space diagram (Figure 2) that relates bed degradation or aggradation to increases or decreases in cross-sectional area. The proposed phase-space diagram builds on a channel-stability diagram (Watson et al. 2002) and a geomorphic covariance diagram (Brown and Pasternack 2017). A key advance in our phase-space diagram is delineation of a nine 'phase-space domains' that represent different styles and stages of morphological evolution. For example, one domain (diagonal line in Figure 2) represents uniform aggradation or degradation across the width of an initial reference channel—that is, changes in bed elevation that mimic piston-like upward or downward motion. Channel changes in most domains, however, are dominated by impacts of lateral morphological adjustments. Identification of these 'phase-space domains' supports deeper insights concerning geomorphic processes responsible for long-term channel evolution.

Unlike a linear-response model described by Meyer and Martinson (1989), our analysis reveals channel development has been distinctly nonlinear and non-sequential. Rather than following a linear and sequential trajectory of (1) channel initiation and incision, (2) aggradation and widening, and (3) episodic scour and fill with little change in bed elevation, long-term channel evolution has been more complex with vertical and lateral adjustments intertwined throughout. Phase-space diagrams for cross sections along upper NFTR channel (e.g., Figure 3) show that (1) channel evolution has followed a complex trajectory that has migrated through several phase-space domains non-sequentially, featuring (i) degradation with both widening and narrowing, (ii) aggradation with both widening and narrowing, (iii) bed fluctuations with little change in cross-section area, and (iv) changes in cross-section area with little change of bed elevation; and that (2) lateral adjustments became predominant after the late 1980s to mid-1990s when vertical bed adjustments largely diminished and the channel long profile largely stabilized (Zheng et al. 2014). Documented nonlinearity in long-term evolution of upper North Fork Toutle River channel is consistent with a stream-evolution model proposed by Cluer and Thorne (2014) (see also Zheng et al. 2017). Persistent channel and valley widening, and reworking of the channel bed, are responsible for maintaining sediment delivery from this basin at levels elevated relative to pre-eruption conditions. Elevated sediment loads will likely persist until the valley-

floor width greatly exceeds the active channel-migration zone, and/or channel slopes and valley walls stabilize.

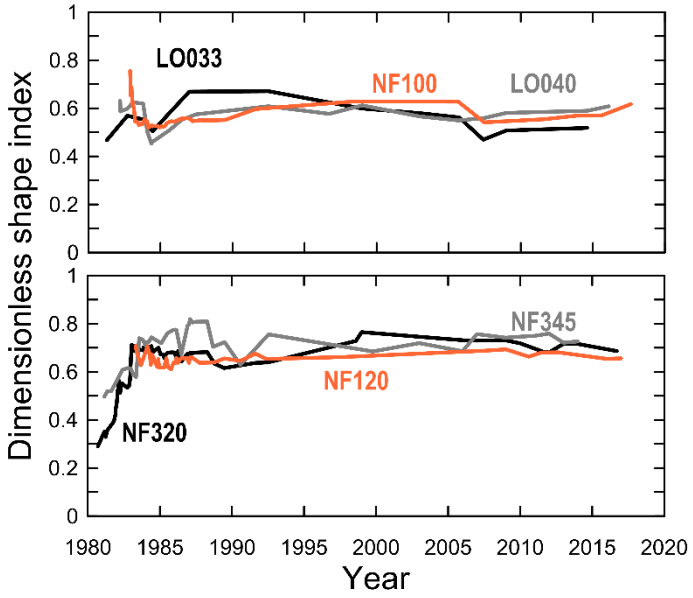

Figure 1. Examples of temporal trends in cross-sectional shape indices derived from cross-section profiles in erosional (top graph) and transitional (bottom graph) domains in upper North Fork Toutle River. The shape index is defined as the area of a cross section relative to a hypothetical rectangular area eroded uniformly across the section top width to the channel-thalweg elevation. Highly entrenched geometries (quasi-V-shaped) have shape indices ~≤0.5. Sections having more U-shaped or box-like geometries have indices >0.5.

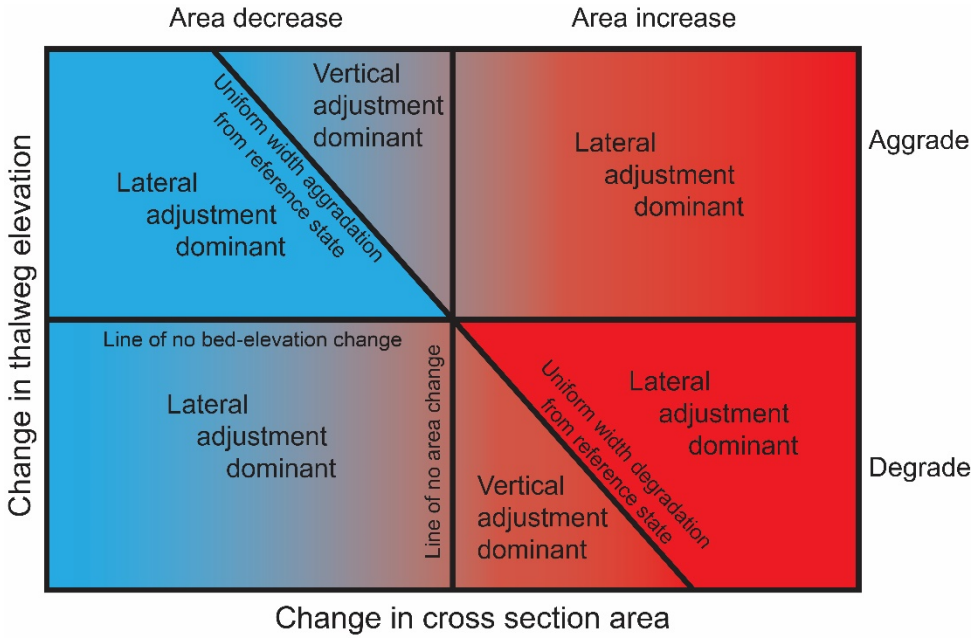

Figure 2. Alluvial phase-space diagram illustrating relations between vertical and lateral adjustments and changes in cross-sectional area. Nine 'phase-space domains' (3 lines, 6 regions) depict varying dominance of vertical (degradation or aggradation) and lateral (widening by erosion, narrowing by deposition or erosional entrenchment) adjustments. Color gradients illustrate gradual changes in process dominance between phase-space domains.

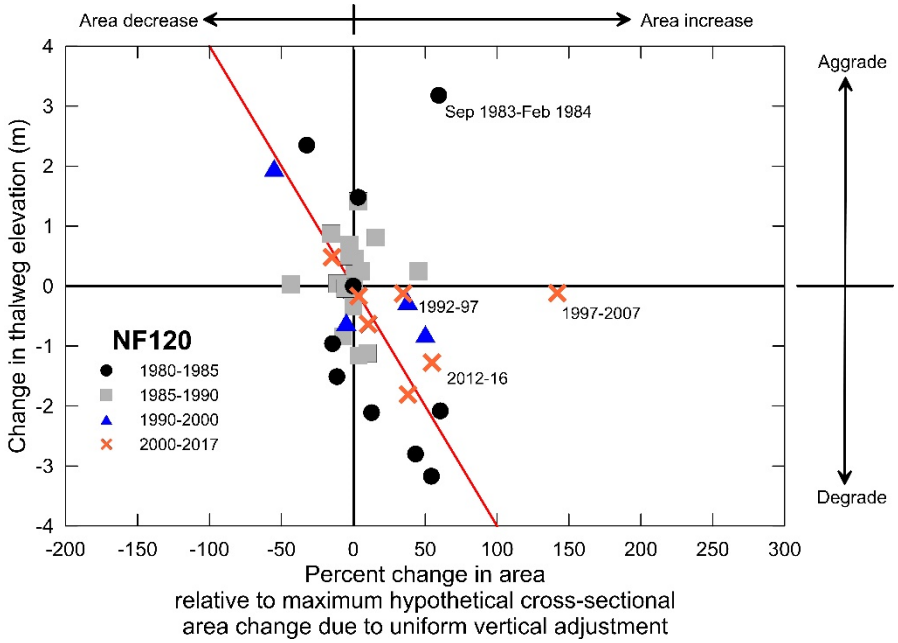

Figure 3. Example alluvial phase-space diagram for North Fork Toutle River cross-section NF120. Diagram depicts relations between change in bed elevation and percent change of cross-sectional area relative to a maximum hypothetical change of area under constant-width aggradation or degradation from an initial reference state. Red diagonal line represents a hypothetical linear relation between changes in bed elevation and cross-section area under uniform-width conditions. Data reflect changes between consecutive surveys and are categorized by time after the 1980 eruption. Times elapsed between selected surveys are highlighted.

References

Brown, R.A., and Pasternack, G.B. 2017. "Bed and width oscillations form coherent patterns in a partially confined, regulated gravel–cobble-bedded river adjusting to anthropogenic disturbances", Earth Surface Dynamics, 5:1-20.

Cluer, B., and Thorne, C. 2014. "A stream evolution model integrating habitat and ecosystem benefits", River Research and Applications, 30:135-154.

Meyer, D.F., and Martinson, H.A. 1989. "Rates and processes of channel development and recovery following the 1980 eruption of Mount St. Helens, Washington", Hydrological Sciences Journal, 34:115-127.

Watson, C.C., Biedenharn, D.S., and Bledsoe, B.P. 2002. "Use of incised channel evolution models in understanding rehabilitation alternatives", Journal of the American Water Resources Association, 38:151-160.

Zheng, S., Thorne, C.R., Wu, B.S., and Han, S. 2017. "Application of the Stream Evolution Model to a volcanically disturbed river: The North Fork Toutle River, Washington State, USA", River Research and Applications, 33(6):937-948.

Zheng, S., Wu., B., Thorne, C.R., and Simon, A. 2014. "Morphological evolution of the North Fork Toutle River following the eruption of Mount St. Helens, Washington", Geomorphology, 208:102-116.

Geomorphic Trends of the Mississippi River Revealed by Specific Gage Records and Channel Geometry Changes

David S. Biedenharn, Research Hydraulic Engineer, USACE, ERDC-CHL, Vicksburg, MS, david.s.biedenharn@usace.army.mil
Travis A. Dahl, Research Hydraulic Engineer, USACE ERDC-CHL, Vicksburg, MS, Travis.A.Dahl@usace.army.mil
Charles D. Little, Hydraulic Engineer, Mendrop Resources Engineering, Ridgeland, MS, clittle@mendrop.net

Extended Abstract

The Mississippi River between Cairo, IL and the Old River Control Complex, LA is a vital conduit for both commercial navigation and waters draining from much of the United States. Any changes to the hydraulic conveyance of this system are, therefore, of national importance. In this study, we describe our recent efforts to identify patterns and trends in the conveyance of the system. We developed specific gage records for a range of flows at 19 stations along the Mississippi River. The specific gage trends differed both between gages and, at some locations, between flows at the same gage. We also compared the regional trends from the specific gage records with trends in channel geometry, including cross-sectional and volumetric change, to help determine the source of the stage trends.

The development of the Mississippi River and its floodplain for navigation and flood control has been ongoing since the eighteenth century, with the most concerted efforts occurring as a result of the Flood Control Act (FCA) of 1928 (U.S. Congress 1928) following the Great Flood of 1927. With the complex requirements in navigation, flood risk reduction, and environmental restoration, all with multiple stakeholders, future Mississippi River management will require the most advanced knowledge available. The Mississippi River Geomorphology & Potamology (MRG&P) Program was developed in recognition of this challenge. The MRG&P Program is a joint effort of the U.S. Army Corps of Engineers (USACE), St. Louis, Memphis, Vicksburg, and New Orleans Districts and is conducted with the oversight of the Mississippi Valley Division (MVD) and benefits from technical contributions from the U.S. Army Engineer Research and Development Center. The study reported herein is just one of many components of the MRG&P Program (Lewis et al. 2019).

The objectives of this study were to examine the morphologic trends from the mid-1970s to present along the Lower Mississippi River (LMR) between Cairo, IL, (RM 954) and the Old River Control Complex, LA (RM320). The study area is illustrated in Figure 1. This was accomplished by means of analysis of specific gage trends and comparison of channel geometry. This study reflects an integration of two recently completed MRG&P reports by Biedenharn et al. (2017), and Little et al., (2017).

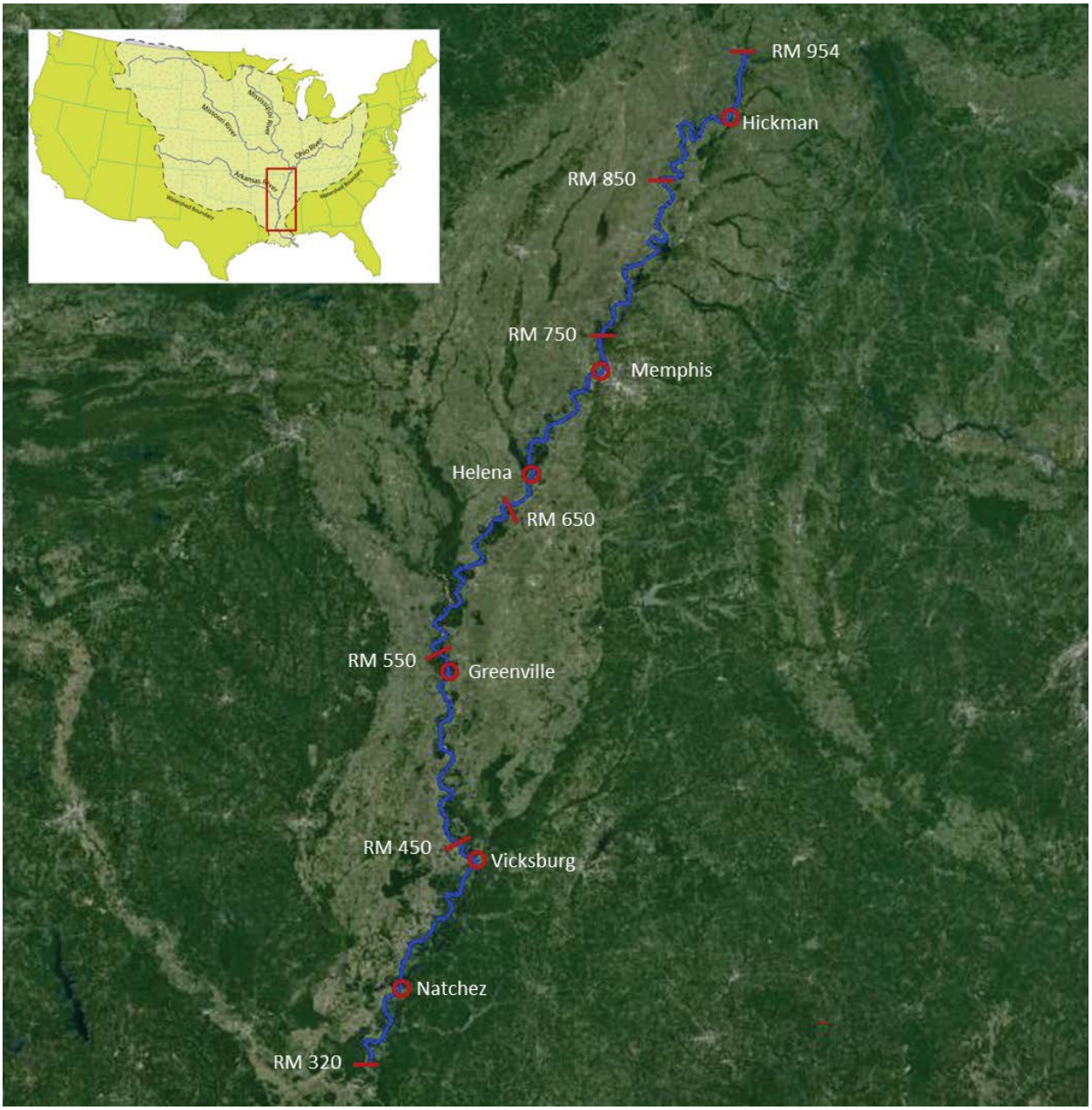

Figure 1. Map of the study area along the LMR from Cairo, IL (RM 954) at the upstream end to the Old River Control Complex, LA (RM 320) at the downstream end.

A geometric data analysis was conducted for the study reach to document long-term trends in the dimension, pattern, and profile of the LMR channel within the study reach. Hydrographic survey data for the years 1975, 1989, 1996, 2002, 2004, and 2013 were used to determine spatial and temporal variations in channel geometry and volume. Trends of geometric change (area, depth, width, conveyance, and channel volume) were identified along defined geomorphic reaches of the river (Little et al., 2017). Although there was considerable local variability in the survey comparisons, broad-scale trends were clearly evident. For the period 1975 to 2013 there was a consistent loss of cross sectional area and channel volume (aggradation) for the most downstream reach extending from about RM 320 (near ORCC) to about RM 435 (near Vicksburg, MS). For

the majority of the reach between RM 435 and RM 592 near Rosedale, MS, the geometry comparisons fluctuated but remained relatively constant, indicating no significant net erosion or deposition (dynamic equilibrium). However, there was a short reach extending from the vicinity of Greenville, MS (RM 530) to near Arkansas City, AR (RM 560), that revealed a slight erosional trend. The channel geometry comparisons indicated that the entire reach from about RM 592 to near Cairo, IL (RM 954) was gaining in cross sectional area and volume, indicating an erosional regime.

Morphologic trends along the LMR were also examined using specific gage records. Specific gage records were developed at the following 19 gaging stations along the LMR: Columbus, KY; Hickman, KY; Tiptonville, TN; Caruthersville, TN; Osceola, TN; Fulton, TN; Memphis, TN; Star Landing, MS; Mhoon Landing, MS; Helena, AR; Fair Landing, AR; Rosedale, MS; Arkansas City, AR; Greenville, MS; Lake Providence, LA; Vicksburg, MS; St. Joseph, LA; Natchez, MS; and Red River landing, LA (Biedenharn et al., 2017). Analyses of the historical specific gage records extending back into the mid-1800s, have shown that the meander cutoffs (which were mostly performed during the 1930s and early-1940s) resulted in larger and more abrupt stage reductions than those associated with any other event that has impacted the Mississippi River during at least the last 100 years. In some reaches, stage decreases of 15 feet were observed immediately following the cutoffs. During the post-cutoff period, the river has continued to adjust to the cutoffs, though stage changes have been much less abrupt than those during the cutoff period. However, this relatively simple pattern of response is complicated because the river is also adjusting to the impacts of other factors such as the dikes, revetments, levees, diversions, upstream reservoirs, maintenance dredging, tributary improvements, sediment yield reductions in the basin, and hydrologic extremes, all of which act to modify these broad-scale trends driven by the cutoffs.

For this study, we compared the trends generated by specific gage records and channel geometry analysis. Comparing these trends required that comparable flow regimes be considered. Examination of the specific gage records reveals there is often a contrast between high (overbank) flows and low to mid-range (in-bank) flows, with low to mid-range flow trends being indicative of channel scour and fill while high flow trends reflect the additional influences of overbank and floodplain processes. The channel geometry trends reported herein did not consider the overbank areas, and therefore, reflect conditions below top bank. Therefore, the specific gage records for the low to mid-range flows were selected for comparison with the channel geometry analyses. Both specific gage and channel geometry analyses indicate that the river is continuing to respond to the cutoffs through degradation that is migrating upstream, while aggradation is persisting in the reaches further downstream. These broad-scale trends, as indicated by both specific gage records and channel geometry analyses, are shown in Table 1. The specific gage trends are generally consistent with the trends indicated by the channel geometry comparisons.

Understanding historical and present-day fluvial processes and morphological responses in the LMR is essential to designing and delivering long-term management of the system for flood control, navigation, and ecology that is cost-effective, adaptable, and sustainable. Specific gage records and channel geometry analysis are important components of river engineering and geomorphic assessments aimed at developing a better understanding of the complex fluvial processes that drive the morphology of large rivers.

Table 1. Observed in-bank morphologic trends as determined by channel geometry comparisons and specific gage records for the mid-1970s to present time period.

Approximate Reach Limits	Observed Morphologic Trends	
	Channel Geometry	Specific Gage Records
RM 325 AHP to RM 435 AHP	Aggradation	Aggradation
RM 435 AHP to RM 600 AHP	Dynamic Equilibrium to Slight Degradation	Dynamic Equilibrium
RM 600 AHP to RM 954 AHP	Degradation	Degradation

References

Biedenharn, D.S., Allison, M.A., Little, C.D., Thorne, C.R., and Watson, C.C. 2017. "Large-scale geomorphic change in the Mississippi River from St. Louis, MO, to Donaldsonville, LA, as revealed by specific gage records," U.S. Army Corps of Engineers, Mississippi Valley Division, MRG&P Technical report No. 10.

Little, C.D., Biedenharn, D.S., Allison, M.A., McCullough, T., and Wofford, K. 2017. "Channel geometry trends of the Mississippi River, Old River Control Complex to St. Louis, Missouri," U.S. Army Corps of Engineers, Mississippi Valley Division, MRG&P Technical report No. 11.

Lewis, J.W., Dahl, T.A., Biedenharn, D.S., Killgore, J., Murphy, C., and Wamsley, T.V. 2019. "The Mississippi River Geomorphology & Potamology Program: Improving understanding of rivers by combining data collection, modeling, and geomorphic analysis," Proceedings of the SEDHYD 2019 Conference, Reno, NV.

Hickman Hardpoint Potamology Study Mississippi River at River Mile 921

Roger Gaines, Research Civil Engineer, USACE, Memphis, TN, roger.a.gaines@usace.army.mil
David Biedenharn, Research Hydraulic Engineer, ERDC-CHL, Vicksburg, MS, david.s.biedenharn@usace.army.mil
Heidi Wadman, Research Oceanographer, ERDC-FRF, Duck, NC, Heidi.w.wadman@usace.army.mil
Jesse Mcninch, Research Oceanographer, ERDC-FRF, Duck, NC, jesse.e.mcninch@usace.army.mil
Jarrell Smith, Research Physical Scientist, ERDC-CHL, Vicksburg, MS, stanley.j.smith@usace.army.mil
Anthony Priestas, Research Physical Scientist, ERDC-CHL, Vicksburg, MS, Anthony.m.priestas@usace.army.mil

Introduction

Background

The Mississippi River has been utilized as a means for transportation by European settlers since the early 1600's. This led to settlement along the river. Increasing population and development along the river over time resulted in various ad hoc measures being implemented to improve navigation and to reduce flood damages. Beginning in the 1700's a more systematic approach for these improvements was being developed. The Flood Control Act of 1928 authorized construction of a system of improvements within the lower Mississippi River (from Cairo, IL and downstream) to reduce flood impacts and to improve navigation which is known as the Mississippi River and Tributaries Project (MR&T). One significant feature implemented under the MR&T was a series of channel cut-offs constructed to accelerate evacuation of floodwaters and to improve navigation alignments. Winkley (1977) provides descriptions of the cutoffs made and the subsequent river response.

Winkley (1977) reports that between 1929 and 1942 there were 16 cutoffs made as part of the MR&T system of improvements, 14 were man-made and two that developed naturally, which shortened the river by 151.9 miles. The river has been adjusting to the increased slope imposed by the cutoffs since their original implementation—over some 80 years ago. In general terms, Winkley (1977) described three response mechanisms observed for cutoffs as presented by Lane (1947): 1) downstream of a cutoff aggradation occurs, 2) at/near a cutoff an over steepened slope develops, and 3) upstream of a cutoff degradation occurs. Data show that the Mississippi River follows these general trends. Data also show that the degradational response to the 16 MR&T cutoffs has recently progressed upstream to about New Madrid, MO at River Mile (RM) 899. The rate of upstream adjustment has been impacted by various geologic controls. One such control exists at RM 921 near Hickman, KY—referred to as the Hickman Hardpoint (Figure 1).

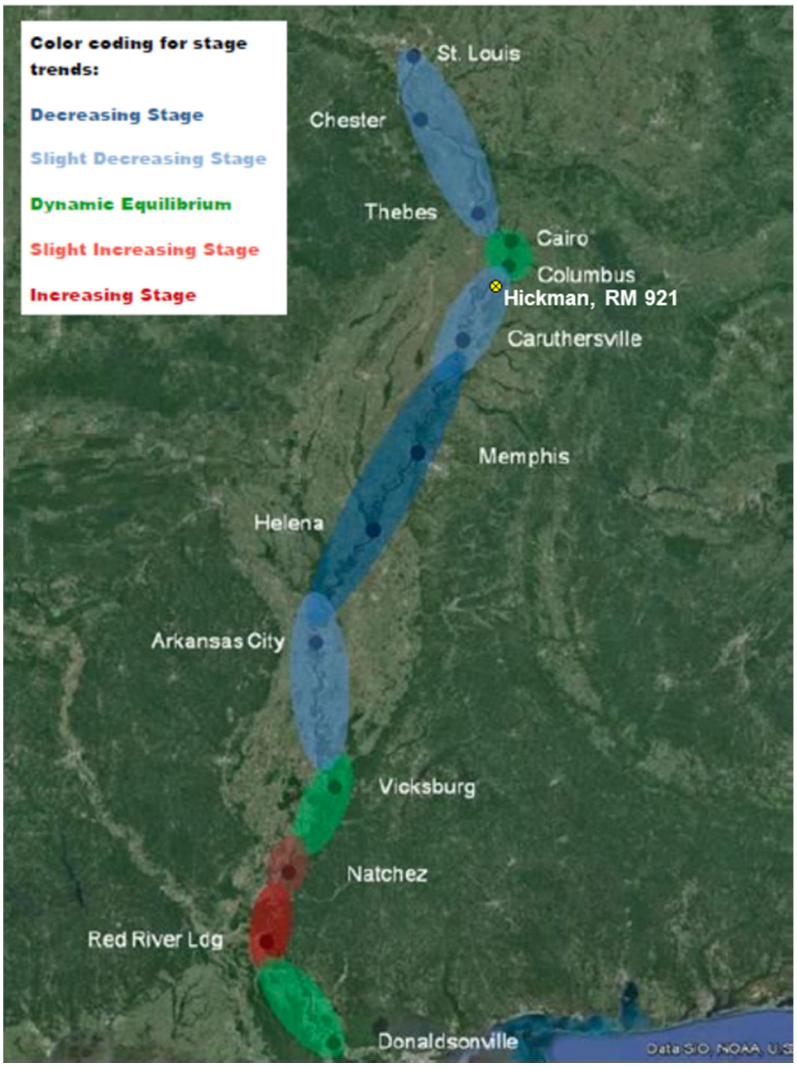

Figure 1. Low-water stage trends along the Mississippi River (from Biedenharn et al. (2015).

The Hickman Hardpoint is an erosion resistant layer at and beneath the river bed immediately downstream of the Hickman Harbor. During extremely low water in 2012 there were several reports of groundings in the vicinity of the Hardpoint's location. The grounding reports indicated impacts by vessels or barges with the bed with no known damage or lost-time reports. There is concern that such groundings may become a hazard to navigation especially during future low water periods. This implies that some improvements may be sought to remove parts of the resistant layer either through dredging within the navigation channel or other means to reduce the risk of grounding. One concern with changing the existing bed elevation across the resistant layer pertains to potential upstream consequences. In effect, lowering the bed at a geologic control results in the same response as a constructed cutoff by creating a steeper slope within the immediate vicinity of the control. The Hickman Hardpoint Potamology Study sought to develop data defining characteristics and extent of the Hardpoint, to explore reach stability both in short-term and long-term horizons, and to assess the potential for upstream impacts with its removal or modification.

Geomorphic Setting

The Lower Mississippi Alluvial Valley (LMV), is a gently sloping, broad, relatively flat plain comprised of unconsolidated or partially consolidated gravels, sands, silts, and clays (alluvium) deposited within the Mississippi Embayment. Depositional environments of the recent alluvium are complex and consist of abandoned channels, point bars, backswamps, natural levees, and relict braided alluvial fans. Much of the alluvium has been deposited and re-worked by channel migration. Tertiary deposits underlie the alluvium at depths ranging from a few feet to as much as 200 feet (Saucier 1964) owing to the entrenched valleys of previous Ohio River courses during Pleistocene interglacial stages when sea level was several hundred feet lower than present. Thus, Tertiary deposits can be found well below the maximum channel depth of the modern Mississippi River, or may occasionally intersect the thalweg.

The river has undergone continual change to seek a state of quasi-equilibrium between water and sediment inputs, the channel geometry and planform, and external boundary controls. Channel migration which included meanders and natural cutoff formation was the predominant response to maintain a certain degree of balance between inputs and boundary constraints. Cutoffs occurred as meander belts became more and more tortuous, ultimately cutting through increasingly narrow banks that separated the channels or short circuiting the main flow path through formation of chutes often during floods. Upon introduction of man-made changes beginning in the 18th century the river became more constrained in its ability to meander.

The River's Historical Response to cutoffs: The River's historical response to cutoffs was dependent on general characteristics of the Mississippi River including any geologic controls in the river valley. These controls included rock outcrops, gravel and coarse alluvium concentration, clay plugs, the general stratification of soils, valley slope and fault zones resulting from tectonic activity. The geologic history of the Lower Mississippi Valley has been written about extensively with one of the more complete records presented by Fisk (1944). Fisk states that the Lower Mississippi has shown no tendency to aggrade or degrade its channel since it joined the Ohio River in its present location. Fisk dated the current meander belt at 2000± years old. Saucier (1974) presented similar variation in the time of activity and sequencing of the present meander belt as Fisk but at different rates of change. Winkley (1970) suggested that due to flow adjustments and shifts in the location of the belt and delta, the riverbed had not reached a condition of regime until approximately 500 years prior to man's first attempts to regulate the river in the 18th century. During this 500 year period, the river averaged 14 cutoffs per hundred years and seemed to take 30-80 years for a local adjustment to any individual cutoff. The wide range of response time resulted from local slope variations, number of cutoffs in a particular reach, soil variability and tributary influences. Even though Winkley described the 500 year period as having an in-regime state, there was a general thought that the valley was aggrading.

Winkley (1977) goes on to raise the question of response time for a series of quickly implemented cutoffs. Considering the historical rate of cutoff formation of 14 per 100 years, Winkley suggests that 16 cutoffs artificially made in a 13-year period between 1929 and 1942 effectively represents a single change imposed on the river—that is, the multiple cutoffs behave as if they were a single cutoff. With this viewpoint, Winkley conjectured that it would take at least 55 years (or until 1997 at the time of his publication) for the river to recover from the dramatic shortening from 16 cutoffs. He caveats this projection with significant uncertainty because it assumes the river would be allowed to regain its length, sinuosity and bar spacing

during that 55 year period which had not been the case. Therefore, Winkley expected that the recovery period would be much longer.

Current River's equilibrium state: The relevance of the cutoff program and subsequent river response to the Hickman Hardpoint is two-fold. First, the constructed cutoffs resulted in channel degradation trends in reaches upstream from the cutoffs. The degradation has resulted in major downward shifts in stage-discharge rating curves over time at points upstream of Helena, AR currently extending to New Madrid, MO. The upstream progression of the degradational trends will soon result in significant increases in slope as the Hickman Hardpoint becomes more of a hydraulic control. Secondly, the response is persistent in that the channel upstream of the combined cutoff reach would not be expected to rebound even after an extended time period. Specific gage records support the conclusion that degradation upstream of the cutoffs do not rebound, at least not in the sense of engineering time scales.

Biedenharn et al. (2015) presented stage trends along the Lower Mississippi River using specific gage records. Biedenharn et al.'s results revealed that the Lower Mississippi River is still responding to the meander cutoffs with degradation migrating upstream of the cutoff reach. The most pronounced degradation was reported for the reach just south of Helena, AR to near Osceola, AR. Recent data show the degradation has begun to migrate further upstream to just south of Cairo, IL (Figure 1). Biedenharn also prepared an overlay of thalweg elevations with Tertiary elevation data obtained from Waterways Experiment Station geologic maps of the Mississippi River (Kolb et al, 1975; Saucier 1964, 1969, 1994; Smith and Russ 1974; Smith and Saucier 1971). There are a number of locations (Figure 2) where Tertiary layers intersect the channel boundary. At these locations the river's response was influenced by the characteristics of the Tertiary layer. For example, the relatively stable trend between 1950 and 1970 for specific gage record at Memphis, TN (Figure 3).

Notably, the downward trend has just begun at Hickman, KY (Figure 4) indicating that response to the 1929-1942 cutoff program continues to work its way upstream. The presence of geologic controls seem to have the major influence on the rate of upstream movement in channel degradation as the river continues to respond to the cutoffs.

The Hickman Rating Curve has remained relatively consistent over time partly due to the presence of the Hardpoint layer which is just downstream of the discharge range. It is also partially due to the delay in channel degradation response for reaches downstream of Hickman. Beginning around 2000, the steady trend at Hickman begins to change. From Figure 3 and Memphis Rating Curves, there has been a downward shift of more than 10 feet at lower stages at the Memphis gage. The downward shift for the lowest flows at Memphis appears to have leveled out since about 2010, but bankfull (1 million cfs) and higher discharges do not show signs of balancing out yet. Based on data from downstream stations it is conjectured that at least 10 feet of lowering for in-channel flows can be expected at Hickman. This amount of channel lowering poses a significant concern with respect to the Hickman Hardpoint. If the Hardpoint materials are similar to other erosion resistant Tertiary layers at Helena, Memphis and other locations downstream of Hickman, then the degradation will be slowed, but will eventually move upstream past Hickman. However, if the Hardpoint material can withstand the erosive forces, either the channel will develop an alternate path, most likely toward the westward, right hand side of the existing channel or there will be some major failure in the revetment along the left bank.

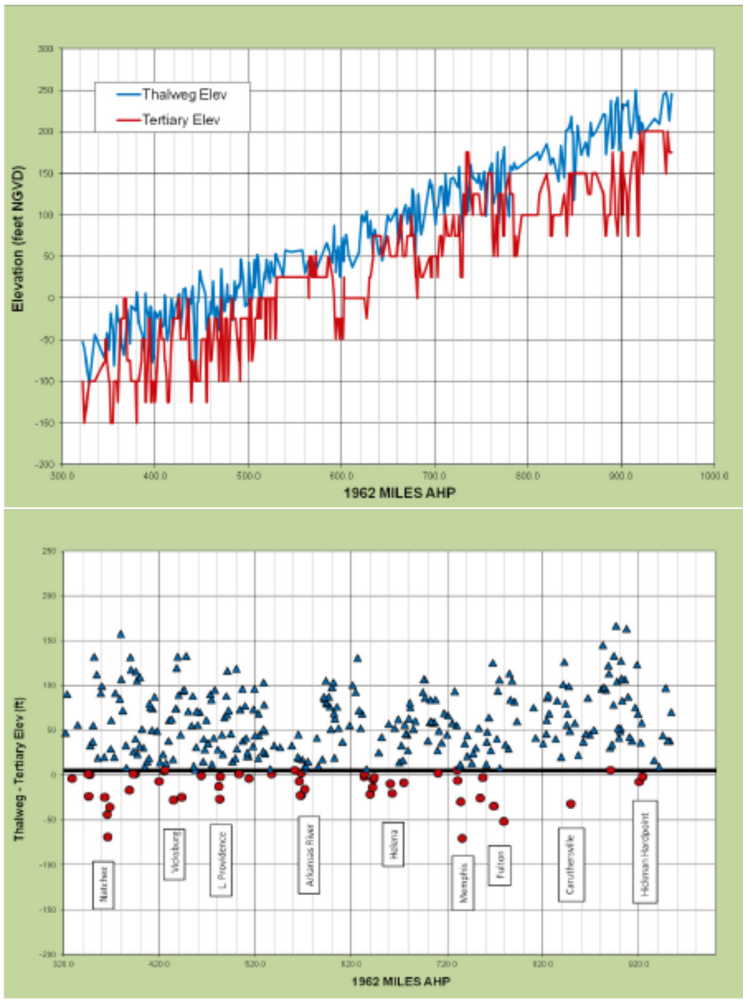

Figure 2. Top: Comparison of thalweg and Tertiary layer elevation; Bottom: Thalweg elevation minus top of Tertiary layer elevation with Red Dots indicating locations where the Tertiary layer is within 5 feet of the thalweg. (Biedenharn et al. 2015). River Miles given in 1962 Above Head of Passes (AHP).

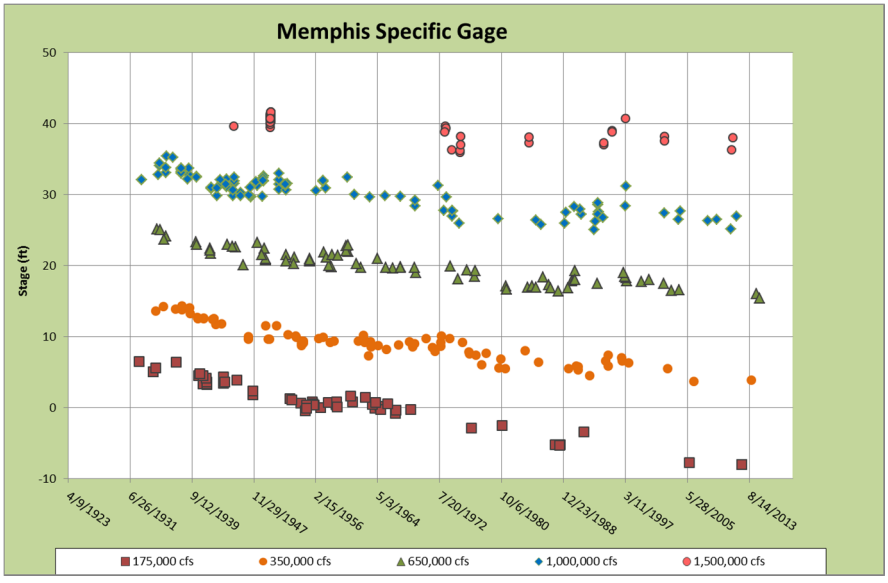

Figure 3. Specific Gage Record for Memphis, TN at RM 734.7 (Biedenharn et al., 2015)

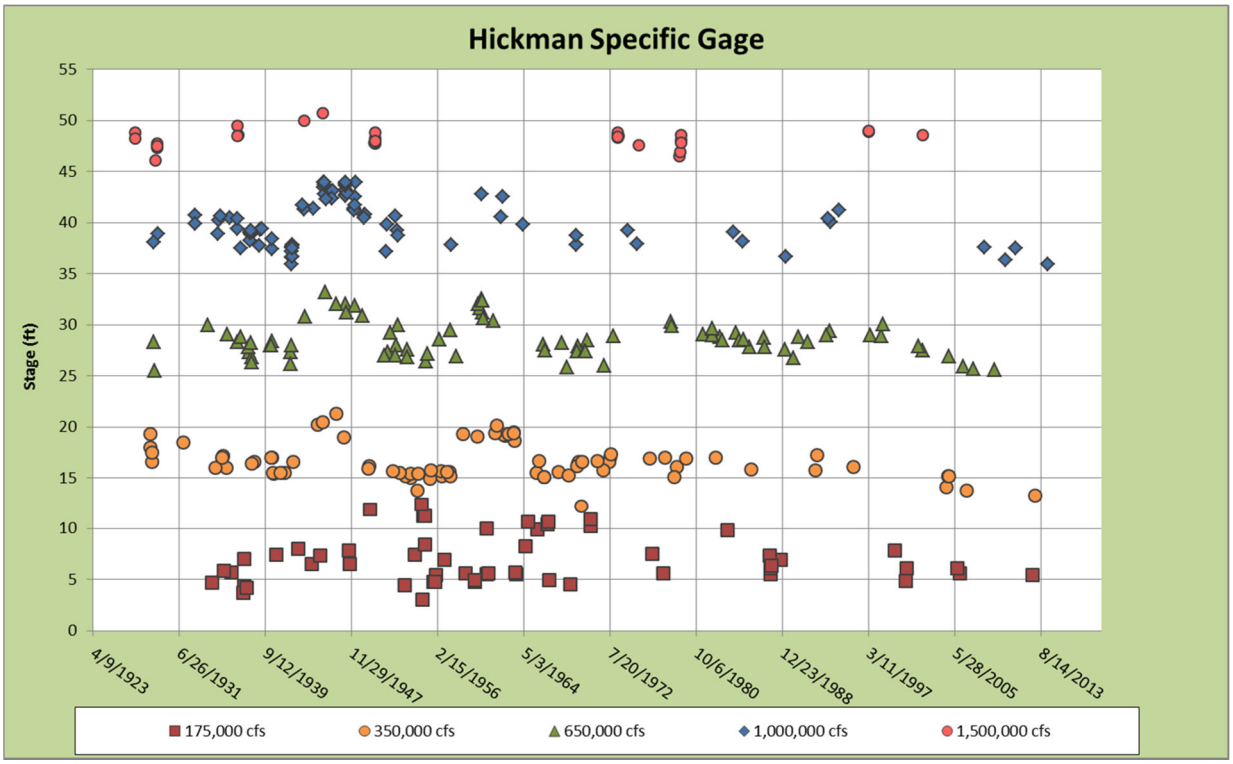

Figure 4. Specific Gage Record for Hickman, KY at RM 922 (Biedenharn et al., 2015)

Hickman Hardpoint as a Geologic Control

Location of the Hickman Hardpoint

The geologic control referred to as the Hickman Hardpoint is located at RM 921 about 1 mile downstream of the Hickman Harbor entrance and along the left descending bank of the Mississippi River. The characteristic feature at this location is presence of a resistant layer that extends across the left most one-third to one-half of the channel bed with an uncharacteristic deep scour hole immediately downstream of the layer (Figure 5). There are actually two outcroppings of this material, one at RM 921 referenced as HP1 and another just upstream near the harbor entrance referenced as HP2. The scour hole has the appearance of a plunge pool typically located downstream of a geologic control (i.e. a head cut), and extends approximately 100 to 120 feet below the thalweg elevation upstream or downstream of the hole. The presence of the plunge pool was first detailed with the advent of multi-beam surveys taken in 2006. Prior to that, hydrographic surveys were conducted using transects (or survey ranges) at 1,000 foot intervals. Coincidently, the 1,000 foot ranges transected this area just upstream of and just downstream of the plunge pool limits. After initial multi-beam survey data revealed the presence of the scour hole, a closer review of historic hydrographic surveys revealed contours that cut across the downstream limit of the scour. While details of the deepest part of the pool were not available from earlier hydro surveys, evidence indicated that some type of scour existed beginning as early as the 1960s.

Long term persistence of the Tertiary layer along with the presence of the downstream scour indicated that this geologic control exhibited a different behavior than observed at other locations where Tertiary layers intersected the channel bottom. The Hickman area is also near

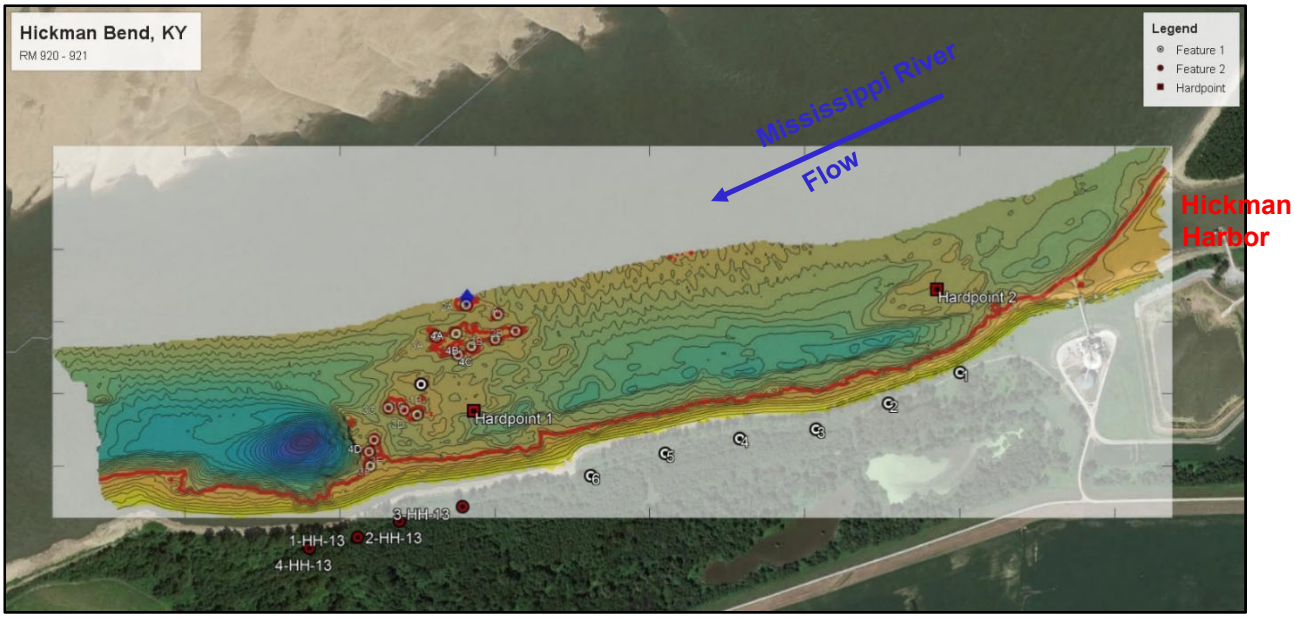

Figure 5. Inset image: Scour hole (dark blue) downstream of resistant layer (higher yellow shades) at Hickman. Markers along the left descending bank show locations of 1949 revetment borings (white) and rotosonic borings from 2013 (red). Markers within the channel show locations of 2017 drag samples (Background map by Google Earth ™).

the area impacted by major earthquakes along the New Madrid fault in the early 1800s. Steps were therefore taken to identify the geotechnical and geologic characteristics of the outcrop material.

While surface details of the resistant layer can be seen from multi-beam survey data, the full extent of the layer cannot be determined from conventional surveys where point bar deposits exist along the right side of the channel. In order to evaluate the full spatial extent of the Tertiary outcrop, seismic survey techniques were employed in an attempt to penetrate through alluvial sand and gravel deposits.

Geology of Hickman Hardpoint Sediments

Geomorphic and geologic data were evaluated in the Hickman, KY area to better understand the influence of geologic controls on the bed and banks of the river. The Tertiary stratigraphy underlying the substratum sands at RM 921 is primarily Eocene sands and silty sands of the Jackson Formation. This stratigraphy is confirmed by deep rotosonic boring obtained by Memphis District in 2013. Rotosonic boring No. 4 contained the presence of stiff Tertiary clay which may denote a paleo-surface valley or unconformity as compared to other borings. Deep vertical erosion into the Jackson Formation in the scour pool is coincident with the transition in soil texture in the river channel bottom from fine-grained to coarse-grained as the thalweg of the river meets the convex side of the old abandoned channel on the south bank.

The river at Hickman is eroding older point-bar and abandoned channel deposits of the Mississippi River. The abandoned channel that is present in the south bank contains a variably thick (between 20 to 50 feet), fined-grained topstratum, underlain by 50-60 feet of substratum sands and gravels. Bathymetric survey data from 2013 indicate that the river has scoured through the substratum sands and into the underlying Tertiary deposits to elevation 140 feet, thus scouring into the Tertiary deposits as much as 75 feet.

In addition to the 2013 rotosonic borings, in-channel samples were obtained in 2017 using an experimental floating rig with core sampler and with a pipe dredge sampler (Figure 6).

Questions about their long-term survivability prompted investigations into their erosion potential and the likelihood and timeframe that they would be removed by natural river forcings. To evaluate the erosion potential samples were needed of the material. Attempts to core the Hardpoint's surface to perform erosion experiments failed because of the very high compressive strength encountered. Instead, only fragments of the Hardpoint were collected using a drag pipe sampler.

Possible Origins of the Hickman Hardpoint: The resistant outcrops of the Hickman Hardpoint were originally presumed to be the exposed clay fills of abandoned channels, or clay plugs as referred to by Fisk (1944). However, the samples retrieved from site HP1 were not consistent with the description provided for such a deposit; samples from site HP2 could be although this remains uncertain. Identifying the geologic units to which they belong may provide some insight into their extent and potential thickness. There appeared to be two possible explanations for the origins of the Hardpoint formations. These were: 1) the eroded remnants of Tertiary bluff deposits, or 2) relict alluvium consisting of point bar and/or abandoned channel deposits. Evidence to suggest or reject these proposals are examined further.

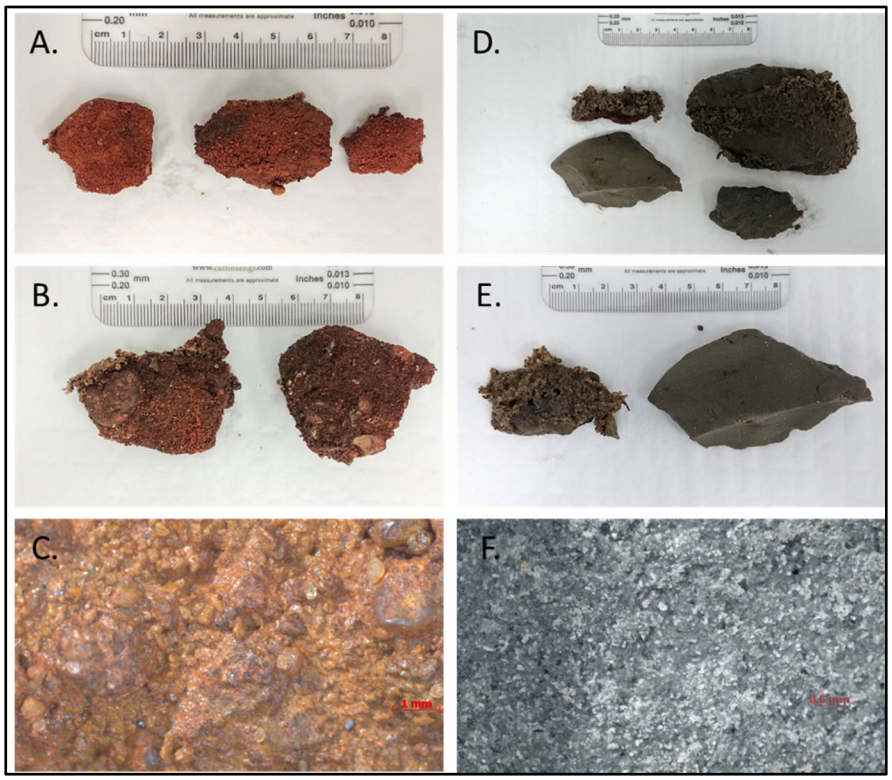

Figure 6. Photographs of representative samples collected from HP1 (A-C) and HP2 (D-F). Note the presence of caddislfly silk retreats (caddisfly silk retreats most visible along sample margins in B and E), which indicates the stability of these formations.

Faulted vs. Mass Movement Hypothesis: A suspicion that the hardpoints were remnants of eroded bluff deposits arose from the lithological resemblance of HP1 to that of the Lafayette Formation, both of which are a kind of ferricrete. If HP1 was associated with the Lafayette Formation then the difference in stratigraphic position between the bluff and river bed could be due to either faulting, large-scale mass wasting, or both.

Erosion Testing of Hickman Hardpoint Sediments

One objective of this study was to determine the surface erodability of Hardpoint sediments to better understand their resistance to the erosion by the river. High-shear erosion testing is conducted with the Sedflume (McNeil et al., 1996).

Sedflume: Sedflume is a field- or laboratory-deployable flume for quantifying cohesive sediment erosion. The USACE-developed Sedflume is a derivative of the flume developed by researchers at the University of California at Santa Barbara (McNeil et al. 1996). The flume includes an 80-cm-long inlet section (Figure 7) with a 2 × 10 cm rectangular cross section for uniform, fully developed, smooth-turbulent flow. The inlet section is followed by a test section with a 10-cm diameter open bottom. Coring tubes and flume test section, inlet section, and exit sections are constructed of clear polycarbonate materials to permit observation of sediment-water interactions during the course of erosion testing. The flume includes a port over the test section to provide access to the core surface for physical sampling. The flume accepts sediment cores up to 80-cm in length.

Prior to the erosion testing, descriptions of the sediment were recorded, including length, condition of the core surface, biological activity, and any visual evidence of layering. Cores were typically inserted into the testing section of Sedflume and a screw jack was used to advance the plunger such that the core surface became flush with the bottom wall of the flume. Flow was directed over the sample by diverting a portion of the pump discharge through a 5-cm inner diameter hose into the flume. The flow through the flume produced shear stress on the surface of the core. (Numerical, experimental, and analytical analyses have been performed to relate flow rate to bottom shear stress.) Erosion of the surface sediment was initiated as the shear stress increases beyond the critical stress for erosion, τ_c. As sediment eroded from the core surface, the operator advanced the screw jack to maintain the sediment surface flush with the bottom wall of the erosion flume. Figure 7 included a photograph of the flume, a close-up photograph of the test section, and a table of flow rate/shear stress relationships. The shear stress relationship for this study was extended to 25 Pa, which corresponds to 8.5 L/s (135 gpm) of flow through the channel.

Testing: The clear water erosion testing resulted in no measureable erosion after 5 hours of exposure at 23.6 Pa. The most notable change in the specimen occurred in the first hour, during which sand imbedded in the caddisfly webbing was washed away. No measureable changes in specimen mass was detected (at a detection limit of 0.1g) over the 5-hour testing period. At the end of the clear-water erosion testing, most if not all of the caddisfly webbing was still attached to the specimen surface.

The sand suspension testing yielded similar results. After 5 hours of exposure at 23.6 Pa and 3g/L of suspended sand, no measurable changes in the specimen surface or weight were detected. Much of the caddisfly webbing remained intact after testing, and no visible erosion of the sediment surface had occurred.

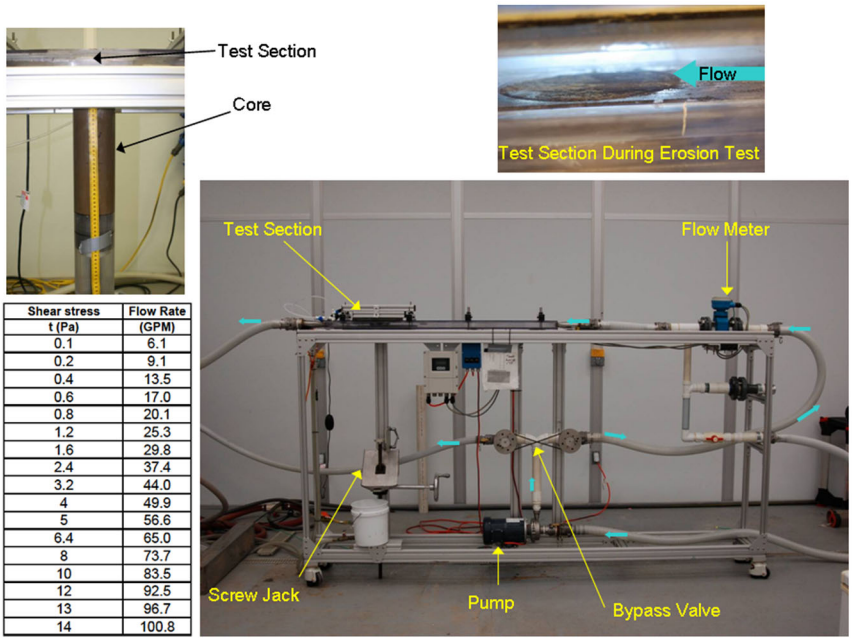

Shear stress t (Pa)	Flow Rate (GPM)
0.1	6.1
0.2	9.1
0.4	13.5
0.6	17.0
0.8	20.1
1.2	25.3
1.6	29.8
2.4	37.4
3.2	44.0
4	49.9
5	56.6
6.4	65.0
8	73.7
10	83.5
12	92.5
13	96.7
14	100.8

Figure 7. Sedflume erosion flume (lower right). Core inserted into test section (upper left). Core surface flush with bottom of flow channel (upper right). Table of shear stress associated with channel flow rates (lower left).

Subbottom Stratigraphy and Extent of Hickman Hardpoint

Subbottom profiling provided a means to assess the presence of and spatial extent of the hardpoint layer. In subbottom profiling, acoustic signatures or their reflections provide a means to estimate locations of different layers beneath the river bed. Different layers produce different acoustic signatures based on their density and reflectivity of the sound signal(s) being used. In order to identify the acoustic nature of the stratigraphic units associated with the Hickman Hardpoint, the shallow stratigraphy of the region was mapped via shallow acoustic reflection (chirp) sub-bottom imaging throughout the study area (Figure 8) in October of 2016, and February of 2017.

The resolution of stratigraphic layers, as well as the depth below the riverbed to which the acoustic data could penetrate, is a function of the geology being mapped, and both the frequency used as well as the amplification power contained within the chirp towfish. Briefly, an acoustic reflection chirp profiler generates a sound source (or pulse) containing a range of acoustic frequencies, similar in audible sound to a bird chirp. The sound is reflected back to receivers either embedded in the chirp towfish or towed behind the survey vessel when it encounters a change in the acoustic impedance below it (see Figure 9).

Reflection Surfaces: The single-most dominant reflection surface observed in the study site was digitized as R01. This reflection surface was characterized by the highest amplitude returns, frequently exhibited bowtie artifacts near the surface, and was smudged at depth, all of which indicate a very dense (hard) geologic unit. In addition, reflection surfaces were only rarely observed below R01, though that could in part be due to the pulse frequency and record length, towfish power, or vessel speed. Steep changes in the subsurface elevation R01 were commonly

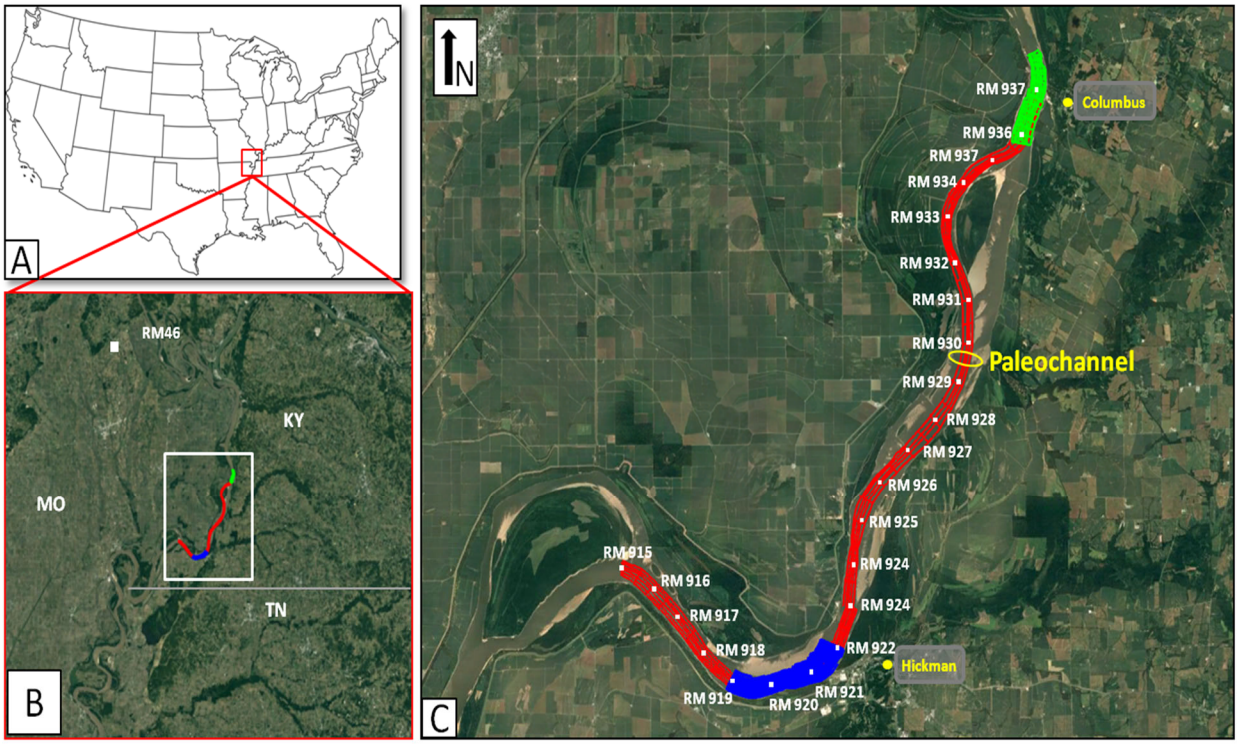

Figure 8. Location of the study area near Hickman, KY. (A) General location of the Hickman Hardpoint in the U.S., and (B) region. (C) Survey lines in the Mississippi River. The different colors reference different surveys. River Mile (RM) locations are plotted in white.

observed. Specifically, the unit would be found near the riverbed, and then plunge rapidly, often exhibiting depth changes of >12 ft. over a horizontal distance of only ~100 ft. All of these observations suggest that R01 is a very dense unit, sufficiently lithified to allow such steep gradients in topography and only minimal acoustic penetration below it. The unit was also spatially adjacent to regions mapped as HP1 and HP2.

Although R01 was exposed occasionally as part of the HP1 and HP2 units, it was most frequently observed at depth in the seismic profiles, with an average depth of ~11 ft. below the riverbed. The shallowest elevations of R01 were nearly always observed spatially adjacent to outcrops of HP1 and HP2. It should be noted that R01 was frequently lost below the bottom multiple in the seismic profile, and that lack of data showing R01 at depths greater than ~20 ft. does not imply R01 is not present at depth, merely that the towfish either 1) lacked the transmitting power or 2) had a sufficiently low acoustic frequency pulse that failed to detect R01 at depths exceeding ~15 ft. below the riverbed.

Channel Geometry Trends

Multi-beam hydrographic survey data from 2006 through 2014 provided detailed elevation data that facilitated an analysis of upstream movement of the scour hole over time using longitudinal profiles and changes in scour hole width over time using cross-sections. There is a steep, almost vertical erosion face at the downstream limit of the Tertiary outcrop followed by a deep scour hole. Biedenharn et al. (2015) likens this to a knick point found in smaller tributaries that are

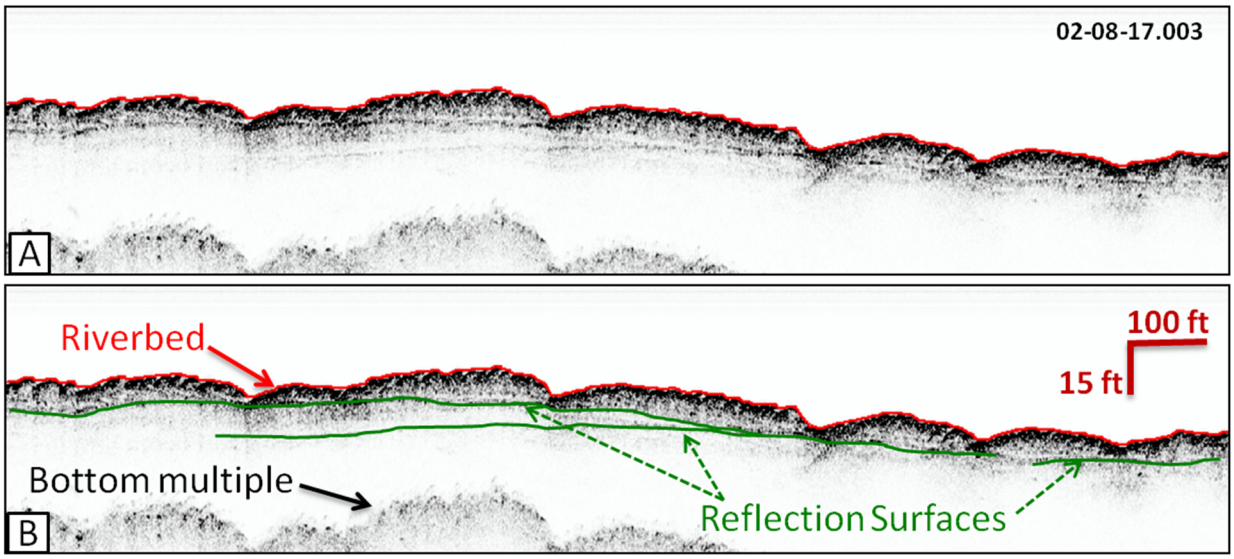

Figure 9. Example seismic profile from the Hickman Hardpoint study. The upper panel (A) is an un-interpreted image of the seismic profile. The lower panel (B) shows interpretation of the riverbed, pertinent reflection surfaces, and horizontal and vertical scale.

experiencing degradation through head cutting. The scour hole only persists on the left one-third to one-half of the channel immediately downstream of the Tertiary outcrop. Elsewhere and beyond the known outcrop limits, the channel and sand bar bed elevations exhibit values consistent with typical riverbed response. To evaluate the stability in position of the scour hole five profiles were evaluated (Figure 10). The profiles extended from the lowest elevations within the scour hole to a point upstream that was beyond the Tertiary outcrop referred to as the Hardpoint.

The profiles show that over time there is a relatively slow upstream migration of the steep vertical face at the Tertiary layer (Figure 11). Over the time period between 2006 and 2015 the scour advanced upstream approximately 10 feet, or at an average rate of about 1 foot per year. However there was some oscillation in the position between 2010 and 2014 with conjecture that the record flood in 2011 which included activation of the Birds Point/New Madrid floodway introduced significant sediment volumes to the reach that are only now being readjusted.

Overall the cross-section (X-6) across the Hardpoint remained constant over the 2006-2015 period showing only signs of river sediments being transported through the reach (Figure 12). The cross-section (X-2) through the deepest part of the scour hole indicates a lowering trend on the right side; the left side of the section does not change appreciable due to the presence of bank revetment. The elevations near the bottom of the scour hole also remain relatively unchanged over time which could be due to presence of the Tertiary layer, limiting shear stresses at that depth, or some combination of these.

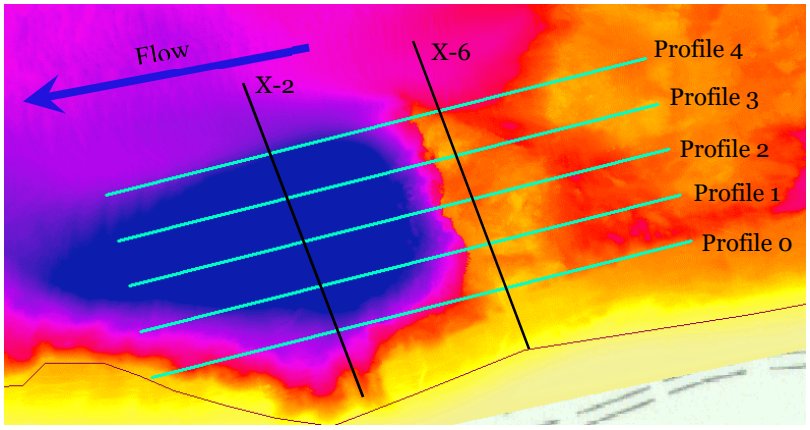

Figure 10. Longitudinal profile and cross-section locations through scour hole (deepest blues) and Tertiary outcrop (yellows within channel bottom) at RM 921.

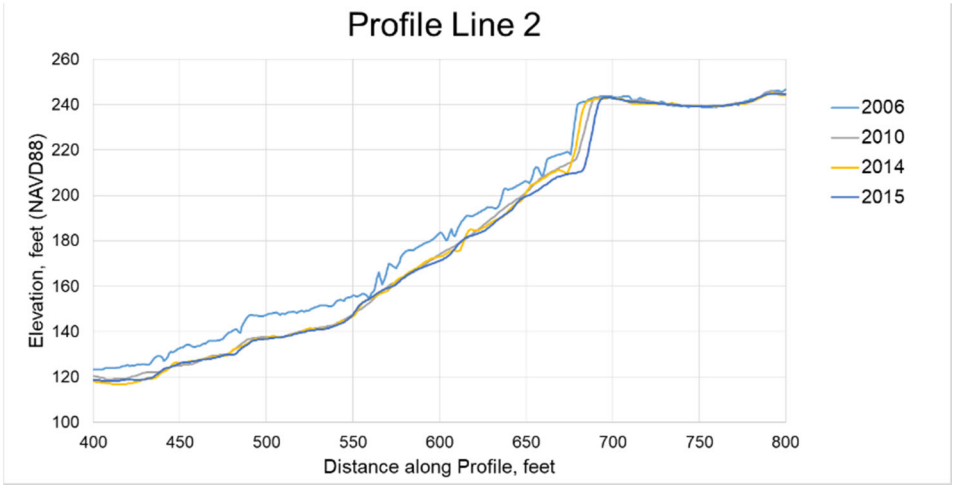

Figure 11. Profile through scour hole (Hickman Hardpoint at Distance 695).

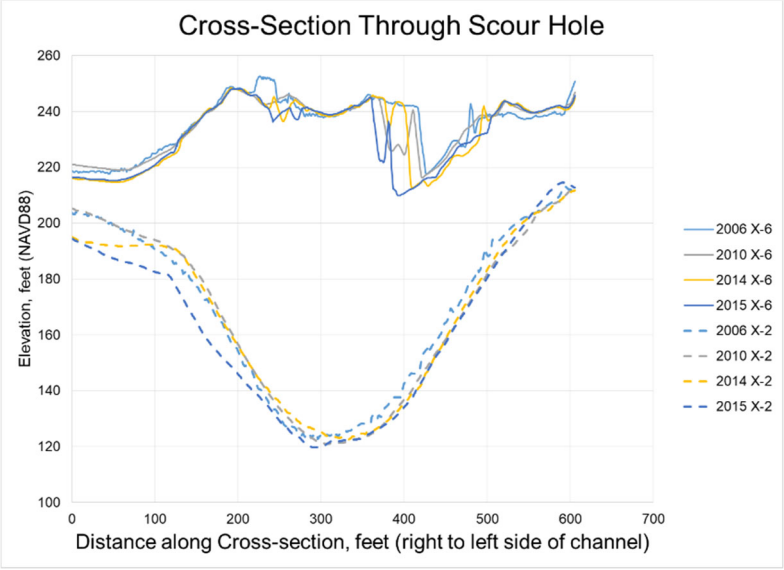

Figure 12. Cross Sections through scour hole (Hardpoint located at X-6)

Numerical Model Sediment Transport Simulations

An existing HEC-6T model was used to perform simulations to evaluate long-term trends with and without the Hardpoint. In order to get a sense of extended bed response, model simulations were made using a period of 250 years. Typically numerical sediment transport simulations are limited to about 50 years or less. Simulations for such an extended period of time have many uncertainties; however, it was thought that projecting upstream response for systematic bed lowering from the 1929-1942 cutoff program would require a timeframe on the order of centuries and not decades. Model results indicated that expected degradation upstream of Hickman could be on the order of 15 to 20 feet up to the Ohio Confluence. That amount of degradation would continue up the Middle Mississippi until approximately Thebes, IL where bedrock is exposed in the river bed. On the Ohio, expected degradation amounts are significantly less due to the sediment characteristics and morphology of the Ohio River.

Conclusions

The Hickman Hardpoint provides a measure of grade control at RM 921. Geologic records, soil boring data, seismic acoustic data analysis, and field sampling of the erosion resistant layer indicate that the control is provided by an outcropping of a very resistant Tertiary layer. Surface erosion tests provide the best insight and show no loss of material under excessively high shear stresses—well beyond stresses imposed by the river. The long-term stability of the rating curve at Hickman also supports this claim. Because the downstream channel has only recently seen degradation from downstream cutoffs constructed between 1929 and 1942, impacts to navigation from the Hardpoint control have been minimal. As downstream degradation continues to occur the outcrop will increasingly influence navigation. Projecting the 10+ feet of lowering experienced at Memphis at RM 734.7 to the Hardpoint at RM 921 presents a significant hurdle to Navigation in the next 10 to 20 years. The erosion test results conducted for this study indicate that the Hardpoint will not be removed naturally by surface erosion. Similarly, analysis of profiles through the main path of scour downstream of the Hardpoint shows a very slow rate of failure due to undercutting of the resistant layer—only about 1 foot per year. The extent of the Hardpoint upstream of the scour hole varies in elevation, but is more or less continuous for a distance approaching 1 mile. Considering the immediate distance between downstream and upstream limits at the brink of the scour hole of 100 feet and a failure rate of 1 foot per year, it could take about a century to cut through this one feature by natural channel response. Nonetheless, any future modifications required to sustain low flow navigation should be directed to dredge along the right side sand/gravel bar of the existing channel with no modification of the resistant layer. By dredging along the right perimeter of the hardpoint material sufficient navigation depths can be obtained without permanently removing the control. This approach may result in a different channel stabilization scheme than currently exists along the Hickman harbor reach.

References

Biedenharn, D.S., Dunbar, J.B., Gaines, R.A., and Little, C.D. Jr. 2015. The Influence of Geology on the Morphologic Response of the Lower Mississippi River, MRG&P Report No. August, US Army Corps of Engineers, Vicksburg, MS, 46 p.

Fisk, H.N. 1944. Geological Investigation of the Alluvial Valley of the Lower Mississippi River, Mississippi River Commission, Vicksburg, MS.

Kolb, C.R., Smith, F.L., and Silva, R.C. 1975. Pleistocene sediments of the New Orleans-Lake Ponchartrain area, Technical Report No. S-75-6, US Army Corps of Engineers, Waterways Experiment Station, Vicksburg, MS, 57 p.

Lane, E.W. 1947. "The Effect of Cutting Off Bends in Rivers," University of Iowa Studies in Engineering, Proceedings of the Third Hydraulics Conference, J.W. Howe and J.S. McNown, eds., Bulletin 31, University of Iowa, Iowa City, IA, pp 230-240.

McNeil, J., Taylor, C., and Lick, W. 1996. "Measurements of erosion of undisturbed bottom sediments with depth,' *Journal of Hydraulic Engineering*, 122(6), pp 316-324.

Saucier, R.T. 1964. Geological investigation of the St. Francis Basin, Technical Report No. 3-659, US Army Corps of Engineers, Waterways Experiment Station, Vicksburg, MS, 96 p.

Saucier, R.T., 1969. Geological investigation of the Mississippi River area: Artonish to Donaldsonville, LA, Technical Report No. s-69-4, April, US Army Corps of Engineers, Waterways Experiment Station, Vicksburg, MS, 24 p.

Saucier, R.T. 1974. "Quaternary Geology of the Lower Mississippi River Valley," Research series No. 6, Arkansas Archeological Survey, Fayetteville, AR.

Saucier, R.T., 1994. Geomorphology and quarternary geologic history of the Lower Mississppi Valley, Two Volumes, December: text, 398 p (Volume I) and 26 oversized maps (plates) in six series (Volume II); US Army Corps of Engineers, Waterways Experiment Station, Vicksburg, MS.

Smith, F.L. and Saucier, R.T. 1971. Geological investigation of the Western Lowlands area, Lower Mississippi Valley, Technical Report No. S71-f, US Army Corps of Engineers, Waterways Experiment Station, Vicksburg, MS, 94 p.

Smith, F.L. and Russ, D.P. 1974. Geological investigation of the Lower Red River-Atchafalaya Basin area, Technical Report No. S-74-5, July, US Army Corps of Engineers, Waterways, Experiment Station, Vicksburg, MS, 182 p.

Winkley, B.L. 1970. "Influence of Geology on the Regimen of a River," Meeting Preprint 1078, American Society of Civil Engineers, New York, NY.

Winkley, B.R. 1977. Man-made cutoffs on the Lower Mississippi River, conception, construction, and river response, Potamology Investigations Report 300-2, March.; US Army Corps of Engineers, Waterways Experiment Station, Vicksburg, MS, 219 p.

Interpreting Flux-Based Sediment Budgets in a Habitat Context: Linking Precise Temporal-Resolution Measurements of Sediment Flux to Spatially Robust Characterization of Channel Change

Christina M. Leonard, Ph.D. Candidate, Utah State University, Logan, UT, Christina.leonard@aggiemail.usu.edu
John C. Schmidt, Professor and Director of the Center for Colorado River Studies, Utah State University, Logan, UT, jack.schmidt@usu.edu
David J. Topping, Research Hydrologist, Grand Canyon Monitoring and Research Center, U.S. Geological Survey, Flagstaff, AZ, dtopping@usgs.gov
Ronald E. Griffiths, Hydrologist, Grand Canyon Monitoring and Research Center, U.S. Geological Survey, Flagstaff, AZ, rgriffiths@usgs.gov

Abstract

Continuous measurements of sediment transport at reach-bracketing gaging stations allow for the construction of continuous mass-balance sediment budgets for the intervening reach. Although these budgets identify periods of sediment surplus (net deposition) or sediment deficit (net erosion), such analyses cannot identify the locations within the reach where channel change occurs. Because channel change and associated changes in habitat are of greater interest to river managers than the precise value of reach-scale loss or accumulation of sediment, it is important to explicitly link reach-scale changes in sediment mass balance to field measurements of channel change. In this study we evaluated the relationship between the magnitude of the sediment mass imbalance measured by acoustic-Doppler profilers and the resulting channel change on the Yampa River in Dinosaur National Monument.

Introduction

Maintenance and enhancement of in-channel and floodplain habitat are essential components of efforts to recover endangered big-river fish in the Colorado, Green, and San Juan rivers. In some cases, reservoir releases have been changed to be consistent with aspects of the life-history strategy of the target species, including providing favorable conditions for spawning, larval drift, and access to nursery habitat. However, clear-water reservoir releases also have the potential for unintended geomorphic consequences, because any reservoir release also transports fine sediment that is delivered to the mainstem channel from tributary watersheds or eroded from the channel bed and banks. Thus, reservoir releases for endangered-fish management have the potential to exacerbate or ameliorate perturbations to the sediment mass imbalance originally caused by the construction and operations of the region's large dams, and these perturbations have the potential to adversely affect in-channel habitat. These unintentional consequences are especially of concern with respect to controlled floods.

River and habitat managers are especially concerned with the efficacy and efficiency of fish-management reservoir releases. In other words, managers want to know whether such releases achieve their intended goals and whether there are adverse consequences. For these reasons, it is useful to measure sediment transport and to determine whether these reservoir releases

improve or degrade habitat conditions caused by changes in channel form and geomorphology. Measurements of reach-scale sediment influx and efflux allow changes in streamflow, whether caused by reservoir reoperations or climate change, to be related to sediment transport and changes in sediment mass balance. Computation of sediment mass-balance perturbation – whether surplus or deficit – implies, but does not directly measure, changes in river channel form or habitat.

The Green River in Dinosaur National Monument and the Uinta Basin is one such area where there is interest in linking decisions about upstream reservoir operations at Flaming Gorge Dam with downstream changes in within-channel and floodplain habitat. The existence of this linkage has inspired the National Park Service and the Upper Colorado River Endangered Fish Recovery Program to fund direct measurements of sediment transport at gaging stations in the upper and middle Green River affected by operations of Flaming Gorge Dam, as well as at gaging stations in the lower Yampa River (Figure 1). This sediment-transport measurement program is conducted by the U.S. Geological Survey Grand Canyon Monitoring and Research Center (USGS/GCMRC) using a novel approach of acoustic-Doppler side-looking profilers to measure suspended-sediment concentration and grain size at 15-minute intervals and episodic measurements of dune migration to estimate bedload transport of sand (Topping et al., 2018). These measurements are used to construct flux-based continuous mass-balance sediment budgets. Although these budgets allow for the determination of whether specific river segments are in sediment deficit or surplus, no studies have been conducted to link the magnitude of sediment mass imbalance with on-the-ground changes in habitat and other river resources. As part of this ongoing research program we ask, “What is the magnitude of sediment deficit or surplus that produces significant within-channel and floodplain changes, some of which may be of concern to river resource managers?”

We use measurements of sediment mass imbalance and geomorphic analysis of channel change to evaluate the links among sediment flux, streamflow, and changes in channel morphology on the lower Yampa River (Figure 1). This part of the Yampa River is ideal for developing a methodological framework to link sediment transport measurements to channel change. Future work will apply this framework to longer river segments on the Green River and evaluate how reservoir releases from Flaming Gorge Dam affect habitat availability.

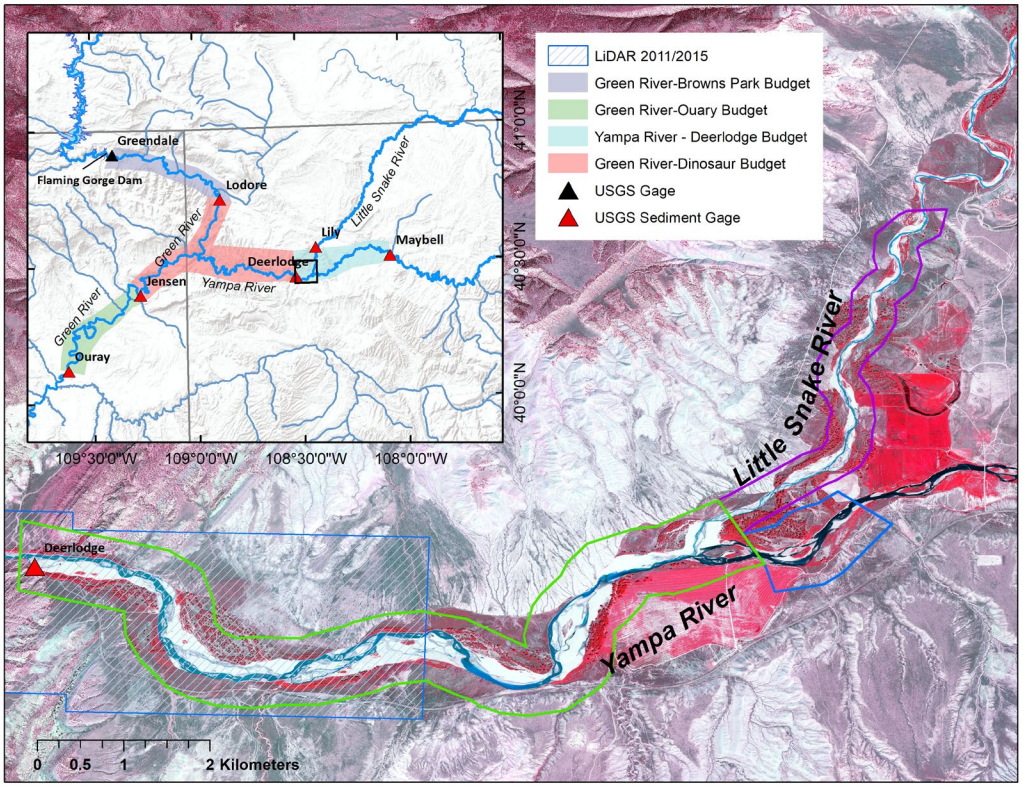

Figure 1. Map showing the locations of the study area near Dinosaur National Monument on the Yampa and Little Snake Rivers. The study area is part of a larger area that encompasses a sediment-transport monitoring network at USGS gaging stations (i.e., sediment gages) that defines four flux-based sediment budget segments in the region (see inset map). In the study area shown in this figure, volumetric change in storage was divided into three reaches: (1) Yampa River ~1 km upstream of the Little Snake River, (2) Yampa River downstream of the Little Snake River to the Deerlodge sediment gage, and (3) Little Snake River ~4 km upstream of the Yampa River, but we focus on results from the Yampa River downstream of the Little Snake River.

On the Yampa River in Deerlodge Park, channel morphology, and within-channel habitat, are a consequence of fine-sediment (e.g., sand, silt, and clay) transport. Sand transport is affected by rare pulses of fine sand that originate from Sand Creek, a tributary of the Little Snake River (Figure 1; Topping et al., 2018). These episodic inputs of sand cause the beds of the Little Snake, Yampa, and middle Green rivers to become finer (Topping et al., 2018). In the intervening periods between these pulses, bed winnowing coarsens the bed. Thus, the sand-transport capacity is controlled by two processes: bed-sand grain-size adjustment and changes in channel form. Flux-based measurements show that the efflux of sand exceeded the influx in every year since 2012, resulting in a sand deficit of 470,000 ± 320,000 metric tons, which corresponds to between 0.04-0.20 m of erosion averaged over a channel length of 12.5 km. The influx and efflux of silt and clay during the same period were in balance.

We hypothesize that the total mass of erosion or deposition measured in the segments between the sediment gages cannot be used to predict detailed channel response and habitat change, because these flux-based sediment budgets do not account for different patterns of storage of different grain sizes in the channel. For example, when the mass of erosion was partitioned by sand size classes, fine to coarse sand was found to have been continuously in deficit since 2012, but very fine sand had accumulated in 2014 and since 2016 (Figure 2). Thus, any segment scale, net change in channel geometry must primarily involve those geomorphic units where fine to

coarse sand was eroded and very fine sand was deposited. Conversely, there should be relatively little net change in geomorphic units that are primarily composed of mud, because the influx and efflux of silt and clay were in balance.

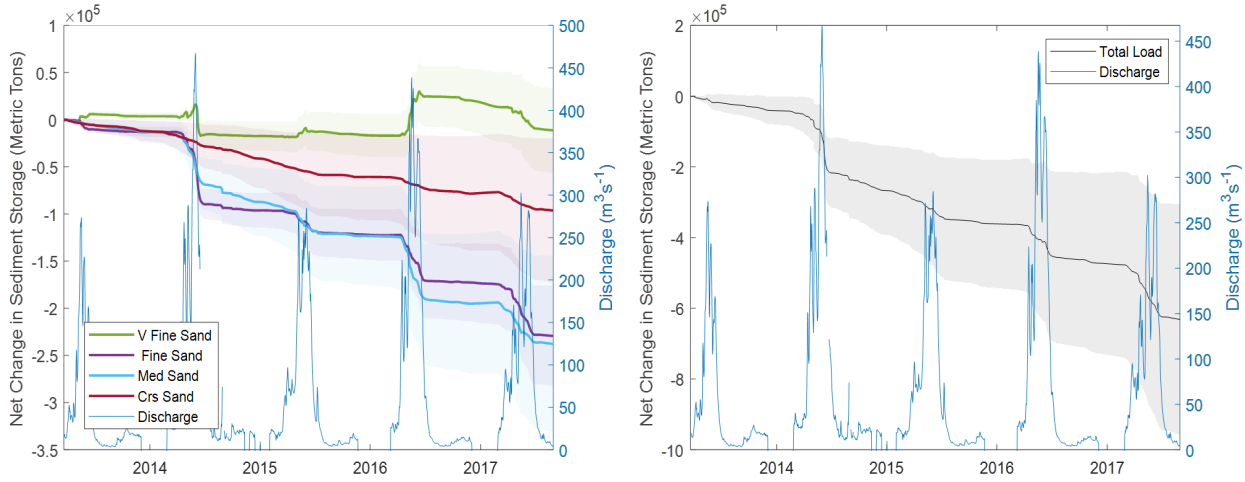

Figure 2. Partitioned and total flux-based sand budget.

Methods and Results

To characterize where sediment was stored or evacuated from different reaches, we used repeat aerial images to quantify channel change and a probabilistic method to account for uncertainty in digitizing and image co-registration. Planform channel adjustments were converted to a volumetric change in sediment storage using a Bayesian model to estimate heights of different geomorphic surfaces from a terrain model that covered part of the study area (Figure 1).

LiDAR topography data were acquired with laser pulses in the near-infrared wavelength and provide no bathymetric data. To calculate bathymetry, we derived estimates of wetted channel depth using multi-spectral aerial images following the methods of Legleiter (2015), which do not require field measurements of water depth at the time of image acquisition. Legleiter (2015) developed the Flow Resistance Equation-Based Imaging of River Depths (FREEBIRD[1]) algorithm to derive a linear relationship between image pixel depth and the natural log of a ratio of two image bands (i.e., red, green, blue, and NIR wavelengths). FREEBIRD is based on a cross-sectional average velocity calculated from a Manning-like flow resistance equation that includes a single, quasi-universal conductance coefficient. FREEBIRD links image data to channel hydraulics by substituting the band ratio for depth in a series of incremental distances (i.e., pixels) along a cross-section to produce unit discharges that are summed to estimate the total discharge. A separate algorithm minimizes the differences in discharge between cross-sections and the known discharge at the time of image acquisition by iteratively adjusting the slope and y-intercept of the image pixel depth-to-band ratio relationship. The final terrain model was generated by subtracting image-derived estimates of depth from LiDAR-derived water-surface elevations, then combining the resultant bed elevations with LiDAR elevations of terrestrial surfaces (Hicks et al., 2006; Legleiter, 2012).

[1] Any use of trade, product, or firm names is for descriptive purposes only and does not imply endorsement by the U.S. Government

Aerial-image-derived volumetric changes in storage showed that the volume of bank erosion exceeded the volume of deposition along the channel margin on the Yampa River downstream from the Little Snake confluence in every year (Figure 3). At the same time, vegetated island expansion exceeded erosion (Figure 3). These results demonstrate that, in this river segment, the flux-determined sand deficit is driven by bank erosion, with partial offset by vegetated-island expansion. Grain-size measurements suggest that the sand-size material in the channel banks is composed of fine to coarse sand, and vegetated islands are dominated by very fine to fine sand (Figure 4). The fine to coarse size sand evacuated from the banks and fine to very fine sand stored on vegetated islands can thus be linked to the partitioned flux-based sediment budget, which showed that fine to coarse sand was in deficit, and very fine sand accumulated.

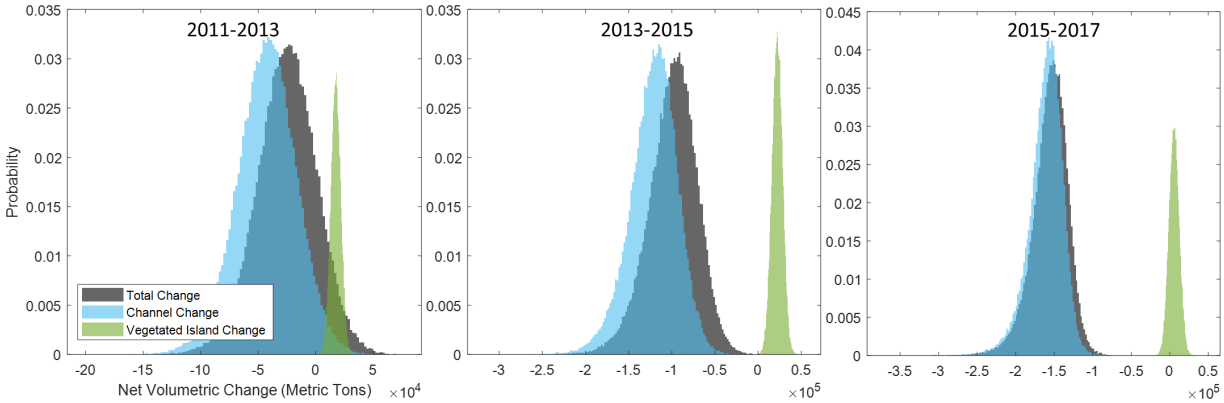

Figure 3. Volumetric change in sediment storage between repeat aerial images on the Yampa River downstream of the Little Snake confluence (Figure 1).

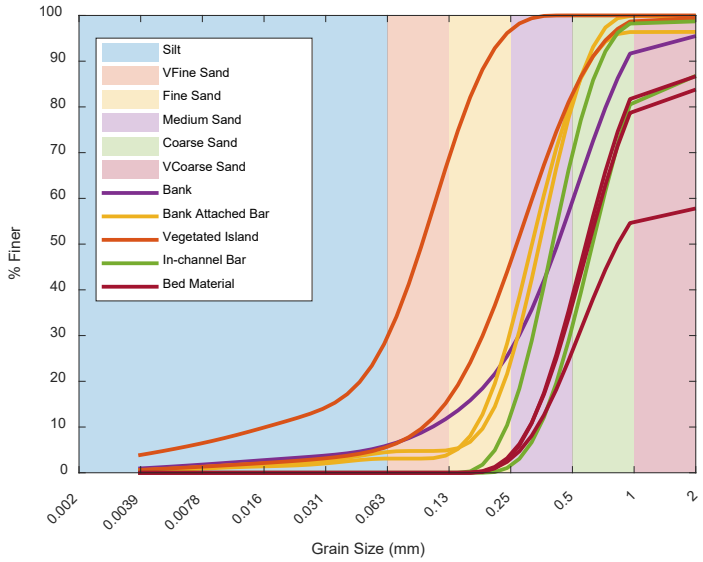

Figure 4. Grain size distribution of geomorphic units used to calculate volumetric change in storage between repeat aerial images. Vegetated islands are composed of the finest sand-size fractions and the bank is composed of fine to coarse sand.

Calculations of channel width from aerial images showed that the channel narrowed from 2011 to 2015 and slightly widened from 2015 to 2017 (Figure 5). Channel narrowing has primarily occurred by vegetated island expansion and bank attached bar deposition prior to 2015. Following 2015, vegetated islands continued to expand, but narrowing in these areas was offset by localized large areas of bank erosion. Thus, the flux-determined sand deficit can be linked to

a reduction in channel width caused by within-channel storage of very fine sand followed by a slight increase in channel width associated with bank erosion and evacuation of coarser-size sand. It is likely that channel narrowing from 2011 to 2015 was a recovery response from the second largest flood of record, which occurred in 2011 before the aerial image was acquired. Presumably, the 2011 flood widened the channel and subsequent channel narrowing from 2011 to 2015 was caused by channel recovery to pre-2011 widths. Future work will extend the aerial photo analysis to 1938 to confirm whether channel narrowing is a long-term trend or short-term response to the 2011 flood.

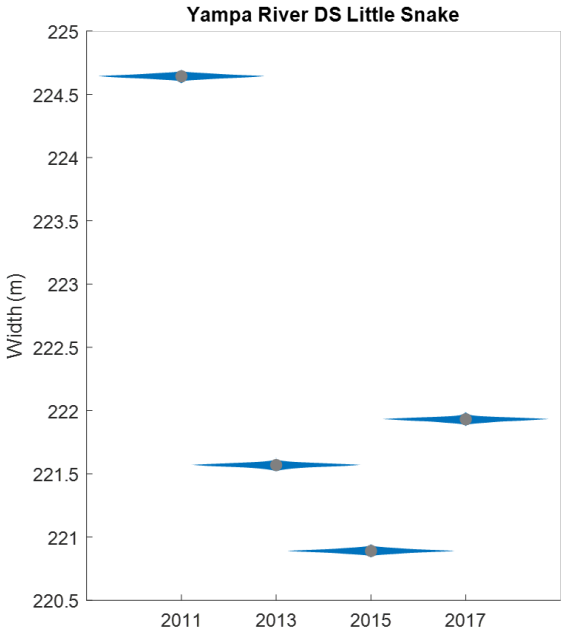

Figure 5. Channel width on the Yampa River downstream of the Little Snake confluence (Figure 1). Width was calculated by subtracting the vegetated island area from the channel area and dividing by the centerline length.

These results demonstrate that it is possible to explicitly link new channel change with sediment-transport measurements to understand where and why channel change occurs. Future work will extend this analysis to the Green River and aims to link changes in reservoir operations at Flaming Gorge Dam with changes in channel form through sediment transport measurements in order to evaluate changes in habitat availability.

References

Hicks DM, Shankar U, Duncan MJ, Rebuffe M, Abele J. 2006. Use of remote sensing technologies to assess impacts of hydro-operations on a large, braided, gravel-bed river: Waitaki River, New Zealand. Braided Rivers, Processes, Deposits, Ecology and Management. International Association of Sedimentologists, Special Publication **36** : 311–326.

Legleiter CJ. 2012. Remote measurement of river morphology via fusion of LiDAR topography and spectrally based bathymetry. Earth Surface Processes and Landforms **37** : 499–518. DOI: 10.1002/esp.2262

Legleiter CJ. 2015. Calibrating remotely sensed river bathymetry in the absence of field measurements: Flow REsistance Equation-Based Imaging of River Depths (FREEBIRD). Water Resources Research **51** : 2865–2884. DOI: 10.1002/2014WR016624

Topping, D.J., Mueller, E.R., Schmidt, J.C., Griffiths, R.E., Dean, D.J., and Grams, P.E., 2018, Long-term evolution of sand transport through a river network: Relative influences of a dam versus natural changes in grain size from sand waves, Journal of Geophysical Research: Earth Surface **123**: 1879-1909, https://doi.org/10.1029/2017JF004534.

Interpreting Topographic Change on the Lower American River in California

Matthew Weber, Ecohydrologist, cbec, inc. eco engineering, West Sacramento, CA, m.weber@cbecoeng.com
Chris Bowles, Managing Director / Ecoengineer, cbec, inc. eco engineering, West Sacramento, CA, c.bowles@cbecoeng.com
Chris Hammersmark, Director / Ecohydrologist, cbec, inc. eco engineering, Santa Cruz, CA, c.hammersmark@cbecoeng.com
Tom Gohring, Executive Director, The Sacramento Water Forum, Sacramento, CA, tgohring@waterforum.org
Dan Tibbitts, Principal Engineer, The Sacramento Area Flood Control Agency, Sacramento, CA, tibbittsd@saccounty.net

Abstract

The commercial availability of topobathymetric LiDAR (i.e., cost-effective LiDAR with near-infrared and green sensors that can map topography and bathymetry) has rapidly advanced topographic change detection (TCD) analyses. LiDAR provides the detail necessary to develop robust uncertainty analyses and resolve topographic change at the feet-scale over large spatial extents. In this study, a 2017 topobathymetric LiDAR survey was used to conduct a TCD analysis from 2006/2008 to 2017 for the ~23-mile lower American River in Northern California. This time period experienced a prolonged drought with only moderate flows of ~30,000 cfs in 2011 (~2-3 year event) and a series of high flows in 2017 (63,000 cfs and 82,000 cfs, ~10-yr events). The goals of this study were to: (1) assess topographic change by comparing the 2017 survey to an earlier survey from 2006/2008; (2) implement a robust topographic uncertainty analysis for each survey data set by accounting for point density, landcover, slope, surface roughness, and survey method; (3) quantify the amount of sediment exported out of the system due to lack of sediment connectivity below Nimbus and Folsom Dams; (4) compare and contrast the topographic change results between different geomorphic reaches to understand how the river is behaving; and (5) compare the results to a previous TCD that was conducted from 1997 to 2006/2008 to inform how different flood magnitudes influence the results. Results showed that from 2006/2008 to 2017, the lower American River exported approximately 330,000 cubic yards of sediment to the Sacramento River (average of 31,000 yd^3/yr). Much of this sediment was eroded from the channel bed (i.e., within the channel banks), with little sediment connectivity between the channel and the floodplain. During the preceding decade, from 1997 to 2006/2008, the lower American River exported approximately 170,000 cubic yards of sediment (average of 19,000 yd^3/yr). This earlier time period experience only small floods of 2-3-year recurrence intervals. During both periods, the river scoured the most sediment in the reach below Nimbus Dam (Sunrise reach) with neutral to aggrading conditions in the widest reach (Riverbend reach). These findings play an important role in informing ongoing remediation efforts to provide gravel augmentation to sites below Nimbus Dam, assess erosion vulnerabilities of banks and levees that may be at risk, inform design of bank and levee erosion protection, and enhance/create salmonid spawning and rearing habitat.

Lake Providence to Old River Geomorphic Assessment

Waleska Echevarria-Doyle, Research Hydraulic Engineer, U.S. Army Engineer Research and Development Center, Coastal and Hydraulics Laboratory, Vicksburg, MS, Waleska.Echevarria-Doyle@usace.army.mil

David S. Biedenharn, Research Hydraulic Engineer, U.S. Army Engineer Research and Development Center, Coastal and Hydraulics Laboratory, Vicksburg, MS, David.S.Biedenharn@usace.army.mil

Charlie D. Little Jr., Civil Engineer, Mendrop Engineering Resources, LLC, Vicksburg, MS, clittle@mendrop.net

Abstract

This study integrates information from previous geomorphic studies coupled with new analysis to provide a comprehensive geomorphic characterization of the Lake Providence (River Mile [RM] 487.2 Above Head of Passes [AHP]) to Old River Control Complex (ORCC), (RM 317 AHP) reach from the early 1800s to present. Individual components of this study included: historical geomorphic studies, development of an event timeline, specific gage records, trends in water surface slopes, bed material studies, channel geometry data, and effects of channel improvements (cutoff, dike, revetment, and dredging). These individual assessments were consolidated to develop an overall assessment of how the study reach has evolved since the early-1800s.

Introduction

The Mississippi River has been molded by anthropogenic and natural factors for thousands of years. Early effort by the U.S. Army Corps of Engineers (USACE) to manage the river for navigation began in the early-1800s, with the most comprehensive efforts occurring as a result of the Flood Control Act (FCA) of 1928 following the Flood of 1927. The Mississippi River & Tributaries (MR&T) Project that was authorized from the FCA of 1928 has produced a massive, comprehensive system for flood protection and channel stabilization that includes levees, channel modifications, and floodways, as well as tributary reservoirs and other basin improvements. The first official “Potamology Investigations” were initiated in the mid-1940s. These potamology studies continued as an integral component of the MR&T Program until the 1980s when the program ended. Then, after lost decades of continued potamology advancement and technical expertise, the Mississippi River Geomorphology and Potamology (MRG&P) program was created by the USACE Mississippi Valley Division (MVD) in 2014. MRG&P studies are designed to provide a comprehensive analysis of physical and anthropogenic factors that influence the flood conveyance, navigability, and environmental quality of the Mississippi River. The report presented herein represents one component of the MRG&P Program. This study represents an integration of numerous individual studies that addressed various geomorphic aspects of the Mississippi River combined with new analyses to weave together a more comprehensive understanding of the geomorphic character specifically for the river reach between Lake Providence, LA (RM 487.2 AHP) and the ORCC, (RM 317 AHP). The 1962 river mile system, which reflects miles above the Head of Passes (AHP), is used throughout the report.

Geomorphic Changes Early 1800s to Present

Event Timeline

A chronology of the major river engineering, hydrologic, and anthropogenic events within the study reach was developed for the study time period. The timeline is presented to add insight into the interpretation of the results from other analyses presented in this report. Table 1. summarizes the main events from the early 1800s to present.

Table 1. Major Event Timeline from the early-1800s to present.

Early-1800s to late-1800s	Late-1800s to early- 1900s	Mid-1900s to late-1900s	Late-1900s to present
1) Massive clearing of streambanks and riparian areas for wood burning steamboats and agriculture. 2) 1811-1812: New Madrid Earthquakes. 3) 1849-1850: Repeated flooding along the Mississippi River Valley. 4) Flood of 1874-Results in creation of Levee Commission. 5) 1879-Mississippi River Commission (MRC) created.	1) 1879-1928: Levees only policy adopted by MRC. 2) 1884-1929: MRC adopts policy to prevent natural neck cutoffs from forming. Natural chute cutoffs were allowed to continue during this period. 3) 1890, 1913, and 1927 Floods. 4) 1928-FCA of 1928 results in creation of the MR&T Project. 5) 1929-MRC allows the Yucatan cutoff to occur naturally, the first natural neck cutoff to occur since 1884.	1) 1930-1934: Low water period. 2) 1931-1942: Cutoff Period (14 neck cutoffs between just south of Natchez, MS and just north of Helena, AR). 3) 1937 Flood. 4) 1940s-Studies indicate potential of Atchafalaya capturing Mississippi River Flow. 5) 1940-1944 and 1952-1972: Low water periods. 6) 1950s-Mid-1990s: Major bank stabilization period. 7) Mid-1960s-early-2000s: Major dike construction period.	1) 1963 ORCC Low Sill Structure in operation 2) 1975 Flood. 3) 1984-1988: Low water period. 4) 1986-ORCC Auxiliary Structure in operation. 5) 1990-ORCC Hydropower Unit in operation. 6) 1993-Flood on upper Mississippi River. 7) Mid-1990s-Dike notching program begins. 8) 1997 Flood. 9) 2000-Low water year. 10) 2008 Flood. 11) 2011 Flood. 12) 2012-2014: Low water period.

Pre-Cutoff Period (early 1800 to 1929)

Early 1800s to 1880s: The early 1800s was a period of rapid expansion into the Lower Mississippi River (LMR) Valley, and navigation along the waterways was the key to the growth of this region. At the time, the Mississippi River was experiencing substantial geomorphic changes as a result of both natural and anthropogenic factors during this initial period of expansion. According to Winkley (1977), the New Madrid earthquakes (1811 to 1812) contributed to substantial bank instabilities throughout the river causing excessive sediment supply, bar growth and other problems that impacted navigation. Additionally, wood burning steamboats along the Mississippi River were introduced in the early 1880s. These steamboats required

massive amounts of fuel (wood) which was supplied from the numerous woodyards that sprung up along the river during this period and resulted in thousands of acres of streambanks being cleared. This land clearing combined with agriculture along the natural levees accelerated bank erosion and sediment supply to the system (Winkley, 1977).

Six natural neck cutoffs occurred in the study reach between 1776 and 1884, shortening the river by approximately 78 miles (Table 2). Although specific years are listed in Table 2, it should be recognized that these cutoffs typically did not develop instantaneously, but rather, generally took many years to completely develop. Meanwhile, the river was obtaining additional length elsewhere through meander growth, such that, according to Winkley (1977), the overall river lengths for the entire Lower Mississippi River in 1765 (the first map of the Mississippi River) and 1884 were nearly the same.

Table 2. Natural Neck Cutoffs from Lake Providence, LA to Old River between 1776 and 1884 (Modified from Winkley, 1977).

Natural Cutoff	1962 River AHP Mile	Year Cutoff Occurred	River Length Reduction by Cutoff (Miles)
Terrapin Neck	462	1866	16
Yazoo	442	1799	12
Centennial Lake	438	1876	6
Davis or Palmyra	422	1867	19
Waterproof	377	1887	12
Homochitto	322	1776	13
			Total = 78

The dramatic changes occurring during this time period indicate that the channel was in a period of morphologic adjustments to regain dynamic equilibrium. The magnitude of these changes is illustrated in Figure 1, which shows changes in the average top bank width for the reach of river between Vicksburg (RM 435 AHP) and the Red River (RM 312 AHP). Even with the uncertainty in the surveys during these older time periods, a good approximation of the order of magnitude of the width changes in the river was estimated. Comparison between the 1821 survey with the survey of 1880 showed that the average top bank width in this reach increased approximately 91%. Width increases of this magnitude would not be compatible with the natural meandering processes of a river in dynamic equilibrium but rather would be indicative of a river experiencing severe system instabilities. Identifying all the causes for this systematic instability is difficult, but the New Madrid earthquakes (Winkley, 1994; Winkley, 1977; Schumm et al., 1994), coupled with the clearing of the streambanks and adjacent riparian areas, appear to be the dominant factors during this period.

Flood protection began in the LMR Valley in the early 1700s, but it was localized and discontinuous. Prior to building levees, the LMR Valley was a delta that carried high as well as lower flows into various lowland basins. After the disastrous flood of 1874, a levee commission was created to evaluate and make recommendations for an integrated levee system (D. O. Elliot, 1932). However, it was not until the creation of the Mississippi River Commission (MRC) in 1879 that a more comprehensive approach was adopted.

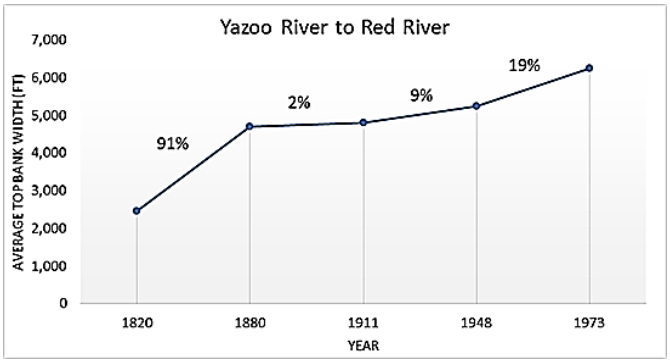

Figure 1. Change in Mississippi River Top Bank Width between 1820 and 1973 (Adapted from Winkley, 1994).

Early 1880s to 1927: The MRC, established in 1879, was created to plan and execute projects to improve navigation along the LMR. Federal funds were assigned to MRC for the construction of levees as part of the navigation improvement program. Other approaches considered included reservoirs, outlets, and cutoffs. After considerable debate, the MRC settled on a "Levee Only Policy". This approach was based on the assumption that the construction of levees would deepen the channel, thereby providing adequate navigation depths. The construction of levees started in 1882 to complete the gaps along the existing levee system. As the average levee height and crevasses became less pronounced, peak annual stages at Natchez, MS began to increase in the early 1900s up to the 1930s (Winkley, 1977).

In 1884, the MRC adopted the "no cutoff" program with the goal of preventing natural neck cutoffs from occurring. Natural neck cutoffs occur when the river flow breaches between the two bends of a meander creating a new channel alignment. This was accomplished by implementing bank stabilization in areas where a natural neck cutoff was considered likely. As a result of this program, the Waterproof cutoff (RM 377 AHP), which occurred naturally in 1884, was the last neck cutoff allowed until 1929. Since six natural neck cutoffs occurred in the 108 year period prior to 1884, it is reasonable to assume that more natural neck cutoffs would have occurred in the 45 year period between 1884 and 1929 without the intervention of the MRC program. Chute cutoffs were allowed during this period. According to Winkley (1977), chute cutoffs occur as a result of recurring large flows across the inside of point bars. The chute cutoffs shortened the river by approximately 45 miles from Cairo, IL to Vicksburg, MS. As a consequence, the river only increased in length in this reach by approximately 14 miles between 1884 and 1929 (Winkley, 1977).

Winkley (1977) suggested that the LMR prior to 1927 was losing channel capacity (due to aggradation) at all gages. Specific gage records, developed at Lake Providence and Vicksburg were examined to determine if aggradational trends were evident during this period at high flows. Unfortunately, historical data prior to the 1930s were not available at the St. Joseph and Natchez gages. As shown in Figure 2, the channel does appear to be slightly aggradational at high flows (1,500,000 cubic feet per second [cfs]) prior between 1900 and 1930.

Numerous floods occurred during this period, and although there were some issues, the overall levee system under the Levee-only approach seemed to perform satisfactorily. This all changed with the devastating flood of 1927. As a result of this major flood, the MRC recognized that a more comprehensive approach was going to be needed to provide adequate flood protection and navigation on the LMR.

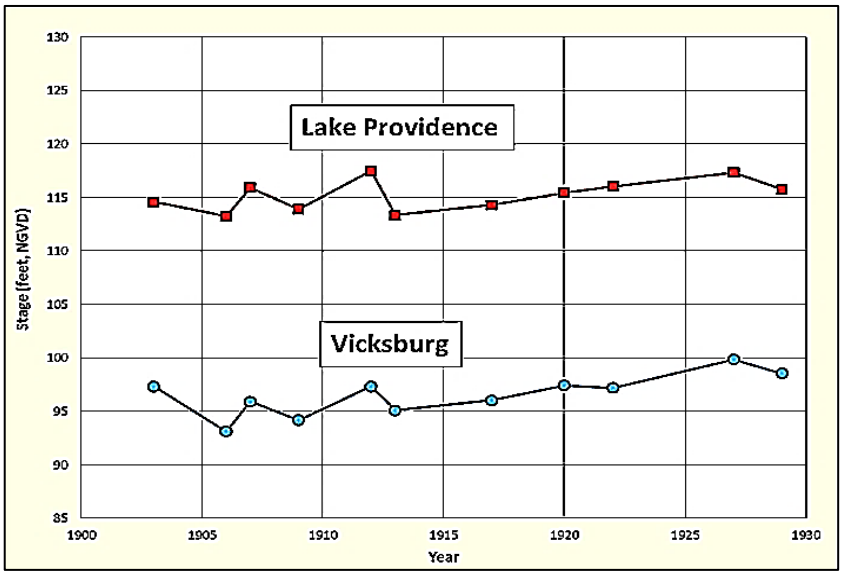

Figure 2. Specific gage records at Lake Providence and Vicksburg in the Pre-cutoff Period for 1,500,000 cfs.

Cutoff Period (early 1929 to 1942)

The advantages and disadvantages of artificial cutoffs on the Mississippi River had been debated without consensus by river engineers since the mid-1880s. However, following the 1927 flood, the MRC again revisited the idea of incorporating artificial cutoffs on the river as one component of the MR&T Project. In 1929, the first natural neck cutoff since 1884 was allowed to occur at the Yucatan Bend downstream of Vicksburg as part of a study to evaluate the response of the river to a neck cutoff. After monitoring the Yucatan cutoff for 2 years, the MRC initiated the cutoff program in 1931. Through this program, the USACE constructed 14 artificial cutoffs and allowed 2 natural cutoffs (Yucatan and Leland) to develop between 1929 and 1942 on the LMR (Table 3). These cutoffs shortened the river between Memphis, TN, and Old River, LA, by approximately 152 miles. Since 1942, no neck cutoffs have been constructed or allowed to develop. However, between 1932 and 1955, chute cutoffs were constructed at 40 locations between Cairo, IL, and Natchez MS, further shortening the river by another 55 miles. Following the artificial cutoffs, meander migration continued as the river attempted to regain some of its length. This continued until the 1960s when further meander migration was essentially terminated by the revetment program. However, according to Winkley (1977), these length increases were offset by the chute cutoffs so that the river is still approximately 150 miles shorter today than prior to the cutoffs.

The study reach (Lake Providence to ORCC) included 7 cutoffs: Willow, Marshall, Diamond, Yucatan, Rodney, Giles, and Glasscock. These cutoffs shortened the study reach by approximately 62 miles. However, during the cutoff period, the dominant response was channel degradation. Winkley (1977) presents specific gage records that show the stage reductions at Vicksburg were in the range of 10 to 12 ft, while farther downstream at Natchez, the stage reductions were slightly less (5 to 7 ft).

Table 3. Man-made neck cutoffs, 1929-1942 (adapted from Winkley [1977]).

Cutoff Name	River Mile	Year Opened	Distance River Shortened (Miles)
Hardin	678	1942	16.9
Jackson	628	1941	8.7
Sunflower	625	1942	10.4
Caulk	575	1937	15.2
Ashbrook	549	1935	11.4
Tarpley	541	1935	8.6
Leland*	539	1933	9.8
Worthington	514	1933	4.3
Sarah	504	1936	5.3
Willow	463	1934	7.7
Marshall	448	1934	4.2
Diamond	424	1933	12
Yucatan*	408	1929	9.6
Rodney	388	1936	5.9
Giles	366	1933	11.1
Glasscock	343	1933	10.8
* Natural Cutoffs			Total = 151.9

Post-Cutoff Period (1943 – present)

Channel Improvements (revetments, dikes, and dredging): The period from the mid-1940s through the mid-1960s was one of extensive adjustments on the LMR as the river responded to the cutoffs. As the river was adjusting to a higher channel slope and stream power after the cutoffs, bank erosion increased as the channel attempted to regain channel length. During this initial period following the cutoffs, the revetment program was initiated in an attempt to stabilize channel alignments. The revetments construction began in the 1940s, reaching a peak in the 1950s and 1960s. By the mid-1960s, most of the major meander bends had been stabilized, thereby fixing the alignments in place. After the mid-1960s, construction was mostly associated to extensions of existing revetments. Winkley (1973) presents accumulated annual average bank caving volumes for the Arkansas River to Old River LMR reach during three time periods: 1877 – 1892, 1931 – 1942, and 1965 – 1972 (Figure 3). These curves were developed by calculating the area associated with the bankline movement between surveys. An average bank height of 40 ft was assumed for the volumetric computations. Using these curves, an estimate of the average annual bank caving volumes in the reach from Lake Providence to the ORCC were reduced approximately from 350,000,000 cy/year in the pre-revetment period (average of the two time periods 1877 - 1892 and 1931 – 1942) to approximately 30,000,000 cy/year in the post-revetment period. This is a reduction in sediment delivery from the channel banks to the system of approximately 90%. However, because the size distribution of these sediments was not reported, the significance of these sediment reductions on the morphological changes in the river system is not clear.

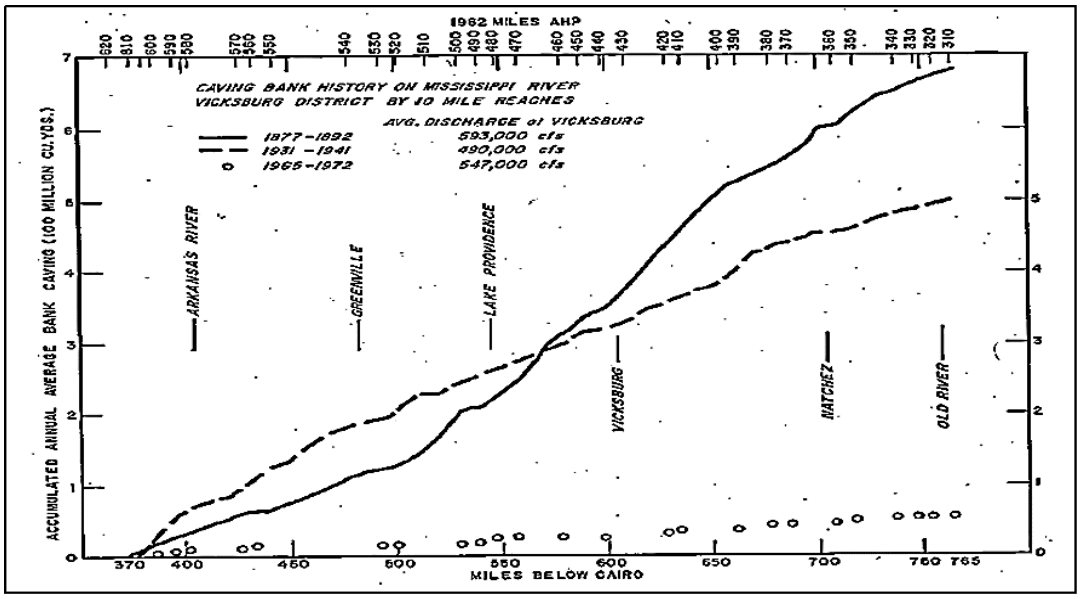

Figure 3. Accumulated annual average bank caving volumes from the Arkansas River to the ORCC (Winkley, 1973).

The cutoffs also imposed a new alignment on the channel system that altered the historic crossing patterns in the river. These alignment changes combined with the increased sediment delivery from bed material upstream resulted in increased maintenance dredging throughout the system. After 1970, the amount of maintenance dredging began a long-term decreasing trend on the LMR as a result of two interrelated factors. The first was the revetment program, which imposed planform alignments with more orderly pool-crossing patterns. The next, and most important factor, was the construction of dikes. The purpose of these dike structures is to provide adequate navigation depths by constricting the channel width, closing off secondary channels and chutes to reduce divided flow, and adjusting channel alignment.

Specific gage records: Specific gage analysis is an effective tool used by river engineers and scientists to assess the historical behavior of rivers. Watson et al. (2013) provides a detailed description of the specific gage analysis. Fundamentally, a specific gage record is simply a plot of river stage versus time for a specific discharge. The specific gage records in this study were developed using the *rating curve method*. Stage data recorded at the Lake Providence gage (secondary station, RM 487.2 AHP, bankfull stage = 37 ft) were combined with discharges measured at Vicksburg (RM 435.7 AHP) using a 1-day lag time to generate the specific gage record from 1906 to 2014 (Figure 4). The channel degradation, which began in the early-1930s after the cutoffs, continued through the late-1940s to early-1950s. Since the 1950s, there have been some fluctuations in stage, but overall stages have remained relatively stable. The specific gage analysis for the Vicksburg gage (primary station, RM 435.7 AHP, bankfull stage = 43 ft) extends from 1903 to 2016. An abrupt decrease in stages for all flows occurred during the early-1930s, and this decreasing trend continued throughout the 1940s and early-1950s. Since then, stages for all flows greater than 200,000 cfs have fluctuated around what appears to be a generally increasing trend. In contrast, stages for a discharge of 200,000 cfs have been relatively stable since the 1950s. The specific gage analysis for the St. Joseph gage (secondary station, RM 396.4 AHP, bankfull stage = 40 ft) extends from 1935 to 1996. The specific gage record was developed by coupling daily stages observed at St. Joseph with discharges measured at Natchez using a 1-day time lag. As shown in Figure 4, a decreasing trend in stages began in the mid-1930s and persisted into the early-1940s. Between the mid-

1940s and the end of the period of record in the mid-1990s, stages for all but the lowest discharge exhibited an increasing trend. Stages for 200,000 cfs remained relatively stable. The specific gage analysis for the Natchez gage (primary station, RM 393.3 AHP, bankfull stage = 48 ft) extends from 1935 to 2016. The stages for all flows at this gage decreased abruptly in the late-1930s and continued to display a downward trend during the early-1940s. Since the mid-1940s, a general, increasing trend is evident in the stages associated with all selected flows.

The study reach is responding in an expected manner following a series of cutoffs. At the upstream end of the reach, represented by the Lake Providence gage, the stages have been relatively stable since the early-1950s. Moving farther downstream, the gages (Vicksburg, St. Joseph, and Natchez) become progressively more aggradational. This suggests that the reach from Lake Providence to Vicksburg may be a transition reach between dynamic equilibrium and the aggradational trends that exist farther downstream.

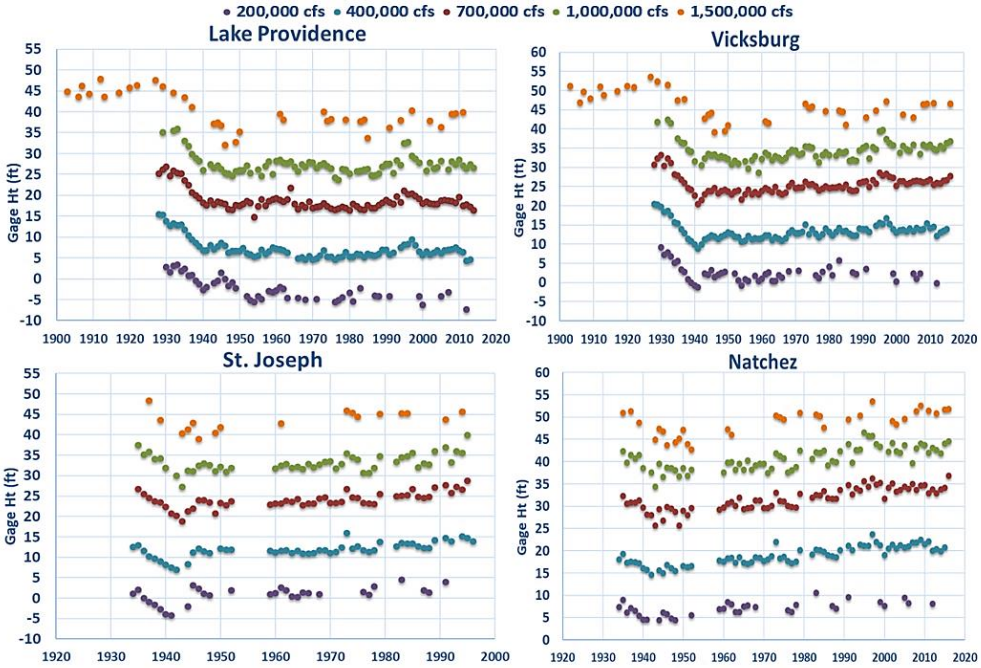

Figure 4. Specific gage record at Lake Providence, Vicksburg, St. Joseph, and Natchez gages.

Water surface slope trends: Water surface slope provides a representation of the energy in a channel system. Slope is closely associated with the sediment transport capacity. Therefore any changes in channel slope can be used to infer morphologic changes in a channel system. Slope trends on the LMR are extremely important because of the substantial increases that occurred immediately after the cutoffs. Tracking these slope changes in the Pre- and Post-cutoff Periods provides valuable insight into the morphology of the study reach. Water surface slopes were calculated between the following sub-reaches: (1) Lake Providence to Vicksburg; (2) Vicksburg to St. Joseph; (3) St. Joseph to Natchez; and (4) Vicksburg to Natchez. Daily water surface slopes were calculated using daily stage data and the distance between the gaging stations. Average annual slope values were then calculated for each year.

Figure 5 shows the trends in average annual water surface slopes for the Lake Providence to Vicksburg, Vicksburg to St. Joseph, St. Joseph to Natchez, and Vicksburg to Natchez. The events

that caused the distance change between the gages (cutoffs, meander activity, gage location change, etc.) and their respective time periods were taken into consideration to estimate the water surface slope. Beginning in the mid-1930s and continuing through the mid-1940s, there was a dramatic increase in slope in the Lake Providence to Vicksburg reach (Figure 5). During this period, slopes increased from approximately 0.000054 to 0.000078, an increase of approximately 44%. From the mid-1940s through the mid-1970s to early-1980s, the slopes fluctuated but generally exhibited a decreasing trend. Since the early-1980s, the slopes have been relative stable, with an average slope of approximately 0.000063. The present-day slopes (early-1980s to present) are approximately 16% higher than the pre-cutoff slopes.

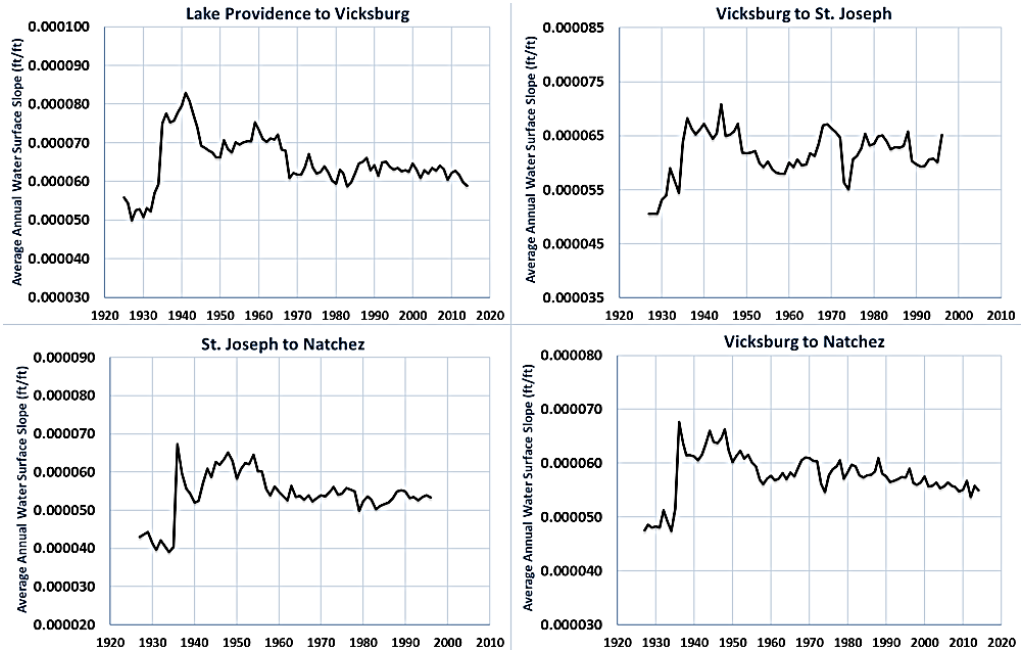

Figure 5. Average annual surface slopes for: 1) Lake Providence to Vicksburg, 2) Vicksburg to St. Joseph, 3) St. Joseph to Natchez, and 4) Vicksburg to Natchez.

The changes in the average annual water surface slopes for the Vicksburg to St. Joseph reach are also shown in Figure 5. Note that there are no data after 1996 due to the discontinuance of the St. Joseph gage. Water surface slopes increased dramatically between the mid-1930s and the mid-1940s. The channel slopes were approximately 24% higher immediately after the cutoffs (mid-1930s to mid-1940s) compared to the Pre-cutoff slopes. After the mid-1940s, the slopes began a decreasing trend, which generally continued until the early 1960s. From the early-1960s to 1995, channel slope exhibited alternating periods of increasing and decreasing trends but remained within an approximate range between 0.00006 and 0.000067 with an average slope of approximately 0.000063. Comparison of the Pre-cutoff and Post-cutoff (mid-1980s to 1995) data shows that the Post-cutoff slopes are still approximately 17% higher than the Pre-cutoff slopes. Following the cutoffs in the mid-1930s, the slope from St. Joseph to Natchez increased abruptly reaching a peak in approximately 1936. After this, the slopes decreased until approximately 1940 when the slope began to increase again. The slopes remained elevated until the mid-1950s when they decreased again. These initial slope increases, which persisted through the mid-1950s, were approximately 45% higher than the Pre-cutoff slopes. Since the mid-1960s up to 1996, the slopes have remained relatively stable with an average slope of approximately 0.000053, which is approximately 29% higher than the Pre-cutoff slopes.

Figure 5 also shows the slope trends for the Vicksburg to Natchez reach. The advantage of considering the Vicksburg to Natchez reach is that it has a much longer period of record than the St. Joseph gage. However, it must be recognized that the slope calculations cover a much longer reach and therefore represent a somewhat more broad-scale view of the system. The Pre-cutoff slopes in this reach averaged approximately 0.000049. In the mid-1930s, the slopes increased and remained elevated through the late-1940s with an average slope of approximately 0.000064. This was an increase of approximately 31% relative to the Pre-cutoff slopes. Between the late-1940s and late-1960s, there was a decreasing trend in the slopes. From the late-1950s through the late-1980s, the slopes exhibited some fluctuations but were overall relatively stable. Since the late-1980s, the slopes appear to have been on a slightly decreasing trend with an average slope of approximately 0.000056. The present day slopes (late-1980s to present) are approximately 16% higher than the slopes in the Pre-cutoff Period.

In summary, initial increases in water surface slopes after the cutoffs ranged from approximately 24% to 45%. These increases in slope also increased sediment transport capacity, resulting in channel degradation throughout the reach. Although the slopes have decreased from their initial peak conditions immediately after the cutoffs, the present-day slopes in the study reach are still higher (generally approximately 17%) than in the Pre-cutoff Period.

Bed material characteristics: Gaines and Priestas (2016) compared bed material gradations collected in 2013 to bed material gradations for 1932 (WES 1935) and 1989 (Nordin and Queen 1992). The findings documented in the report are based on 754 bed material samples collected in November 2013 at 496 locations spaced at intervals of 2 to 3 miles along the Mississippi River between Grafton, IL, and Head of Passes, LA. Data collection procedures in 2013 were matched as closely as possible to the procedures used for the collection of bed material samples in 1932 and 1989. Figure 6 shows the downstream trends in median (D_{50}) grain sizes measured in November 2013 in the LMR between Cairo, IL, and Head of Passes, LA. River miles between Lake Providence and Old River are within the red box. According to the regression line in Figure 6, the D_{50} at Vicksburg and Natchez is approximately 0.36 and 0.3 mm, respectively. Additionally, Gaines and Priestas (2016) compared bed material grain size distributions in the LMR in 1932, 1989, and 2013. Based on this comparison, the study reach had a higher amount of very coarse sand and gravel (2 mm or larger) in 1932 when the bed material grain size distributions are compared with the 1989 and 2013 gradations. It is also noticed that very fine sand (0.0625 mm – 0.125 mm), coarse silt (0.004 mm – 0.062 mm), and clay (< 0.004 mm) have decreased over time. In fact, in 1989 and 2013, there was essentially no bed material finer than very fine sands in the bed, with the exception of a very small amount near the downstream end of the reach in 1989. However, the amount of medium sand within the study reach has increased relative to the 1932 sampling.

Robbins (1977) published a study of the suspended sediment and bed material trends within the Vicksburg District reach to identify possible trends in the datasets that might have relevance for navigation and flood control. Using the Robbins (1977) data, Thorne et al. (2017) conducted a detailed analysis of the spatial and temporal bed material trends. The data presented herein are summarized from these two reports. As part of the USACE Vicksburg District's Potamology Program, the Vicksburg District reach was divided into 25 potamology reaches. Between 1966 and 1974, the district conducted extensive data collection and analyses in these reaches. Typically, data that were collected (sometimes several times per year) included hydrographic surveys, suspended sediment samples, bed material samples, slope measurements, and discharge measurements. Fourteen of the 25 reaches were included within the study reach

between Lake Providence and Old River. In each reach, bed sediment samples were collected at specific sediment study ranges. At each range, between 4 and 12 bed material samples were collected, depending on the width of the cross section. The extensive sampling conducted in the potamology reaches over the 9 year period provides valuable insight into the variability of the bed material composition.

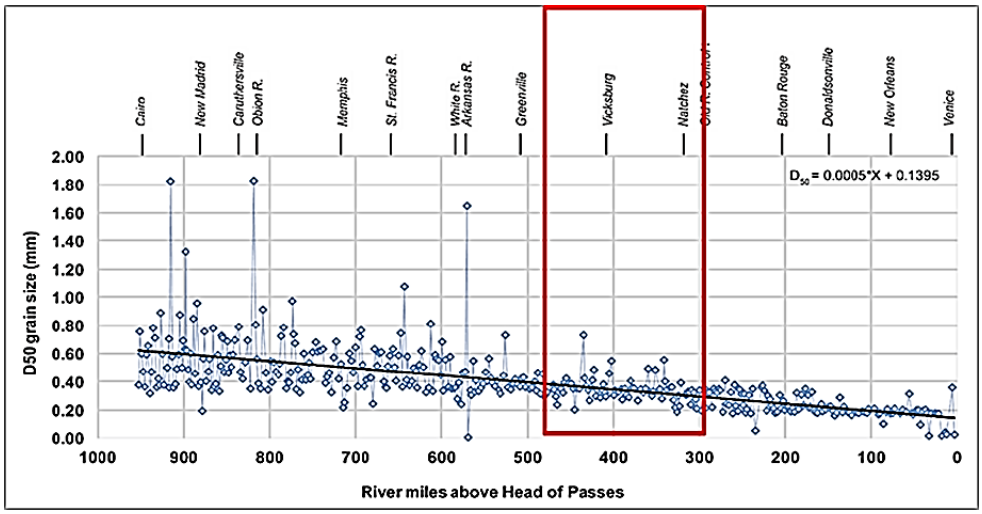

Figure 6. Downstream trends in D50 in November 2013 – Study reach outlined in red (Gaines and Priestas, 2016).

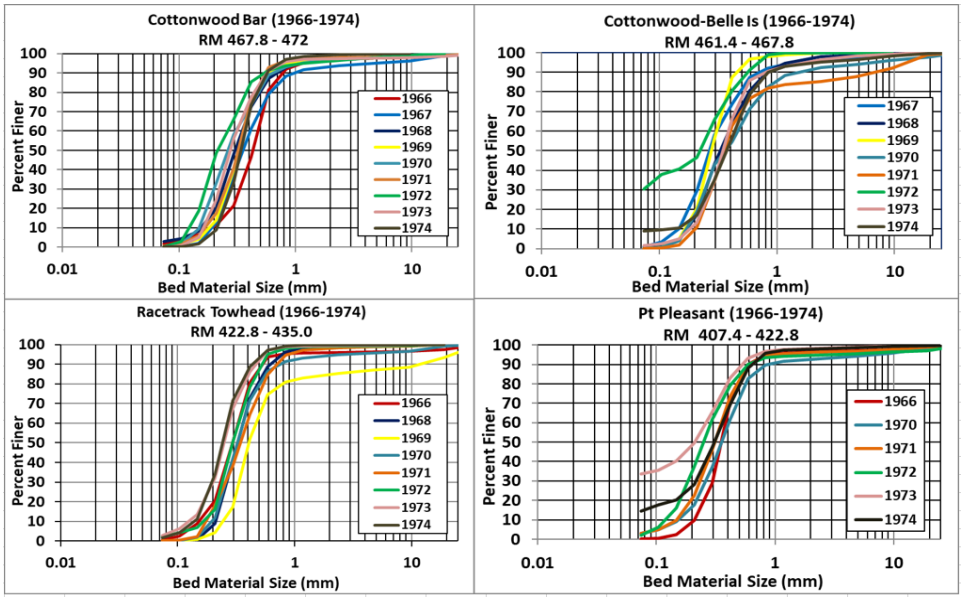

Figure 7. Selected bed material gradation curve in the research study.

Figure 7 shows the variability between years in the bed material gradations for four selected reaches. Examination of these plots clearly shows that there is considerable temporal variability in the bed material gradation. However, no downstream, decreasing trends in the data were observed. The Robbins (1977) data indicate that the dominant bed size is sand with an average D50 of approximately 0.31 mm.

Channel geometry trends: Little et al. (2017) conducted a detailed geometric data analysis for the Mississippi River from ORCC to St. Louis, MO, or approximately RM 325 AHP to RM 180 Above Mouth of the Ohio River. This study documented the long-term trends in the dimension, pattern, and profile of the LMR and Middle Mississippi River. Hydrographic survey data from 1975 to 2013 were used to determine spatial and temporal variations in channel geometry and volume. Trends of geometric change (area, depth, width, conveyance, and channel volume) were identified along defined geomorphic reaches of the river. The following is a brief summarization of the results specifically for the Lake Providence to Old River reach.

Little et al. (2017) reported a decreasing trend for the period 1975 to 2013 in channel area, hydraulic depth, conveyance, and channel volume for the portion of the study reach from approximate RM 325 AHP to RM 435 AHP in the vicinity of Vicksburg. In this study, they examined the pools and crossings individually and found the patterns of decreasing trends to be similar for both. They attributed these decreases to the general depositional trends in this portion of the river. The absence of significant cross-sectional and volumetric changes in the reach from approximately Vicksburg (RM 435 AHP) to Lake Providence (RM 487 AHP) led Little et al. (2017) to classify this reach as a transition zone from the depositional trends downstream to more stable conditions (dynamic equilibrium). The cumulative volume change plots developed by Little et al. (2017) help visualize the observed trends discussed above. These plots allow the spatial extent of the average volumetric change rates over time to be readily determined. The cumulative volume change plots referenced to the Low Water Reference Plane (LWRP) for the entire Vicksburg District reach are shown in Figure 8. The study reach is highlighted in the red box. A negative slope of the cumulative volume change curve indicates deposition (negative cumulative volume change) while a positive slope indicates erosion (increasing cumulative volume). If the cumulative volume change curve is neither increasing nor decreasing over some time period, then this is an indication of dynamic equilibrium. As shown in Figure 8, the reach from approximately RM 325 AHP to approximately RM 425 AHP near Vicksburg exhibited a consistent rate of channel volume decrease (negative slope) for the 1975 to 2013 time period, indicating that this was a depositional zone during this period. From Vicksburg (RM 435 AHP) up to Lake Providence (RM 487 AHP), the cumulative channel volume change fluctuated but remained fairly constant in magnitude, indicating that there was no significant net erosion or deposition during this time period.

In summary, the analysis of the channel geometry parameters indicate that the river channel in the lower portion of the study reach (RM 325 AHP to near Vicksburg RM 435 AHP) was in a depositional or aggradational state for the 1975 to 2013 time period. The reach upstream of Vicksburg to Lake Providence appears to be a transition reach of little to no change in the channel geometry. This suggests that this reach may be approaching dynamic equilibrium.

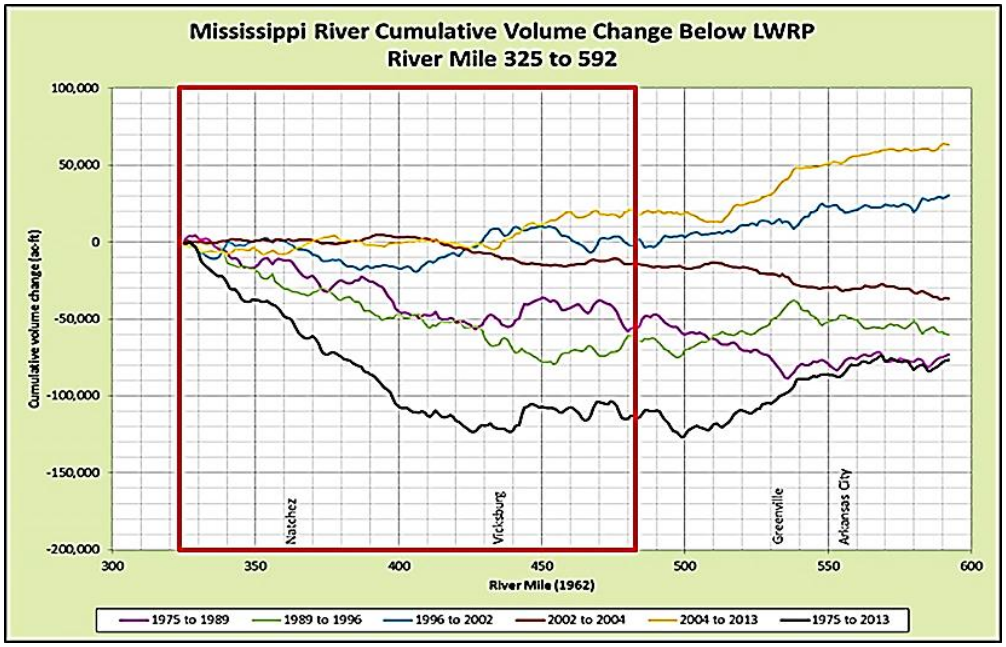

Figure 8. Cumulative volume change curves for the Vicksburg District. Study area outlined in red.

Summary

Pre-cutoff Period: The LMR between the early-1800s to the late-1870s was undergoing substantial morphological changes as a result of both natural and anthropogenic factors during this initial period of expansion. The instabilities in the river aggravated early navigation problems making navigation in the LMR a challenge. In an effort to improve the existing levee system and the assumption that a more robust levee system would deepen the channel to improve navigation, the MRC settled on a Levees-Only policy. Later in 1884, the MRC adopted a no-cutoff program to prevent natural neck cutoff from occurring. As a result, Waterproof cutoff was the last neck cutoff allowed until 1929 when the MRC decided to allow the Yucatan cutoff just south of Vicksburg to develop. The river in the post-1880s was still a dynamic river; although compared to the pre-1880s period, the rates of change had slowed considerably. Although data are sparse in this period, it does appear, based on specific gage records and historical references (Winkley 1977), that the river in the study reach was slightly aggradational during this period. As a result of the 1927 flood, the MRC decided to revise the levees-only approach. With the FCA of 1928, the MR&T was initiated. The MR&T produced a massive, comprehensive system for flood protection and channel stabilization that includes levees, channel modifications, and floodways as well as tributary reservoirs and other basin improvements.

Cutoff Period: The advantages and disadvantages of artificial cutoffs on the Mississippi River had been debated without consensus by river engineers since the mid-1880s. In 1929, the first neck cutoff since 1884 was allowed to occur at the Yucatan Bend downstream of Vicksburg as part of a study to evaluate the response of the river to a neck cutoff. After monitoring the Yucatan cutoff for 2 years, the MRC initiated the cutoff program in 1931. Through this program, the USACE constructed 14 artificial cutoffs and allowed 2 natural cutoffs (Yucatan and Leland) to develop between 1929 and 1942 on the LMR. Seven cutoffs were constructed in the study

reach between Lake Providence and just south of Natchez. These cutoffs shortened the reach by approximately 62 miles. During the cutoff period between 1929 and 1942, the dominant response in the study reach was channel degradation and slope increase. The stage reductions due to degradation after the cutoffs were in the range of 10 to 12 ft at Lake Providence and Vicksburg. Farther downstream at St. Joseph and Natchez, the stage reductions were slightly less, in the 5 to 7 ft range. Substantial slope increases in the study reach occurred after the cutoffs. Initial increases in water surface slopes ranged from approximately 25% to 45%. These increases in slope increased sediment transport capacity significantly, resulting in channel degradation throughout the reach.

Post-cutoff Period: The period from the mid-1940s through the mid-1960s was one of extensive adjustments on the LMR as the river responded to the cutoffs. As the river was adjusting to a higher channel slope and stream power after the cutoffs, bank erosion increased as the channel attempted to regain channel length. It was during this initial period following the cutoffs that an aggressive revetment program was initiated in an attempt to stabilize channel alignments. By the mid-1960s, most of the major meander bends had been stabilized, thereby fixing the alignments in place. The revetment program not only provided for an improved and stable channel alignment but also significantly reduced the sediment loading to the river from streambank erosion (Winkley, 1973). Further studies are needed to determine what percentage of this material would be considered wash load or bed material load in the river system.

The cutoffs imposed a new alignment on the channel system that altered the historic crossing patterns in the river. These alignment changes combined with the increased bed sediment delivery from upstream resulted in increased maintenance dredging throughout the system, which peaked in the late-1970s. After 1970, the amount of maintenance dredging began a long-term decreasing trend as a result of two factors: (1) the revetment program imposed much better planform alignments with more orderly pool-crossing patterns and (2) the construction of training structures (dikes).

At the upstream end of the reach, represented by the Lake Providence gage, the specific gage trends have been relatively stable since the early 1950s. Moving farther downstream, the gages (Vicksburg, St. Joseph, and Natchez) become progressively more aggradational. This suggests that the reach from Lake Providence to Vicksburg may be a transition reach between dynamic equilibrium and the aggradation trends that exists farther downstream. The analysis of channel geometry parameters between 1975 and 2013 support these same trends. As previously noted, initial channel slopes increased substantially after the cutoffs (25% to 45%). Although these slopes have decreased from their peak conditions in the 1940s, the present-day slopes in the study reach are still higher (generally, approximately 17%) than in the Pre-cutoff Period.

Analysis of bed material data indicates that the bed throughout the study reach is predominantly formed of sand, with the D_{50} being squarely in the medium sand range. Long-term (decadal) scale analysis by Gaines and Priestas (2016) showed a significant reduction in the amount of gravel in the 1989 and 2013 surveys relative to the 1932 sampling. The Gaines and Priestas (2016) analysis also showed that while the 1932 bed did contain sediments in the very fine sand, silts, and clay ranges, these fine sediments were not found in any appreciable amounts in the 1989 and 2013 data. It is difficult to assign definitive causal links between the observed bed material changes and natural and anthropogenic factors. The slopes today are almost 20% higher than they were in 1932. With slope increases of this magnitude, it is very conceivable that the finer sediments (very fine sand and finer) are being transported through the reach acting as wash load and are therefore not being found in the bed in appreciable quantities.

References

D. O. Elliot.1932. The Improvements of the Lower Mississippi River for Flood Control and Navigation. Volume No. 1. and No. 2. Vicksburg, MS: U.S. Army Corps of Engineers.

Gaines, R.A., and A. M. Priestas. 2016. *Particle Size Distributions of Bed Sediments along the Mississippi River, Grafton, Illinois, to Head of Passes, Louisiana, November 2013*. MRG&P Report No. 7. Vicksburg, MS: U.S. Army Engineer Research and Development Center.

Little Jr., C. D., D. S. Biedenharn, M. A. Allison, K. Wofford, and T. McCullough. 2017. *Channel Geometry Trends of the Mississippi River, Old River Control Complex to St. Louis, Missouri*. MRG&P Report No. 11. Vicksburg, MS: U.S. Army Engineer Research and Development Center.

Nordin, C. F., and B. S. Queen. 1992. *Particle Size Distributions of bed Sediments along the Thalweg of the Mississippi River, Cairo, Illinois, to Head of Passes, September 1989*. Report 7, Potamology Program (P-1). Vicksburg, MS: U.S. Army Corps of Engineers, Lower Mississippi Valley Division.

Robbins, L. G. 1977. *Suspended Sediment and Bed Material Studies on the Lower Mississippi River*: *Potamology Investigations*. Report 300-1.Vicksburg, MS: U.S. Army Corps of Engineers, Lower Mississippi Valley Division.

Schumm, S. A., Rutherfurd I. D. and John Brooks 1994. *Pre-Cutoff Morphology of the Lower Mississippi River: The Variability of Large Alluvial Rivers*. Chapter 2. American Society of Civil Engineers Press.

Thorne, C. R., D. S. Biedenharn, C. D. Little, K. Wofford, T. McCullough, and C. C. Watson. 2017. *Bed Material Sizes, Variability, and Trends in the Lower Mississippi River and Their Significance to Calculated Bed Material Loads*. MRG&P Report No. 16. Vicksburg, MS: U.S. Army Engineer Research and Development Center.

Waterways Experiment Station (WES). 1935. *Studies of river bed materials and their movement with special reference to the Lower Mississippi River*. Paper 17. Vicksburg, MS: U.S. Army Corps of Engineers, Waterways Experiment Station.

Watson, C. C., D. S. Biedenharn, and C. R. Thorne. 2013. Analysis of the Impacts of Dikes on Flood Stages in the Middle Mississippi River. *Journal of Hydraulic Engineering* 139(10):1071-1078. DOI: 10.1061/ (ASCE) HY.1943-7900.0000786.

Winkley, B. R. 1994. *Response of the Lower Mississippi River to Flood Control and Navigation Improvements: The Variability of Large Alluvial Rivers*. Chapter 3. American Society of Civil Engineers Press.

Winkley, B. R. 1977. *Man-Made Cutoffs on the Lower Mississippi River, Conception, Construction, and River Response*: *Potamology Investigations*. Report 300-2. Vicksburg, MS: U.S. Army Corps of Engineers, Lower Mississippi Valley Division.

Winkley, B.R. 1973. *Metamorphosis of a River, a Comparison of the Mississippi River before and after Cutoffs*. Mississippi State University, MS: Water Resources Research Institute.

Measuring Fluvial Sediment Transport with Tracer Stones

D. Nathan Bradley, Sedimentation and River Hydraulics, USBR, Denver, CO, dnbradley@usbr.gov

Abstract

Tracing the motions of individually identifiable sediment particles over multiple floods offers a unique and detailed view of fluvial sediment transport processes. Individual particle trajectories can be used to identify the flows required to initiate sediment transport, to measure particle travel distances and the duration of immobile periods, to estimate sediment flux, and to illuminate the interaction between channel morphology and sediment transport. In particular, coarse sediment equipped with radio frequency identification (RFID) technology in the form of passive integrated transponder (PIT) tags allow individual particles to be tracked over many years with very high recovery rates. The PIT tags equip each clast with a unique identifier that can be detected from a distance with little interference from water or sediment, allowing particles to be located and identified without disturbing the stream bed. I describe and discuss RFID tracer experiments in several rivers including Halfmoon Creek in Colorado (investigating the nature of fluvial sediment dispersion), the Methow River in Washington (assessing the mobility of gravel bars along a large river), and the Bighorn River in Montana (the maintenance and sustainability of side channels on a regulated river).

Introduction

Tracking the trajectories of individually labeled bedload particles provides a uniquely detailed view of fluvial sediment transport. Knowledge of individual particle trajectories can be used to identify transport thresholds, to measure travel distances and storage times, to estimate bedload fluxes, and to observe the feedbacks between channel morphology and sediment transport.

Radio Frequency Identification technology (RFID) in the form of small, inexpensive Passive Integrated Transponder (PIT) tags can be used to equip gravel-sized and larger bedload clast with an identifying number that can be detected and read out at a distance with little interference from water or sediment. The exact detection range depends on the size and type of antenna used to energize the tag, but is generally on the order of 0.5 – 2m. The antenna provides the power the PIT tags use to transmit the unique identifier when within range (hence the term ‘passive’), so the tags require no battery and can last for decades. The use of PIT tagged gravels to investigate gravel transport dynamics was introduced about a decade ago and studies in relatively small, wadeable streams have produced tracer recovery rates above 90% for years after tracer installation. In this extended abstract, I discuss one of these early RFID tracer studies and two ongoing tracer experiments.

Halfmoon Creek Tracer Experiment

In May 2007, Greg Tucker of the University of Colorado and I deployed 893 PIT tagged tracer stones in Halfmoon Creek, a small alpine watershed in the Upper Arkansas Basin near Leadville, CO. The study was designed to investigate nature of the probability distributions of travel distances and storage times that govern tracer dispersion. We surveyed the positions of the tracers every summer following the spring snowmelt flood from 2007 to 2016, resulting in a decade long record of tracer transport observations. Recovery rates exceeded 90% in all years but one.

Early results showed that tracer transport distributions were best described by a thin-tailed probability distribution (Figure 1a) [Bradley et al., 2010] a result that was later confirmed [Bradley, 2017]. Similar studies have reached the same conclusion, ruling out heavy-tailed step lengths as a cause of anomalous diffusion [e.g. Phillips et al., 2013]. Later results showed anomalous super-diffusion caused by an observable heavy-tailed distribution of tracer storage times (Figure 1b) [Bradley, 2017], confirming what had been suspected [Martin et al., 2012; Phillips et al., 2013; Voepel et al., 2012] for several years. I attribute the high probability of long storage times to trapping by gravel bars (Figure *2*).

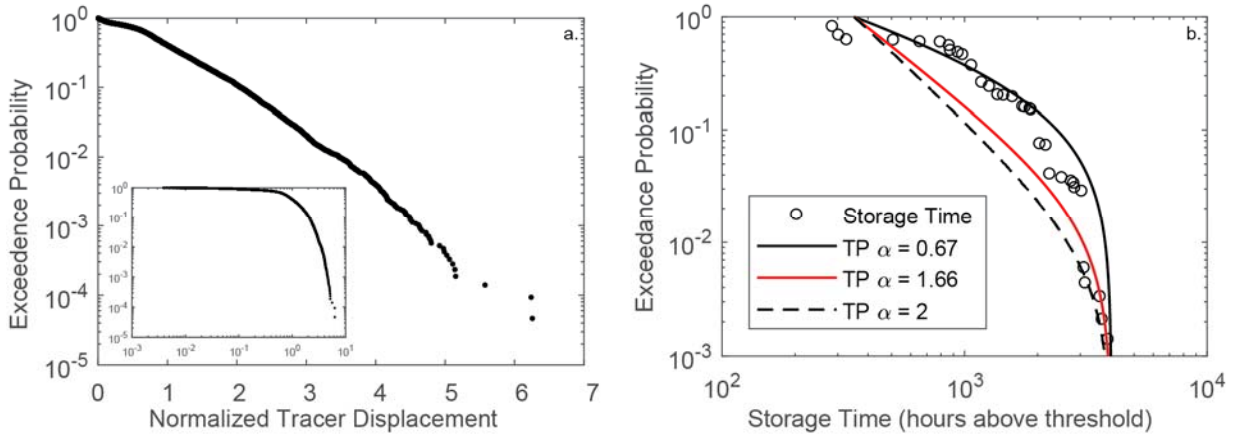

Figure 1. a) The distribution of tracer travel distance is thin-tailed. Tracer displacements are normalized by the mean displacement over that interval. b) The distribution of tracer storage times are best modeled by a truncated Pareto (TP) distribution with a tail parameter of 0.67. Modified from Bradley [2017].

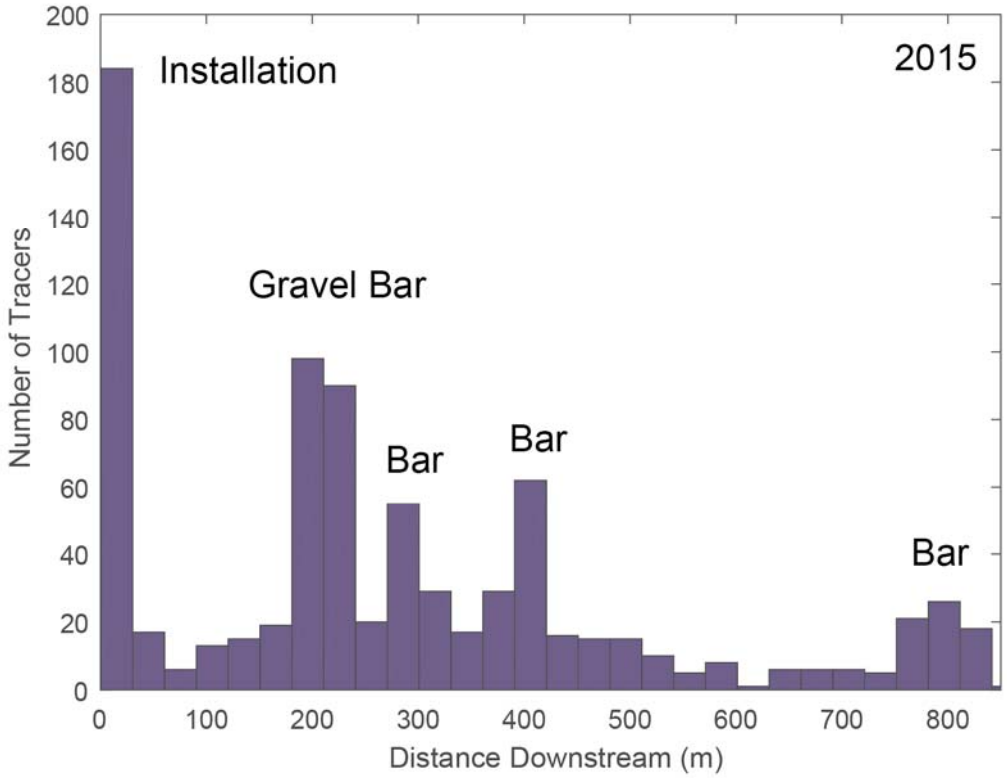

Figure 2. The peaks in PIT-tagged gravel tracer concentration in Halfmoon Creek correspond to the locations of gravel bars, highlighting the role stream morphology plays in modulating gravel transport.

Methow River Sugar Levee Gravel Bar Mobility

The Methow River near Twisp, WA is confined by the Sugar Levee along the right bank upstream of a very large right bank point bar Figure 3. Across from the point bar, the river is rapidly eroding into private property. My hypothesis is that the levee is limiting the sediment depositions space on the point bar across from the levee, causing sediment to move rapidly through the levee reach and accumulate on the downstream point bar. If the levee were removed or set back, the river would be able to move to the right and gravel could accumulate on the opposite point bar, possibly reducing annual deposition on the downstream point bar and slowing bank erosion. To test this hypothesis and gain a better understanding of the movement of sediment through this reach, Reclamation deployed 600 RFID tagged gravel and cobble clasts on bars upstream of and across from the levy in the summer to 2018. The positions of the tracer stones will be surveyed annually following the spring snowmelt for 3 years. Direct observation of where tracer gravel accumulates (and does not accumulate) will provide insight into the interaction between the levy and the sediment dynamics.

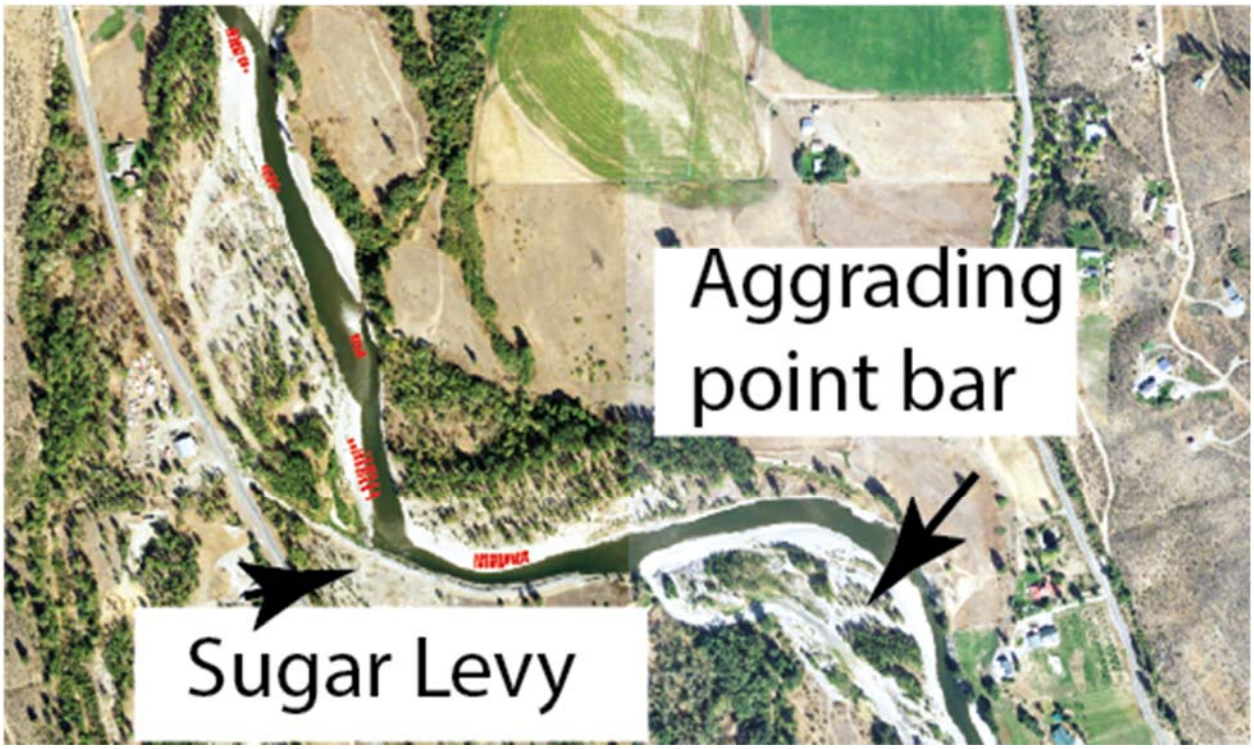

Figure 3. The Methow River near Twisp, WA. Tracer locations are shown by red dots. Each dot represents 3 tracers.

Bighorn River Side Channel Sediment Transport

Reclamation deployed 400 RFID tracer stones in side channels of the Bighorn River below Yellowtail Dam in Montana in the winter of 2012 as a part of an effort to evaluate sediment transport through side channels and side channel longevity {Hilldale, 2012}. Side channels provide important fish habitat and the factors that contribute to their persistence are not well understood. The tracers were recovered for several years and their motion was used to evaluate incipient motion thresholds in the context of the flows released from Yellowtail Dam. Reclamation will re-survey the tracer locations again in 2019 and 2020 as a part of study to evaluate how the Bighorn River side channels have responded to several years of high flows since the end of the original study.

References

Bradley, D. N. (2017), Direct observation of heavy-tailed storage times of bedload tracer particles causing anomalous super-diffusion, Geophysical Research Letters, doi: 10.1002/2017GL075045.

Bradley, D. N., G. E. Tucker, and D. A. Benson (2010), Fractional dispersion in a sand bed river, J. Geophys. Res., 115, 33-52, doi: 10.1029/2009jf001268.

Hilldale, R.C., 2012, Bighorn River Side Channel Investigation: Hydraulic and Sediment Transport Analysis, Bureau of Reclamation Technical Service Center Report No. SRH-2012-26.

Martin, R. L., D. J. Jerolmack, and R. Schumer (2012), The physical basis for anomalous diffusion in bed load transport, J. Geophys. Res., 117(F1), doi: 10.1029/2011jf002075.

Phillips, C. B., R. L. Martin, and D. J. Jerolmack (2013), Impulse framework for unsteady flows reveals superdiffusive bed load transport, Geophysical Research Letters, 40(7), 1328-1333, doi: 10.1002/grl.50323.

Voepel, H., Schumer, R., & Hassan, M. A. (2013). Sediment residence time distributions: Theory and application from bed elevation measurements. Journal of Geophysical Research: Earth Surface, 118, 2557–2567. https://doi.org/10.1002/jgrf.20151.

Post-Dredge Monitoring of Channel Adjustment in a Gravel-Bedded River

Peter Brooks, Senior Hydraulic Engineer., Northwest Hydraulic Consultants, Seattle, WA, pbrooks@nhcweb.com
Kevin Geoghegan, Hydraulic Engineer, Northwest Hydraulic Consultants, Seattle, WA, kgeoghegan@nhcweb.com
Joseph Farah, Civil Engineer, City of Renton Surface Water Utility, Renton, WA, jfarah@rentonwa.gov

Introduction

The Cedar River has a contributing basin area of 184 square miles and travels 45 miles westward from the Cascade Mountains to Lake Washington in the City of Renton, Washington. The river serves as a drinking water supply for the City of Seattle and is populated by several species of anadromous salmonids, including Chinook, sockeye, coho, and steelhead. The greater Lake Washington basin, including the lower Cedar River (Figure 1), has been highly altered over the past century (Chrzastowski, 1983). These alterations included the lowering of Lake Washington by approximately 9 feet and the abandonment of the lake's previous outlet channel, the Black River, which flowed southward to the nearby Green River. Historically, the lower Cedar River was located on an active alluvial fan over what is today downtown Renton and discharged directly to the Black River. Since 1912, the Cedar River has been channelized and directed to Lake Washington. Owing to the ongoing sediment delivery from upstream and the depositional nature of this reach, periodic dredging, typically on a decadal timescale, is required to maintain flood conveyance along what is now an economically vital and urbanized corridor (USACE, 1997).

In summer 2016, the lower 1.2 miles of the Cedar River was dredged. Near the upstream dredge extent, the channel gradient was steepened to approximately 0.6% to tie into the existing channel grade. Referred to as the transition zone, it was anticipated that this steepened reach would undergo adjustment through a rotational headcutting process. As requested by stakeholders and required by permitting agencies, a focused monitoring program was implemented in the reach immediately upstream of the dredge project to document channel adjustment and potential impacts to salmonid spawning areas. Presented herein are the methods and findings of monitoring efforts conducted over the course of four flood seasons immediately before and after the 2016 dredging of the lower Cedar River.

Methods

Four monitoring sites were established on the lower Cedar River as part of this study (Figure 1). Three sites were located between River Mile (RM) 1.23 and 1.69 to evaluate conditions immediately upstream of the dredge project. A fourth site, located outside the anticipated area of project influence near RM 2.10, was established as a control site. A key component of the monitoring involved the use of buried scour chains equipped with accelerometers following the methodology of Gendaszek et al (2013).

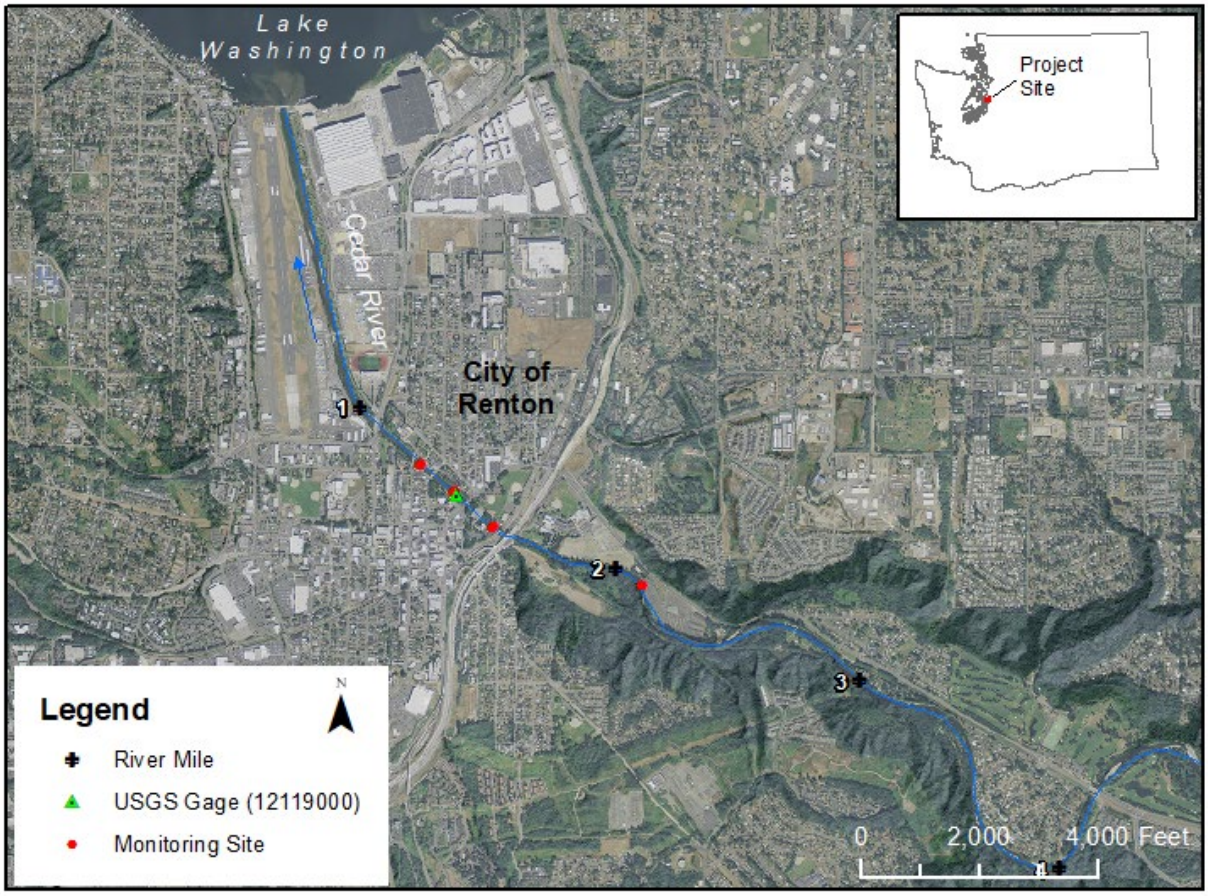

Figure 1. Project vicinity map

Scour chains were constructed with HOBO® Pendant™ G Data Loggers (accelerometers) wrapped with lead to counteract buoyant effects, then encased within an 8-cm-long PVC pipe sleeve to provide impact protection (Gendaszek et al, 2013). Three accelerometer units were connected by crimped cable at fixed depths along a single chain and record movement when a unit is exposed by bed scour. Following Gendaszek et al (2013), each accelerometer was set to record its orientation at 20-minute intervals, and movement owing to natural scour or burial forces was determined when the recorded vertical (z) tilt of an accelerometer changed by more than 15 degrees. Accelerometers were attached at depths of approximately 4, 19, and 45 cm (Figure 2), corresponding to the approximate center of the 8 cm PVC sleeve length. The accelerometer placed at the 4 cm depth was intended to measure surface armor layer movement. Depths of 19 and 45 cm below the bed surface correspond to the upper limit of spawning disturbance depth for Sockeye salmon (DeVries, 1997), and the upper and lower limits of spawning disturbance depths for Chinook salmon (Gendaszek et al, 2013). Scour chains were installed vertically into the streambed using a manual hollow-core driver-pipe apparatus. Three scour chains equipped with accelerometers were installed along a transect at each monitoring site spanning the estimated active channel. Scour chains were typically installed during the fall and retrieved the following summer.

Figure 2. Three scour chains equipped with accelerometers prior to installation

In addition to scour chain installation, field data collection included bathymetric surveys and surface bed material sampling. Bathymetric surveys were conducted using a combination of real time kinematic-global positioning system (RTK-GPS) and total station survey equipment. Surveys extended approximately 100 feet upstream and downstream of the established transect at each monitoring site. Survey data were processed to create digital elevation models (DEMs) and evaluate bed level changes between flood season. Sampling of surface bed material was conducted to characterize spatial and temporal variation of grain size distributions at each of the four monitor sites. Samples were collected in the central portion of the channel where scour chains were installed using a traditional random-walk pebble count methodology.

River discharge was obtained from a nearby USGS stream gage (Figure 1, USGS 12119000, Cedar River at Renton, WA). River hydraulics were computed with a one-dimensional HEC-RAS model of the project reach. This model was calibrated and is updated annually with channel geometry data to assess the effects of channel aggradation on flood profiles along the lower Cedar River.

Results

River flows during three of the four years monitored were hydrologically uneventful (Figure 3) with peak discharges below the estimated 2-year return period flow of 3,150 cfs (Tetra Tech, 2017). During Water Year (WY) 2016, however, the 2-year flow was approached or exceeded during three separate events, and the maximum peak discharge of 5,460 cfs exceeded the estimated 5-year return period discharge of 4,790 cfs (Tetra Tech, 2017).

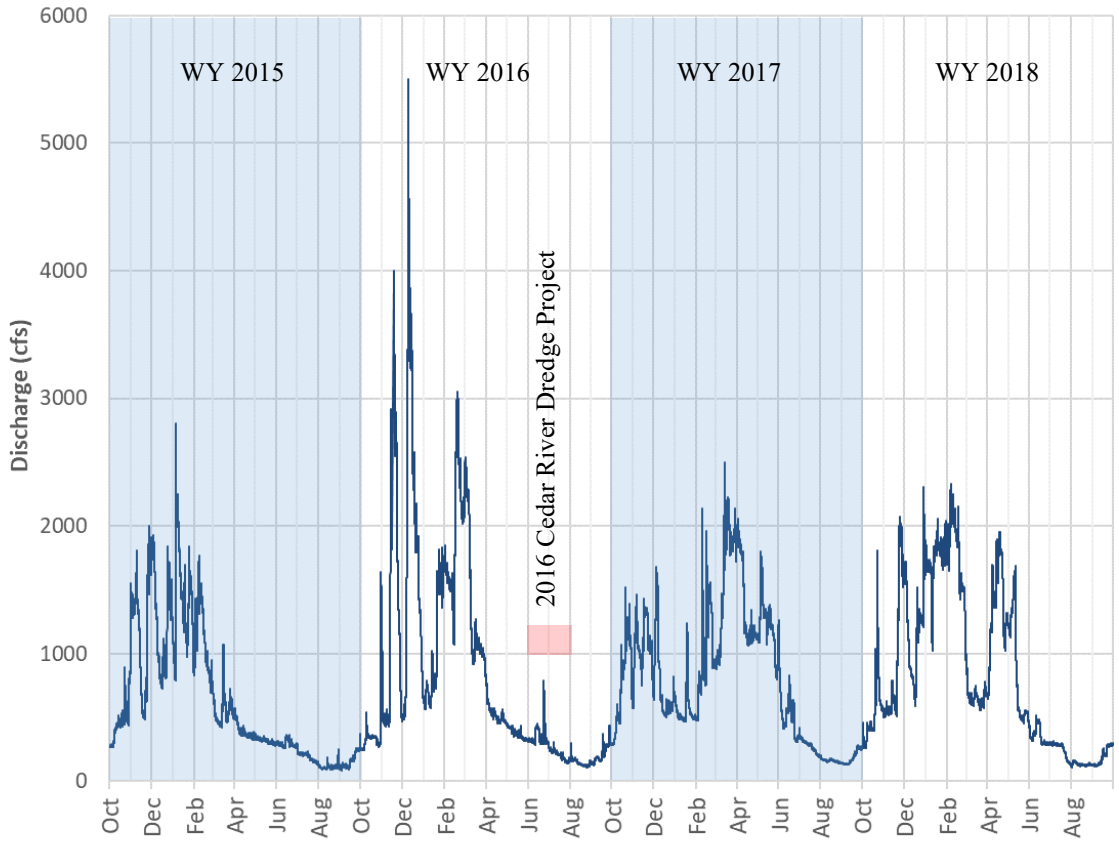

Figure 3. 15-minute Cedar River discharge for Water Years 2015-2018 (USGS 12119000 CEDAR RIVER AT RENTON, WA)

Scour monitoring results showed little activity during the first year (WY 2015), with motion of the surface accelerometer (4 cm depth) measured at only four of the 12 chains installed. Motion coincided with a single peak event occurring in early January 2015, at a discharge of 2,630 cfs, and was limited to the upstream two monitoring sites. During the second year of monitoring (WY 2016) higher peak discharges resulted in the motion of a similar number of accelerometers; however, motion was recorded during multiple events, and at intermediate units (17 cm depth). In addition, motion at the two downstream monitoring sites was recorded.

In summer 2016, the lower Cedar River was dredged, and monitoring results from WY 2017 indicate that channel adjustment began shortly after the beginning of the flood season. Immediately upstream of dredge project limit, at the downstream-most monitoring site, motion of the surface accelerometers began in October at a relatively low flow of 1,500 cfs. Further upstream, at the remaining three monitoring sites, motion was recorded at discharges ranging from 1,900 to 2,100 cfs. Channel adjustment was also apparent in the bathymetric survey and bed material data collected. Channel degradation of up to four feet was observed at the downstream monitoring site but decreased in magnitude in the upstream direction. Coarsening of the surface armor layer was also observed. In the second flood season following the dredging (WY 2018), peak flows over 2,000 cfs were achieved, but scour monitors did not record motion. Bathymetric surveys indicated that aggradation was beginning to occur at the downstream

monitoring sites with limited degradation observed upstream. Figure 4 shows average bed profiles from annual surveys of the lower Cedar River and illustrates headcut rotation following the 2016 dredging.

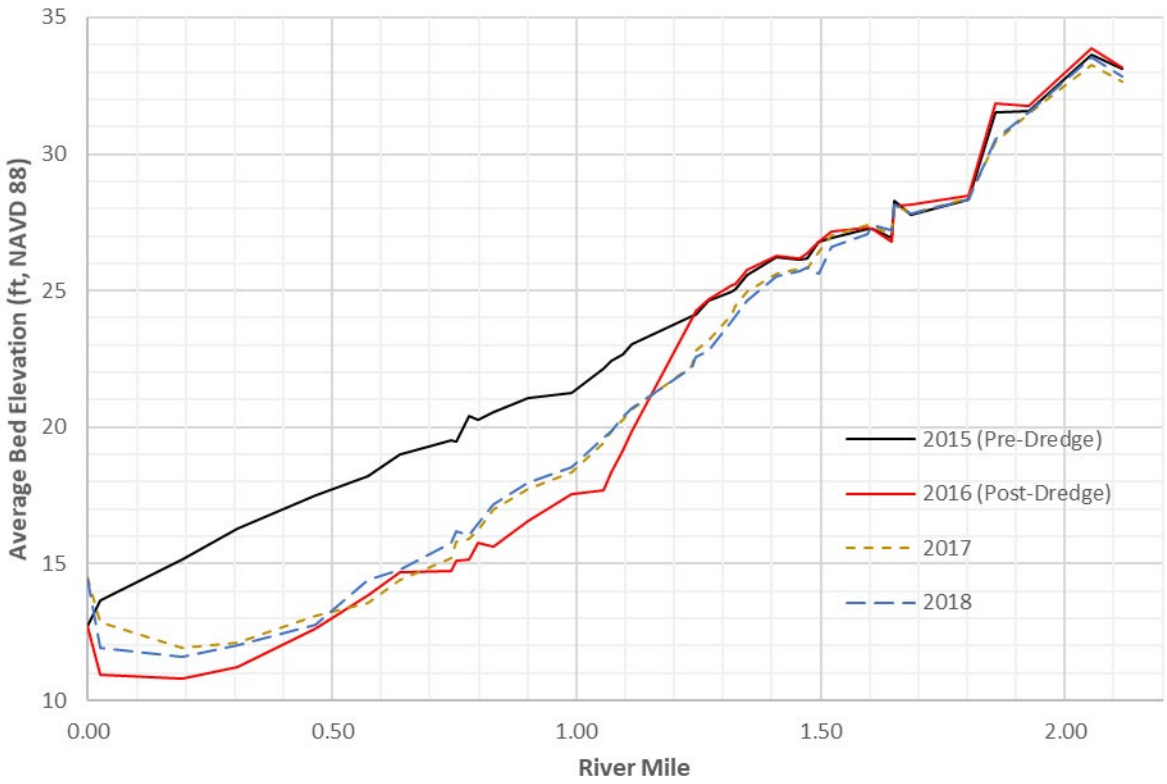

Figure 4. Lower Cedar River average bed level profiles surveyed 2015-2018

Conclusion

Prior to the 2016 dredging, the lower Cedar River, downstream of RM 1.6, exhibited a forced plain-bed morphology, evidence of alternative bar formation, and a uniform slope of approximately 0.15-percent. Median (D50) particle diameters ranged from 29-60 mm and D90 particles ranged from 78-115 mm. Interestingly, between RM 1.2 and 1.6, grain sizes tended to increase in the downstream direction suggesting selective transport of finer materials in a generally aggrading reach. Under these conditions, scour chain monitoring indicated that incipient motion occurred under flows ranging from 2,000 to 3,000 cfs (1.5- to 2-year return period) and scour depths limited to approximately 0.5 feet (17 cm). The latter is consistent with disturbance depths observed at twice the surface D90 (DeVries, 2002).

As a result of the 2016 dredging, and particularly the grading of a localized over-steepened (0.6-percent) sub-reach between RM 1.1-1.3 (i.e. the transition zone, Figure 4), the channel has adjusted through a process of headcut rotation with relatively symmetric degradation extending upstream and aggradation downstream (Brush and Wolman, 1960). Given the noncohesive gravel-cobble composition of the bed material, this process initiated rapidly and after two flood seasons the channel profile is approaching a slope 0.30-percent. From here, it is anticipated

that the lower Cedar River has responded to the 2016 dredging and will begin to aggrade uniformly.

Acknowledgements

The authors would like to thank Andrew Gendaszek (USGS-WA) and Chris Magirl (USGS-AZ) for assistance with initiating this monitoring study, as well as the City of Renton, WA and King County Flood Control District who provided oversight and funding.

References

Brush, L.M. and Wolman, M.G. 1960. "Knickpoint Behavior in noncohesive material: a laboratory study," Bulletin of the GSA, January, Vol. 71, pp 59-74.

Chrzastowski, M.J. 1983. Historical Changes to Lake Washington and Route of the Lake Washington Ship Canal, King County, Washington. USGS open File Report 81-1182.

DeVries, P. 1997. Riverine salmonids egg burial depths: review of published data and implications for scour studies. Canadian Journal of Fisheries Aquatic Science. 54: 1685-1698.

DeVries, P. 2002. Bedload layer thickness and disturbance depth in gravel bed streams. Journal of Hydraulic Engineering, 128/11: 983-991.

Gendaszek, A.S., Magirl, C.S., Czuba, C.R., and Konrad, C.P. Klingeman, P.C. 2013. "The timing of scour and fill in a gravel-bedded river measured with buried accelerometers," Journal of Hydrology, 495 (2013) 186-196.

Tetra Tech. 2017. Cedar River Section 205 Levee System Determination of the 100-year Return Period Flow. Draft report prepared for the City of Renton. October.

U.S Army Corps of Engineers (USACE). 1997. Final Detailed Project Report and Environmental Impact Statement, Cedar River Section 205, Renton Washington. June.

The Upcoming NASA SWOT Mission and Its Potential to Advance Fluvial Geomorphology and Applied Hydraulics

J. Toby Minear, Research Hydrologist, University of Colorado, Boulder, Colorado, tminear@colorado.edu
Michael Durand, Associate Professor, Ohio State University, Columbus, Ohio, durand.8@osu.edu
& Tamlin M. Pavelsky, Associate Professor, University of North Carolina, Chapel Hill, North Carolina, pavelsky@unc.edu

Extended Abstract

NASA has several next generation high-resolution satellite missions to study the hydrologic cycle that are launched or soon to be launched, yet these missions remain relatively unknown to most users of water data. Several of these missions were conceived in part to measure different aspects of surface water: The Surface Water and Ocean Topography (SWOT) Mission to measure water surface elevations and extents, the NASA ISRO Synthetic Aperture Radar (NISAR) Mission to study wetland and floodplain inundation; and the ICESat-2 Mission to measure surface elevation and shallow bathymetry. In this talk, we will focus on the aspects of SWOT that make it particularly appealing to users of water data.

The upcoming SWOT Mission will provide first-of-its-kind satellite swath altimetry with simultaneous water surface elevations (WSE) and water extent data for wetlands, rivers, lakes, tidal zones and oceans. Scheduled for launch in 2021, SWOT utilizes a Ka-band (~8mm wavelength) interferometric synthetic aperture radar to simultaneously collect sub-decimeter simultaneous water surface elevation, slope, and extent. SWOT data will cover a large, 120km swath (Figure 1a), with repeat times at most locations of two to three times per 21-day orbit cycle in temperate latitudes (Figure 1b). While the initial point cloud of water surface elevations will contain a fair amount of scatter, the river center line averaged 'node' product will be much cleaner and likely will be used by most users. SWOT mission requirements are that WSE measurements are within ten centimeters of true WSE (1σ, 1km^2 area), river slopes are within 1.7 cm/km (17 μrad, 1km^2 area), and surface water extents are within 15% of true extent (1km^2 area). As these satellite measurements are as good or better than conventional ground surveys, are near instantaneous for large swaths of inland waters, have unprecedented temporal and spatial coverage, and will provide data over the three-year planned mission life, these are clearly large advances for user of water data. And the data are free.

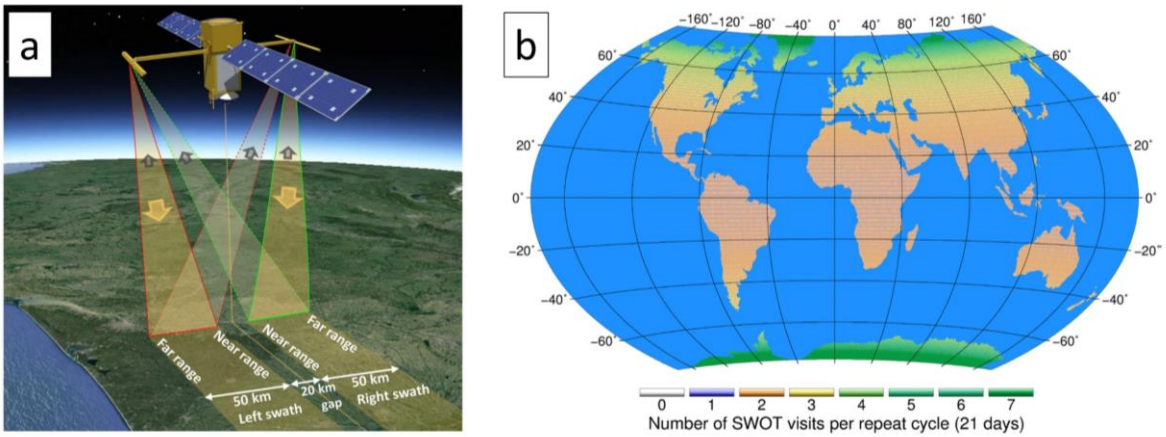

Figure 1a,b. a.) Schematic of the SWOT instrument with 120km wide ground swath shown (from *Biancamaria et al. 2016*). b.) temporal repeat coverage of SWOT per 21-day repeat cycle (~two to three times per 21 days for temperate latitudes; from *Biancamaria et al. 2016*).

Clearly, the SWOT Mission has great potential to advance global hydrology, particularly in locations lacking sufficient hydrologic measurements (e.g., lacking river gages, etc.). In areas with gage data, SWOT also has potential to advance our understanding of inland surface water processes. In particular, the two related fields of fluvial geomorphology and applied hydraulics will be able to benefit from SWOT measurements. Some examples include: 1.) developing and calibrating large-scale hydraulic and hydrologic models such as the National Water Model (an expensive proposition at present), 2.) determining hydraulic resistance at existing gage locations, 3.) creating bathymetry for hydraulic models, 4.) determining local geomorphic units (pools, riffles, etc.) and local estimates of hydraulic parameters, and 5.) calculating depth-slope products to estimate sediment transport rates.

In this talk, we will make the case that SWOT data can be used to advance applications within the fields of fluvial geomorphology and applied hydraulics, using a compilation of recently published SWOT papers, recent SWOT simulation data and AirSWOT (a SWOT-like prototype plane) data collections in 2015 and 2017, along with contemporary water- and ground-surface measurements. Of particular focus will be the utility of using SWOT data to create an inland bathymetry dataset, called the “Inland Bathymetry Estimates from SWOT” or IBES dataset. In addition, we will discuss using direct SWOT measurements (relative depth and slope) to calculate shear velocities at reach scales for sediment transport calculations, and the potential to do so at geomorphic unit scale (e.g., riffles, pools, etc.) using smoothing techniques. In all, SWOT has great potential for many types of users of water data.

References

Biancamaria, S., Lettenmaier, D.P., and Pavelsky, T.M., 2016. The SWOT Mission and Its Capabilities for Land Hydrology. Surveys in Geophysics, 37:307-337.

Channel Modification and Evolution Alters Hydraulic Connectivity in the Atchafalaya River Basin Increasing Vulnerability to Sea-Level Rise

Daniel E. Kroes, Research Ecologist, U.S. Geological Survey, Lower Mississippi-Gulf Water Science Center, Baton Rouge, LA, dkroes@usgs.gov
Richard Day, Geographer, U.S. Geological Survey, Wetland and Aquatic Research Center, Lafayette, LA, dayr@usgs.gov
Charles Demas, Emeritus, U.S. Geological Survey, Baton Rouge, LA, crdemas@gmail.com
Yvonne Allen, Geographer, U.S. Fish and Wildlife Service, Baton Rouge, LA, Yvonne_allen@fws.gov
Steve Roberts, Biologist, U.S. Army Corp of Engineers, New Orleans, LA, steve.w.roberts@usace.army.mil

Abstract

Channel dredging and erosion in the Atchafalaya River basin have resulted in changes to the hydraulic connectivity of this floodplain swamp that have not been previously quantified. In this study, analyses were conducted to determine hydraulic and geomorphic factors that have changed since channel closure in 1962. Results indicated changes occurred in the Atchafalaya main channel cross-section between 1962 and 2010, and hydraulic and geomorphic changes were detected in portions of the interior eastern basin floodplain. Analyses of hydrographs in relation to floodplain elevations indicated that there was a lack of mineral sediment deposition sufficient to offset subsidence and rising sea level. This deficit has resulted in extended hydroperiods over the floodplain which could prevent tree regeneration and promote hypoxia.

Introduction

The Atchafalaya River (AR) basin (Figure 1) is the largest remaining forested wetland in the contiguous United States. Many changes have occurred in the basin since channel closure in 1962 and the end of channel dredging in 1968. Channel dredging and erosion have resulted in changes to the hydraulic connectivity of this floodplain swamp that have not been previously quantified. In portions of the East side, decreased tree regeneration has occurred (Faulkner et al. 2009) due to changes in the water level and hydroperiod over the floodplain. Numerous studies indicate widespread hypoxia (Sabo et al., 1999a; 1999b; Kaller et al., 2011; Pasco et al., 2015) and fish populations indicate worsening oxygen concentrations over time (Bennet and Kozak, 2016).

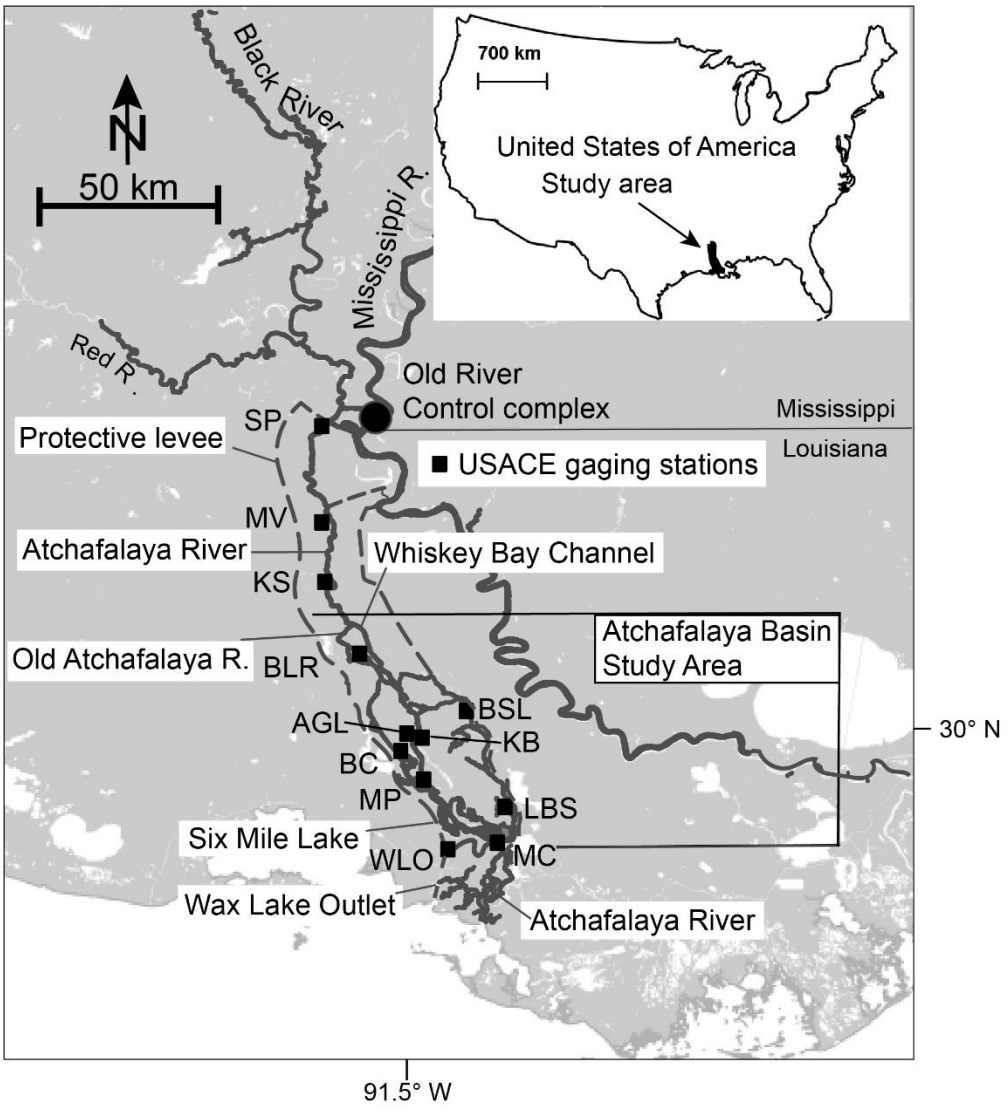

Figure 1. The Atchafalaya River basin study area is located within the Atchafalaya Basin Protective levees and extends from the head of the Whiskey Bay Channel to Morgan City. Squares show the location of the U.S. Army Corps of Engineers streamgage stations. See Table 1 for definitions of the station codes. Shaded base map created using ArcGIS software by ESRI, modified from Kroes et al., 2015. USA base map modified from Kroes and Brinson, 2004.

Table 1. U.S. Army Corps of Engineers (USACE) streamgage stations. [USGS, U.S. Geological Survey; --, no available data.

USACE station name (partial)	Station code (see Fig. 1)	USACE streamgage number	USACE period of record	USGS station number	USGS period of record
Simmesport	SP	03045	1930-	07381490	2009-
Melville	MV	03060	1911-	07381495	2015-
Krotz Springs	KS	03075	1934-	--	--
Butte La Rose	BLR	03120	1930-	07381515	1996-
Arm of Grand Lake	AGL	49197	1976-	300312091320000	2003-
Buffalo Cove	BC	49235	1976-	07381567	1996-
Keel Boat	KB	03615	1957-	--	--
Bayou Sorrel Lock	BSL	49630	1942-	--	--
Chicot Pass at Millet Point	MP	03540	1963	073815450	1996-
Little Bayou Sorrel	LBS	49725	1970-	--	--
Morgan City	MC	03780	1932-	07381600	1992-
Wax Lake Outlet	WLO	03720	1942-	07381590	1995-

We examined: 1) channel and bank hydrographic surveys from 1962, 1974, and 2010; 2) surface-water elevation/streamflow relationships from 1960-2015; 3) flow distribution to the swamp comparing synoptic streamflow measurements from 1958-1974 to 2001-2017; 4) total subsidence rates (preliminary) 5); sediment deposition rates (preliminary); and 6) the hydroperiod required for tree regeneration. These analyses were conducted to determine hydraulic and geomorphic factors that have changed since channel closure that may contribute to worsening oxygen and fisheries conditions. Once the changed factors are identified, ongoing restoration projects may capitalize on remediating the identified factors that degrade water quality.

Methods

Channel cross-sectional areas were analyzed using channel bed elevations from transects of hydrographic surveys conducted by, or for, the USACE for the main channel(s) of the AR. Hydrographic surveys used for this analysis were conducted from 1962-64 (hereafter 1962, USACE, 1967), 1974-76 (hereafter 1974, USACE, 1977) and 2010 (USACE, 2012). Bank morphology for the 2010 survey was determined using 2010 light detection and ranging (LiDAR). The top of the bank of the channel transect was defined as the mean of bank heights as determined by the surveyed topographic breaks or the tops of point bars.

Stage relative to streamflow was analyzed for an approximate 1.5-yr high, mean streamflow, and 1.5-yr low to approximate a range in stages that could be expected to occur. Flow distribution divergent from the main channel was calculated using streamflow measurements made by the Corp of Engineers for the period 1959-1968 (USACE, 1977) and from measurements made by the USGS for the period 2001-17 for a range of streamflows that could be considered normal: 2,700 m^3/sec to 11,500 m^3/sec (1.5-yr low to 1.5-yr high). Streamflow data collected by the USGS are available from the National Water Information System web interface (U.S. Geological Survey, 2019).

Rod-type surface elevation tables (SETs) were installed in 2010 and read yearly through 2017. SET rods were surveyed using real-time kinematic global positioning system surveying devices and optical levels to determine elevation in 2010 and 2017.

Deposition in the area previously identified as interior east and interior isolated east by Hupp et

al. (2019) was measured using a ceramic tile marker horizon on the near permanently flooded floodplain surface. Samples of the semi-fluid deposition were collected above the marker horizon using a 51-mm diameter clear plastic tube, measured in-situ and in the tube, and the volume of sample was calculated. Samples were dried, and mass was determined. Deposition in mm/yr was calculated by dividing the mass of sample by the average density of deposition of 0.8 g/cm^3 from Hupp et al. (2008).

Hydroperiods were examined relative to the areas determined by Faulkner et al. (2009) to be non-regenerative for trees even if planted. The elevations of the areas found to be non-regenerative were determined and then compared with the closest gage hydrograph to calculate the percentage of the year that the floodplain was above water.

Results

From 1962 to 2010, the Atchafalaya River main channel doubled in cross-sectional area (Figure 2), half of the increase occurred (1962 – 1974) because of dredging and erosion, whereas the remaining increases (1974- 2010) resulted from erosion only. This increase in cross-sectional area lowered the surface-water elevation of a 1.5-yr flood (11,500 m^3/sec) at the Butte La Rose gaging station (USGS station no. 07381515) from 1 m above bank height to 2.4 m below the bank height (Figure 3). The bankfull streamflow increased from 6,400 m^3/sec (1960) to more than 17,500 m^3/sec (2011). Reduction in surface-water elevation and distributary blockage has reduced the volume of water leaving the main channel since 1968 when channel dredging was completed (USACE, 1979; Kroes, 2012; USGS 2019). Flow leaving the river does not indicate flow across the swamp floor as numerous spoil banks exist that inhibit or block flow through the forested portions while encouraging flow through the many over competent channels that exist on this floodplain.

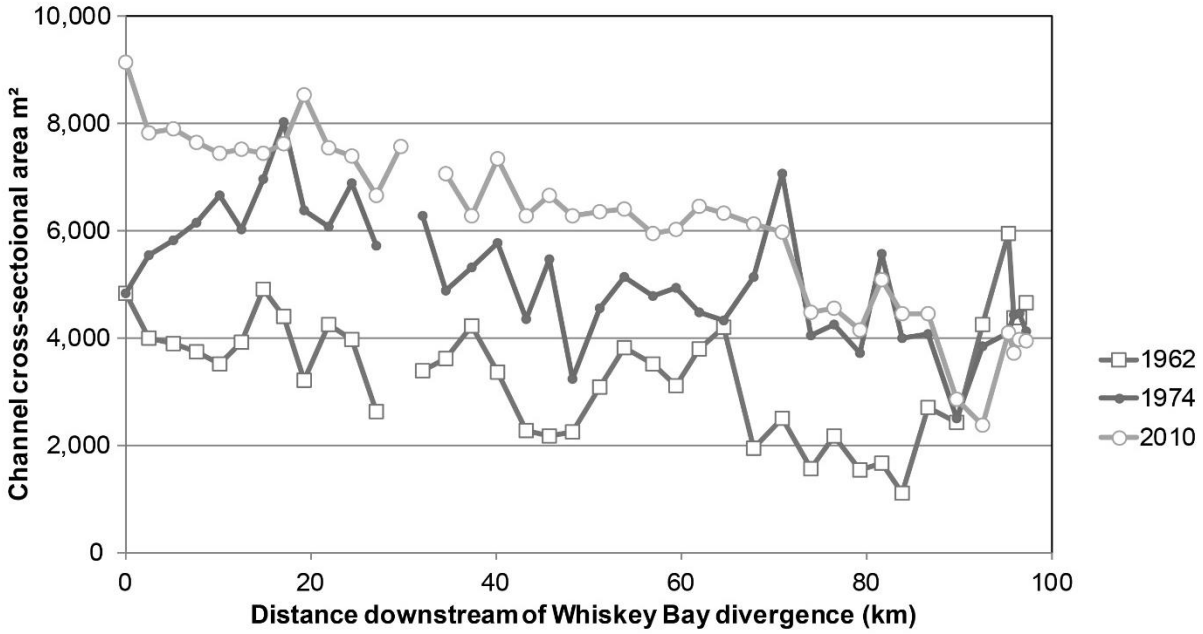

Figure 2. Atchafalaya River channel cross-sectional areas from the head of the Whiskey Bay Channel to Morgan City from 1962, 1974, and 2010 channel surveys. Gaps in the graph are where the Whiskey Bay and Old Atchafalaya River channels rejoin creating an abnormal scour feature. Mean bank height was determined from the surveyed topographic breaks and/or the tops of point bars.

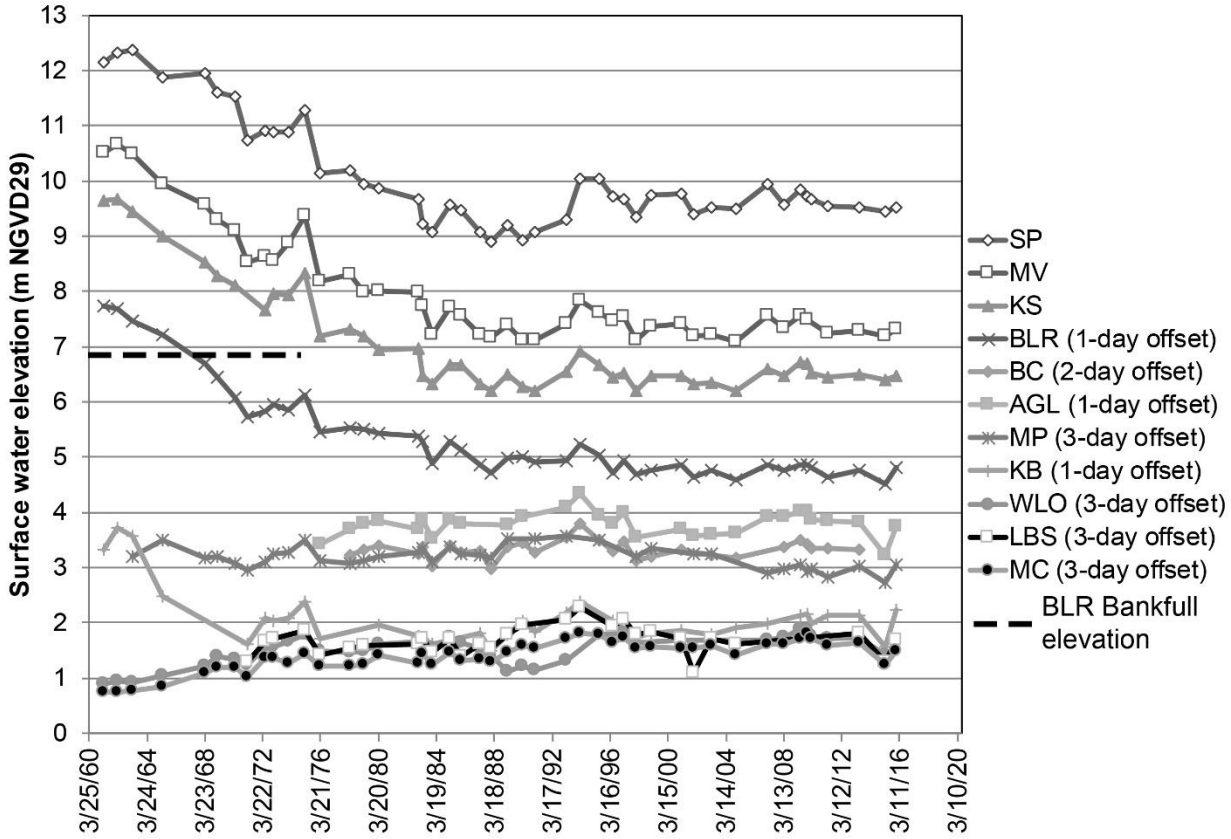

Figure 3. Changes in surface-water elevation of a 1.5-year flood at select streamgage stations in the Atchafalaya River basin study area. [NGVD, National Geodetic Vertical Datum of 1929; Station codes from Table 1].

Subsidence rates (shallow and deep) were monitored from 2010-17, indicating lower subsidence rates in the west part of the Basin (1 mm/yr) and the north part of the Basin (15 mm/yr, Figure 4). Greater subsidence rates (21 to 26 mm/yr) were observed on the east and southern portions of the Basin. Hupp et al. (2019) found hydraulic connectivity to be least in the area where subsidence was the greatest. The reduced connectivity was manifested in low sediment deposition rates in the interior east and isolated interior east side of the Basin (approximately at an average of 3.8 mm/yr assuming density of 0.8 g/cm^3).

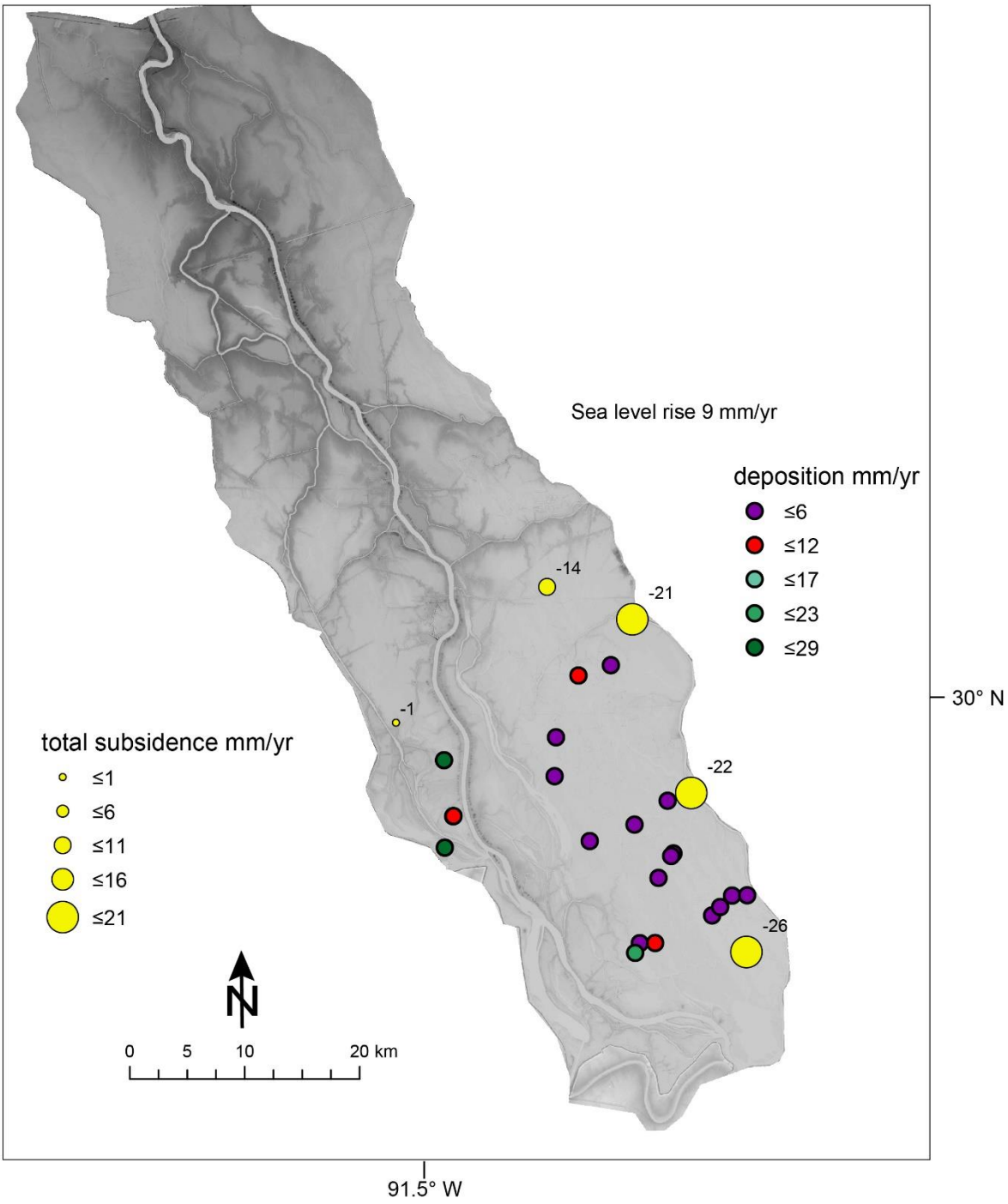

Figure 4. Subsidence and deposition measurements for the lower Atchafalaya River basin. Base map derived from 2010 LiDAR (USGS 2012) using ArcGIS software by ESRI.

The reduction of hydraulic connectivity between the Atchafalaya main channel and its floodplain swamp has resulted in several conditions. For large portions of the east side of the Basin, sediment deposition rates are insufficient to keep up with subsidence (preliminary, avg 21 mm/yr) and sea-level rise (9.7 mm/yr, National Oceanic Atmospheric Agency tide gage no. 8761724 NOAA, 2018). Our analyses indicated that in this system the floodplain requires an

unflooded sediment surface for tree regeneration between 46 to 55 percent of the year. However, the estimated sediment deficit has resulted in a large area of floodplain (approx. 400 km^2) that either may soon lack or no longer has, sufficient dry time for woody plants to successfully regenerate.

Conclusions

Much of the swamp no longer receives headwater flow (upstream to downstream) or receives too little flow to alleviate backwater stagnancy and hypoxia at lower surface-water elevations because of blocked distributaries, increased channel cross-sectional area, and spoil banks. Interior areas of the swamp are lacking the sediment deposition rate required to keep up with subsidence and sea-level rise. Large portions of the Basin have low water levels that are now controlled by the Gulf of Mexico (Figure 5), resulting in extended inundation that inhibits or precludes tree regeneration and may eventually result in currently forested floodplain becoming open water.

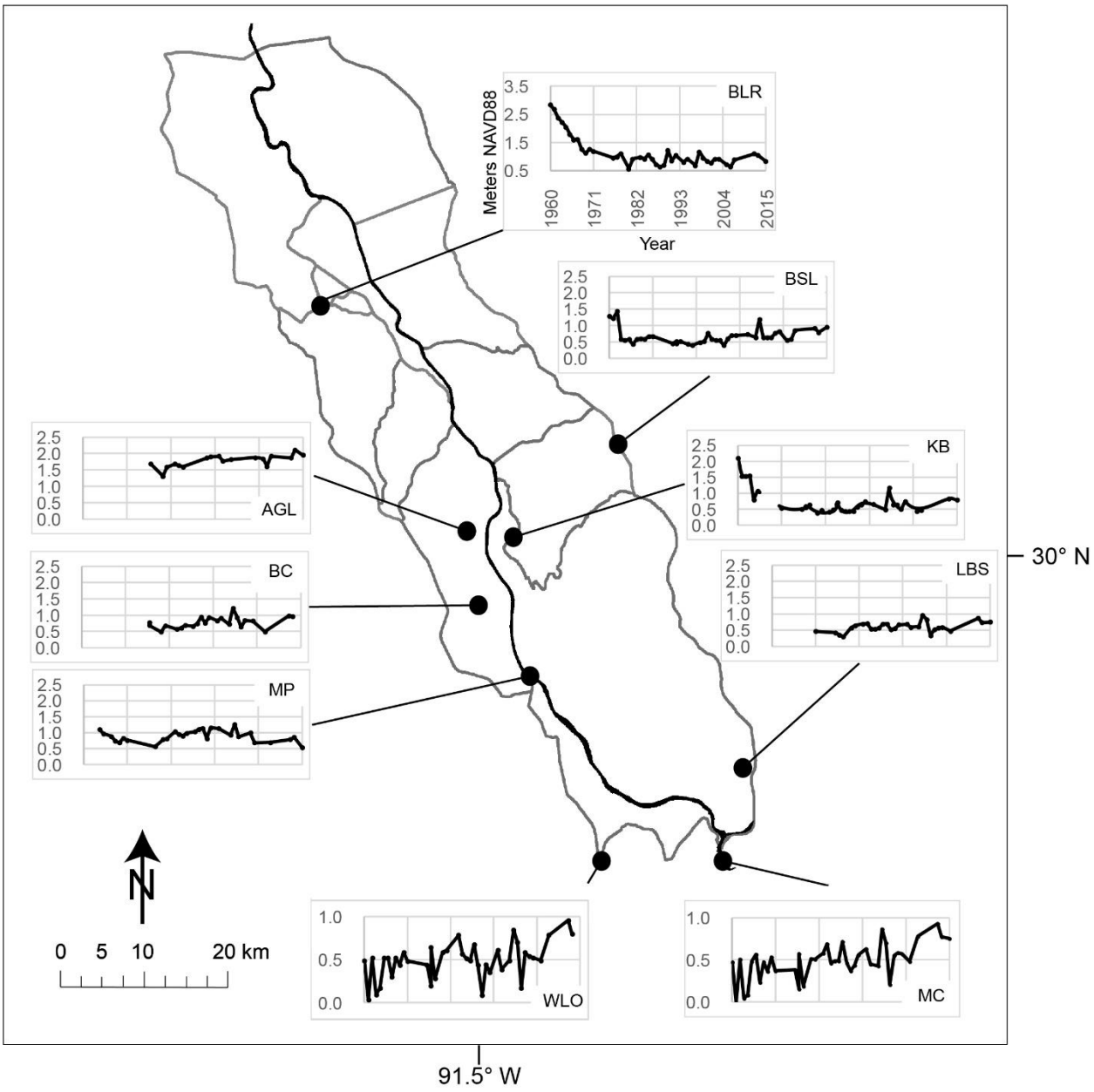

Figure 5. Surface-water elevation of a 1.5-year drought at select streamgage stations in the Atchafalaya River Basin study area. Gage datum for these observations were converted to North American Vertical Datum 1988 (NAVD88) because of the increased accuracy needed for comparison of observed small differences in elevation. Base map from Allen et al, 2008.

Disclaimer

Any use of trade, product, or firm names in this publication is for descriptive purposes only and does not imply endorsement by the US Government.

References

Allen, Y.C.; Constant, G.C.; Couvillion, B.R. 2008. Preliminary Classification of Water Areas within the Atchafalaya Basin Floodway System by Using Landsat imagery; Open-File Report 2008–1320; USGS, Reston, VA.

Bennett, M.G., Kozak J.P. 2016. Spatial and temporal patterns in fish community structure and abundance in the largest U.S. river swamp, the Atchafalaya River floodplain, Louisiana. Ecology of Freshwater Fish 25:577–589.

Environmental Systems Research Institute (ESRI). 2015. ArcGIS. Version 10.7. Redlands, CA.

Faulkner, S.P., Bhattarai P., Allen Y., Barras J., Constant G. 2009. Identifying bald cypress-water tupelo regeneration classes in forested wetlands of the Atchafalaya Basin, Louisiana. Wetlands, 29:809-817, doi: 10.1672/08-211.1.

Hupp CR, Demas CR, Kroes DE, Day RH, Doyle TW. 2008. Recent sedimentation patterns within the central Atchafalaya Basin, Louisiana. Wetlands 28, pp. 125-140.

Hupp, C.R., Kroes, D.K., Schenk, E.R., Noe, G.B., Day, R. 2019. Sediment trapping and carbon sequestration in floodplains of the lower Atchafalaya Basin, LA: Allochthonous vs. autochthonous carbon sources. J of Geophysical Research, doi: 10.1029/2018JG004533

Kaller, M.D., Kelso W.E., Halloran, B.T., Rutherford, D.A. 2011. Effects of spatial scale on assessment of dissolved oxygen dynamics in the Atchafalaya River Basin, Louisiana. Hydrobiologia 658:7–15.

Kroes, D.E., Brinson, M.M. 2004. Occurrence of riverine wetlands on floodplains along a climatic gradient. Wetlands: 24:167–177

Kroes, D.E. 2012. 20120914_update_Synoptic Surveys. GIS layer. Accessed online Nov. 15, 2017 at https://abp.cr.usgs.gov/Library/DownloadFile.aspx?id=514.

Kroes, D.E., Schenk, E.R., Noe, G.B., Benthem, A.J. 2015. Sediment and nutrient trapping as a result of a temporary Mississippi River floodplain restoration: the Morganza Spillway during the 2011 Mississippi River Flood. Ecological Engineering 82:91–102.

NOAA, 2018b. Sea Level Rise Viewer. Accessed 10 Sept 2018 at https://coast.noaa.gov/digitalcoast/tools/slr.html.

Pasco, T.E., Kaller, M.D., Harlan, R., Kelso, W.E., Rutherford, D.A., Roberts, S. 2015. Predicting floodplain hypoxia in the Atchafalaya River, Louisiana, USA, a large, regulated southern floodplain river system River Res. Appl., 32:845-855.

Sabo, M.J., Bryan, C.F., Kelso, W.E., Rutherford, D.A. 1999a. Hydrology and aquatic habitat characteristics of a riverine swamp: I. Influence of flow on water temperature and chemistry. Regulated Rivers 15: 505-523.

Sabo, M.J., Bryan, C.F., Kelso, W.E., Rutherford, D.A. 1999b. Hydrology and aquatic habitat characteristics of a riverine swamp: II. Hydrology and the occurrence of chronic hypoxia. Regulated Rivers: Research and Management 15:525–544.

U.S. Army Engineer District, New Orleans, (USACE) 1967. "Atchafalaya River Hydrographic Survey, 1962-1964; Old River to Atchafalaya Bay Including Main Channel and Distributaries," New Orleans, La.; prepared for Mississippi River Commission, Vicksburg, MS.

U.S. Army Engineer District, New Orleans, (USACE) 1977. Atchafalaya River Hydrographic Survey, 1974-1976; Old River to Atchafalaya Bay Including Main Channel and Distributaries," New Orleans, La.; prepared for Mississippi River Commission, Vicksburg, MS.

U.S. Army Corps of Engineers (USACE), 1979. Atchafalaya Basin Floodway Draft Environmental Statement. New Orleans, La., U.S. Army Corps of Engineers. 6 volumes.

U.S. Army Engineer District, New Orleans, (USACE) 2012. Atchafalaya River and Outlets to Gulf of Mexico. New Orleans, La.; prepared for Mississippi River Commission, Vicksburg, MS.

U.S. Geological Survey (USGS). 2013. 2010 U.S. Geological Survey Topographic LiDAR:

Atchafalaya Basin, Louisiana. Available at https://abp.cr.usgs.gov/Library/DownloadFile.aspx?id=376.

U.S. Geological Survey, 2019, National Water Information System—Web interface. Accessed 2 April, 2019 at http://dx.doi.org/10.5066/F7P55KJN.

Role of Physical Processes and Fish Passage in Reservoir Operations at Marble Bluff Dam, Truckee River, Nevada

Jennifer Bountry, Hydraulic Engineer, Bureau of Reclamation, Denver, CO, jbountry@usbr.gov
Nate Bradley, Geologist, Bureau of Reclamation, Denver, CO, dnbradley@usbr.gov
Jeanne Godaire, Geologist, Bureau of Reclamation, Denver, CO, jgodaire@usbr.gov

Abstract

Over the last century, upstream water withdrawal has resulted in a rapid lowering of Pyramid Lake where the Truckee River terminates in Nevada, USA. Lake lowering initiated up to 90 ft of channel incision and the formation of high terraces composed of lacustrine sediment. In 1976 Marble Bluff Dam was constructed by the Bureau of Reclamation about 4 miles upstream of the confluence with Pyramid Lake to halt the upstream progression of channel incision (Figure 1). and help limit erosion of upstream agricultural lands, tribal resources, and infrastructure. Since construction, an additional 40 ft of lake and subsequent channel lowering has occurred. In the 1990s a grade control structure was built to ensure headcut progression would not reach the base of the dam. In 2016, Pyramid Lake had dropped to elevation 3796 ft (NAVD88), a level similar to 1994 (elevation 3797), but not as low as the 1960s when the lake was at elevation 3787 ft. To complicate matters, the downstream river experiences lateral migration, especially where a delta forms at the confluence with Pyramid Lake. Sedimentation in the delta results in shallow channels that pose challenges to endangered Cui-ui and threatened Lahontan Cutthroat Trout (LCT) that migrate into the upstream river each year for spawning. The fish must either migrate through the shallow delta channels that are subject to predation by pelicans, and then through a fish lock at the dam, or utilize a fish bypass channel that allows fish to avoid the shallow delta area during low lake levels. Once released into the reservoir, the fish must navigate upstream to find suitable spawning grounds. This is particularly challenging for Cui-ui that are not as strong of swimmers as LCT. The original operating manual for the dam recommends year-round flushing of sediment through radial gates to prevent reservoir sedimentation, but when fish need to be released into the reservoir the gate must be shut to prevent fish from being swept back downstream. The reservoir is now nearly filled with sediment and there is concern that released fish cannot effectively swim upstream with the shallow water depths without risking being swept back downstream over the dam. The fish can access a main channel, but this path currently flows parallel to the dam crest before turning upstream. One side channel exists near the fish release point upstream of the dam, but depth and velocity during critical fish passage flows are not within the desired range for Cui-ui. Dam operators and fish passage managers requested a geomorphic and modeling study to inform adaptive management options to assist with long-term planning of reservoir sedimentation and downstream channel grade control. To address the study questions, we collected topographic data from 2016 to 2018, sediment gradation samples, and aerial and satellite imagery; we installed time-lapse cameras and conducted two-dimensional modeling and geomorphic mapping. We also investigated available literature and documented historical dam operations to identify options for reservoir sediment management and downstream grade control. The study was done in collaboration with Reclamation Lahontan Basin Area Office, U.S. Fish and Wildlife (Reno, NV) and the Pyramid Lake Paiute Tribe.

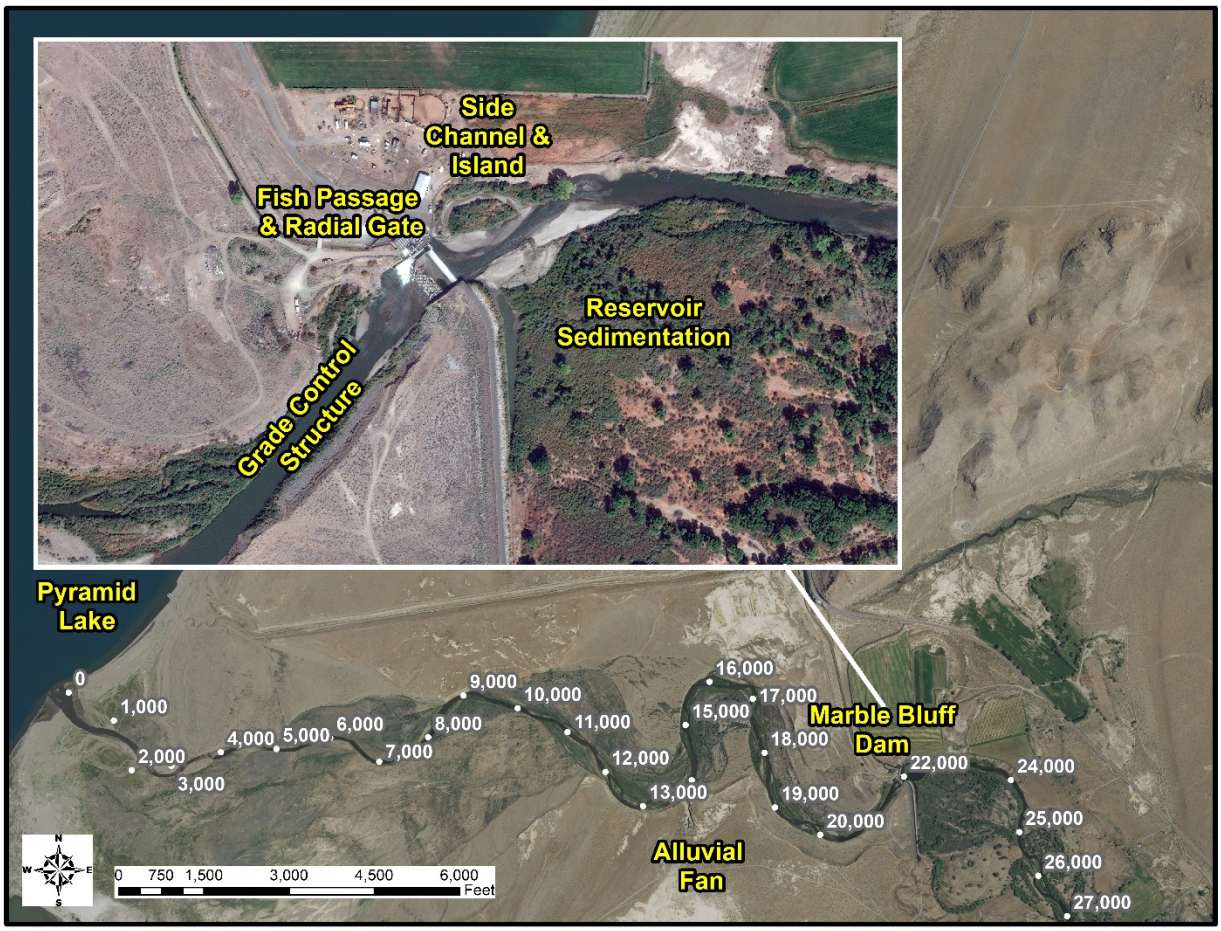

Figure 1. Location map of Marble Bluff Dam and relevant features on 2015 aerial photograph for large map and 2018 aerial photograph for inset.

Setting

The study area extends for about 9 miles from the terminus of the Truckee River in Pyramid Lake upstream to Numana Dam. The Truckee River is about 4.2 miles in length downstream from Marble Bluff Dam to Pyramid Lake based on the 2016 channel but can be shorter or longer depending on sinuosity and the amount of backwater from the lake. Geologic deposits located in the study area include Pleistocene lacustrine deposits of Lake Lahontan and Pyramid Lake. Shorelines record former lake levels from the late Pleistocene high stands as well as a more recent high stand from 1906. Holocene alluviation along the Truckee River has eroded the lacustrine deposits closest to the river, forming a set of three terraces ranging from historical to late Holocene (<2ka) in age that are composed of clay, sand and silt as well as well-rounded gravels and cobbles (Bell et al., 2005). Upstream of Marble Bluff Dam, an older and extensive early to middle Holocene terrace is mapped adjacent to the late Holocene terraces. The terrace is composed of fluvial sediment that was being reworked as the lake level receded during the Holocene. Drill holes during construction of Marble Bluff Dam found no bedrock and the first substantial clay layer was only a couple feet thick and about 45 ft below the surface. The only

known bedrock exposed in the channel bottom is located at Numana Dam, about 9.3 miles upstream of Pyramid Lake (Adams, 2012).

Pyramid Lake has a volume of 22.4 to 30.6 million acre-ft at a lake elevation of 3810 to 3874 (NAVD88), respectively (pers. Comm. Donna Marie Noel, Pyramid Lake Paiute Tribe). Lake stage fluctuates due to changes in incoming river discharge, evaporation, and other hydrologic factors such as surface runoff. Floods on the Truckee River are major catalysts for channel change on this section of river and occur largely in winter months. Flood frequency values for regulated conditions (upstream dam operations) in the reach between Numana Dam and Pyramid Lake are 20,100 ft^3/s for the 100-year flood, 7,800 ft^3/s for the 10-year flood, and 6,800 ft^3/s for the 5-year flood (USACE, 2013). The flood of record in 1997 peaked at 21,200 ft^3/s (slightly greater than 100-year flood). During the 1997 flood, water levels peaked at about 1.5 ft below the parking lot at the Marble Bluff Dam facility. The next five largest floods occurred in 1955 (14,000 ft^3/s), 1963 (14,400 ft^3/s), 1986 (16,300 ft^3/s), 2006 (12,700 ft^3/s), and 2017 (13,500 ft^3/s). Historical accounts and early measurements between 1844 and 1905 suggest Pyramid Lake fluctuated about 20 ft between elevation 1864 and 1884 ft (elevations in NAVD88; Born and Ritter, 1970). Between 1910 and 1966 Pyramid Lake had an overall trend of declining lake elevation dropping 86 ft, resulting in an equivalent lowering of the Truckee River where it enters the lake (USGS Gage 10336500). The lake lowering is attributed to substantial increases in water diversion in the upstream Truckee River after construction of Derby Dam in 1905, reducing the annual volume of water contributed to Pyramid Lake by approximately 0.25 million acre-ft (Born and Ritter, 1970). With the current water management allocations in a normal water year about 80% of the Truckee River flow passes into Pyramid Lake, but in a drought year this can reduce to 33% (tmwa.com/your-water/topics-facts/truckee-river-users).

Historical terrace formation on the Truckee River downstream of Numana Dam is described in Born and Ritter (1970) and Adams (2012). The timeframes for each terrace unit represent the time period over which a particular surface was actively being reworked by fluvial processes along the Truckee River. Abandonment of a given surface occurred following the youngest date of the unit, in which the channel incised beyond a stage threshold required to inundate and modify the surface, forming the historical terrace. Adams (2012) defines a total of 12 separate terraces that were formed between 1938 and 2008, expanding upon the six terraces identified in Born and Ritter (1970) that formed between 1938 and 1965. Born and Ritter (1970) propose the rapid rate of channel incision and terrace formation in this reach (years to decades) is related to:

> "*a combination of hydrologic and geologic conditions which allow for rapid development of a well-defined, erosional terrace sequence: (1) steady, although intermittent, lake-level decline; (2) degradation of the main river channels in response to lowering local base level; (3) periodic and extensive lateral erosion associated with high discharge and elevated river stage; and (4) stranding of lateral elements of the valley bottom as a result of renewed downcutting by the river.*"

Adams (2012) concluded that Pyramid Lake level "approached its historical lowstand in 1967, the planform and long profile of the Truckee River evolved from one that was relatively sinuous and gentle to one that was straighter, shorter, and steeper." Adams (2012) added that "the gradient of the channel would likely lessen through time if there were a stable base level, thereby decreasing the sediment transport rate as the system approached a new equilibrium. A version of this process may already be occurring below Marble Bluff Dam, where the river has been flattening its gradient since installation of the dam in 1975."

Methods

Longitudinal profiles of the Truckee River were compared over time to further understand trends in channel incision and flattening in response to Pyramid Lake levels and occurrence of floods. To temporally expand the Adam (2012) longitudinal profile analysis, we used 2010 survey data from U.S. Army Corps of Engineers, collected 2016 to 2018 channel profiles, and incorporated channel survey data from 1961 and 1971 collected for the design of Marble Bluff Dam. Because the extent of delta deposition is affected by lake level, a USGS discharge gage (10351700) was used with data since 1958 near Nixon, NV (upstream of Marble Bluff Dam and Pyramid Lake) along with intermittent measurements of Pyramid Lake stage (USGS gage 10336500).

Terrace mapping from Adams (2012) has been modified to show the 2015 position of the Truckee River channel and thus has altered the shape of some of the polygons that were mapped in the 2012 study. For the purposes of this study, some of the historical terraces from Adams (2012) have been combined to reduce the number of historical terraces. In addition to refinement of terrace mapping, other channel features were mapped to identify the 2015 active channel and floodplain features. In 2017, the river channel laterally migrated extensively and further eroded historical terraces which was mapped using field survey data and satellite imagery.

Two-dimensional (2D) hydraulic models were developed for the study reach downstream of Marble Bluff Dam to Pyramid Lake and upstream of Marble Bluff Dam. The hydraulic models are based on a topographic surface developed from new bathymetric surveys and from LiDAR collected by the Army Corp of Engineers (ACOE) in 2010 and 2011. Reclamation and USFWS staff performed bathymetric surveys in 2016, 2017, and 2018. In 2016 about 93 cross sections were surveyed in the unvegetated active channel with RTK GPS and where not wadable, a Sonarmite single beam depth sounder mounted on an inflatable kayak. Approximately 23,000 feet of stream length was surveyed over a total area of 4.44 million square feet of active channel. The average cross section spacing was about 250 feet. Sonar points were collected every 5 feet where water depth allowed. Additional surveys of only a longitudinal profile and limited repeat cross-sections were performed in 2017 and 2018 downstream of Marble Bluff Dam, and of the reservoir backwater area upstream of Marble Bluff Dam to evaluate potential changes in reservoir sedimentation.

Sediment data was collected in Marble Bluff Reservoir side channel and island area and in unvegetated exposed bars of the Truckee River downstream of Marble Bluff Dam. Sediment samples were taken to a lab for gradation analysis. Additional sediment gradation data in the Truckee River active channel downstream of Marble Bluff Dam was provided by USFWS. Other data utilized include time-lapse cameras to document changes in upstream reservoir sedimentation due to radial gate operation, documentation of fish swimming capacity from USFWS, and documentation of radial gate operation by USFWS staff.

Results Downstream of Marble Bluff Dam

Annual discharge volume was plotted over time to better understand how lake stage responds to variations in incoming flow from the Truckee River as context for interpreting longitudinal profile changes discussed later (Figure 2). Between 1958 and 2018, Pyramid Lake experienced

four periods of lowering and four periods of rising with differences ranging between 10 and 30 ft. The lake lowering happened slowly over several years at an approximate rate of 1.5 to 3 ft/yr with the minimum stage occurring in 1966. When Marble Bluff Dam was built in 1976 the lake had been rising slowly at about 1.6 ft/yr, but after construction the lake entered another declining period. The other three lake rise periods were more rapid at 6 to 6.5 ft/yr, occurring in years where the Truckee River had high annual water volumes. The largest annual lake increase of 13 ft happened in 1983, which had the highest annual flow volume of 1.9 million acre-ft, which is nearly five times the mean. This period also had high annual flow volumes in 1982, 1984 and 1986 with at least 0.9 million acre-ft per year. Another lake rise period occurred in the late 1990s when a large flood peak occurred in January 1997 combined with three additional years of high annual discharge volumes. When we started this study in 2016, the lake was in a declining phase and only 8 ft above the minimum stage measured in 1967 (elevation 3796 and 3787, respectively). Large floods combined with a large spring snowmelt in 2017 resulted in the second highest annual flow volume, since 1958, of 1.5 million acre-ft (nearly 4 times the mean), reversing the declining trend and increasing lake stage 9 ft (elevation 3797 to 3806; see Figure 2). Water year 2018 had a moderate annual volume, enough to bump the lake stage up a couple more feet (elevation 3806 to 3808 ft).

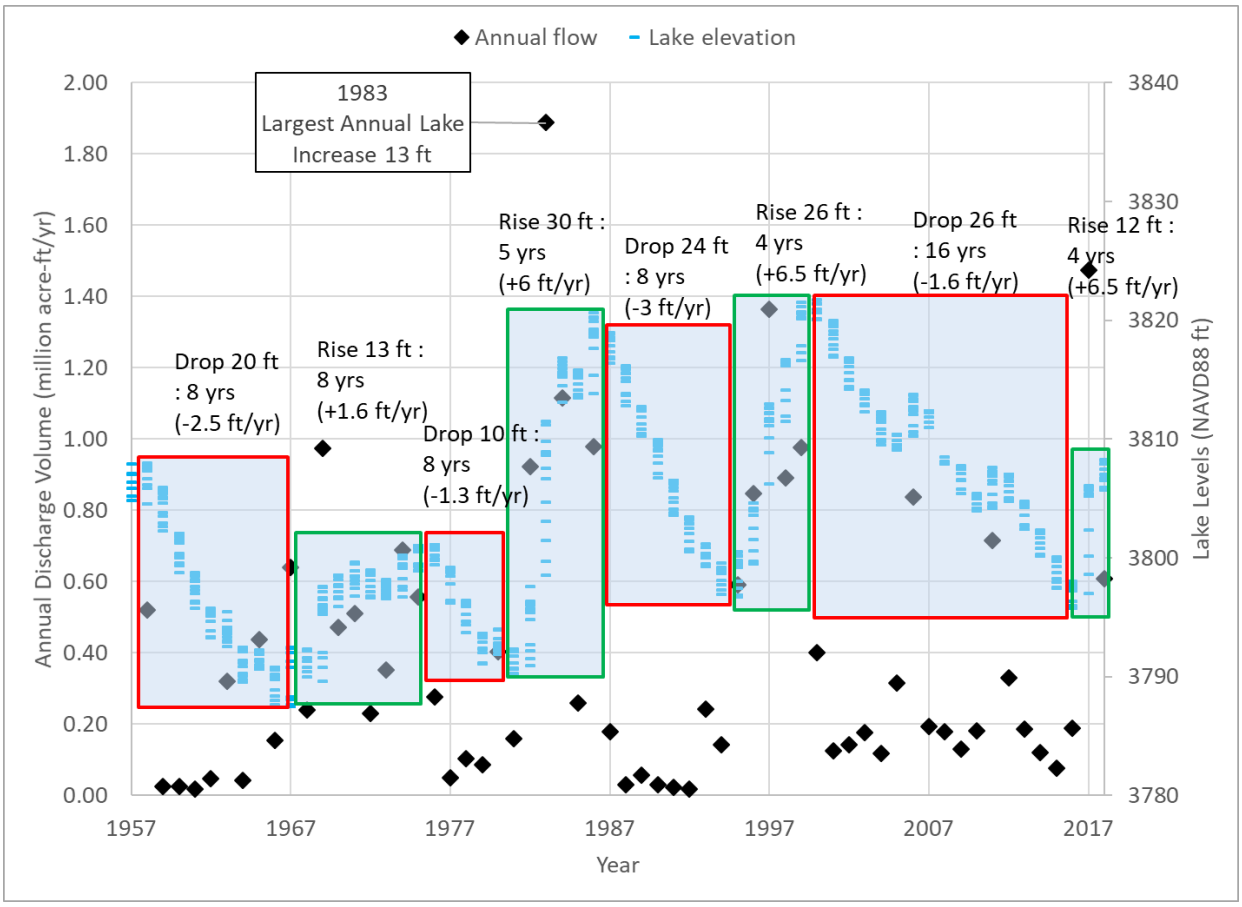

Figure 2. Pyramid Lake elevation rise and fall periods since 1958 correlated with annual discharge volume on the Truckee River upstream of Marble Bluff Dam.

As a result of the last century of Pyramid Lake lowering and continued floods, the Truckee River has had many phases of channel incision and lateral widening that have contributed large sediment volumes. Adams (2012) estimates 78.5 million cyds^3 of sediment have been released

into Pyramid Lake over the past 120 years (through 2008) just from terrace erosion, which doesn't account for the additional suspended sediment or bed-material load. Born and Ritter (1970) propose lateral bank failure on the Truckee River is likely due to a combination of, "(1) local undercutting by the river resulting in slope instability and consequent failure of the banks, (2) corrasion by the flood waters, and (3) failure related to changes in pore-water pressure conditions in stream-bank sediments due to changes in river stage." The typical bed-material is 10 to 20 mm. The coarsest sediment supplied to the channel was from an alluvial fan with a D_{50} of 22.6 mm (see Figure 1). At the current slope, 2D model results indicate sediment of this size is mobile at the bankfull discharge of 5,000 cfs over more than 50% of the channel. Around station 8,000 there is a small alluvial fan that contributes some larger sized gravel and cobble (see Figure 1). Historically there was an instance where the fan delta was so large it completely filled the Truckee River channel. However, the river eventually flushed out this material during a subsequent flood indicating the alluvial fan sediment may only temporarily slow headcut progression and channel incision during low flow periods.

Adams (2012) used relative elevation differences in historical terrace mapping (Figure 3) to estimate the change in channel gradient as the lake lowered (Figure 4). Because there is no resistant layer such as bedrock outcrops in the river bed, the upstream channel dramatically decreased in slope between 1938 and 1977. U.S. Fish and Wildlife staff have anecdotally observed clay knickpoints in the Truckee River channel downstream of Marble Bluff Dam while doing fish surveys. These knickpoints likely occur during channel incision resulting from lake lowering but are easily eroded during subsequent high flow periods; knickpoints were not observed during 2016 to 2018 surveys in the downstream channel.

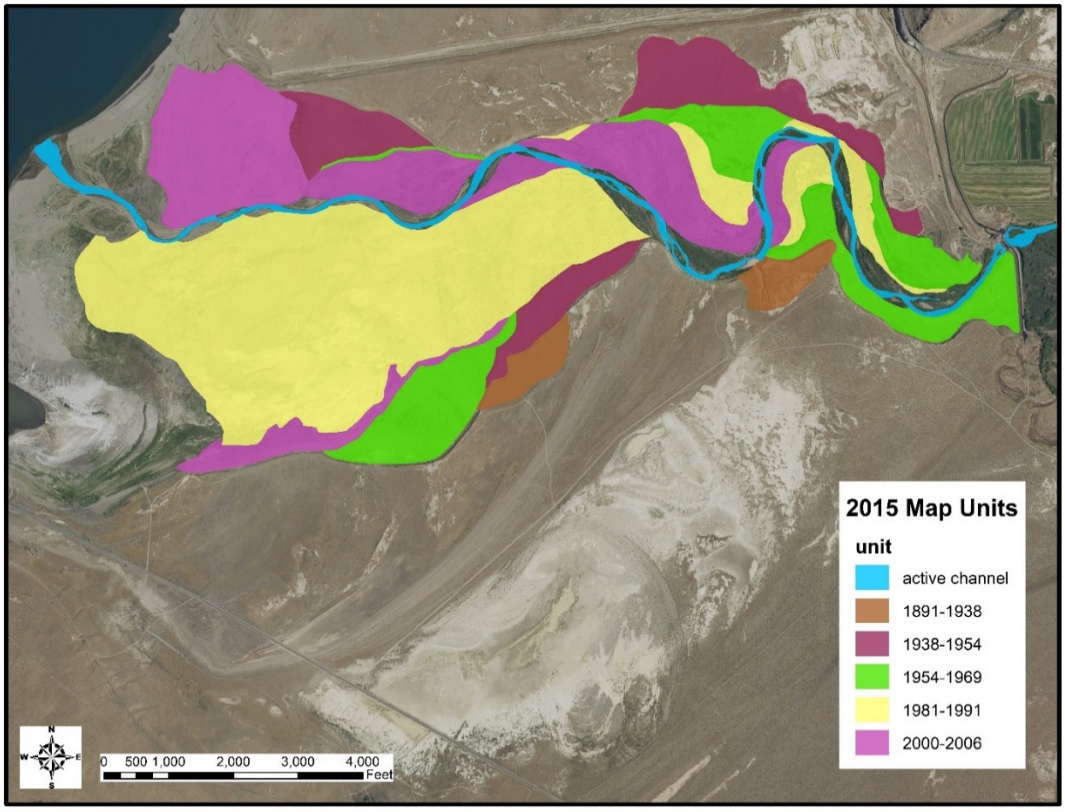

Figure 3. Updated surficial geologic map of Truckee River terraces and 2015 channel downstream of Marble Bluff Dam. Historical mapping modified from Adams, 2012.

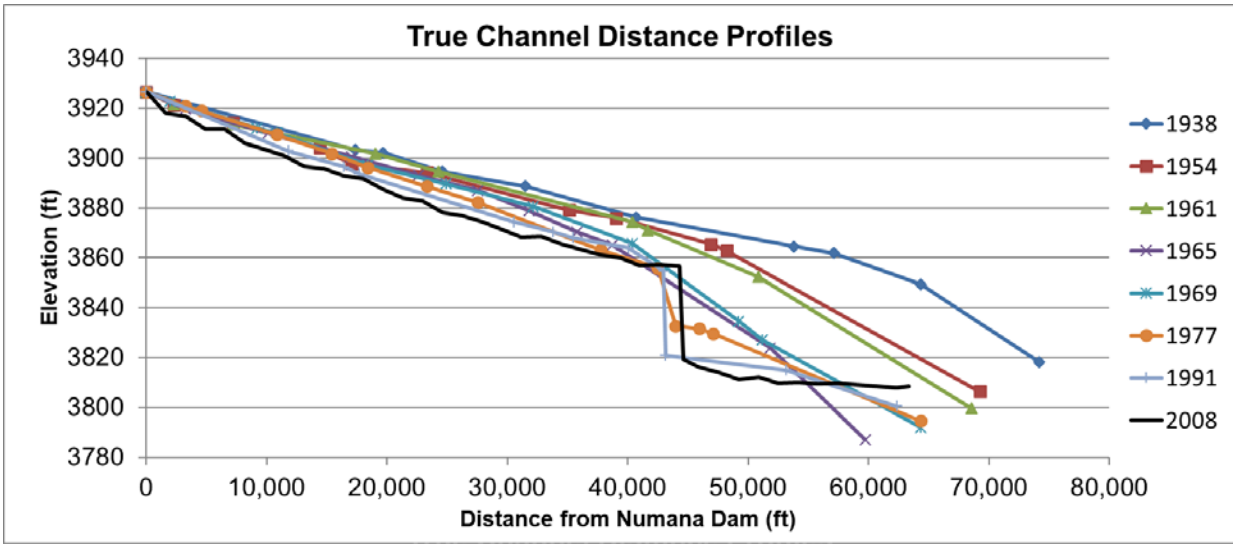

Figure 4. Reproduced in English units with permission from Adams (2012) Figure 10.

The 1961 and 1971 design data validate the tens of feet of channel lowering immediately below Marble Bluff Dam documented in Adams (2012) and provides more detail about the 1971 slope (Figure 5). The 1971 data indicates the steeper slope intercepted the downstream channel around station 10,000 (see Figure 1). Since 1971, the channel between station 0 (Marble Bluff Dam) and 10,000 has flattened to about 0.001 from Marble Bluff Dam to Pyramid Lake. In the late 1990s, a grade control structure of rock riprap was placed for about 1,000 ft downstream (see Figure 1) to ensure future headcut progression did not reach the spillway toe of Marble Bluff Dam (elevation 3800 ft). In 2016, the question was raised as to whether the slope could decrease further, and what would happen if Pyramid Lake lowered another 10 feet or more, similar to the stage in 1967. Fortunately, in 2017 a high-water year caused an increase in Pyramid Lake stage leading to delta deposition rather than incision. There did appear to be a minor break in slope around station 10,000 in 2016, similar to the location of the break in slope in 1971 but with a much smaller change in slope upstream to the dam (see Figure 5).

The historical response of the Truckee River to falling Pyramid Lake levels is to incise and straighten the channel resulting in a steeper slope as evidenced from the 2016 profile and 2015 channel alignment. If Pyramid Lake had dropped another 10 feet to 3784 from the 2016 elevation (3794 ft), the river would be expected to further incise and increase the slope. If Pyramid Lake remained at a lower stage long enough, the channel would have the potential to flatten the slope through subsequent headcut progression. In 2017 a large flood occurred that increased lake stage and resulted in new delta deposition. In 2018 minimal flooding occurred and lake stage and channel bottom elevations were maintained at the higher levels created in 2017. The Truckee River downstream of Marble Bluff Dam had significant lateral erosion and an increase in channel sinuosity as a result of the 2017 flood (Figure 6).

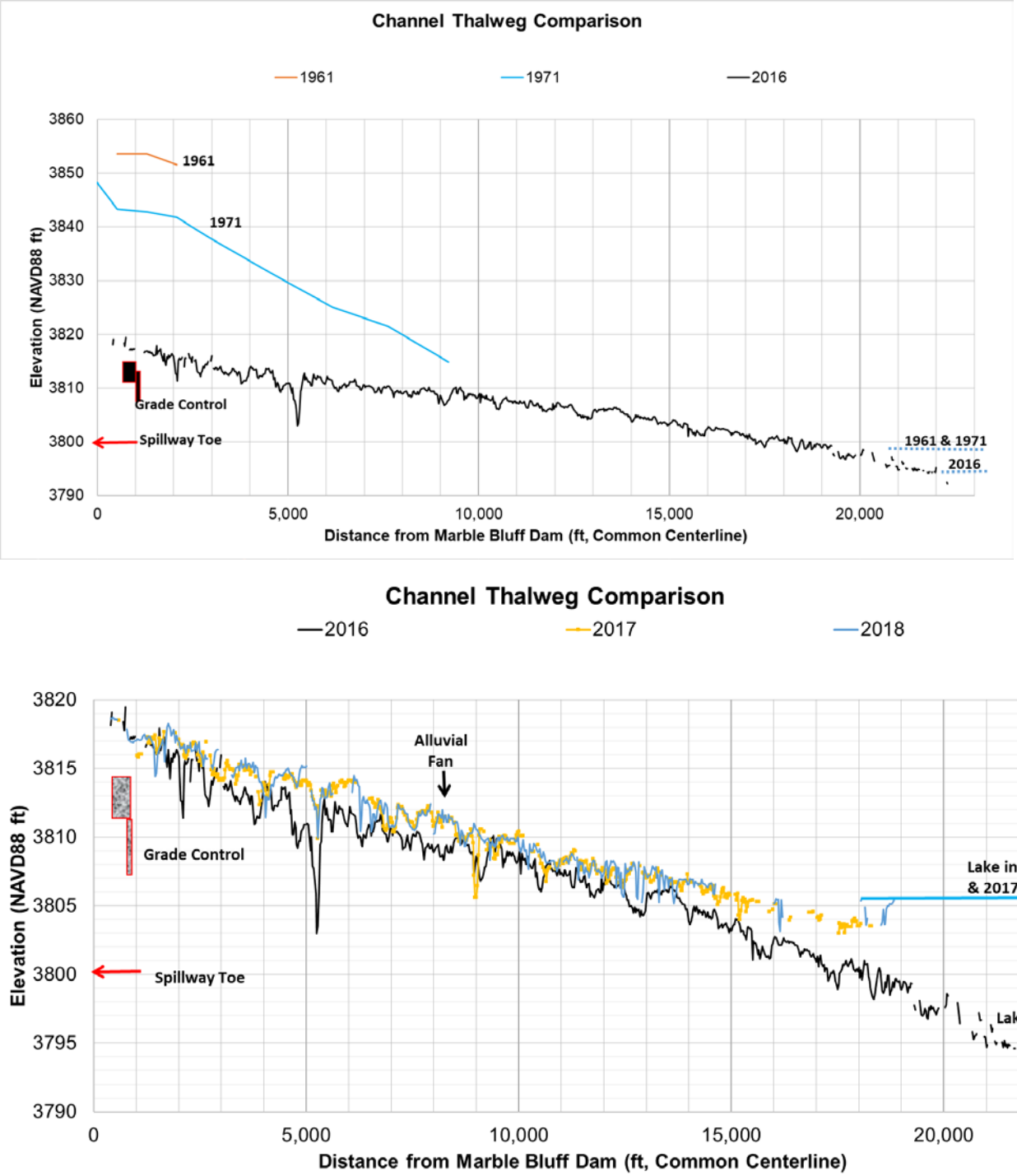

Figure 5. Channel thalweg data comparison of2016 data with 1961 and 1971 (top), and of 2016, 2017 and 2018 (bottom) and associated Pyramid Lake elevations during the same time periods. Grade control placed in the 1990s and the spillway toe of Marble Bluff Dam are shown for reference.

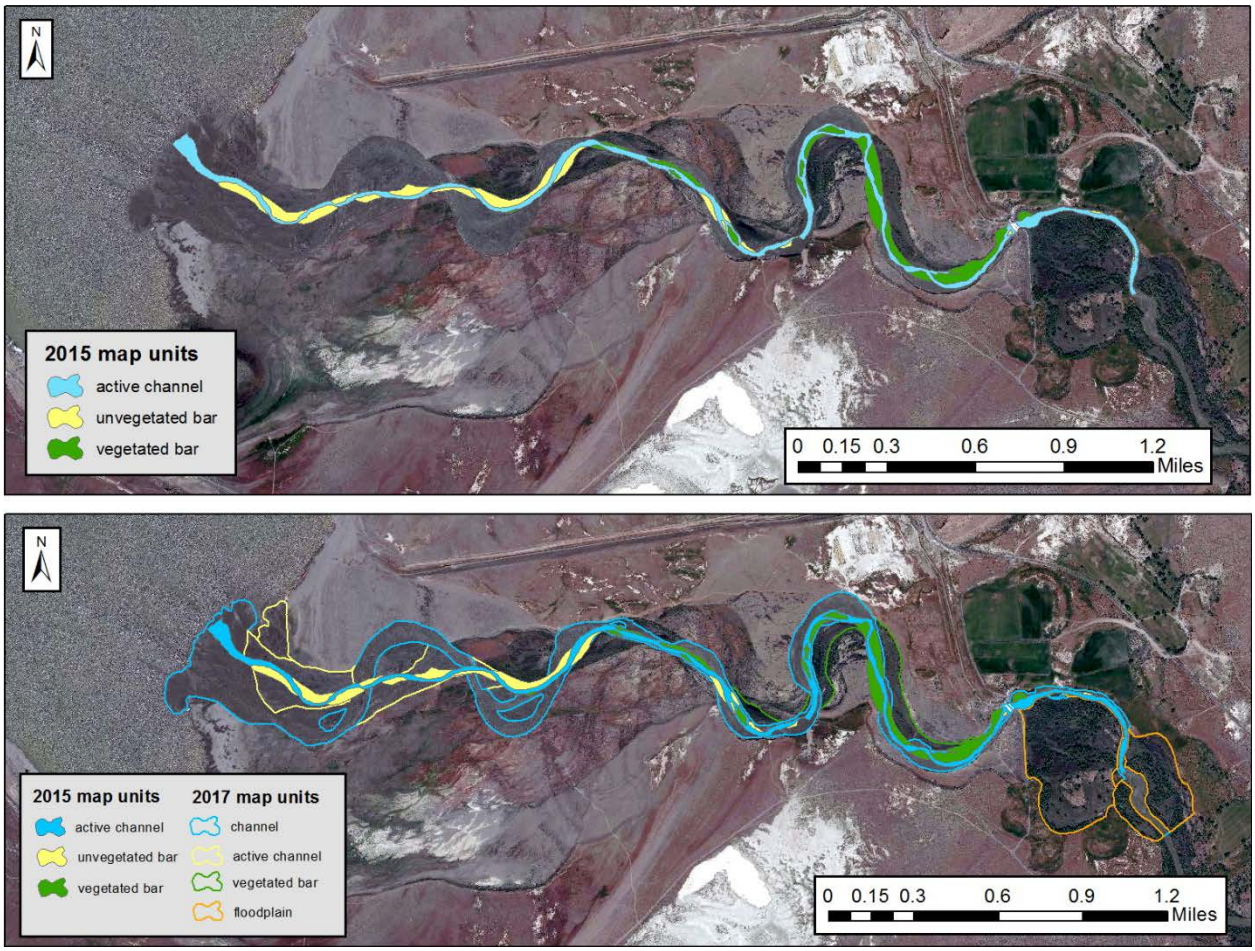

Figure 6. Lateral migration and expansion of the active channel between 2015 and 2017 due to high flows and increasing Pyramid Lake stage in water year 2017.

Results in Marble Bluff Reservoir

Upon its completion in 1976 Marble Bluff Dam had a storage capacity of 300 acre-ft, which is less than 1% of the annual flow volume (Figure 7). Although not intended for water storage, the dam backed up surface flow for a distance of approximately 3/4 mile upstream of Marble Bluff Dam. At the time of construction, the active channel in the vicinity of Marble Bluff Dam was braided with sparse vegetation due to recent high flows, channel incision, and high sediment loads from upstream erosion. Continued sedimentation upstream of Marble Bluff Dam rapidly filled the reservoir area, progressing downstream from the upstream end, and forming a braided network of channels between 1977 and 1981. Vegetation encroachment in floodplain and active channel areas coupled with regulated flows from upstream encouraged narrowing of the active channel to a single channel or split flow channel morphology. Based on mapping from aerial photography, the reservoir appears to have filled in with sediment within about 20 years following its construction. Operation of a small radial gate was intended to minimize filling of the reservoir, but it likely only slowed the sedimentation rate.

Since the 1990's, the reservoir area has continued to change with the development of islands and bars near the dam and just upstream from the dam (Figure 8). While the general location of the active channel has remained very similar, local bar features have highly influenced the position of the thalweg, active channel and side channels near the dam. The first glimpse of a mid-

channel bar/island forming near the dam is from the 1994 aerial photography, where a small vegetated island had formed just upstream of the dam. While the thalweg cannot be seen in the aerial photography, it was likely located along the right (north) bank as it entered the diminished reservoir area. The linear character of the channel in this location suggests that the channel may have been dredged recently to remove sediment and/or direct the channel toward the radial gate. Several unvegetated bars are mapped in the aerial photography; former channel paths can also be viewed in the 1994 aerial photography that had not been filled completely with sediment or vegetation. By 2004, many of these channel paths as well as the unvegetated bars had been filled in with vegetation and likely sediment as well. The channel thalweg had moved toward the center of the dam, with vegetated bars becoming more prevalent within the reservoir area and upstream of the reservoir. On the southern side of the reservoir, a side channel had formed around a large unvegetated bar deposited upstream of the left embankment, while lateral erosion was the dominant process along the right bank near adjacent agricultural fields. Aerial photography flown in 2006 shows continued changes, with a small incipient unvegetated mid-channel bar forming in the reservoir area upstream from the radial gate and vegetation increasing on the 2004 unvegetated bar on the south side of the reservoir. This mid-channel bar continued to grow in size through 2010, which shows the advanced development of the side channel and vegetation on the mid-channel island. The channel near the reservoir continued to decrease in complexity through sedimentation and vegetation encroachment, filling in the southern side channel as well as other side channels just upstream of the reservoir area. The island near the radial gate continued to grow in size; in addition, sediment can be seen filling the mouth of the side channel associated with the island. Between 2010 and 2016 the radial gate was rarely operated, usually only for a few hours to days to check it was working. Aerial photography in 2015 shows little change from the 2013 channel configuration.

In 2016, 7 to 10 ft of reservoir sedimentation was documented in the side channel and island above the radial gate outlet (Figure 9). Radial gate operation was recommended to test if reservoir sediment could be flushed out of the side channel area. To operate the fish passage facility at Marble Bluff Dam the radial gate must be fully shut,, but the gate could be opened outside fish passage periods (typically January to June). Despite repeated attempts to sluice through the radial gate and the high flow in 2017, only minor erosion of the island occurred and no erosion of the side channel happened. In fact, after the 2017 flood, 1 to 3 ft of deposition occurred in the side channel and 4 to 5 ft on the opposite side of the reservoir due to the higher stage and likely higher incoming sediment loads (Figure 10). To improve understanding we applied a 2D model in the reservoir. When higher flows occurred, the reservoir backwater increased, decreasing the opportunity to sluice sediment even when the radial gate was operated. The vegetation on the island also limited potential for erosion of the sediment. Additionally, the upstream channel had further migrated into the right bank and one large cottonwood tree remained on an exposed surface that acted like a jetty. This jetty actually steered the low-flow channel away from the side channel creating a depositional zone and further reducing the likelihood of any erosion (Figure 11).

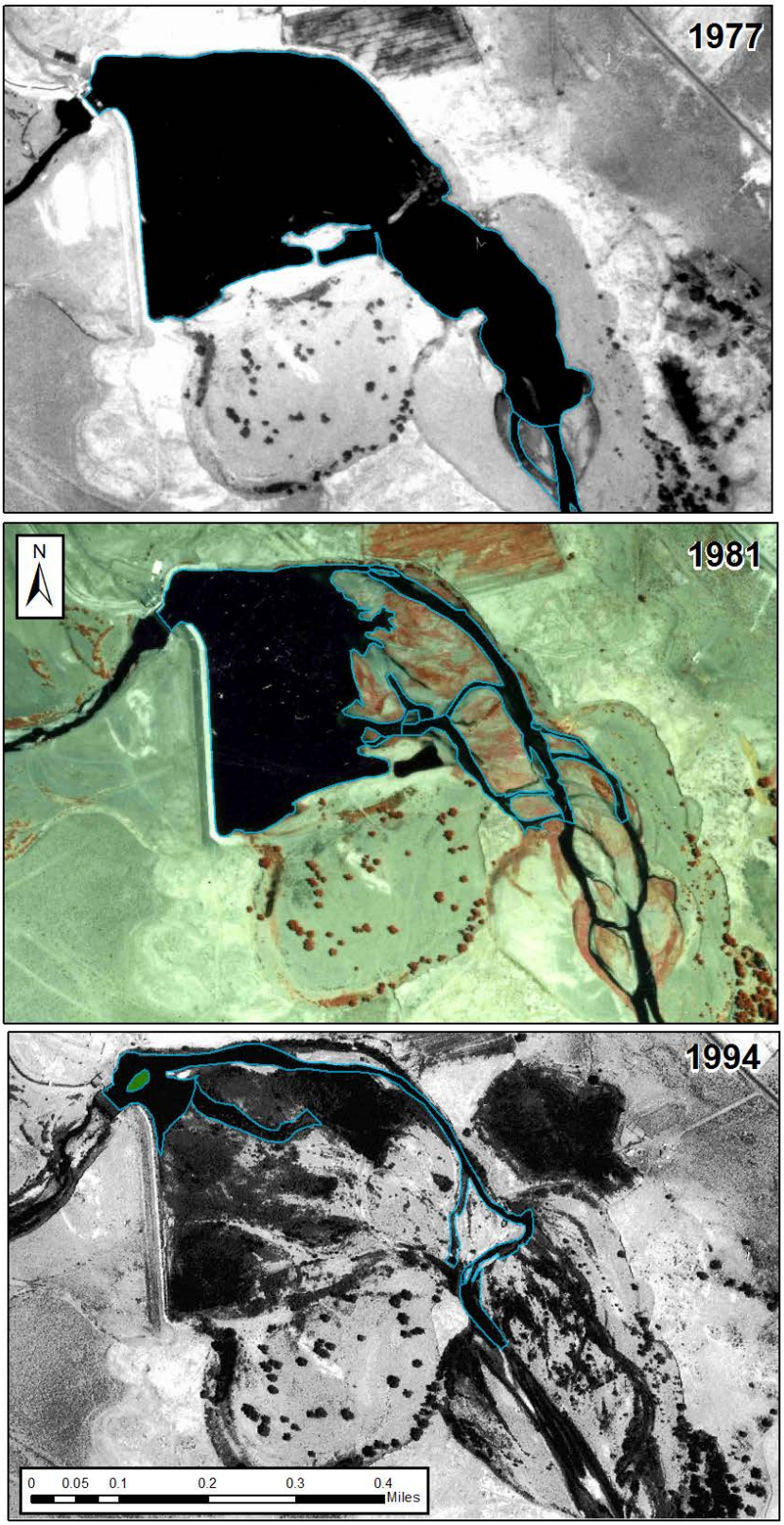

Figure 7. Sedimentation of Marble Bluff Reservoir from 1977 to 1994.

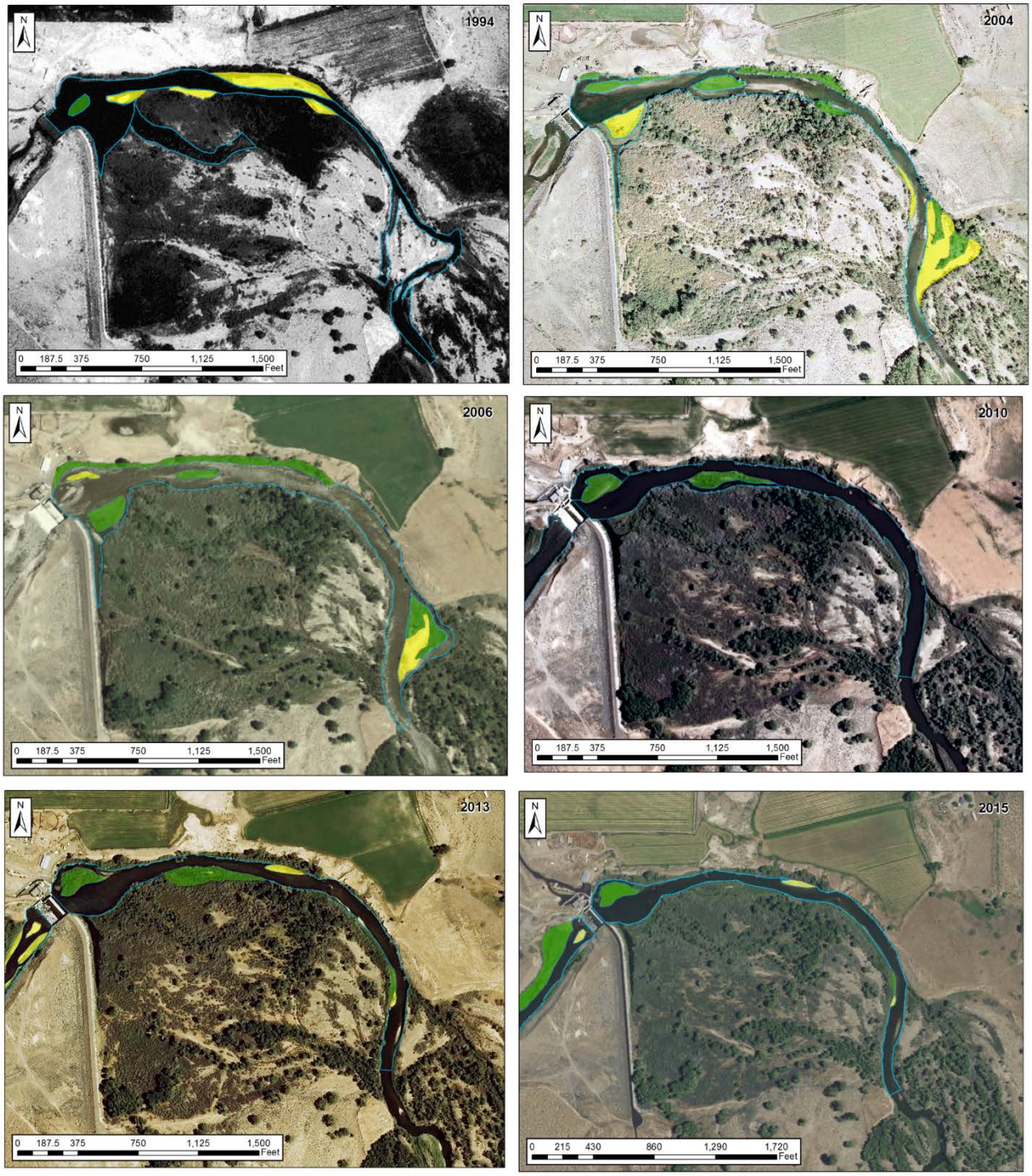

Figure 8. Channel changes in Marble Bluff reservoir area, 1994-2015. Active channel is designated by the blue line; unvegetated bars are shown in yellow; vegetated bars are shown in green.

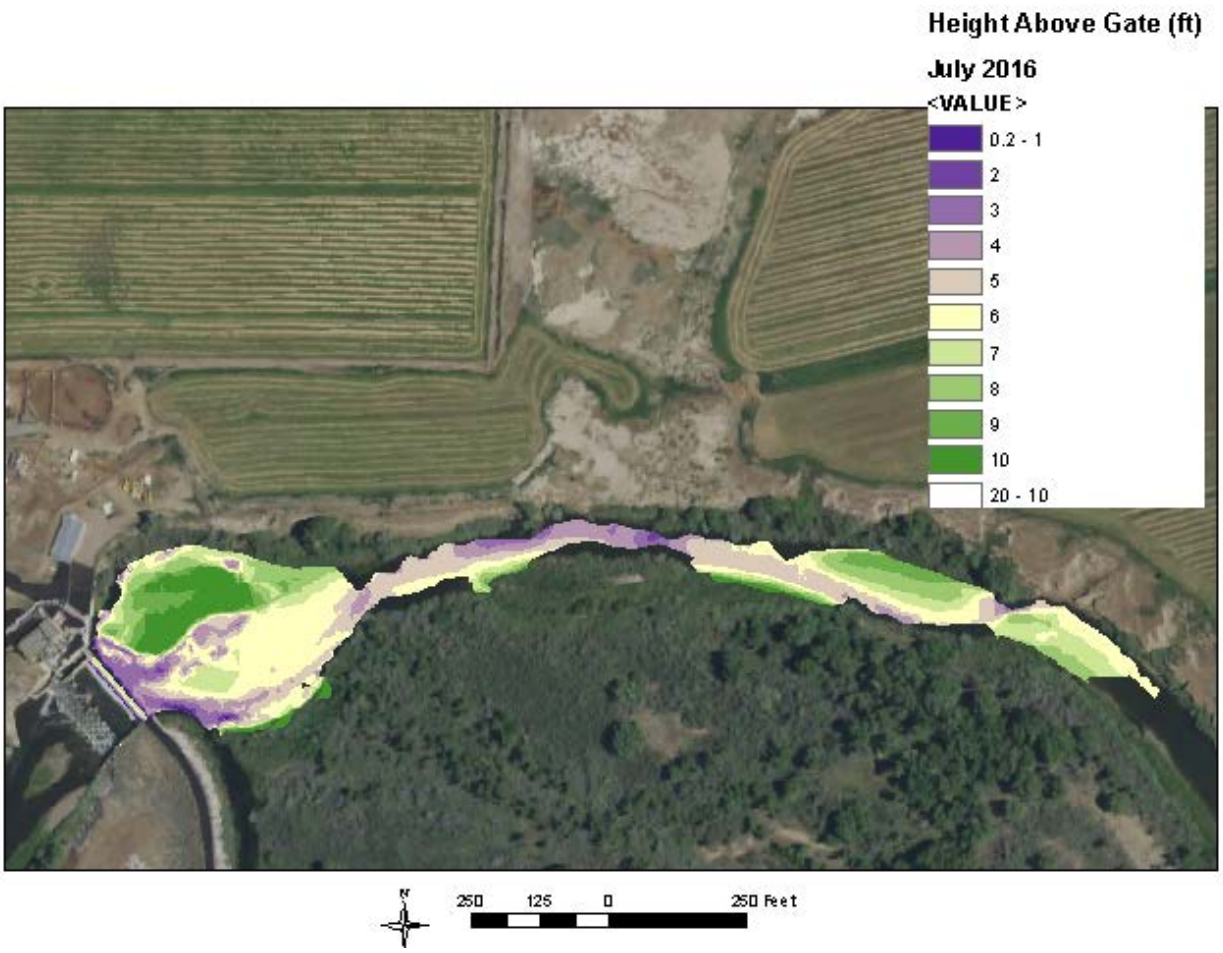

Figure 9. Sediment thickness based on 2016 survey relative to bottom of radial gate used for sluicing at Marble Bluff Dam.

Figure 10. Upstream view of reservoir sedimentation following 2017 flood in vicinity of fish passage release and radial gate.

Figure 11. 2017 aerial photograph showing channel changes upstream of Marble Bluff Dam as a result of the 2017 flood.

Discussion

Annual monitoring is recommended to further understand river channel profile, alignment, and sedimentation response downstream of Marble Bluff Dam from Pyramid Lake level changes and occurrence of river floods or low water years. If Pyramid Lake lowers below the 2016 level and channel incision progresses upstream of the break in slope at station 10,000 immediate monitoring of the grade control structure is recommended and possible enhancement if needed. Monitoring of the channel bed to determine whether the river is in equilibrium or could further flatten is important to ensure fish can enter the passage facility at the base of the dam.

Within Marble Bluff Reservoir, the river is unlikely to erode the vegetated island and side channel sedimentation from radial gate operation alone. However, if lateral migration continues on the upstream right bank and more flow goes behind the remaining cottonwood tree, the river could erode more of the side channel sediment. We ran 2D models with various excavation scenarios to determine if removal of the side channel and island sediment would result in viable pathways for fish passage. The goal is to have the fish avoid swimming in front of the dam and risk being swept back downstream. An estimated removal of 10,000 yds^3 of sediment is recommended to improve hydraulics for fish passage. Sediment quality testing must occur first to ensure the sediment is not contaminated above thresholds, which would require different mitigation requirements to excavate and dispose. Sediment sampling and quality testing is planned for fall 2019. To address the upstream bank migration, design options will be evaluated that could slow the rate of migration and prevent the river from outflanking the cottonwood tree or downstream infrastructure. With some concerns being raised about the possibility of the tree being uprooted and getting trapped in the downstream radial gate or on the dam spillway which can result in damage and poor hydraulic conditions, tree removal is also recommended.

Summary

Lowering of Pyramid Lake has resulted in a complex river system that has evolved rapidly in the last several decades. Channel incision and headcut progression was stalled in 1976 through the construction of Marble Bluff Dam, but downstream of the dam channel incision continues to occur. The dam is now vital to maintain endangered fish passage and prevent further erosion in upstream tribal lands. Downstream of the dam, channel incision has progressed over the years such that the slope appears flat enough to be near equilibrium. Because the slope is so low, any further lowering of Pyramid Lake level would result in further incision that could prevent successful fish passage at the dam. Though grade control was installed to limit upstream headcut progression, monitoring was recommended to ensure channel incision does not undermine it and to identify enhancement needs to keep it functioning as designed." In the upstream reservoir, sedimentation has reduced viable fish pathways to migrate upstream and spawn. The radial gate intended for sediment sluicing has not been effective due to the configuration of the channel and vegetation establishment on the sediment deposit. Excavation is recommended to re-establish viable fish pathways that allow a route into a side channel away from the dam crest. Investigation of sediment quality will occur in 2019 to help inform sediment management options for excavation activities planned in 2020.

References

Adams, K.D.. 2012. “Response of the Truckee River to lowering base level at Pyramid Lake Nevada, based on historical air photos and LiDAR data,” Geosphere; June 2012; v. 8; no. 3; p. 607–627; doi:10.1130/GES00698.1

Bell, J.W., House, P.K., and Briggs, R.W. 2005. Geologic map of the Nixon area, Washoe County, Nevada, Nev. Bureau of Mines and Geology.

Born, S.M. and Ritter, D.F. 1970. Modern Terrace Development Near Pyramid Lake, Nevada, and its Geologic Implications, Geological Society of America Bulletin, v.81, p.1233-1242.

Lebo, M.E., Reuter, J.E. and Meyers, P.A. 1994. “Historical changes in sediments of Pyramid Lake, Nevada, USA: consequences of changes in the water balance of a terminal desert lake,” Paleolimnology, 12: 87. https://doi.org/10.1007/BF00678089.

USACE. July 22, 2013. Truckee Meadows Flood Control Project, Reno, Nevada, Attachment B – Hydraulic Design, Sacramento District, USACE

The Geography of Fluvial Geomorphic Hazards in River Corridors

Joel Sholtes, Instructor, Colorado Mesa University, Department of Engineering, Grand Junction, CO, jsholtes@coloradomesa.edu
Katie Jagt, Water Resources Engineer, Watershed Science and Design, Boulder, CO katiejagt@watershedscienceanddesign.com
Michael Blazewicz, Fluvial Geomorphologist, Principal, Round River Design, Salida, CO michael@roundriverdesign.com

Abstract

The natural and human-influenced river processes of avulsion, erosion, and deposition change the boundaries of a river, its valley margins, and its floodplain. These fluvial geomorphic processes, which may occur gradually over time or abruptly during a flood, become hazards when they interact with human infrastructure located within stream corridors. Fluvial geomorphic hazards can lead to unexpected and unmitigated flood impacts that traditional floodplain mapping ignores. From deposition of sediment at alluvial fans, to scour of hillslopes in steep mountain streams, to braiding of wandering sand bed rivers, a wide variety of fluvial geomorphic hazards exist across Colorado and within the western United States. We provide an overview of how streams and rivers move, influence the river corridor, and identify the geographic settings where they are most severe. This geography of fluvial geomorphic hazards can inform floodplain management in hope of avoiding future damages and improving resilience to natural disasters within our communities.

Introduction

Floodplain management in the U.S. has characterized hazards within a river or stream corridor by mapping zones of potential inundation from a flood (i.e., the flood insurance rate map, FIRM, FEMA 2019). These are federally and locally regulated maps that inform the need for and cost of flood insurance and as well as land use planning within stream corridors. Since 1978, approximately 49% of all National Flood Insurance Program claims in Colorado have come from insurance policies written outside the high-risk area depicted on the Federal Emergency Management Agency (FEMA) FIRMs (i.e., the 1% annual chance flood or 100-year floodplain, Matthew Buddie, FEMA Region 8, personal communication, October 25, 2017). This is may be due to inaccuracies or (unpublished) uncertainties in the hydrology and hydraulics associated with this inundation mapping (Merwade et al., 2008), the occurrence of floods with annual chances smaller than 1%, as well as lack of representation of dynamic stream processes occurring gradually over time and associated with flood events (FEMA 1999). Because they only identify inundation hazards and assume that the stream channel and floodplain are topographically static, FIRM maps fall short of characterizing all hazards associated with stream corridors, defined as the stream, its floodplain, and adjacent valley margins.

Stream corridors are naturally dynamic environments. Fluvial geomorphic processes are those created by moving water that involve the erosion, transport, and deposition of sediment and organic matter. These physical processes, which may occur gradually over time or abruptly during a flood, become hazards when they interact with human infrastructure located within stream corridors. These interactions may include damage beyond simple wetting associated with inundation flooding and as previously mentioned may extend beyond the mapped and regulated

floodplain areas designated in FEMA FIRMs. Because of these issues, the State of Colorado's Water Conservation Board (a state agency located within the Department of Natural Resources) is developing a protocol for mapping the Fluvial Hazard Zone (FHZ), defined as the area a stream has occupied in recent history, may occupy, or may physically influence as the stream stores and transports water, sediment and debris.

The process for mapping FHZs in Colorado is built on a body of work and developed in other regions in the U.S. including the States of Washington (Olson et al., 2014, Rapp and Abbe 2004), Vermont (VT DNR 2017), Montana (MT ARS, 2017), as well as arid and semi-arid municipalities such as Maricopa County (Maricopa County, AZ 2013). A review of these methodologies was conducted for the State of Colorado FHZ program by Jagt et al. (2015).

In this paper, we discuss the physiographic contexts – geologic, hydrologic, and geomorphic – that drive fluvial geomorphic hazards from the watershed to reach scales and inform the spatial character, or geography, of fluvial geomorphic hazards. Evaluating the physiographic context of a study area sets up a framework and context for describing and ultimately mapping fluvial geomorphic hazards. Geologic context can inform valley form and slope, erodibility of valley margins, and sediment supply. Climatic context informs flow regime variability, fire regime, and vegetation type and prevalence. Finally, geomorphic context integrates these other contexts to inform how a river corridor has evolved over human time scales, inform how it responds to flood events, and to predict the trajectory of its form and sensitivity to change over the decades to come.

We first describe how these various contexts influence fluvial geomorphic processes, and hence hazards, over a range of temporal and spatial scales. We then integrate these contexts to create a framework for describing the geography of fluvial geomorphic hazards. Finally, we apply this framework to a case study on East Plum Creek, Douglas County, CO.

Physiographic Context

The physiographic context is defined by the dominant geologic, topographic, and climatic conditions which influence its form, associated physical processes, and magnitude and frequency of dynamism. Physiographic regions have been defined by Fenneman and Johnson (1946) and since refined and expanded upon (e.g., NRCS, 2006). These regions (Figure 1) delineate areas within which geology and climate are relatively homogenous.

The entirety of a study area will not necessarily lie within the same physiographic setting. Longer reaches of streams may span two or more regions or subregions. Examples of this are many streams on the Colorado Front Range that begin in the Southern Rocky Mountains region and flow into the Colorado Piedmont and Great Plains regions. Major rivers such as the Yampa, Gunnison, Arkansas, and Colorado also flow through two or more physiographic regions from their headwaters to their mainstems.

Geologic Context

The geologic context controls a suite of variables pertinent to geomorphic response of stream systems ranging from sediment supply, valley confinement, erodibility of channel and valley margins, vegetation, and hydrology (Brierley and Fryirs, 2005). This geologic setting will inform the watershed- to reach-scale geomorphic context of the study area. For example, many basins in Colorado's Rocky Mountains were glaciated or influenced by glacial events. As glaciers retreated, they produced meltwater flows and sediment loads exceeding contemporary flows and

sediment loads (Church and Ryder, 1972). Along the Colorado Front Range Piedmont, and in other areas such as the piedmont of the Sangre de Cristo Mountains in the San Luis Valley, deposits formed from glacial outwash material, sometimes creating alluvial fans (McCalpin, 1982). The glaciers also deposited terminal and lateral moraines with which contemporary stream corridors interact. Headwater streams located within or downstream of glaciated valleys may be considered "underfit" if the existing stream is not responsible for forming the broad valley or corridor within which the present stream now resides (Drury, 1964).

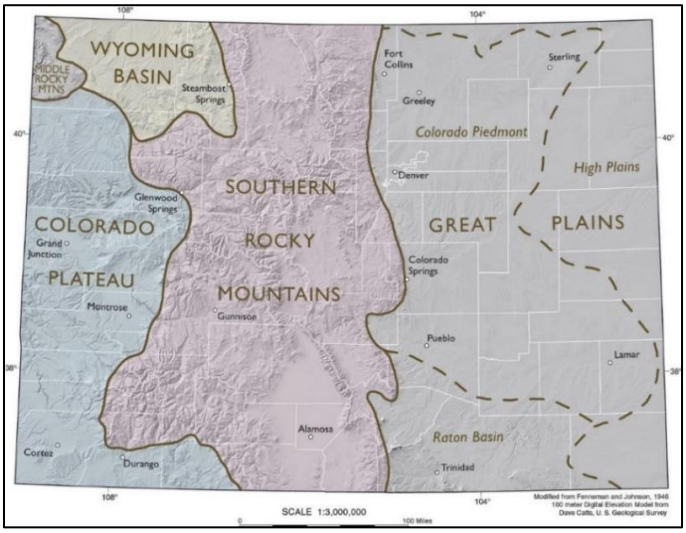

Figure 1. Physiographic regions of Colorado (from Colorado Geologic Survey, 2019)

During the present inter-glacial period, many of these former depositional environments are now degradational eroding into glacial outwash deposits and forming alluvial terraces as they abandon former floodplains. These terraces may comprise the valley margins of these streams. In many regions within the Colorado Piedmont, terraces margins comprised of glacial outwash are composed of sand and gravel and are highly erodible. In other cases, such as along the Eagle River, headwater tributary to the Colorado River, alluvial terraces comprised of cobble- and boulder-sized material may be less erodible (Lidke, 2002).

Other geologic features that may be important to the geologic context are the presence of faults, dykes, and kickzones, which may provide local topographic and valley morphology controls. Aeolian deposits (i.e., loess) and sand dunes may represent more erodible material present within a river corridor. Ultimately, as these examples indicate, the identification of the regional geologic context is important to identify and understand.

To characterize the geologic context, surficial geology maps can be used to identify geologic formations within a study area and along study reaches (Figure 2). Other geologic studies may also be available including local geologic hazard reports. Available surficial geology maps are posted to the National Geologic Map Database (U.S.G.S. 2019). The 1:24,000 scale of the most detailed geologic maps limits their accuracy at smaller scales (i.e., < 1:1000). They may also not account for fill material imported into the floodplain from recent development. Finally, because a geologic map designates a particular surface as a type of bedrock unit, this does not necessarily mean that a bedrock outcrop exists along the entire mapped unit. Rather, erodible mantles

comprised of colluvium or a soil may exist. As such, field verification is required to ground truth surficial geology.

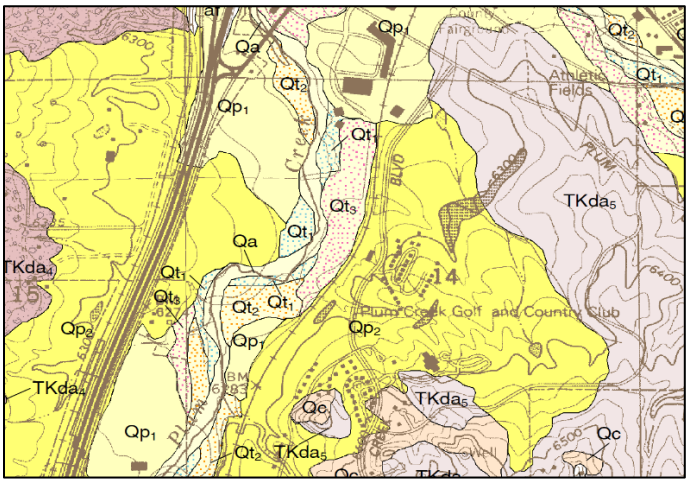

Figure 2. Example of 1:24,000 scale geologic map (Castle Rock South quadrangle, Thorson, 2004). Presence of "Q" units within the East Plum Creek corridor indicate alluvial deposits of varying ages and a highly erodible corridor. In some cases, approximate ages of different "Q" units provided within geologic maps can be used to differentiate between active floodplain and terrace features. The Dawson Formation is represented by units labeled "TKda".

Surficial geologic maps can be useful for identifying erodible units such as Holocene or Pleistocene alluvial, colluvial or aeolian deposits (Morse, 1976; Crifasi, 1992) or those created in lacustrine environments such as within the Roan Plateau on the Western Slope (Hail, 1992). These erodible sedimentary formations are typically composed of sandstones and claystones along with conglomerates. The Dawson Formation, located around Castle Rock and the Palmer Divide area, is an example of this type unit (Figure 2, Thorson, 2004). Composed of weakly consolidated sandstone, claystone, and conglomerate, the Dawson Formation is particularly prone to gullying and constitutes a large upland sediment supply to streams in this area.

Hydrologic Context

The timing and magnitude of runoff as a result of a precipitation event is complex. It can be related to the slope and size of the contributing watershed (Dunne and Leopold, 1978), density of the upstream channel network (Gregory and Walling, 1968), the infiltration capacity and antecedent soil moisture conditions surfaces within the watershed, wildfires or development in the watershed (Holman-Dodds et al., 2003; Ebel and Moody, 2013), as well as rate and timing of precipitation or snowmelt (Berghuijs et al., 2018).

Topography, including regional orographic effects, elevation, and local conditions such as slope and aspect, plays a large role in climatology and flood meteorology (Doesken et al., 2003). Colorado straddles the continental divide and hosts a diverse topography over a wide range of elevations. Because precipitation quantity and intensity are influenced in part by elevation as well as by which side of the continental divide a study area's watershed lies (Capesius and Stephens, 2009), the flood climatology of Colorado is quite variable across the state. Colorado flood geography has been summarized by the United States Geological Survey (USGS) in their regional flood frequency analyses (Capesious and Stephens, 2009; and Cohn et al., 2016). It has also been summarized by the Colorado Dam Safety Office in a related study of regions within

which flood-producing precipitation events are relatively homogenous in terms of their magnitude (duration, intensity, and depth) and scale (Figure 3, Colorado Dam Safety, 2018).

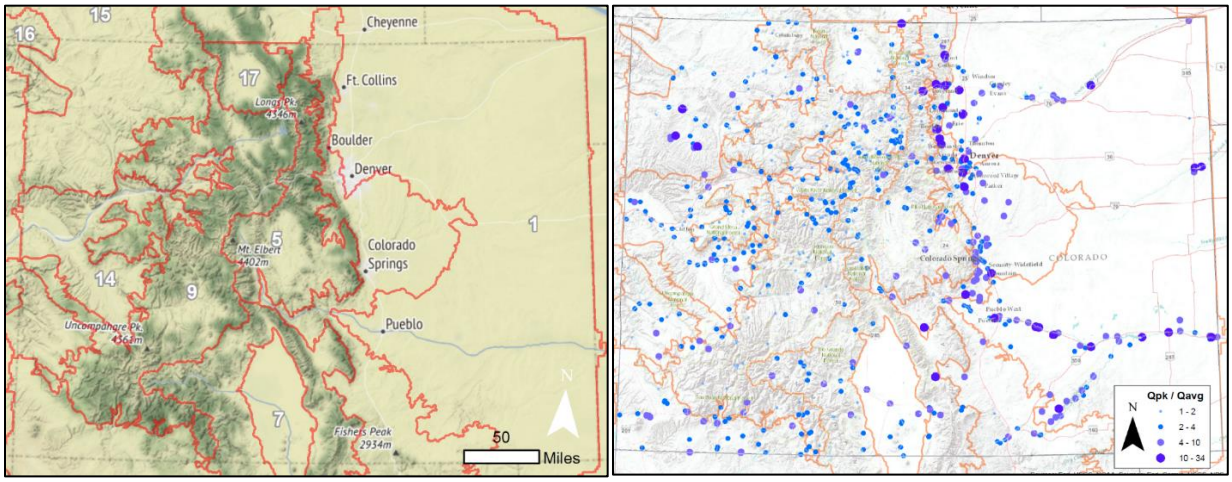

Figure 3. (Left) Regions of homogenous extreme precipitation events. Red boundaries represent "storm transposition units" within which extreme precipitation events at different scales are considered homogenous and therefore may be transposed to other locations within these bounds (Colorado Dam Safety Office, 2018). (Right) Map depicting location of UGSG peak discharge measurements across Colorado with ≥ 10 years of data. Dots represent the intensity of recorded flood events enumerated as the annual maximum discharge (Q_{pk}) normalized by the average of the annual maxima for a gage (Q_{avg}). Larger, more purple dots indicate extremely flashy or intense floods. Value ranges reported in the legend represent annual maximum peak discharge values formalized by the mean of the peak discharge values as measured at USGS gages.

Flooding in Colorado occurs primarily as a result of intense and persistent rainfall events from small to large scales (Doesken et al., 2003). In an analysis of flood peak intensity, defined as a high ratio of annual maximum peak discharge to average annual maximum peak discharge, the majority of intense floods have been observed along the Colorado Piedmont (Front Range) and along the Arkansas and Purgatorie Rivers (Figure 3). Smaller-scale flooding from intense rainfall has been observed along the Roan Plateau and in the southwest of Colorado. Snowmelt driven floods also occur in years of heavy snow pack. Snowmelt floods are typically less intense but can have very long durations resulting in significant geomorphic work on the channel and floodplain. Rainfall over an existing snowpack can rapidly melt snow recruiting greater quantities of runoff for a flood on top of a spring snowmelt hydrograph resulting in relatively large flood magnitudes. In a review of trends for "rain-on-snow" events in the western U.S. (McCabe et al., 2007), significant positive temporal trends in their frequency were found at higher elevation sites (> 6,500 ft) and significant negative trends where found at lower elevation sites (< 6,500 ft). Rain-on-snow events decrease with warmer temperatures up to a certain elevation: under hotter conditions, there is less snow on the ground and therefore less opportunity for rain-on-snow events. However, rain-on-snow events may be increasing for higher elevation sites where snowpack is expected to remain (McCabe et al., 2007).

At watershed to sub-watershed scales, the hydrologic context of a study stream is important to evaluate as changes in hydrology—as a result of land use change or flow regulation—can disrupt the water-sediment balance in stream systems thus informing fluvial processes and trajectories. Enhanced stormwater runoff from development, for example, may increase the volume and peak runoff rate of stormflow leading to erosion, incision, and channel widening, particularly in smaller drainage areas (Vietz et al., 2016). Similarly, wildfire may significantly increase the volume and amount of water and sediment delivered to a channel and change the

timing of runoff (Pierson et al., 2001).

Conversely, reductions in flow either from diversions or impoundment can cause a stream to narrow over time as vegetation encroaches and sediment accumulates (Church, 1995). This in turn may lead to increased channel erosion and bank failure during large flood events when diversions and impoundments are bypassed, and the channel regains its latent footprint. In fact many of Colorado's streams have flow regimes that are moderately to severely impacted by regulation from dams. This flow regulation typically results in the reduction of peak flows as compared to the hydrograph prior to regulation. Flow regulation may reduce the migration rate of a stream downstream (i.e., Shields et al., 2000). It may also result in channel narrowing as vegetation encroaches on surfaces that are no longer disturbed by semi-frequent floods events (Surian, 1999; Grams and Schmidt, 2002). The existence of a dam upstream of a study area does not preclude the possibility of geomorphically-significant flow events downstream. Indeed, runoff upstream of a reservoir can exceed that reservoir's capacity resulting in spillway or outlet works releases exceeding the channel capacity. The 2013 Colorado Front Range flood overwhelmed several reservoirs in the affected region resulting in uncontrolled spillway releases, such as on the St. Vrain Creek upstream of Lyons. Another recent example, the Oroville Dam in 2017 on the Feather River in California, resulted in widespread geomorphic change to the receiving channel and banks downstream.

Many sources of data exist to aid in evaluating the hydrologic context of a study area. A regional analysis of stream gage data (i.e., annual maximum floods) can inform the level of intensity of flooding in a region of interest. Hydrologic studies associated with floodplain mapping within or nearby the study area can also provide useful information. The National Oceanic and Atmospheric Administration maintains an atlas of extreme precipitation depths for the nation (NOAA Atlas 14, i.e., Bonnin et al, 2011). The USGS' StreamStats (2019) online tool can be used to provide reach-scale drainage area and flood frequency estimates based on regional regression equations. Finally, descriptions of the geographic distribution of extreme precipitation across a state may be available (e.g., Capesious and Stephens, 2009, Colorado Dam Safety Office, 2018).

Geomorphic Context and Trajectory

The geomorphic context integrates physiographic factors (geology, hydrology, biology) and human factors and considers these in the existing morphology (i.e., form) of the reach. These factors may include land use history at the reach to watershed scale, floodplain development, channel modifications, biotic factors such as riparian vegetation, beaver, large wood, and alterations to the flow regime. Analysis of the geomorphic context provides a better understanding of what fluvial processes are actively working on the channel and its margins as well as the types of flood responses and hazards that exist within the study area.

Geomorphic trajectory refers to how channel and floodplain form and process may evolve in the future based on current and past states, active processes and external stressors. Geomorphic history is important to understanding trajectory as it can provide context to understanding contemporary geomorphic processes and their influence on channel evolution and flood response. The combination of these spatial and temporal characteristics creates a geomorphic context that governs the contemporary form of the active river corridor and the mechanisms and rate at which fluvial processes occur (Wohl, 2018).

Temporal Scale

The concept of a stream's slope and cross-sectional shape in equilibrium with its flow regime and sediment supply has been a theoretical foundation of fluvial geomorphology (Gilbert, 1914; Mackin, 1948). However, contemporary investigators have found that in many cases, the streams may never truly achieve equilibrium (Graf, 1983; Pizzuto, 1986) but rather they perpetually adjust in response to short and long terms forcing. Streams may be adjusting to changes in flow or sediment regimes over the short (1's to 10's of years) or long (100's to 1,000's of years) term. They may also be adjusting from past flood events (i.e., Friedman and Jones, 2000) or human interventions such as channel straightening and armoring, constrictions and fill, and floodplain disconnection. Examples of short-term adjustment are channel widening then narrowing in response to a flood, channel widening and braiding from augmented mainstem sediment supply from a forest fire, and channel incision and widening in response to urbanization.

Examples of long-term adjustment include the net denudation of the Rocky Mountains and up-canyon knickpoint migration along the Front Range (Anderson et al., 2006), net erosion of glacial outwash alluvium in mountain piedmont settings (Church and Ryder, 1972), and channel and valley response to floodplain encroachment by alluvial or debris fans (Lancaster and Casebeer, 2007). Long-term adjustments typically occur over larger scales and influence channel and floodplain processes over tens to hundreds of miles (Montgomery and Buffington,1997). The context of the watershed and its history may illuminate these various adjustment scenarios. An objective assessment of the next phases of channel and landscape evolution, given potentially altered hydrologic characteristics due to development, transbasin diversions, wildfire, and climate change, may be influential on geomorphic processes in the coming decades. However, the hydro-geomorphic regime of the geologic past sets the stage for these processes to play out. Consultation with geologists can bring appropriate perspective to this question.

Geomorphic form and process are influenced by and occur within a framework of nested scales (Brierly and Fryirs, 2005). The following is a discussion of how the mediators of fluvial geomorphic hazards, such as geology, hydrology, land use, and landforms, play out at the landscape, valley, and reach scales. These scales should be delineated and classified to inform the geomorphic context of the study area.

Landscape Spatial Scale

A watershed of interest may be divided into "landscape units" broadly defined by their position within a watershed and the prevailing sediment transport processes of net erosion, transfer, or accumulation (Brierley and Fryirs, 2005; Figure 4). In mountains to plains settings, such as on the Colorado Front Range, landscape units might be grouped as steep headwater channels (sediment source or net erosional streams); canyon reaches (transport and erosional reaches); foothills reaches (transport / response reaches), and plains reaches (transport and depositional reaches). Within each landscape unit, prevailing sediment transport processes influences the types of channel response to floods. Source or erosional units will most likely respond to floods through channel incision, and hillslope failure. Transport dominated zones will respond with channel widening, some incision and hillslope failure, as well as lateral meander migration. Net transfer, or accumulation zones will exhibit some channel widening, but lateral migration and avulsion will likely dominate stream response.

Valley Spatial Scale

Valley setting is the next level of classification nested within each landscape unit. At this scale one considers the slope of the valley, the amount of room that exists between the stream channel(s) and the confining valley margins, as well as the proportion of valley length stream channels are in contact with valley margins (Fryirs et al., 2016). Confined valleys have walls that extend down to the stream banks or have only narrow floodplain benches. Partially-confined channels have valley walls set back from the channel and a continuous floodplain may exist. Unconfined channels have wide valleys, or no valley margins at all, allowing for ample meander room. Valley confinement ratios (valley floor width: average channel width) associated with confinement classifications are not firm and may vary depending on the stream system.

Valley margin steepness and erodibility may also be an important factor to consider particularly when the channel is coupled with that feature (Whiting and Bradley, 1993). Hillslope channel-coupling means that debris flows or hillslope failures can introduce coarse sediment into the channel. This excess material may cause a geomorphic response locally as a valley constriction and as punctuated sediment supply that can create local and downstream hazards.

Figure 4. Example of landscape units and dominant flood response within a watershed from mountain headwaters to plains. A) A confined reach in the canyons of the Colorado Front Range Foothills responds to a flood with incision and widening, though braiding and deposition can occur at smaller scales in floodplain pockets. B) A partially confined reach at the transition from canyons to plains responds with lateral migration and braiding. C) an unconfined reach in the plains responds with bank erosion and avulsion. Here the light blue line designates the main channel and the yellow dashed line the avulsion pathway. Adapted from Brierley and Fryirs (2005).

Reach Spatial Scale

Stream reaches are geomorphically homogeneous lengths of stream within landscape units and valley settings. Channel and floodplain geomorphology (e.g., stream width, depth, slope, and sinuosity) may vary from year to year over mean values but maintain a dynamic equilibrium over time given a stable flow regime and sediment supply (Leopold, 1994). For example, a meandering stream may gradually migrate down valley via erosion of the outer bank. Concomitant deposition on point bars maintains a stable width during this process. Outward meandering and an increase in sinuosity (reduction in channel slope) are balanced with meander cutoffs, which shorten the reach length, reduce sinuosity, and increase slope. A disturbance, such as a flood event, may temporarily alter this dynamic equilibrium, but channel form adjusts towards pre-disturbance conditions over time as dictated by the geomorphic context. The relaxation time, the time required to return to equilibrium conditions after a disturbance, may be longer or shorter than the average frequency of disturbances, dictating if and how long a system may achieve dynamic equilibrium (Wolman and Gearson, 1978).

Changes in sediment supply from a tributary or valley confinement or valley slope that may occur from reach to reach can influence geomorphic response to floods. Longitudinal variation in reach-scale properties, anthropogenic influences such as undersized crossings that act as sediment and debris traps, natural debris jams, and other factors can influence geomorphic responses to floods on the reach-scale basis. For example, reaches located at a trough or at the toe of a longitudinal profile of unit stream power at the peak of the 2013 flood exhibited wider widths of fluvial disturbance than other reaches studied along the Front Range (Sholtes et al., 2018). Troughs or toes in units stream power may occur at the valley to landscape scales along where milder slopes and/or wider valley bottoms occur downstream of steeper slopes and/or narrower valley bottoms. In these cases, upstream reach properties can influence downstream response at the reach scale.

Framework for Mapping Fluvial Geomorphic Hazards

The physiographic and geomorphic contexts can be synthesized to identify the type and magnitude of fluvial geomorphic hazards to characterize in a study area as is further explored in the fluvial hazard mapping protocol developed for the State of Colorado (CWCB, 2019). Under this protocol, the fluvial hazard zone is defined as the active river corridor (ARC) (i.e., the geomorphic floodplain) with an adjoining fluvial hazard buffer. The active river corridor is land adjacent to a stream that has been shaped by stream erosion and deposition under the prevailing flow and sediment regimes. The fluvial hazard buffer accounts for erosion prone land located beyond the ARC, such as hillslopes and terraces, that may be susceptible to failure as a result of toe erosion. Auxiliary FHZ units include the avulsion hazard zone, which identifies pathways a channel might occupy during a flood event outside of the ARC. Alluvial and debris fans within the stream corridor are also identified; however, hazards within a fan are not explicitly characterized.

The ARC represents the primary component of the FHZ. In steep to moderately sloped streams (3% to 0.1%) that are confined to partially confined and have developed (though potentially discontinuous) floodplains, the ARC is delineated by identifying topographic signatures of active fluvial geomorphic processes in the stream corridor using LiDAR-derived topographic data, aerial photographs, and geologic maps. This method follows in part what is outlined by the State of Washington (WA Department of Ecology, 2014). In meandering rivers and streams in broad, mild-sloped valleys that are unconfined (valley margins are beyond the meander belt), the ARC may be delineated as a buffer from a meander centerline closely following methods developed by the State of Vermont (VT ANR (2017). Finally, special considerations are taken when

delineating the ARC in urbanized areas where floodplain fill, channel straightening, and bank revetment all may affect a stream's response to floods and in headwater streams where fluvial signatures have not yet formed.

A study of hillslope erosion and mass wasting as a result of past flood events was conducted in support of the creation of this FHZ mapping protocol. Buffer widths, appended to the outside of ARCs, are typically factors of channel or floodplain width and are a decreasing function of the ratio of valley to channel width: more confinement (a smaller ratio) results in a wider buffer.

Case Study: East Plum Creek, Douglas County, Colorado

East Plum Creek (EPC), a tributary to the South Platte River, drains the north side of the Palmer Divide along the southern border of the Denver Metropolitan region along the Front Range of the Colorado Rocky Mountains. The study reach runs through the Town of Castle Rock, which has experienced rapid growth over the last 20 years, some of which has occurred adjacent to the stream corridor. Streams in this region are typically sand bedded and entrenched within valley margins composed of alluvial material as well as the weakly consolidated sandstone, claystone, and conglomerate of the Dawson formation (Figure 2, Thorson, 2004). Ongoing development on alluvial terraces adjacent to the stream corridor may be susceptible to fluvial hazards associated with hillslope failures due to channel migration and channel widening. As such, the Town of Castle Rock volunteered to participate in a pilot fluvial hazard mapping program with the Colorado Water Conservation Board.

Physio-Geographic and Geologic Setting

East Plum Creek, our case study stream, lies within the Colorado Piedmont subregion within the Great Plains physiographic region (Figure 1). The evolution of the Great Plains of Colorado begins during the Laramide orogeny when the uplifting Rocky Mountains resulted in downwarped structural basins east of the mountain front. As uplift continued though the Cretaceous and Eocene, packages of synorogenic clastic sediments accumulated in these basins. The end of the Laramide orogeny was followed by a period of low sedimentation during the Oligocene and early Miocene. During the late Eocene, the Rocky Mountains and Great Plains were again uplifted, possibly by the East Pacific Rise to the west. This resulted in a gentle, eastward-dipping surface on which sediments of the Miocene Ogallala Formation were deposited (High Plains). Later incision and transport of sediment by the South Platte and Arkansas rivers and their tributaries removed the Miocene and younger sediments resulting in an eroded region called the Colorado Piedmont (CWCB, 2019).

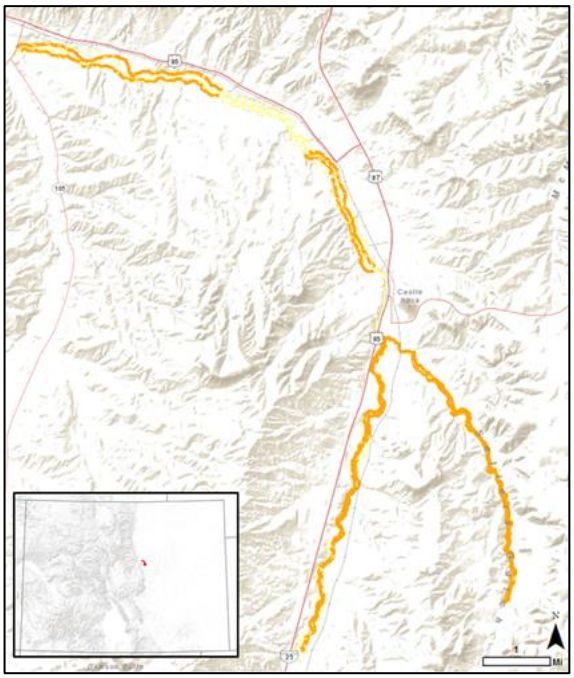

Figure 5. East Plum Creek and Sellers Gulch (eastern tributary) fluvial hazard zone mapping study area with location relative to the State of Colorado in inset map (red area).

The East Plum Creek watershed is bounded by the Palmer Divide (a caprock escarpment) to the south and drains to the north joining West Plum Creek then the South Platte river at Chatfield Reservoir. Interstate 25 runs along the length of its corridor to the west (Figure 5). The maximum basin elevation is 9370' above sea level and the mean basin elevation is 7045'. Annual precipitation is approximately 15 inches resulting in a semi-arid climate with sparse shrubby vegetation in the uplands and willow and cottonwood along the riparian corridor. The drainage area across the study area ranges from 85 mi^2 to 115 mi^2.

The valley bottom and margins along the study reaches are primarily composed of unconsolidated alluvial deposits (Morgan et al., 2004). This alluvial material contains sediment with size classes that include silt, sand, and gravel. Alluvium in the terraces that comprise the valley margins was generally deposited by streams flowing east from the Rockies during late-glacial and interglacial periods dating back to the early to middle Pleistocene epoch. Other alluvial deposits include more recent debris fan deposits with similar grain sizes as well as pediment gravel deposits, which contain coarser material in the gravel to cobble size range.

The study reaches have since incised within this alluvial material (Figure 6) likely as a combined result of large flood events, historic extirpation of beavers from the system, channel straightening and floodplain fill, and changes in the hydrology of the contributing watersheds (specifically as a result of urbanization). Sporadic outcrops of conglomerate and interbedded sandstone material are mapped along the river corridor but are discontinuous and were not observed to provide grade or valley margin control along the study reaches. Anthropogenic fill material has been introduced into the stream corridor to provide for development along its margins. It is assumed that this fill material has a similar erodibility as native material.

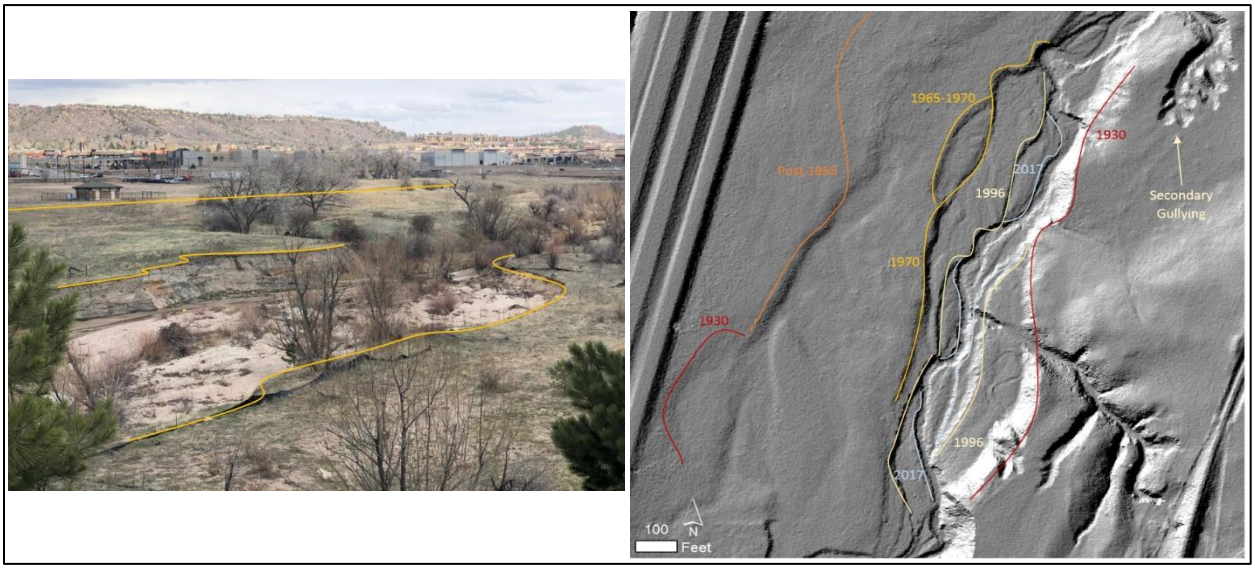

Figure 6. (Left) East Plum Creek with alluvial terrace edges highlighted. Terrace material, which forms valley margins, is highly erodible. (Right) Planview of hillshade image of East Plum Creek with approximate dates of when terrace margins formed (i.e., when river incised and abandoned these surfaces as floodplains) based on historic aerial imagery analysis. Channel has incised approximately 12 feet since 1930 in this area.

Hydrologic Context

Colorado's most intense large-scale rainfall events occur over the Great Plains Region, especially along the Colorado Piedmont (Doesken et al., 2003). Precipitation in the Colorado Piedmont averages 15 inches annually, most of which falls as snow in the early spring and rainfall during

the summer months. As such, natural vegetation is limited to grass, shrubs, and evergreen trees in upland areas with deciduous riparian vegetation such as cottonwood and willow in stream corridors (Hansen, 1978). Here small-scale, short duration to regional-scale, long duration extreme precipitation events occur in the late summer and early fall as moisture is forced to uplift along the Front Range (i.e., Gochis et al., 2014). This extreme rainfall along with the alluvial deposits that form much of the Colorado Piedmont, as well as the aeolian deposits further east, result in highly dynamic stream systems.

East Plum Creek is primarily intermittent, flowing seasonally with low-elevation snow melt and in response to summer and fall rainstorms. Portions are perennial where waste water treatment plant effluent outflows contribute. Monsoons and convective rainfalls occurring in the summer and fall are responsible for the most extreme floods in the region (Jarrett and Costa 1988, Pitlick 1994, Mahoney et al., 2015, and Figure 3, above). Regional-scale heavy rainfall over extended durations was responsible for the 1965 and 2013 floods along the Front Range and Eastern Plains, both of which resulted in catastrophic damage over large areas (i.e., multiple HUC-8 basins). Smaller-scale convective rainfall events that result in localized flood damages are more common. These floods typically influence one or more smaller basins (HUC-14) or a single larger basin (HUC-8). Runoff from rainfall events can augment the small to nonexistent baseflow to 1000's of ft^3/s. The 1% annual exceedance flood for East Plum Creek along the study reach is 16,650 ft^3/s (UDFCD 2016). The propensity for such large extremes in flood flows and history of extreme rain events in this region led to the construction of Chatfield Reservoir downstream of the study reach by the U.S. Army Corps of Engineers following the 1965 flood that impacted this watershed and others in the region.

Geomorphic Context

Both the East Plum Creek and Sellers Gulch are primarily comprised of sinuous sand and gravel bedded reaches of moderate slopes (0.5-2.5%). Some reaches are comprised of wide valleys with multi-threaded, willow-dominated, wetland-like zones where no dominant channel exists. Evidence of beaver activity has been observed in these reaches. Other reaches have sinuous and wandering channels entrenched within alluvial terraces ranging from 10 to 30 feet, increasing in height downstream. The reaches of the study area are partially to fully confined. Estimating an average width of the channel proves challenging as it is highly variable longitudinally and is also a strong function of time since the last major flood (i.e., Friedman and Jones, 2000). As discussed under the previous sections, a combination of high sediment supply, erodible valley margins, and flashy hydrology results in East Plum Creek being geomorphically dynamic, especially under floods.

The East Plum Creek watershed has experienced several extreme flood events over the last 100 years that have reconfigured the channel, floodplain, and valley resulting in a broad braided channel post flood. Aerial photo analysis, confirmed with gauge data, indicate that the 1965 flood was the most recent of these significant floodplain-altering events for the mainstem of East Plum Creek. Since then, vegetation in the active river corridor of the study area has largely re-established and the post-flood braided channels have narrowed back into a small single-thread channel. Due to the highly erodible nature of the valley margin, large flood events may result in hillslope retreat on the order of 10's to 100's of feet (Figure 7).

Analysis of historic aerial imagery coupled with contemporary digital elevation models indicates that East Plum Creek has been incising over at least the last century and perhaps longer (Figures 6 and 7). Beaver extirpation from the Front Range during the mid-1800s may have aided in channel incision (Goldfarb, 2018). Since 1930, the channel has incised up to 12 feet in some locations resulting in a series of alluvial terraces (Figure 6). The presence of erodible sands and

gravels of alluvial terrace margins along with the lack of the bedrock to provide natural grade control has resulted in a net export of sediment from these study reaches and a continual lowering of the channel bed and floodplain over time. Changes in land cover from historic ranching then urbanization in the watershed may have also exacerbated channel incision and sediment loads to the study area. However, the ranching itself may have contributed to this. Gullying can be observed throughout the study area along ephemeral side drainages (Figure 6).

Incisional processes in East Plum Creek compounds geomorphic hazards associated with valley margins, which are prone to mass-wasting as a result of direct fluvial scour and over-steepening. Urbanization along the center of the study area has led to moderate and heavily alteration to the stream corridor including increased constriction of the channel by floodplain fill. Therefore, in addition to lateral hillslope erosion during floods, chronic channel incision and floodplain fill may contribute to geomorphic hazards associated with the instability of valley margin terraces. The geomorphic trajectory of the East Plum Creek study area is likely continued channel incision along with episodic, valley-scale widening as a result of low-frequency, extreme flood events.

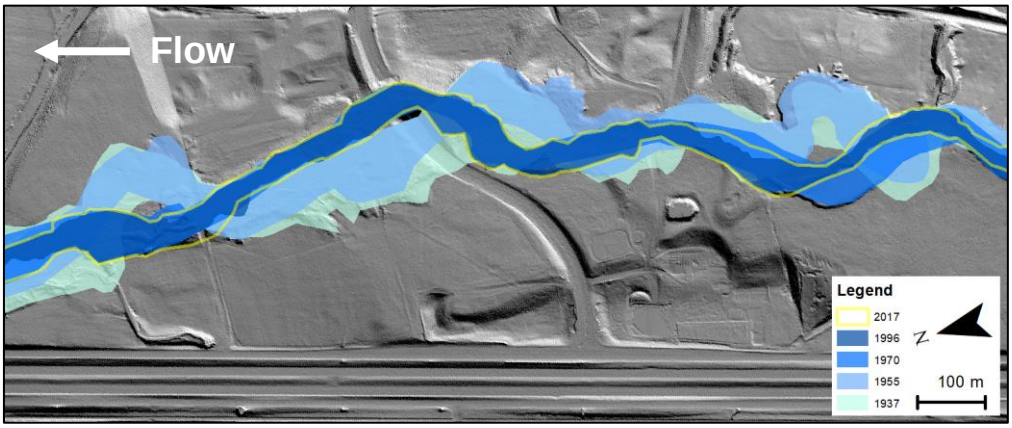

Figure 7. Illustration of valley-wide channel migration and valley margin erosion on East Plum Creek, north of the Town of Castle Rock. Shaded polygons demark the active river corridor (channel and geomorphic floodplain) for each year. Since this event (1970-1996), several moderate-sized flood events have occurred resulting in gradual (tens of feet) erosion of valley margins.

Mapping Fluvial Geomorphic Hazards on East Plum Creek

Mapping fluvial geomorphic hazards along East Plum Creek begins with defining the active geomorphic floodplain, also known as the active river corridor (CWCB, 2019). Based on historic evidence of valley-wide expansion of the creek during extreme flood events, the ARC was typically delineated from toe to toe of the valley margin. Given the multiple incisional events that have occurred over the past century and the numerous terrace margins bordering the active river corridor at different elevations, defining the valley margin proved to be a non-trivial task (Figure 7). Use of a LiDAR-derived relative elevation models coupled with hillshade imagery allowed for initial active river corridor delineation, later refined with field observations used to verify which terraces could be within the ARC.

A wide fluvial hazard buffer, extending from the edge of the ARC to some distance into the valley margins, was deemed necessary based on observations of dramatic lateral erosion into valley margins. Median values for the width of lateral erosion into valley margins as a result of the 1965 flood event averaged one half of the width of the ARC (100 ft) (CWCB, 2019). However, as noted above, East Plum Creek has incised over ten feet in the last century resulting in much higher terrace valley margins in many locations. A flood event of similar magnitude as the 1965 flood in

the contemporary stream corridor may not accomplish such wide margins of erosion given its greater degree of entrenchment. To delineate the FHB, a buffer of two ARC widths was made on either side of the valley centerline. The FHB was defined as the area of the buffer extending beyond the ARC. A minimum of one channel width from the ARC defines the FHB where the ARC intersects this meander centerline buffer (Figure 8). Site-scale geologic or geotechnical studies may be used to validate the width of this buffer and determine if some valley margins are more competent than assumed in this delineation.

The fluvial hazard zone, then is defined as the sum of the active river corridor and the fluvial hazard buffer. Fans identified within the stream corridor along with potential avulsion pathways are identified as auxiliary hazard units.

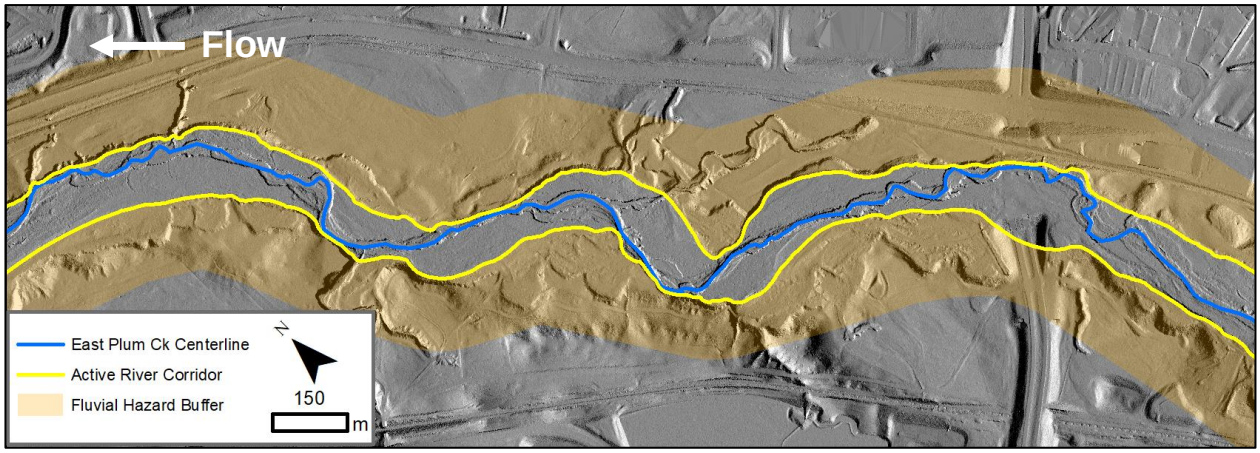

Figure 8. In a highly erosive system like East Plum Creek the fluvial hazard buffer is determined by delineating a buffer (orange polygon) of two ARC widths on either side of the valley centerline.

Summary and Conclusions

In this paper we have described the various components of the physiographic and geomorphic contexts that influence fluvial geomorphic hazards along stream corridors. This context is important in understanding the geomorphic trajectory of the stream corridor and its sensitivity to disturbances. This in turn informs how a fluvial hazard zone can be mapped to delineate existing fluvial geomorphic hazards. We provide a case study on East Plum Creek in the Colorado Front Range Piedmont region in which we define the physiographic and geomorphic contexts and apply them to a fluvial hazard zone delineation. We are grateful for the contributions of Matthew Morgan and Kevin McCoy of the Colorado Geologic Survey and for the support and funding of the Colorado Water Conservation Board.

References

Bonnin, G.M., Martin, D., Lin, B., Parzybok, T., Yekta,M., Riley, D. 2011. NOAA Atlas 14 Precipitation-Frequency Atlas of the United States. Volume 1 Version 5.0: Semiarid Southwest. U.S. Department of Commerce. National Oceanic and Atmospheric Administration, National Weather Service. Silver Spring, Maryland, 265p.

Church, M., 1995. Geomorphic response to river flow regulation: Case studies and time-scales. Regulated Rivers: Research & Management, 11(1), pp.3-22.

Colorado Water Conservation Board. 2019. “A Protocol for Mapping the Fluvial Hazard Zone”. DRAFT Report. Colorado Department of Water Resources. Denver, CO. 145p.

Colorado Geologic Survey. 2019. "Physiographic Provinces of Colorado," http://coloradogeologicalsurvey.org/colorado-geology/topography/physiographic/ , Accessed February 2, 2019.

Doesken, N.J., Pielke, Sr., R.A., Bliss, O.A.P. 2003. Climate of Colorado, Climatography of the United States No. 60. Prepared by Colorado Climate Center, Atmospheric Science Department, Colorado State University, Fort Collins, CO. 14p.

Fenneman, N.M., and D.W. Johnson. 1946. "Physical divisions of the United States," U.S. Geological Survey Map.

Federal Emergency Management Agency (FEMA). 2019. https://www.floodsmart.gov/. Accessed April 12, 2019.

Federal Emergency Management Agency. 1999. Riverine Erosion Hazard Areas Mapping Feasibility Study. Technical Serices Division, Hazards Branch. Washington DC. 171p.

Fryirs, K.A., Wheaton, J.M. and Brierley, G.J., 2016. An approach for measuring confinement and assessing the influence of valley setting on river forms and processes. Earth Surface Processes and Landforms, 41(5), pp.701-710.

Gilbert, G. K. 1914. The Transportation of Débris by Running Water. U.S. Gov't Printing Office.

Graf, W. L. 1983. Downstream Changes in Stream Power in the Henry Mountains, Utah. Annals of the Association of American Geographers, 73(3), 373–387.

Hansen, W.R., Chronic, J., Matelock, J. 1978. Climateography of the Front Range Urban Corridor and Vicinity, Colorado. U.S. Geological Survey Paper 1019. Washington D.C., 59p.

Jagt K., M. Blazewicz, J. Sholtes. 2015. Fluvial Hazard Delineation: A Framework for Mapping Channel Migration and Erosion Hazard Areas in Colorado. Colorado Water Conservation Board. Denver, Colorado. 65p.

Mackin, J. H. 1948. The concept of a graded river. Geological Society of Am. Bulletin, 59(5), 463.

Maricopa, County of 2013. Drainage Design Manual. Maricopa County Flood Control District. Phoenix, AZ. Chapter 11, Sedimentation.

Merwade, V., Olivera, F., Arabi, M. and Edleman, S., 2008. Uncertainty in flood inundation mapping: current issues and future directions. J. of Hydrologic Engr., 13(7), pp.608-620.

Montana Aquatic Resources Services. 2017. Channel migration easements in Montana: how conservation easements and rivers can work together. Bozeman, MT. 49p.

Natural Resources Conservation Service (NRCS). 2006. "Land Resource Regions and Major Land Resource Areas of the United States, the Caribbean, and the Pacific Basin," United States Department of Agriculture, Handbook 296. 682p.

Olson, P.L., Legg, N.T., Abbe, T.B., Reinhart, M. A. Reinhart, J. K. Radloff. 2014. A Methodology for Delineating Planning-level Channel Migration Zones. Washington State Dept. of Ecology. Olympia, WA. 83p.

Pierson, F.B., Robichaud, P.R. and Spaeth, K.E., 2001. Spatial and temporal effects of wildfire on the hydrology of a steep rangeland watershed. Hydrol. Processes, 15(15), pp.2905-2916.

Pizzuto, J. E. 1986. Flow variability and the bankfull depth of sand-bed streams of the American midwest. Earth Surface Processes and Landforms, 11(4), 441–450.

Rapp, C.F. and Abbe, T.B., 2003. A framework for delineating channel migration zones (No. Ecology Publication# 30-06-027).

U.S.G.S. 2018. National Geologic Map Database. https://ngmdb.usgs.gov Accessed 4-18-2018.

U.S.G.S. 2019. The StreamStats program for Colorado, online at http://water.usgs.gov/osw/streamstats/colorado.html, accessed on (April 20, 2019)

Vietz, G.J., Walsh, C.J. and Fletcher, T.D. 2016. Urban hydrogeomorphology and the urban stream syndrome: Treating the symptoms and causes of geomorphic change. Progress in Physical Geography, 40(3), pp.480-492.

VT ANR (2017). Department of Environmental Conservation Flood Hazard Area and River Corridor Protection Procedure. 40 p. Montpelier, VT. 40p. http://dec.vermont.gov/sites/dec/files/documents/DEC_FHARCP_Procedure.pdf

Whiting, P. J., & Bradley, J. B. 1993. A process-based classification system for headwater streams. Earth Surface Processes and Landforms, 18(7), 603–612.

The Mississippi River Geomorphology & Potamology Program: Improving Understanding of Rivers by Combining Data Collection, Modeling, and Geomorphic Analysis

James Lewis, Mississippi River Science and Technology Office Director, U.S. Army Corps of Engineers, Vicksburg, MS, James.W.Lewis@usace.army.mil
Ty Wamsley, Director of the Coastal and Hydraulics Laboratory, U.S. Army Corps of Engineers, Vicksburg, MS, Ty.V.Wamsley@usace.army.mil
Travis Dahl, Research Hydraulic Engineer, U.S. Army Corps of Engineers, Vicksburg, MS, Travis.A.Dahl@usace.army.mil
David Biedenharn, Research Hydraulic Engineer, U.S. Army Corps of Engineers, Vicksburg, MS, David.S.Biedenharn@erdc.dren.mil
Jack Killgore, Research Fisheries Biologist, U.S. Army Corps of Engineers, Vicksburg, MS, Jack.Killgore@usace.army.mil
Catherine Murphy, Research Fisheries Biologist, U.S. Army Corps of Engineers, Vicksburg, MS, Catherine.E.Murphy@usace.army.mil

Introduction

The primary purpose of the Mississippi River Geomorphology and Potamology (MRG&P) Program is to develop the understanding, tools, and techniques required for achieving the U.S. Army Corps of Engineers (USACE) mission of efficient management and operation of the Mississippi River to provide navigation and flood risk management in an environmentally responsible manner. The program will advance the Mississippi River Commission (MRC) 200-year working vision for the Mississippi River watershed through science investigation and technology development. The MRC recognizes that science and technology are critical to improving our understanding of the evolving geomorphology and potamology of the Mississippi River, accomplishing the USACE mission, and achieving their vision. The MRG&P Program strives to bring the best science to bear in answering today's questions as well as to develop the understanding and enabling capabilities that will allow USACE and MRC to advance, operate, and maintain the Mississippi River and Tributaries (MR&T) Project over the next 100 years. The MRG&P Program addresses the critical need of USACE to have access to the most up-to-date and technically competent scientific data and analysis for providing navigation and flood risk management in an environmentally responsible manner.

The MRG&P Program is a regional effort of USACE Mississippi Valley Division, with participation from the St. Louis, Memphis, Vicksburg, and New Orleans Districts, and conducted with technical contributions from the Engineer Research and Development Center. The program study area extends from the confluence of the Missouri River (specifically the sediment gage at Grafton, Illinois) to the Gulf of Mexico. The middle Mississippi River is defined as the area from the Upper Mississippi River's confluence with the Missouri River and extends 190 miles to its confluence with the Ohio River near Cairo, Illinois. From the confluence of the Ohio River to the Gulf of Mexico, the lower river is approximately 1000 miles. The lower Mississippi River valley is a relatively flat plain which has about 35,000 square miles of alluvial lands bordering the river. This valley begins just below Cape Girardeau and extends to the Gulf

of Mexico. The valley varies in width from 30 to 125 miles and includes parts of seven states; Missouri, Illinois, Tennessee, Kentucky, Arkansas, Mississippi, and Louisiana.

Following the 2011 flood, the Mississippi Valley Division and its Districts conducted a damage assessment which identified areas (levees, channels, structures, etc.) which were damaged and/or revealed weaknesses that need to be addressed before future floods occur. It also became apparent that the river channel itself changed and adjusted prior to and during the flood. At many locations, stages were different than historical discharges would suggest, and sediment transport and deposition occurred in patterns different than expected, leading to the need for updated river geomorphology. The 2011 flood again made it evident that on-going scientific studies are necessary to ensure that the USACE has access to the most up-to-date and technically competent scientific data and analysis, both during emergency operations and in the day-to-day decisions concerning the management and operation of the river for providing navigation and flood risk management in an environmentally responsible manner. The sporadic sampling programs of the past have left major data gaps and data collections errors undiscovered for decades, thus highlighting the need for a continuous science program. The MRG&P Program is required to support this need.

By integrating data collection, modeling, and analysis, the MRG&P program is improving the overall understanding of changing ecology, hydraulics, hydrology, channel geometry, and other issues related to rivers. MRG&P is a long-term program aimed at developing and maintaining our understanding of the river and continually developing the technology required to apply that knowledge for the practical management of the river. The Mississippi River is a complex, dynamic natural system that requires systematic study of the natural and engineered systems. As new science questions arise, study elements may be modified to respond to evolving needs.

Research Areas

Recent research projects are categorized in the following scientific areas, although several projects cross-over between multiple areas.

Data Collection

Work units in this area obtain important data, develop new measurement techniques, or improve the consistency or accuracy of existing data collection methods. Work units could also focus on identifying sources of errors and quantifying uncertainty in existing data collection practices. Recent project examples include bed-load, discharge, water surface slope, water quality, fish, macroinvertebrate, and sediment measurement data.

Serving Data and Tools

Work units in this area will make important data or tools available to others. This could include improving the service of existing data, developing a method for serving new data, creation of a new tool for analyzing the data, or adding capabilities to existing software. Activities seek to leverage advances in data integration that are rapidly developing in the information technology world as well as invest in modeling advancements and management of numerical models. The MRG&P Program seeks to facilitate compiling complete and accurate data, both measured and modeled, and streamline how it and other data is applied for project execution. Work units will advance numerical modeling capabilities specifically required for management and operation of

the MR&T. These activities will leverage and collaborate with work being conducted in USACE research and development programs as well as advancements being made by others, including other Federal agencies such as NOAA and academia. Numerical models developed and applied for the river all have a specific purpose and, depending on the problem to be solved, different models are the appropriate tool to be applied. Processes will also be supported to keep models active and up to date to the extent possible.

Geomorphology

The dominant morphological processes that shape the Mississippi River channel can operate over a very large range of spatial and temporal scales. There are many factors, both natural and man-induced, that can contribute to these processes. The effects of large flood events, changing sediment loads and characteristics, channel maintenance activities, dredging practices, diversions (natural and man-made), and relative sea level rise are just a few such factors. Accurate assessment of river morphology over these large scales requires evaluation of long-term trends in geometry adjustment, flow distribution, and sediment loading based on observed data. Morphologic changes have important implications related to flood risk management, navigation and maintaining a productive ecosystem. Work units include hydraulic, geomorphic, and sedimentation studies on the Mississippi River to determine trends and river processes for better long-term management of the Lower Mississippi River.

Ecohydrology

Ecohydrology is an interdisciplinary field studying the interactions between water and ecosystems. The MRC 200 year vision calls for a system that addresses the needs of environmental sustainability and allows for people to enjoy the fauna, flora, and forests surrounding the river while hunting, fishing, and recreating. Work units will collect data and evaluate system-wide relationships between hydro-geomorphic processes and biodiversity of fish and other aquatic organisms; identify environmental variables that can be used to predict biotic response of riverine and floodplain dependent species; and recommend conservation and restoration measures to mitigate adverse impacts of river regulation and protect important aquatic resources. MRG&P efforts will complement regular, ongoing District data collection and conservation efforts.

Endangered Species

Section 7(a)(1) of the Endangered Species Act requires federal agencies to use their authority as appropriate to carry out programs for the conservation of endangered and threatened species. Essential data collection and study on threatened species is required to implement conservation measures to maintain and improve habitat values within the Lower Mississippi River for recovery of species inhabiting the river channel. In addition, the non-jeopardy biological opinion (bi-op) negotiated with the US Fish and Wildlife Service in 2013 requires monitoring of the three species considered in the bi-op: pallid sturgeon, fat packet book mussel and the interior least tern. The secondary channels are very important to their survival, so monitoring them is also a priority. Work units include scientific system-wide field studies and monitoring to support the preparation of conservation plans. MRG&P efforts will complement regular, ongoing District data collection and conservation efforts.

Coastal Interaction

The interaction of riverine and coastal processes is complex with significant implications for navigation and risk of flood stages overtopping the Mississippi River levees. Antecedent river conditions have a tremendous effect on storm surge elevations in the river. Measurements have shown surges extend well beyond Baton Rouge. In addition, proposed diversions for sustaining coastal wetlands will influence the Mississippi River channel as well as the levees near the location where diversions are sited. Work units will investigate these interactions and develop tools to address Mississippi River issues influenced by coastal processes.

Watershed Change

Hydrologic processes can be sensitive to changes in land use, temperature (which can affect the form of precipitation), precipitation intensity and volume, the timing and volume of runoff, and conditions that cause or enhance drought. USACE policy and guidance requires consideration of climate change to reduce vulnerabilities and enhance the resilience of our water-resource infrastructure and ensure reliable services in changing conditions. Observed watershed change and variability have affected MR&T operations. Work units conduct scientific investigations and develop the tools required to adequately consider watershed change in the operation and maintenance of the MR&T system.

Communication of Data and Findings

The program effectively uses technology transfer mechanisms to share with the general public, academia and within the Corps of Engineers itself both the wealth of historical information on the middle and lower Mississippi River and the new information developed by the program. An MVD river science report, technical note, and fact sheet series has been established to highlight and summarize important research findings; these are made available in the national library system. Information and publications will also be available on the MVD Mississippi River Science and Technology website (https://www.mvd.usace.army.mil/mrgp.aspx).

The Relationship of Channel Planform and Point Bar Architecture on a Reach of the Wabash River near Grayville, Illinois

Taylor Rowley, Pathways Student Hydrologist, U.S. Geological Survey, Lower Mississippi-Gulf Water Science Center, Baton Rouge, LA, trowley@usgs.gov
Kory Konsoer, Assistant Professor, Louisiana State University, Baton Rouge, LA, kkonsoer@lsu.edu
Mick Ursic, Civil Engineer, Agricultural Research Service-U.S. Department of Agriculture, Oxford, MS, Mick.Ursic@ars.usda.gov
Eddy Langendoen, Research Hydraulic Engineer, Agricultural Research Service-U.S. Department of Agriculture, Oxford, MS, Eddy.Langendoen@ars.usda.gov

Introduction

The erosional and depositional characteristics of meandering rivers lead to the formation and maintenance of point bars along the inner banks of meander bends. Point bars are composed of sediment layers in patterns resulting from the rate and style of channel migration, hydrodynamics, and sediment transport and deposition within the river system (e.g. Jackson, 1976; Dietrich and Smith, 1984; Dietrich, 1987, Abad and Garcia, 2009). The distribution of the sediments preserved in the internal architecture of a river point bar provides a record of channel planform evolution. Geophysical methods are used to gain a large-scale visualization of the subsurface and aid in the interpretation of historic channel patterns (Best et al., 2003; Woodward et al., 2003; Sambrook Smith et al., 2006). Comparing known surficial extents of the point bar to features identified in the subsurface can also enhance the understanding of historic channel planform.

This study investigates two point bars along bends with different styles of migration, Maier and TB3, in a well-documented reach of the Wabash River near Grayville, IL. Evidence from historic aerial photography, modern lidar, photogrammetry, and geophysical surveys were used to determine the relationship between the point bar architecture and channel planform. Airborne lidar was flown in 2011 and is used to create the 2011 point bar surface. In 2017, a terrestrial lidar and Real Time Kinematic-Global Navigation Satellite System (RTK-GNSS) topographic survey were combined to create the surface for TB3. In 2018, a photogrammetric survey collected with a small unmanned aerial system (sUAS) was used to create a structure-from-motion (SfM) derived surface for Maier bend. The 2018 survey-based point bar surfaces were differenced from the 2011 point bar surfaces to get a Digital Elevation Model (DEM) of difference (DoD) to visualize areas of erosion and deposition. In addition, geophysical surveys using ground penetrating radar (GPR) were conducted in transverse and streamwise lines across the point bars in 2018. Elevation profiles from the 2011 point bar surfaces are extracted and overlain onto the 2018 GPR images to determine how the point bar is preserving the structure of sediments previously deposited. Results from this study provide an update to current models of point bar architecture.

Study Area

Maier bend and TB3 are point bars along the Wabash River near Grayville, Illinois that are located in a reach of consecutive bends that have been studied for several years (e.g. Jackson, 1976; Konsoer et al., 2016a, b) (Fig. 1). Bankfull widths and depths for this reach of the Wabash

range between 225-350 m and 5-8 m, respectively. In areas of rapid bank erosion, Maier and TB3 are migrating at rates of approximately 14 and 9 m yr^{-1}, respectively. Maier bend is extending, whereas TB3 is rotating and extending into the floodplain through outer bank erosion and point bar extension. The point bar on Maier is wrapped around much of the apex of the bend, and shows extension downstream of the apex, adjusting to the erosion of the outer bank. The bar associated with TB3 is skewed downstream of the apex and has a detached bar tail. Medium gravel dominates the upstream ends of the point bars and fine to medium sand dominates the downstream ends.

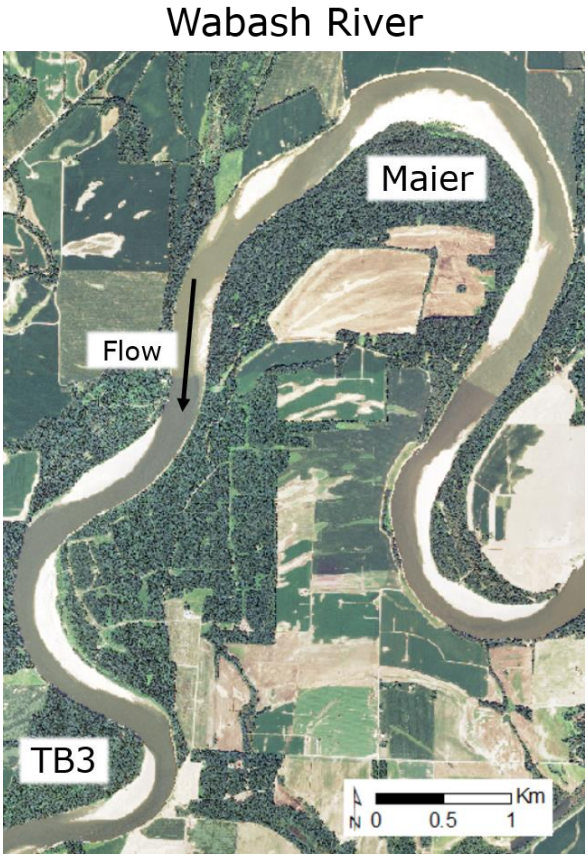

Figure 1. The 10 km study reach along the Wabash River. TB3 is approximately 8 km downstream of Maier.

Methods

Ground penetrating radar information was collected by pulling a PulseEkko Pro SmartCart GPR unit, with 100 MHz antennae, along predetermined transects perpendicular to the river centerline at approximately a 200 – 300 m spacing, and three longitudinal transects parallel to stream flow for the length of the bar (Fig. 1A and 2A). Each GPR line was surveyed with an RTK-GPS to properly align the topography and position. GPR data were collected in smaller grids along ten perpendicular and three longitudinal lines at an approximately 10-meter spacing at the upstream, apex, and downstream areas of the point bars. Focusing on the point bar head, apex, and tail, areas provide more detailed information on how planform change is reflected in point bar architecture.

GPR data from each transect were post-processed using Ekko Project. Dewow and bandpass filters along with deconvolution and migration were applied to each line to better visualize

reflectors for interpretation. Depth of penetration was calculated using an assumed velocity of 0.055 m ns^{-1} to get average depths of 2-3 m (Woodward et al., 2003; Robinson et al., 2013). Point bar surfaces were derived from airoborn lidar for the 2011 extent of Maier and TB3, terrestrial lidar and RTK-GNSS topographic surveys for the 2017 bar extent on TB3, and SfM for the 2018 extent of Maier. The surfaces show the planform evolution of the meander bends, whereas DoD maps were created to understand patterns of erosion and deposition.

Results

Evidence is seen in the DoD where upstream erosion, up to two meters, and downstream deposition, over three meters, has occurred between 2011 and 2017 (Fig. 2A). GPR penetration depths of 2-3 m are sufficient to capture the deposition on the downstream end. Along the downstream line (DS) for TB3, two major reflectors in the GPR data dip away from the water's edge, indicating movement in the opposite direction, corresponding to the hatched area in Figure 2A, and show evidence of progradation. TB3 has a rapidly extending bar tail created by large bar fronts moving across the bar top to extend the tail. The bar tail is detached and progradation has been away from the channel toward the floodplain.

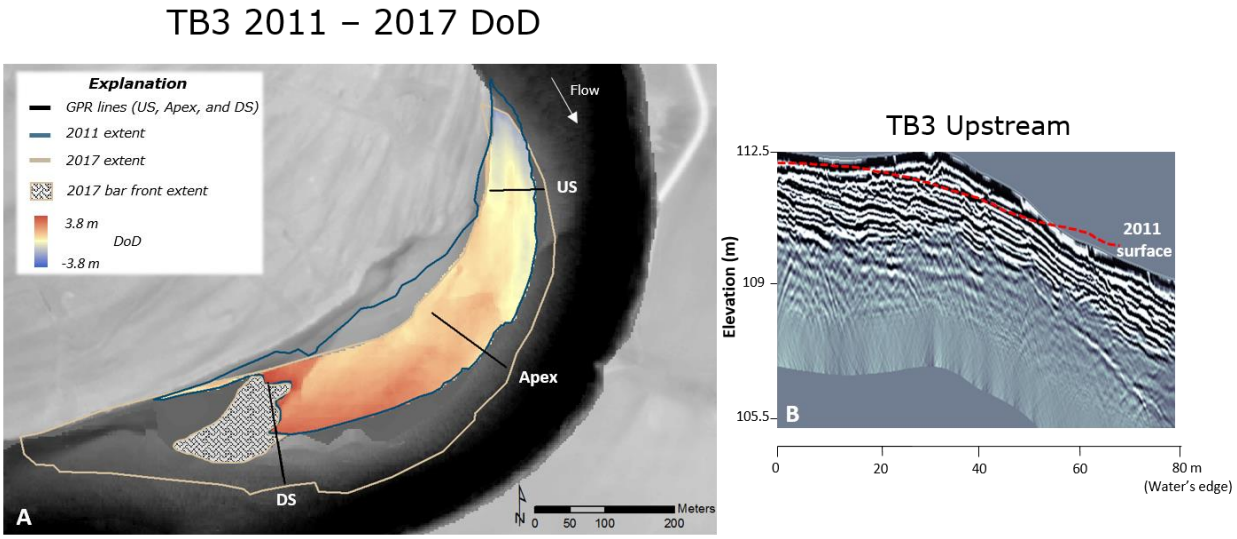

Figure 2. (A) TB3 DEM of Difference (DoD) between 2011 and 2017 using aerial Lidar for the 2011 bar extent and a combination of RTK-GNSS and terrestrial Lidar for the 2017 extent. Red indicates areas of deposition, while blue indicates erosion. (B) Upstream GPR line for TB3. [US, upstream; DS, downstream; m, meters].

The upstream GPR output reveals dipping reflectors on the bar top (0-40 m) inferred as lateral accretion surfaces that form as the bar progrades outward toward the thalweg. The lower part of the point bar (40-80 m) has continuous lateral and horizontal reflectors that represent reworked sediments as erosional surfaces as the bar head progresses downstream (Fig. 2B). To corroborate this, the 2011 aerial-lidar based surface elevation, in red, was overlain onto the 2017 GPR line to evaluate what has been preserved in the architecture. Reflectors that extend above the 2011 surface correspond to deposition interpreted from the DoD output. In contrast, the facies architecture on the lower part of the point bar has been modified by erosion where the bar surface in 2011 was higher than in 2017.

DoD results at Maier bend indicate that since 2011, up to 2.5 meters of sediment has deposited in the apex region, whereas the bar head and tail areas have experienced up to 1.5 meters of

erosion (Fig. 3A). GPR results at the apex show lateral accretion surfaces that directly relate to bar expansion and deposition in the apex region. The upstream GPR transect is composed of indiscriminate reflectors inferred as dune and ripple facies. The downstream GPR transect supports field observations that the downstream tail is somewhat locked in place because of an exposed bedrock bench along the outer bank. The bank cannot expand, thus the point bar should not expand. However, adjustment on the bar top is seen in the undulating reflectors indicating cycles of erosion and deposition, likely a result from the limited movement of the bar in the area (Fig. 3B). The 2011 elevation profile, in red, was overlain onto the downstream 2018 GPR line and sits above the 2018 surface, corroborating the erosion seen in the DoD.

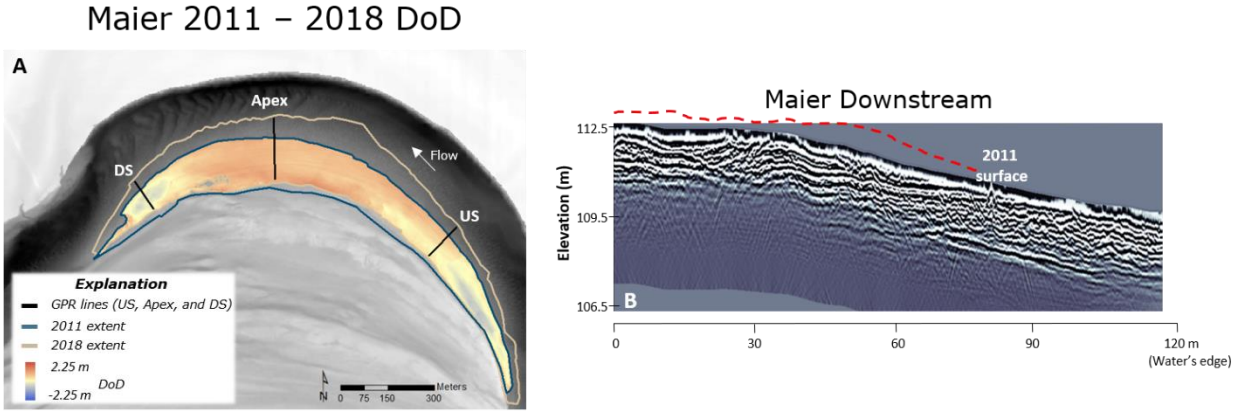

Figure 3. (A) Maier DEM of Difference (DoD) for 2011 to 2018 using aerial Lidar for the 2011 bar extent, and Structure-from-Motion for the 2018 extent. Red indicates areas of deposition, while blue indicates erosion. (B) Downstream (DS) GPR line for Maier.

Conclusion

Preliminary analyses confirm that the findings from GPR data collection and point bar elevation surfaces in 2017 at TB3 and 2018 at Maier bend can be compared with 2011 elevation surfaces generated from aerial lidar data. Moreover, the two datasets can be combined to offer a more complete interpretation of the point bar dynamics and resulting facies architecture. The rapid migration of both TB3 and Maier offer the chance to directly relate the point bar architecture to planform evolution over a short timescale. The combined use of DoDs and GPR data reveal a clearer picture of the different styles of point bar evolution at these two sites: TB3 is rotating in the downstream direction as it progrades out into the channel and shows large bar fronts moving across the bar with lateral accretion sets dipping in the direction of the front rather than the channel thalweg. In contrast, Maier bend is expanding more symmetrically, without rotating, and shows lateral accretion surfaces in the apex region, where the most rapid migration is occurring. Findings from this study help characterize and relate the style of planform evolution to point bar architecture.

References

Abad, J.D., Garcia, M.H., 2009. Experiments in a high-amplitude Kinoshita meandering channel: 2. Implications of bend orientation on bed morphodynamics. Water Resources Research 45, 1-14.

Best, J.L., Ashworth, P.J., Bristow, C.S., and Roden, J., 2003. Three-dimensional sedimentary

architecture of a large, mid-channel sand braid bar, Jamuna River, Bangladesh. Journal of Sedimentary Research 73, 516-530.

Dietrich, W.E., 1987. Mechanics of flow and sediment transport in river bends. 179-224.

Dietrich, W.E., Smith, J.D., 1984. Processes controlling the equilibrium bed morphology in river meanders. Am. Soc. Civ. Eng.: New York, NY, United States, United States, pp. 759- 769.

Jackson, R.G., 1976. Depositional model of point bars in the Lower Wabash River. Journal of Sedimentary Petrology 46, 579-594.

Konsoer, K.M., Rhoads, B.L., Best, J.L., Langendoen, E.J., Abad, J.D., Parsons, D.R., and Garcia, M.H. 2016a. Three-dimensional flow structure and bed morphology in a large elongate meander loops with different outer bank roughness characteristics. Water Resources Research 52(12), 9621-9641.

Konsoer, K.M., Rhoads, B.L., Langendoen, E.J., Best, J.L., Ursic, M.E., Abad, J.D., and Garcia, M.H. 2016b. Spatial variability in bank resistance to erosion on a large meandering, mixed bedrock-alluvial river. Geomorphology 252, 80-97.

Robinson, M., Bristow, C., McKinley, J., and Ruffell, A., 2013. Ground penetrating radar, British Society for Geomorphology, Geomorphological Techniques, part 1, section 5.5, pp. 1-26.

Sambrook Smith, G.H., Ashworth, P.J., Best, J.L., Woodward, J., and Simpson, C.J., 2006. The sedimentology and alluvial architecture of the sandy braided South Saskatchewan River, Canada. Sedimentology 53, 413-434.

Woodward, J., Ashworth, P.J., Best, J.L., Sambrook Smith, G.H., and Simpson, C.J., 2003. The use and application of GPR in sandy fluvial environments: methodological considerations. Geological Society Special Publications 211, 127-142.

The Role of Dynamic Ice-Breaup on Bank Erosion and Lateral Migration of the Middle Susitna River, Alaska

Renee Vandermause, **EIT,** Tetra Tech, Inc., renee.vandermause@tetratech.com
Mike D. Harvey, PhD, Tetra Tech, Inc., mike.harvey@tetratech.com

Abstract

Rivers in northern, boreal regions experience winter ice formation that influences several geomorphic processes including bank erosion and lateral channel migration. Not only are the ice-driven processes complex and highly variable in time and space, but they are difficult to observe due to the logistical challenges of conducting fieldwork when the rivers are frozen in the winter and during ice breakup in the spring. Characterizing and quantifying the processes that drive bank erosion, whether during the summer open-water period or when ice is in the channel, is important for predicting channel dynamics in boreal rivers where there is a mixed ice-fluvial regime that is sensitive to on-going climate change. Of particular importance is understanding the erosional processes that form or maintain complex channel and riparian systems which in turn provide diverse aquatic habitat for a range of salmonid species. This study utilized an extensive set of field data and observations, to quantify the extent to which channel change is driven by ice and fluvial processes on the Susitna River, a large gravel-cobble bed river in south-central Alaska. Surprisingly, given the apparent dynamic nature of the river, longer-term rates of bank erosion (evaluated over 61 years) along the Middle Susitna River determined by aerial photo analysis (1951 – 2012) are relatively low in comparison to bank erosion rates reported along gravel-bed rivers, in general.

Aerial photography and videography over two one-year periods, 2011 to 2012 (included a thermal ice-breakup) and 2012 to 2013 (included a dynamic ice-breakup), were used to identify short-term erosion rates for distinct geomorphic reaches (single channel and multi-channel), determine the amount of erosion by the type of geomorphic surface and quantify when most bank erosion occurred annually; whether during the open-water season or when ice was in the channel, particularly during ice-breakup. The aerial imagery was supplemented by field observations and data collected along the Middle Susitna River over two field seasons and output from a 2-D (SRH-2D) depth-averaged hydraulic model.

The majority of bank erosion (measured as conversion of vegetated floodplain to unvegetated channel), 54 to 61 percent in single channel and multi-channel subreaches, respectively, occurs or is initiated over a short period of time during dynamic breakup of the river's ice cover in the Spring. The erosion is attributable to the combined effects of relatively high-water discharge and the presence of ice floes and ice rubble. Lower elevation vegetated bars as well as higher elevation fluvial terrace margins were the most susceptible to bank erosion, notably by impacting ice floes. Mid-elevation, active, densely vegetated floodplain surfaces, with margins partly protected by cantilevered vegetated rootmats, were much less susceptible to erosion.

The relatively low long-term erosion rates for the Middle Susitna River may partly be explained by the low frequency of dynamic, ice-breakup events that initiate large-scale bank erosion. Additionally, the longer term impacts of ice processes that result in the formation of gravel-cobble pavements at bank toes that reduce the potential for toe scour, and the extensive presence of cantilevered vegetation root mats that protect the vulnerable sand and silt

layers that overlie the lower bank gravels from fluvial erosion, limit the potential for bank erosion and lateral channel migration during the open-water period of the year.

Introduction

Understanding the processes that drive geomorphic changes is important for predicting future channel changes, especially for rivers in boreal regions that are particularly sensitive to a warming climate. The amount of erosion that is driven by the presence of an ice-regime has been quantified for some boreal rivers such as the Colville River, Alaska (Walker, 1973; Walker and Hudson, 2002) and Mackenzie River, Northwest Territories, Canada (Outhet, 1974), both rivers inset within permafrost terrain, where the majority of erosion occurs during or shortly after the ice-breakup period. The importance of the ice-regime and erosion on other boreal rivers such as rivers on Banks Island, Canadian Arctic (Miles, 1976), seems to be of less importance, where the majority of the erosion occurs during the open-water runoff period due to summer rain storms. Permafrost and drainage size may be indicators of the importance of an ice-regime on bank erosion processes (Scott, 1978) yet the importance of the ice-regime remains unknown for many rivers in boreal regions. Reported observations of the effects of ice on bank erosion on northern rivers (Marusenko, 1956; Smith, 1980; Beltaos, 1995; Zabilanksy et al., 2002; Prowse and Culp, 2003) include increased erosion during the ice-breakup period from ice run gouging, abrasion (Ettema and Kempema, 2012), and ice-jam release waves (Beltaos, 2018).

This investigation of erosional processes was conducted as part of a proposed hydroelectric project (Alaska Power Authority [APA] 1984, Alaska Energy Authority [AEA] 2012) on the Susitna River, Alaska. The objective of the investigation, using a synthesis of current and historical data and short-term erosion analysis over two one-year periods with distinctly different ice breakup regimes and open-water flows, was to characterize the extent channel change and lateral migration are driven by ice and fluvial processes.

Study Area and Background

The Susitna River is a predominantly gravel- and cobble-bed river, subject to long, frigid winter weather conditions. As shown in Figure 1 the river originates in the Alaskan Range and has been sub-divided into four large-scale geomorphic segments referred to as, Above Maclaren, Upper River, Middle River and Lower River, as it flows approximately 580 km to Cook Inlet near Anchorage, Alaska (Tetra Tech, 2015a). The most downstream, southerly geomorphic segments, including the Lower and Middle Susitna Rivers, do not flow through permafrost terrain.

The geomorphic segment analyzed for this study of bank erosion is referred to as the Middle River and extends 135 km downstream from the proposed dam site (RK 301) to the Susitna River confluence with its next two major tributaries, the Chulitna and Talkeetna Rivers, referred to as the Three Rivers Confluence (RK 165). Through this segment, the river alternates between primarily confined single channel reaches and multi-channel reaches in valley floor expansions zones. The active channel is between 260 m and 300 m wide, while the valley bottom width ranges from 625 m to about 720 m. A railroad on the east side of the river provides some, though limited, lateral constraint through a portion of the reach. The surface bed material, sampled at the heads of mid-channel bars and islands, is composed of gravel and cobbles with a median grain size (D_{50}) of 60-65 mm. Sampling of the bed material beneath the ice cover along the thalweg of the channel during winter, , yielded somewhat higher D_{50} values of 65 mm to 94 mm (Tetra Tech, 2014a).

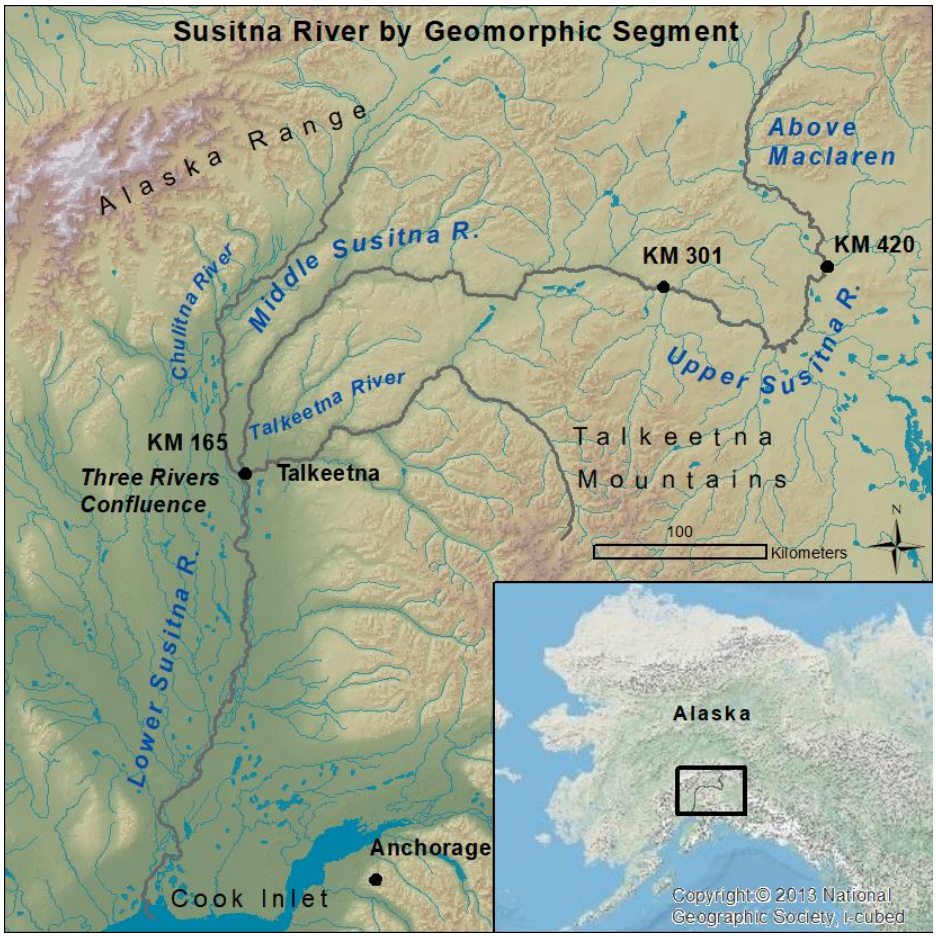

Figure 1. Geomorphic Segments along the Susitna River, Alaska (Vandermause, 2018).

Two reaches with different morphologies were selected for analysis within the Middle River. River kilometer (RK) 225.4 to RK 197.5 (Reach 6), and RK 197.5 to RK 173.6 (Reach 7). Reach 6 is a multiple channel reach with sediment storage in mid-channel bars, vegetated islands, and continuous floodplain segments. Reach 7 is a primarily single channel reach with limited sediment storage in mid-channel bars, vegetated islands, and non-continuous bank-attached floodplain segments. Wider valley bottom reaches with multiple channels and a suite of depositional lower-, mid-, and higher elevation surfaces are located upstream of valley floor constrictions. Multi-channel reaches are areas of higher ice activity which include larger sizes and numbers of ice-jams and ice runs, compared to single channel reaches (Beltaos, 1995).

The latest geomorphically-significant event in the Susitna River Basin was during the Little Ice Age, a Holocene-age glacial event that peaked in 1750 and begin to recede sometime between 1800 to 1850 (Luckman, 2000; Calkin et al., 2001; Reyes et al., 2006). Dendrochronology of present-day terrace surfaces along the Middle River is consistent with the timeline of glacial retreat. Terrace surfaces were defined as surfaces above the 100-yr open water elevation (Tetra Tech, 2015b). Channel degradation since glacial retreat has resulted in the development of terrace surfaces which occupy more than one-half of the non-channel valley bottom area. Meadows, open spruce-poplar forests and open spruce-paper birch woodlands are common vegetation types on terrace features. Less than one-half of the valley bottom area is composed of surfaces linked to the active hydrologic regime. The geomorphically-active river corridor is characterized by depositional surfaces categorized by elevation and top-of-bank vegetation

(Figure 2). As shown in Figure 2, there is a vertically-differentiated continuum that is dependent primarily on vertical accretion of the geomorphic surfaces over time (Leopold and Wolman, 1957). Vegetated bars at lower, more frequently inundated locations (overtopped between the 2-yr to 5-yr open water flows and comparable to the bank-full event) are colonized by willow-alder shrub vegetation which develop into poplar forests on low-to mid- elevation young floodplain surfaces (overtopped at approximately the 5-yr open water flow). With time and continued deposition, low elevation surfaces shift into mid-elevation mature floodplain surfaces (overtopped between the 20-yr to 50-yr open water flows) and slightly higher-elevation old floodplain surfaces (overtopped around the 50-yr open water flow) that are colonized by spruce-poplar forests and spruce-paper birch forests with increasing age.

Comparison of channel survey data since the 1980s along the active river corridor indicates no reach-wide degradation or aggradation trends (Tetra Tech, 2014e). Since the first period of aerial photography record, starting in 1951, the Middle Susitna River has experienced rather modest, reach-scale bank erosion and lateral migration. The channel has essentially maintained its planform, and only rarely have entire islands been completely eroded. Long-term rates of channel change over two 30-year periods (1951-1983 and 1983-2012), determined from aerial photography overlays (Tetra Tech, 2014b), are relatively low compared to the size of the river (approximately 5 percent of the total reach area or less). Long-term rates of lateral bank retreat are also low, averaging approximately 10 percent or less of the channel width over two 30-year periods. Long-term erosion rates compared to a compilation of channel migration rates for a number of similar sized gravel-bed rivers (Lagasse et al. 2004) indicate that bank erosion along the Middle Susitna is a factor of 10 less than for comparable channel systems (Vandermause, 2018). For contrast, vegetated islands on the unregulated, gravel-bed Fiume Tagliamento River (Italy), with a pluvio-nival snow regime, are typically eroded in 20 years or less (Gurnell et al., 2001).

The contributing drainage area of the Middle Susitna River at the closest gaging station (Gold Creek Station; USGS Gage No. 15292000) is approximately 16,000 km^2. The average annual flow of the Susitna River at Gold Creek is 277 m^3/s with high seasonal variability (Tetra Tech, 2013a). Flows decrease with receding temperatures through the late fall. Flows remain low through the ice-covered period when temperatures fluctuate between -4^0C and -12^0C, with an average monthly low in March of approximately 40 m^3/s. As temperatures rise and ice begins to melt within the basin, the ice breakup period typically occurs between late April and late May and consists of either thermal ice-breakups, dynamic ice-breakups, or a combination of the two (HDR Alaska, Inc. 2015). Peak flows correspond with the rise in temperature and melting of snow through the basin, with an average monthly flow of 745 m^3/s in June.

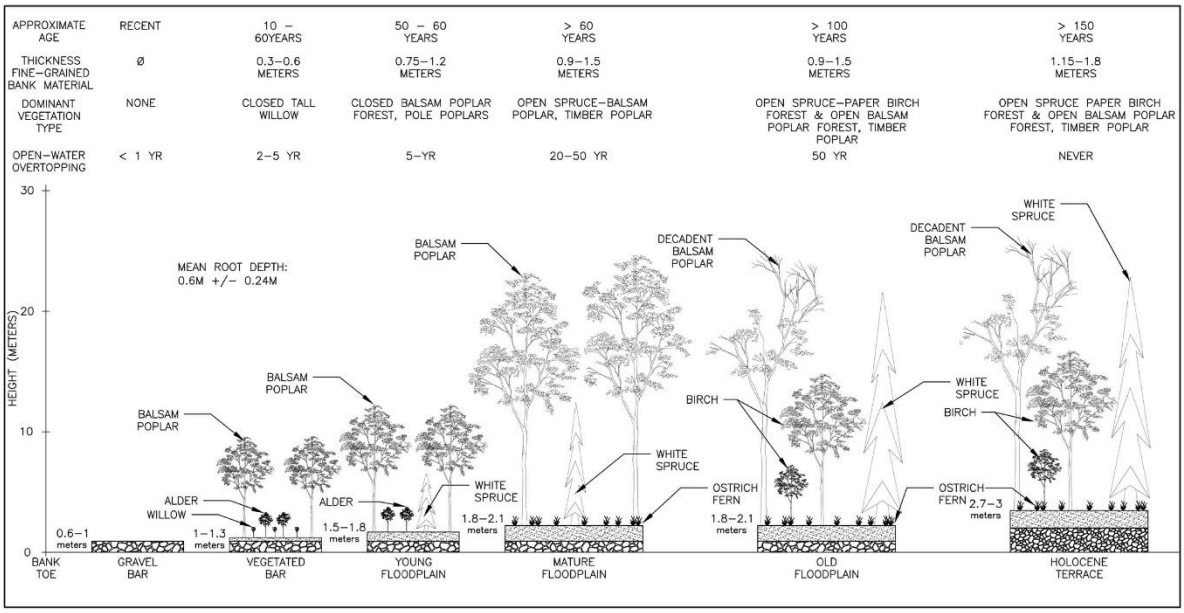

Figure 2. Geomorphic and vegetative succession of typical geomorphic surfaces in the Middle Susitna River (Vandermause, 2018).

Methods

Geomorphic mapping, field measurements, material sampling and observations were used to characterize geomorphic surfaces, bank height and morphology and stratigraphy (Figure 1) as well as the presence/absence of erosion and the primary modes of bank failure. Average open-water inundation frequency for each of the identified geomorphic surfaces was determined from a 2-D hydrodynamic model (SRH-2D) using the flow record from the USGS Gold Creek gage (No. 15292000).

Analysis of time-sequential aerial photographs and aerial videography was used to identify and measure short-term erosion, by geomorphic surface. The short-term erosion analysis was performed over two, one-year periods with distinctly different hydrologic regimes including varying open-water peak flow events and types of ice-breakup. The first period of analyses, shown in Figure 3, was between May 2011 through September 2012 and included two approximately 2-year flows, one flow between the 2-yr to 5-yr recurrence interval and a thermal ice-breakup. The second period of analysis, shown in Figure 4, was between September 2012 to September 2013 and included one 2-yr flow, one approximately 20-yr flow, one near 50-yr flow, and a dynamic ice-breakup.

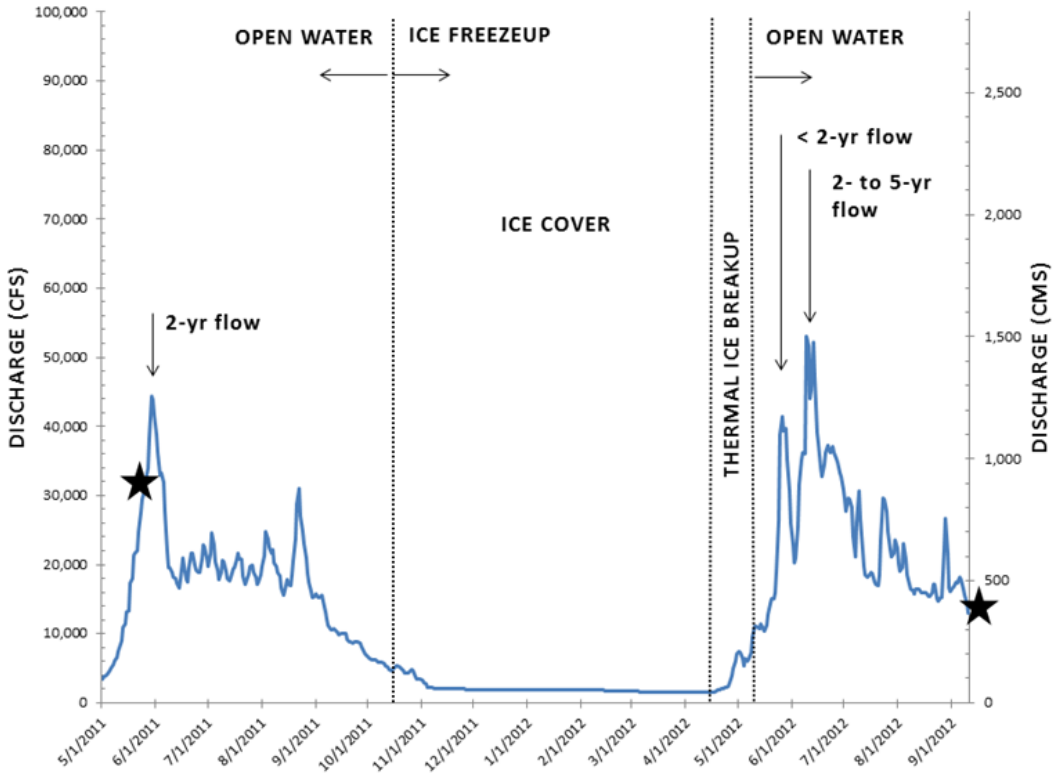

Figure 3. Mean daily discharge between 2011 and 2012 aerial imagery flights at Gold Creek gage. The black stars represent date of aerial photography flight.

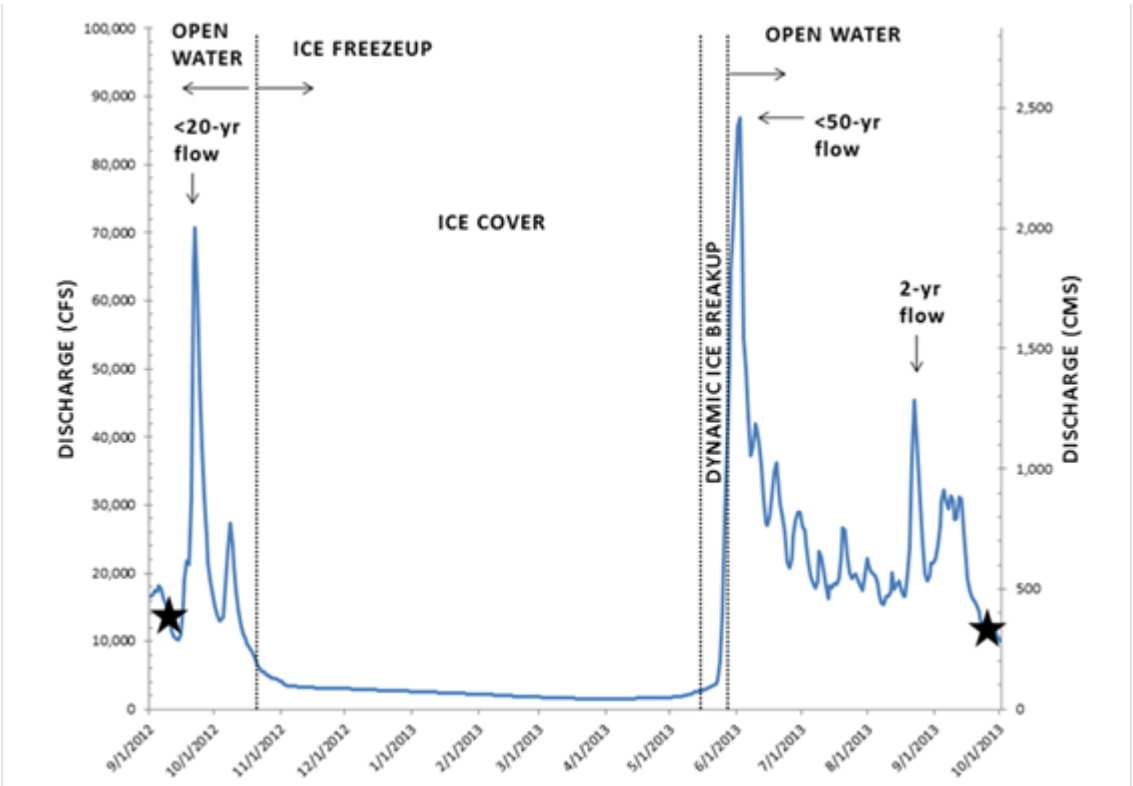

Figure 4. Mean daily discharge between 2012 and 2013 aerial imagery flights at Gold Creek gage. The black stars represent date of aerial photography flight.

Channel changes between the aerial photographs were categorized into approximate time period "bins" within the year: ice freeze-up, ice breakup, and the open-water period. Aerial reconnaissance videos flown periodically between the aerial photography flights, collected during ice-freeze up, ice-cover, ice-breakup, and post ice-breakup, were reviewed to attribute channel change to a specific time period within the year. Changes within the channel over each one-year period for both the geomorphic reaches (Reach 6, Reach 7) were categorized into two types of change: (1) Erosion: i.e., conversion from vegetated bar or floodplain to un-vegetated channel; and (2) Vegetation reset: the area of mature vegetation on a vegetated bar or floodplain that is converted to low-lying vegetation. Channel change was also linked to the identified geomorphic surfaces (Figure 2) in order to relate erosion to varying degrees of bank-resistance; where bank resistance is based on bank height, sediment composition and top-of-bank vegetation type.

Finally, short-term erosion rates and erosion by geomorphic surface over the two, one-year periods were compared to long-term erosion rates and erosion by geomorphic surface over two 30-year periods from 1951-1983 and 1983 to 2012.

Results and Discussion

Part 1 Bank Observations by Geomorphic Surface

The tops of all banks through Reaches 6 and 7 were vegetated with trees and shrubs, with the exception of very old floodplain surfaces or terraces where the tree vegetation succession has reached a point where trees are sparse and have been replaced by low-lying shrubs, grasses, and ostrich ferns. The absence of hydro-geomorphic conditions required for recolonization by the tree-dominated vegetation community precludes re-establishment of forest species.

The vegetated bars are composed of an approximately 1 m thick basal gravel unit overlain with about 30 cm of primarily sand. The bank toe is frequently paved or armored with gravels and cobbles, the bank profile is gradually sloping, and bank-top vegetation is composed of alders and willows. The vegetation is often disturbed by ice-push, but is resilient and able to regrow from an established root network.

The floodplain surfaces are composed of an approximately 1 m thick basal gravel unit overlain by about 80cm (young floodplain surface) to 1.2 m (mature floodplain surface) of interbedded sand and silt units that form a vertically-fining stratigraphic sequence that is typical of fluvial systems. The bank-top vegetation, composed primarily of dense poplars and spruces, develops extensive root mats that tend to provide effective cohesion to the low-cohesion sands and silts. The extensive root mats stabilize the upper bank (Simon and Collison 2002; Pollen and Simon, 2005) and buffer the abrasive effects of ice rubble moving along banks.

Erosion of the underlying, non-root reinforced sand and silts, causes the root mats to hang down over the bank faces forming what has been termed vegetation rip rap (Church and Miles, 1982) (Figure 5).

The extensive presence of overhanging vegetated rootmats along the Middle Susitna River indicates that these features persist for some time in stabilizing the bank, and thereby preventing significant lateral retreat during the open-water season. This reinforcing effect is, however, time-limited. In the short-term, protective rootmats can be removed by mechanical shearing of ice. However, the main time-limiting factor is the vegetation succession (Figure 2) where the trees reach the end of their life cycle and die off, that then leads to a lack of root reinforcement for the

upper bank. Accordingly, the bank profile for the old floodplain and terrace surfaces will again be partially or completely exposed, and therefore becomes more susceptible to the erosive effects of ice and water flow.

Almost all banks showed some sign of ice disturbance. Ice effects, as expected, were more common and often more damaging to the overbank vegetation on lower geomorphic surfaces including vegetated bars and young floodplains. These lower geomorphic surfaces were often characterized by large swaths of ice-bulldozed vegetation or leaning pole poplars. While the effects of ice were present on higher surfaces including mature floodplains, old floodplains, and terraces, the effects were less pervasive than on the lower geomorphic surfaces and included tree ice-scars, ice-deposited cobbles or gravels on top of the bank, or pockets of bent and leaning trees.

The cantilevered bank is one of the most common bank forms along the Middle Susitna River. Erosional processes that contribute to this feature can be caused by water flow, ice-processes, or a combination of the two. Bank retreat occurs when the stress on the river's banks from applied external forces exceeds the bank's resistive properties. The location, magnitude and duration of applied external force are functions of a suite of variables: regional and local climate, water level, water depths, velocity, shear stress, presence of in-channel ice, and strength of in-channel ice. The effect of each variable changes throughout the year, but can generally be categorized based on the primary hydrologic regime. A schematic of erosional processes observed to occur along the Susitna River during each of the primary hydrologic regimes and associated values for discharge, velocity, bank condition, and ice-breakup type is presented in Figure 6. Ice-breakup type (i.e. thermal versus dynamic) is used as a proxy term indicating the strength condition of river ice.

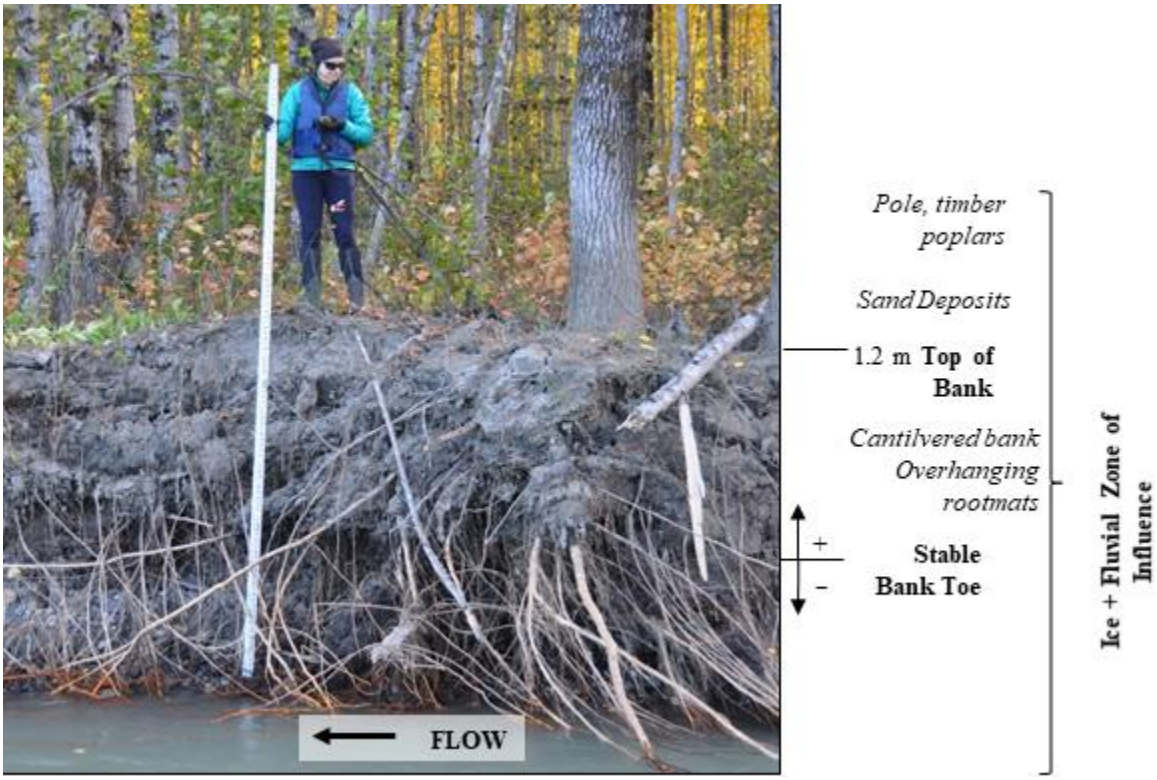

Figure 5. Photograph and schematic of cantilevered bank on active floodplain surfaces.

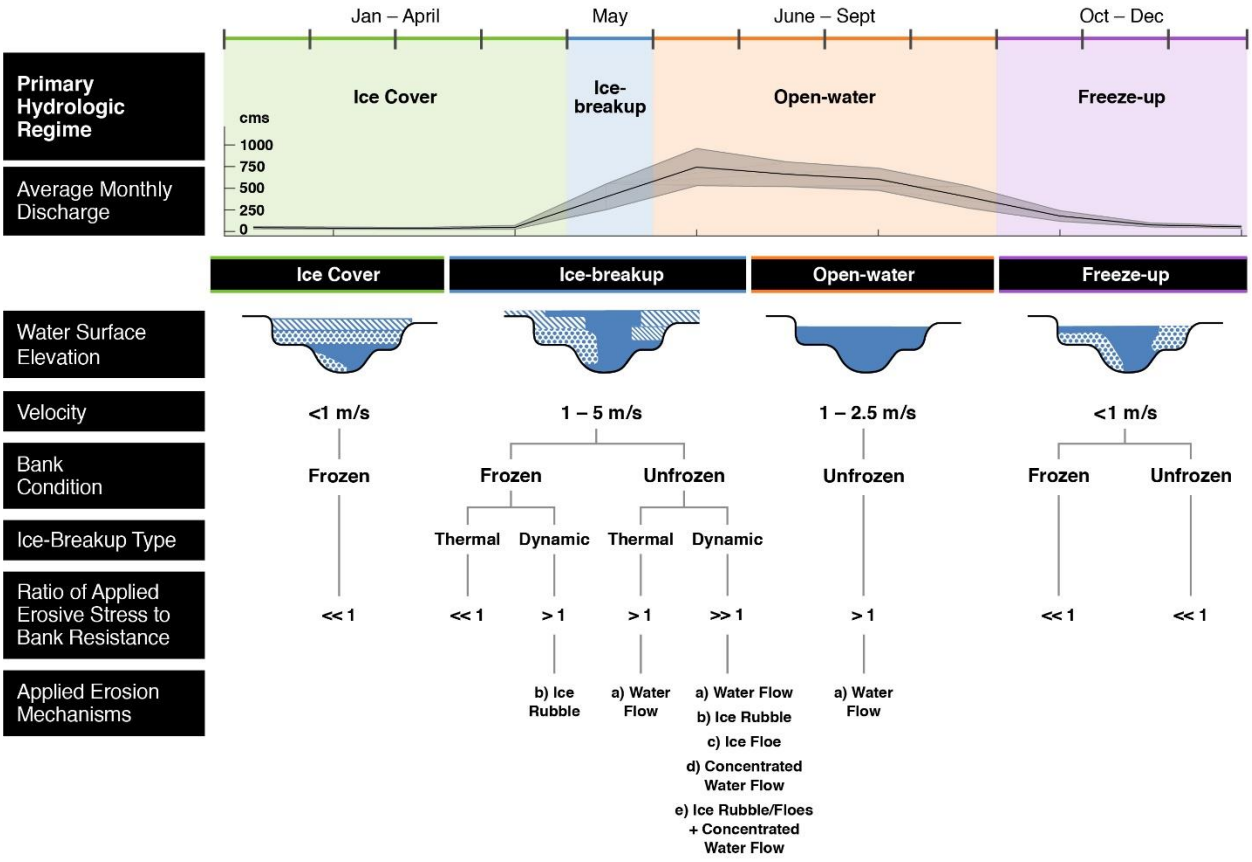

Figure 6. Schematic of hydrologic, hydraulic, bank conditions, and applied erosion mechanisms throughout the year (Vandermause, 2018)

Incipient motion calculations derived from the 2-D model results, indicate that fluvial shear stresses (even at the 100-yr recurrence interval) are unable to mobilize the bank toe sediments at many locations along the Middle Susitna River that have historically eroded (Tetra Tech, 2015c). Therefore, fluvial erosion can only occur when the shear stresses are sufficiently high to erode the sands and silts that are located above the basal gravel toe. This leads to cantilever failure of the upper bank materials (Thorne and Tovey, 1981; Church and Miles 1982; Collins, 1990).

The manner whereby river ice forms and moves along the river creates additional processes that may cause bank erosion. As erosional processes involving ice act in conjunction with water flow, making it difficult to differentiate effects due solely to ice or water flow, the combined effects are referred to as the "ice-driven regime." As summarized in Vandermause (2018), when ice blocks accumulate or are shoved along a bank, and are directly in contact with a bank, several factors may cause large-scale bank erosion along a root-reinforced cantilevered bank. From a synthesis of historical ice observations (during the 1980s), current ice observations (2012-2015), review of reconnaissance videos during the 2013 dynamic ice-breakup, results of 2D hydrodynamic modeling, and results from a numerical analysis of possible impact stresses exerted by ice, four ice-driven erosion processes were identified along the Middle Susitna River.

Erosion Process 1: Ice rubble (i.e., small ice blocks typically 10m or less wide and approximately 1m thick) abrasion and gouging. Ice rubble is conveyed downstream, largely parallel to banks, and shearing along bank faces. As most banks are protected with an upper layer of rootmats, this process was observed to scar, break, or remove some rootmats completely. Rubble impact

appears to be more severe for banks at the head (i.e. upstream end) of the island or bar where ice rubble is conveyed directly into the bank. Removal of vegetation rootmats, exposes the unconsolidated fine-grained material above the gravel core to further entrainment by fluvial erosion. Overall this process was found to locally scar vegetation but results in limited lateral bank retreat.

Erosion Process 2: Ice floe (i.e., large blocks of ice ranging from greater than 10m to over 100m in width and approximately 1m thick) allision with banks and ride up onto low islands. Ice floes are capable of greater impact stresses than ice rubble, and were observed to bulldoze and completely removing top-of bank vegetation, in particular on low-elevation vegetated bars. While this process was found to significantly modify vegetation succession regimes (i.e. reset the vegetation succession), it had a more limited effect on bankline migration.

Erosion Process 3: Increased bed shear stresses due to flow constrictions or diversions from in-channel ice. While 1-D modeling of flow under an ice-cover on the Susitna River identified increased velocities (HDR Alaska, Inc., 2014b), shear stress values still did not exceed values required for bank toe mobilization. Observations during the 2013 ice-breakup revealed large main channel jams diverting all upstream flow into secondary channels, causing the banks to overtop and overbank flow on geomorphic surfaces that are not inundated during the same discharge under open-water conditions. While this process may cause entrainment of the surficial non-consolidated fine-grain material above the basal core, fluvial modeling of the diversion of water flow into secondary channels at a range of flows common during the ice-breakup period, did not produce shear stresses capable of exceeding critical shear at the bank toe (Vandermause, 2018). It is possible that flow surges from ice-jam breaks may cause sufficient bed shear stresses to mobilize the bed and bank (HDR Alaska, 2014d). Observations and modeling on other boreal rivers indicate surges released from ice-jam breaks have reached velocities not observed in open-water conditions (Beltaos and Burrell, 2005; Beltaos et al., 2018; Beltaos, 2018).

Erosion Process 4: Process 4 is a combination of ice rubble (Process 1), ice floes (Processes 2), and increased or diverted water flow (Process 3). While fluvial bed-shear stresses at unconstricted and constricted/diverted flows do not exceed critical shear values for bank toe mobilization, increased fluvial stresses coupled with ice-induced shear stresses are likely to cause bank erosion and consequent lateral retreat, as was observed during the 2013 ice-breakup.

Part 2 Erosion Analysis

Between 2011 and 2012 (thermal ice-breakup year) only 4 locations had identifiable lateral retreat. The locations of bank retreat were along the sides of mid-channel islands or bank-attached floodplain units and the distances did not exceed 10 m. Between 2012 and 2013 (dynamic ice-break up year), 63 locations had identifiable lateral retreat. The locations of bank retreat were along the sides of mid-channel islands, and bank-attached floodplain or terrace units and ranged from 10m to nearly 100m in distance (Table 1).

Overall, a majority of erosion in the two geomorphic reaches (61 percent of erosion in Reach 6 and 53 percent of erosion in Reach 7), and all vegetation scour, occurred predominantly during ice breakup or during both ice breakup and the open-water regime immediately after ice breakup. In Reach 6, only 3 percent of the eroded area (corresponding to one location) could be attributed solely to fluvial processes (i.e., occurring pre-freeze up during the open-water season). Given the hydrologic record during the fall of 2012 prior to freeze-up, it is likely that this bank eroded during the nearly 20-year flow event in late September. In Reach 7, no areas of erosion could be attributed solely to fluvial processes.

For both reaches, erosion during 2012-2013 was nearly 4 to 8 times the historical erosion rates, while erosion during 2011-2012 was minimal. Total erosion during 2012-2013 ranged from 10 to 30 percent of the total amount of historical erosion from 1951-2012. Between 2011-2012 erosion rates and total erosion were small fractions of historic rates of erosion. These rates indicate that large-scale erosion is episodic.

Table 2 summarizes the timing and likely erosion regime (i.e., fluvial or ice-related) for erosion occurring between 2012 and 2013. In Reach 6, about 40 percent of the erosion occurred in the ice-breakup window (May 25, 2013 – May 29, 2013). Another 20 percent, categorized as "Ice-breakup through fall", occurred sometime between the onset of ice-break up (May 25, 2013) and when the next imagery set was flown (September 2013). These locations were categorized within this larger time frame because the reconnaissance videos and photographs did not provide sufficient evidence that the location eroded during a specific event (i.e., only during breakup). Some of the videos taken during ice breakup viewed the locations via oblique angles of observation, thus hampering definitive categorization of erosion during ice breakup. Additionally, erosion at these locations was likely exacerbated by the subsequent high-flow event (nearly 50-year event) following breakup. However, review of the videos and photographs indicated that, for many of the locations that eroded during the ice-breakup to fall period, erosion was likely initiated during ice-breakup. This conclusion was determined based on the aerial flight images and on-the-ground photographs where trees were significantly ice-scarred and leaning over and lateral bank retreat was significant, ranging from 10 to 30 m. It is likely that open-water erosional processes also contributed to the prevalence of cantilevered banks along the Middle River; however, it is unlikely that open-water erosional processes contribute to large-scale bank retreat. This conjecture is based on an analysis of bank retreat at surveyed cross-sections. From a comparison of 60 cross-sections surveyed in 2012 and 2013 with 2014 LiDAR-based topography, only one location had identifiable, substantial erosion. During this time period, all cross-sections were subjected to a 2-year peak flow where the water-surface elevation was above the basal gravel core and adjacent to the non-cohesive sand and silt bank sediments and 60 percent of the cross-sections were subjected to a nearly 50-year peak flow that inundated the entire bank face.

Table 1. Total area of valley bottom-land, total eroded area, and erosion rates for Reaches 6 and 7 over four time periods.

Time Period	Valley Bottom Land Area (m^2)	Total Eroded Area (m^2)	Eroded Percent of Total Valley Bottom Land Area	Erosion (m^2/km)	Erosion Rate (m^2/km/yr)	Erosion (m/y)	Eroded percent of 1951-1983 Erosion	Eroded percent of 1983-2012 Erosion
Reach 6								
1951-1983	13,306,400	1,192,800	9.0%	42,800	1,300	1.3		
1983-2012	13,844,000	538,700	3.9%	19,300	700	0.7		
2011-2012	14,694,600	6,500	0.04%	200	200	0.2	0.5%	1.2%
2012-2013	14,694,600	158,100	1.1%	5,700	5,700	5.7	13.3%	29.3%
Reach 7								
1951-1983	9,471,200	318,200	3.4%	13,300	400	0.4		
1983-2012	9,418,000	151,100	1.6%	6,300	200	0.2		
2011-2012	9,978,800	0	0.0%	0	0	0.0	0.0%	0.0%
2012-2013	9,978,800	33,900	0.3%	1,400	1,400	1.4	10.7%	22.4%

Note:
1. All values are rounded to the nearest hundred
2. Valley Bottom Land Area is determined from the land area from 1951 for 1951-1983, from 1983 for 1983-2012, and from 2012 for both 2011-2012 and 2012-2013
3. Data sources for valley bottom land area and historical erosion rates can be found within Tetra Tech (2014c)

Table 2. Total Erosion from 2012-2013 (dynamic ice breakup year) categorized by time period of erosion.

Time, Regime (Duration of Period)	Reach 6	Reach 7
	Percent of Total Erosion from 2012-2013	
Fall through Pre-freeze-up, (~30 days)	3%	0%
Ice Breakup, Ice/Fluvial, (~5 days)	41%	7%
Ice Breakup Through Fall, Ice/Fluvial (~150 days)	20%	46%
Unclear	36%	46%

The magnitude of erosion by geomorphic surface is summarized in Table 3. Generally, there are similar trends in the magnitude of erosion for the three categories of geomorphic surfaces over the various time periods for each geomorphic reach. In Reach 6, excluding erosion that occurred between 2011 to 2012, the erosion of terrace surfaces (i.e., high banks with minimal upper bank root-reinforcement) was 40 to 50 percent of the total erosion during each time period. In Reach 7, 40 to 50 percent of the historical erosion also occurred on terrace surfaces. Between the time periods that vegetated bar surfaces were linked to erosion data (i.e., 1983-2012 and 2012-2013), erosion of vegetated bars composed nearly 25 percent of the total erosion while the active floodplain surfaces composed 25 to 33 percent of total erosion. The anomaly to this trend was in Reach 7; between 2012 to 2013, only 4 percent of the total eroded area occurred on terrace surfaces and 76 percent occurred on vegetated bars. Notably, for both reaches, excluding the period 2011 to 2012, approximately 75 percent of the total erosion was either on higher geomorphic surfaces or on vegetated bars, while approximately 25 percent of total erosion was on active floodplain surfaces. These findings indicate that most erosion occur on surfaces with less relative root reinforcement than the more active floodplains surfaces; for the terrace surfaces, root reinforcement, if present, is higher on the bank and less able to form “vegetation rip-rap” while vegetated bars are typically low enough in the channel to be overridden by ice, thereby negating protective qualities provided by root reinforcement.

The overall magnitude of bank erosion and erosion as percentage of valley bottom area by reach, was greater in the multi-channel reach (Reach 6) compared to the single channel reach (Reach 7). This is likely the result of more geomorphic surfaces susceptible to erosion including low-elevation vegetated bars and older, high-elevation old floodplains that are less protected by root-reinforced upper banks. Additionally, it is a result of the higher ice activity in multi-channel reaches upstream of constrictions that are more prone to ice-jam formation and consequently ice-induced diversion of flow and ice rubble, and ice jam breaks.

Table 3. Percent short-term and long-term erosion that eroded from terrace surfaces, active floodplain surfaces, and low-lying vegetation.

Time Period	Total Eroded Area (m^2)	Percent Erosion of Terrace Surfaces[1]	Percent Erosion of Active Floodplain Surfaces[2]	Percent Erosion of Low-lying vegetation[3]
		Reach 6		
1951-1983	1,192,200	45%	55%	n/a
1983-2012	538,400	53%	26%	22%
2011-2012	6,500	31%	69%	0%
2012-2013	158,000	39%	35%	25%
		Reach 7		
1951-1983	318,000	41%	59%	n/a
1983-2012	151,000	53%	20%	27%
2011-2012	0	0%	0%	0%
2012-2013	33,900	4%	20%	76%

Note:
1 Terrace surfaces were defined as land units within the valley bottom that were 1.5m higher than the 100-year water-surface elevation (Tetra Tech, 2015b).
2 Active floodplain surfaces were defined as land units within the valley bottom that were vegetated with mature tree-stands. For the 2011-2012 and 2012-2013 periods this was determined during the sequential aerial photography analysis. This constituted all of the area that was not terrace surfaces between 1951-1983 as there was no reliable method to determine what were mature tree stands or low-lying vegetation. For the 1983-2012 period this was determined by subtracting the total area of low-lying vegetation from the total area that eroded that was not a terrace surface.
3 For the periods 2011-2012 and 2012-2013, low-lying vegetation was determined during the sequential aerial photography analysis. For the period 1983-2012, low lying vegetation that eroded was determined as the amount of vegetation that established between 1951-1983 and subsequently eroded during 1983-2012.

Conclusions

Short-term erosion over a one-year period with a dynamic ice-breakup comprised 10 to 30 percent of long-term erosion (over two 30-year periods). Minimal lateral bank retreat occurred during a one-year period with a thermal ice-breakup. While both one-year periods of short-term erosion analysis experienced several flows above the 2-year recurrence interval and flows near the 20-year and 50-year recurrence interval, 2D depth-averaged fluvial modeling indicated shear stress at the bank toe often does not exceed the shear stress required for sediment mobilization even at the 100-year recurrence interval. Thus, a major driver for fluvial erosion is generally absent, most likely the result of long-term ice armoring and compaction of the bed material. A majority of erosion from 2012 to 2013 (53% to 61% for Reaches 7 and 6, respectively) was attributed to the ice-breakup regime. High short-term erosion rates during a dynamic ice-breakup year, minimal erosion during a thermal ice-breakup year, insufficient fluvial shear stresses even at high flows, and observation of erosion during the ice-breakup regime indicates that erosion, when it occurs, is episodic and driven by dynamic ice-breakups.

Low rates of channel change have been observed on other boreal rivers (Brice, 1971; Lewis and McDonald, 1973; Scott, 1978). Scott (1978) suggests that overall low long-term rates of erosion

may be due to the timing of erosion where most erosion occurs in small increments during the annual spring breakup flooding. In contrast, this investigation of erosion on the Middle Susitna River indicates that the majority of erosion is episodic (at least 53 to 61 percent in both reaches), and occurs infrequently, the result of dynamic ice-break up. This finding has important implications for the maintenance of geomorphic complexity as a changing climate may affect the intensity and frequency of dynamic break up events.

References

Alaska Energy Authority (AEA), 2012. Revised Study Plan. Susitna-Watana Hydroelectric Project, FERC Project No. 14241 Submittal: December 14, 2012.

Alaska Power Authority, (APA) 1984. Draft Environmental Impact Statement. Susitna Hydroelectric Project, FERC Project No. 7114 – Alaska. Volume 1 – Volume 7. May 1984. ARLIS document number "APA 1653" at http://www.arlis.org/susitnadocfinder/.

Beltaos, S., 1995. *River ice jams*, Water Resources Publications, Highlands Ranch, Co., U.S.A.

Beltaos, S., 2018. Erosion potential of dynamic ice breakup in Lower Athabasca River. Part II: Field data analysis and interpretation. *Cold Regions Science and T echnology*, 148, pp.77–87.

Calkin, P.E., Wiles, G.C., Barclay, D.J., 2001. Holocene coastal glaciation of Alaska. *Quaternary Science Reviews*, 20(1), pp.449-461.

Church, M., Miles, M.J., 1982. Discussion on Processes and mechanisms of bank erosion. In: Hey, R.D, Bathurst, J.C., Thorne, C.R. (Eds), *Gravel-bed Rivers: fluvial processes, engineering, and management,* John Wiley & Sons.

Gurnell A.M., Petts, G.E., Hannah, D.M., Smith, B.P.G., Edwards, P.J., Kollmann, J., Ward, J.V. and Tockner, K., 2001. Riparian vegetation and island formation along the gravel-bed Fiume Tagliamento, Italy. Earth Surface Processes and Landforms, 26, 31-62.

HDR Alaska, Inc., 2015. 2014-2015 Study Implementation Report, Ice Processes in the Susitna River, Study 7.6. Susitna-Watana Hydroelectric Project, FERC No. P-14241 Filing: November 9, 2015. Prepared for Alaska Energy Authority, Anchorage, Alaska.

Leopold, L.B., and Wolman, M.G., 1957. River Channel Patterns: Braided, Meandering and Straight. U.S. Geol. Surv. Paper. 282-B.

Luckman, B.H., 2000. The Little Ice Age in the Canadian Rockies. *Geomorphology*, 32(3), pp.357-384.

Marusenko, Y. I., 1956. The Action of Ice on River Banks. *Priroda*, 12, pp.91-93. *In Russian*.

Outhet, D.N. 1974. Progress Report on Bank Erosion Studies in the Mackenzie River Delta, N.W.T. In: Hydrological Aspects of Northern Pipeline Development. Environmental Social Committee, Northern Pipelines, Task Force on Northern Oil Development, Report No. 74-12.Pollen, N., Simon, A., 2005. Estimating the mechanical effects of riparian vegetation on stream bank stability using a fiber bundle model. *Water Resources Research*, 41(7).

Prowse, T.D. Culp, J.M., 2003. Ice breakup: a neglected factor in river ecology. *Canadian Journal of Civil Engineering*, 30(1), pp.128–144.

Scott, K.M. 1978. Effects of Permafrost on Stream Channel Behavior in Arctic Alaska. Geological Survey Professional Paper 1068.

Simon A, Collison A.J.C, 2002. Quantifying the mechanical and hydrologic effects of riparian vegetation on streambank stability. *Earth Surface Processes and Landforms*, 27(5), pp.527-546.

Smith, D.G., 1980. River ice processes: thresholds and geomorphic effects in northern and mountain rivers. In: Coates, D.R., Vitek, J.D. (Eds), *Thresholds in Geomorphology*, George Alleen and Unwin, London, pp.323-345.

Tetra Tech, 2015a. Geomorphic Reach Delineation and Characterization, Upper, Middle, and Lower Susitna River Segments – 2015 Update Technical Memorandum. Attachment 1 to 06.05 Geomorphology Study 2014-2015 Study Implementation Report. Susitna-Watana Hydroelectric Project, FERC No. P-14241 Filing: November 2015. Prepared for Alaska Energy Authority, Anchorage, Alaska. 37 p.

Tetra Tech, 2015b. 2014-2015 Study Implementation Report, Geomorphology Study, Study Plan Section 6.5. Susitna-Watana Hydroelectric Project, FERC No. P-14241 Filing November 9, 2015. Prepared for Alaska Energy Authority, Anchorage, Alaska.

Tetra Tech. 2015c. 2014 Fluvial Geomorphology Model Development. Susitna-Watana Hydroelectric Project, FERC No. P-14241 Filing: November 2015; Study Completion and 2014/2015 Implementation Reports. Attachment 1 to 06.06 Fluvial Geomorphology Modeling below Watana dam 2014-2015 Study Implementation Report. Prepared for Alaska Energy Authority, Anchorage, Alaska. 100 p.

Tetra Tech. 2014a. Winter Sampling of Main Channel Bed Material. Susitna-Watana Hydroelectric Project, FERC No. P-14241 Filing: September 26, 2014; Technical Memorandum. Prepared for Alaska Energy Authority, Anchorage, Alaska. 68 p.

Tetra Tech, 2014b. Susitna River Historical Cross Section Comparison. Susitna-Watana Hydroelectric Project, FERC No. P-14241 Filing: September 17, 2014; Technical

Tetra Tech, 2014c. Mapping of Geomorphic Features and Turnover within the Middle and Lower Susitna River Segments from 1950s, 1980s, and Current Aerials. Susitna-Watana Hydrolectric Project, FERC No. P-14241 Filing: September 26, 2014; Technical Memorandum. Prepared for Alaska Energy Authority, Anchorage, Alaska.

Tetra Tech. 2013. Stream Flow Assessment. Susitna-Watana Hydrolectric Project, FERC No. P-14241. Prepared for Alaska Energy Authority, Anchorage, Alaska. 103 p.

Vandermause, R. 2018. The Role of Dynamic Ice-Breakup On Bank Erosion And Lateral Migration Of The Middle Susitna River, Alaska. Master's thesis. Colorado State University, Fort Collins, CO

Walker, J.H., Hudson, P.F., 2003. Hydrologic and geomorphic processes in the Colville River delta, Alaska. *Geomorphology*, 56(3), pp.291–303.Zabilanksy, L.J., Ettema, R.J. Wuebben, J. and Yankielun, N.E., 2002. Survey of River-ice Influences on Channel Bathymetry along the Fort Peck Reach of the Missouri River, Winter 1998-1999. United States Army Corps of Engineers, Cold Regions Research and Engineering Laboratory, Hanover NH, Contract Report.

Sedimentation, Bankfull Flow, and River Floodplain Connectivity across Topographically Distinct Floodplains and their Implication for Floodplain Management

John T. Schubert, Undergraduate Research Assistant, Virginia Tech, Blacksburg, VA, johnts@vt.edu
Sumaiya, Graduate Research Assistant, Virginia Tech, Blacksburg, VA, sumaiya18@vt.edu
Jonathan A. Czuba, Assistant Professor, Virginia Tech, Blacksburg, VA, jczuba@vt.edu

Abstract

High-resolution topographic data reveal pronounced variability in floodplain topography. This includes common features such as oxbows, chute channels, and scroll bars, but also surprisingly long and interconnected floodplain channels. In this work, we compare the hydrodynamics on several different floodplains with various degrees of topographic variability and river-floodplain connectivity. These river-floodplain systems include the East Fork White River (in two locations) and the Tippecanoe River in Indiana, and the South River in Virginia. We constructed two-dimensional numerical models using 2-D HEC-RAS of these river-floodplain systems from LiDAR data to investigate floodplain hydrodynamics over a range of flows.

Specifically, we extracted shear stresses from the 2D HEC-RAS models across a range of flows in both the channel and the floodplain to estimate the location of erosion and deposition of specific sizes of sediment based on the Rouse number. This allows us to determine the mobility of particular size classes of sediment, and used in conjunction with a path dependent model for sedimentation based on flow pathways, we identify areas of sedimentation and erosion in the floodplain by grain size at various flows. We then compare overall erosive and depositional potential across each floodplain relative to flow recurrence to determine if these floodplains are net erosional versus net depositional. We further ask, is the degree of topographic variability of these floodplains related to its erosional or depositional potential, and how does the supply of incoming sediment affect this relation? Specifically, in the East Fork White River, it is hypothesized that the long, interconnected floodplain channels (described by David et al. 2017, 2018; Czuba et al. 2019) persist because of low incoming sediment concentrations and erodible agricultural fields in the Spring prior to crop growth and when flows are often high.

We also compared bankfull flow across each river-floodplain system to determine the proportion of flow that leaves the channel prior to overtopping the bank. Does a definitive bankfull flow exist in any of these systems, or does the proportion of water leaving the channel prior to overtopping the banks vary with floodplain topography? We find that river-floodplain systems with long, interconnected floodplain channels (e.g., the East Fork White River) have a greater capacity to exchange water prior to overtopping their banks. Thus, in such systems, a definitive bankfull flow does not exist that completely fills the channel prior to spilling out onto the floodplain. Furthermore, we quantified this surface-water exchange flux across the river-floodplain boundary and also quantified the surface-water residence time of floodwaters on the floodplain (for methods see Czuba et al. 2019). We suspect that floodplains with long, interconnected floodplain channels have a higher capacity to exchange water between the river

and floodplain and perhaps remove a considerable proportion of nitrate from floodwaters due to its residence time than those without floodplain channels.

References

Czuba, J.A., S.R. David, D.A. Edmonds, and A.S. Ward (2019), Dynamics of surface-water connectivity in a low-gradient meandering river floodplain, Water Resources Research, 55(3), 1849-1870, doi:10.1029/2018WR023527.

David, S.R., Czuba, J.A., and Edmonds, D.A. 2018, "Channelization of meandering river floodplains by headcutting," Geology, 47(1):15-18, doi:10.1130/G45529.1

David, S.R., Edmonds, D.A., and Letsinger, S.L. 2017, "Controls on the occurrence and prevalence of floodplain channels in meandering rivers," Earth Surf. Process. Landforms, 42(3):460–472. doi:10.1002/esp.4002

The Sedimentological Imbalance of a *São* Francisco River Longitudinal Segment, Brazil

Geraldo Wilson Junior, Docteur d'Etat, COPPE/UFRJ
Federal University of Rio de Janeiro, Rio de Janeiro, Brazil. jrwilsong@gmail.com
Fernando Roversi, DSc., COPPE/UFRJ
Federal University of Rio de Janeiro, Rio de Janeiro, Brazil. fernandoroversi@gmail.com **Mario Grüne de Souza e Silva,** DSc., COPPE/UFRJ
Federal University of Rio de Janeiro, Rio de Janeiro, Brazil. mariosilva@poli.ufrj.br

Abstract

The hydrodynamic, sedimentological and morphological aspects of a longitudinal segment of the *São Francisco* River, on the border of *Minas Gerais* and *Bahia* States, Brazil, were considered at the SEDHYD2015 conference, in Reno, Nevada, USA. The *Iuiú* Irrigation Basic Project, which is located at the mouth of *Verde Grande* Tributary, was conceived in 2000 for the agricultural development of a 500 km² area. The 10.0 km studied reach of the *São Francisco* River project is located between two hydro-sedimentological stations: *Manga* 30.0 km upstream in *Minas Gerais* State, and *Carinhanha*, 20.0 km downstream, in the *Bahia* State. This longitudinal segment is not uniform; its cross sections are asymmetric. Due to the streamflow variations ($Q_{min} \cong 1{,}000$ m³/s; $Q_{max} \cong 12{,}000$ m³/s), varied bed forms, bars, islands and sediment deposits have been observed *in situ* and on satellite images. Assisted by remote sensing techniques between 1985 and 2011, six sediment bars were analyzed. Annual images showed that some of the sediment bars were intermittent, while others were permanent. It also showed that some bars migrated downstream, while others remained stationary but had annual morphological modifications. Three bars have been in the same position and were always present in the 26 analyzed images. One other bar can also be considered permanent, although it has only reached the *Iuiú*' area in 2001; it was outside the study reach, but later extended downstream. The last two bars represented intermittent movable deposits, common on some Brazilian rivers of the *Amazonas* and *Prata* Basins, which arise during some years, generally after flood seasons, but which are gradually eroded on the subsequent periods. A great challenge, and, consequently a great motivation to continue the morphodynamical studies on the *São Francisco* River, has been to explain the formation and disappearances of these movable bars. The main objective of this paper is to expand the 2000 study to include data from 2011 to 2018. The results are conclusive and surprising: (i) Numerous diversion projects were installed along tributaries of the *São Francisco* River; (ii) several tributaries dried up including the *Verde Grande* River, due to uncontrolled water diversions for agricultural development; (iii) numerous sediment bars appeared in the 60.0 km *São Francisco* River stretch from *Manga* to *Carinhanha*; (iv) the 10.0 km of the *Iuiú* Project, which was in sediment balance between 2003 and 2011, presented new sediment bars and tendencies to braiding; (v) forests were replaced by mechanized grain plantations, and (vi) conflicts arose between large landowners and peasants. The evolution of the watershed and channel-morphology, that has occurred in the *São Francisco* River' region, during this same period will be further evaluated using Landsat-5 and -8 images and Google Earth Engine JavaScript Application Programming Interface (Wilson-Jr. *et al.*, in prep).

Introduction

The incipient motion of the sediments in the watercourse beds or in their watersheds, the transport, dispersion and deposition of their grains, characterize sedimentological processes. These are associated with morphological processes, which consist of changes in the geometric characteristics of watercourses, because of disruptions in the dynamic balance of sediment movement (Motta, 1978). In rivers, estuaries and waterways, a very common change is the position and size of the sandbars, which often result in costly repairs and maintenance of the managed waterway system.

When the solid grains of a river bed have physical and chemical properties like those of the grains that are in motion, the bed is called alluvial. The shape and dimensions of the sediments are determined by a condition of equilibrium between the upstream solid feed and the carrying capacity of the streamflow. In alluvial reaches, sediment balance depends on the length of the reach and the period considered, define the spatial and temporal scales of the morphological process.

According to Einstein (1972), when the mass of sediment that is transported through a watercourse is equal to the mass that leaves it in a certain period, it is in sedimentological equilibrium. However, natural and anthropogenic adjustments may still occur in equilibrium reaches during the hydrological cycle, including formation of beaches on the margins, bars and other bed forms in the channel, development of cut-offs and dead arms, planform adjustments including braiding and meandering and others.

Anthropogenic modifications of the river bed and in the watershed add to these phenomena, which must be diagnosed and controlled, since they modify the sedimentological equilibrium, with severe impacts to environmental and civil works projects in general (Vieira da Silva and Wilson-Jr. 2005).

Principle of Self Adjustment

The sediment balance, also called regime or dynamic equilibrium (Blench, 1970), is governed by the Self Adjustment Principle, which establishes that, along an alluvial reach, subject mainly to unidirectional flows, there is a relationship between the independent variables - water discharge (Q) and sediment discharge (Q_b), and the dependent - width (B), depth (h) and longitudinal mean slope (S) of the reach.

If a dependent variable undergoes a change and the independent quantities remain constant, the flow will tend to restore to the changed quantity, its original equilibrium value. Conversely, if the altered quantity is an independent variable, the dependent quantities will tend to adjust towards new equilibrium values.

The concept of Self-Adjustment was initially established for irrigation channels designed to operate with constant water discharge. The concept was subsequently expanded to include rivers subject to non-permanent discharge during the hydrological cycle and with a fourth degree of freedom: that of forming meanders (Motta, 1978). But there is still a fifth degree of freedom, since the water flow has the capacity to sculpt or mold sand bed forms, as plane bed, ripples, bars, dunes, transition forms, anti-dunes, chutes and pools configurations.

Meanders can be defined by their wavelength (λ), which corresponds to the average distance between two consecutive curves on the same side of the flow, and the bed's forms, by their mean amplitude (h_d), equal to the average distance between the crest and the bottom of the configurations (Wilson-Jr. 1996).

Lane's Proportionality Relation (1955)

According to Lane (1955), there is a relationship between the sedimentological characteristics of the river's reach studied, represented by the bed material discharge, Q_b, and the median diameter of bed sediment particles, D_{50}; and the hydrodynamic characteristics, represented by the water discharge, Q, and the longitudinal slope of the water surface, S_o:

$$Q_b \times D_{50} = k \times Q \times S_o \quad (1)$$

where k is a dimensional proportionality coefficient to be determine with field measurements (Figure 1).

The equation is widely used in Environmental Impact Studies and Reports of Hydraulic Works Impact on the Environment (*EIA-RIMA, in Portuguese*). It quickly provides a qualitative prognosis of river' reaches subject to natural and anthropic actions.
If one of the four variables of the Equation (1) is modified, the equation generally predicts the response in one or more of the three remaining variables, for the restoration of the stretch's sedimentary equilibrium, which can be done naturally or by human action.

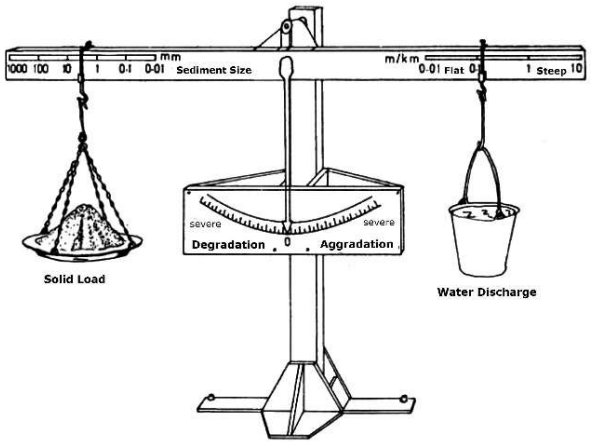

Figure 1. Sedimentological equilibrium in river flows. (Lane, 1955; Vieira da Silva & Wilson-Jr. 2005)

Stability of a River Reach (Schumm, 1960)

Evaluation of the morphological evolution of the fluvial reaches is facilitated by considering the possible modifications imposed to independent and dependent variables, based on qualitative relationships which were presented by Schumm (1960):

$$Q \ \alpha \ \frac{B, h, \lambda}{S} \quad (2)$$

$$Q_b \ \alpha \ \frac{B, S, \lambda}{h, P} \quad (3)$$

where: P is the flow sinuosity coefficient, defined as the ratio between the lengths of the water course and the river valley; λ is the wavelength of the meanders and S is the longitudinal slope of the energy line. Other variables could also be considered, such as: amplitude of the bed forms (h_d); ratio between the width and depth of the watercourse (F), and, the percentage of clay and silt present in the riverbed (M).

Quantitative relationships from Equations (2) and (3), can only be obtained through a methodology that encompasses observations and systematic field measurements, over the course of at least one hydrological cycle. However, as qualitative relationships, those are fundamental for the study of the susceptibility of fluvial reaches to morphological variations caused by erosion and sedimentation. Figure 2 shows the consequences of the simultaneous variations of the independent variables (Q and Q_b) on channel morphology. The symbols ⇧ and ⇩ indicate increases and decreases of the variables' values in response to altered conditions, respectively (Schumm, 1960; Vieira da Silva & Wilson-Jr. 2005).

		Width B	Depth h	Meander λ	Slope S	Sinuosity P	Ration F B/h
CASE I (Normal watercourse; increase of the watershed sediment yield)							
Water Discharge, Q	⇧	⇧	⇧	⇧	⇩	⇩	⇧
Solid Discharge, Q_B	⇧		⇩		⇧		
CASE II (Upstream of dams; confluence with larger river; entrance of lakes and bays)							
Water Discharge, Q	⇩	⇩	⇩	⇩	⇧	⇧	⇩
Solid Discharge, Q_B	⇩		⇧		⇩		
CASE III (Sediment retention in lake and reservoir; water supply from another source)							
Water Discharge, Q	⇧	⇧	⇧	⇧	⇩	⇧	⇩
Solid Discharge, Q_B	⇩	⇩		⇩			
CASE IV (Derivation of water for irrigation and increase of sediment yield due to agricultural exploitation, for example)							
Water Discharge, Q	⇩	⇩	⇩	⇩	⇧	⇩	⇧
Solid Discharge, Q_B	⇧	⇧		⇧			

Figure 2. Morphological trends of river stretch as a function of independent variables. (Schumm, 1960)

The Challenge and Motivation

Using annual LANDSAT-5 TM images, Wilson-Jr. & Souza e Silva (2015) studied a stretch along the São Francisco River planned for the *Iuiú* Irrigation Basic Project water intake. The authors described the evolution of six sediment bars between 1985-2011. Some were intermittent while others were permanent; some bars migrated to downstream while others remained stationary, while undergoing annual morphological modifications. A first challenge has been to explain the formation, displacements and disappearance of these landforms.

The *Iuiú* Basic Irrigation Project is located Southwest of *Bahia* State, on the border of *Minas Gerais* State, near the mouth of the *Verde Grande* River (Figures 3 and 4). It was elaborated in 2000 and intended for the agricultural development of an area of 500 km². The expected liquid discharge for the *Iuiú* Project 29.7 m³/s of water from the *São Francisco* River. The project is located between two hydro sedimentological stations: *Manga* 30.0 km upstream in *Minas Gerais*, and *Carinhanha*, 20.0 km downstream, in *Bahia* State. Figure 4 highlights the river stretch that has been studied for the *Iuiú* Irrigation Project (the project has not yet been implemented), the location of the hydro-sedimentological stations, the alternatives for water intake and the sediment bars that were analyzed during the period of 1985 to 2011. Hydro-sedimentological data collected by Wilson-Jr. (2000), was collected during a drought, when recorded discharge was 1,045 m³/s, close to the annual minimum mean discharge of the river. The *São Francisco* River in the vicinity of the project's water intake is not rectilinear. Its cross sections are asymmetric and because of the water discharge variations during the hydrological cycle ($Q_{min} \cong 1{,}000$; $Q_{max} \cong 12{,}000$ m³/s), varied bed forms, islands and sediment deposits can be observed *in-situ* and on the satellite images.

During periods of drought, the sediment deposits emerge as bars, enabling the development of subsistence farming by the riverside population. With the arrival of the rainy season, the water level of the river rises, floods and washes most of the plantations. Flooding modifies the bars and islands by eroding and depositing sediments, and altering the river bed's planform and

morphology. It also fertilizes the soil. During the field visit of July 2000, three sediment bars were observed (2, 4 and 6, Figure 4). Remote sensing techniques were used to identify three other sediment bars (1, 3 and 5, Figure 4) that were created between 1985 to 2011 (Wilson- Jr. & Souza e Silva, 2015).

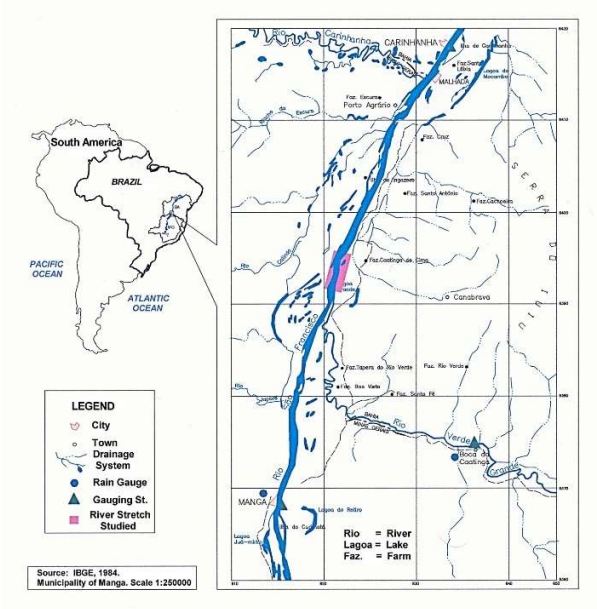

Figure 3. Semi-arid region of the *São Francisco* River watershed (Wilson-Jr. 2003)

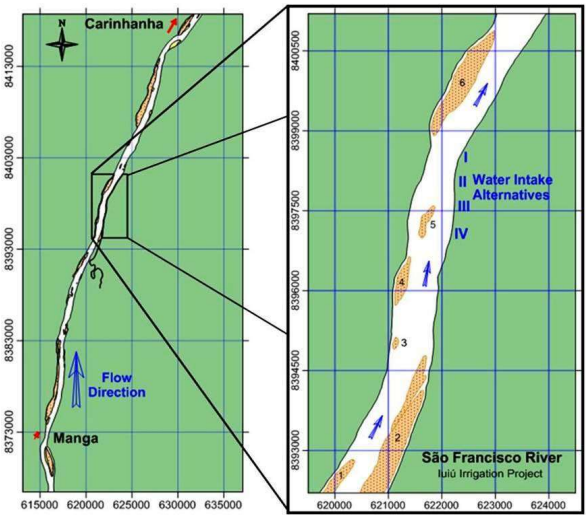

Figure 4. Reach of the Irrigation project *Iuiú*, alternatives of the water intakes, sediment bars localization. (Souza e Silva, 2013)

However, since 2012, streamflow discharge from once perennial tributaries of the *São Francisco* River in the northern region of the state of *Minas Gerais* and south of *Bahia*, such as the *Verde Grande* River, has decreased and some became intermittent, presenting beds completely dry during the hydrological cycle (Figures 5 and 6). The primary causes of these changes include the occupation of the soil and the diversion of water for the mechanized irrigation of large agricultural plantations. Therefore, conflicts emerged between large farmers who adopt a mechanized cultivation, and the small pioneer owners with subsistence operations that include livestock (https://www.metropoles.com/materias-especiais/ribeirinhos-e-fazendeiros-travam-batalha-na-bahia-por-escassez-de-agua). *São Francisco* River discharge also decreased from the year 2013; discharge measured in *Manga* Station, for example, was reduced 50% compared to previous years (Figures 7 and 8). These events led us to examine the satellite images of the *São Francisco* River basin and channel, between the *Manga* and *Carinhanha* Stations, to evaluate the increase in the number of bars exposed in the riverbed during the dry season (Figures 9 and 10).

Figure 5. A reach of *Verde Grande* River in 2012 (Photo Dêniston Diamantino)

Figure 6. A reach of *Verde Grande* River in 2013 (Photo Dêniston Diamantino)

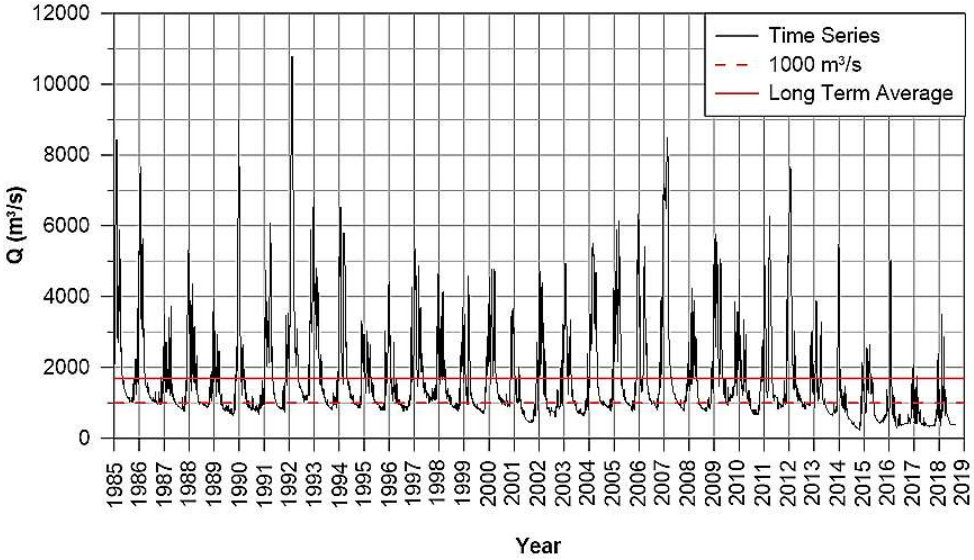

Figure 7. Daily liquid discharges of the *São Francisco* River in the Hydro-Sedimentological Station of *Manga*, MG (ANA, 2018).

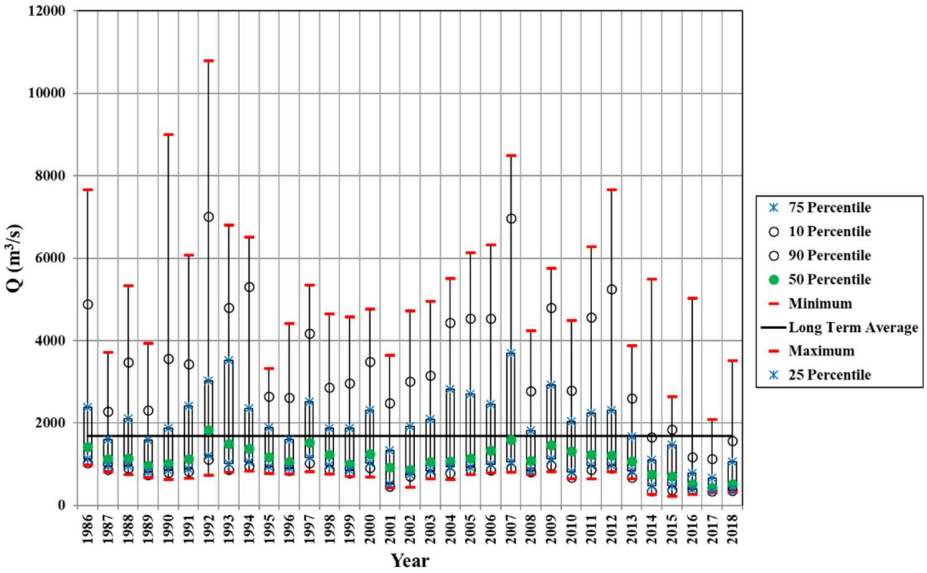

Figure 8. Statistic values box-plot of the daily streamflow discharges of the *São Francisco* River at *Manga* Station, MG.

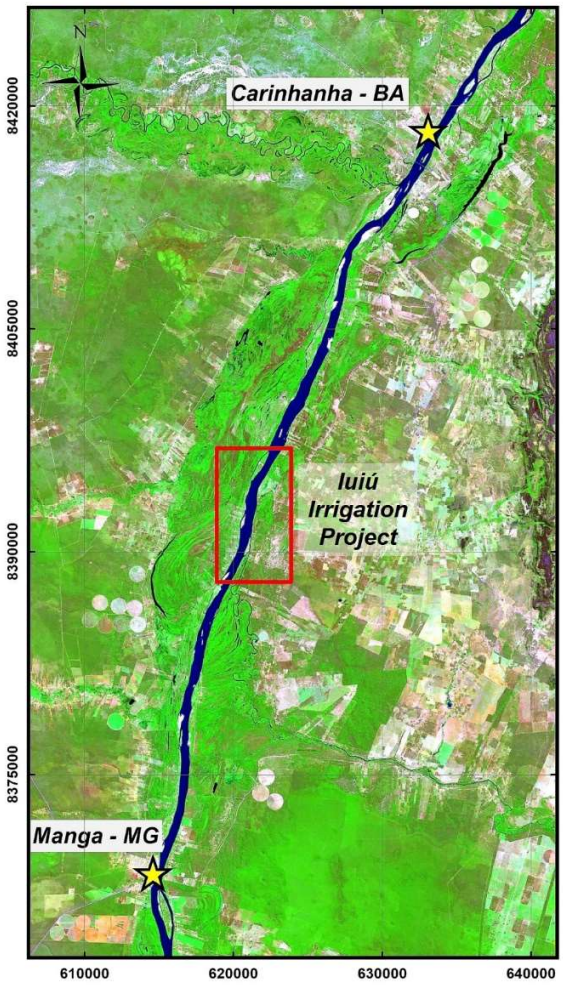

Figure 9. *São Francisco* River between *Manga* and *Carinhanha* Stations. 2011-06-24 Landsat-5TM Image.

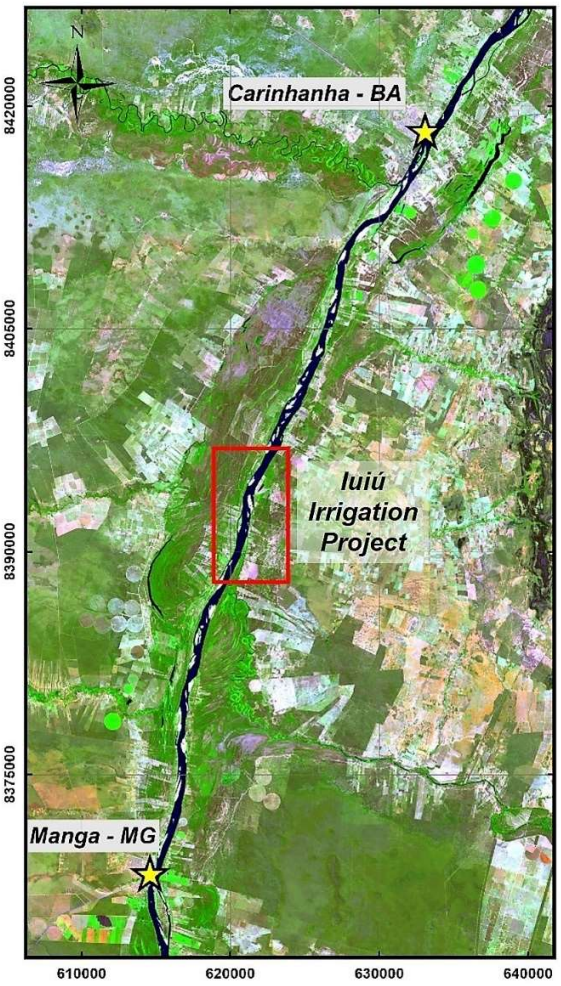

Figure 10. *São Francisco* River between *Manga* and *Carinhanha* Stations. 2018-07-29-Landsat-8TM Image.

Objectives

The main objectives of this study are to:

1. Present the sedimentological and morphological characteristics observed during a field visit, of an approximately 10.0 km long reach along the *São Francisco* River, on the border of the States of *Minas Gerais* and *Bahia*, and downstream from the *Verde Grande* River confluence.
2. Show that the evolution of mobile bars and river banks can be analyzed using medium resolution (30.0 m) satellite images (Landsat-5 and -8 TM).
3. Recommend the use of these images and/or of higher resolution (≤ 1.0 m) in the descriptive methodology of sediment movement in open channel flows.
4. Compare the morphological behaviors of a reach along the *São Francisco* River that occurred between 1985-2011 (Wilson-Jr. & Souza e Silva, 2015), and between 2011-2018, when significant land use changes including irrigation diversion occurred in the basin.

Methodology

Wilson-Jr. & Vukmirović (1980) and Wilson-Jr. (1999, 2009) developed a three simultaneous steps methodology for qualitatively and quantitatively describing, sediment movement in open channel flows, using topobathymetry surveys, use of tracers, remote sensing techniques and GIS: (1) know and describe the watershed delimited by the project; (2) *in-situ* measurements of the solid motion in a representative reach of the flow; and (3) determine the hydrodynamic, sedimentologic and hydrometeorological characteristics of the representative watershed segment.

First Step: Knowledge of the Watershed Basin

The knowledge of the watershed involves the understanding of its geographic, geologic, hydro-meteorological, sedimentologic, socio-economic and historical characteristics, among others. In this step, aerial photography, satellite images and GIS techniques are very useful.

Second Step: In-situ Measurements Campaigns

The study section was chosen based on its location and to provide technical subsidies for selection of water intake alternatives for the *Iuiú* Basic Irrigation Project. To quantify sediment movement through the study reach, three superposed measurement campaigns are necessary: daily, periodic and intensive.

Daily measurements consist of the water level record and water sample collection to determine the concentration and granulometry of the suspended sediment, which, along with the pluviometry and evaporation data, characterize the hydrologic cycle.

Periodic measurements complement to the daily observations and are taken in response to the hydrometeorological events. They include streamflow velocity and discharge; watershed morphology including erosion and aggradation; detailed sampling of the sediments and bathymetric surveys including the longitudinal waterline and bed slopes, flood levels, and bedform morphology.

The periodic measurements are used to define the analytical relations between hydrodynamic and sedimentological quantities for the representative river reach. The daily measurements are used to extrapolate the relations across the hydrological cycle(s).

Intensive measurements campaign is performed in well-defined hydrological conditions, generally during the rainy season, when rates of sediment production and transport are high, or during the average discharge period when bedforms are created. They include longitudinal bathymetry of the stretch, bed forms records and special measurements of the bed sediment discharges.

Third Step: Hydrometeorological Characteristics

The data collected- especially those collected as part of the intensive measurement dataset, are limited in time and to defined hydrometeorological conditions, which need to be well known, so the data can be extrapolated.

Special Measurements of the Sediment Movement

The special measurements are the ones that enable the calibration and validation of the models. In this paper, hydrodynamic and sedimentological measurements, topographic and bathymetric surveys, remote sensing technique and GIS are the special measurements considered for the knowledge of hydrodynamic regimes, watershed characteristics, and evolution description of bedforms and of the *São Francisco* River's morphology along the *Iuiú* Irrigation Project.

Morphological Characterization of the *Iuiú* Project Stretch

The HEC-RAS Software Application

Data for this study were obtained through the following field measurements: (i) GPS contours of the segment, bars and islands; (ii) cross sections measurements with sonic sounder and GPS positioning; (iii) longitudinal bathymetric bed configurations records (Wilson-Jr., 2000, 2003).

The *São Francisco* River stretch contours were recorded by boat, navigating as close as possible to the margins with GPS equipment. In the consolidated bars and islands, the geographic and morphologic records were performed walking around the beaches, bars and islands. The final product of the records was a detailed geographic map of the 10 km long *São Francisco* stretch, downstream from the *Verde Grande* River confluence, part of which constitutes an accurate record of the *São Francisco* River stretch during the dry period, prior to 2011 (Figure 11).

The *HEC-RAS* software (USACE, 1997) was used to estimate longitudinal variations of water levels (Figure 12). The analysis entailed two calibrations a one simulation:

In the first calibration attempted to reproduce the longitudinal profile of the open surface, using values of the flow resistance coefficient obtained as a function of the bed material grain size. However, since the results obtained in this stage did not correctly reproduce the water levels observed in the fourteen cross sections of the studied stretch (Figure 11), a second calibration was performed.

The second calibration attempted to determine, within the range of values related to the riverbed material size and for each cross section, the values of the Manning coefficients that best reproduced the water levels observed in the field. The values of the hydraulic parameters measured in the Alternative 3's Cross Section and calibrated with the *HEC-RAS*, are presented in the Table 1 (Guimarães & Wilson-Jr, 2002).

In the final phase, 30 simulations were run, varying the water line slope, the flow resistance coefficient, and considering the following water discharges: 1,045.2; 2,000.0; 5,000.0; 8,000.0 and 12,000.0 m^3/s. The water discharge Q = 5,000.0 m^3/s corresponds to the overflow in some cross sections, or the flood discharge initial limit.

For the first fourteen simulations, in which the flow remains in the river channel, the cross sections used were measured in the field. In the simulations where flows spread out onto the floodplain, it was assumed that the sections would reach a quota of 5.0 m above the largest quota values already observed in each margin, for distances of 1,000 m from the extremities of the measured water surfaces during the day of the field visit. Figures 13 and 14 present the HEC-RAS sketches of Section 9, Normal and Prolonged, for Q = 1,045.2 and 8,000.0 m^3/s, respectively, highlighting the verticals of equal velocity (Guimarães & Wilson-Jr, 2002).

Figures 15 and 16 present the qualitative longitudinal flow profiles in perspective, from the upstream section 14, on the left side of the figures, to section 1, on the right side (downstream). Figure 15 shows results in which the flow is contained within the banks of the active channel, while the results of Figure 16, for water discharges higher than Q = 5,000.0 m³/s, represent overbank flooding conditions.

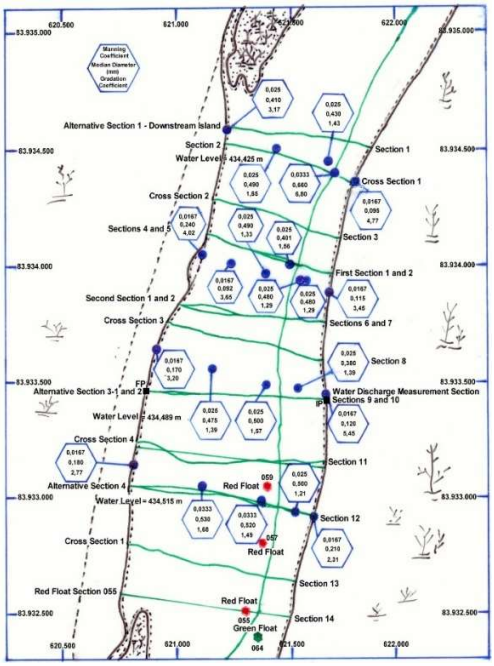

Figure 11. Geographic map of the water intake alternative sections on the *São Francisco* River. *Iuiú* Irrigation Project. (Wilson-Jr., 2000)

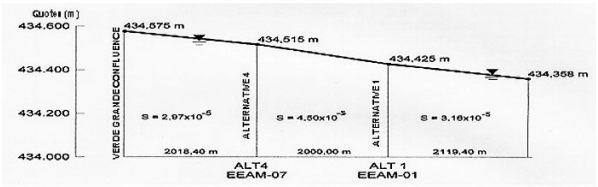

Figure 12. Quotes of water surface levels in the *São Francisco* River reach (Wilson-Jr., 2000).

Table 1. Hydraulic parameters measured in the section 9 and calibrated with *HEC-RAS* model. (Wilson-Jr., 2000; Guimarães & Wilson-Jr, 2002).

Variables	Units	Measured	Calibrated
Water discharge	m³/s	1,045.20	1,045.20
Water level elevation	m	434.489	434.49
Upper section width	m	789.08	777.67
Flow area	m²	1,566.65	1,477.73
Wet perimeter	m	789.64	778.34
Hydraulic radius	m	1.984	1.90
Flow velocity	m/s	0.667	0.71
Manning coefficient	$m^{-1/3}$. s	0.0159	0.0167
Channel slope	cm/km	4.50	4.50
Shear stress	N/m²	0.876	1.10
Froude number		0.15	0.16

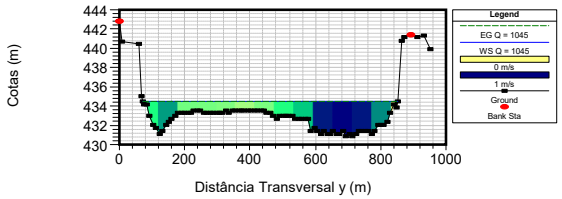

Figure 13. Normal Cross Section 9 for Q = 1,045.2 m³/s. (Guimarães & Wilson-Jr, 2002).

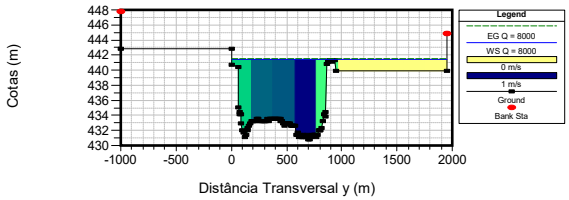

Figure 14. Prolonged Cross Section 9 for Q = 8,000.0 m³/s. (Guimarães & Wilson-Jr, 2002).

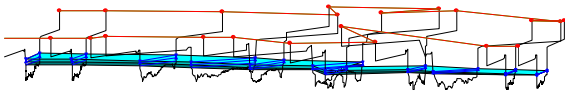

Figure 15. Longitudinal Profiles of the *São Francisco* River Stretch (Q = 1,045.2 m³/s; Contour Conditions: Water Levels in Sections 14 to 1). (Guimarães & Wilson-Jr, 2002).

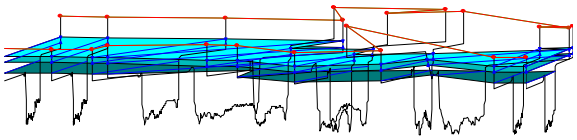

Figure 16. Longitudinal Profiles of the *São Francisco* River Stretch (S = 9,0 x 10^{-5}. Q = 5,000.0; 8,000.0 and 12,000.0 m³/s). (Guimarães & Wilson-Jr, 2002).

Remote Sensing Results

The Period of 1985 to 2011: Wilson-Jr. & Souza e Silva (2015) showed that Landsat-5 TM images have sufficient resolution to reproduce the contours of the margins and sediment bars of a river stretch of the same size of the *São Francisco* River, with a maximum discrepancy between the areas raised in the field and from the satellite image of less than 7 percent.

To evaluate the morphological evolution of the *Iuiú* Project region, 26 satellite images taken between 1985-2011 during the dry season ($Q \cong 1{,}000\ m^3/s$) were used (an adequate Landsat-5 image was not available for the 2002 dry season). The sum of the emergent areas of the six sediment bars on each image, named Dry Area; and the complement of this sum in relation to the delimited domain of the *São Francisco* River stretch, named Wet Area, were used to estimate the sedimentological behavior of the reach. The results are shown in Figure 17, hereafter.

Results document an increase of the Dry Area and a corresponding decrease of the Wet Area throughout the first 17 years (1985-2001). This finding suggests that the Irrigation *Iuiú* Project's stretch was not in sedimentological equilibrium; measurements suggest aggradation on the order of 7.70 % relative to 1985's recorded area. In contrast, the dry and wet areas oscillated around constant values between 2003-2011, indicating that the *São Francisco* River stretch reached a sedimentological equilibrium during this second period.

The aggradation of the river stretch becomes even more evident when the temporal variations of the dry area of each sediment bars are analyzed. Figure 18 shows the annual variations of dry area of the six bars. The presentation of the bars was made in ascending order of dry area values in relation to the total area of the studied stretch, so the highest values stay on the back of the figure and do not hide the value of the smaller bars.

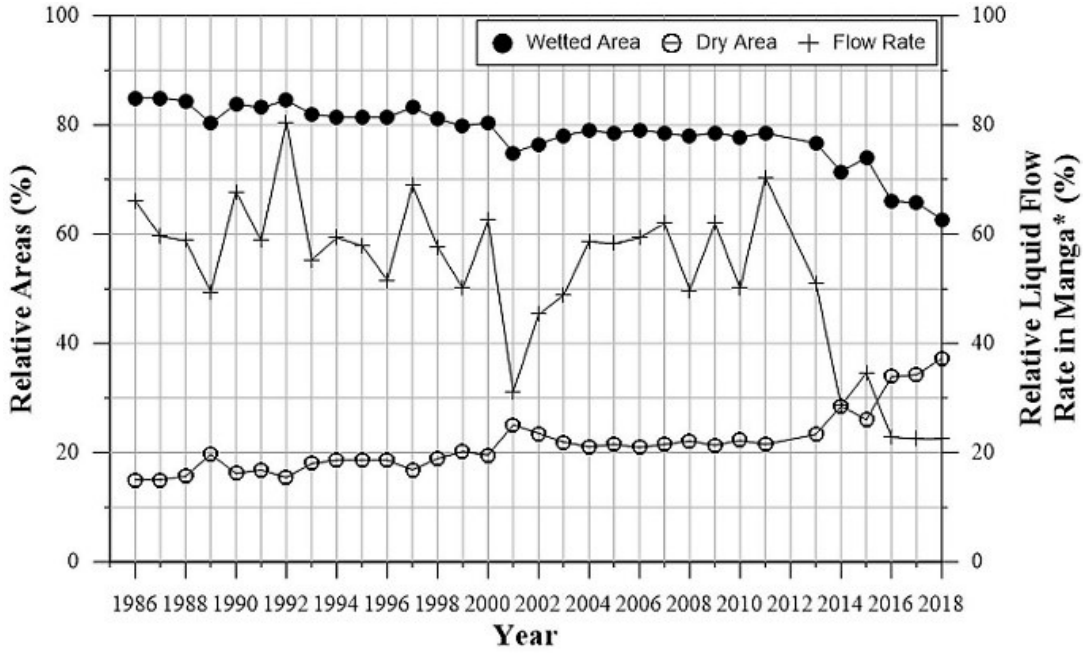

Figure 17. Annual evolutions of the relatively dry and wet areas of the *Iuiú* Project in the *São Francisco* River.

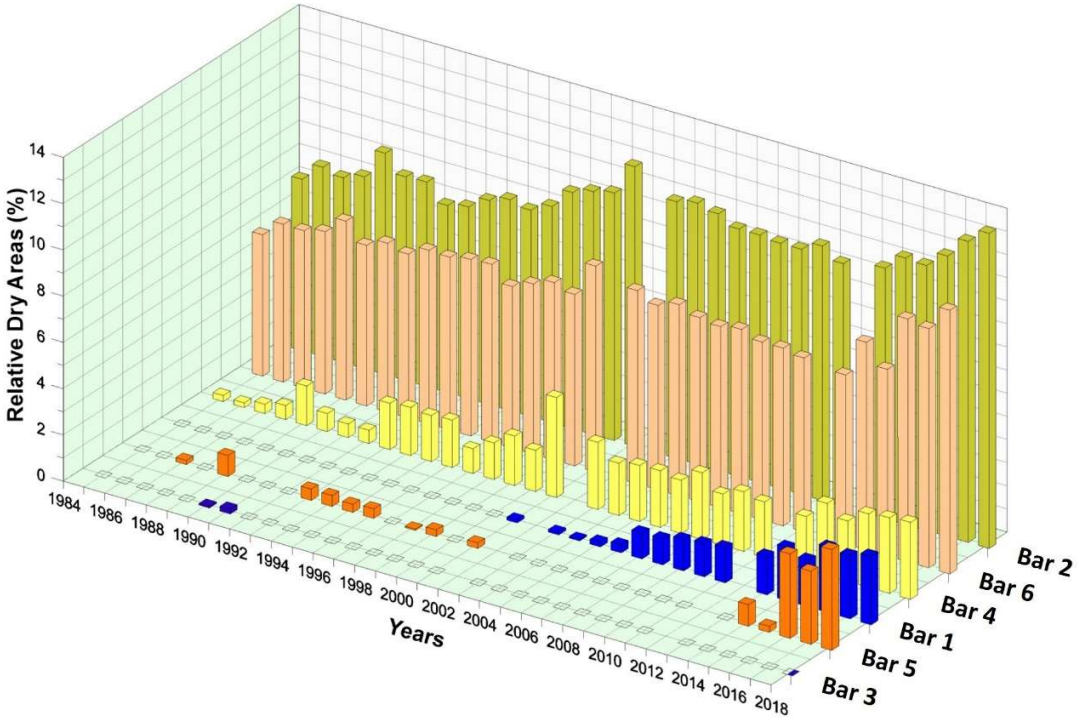

Figure 18. Morphological evolution of the São Francisco's sediment bars, from 1985 to 2018.

The Period of 2011 to 2018: The previous analysis (1985-2011) of the annual images showed that some of the sediment bars are intermittent, while others are permanent. It also showed that some bars migrate downstream, while others remained stationary but had annual morphological modifications. Bars 2, 4 and 6 of Figures 4 and 19, are permanent and present in all the first 26 analyzed images. Bar 1 can also be considered permanent, although it had only reached the *Iuiú*' area in 2001. Before then, the bar fell outside the map's limits, but as Bar 2 it later extended itself downstream. Bars 3 and 5 represent intermittent movable deposits, which arise during some years, generally after flood seasons, but are gradually eroded on the subsequent periods, with lower water levels. Bar 3 was only present in 1990 and 1991, while Bar 5 emerged in 1987, 1989, of 1993 to 1996, and again in 1998, 1999 and 2001.

Results of our analysis of the later period (2011-2018), combined with anecdotal reports of the riverside fishermen, indicated a considerable reduction of the streamflow after 2013 (Figures 7, 8, 17 and 18). The six bars, among others most recent (Figures 17 to 19), have developed and consolidated, hindering navigation.

According to the Self Adjustment Principle, the reduction of the value of the independent variable Q at the Manga Station caused changes in the one or more of the dependent variables, B, h, S, λ and h_d, downstream of this section. Lane's Equation (1) and Figure 1 indicate that the system responded to an in-water discharge (Q) by decreasing the bed material discharge, Q_b, and/or decreasing median grain size, D_{50}, causing aggradation along the downstream reach. Similarly, the Schumm's Equation (2) and Figure 2 indicate that the most likely variables to be altered (⇩) are B, h, as well as the longitudinal mean length λ of the meanders. Some of these modifications can be seen in Figure 19.

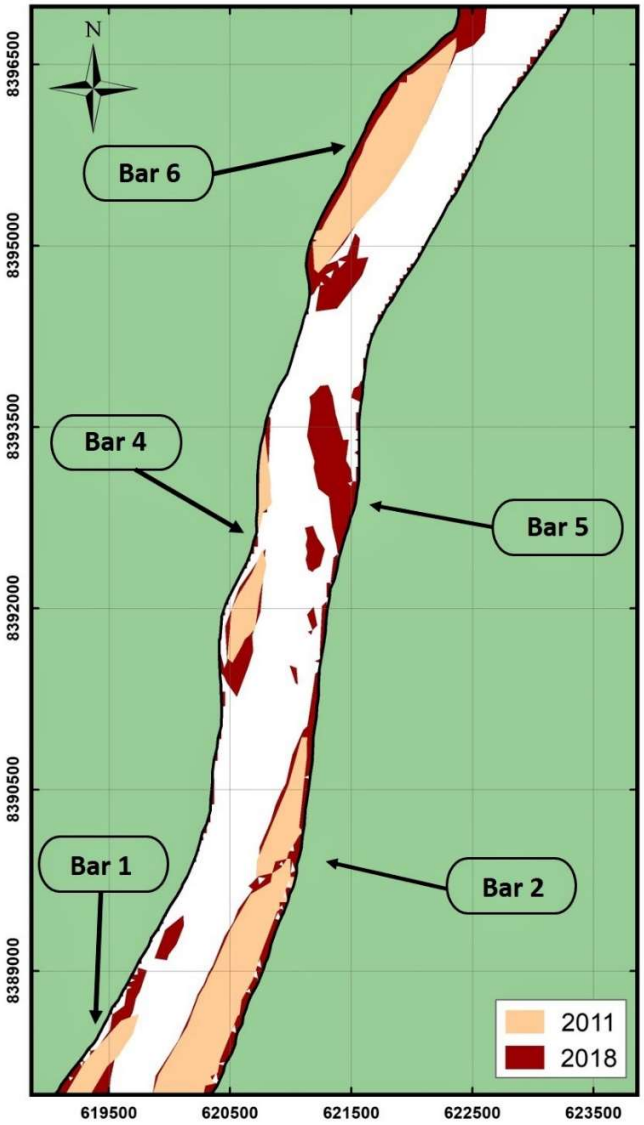

Figure 19. *São Francisco* River' sediment bars on 2011 and 2018.

Conclusions and Recommendations

Although conceived in the year 2000, the *Iuiú* Irrigation Project has not yet been approved due to the large liquid discharge (Q = 29.7 m^3/s) that would be diverted from the *São Francisco* (*SF*) River. However, the authors verified through field visits, satellite image analysis, and riverine information that from 2011 to 2018 there was a gradual increase in water withdrawal for numerous irrigation projects which were easier installed along tributaries of the *SF* River.

Between 2001-2013, the *São Francisco* River was in sedimentological equilibrium in the Iuiú's Project reach. During dry seasons, islands of sandy and cohesive sediments were deposited in the *São Francisco* River. These deposits constituted a fertile soil such that the islands were temporarily cultivated, for subsistence, by the riverside habitants. Higher streamflow during the wet season deposits submerged and scoured the bars and caused them to migrate wholly or partially downstream. In the following hydrological cycle, the deposits were restored during the

rainy seasons, and reemerged in the dry season: when the stretch is in sedimentological equilibrium.

Since 2013, however, excessive diversions for irrigation and pasture for livestock dried up important tributaries, decreasing streamflow discharge and disrupting the sedimentological balance along the study reach.

Topographic and bathymetric surveys of the stretch, hydrodynamic and sedimentological measurements campaigns, hydrodynamic models such as HEC-RAS and the use of remote sensing and GIS, are recommended tools for the studies of sedimentological and morphological processes in open channel flows. In addition to the common view from the margins, limited in time and space, the observer possesses the most, a dynamic perspective, and a top and detailed description of the watershed, the river stretches and even of the river bottom.

Additional studies are planned that will use the methods outlined in this paper, to continue to evaluate the impacts of land changes including deforestation, on sedimentological equilibrium *São Francisco* River basin.

References

ANA – Agência Nacional de Águas, 2018. "Portal HIDROWEB. SNIRH: Sistema Nacional de Informações sobre Recursos Hídricos", Acervo de Dados Hidrológicos. www2.ana.gov.br/.

Blench, T., 1970. "Regime theory design of canals with sand beds". J. Irrig. Drainage Div. ASCE, 96(IR2), pp. 205-213, June.

Einstein, H.A. 1972. "Relatório sobre o transporte de sedimentos no *Rio Paraná*". *In*: Eletrobrás e ANDE, 1974. Appendix A – Hydrology and Meteorology, Final Draft - Rio Paraná Study.

Guimarães, M.M. & Wilson-Jr., G. 2002. Hydrodynamics and sedimentological studies of *São Francisco* River stretch with the HEC-RAS model. V ENES, V. 1, p. 219-235. São Paulo, Brasil.

Lane, E.W. 1955. "The importance of fluvial morphology in Hydraulic Engineering". Proceedings of the ASCE, Vol. 84, Nº 745.

Motta, V.F. 1978. "Processos sedimentológicos e morfológicos em estuários". Nota Técnica, Área de Engenharia Costeira do PENO/COPPE/UFRJ. 9p. Rio de Janeiro, Brasil.

Schumm, S.A. 1960. "The shape of alluvial channels in relation to sediment type". U.S. Geological Survey Prof. Paper 352-B, pp. 17-30. USA.

Souza e Silva, M.G. 2013. "Análise de processos hidrossedimentológicos em escoamentos com superfície livre: trecho do projeto de irrigação *Iuiú* no Rio São Francisco". Dissertação de M.Sc. PENO-COPPE-UFRJ. Rio de Janeiro, Brasil.

USACE - (U.S. Army Corps of Engineers) 1997. "HEC-RAS: Hydrologic Engineering Center - River Analysis System". Davis, CA. USA.

Vieira da Silva, R.C. and Wilson-Jr., G. 2005. "*Hidráulica Fluvial II*". COPPE/UFRJ. *Rio de Janeiro,* Brasil.

Wilson-Jr., G. 1996. "Diagnóstico do movimento sedimentar da Bacia Hidrográfica do Rio Iguaçu". COPPETEC, PINUD, Vols. I, II, III, 535 p., 343 photos. Rio de Janeiro, Brasil.

Wilson-Jr., G. 1999. "Estudo do movimento sedimentar em escoamentos com superfície livre". *XIII Simpósio Brasileiro de Recursos Hídricoso*. ABRH. Belo Horizonte, MG. Brasil.

Wilson-Jr., G. 2000. "Estudos hidráulicos e sedimentológicos referentes às alternativas de tomada d'água do Rio São Francisco para o Projeto de Irrigação *Iuiú"*. COPPETEC-PENO-UFRJ. V.1, 198 *p.il.*, Rio de Janeiro, Brasil.

Wilson-Jr., G. 2003. “Hydrodynamic, sedimentological and morphological aspects of a *São Francisco* River stretch, Brazil”. Proceedings of the Ninth International Symposium on River Sedimentation. Vol. III, p.1602-1609. Tsinghua University Press. Yichang, China.

Wilson-Jr., G. 2009. “Evolução morfológica de trechos hidroviários”. *6º Seminário de Transporte e Desenvolvimento Hidroviário Interior*. SOBENA. Rio de Janeiro, RJ, Brasil.

Wilson-Jr., G. & Souza e Silva, M.G. 2015. “Morphological evolution of fluvial and estuarine segment flows”. *SEDHYD Conference*. Reno, Nevada, USA.

Wilson-Jr., G. & Vukmirović, V. 1980. “Sediment transport on the *Ivai* River, Brazil”. *Symposium on River Engineering and its Interaction with Hydrological and Hydraulic Research*. IARH. Belgrade, Yugoslavia.

Acknowledgments

The authors express their gratitude to PENO/COPPE/UFRJ, COPPETEC/UFRJ, CAPES, FAPERJ and CNPq for their institutional support, without which, the realization of this work would not have been possible.

Julia Grim and Troy Lyons deserve our special thanks for their valuable suggestions and thorough revision of the text.

Extended Abstract: Tracking a Riverbed's Response to Channel Mining on the Lower Missouri River

Heather Shaughnessy, Hydraulic Engineer, United States Army Corps of Engineers, Kansas City, MO, Heather.H.Shaughnessy@usace.army.mil
John Shelley, Hydraulic Engineer, United States Army Corps of Engineers, Kansas City, MO, John.Shelley@usace.army.mil

Introduction

Since the 1930s, large stretches of the lower Missouri River have experienced in-channel commercial sand and gravel mining with annual totals over the last 20 years of more than 5 million tons. As part of a study to understand the localized, short-term impacts of mining on the river, the acute depression in the riverbed caused by a cutter head dredge was surveyed using a multibeam echosounder. Multiple surveys were collected over the course of two weeks until the depression was no longer evident. Repeated, detailed surveys of a marked removal of a known quantity of bed material provides a visible depiction of the channel's localized geomorphic response to the dredging disturbance. This extended abstract documents the lateral extent, depth, and location of the depression over time and provides insight into the morphological behavior of this large, sand bed river.

Methods

In order to assess the spatial and temporal changes that dredging induces in the river bed in the immediate area of the dredging operation, daily multibeam hydrographic surveys were collected immediately following and in the localized vicinity of a discrete dredging event. As conditions and schedules allowed, daily surveys were continued until effects of dredging were no longer evident. The multibeam survey crew mobilized immediately following cessation of dredging at an actively dredged location. The area surveyed within the channel extended from 0.2 miles upstream to 0.2 miles downstream of the dredge location.

The Lexington Reach from river mile (RM) 315-317.5 was the area targeted for this survey effort. The depression created from a commercial suction cutter head dredge is the focus of this analysis. This data provides information for management actions on regulation of commercial dredging.

The survey equipment for this effort includes a sounding system comprised of an R2Sonic 2024 multibeam echo sounder with user selected frequency from 200 kHz to 450 kHz and 700 kHz UHR with capability to log Water Column and True Pix (side scan), POS MV 320 V5 inertial aided DGPS with optional RTK. Sound velocity measurements are obtained from Odom Digibar Pro SV profiler and a Valport Mini SV Probe at the head. Navigation and data collection are accomplished with HYPACK/HYSWEEP. This data was collected to yield 1-foot point spacing in the resulting point cloud.

Results

The extraction location, extraction quantity, the extents, the depth, and depression location for a dredge event occurring on 16 July was tracked over time at Lexington Bend at RM 316.2. Surveys were collected starting on 16 July 2018 and ending on 6 August 2018. No additional dredging occurred in the surveyed area during the 22 days following the 16 July survey event. While the depressions from several dredging events from a week prior to the 16 July event are evident in the survey data, the dredge hole resulting from the 16 July dredge event, which occurred a few hours prior to the hydrosurvey, is the focus of this analysis. Also, note that the surveys were collected during a time of fairly constant water surface elevations that dropped no more than 2 feet over the course of the surveys (Figure 1).

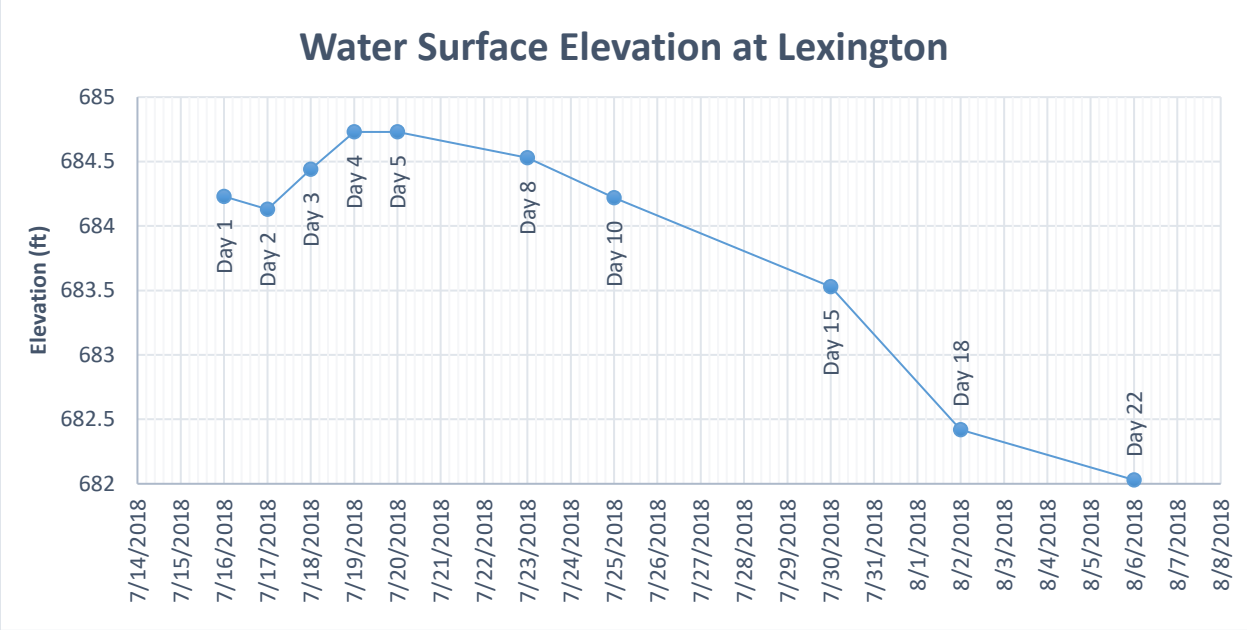

Figure 1. Water Surface Elevation at Lexington on surveyed days (Day 1 = day of dredging event)

The translation and attenuation of the dredge hole occurs in a very dynamic system. For example, natural variability in bed elevations, as indicated by repeated cross section, single beam surveys under steady flow conditions, can be as high as 6 feet. Notwithstanding, the multibeam surveys employed for this analysis provide sufficient resolution to describe the dredge hole's initial dimensions as well as its translation and attenuation over time. This dredge hole analysis uses multibeam data with 1-ft bed elevation spacing and captures more of the bedform scale features that are not evident in cross section based data. For instance, dune heights up to 3 feet are apparent in this multibeam survey data. While the spatial scale is relatively small in this analysis, it is important to keep in mind the natural trends that are occurring at the larger scale. This analysis aims to characterize the effects of one discrete dredging event and will be used to develop a methodology for future surveys which will ultimately provide a better understanding of the effects of commercial dredging on the Missouri River system as a whole.

Extraction Location and Quantity

A total of 750 tons was removed from the bed during this targeted dredge event. The initial dredge depression extended about 230 feet upstream to downstream and averaged about 25 feet wide. Typical cutter head suction dredges start downstream and pull themselves upstream by the use of anchors as the dredge cuts into the bed. The two points plotted in the graphic below (Figure 2) mark the start (downstream) and stop (upstream) location of the dredge path. About 3 tons per linear foot were dredged at this location.

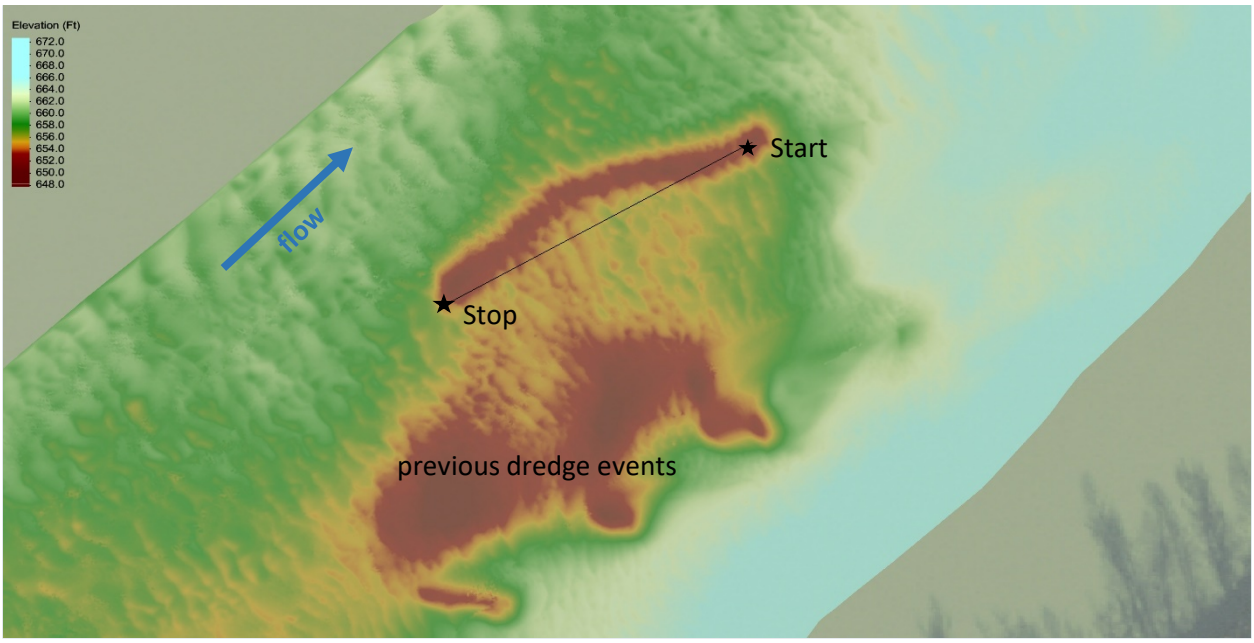

Figure 2. Day 1 Dredge Hole Survey at Lexington with Dredge Start/ Stop Locations

Extents and Depth

The extent and depth of the depression were measured for each subsequent survey. Days 1-8 are plotted below (Figure 3). Surveys collected after Day 8 are not shown because the effects of dredging were no longer evident. Over time the depression migrates downstream, reduces in depth, segments, and widens laterally.

At an average river discharge of about 100kcfs, the surveys show that each day the dredge hole migrated downstream about 20-40 feet and widened about 10 feet until the hole completely attenuated. The downstream travel distance from Day 1 to Day 8 is approximately 200 feet. The dredge hole depth attenuated about 1 foot per day until the hole depth was about 3 feet and then attenuated at a much slower rate for the next 5 days. Where the dredge hole overlaps with the hole from prior dredging events, it appears the downstream migration distance increased. The initial depression immediately following dredging is narrow, long, and deep. Over time the depression becomes shallower and widens which increases the impacted footprint across an area more than double that of the initial depression.

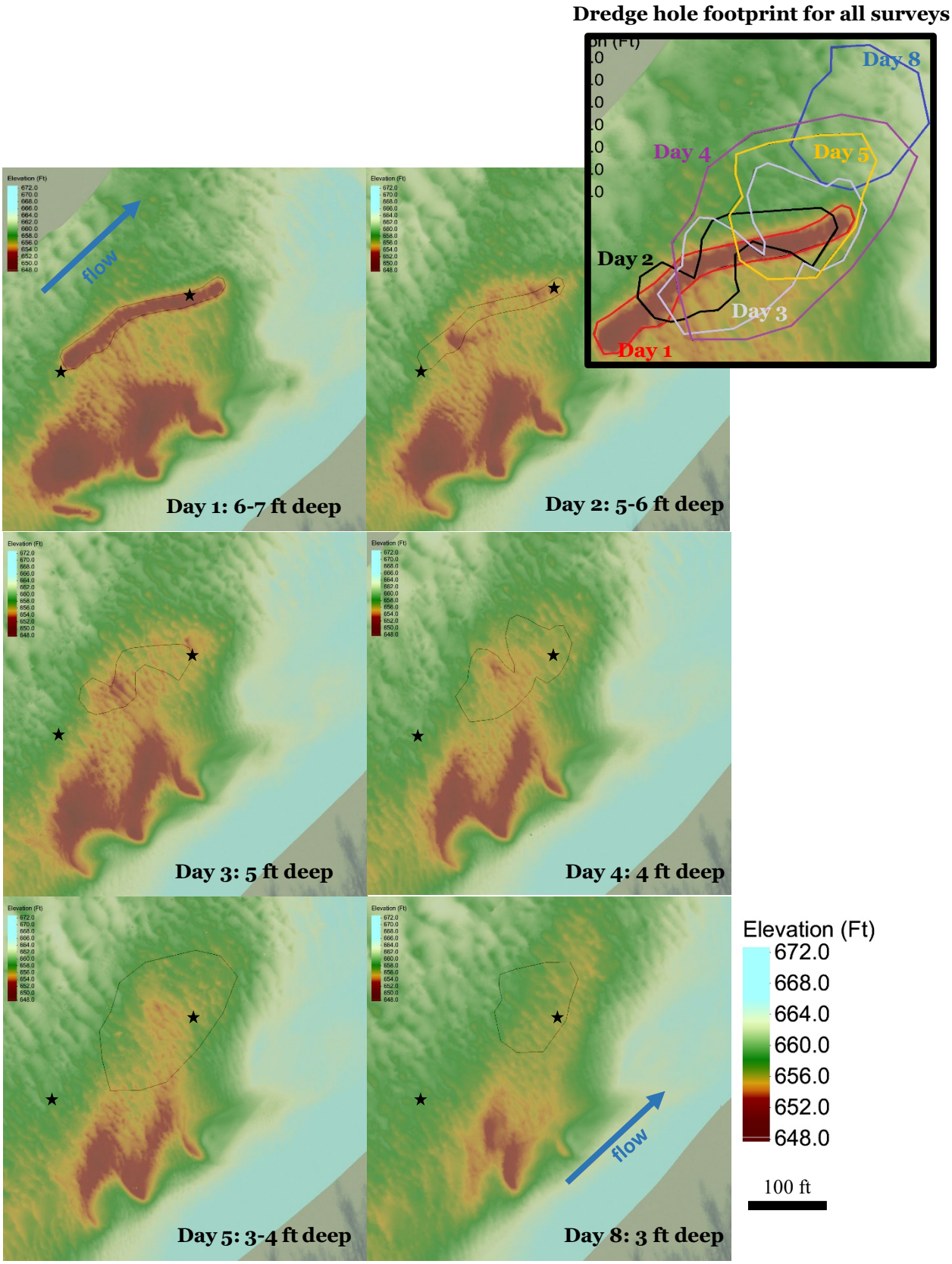

Figure 3. Dredge hole migration. Outline indicates preceding survey's dredge hole extents.

Limitations

The information presented in this abstract documents the attenuation of a single dredge hole under a specific set of conditions. Further data are required to generalize rates of attenuation to other dredge hole sizes, configurations, locations, discharge conditions, and dredging methodologies. Furthermore, this analysis only describes the localized, short-term effects of channel mining, not the long-term, reach-scale cumulative effects of multiple dredging events over years.

Conclusions

At a fairly constant river discharge of about 100kcfs, the depression created from a dredge event that removed 750 tons from a narrow 230 foot long segment of the riverbed persisted for over 8 days. The depression migrated 200 feet downstream, reduced in depth, and widened in lateral extents, resulting in an impacted area nearly double the size of the initial footprint. This information along with future examination of other dredge holes provides insight to the localized, short-term geomorphic response of the sandbed to commercial sand and gravel mining.

Forecasting

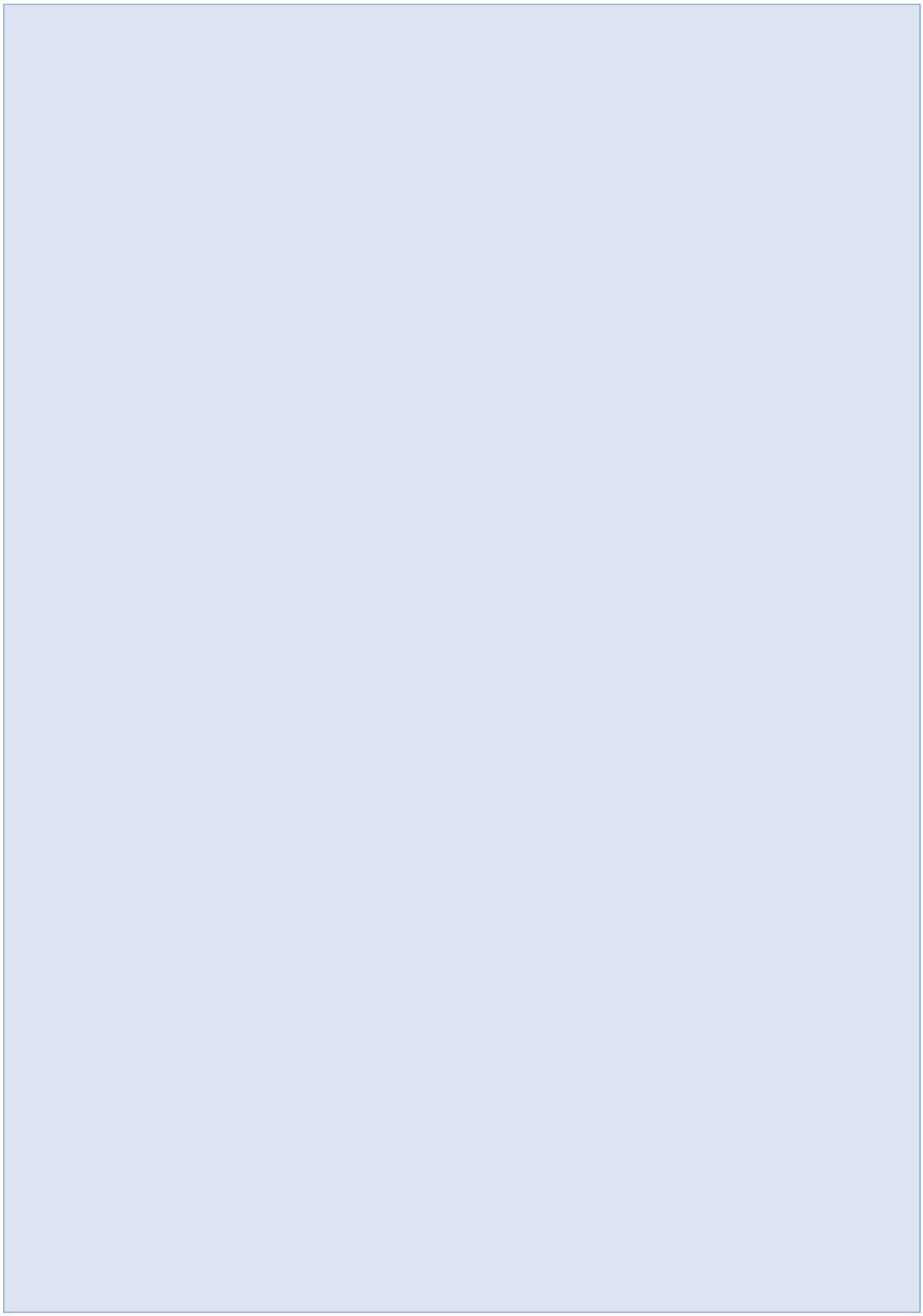

Multi-Agency Niagara River Short Term Forecasting Model

Katherine Labuhn, Hydraulic Engineer, U.S. Army Corps of Engineers, Detroit, MI, katherine.a.labuhn@usace.army.mil
Tim Calappi, Hydraulic Engineer, U.S. Army Corps of Engineers, Detroit, MI, tim.j.calappi@usace.army.mil
Drew Gronewold, Hydrologist, NOAA- Great Lakes Environmental Research Lab, Ann Arbor, MI, drew.gronewold@noaa.gov
Alison Macneil, Hydrologist, National Weather Service – Northeast River Forecast Center, Taunton, MA, alison.macneil@noaa.gov

Abstract

The Niagara River is the natural outlet of Lake Erie and drains four of the five Great lakes. The river is used to move commerce and is home to both sport fishing and tourism industries. It also provides nearly 5 million kilowatts of hydropower for approximately 3.9 million homes. Due to a complex international treaty, and the necessity of balancing water needs for an extensive tourism industry, the power entities operating on the river require detailed and accurate short-term river flow forecasts to maximize power output. A new forecast system was implemented that took advantage of several previously independent components including the NOAA Lake Erie operational Forecast System (LEOFS), a previously developed HEC-RAS model and input from the New York Power Authority and Ontario Power Generation. The Corps of Engineers updated the HEC-RAS model of the upper Niagara River to use the output forcing from LEOFS and a planned Grass Island Pool elevation provided by the power entities. The entire system is integrated at the NOAA Northeast River Forecast Center; it is run multiple times per day. The new model helps improve discharge forecasts by better accounting for dynamic conditions on Lake Erie.

This work focuses on choosing appropriate boundary conditions given the complexities of the system and the sensitivities of overlapping, real-time energy markets.

Introduction

The Great Lakes and the channels which connect them, contain approximately 20-percent of the world's supply of fresh water and provide numerous recreational and economic opportunities such as: commercial navigation providing over $18-billion annually to the region (Lre.usace.army.mil, 2019), commercial and sport fishing which generates over $5-billion annually (glerl.noaa.gov/education/ourLakes/Economy). The Niagara River is the natural outlet of Lake Erie and drains four of the five Great lakes. The river is used to move commerce (on the upper Niagara) and is home world class sport fishing and tourism industries. It also provides nearly 5 million kilowatts of hydropower for approximately 3.9 million homes. Due to a complex international treaty, and the necessity of balancing water needs for an extensive tourism industry, the power entities operating on the river require detailed and accurate short-term river flow forecasts to maximize power output.

A new forecast system was implemented that took advantage of several previously independent components including the National Oceanic and Atmospheric Administration (NOAA) National Ocean Service (NOS) Lake Erie Operational Forecast System (LEOFS), a previously developed HEC-RAS model and input from the New York Power Authority and Ontario Power Generation. The U.S. Army Corps of Engineers (USACE) updated the HEC-RAS (Hec.usace.army.mil, 2019), model of the upper Niagara River to use the output forcing from LEOFS and a planned Grass Island Pool elevation provided by the power entities. The entire system is integrated at the NOAA Northeast River Forecast Center; it is run multiple times per day.

The new model helps improve discharge forecasts by better accounting for dynamic conditions on Lake Erie. LEOFS captures seiche events on the lake that are often several meters of displacement from still water level. These seiche events translate into flow spikes HEC-RAS routes downstream. Knowledge of the peak arrival time and flood wave attenuation parameters helps improve operational decisions at the Grass Island Pool.

Model Development

Hydraulic Model

The HEC-RAS model for this project was based on a previous HEC-RAS model constructed by the USACE Buffalo District. That model is a steady state model with 117 cross sections, (figure 1) and limited information about bridge crossings. The model was used to help answer questions pertaining to general planning studies and did not require forecasted boundary conditions. The updates to original model are described below.

There are three bridges currently included in the model. All three bridges have low chord deck elevations that are unlikely to impact the flow in the river at any discharge but they are all resting on piers that obstruct the flow in the river. So instead of modeling the bridges using the bridges option they were modeled simply using the blocked obstruction option at two cross sections, one on the upstream face of the bridge and one on the downstream face of the bridges. The three bridges modeled this way were the International Railroad Bridge, the I-90 Bridge and the Peace Bridge. The stations and dimensions of the piers for I-90 Bridge and the Peace Bridge were estimated using Google Earth while the International Railroad Bridge data was included in the original model.

The Manning's n values for the model were set as 0.03 for all cross sections and then the seasonal roughness calibration tool was used in HEC-RAS version 5.0 to adjust them. The calibration section of this report has additional information.

The bathymetry used for the updated model consisted of a number of different sets of data and were all obtained from the USACE Buffalo District Office except for the TVGA survey of the Grass Island Pool for the New York Power Authority. These datasets consist of various resolutions, projections, datums and collection methods.

Once all the datasets were projected as needed, they were combined to create a Triangulated Irregular Network (TIN) surface that best represents the upper Niagara River to use with HEC-GeoRAS to update the existing cross sections from the model provided by the Buffalo District and also to add new cross sections where necessary.

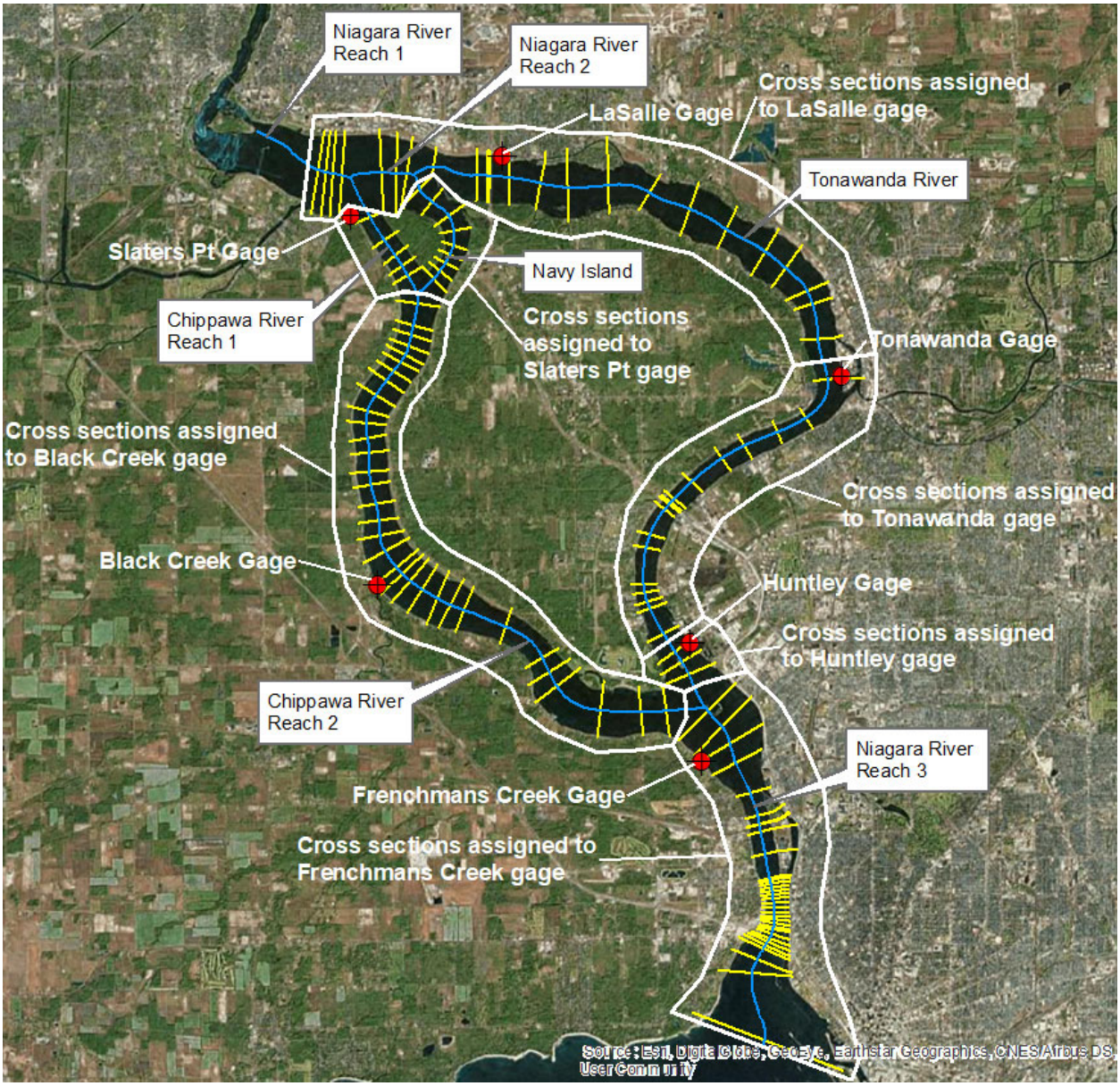

Figure 1. Map showing model layout, cross sections, gauge locations and automated calibration reach assignments

Calibration

Development of this model requires two sets of boundary conditions. One set for calibration, the other for operations. Both the upstream and downstream boundary conditions are straight forward for calibration. The boundary conditions for the operational forecast required more work.

Upstream Boundary Condition: The model currently extends from the outlet of Lake Erie downstream to the location of the Material Dock water level gage in the Grass Island Pool (GIP). During calibration, the upstream boundary condition is a flow time series based on the water level in Lake Erie. In order to calibrate the model the historic water level data at the

Buffalo water level gage was downloaded from the NOAA Tides and Currents website and converted to flow using the Buffalo rating equation shown below (U.S. Army Corps of Engineers, 2018).

$$Q = 643\ (Buffalo\ Water\ Level\ - 169.78)^{1.5}$$

For operational forecasting the upstream boundary condition is produced by LEOFS. LEOFS is a real-time, fully operational forecasting system built on the Finite Volume Community Ocean Model (FVCOM) (Chen, 2019) with roughly 6,000 nodes, 11,500 elements, 20 vertical layers, and grid sizes that vary in scale from 400m to 3.5km. Meteorological and hydrodynamic conditions are forecast every hour for each of these grids over a 120-hour forecast horizon with time increments of 60 minutes.

The authors evaluated water level simulations across a series of nodes near the outlet of Lake Erie, Figure 2, and isolated those that best represented what were believed to be actual water level fluctuations, using the nearby Buffalo, New York water level gaging station as a reference. Those nodes were then considered the best representation as the upstream boundary condition for the Niagara River HEC-RAS model in forecast mode.

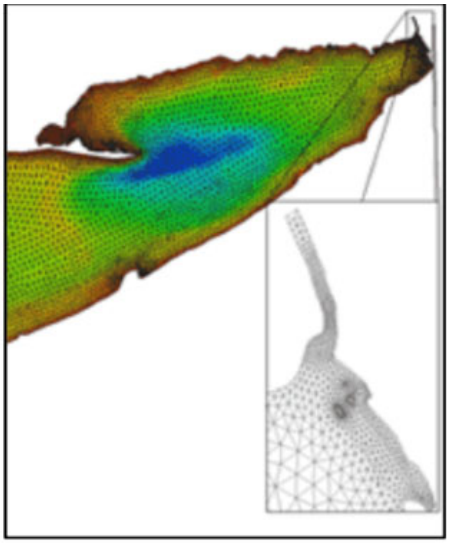

Figure 2. PLACEHOLDER GRAPHIC Detail of FVCOM grids within LEOFS in the eastern end of Lake Erie. Detailed insert shows grids in the transition between the Lake Erie outlet and the upstream section of the Niagara River

Downstream Boundary for Calibration:

The downstream boundary condition is a water level time series from the power entities' Material Dock water level gage for calibration. This gauge implicitly captures all of the operations affecting the water level in the GIP and makes it unnecessary to know the hourly operations affecting the pool.

The forecasting downstream boundary is complex and required extensive testing and sensitivity analysis to determine an appropriate amount of simplification. One of the complicating factors is the requirement for the boundary condition to be forecasted out several days. The following four boundary conditions were reviewed to determine accuracy and suitability.

1. The long term average monthly water level of the GIP
2. The estimated water level in the GIP computed by the Niagara River Control Center (NRCC) after all hydropower diversions and treaty regulated flows over Niagara Falls (referred to as the "Plan")
3. Normal depth
4. Using the Rules function in HEC-RAS to set the flow out of the model using information on the NRCC gated control structure, date, time of day and the amount of water withdrawn for hydropower usage

The ideal downstream boundary condition would be the fourth option which would extend the existing model past the GIP downstream to Niagara Falls. The Rules option would be coded to include frequent updates to flows through the River Control Structure gates and the combined flow diverted to the U.S. and Canadian hydropower plants. Due to the competing electrical markets, these forecasted operational flow data are sensitive and steps must be taken to ensure each hydropower entity's forecast is not made available to the other. Thus, this boundary condition was not considered for the real-time operational forecast model. However, for the purposes of calibration, the actual water level of the GIP were used as the boundary condition. This implicitly captures all of the complexity of the operations in the GIP.

There are six water level gages throughout the model domain that were used for calibration purposes. Figure 1 shows the locations of the gages. The Manning's n values were calibrated on a monthly basis using the automated roughness calibration tool now available in HEC-RAS version 5.0.1. All Manning's n values in the channel were set to a standard value of 0.03 in the geometry file and the seasonal roughness factors option was used to let HEC-RAS change the channel Manning's n value by month.

The automated roughness calibration tool works by assigning ranges of cross sections to an observed water level gage and then letting HEC-RAS vary the Manning's n value for the cross sections to match as close as possible the observed water level data at the gage. Figure 1 shows how the cross sections were assigned to the water level gages.

The model was run for each month and year in which gage data was available. Table 1 lists the available data by gage.

Table 1. Gage data available for calibration

Gage Name	Start Date	End Date
Frenchmans Creek	01 December 2003	18 June 2013
Huntley	12 February 2004	25 June 2012
Tonawanda	14 January 2004	23 June 2013
LaSalle	01 December 2003	19 June 2013
Black Creek	01 December 2003	18 June 2013
Slaters Point	01 December 2003	19 June 2013

The model was calibrated for the months of April to November. Although HEC-RAS has some ice modeling capabilities there are no relationships developed between ice cover/thickness and gage data for the Niagara River so the seasonal roughness values for December were set to be the same as November and the values for January to March were the averages between the November and April values.

Calibration Methodology

The model was run for the each month between April and November for the years of gage data available. Then the absolute differences between the model values and the gage values were calculated and averaged for each calibration month of each year. The results for each year were then reviewed against the following criteria:

1. The best calibration (lowest average departures between model and measured) for the Slaters Point and LaSalle gages since they are the closest gages to the GIP
2. The best overall calibration, defined by minimum average difference between model elevation and gage elevation, equation 1.

$$\min(average\ (modeled - measured)) \tag{1}$$

For example, Figure 3 shows the results for each April for the calibration years. As shown on the figure, the year 2004 had very low average errors for Slaters Point and LaSalle and also had the lowest difference between the six gages.

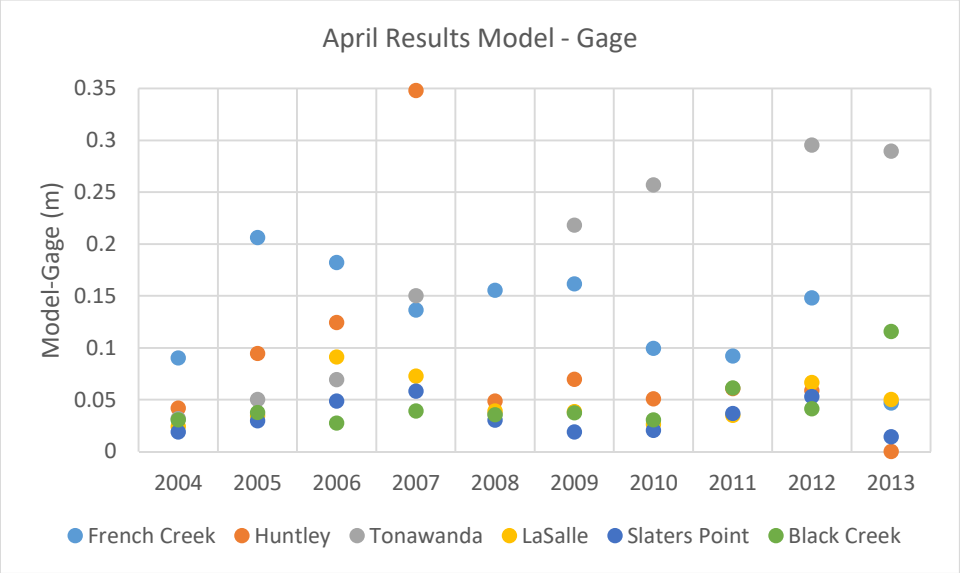

Figure 3. Calibration results for each April at all gauge locations

Based on the results above, the roughness factors calculated by HEC-RAS for April 2004 were set to be the seasonal roughness factor for April. Figures 4 through 9 show the results of using the April 2004 values at the six gages.

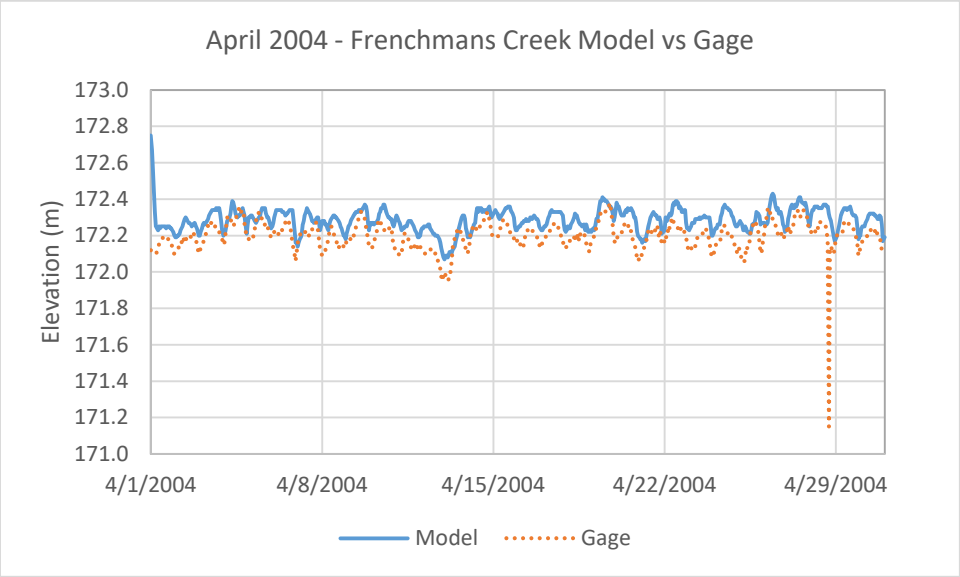

Figure 4. April 2004 Model Results vs Gage at the Frenchmans Creek Gage

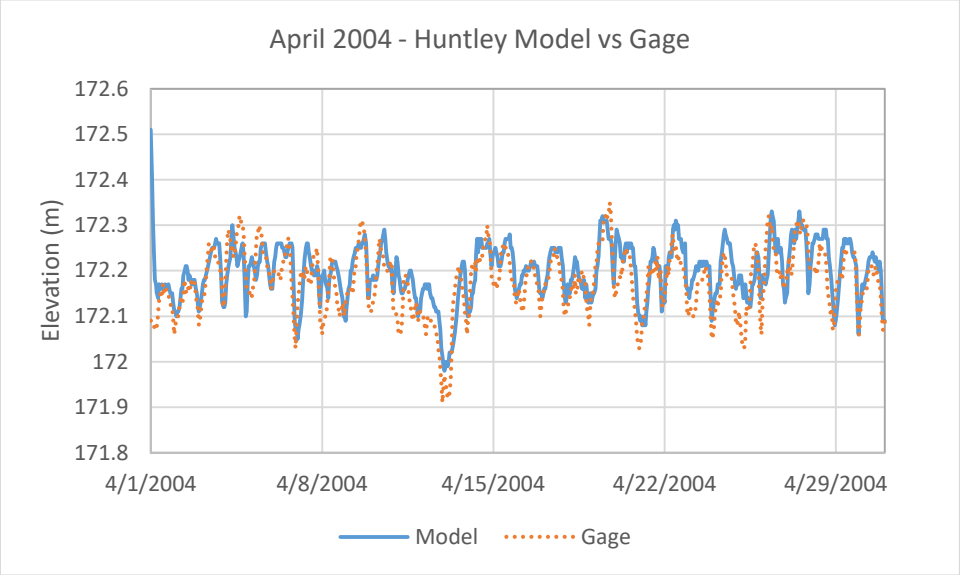

Figure 5. April 2004 Model Results vs Gage at the Huntley Gage

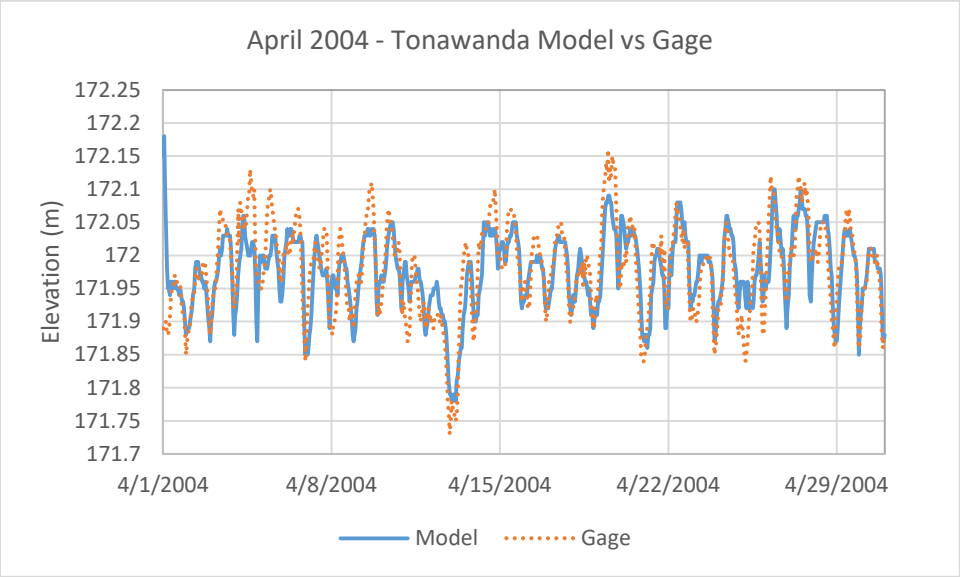

Figure 6. April 2004 Model Results vs Gage at the Tonawanda Gage

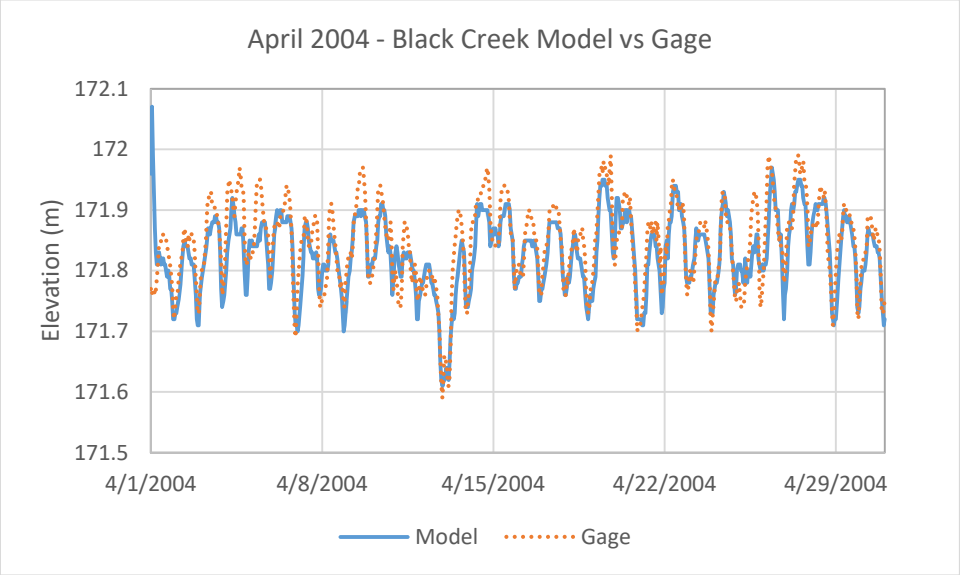

Figure 7. April 2004 Model Results vs Gage at the Black Creek Gage

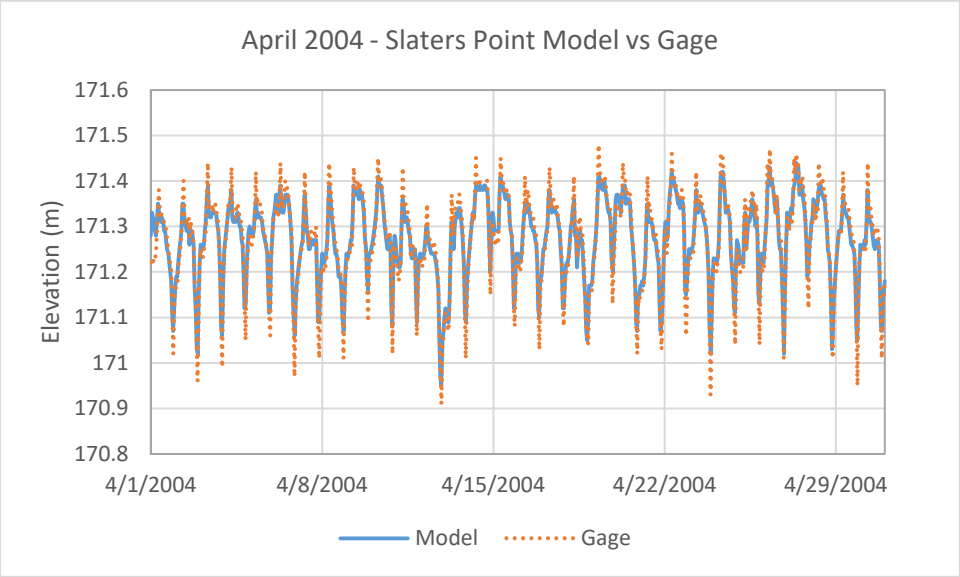

Figure 8. April 2004 Model Results vs Gage at the Slaters Point Gage

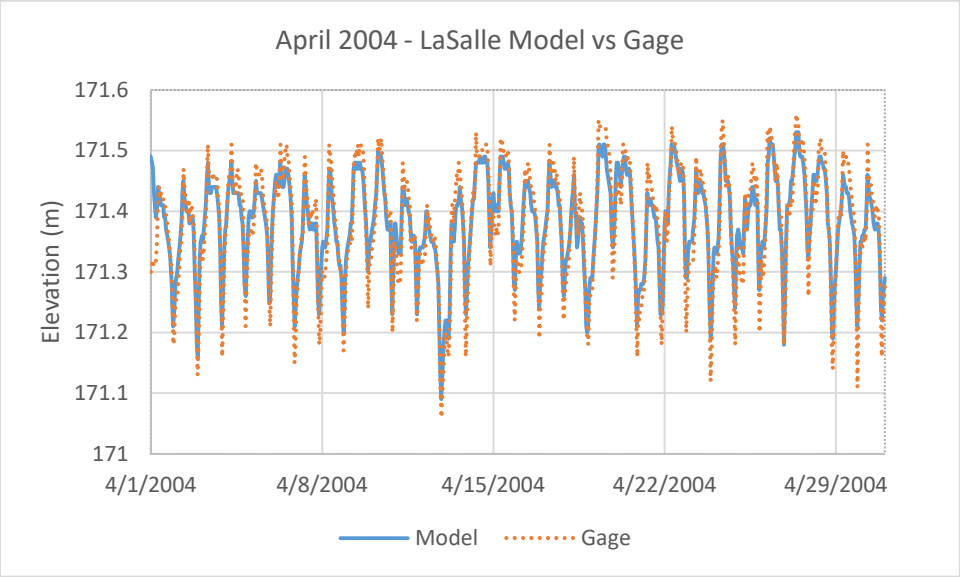

Figure 9. April 2004 Model Results vs Gage at the LaSalle Gage

The same methodology was used to determine the roughness factors for the months of May through November.

Forecasted Downstream Boundary

Long Term Average:

The long-term monthly average of the water level as reported at the Material Dock gage was considered as a static downstream boundary. While this boundary condition is easily forecastable it does not provide any temporal information about hydropower operations and is too simplistic for the purpose of forecasting discharge on the Niagara River.

The Plan:

The River Control Center develops estimates of GIP water levels at hourly resolution for an entire year. Each 24 hour period has the same cycle of water levels and the cycle changes each month. Using the GIP Plan as the downstream boundary condition has the advantage of a temporally varying boundary condition that can be reasonably well forecasted to coincide with the forecasted inflows at the upstream end of the model. Deviations are expected and at times are significant but the Plan has the advantage of informing the HEC-RAS model with a more likely, independent, temporally varying downstream boundary condition.

Normal Depth:

HEC-RAS can also use normal depth as a downstream boundary condition with a user specified slope. Normal depth occurs when the bottom slope of the river matches the slope of the water surface profile. While the normal depth boundary condition is best applied to sections with uniform flow, it is frequently applied to natural systems such as the Upper Niagara. Applying normal depth as the downstream boundary on the Niagara River does allow for a temporally varying boundary condition but only insofar as normal depth is a function of discharge and the discharge varies temporally. The probability of the water surface slope matching the bottom slope, especially during a flood wave associated with a seiche, is low. Normal depth also makes no attempt to capture the effects of independent, temporally varying hydropower operations.

Comparison of the Boundary Conditions:

The model was also run using the Material Dock water level gauge as the downstream boundary. For this modeling exercise, these flows were considered most representative of the actual flows entering the Grass Island Pool. Each of the three viable downstream boundary conditions for forecast operations were evaluated against model runs with Material Dock as the downstream boundary. Figures 10 through 12 show the model calculated flows at the upstream end of the GIP for April, July and November 2015.

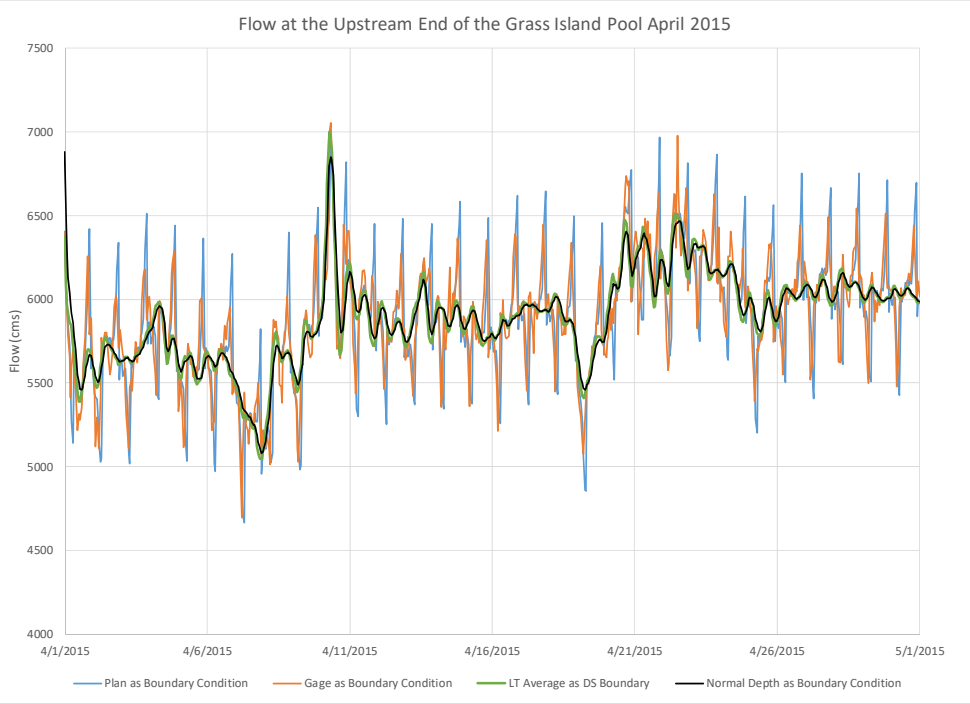

Figure 10. Modeled Flow at the Upstream End of the GIP April 2015 for 3 Boundary Conditions and the Material Dock Gage Data

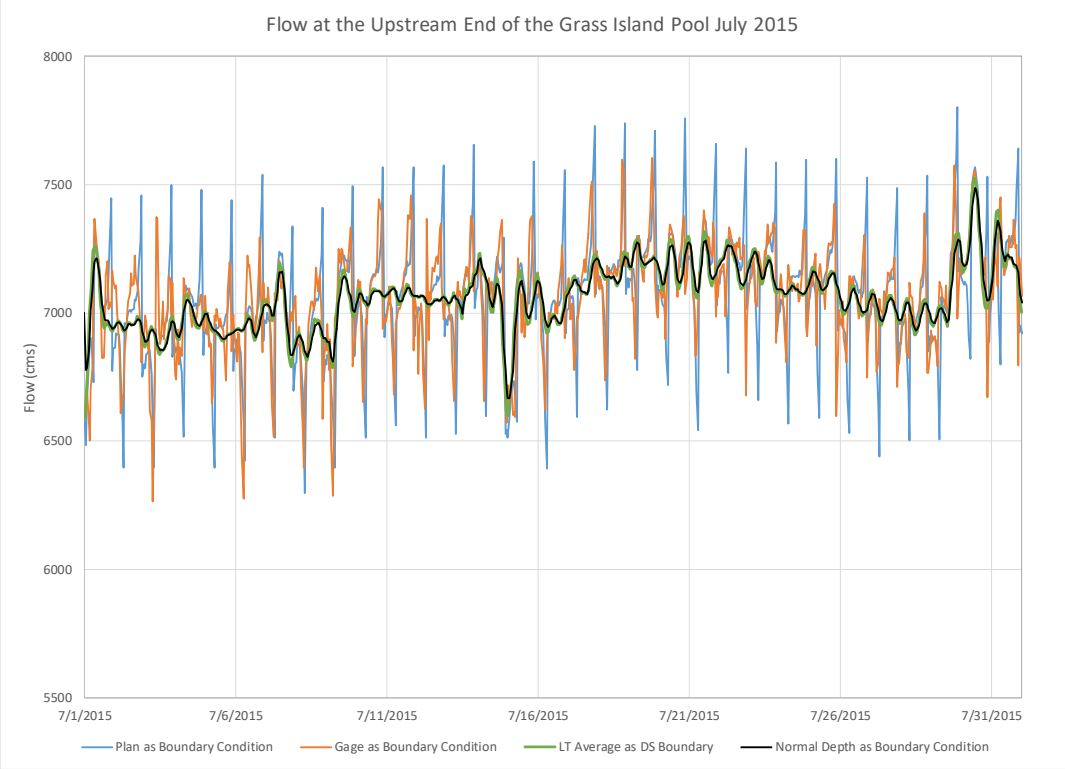

Figure 11. Modeled Flow at the Upstream End of the GIP July 2015 for 3 Boundary Conditions and the Material Dock Gage Data

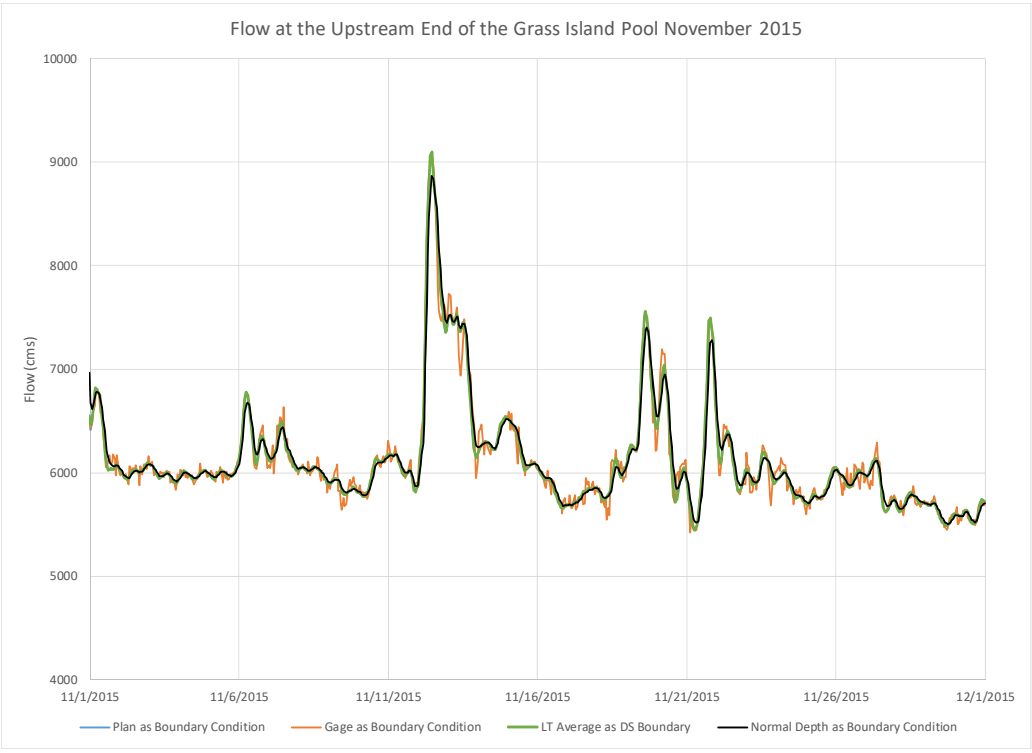

Figure 12. Modeled Flow at the Upstream End of the GIP November 2015 for 3 Boundary Conditions and the Material Dock Gage Data

The results for the two tourist season months (April and July) show that modeled discharges consistently underestimate peak flow and underestimates low flow when compared to modeled output using actual gauge data for the downstream boundary condition. The same is true when compared to modeled results with the long term average GIP as the downstream boundary condition. The results for the non-tourist season month (November) also show that modeled discharges underestimate peak flow for both the Plan and the long term average but to a lesser extent when compared to the tourist season. Using normal depth as the downstream boundary provides the smallest estimate of discharge into the GIP when compared to models with alternative downstream boundary conditions.

Recommendations

Based on the sensitivity analyses performed, it is the authors recommendation to use the Plan as the downstream boundary condition. Using the Plan adds a temporal variation component in the downstream boundary conditions. It enables the model to capture the cyclic nature of flow associated with regular hydropower operation, although it regularly under-predicts the high and low flow; it does, however, perform well under seiche events on Lake Erie, provided the LEOFS is forced with accurate meteorology.

The Niagara River HEC-RAS forecast model continues evaluation and improvement; the current version continues evaluation in operational mode at the National Weather Service, Northeast River Forecast Center. Forecasts are currently shared with the Niagara River Control Center and provide another tool to help regulate the water level in the Grass Island Pool at the head of Niagara Falls. Upon completion of model development, validation and implementation, results will be publically available.

References

Chen, Changsheng (2019). School for Marine Science & Technology - UMass Dartmouth Professor & Montgomery Charter Chair. [online] Umassd.edu. Available at: https://www.umassd.edu/directory/c1chen/ [Accessed 1 Apr. 2019].

Glerl.noaa.gov (2017). [online] Available at: glerl.noaa.gov/education/ourLakes/Economy [Accessed 15 Feb 2017]

Hec.usace.army.mil. (2019). HEC-GeoRAS. [online] Available at: https://www.hec.usace.army.mil/software/hec-georas/ [Accessed 1 Apr. 2019].

Hec.usace.army.mil. (2019). HEC-RAS. [online] Available at: https://www.hec.usace.army.mil/software/hec-ras/ [Accessed 1 Apr. 2019].

Lre.usace.army.mil. (2019). Great Lakes Navigation System: Economic Strength of the Nation. [online] Available at: https://www.lre.usace.army.mil/Portals/69/docs/Navigation/GLN_Strength%20to%20the%20Nation%20Booklet2013v2_final2w.pdf [Accessed 1 Apr. 2019].

U.S. Army Corps of Engineers, 2018, Review of Buffalo rating equation for Niagara River flows and discharge measurements made near the International Railway Bridge

Forecast-Informed Reservoir Operations: Lessons Learned from a Multi-Agency Joint Research and Operations Effort

Cary Talbot, Division Chief, Coastal & Hydraulics Laboratory, US Army Corps of Engineers, Vicksburg, MS, Cary.A.Talbot@usace.army.mil
Marty Ralph, Director, Center for Western Weather & Water Extremes, La Jolla, CA, mralph@ucsd.edu
Jay Jasperse, Chief Engineer, Sonoma Water, Santa Rosa, CA, Jay.Jasperse@scwa.ca.gov

Abstract

In May 2016, the US Army Corps of Engineers (USACE) updated Engineer Regulation 1110-2-240 which governs water control management throughout the agency. Included in the update is language that allows forecast information to be used for planning future operations which represents a significant change from the decades-long policy of operating solely to "water on the ground." Since 2014, a multi-agency research and development effort called Forecast-Informed Reservoir Operations (FIRO) has been exploring how advances in weather prediction and observations can inform operations and policy decisions at Federal, State and Local water management agencies with the collaborative engagement and support of researchers, engineers, operators and stakeholders. The FIRO Steering Committee consists of scientists, engineers and operators from research and operational elements of the National Oceanographic and Atmospheric Administration and the USACE, researchers from the US Geological Survey and the US Bureau of Reclamation, the state climatologist from the California Department of Water Resources, the chief engineer from Sonoma Water, and the director of the Scripps Institution of Oceanography's Center for Western Weather and Water Extremes at the University of California-San Diego. Viability assessments have demonstrated the potential for significant and simultaneous improvements in water supply, flood risk management and ecological benefits using current forecast skill. FIRO also includes efforts to improve forecast skill, particularly for atmospheric river events in the Western US, with the promise of increased benefit to water operations. Lessons learned from the formation of the FIRO steering committee, a research and development work plan and its execution, and the interfacing of the effort with the participating agencies' water management roles and stakeholders will be presented.

Introduction

A Key Policy Change

In May 2016, the US Army Corps of Engineers (USACE) updated Engineer Regulation (ER) 1110-2-240, Water Control Management (USACE, 2016). In section 3.3, Evacuation of Impounded Water, two key sentences are found at the end of the first paragraph in Sub-Section 3.3a. The first is a restatement of the principle of making water management operational decisions based on "the principle of water on the ground which is observed precipitation or observed snowpack" – a principle by which USACE has conducted water management operations for decades. However, the May 2016 update adds another sentence that has not previously been found in USACE guidance. It reads: "Forecasted conditions may be used for

planning future operations, but releases should follow the water control operations plan based on observed conditions within the watershed to the extent practicable." The inclusion of the phrase "forecasted conditions" opens the door for the concept of forecast-informed operations at USACE water control projects. However, like all ERs, guidance is provided about what can and cannot be done but details about how it is to be done are left for other guidance documents such as Engineer Manuals, Engineer Circular Bulletins, etc. Additionally, the change in policy in ER 1110-2-240 re-emphasizes the importance of the "water control operations plan" which, in most cases, is the Water Control Manual (WCM) for each project. However forecasted conditions are to be used for planning future operations at a particular water control project, the WCM for that project will need to be updated to reflect those procedures. Research and investigation into appropriate measures for incorporating forecasted conditions into water operations was therefore needed to determine how this policy change can be safely and effectively implemented.

Forecast-Informed Reservoir Operations

Since 2014, a multi-agency research and development effort called Forecast-Informed Reservoir Operations (FIRO) has been exploring how advances in weather prediction and observations can inform operations and policy decisions at federal, state and local water management agencies with the collaborative engagement and support of researchers, engineers, operators and regulators. A steering committee guides the FIRO effort for the pilot reservoir, Lake Mendocino in the Russian River watershed in northern California, and is comprised of scientists, engineers and operators from research, regulatory and operational elements of the National Oceanographic and Atmospheric Administration (NOAA) and the USACE, researchers from the US Geological Survey (USGS) and the US Bureau of Reclamation (USBR), the state climatologist from the California Department of Water Resources, the chief engineer from Sonoma Water (SW), and the director of the Scripps Institution of Oceanography's Center for Western Weather and Water Extremes (CW3E) at the University of California-San Diego. This paper will describe the formation and operation of the Lake Mendocino FIRO steering committee and research effort that has been conducted over the past four years, including lessons learned from engaging research, operations and regulatory perspectives in formulating, planning and carrying out the FIRO effort. Products including reports, tools and WCM deviations to allow for testing of FIRO approaches will be discussed along with the path forward for FIRO in helping define how forecasted conditions can be safely and effectively used in planning future water control management operations for the USACE and other agencies.

Background

Severe Drought in California

The water years 2012-2014 (October 2011 – September 2014) were the driest 3-year period in California history (Jones 2015). By early 2014, strict water conservation measures were enacted by local and state governments. Concerns arose over balancing agricultural water allocation reductions with associated job losses, and potential threats to the survival of endangered fish species. State and federal administrators and politicians took many actions, including the Governor's Drought Task Force visiting the Russian River's Lake Mendocino to highlight the drought crisis and announce water restrictions.

Russian River Watershed

Watershed Characteristics: The Russian River watershed is a 1485 mi² (0.95 M acre) watershed located north of the San Francisco Bay area in Sonoma and Mendocino counties in northern California (see Figure 1). The Russian River has an annual average discharge of 1.6 M acre-feet (ac-ft) with a main stem length of approximately 110 mi. There are two reservoirs located on tributaries of the Russian River: Lake Sonoma on Dry Creek in the western part of the watershed and Lake Mendocino on the East Fork in the northeast portion of the watershed. Both reservoirs are formed by dams that are owned by the USACE and are operated as multi-purpose reservoirs primarily for flood risk management in the winter by the USACE but in the warm seasons primarily for water supply by SW.

Atmospheric Rivers: Water management in the Russian River region is keyed to the existence or absence of large winter storms. The watershed is winter rain-driven, with a few atmospheric river (AR) storms each year bringing 40-50% of the annual rainfall. Atmospheric rivers (see Figure 2) are defined by the American Meteorological Society (AMS) as "a long, narrow, and transient corridor of strong horizontal water vapor transport that is typically associated with a low-level jet stream ahead of the cold front of an extratropical cyclone. The water vapor in atmospheric rivers is supplied by tropical and/or extratropical moisture sources. Atmospheric rivers frequently lead to heavy precipitation where they are forced upward—for example, by mountains or by ascent in the warm conveyor belt. Atmospheric rivers are the largest "rivers" of fresh water on Earth, transporting on average more than double the flow of the Amazon River" (AMS 2016). The two multi-purpose reservoirs in the Russian River watershed provide storage for warm-season uses, and there is little to no snow pack to extend the runoff season. The same ARs that provide beneficial water supply can also cause flooding when ARs stall. Analysis of National Flood Insurance Program claims over the past 40 years, correlated with a 70-year catalog of AR events in the western US reveals that 84.2% of all

Figure 1. The Russian River watershed with location of Lake Mendocino and Lake Sonoma reservoirs and the Potter Valley Project depicted.

Figure 2. Color shaded contours of Integrated Vapor Transport (IVT), a measure of AR strength, from a global weather model forecast run. *Figure courtesy CW3E.*

insured losses in the western U.S. are associated with ARs (Corringham et al. 2019). In Sonoma County, the county which experienced the greatest losses of all 414 counties in the West, this figure is 99.8%.

Russian River Challenges: The Russian River provides water for over 650,000 people in Sonoma, Marin, and Mendocino counties in California in addition to supporting Sonoma and Mendocino County wineries, one of the most valuable agricultural areas in the U.S. and a major tourist area. The river also supports 3 salmonid species listed under the federal and state Endangered Species Act. Consequently, the Russian River is the focus of a biological opinion from NOAA's National Marine Fisheries Service (NMFS) and California Department of Fish and Wildlife aiming to restore species viability while balancing water supply and flood management operations by the USACE and SW (USGS 2017). The multiple purposes, which often seem to be in conflict with one another, are exacerbated by droughts and water shortages. The combination of flood risk and sustained drought conditions represents a major challenge to water managers, agriculture, endangered species and tourism in the Russian River watershed. It is for these reasons that this watershed is a National Integrated Drought Information System (NIDIS) pilot activity area, as well as an Integrated Water Resources Science and Services (IWRSS) demonstration area, the NOAA Habitat Blueprint demonstration watershed, and a Hydrometeorology Testbed for NOAA.

Potter Valley Project: An additional challenge in managing water resources at Lake Mendocino is a reduction in the inflow to the reservoir that has historically come from an inter-basin water transfer from the nearby Eel River to the headwaters of the East Fork of the Russian River through the Potter Valley Project, a power generation operation owned and operated by Pacific Gas & Electric (PG&E)(See Figure 1). In 2004, relicensing of the Potter Valley Project by the Federal Energy Regulatory Commission placed limits on the amount of diverted water, reducing the average annual inflow by 57%, from ~150,000 ac-ft to ~90,000 ac-ft. Given that the winter-time water supply capacity of Lake Mendocino is 68,400 ac-ft and the WCM for the reservoir was developed based on the historic larger Eel River diversion, this significant reduction in inflow indicates an existing need to update the WCM for Lake Mendocino.

FIRO Steering Committee

Participation in IWRSS activities for the Russian River demonstration area led to discussions among federal, state, local and academic partners regarding how a new approach, building on improvements in AR science, and in response to the continuing drought, could explore the potential viability of using forecasts to inform operations at reservoirs, using Lake Mendocino as a pilot. The steering committee formed to guide the project, is comprised of leading civil engineers, hydrologists, meteorologists, climatologists and biologists, including the engineers responsible for day-to-day operation of Lake Mendocino. Committee membership was purposefully chosen to bring together representatives from the relevant organizations that had responsibility for operations and regulation at Lake Mendocino but also for conducting research into the relevant physical processes that impact water management operations, namely meteorological forecasts and hydrologic and hydraulic modeling.

The Lake Mendocino FIRO Steering Committee (SC) is co-chaired by the CW3E director, representing leading academic research into improving the understanding and prediction of atmospheric rivers in the west, and the SW Chief Engineer, representing a local agency that operates Lake Mendocino for water supply and ecological compliance purposes. The committee

is further comprised of the State Climatologist from the California Department of Water Resources (CA-DWR), representing the state perspective of water resources from a seasonal perspective, the Hydrologist-in-Charge from the California-Nevada River Forecast Center (CNRFC) of the National Weather Service (NWS), representing the federal agency responsible for operational river flow forecasts across the region, a senior fisheries expert from the West Region office of NOAA NMFS, representing the regulatory perspectives of enforcement of the biological opinion for salmonids in the Russian River, the Director of the Physical Sciences Division in NOAA's Earth System Research Laboratory, representing the research perspective from the federal agency responsible for providing weather forecasting capability, the senior water management chiefs from the USACE Sacramento and San Francisco Districts, representing the operations perspectives of the federal agency tasked with flood risk management of reservoirs in central and northern California, the program manager from the USACE Engineer Research and Development Center (ERDC), representing the research perspectives of the federal agency responsible for managing flood risk, the head of research from the USBR, representing the perspective of the federal agency responsible for managing, developing and protecting water resources in the west, and the senior atmospheric science researcher from the USGS, representing the research perspective from the federal agency responsible for providing reliable scientific information for managing water resources.

The first full meeting of the Lake Mendocino FIRO SC was held in December 2014 and terms of reference for the committee were agreed upon. The committee agreed to meet at least quarterly but smaller subcommittees would meet and interact more frequently as needed to ensure delivery of products of the effort. It was also determined that a work plan was needed to guide the research effort in exploring the viability of using forecast information in an operational setting. It was also recognized that the input and interaction between engineers, scientists, operators and regulators would be crucial to the success of the development of the work plan as well as the execution of that work plan over the course of the effort. Between December 2014 and September 2015, a 5-year work plan was developed and published in October 2015 (Jasperse et al. 2015). The work plan serves to provide the road map for the effort as it has progressed from the initial concept through to all stages of the effort that will be described in the following sections.

Preliminary Viability Assessment

Designing the Assessment

The Lake Mendocino FIRO work plan laid out a multi-step strategy to assess the viability of FIRO. The first step in the plan was to carry out a Preliminary Viability Assessment (PVA), conducted over two years, to be followed by a Full Viability Assessment (FVA), which would require substantial additional effort over roughly another three years. The PVA considered the following questions:

1. If FIRO is implemented, will reservoir operation improve reliability in meeting water management objectives and the ability to meet environmental flow requirements, and to what extent?
2. If FIRO is implemented, will reservoir operation adversely affect flood risk management in the system? If so, where and to what extent can that be mitigated?
3. What meteorological and hydrological forecast skill is required to enable FIRO to be implemented? Is current forecast skill for landfalling ARs (and their associated heavy precipitation and runoff) and other extreme precipitation events adequate to support

FIRO, and what improvements would be needed to enable full implementation of FIRO for Lake Mendocino?

The SC's strategy for decision making was this: If the PVA suggested FIRO would be viable, the project team would move forward with the FVA. Due to the preliminary nature of the analysis, the PVA relied on representations of FIRO system components, reasonable simulation of performance of those components, and anticipated flexibility in operation of Lake Mendocino under FIRO. In the subsequent FVA, candidate components of the Lake Mendocino FIRO system would be identified; the forecast parameters and associated forecast skill requirements would be quantified; research to improve forecast skill to meet those requirements would be conducted; alternative components formulated, assessed, and compared; and a plan for implementation developed. If necessary components do not exist, research and development (R&D) programs would be identified in the FVA, and work initiated to develop the components. Finally, necessary changes to the operation rules, as defined in the project's WCM, and the process for modifying the rules would be identified in the FVA consistent with USACE procedures and protocols to support consideration of a WCM update. If the PVA found FIRO implementation not viable, the project team would identify scientific and operational enhancements necessary to make FIRO viable. The team then would initiate an R&D effort to provide those enhancements (FIRO Steering Committee 2017).

Conducting the Assessment

The PVA was undertaken in three parts: analysis of the hydrometeorological forecast requirements and assessment of current forecast skill; a study to determine whether forecast informed operation could improve reliability of meeting water management objectives; and a parallel coordinated study to demonstrate whether forecast informed operation could improve reliability of meeting water management objectives while not increasing flood risk.

Assessing Current Forecast Requirements and Skill: For the first part of the study, to support anticipated changes in operational decision making, SC members quantified forecast skill requirements. They determined that 5-7 days lead time is needed on forecasts of 2 inches of rain above Lake Mendocino in 24 hours, which requires accurate prediction of AR landfall location, strength, and timing as well as runoff efficiency and timing. They also assessed current skill. This analysis determined that prediction of AR landfall and streamflow has meaningful skill, from a flood risk management standpoint, out several days, but improvements are needed in forecasting timing, location, strength and duration, while extended periods of dry weather were found to have greater predictability than the details of AR landfall and runoff.

Assessing If FIRO Can Improve Water Management Reliability: For the second part of the PVA, SW analysts developed and used mathematical models to assess improvements to reliability of meeting water management objectives and ability to meet environmental flow requirements. For a range of meteorological and hydrologic conditions, they simulated Lake Mendocino operation with a variety of FIRO alternatives. The Perfect Forecast Operations alternative represents flexibility in operation rules and assumes perfect forecast skill (using the inflows that actually occurred as the forecasts), which establishes a theoretical maximum benefit. The Ensemble Forecast Operations (EFO) alternative represents the same flexibility in operation rules but reflects current forecast skill and is thus more realistic. The Hybrid Operations (HO) alternative represents an initial or interim implementation of FIRO by providing a band of storage – up to 10% of current storage during the winter months – that offers the operators flexibility to selectively store or release water according to forecasted and

observed conditions in the watershed. The SW analysis used a "risk-based" decision process to determine releases, considering probability of future failures to satisfy targets. Performance metrics used for the SW analysis include:

- End of water year storage
- Dry season environmental flows
- Discharge at Hopland and Healdsburg
- Uncontrolled spill from Lake Mendocino.

Assessing FIRO Flood Risk Impacts: For the third part of the PVA, analysts from the USACE Hydrologic Engineering Center (HEC) focused on flood risk impacts. To do so, they simulated Lake Mendocino flood operation for a wide range of meteorological and hydrologic conditions, accounting for flow requirements for water management objectives and environmental purposes. HEC analysts also considered a variety of FIRO alternatives. The Encroach alternative represents a simple FIRO alternative based on perfect precipitation forecasts. The Combined alternative represents a more complex FIRO alternative based on perfect forecasts of several types of data. The EncroachWIF (with imperfect forecast) alternative is the same as the Encroach alternative but is assessed using imperfect precipitation forecasts. Streamflow forecast uncertainties, however, were not included in this analysis. Performance metrics used for the flood risk analysis include:

- End of water year storage
- May 10 storage (when maximum conservation storage becomes available each year)
- Expected annual damage (EAD) and average annual damage (AAD) reduction
- Discharge and stage frequency at Hopland, Healdsburg, Guerneville, and Lake Mendocino
- Uncontrolled spill from Lake Mendocino.

PVA Results and Findings

The analyses completed for the PVA demonstrated forecast informed operation, as simulated in the studies, improved reliability of meeting water management objectives without adversely affecting flood risk management in the basin.

Forecast Skill Analysis: Overall, CW3E found forecasts to support FIRO were available or could be produced with enhancements that will be available through additional research. Skill in precipitation forecasting was best during extended dry periods, and appears viable for use in FIRO; however, significant errors remain during stormy periods. Current and ongoing efforts seek to study (1) the predictive skill of transitions from extended dry periods into wet periods and (2) the predictive skill of ensemble-based forecasts of atmospheric water vapor flux during AR-type storm events. Individual cases of past events illustrate meaningful skill in (1) transitions out to 3 days lead time on average and up to 5 to 7 days leads for individual cases and (2) ensemble-based water vapor flux forecasts out to 5–6 days lead time on average and up to 9 days lead for individual cases.

Analysis of the river channel geometry and operating release rates from Lake Mendocino showed that it would likely take roughly 2 days to release up to 10,000 ac-ft without exceeding the established target flow rate and then 2 to 3 days for that release to move downstream past the flood-prone town of Guerneville. Thus, skill is required at 5-days lead time for prediction of landfalling ARs and their associated heavy precipitation and runoff.

The PVA reaffirms that ARs are the key to flooding on the Russian River, and errors in their prediction are the primary source of uncertainty in the prediction of major precipitation and runoff events affecting Lake Mendocino, its watershed, and the Russian River. The PVA demonstrates that errors in precipitation and streamflow forecast result partly from errors in the timing, duration, intensity, and location of landfalling ARs, mesoscale frontal waves (a disturbance that forms offshore and can change the locations and duration of AR landfall and associated heavy precipitation), and inaccuracies in the representation of clouds and precipitation.

The PVA identifies the need for efforts targeted at the development of weather prediction models tailored toward improving forecasts of precipitation and landfalling ARs over the Russian River, such as the development of a specialized version of the Weather Research and Forecasting model (WRF)(Skamarock et. al, 2008), called "West-WRF" which is being developed at CW3E. Also identified are (1) the need for additional unique performance and model evaluation metrics for precipitation and landfalling ARs that illustrate trends and improvements in forecast skill of existing models and derived decision support tools, and (2) additional integration of existing and reconnaissance-based observational datasets (e.g., mesonets and aircraft data offshore, respectively) that serve to improve the potential viability of FIRO at Lake Mendocino or any other potential location.

SW Analysis: The SW analysis with FIRO alternatives showed significant additional storage that resulted in improved reliability of meeting water management objectives. Compared with existing operations, additional water was stored and available for delivery for nearly all years simulated. Table 1 shows the median end of water year storage for the 1985-2010 period for existing operations and each FIRO alternative. Increases attributable to FIRO as modeled range from 8,633 ac-ft to 27,780 ac-ft, or up to a 49% increase for the Perfect Forecast Operations scenario.

Table 1. Potential improved reliability in meeting water management objectives achieved by FIRO alternatives in terms of increase in median end of water year storage based on simulation results for 1985-2010

FIRO Alternative	Median End of Water Year Storage (ac-ft)	Increase over Existing Conditions (ac-ft)	Percent Increase
Existing Operations	56,220	-	-
Perfect Forecast Operations	84,000	27,780	49%
Ensemble Forecast Operations	76,277	20,057	36%
Hybrid Operations	64,853	8,633	15%

HEC Analysis: The HEC analysis showed no significant loss of ability of the system to manage flood risk for the Russian River basin. HEC assessed risk in terms of AAD and EAD. AAD was computed from a continuous simulation over the Period of Record (PoR), 1951 – 2010. EAD was computed from a probabilistic Monte Carlo assessment of 5,000 events. Table 2 lists the computed AAD and EAD for the existing operations and the tested FIRO alternatives.

Table 2. AAD computed from a continuous Period of Record (PoR)(1951-2010) and EAD computed from a probabilistic Monte Carlo Flood Risk Analysis (FRA) using 5,000 events

	PoR Compute (60 years, 1951-2010)		FRA Compute (5,000 events)	
FIRO Alternative	AAD ($ million)	Increase in AAD from existing ($ million)	EAD ($ million)	Increase in EAD from existing ($ million)
Existing Operations	6.10	-	10.4	-
Combined (complex, perfect forecast)	6.10	0	10.4	0
Encroach (simple, perfect forecast)	6.10	0	10.5	0.10
EncroachWIF (simple, imperfect forecast)	6.10	0	10.5	0.10

PVA Recommendations

As a result of conducting and reviewing the findings of the PVA, the FIRO Steering Committee's recommendations are to:

1. Conduct a full viability investigation in detail, considering and selecting components of the system and FIRO strategies that could be implemented in the near-term using current technology and scientific understanding (e.g., forecast of near-term dry conditions); and
2. identifying and developing new science and technologies that can ensure FIRO implementation is safe and successful, and to enhance FIRO where possible; and
3. working with USACE and SW, the SC should develop a plan for utilizing major deviations to the WCM for each of the next few years. Each deviation request by the SC to USACE would be designed to explore the viability of implementing certain FIRO strategies using current forecast skill and technology with the appropriate constraints and limitations that meet USACE conditions for deviations per USACE South Pacific Division (SPD) policy. It is anticipated that each subsequent deviation request will build on the prior years' experience and will be modified as appropriate with the concurrence of USACE, SW and the SC. The SC should also work with USACE and SW to determine what types of changes to reservoir operation rules are most effective to allow various levels and components of FIRO implementation, and what types of changes to reservoir operation rules will be acceptable to USACE (for example, rules that shift to accommodate forecasts of an extreme event). To achieve permanent implementation of FIRO, USACE approval will be required through an update of the WCM.

The PVA process also identified additional areas of investigation to be conducted as part of the recommended Full Viability Assessment (FVA). These areas include:

- Although elements of the PVA considered the possibility of encroaching into the conservation pool prior to a predicted flood-producing storm, the PVA mostly emphasized consideration of retaining extra water to reduce drought impacts. A greater emphasis should be put on exploring how changes to the operating rules to permit pre-releases before a major landfalling AR could enhance the flood risk mitigation capacity of Lake Mendocino.
- What forecasting methods and technology (e.g., meteorological and watershed observations and models) must be enhanced to enable implementation of FIRO? While hydrometeorological forecasts of sufficient accuracy may be available for the Russian

River watershed in many instances, important gaps remain in the details, even for shorter lead times. In addition to better skill in the details of extreme event prediction at short lead times (up to 5 days), enhancements are also required for forecasting with longer lead times (5 days to several weeks) to fully realize the potential improved reliability in meeting water management objectives.

- In addition to forecasts, successful FIRO depends on whatever knowledge is available regarding the current hydrologic state of the reservoirs, river (and tributaries), and watershed at the time of decisions. Scientific inquiry and plans to ensure that monitoring of the state of the system is adequate, or to improve monitoring, is needed.
- Evaluation of emerging watershed and runoff forecast systems such as NOAA's National Water Model and USACE's Gridded Surface Subsurface Hydrologic Analysis (GSSHA) model run at temporal and spatial scales that directly support FIRO goals and objectives. GSSHA is particularly suited to potentially provide benefit to water management decisions given its spatially distributed nature and the coupling of groundwater with hydrologic flow processes.
- Needed software enhancements to the suite of tools used in USACE water management, the Corps Water Management System (CWMS), such as the ability to evaluate reservoir inflow and downstream flow forecasts based on ensemble rather than deterministic forecasts, were identified. Eventual implementation of FIRO will require that these tools be added to CWMS.

Full Viability Assessment

Elements of Viability Assessment

The FVA is being conducted at this time under direction from the FIRO SC and in coordination with senior leaders from USACE Headquarters and SPD who have purview over water management. The FVA consists of several elements, some of which are described in detail in the following sections.

Interim Operations: The Hybrid Operations scenario, developed in the PVA, was used as a basis for the FIRO SC to request a Major Deviation to the operations at Lake Mendocino for Water Year 2019. This request was supported by PVA study findings in addition to "virtual operations" – operations that were conducted and tracked only virtually – during Water Year (WY) 2017 for Lake Mendocino. WY 2017 was the wettest water year on record according to CA-DWR's eight-station precipitation index, which tracks conditions in the largest Central Valley watersheds important to water supply (CA-DWR 2017). The west coast was hit by an unusually high number of ARs – 49 in total – with 16 being either strong or extreme in intensity. Given these extreme conditions, it was especially informative to have virtual operations tracking how FIRO might impact flood risk during the wet season as well as end-of-year water supply. Figure 3 plots the Hybrid Operations (HO) against the actual operations conducted that year. Note that a minor deviation, requested by SW, was in place at the time and which allowed for a 5% increase in the top of water conservation pool from mid-January until mid-March 2017, as noted by the purple dashed line in Figure 3. The green dashed line in Figure 3 depicts the modified guide curve which is a 10% increase over the guide curve defined in the current WCM for Lake Mendocino (dashed yellow line). A 10% increase is the maximum allowed deviation in a Major Deviation request according to USACE policy.

Note in Figure 3 that due to the forecast-informed nature of the HO, releases ahead of large precipitation events, which caused significant rises in reservoir storage in the actual operations, allowed the HO scenario to consistently have significantly lower peak storage values throughout the rainy winter, representing an improved condition from a flood risk management perspective. Additionally, the late-season rains were captured and stored by the HO, providing for an additional 5500 ac-ft in end-of-season storage compared to the actual operations. These virtual operations demonstrated that the potential for improving both flood risk and water supply management objectives is possible by using a FIRO scenario, even in a record-setting wet year.

Figure 3. Plot of actual (observed) operations and the virtual FIRO-developed Hybrid Operations scenario at Lake Mendocino during a portion of Water Year 2017. *Figure courtesy Sonoma Water.*

The requested Major Deviation was approved by SPD in early November 2018 and the reservoir operated with the modified guide curve (dashed green line in Figure 3) in WY 2019. Valuable data regarding how decisions are made by the water managers at Lake Mendocino while operating under the HO in WY 2019 will be used to make modifications to additional Major Deviation requests in coming seasons until a final WCM update request is made at the conclusion of the FIRO effort at Lake Mendocino.

Decision Support System: A decision support system (DSS) was developed to provide water managers with a set of tools to bring together the various pieces of data, including ensemble forecasts of AR conditions from West-WRF and other atmospheric models, CNFRC inflow forecasts, and watershed, reservoir and downstream conditions. With all of these various pieces of data together in one place, water managers have ready access to more information upon which to make operational decisions. A schematic of how the FIRO DSS works in practice is shown in Figure 4. The California Data Exchange

Figure 4. Schematic of FIRO Decision Support System elements and how reservoir operators can use it to inform release decisions. *Figure courtesy Sonoma Water.*

Center (CDEC) in the figure is a state-wide clearinghouse for water resources data and is operated by the CA-DWR. Lake Mendocino operators were trained in the use of the FIRO DSS at the start of WY 2019.

Technical Studies: In order for FIRO to be incorporated into standard USACE water operations, capabilities of the functional components of CWMS are being added to allow, among other things, for the ability to link to and evaluate reservoir inflow and downstream flow forecasts based on ensemble rather than deterministic forecasts. These capabilities will aid in conducting the FVA at Lake Mendocino and other candidate reservoirs but will also provide a means of carrying out FIRO at reservoirs in an operational context.

Full viability assessment of FIRO at Lake Mendocino requires the evaluation of FIRO under extreme conditions, including historical peak flows (e.g. 1964 for Lake Mendocino). This will require simulation of forecasts and flows that are outside the record of past forecast information archived by the CNRFC (the current archive reaches back to approximately 1980). A process for generating synthetic forecasts for past events that are beyond the extent of the CNRFC archive is being developed and will be used to provide forecast information that will enhance the FVA of FIRO at Lake Mendocino.

The PVA evaluated the flood risk management impacts of FIRO from the perspective of maximizing water supply without increasing flood risk. Another technical study that is being conducted in the FVA will quantify the flood risk benefits that come from FIRO pre-releases similar to what was demonstrated in the WY 2017 virtual operations shown in Figure 3. Quantifying the impact of FIRO from flood damages prevented, and ecological, agricultural, socio-economic, and water management reliability benefits will be an important factor in conveying the full benefits of implementing FIRO at this and other locations.

Scientific Research: Since the inception of the FIRO effort in 2014, the largest investment of research effort has been made in improving forecast skill, particularly with respect to ARs given their importance to water management issues in the western US. This investment continues with efforts focused on continued West-WRF development and scientific investigations into fundamental questions regarding AR formation, intensification, migration and dissipation. AR research is aided by an investment into a campaign of AR reconnaissance missions made possible through a multi-agency collaboration of atmospheric researchers led by a steering committee comprised of leading scientists engaged in collecting and analyzing atmospheric data. In the rainy winter months during 2016, 2018 and 2019, AR

Figure 5. Flight plan for AR reconnaissance mission in January 2018 using two Air Force C-130 and the NOAA G-IV research aircraft. *Figure courtesy CW3E.*

reconnaissance missions were conducted using US Air Force Reserve C-130 aircraft from the 53rd Weather Reconnaissance Squadron, aka "The Hurricane Hunters", and the NOAA Gulfstream G-IV research aircraft. When operational, the AR Recon SC meets to evaluate weather forecasts, calling for recon missions to have ARs probed with aircraft releasing dropsondes along strategically planned routes (see Figure 5). These missions collect atmospheric data to feed into global weather models providing key data from areas of the globe where observation data is often absent and where atmospheric dynamics are influencing the location, intensity and duration of ARs that are poised to impact the western US.

Figure 6. Map of data collection stations located above Lake Mendocino in the Russian River watershed. *Figure courtesy CW3E.*

In addition to the aircraft-based AR recon efforts, land-based efforts are also conducted which include releases of weather balloons carrying radiosonde instruments from key locations as ARs approach and strike along the coast. Surface meteorology data (temperature, pressure, relative humidity, precipitation) and soil conditions (moisture and temperature) at 6 depths up to 1m below the surface are also collected from six stations spread throughout the Russian River watershed as shown in Figure 6. This instrumentation augments the NOAA's 14 existing hydrometeorological testbed stations which measure the same parameters. Two of the sites installed by CW3E in the Russian River also include vertically pointing radars, disdrometers that measure size and velocity of hydrometeors, and GPS-Met sensors that measure the amount of integrated water vapor in the atmospheric column. These two sites support both the radiosonde and the hydrometeorological components of the project. FIRO also sponsored the installation of ten additional stand-alone precipitation gauges and six stream gauges (see Figure 6).

At the inception of the FIRO effort, ERDC researchers began constructing GSSHA models of varying resolution and scale within the Russian River watershed to test its ability to provide additional information to operational decisions. The spatially distributed and physical process-based formulation of GSSHA, coupled with the data collected from the extensive network of gages and stations in the Russian River watershed, provides the ability to computationally track water as it moves through every part of a watershed and the FIRO effort provides a unique opportunity to test the ability of this model to provide added insight to water managers and operators that can impact decisions. Results from the GSSHA models in this study, compared to current CWMS and water management tools, will provide insight into future water management benefits to be realized from the use of GSSHA.

Path Forward and Lessons Learned

Lake Mendocino FIRO FVA Report

The Lake Mendocino FIRO effort will be documented in the FVA report which will include recommendations for a Lake Mendocino WCM update that will incorporate FIRO based on lessons learned during the Major Deviation tests explored under the FVA. The FVA report will include the needed elements required for a WCM update according to USACE policy.

FIRO Transferability

Prado Dam: The transferability of FIRO to additional reservoirs will be explored first at Prado Dam on the Santa Ana River in southern California. This dam was selected after careful consultation with water management technical leaders, engineers and operators within the USACE Los Angeles District and the SPD. Additionally, the selection of a dam in this area was supported by the FIRO atmospheric science team members based on the differences in how atmospheric rivers behave in southern California verses northern California, and on the differences in watershed characteristics that would yield new insights into FIRO potential. The Santa Ana River watershed is highly urbanized with fast hydrological response and a large elevation difference from the upper to lower watershed, including some snow-impacted areas. An additional important difference is that direct groundwater recharge, as opposed to surface storage, is a key water management practice in this basin. A steering committee for FIRO at Prado Dam has been formed, following the model used at Lake Mendocino, and is comprised of representatives from the key federal, state and local agencies and stakeholders that interact regarding water management and ecological decisions at Prado Dam and in the Santa Ana River watershed. As with Lake Mendocino, the Prado Dam FIRO SC is comprised of engineers, water managers, regulators, researchers and scientists, providing the blend of research and operations that has enabled the success of FIRO at Lake Mendocino.

Additional Reservoirs: Additional reservoirs beyond Prado Dam will be chosen for assessments of FIRO viability based on criteria that include factors such as dams and/or reservoirs, and watershed/regions where:
- there is potential that a suitable level of atmospheric river forecast skill could be achieved that would likely enable FIRO to be viable
- there are gaps in atmospheric prediction and watershed challenges in the region that have not yet been addressed in other pilot areas (e.g. high elevation, snow-impacted systems, etc.)
- there is capacity in the downstream channel to allow for a wide range of flows
- a favorable management context exists, (i.e., local stakeholders have key technical expertise, strong partnerships exist between stakeholders with a culture of innovation and compromise)
- a modification to the water control manual is needed and/or is being planned due to water budget changes, dam modifications, etc.

Screening Level Assessments: All or parts of the western states are impacted by atmospheric river events, some to greater degrees than others. Through the process of applying FIRO to Prado Dam and the other reservoirs that will be selected, a procedure for conducting screening-level FIRO assessments will be developed and applied to additional dams in the states where atmospheric rivers affect water management operations. The criteria for selecting these dams will be similar to that used for selecting additional reservoirs for full FIRO assessments.

The screening level assessment will not be as detailed or complete as the full viability assessments for Lake Mendocino, Prado Dam, or the other full assessments. However, the screening level assessment will provide important guidelines for how FIRO viability can be assessed at potential candidate reservoirs in the West and across the rest of the United States. This approach will systematically grow the scientific and engineering knowledge base needed to perform well-founded future assessments of FIRO applicability across a much broader range of conditions than has been explored in the first pilot reservoir, Lake Mendocino. These guidelines will assist water management agencies in deciding where and how FIRO principles and tools can be incorporated into future water control manual updates.

Key Lessons Learned

The success of the FIRO effort is due in large part to the formation of the FIRO SC and the development of its internal culture and processes which has successfully brought together groups with often competing missions and interests, but with a common vision that better operations could be possible through cooperation and advances in science and engineering. Additionally, with the connection and interaction of FIRO SC members and staff from the respective organizations who are engaged in the research and operations aspects of water management, the FIRO effort has eliminated the gap that can exist between research that investigates and makes scientific advances and operations who need tools that are ready for application to real world problems with requisite reliability and assurance. Research, operations and regulatory perspectives have blended in every element of the FIRO effort to produce science to inform policy and bring about improved efficiency in water management for the simultaneous benefit of flood risk management, water supply and ecologic concerns.

References

AMS 2016. *Atmospheric river*. Glossary of Meteorology. Available at http://glossary.ametsoc.org/wiki/Atmospheric_river.

California Department of Water Resources 2017: Water Year 2017: What a Difference a Year Makes, Available from https://water.ca.gov/

Corringham, T.W., A. Gershunov, D. R. Cayan, C. A. Talbot, and F. M. Ralph 2019: Atmospheric Rivers Drive Flood Damages in the Western United States *(submitted)*.

FIRO Steering Committee (2017). Preliminary viability assessment of Lake Mendocino. Available from: http://escholarship.org/uc/item/66m803p2

Jasperse, J., F.M. Ralph, M. Anderson, L. Brekke, M. Dillabough, M. Dettinger, R. Hartman, C. Jones, P. Rutten, C. Talbot, R. Webb, D. Ford, A. O'Donnell and A. DuBay 2015: A comprehensive plan to evaluate the viability of forecast informed reservoir operations for Lake Mendocino. *Sonoma County Water Agency report*, 1-374.

Jones, J. 2015. *California's most significant droughts: comparing historical and recent conditions*. California Department of Water Resources.

Skamarock, W. C., J. B. Klemp, J. Dudhia, D. O. Gill, D. M. Barker, M. G Duda, X.-Y. Huang, W. Wang, and J. G. Powers, 2008: A Description of the Advanced Research WRF Version 3. *NCAR Tech. Note NCAR/TN-475+STR,* 113 pp. doi:10.5065/D68S4MVH

USACE 1982. "Water Control Management," Engineer Regulation ER 1110-2-240, dated 30 May 2016. Available at https://www.publications.usace.army.mil/.

USGS 2017. "Coping with Drought in the Russian River Watershed," A California Water Science Center Regional Hydrology Project, dated 30 November 2017. Available at https://ca.water.usgs.gov/projects/reg_hydro/drought-russian-river-watershed.html

Forecast Informed Reservoir Operations Using Ensemble Streamflow Prediction for a Multi-Purpose Reservoir in the Russian River Watershed

Chris Delaney, Engineer, Sonoma Water, Santa Rosa, CA, chris.delaney@scwa.ca.gov

John Mendoza, Engineer, Sonoma Water, Santa Rosa, CA, john.mendoza@scwa.ca.gov

Robert Hartman, Consultant to Sonoma Water, Folsom, CA, hydrologic.prediction@gmail.com

Cary A. Talbot, Division Chief, Engineer Research and Development Center, US Army Corps of Engineers, Vicksburg, MS, cary.a.talbot@erdc.dren.mil

Abstract

Forecast Informed Reservoir Operations (FIRO) is a proposed alternative management strategy that aims to use data from watershed monitoring and state of the art weather and water forecasting to adaptively manage reservoir storage levels by incorporating forecasts of available water to improve water supply reliability without impairing flood protection. The first testbed for this strategy is Lake Mendocino, which is located in the East Fork of the 1485 mi² Russian River Watershed (Figure 1) in northern California. This project was guided by the Lake Mendocino FIRO Steering Committee (Steering Committee), which consists of water managers and scientists from several federal, state, and local agencies, and universities including the U.S. Army Corps of Engineers (USACE), Sonoma County Water Agency, National Oceanic and Atmospheric Association (NOAA), and the Center for Western Weather and Water Extremes (CW3E) at Scripps Institute. The Steering Committee shares a vision that operational efficiency can be improved by using monitoring and forecasts to inform decisions about releasing or storing water.

In July 2017 the Steering Committee completed a preliminary viability assessment (PVA) of FIRO for Lake Mendocino (FIRO Steering Committee, 2017). This study found that a forecast based decision support system could be a viable solution to meet project goals of improving the water supply reliability of Lake Mendocino without increasing the flood risk to downstream communities. Model simulation results presented in this abstract are from a study completed by Sonoma Water (Delaney & Mendoza, 2017) to support the PVA.

Lake Mendocino is a reservoir located in Mendocino County, California, about 110 miles north of the City of San Francisco. This small 116,500 acre-foot reservoir releases water into the Russian River and provides both flood protection and water supply to downstream communities. Lake Mendocino is cooperatively managed by 2 government offices: the USACE manages flood operations and the Sonoma County Water Agency manages water supply operations. The lake receives inflow from natural runoff as well from an adjacent river system, the Eel River, through a hydroelectric facility (Potter Valley Project) a short distance upstream of the lake. Recent changes in the operations of this hydroelectric facility have drastically reduced the average annual inflow of Lake Mendocino by 45%, contributing to a water supply crisis for the region. This crisis, among other reasons, made Lake Mendocino an excellent

location as a first pilot project to evaluate the concepts of FIRO in an effort to recover lost water supply reliability.

Lake Mendocino, like many other reservoirs, is currently operated using a rule called the storage guide curve (Figure 2), which determines the maximum water supply storage level of the reservoir. This seasonally varying guide curve provides increased flood capacity in the wet months (November – February) and increased water supply capacity during the dry months (May – September). This design works well during years with sufficient springtime (March – May) rainfall to fill the reservoir as the guide curve increases, but dry spring years can be challenging for water supply because the region typically receives very little precipitation during the summer and fall. Under FIRO, the objective is to detain wet season runoff above the guide curve level until forecasts indicate water should be evacuated to provide adequate volume for predicted flood events. Stored water released in advance of a forecasted flood event would be recovered by inflows from the flood event and held in the reservoir for water supply.

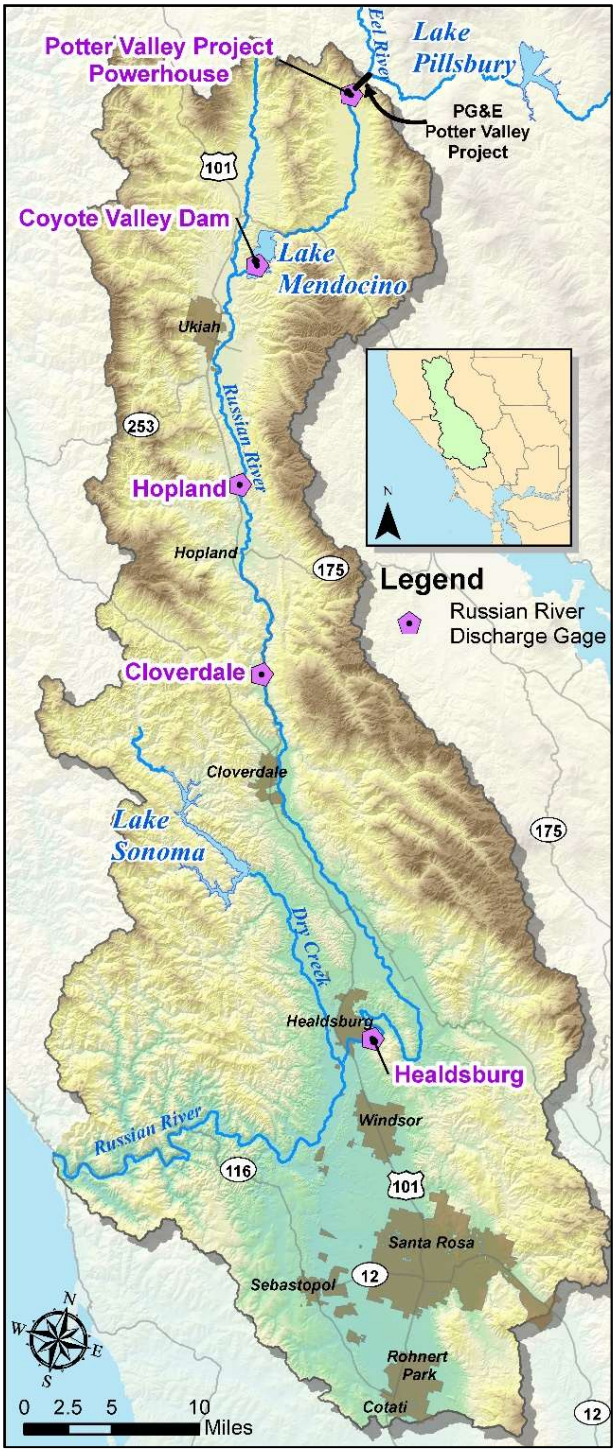

Figure 1. Map of the Russian River watershed including the Potter Valley Project.

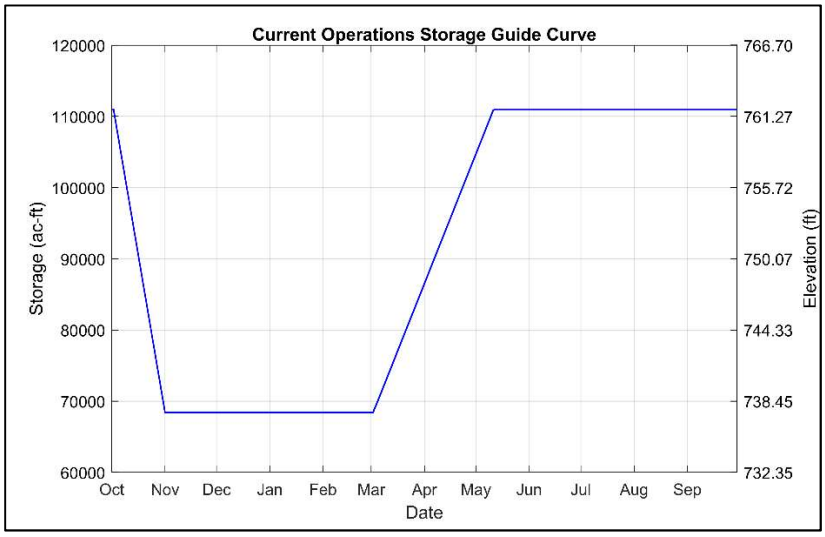

Figure 2. Currently used reservoir storage guide curve defines maximum water supply capacity.

A central challenge for this project is to develop new operational methodologies that incorporate forecast information to make reservoir release decisions to meet the project goals. One such methodology that is being evaluated for Lake Mendocino is called Ensemble Forecast Operations (EFO), which uses the Hydrologic Ensemble Forecast System (HEFS) ensemble forecast prepared by the California Nevada River Forecast Center (CNRFC) to evaluate the risk of reaching 111,000 acre-feet, which is maximum conservation storage level of the reservoir and jut 3 feet below the emergency spillway crest.

With the EFO methodology each hydrologic ensemble member is independently modeled to forecast reservoir storage assuming no water is released. Forecasted risk is evaluated for each timestep in the forecast horizon as the percentage of ensemble members that exceed the maximum storage level (111,000 acre-feet). The top panel of Figure 3 provides an example of a storage forecast with a 15-day forecast horizon and the maximum storage level shown as the black dashed line. The bottom panel of Figure 3 provides an example of the risk forecast shown as the red line. A key component of the EFO methodology is something called the risk tolerance curve, which is shown in the bottom panel as the blue dashed line. This curve defines the maximum allowable risk for each forecast timestep.

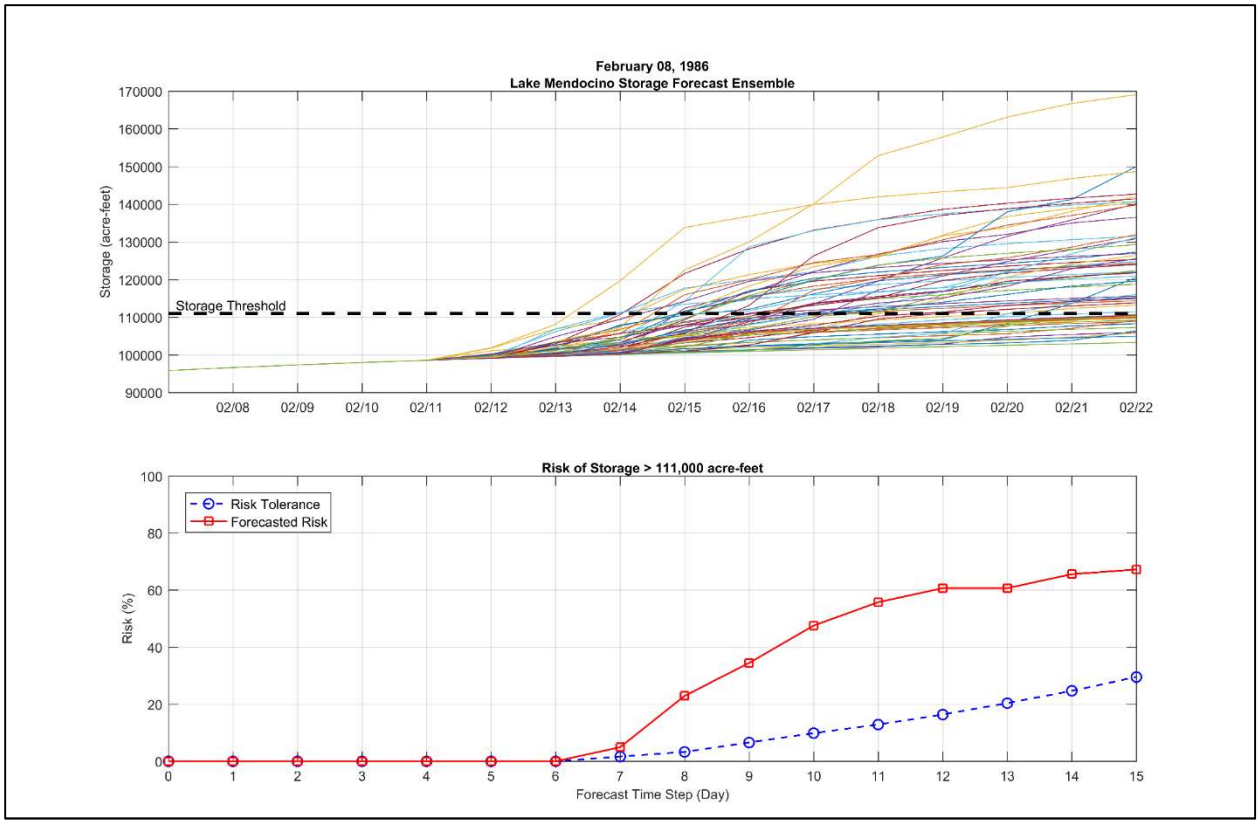

Figure 3. (top) Storage forecast ensemble assuming zero releases; (bottom) risk of exceeding storage threshold, and operational risk tolerance level.

If forecasted risk exceeds the risk tolerance curve, as in our example, a release schedule is developed that mitigates the forecasted risk at or below the curve. For this example, the model simulated a release of 1,940 cubic feet per second (cfs) to reduce the forecasted risk to the risk tolerance level. This is illustrated in the Figure 4 showing forecasted risk and storage levels after the release schedule has been applied. The model completes this process, updating release schedules each day as a new forecast is issued by the CNRFC. With the EFO methodology evaluated in this study, the storage guide curve (Figure 2) used under existing operations is not considered, therefore storage levels can encroach into the existing flood control pool or be released below the existing top of conservation pool if forecasted risk warrants such release decisions.

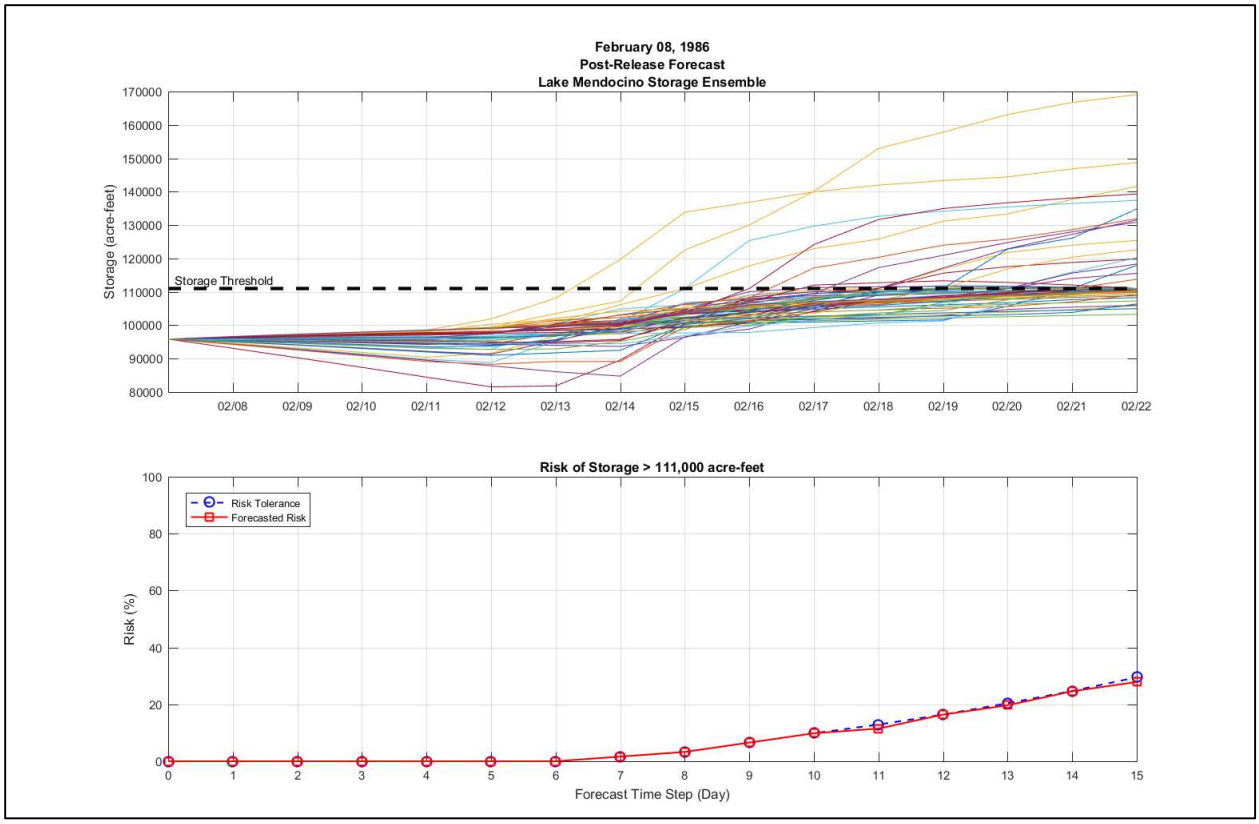

Figure 4. (top) Storage forecast ensemble after reservoir release schedules are calculated; (bottom) the resulting risk of exceeding the storage threshold matches the EFO risk tolerance policy.

A thorough analysis of the EFO methodology was made possible by an ensemble flow hindcast dataset from the HEFS prepared by CNRFC for the Russian River Basin. The hindcast study allowed estimating what the forecast would have been for each day from 1985 to 2010, given their current forecasting skill. This allowed the simulation of reservoir operations and flows for points downstream under a variety of hydrologic conditions including the 1986 flood, on the largest recorded events for the Russia River basin. An additional scenario was simulated, called Perfect Forecast Operations, which computes reservoir releases consistent with the EFO methodology, but substitutes observed flows in place of the hindcasted HEFS flows and simulates the maximum possible benefit from EFO alternative. All simulations of reservoir operations were constrained by the physical limitations of the outlet structures and the maximum and minimum release requirements established in the reservoir Water Control Manual (USACE, 2003) and other operational guidance regulations.

Model simulation results show significant increases in storage levels (Figure 5) for almost the entire simulation period, with a 35 - 40% increase in end of water year (September 30) storage levels of the EFO scenario compared to simulated existing operations for the median to driest years in the simulation period. The Perfect Forecast Operations scenario demonstrates a 49 - 70% increase in end of water year storage compared to simulated existing operations for the median to driest years.

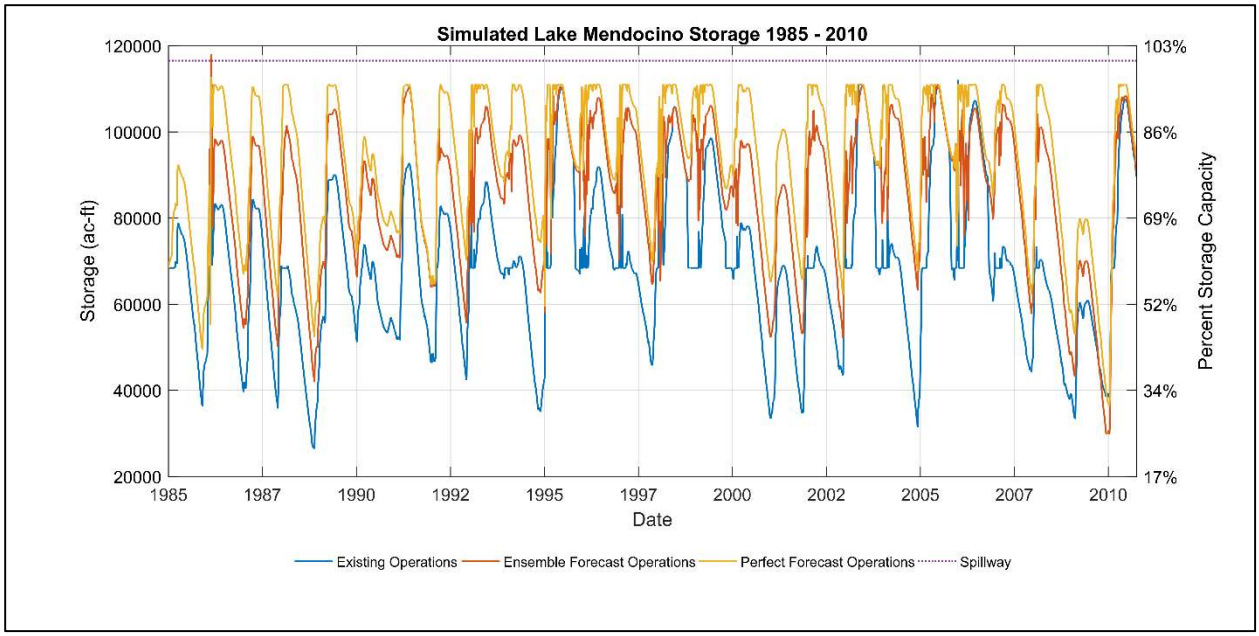

Figure 5. Storage levels for existing operations, EFO and Perfect Forecast Operations scenarios.

Despite the generally increased storage levels, hindcast simulation results do not demonstrate any increased flood risk, with no instances of increased flow levels above flood stage. Figure 6 shows flows plotted as percent exceedance for the most flood prone region immediately downstream of Lake Mendocino.

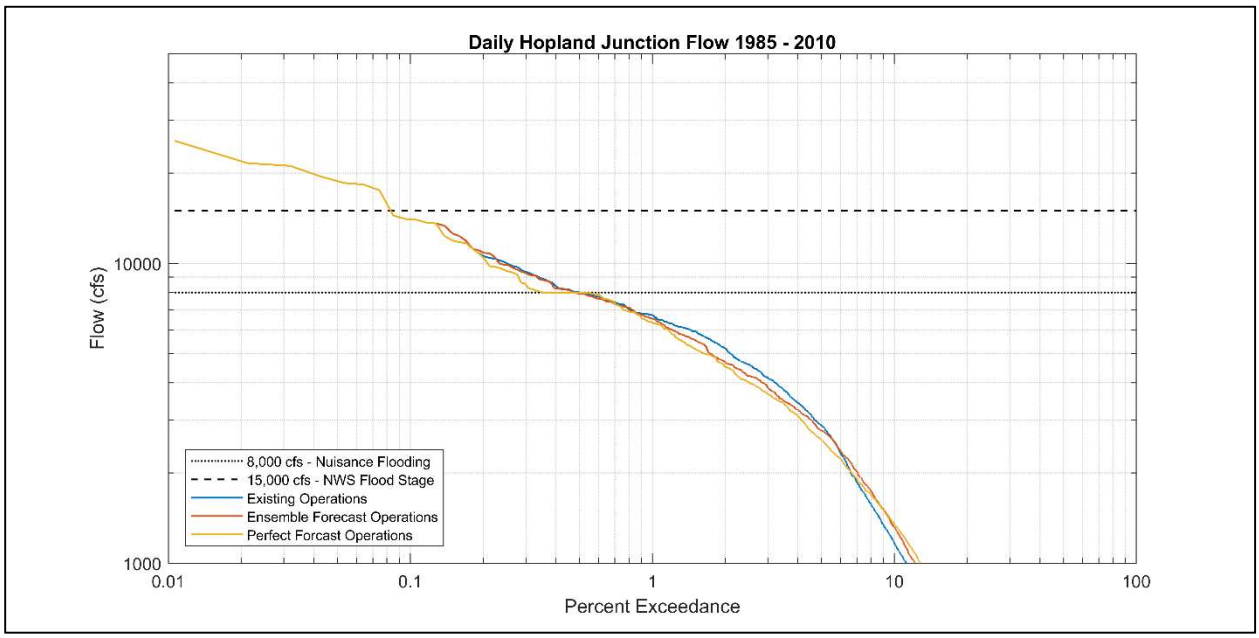

Figure 6. The distribution of downstream flows for Existing, EFO, and Perfect Forecast Operations scenarios, showing that no significant increase in the risk of downstream flood-level flows.

The results of this study demonstrate that the implementation of the EFO methodology will likely achieve the goals of the FIRO Lake Mendocino pilot project – to improve water supply reliability without increasing flood risk to downstream communities. Additionally, results of the

Perfect Forecast Operations scenario indicate that future improvements forecasting skill could improve the water supply and flood protection benefits of the EFO alternative.

Following the positive outcomes of the PVA, the Steering Committee has been working with the USACE to implement a revised version of the EFO methodology for the 2019 water year through a major deviation of the Water Control Manual. Additionally, further research and analysis of the EFO alternative is currently being pursued for a final viability assessment (FVA) that is being prepared by the Steering Committee. The research of the FVA will provide the foundation for the USACE to implement FIRO through permanent changes to the Water Control Manual.

References

Delaney, C.J., Mendoza, J.R. (2016). Forecast Informed Reservoir Operations, Lake Mendocino Demonstration Project, Evaluation of Ensemble Forecast Operations. Santa Rosa, CA. Sonoma Water.

FIRO Steering Committee. (2015). A Comprehensive Plan to Evaluate the Viability of Forecast Informed Reservoir Operations (FIRO) for Lake Mendocino.

FIRO Steering Committee. (2017). Preliminary Viability Assessment of Lake Mendocino Forecast Informed Reservoir Operations. (http://cw3e.ucsd.edu/firo-preliminary-viability-assessment-for-lake-mendocino/#TOP)

USACE. (2003). United State Army Corps of Engineers, Coyote Valley Dam and Lake Mendocino, Russian River, California, Water Control Manual: Appendix I to master water control manual Russian River basin, California. Sacramento (CA): U.S. Army Corps of Engineers, Sacramento District.

Implementation of HEC-RTS for Rapid Flood Forecasting and Online Mapping

Barnard Mondal, Staff Engineer, WEST Consultants, Inc., San Diego, California, bmondal@westconsultants.com
Martin Teal, Senior Vice President, WEST Consultants, Inc., San Diego, California, mteal@westconsultants.com
David Smith, Project Manager, WEST Consultants, Inc., San Diego, California, dsmith@westconsultants.com
Rosa Smith, Staff Engineer, WEST Consultants, Inc., San Diego, California, rsmith@westconsultants.com
Rand Allan, Associate Meteorologist, San Diego County Flood Control District, San Diego, California, Rand.Allan@sdcounty.ca.gov

Abstract

The U.S. Army Corps of Engineers Hydrologic Engineering Center (HEC) created and maintains the Real Time Simulation (RTS) software. HEC-RTS integrates the suite of HEC hydrologic and hydraulic software for real-time simulation and forecasting of reservoir and riverine water surface elevations. These forecasts provide stakeholders, such as local and federal governments, with a tool to promote public safety. The San Diego River and the San Luis Rey River watersheds (430 and 560 square miles, respectively) in San Diego County, California receive storms which inundate major road crossings and pose a threat to public safety during the rainy season. Flood forecasting is expected to improve decision-making for the closing of bridge and culvert crossings throughout these watersheds during flood events. The San Diego County Flood Control District (SDCFCD) and WEST Consultants, Inc. (WEST) have implemented HEC-RTS for the San Diego River and San Luis Rey River watersheds. Forecast stage results for selected crossings of interest are made available online through a webpage specific to each watershed along with corresponding flood maps. The static maps were developed for a range of water surface elevations at fixed intervals from several feet below the low cord to several feet above the high cord of the crossing. Users can read the forecasted water surface elevation for a crossing for the forecasted time period and view inundation maps which show the predicted flooded areas. SDCFCD is able to forecast flooding in a timely manner and provide information to users through this approach using HEC-RTS.

Introduction

Flood Forecast Model Background

SDCFCD is responsible for providing San Diego County with relevant flood warnings and coordination of personnel and resources to protect public safety during flood events. In 2016, SDCFCD and WEST developed a flood warning system for the San Diego River using HEC-RTS (HEC, 2017) which utilized both observed and forecasted precipitation to simulate future river stages. The components of the HEC-RTS model included separate hydrologic modeling system (HEC-HMS) and unsteady hydraulic river analysis system (HEC-RAS) models (HEC 2016b, 2016c). Because the hydraulic model included multiple reaches, each forecast simulation took

over thirty minutes to compute. The forecaster was limited in performing simulations and calibrations of the model due to the computation time.

In order to improve usability, the flood warning system was simplified by replacing the hydraulic routing with an unsteady HEC-RAS model with hydrologic routing in an HEC-HMS model. In 2018, the HEC-RTS model for the San Diego River was updated with this change and an additional HEC-RTS model was developed for the San Luis Rey River. The simulation time for both of the current HEC-RTS models is generally less than a minute for each day in the forecast period.

San Diego County Hydrology

The average annual precipitation within San Diego County varies from eight inches along the coast, to thirty inches over the mountains, to less than four inches in the deserts (PRISM, 2012). The majority of rainfall occurs between December through March of a given water year. The San Diego River and San Luis Rey River watersheds are two of the major basins in the county. Each river originates in the mountains and flows west through unincorporated areas of San Diego County before entering the Pacific Ocean.

HEC-RTS Model Development

Model Components

The data requirements for HEC-RTS are observed precipitation, forecasted precipitation, and observed stream flow. The data is retrieved using scripts within HEC-RTS and stored in HEC-DSS (Data Storage System) files (HEC, 2009). The HEC-produced GageInterp program (HEC, 2016a) is used to transform the observed and forecasted point precipitation to gridded precipitation using the inverse distance weighting method.

The components of the HEC-RTS model for both the San Diego River and San Luis Rey River are an MFP (Meteorologic Forecast Processor) model (HEC, 2017) to organize gridded precipitation data and an HEC-HMS model which computes the precipitation loss, precipitation transformation, and hydrologically routes flow downstream.

After acquiring data in HEC-RTS, the user defines the start time, forecast time, and end time for a simulation. The user then runs the simulation to compute river flow and flood elevations for major stream crossings. An HEC-RTS script processes and summarizes the relevant results for the user. See Figure 1 for a schematic of the HEC-RTS model. The elevation threshold graphic result summary is displayed within the HEC-RTS software window while the threshold warning message and web display are viewed outside the HEC-RTS software window.

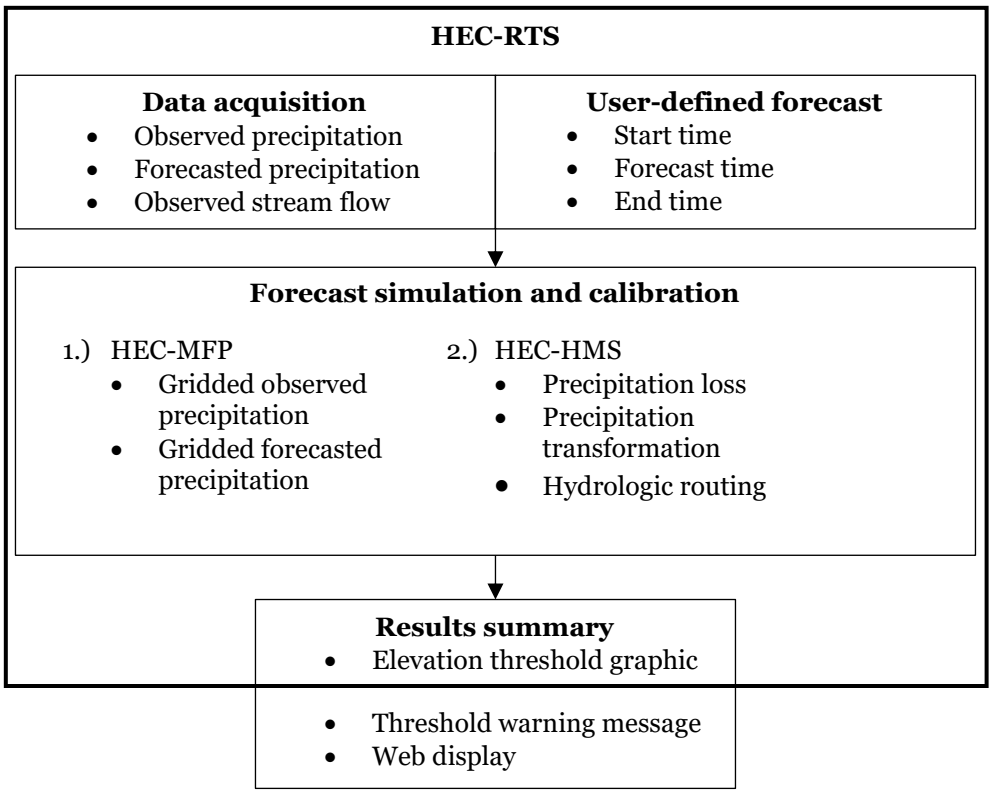

Figure 1. Schematic of HEC-RTS model with web display for San Diego River and San Luis Rey River

Hydrologic Model

The stream crossings of interest as defined by SDCFCD correspond to subbasin junctions of the HEC-HMS hydrologic model of the San Diego River and San Luis Rey River watersheds (Figure 2). Elevation-discharge curves for each of the crossings were computed using HEC-RAS models of the watershed stream networks. In this way HEC-HMS flow results could be converted to water surface elevations.

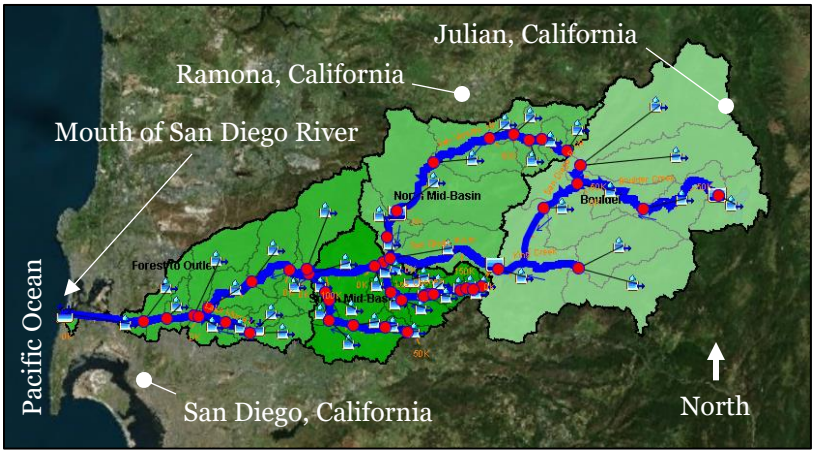

Figure 2. Hydrologic model map of San Diego River watershed in HEC-RTS window

Major reservoirs in the watershed are simulated within the HEC-HMS model as one-dimensional storage areas defined by an elevation-storage relationship. The hydrologic models for both watersheds were calibrated to three major storms. However, the user is advised to calibrate the look-back period of a given forecast simulation by modifying the precipitation loss rates and/or baseflow values.

Precipitation Loss: The deficit and constant loss method was used to model precipitation losses for the San Diego River and San Luis Rey River watersheds. This method provides users limited parameters to calibrate (initial deficit, maximum storage, and constant loss rate), of which the initial deficit is primarily modified to match the approximate antecedent moisture conditions.

Precipitation Transformation: The Modified Clark transformation method (HEC, 2000) is used in the hydrologic model to convert gridded precipitation excess to flow at each subbasin outlet.

Hydrologic Routing: The Modified Puls routing method (HEC, 2000) is used in the hydrologic model to route flood hydrographs downstream. This method is based on the hydraulic relationship between the storage and discharge along a reach of river. The storage-discharge relationship for each reach was determined with an HEC-RAS hydraulic model for both the San Diego River and San Luis Rey River watersheds. A steady flow HEC-RAS model was used to develop the storage-discharge curves for elevations ranging from the channel invert to several feet above the overbanks to ensure that the model could route a range of flows at each reach.

River Stage Forecast Process

Data Acquisition

All data which is acquired and formatted for application in the HEC-RTS model is publicly available. San Diego County and several Indian reservations own and operate precipitation gages throughout the county. The observed precipitation is recorded and made publicly available in real time through the county OneRain website (SDCFCD, 2019). Precipitation forecasts for the county are published by the National Weather Service (NWS) as quantitative precipitation forecasts (QPF) at numerous sites (NWS, 2019). The NWS QPF spans three days into the future and is published if precipitation is forecasted. Observed stream flow and stage data is published by the U.S. Geological Survey (USGS, 2019).

Observed Precipitation: There are 25 and 42 precipitation gages in the San Diego River and San Luis Rey River watersheds, respectively. Real time records are acquired in HEC-RTS and converted to grid-set data. The precipitation grid is entered into the forecast simulation for the purpose of calibrating simulated to observed flow (Figure 3).

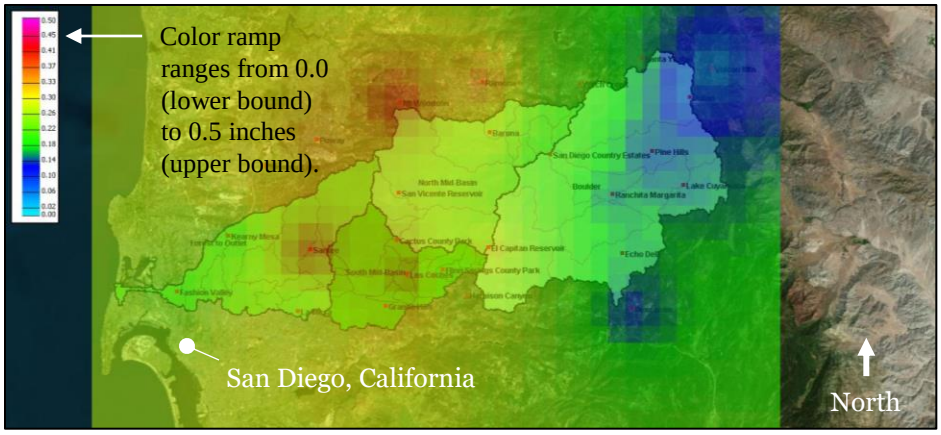

Figure 3. Observed accumulated precipitation map in HEC-RTS window

Precipitation Forecast: There are ten locations in or near the San Diego River watershed and seven locations in or near the San Luis Rey River for which QPFs are published. Similar to converting the point precipitation to a grid set data, the QPF point specific time series precipitation is transformed into a grid set data. The QPF grids are used in HEC-RTS to simulate flow for the user-defined forecast period.

Observed Stream Flow: The USGS operates three stream gages in the San Diego River watershed and one gage in the San Luis Rey River watershed. Additionally, SDCFCD operates six stream gages which measure stage along the San Luis Rey River. The observed flow is the reference in HEC-RTS for calibration of the hydrologic model.

Forecast Simulation and Calibration

Once the user specifies the start time, forecast time, and end time of the simulation, the acquired observed and forecasted data is applied to the forecast model to compute the resulting flow over the period specified. The observed flow data can be viewed for the corresponding junction within the forecast map viewer along with the simulated flow. The user can modify the loss parameters by either subbasin or by zone (group of subbasins) to calibrate the simulated flows to match the observed flows. Once the look-back period (start time to forecast time) is calibrated, the forecaster can then expect reasonable results for the forecast period (forecast time to end time).

Results Summary

Of the results from the forecast simulation of flow and water surface elevation, SDCFCD is primarily concerned with the time at which flooding overtops major river crossings and the approximate inundation areas that might be expected for certain sites. A script within HEC-RTS reads the results of the forecast simulation from HEC-DSS files and summarizes the results for the user in the form of an elevation threshold graphic, a text file listing all the river crossings which are expected to be overtopped and the expected time of overtopping, and files for web display of the inundation maps. The text file and files for web display are viewed outside of the HEC-RTS platform.

Figure 4 is an example stage forecast result from the HEC-RTS model for the San Luis Rey River gage at Oceanside, California for the February 15, 2019 storm event which also shows the USGS stage record (adjusted to reference the North American Vertical Datum of 1988 (NAVD 88)). The event did not reach the threshold flood stage but the example plot indicates that the timing of the forecasted peak stage approximately matches the recorded event. The forecast was calibrated at 08:30 Pacific Standard Time (PST) and resulted in a forecasted peak stage which was 1.14 feet less than the observed peak stage and arrived 5 minutes later.

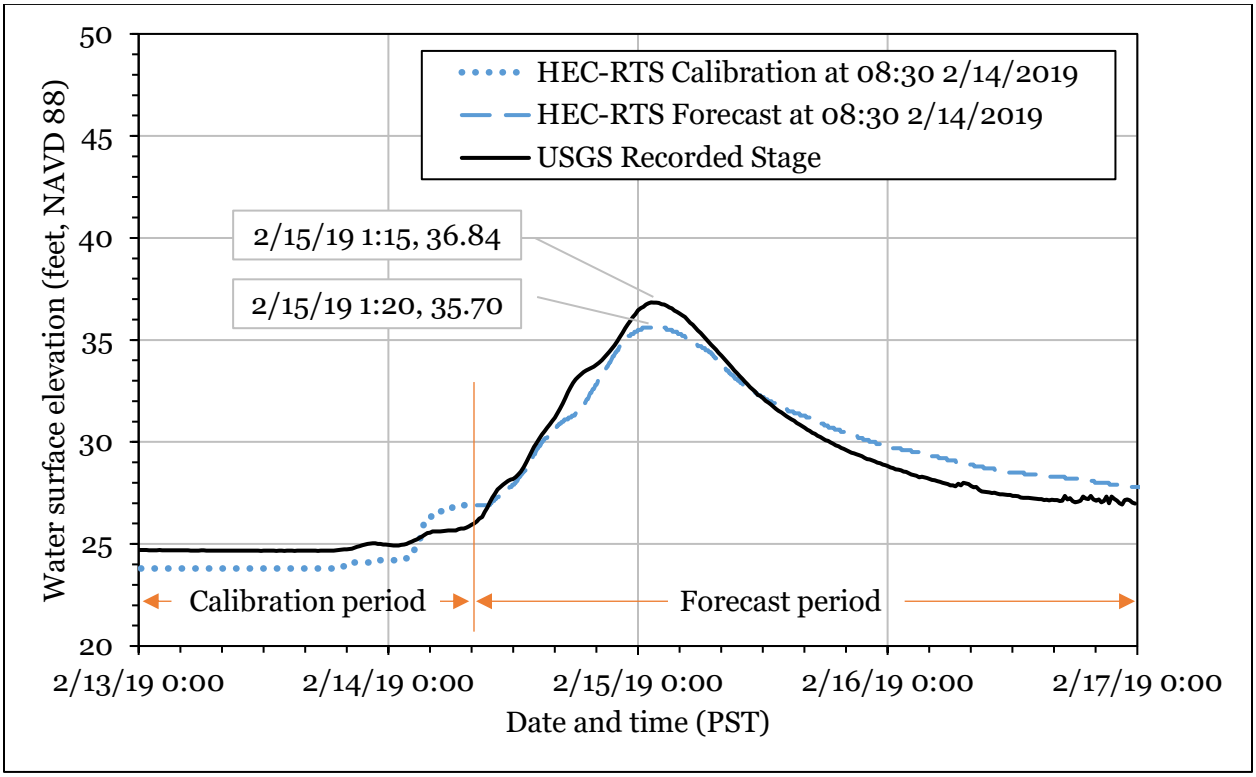

Figure 4. Comparison of forecasted and observed stage of San Luis Rey River at Oceanside, California USGS gage

Flood inundation maps were generated using the same HEC-RAS models used to develop the elevation-discharge and storage-discharge curves within HEC-RTS. The maps were created for seven sites within the San Diego River and San Luis Rey River watersheds which SDCFCD designated as points of interest. Once the results summary script is run in HEC-RTS the inundation maps can be viewed online and the user can immediately estimate the extent of flooding.

HEC-RTS Limitations

The simplifications for the San Diego River and San Luis Rey River HEC-RTS models improve usability yet limit the computation of flow and elevation to subbasin junctions. In the previous version of the San Diego River flood forecasting model, results were computed for each cross-section of the HEC-RAS model, giving the user more information. Though hydrologic routing parameters and rating curve results from HEC-RAS can be readily updated in HEC-HMS, adding points of interest to the current forecast model would require delineating new subbasins and determining hydrologic parameters for the new subbasins.

Additionally, in the current implementation of HEC-RTS for flood forecasting, the calibration of forecast simulations is limited by the availability of stream gage flow data. Adding stream-gages to the San Diego River and San Luis Rey River could improve calibration efforts but would require delineating new subbasins in the hydrologic model.

Summary

Despite the limitations of the HEC-RTS models, the implementation described in this paper incorporates observed and forecasted precipitation throughout the San Diego and San Luis Rey River watersheds to forecast river stage and display forecasted impacts in a timely manner. The San Diego River and San Luis Rey River flood forecast models are in the process of being applied by SDCFCD. The accuracy of flood forecasts will be reviewed as major storms occur over the San Diego River and San Luis Rey River watersheds. The lead time provided by the model forecasts will allow the County to send crews to close roads prior to overtopping and estimate inundated areas prior to the actual event. These and other benefits provided by the models enhance public safety.

References

Hydrologic Engineering Center (HEC). 2017. Real-Time Simulation (HEC-RTS) User's Manual, Version 3.0.3. U.S. Army Corps of Engineers, Davis, California.

Hydrologic Engineering Center (HEC). 2016a. GageInterp: A Program for Creating a Sequence of HEC-DSS Grids from Time-Series Measurements, User's Manual, Version 1.6.Draft. U.S. Army Corps of Engineers, Davis, California.

Hydrologic Engineering Center (HEC). 2016b. Hydrologic Modeling System (HEC-HMS) User's Manual, Version 4.2. U.S. Army Corps of Engineers, Davis, California.

Hydrologic Engineering Center (HEC). 2016c. River Analysis System User's Manual, Version 5.0. U.S. Army Corps of Engineers, Davis, California.

Hydrologic Engineering Center (HEC). 2009. Data Storage System Visual Utility Engine (HEC-DSSVue) User's Manual, Version 2.0. U.S. Army Corps of Engineers, Davis, California.

Hydrologic Engineering Center (HEC). 2000. Hydrologic Modeling System (HEC-HMS) Technical Reference Manual. U.S. Army Corps of Engineers, Davis, California.

National Weather Service Forecast Office (NWS). 2019. Quantitative Precipitation Statement. U.S. Department of Commerce, National Oceanic and Atmospheric Administration. San Diego, California. Available online at: https://www.wrh.noaa.gov/sgx/display_product.php?sid=SGX&pil=QPS

PRISM. 2012. 30-Year Normals, 800 meter, Annual Precipitation. Northwest Alliance for Computational Science & Engineering, Oregon State University, Corvallis, Oregon.

San Diego County Flood Control District (SDCFCD). 2019. San Diego County Rainfall and Stream Level Information System. San Diego County. San Diego, California. Available online at: https://sandiego.onerain.com/home.php

U.S. Geological Survey (USGS). 2019. Current Water Data for California. U.S. Department of the Interior. Available online at: https://waterdata.usgs.gov/ca/nwis/rt

Improving Seasonal Forecasting to Support Operational Decision-Making and Policy within Bureau of Reclamation Service Areas

Flavio Lehner: Research Applications Laboratory, National Center for Atmospheric Research, Boulder, CO, USA; flehner@ucar.edu
Dagmar Llewellyn; Albuquerque Area Office, Bureau of Reclamation, Albuquerque, NM, USA dllewellyn@usbr.gov.
Andrew W. Wood: Research Applications Laboratory, National Center for Atmospheric Research, Boulder, CO, USA; andywood@ucar.edu
Douglas B. Blatchford: Lower Colorado Regional Office, Bureau of Reclamation, Boulder City, NV, USA (retired)
Angus Goodbody: National Water and Climate Center, Natural Resources Conservation Service, Portland, OR, USA; angus.goodbody@por.usda.gov
Florian Pappenberger: Forecast Department, European Centre for Medium-Range Weather Forecasts, Reading, UK; florian.pappenberger@ecmwf.int

Abstract

In semi-arid and snow-melt dominated watersheds of the American Southwest, such as the Colorado River or Rio Grande, water managers and policy makers are reliant on seasonal streamflow forecasts, termed water supply forecasts (WSFs). These forecasts are issued several months ahead of the main runoff season when agriculture and municipalities have the greatest water demands and provide a fundamental basis for planning reservoir management, water resource allocations, and conservation efforts. All of these planning steps involve inter-agency communication and policy discussion, elevating WSFs to being a policy-relevant tool.

Recent studies have documented the influence of increasing temperature on streamflow across the American West. At the same time, some basins are reporting decreasing skill in WSFs over the recent decades, in part linked to the changing hydrological cycle with warming. Here we show that incorporating seasonal temperature forecasts from operational global climate prediction models into WSFs adds prediction skill for watersheds in the headwaters of the Colorado and Rio Grande River basins. Such predictions can increase the resilience of streamflow forecasting and water management systems in the face of continuing warming as well as decadal-scale temperature variability and thus help to mitigate the impacts of climate non-stationarity on streamflow predictability. In addition to the scientific analysis of the improved WSFs, implications for decision-making and policy within the Bureau of Reclamation are also discussed.

Introduction

With growing populations and rising temperatures, the pressure on water resources in the southwestern United States (US) is increasing and expected to continue to do so over the coming decades (Reclamation 2016). Water resources in this region are currently entirely allocated for agricultural, industrial and municipal uses and are heavily managed, with seasonal streamflow forecasts being a key tool used to inform this management. Seasonal streamflow forecasts for a range of lead times are among the most economically valuable streamflow predictions made in

the US and around the world, given their significance for water management (Hamlet et al. 2002; Pierce 2010; Raff et al. 2013).

Seasonal streamflow forecasts in the Upper Rio Grande basin, for example, are used to predict the annual water delivery requirements between Colorado, New Mexico, and Texas under an interstate river allocation agreement, the Rio Grande Compact, to plan for water storage and to inform associated reservoir management decisions. Seasonal streamflow forecasts also indicate the likely supplemental water needs for endangered species, and the storage needs of Native American Pueblos to assure they receive adequate water to meet their Prior and Paramount water rights. The forecasts in combination with those decisions enable projections of the water supplies that will be available to farmers, which in turn can influence cropping decisions. In addition, supplemental water supply to the Upper Rio Grande basin is imported each year from the Colorado River system through trans-basin diversions. Forecasts of the water available for diversion are used to estimate the portion of the imported water that will be available for purchase by the Federal government to support the needs of endangered species, as well as for planning of drinking water operations in major municipalities. On the much larger Colorado River system, as well, water supply forecasts issued in spring are essential to make reservoir storage and release decisions that help avoid shortage conditions in Lake Mead and Lake Powell, and that determine water and hydropower allocations affecting 7 southwestern US states. These decisions influence water and energy costs for major American cities such as Los Angeles, Las Vegas and Phoenix, and major irrigation regions such as California's Imperial Valley and Arizona's Welton Mohawk Irrigation and Drainage District.

Seasonal streamflow forecasts in snowmelt driven basins derive skill from the stability of relationships between winter precipitation and snow water equivalent (SWE) with spring to summer melt season runoff (e.g., April-July streamflow). The simplest operational form of seasonal streamflow prediction relies on statistical models that quantify these relationships, such as principal component regression (PCR) models trained on observed in situ data records of ~30 years (Garen 1992). These 'water supply forecasts' (WSFs) have traditionally been made beginning in January of the same year with updates on the first day of each month to incorporate new precipitation and SWE observations (Pagano et al. 2014b). Operational forecasts are published by regional River Forecasting Centers and the US Department of Agriculture National Resources Conservation Service (NRCS). A second common form of seasonal streamflow prediction involves the use of dynamic watershed models to predict future watershed states and fluxes (Day 1985; Pagano et al. 2014a).

The skill of statistical WSFs varies with lead time and also on decadal time scales, with basins such as the Upper Colorado River (UC) and Upper Rio Grande (URG) showing declining skill since the 1980s (Pagano et al. 2004; Pagano and Garen 2005). The proximate causes of variations and trends in forecast skill, at least from a hydroclimate perspective, are internal climate variability (e.g., the sequencing of wet and dry years and the timing of accumulation and melt relative to the forecast issue date) and secular trends due to more systematic changes in climate (e.g., warming leading to more evapotranspiration and changes in the snow-rain partitioning), as illustrated by numerous attribution studies (Woodhouse et al. 2016; Lettenmaier and Gan 1990; Barnett et al. 2005; Mote et al. 2005; Nowak et al. 2012; Vano et al. 2012; Christensen et al. 2004; Griffin and Friedman 2017; Udall and Overpeck 2017; Lehner et al. 2017a, 2018; Chavarria and Gutzler 2018). As a consequence, the relationship between winter moisture accumulation (precipitation and SWE) and summer streamflow is evidently non-stationary and influenced by changing temperature and other climatic factors. The influence of temperature on streamflow is problematic for WSFs in light of their underlying stationarity assumptions with regard to the background climate during the forecast period.

In comparison to their value, the costs of enhancements to operational water supply forecasting are small, especially when they represent an extension of the current forecasting approaches. In recent decades the western US has seen strong hydroclimatic trends and decadal variability, leading to variable streamflow forecasting skill and a likelihood of sub-optimal management decisions (Pagano and Garen 2005). To better grapple with water resource management challenges arising from hydroclimate non-stationarity and increasing water demands, improved efficiency in water management practices is critically needed (Milly et al. 2008; Lins and Cohn 2011; Steinschneider and Brown 2012).

With the advent of seasonal predictions by dynamical climate models, an opportunity arises to combine seasonal climate forecasts with traditional WSF based on snowpack observations. While seasonal forecast skill for precipitation remains limited, temperature has been shown to be skillfully forecasted for lead times of several months (Becker et al. 2014; Slater et al. 2016; Lehner et al. 2017b). Here we investigate whether including temperatures (as predicted by seasonal climate prediction models) in WSFs improves seasonal streamflow forecasting skill. To that end, we generate WSFs via the current operational strategy, termed 'baseline forecast', as well as WSFs that include seasonal temperature forecasts as a predictor, termed 'temperature-aided forecast'. The comparison of the two approaches enables us to assess the potential to improve streamflow forecasting skill by including temperature forecasts.

Data and methods

To best mimic the current operational WSF, we largely use the same underlying data as the NRCS. Estimates of naturalized monthly streamflow at 20 gages across the UC and URG are obtained from the NRCS. Observations of water year-to-date cumulative precipitation and instantaneous SWE at the 1st of January, February, March, April, and May are extracted from snow telemetry monitoring (SNOTEL) stations. Monthly mean temperature is taken from the Parameter Elevation Regression on Independent Slopes Model (PRISM) data set (Daly et al. 2008) averaged over 35.5-39.5°N, 108.5-105.0°W.

Seasonal temperature forecasts are derived from 8 initialized coupled climate models that produce seasonal climate forecasts. These models issue forecasts each month for lead times of up to 12 months with various numbers of ensemble members (10-51). Since we are interested in extracting the seasonally predictable signal, we use each model's ensemble mean (rather than all its individual ensemble members) of monthly mean 2-m temperature hindcasts, averaged over the same area as indicated above. We then use an equal-weights multi-model mean across the 8 models.

The WSF procedure is detailed in Garen (1992) and Lehner et al. (2017b) and summarized briefly here. The SNOTEL data is used in a principal component regression (PCR) trained on 30 years (1987-2016) of observed naturalized streamflow of the respective target period and cross-validated with a leave-one-out procedure (hereafter 'baseline forecast'). We then reforecast the same time period using the same information, but add the ensemble mean temperature anomaly of the 8 seasonal forecasting models as an additional predictor to the PCR (hereafter 'temperature-aided forecast'). Comparing the 'temperature-aided forecast' with the 'baseline forecast' allows us to determine whether there is skill improvement from adding temperature as a predictor to the WSF.

Results

The 'temperature-aided forecast' is more skillful than the 'baseline forecast' for most gages, skill metrics, and forecast lead times (Figure 1). The forecast skill is improved in terms of better capturing the year-to-year variability ('correlation') as well as in an mean error sense (relative root mean squared error , 'rRMSE'). While the improvements are modest (~5%), they are robust in a bootstrapping-with-replacement exercise (not shown). The same holds true for an evaluation of the probabilistic forecast skill (cumulative rank probability skill score, 'CRPSS') illustrating that the 'temperature-aided forecast' better depicts the observed probability distribution of streamflow values. The only skill metric that does not show unanimous improvement is a probabilistic skill score aimed at low flow years (brier skill score for the lowest tercile, 'BSS'). It shows that for some gages and lead times, adding temperature to the WSF does not improve the forecast skill for years of flow below the 33rd percentile of the climatological distribution. We also test how much skill improvement derives simply from the long-term warming trend by including the observed linear temperature trend over the study time period as a predictor (1987-2016), thereby excluding information on the interannual temperature variability. It is shown that the trend itself adds most of the skill. Thus, the interannual temperature variability, despite being forecasted skillfully, adds little additional streamflow forecasting skill above the secular warming trend.

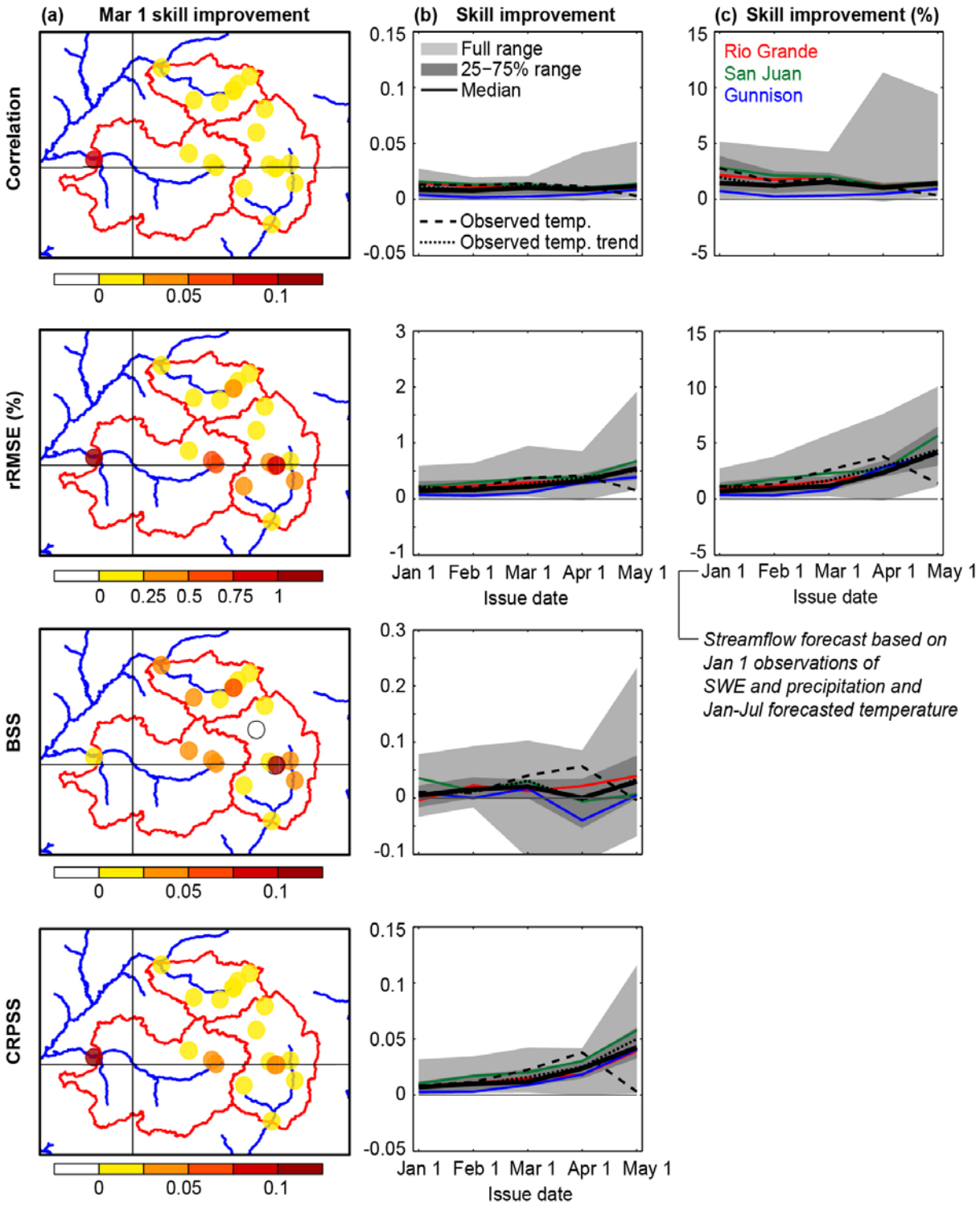

Figure 1. (a) Absolute skill improvement of the temperature-aided forecast relative to the baseline forecast at individual gages for issue date 1st March as an illustrative example. (b) Absolute skill improvement for all gages as a function of issue date. (c) Relative skill improvement for all gages as a function of issue date. Solid lines are the median across (black) all gages and (colors) the three basins. Dashed line is the median across all gages when using observed temperature, mimicking the hypothetical case where the future temperature is known at the time of forecast issue, and dotted line is the median when using only the linear trend of observed temperature (after Lehner, et. al., 2017b).

Conclusions, Implications, and Next Steps

The skill improvement demonstrated here for seasonal streamflow forecasts in the Upper Rio Grande and Upper Colorado River basins can be of significant value to State and Federal water managers, which, in turn, can benefit water users throughout these basins (Carolyn Donnelly, Bureau of Reclamation, Albuquerque, New Mexico and Craig Cotton, Colorado Division of Water Resources, personal communication). Despite its limited spatial extent, the study here is of relevance for other snow-melt driven basins across the US and the world, since streamflow forecast skill in such basins is often driven by the same temperature-sensitive processes.

We leverage the fact that current seasonal climate prediction models are skillful in forecasting seasonal temperature for this region. This temperature information adds skill to existing 'water supply forecasts' (WSFs), mitigating some of the forecast errors introduced through climate non-stationarity, and moving the WSFs closer to their maximally expected forecast skill based on relationships between observed snow, precipitation, and temperature.

It is important to note that the largest source of forecast error remains the (unknown) precipitation that falls after a forecast issue date (i.e., spring and summer precipitation). Thus, additional streamflow predictability might be available once seasonal precipitation forecasts become more skillful, although expectations for such skill are damped by the established theory of stochastic weather variability at lead times greater than a couple of weeks for this region of the world. Meanwhile, so-called sub-seasonal climate forecasts (lead time of a few weeks) are an interesting new tool to bridge the gap between the lead times of conventional weather forecasts and the longer lead times of seasonal climate forecasts used here.

Other conventional forecasting approaches based on hydrologic models (such as Ensemble Streamflow Prediction, or ESP, a popular operational method that is not discussed in this paper) are also commonly dependent on climate stationarity assumptions and thus are also likely to benefit from additional temperature forecast information. In the US Southwest, and similar hydroclimates around the world, expanding the use of model-based seasonal climate predictions, and particularly temperature forecasts, appears to be one pragmatic strategy for improving streamflow prediction skill in the face of a non-stationary climate.

Despite the evidence of forecast skill improvement through inclusion of temperature, this study does not support detailed conclusions regarding the hydrologic processes that underpin changes in prediction skill, as the temperature influence on streamflow can be dampened or amplified due to other effects and non-linear interactions (e.g., related to groundwater use or vegetation alterations or the co-variance with precipitation itself). Similarly, using low-dimensional statistical models only, we are unable to disentangle why certain gages show greater improvement than others. Process-based observation and modeling studies tackling this question may therefore be a valuable next step for the hydrologic forecasting community.

Beyond the direct improvement of streamflow forecast skill, better climate information (on seasonal and longer time scales) also has the potential to inform decisions related to daily water management operations. Streamflow forecasts today provide an estimate of the seasonal flow total, but not of the shape of the associated hydrograph. Water agencies often rely on analogs from historically observed hydrographs to anticipate the timing and shape of a given year's forecasted streamflow total. However, in an inherently non-stationary climate, historical hydrographs might be suboptimal analogs for next year's hydrographs. Due to systematic changes in the melt behavior and overall lengthening of the growing season (Musselman et al.

2017), hydrographs might look different even in cases where a forecasted flow total happens to have a historical analog. Here, seasonal climate forecasts could help create synthetic hydrographs that better reflect current climate-hydrology dynamics to be used in daily operations of water agencies.

References

Barnett, T. P., J. C. Adam, and D. P. Lettenmaier, 2005: Potential impacts of a warming climate on water availability in snow-dominated regions. *Nature*, **438**, 303–309, doi:10.1038/nature04141.

Becker, E., H. Van den Dool, and Q. Zhang, 2014: Predictability and forecast skill in NMME. *J. Clim.*, **27**, 5891–5906, doi:10.1175/JCLI-D-13-00597.1.

Chavarria, S. B., and D. S. Gutzler, 2018: Observed Changes in Climate and Streamflow in the Upper Rio Grande Basin. *J. Am. Water Resour. Assoc.*, **54**, 644–659, doi:10.1111/1752-1688.12640.

Christensen, N. S., A. W. Wood, N. Voisin, D. P. Lettenmaier, and R. N. Palmer, 2004: The effects of climate change on the hydrology and water resources of the Colorado River basin. *Clim. Change*, **62**, 337–363, doi:10.1023/B:CLIM.0000013684.13621.1f.

Daly, C., M. Halbleib, J. I. Smith, W. P. Gibson, M. K. Doggett, G. H. Taylor, J. Curtis, and P. P. Pasteris, 2008: Physiographically sensitive mapping of climatological temperature and precipitation across the conterminous United States. *Int. J. Climatol.*, **28**, 2031–2064, doi:10.1002/joc.1688.

Day, G. N., 1985: Extended Streamflow Forecasting Using NWSRFS. *J. Water Resour. Plan. Manag.*, **111**, 157–170, doi:10.1061/(ASCE)0733-9496(1985)111:2(157).

Garen, D. C., 1992: Improved Techniques in Regression-Based Streamflow Volume Forecasting. *J. Water Resour. Plan. Manag.*, **118**, 654–670, doi:10.1061/(ASCE)0733-9496(1992)118:6(654).

Griffin, E. R., and J. M. Friedman, 2017: Decreased Runoff Response to Precipitation, Little Missouri River Basin, Northern Great Plains, USA. *JAWRA J. Am. Water Resour. Assoc.*, **80526**, 1–17, doi:10.1111/1752-1688.12517.

Hamlet, A. F., D. Huppert, and D. P. Lettenmaier, 2002: Economic Value of Long-Lead Streamflow Forecasts for Columbia River Hydropower. *J. Water Resour. Plan. Manag.*, **128**, 91–101, doi:10.1061/(ASCE)0733-9496(2002)128:2(91).

Lehner, F., E. R. Wahl, A. W. Wood, D. B. Blatchford, and D. Llewellyn, 2017a: Assessing recent declines in Upper Rio Grande runoff efficiency from a paleoclimate perspective. *Geophys. Res. Lett.*, **44**, 4124–4133, doi:10.1002/2017GL073253.

——, A. W. Wood, D. Llewellyn, D. B. Blatchford, A. G. Goodbody, and F. Pappenberger, 2017b: Mitigating the Impacts of Climate Nonstationarity on Seasonal Streamflow Predictability in the U.S. Southwest. *Geophys. Res. Lett.*, **44**, 12,208-12,217, doi:10.1002/2017GL076043.

——, C. Deser, I. R. Simpson, and L. Terray, 2018: Attributing the U.S. Southwest's Recent Shift Into Drier Conditions. *Geophys. Res. Lett.*, **45**, 6251–6261, doi:10.1029/2018GL078312.

Lettenmaier, D. P., and T. Y. Gan, 1990: Hydrologic sensitivities of the Sacramento-San Joaquin River Basin, California, to global warming. *Water Resour. Res.*, **26**, 69–86, doi:10.1029/WR026i001p00069.

Lins, H. F., and T. A. Cohn, 2011: Stationarity: Wanted dead or alive? *J. Am. Water Resour. Assoc.*, **47**, 475–480, doi:10.1111/j.1752-1688.2011.00542.x.

Milly, P. C. D., J. Betancourt, M. Falkenmark, R. M. Hirsch, Z. W. Kundzewicz, D. P. Lettenmaier, and R. J. Stouffer, 2008: Climate change. Stationarity is dead: whither water management? *Science*, **319**, 573–574, doi:10.1126/science.1151915.

Mote, P. W., A. F. Hamlet, M. P. Clark, and D. P. Lettenmaier, 2005: Declining mountain snowpack in western north America. *Bull. Am. Meteorol. Soc.*, **86**, 39–49,

doi:10.1175/BAMS-86-1-39.

Musselman, K. N., M. P. Clark, C. Liu, K. Ikeda, and R. Rasmussen, 2017: Slower snowmelt in a warmer world. *Nat. Clim. Chang.*, **7**, 214–220, doi:10.1038/NCLIMATE3225.

Nowak, K., M. Hoerling, B. Rajagopalan, and E. Zagona, 2012: Colorado River Basin Hydroclimatic Variability. *J. Clim.*, **25**, 4389–4403, doi:10.1175/JCLI-D-11-00406.1.

Pagano, T., D. Garen, and S. Sorooshian, 2004: Evaluation of Official Western U.S. Seasonal Water Supply Outlooks, 1922–2002. *J. Hydrometeorol.*, **5**, 896–909, doi:10.1175/1525-7541(2004)005<0896:EOOWUS>2.0.CO;2.

——, A. Wood, K. Werner, and R. Tama-Sweet, 2014a: Western U.S. water supply forecasting: A tradition evolves. *Eos (Washington. DC).*, **95**, 28–29, doi:10.1002/2014EO030007.

Pagano, T. C., and D. Garen, 2005: The recent increase in Western US streamflow variability and persistence. *J. Hydrometeorol.*, **6**, 173–179, doi:10.1175/JHM410.1.

——, and Coauthors, 2014b: Challenges of Operational River Forecasting. *J. Hydrometeorol.*, 140516115449007, doi:10.1175/JHM-D-13-0188.1. http://journals.ametsoc.org/doi/abs/10.1175/JHM-D-13-0188.1.

Pierce, J. A. S., 2010: *A Measure of Snow: Case Studies of the Snow Survey and Water Supply Forecasting Program*. Salt Lake City, UT, 109 pp. https://www.wcc.nrcs.usda.gov/ftpref/downloads/factpub/MeasureofSnowFullReport.pdf.

Raff, D., L. Brekke, K. Werner, A. Wood, and K. White, 2013: *Short-Term Water Management Decisions: User Needs for Improved Climate, Weather, and Hydrologic Information*. 231 pp. http://www.ccawwg.us/.

Reclamation, B. of, 2016: *Climate Change Adaptation Strategy*. 33 pp. https://www.usbr.gov/climate/docs/2016ClimateStrategy.pdf.

Slater, L. J., G. Villarini, and A. A. Bradley, 2016: Evaluation of the skill of North-American Multi-Model Ensemble (NMME) Global Climate Models in predicting average and extreme precipitation and temperature over the continental USA. *Climate Dynamics*.

Steinschneider, S., and C. Brown, 2012: Dynamic reservoir management with real-option risk hedging as a robust adaptation to nonstationary climate. *Water Resour. Res.*, **48**, 1–16, doi:10.1029/2011WR011540.

Udall, B., and J. Overpeck, 2017: The 21 st Century Colorado River Hot Drought and Implications for the Future. *Water Resour. Res.*, doi:10.1002/2016WR019638.

Vano, J. A., T. Das, and D. P. Lettenmaier, 2012: Hydrologic Sensitivities of Colorado River Runoff to Changes in Precipitation and Temperature. *J. Hydrometeorol.*, **13**, 932–949, doi:10.1175/JHM-D-11-069.1.

Woodhouse, C. A., G. T. Pederson, K. Morino, S. A. McAfee, and G. J. McCabe, 2016: Increasing influence of air temperature on upper Colorado River streamflow. *Geophys. Res. Lett.*, **43**, 2174–2181, doi:10.1002/2015GL067613.

Managing Uncertainty in Reservoir Operations Using Ensemble Inflow Forecasts

Caleb Erkman, PE, Project Manager, Precision Water Resources Engineering, Loveland, Colorado, caleb@precisionwre.com
Shane Coors, PE, Principle, Precision Water Resources Engineering, Loveland, Colorado, shane@precisionwre.com
Dave Wathen, Assistant Water Master, U.S. Water Master Office, Reno, Nevada, dwathen@uswatermaster.org

Abstract

The Truckee River system in eastern California and western Nevada contains seven reservoirs that are operated collectively as prescribed by the Truckee River Operating Agreement (TROA). TROA allows the stakeholders in the basin to store water in the basin's seven reservoirs to achieve each of their unique objectives as well as possible. Given the complex operations that are both required and allowed by TROA, a state of the art RiverWare© reservoir operations and accounting model is necessary to support decision making. Uncertainty in the short-to-seasonal forecasted basin inflows complicates the decision-making required under TROA. The California-Nevada River Forecast Center (CNRFC) ensemble streamflow prediction forecasts (ESP) are used in conjunction with Natural Resources Conservation Service (NRCS) forecasts and historical inflow data to quantify the likelihood that various events will occur, and thus evaluate the effectiveness and risks associated with operational strategies. This methodology determines the risk associated with uncertainty in future seasonal inflow volumes as well as other more abstract quantities such as the shape of runoff hydrograph, the largest likely event by season, abnormal temperature patterns, etc. How ensemble-forecast methods improve reservoir operational decision making compared to more traditional most probable inflow and other single or few trace forecasting methods will be discussed.

Two case studies will be examined that show how ensemble-forecast methods have been used to support reservoir operational decisions. The first, will be a discussion of how ensemble-forecasts are incorporated into the monthly decision-making process. As a part of monthly meetings of basin stakeholders and decision makers, ensemble-forecasts are used to quantify the probabilistic range of potential outcomes based on the latest hydrologic forecasts and to coordinate operational plans. During these meetings the risk of undesirable outcomes in the future are identified and discussed in an effort to mitigate impacts and increase the likelihood of desirable outcomes when possible. A second case study will summarize how probabilistic decision support was used to determine release rates from Lake Tahoe in 2017 and 2018 to ensure that the reservoir would fill without, in-so-far as practicable, exceeding the established upper elevation limit. With this method operational decisions were made to reduce the likelihood of negative outcomes due to releases being either too large or too small.

Introduction

Truckee River System and the Truckee River Operating Agreement (TROA)

The Truckee River Basin covers roughly 2720 square miles in eastern Nevada and Western California. Originating in California's Sierra Nevada range, the Truckee River begins at Lake Tahoe and flows approximately 105 miles across the state line, through the Truckee Meadows and the Reno-Sparks metropolitan area, terminating in Pyramid Lake in the Great Basin. The waters of the Truckee River are highly regulated with seven upstream California reservoirs controlling nearly 70% of the total inflows to the basin. The majority of the water usage is in Nevada and consists of irrigation, municipal and

industrial, and environmental water right holders. One notable usage of the Truckee basin water is for the Newlands project, a trans-basin irrigation project in the neighboring Carson River Basin, which diverts water through the Truckee Canal at Derby Dam and was the United States Bureau of Reclamation's first project in 1903. Due to the semi-arid nature of the basin and the multitude and diversity of uses of the water, the history of the Truckee River has been full of conflict and litigation.

As a result of the intense and protracted conflict in the basin, Public Law 101-618 was enacted in 1990 directing the United States Secretary of the Interior to facilitate negotiations for a new operating agreement for the Truckee. After thirty years of negotiations among the major parties in the basin, the Truckee River Operating Agreement (TROA) was signed into law in 2008. After a series of legal challenges were resolved, the agreement began to be implemented in December 2015. The purpose of TROA is to improve operational flexibility and efficiency of Truckee River Reservoirs while satisfying water rights in conformance with existing decrees.

Evolution of water management

Ever since the early 1900's and the pioneering work of Dr. James E. Church, measurements of snowpack and more specifically the water content within the snowpack have been used to predict seasonal water supply. Dr. Church concluded early on in his work that… "it was quickly seen that the winter snow in percentage of its normal equaled that of the summer rise of the lake (Lake Tahoe). Rivers followed the same rule, but more closely." (Church 1937) Beginning in the mid 1930's the USDA Soil Conservation Service (SCS) – now the Natural Resources Conservation Service (NRCS) – has been charged with collecting monthly snow survey measurements and issuing seasonal water supply forecasts for areas all over the western United States. The NRCS data collection network has expanded from initially consisting of just the manual snow courses, to an extensive automated network of snow telemetry (SNOTEL) stations.

Just as the water supply forecasts have evolved and improved over the years, so has the Water Master's use of the data and reliance on these forecasts. In the early years of water management on the Truckee River, water managers and specifically the Water Master put little faith in water supply forecasts issued in the early period of the accumulation season. Claude Dukes (Truckee and Carson River Water Master, 1959 – 1984), is remembered as saying this quote when asked about an early season water supply forecast… "No Water Master worth his salt would make a projection before April 1st." Dukes' thoughts on this subject are understandable considering every year on the eastern slopes of the Sierra Nevada seems to be unique in its own way. Not unlike many areas, the eastern slopes of the Sierras can experience extreme variability from year to year with regards to how precipitation accumulates over the season. Even with an April 1 forecast in hand where confidence is high with regards to the volume of water in the snowpack, there is still the challenge as to how the runoff will be distributed over the summer.

Before the aid of any computing resources and sophisticated hydrologic modeling software, the Water Master had to rely mainly on years of experience in the basin. As the years of inflow and runoff data were collected and analyzed, certain metrics were derived that are characteristic to the basin. For example, the Truckee River below Lake Tahoe has multiple tributaries contributions including four of which that are regulated by reservoirs; two of these being the Little Truckee River and Prosser Creek. On average, the Little Truckee will produce approximately 35% of the April through July forecasted volume expected at the Truckee River at Farad forecast point. Prosser Creek on average will produce approximately 16% of the total volume. Another key metric that proved to be of value was analysis of recession rates after the peak runoff streamflow had occurred. It was found that regardless of the volume forecast – whether it be a very large volume or not — once the peak has occurred the recession limb of the hydrograph typically drops at the same average rate over time from year to year.

Forecasting Methods

Current operations of the Truckee River system rely on hydrologic forecasts that are coordinated between the NRCS and the California Nevada River Forecast Center (CNRFC). These hydrologic forecasts are inputted into the TROA RiverWare Operations model that is used to forecast reservoir operations for the

remainder of the year. Methodologies for each of these forecasts will be discussed in more detail in the following sections.

NRCS Forecasts

“Most of the annual streamflow in the western United States originates as snowfall that accumulates in the mountains during the winter. As the snowpack accumulates, hydrologists can estimate the runoff that will occur when the snow melts. Measurements of snow water equivalent (SWE) at snow courses and SNOTEL sites, along with precipitation, antecedent streamflow, and El Niño / Southern Oscillation indices are used in computerized statistical models to produce streamflow runoff forecasts. Forecasts … give the total volume of water expected to flow past a location during a specified period, such as April 1 to July 31. … Forecasts of any kind are not perfect. Streamflow forecast uncertainty arises from three primary sources: (1) uncertain knowledge of future weather conditions, (2) uncertainty in the forecasting procedure, and (3) errors in the data. The forecast, therefore, must be interpreted not as a single value but rather as a range of values with specific probabilities of occurrence. The middle of the range is expressed by the 50% exceedance probability forecast. There is a 50% chance that the actual flow will be above, and a 50% chance that the actual flow will be below, this value." (Anderson 2019)

CNRFC Forecasts

The Ensemble Streamflow Prediction (ESP) forecasting method uses historical time series of precipitation and temperature as input to NWSRFS Hydrologic Models in conjunction with current conditions for snowpack, soil moisture, reservoir storages and streamflow to produce daily timestep streamflow forecasts. These ESP forecasts can be used to compute a distribution of seasonal water supply runoff volumes. The ESP forecasts have the added benefit of providing forecasted flows at the daily timescale. Because the ESP forecasts are based on observed climate over a relatively long period of time (the CNRFC currently uses climate from the years 1950 through 2008), ESP forecasts provide a range of reasonable streamflow forecasts for a wide variety of hydrologic quantities such as: peak reservoir inflow by month, summer base flow, streamflow peak date, runoff recession rate, inflow variability between subbasins, etc. These forecasts are particularly helpful for reservoir operational forecasting which is often driven by hydrologic quantities other than seasonal runoff volume. While these forecasts provide valuable information, they only provide information on the uncertainty associated with future temperature and precipitation. These forecasts are also output of hydrologic models which require on-going tuning and may provide unreasonable results in some circumstances. (Hartman 2008)

Reservoir Operations Model

The TROA Operations and Accounting RiverWare model was developed to model the Truckee - Carson River reservoir and river system including all of the accounting and operational rules specified by TROA. The RiverWare model is a 15-month daily timestep model that utilizes the observed water-year-to-date stream flows and reservoir elevations and then uses forecasted inflows to project reservoir operations through the end of the calendar year. The RiverWare model was developed with heavy coordination and input of basin stakeholders beginning in 2005 until TROA was implemented in 2015. In 2015, the model was adopted by the Water Master as the tool that is used to compute the official accounting record for the basin (observed period) and to facilitate the monthly scheduling process (seasonal forecast).

Deterministic forecasts of the remaining years reservoir operations are developed utilizing operator judgement, similar year CNRFC ESP traces, and median NRCS seasonal volume forecasts. Multiple times per week the Water Master will import the latest observed flows and reservoir elevations into the model and use the model to compute the storage and release accounting for these observed flows based on the requirements of TROA, the current operational objectives, and stakeholder goals. The model then seamlessly transitions into an operational forecasting model advising the Water Master of anticipated operational changes that may be necessary. The deterministic inflow forecast is updated periodically as meteorological conditions change as reflected in the latest median CNRFC ESP traces.

For this paper we will carefully define a median inflow forecast as "deterministic forecast or median forecast", in some cases such forecasts are referred to as “normal, "most probable" or "most likely" forecasts. These terms can be misleading because having near median inflow is only most probable if the expected statistical distribution is normal. Forecasted hydrologic inflow is very rarely normal because they have a fixed minimum of zero and an unbounded maximum (statistical skew). **Error! Reference source not found.** shows that for a normal distribution the most likely half-standard of deviation bin is in fact the bin that includes the median inflow so the "most likely" could be used interchangeably with median. However, when considering the CNRFC traces the most likely bin is the from -0.75 to -0.25 standard of deviations from the median. In fact, the runoff volume is 15% more likely to be in this bin than in the bin surrounding the median. It is also of note that the likelihood of inflow being within 0.25 standard deviations of the median is 22%, leaving a 78% likelihood that the inflow will be outside of this interval. Because of these effects, describing the median inflow as “normal, "most likely" or "most probable" should be avoided to avoid misrepresentation of results.

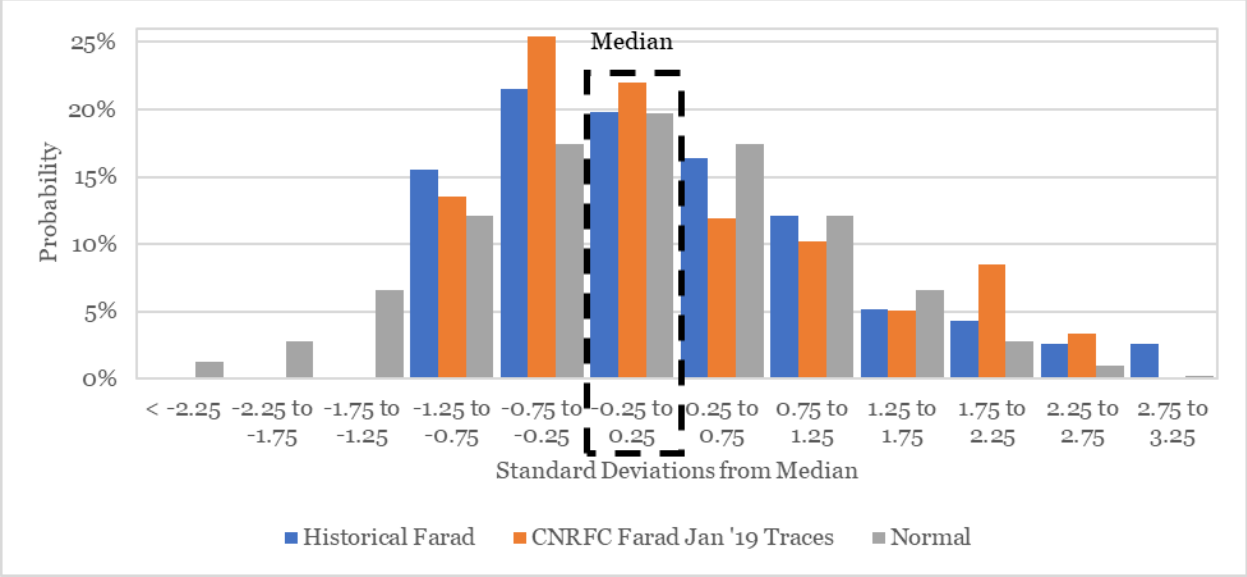

Figure 1. Comparison of probability distribution function of Truckee River at Farad Apil through July Volume

Reservoir operations can be non-linearly with seasonal inflow volumes in many cases. A simple example would be a reservoir that has available storage capacity equal to the forty-percent exceedance seasonal inflow. A deterministic forecast equal to the median forecasted inflow (fifty-percent exceedance) would not fill the reservoir, however the reservoir would have approximately a forty-percent likelihood of filling. It would be misleading to say that the "most probable" peak reservoir storage is something less than full because the reservoir would have a forty percent likelihood of filling then a total of sixty-percent likelihood distributed over the space of nearly full to not filling at all. Several other more complex operational objectives can lead to non-linearity in reservoir operations such as release thresholds, reservoir storage thresholds, etc. Reservoir operators often need to be aware of potential negative outcomes such as reservoir elevations or stream flows going outside of accepted ranges. While knowing that these constraints are met based on the median inflow forecast is of some comfort, a median forecast alone cannot specify a likelihood that these constraints will be violated. In some cases, a constraint may be violated if the same seasonal runoff were to occur in a different way such as with a sharper runoff peak, with more out of season storms, or any number of other perhaps unknown secondary characteristics of the runoff. With these considerations it is vital for reservoir operators and basin stakeholders to have a method to determine the risks of outcomes (positive or negative) which may be driven by uncertainty in runoff volume and other important characteristics of the hydrology.

The CNRFC ESP forecasts are particularly adept at addressing these issues because many of the other characteristics of the hydrograph are driven by a combination of temperature and/or precipitation. For example, runoff peak date is primarily driven by the temperature, while maximum March inflow is driven by a combination of snowpack, precipitation and temperature (for March). The CNRFC traces have the advantage over comparison to historical inflows that they are consistent with the current state of the snowpack and soil conditions. While CNRFC ESP traces give a good representation of the uncertainty in runoff based on uncertainty in future precipitation and temperature, they do not fully account for the uncertainty associated with other parameters such as antecedent conditions, and model bias. The CNRFC staff do much to address these issues, but it is helpful to utilize the NRCS statistical inflow forecasts to validate the seasonal runoff volume produced by the CNRFC traces. Some strengths of the NRCS statistical forecast methodology include: they are long standing and well accepted, they are based on some parameters independent of the parameters CNRFC traces are based on, and they account for uncertainty in parameters other than precipitation and runoff. Given the strengths of the NRCS volume forecast (which are coordinated with CNRFC forecasters) it is preferred to utilize the NRCS seasonal runoff distribution for risk analysis. The CNRFC ESP traces are transformed to match the distribution forecasted by NRCS.

The transformed CNRFC ESP is utilized to determine the likelihood of reservoir operational outcomes. The TROA Ops RiverWare Model is run with each trace in the transformed ensemble and the outputs from each of these model runs are compiled. Statistics are computed based on the ensemble of results. The results can be visualized in a variety of ways that will be discussed in more detail in Case Study 1: Monthly TROA Scheduling Process.

Case Study 1: Monthly TROA Scheduling Process

TROA requires that basin stakeholders provide scheduling to the TROA Administrator (TROA 2008, Section 11). This scheduling is implemented through a monthly scheduling process. The steps that occur as part of the scheduling process are outlined in Figure 2. The first case study discuss how uncertainty management is integrated into the monthly process. This process generally occurs over a two-week period beginning with the issuance of a first of month forecast by the NRCS. As part of the meeting preparation the TROA Administer runs the transformed ensemble through the RiverWare model. From the results of this analysis, the TROA Administrator compiles a presentation that quantifies the expected range of outcomes for various reservoir operations for the remainder of the water year. These outcomes include expected reservoir levels, party (stakeholder) account storages, stream flows in critical reaches, likelihood that party objectives will be achieved, and risks of negative outcomes. The results are presented and discussed at the TROA Scheduling Meeting highlighting any other relevant reservoir operational issues. Stakeholders may adjust their operational plans based on the information provided in the meeting or the information may be used to inform operational scheduling in future months for less urgent issues. These presentations have been designed, and are constantly adjusted to identify the risks of negative outcomes that may occur based on current conditions, party scheduling, maintenance plans, etc. There is also an emphasis to present results in a way that reduces the likelihood that results are misinterpreted especially if they will be disseminated to a non-technical audience. A sample of the quantities and visualizations used for this purpose are discussed below.

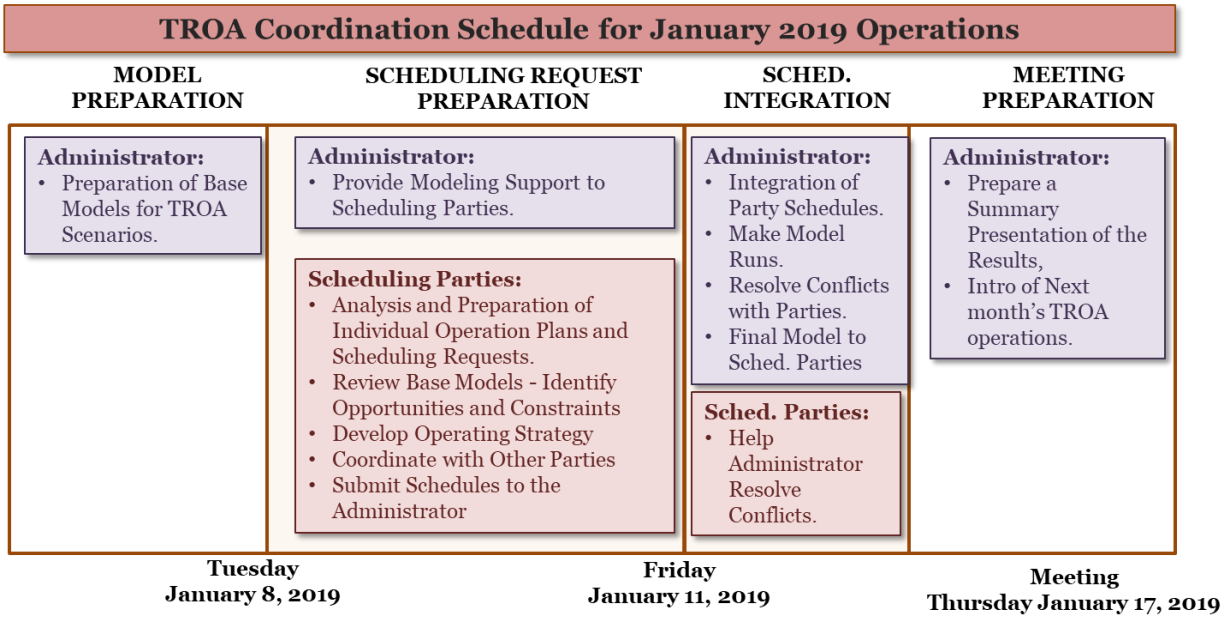

Figure 2. Typical TROA monthly scheduling process

The types of graphics presented and discussed at these meetings include: spaghetti plots, histograms, heat maps, exceedance curves, and parameter vs runoff volume plots. A sample of each output graphic will be shown and the typical uses of each will be discussed. All of the output shown are from the forecast made in December 2018.

Spaghetti Plot

A time series plot showing the outcome from each CNRFC ESP trace for a particular quantity is commonly referred to a "spaghetti plot". A sample of these plots showing the expected pool elevation of Lake Tahoe is shown in Figure 3. These plots can be helpful to show the possible range of outcomes and tend to draw focus on the extremes. The plot below includes a "median" line (thick red) which notes the elevation that fifty-percent of the traces are below and fifty percent of the traces are above as a function of time. These plots can be helpful to show a qualitative look at how likely thresholds are to be met. For example, the dotted black line marks the maximum operational elevation of Lake Tahoe. From this plot it can be seen that no traces meet this level during the remaining winter and spring months, several meet this level during the summer, and only one exceeds this level in the November-December. Methods to manage uncertainty when setting releases to meet this objective will be discussed in detail in section Case Study 2: Managing Uncertainty when setting releases to maintain elevations on Lake Tahoe. Overall these plots can be helpful to examine any quantity where the expected range of outcomes is particularly important, or a quantity where it is desired to avoid making a statement about a precise expected outcome.

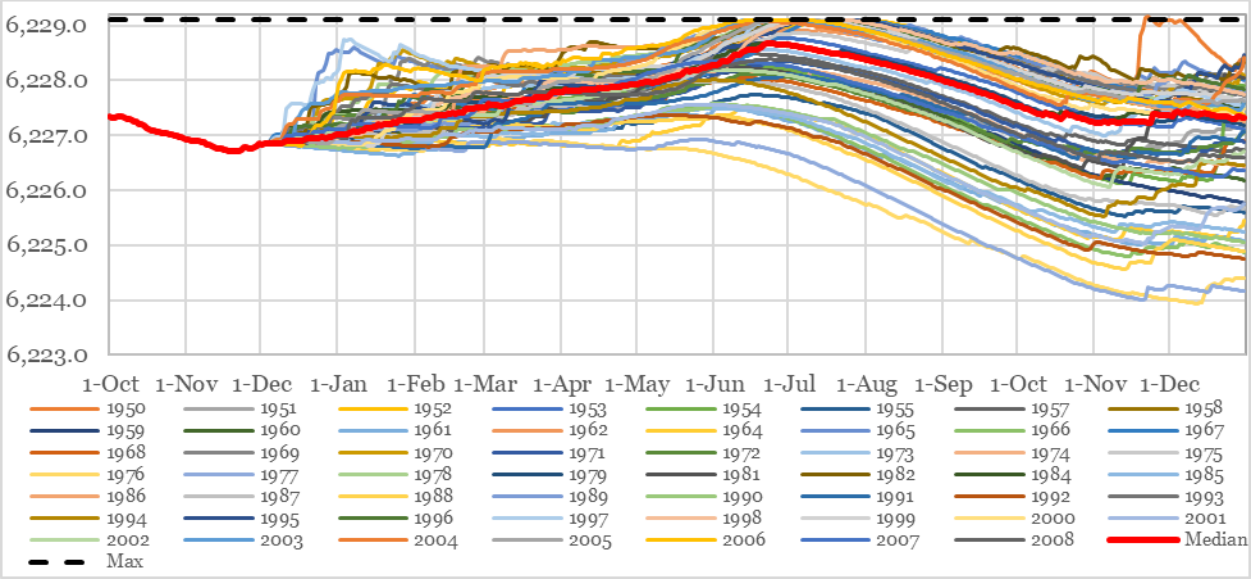

Figure 3. Example spaghetti plot showing the forecasted water year 2019 pool elevation of Lake Tahoe

Histogram

A histogram can be computed to evaluate the expected range of any parameter that can be represented by a single value computed from the model results from each CNRFC ESP trace. Quantities that this can be useful to represent include: volumes of flow over a specified period, maximum values for a quantity over a period (such as reservoir elevation or stream flow), period of time that a threshold will be exceeded, or likelihood that an important operational threshold will be met. In Figure 4, the probability that water will need to be released from Boca reservoir without a demand (operational spill which is commonly called spill) at some point in the remainder of water year 2019 is shown. For this metric, the likelihood of either zero or a small amount of spill is of interest (24% and 17%, respectively). Using this information, a party may choose to avoid storing water in Boca reservoir for water year 2019 because the risk of the water spilling is higher than other locations. This graphic is extremely useful to provide a quantitative calculation of the risk or extent that a specific outcome will occur. In some cases, a histogram can be computed for the benefits and the risks associated with a decision allowing the decision maker to objectively weigh the risk-reward relationship and make a well-informed decision.

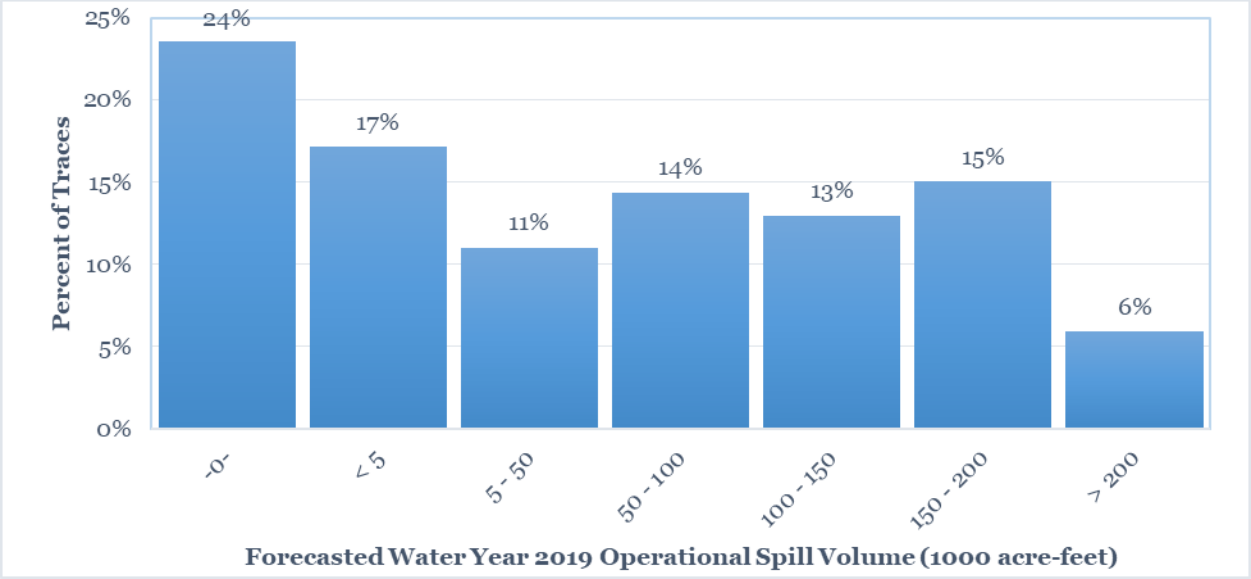

Figure 4. Histogram showing the volume of operational spill from Boca reservoir for water year 2019.

Daily Exceedance Plots

A common derivative of the spaghetti plot is an exceedance plot. Where values that are exceeded by a specified percentage of traces for several different exceedance thresholds are displayed. Figure 5 shows the forecasted exceedance probabilities for Fish account storages for the exceedances of 5%, 20%, 50%, 80% and 95%. These plots can be helpful to portray quantitative results over the course of the year but should be used cautiously because they are prone to mis-interpretation. Much of this mis-interpretation comes from the fact that unlike the spaghetti plot, the lines on an exceedance plot are not hydrographs! A viewer of Figure 5 may conclude that there is approximately a 20% likelihood of reaching the maximum storage (212,400 acre-feet), because the 20% exceedance line barely reaches the maximum level in mid-July. In reality 45% of traces reach this level at some point in the summer and only 25% of traces are still at this level on July 15. This discrepancy is driven by variability in the timing of the runoff peak which is largely a function of spring and summer temperatures and operational criteria. These plots actually show the distribution of the expected storages for each day of the year.

There is also a tendency for casual viewers to associate the lower exceedance curves with the lower exceedance runoff volumes, which is not necessarily the case due to the non-linearity of some reservoir operations. This phenomenon will be discussed in more detail in the following Section: Parameter versus runoff volume plot. The maximum storage example illustrates a way that this plot can be misinterpreted when representing storage values because of the temporal variability of the quantity. The potential for misrepresentation is much greater if streamflow data is plotted in an exceedance plot because streamflow data often changes significantly from day to day. The heat map can be an effective alternative method to display ensemble streamflow data. Due to the tendency for these plots to over simplify the results leading to misinterpretation, these plots should be used sparingly and primarily for quantities that have low short-term temporal variability (such as the elevation of a large reservoir or lake that changes gradually over several weeks to months).

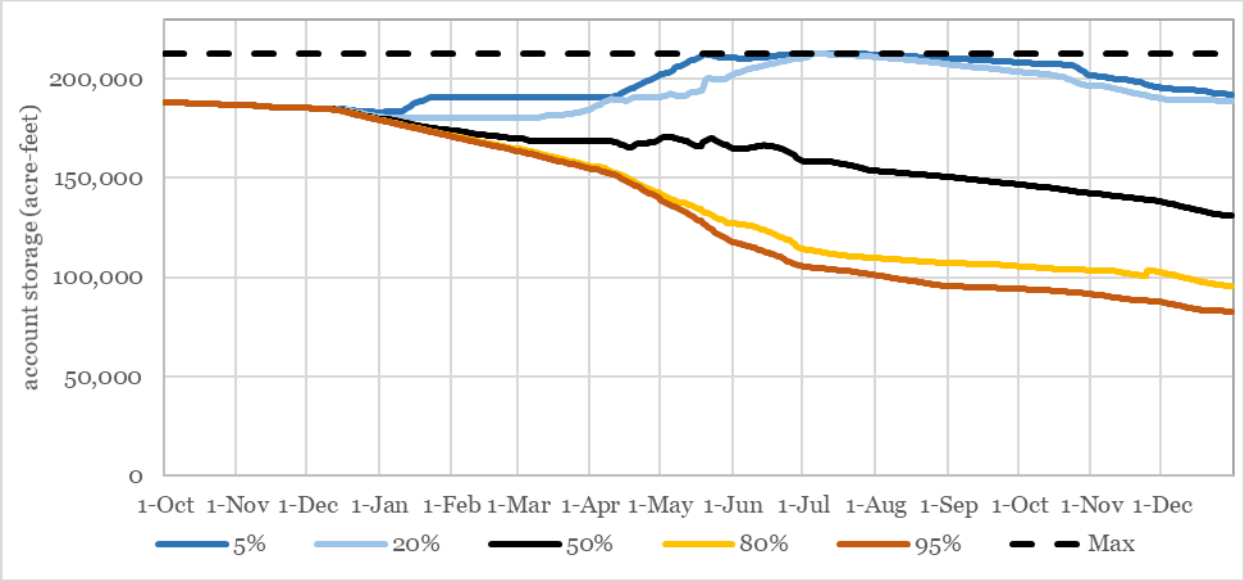

Figure 5. Forecasted 2018-19 total of FishW account storage in all Little Truckee River reservoirs

Heat Maps

Some of the challenges with visual representation of the uncertainty associated with flow data was discussed in the section Daily Exceedance Plots. The primary issue is that stream flows can change rapidly over short-term periods (hours to days) and these rapid changes could occur at any time but are unlikely to occur at a particular time (unless driven by reservoir operations). For example, there is an 80% likelihood that the natural flow above Farad will exceed 1000 cfs at some point in the winter. However, there is only a 15% likelihood that the natural flow exceeds 1000 cfs on January 1. Because of this an exceedance plot of the natural flow above Farad would give the false impression that 1000 cfs is an extreme flow for the winter time period. This illustrates a factor that a forecaster should take into careful consideration when constructing a deterministic reservoir inflow forecast.

The heat map utilizes color formatting to illustrate how likely each output bin (vertical axis) will occur as a function of time (horizontal axis, in this case days). The largest advantage of this output method is that there are no lines to misinterpret as hydrographs! The genesis of this display method came from the need to represent uncertainty in flow forecasts. An example of this is that recreational flow targets in the reach below Lake Tahoe are between 200 and 500 cfs from July 4th through Labor Day. From Figure 6, it is apparent that flows are likely to be within the recreational range but may deviate from this range (either high or low) during these months.

Heat maps may also be used to display any parameter where the goal is to qualitatively show the uncertainty associated with a parameter and avoid making strong statements about the "most probable" or "most likely" outcome. So, the answer to the question “Will there be recreational flows this summer?” can be… the probability is blue (lower probability) early in the season – and increasing to red (higher probability) later in the season, instead of… the most likely model indicates there will be rafting flows all season. This answer more accurately describes our knowledge of the future.

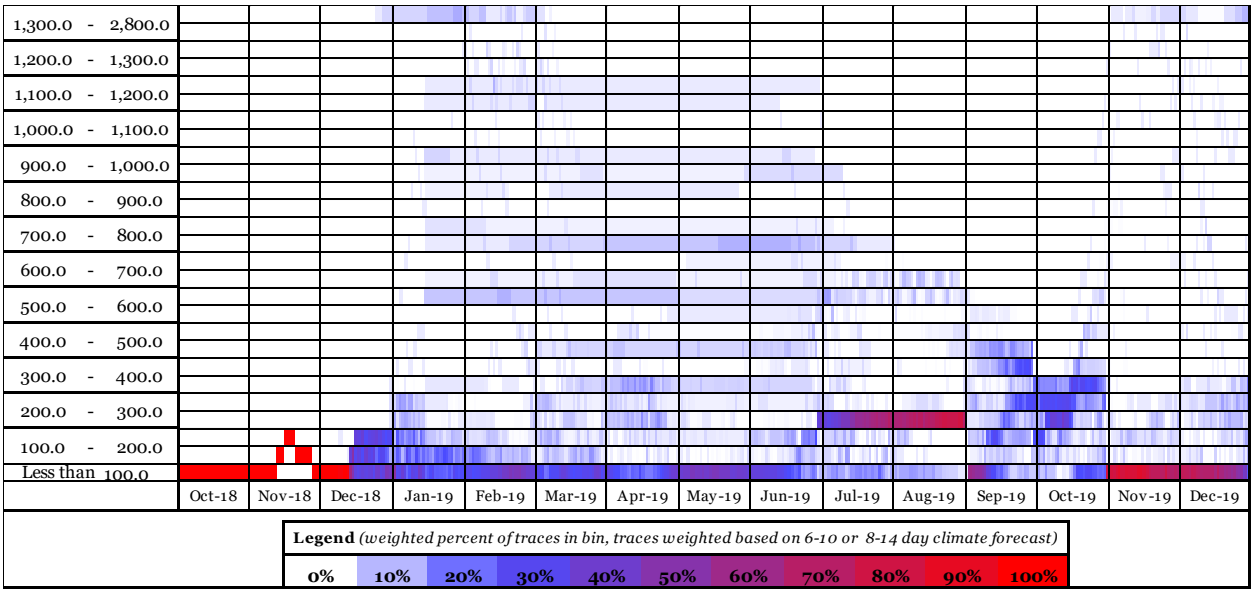

Figure 6. Tahoe outflow heat map for water year 2019. Color formatting based on the density of ESP traces in each bin.

Parameter versus Runoff Volume Plot

In many cases it can be helpful to determine the relationship between a forcing parameter and an output parameter. This can help decision makers answer questions such as: what would the seasonal runoff need to be to require an operational spill? Or, what seasonal runoff would cause a shortage? Or, what seasonal runoff volume produces the largest amount of credit water storage? Answers to these questions can give operators simple reference thresholds that identify when action needs to take place or satisfy academic curiosity. In many cases stakeholders may hold a simplistic view of how reservoir operations are related to season runoff. Some common simplifications include: higher inflow leads to higher storage, higher inflow leads to larger releases to maintain storage thresholds, or higher seasonal runoff leads to higher downstream flows. While many of these assumptions hold true in first order approximations for many reservoir systems, there are many examples where the respective outcome is not as well correlated with seasonal runoff volume as one might expect. The lack of correlation can be caused by many different things as discussed in Section Forecasting Methods. Figure 7 displays the relationship between the expected volume of operational spill and the season inflow volume (displayed in the gates closed rise "GCR" in feet which is the volume required to fill the lake one foot if not water is released.) for Lake Tahoe. Note that there are no traces with a GCR less than 1.4 feet that require operational spill. For the traces that do require operational spills the volume of spill is far from linear. In many cases plotting a parameter versus the runoff volume can be a helpful way to build understanding on how parameters are related to runoff and establish thresholds where action is necessary.

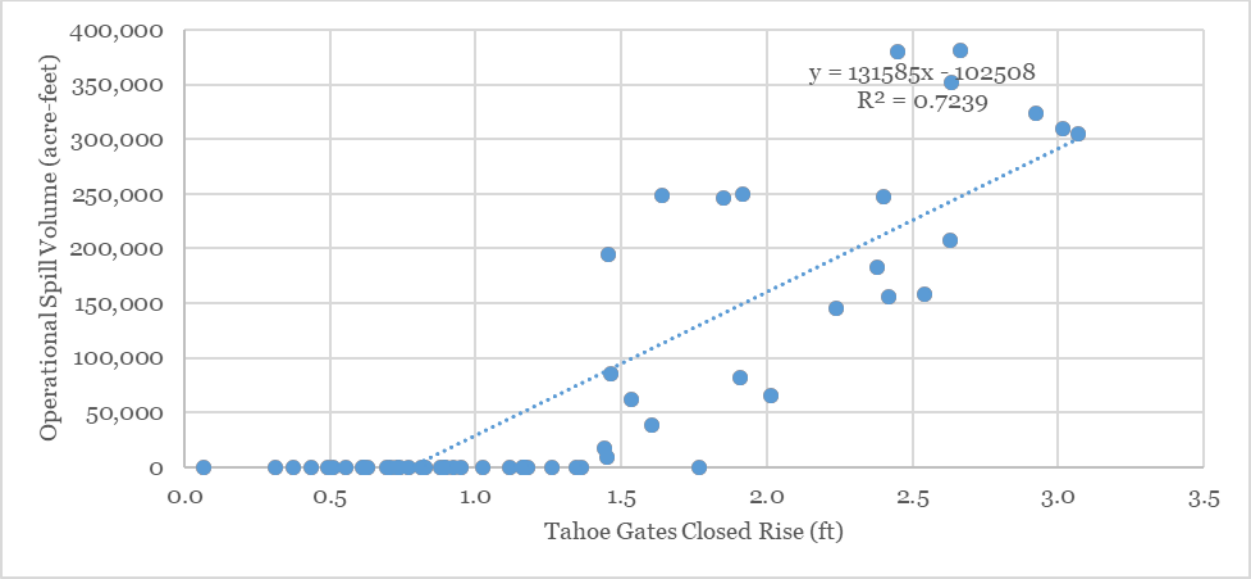

Figure 7. Scatter plot of anticipated operational spill volume from Lake Tahoe in water year 2019 versus the Tahoe April to High Gates Closed Rise (a metric of the seasonal runoff volume).

Case Study 1 Conclusion

Routine computation of the likely reservoir outcomes using a well-considered compilation of metrics can be helpful to identify potential issues early enough for action to occur. An example of this is that a river restoration project was planned in the upper Truckee River during October 2018. Forecasts several months prior to the project showed some risk that flows may be too high for the project to occur. The planned operations for reservoirs upstream of the project location were altered to increase the likelihood that the stream flow would be low enough to allow the project to occur, without having negative outcomes for the water right holders. Computation of the risk associated with these altered operations gave the water right holders confidence that they could accommodate the lower flow requests without negatively impacting their own interests. Overall regular discussion of the range in potential reservoir operational outcomes enables parties to be more cooperative, identifies negative outcomes further in advance, and enables better informed decision making.

Case Study 2: Managing Uncertainty when setting Releases to Maintain Elevations on Lake Tahoe

Lake Tahoe Operational Requirements

Lake Tahoe is a large natural lake sitting on the border between California and Nevada which forms the headwaters of the Truckee River. There is a small dam that allows regulating an additional 6.1' of storage above the Lake's natural rim which sits at elevation 6223'. This dam impounds 744,650 acre-feet of storage when full. Releases from Lake Tahoe are the primary means of supplementing the natural inflow to maintain the Floriston Rate (FR)—a flow target at the Nevada-California state line. The only other storage available to supplement natural inflow in meeting the FR (which has an annual demand of approximately 167,000 AF) is Boca reservoir which can store up to 40,000 acre-feet. Thus, water stored in Lake Tahoe is 95% of the reservoir capacity available for FR and is the primary method of maintain FR in low inflow years. Because of this, Lake Tahoe storage is a critical component in the reliability of meeting FR which serves all of the Nevada water rights on the Truckee River.

The reservoir portion of Lake Tahoe is unique from other similar volume reservoirs for many reasons. Perhaps the most significant difference is that the depth of water behind the dam is only 6.1 feet. Blue Mesa reservoir in Colorado has a similar volume but has a much greater depth of 502 feet. Reservoir outlet works capacity would often be designed as a function of the inflows to the basins which is a function of drainage area and the climate. As an example, if 1" of rain occurred over all of Lake Tahoe's basin it would take 6.5 days to evacuate the inflow. In comparison if 1" of rain occurred over the Blue Mesa basin it would take only 2.4 days to evacuate the water even though the drainage area of Blue Mesa is nearly seven times the drainage area of Lake Tahoe. Unlike many other large reservoirs, Lake Tahoe's release capacity if limited to 17-gates that are build into the dam structure and it does not have a spillway structure (regulated or unregulated). The outlet works capacity listed in Table 1 for Stampede and Blue Mesa does not include the unregulated spillway that added additional release capacity when the reservoir is surcharged. Therefore, releases to maintain elevations on Lake Tahoe (spills) need to begin very far in advance. However, because Lake Tahoe is so critical to meet demands for the FR, operational spills should be limited as much as possible.

Table 1. Characteristics of several reservoirs. (Projects and Facilities 2017).

	Lake Tahoe	**Boca Reservoir**	**Stampede Reservoir**	**Blue Mesa**
Capacity (acre-feet)	732,000	40,000	226,000	748,430
Depth behind dam (ft)	6.1	93	239	502
Outlet Works Capacity and Regulated Spillway Capacity at Full (cfs)	2,600	9,200	2,684	39,000
Drainage Area (sq. mi)	505	172	136	3,470
Volume of 1" of rain on basin (acre-feet)	26,933	9,173	7,253	185,067
Days to pass 1" of rain on basin	6.5	0.5	1.4	2.4
Unregulated spillway	No	No	Yes	Yes

TROA requires that releases from Lake Tahoe be made to maintain elevation 6229.1' "in-so-far as practicable" and specifies when such releases should begin. (TROA 2008) When determining releases to maintain elevation 6229.1', the uncertainty in seasonal runoff is often a significant portion of the amount of water that will need to be spilled. There are also competing objectives of not allowing the lake to rise above 6229.1' and avoid releasing any more water than necessary to maximize the water supply available to meet FR in coming years. In order to meet these competing objectives, it is necessary to consider the uncertainty in seasonal runoff when determining release rates.

Operating to Reduce Risks

For Lake Tahoe spill operations there are negative outcomes associated with releasing too much or releasing too little, both of which should be avoided if possible. Each time that a release rate is determined there is some practical fixed amount of time until the next change will be made. This amount of time may vary, but it is generally based on how much time needs to pass before the operator has enough new knowledge to make a change. Given that spill releases need to occur well in advance for Lake Tahoe, this time period is often the period between NRCS seasonal runoff forecasts which are usually published twice a month. CNRFC ESP traces are updated daily, but generally only give significant new information if conditions have changed dramatically –usually caused by a significant rain or snow fall event. Establishing a duration that releases will remain in effect allows computation of what the remaining release would need to be after that period to still perfectly fill the lake. This computation can be made using each of the CNRFC ESP traces and the percentage of traces outside of the acceptable range tallied.

The release rate for the fixed period can then be adjusted to ensure that it is still possible to adjust and fill the lake for the entire distribution of CNRFC traces. In some cases, it may not be possible to eliminate the risk of either exceeding 6229.1' or not filling. When this occurs, the operator needs to determine if one outcome is more important and adjust accordingly. This methodology also allows the operator to introduce other secondary objectives to be achieved as long as such operations do not increase the risk of failing to meet the primary objectives. Some secondary objectives that were considered in 2017 and 2018 include: limit large changes in release, limit releases that exceed flood stage downstream, avoid decreasing the release then going back up, and finally maintaining releases conducive to recreation (between 200 and 500 cfs from July 4th through Labor Day).

Water year 2017 brought historic precipitation and runoff to the Truckee River basin. The low to high GCR was 8.7 feet (TIS 2019), which exceeded the previous record of 6.9' from 1983 by 27%! This historic inflow allowed Lake Tahoe to fill from below the natural rim to the maximum elevation in a single year, something that had never occurred since the dam was constructed in 1913 (TIS 2019) (Projects and Facilities 2017). These high inflows necessitated development of a method to determine releases to fill the lake that reduce the risk of exceeding the maximum elevation while filling the Lake as nearly as practicable. These methods were refined by trial and error over 2017 and 2018 as different release schedules were evaluated to determine which schedules have lower risks based on the forecasted inflow distribution at that time. This approach is compared to an alternative and more traditional method which is to set releases based on the median inflow forecast and adjust appropriately as the median inflow forecast changes. The risk associated with these two methods are compared in Figure 8. In Figure 8, the releases that were set to minimize risk are shown in the "Obs." and the releases that would have been set if median forecasted inflow had been used to determine the releases is shown as "Median".

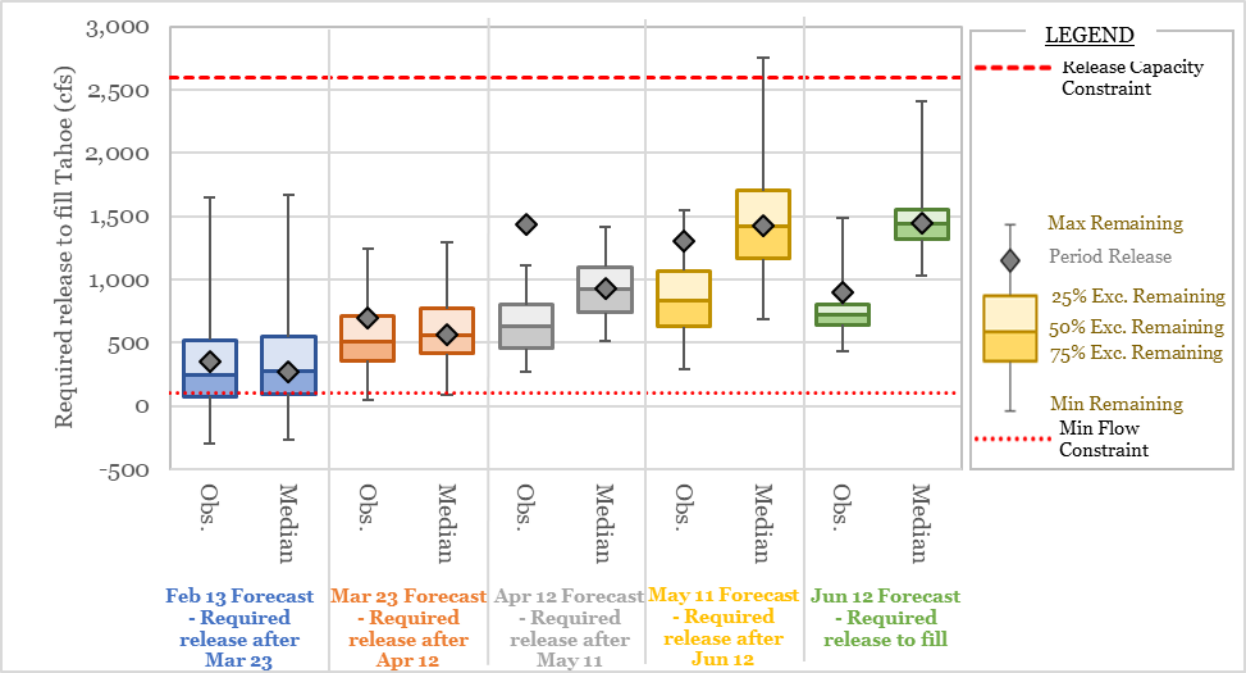

Figure 8. Tahoe releases and associated remaining season release required to fill Lake Tahoe in 2017 based on monthly forecasts ranging from February 13 through June 12, 2017.

Figure 8. Tahoe releases and associated remaining season release required to fill Lake Tahoe in 2017 based on monthly forecasts ranging from February 13 through June 12, 2017.These values assume that a release would be set until the next forecast date (grey diamond), then the range of the remaining release after the set period is computed (box and whisker plots). For example, for the April 12 forecast (grey) the release between April 12 and May 11 was set to 1,430 cfs and based on the April 12 volume distribution the release from May 11 to the day that Lake Tahoe filled would need to be between 1,100 cfs and 275 cfs with

a median of 630 cfs. For all of the Median methods the release from the forecast date to the next forecast date will be the same as the median release required after the next forecast date. If the required release is outside of the red constraint lines this denotes a risk of failure. For this analysis only, monthly forecasts are shown for simplicity, in practice several mid-month forecasts were considered to inform release changes based on mid-Month NRCS forecasts and the latest CNRFC ESP Traces.

The result of these considerations was to release as much as possible as early as possible while ensuring the release constraints could still be satisfied. In doing this, the amount of water that needed to be released in the later part of the season was reduced. This was particularly beneficial for the June 12th forecast when the uncertainty in the date that the peak elevation would occur was over three weeks (between June 28 and July 16). The uncertainty in the peak date has a significant impact in the uncertainty of the release required when the remaining time in the runoff season is short. With these operations the range in release required was reduced from 1,380 cfs (if operations were made to the median) to 1,050 cfs (24% reduction). The interquartile range was reduced from 240 cfs to 157 cfs (35% reduction)–meaning there was a much higher likelihood that releases could be managed within a small range during the final days of the runoff as Lake Tahoe approached its peak elevation for the year. In the Median scenario, the maximum remaining release exceeded the release capacity constraint for the May forecast and was near the constraint for the June forecast. So, there would have been a risk of exceeding the maximum elevation had releases been set based on the median forecasted inflow, this risk was avoided in the Obs. scenario.

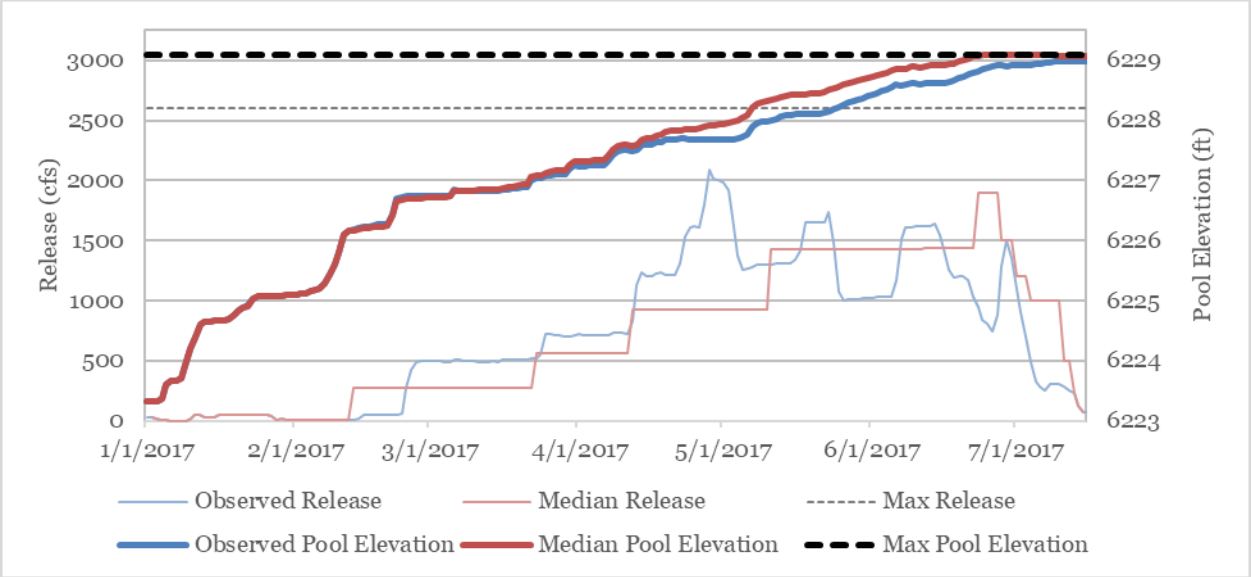

Figure 9. Lake Tahoe elevation and release comparison for summer 2017 comparing the observed release and resultant pool elevations, to the releases resultants pool elevations that would have occurred if releases were set based on the median forecasted inflow for each month.

Another benefit of operating the reservoir to reduce risk was that space was maintained in Lake Tahoe longer in comparison to the Median scenario. This extra space provided a buffer in case inflow exceeded any inflow that was represented in the CNRFC traces. For example, if an average of one inch of net precipitation occurs over the Lake Tahoe basin, it would require six and a half days of maximum releases from the lake to pass this inflow (Table 1) so additional space is particularly valuable. The additional space and altered release pattern in the two scenarios are shown in Figure 9. Note that even though the median release is nearly the same for May and June, release increases would have been necessary around June 20 to avoid overfilling the lake. Another result of operating to the median forecasted inflow is that the release trends will follow the trends in precipitation. Which is shown that the median release increases each month from February through May because the precipitation in each of the preceding months exceeded the median precipitation for those months. If below median precipitation had

consistently occurred than the opposite trend in forecasted releases would have occurred. Utilizing these methods operators were also able to achieve some secondary objectives that would not have been achieved if operations were set based on the median inflow forecast. These secondary objectives include: limit releases that exceed flood stage downstream and have releases conducive to recreation over the Fourth of July weekend (between 200 and 500 cfs).

Conclusion

Seasonal runoff forecasting science has made significant improvements from the genesis of the snow survey program in the early 1900 through the ongoing work by agencies such as NRCS and CNRFC. Despite these improvements, hydrologic forecasting remains an imperfect science and uncertainty in runoff forecasts results in significant uncertainty in seasonal reservoir operational planning.

As discussed in Case Study 1: Monthly TROA Scheduling Process, quantification of risk and uncertainty in routine operational forecasting provides benefits to basin stakeholders. Some of these benefits include: more accurate communication of uncertainty, improved peace of mind which can lead in fewer overly conservative decisions, identification of risks further in advance, and it removes barriers of cooperation between parties.

In Case Study 2 we examined how consideration of uncertainty improved operations to fill Lake Tahoe and reduced the risk that the maximum elevation threshold would be exceeded. These improvements allowed the operator to consider the risks associated with operational plans and consider contingency plans to enact if runoff were to occur in any of a wide range of potential futures that were represented by the CNRFC ESP Traces.

References

Anderson, Jeff. 2019. "Snow Survey." *Natural Resources Conservation Service*. 1. Accessed 1 1, 2019. https://www.nrcs.usda.gov/wps/portal/nrcs/main/nv/snow/.

Church, J.E. 1937. "The Human Side of Snow." *Scientific Monthly* 44 (2): 148.

Hartman, Rob. 2008. "Publications." *California Nevada River Forecast Center*. April 29. Accessed 1 1, 2019. https://www.cnrfc.noaa.gov/publications/hepex1_rhartman.pdf.

National Oceanic Atmospheric Admistration;. 2019. "Truckee River - Farad." *California Nevada River Forecast Center*. Accessed 1 22, 2019. https://www.cnrfc.noaa.gov/ensembleProduct.php?id=FARC1&prodID=7&year=2018&briefing=0.

2017. "Projects and Facilities." *Reclamatition*. 4 25. Accessed 1 14, 2019. https://www.usbr.gov/projects/facilities.php?type=Dam.

TIS. 2019. *TROA Information System*. Accessed 1 22, 2019. http://www.troa.net/tis/.

2008. "TROA." *Truckee River Operating Agreement*. September 6. http://www.troa.net/documents/TROA_Sep2008/troa_final_09-08_full.pdf.

Overcoming the Challenge of Initial Parameter Estimation for Event-Based Hydrological Models

Luciana K. Cunha, Project Manager, WEST Consultants, Folsom, CA,
lcunha@westconsultants.com
David C. Curtis, Sr. Vice President, WEST Consultants, Folsom, CA,
dcurtis@westconsultants.com
Travis Stanford, U.S. Army Corps of Engineers, Fort Worth District, Fort Worth, TX,
Travis.W.Stanford@usace.army.mil
Jerry Cotter, U.S. Army Corps of Engineers, Fort Worth District, Fort Worth, TX,
Jerry.L.Cotter@usace.army.mil

Abstract

An innovative approach that bridges the gap between event-based hydrological modeling and continuous soil moisture accounting approaches is discussed. Hydrologic Engineering Center (HEC) Hydrological Modelling System (HMS), developed by the US Army Corps of Engineers (USACE), is one of the most widely used hydrologic modeling programs in the world. HMS was used in the project, but the developed methodology can be extended to any event-based hydrological model.

HMS is applied to forecast reservoirs operations both by the USACE and outside agencies. While HMS can be ran continuously, it is mainly applied operationally in its event-based configuration to avoid the need of continuous maintenance. Event-based hydrological models do not explicitly address hydrologic processes that take place between storms such as evapotranspiration and percolation of water through the soil column. In HMS, hydrologic losses from incident rainfall are modeled simplistically using an initial loss and a continuing loss parameter. In an operational environment, these parameters are adjusted once catchment response is observed and compared to the HMS response. Time spent waiting for the initial catchment response needed to adjust the HMS loss parameters is time lost for flood mitigation or planning reservoir operations.

An innovative approach was developed that applies simulated soil moisture obtained from the Noah North American Land Data Assimilation System version 2 (NLDAS-v2) to update HMS parameters before an event is initiated. The application of NLDAS-v2 allows the estimation of initial losses after long dry periods when flow and rainfall indices are likely to be zero. NLDAS-v2 has the advantage of being continuously updated and publicly available online.

The methodology was applied for 24 reservoirs in the Ft. Worth District of the USACE. For each reservoir, statistical analyses were performed to determine the best soil moisture indicators and to define the relationships between initial moisture condition, rainfall, and runoff. A spreadsheet tool was developed that incorporates the NASA soil moisture data and information on historical storms to provide improved estimates of initial and continuous loss parameters for HMS in a real-time river forecast environment.

Introduction

The US Army Corps of Engineers (USACE) Fort Worth District (SWF) routinely produces inflow forecasts for each of the District's dams that support decisions related to reservoir operations. Historically, one of the challenges to accurately forecast inflows to District reservoirs is the estimation of hydrologic losses. Current methods in use by the Fort Worth District to estimate hydrologic losses involve simple nomographs and HEC-HMS hydrologic modeling software which provides information regarding timing, rate of rise, and peak pool elevation. Both methodologies are supported, in large measure, by professional judgement. The general consensus from the District's hydrologic forecasters is that the current methods are inadequate, especially for rainfall events occurring after prolonged dry periods or for multiple storm events occurring in series.

The goals of the project was to develop and implement an easy-to-use method for predicting losses associated with storm events that contribute runoff to 24 dams of interest (Figure 1). A methodology was developed to bridge the gap between event-base hydrological models commonly used by the USACE and the need for timely and accurate runoff forecasts even after long dry periods. The method takes advantage of existing systems continuously operated by NASA or NOAA. For this project, the North America Land Data Assimilation System (NLDAS) was applied. The National Water Model (NWM) operated and maintained by the National Oceanic and Atmospheric Administration (NOAA) can also be used, but at the time of the project the NWM reanalysis period was not available.

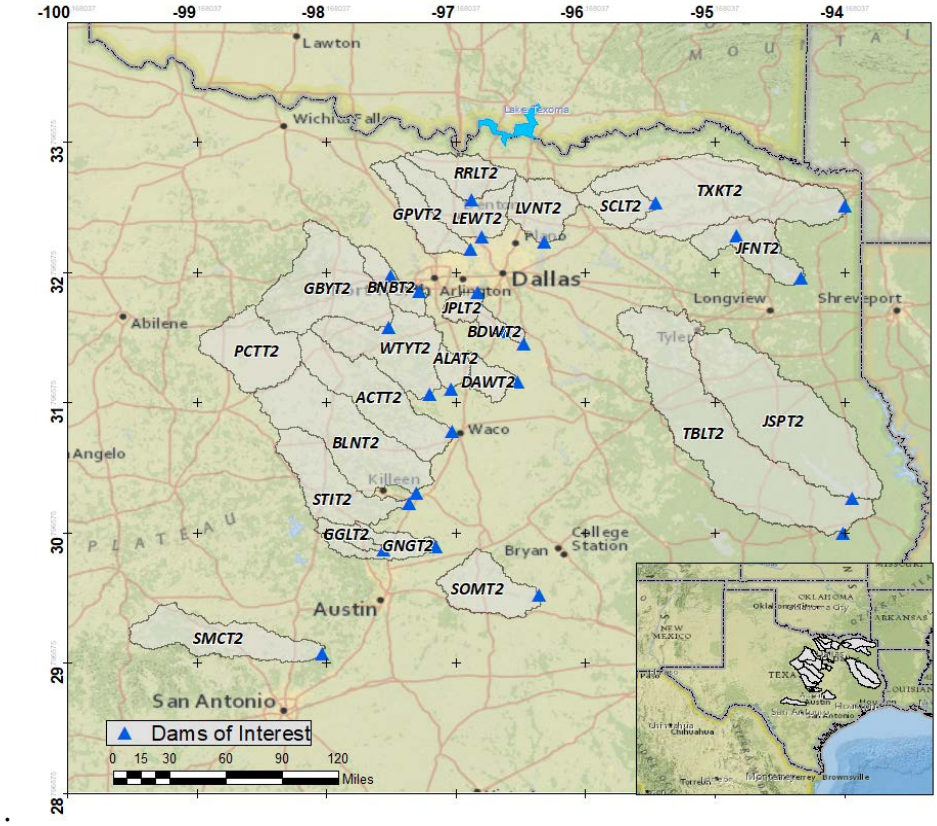

Figure 1. Location of the dams of interest

Datasets

Daily runoff time series were provided by the SWF for all sites of interest. The period of record available varies for each location, but all time series cover the period of 1981 to 2016. Basin average rainfall values were calculated based on the Parameter-elevation Regression on Independent Slopes Model (PRISM) AN81d (Daly and Bryant, 2013). PRISM accounts for topographic influences on precipitation patterns and amounts.

Soil moisture conditions for each watershed was characterized by the North American Land Data Assimilation System version 2 dataset (NLDAS-v2). NLDAS-v2 datasets are available at the hourly scale for the period of 1979 to present and are updated daily with a latency of 3 or 4 days. The spatial resolution of the NLDAS dataset is 13 km in space (Xia et al 2016).

NLDAS-v2 provides the results of four land surface models forced by the best available observations. For a review of these models refer to Cai et al (2014). The results from Noah-2.8 and VIC-4.0.5 are applied in this report. Noah-2.8 was selected since this model is used as the land surface component in multiple weather forecast systems[1]. The Noah-2.8 model was developed as the land component of the NOAA NCEP mesoscale Eta model (Xia et al 2012). VIC was selected since it is the model currently used to generate CMIP5 hydrology projections over the contiguous U.S. by the U.S. Bureau of Reclamation and collaborators (U.S. Bureau of Reclamation, 2014). This dataset can be potentially used to better understand the effects of climate change on runoff generation. VIC was also included in the project to verify if the methods applied in this project are sensitive to the land surface model applied.

Data for the period 1981 to 2016, which correspond to the period of available daily runoff data, were applied. The Noah-2.8 soil moisture variables used in this project include: soil moisture content (SOILM) for soil depths of 0 to 40 in, 0 to 80 in, 4 to 16 in, 16 to 40 in and 40 to 80 in; liquid soil moisture content (LSOIL) for soil depths of 0 to 4 in, 4 to 16 in, 16 to 40 in and 40 to 80 in; and moisture availability (MSTAV) for soil depths of 0 to 40 in and 0 to 80 in.

The VIC-4.0.5 model is a macroscale, semi-distributed, grid-based, hydrologic model developed at the University of Washington and Princeton University (Wood et al., 1997). NLDAS-2 applies the full water and energy balance version of VIC (version 4.0.5). The model includes three soil layers, with a 10 cm top layer (SOILM 1) and four deeper layers of spatially varying thicknesses (SOILM 2 and 3). Soil moisture (SOILM) and moisture availability (MSTAV) for the 0-40 inches layer (SOILM 0-40) and for the total column (SOILM Total) are also provided. The VIC model utilizes sub-grid vegetation tiles, and includes a two-layer energy balance snow model (Cherkauer et al., 2003) that uses sub-grid elevation bands to represent the impact of elevation on temperature, precipitation, and snow.

The time series of basin average precipitation and Noah 16-40 inch layer liquid soil moisture content (LSOIL) for the Benbrook Lake Reservoir for a dry (2011) and a wet (1991) year show the influence of initial soil moisture on runoff generation (Figure 2). LSOIL was similar in the beginning of both years. However, LSOIL decreased significantly in 2011 due to low precipitation and high temperature. By October 2011, LSOIL was significantly below average, while in October 1991 LSOIL was near average. For both years, a significant rainfall event (more than 4 inches/day) was registered in October. The resultant maximum peak inflow for this event was only 0.04 inch/day in 2011, while in 1991 a maximum peak inflow of 2.23 inch/day was observed.

[1] Weather Research and Forecasting (WRF) regional atmospheric model, the NOAA NCEP coupled Climate Forecast System (CFS) and the Global Forecast System (GFS)

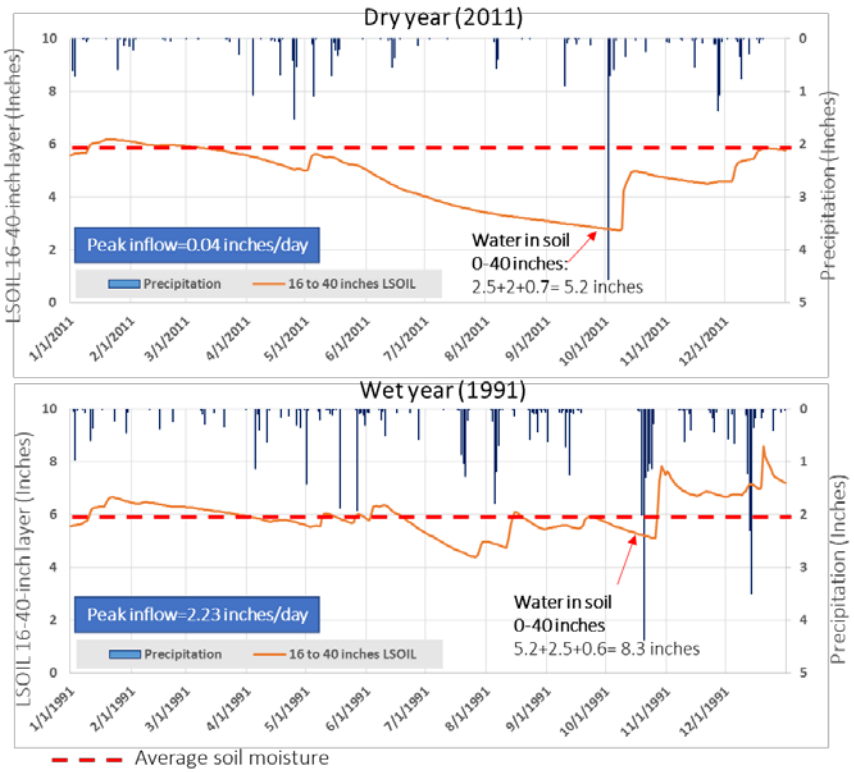

Figure 2. Time series of basin average precipitation and Noah 16-40 inch layer liquid soil moisture content for the Benbrook Lake Reservoir for a dry (2011) and a wet (1991) year.

Methodology

The HMS deficit and constant loss model (DCLM) applies an initial value of loss at the beginning of the rainfall event, prior to the beginning of surface runoff, which is a function of the current moisture state (MS) of the watershed. Interception loss (IL) accounts for rainfall intercepted by vegetation, retention on the surface (depression storage) and initial infiltration into the soil. As the watershed becomes saturated, the initial loss approaches zero. The drier the MS of the watershed, the higher IL will be.

Continuing loss (CL) is the average rate of loss throughout the rest of the storm and accounts for infiltration, percolation and evaporation. CL reflects the physical properties of the watershed (e.g. soil, land cover, topography) and the storm event (e.g. rainfall intensity, duration, spatial and temporal distribution). For the same watershed, CL varies only based on the properties of the rainfall event (RE).

From the start of the rainfall event, the water balance equation can be expressed as:

$$P = IL(MS) + CL(RE) * t + QF$$

where *P* is precipitation, *IL(MS)* is initial loss as a function of the moisture state of the watershed, *CL* is continuous loss as a function of the rainfall event properties (*RE*), t is the time for which rainfall is larger than zero and QF is the runoff resulting from the rainfall event. *QF* is expressed as the total inflow to the reservoir minus baseflow (BF). BF is the portion of the inflow that comes from the sum of deep subsurface flow and delayed shallow subsurface flow. *P*, *IL(MS)*, and *QF* are measured in inches, while *CL(RE)* is measured in inches per day.

Initial and continuous losses were estimated using daily basin average precipitation estimated from PRISM AN81D and runoff data provided by the SWF. The methods applied, as well as the results, are presented in the following sections.

Initial Loss Estimation: Initial loss is a function of the current state of saturation of the watershed. In the DCLM, the current moisture state of the watershed is specified as water deficit. The model requires the definition of two parameters: maximum soil deficit and soil deficit at the beginning of the simulation. In this section, a methodology to estimate maximum soil deficit and soil deficit as a function of the current moisture state of the watershed is presented.

From the available discharge and precipitation time series, it is possible to retrieve several indicators of hydrologic conditions prior to the flood events. To determine the optimal indicator for the hydro-meteorological conditions, multiple indicators were initially calculated and tested. These included: base flow at the beginning of each event, accumulated precipitation and discharge for 5, 15, and 30 days prior to the flood, the antecedent precipitation index (API) and antecedent flow index (AFI). Continuous time series of all indicators were generated.

Both rainfall and runoff present advantages and disadvantages when used to estimate soil moisture. Rainfall has the advantage of accounting for storm events even when no runoff is generated. Runoff has the advantage of being the result of the integration of multiple hydrologic processes at multiple spatial and temporal scales (rainfall, infiltration, evapotranspiration, flow transport), and therefore represents the overall state of the watershed. However, runoff indices are affected by season and do not necessarily reflect changes caused by rains during the previous week.

While rainfall and runoff indicators are suitable in many regions, that is not the case for Texas. All regions in Texas experience long periods of droughts, and during these periods rainfall and runoff indicators tend toward zero and are not able to capture the severity of the drought. To overcome this limitation, in this project soil moisture time series generated based on land surface models are applied. While measured soil moisture information is not readily available, simulated soil moisture data is available as output from land surface models. Since the soil moisture data is the output of a model, it is subject to model and data uncertainties. However, these datasets can be very useful since land surface models take into consideration other processes (e.g. evapotranspiration, soil percolation) that are not directly accounted for when applying observed precipitation and runoff datasets to estimate moisture indices.

To improve the real-time estimation of initial loss, relationships that relate initial losses to the current state of the watershed were developed. Various relationships were developed based on multiple moisture indicators with the goal of selecting the relationship that provides the best estimate of initial losses for each watershed.

Initial losses were estimated by evaluating historical rainfall-runoff events. Storm events that generated no or insignificant runoff were selected. To quantify insignificant runoff, a threshold was defined. The initial losses for these events were plotted against soil moisture indicators and linear or exponential relationships were fit to the data. Two examples are shown for the Benbrook Lake watershed based on (A) AFI and (B) Noah liquid soil moisture content (0 to 40-inch) (Figure 3). In this plot, different seasons are represented by markers of different shape and color. In general, the initial losses decrease as moisture conditions increases.

A methodology to extract semi-envelope curves was applied. An envelope curve of a series of points is represented by the smooth curve that outline all extreme points. The semi-envelope curves were derived by relaxing the requirement that all extreme points should be below the

curve. The semi-envelope curve focuses on the decay rate of the data, instead of encompassing all extreme points.

Semi-envelope curves are used instead of envelope curves since initial losses that result in saturated or almost saturated soils were probably not observed for the full range of initial states of the watershed. Moreover, uncertainties arise from using daily instead of hourly precipitation and runoff data as well as from including multiple day events without a more robust representation of evapotranspiration.

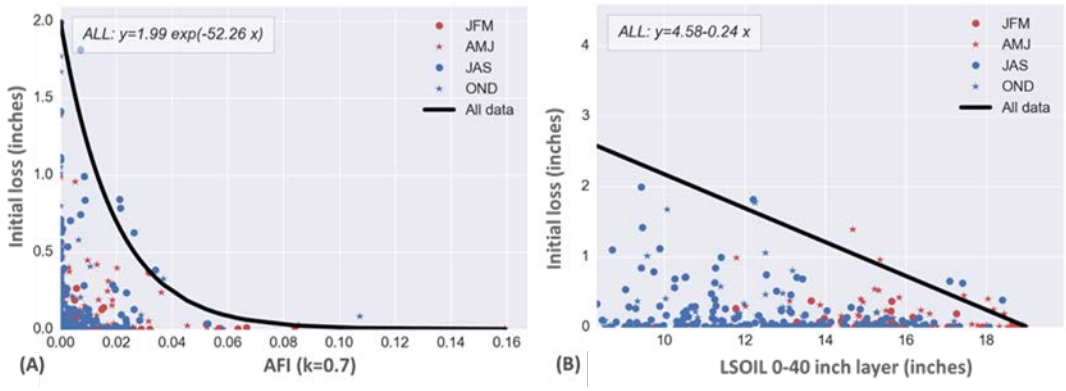

Figure 3. (A) AFI and (B) liquid soil moisture content at the 0 to 40-inch soil layer versus initial loss data (inches) for BNBT2. Values for different seasons are identified by color and marker shape. JFM: January, February, and March; AMJ: April, May and June; JAS: July, August and September, and OMD: October, November and December.

Continuous and total loss estimation: Storm events generating significant runoff were selected from the available time series of precipitation and runoff. For each event, initial loss was estimated using the soil moisture indicator for the beginning of the event and the exponential or linear curves described in the previous section. Once the initial loss is known, continuous loss can be calculated as a function of known properties of the event, including total rainfall, number of days with rain, average daily rainfall and the moisture condition in the beginning of the event. An optimization procedure was implemented to determine which moisture indicator best describes initial losses for the basins of interest, and which characteristics of the rainfall event best predict continuous loss.

The procedure to estimate initial and continuous losses is schematically represented in Figure 4. The goodness of fit of the relationships are evaluated based on the coefficient of determination ($\rho 2$) and the normalized RMSE (CVRMSE). The coefficient of determination ($\rho 2$) is a number that indicates the proportion of the variance in the dependent variable that is explained by the independent variable(s). The root mean squared error (RMSE) provides a measure of the differences between predicted and observed values. The normalized RMSE (CVRMSE) is adopted since allows for the direct comparison of different datasets or models.

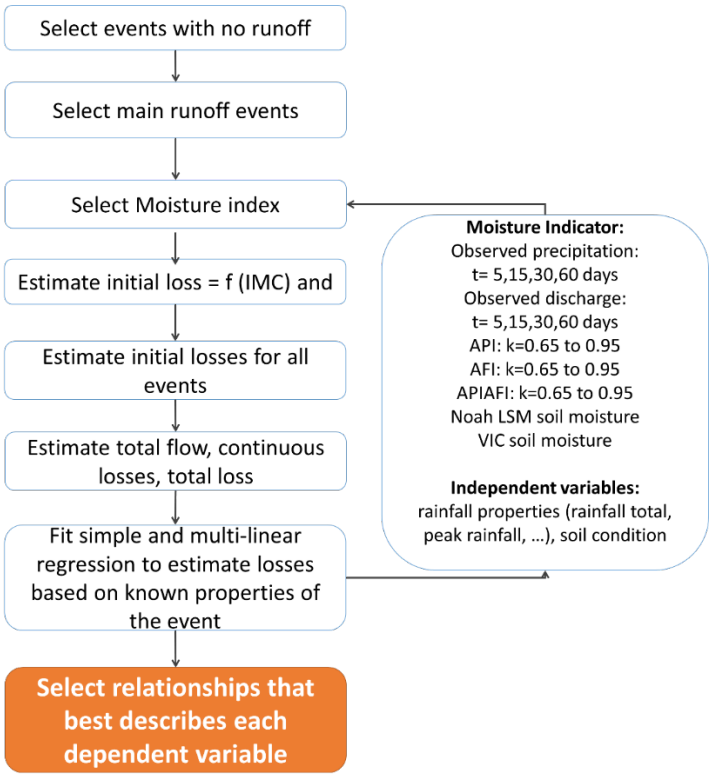

Figure 4. Optimization procedure to select the best moisture indicator and relationships to predict the characteristics of flood events (dependent variables)

Runoff event selection: Figure 5 shows a schematic representation of the procedure used to select main runoff events. The figure contains all the steps required to define the events.

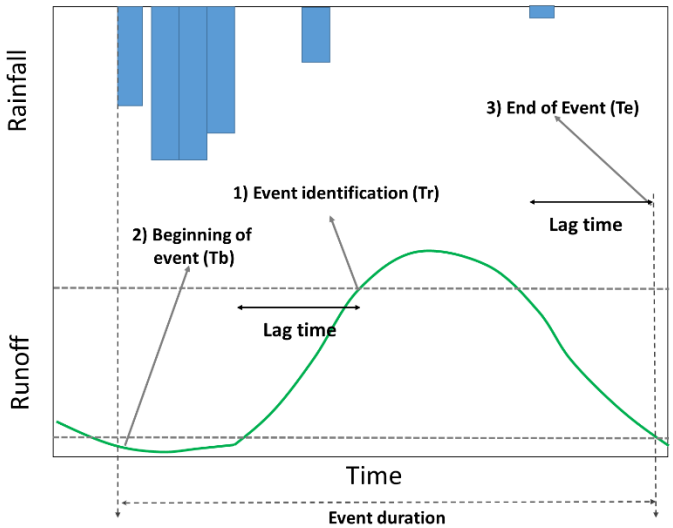

1) **Event identification:** identify runoff that is larger than the 98th runoff percentile;
2) **Beginning of event (Tb):** look backwards from Tr minus concentration time and identify two days with rainfall equal to zero or the end of the previous event;
3) **End of event (Te):** look forward from Tr and identify the time for which the three criteria are valid:
    3.1) Runoff less than half of the 98th runoff percentile
    3.2) No significant rainfall for the last Tc days
    3.3) No significant decay in runoff for 2 consecutive time steps

Figure 5. Runoff event selection process: schematic representation

Event-Based Hydrological Analysis: Results

Initial and Continuous Loss Estimation: The best soil moisture indicator varied for each basin and variable being predicted. To be consistent and to allow the direct comparison among different basins of interest a unique soil moisture indicator was selected for all sites. The Noah SOILM 0-40 inches layer was selected since its performance for all basins and variables does not differ significantly from the performance obtained with the best NLDAS soil moisture indicator.

Statistically significant relationships between hydrological losses and the following variables were identified: a) Soil moisture state at the beginning of rainfall; b) Storm total rainfall volume; c) Duration of rainfall; and d) Peak day rainfall intensity.

The r-squared and CV(RMSE) for relationships to estimate total loss, total continuous loss, and peak runoff based on Noah SOILM 0-40-inch data are shown in Figure 6. For all watersheds, the NLDAS relationships explained from 73% (LEWT2) to 96% (WTYT2) of the variation in total loss, 61% (PCCT2) to 95% (GGLT2 and WTYT2) of the variation in total continuous loss and 32% (JFNT2) to 75% (BNBT2) of the variation in peak flow. CVRMSE is shown in Figure 7. Total loss and total continuous loss present similar errors, while errors for peak flow are considerable higher. This is expected since the estimation of peak flow using daily data is limited especially for small watershed with lag time of 1 day or less.

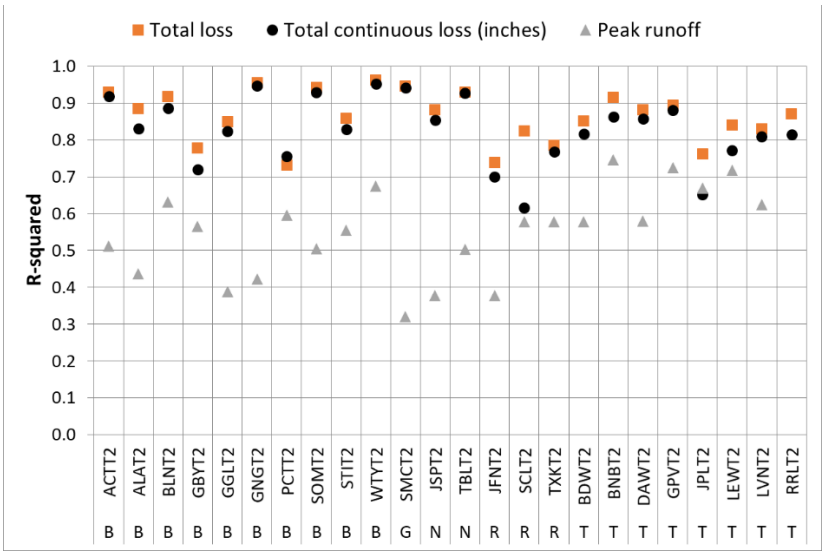

Figure 6. R-squared for relationships to estimate total loss, total continuous loss, and peak runoff based on soil moisture data (Noah SOILM 0-40) for watersheds of interest (Figure 1). Sub-basins are identified in Figure 1. Watersheds are identified by B: Brazos; G: Guadalupe; N: Neches; R: Red and T: Trinity watershed.

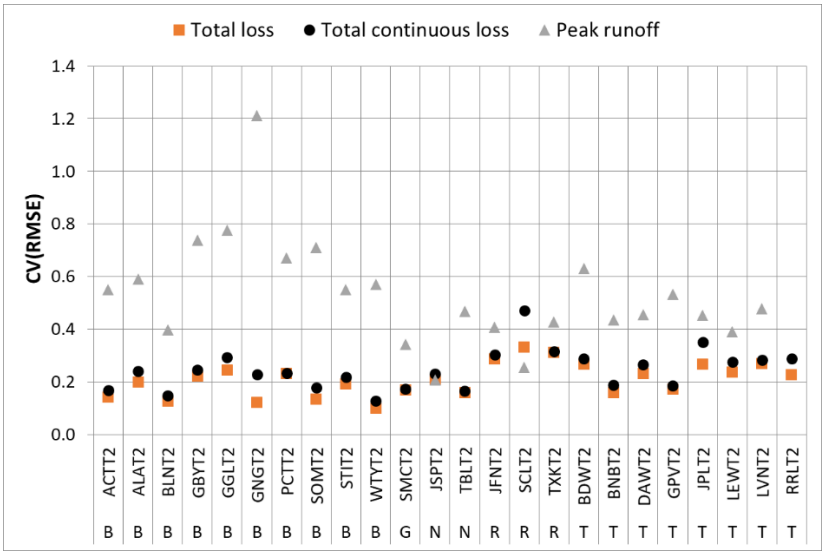

Figure 7. CV(RMSE) for relationships to estimate total loss, total continuous loss, and peak runoff based on soil moisture data (Noah SOILM 0-40). Sub-basins are identified in Figure 1. Watersheds are identified by B: Brazos; G: Guadalupe; N: Neches; R: Red and T: Trinity watershed.

Operational Tools: The results for all watersheds are provided in two main products developed to support event-based forecast:

1. Summary sheet: an individual summary sheet was created for each basin containing all the relevant information generated in this project. The summary sheet was designed taking into consideration forecasters need in the advance of an event. The document can be used to evaluate the current condition of the watershed in comparison to past conditions, and to make predictions if a computer is not available. The document can also be used to compare the response of different watersheds.

2. Total Runoff Tool: The results of the regression analyses were compiled in Excel files designed to support event-based runoff estimation at the daily scale. The Excel files are referred as the "Total Runoff Tools" (TRT). The TRTs contain basically the same information shown in the Summary Sheets in a way to support automated calculations for real time operations.

For brevity, the summary sheet for only one watershed will be discussed and included in this paper. Figure 8 and Figure 9 contain the first and second pages of the Benbrook Lake Watershed summary sheet. The following sections are included in the summary sheet:

1. General Statistics (Figure 8): This section contains general characteristics of the watershed, including the SHED code, name of the dam it drains to, USGS Site ID number, drainage area, mean annual precipitation, mean annual flow, mean annual loss, lag time, curve number, main land use, the 1, 5, 25, 50, 75, 95, and 99 quantiles for daily rainfall, daily runoff, initial condition, and seasonal initial condition. It also shows a map of the basin location.
2. Daily changes (Figure 8): This section contains two plots that show how initial soil moisture affects daily changes in runoff and soil moisture:
3. The plot on the left shows daily change in runoff as a function of initial soil moisture condition (x-axis) and accumulated rainfall for the lag time in days plus one (color-coded). This plot can be applied to understand the limits of daily runoff change as a function of the current soil moisture condition of the basin.
4. It is important to note that significant daily change in runoff does not occur when the soil is dry, but dry soil conditions vary from basin to basin. For example, for BNBT2 the maximum observed daily change in runoff is 2-inch/day and it occurred when soil moisture condition (SOILM 0-40-inch layer) was approximately 13.7 inches. For LVNT2 the maximum observed daily change in runoff is 3.8-inch/day and it occurs when soil moisture condition was approximately 14.4. For both basins the maximum daily runoff change occurred when the 2-day accumulated precipitation was higher than 4-inch. For TBLT2, the maximum observed daily change in runoff is approximately 0.23 inches/day, even when the soil is close to saturation.
5. The plot on the right shows the 4-day change in soil moisture as a function of initial soil moisture condition (x-axis) and the 4-day accumulated rainfall (color-coded). This plot allows the operator to estimate minimum and maximum changes in soil moisture that might have occurred during the NLDAS latency period. This plot can be used to obtain an initial estimation of the updated soil moisture. This plot also provides an estimation of the physical limits of continuous losses for each initial soil moisture condition. This information should be used with caution since the results shown in the plot are for simulated soil moisture properties over the entire watershed on the period of 4 days as simulated by a land surface model. Therefore, this information should not be used to determine the maximum infiltration over a short period of time and at a specific location in the basin.
6. Soil moisture and daily runoff (Figure 8): This section contains two plots that show how initial soil moisture affects daily runoff and how soil moisture distribution changes with the day of the year:
    a. The plot in the left shows daily runoff as a function of initial soil moisture condition (x-axis) and accumulated rainfall for the lag time in days plus one (color-coded). This plot can be applied to understand the limits of daily runoff as a function of the current soil moisture condition of the basin. Daily runoff

increases as soil moisture increases. Maximum daily runoff also varies significantly from basin to basin.

b. The plot in the right presents the distribution of soil moisture for each day of the year based on the period of 1981 to 2016. Shaded areas define the minimum and maximum, the 5th and 95th percentile, and the 25th and 75th percentile of soil moisture for each day of the year. The black line indicates the mean soil moisture for each day. This figure allows the operator to contextualize the current state of the soil in relation to what has been observed in previous years. This plot is also useful during drought situations to better understand current drought intensity.

7. Initial condition update (Figure 9): This section presents the equations to update the soil moisture condition as a function of the current soil moisture and the accumulated rainfall for latency period of 3 or 4 days.
8. Runoff relationships (Figure 9): This section presents the equations to estimate initial loss, continuous loss, total loss and peak runoff for a storm event. The section also contains a plot that allows the forecaster to visually estimate an approximate value of total runoff as a function of total rainfall, initial soil moisture (color-coded) and peak rainfall intensity (marker size). Automated calculations based on these equations can be performed in the TRT.
9. Spatial variability (Figure 9): This section contains maps that allow the forecaster to evaluate the spatial variability of hydrological losses in the basin of interest. The map on the left shows spatial variability of hydrological losses for each HUC 12. The map on the right shows the loss spatial factor k, which represents the percentage of hydrological losses that occurs in each sub-area. This maps can be used to estimate uncertainties in the quantification of losses depending on the location of the storm in the basin.

Conclusions

A novel methodology to estimate hydrologic losses and total runoff at the event scale incorporating daily data was developed and encoded in Excel spreadsheets for operational use. The methodology relies on the analytical results derived from daily runoff, precipitation, and soil moisture indicator data. Rainfall events generating little or no runoff were used to establish relationships to estimate initial losses. Significant runoff events were used to establish relationships to estimate continuous and total losses based on the properties of the rainfall and initial soil moisture conditions. The results provides two main products to support event-based forecast, a summary sheet, and a Total Runoff Tool. The proposed methodology offers a significant improvement over current methods used to estimate hydrologic losses.

BNBT2: Benbrook Lake USGS: 08046500 Drainage area: 430 mi² 1/2

General Statistics

Trinity basin
Mean annual precipitation = 35.42 inches
Mean annual flow = 4.73 inches
Mean annual loss = 87.4%
Lag Time= 1 day
CN = 79.8
Main land use = Grasslands 61.0%
Open water and wetlands 2.8%

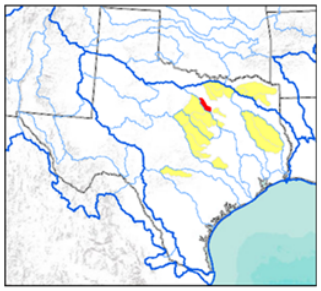

	Quantiles (units: inches)						
Statistics	1	5	25	50	75	95	99
Daily rainfall (>0)	0.01	0.01	0.05	0.17	0.47	1.36	2.55
Daily runoff	0.01	0.01	0.01	0.02	0.04	0.1	0.52
Initial condition	5.53	6.34	8.06	9.39	10.48	11.55	12.29
Initial condition (JFM)	6.37	7.86	9.44	10.35	10.98	11.7	12.25
Initial condition (AMJ)	7.26	7.76	9.04	9.96	10.72	11.85	12.64
Initial condition (JAS)	5.56	5.88	6.91	7.78	8.9	10.32	11.2
Initial condition (OND)	5.21	6.16	7.92	9	10.16	11.46	12.25

Daily changes

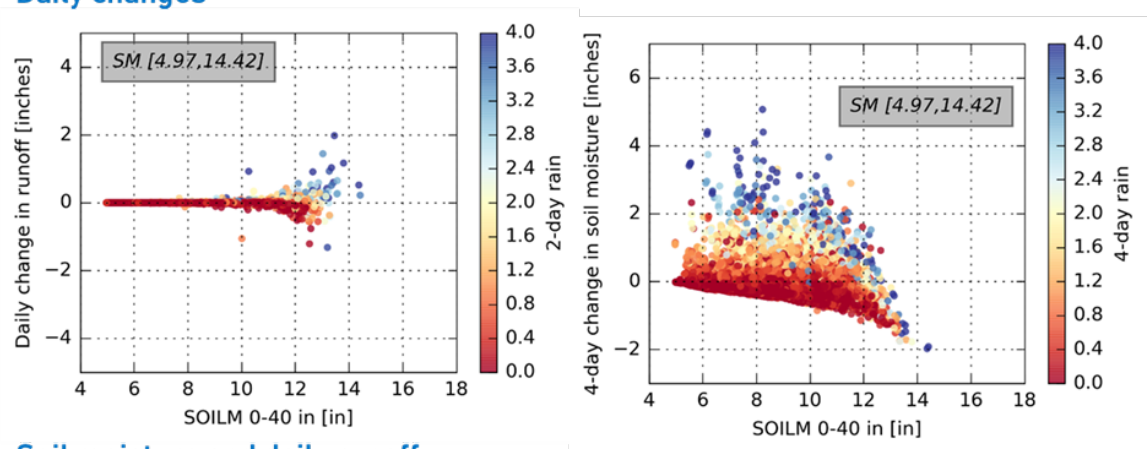

Soil moisture and daily runoff

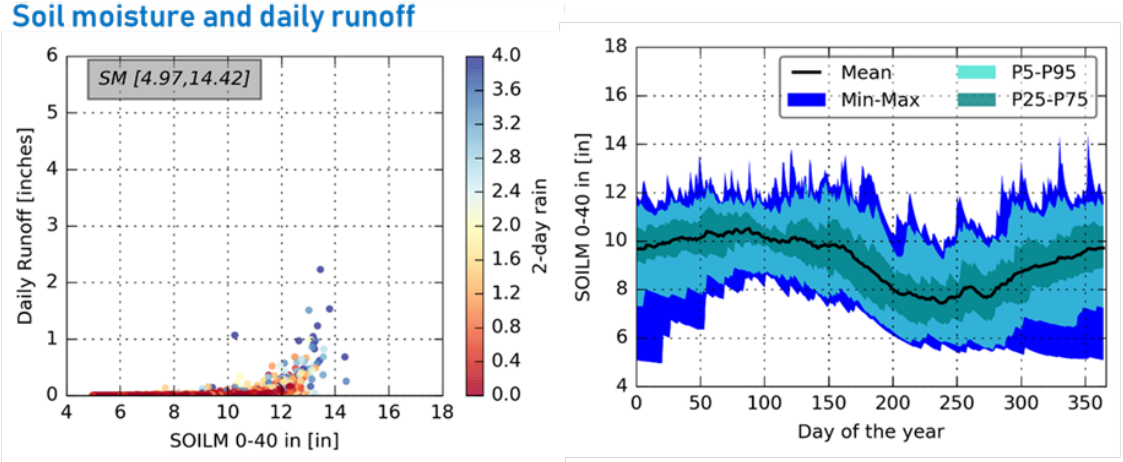

Figure 8. Runoff event selection process: schematic representation

BNBT2: Benbrook Lake, USGS: 08046500 Drainage area: 430 mi^2 2/2

Initial condition update

Latency	Rain=0	Rain>0
3-day	$IC = 0.96\,x\,IC_{(t-3)} + 0.15$	$IC = 0.43\,x\sum_{-1}^{-3} R_{(t)} + 0.95\,x\,IC_{(t-3)} + 0.36$
4-day	$IC = 0.95\,x\,IC_{(t-4)} + 0.19$	$IC = 0.43\,x\sum_{-1}^{-4} R_{(t)} + 0.93\,x\,IC_{(t-4)} + 0.45$

Runoff relationships

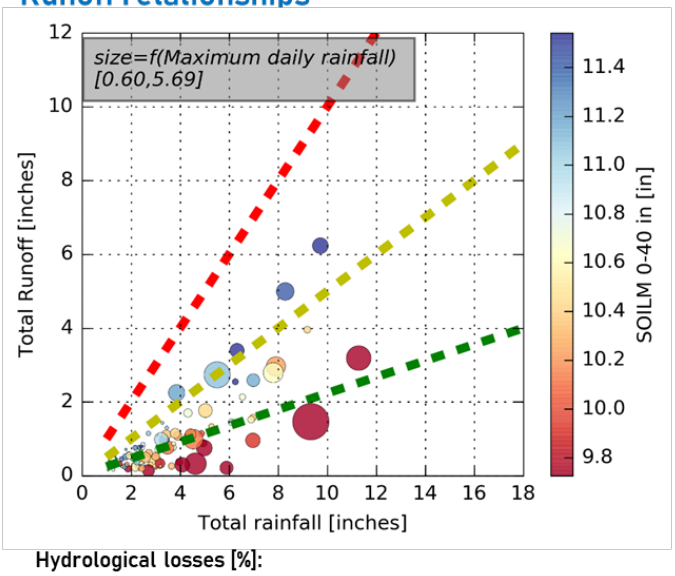

$Number\ of\ events = 93$

$Average\ event\ duration = 5 - days$

$IL = 5.75 - 0.54\,x\,IC$

$CL = 1.58 + 0.54\,x\,TR\ -0.11\,x\,IC$

$TL = IL + CL \quad Or$

$TL = 5.93 + 0.55\,x\,TR\ -0.50\,x\,IC$

$TRun = TR - TL$

$PRun = -2.16 + 0.31\,x\,PR\ +0.18\,x\,IC$

IC=Initial condition based on NLDAS-v2 NOAH SOILM 0-40 inches layer (in); IL= Initial loss (in); TR=Total rainfall (in); CL=Continuous loss (in); ND=Number of days rainfall ;TL=Total loss (in); TRun=Total runoff (in); PR= peak rainfall (in/day); PRun = peak runoff (in/day); AR=Average daily rainfall (in/day)

Spatial variability

HUC 12 - Losses

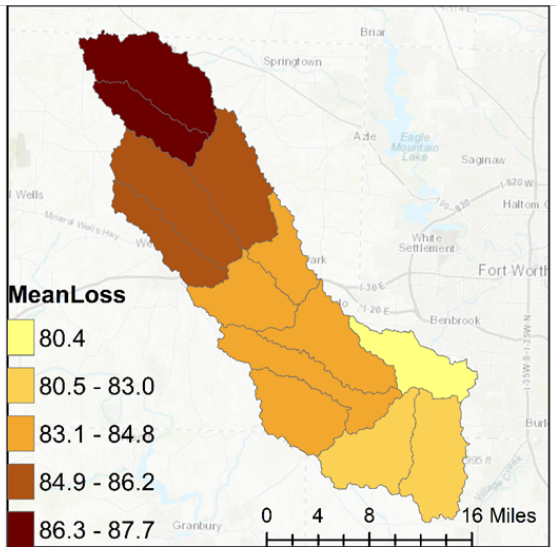

Loss spatial factor (k)

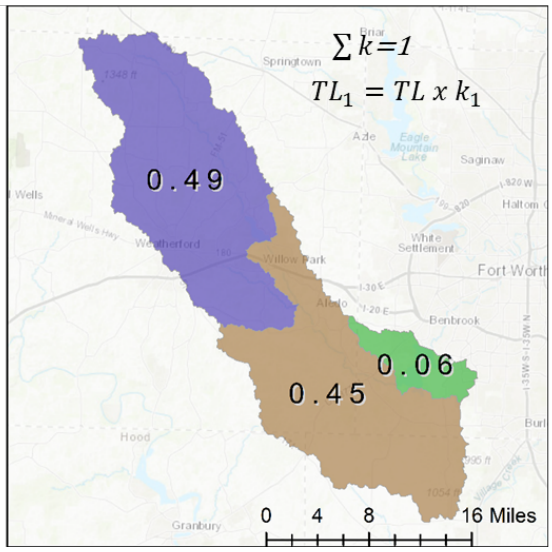

Figure 9. Runoff event selection process: schematic representation

References

Cai, Xitian, et al. Assessment of simulated water balance from Noah, Noah-MP, CLM, and VIC over CONUS using the NLDAS test bed. Journal of Geophysical Research: Atmospheres 119.24 (2014): 13-751.

Cherkauer, K. A., L. C. Bowling, and D. P. Lettenmaier (2003), Variable infiltration capacity cold land process model updates, Global Planet. Change, 38(1–2), 151–159, doi:10.1016/S0921-8181(03)00025-0.

Daly, C., Bryant, K. The PRISM climate and weather system – an introduction. Cai et al (2014) Available at: http://www.prism.oregonstate.edu/documents/PRISM_history_jun2013.pdf. Accessed on 06/2015.

U.S. Bureau of Reclamation (2014). Downscaled CMIP3 and CMIP5 climate and hydrology projections: release of hydrology projections, comparison with preceding Information, and summary of user needs, prepared by the U.S. Department of the Interior, Bureau of Reclamation, Technical Services Center, Denver, Colorado. 110 pp.

Wood, E. F., D. Lettenmaier, X. Liang, B. Nijssen, and S. W. Wetzel (1997), Hydrological modeling of continental-scale basins, Annu. Rev. Earth Planet. Sci., 25, 279–300, doi:10.1146/annurev.earth.25.1.279.

Xia, Y., Mitchell, K., Ek, M., Sheffield, J., Cosgrove, B., Wood, et al. (2012). Continental-scale water and energy flux analysis and validation for the North American Land Data Assimilation System project phase 2 (NLDAS-2): 1. Intercomparison and application of model products. Journal of Geophysical Research: Atmospheres, 117(D3).

Xia, Youlong, Brian A. Cosgrove, Kenneth E. Mitchell, Christa D. Peters-Lidard, Michael B. Ek, Michael Brewer, David Mocko, Wei, H., Meng, J. and Luo, L.,. Basin-scale assessment of the land surface water budget in the National Centers for Environmental Prediction operational and research NLDAS-2 systems. Journal of Geophysical Research: Atmospheres121, no. 6 (2016): 2750-2779.

Predicting Post-Fire Hillslope Erosion and Small Watershed Response with Online Interfaces Using WEPP Technology

Peter R. Robichaud[1], Marianna Dobre[2], Roger Lew[2] William J. Elliot[1], Erin Brooks[2], Mary Ellen Miller[3], Dylan Quinn[2]

[1]USDA-Forest Service, Rocky Mountain Research Station, Moscow, Idaho, [2]University of Idaho, Moscow, Idaho, [3]Michigan Technology Research Institute, Michigan Technological University, Ann Arbor, Michigan. probichaud@fs.fed.us; mdobre@uidaho.edu; rogerlew@uidaho.edu; welliot@fs.fed.us; ebrooks@uidaho.edu; memiller@mtu.edu; quinnd@uidaho.edu

Wildfires continue to be a frontline priority for forest management throughout the western US. The threat of erosion, flooding and debris flows after fire is a major concern for land managers and water purveyors around the world. Decision support tools that incorporate the range of burn severity conditions are essential to accurately determine the risk of erosion and flooding. Various online interfaces have been developed using the Water Erosion Prediction Project (WEPP) model as the engine; aimed to evaluate the risks of upland erosion, sediment delivery and flood flows from forest and rangeland watersheds smaller than 5000 ha. Considerable efforts have been made to improve model algorithms and input parameters, and the interfaces restructured to be meaningful and end-user-friendly for post-fire assessments. Various interfaces allow users to run simulations for hillslopes and watersheds and even employ cloud computing power with online GIS or in ArcGIS environments. After a wildfire, managers develop a soil burn severity map from remotely sensed imagery and ground surveys. The spatially explicit map showing the distribution of soil burn severity on the landscape can be easily uploaded as a raster layer for model use. The various interfaces allow the user to run WEPP with menu-driven input selections to access databases of topography, soils and climate layers for the areal extent of the burned area. Numerous erosion prediction calculations are automatically carried out then results are displayed in both spatial and tabular data formats, and a graphical display of hillslope erosion rates is color-coded for ease in visualizing high erosion risk areas. Batch programs allow for assessment over large burned areas and can easily compare mitigation treatments (e.g. mulching) on reducing hillslope erosion. Outputs are available for return interval comparisons at hillslope or watershed scales and can be sorted by precipitation, total runoff or peak flow. Validation efforts have been completed at various hillslope- and small watershed-scale burned areas with satisfactory results.